Andreas H. Mahnken · Kai E. Wilhelm
Jens Ricke *Editors*

CT- and MR-Guided Interventions in Radiology

Second Edition

Springer

CT- and MR-Guided Interventions in Radiology

Andreas H. Mahnken • Kai E. Wilhelm
Jens Ricke
Editors

CT- and MR-Guided Interventions in Radiology

Second Edition

Springer

Editors
Andreas H. Mahnken
Department of Diagnostic and
Interventional Radiology
University Hospital
Marburg
Germany

Philipps University of Marburg
Marburg
Germany

Kai E. Wilhelm
Department of Radiology
University Hospital Bonn
Bonn
Germany

Jens Ricke
Department of Radiology and
Nuclear Medicine
University Hospital Magdeburg
Magdeburg
Germany

ISBN 978-3-642-33580-8 ISBN 978-3-642-33581-5 (eBook)
DOI 10.1007/978-3-642-33581-5
Springer Heidelberg New York Dordrecht London

Library of Congress Control Number: 2012953476

Printed on acid-free paper

Springer is part of Springer Science+Business Media (www.springer.com)

Dedicated to our teaches, mentors, families and friends.
Forwarding Interventional Radiology

Foreword

There has been an increasing interest in and need for CT- and MR-guided nonvascular applications in Interventional Radiology in the past few years. The rapid development, progress and clinical demand in this field explain that 3 years after the publication of the first successful edition in 2009, the current authors – Andreas Mahnken from my former department at Aachen University, Jens Ricke from Magdeburg University and Kai E. Wilhelm from Bonn University – present an attractive second edition which has been revised, updated and enlarged by including new data and new aspects. CT- and MR-guided interventions belong to the very few still Radiology-dominated fields, and thus, interventional radiologists should continue to play an eminent role there without neglecting ultrasonography as a competing as well as an adjunctive modality.

A book like this helps propagating the ideas of nonvascular interventions and serves as a textbook as well as a source of valuable information and guidance for our daily practice. It covers a comprehensive spectrum of CT- and MR-guided nonvascular interventions with a special focus on Interventional Oncology and reflects the high expertise of the authors involved. I am sure that the second edition, too, will be a most valuable clinical companion in a rapidly developing and most promising part of Interventional Radiology.

Berlin, Germany
January 2013

Rolf W. Günther, M.D.

Contents

Contributors

Thierry de Baère Department of Interventional Radiology, Institut Gustave Roussy, Villejuif, France

Reto Bale SIP – Department for Microinvasive Therapy/Department of Radiology, Medical University Innsbruck, Innsbruck, Austria

Alexander Beck Klinik für Strahlenheilkunde, Charité Campus-Virchow-Klinikum, Berlin, Germany

Philipp G.C. Begemann Röntgeninstitut Düsseldorf, Düsseldorf, Germany

Oliver Beuing Department of Neuroradiology, University Hospital Magdeburg, Magdeburg, Germany

Deniz Bilecen Department of Interventional Radiology, University of Basel, Basel, Switzerland

Mathias Bosch Boston Scientific Medizintechnik GmbH, Ratingen, Germany

Roland Bruening Roentgeninstitut Asklepios Klinik Barmbek, Hamburg, Germany

Philipp Bruners Department of Diagnostic and Interventional Radiology, University Hospital, RWTH Aachen University, Aachen, Germany

Arno Bücker Department of Diagnostic and Interventional Radiology, University Hospital Saarland, Homburg, Germany

Stephan Clasen Department of Diagnostic and Interventional Radiology, Eberhard-Karls-University Tübingen, Tübingen, Germany

Philip Ditter Department of Radiology, University of Hospital Bonn, Bonn, Germany

Markus Düx Department of Radiology and Neuroradiology, Krankenhaus Nordwest, Frankfurt am Main, Germany

Katrin Eichler Department of Diagnostic and Interventional Radiology, University of Frankfurt/Main, Frankfurt am Main, Germany

Joseph P. Erinjeri Department of Radiology, Interventional Radiology Service, Memorial Sloan-Kettering Cancer Center, New York, NY, USA

Dimitris Filippiadis 2nd Department of Radiology, National and Kapodistrian University of Athens Medical School, University General Hospital «Attikon», Athens, Greece

Roman Fischbach Department of Radiology, Asklepios Klinik Altona, Hamburg, Germany

Thomas Gast Interventional Radiology Service, Memorial Sloan-Kettering Cancer Center, New York, NY, USA

Thomas Helmberger Department of Diagnostic and Interventional Radiology and Nuclearmedicine, Klinikum Bogenhausen, Munich, Germany

Susanne Hengst Klinik für Strahlenheilkunde, Charité Campus-Virchow-Klinikum, Berlin, Germany

Dietrich Henzler Departments of Anesthesia and Critical Care, QE II Health Science Centre, Dalhousie University, Halifax, NS, Canada

Jan Hoeltje Roentgeninstitut Asklepios Klinik Barmbek, Hamburg, Germany

Ralf-Thorsten Hoffmann Department of Clinical Radiology, Großhadern Campus, Ludwig-Maximilians-University Munich, Munich, Germany

Christian Hohl Department of Diagnostic and Interventional Radiology, HELIOS Hospital Siegburg, Siegburg, Germany

Dagmar Honnef Department of Diagnostic and Interventional Neuroradiology, University Hospital, RWTH Aachen University, Aachen, Germany

Augustinus L. Jacob Department of Interventional Radiology, University of Basel, Basel, Switzerland

Bruno Kastler Department of Radiology and Laboratoire d'Imagerie et d'Ingenierie, University of Besançon, CHU Minjoz, Besançon, France

Marcus Katoh Department of Diagnostic and Interventional Radiology, HELIOS Hospital Krefeld, Krefeld, Germany

Alexis Kelekis 2nd Department of Radiology, National and Kapodistrian University of Athens Medical School, University General Hospital «Attikon», Athens, Greece

Sebastian Kos Department of Interventional Radiology, University of Basel, Basel, Switzerland

Gabriele A. Krombach Department of Radiology, University Hospital Gießen, Gießen, Germany

Andreas Lubienski Radiology Health Care Centre Minden, Minden, Germany

Martin G. Mack Department of Diagnostic and Interventional Radiology, University of Frankfurt/Main, Frankfurt am Main, Germany

Andreas H. Mahnken Department of Diagnostic and Interventional Radiology, University Hospital, Marburg, Germany

Philipps University of Marburg, Marburg, Germany

Jean-Baptiste Martin GIC-Geneva Imaging Center Sàrl, Genève, Switzerland

Robert C.G. Martin Division of Surgical Oncology, University of Louisville School of Medicine, Louisville, KY, USA

Peter Messmer Department of Interventional Radiology, University of Basel, Basel, Switzerland

Bernhard C. Meyer Department of Diagnostic and Interventional Radiology, MH Hannover, Hannover, Germany

Konrad Mohnike Klinik für Radiologie und Nuklearmedizin, Universitätsklinikum Magdeburg, Magdeburg, Germany

Michael Murphy Departments of Anesthesia and Critical Care, QE II Health Science Centre, Dalhousie University, Halifax, NS, Canada

Philippe L. Pereira Department of Radiology and Nuclear Medicine, Klinikum Am Gesundbrunnen, Heilbronn, Germany

Ulf Redlich Department of Radiology and Nuclear Medicine, University Hospital Magdeburg, Magdeburg, Germany

Jens Ricke Department of Radiology and Nuclear Medicine, University Hospital Magdeburg, Magdeburg, Germany

Christian Rosenberg Department of Diagnostic Radiology and Neuroradiology, Ernst Moritz Arndt University, Greifswald, Germany

Arnd-Oliver Schäfer Department of Diagnostic Radiology, University Hospital Freiburg, Freiburg, Germany

Suzanne C. Schiffman Division of Surgical Oncology, University of Louisville School of Medicine, Louisville, KY, USA

Günther Schneider Department of Diagnostic and Interventional Radiology, University Hospital Saarland, Homburg, Germany

Simone Schrading Department of Diagnostic and Interventional Radiology, University Hospital, RWTH Aachen University, Aachen, Germany

Martin Sedlmair Siemens Healthcare, CT, Forchheim, Germany

Jens-Peter Staub MVZ Schießstattweg, Passau, Germany

Holger Strunk Department of Radiology, University Hospital Bonn, Bonn, Germany

Patrick Stumpp Department of Diagnostic Radiology, University Hospital Leipzig, Leipzig, Germany

Toshihiro Tanaka Department of Radiology, Nara Medical University, Kashihara, Japan

Christoph Thomas Department of Diagnostic and Interventional Radiology, Eberhard-Karls-University Tübingen, Tübingen, Germany

Christoph Gregor Trumm Department of Clinical Radiology, Großhadern Campus, Ludwig-Maximilians-University Munich, Munich, Germany

Bernd Turowski Department of Neuroradiology, Heinrich-Heine-University, Düsseldorf, Germany

Thomas J. Vogl Department of Diagnostic and Interventional Radiology, University of Frankfurt/Main, Frankfurt am Main, Germany

Markus Völk MVZ Theresientor, D-Straubing, Germany

Frank K. Wacker Department of Diagnostic and Interventional Radiology, MH Hannover, Hannover, Germany

Gerlig Widmann SIP – Department for Microinvasive Therapy/Department of Radiology, Medical University Innsbruck, Innsbruck, Austria

Gero Wieners Department of Radiology and Nuclear Medicine, University Hospital Magdeburg, Magdeburg, Germany

Joachim E. Wildberger Department of Radiology, University Hospital Maastricht, Maastricht, The Netherlands

Kai E. Wilhelm Department of Radiology, University Hospital Bonn, Bonn, Germany

Oliver Wüsten Radiologie im Liebig-Center, Bahnhofstraße, Gießen, Germany

Part I

Basics

Pre- and Postinterventional Imaging

1

Marcus Katoh, Günther Schneider, and Arno Bücker

Contents

1.1 Introduction

Every intervention starts with the visualization of the target organ or lesion and planning of the path to the chosen target. In principle, any imaging modality that provides images with adequately high spatial resolution and contrast can be used for pre- and postinterventional imaging. The image contrast needed encompasses visualization of the target lesion as well as the surrounding anatomy, particularly critical structures along the intended needle path. This is a prerequisite for defining the ideal path to the lesion and for monitoring the interventional procedure. During the intervention, real-time imaging would be the ideal solution, but near real-time imaging usually will suffice.

X-ray fluoroscopy provides real-time images with high spatial resolution. Until now, X-ray fluoroscopy in combination with iodine contrast medium application is regarded as the gold standard for vascular intervention. It is also used for guiding musculoskeletal procedures like percutaneous osteosynthesis or arthrography. For other indications, however, X-ray fluoroscopy is less suited to monitor interventions due to the low intrinsic soft tissue contrast and the lack of three-dimensional information in projection images.

Similar to X-ray fluoroscopy, ultrasound offers (near) real-time image acquisition with high spatial resolution. In addition, contrast agents can be applied to improve image contrast or to acquire dynamic perfusion information (Wells 2006; Delorme et al. 2006). However, the field of view is limited. Furthermore, bone and air may impair

M. Katoh, M.D. (✉)
Department of Diagnostic and Interventional Radiology,
HELIOS Hospital Krefeld,
Lutherplatz 40, Krefeld D-47805, Germany
e-mail: marcus.katoh@helios-kliniken.de

G. Schneider, M.D. • A. Bücker, M.D.
Department of Diagnostic and Interventional Radiology,
University Hospital Saarland,
Kirrbergerstr. 1, Homburg D-66421, Germany

A.H. Mahnken et al. (eds.), *CT- and MR-Guided Interventions in Radiology*,
DOI 10.1007/978-3-642-33581-5_1, © Springer-Verlag Berlin Heidelberg 2013

the visualization of the target as they prevent ultrasound penetration. Moreover, ultrasound monitoring of hyperthermal ablation procedures is limited due to air bubbles caused by vaporization. Therefore, ultrasound guidance is mostly used for superficial lesions that can be easily reached without the risk of injuring adjacent organs or vessels. Dedicated interventional ultrasound probes with a central perforation may be used, which allow the accurate delineation and positioning of dedicated interventional devices. Alternatively dedicated needle holders are available for aligning the puncture needle to the position of the ultrasound transducer, thereby facilitating ultrasound-guided procedures.

In contrast, cross-sectional imaging modalities like computed tomography (CT) and magnetic resonance (MR) imaging provide excellent overviews with the capability of three-dimensional reconstructions due to the volumetric data set. Intestinal or vascular structures can be clearly identified. In addition, the same slice orientation can be imaged multiple times, which in turn allows for precise planning of the path to the lesion even in deeper areas of the body. This chapter deals with general considerations for pre- and postinterventional imaging and provides the basic knowledge for successful periinterventional CT and MR imaging.

1.2 Materials and Techniques

1.2.1 Pre-interventional CT Imaging

For pre-interventional CT imaging, one should consider the patients' orientation and position if the lesion site is already known, e.g., the patient should be moved to the left of the CT gantry, if the right liver lobe is going to be targeted. In addition, table position should be lowered in order to gain space above the patient. This allows for the use of longer instruments and helps to avoid collision of instruments with the gantry during controls, which is of particular interest in obese patients.

Oral or rectal contrast medium should be applied to delineate adjacent intestinal structures. However, barium-containing contrast agents should not be used to avoid potential complications such as barium peritonitis (de Feiter et al. 2006). In addition, i.v. contrast medium application might be necessary (sometimes even repetitively) to visualize arterial and venous vessels or to better delineate the lesion. Contrast medium is also invaluable to identify hyperperfused lesions or vascular tumors, which may represent contraindications for biopsies (Fig. 1.1).

In general, routine CT protocols and reconstructions, which are used for daily diagnosis, can be used for pre-interventional CT imaging.

For thoracic and abdominal lesions, a spiral CT should be performed with a minimum slice thickness of ~5 mm and an increment of ~4 mm. For cervical and peripheral bone or soft tissue lesions, the reconstructed slice thickness and increment should not exceed 3 and 2 mm, respectively. Sequential CT techniques are not recommended to avoid misregistration of the lesion due to varying breathing volumes and consequently different organ and lesion positions in between different breathholds. The breathing commands should be the same as required for later intervention. In praxis, examinations during exspiration are more favorable as exspiration allows the patient to hold the position of the diaphragm at the same level more easily.

After scanning, different reconstructions are required depending on the lesion site. For thoracic lesions, e.g., data needs to be reconstructed using soft tissue (window width: ~350 HU; level: ~50 HU) as well as lung (window width: ~1,500 HU; level: ~−600 HU) algorithms to evaluate the proximity to vessels and pleural space. It is helpful to use a small field of view limited to the lesion and the skin in the area of the anticipated skin entry point.

For thoracic lesions, one may consider the following points (Fig. 1.2):

- For pulmonary lesions, the cranial border of the ribs should be used as an entry point to avoid injury of the intercostal artery.
- The pleura (including the horizontal and oblique fissures) should be passed only once in order to keep the risk of pneumothorax as low as possible.
- Lesions in front of a vessel should be targeted from the side (tangential orientation of the biopsy path toward the vessel) to avoid accidental vessel injury.

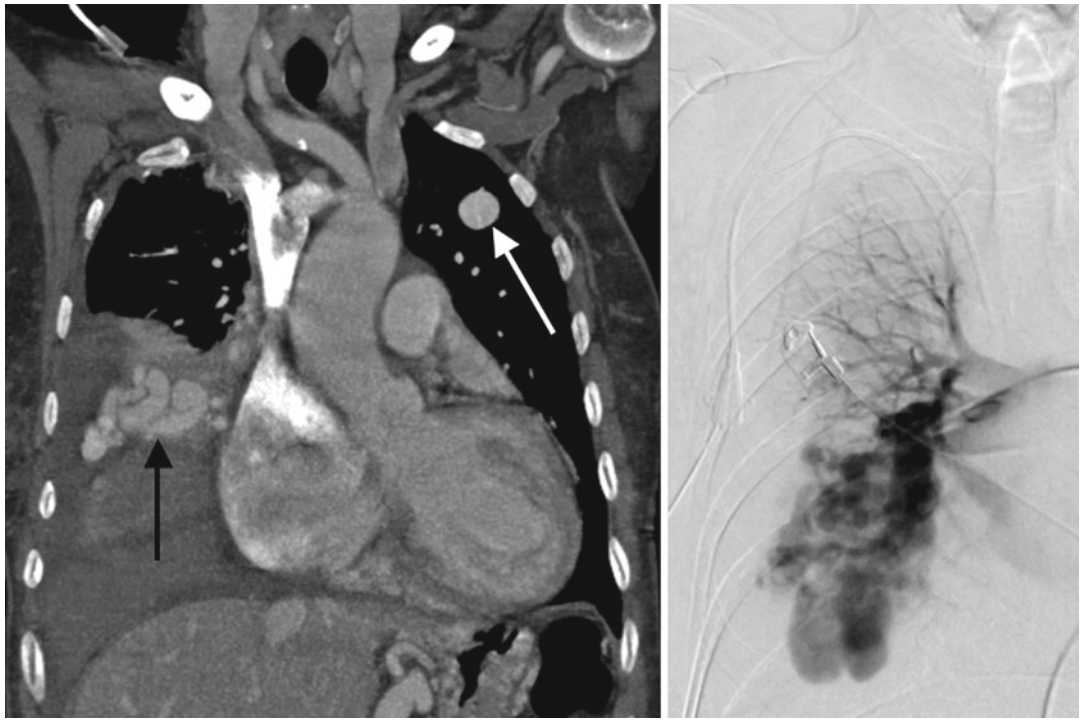

Fig. 1.1 Coronal reconstruction of an i.v. contrast-enhanced spiral-CT data set demonstrating multiple pulmonary AV-malformations (*arrows*) in a 75-year-old female patient (*left image*). Prior to this control CT, patient underwent CT-guided biopsy (without contrast medium application) on the right side since a solid tumor was suspected. This intervention led to massive bleeding. The corresponding X-ray angiography shows nicely the extension of the AV-malformation (*right image*)

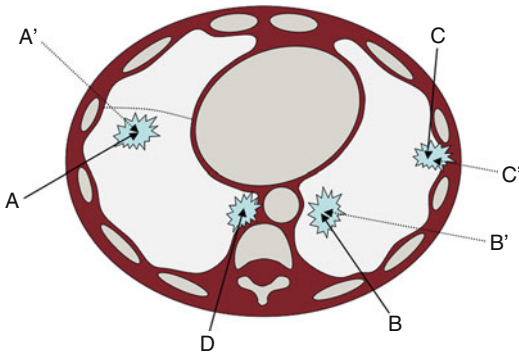

Fig. 1.2 Schematic drawing of a cross-sectional image at the level of the heart illustrates some aspects that should be considered for reaching pulmonary lesions. The pleura should be passed only once (*A*) instead of passing it multiple times (*A′*). Another access should be chosen (*B*) if a vessel is located behind the lesion (*B′*). For subpleural lesions, an indirect access is more favorable (*C*) than a direct path (*C′*) to decrease the risk of a pneumothorax. Passing the pleura can often be completely avoided for mediastinal and paramediastinal/paravertebral lesions (*D*)

- Subpleural lesions should be targeted tangentially to the pleura. Furthermore, an aspiration biopsy should be performed rather than a cutting biopsy to avoid pneumothorax.
- Mediastinal, paramediastinal/paravertebral lesions may be reached without passing the pleura; mediastinal widening by injection of NaCl solution can be helpful.

For abdominal lesions, one may consider the following points:

- In case of subphrenic lesions, one should avoid passing the pleura.
- Subcapsular liver lesions should be targeted indirectly (passing normal liver parenchyma first) to avoid abdominal bleeding.
- Renal and especially splenic lesions are prone to bleeding.
- The stomach and the small bowel can safely be passed if a lesion is located behind it.

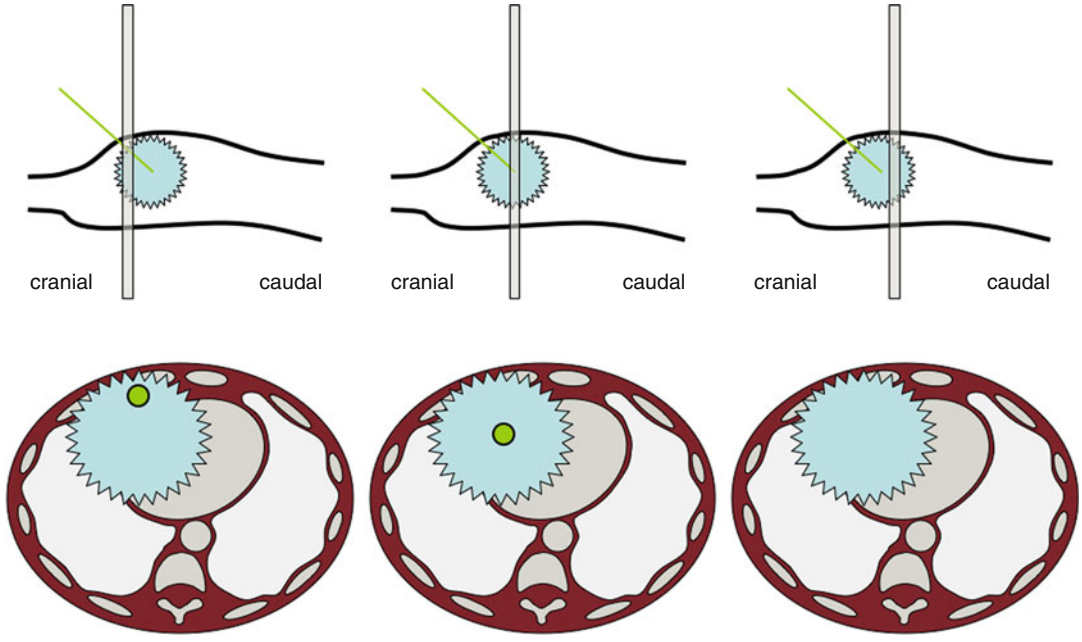

Fig. 1.3 This diagram shows schematically the position of a needle (*green line*) inside of a target lesion (*blue*, *upper row*). Repositioning of the axial slices (*gray*) will allow to exactly locate the tip of an interventional instrument on the axial images (*lower row*). Note the fact that an axial slice through the tip of a needle will look very similar

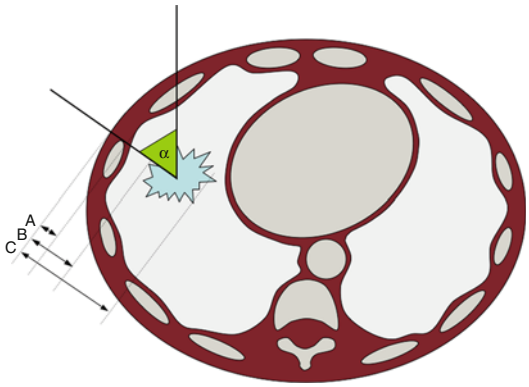

Fig. 1.4 Schematic of a cross-sectional image at the level of the heart demonstrating the measurements that should be performed before intervention: angle between a vertical line (alternatively a horizontal line) and a line connecting the entry point and the lesion (α), distance from the skin to the pleura (or peritoneum) (*A*), distance from the skin to the beginning of the lesion (*B*), and the distance from the skin to the end of the lesion (*C*)

For lesions of the upper or lower extremities, one may consider the following points:

- If a malignant lesion is expected, only the compartment in which the lesion is located should be opened/passed.
- The path of intervention, e.g., for biopsy, should be the same as the potential operative access in order to allow easy resection of the biopsy path in case of malignant lesions prone to metastases along the biopsy path.

In general, intervention is facilitated if the access to the lesion is planned parallel to the gantry as the whole instrument can be visualized at once on one axial slice. Otherwise, the instrument (particularly the tip of the instrument) must be identified by acquiring multiple axial slices along the instrument (Fig. 1.3).

If an adequate image slice was chosen for intervention, the following points should be determined (Fig. 1.4):

- Slice position
- Angle between a horizontal/vertical line and a line connecting the entry point and the lesion
- Distance from the skin to the pleura, peritoneum, liver capsule, or any other structure in need of thorough local anesthesia
- Distance from the skin to the beginning of the lesion
- Distance from the skin to the end of the lesion

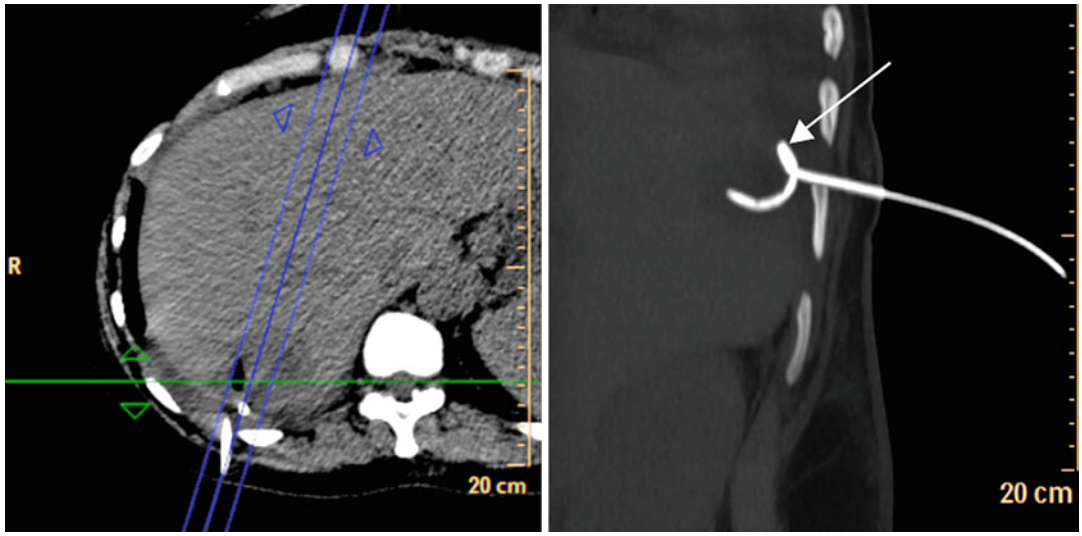

Fig. 1.5 Control CT after insertion of a drainage catheter for the treatment of a liver abscess. The *left image* shows an axial image at the level of the abscess. The corresponding parasagittal maximum intensity projections (MIP) reconstruction on the *right* demonstrates that the drainage passes the pleura with a loop in it (*arrow*)

1.2.2 Postinterventional CT Imaging

Immediately after the intervention, a control scan should be performed. An additional contrast medium application is usually not necessary.

The following issues should be confirmed or ruled out (Fig. 1.5):

- Pneumothorax
- Bleeding
- Position of the drainage or other interventional materials

Even if there is no obvious complication, it has to be decided on a case-by-case basis to carry out follow-up examination, e.g., chest X-ray, 2 and 4 h after thoracic interventions to rule out pneumothorax and intraparenchymal or pleural hemorrhage. Postinterventional hemoptysis might be observed in some cases. The expectoration of blood, however, should significantly decrease within the next few hours. Massive bleeding as defined by hemoptysis of more than 200 ml in 1 h requires immediate control.

After abdominal interventions, ultrasound can sufficiently identify bleeding or free abdominal fluid. In patients with impaired echoic window, a repeat CT scan might be considered. In some cases, the hemoglobin level might be controlled.

1.2.3 Pre-interventional MR Imaging

Besides imaging without ionizing radiation, MR imaging offers advantages such as high soft tissue contrast, multiplanar imaging without reconstructions, and ability to measure multiple physical or functional parameters including flow, perfusion, diffusion, and temperature. Space for intervention, however, is more limited in a MR scanner compared to a CT scanner. The bore diameter of a commercial closed-bore MR scanner measures about 60 cm. Therefore, patient accessibility is limited, which may complicate some MR-guided interventions and orientation as well as positioning of the patient must be considered more carefully. To overcome the drawback of limited space, open-bore systems were developed with a vertical or horizontal gap between the magnets (Lamb and Gedroyc 1997; Adam et al. 1998). Depending on the magnet design, space is infinite at least in one direction offering wide lateral or frontal access. Obese and particularly claustrophobic patients appreciate these open-bore scanners. Advantages exist also for pediatric or emergency patients who require ventilation. To date, the field strength of a commercial open-bore system is limited to a maximum of 1.0 T (GE, Signa Ovation HD

(0.35 T); Toshiba, Opart (0.35 T); Philips, Panorama HFO (1.0 T)). An alternative scanner design is presented by Siemens (Espree) offering a short-bore 1.5 T system with a bore length of only 125 cm and a bore width of 68 cm.

Even though MR-guided interventions have the potential to replace high-cost, open surgery procedures, the implementation is still limited to a few centers. The most promising clinical application for MR-guided intervention seems to be brain, breast, liver, prostate, and bone, which will be discussed in detail later in this book.

In principle, every sequence type and image weighting (T1, T2, PD, diffusion weighing, and fiber tracking) can be used that delineates the lesion in question with adequately high spatial resolution and contrast. Besides sufficient in-plane resolution, slice thickness is of considerable significance. Image slices should be thin enough to delineate the lesion accurately but thick enough to obtain reasonable signal-to-noise ratios (SNR), i.e., 3–5 mm. 3D imaging or overlapping slice techniques are preferable, while gaps between the slices should be avoided. If 2D imaging techniques are applied, the same sequence should be acquired in two different slice orientations to visualize the lesion.

For thoracic and abdominal lesions, breath-hold maneuvers are necessary to prevent respiratory motion artifacts and spatial misregistrations. Moreover, respiratory motion correction techniques (e.g., navigator, respiratory sensor) can be applied to perform MR imaging during free-breathing and to increase spatial resolution.

Considering the appearance of malignant lesions using MR imaging, which are mostly hyperintense on T2-weighed and hypointense on T1-weighed sequences, T2-weighed sequences are more favorable for pre-interventional and interventional imaging as dark-appearing instruments are better distinguishable from usually hyperintense pathologic lesions.

For localizing alien elements, "passive" visualization based on signal void due to spin replacement and susceptibility artifacts is usually used (Bakker et al. 1997). Magnetic susceptibility describes the degree to which a substance becomes magnetized in response to an external magnetic field, resulting in local field disturbances. This effect is influenced by several factors. In general, stronger magnetic fields cause more (or more severe) artifacts (Frahm et al. 1996). Gradient-echo (GRE) sequences are sensitive to susceptibility artifacts particularly with increasing echo-time (TE). In contrast, susceptibility artifacts are decreased in spin-echo (SE) sequences due to the refocusing pulses. Furthermore, the size of susceptibility artifacts is greatly affected by the orientation within the B_0-field and the choice of the frequency- and phase-encoding direction (Ladd et al. 1996) (for more details, see Chap. 3). Hence, T2-weighed SE or fast imaging using turbo-spin-echo (TSE) sequences might be the adequate imaging technique for planning the intervention. Alternatively, steady-state free-precession (SSFP) imaging can be performed, which provides high SNR and an image contrast, which is characterized by the ratio of T2/T1. SSFP has the added advantage that this sequence is flow compensated due to the symmetric shape of the gradient pulses in all three spatial dimensions.

In some cases, i.v. contrast medium administration might be necessary to better delineate the extent of the lesion. The choice of contrast agent will be determined by the longest lasting effect of contrast enhancement of the particular agent.

The most important benefit of MR imaging over CT is the ability to acquire images in any arbitrary orientation. Moreover, even with MR imaging, intervention can be controlled more easily and safely, if one of the main axis (axial, coronal, or sagittal) is used for intervention guidance.

If an adequate image slice was chosen, the same measurements as in CT should be performed to control every step during intervention (see Sect. 1.2.1).

1.2.4 Postinterventional MR Imaging

At the end of the procedure, MR imaging should be performed to rule out potential complications like acute bleeding using T2-wheighed SE/TSE or SSFP sequences. Using the same sequence, treatment efficacy or the position of materials like drainage and markers can be confirmed, too.

Chest X-ray and ultrasound can be performed in addition to MR imaging comparable to the follow-up after CT-guided intervention.

Appraisal

There are various imaging modalities available for pre- and postinterventional imaging as well as for interventional navigation.

X-ray fluoroscopy, which provides real-time images with high spatial resolution, is regarded as the gold standard for vascular intervention and is also used for some musculoskeletal procedures. The soft tissue contrast, however, is very limited.

Ultrasound also provides real-time images with high spatial resolution. However, ultrasound-guided interventions are restricted by bone, air, and due to the small field of view.

CT is widely available and provides an excellent overview with the capability of three-dimensional reconstructions due to the volumetric data. In addition, intestinal or vascular structures can be clearly identified using iodinated contrast media. CT is the most valuable imaging modality for abdominal and particularly thoracic targets. Image quality can be impaired by metal artifacts.

MR imaging provides similar overview and even better soft tissue contrast compared to CT. It has the added advantage of multiplanar imaging without the need for multiplanar reformats. Patient access and space for intervention, however, is more limited due to a smaller bore size compared to CT. In addition, the availability of MR scanners is much more restricted. Therefore, MR-guided interventions are still limited to a few numbers of research centers.

Key Points

- For pre- and postinterventional imaging as well as for interventional navigation, the imaging modality should be used that visualizes the lesion or the target organ best.
- CT is suited to navigate abdominal and particularly thoracic interventions. MR imaging needs to be applied where a high soft tissue contrast is mandatory and for lesions only visible by this technique (e.g., breast lesions).
- Patient position and breathing depth should be considered before imaging to allow correct planning and safe access to the lesion.
- Using CT, oral, rectal, or i.v. contrast medium application might be necessary to visualize adjacent organs or vessels. Data reconstruction with different (soft tissue, lung, bone) algorithms can be helpful to plan the access route.
- For MR-guided interventions, T2-weighed SE or TSE sequences as well as SSFP sequences are well suitable for distinguishing target lesions from instruments.
- Postprocedural radiography or ultrasound examination can be used to rule out complications like pneumothorax or bleeding.

References

Adam G, Bucker A, Glowinski A et al (1998) Interventional MR tomography: equipment concepts. Radiologe 38:168–172 [German]

Bakker CJ, Hoogeveen RM, Hurtak WF et al (1997) MR-guided endovascular interventions: susceptibility-based catheter and near-real-time imaging technique. Radiology 202:273–276

de Feiter PW, Soeters PB, Dejong CH (2006) Rectal perforations after barium enema: a review. Dis Colon Rectum 49:261–271

Delorme S, Krix M, Albrecht T (2006) Ultrasound contrast media – principles and clinical applications. Rofo 178:155–164 [German]

Frahm C, Gehl HB, Melchert UH et al (1996) Visualization of magnetic resonance-compatible needles at 1.5 and 0.2 Tesla. Cardiovasc Intervent Radiol 19:335–340

Ladd ME, Erhart P, Debatin JF et al (1996) Biopsy needle susceptibility artifacts. Magn Reson Med 36:646–651

Lamb GM, Gedroyc WM (1997) Interventional magnetic resonance imaging. Br J Radiol 70:S81–S88

Wells PN (2006) Ultrasound imaging. Phys Med Biol 51:R83–R98

CT-Guided Interventions: Indications, Technique, and Pitfalls

2

Philipp G.C. Begemann

Contents

P.G.C. Begemann
Röntgeninstitut Düsseldorf,
Kaiserswerther Straße 89, Düsseldorf D-40476, Germany
e-mail: p.begemann@roentgeninstitut.de

2.1 Introduction

Over the last 30 years (Haaga 2005), computed tomography (CT) has developed into a well-accepted and widely used guiding tool for a broad range of percutaneous interventions. It can be used either as an alternative to sonography or fluoroscopy or if interventions cannot be done under sonographic or fluoroscopic guidance. In general, CT-guided interventions may be divided into diagnostic interventions and therapeutic interventions, although there are overlaps.

Typical diagnostic interventions are biopsies, which can be done as aspiration or fine-needle biopsies, punch biopsies, or drill biopsies, depending on the region, the access, or the material that has to be biopsied. Aspiration or fine-needle biopsies are used to acquire either liquid material for a microbiological analysis to search for infection (Fig. 2.1a, b), for example, in patients with acute pancreatitis, or to obtain material for cytological examination, for example, in small pulmonary nodules or in regions that cannot be reached or safely approached with punch biopsies. The latter is carried out if larger amounts of tissue are needed for pathologic or histological examinations, for example, punch biopsies of lymph nodes or soft tissue masses to identify or classify tumors before treatment (Fig. 2.1c–e) or to search for remaining living tumor cells after chemotherapy in persistent lymph nodes or tumor masses. Punch biopsies can also be done in parenchymal organs or large pulmonary or pleural

A.H. Mahnken et al. (eds.), *CT- and MR-Guided Interventions in Radiology*,
DOI 10.1007/978-3-642-33581-5_2, © Springer-Verlag Berlin Heidelberg 2013

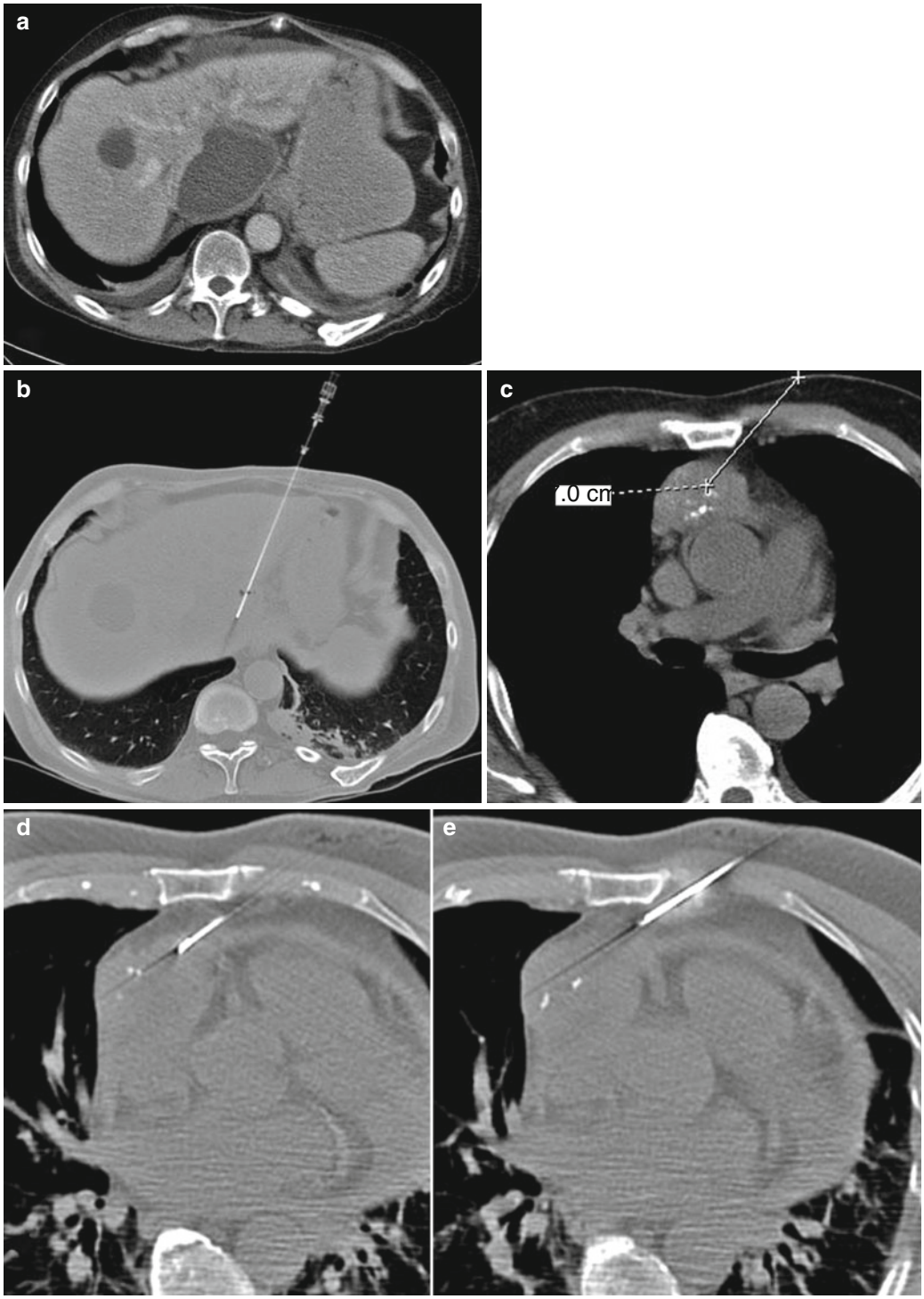

Fig. 2.1 (**a**, **b**) A fine-needle aspiration of a liquid structure behind the left liver lobe after liver surgery, which turned out to be a seroma without superinfection. (**c**–**e**) An example of a punch biopsy of a retrosternal mass, turning out to be a squamous cell carcinoma. (**f**–**h**) A drill biopsy of a bone metastasis in a vertebral body (L3)

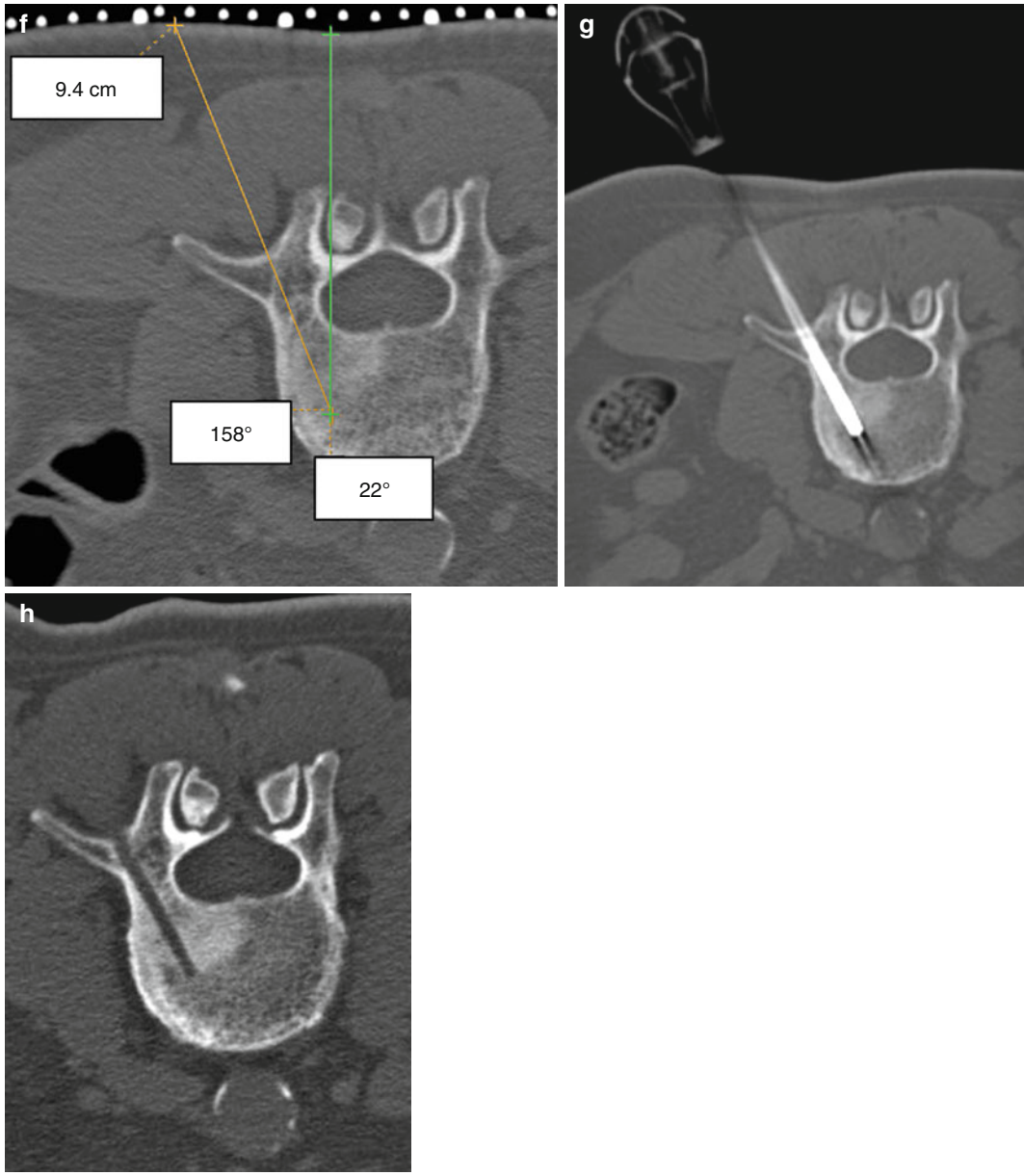

Fig. 2.1 (continued)

masses. Drill biopsies are usually done in bones to classify bone tumors or soft tissue tumors within bones (Fig. 2.1f–g). Further diagnostic interventions that can be done under CT guidance include discographies or localization techniques, for example, coil or wire placement prior to video-assisted thoracoscopy surgery of small lung nodules (Fig. 2.2d–f) or before partial nephrectomy of small renal cell carcinomas or suspect renal lesions (Fig. 2.6).

Drainages are partly diagnostic, partly therapeutic. Most drainage procedures are done to evacuate abscesses as an established alternative method to surgical intervention (Fig. 2.2a–c). But also other liquid-filled structures can be drained, such as bilioma, hematoma, seroma,

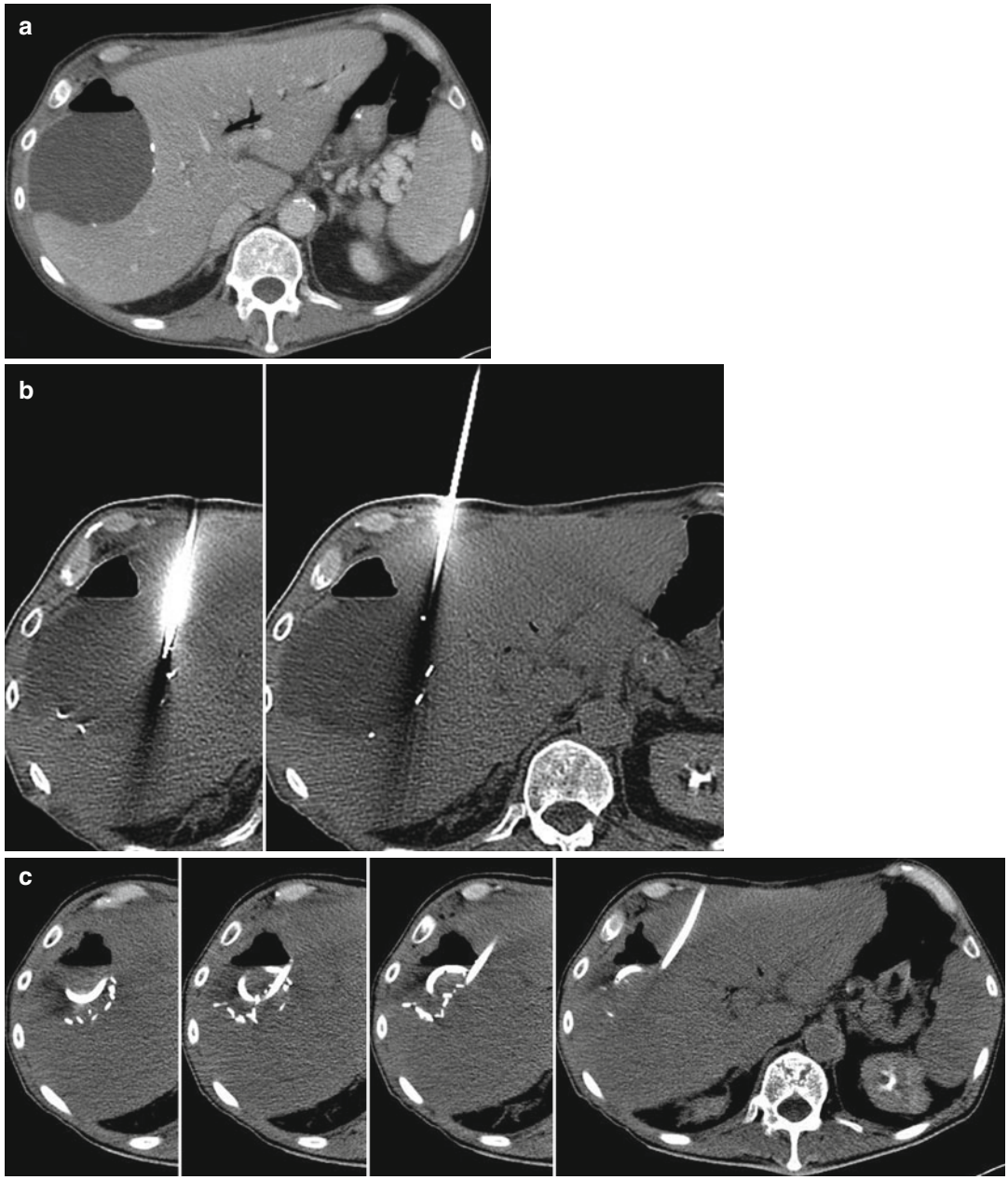

Fig. 2.2 (**a**–**f**) Drainage of a large liver abscess after surgery. The 12-F drainage catheter was placed with the trocar technique. (**d**–**f**) An example of a localization of a small lung nodule before video-assisted thoracoscopy surgery ((**f**) is a sagittal thick slice multiplanar reformation)

urinoma, cysts, pseudocysts, pleural effusion or empyema, the renal pelvis, and the urinary bladder. Depending on the access path, drainages can generally be placed in two different ways: (1) with the trocar technique, where the fluid collection is punctured directly with the drainage placed on a mandrin with a cutting edge (Fig. 2.2b), (2) or with Seldinger's technique, where the fluid collection is first punctured with a thin hollow needle before a guide wire is placed

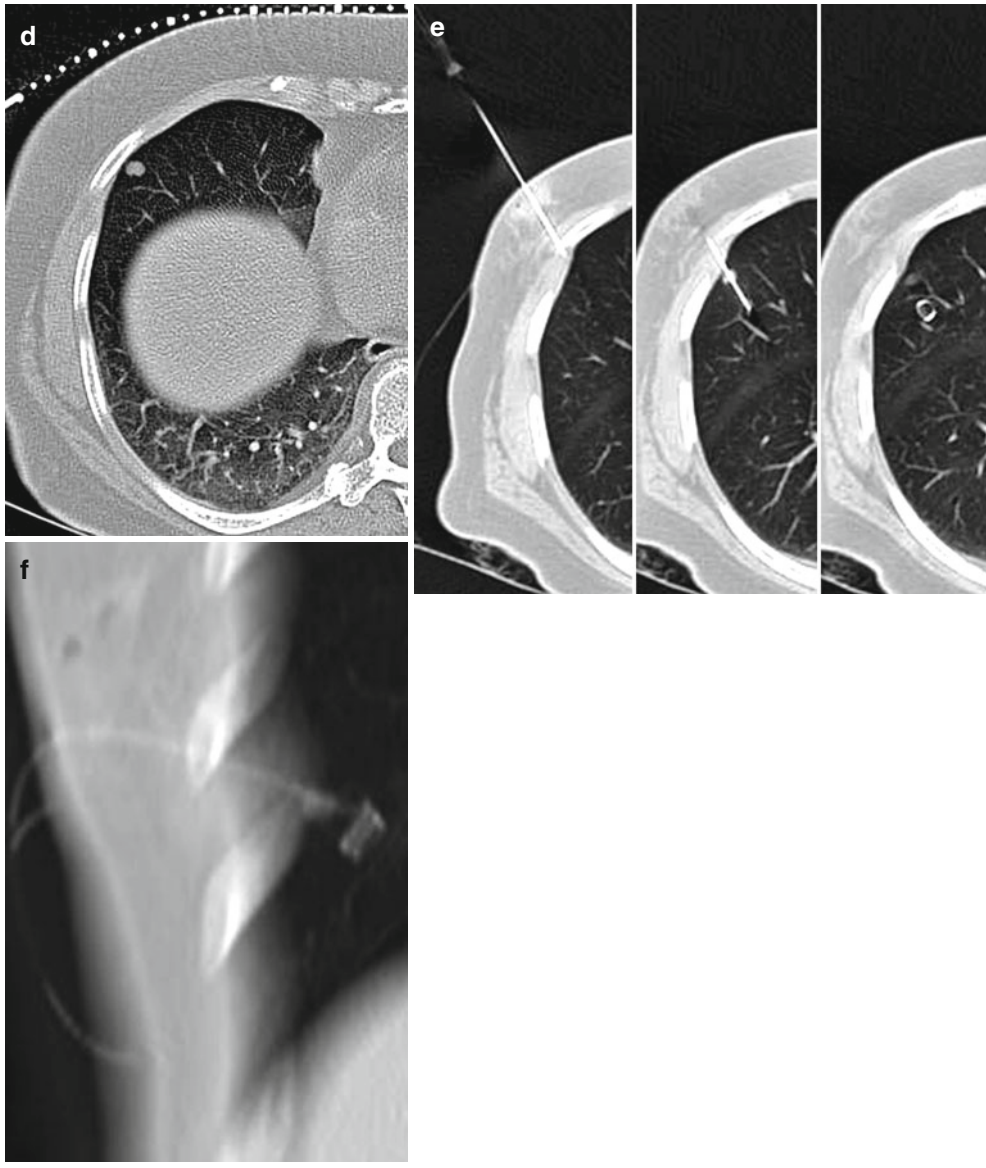

Fig. 2.2 (continued)

within the collection. Finally, the drainage catheter is inserted over the wire.

Percutaneous tumor therapy, including radiofrequency ablation or laser interstitial thermal therapy, percutaneous ethanol injection, or local radiation therapy, can be performed under CT guidance as curative or palliative tumor therapy for primary or metastatic tumors in virtually all regions of the body. Another large field of therapeutic interventions is pain management by the use of neurolysis or injection therapy of local anesthesia with or without corticoids. CT-guided thermal ablation of osteoid osteoma has even become established as the curative treatment of choice. Many other skeletal interventions are also routinely performed under CT guidance, including vertebroplasty and osteoplasty as well as percutaneous osteosynthesis, for example, percutaneous screw insertion of the

Table 2.1 Overview of the most common computed tomography (CT)-guided interventions and their indications

Type of intervention	Indications	Examples
Fine-needle biopsy	Cytology	Small lymph nodes (<1 cm)
		Pulmonary nodules
		Difficult access (i.e., transgastral)
		Suspected malignant effusion
	Microbiology	Suspected superinfection
Punch biopsy	Histology	Lymph nodes
		Solid masses
Drill biopsy	Histology	Bones
		Bone tumors
		Soft tissue tumors within bones
Drainages	Microbiology	Every type of superinfected fluid collection
	Therapy	Abscess
		Necrosis
		Fluid collections (bilioma, seroma, etc.) (gastrostomy)
Localization techniques	Surgery preparation	Lung nodules before video-assisted thoracoscopy surgery
		Intraparenchymal kidney tumors
Tumor/ablation therapy	Palliative or curative tumor therapy	Primary cancers (hepatocellular carcinoma, renal cell carcinoma, lung cancer, etc.)
		Metastasis (liver, kidney, adrenal, lung, etc.)
Neurolysis	Pain management	Tumor-induced pain (sympathetic chain, ganglion celiacum, etc.)
		Neuralgia [Gasserian (trigeminal) ganglion, etc.]
Anesthesia injection	Pain management	Periradicular therapy (disc herniation, etc.)
Skeletal interventions	Trauma management	Vertebroplasty, sacroplasty, percutaneous screw insertions, etc.

pelvis after divulsion of the iliosacral joint. Cysts or parasitic cysts can be sclerosed with CT guidance, and even CT-guided gastrostomies are routinely done now. The different types of intervention, their indications, and typical examples are summarized in Table 2.1 (Feuerbach et al. 2003).

2.2 Materials and Techniques

2.2.1 Equipment

Generally every type of CT scanner (single slice or multislice) can be used for CT-guided interventions. There should be enough space in the scanner room for the radiologist, one or two assistants, the sterile table with the required instruments, and possible further equipment (e.g., for anesthesia or even general anesthesia, radiofrequency generators). Some interventions, for example, complex CT-guided skeletal interventions, like CT-guided percutaneous osteosynthesis, require even more space and ideally laminar airflow to achieve definite sterile conditions similar to those in surgical operating rooms. This needs to be considered when selecting the room for the planned procedure.

Before every intervention, the scanner room has to be carefully cleaned and disinfected with antibacterial, antifungal, and/or antiviral agents, especially the CT table and the gantry. A movable instrument table has to be covered with sterile sheets and equipped with syringes of

different size (5, 10, and 20 ml) with and without Luer-Lock, hypodermic, and 20G syringe needles for local anesthesia, anesthetics, saline solution, sterile pads, sterile clear tape to cover the CT gantry's control panel, and sterile sheets for interventional purposes. Furthermore, the procedure-specific materials such as puncture needles, drainages, sample tubes, and specific drugs need to be placed on the table. The radiologist has to perform a medical hand washing and wear a surgical cap and mask, sterile gloves, as well as a lead apron. In complex interventions as well as in all skeletal interventions, the interventionalist needs to wear a sterile coat.

Different technical specifications or technical tools make the procedure easier or even safer. A list of desirable equipment for successful CT-guided interventions is given below:

- Multislice CT scanners with wide detector arrays are preferable, since detectors with a width of, for example, 16×1.5 mm (24 mm) or 64×0.625 mm (40 mm) are mostly able to cover the whole range of the intervention site in the *z*-direction. This not only permits one to easily recognize needle deviations into cranial and caudal direction but also permits adaptation of the puncture direction to organ shift (e.g., due to breathing) during the intervention.
- A monitor within the scanner room is almost mandatory for the radiologist to monitor the procedure.
- A foot pedal to start sequential scans or fluoroscopy makes the radiologist more independent during the procedure and helps to speed up the intervention.
- The patient table can be either moved after covering the control panel with sterile clear tape or pushed directly after manually releasing the table. Newer CT systems also offer a complete control panel fixed at the side of the patient table, where all scanner actions can be carried out by the radiologist under sterile conditions.
- CT scanners with a larger bore (Fig. 2.3), for example, 85 cm, are very practical for CT-guided interventions since they at least partly overcome the narrowness of normal-size CT scanners with a typical gantry bore of 70 cm. CT scanners with a big gantry bore are offered by different CT vendors, for example, Philips (Brilliance CT Big Bore Radiology, 85-cm bore size, 60-cm true scan field, 16-slice configuration), Siemens (Somatom Sensation Open, 82-cm bore size, 50-cm scan field of view, 82-cm extended field of view, 24- or 40-slice configuration), Toshiba (Aquilion Large Bore, 90-cm bore size, 70-cm field of view, 85-cm field of view optional, 16-slice configuration), and GE Healthcare (Light Speed RT 16, 80-cm bore size, 65-cm display field of view, 16-slice configuration).
- For difficult double-angulated interventions, the use of commercially available tracking or navigation systems can be considered (see Chap. 7).

A typical CT room suitable for CT interventions is shown in Fig. 2.4 with a 64-slice CT scanner with a foot pedal and a monitor inside the scanner room. Additionally, the system should be capable of CT fluoroscopy.

2.2.2 CT-Guided Puncture: Step by Step

CT-guided punctures follow a very similar course of action as is described in theory and in a sample procedure where a CT-guided localization of a renal tumor is described (Fig. 2.3).

The general course of a CT-guided intervention is as follows:

1. The first mandatory step is the review of the radiological examinations that have been done to the patient so far. It is the decision of the radiologist whether he/she will perform the puncture or if alternative approaches (i.e., surgery) have to be considered. If the puncture is determined, the patient needs to be informed about the course, the risks, and the possible complications of the procedure (Table 2.2) ideally the day before the procedure. Depending on local laws, written consent may be required.
2. The knowledge of the patient's blood clotting capabilities (international normalized ratio (INR), platelet count, previous taking of platelet inhibitors, i.e., aspirin) is obligatory

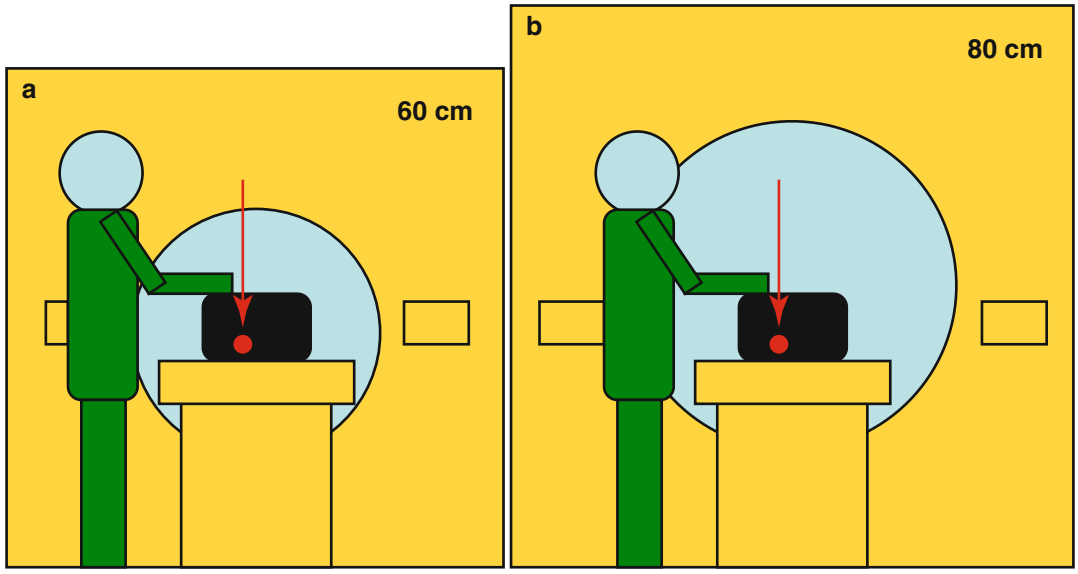

Fig. 2.3 The space in the bore when using a diameter of 60 cm and a diameter of 80 cm. (**a**) The device shown (*red arrow*, e.g., a drainage on a trocar) could not be placed within the bore to control the localization or to use computed tomography (CT) fluoroscopic guidance. Using a CT scanner with a larger bore, (**b**) can overcome this limitation

Fig. 2.4 A typical CT scanner room suitable for CT interventions equipped with a 64-slice CT scanner with a foot pedal, a monitor, and the option to perform fluoroscopic interventions

Table 2.2 Typical risks and complications of CT-guided interventions

General complications	Drug reaction due to local anesthesia or contrast media
	Nerve lesion with numbness or paralysis
	Infection, abscess, sepsis
	Bleeding, hematoma
	Surgery
	Death
Procedure-specific complications	
Thoracic procedures	Pneumothorax
	Air embolism (arterial and venous) with arterial infarction (i.e., myocardial infarction, stroke)
Abdominal procedures	Pneumothorax (upper abdomen)
	Injury of parenchymal organs of the abdomen (i.e., liver, spleen, kidneys)
	Arteriovenous fistula in parenchymal organs
	Injury of the intestine
	Peritonitis
Osseous procedures	Fracture
	Osteomyelitis
Tumor ablation	Large necrosis with abscess formation and sepsis
	Bilioma (after liver ablation)
	Injury of adjacent organs or structures
	Bleeding

before starting the procedure. Generally the INR should be below 1.7 and the platelet count above 50,000/mm^3.

3. Before the procedure, the CT room should be cleaned and the sterile table prepared.
4. The patient is placed on the CT table in a position that facilitates the preinterventionally determined access route. For most interventions, a spiral scan of the region of the intended procedure is done for further planning. The scan can be done with or without the use of contrast material to identify vascular structures and/or areas of abnormal or pathologic contrast enhancement behavior. Furthermore, it has to be decided whether the procedure has to be done in inspiration, expiration, or free breathing, depending on the area and the compliance of the patient. Ideally, a radiopaque grid (e.g., Seegrid; AprioMed, Uppsala, SE) has already been fixed on the patient's skin (Fig. 2.1f). Instead of a commercially available grid, custom-made grids from angiographic catheters or injection needles may be used. Alternatively, barium paste may also serve as skin marker. The anticipated puncture tract can be assessed either on the axial images or on multiplanar reformations if procedures are needed to be angulated to the *z*-direction. Preferably, the intervention is planned in a plane perpendicular to the *z*-axis, which makes the procedure much easier to perform and to monitor. If double-angulated punctures are necessary, the gantry can be tilted for surveillance in order to provide images parallel to the direction of the puncture tract.
5. The intended pathway of the puncture can be measured (length and angle; Fig. 2.1f).
6. The radiologist performs a medical hand washing and dresses with a surgical cap and mask and sterile gloves. A sterile coat is used in complex as well as in all skeletal interventions. The skin area of the procedure is disinfected, and the patient covered with sterile sheets.
7. After another disinfection of the skin, local anesthesia is performed. Using the syringe needle for the local anesthesia, one approaches the intended target for the first time. This step can already be done with CT guidance using the techniques described below. Careful local anesthesia is mandatory for the patient, especially in bone punctures.

8. After the target has nearly been reached with the anesthesia needle, the procedure is repeated with the interventional device (i.e., drainage, puncture device, RF ablation device, etc.). If a thicker device is used, a small incision of the skin using a scalpel is necessary.
9. After the procedure has been finished, the skin lesion is bandaged. A CT scan of the target region is performed to exclude immediate complications and, if necessary, to control the position of drainage catheters, coils, or localization needles.
10. Depending on the procedure, the patient should typically maintain bed rest for 2–4 h, ideally lying on the punctured site. During that time, he or she should be regularly monitored. After pulmonary punctures, at least one chest X-ray should be performed after approximately 2 h to exclude pneumothorax (see Chap. 1). After punctures in the upper abdomen, a chest X-ray can be considered depending on the course of the intervention (e.g., if a pleural recess has been passed). After difficult interventions, further CT scans may be required during short-term follow-up. In patients with reduced blood clotting capabilities or after punctures with a bleeding risk, further controls of the blood hemoglobin are needed.

Generally two different techniques of CT surveillance are used: sequential scans or CT fluoroscopy.

2.2.3 Sequential CT Guidance

Whenever it is necessary to control the position of the puncture device, the patient is moved into the CT gantry, positioned according to the laser marker, and sequential scans of the region are performed either by the technician or by the radiologist using the foot pedal. With use of multislice CT, with every sequential scan, several images with a section thickness of approximately 2–5 mm can be displayed on the monitor. If small lesions are punctured, the slice thickness has to be adjusted accordingly, so as not to miss the lesion owing to partial volume artifacts. Every interventional step between the sequential scans is planned on the preinterventionally acquired images. The navigation of the puncture device can be done either as a freehand procedure or with the help of one or two assistants if angulated or double-angulated procedures have to be done. The angles are measured on the previous scans. In angulated procedures, one assistant is positioned either opposite the radiologist or at the bottom of the CT table and monitors the angulation using a goniometer. In the case of a double-angulated procedure, two assistants are positioned opposite the radiologist and at the bottom of the CT table (Fig. 2.5).

2.2.4 CT Fluoroscopy

CT fluoroscopy was first reported in 1993 using a modified single-slice CT scanner with good clinical results (Katada et al. 1996). With technical improvements of the CT scanners and development of multislice CT, increasing hardware and software performance, CT fluoroscopy became a routine option for CT scanners provided by all manufacturers.

Technically, axial CT images are acquired and concurrently reconstructed with a reduced spatial resolution at a frame rate of up to ten images per second, whenever the performing radiologist presses the foot pedal. Thereby real-time visualization of the direction and pathway of the interventional tool during the procedure became possible. One to six images can be displayed on the monitor; the slice thickness of the fluoroscopic images can be chosen according to the scanner's specifications. Major advantages of CT fluoroscopy are the improved sensitivity for proving neoplastic lesions with small tumor size, the increase in patient safety, and a shortening of the procedure time and thus reduction of in-room time for the patient and the interventionalist.

Reasonably, CT fluoroscopy is used, if the procedure aims at moving targets, especially in the lungs, near the heart and the upper abdomen; if the procedures are performed within difficult anatomic regions; or if interventions need to be done with incompliant patients. Technically, the procedure has to be performed within the CT bore, which leads to the major disadvantage of CT fluoroscopy, a relatively high radiation exposure to the interventionalist, which will be discussed in Sect. 2.4.

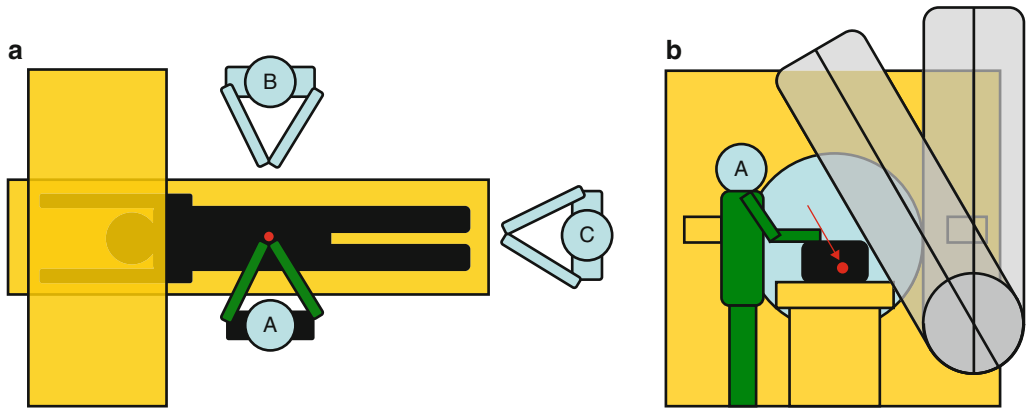

Fig. 2.5 (**a**) The positions of the radiologist (*A*) and two assistants (*B* and *C*) for a goniometer-guided double-angulated procedure. (**b**) The view of assistant *C* with the goniometer and the accordingly angulated puncture device

2.2.5 Pictorial Sample Procedure

As a pictorial sample procedure, a CT-guided localization of a small renal mass is described:

1. On an initial CT scan, a suspect, 2-cm noncystic renal lesion with irregular contrast enhancement is diagnosed in the dorsomedial parenchyma of the right kidney which does not bulge out the renal surface. Instead of total nephrectomy, organ-sparing surgery was planed, and it was requested to localize the tumor prior to surgery (Fig. 2.6a). It was decided to use a breast lesion coil to be placed directly behind the tumor in the perirenal fat.
2. The patient is placed on the CT table in a way that there is good access to the target region. In this case, the patient was placed in prone position.
3. A contrast-enhanced (spiral) scan is acquired to plan the procedure (Fig. 2.6b). In this example, the easiest way to reach the perirenal fat next to the tumor would be from dorsal paravertebral direction. Since the dorsal pulmonary recessus is behind the lesion and a transpleural puncture should be avoided, either an angulated caudocranial access or lateral access is possible. To stay in the *xy*-plane without angulation in the *z*-direction, it was decided to use the lateral access. The distance from the skin to the lesion and the entrance angle are measured.
4. Local anesthesia is performed with a 7-cm 22G needle (Fig. 2.6c), and the direction is controlled.
5. After incision of the skin, it was changed to an 18G hollow needle. With use of sequential CT scans for image guidance, the needle tip was placed directly behind the renal lesion (Fig. 2.6d).
6. A breast localization coil was positioned directly behind the tumor via the hollow needle (Fig. 2.6e, f).
7. The postinterventional spiral scan excluded immediate complications such as pneumothorax (Fig. 2.6g) or bleeding and showed the correct coil localization directly behind the tumor also in the multiplanar reformations (Fig. 2.6h).

2.3 Tips & Tricks

To avoid unwanted incidents such as bleeding, infection, pneumothorax, or nerve injury, the following precautions have to be taken:

- The whole procedure has to be performed under sterile conditions to prevent intervention-related iatrogenic infections especially in skeletal interventions.
- The patient's blood clotting capabilities must be known to prevent bleeding.
- Before the intervention starts, the initially acquired CT images have to be analyzed carefully to identify the safest path to the target. Extensive knowledge of the anatomy of the region of intervention is mandatory to avoid injury of neural structures or blood vessels, especially arteries. Transpleural pathways to

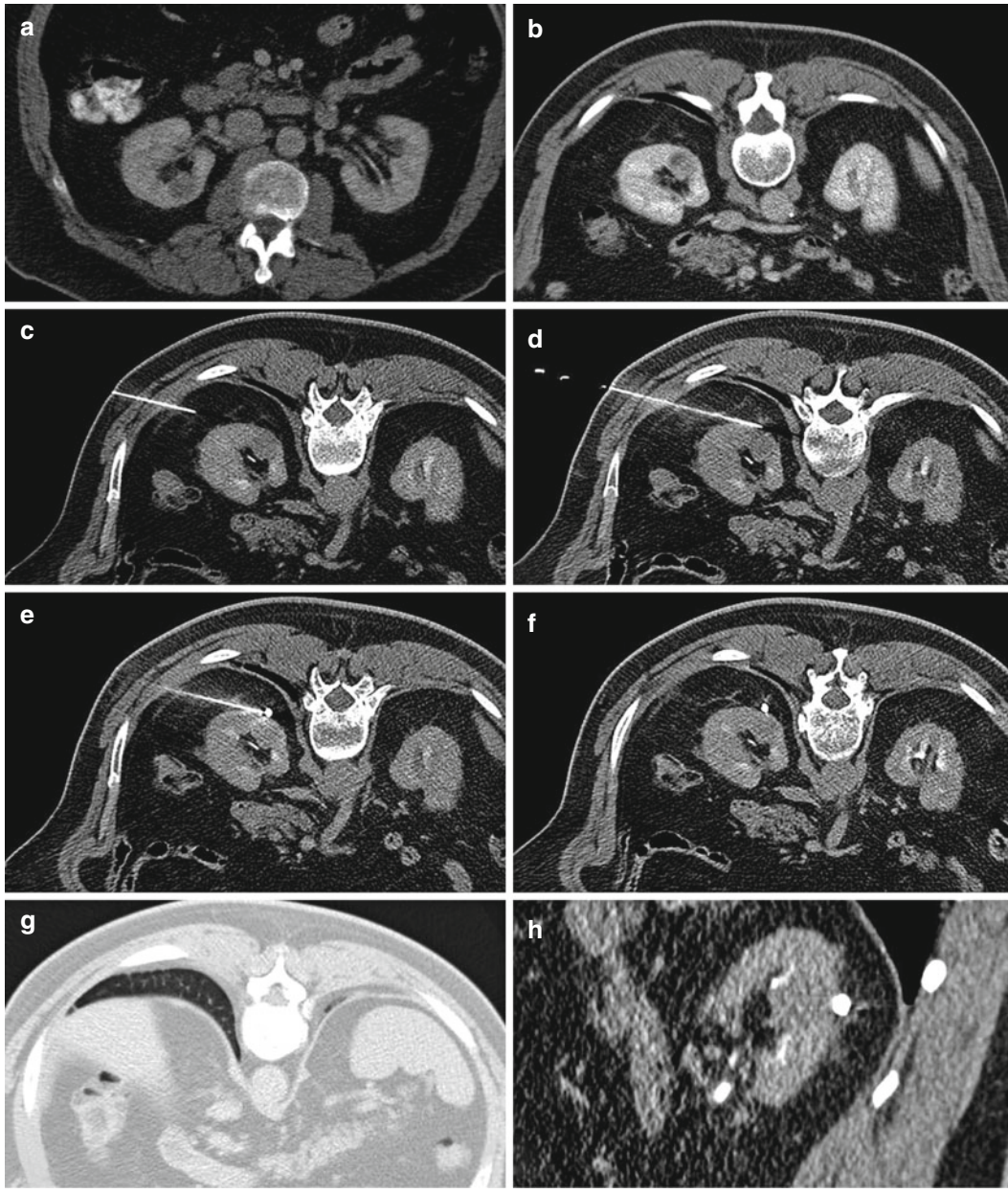

Fig. 2.6 (**a**–**h**) Localization procedure of a small renal tumor before organ-sparing surgery. The complete procedure is described in Sect. 2.2.5

access targets, for example, within the liver or kidneys, should be avoided to prevent pneumothorax or spreading of infection or tumor from the abdomen into the thorax. Transgastral fine-needle biopsies or punctures for pain therapy are generally possible, but the patient has to be fasting, and periinterventional antibiotics should be administered. The same holds true for the passage of the small bowels (see Chap. 6).

- The direction of the puncture should not head toward organs sensitive to damage, that is,

aorta, coronary arteries, etc., especially when performing punch biopsies.

- In order to avoid contact of the puncture device with the gantry, especially when long devices are used, the procedure should be done with the patient table in the lowest position in order to gain more space in the gantry bore. This is even more important if the patient is positioned on his/her side, for example, on the left side, if the liver is punctured.
- Interventions of the lung or breath-dependent organs have to be done with careful coordination with the patient to prevent failed puncture. If this is not possible, the use of CT fluoroscopy helps to avoid repeated punctures.
- Biopsies or drainages of parenchymal organs should be done with parenchymal bridging of the access path to prevent bleeding or spreading of infection into the peritoneum or retroperitoneum.
- Liver punctures in patients with ascites should be avoided, if possible, owing to a higher bleeding risk, especially in patients with liver cirrhosis. Preinterventional drainage directly prior to the intervention may be used to provide safe access to the target without interposition of fluid.
- If large tumor masses are biopsied, samples from the center and from the periphery of the tumor have to be taken to gain enough, reliable material for histological workup, since many tumors are necrotic at their center.
- For forensic reasons, the radiation dose should be documented in the report or in the hospital information system.

2.4 Radiation Dose

A relevant disadvantage of CT guidance is the exposure of the patient and the interventionalist to radiation. The dose which will be administered to the patient shows broad variations and can be effectively influenced by the interventionalist. Since there are usually previous CT or magnetic resonance images, the planning scan as well as the control scan after finishing the procedure should be limited to the minimum scan range needed. The dose settings (kilovolts and milliampere seconds) should be limited to an acceptable level to identify the important structures and to monitor complications, and the number of sequential scans should be kept as low as possible.

In CT fluoroscopy, the dose issue is even more relevant. During fluoroscopic procedures, not only the patient is exposed to ionizing radiation but also the hands of the operator, which might be within the gantry during the intervention. To avoid direct exposure of the interventionalist's hands, different techniques are available. One is to use specific needle holders that the interventional device can be controlled without the need of operating within the CT gantry. Another possibility has been investigated by Hohl et al. (2008), the so-called angular beam modulation, where the X-ray exposure is switched off in a predefined segment of the gantry rotation, since only a rotation angle of 240° is needed for image reconstruction. With that method, the effective dose of the patient can be reduced by 35 %, the skin dose by 75 %, and the dose to the operator's hands between 27 and 72 % without reduction of the image quality. Nevertheless, in reviewing the literature, quite high patient's doses were reported, and the contribution to the occupational radiation exposure cannot be neglected. Therefore, during fluoroscopic procedures, it is even more important to minimize the X-ray time.

Appraisal

CT offers the possibility to safely guide interventions. CT is widely available, and generally CT-guided interventions can be performed with every type of scanner. No special interventional equipment is needed, which is an important advantage over magnetic resonance guidance. The radiation exposure during CT-guided interventions has to be mentioned, and every procedure should be performed in a dose-saving manner, especially if CT fluoroscopy is used.

Key Points

- CT is a widely available tool to monitor interventions.
- The patients have to be informed about the complications, and the patient's blood clotting capabilities must be known.
- The procedures have to be done under sterile conditions.
- Knowledge of the anatomy and accurate planning of the procedure are mandatory to avoid complications. After the procedure, the patients have to be carefully monitored.
- Dose issues should be considered while planning and performing the procedure.

References

Feuerbach S, Schreyer A, Schlottmann K (2003) Standards in radiographically guided biopsies – indications, techniques, complications. Radiol Up2date 3: 207–223

Haaga JR (2005) Interventional CT: 30 years' experience. Eur Radiol 15(Suppl 4):D116–D120

Hohl C, Suess C, Wildberger JE et al (2008) Dose reduction during CT fluoroscopy: phantom study of angular beam modulation. Radiology 246:519–525

Katada K, Kato R, Anno H et al (1996) Guidance with real-time CT fluoroscopy: early clinical experience. Radiology 200:851–856

MR-Guided Interventions: Technique, Pitfalls, and Indications

3

Arno Bücker and Marcus Katoh

Contents

3.1 Introduction

Different techniques have proved to be valuable for guidance of interventional procedures, namely, ultrasound (US), computed tomography (CT), and magnetic resonance (MR) imaging. For many indications, all these techniques are "me too" alternatives. In case there is no medical reason to prefer one imaging modality over the other factors like availability, simplicity and cost are of great importance. Looking at any of those cofactors, it is evident that MR imaging is the least likely method to be initially favored for guidance of interventional procedures. In this chapter, only nonvascular interventions will be considered like imaging-guided punctures/markings, drainages, and tumor ablations. Each radiologist performing any of these procedures should be familiar not only with the standard techniques of US and CT guidance but also with guidance technique exploiting the imaging features of MR imaging. This is true despite the fact that there are so far only rare indications, which definitely require MR imaging as a guidance tool. But some lesions, which are only detectable by MR imaging, require MR guidance or MR-guided localization and marking (Solomon et al. 2002). Among these, breast lesions are the most common, and the continuously growing role of MR imaging in this field will lead to an incline in numbers of breast lesions, which can only be biopsied or marked by MR guidance (Malhaire et al. 2010).

A. Bücker, MD (✉)
Department of Diagnostic and Interventional Radiology,
University Hospital Saarland,
Kirrbergerstr. 1, Homburg D-66421, Germany
e-mail: arno.buecker@uks.eu

M. Katoh, MD
Department of Diagnostic and Interventional Radiology,
HELIOS Hospital Krefeld,
Lutherplatz 40, Krefeld D-47805, Germany
e-mail: marcus.katoh@helios-kliniken.de

A.H. Mahnken et al. (eds.), *CT- and MR-Guided Interventions in Radiology*,
DOI 10.1007/978-3-642-33581-5_3,

3.2 Materials and Techniques

3.2.1 Magnetic Resonance (MR) Scanner

The ideal MR scanner will allow complete open access to the patient. Current MR scanners do not allow for this, but there is a distinct difference between closed-bore and open-bore MR scanners (Adam et al. 1998). The best patient access so far offers a magnet, which consists of two halves; the space between those two can be occupied by the interventionalist. This double doughnut concept creates a field strength of 0.5 T in the imaging area, demonstrating the fact that MR scanner offering better patient access usually has lower-field strengths ranging from 0.064 to 1 T. MR scanners up to 3 T have been evaluated for MR guidance of interventions (Paley et al. 2001).

Considering high image quality along with high imaging speed as a demand for interventional MRI, the need for surface coils is obvious. While they are not always necessary, they will offer advantages like better SNR and the ability to apply parallel imaging techniques. Many surface coils are ring coils allowing access to the imaged area through the open center part of the surface coil. In addition, dedicated devices are available for MR-guided breast interventions (Floery and Helbich 2006), although the ability to perform MR-guided breast interventions with standard surface coils has been proved (Daniel et al. 1998). Even dedicated robotic systems have been developed to perform the intervention inside a high-field closed-bore MR scanner (Kaiser et al. 2000). It will depend on numbers of interventions performed at one institution and on the skill of the interventionalist, if the additional investment of a dedicated interventional coil is justified. However, a recent interdisciplinary consensus paper supports performing MR-guided vacuum-assisted breast biopsy (Heywang-Köbrunner et al. 2009).

If one considers vascular interventions, the need for fast imaging capabilities requires preferably high-field strength MR scanners (Buecker et al. 2002b; Mahnken et al. 2004b; Spuentrup et al. 2002), although midfield systems have been used from the very beginning to perform vascular interventions as well (Wildermuth et al. 1997). Looking at nonvascular interventions, patient access might be of more importance compared to imaging speed. Furthermore, lower-field strength will lead to smaller susceptibility artifacts, which can be advantageous when metallic instruments are used (Frahm et al. 1996a; Gehl et al. 1996). Consequently, punctures and biopsies have been performed on a wide range of MR scanner from low to high field proving the ability for all these scanners to reliably perform MR-guided interventions (Adam et al. 1999; Barentsz 1997; Buecker et al. 1998; Frahm et al. 1996b; Hall et al. 1999b; Heywang-Kobrunner et al. 2000). Therefore, individual factors of the single institution will influence the choice of the field strength more than the fact that MR-guided interventions are being planned for the future.

Planning interventions within the MR room, one should establish double doors to allow shielded access to the scanning room even during image acquisition. Furthermore, an in-room monitor and console will be very helpful. Any change of geometry data of an imaging sequence with on the flight angulation of the imaging slice should be possible from within the MR room without the need for the usually applied time-consuming preparation phases of standard diagnostic imaging sequences. Furthermore, switching between different sequences should be possible as well, and the orientation of the actual imaging plane should be indicated on images of other orientation. This should allow easy planning of the imaged slice through any desired path, allowing for visualization of the imaged interventional instrument in its full length. For nonvascular interventions, a reliable means of communication from within the MR room to console outside might seem a possible alternative, but the noise of any imaging sequence will make this task quite difficult to achieve. Considering the generally available options of all major vendors for in-room equipment, direct manipulation of imaging sequences inside the MR room should be standard for any MR scanner, where interventions are being performed.

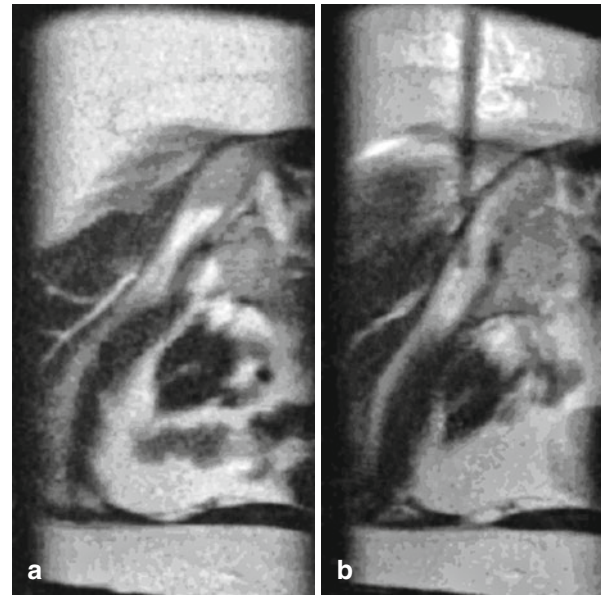

Fig. 3.1 Figure a depicts a region of bone edema of the pelvis on a T2-weighted image acquired in 600 ms (**a**). A 14-G bone drill was used to biopsy this lesion (**b**), which turned out to be a chronic osteomyelitis. Excellent contrast between the lesion and the instrument is achieved on the T2-weighted image

3.2.2 Imaging Sequence: General Considerations

The originally very slow technique of MR imaging has by now developed into a technique allowing even for real-time control of vascular interventions with a high temporal resolution while maintaining a combination of adequate spatial resolution and good contrast (Buecker et al. 2002a). Considering nonvascular interventions, fast spin-echo sequences and gradient-echo sequences have been initially applied for this purpose (Adam et al. 1997). Due to the contrast between vessels and surrounding tissue and the speed of steady-state free precession sequences, this technique is widely used for MR guidance of vascular interventions (Duerk et al. 1998). One disadvantage of SSFP imaging is the substantial noise produced by this technique, causing not only problems for communication but also discomfort to the anxious patient. In general, the ideal sequence for MR guidance of biopsy procedures encompasses the following features:

1. Good contrast between lesion and interventional instrument
2. Sufficiently high temporal and spatial resolution to visualize all lesions to be targeted and to be performed during an easy patient breath hold if not faster
3. Sufficient field of view to avoid back folding enabling switching of phase and frequency encoding directions
4. Preferably low acoustic noise
5. Preferably no additional hardware requirements

Add 1: T2-weighted sequences will usually be advantageous compared to T1 weighted because the susceptibility artifact of metallic instruments causes a signal drop on all sequences. The same is true for signal void caused by nonmetallic materials like ceramic instruments. The usually high signal intensity of pathologic lesions on T2-weighted images yields a good contrast between low signal instrument and high signal lesion (Fig. 3.1) (Bucker et al. 1997).

Add 2: Many articles have published so-called real-time imaging sequences. Considering the imaging frames of 15 per second for a video, this demand is rarely ever met by MR imaging sequences. But nonvascular interventions do not require such a high temporal resolution. Considering the greater importance of high contrast and high spatial resolution, some imaging time should be invested into these parameters. Nonetheless, an easy patient breath hold should be the maximum time needed to acquire an image or an image series. Imaging rates of one image every 10–15 s fulfill this requirement. But looking at the length of a procedure, the

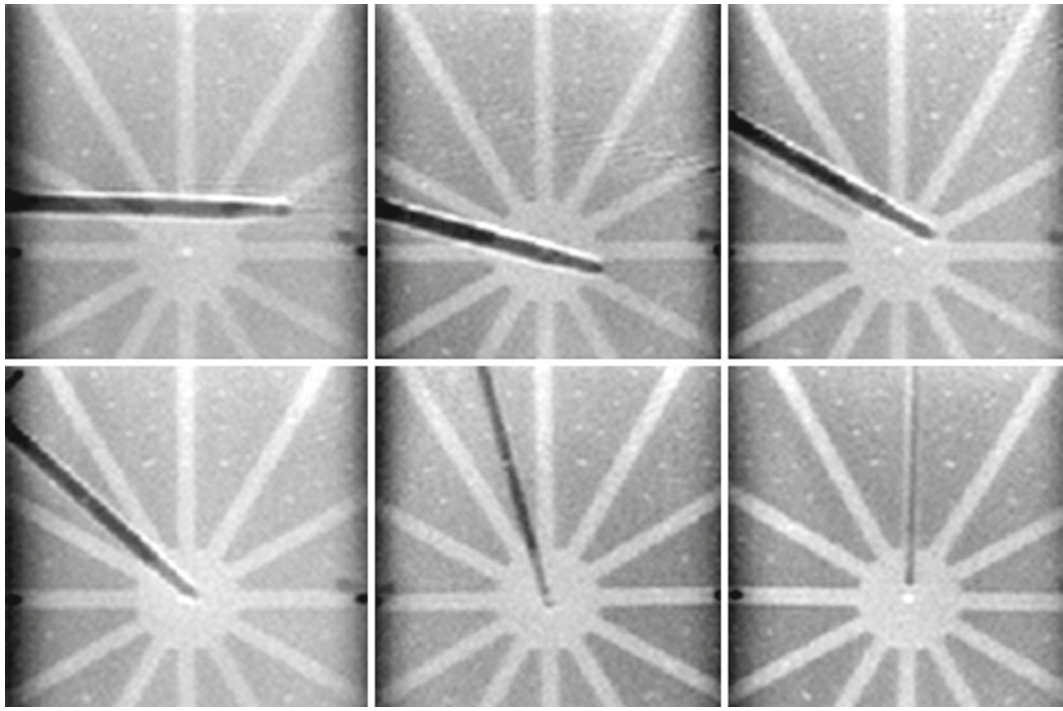

Fig. 3.2 The orientation of an 18-G needle positioned in a water bath is stepwise changed from horizontal to vertical. The change of needle position from the first to the last image is identical in its influence on the susceptibility artifact to switching the phase and frequency encoding direction

demand for faster imaging becomes obvious. The shorter the acquisition time for a single image, the shorter the time of discomfort for the patient and the lower the risk of inadvertent misplacement of a biopsy needle due to patient movement – not to speak about the procedure time and the related cost.

Using the current software implementations, it would be easily possible to adapt the imaging sequence to each single indication and the patient's compliance. But in general, it will be better for the interventionalist to be familiar with one imaging sequence and its contrast and spatial resolution. Therefore, one should try to establish two general biopsy sequences, which are suitable for all interventions; one imaging sequence should be T2 weighted and the other T1 weighted to allow easy switching between these two contrasts depending on the lesion characteristics. Later it will be discussed how different imaging parameters along with the field strength will influence the appearance of our instruments, and tips will be given how to set up the ideal imaging sequences for the individual situation of each institution.

Add 3: The susceptibility artifact of a metallic instrument will depend on the relationship of its axis to the phase and frequency encoding direction. Switching of phase and frequency encoding is easily possible without any changes to the imaging contrast or imaging speed, if the initially acquired field of view is large enough to cover the complete area of interest. This in turn allows for fast changing of the artifact size of metallic instruments (Fig. 3.2).

Add 4: During any biopsy procedure, the patient has to tolerate an individual amount of stress due to the pain induced and especially due to the unknown situation. Any additional stress factors should be avoided for the patient's sake but also to ensure the optimal compliance. Time is of the essence here as mentioned above. Another stress factor is acoustic noise, and this should not be neglected, because many patients

describe the noise as the most unpleasant experience of an MR imaging exam, second only to the limited space inside the magnet bore. Therefore, more quiet imaging sequences are preferable if no other disadvantageous like reduced image contrast or speed outweighs these. In addition, very loud imaging sequences like steady-state free precession techniques, for example, can hinder any communication quite dramatically.

Add 5: MR imaging allows different ways of instrument visualization, which can be divided into active and passive methods of instrument visualization (Coutts et al. 1998; Sathyanarayana et al. 2007; Schulz et al. 1999; Staubert et al. 2000; Wildermuth et al. 1998). An in-depth discussion of all the different methods is beyond the scope of this chapter because most of the time one will focus on passive methods for nonvascular interventions.

In short, active methods use one or even more microcoils fixed to the interventional instrument – usually its tip. Using the MR scanner, the positions of the microcoils are determined and projected either onto a previously acquired road map image or onto an anatomic image acquired during the determination of the microcoil position (Buecker et al. 2002a; Wildermuth et al. 1998). This technique requires a modification of the interventional instrument by attaching a microcoil. In addition, the original active visualization technique required the connection of the microcoil to the scanner. This sophisticated technique makes a simple procedure like MR-guided biopsy quite complicated and further safety concerns arise, which are beyond the scope of this chapter. Additional changes of the MR scanner and the software are needed as well. Newer techniques of active visualization exploit so-called fiducial markers (Coutts et al. 1998), which do not require a connection of the interventional instrument to the MR scanner. But still changes of the software are needed to visualize and localize the fiducial marker.

In contrast to the active methods, passive visualization of an instrument is done without any hard- or software changes. The interventional instrument is displayed directly on the acquired anatomical image.

3.2.3 Imaging Sequence: How to Influence the Appearance of Metallic Instruments Respectively Susceptibility Artifacts

Many interventional instruments still consist of metal. Metals have to be nonferromagnetic in order not to be attracted by the strong magnetic field of the MR scanners. This is the case for *most* modern implants, which consist of stainless steel, nitinol alloys, or titanium to name a few. But is any nonferromagnetic device MR safe or MR compatible? There is some confusion concerning these terms. The Food and Drug Administration offered definitions.

MR Compatible: This term indicates that the device, when used in the MR environment, is MR safe and has been demonstrated to neither significantly affect the quality of the diagnostic information nor have its operations affected by the MR device.

MR Safe: This term indicates that the device, when used in the MR environment, has been demonstrated to present no additional risk to the patient but may affect the quality of the diagnostic information.

According to these definitions, a device cannot be named MR compatible without stating the MR environment (viz., the field strength) and the MR imaging indication. A stainless steel coronary stent may be MR compatible according to the above-mentioned definition for a functional MR examination of the heart, but it will be "only" MR safe for imaging of the coronary arteries.

Another safety concern in the MR environment is caused by the nature of metals, which are electrically conducting. Depending on the length of conducting material and the field strength of the MR scanner, an interventional instrument can act as an antenna. Substantial heating of metallic guide wires has been shown to occur during in vitro and in vivo experiments. The radiofrequency energy used to create the MR images can be fed into the instrument, if the instrument is in resonance with the applied radiofrequency power. There is no agreement among the physicists of different groups according

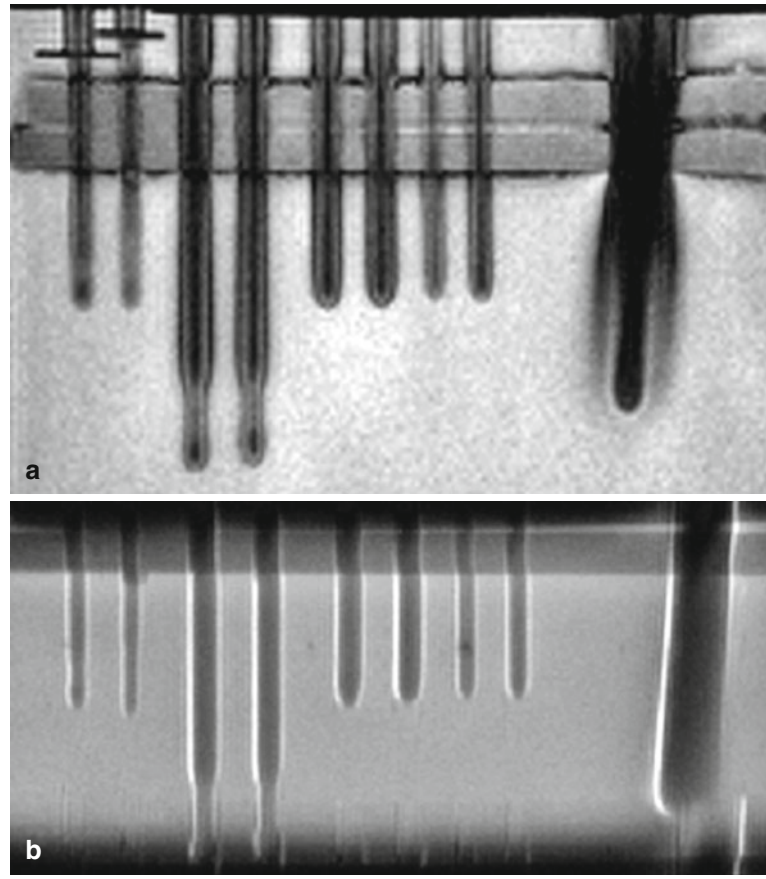

Fig. 3.3 Different MR compatible biopsy needles (18 G trucut, 14 G trucut, 18 G biopsy, 22 G biopsy needle) and one non-MR compatible 22 G needle (last needle on the *right*) are imaged in a water bath with a gradient-echo sequence (**a**) and a spin-echo sequence (**b**)

to the minimum length, at which these safety concerns may appear. The minimal length for occurrence of resonance of a conductive wire is given with 29 cm by one group (Nitz et al. 2001) and 117 cm by another (Armenean et al. 2004). But even for 29 cm, the length of biopsy needles is below the lowest critical threshold for MR scanners with a magnet strength of 1.5 T or less. One needs to be aware of the fact that this length is diminished with increasing field strength of the MR scanner. Consequently, heating phenomena due to resonance are more likely to occur in 3 T MR scanners.

In the following, it will be explained how to manipulate susceptibility artifacts (Ladd et al. 1996). Depending on the field strength, a large artifact might be advantageous compared to a smaller one. While this can be true for low-field strength MR scanners, usually the opposite holds for higher-field strength, requiring minimization of susceptibility artifacts to optimally visualize a metallic instrument and a pathologic lesion. Consequently, the principles will be explained, but no generally true recommendations as to the imaging sequence parameters to be used can be given.

Spin-echo sequences will in general yield a smaller susceptibility artifact compared to gradient-echo sequences (Fig. 3.3). The susceptibility artifact of a gradient-echo sequence will be greatly influenced by the echo time used; the shorter the echo time, the smaller the accompanying artifact (Fig. 3.4).

The orientation of any metallic instrument to the main magnetic field influences the size of the instrument in the image (Fig. 3.2). Usually the ideal approach of a needle to a lesion is predefined and cannot be altered. Nonetheless, one has to be aware of this effect and the possible change of artifact size. Furthermore, a complete switch of

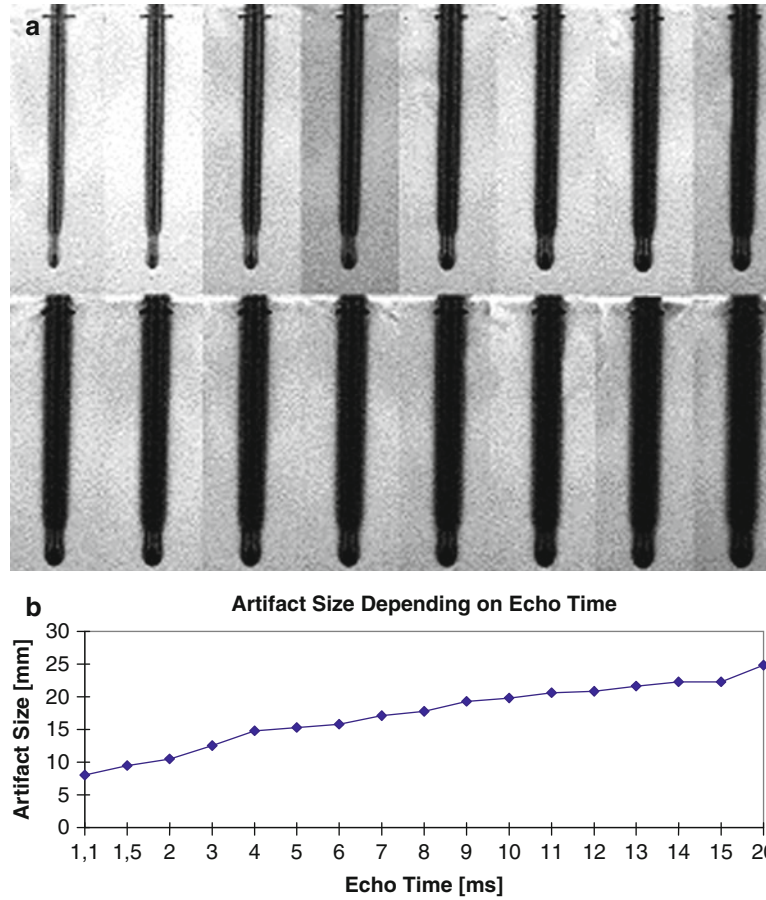

Fig. 3.4 Gradient-echo images of a 14-G biopsy needle acquired with stepwise increasing echo time from 1.5 ms on the *left upper row* to 20 ms on the *right lower row* (**a**) (1.5, 2, 3, 4, 5, 6, 7, 8, 9, 10, 11, 12, 13, 14, 15, 20 ms). The continuous increase in artifact size is also demonstrated by the graph (**b**)

phase and frequency encoding direction can be easily achieved, allowing for a substantial change of the size of susceptibility artifacts. This is demonstrated by the first and last image of Fig. 3.2, which differs by the orientation of the biopsy needle to the main magnetic field; the change of this orientation is equivalent to switching the phase and frequency encoding direction of the imaging sequence.

In order to achieve faster imaging methods, a reduction of the echo read out or partial filling of k-space are sometimes used. If these techniques are applied to sequences used to guide interventions, one has to be aware of a slight change of the form of susceptibility artifacts. One-half of the susceptibility artifact surrounding the metallic instrument will be reduced. While this can be easily detected in an experimental set up imaging a needle within a water bath (Fig. 3.5), it might be much more difficult to visualize with an anatomic background. Usually the needle will be in the center of the signal drop and imaging artifact caused by the difference in susceptibility. This is no longer true, applying partial echo or half Fourier imaging sequences (Fig. 3.5). The amount of metal will also influence the artifact size. Sometimes, this parameter can be changed by removing/inserting a mandrel into a needle.

So far, we only looked at the appearance of the interventional instrument within the imaged slice. The three-dimensional artifact is symmetrically oriented around the physical position of the needle (Fig. 3.6). Therefore, the needle is not centered at the slice position where the needle shape can be depicted best. Instead, the largest artifact will define the image, where the needle is centered exactly in the middle of the imaging plane (Fig. 3.6).

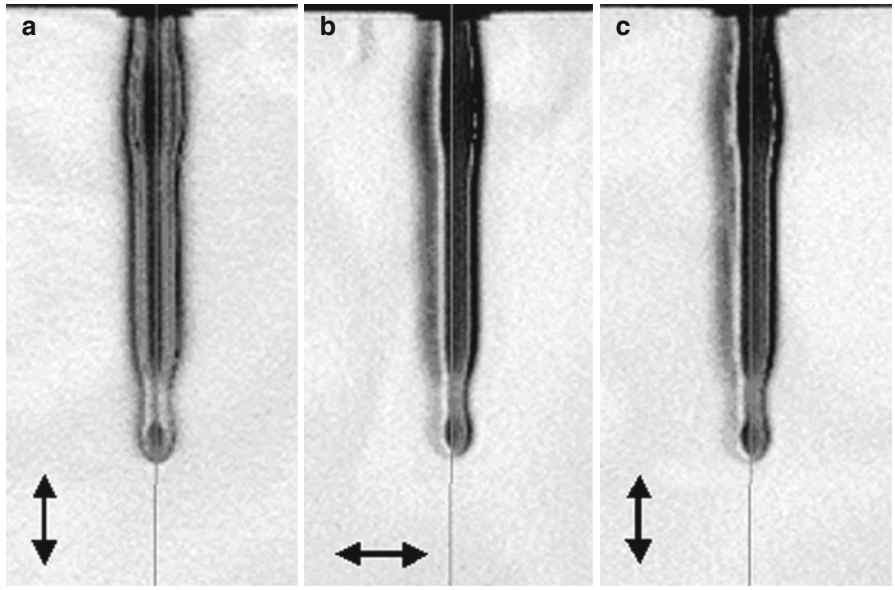

Fig. 3.5 Gradient-echo images of a 14-G needle in a water bath demonstrate the effect of shifting the susceptibility artifact about the true center of the needle, which is marked by the *vertical line*. (**a**) Is acquired without any partial k-space strategies; (**b**) was acquired with 65 % echo read out (partial echo) and (**c**) with partial k-space filling of 65 %. The *black arrows* indicate the phase encoding direction

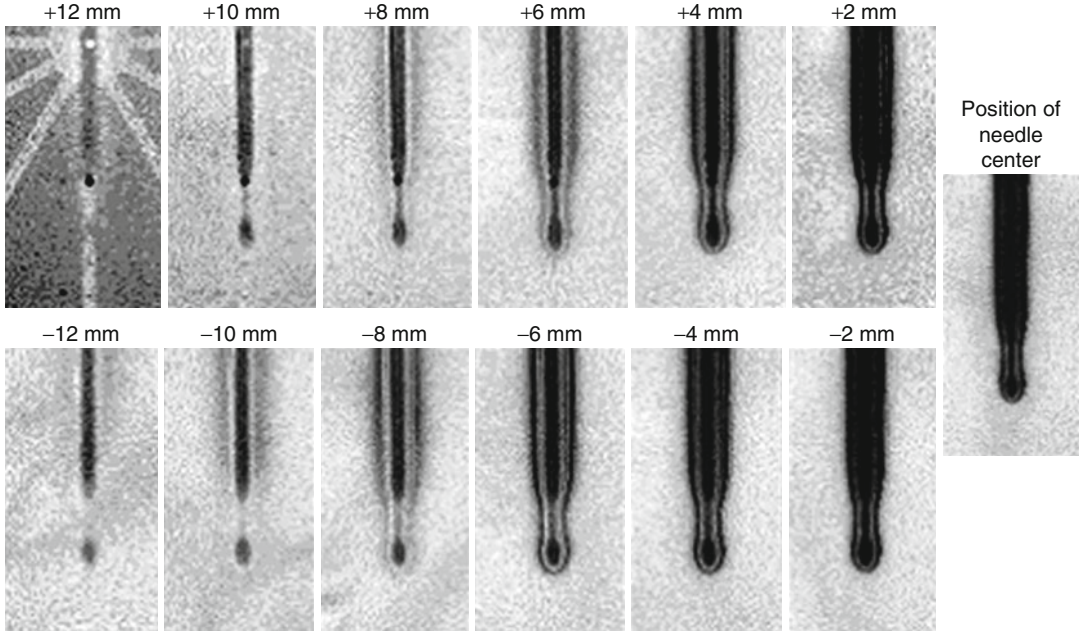

Fig. 3.6 Gradient-echo images acquired with a slice thickness of 10 mm are moved in a stepwise fashion of 2 mm about the physical center of the biopsy needle positioned in a water bath

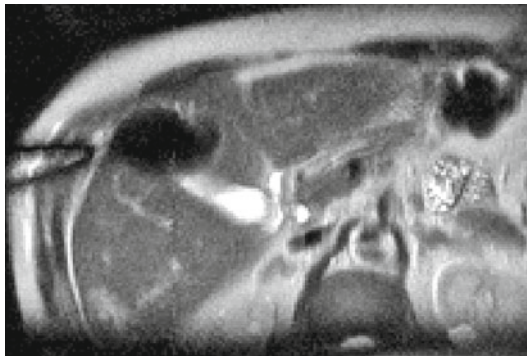

Fig. 3.7 Ice ball formation around two cryoprobes in the liver as depicted on a T2-weighted image acquired in 600 ms (LoLo technique) (Image courtesy of Prof. Dr. med. J. Tacke, Passau Hospital, Germany)

3.2.4 Imaging Sequence: Dedicated Temperature Measurements

Tumor ablation is an increasingly widespread therapy. Different hyperthermal ablation techniques as well as cryoablation are in routine clinical use. Kryotherapy can be easily controlled by MR imaging because the growing ice ball is clearly visualized on standard MR images (Fig. 3.7). The best correlation between the necrotic area and the depicted size of the area of signal void seen on MR images is achieved with T2-weighted spin-echo images (Tacke et al. 2001). Few clinical studies are available on the topic of MR-guided cryosurgery (Mogami et al. 2007; Morin et al. 2004; Wu et al. 2010). This is probably due to the fact that radiofrequency ablation leads to larger lesions compared to cryoablation with identically sized instruments.

Hyperthermal ablation is performed with radiofrequency, laser, microwaves, or focused ultrasound probes (de Jode et al. 1999; Furusawa et al. 2007; Hynynen et al. 1997; Kurumi et al. 2007; Mueller-Lisse and Heuck 1998; Steiner et al. 1998; Vogl et al. 2007). Beside some technical problems for the use of radiofrequency and microwave generators within the MR environment, the visualization of temperature changes by MR are in general possible. Qualitatively this can be achieved by T1-weighted images (Fig. 3.8a), but the control of thermal ablation is not sufficient using the signal drop seen on T1-weighted images. Exploiting the inherent physical properties of the MR technique, it is also possible to semiquantitatively image temperature changes (Fig. 3.8b). These MR techniques are very prone to movement artifacts. Newer real-time sequences for temperature measurements were developed (de Senneville et al. 2007). First clinical trials for MR-guided focused ultrasound treatment of breast lesions (Furusawa et al. 2007; Schmitz et al. 2008) and uterine fibroids (Stewart et al. 2006) have been performed. The current evidence is summarized in a recent comprehensive review on high-intensity focused ultrasound treatment (Hynynen 2010).

3.3 Indication

The relatively complicated technique of MR imaging, the availability, and the cost prohibit a widespread use of MR guidance for interventions, which can be controlled by other imaging modalities like ultrasound or CT. But there are lesions, which can only be seen by MR imaging and consequently can only be biopsied by this technique. Seldom, this is the case for tumors of the liver (Fig. 3.9), but the most common lesions only visible by MR imaging are breast lesions. MR offers the means for simple biopsies and markings (Fig. 3.10) (Dershaw 2000; Heywang-Kobrunner et al. 2000) but also the possibility of excisional biopsies (Gould et al. 1998). Considering the fact that vacuum-assisted biopsy is the method of choice for conventional techniques, the same has to be required for MR-guided procedures (Heywang-Köbrunner et al. 2009). MR-guided brain biopsies have been performed and were proved superior to stereotactic brain biopsy (Hall et al. 1999a). Bone marrow lesions can be very well visualized by MRI, and consequently MR guidance of these lesions can be performed as well (Neuerburg et al. 1998) (Fig. 3.1).

By now, the necessary instruments for biopsies as well as for preoperative marking are available (Floery and Helbich 2006). Besides metallic instruments, nonmetallic devices have been tested as well (Reichenbach et al. 2000), but so far, they

have not replaced metallic instruments. Dedicated breast biopsy devices exist, which fixate the breast and allow an approach from the lateral side (deSouza et al. 1995; Fischer et al. 1995). Techniques without the need for any additional devices have been described as well (Daniel et al. 1998). Usually the procedures are performed with the patient outside of the magnet bore, controlling the advance of the interventional instrument by placing the patient in the scanner bore after advancing the instrument blindly. But automated devices have been developed, which can be used via remote and allow to keep the patient all the time inside the magnet bore, thereby allowing continuous control of the procedure (Kaiser et al. 2000).

Ablative therapy is so far no standard indication for MR guidance. The treatment of uterine fibroids and breast lesions by focused ultrasound requires a direct control of this minimally invasive technique. In this field, MR guidance has been shown invaluable, leading to dedicated focused ultrasound probes integrated into MR tables (Gedroyc and Anstee 2007).

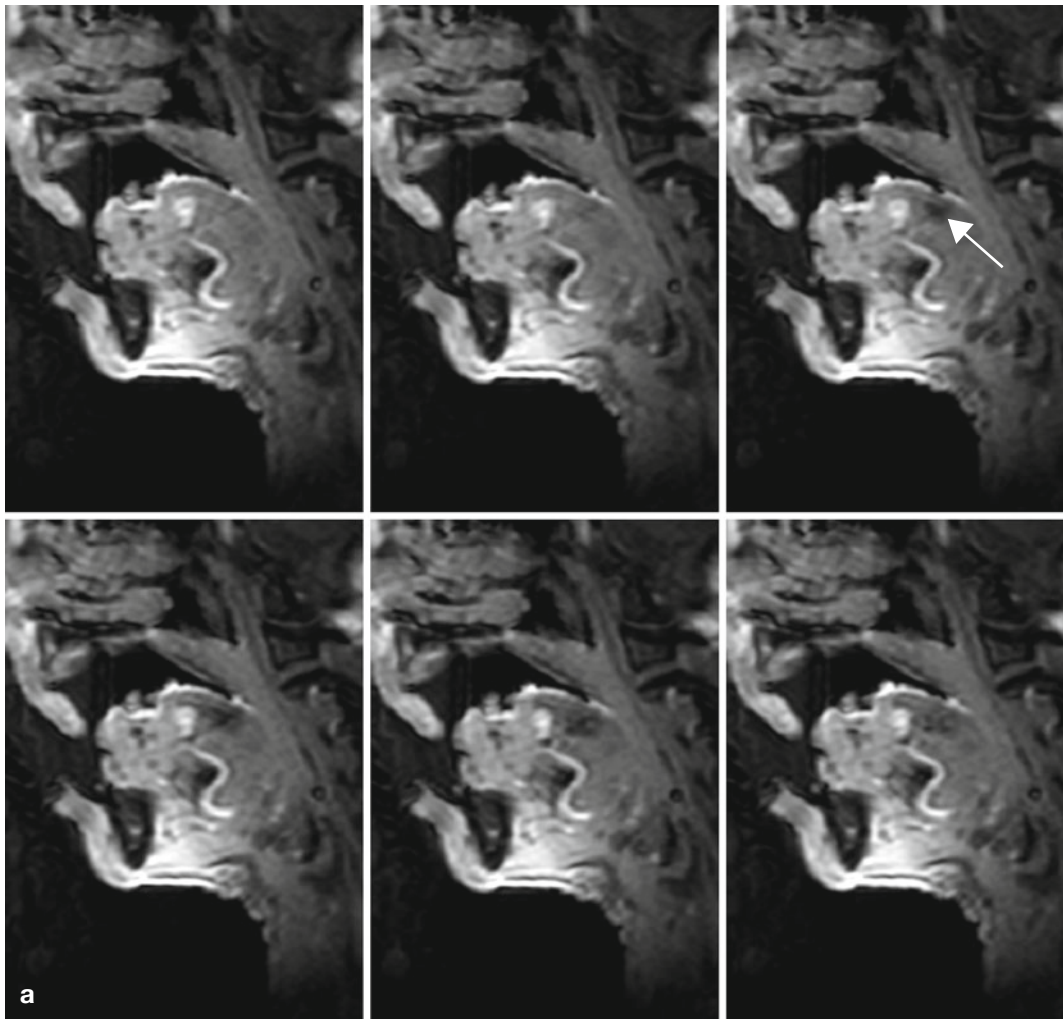

Fig. 3.8 It is difficult to depict the temperature increase around a laser fiber on these T1-weighted gradient-echo images. A slight drop in signal intensity can be seen around the laser tip (*arrow*) positioned in the tongue base tumor (**a**). Using the temperature-dependent change of the phase information of the same MR images, a semi-quantitative depiction of the temperature changes can be projected onto the anatomic images (**b**)

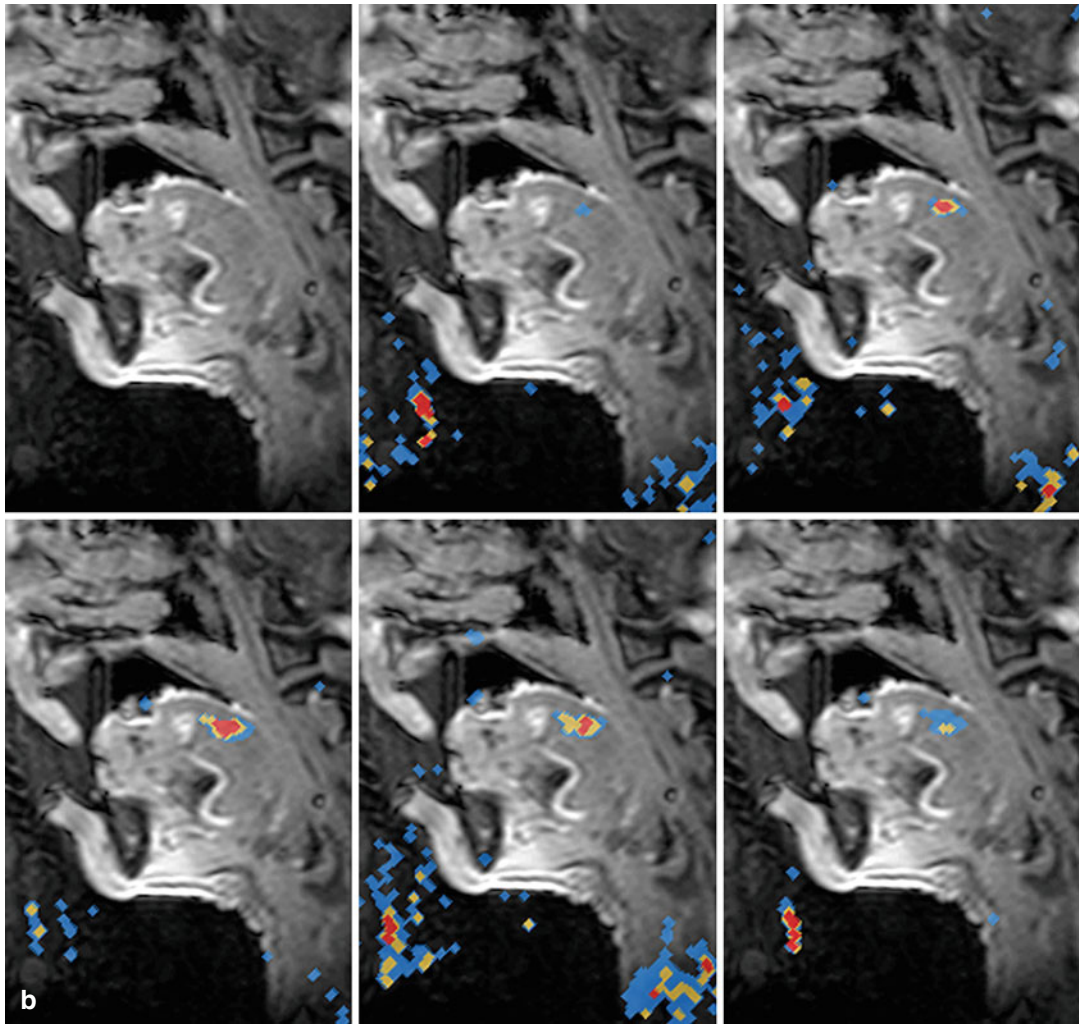

Fig. 3.8 (continued)

MR-guided focused ultrasound treatment of breast lesions (Furusawa et al. 2007) and uterine fibroids (Stewart et al. 2006) has been performed clinically so far. Other techniques of thermoablation like laser and radiofrequency therapy have been applied with MR guidance as well (Mahnken et al. 2004a; Meister et al. 2007; Reither et al. 2000), but for this field, it is not clear, if a broader clinical indication will arise, because standard treatment without direct control of heat spreading is widely available and performed already (Pereira 2007). Other numerous indications like treatment of renal tumors with cryoablation (Mogami et al. 2007) or radiofrequency therapy (Lewin et al. 2004) or microwave therapy (Kurumi et al. 2007) have been performed under MR guidance, but the clinical value of all the different available techniques for different indications remains to be proved yet.

MR imaging is also used for intraoperative guidance of surgical procedures and has been successfully exploited clinically for neurosurgery and endoscopic sinus surgery (Alexander et al. 1995; Buchfelder et al. 2000; Hall et al. 1998; Hsu et al. 1998; Rubino et al. 2000). In the field of clinical neurosurgery, complication rates were found to be acceptable (Hall et al. 2000). New data in this field even suggest a role for 3 T high-field MR scanners (Kim et al. 2009).

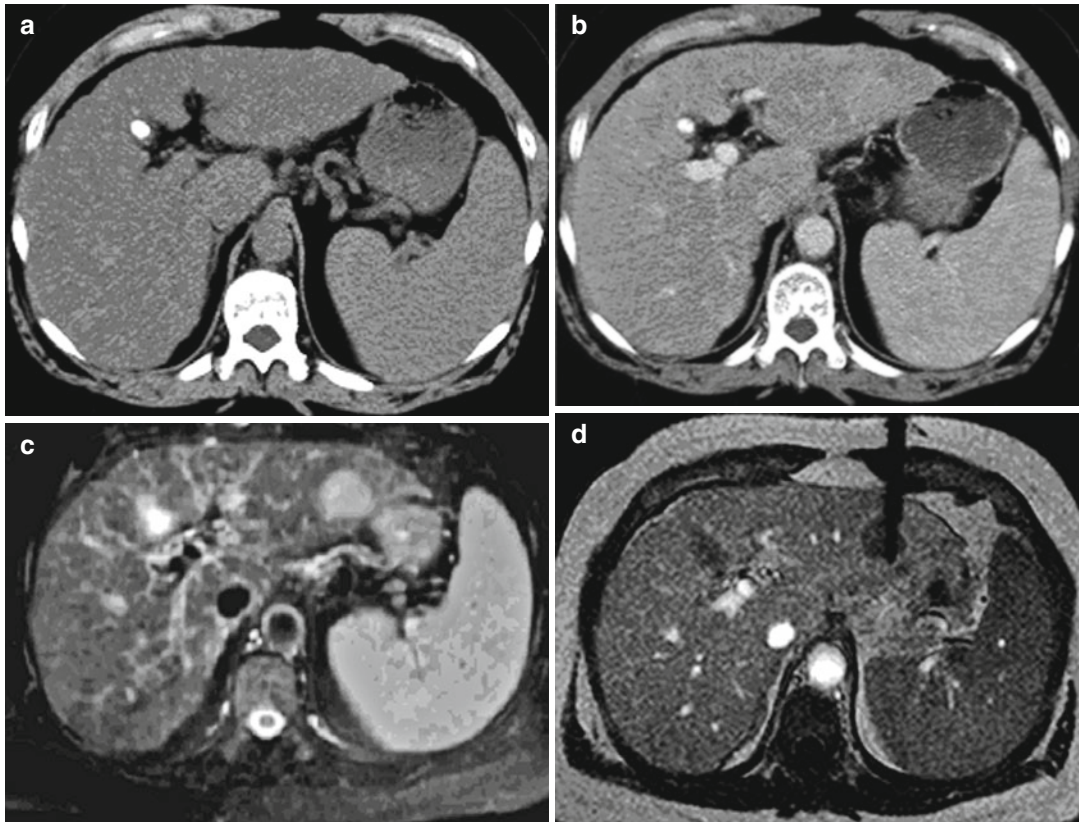

Fig. 3.9 A liver tumor was initially overlooked on the CT images (**a**, **b**). It is clearly visualized on the T2-weighted imaged (**c**) and was biopsied using a T1-weighted gradient-echo sequence (**d**). Histologically, the tumor was proved to be a hepatocellular carcinoma

Appraisal

Despite the fact that MR guidance is cost intensive compared to ultrasound and CT guidance, there is a growing role for MR-guided interventions. Obviously, tumors only visible by MR imaging like breast lesions are one major indication. But beyond this, the imaging feature of MR imaging allowing temperature measurements is by now developed to a state, allowing for clinical use. Especially thermal ablation therapies – and among these high-intensity focused ultrasound – are controlled by MR imaging and offer a truly noninvasive combination of ablation therapy. Clinically, the combination of focused ultrasound and MR guidance is used for breast lesions and uterine leiomyomas, but a growing spread of indications can be expected with further development of focused ultrasound techniques, which will allow even the noninvasive penetration of bone.

Key Points

1. There are dedicated interventional MR scanners with dedicated software.
2. The susceptibility artifacts of metallic instruments can be influenced by changing the imaging sequence; the following parameters lead to smaller susceptibility artifacts:

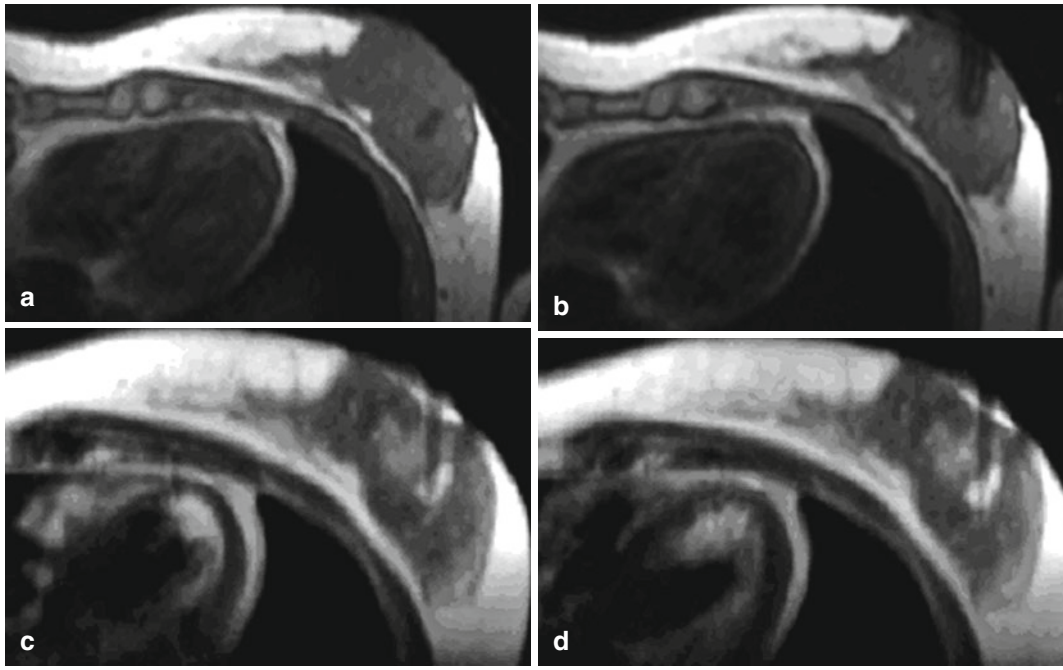

Fig. 3.10 T1-weighted gradient-echo image without contrast agent depicts a breast lesion, which showed a pathologic fast uptake of contrast agent suggesting a malignant tumor (**a**). Using a T1-weighted gradient-echo sequence, the localization wire causes a susceptibility artifact large enough to hide the lesion (**b**). Changing to a T2-weighted spin-echo sequence nicely depicts the needle (**c**) and the marking wire (**d**) within the lesion, which was successfully removed operatively and turned out to be a fibroadenoma

- Spin echo instead of gradient-echo sequence
- Shorter echo time for gradient-echo sequences
- Smaller amount of metal (remove stylet)
- Orientation of the length of the instrument parallel to the frequency encoding direction
- Lower main magnetic field

3. MR compatible means MR safe without disturbing the image quality (depends on the main magnetic field).

   MR safe instruments can disturb the image quality, but are still safe to use (depends on the main magnetic field).

4. Passive visualization: Direct visualization of an instrument in the MR image.

   Active visualization: Use of dedicated microcoils to calculate the position of the microcoil and project this position onto the previously acquired MR image.
5. There is no one and only optimal imaging sequence for MR guidance.
6. MR imaging can depict temperature changes, thereby allowing for control of temperature ablation, especially useful for focused ultrasound therapy.
7. The most demanding indication for MR guidance of nonvascular interventions are breast lesions only visible by MR imaging.

References

Adam G, Neuerburg J, Bücker A et al (1997) Interventional magnetic resonance. Initial clinical experience with a 1.5-tesla magnetic resonance system combined with c-arm fluoroscopy. Invest Radiol 32:191–197

Adam G, Bücker A, Glowinski A et al (1998) Interventional MR tomography: equipment concepts. Radiologe 38:168–172 [German]

Adam G, Bücker A, Nolte-Ernsting C et al (1999) Interventional MR imaging: percutaneous abdominal and skeletal biopsies and drainages of the abdomen. Eur Radiol 9:1471–1478

Alexander E 3rd, Kooy HM, van Herk M et al (1995) Magnetic resonance image-directed stereotactic neurosurgery: use of image fusion with computerized tomography to enhance spatial accuracy. J Neurosurg 83:271–276

Armenean C, Perrin E, Armenean M, Beuf O, Pilleul F, Saint-Jalmes H (2004) RF-induced temperature elevation along metallic wires in clinical magnetic resonance imaging: Influence of diameter and length. Magn Reson Med 52:1200–1206

Barentsz JO (1997) MR intervention in the pelvis: an overview and first experiences in MR- guided biopsy in nodal metastases in urinary bladder cancer. Abdom Imaging 22:524–530

Buchfelder M, Ganslandt O, Fahlbusch R et al (2000) Intraoperative magnetic resonance imaging in epilepsy surgery. J Magn Reson Imaging 12:547–555

Bucker A, Adam G, Neuerburg JM et al (1997) MR-guided biopsies with high-resolution ultrafast T2-weighted turbo spin-echo sequence LoLo: initial clinical experience. Rofo 167:491–495 [German]

Buecker A, Adam G, Neuerburg JM et al (1998) MR-guided biopsy using a T2-weighted single-shot zoom imaging sequence (Local Look technique). J Magn Reson Imaging 8:955–959

Buecker A, Adam G, Neuerburg JM et al (2002a) Simultaneous real-time visualization of the catheter tip and vascular anatomy for MR-guided PTA of iliac arteries in an animal model. J Magn Reson Imaging 16:201–208

Buecker A, Spuentrup E, Grabitz R et al (2002b) Magnetic resonance-guided placement of atrial septal closure device in animal model of patent foramen ovale. Circulation 106:511–515

Coutts GA, Gilderdale DJ, Chui M et al (1998) Integrated and interactive position tracking and imaging of interventional tools and internal devices using small fiducial receiver coils. Magn Reson Med 40:908–913

Daniel BL, Birdwell RL, Ikeda DM et al (1998) Breast lesion localization: a freehand, interactive MR imaging-guided technique. Radiology 207:455–463

de Jode MG, Vale JA, Gedroyc WM (1999) MR-guided laser thermoablation of inoperable renal tumors in an open- configuration interventional MR scanner: preliminary clinical experience in three cases. J Magn Reson Imaging 10:545–549

de Senneville BD, Mougenot C, Moonen CT (2007) Real-time adaptive methods for treatment of mobile organs by MRI-controlled high-intensity focused ultrasound. Magn Reson Med 57:319–330

Dershaw DD (2000) Equipment, technique, quality assurance, and accreditation for imaging- guided breast biopsy procedures. Radiol Clin North Am 38: 773–789

deSouza NM, Kormos DW, Krausz T et al (1995) MR-guided biopsy of the breast after lumpectomy and radiation therapy using two methods of immobilization in the lateral decubitus position. J Magn Reson Imaging 5:525–528

Duerk JL, Lewin JS, Wendt M, Petersilge C (1998) Remember true FISP? A high SNR, near 1-second imaging method for T2- like contrast in interventional MRI at .2 T. J Magn Reson Imaging 8:203–208

Fischer U, Vosshenrich R, Döler W et al (1995) MR imaging-guided breast intervention: experience with two systems. Radiology 195:533–538

Floery D, Helbich TH (2006) MRI-guided percutaneous biopsy of breast lesions: materials, techniques, success rates, and management in patients with suspected radiologic-pathologic mismatch. Magn Reson Imaging Clin N Am 14:411–425

Frahm C, Gehl HB, Melchert UH et al (1996a) Visualization of magnetic resonance-compatible needles at 1.5 and 0.2 Tesla. Cardiovasc Intervent Radiol 19:335–340

Frahm C, Gehl HB, Weiss HD et al (1996b) Technique of MRT-guided core biopsy in the abdomen using an open low-field scanner: feasibility and initial clinical results. Rofo 164:62–67 [German]

Furusawa H, Namba K, Nakahara H et al (2007) The evolving non-surgical ablation of breast cancer: MR guided focused ultrasound (MRgFUS). Breast Cancer 14:55–58

Gedroyc WM, Anstee A (2007) MR-guided focused ultrasound. Expert Rev Med Devices 4:539–547

Gehl HB, Frahm C, Schimmelpenning H et al (1996) A technic of MRT-guided abdominal drainage with an open low-field magnet. Its feasibility and the initial results. Rofo 165:70–73 [German]

Gould SW, Lamb G, Lomax D et al (1998) Interventional MR-guided excisional biopsy of breast lesions. J Magn Reson Imaging 8:26–30

Hall WA, Martin AJ, Liu H et al (1998) High-field strength interventional magnetic resonance imaging for pediatric neurosurgery. Pediatr Neurosurg 29:253–259

Hall WA, Martin AJ, Liu H et al (1999a) Brain biopsy using high-field strength interventional magnetic resonance imaging. Neurosurgery 44:807–814

Hall WA, Liu H, Martin AJ et al (1999b) Comparison of stereotactic brain biopsy to interventional magnetic-resonance-imaging-guided brain biopsy. Stereotact Funct Neurosurg 73:148–153

Hall WA, Liu H, Martin AJ et al (2000) Safety, efficacy, and functionality of high-field strength interventional magnetic resonance imaging for neurosurgery. Neurosurgery 46:632–642

Heywang-Kobrunner SH, Heinig A, Pickuth D et al (2000) Interventional MRI of the breast: lesion localisation and biopsy. Eur Radiol 10:36–45

Heywang-Köbrunner SH, Sinnatamby R, Lebeau A, Lebrecht A, Britton PD, Schreer I (2009) Interdisciplinary consensus on the uses and technique of MR-guided vacuum-assisted breast biopsy (VAB): results of a European consensus meeting. Eur J Radiol 72:289–294

Hsu L, Fried MP, Jolesz FA (1998) MR-guided endoscopic sinus surgery. AJNR Am J Neuroradiol 19: 1235–1240

Hynynen K (2010) MRI-guided focused ultrasound treatments. Ultrasonics 50:221–229

Hynynen K, Vykhodtseva NI, Chung AH et al (1997) Thermal effects of focused ultrasound on the brain: determination with MR imaging. Radiology 204:247–253

Kaiser WA, Fischer H, Vagner V et al (2000) Robotic system for biopsy and therapy of breast lesions in a high-field whole-body magnetic resonance tomography unit. Invest Radiol 35:513–519

Kim PD, Truwit CL, Hall WA (2009) Three-Tesla high-field applications. Neurosurg Clin N Am 20:173–178

Kurumi Y, Tani T, Naka S et al (2007) MR-guided microwave ablation for malignancies. Int J Clin Oncol 12:85–93

Ladd ME, Erhart P, Debatin JF et al (1996) Biopsy needle susceptibility artifacts. Magn Reson Med 36:646–651

Lewin JS, Nour SG, Connell CF et al (2004) Phase II clinical trial of interactive MR imaging-guided interstitial radiofrequency thermal ablation of primary kidney tumors: initial experience. Radiology 232: 835–845

Mahnken AH, Buecker A, Spuentrup E et al (2004a) MR-guided radiofrequency ablation of hepatic malignancies at 1.5 T: initial results. J Magn Reson Imaging 19:342–348

Mahnken AH, Chalabi K, Jalali F et al (2004b) Magnetic resonance-guided placement of aortic stents grafts: feasibility with real-time magnetic resonance fluoroscopy. J Vasc Interv Radiol 15:189–195

Malhaire C, El Khoury C, Thibault F, Athanasiou A, Petrow P, Ollivier L, Tardivon A (2010) Vacuum-assisted biopsies under MR guidance: results of 72 procedures. Eur Radiol 20:1554–1562

Meister D, Hübner F, Mack M et al (2007) MR-thermometrie bei 1,5 T zur thermischen Ablation mittels laserinduzierter Thermotherapie. Rofo 179: 497–505

Mogami T, Harada J, Kishimoto K et al (2007) Percutaneous MR-guided cryoablation for malignancies, with a focus on renal cell carcinoma. Int J Clin Oncol 12:79–84

Morin J, Traore A, Dionne G et al (2004) Magnetic resonance-guided percutaneous cryosurgery of breast carcinoma: technique and early clinical results. Can J Surg 47:347–351

Mueller-Lisse UG, Heuck AF (1998) Steuerung und Monitoring von fokalen Thermotherapien mit der Magnetresonanztomographie. Radiologe 38:200–209

Neuerburg JM, Adam G, Buecker A et al (1998) MRI-guided biopsy of bone in a hybrid system. J Magn Reson Imaging 8:85–90

Nitz WR, Oppelt A, Renz W, Manke C, Lenhart M, Link J (2001) On the heating of linear conductive structures as guide wires and catheters in interventional MRI. J Magn Reson Imaging 13:105–114

Paley M, Mayhew JE, Martindale AJ et al (2001) Design and initial evaluation of a low-cost 3-T research system for combined optical and functional MR imaging with interventional capability. J Magn Reson Imaging 13:87–92

Pereira PL (2007) Actual role of radiofrequency ablation of liver metastases. Eur Radiol 17:2062–2070

Reichenbach JR, Wurdinger S, Pfleiderer SO et al (2000) Comparison of artifacts produced from carbon fiber and titanium alloy needles at 1.5 T MR imaging. J Magn Reson Imaging 11:69–74

Reither K, Wacker F, Ritz JP et al (2000) Laserinduzierte Thermotherapie (LITT) von Lebermetastasen in einem offenen 0,2 T MRT. Rofo 172:175–178

Rubino GJ, Farahani K, McGill D et al (2000) Magnetic resonance imaging-guided neurosurgery in the magnetic fringe fields: the next step in neuronavigation. Neurosurgery 46:643–654

Sathyanarayana S, Aksit P, Arepally A et al (2007) Tracking planar orientations of active MRI needles. J Magn Reson Imaging 26:386–391

Schmitz AC, Gianfelice D, Daniel BL, Mali WPTM, Van den Bosch MAAJ (2008) Image-guided focused ultrasound ablation of breast cancer: current status, challenges, and future directions. Eur Radiol 18: 1431–1441

Schulz T, Schneider JP, Winkel A et al (1999) Der MR-Track-Pointer. Ein wiederverwendbares Instrument zur Lokalisation bei Interventionen. Rofo 171:244–248

Solomon SB, Bohlman ME, Choti MA (2002) Percutaneous gadolinium injection under MR guidance to mark target for CT-guided radiofrequency ablation. J Vasc Interv Radiol 13:419–421

Spuentrup E, Ruebben A, Schaeffter T et al (2002) Magnetic resonance – guided coronary artery stent placement in a swine model. Circulation 105: 874–879

Staubert A, Vester M, Tronnier VM et al (2000) Interventional MRI-guided brain biopsies using inductively coupled surface coils. Magn Reson Med 43: 278–283

Steiner P, Botnar R, Dubno B et al (1998) Radiofrequency-induced thermoablation: monitoring with T1-weighted and proton-frequency-shift MR imaging in an interventional 0.5-T environment. Radiology 206:803–810

Stewart EA, Rabinovici J, Tempany CM et al (2006) Clinical outcomes of focused ultrasound surgery for the treatment of uterine fibroids. Fertil Steril 85:22–29

Tacke J, Adam G, Haage P et al (2001) MR-guided percutaneous cryotherapy of the liver: in vivo evaluation

with histologic correlation in an animal model. J Magn Reson Imaging 13:50–56

Vogl TJ, Lehnert T, Eichler K et al (2007) Adrenal metastases: CT-guided and MR-thermometry-controlled laser-induced interstitial thermotherapy. Eur Radiol 17:2020–2027

Wildermuth S, Debatin JF, Leung DA et al (1997) MR imaging-guided intravascular procedures: initial demonstration in a pig model. Radiology 202:578–583

Wildermuth S, Erhart P, Leung DA et al (1998) Aktive Instrumentenführung in der Interventionellen MR-Tomographie: Einführung in ein neues Konzept. Rofo 169:77–84

Wu B, Xiao Y-Y, Zhang X, Zhang A-L, Li H-J, Gao D-F (2010) Magnetic resonance imaging-guided percutaneous cryoablation of hepatocellular carcinoma in special regions. Hepatobiliary Pancreat Dis Int 9: 384–392

Radiation Protection in CT-Guided Interventions

4

Martin Sedlmair

Contents

4.1 Introduction

Computed tomography (CT) in CT-guided interventions has the advantage of perfect localization and low-contrast detectability in contrast to conventional fluoroscopy. Most current CT-guided interventions are performed using a sequential scan mode, meaning that an acquisition is performed at a single table position and a 3-dimensional stack of images is reconstructed. While state-of-the-art conventional fluoroscopic devices nowadays have 3-dimensional image acquisition features, so called C-arm CT, the image quality and acquisition duration is still inferior to that of conventional CT (Leng et al. 2011). To further improve the interventional workflow in CT-guided interventions, the real-time ability from conventional fluoroscopy has been adapted that combines the benefit of CT image acquisition and reconstruction with real-time imaging of conventional fluoroscopy. This allows a full 3-D visualization of the image data either as multiplanar reformatted slices (MPR) or by using the volume rendering technique (VRT), whereas in conventional fluoroscopy, only a 2-D radiographic projection is acquired and shown. However, it is well known that CT is compared to conventional fluoroscopy, a device with a potential increase in radiation exposure of the patient and the operator (Brenner and Hall 2007). Although CT employs a narrow collimated beam to reduce the entrance dose and applies other dose reduction techniques (e.g., angular beam modulation), it still has a much higher dose rate than conventional fluoroscopy.

M. Sedlmair
Siemens Healthcare, CT,
Siemensstrasse 1, Forchheim D-91301, Germany
e-mail: martin.sedlmair@siemens.com

A.H. Mahnken et al. (eds.), *CT- and MR-Guided Interventions in Radiology*,
DOI 10.1007/978-3-642-33581-5_4, © Springer-Verlag Berlin Heidelberg 2013

Table 4.1 Recommended dose limits in planned exposure situations acc. to ICRP 103

Type of limit	Occupational (mSv/year)	Public (mSv/year)
Effective dose	20, averaged over 5 years, with no more than 50 mSv in any 1 year	1 (exceptionally, a higher value of effective dose could be allowed in a year provided that the average over 5 years does not exceed 1 mSv in a year)
Annual organ doses equivalent to		
Lens of the eye	150	15
Skin	500	50
Hands and feet	500	–

Two important aspects have to be considered in CT-guided interventions:

1. The skin dose of the patient can potentially be very high because the same slice is repeatedly scanned.
2. The operator is often in the direct vicinity of the gantry. Specifically, if CT fluoroscopy is used, the skin of the interventionalist's hand is endangered when it is in the primary beam.

Table 4.2 Estimation of computed tomography fluoroscopy time when the threshold of the deterministic effect and the dose limit for skin is reached (scan parameters 120 kV, 50 mA, 10 mm collimation)

Threshold of deterministic effects at the skin (2 Gy) reached after	7 min (inside the primary beam)
Dose limit for skin/hand for occupational exposure (500 mSv/year) reached after	2 min/200 min (inside/outside the primary beam)

4.2 Dose Considerations

During CT-guided interventions, several regulatory guidelines have to be considered that help to keep the radiation exposure as low as reasonably achievable (ALARA) and to prevent deterministic radiation effects. These guidelines can be seen in the current publication of the International Commission on Radiological Protection (ICRP) in the document ICRP 103 (ICRP 103 2007; Wrixon 2008) and are valid for physicians, the staff, and the patient, likewise. Recommended dose limits for occupational and public individuals from the ICRP 103 report are listed in Table 4.1. To keep the radiation exposure as low as possible, most CT-guided interventions are performed with a reduced tube current-time setting of about 50 mAs or less. Some operators even work with 10 mAs (Paulson et al. 2001), as long as the image quality is sufficient for guiding the intervention. The voltage is commonly set to 120 kV. Unlike in diagnostic CT, severely compromised image quality due to high levels of image noise can be tolerated for CT-guided interventions, as imaging serves the guidance of high contrast objects, rather than diagnostic purposes. The mean fluoroscopy time is about 120 s, but depending on the method and the routine of the operator as well as on the general difficulty of the intervention, the time can vary drastically (Silverman et al. 1999).

4.2.1 Patient Dose

In general, radiation exposure to the patient should be kept as low as possible (ALARA). Since the patient is located in the direct X-ray beam, the radiation exposure needs to be controlled carefully during a CT-guided procedure. The typical dose rate within the beam (120 kV, 50 mA) at the patient's skin is about 5 mSv/s (Nawfel et al. 2000). A rather long intervention with an exposure time of 7 min would lead to a critical threshold of 2 Sv for deterministic effects on the skin (Table 4.2). The effective dose rate to the patient is about 1 % of the dose rate at the skin (Hohl et al. 2008). For a mean fluoroscopy time of 2 min, this would result in an effective dose of 6 mSv. This is a dose similar to that delivered during a diagnostic CT examination.

4.2.2 Operator Dose

The operator's dose limits for occupational exposure must be considered. The international dose limit for the hand is 500 mSv/year (Table 4.1). If the interventionalist's hand is exposed by the beam, the dose received is equal to the dose to the patient's skin, which, given the average values quoted earlier, is about 5 mSv/s. If the operator's hand is not in the primary beam, the radiation exposure is much lower. A few centimeters away from the beam, the radiation exposure of the interventionalist is limited to the scattering generated in the patient. The dose rate rapidly drops from a few millisieverts per second within the beam to 40–50 μSv/s at a distance of 10 cm from the gantry (Nawfel et al. 2000; Stoeckelhuber et al. 2005). If the interventionalist's hand is in the primary beam, the annual dose limit is reached after less than 2 min! If the hand is not in the primary beam, it takes about 200 min to reach the annual dose limit. For common procedures with a duration of 2 min each, 100 procedures can be performed until the dose limit is reached. The dose limit for the effective dose for occupational exposure is 20 mSv/year. Unpublished data from our group indicates that the dose rate at the usual position of the interventionalist next to the gantry is about 2 μSv/s. This results in an effective dose of about 0.02 mSv for a 2-min intervention if the operator wears an apron with a lead equivalent value of 0.35 mm. This calculation considers the shielding of the lead aprons. In this context, it is important to know that X-rays of 120 kV are more penetrating and thus lead to absorption of less than 90 % by the lead apron, when compared to 80 kV where 97 % absorption is achieved. Thus, the amount of radiation which penetrates the lead apron and reaches the interventionalist is greater than in conventional fluoroscopy by a factor of 3. It should be noted that conventional angiography is performed at 80 kV, and thus CT-guided interventions are intrinsically a potential source of a higher amount of radiation exposure. As shown later, the acquisition parameters need to be optimized. The annual dose limit for the effective dose is reached after 2,000 min – e.g., 1,000 interventions with an X-ray exposure of 2 min each. The radiation exposure of the eyes, with the lenses being at risk of cataract formation, is another aspect to be considered carefully. In the literature, the threshold for detectable opacity of the lenses is estimated in the range of 500–2,000 mSv and for visual impairment at 5,000 mSv (Hidajat et al. 2006; Britton and Wholey 1988); hence, eye protection is crucial in CT-guided interventions. The dose limit for the eye lens for occupational exposure is 150 mSv/year. With a dose rate of 2 μSv/s, the limit is reached after 1,500 min (without protective goggles) – i.e., 750 interventions with a duration of 2 min each.

4.3 Radiation Protection in General

Many parameters affect radiation exposure. In general, there is more potential to reduce the radiation exposure to the operator than to the patient. Lead protection applied as a lead cover to the patient greatly reduces exposure of the in-room personnel such as the interventionalist and the technician. It should thus be applied with care before the patient is covered with sterile drape (Simons and Orrison 2004). A dose meter under the lead apron has to be worn inside the scanner room. The interventionalist should wear a ring dose meter in addition because in certain procedures, it is possible that the operator's hand may be directly exposed to radiation (see Sect. 4.2.2). If the scanning parameters are optimized, dose can be reduced considerably. In general, four key parameters define the radiation exposure and image quality in CT and need to be discussed with particular respect to CT-guided interventions.

4.3.1 Collimation

The effect of high entrance doses linearly increases with the selected collimation. This is a particular problem in modern multislice CT scanners with up to 320 collimated sections and a total longitudinal coverage of up to 16 cm. Wide collimations also increase the amount of scatter radiation, which

degrades image quality and is a major source of the operator's radiation exposure. The dose is linearly correlated with the collimation; halving the collimation will result in half the dose applied to the patient. Therefore, the collimation should always be chosen as narrow as possible to gain optimal dose reduction while maintaining the necessary field of measurement for the procedure. Having a dynamically selectable collimation in CT systems is therefore considered as a necessity in conventional fluoroscopic devices, while only few modern CT scanners have a dynamically selectable collimation for interventional procedures.

4.3.2 Tube Voltage

The tube voltage, given in kilovolt (kV), controls the ability of the radiation to penetrate tissue or other materials and to produce a signal at the detector system. Increasing the tube voltage decreases the image noise but also reduces the contrast. Concerning the radiation exposure, the higher the tube voltage, the more radiation exposure is applied to the patient, since the radiation carries an increased potential to create damages during its way through tissue. Reducing the tube voltage from 140 to 120 kV results in a decrease in radiation exposure of more than 30 % (Rogalla and Juran 2004). In general, the tube voltage should be kept as low as possible, but sometimes, metallic instruments or implants prohibit the reduction of the tube voltage due to severe metal artifacts. A new technique in conventional CT-scanning allows for an automatic adaption of the tube voltage for a given reference patient to optimize the contrast-to-noise ratio (CNR) as well as decreasing radiation exposure (Yu et al. 2010), a technique that demands the capability for an automatic adaption of the tube current (see next two sections). Automated tube voltage selection remains to be seen in CT-guided interventional procedures in the future.

4.3.3 Tube Current-Time Product

The tube current-time product, expressed in milliampere-seconds (mAs), defines the amount of photons generated at the X-ray tube. The energy transported by these photons is linearly correlated with the entrance dose of the patient or the operator. Halving the mAs values halves the radiation dose (e.g., using 50 mA instead of 100 mA). Due to differences in scanner characteristics, the mAs value cannot directly be transformed into the respective radiation exposure across different CT scanners, given in milligray (mGy). However, it is possible to measure the correlation between the mAs value and the related radiation exposure for each CT device independently. In CT, this value is expressed as CTDI (computed tomography dose index) and holds the energy deposited per unit mass (mGy/kg) for a given tube voltage setting in a reference phantom (Shope et al. 1981). This reference phantom consists of an acrylic glass cylinder with a diameter of either 16 cm or 32 cm, for head and body, respectively. The CTDI is therefore the only value that allows for comparing the radiation exposure of different CT devices. For longer scan ranges, the CTDI is expressed as the dose length product (DLP) by multiplying the CTDI with the scan length and is defined as mGy×cm. Many application-specific CTDI definitions (e.g., $CTDI_{VOL}$ or $CTDI_{W}$) have been established that respect different acquisitions and measurement techniques (Nagel 2000).

In most currently available interventional applications, the applied radiation exposure is given as the sum of the applied mAs during the whole procedure (Total mAs). Some vendors deliver their CT devices with tables in their manuals to calculate the resulting CTDI from the given total mAs value or show these values directly in the dose report or the real-time displays during a procedure.

4.3.4 Image Noise

Another, often unconsidered, parameter that is controlled by the tube current-time product is image noise. Using the values from the example above, halving the mAs value increases the image noise by a factor of the square root of 2. But also the individual patient thickness has a relevant impact on image noise. As it is well known from X-ray physics, the photon radiation is traveling from the X-ray source through the patient and gets attenuated or absorbed, following an inverse exponential behavior related to the patient thickness

(Starck et al. 2002). This means the radiation dose that produces the signal at the detector is reduced depending on the patient thickness. Increasing the patient thickness by 10 cm, the image noise increases by a factor of about 2.6. To compensate this increase in image noise, the mAs value has to be increased by a factor of about 7. Therefore, state-of-the-art CT scanners have an automatic exposure control (AEC) that respects different patient thicknesses and body regions and adapts the tube current to a predefined reference thickness, accordingly (Kalra et al. 2004). Current CT systems for interventional imaging are currently not equipped with this option. For most interventional procedures, the lack of an AEC is not a problem, since the major concern is dose reduction and not image quality. When comparing the AEC with the automatic tube voltage selection described earlier, it can be seen that automated selection of the tube voltage optimizes the contrast-to-noise ratio, whereas the AEC optimizes the image noise in general. Both optimization features can therefore not be applied independently, because automated kV selection relies on the AEC.

Generally, dose reduction by minimizing tube voltage, tube current, collimation, and fluoroscopy duration is always recommended. Having detailed knowledge about the effectiveness of the tube current-time product or the tube voltage allows for a drastic reduction of radiation exposure to the patient or the operator while keeping image quality at an acceptable level. In certain circumstances, pediatric patients may be treated with different parameters to reduce the radiation dose even more (Donnelly et al. 2001). As shown above, most parameters cannot be adjusted independently. Therefore, suitable settings must be found, applying to the ALARA principle and resulting in adequate image quality, necessary to perform the interventional procedure.

4.4 Radiation Protection by Technical Means

A technical approach to reduce radiation exposure of the interventionalist's hand and the patient's skin dose is to interrupt or reduce the radiation on selected X-ray tube positions (angular beam modulation, ABM) in the upper segment of the gantry (usually between 10- and 2-o'clock positions). This gated fluoroscopy leads to a dose reduction of the operator's hand by 27–72 %, the patient's skin dose by 75 %, and the patient's overall effective dose by 35 % without compromising image quality (Hohl et al. 2008). However, keeping the hand out of the gantry is still most effective. A dose display which the interventionalist can glance at is very useful and is often available in high-end CT devices and shows all important dose and scan parameters during an acquisition (accumulated CTDI and mAs values). Optionally, some vendors also deliver wireless measurement devices that can be worn by the operator and the patient during an interventional procedure. Ideally, a display of the patient's skin dose as a percentage of potential skin dose hazard (2 Gy) should be provided. Current software versions for CT-guided interventions also provide an acoustic or optical warning signal if a predefined dose threshold has been reached (Fig. 4.1).

Two modes are established in CT-guided intervention: a sequential mode with one image (stack) acquired after the other, to verify the needle or instrument position as well as the path to the target lesion, and CT fluoroscopy with a continuous scan during the whole procedure, potentially leading to higher radiation exposure than the sequential mode. Both modes are mostly used for procedures that are directly performed on the patient (e.g., RFA, vertebroplasty) where the physician is in the operating room using in-room acquisition controls like foot switches or wireless control panels (Fig. 4.2). Excessive scans using CT fluoroscopy can therefore lead to a relevant radiation exposure not only for the patient but also to the operator. For this reason, it is recommended to keep in-room time as short as possible or to take appropriate measures for lowering the dose (e.g., lead shields). Sequential and fluoroscopic modes are limited to the longitudinal (z-axis) coverage of the nominal collimation, ranging from one section on older scanners to 320 sections in current high-end scanners with a z-coverage ranging from 0.6 to 160 mm. An additional mode overcomes the limited longitudinal coverage of the previous two modes by applying a continuous spiral acquisition with low-dose settings but has the drawback of not being a real-time acquisition

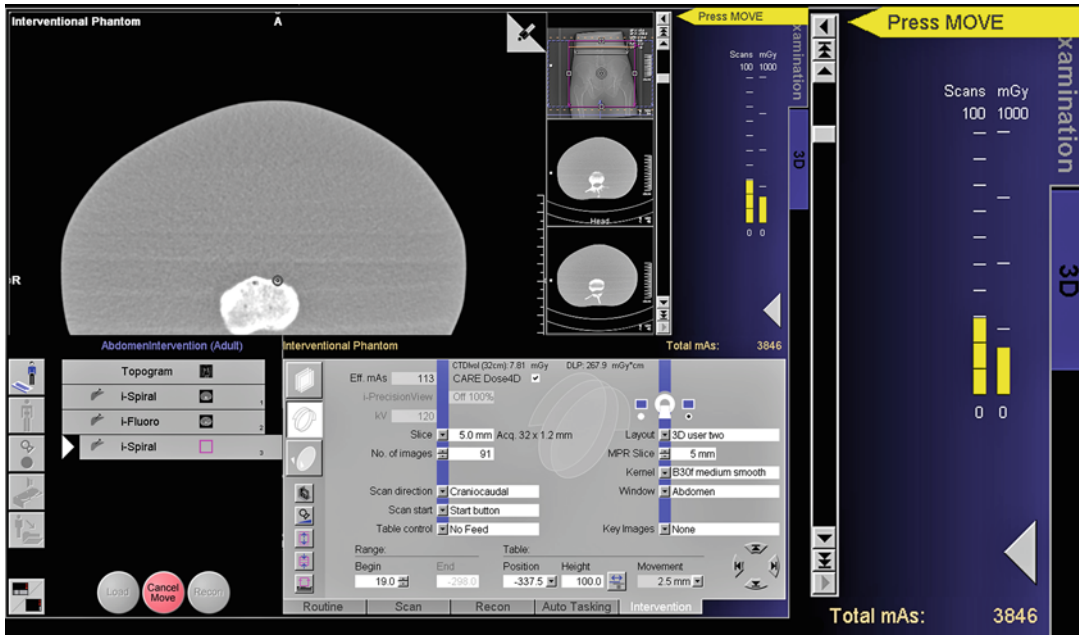

Fig. 4.1 User interface for CT-guided interventions with a dose surveillance monitor on the *upper right side*, shown with two *yellow* bars. One showing the total amount of fluoroscopic acquisitions (*left bar*), the other bar shows the total amount of applied radiation dose in mGy, the total amount of scans, as well as the applied total mAs (*right*). If the number of scans or the amount of applied radiation dose exceeds a predefined value, an alert will appear

anymore. This scan mode is mostly being used for pre- or post-interventional diagnostics.

In addition, many highly sophisticated solutions were suggested to minimize the radiation exposure in CT-guided interventions including laser-guidance, electromagnetic or optical needle tracking, or robotic devices (Cleary et al. 2006; Varro et al. 2004). The basic principle of the mentioned approaches is that an external system assists in finding the right location of the needle entry point and the correct trajectory and angle on pre-interventional scans without having to apply radiation. Thereby, a scan has to be made prior to the interventional procedure itself. The needle path and entry point can be planned without further radiation. After this planning step, the laser or robot device shows or drives the needle to the correct entry point. These solutions not only help to reduce radiation exposure for both, the operator and the patient by up to 76 %, but also reduce the time-consuming process of finding the correct needle position using multiple low-dose acquisitions by up to 40 % (Ohnsorge et al. 2005). Unfortunately for CT-guided interventions, no vendor has currently come up with a practical solution suitable for daily routine practice, since most of the proposed solutions are either prone to interferences (electromagnetic needle tracking), too expensive, too bulky (optical needle tracking), and – since the setup of most devices is cumbersome – not sufficiently integrated in the workflow to reduce the procedure time.

4.5 Radiation Protection of the Interventionalist

X-ray protection of the operator is similar to that for other fluoroscopic interventions where the operator is mostly exposed by the scatter radiation originating from the patient. A lead apron with 0.35-mm lead equivalent must be worn. A thyroid shield as well as protective goggles for the protection of the eye lenses is strongly recommended. To protect the operator from the radiation scattered by the patient, a

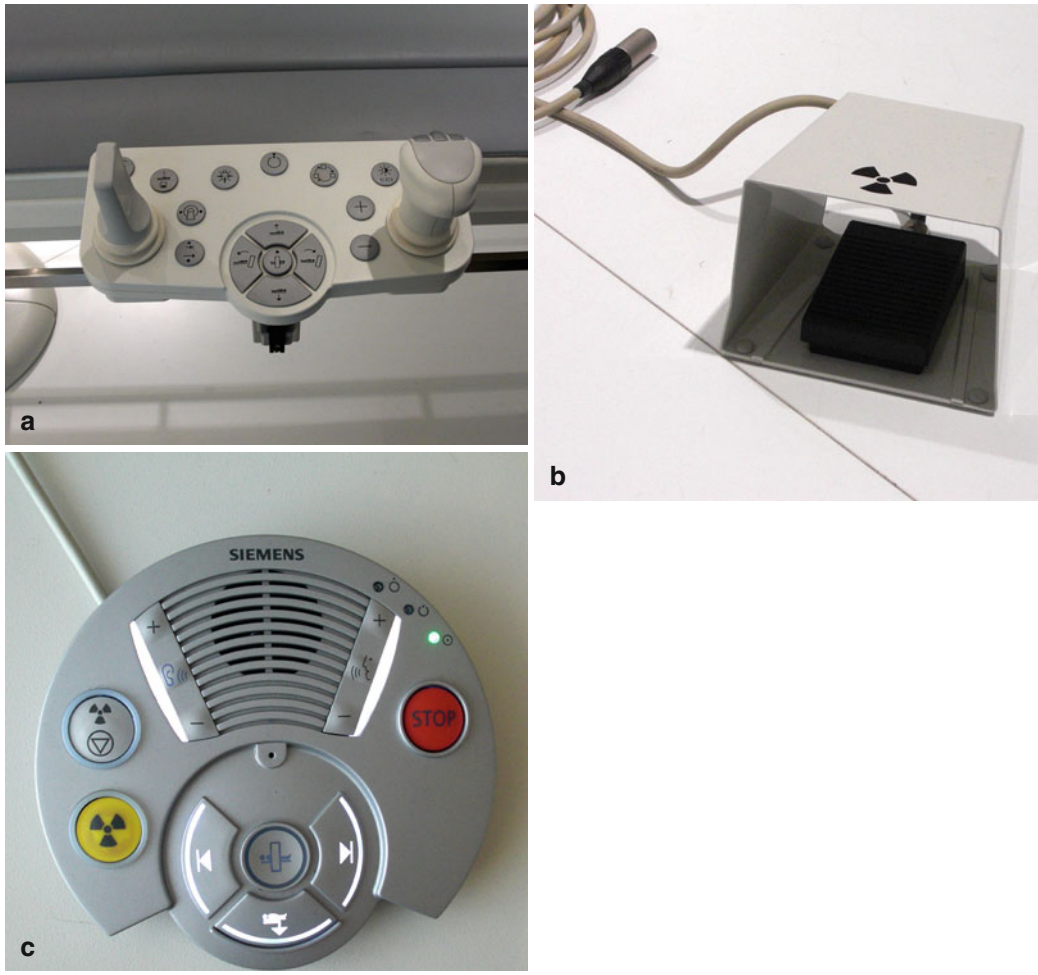

Fig. 4.2 Different operational controls to control the image acquisition and table position. (**a**) In-room control either mounted on the table side support or on a movable trolley. (**b**) In- or out-room foot switch to control the image acquisition. (**c**) Out-room control panel for patient positioning and image acquisition

lead drape should always be placed on the patient close to the scan plane. Thereby, the scatter radiation is reduced by more than 70 % (Nawfel et al. 2000; Stoeckelhuber et al. 2005). To avoid deterministic skin effects at the hand, the use of a needle holder is recommended. The use of lead or bismuth gloves further reduces the radiation exposure but is often uncomfortable and limits the mobility of the hand. Nevertheless, these are effective ways to protect the hand from the primary beam during the intervention and thus to reduce the skin dose by a factor of 100. A plastic instead of a metal needle holder should be used to avoid metal artifacts in the image. Protective gloves, which shield about 50 % of the radiation and have sufficient tactility, may be used in addition.

4.5.1 Operator Location and Distance to the Gantry

One apparent but underused dose reduction potential is the position of the operator or the staff during an acquisition. This fact can be explained by looking at the radiation profile of the gantry and from the patient's scattered radiation which is the dominant source of radiation exposure of the interventionalist (Fig. 4.3a). From Fig. 4.3a, it is obvious that the maximum dose distribution is in front and

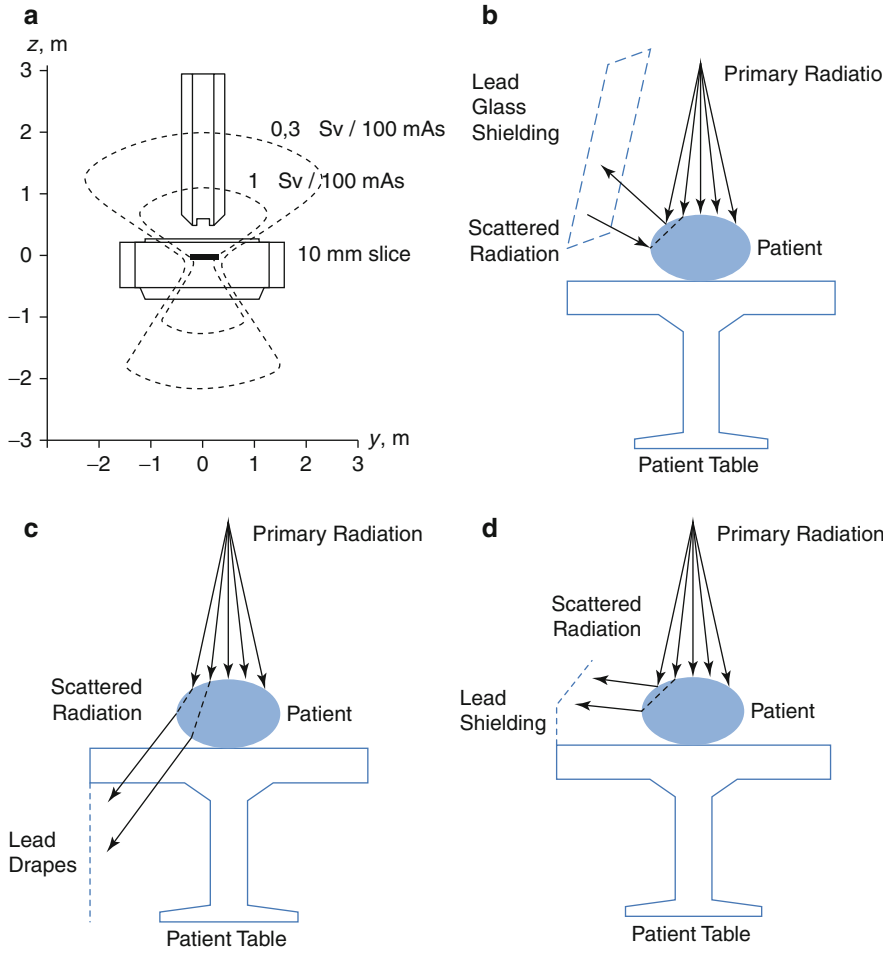

Fig. 4.3 (**a**) Isodose distribution around a computed tomography scanner (Courtesy of Siemens). (**b**) Lead glass shielding mounted on a ceiling support. (**c**) Lead drapes mounted on the lower side of the table. (**d**) Lead shield panels mounted on the upper side of the table support

backside of the gantry opening. Therefore, it is recommended to maximize the distance of the operator to the gantry and the patient and remain in low radiation areas whenever a direct interaction in front or behind the gantry is not necessary.

4.5.2 Shielding Walls

Some vendors for radiation protection equipment also supply acrylic shielding walls (Fig. 4.3b). Most of these devices are mounted on a trolley that can be positioned between the patient and the operator during a procedure. These trolleys are often bulky to use because the trolley is large and hinders to work continuously on the patient. A more convenient solution is a glass shielding that is mounted on the ceiling support and can be moved in and out more easily. Unfortunately, there are almost no studies that show the benefit of using shielding walls for dose reduction in interventional CT.

4.5.3 Lead Curtains Below the Table Support

An effective and simple means for dose reduction of the operator and the staff is lead drapes around the lower side of the patient table and in front of the lower side of the gantry opening (Fig. 4.3c).

The drape can be mounted on the table side rail and may move with the table in the longitudinal direction and the table height. The front side of the drape is aligned orthogonal to the table, so the scatter radiation from the interior part of the gantry can be effectively reduced by about 40 % within a 150 cm radius around the shielding (Mahnken et al. 2012). Some investigators also show the application of lead drapes adjacent to front of the gantry opening which can reduce the amount of primary and scatter radiation up to 97 % but are unhandy when it is necessary to work on the patient inside the gantry (Neeman et al. 2006).

4.5.4 Lead Shields Above the Table Support

Although lead curtains help to reduce the scatter radiation from the patient on the lower side of the patient table, there is still enough scatter radiation from the upper side. For that reason, lead protectors can be mounted on the top support of the patient table (Fig. 4.3d). The special shape of the lead shield reduces the upper part of the scatter radiation. Unfortunately, there are currently no measurements that show how much scatter reduction can be achieved by using this type of shielding.

Summary

As long as the operator performs fewer than about 1,000 biopsies a year, the effective dose and therefore the stochastic effect of radiation is likely to be a minor problem. The main attention has to be drawn to deterministic effects on the patient's and the operator's skin. The dose limit for occupational exposure of the hand is 500 mSv/year. If the operator's hand is frequently hit by the primary beam, this limit is easily reached. In addition, the eye lenses are exposed to scatter radiation. This effect depends directly on the distance between the interventionalist and the gantry and/or the patient and is thus specifically threatening during CT fluoroscopy. It is therefore mandatory to use lead aprons, thyroid shielding, and protective goggles during the whole procedure as general radiation protection measure. The best protection can be achieved by not being exposed to radiation at all by leaving the room during the application of radiation. If in-room presence is necessary, suitable secondary protection (e.g., needle holders, lead drapes) should be used. Reducing radiation exposure by optimizing the scan parameters is recommended in all cases. It is a key toward reducing the dose to the operator and the patient.

Key Points

- Be aware! CT interventions potentially deliver very high doses to the interventionalist, support personnel, and the patient.
- Reduce the dose delivered by careful validation of tube voltage, tube current-time product, collimation, and fluoroscopy time.
- Use sequential images and intermittent fluoroscopy if possible.
- Use a needle holder in CT fluoroscopy.
- Always wear appropriate protection including (undamaged) lead aprons, thyroid shielding, and protective goggles to avoid cataract formation of your eye lenses.
- If available, apply scanner-side radiation protection like lead drapes or gantry curtains, lead glass panels, and table side protections.
- If possible, leave the room or place yourself on the side of the gantry.

References

Brenner DJ, Hall EJ (2007) Computed tomography – an increasing source of radiation exposure. N Engl J Med 357:2277–2284

Britton CA, Wholey MH (1988) Radiation exposure of personnel during digital subtraction angiography. Cardiovasc Intervent Radiol 11:108–110

Cleary K, Melzer A, Watson V et al (2006) Interventional robotic systems: applications and technology state-of-the-art. Minim Invasive Ther Allied Technol 15:101–113

Donnelly LF, Emery KH, Brody AS et al (2001) Minimizing radiation dose for pediatric body

applications of single-detector helical CT: strategies at a large Children's Hospital. AJR Am J Roentgenol 176:303–306

Hidajat N, Wust P, Felix R et al (2006) Radiation exposure to patient and staff in hepatic chemoembolization: risk estimation of cancer and deterministic effects. Cardiovasc Intervent Radiol 29:791–796

Hohl C, Suess C, Wildberger JE et al (2008) Dose reduction during CT fluoroscopy: phantom study of angular beam modulation. Radiology 246:519–525

ICRP 103 (2007) The 2007 recommendations of the International Commission on Radiological Protection. Ann ICRP 37:1–332

Kalra MK, Maher MM, Toth TL et al (2004) Techniques and applications of automatic tube current modulation for CT. Radiology 233:649–657

Leng LZ, Rubin DG, Patsalides A et al (2011) Fusion of intraoperative three-dimensional rotational angiography and flat-panel detector computed tomography for cerebrovascular neuronavigation. World Neurosurg dx.doi.org/10.1016/j.wneu.2011.09.008

Mahnken AH, Sedlmair M, Ritter C et al (2012) Efficacy of lower-body shielding in computed tomography fluoroscopy-guided interventions. Cardiovasc Intervent Radiol. doi:10.1007/s00270-011-0338-0

Nagel HD (2000) Radiation exposure in computed tomography. European Coordination. Committee of the Radiological, Electromedical and Healthcare IT Industry (COCIR), Frankfurt

Nawfel RD, Philip FJ, Silverman SG et al (2000) Patient and personnel exposure during CT fluoroscopy-guided interventional procedures. Radiology 216:180–184

Neeman Z, Dromi SA, Sarin S et al (2006) CT fluoroscopy shielding: decreases in scattered radiation for the patient and operator. J Vasc Interv Radiol 17:1999–2004

Ohnsorge JAK, Siebert CH, Schkommodau E et al (2005) Minimally-invasive computer-assisted fluoroscopic navigation for kyphoplasty. Z Orthop Ihre Grenzgeb 143:195–203

Paulson EK, Sheafor DH, Enterline DS et al (2001) CT fluoroscopy-guided interventional procedures: techniques and radiation dose to radiologists. Radiology 220:161–167

Rogalla P, Juran R (2004) CT-durchleuchtung. Radiologe 44:671–675

Shope TB, Gagne RM, Johnson GC (1981) A method for describing the doses delivered by transmission x-ray computed tomography. Med Phys 8:488–495

Silverman SG, Tuncali K, Adams DF et al (1999) CT-fluoroscopy-guided abdominal interventions: techniques, results, and radiation exposure. Radiology 212:673–681

Simons GR, Orrison WW (2004) Use of a sterile, disposable, radiation-absorbing shield reduces occupational exposure to scatter radiation during pectoral device implantation. Pacing Clin Electrophysiol 27:726–729

Starck G, Lönn L, Cederblad A et al (2002) A method to obtain the same levels of CT image noise for patients of various sizes, to minimize radiation dose. Br J Radiol 75:140–150

Stoeckelhuber BM, Leibecke T, Schulz E et al (2005) Radiation dose to the radiologist's hand during continuous CT fluoroscopy-guided interventions. Cardiovasc Intervent Radiol 28:589–594

Varro Z, Locklin JK, Wood BJ (2004) Laser navigation for radiofrequency ablation. Cardiovasc Intervent Radiol 27:512–515

Wrixon AD (2008) New ICRP recommendations. J Radiol Prot 28:161–168

Yu L, Li H, Fletcher JG et al (2010) Automatic selection of tube potential for radiation dose reduction in CT: a general strategy. Med Phys 37:234–243

Medical Management of the Patient

5

Dietrich Henzler and Michael Murphy

Contents

D. Henzler (✉) • M. Murphy
Departments of Anesthesia and Critical Care,
QE II Health Science Centre, Dalhousie University,
1278 South Park St., 10 West Victoria, Halifax,
NS B3H 2Y9, Canada
e-mail: dietrich.henzler@dal.ca

5.1 Introduction

Substantial progress has been made in the practice of interventional radiology. Such gains would not be possible without adequate medical management of patients. Their well-being may be threatened by such procedures, many of which exceed several hours' duration, during which time patients need to remain totally immobile. Certain procedures may be painful or impose the risk of substantial complications. The patient population subjected to these procedures is tending to the extremes of life: the very young and the very old. These patients tend to be fragile and at times, noncompliant with the demands of the procedure.

This chapter provides an overview of the monitoring techniques that may be used, medications that may prove useful, and the limitations of self-administered sedation.

Before embarking on these discussions, it is crucial that all involved in the planning for these suites understand the requirements imposed by health-care organizations, specialty societies, and building codes with respect to anesthetizing locations. Issues such as the location of piped gas outlets, electrical safety, and air exchanges per hour must be incorporated in the plan to ensure that sedation or occasional anesthesia can be performed in these areas and remain within the applicable laws and standards.

A.H. Mahnken et al. (eds.), *CT- and MR-Guided Interventions in Radiology*,
DOI 10.1007/978-3-642-33581-5_5, © Springer-Verlag Berlin Heidelberg 2013

Table 5.1 Recommended monitoring in sedated patients

	Technique	Normal range
Oxygenation	Pulse oximetry	$SpO_2 > 96$ % on room air
Ventilation	Capnography	10–14 breaths/min, $EtCO_2$ 40–50 mmHg (vol%)
Blood pressure	Noninvasive blood pressure	Systolic 110–150, MAP 60–90 (adult)
Heart rate, arrhythmia, ischemia	ECG	Heart rate 60–100, no QRS/ST changes compared with preprocedural ECG
Sedation and analgesia depth	Verbal response	Mild sedation

SpO_2 O_2 saturation, *$EtCO_2$* end-tidal CO_2, *MAP* mean arterial pressure, *ECG* electrocardiogram

5.2 Materials and Techniques

5.2.1 Monitoring

Ensuring the patient's hemodynamic and respiratory stability may be a major challenge during these procedures, particularly for patients at the extremes of age. Proximity and access to the patient may be limited owing to positioning within the scanner. These factors easily distract one's attention from the monitors, suggesting the need for a second physician or an experienced nurse in the event a timely response to hemodynamic or respiratory deterioration is required. Table 5.1 gives information on recommended monitoring.

5.2.1.1 Hemodynamic Monitoring

Basic hemodynamic monitoring is obligatory for all interventional procedures, particularly in patients undergoing lengthy procedures and those with the following needs or suffering from the following conditions:

- Patients requiring sedation
- Patients with severe claustrophobia
- Patients with labile circulation
- Patients with significant coronary heart disease or arrhythmias

Basic hemodynamic monitoring includes a three-lead electrocardiogram (ECG) and noninvasive blood pressure measurement. It should be noted that built-in ECG devices in computed tomography (CT) and magnetic resonance imaging (MRI) scanners are for cardiac imaging triggering purposes only and may not be approved to monitor and diagnose arrhythmias or ST-segment changes. Separate monitors are recommended, and the output signal of these monitors can be transmitted directly to the scanner for cardiac triggering purposes. In MRI, only one set of ECG leads with short cables and specially approved ECG electrodes may be used to avoid the risk of inflicting burns on the patient when the magnetic field is activated and to prevent image disturbance.

Automatic noninvasive measurement is recommended for accurately and reliably determining blood pressure. Advantages include (1) more time for staff to attend to other tasks, (2) timed repetition of blood pressure measurements, and (3) continuous display of the blood pressure and other parameters (e.g., systolic, diastolic, and mean blood pressure; pulse rate), depending on the machinery.

Modern noninvasive machines employ a detection system based on an oscillometric principle, whereby the blood pressure is electronically determined from the pulse amplitude. The shortcomings of the noninvasive blood pressure technique are those of any cuff measurement technique and usually involve patients with obese arms, uncooperative moving patients, and those with very high or very low blood pressure. Even with these limitations, automatic machines are more accurate, precise, and reliable than auscultation in patients (Murphy and Thompson 2002).

5.2.1.2 Monitoring of Respiration

Respiratory depression is a particular concern in patients undergoing procedural sedation. Unrecognized hypoxia and hypercarbia demand close respiratory monitoring. Patients at particular risk include:

Table 5.2 Expected changes in SpO2 after apnea and recovery

	Time to desaturation (<90 %) after apnea (s)	Time to restoration of SpO_2 > 95 % after recommencement of ventilation
Healthy adult, breathing room air	120–180	3–20 min[a]
Healthy adult, breathing 100 % O_2	180–600	~ 5 s
Morbid obesity, pregnancy, breathing 100 % O_2	60–180	~ 40 s
Children, breathing 100 % O_2	22–45	~ 30 s
Small children (0–2 years), breathing 100 % O_2	20–30	~ 20 s

[a]With unassisted spontaneous breathing

- The massively obese
- Those with manifest or suspected sleep apnea
- The very young and the very old
- Those with preexisting pulmonary disease
- Those with preexisting heart disease such as congestive heart failure, particularly those that are orthopneic

Clinically, respiration is monitored by auscultating breathing sounds and visually observing chest and abdominal excursion. These methods are imprecise and require supplementation with technologies that monitor oxygenation and ventilation of the patient.

Hemoglobin Oxygen Saturation

Hemoglobin oxygen saturation (SpO_2) is monitored by the use of pulse oximetry; it is obligatory for every sedated patient and in unsedated patients during invasive or interventional procedures. Transmission oximetry is based on differences in the optical transmission spectrum of oxygenated and deoxygenated hemoglobin. Misleading values may be obtained in the presence of abnormal hemoglobins (e.g., methemoglobinemia, as seen with topical benzocaine use, or carboxyhemoglobinemia (Murphy and Thompson 2002)). Further limitations to the value of pulse oximetry exist with severe vasoconstriction (e.g., shock, hypothermia), excessive movement, synthetic fingernails and nail polish, and severe anemia. Erroneously high readings (about 3–5 %) and a higher incidence of failure to detect signals have also been reported in dark-skinned races.

Be aware that owing to the sigmoid shape of the O_2 dissociation curve, large changes in the arterial partial oxygen pressure (PaO_2) can occur without much impact on SpO_2 until a saturation of 90 % (corresponding to a PaO_2 of 65 mmHg approximately) is reached, after which small decreases in PaO_2 result in large decreases in SpO_2. While it may take 5–8 min after apnea for SpO_2 to decrease to 95 %, rapid desaturation below 70 % might occur within less than 1 min; in small children, in less than 30 s! Note that once desaturation has occurred, SpO_2 might continue to fall for 10–15 s even with adequate oxygenation and ventilation, and it may take 1–2 min for SpO_2 to rise (Table 5.2) (Heier et al. 2001; Xue et al. 1996; Tanoubi 2006).

Desaturation is more likely to occur in patients with reduced functional residual capacity (the "oxygen reservoir" remaining in the lung at the end of a normal tidal expiration), such as with infants, obese patients, or pregnant women. The administration of oxygen during procedural sedation for invasive procedures is a double-edged sword in that oxygen saturations may remain normal, even in the face of apnea for some time, in effect masking the fact that ventilation has ceased. The addition of end-tidal carbon dioxide ($EtCO_2$) monitoring (see the next section) in these patients aids in the detection of apnea in cases where oxygen administration fails to reveal it.

End-Tidal Carbon Dioxide

Monitoring of $EtCO_2$ will detect clinically occult hypoventilation and is mandatory in all patients at risk for respiratory depression. This includes patients with preexisting pulmonary diseases, older patients, and patients needing deeper sedation to ensure compliance (confused patients, children) or pain control during invasive procedures.

Capnography is the graphic record of instantaneous CO_2 concentrations in the respired gases during a respiratory cycle. Capnometry is the measurement and display of CO_2 concentrations

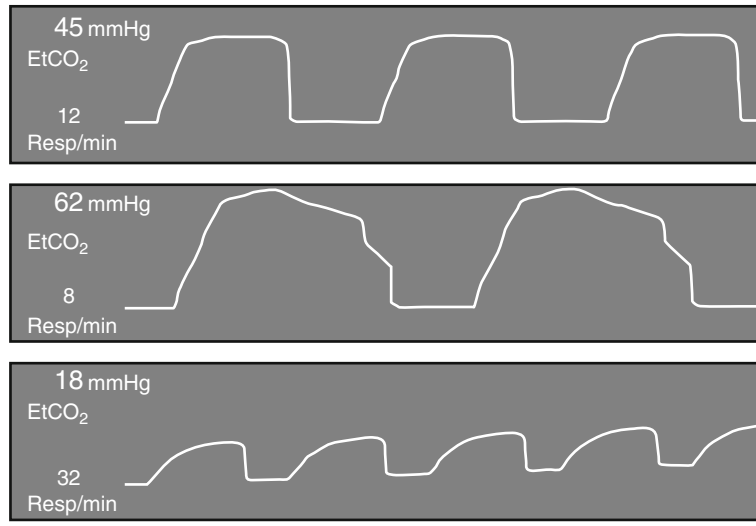

Fig. 5.1 Typical traces of exhaled CO_2: normal (*top*); opioid breathing (*middle*); shallow breathing in deep sedation with slowly increasing levels of CO_2 (*bottom*)

on a visual display, and the usual concentration displayed is the $EtCO_2$ concentration (Murphy and Thompson 2002).

In sedated, spontaneously breathing patients (as opposed to intubated patients), the sampling catheter is incorporated into a nasal prong oxygen delivery apparatus. These devices often also display the respiratory rate as well as the $EtCO_2$ concentration.

Hypoventilation (rising $EtCO_2$ concentration, slowing or cessation of respiratory rate) can be detected early by these devices, prompting immediate corrective interventions (e.g., stimulation of breathing, bag mask ventilation, or sedating agent reversal). Examples of different capnography traces are given in Fig. 5.1.

5.2.1.3 Equipment Issues in the MR Suite

Several manufacturers offer "MR-compatible" monitoring equipment. However, this sometimes refers only to the technical shielding of the monitor against harm from the magnetic field and does not necessarily include demagnetization. These pieces of equipment must not be brought into the room on a portable trolley but have to be installed firmly attached to the wall. Equipment not labeled as MR-compatible may not function properly (i.e., artifacts, misreadings, wrong values) if it is installed inside the MRI room.

When purchasing monitoring equipment, it is important to consider whether procedures will be performed under deep sedation or general anesthesia (see the next section for indications), in which case more portable and compatible (with the anesthesia machine) devices may be required.

5.2.2 Sedation

5.2.2.1 Definitions

The terminology of sedation has undergone considerable evolution over the years. Different medical and dental specialties have used imprecise terms to describe what is being done. It is essential that the lexicon be firmly established and agreed upon in order to ensure unambiguous communication across specialty lines and among practitioners of the same specialty. This is particularly important to investigators as they attempt to make "apples to apples" comparisons and to the readers of such studies for the same reason.

The consciousness continuum spans cognition from "awake and alert" to "death." The continuum is arbitrarily punctuated by points defined as closely as possible by the clinical appearance of the patient (American Society of Anesthesiologists 2009a). As it currently stands:

1. Minimal sedation (anxiolysis, sometimes referred to as "conscious sedation") is a drug-induced state during which patients respond normally to verbal commands. Although cognitive function and coordination may be impaired, ventilatory and cardiovascular functions are unaffected.

2. Moderate sedation/analgesia is a drug-induced depression of consciousness during which patients respond purposefully to verbal commands, either alone or accompanied by light tactile stimulation. No interventions are required to maintain a patent airway, and spontaneous ventilation is adequate. Cardiovascular function is usually maintained.
3. Deep sedation/analgesia is a drug-induced depression of consciousness during which patients cannot be easily aroused but respond purposefully following repeated or painful stimulation. The ability to independently maintain ventilatory function may be impaired. Patients may require assistance in maintaining a patent airway, and spontaneous ventilation may be inadequate. Cardiovascular function is usually maintained.
4. General anesthesia is a drug-induced loss of consciousness during which patients are not arousable, even by painful stimulation. The ability to independently maintain ventilatory function is often impaired. Patients often require assistance in maintaining a patent airway, and positive-pressure ventilation may be required because of depressed spontaneous ventilation or drug-induced depression of neuromuscular function. Cardiovascular function may be impaired. General anesthesia generally involves the presence of an anesthesiologist.

5.2.2.2 The Consciousness Continuum

It is generally agreed that an individual administering procedural analgesia and sedation ought to be capable of managing one level beyond the level desired. For example, if one is attempting to produce moderate sedation, one ought to be competent to manage the physiological concomitants of deep sedation. Having said that, it is well known that individuals have different, and at times unpredictable, responses to the medications employed to produce procedural sedation and analgesia.

5.2.2.3 Sedation, Analgesia, and Dissociation

Sedation and analgesia, for the most part, are separate issues (Murphy 2006a). Sedative hypnotics do not possess analgesic activity and in fact may be antianalgesic. The apparatus of pain transmission is not interrupted by even very deep levels of sedative hypnosis, leading to "wind-up" and postprocedural pain transmission.

Parenteral analgesic agents ordinarily employed in procedural sedation and analgesia possess different degrees of sedating side effects (e.g., morphine, sufentanil) that may be useful in managing individual patients. However, employing an opioid as the primary agent to achieve sedation is rather like attempting to insert a round peg in a square hole: it can be done, but it is a poor fit and often at the expense of ventilatory drive.

Ketamine is an agent that in a dose-dependent fashion produces sedation, amnesia, analgesia, and hypnosis, followed by dissociation. The dissociated state is unique in that patients do not respond to surgical stimuli (i.e., they appear as though they are under general anesthesia), but maintain and protect their airway, and maintain ventilation, hemodynamics, and muscle tone (catalepsy), provided the dose of ketamine is reasonable. In a quantitative sense, they are much like patients in the moderate sedation/analgesia category. So, although qualitatively and cognitively these patients fit the general anesthesia definition, from a "safety" perspective, they conform to the moderate sedation/analgesia definition. This state is called "dissociative sedation" (Murphy 2006a). A similar state is produced by dexmedetomidine, an alpha2-agonist. This agent possesses no analgesic properties. Patients are sedated, yet rousable, and do not demonstrate respiratory depression. Specific caution is warranted in hemodynamically unstable or hypovolemic patients, as dexmedetomidine regularly lowers heart rate and blood pressure, sometimes precipitously.

5.2.2.4 Clinical Approach to Sedation

The best advice is to preemptively determine how deeply sedated the patient will need to be to accomplish what is required in a manner acceptable to the patient. Further, consider the reserve of the patient and whether or not it is sufficient to withstand the effects of the medications that are contemplated, balanced against the stimulation to be inflicted by the procedure. Consider the

aspiration risk, particularly if a deeply sedated or general anesthetic state may supervene. In the final analysis, one must be confident that sedation and analgesia can be safely and effectively undertaken in a manner that is acceptable to the patient and that referral for general anesthesia is unnecessary.

In summary, select the desired state, select the most appropriate medications to get the patient to that end point, and administer them by the safest route. Take into account whether or not the procedure will inflict pain. The following are common end points:

- Minimal sedation (e.g., a mildly anxious patient for a CT scan): PO dosing is acceptable and usual.
- Moderate sedation for nonpainful procedures (e.g., substantially anxious patients for CT and MRI scanning): intravenous titration using "titratable drugs" (see later) is safest, with the probable exception of ketamine.
- Moderate sedation and analgesia for painful procedures: Select a "titratable" opioid (e.g., fentanyl) and titrate it intravenously to establish an acceptable level of analgesia, then utilize a "titratable" sedative hypnotic to titrate the patient to the moderate sedation end point. Avoiding the practice of alternating small doses of sedative hypnotic agents with small doses of opioids, in the author's experience, reduces the risk of sudden and unpredictable apnea. Alternatively, employ ketamine intravenously or by mouth. The use of single doses of any class of medication (sedative hypnotic, opioid, and ketamine) by any route (intravenous, by mouth, intramuscular, subcutaneously, per rectum) is inherently more dangerous (respiratory and cardiovascular depression) than a measured intravenous titration to a defined end point. Some agents have a broader safety profile (ketamine) than others (midazolam, propofol), and some are intermediate in risk (chloral hydrate, dexmedetomidine).

"Titratable" drugs are safer and preferable for intravenous titration to a moderate sedation end point. These drugs have a rapid onset, rapid offset, and a clearly identifiable effect on a dose-by-dose basis (e.g., fentanyl, propofol, ketamine/propofol combinations). They permit one to adjust both the dose and the dosage interval, in a safe and effective manner. Medications such as diazepam are difficult to titrate, and midazolam is of intermediate ease, possessing as much as a 2-min delay to peak effect profile.

Remember to evaluate the "physiologic reserve" of the patient (Murphy 2006b). For the most part, one will be titrating to a "CNS" end point, i.e., degree of sedation and adequacy of analgesia. However, some patients will be too sick or unstable (e.g., a hypotensive patient in ventricular tachycardia; decompensated chronic obstructive pulmonary disease, COPD, patient) to use the CNS end point, and titration will be against ventilatory (e.g., hypoxia, hypercarbia) or cardiovascular (e.g., hypotension) end points. In the very ill, one will use only an amnestic (e.g., a small dose of midazolam) to obtund memory as higher doses may lead to further decompensation.

Administration of the drugs and monitoring should not be undertaken by the same individual performing the procedure if sedation beyond anxiolysis is induced.

A sedated patient must not be left unattended, because the level of sedation can deepen suddenly owing to delayed drug effects or temporary cessation of stimuli!

Drugs commonly used for sedation are benzodiazepines, chloral hydrate, barbiturates, propofol, etomidate, and dexmedetomidine. For dosages and characteristics, refer to Table 5.3. Drugs commonly used for analgesia are opioids, ketamine, and nonsteroidal anti-inflammatory substances. For dosages and characteristics, refer to Table 5.4.

5.2.2.5 Side Effects of Sedation

A freely running and well-secured intravenous cannula is mandatory in all cases. Sedatives should be given intravenously, with some exceptions in children for rectal or nasal application. Oral medication should be given only for baseline analgesic or as premedication. Subcutaneous injections are obsolete, since unreliable reabsorption may lead to a delayed effect or even the maximum of significant drug levels after the procedure in unmonitored situations.

Table 5.3 Sedative drugs

	Dose range	Time to maximum effect	Duration of action	Side effects
Midazolam[a]	0.03 mg/kg i.v. repeat dose 1 mg i.v.	2 min	10–30 min	Paradoxical reaction, apnea
Diazepam (lipid)	5–10 mg i.v.	10 min	20–40 min	Paradoxical reaction, active metabolites >100 h!
Propofol[a]	0.5–1 mg/kg i.v. bolus	30–60 s	4–6 min	Apnea! Hypotension
Propofol[a]	2–4 mg/kg/h infusion	Maintenance	5–10 min after discontinuation	Apnea, hypotension
Etomidate	0.1–0.2 mg/kg i.v.	20–30 s	3–5 min	Apnea, adrenocortical depression, do not repeat
Dexmedetomidine	1 mcg/kg i.v. over 10 min followed by infusion 0.6–1 mcg/kg/h	10–15 min	15–30 min	Bradycardia, hypotension

[a]Only half the dose may be sufficient in patients older than 60 years

Table 5.4 Analgesic drugs

	Dose range	Time to maximum effect	Duration of action	Side effects
Morphine	2.5–10 mg i.v.	2–5 min	4–6 h	Apnea, nausea
Hydromorphone	10–20 μg/kg i.v.	5 min	3–4 h	Apnea, nausea
Piritramide	0.1–0.15 mg/kg i.v.	2–5 min	5–8 h	Apnea, nausea
Fentanyl	1–2 μg/kg i.v.	∪ 60 s	20–30 min	Apnea, nausea
Remifentanil	0.05–0.25 μg/kg/min infusion	2–4 min	2–3 min	Apnea, thoracic rigidity
Ketamine (racemic)[a]	0.5–1 mg/kg i.v.	∪ 60 s	10–20 min	Dysphoria, hallucination, hypersalivation, apnea

[a]For (*S*)-ketamine, use half the dose of racemic ketamine

Respiratory Depression

Opioids act at the central and peripheral opioid μ-receptors, which results in pain relief, nausea, and respiratory depression. It may take up to 15 min after intravenous administration for them to reach their maximum (analgesic and respiration depressant) effect. This may or may not be associated with a decreased level of consciousness. Mild levels of respiratory depression will result in a reduced respiratory rate with deep breaths. Typically, patients will respond when verbally addressed. With higher doses, the respiratory rate decreases further, ultimately leading to apnea. The dose response is very much dependent on age and preexisting medical conditions.

The same opioid dose might be insufficient for pain control in a 40-year-old healthy patient but lead to apnea in a 75-year-old patient.

Patients who are maintained on opioid medication for chronic pain may require higher doses for effective pain control during the procedural sedation as ought to be expected. The dose must be titrated to the desired level of pain control and respiratory function. Note that there are cases where pain control cannot be reached without significant respiratory depression, up to and including apnea. An anesthesiologist may be the best option for patients such as this.

Airway Obstruction

With deepening sedation, especially when opioids and sedative hypnotics are used together, the muscles of the tongue and the upper airway may relax, leading to upper-airway obstruction. This obstruction may be relieved by pulling the mandible forward (Esmarch's procedure) or by employing an oropharyngeal airway (see Sect. 5.3.6).

Confusion

Small doses of any sedative hypnotic agent such as the benzodiazepines, barbiturates, and alcohols (e.g., propofol) are known to produce a "paradoxical" reaction characterized by hyperactivity and agitation. The incidence has been reported to happen in up to 10 % of patients, mostly children and the elderly. A milder degree of confusion (disorientation, ataxia, restlessness) is not uncommon. Repetitive dosing of this class of medications may improve or worsen the agitation, in the latter case causing one to abort the procedure. The most appropriate course of action when confronted by this situation may be to switch agent class.

Hemodynamic Compromise

Hemodynamic compromise is rare in procedural sedation except perhaps in the most fragile of patients or those patients with incipient hemodynamic instability (e.g., those where sympathic tone is reduced or peripheral vasoplegia exists or those with decreased cardiac reserve).

5.3 Medical Management

5.3.1 Preparations

In adult patients, the presedation preparation is similar to that undertaken prior to any surgical procedure or administration of a general anesthetic. A detailed history evaluating the reserve of the vital organ systems (CNS, cardiovascular, and respiratory) as well as that of any chronic disease, of previous interventions, and current medication and allergies should be taken in advance. No food should be permitted up to 6 h before a planned procedure owing to the risk of aspiration of gastric contents, though clear fluids are permitted up to 2 h before.

5.3.1.1 Which Patients Should Be Managed by Anesthesia?

Depending on availability, the organizational structure of the hospital, and the emergency training level of the radiologist, the indication for an anesthesia consult could be liberal or restrictive. The degree of anxiety, the intensity of procedural pain to be endured, or the duration of a procedure that demands total immobility will define the need for and the depth of procedural sedation and analgesia. Patient tolerance for all of these factors must also be factored into the decision. Some patients with cardiac or pulmonary insufficiency may experience severe dyspnea when lying supine, in which case one ought to contemplate an anesthesia consult. Patients with significant sleep apnea should receive special attention during the procedure and should be admitted as an inpatient overnight to a monitored bed according to the hospital's policy.

5.3.1.2 Premedication

Anxiolytic medication may be administered orally to patients who need them. The following benzodiazepines have reasonably quick onset times and relatively short durations of action. Typical doses in adults are:

- Oxazepam, 10 mg p.o.
- Diazepam, 5 mg p.o.
- Lorazepam, 0.5–1 mg p.o., or sublingually if a more rapid onset is desired

Benzodiazepines should not be given as premedication in patients with significant respiratory impairment (e.g., COPD, pulmonary fibrosis, progressive muscular weakness) owing to their muscle-relaxing effects. An alternative may be clonidine (1.5–2 μg/kg body weight p.o.).

Patients at risk for aspiration (chronic reflux, hiatal hernia, gastroparesis, obesity) should additionally receive 150–300 mg ranitidine or a proton pump inhibitor.

Medications the patient takes chronically should generally be continued as usual, with the exception of oral antidiabetics, insulin, and angiotensin-converting enzyme inhibitors/AT-2 blockers. Patients with insulin-dependent diabetes should have an endocrine or anesthesia consult to set up a specific insulin regimen. Any rescue medication carried by the patient (e.g., nitro spray, bronchodilating puffers) should remain immediately available during the patient's entire stay.

5.3.2 Conduct of Sedation

5.3.2.1 Administrative Matters

It is highly advisable to reach agreement with the institution's anesthesia department on which cases/procedures ought to require anesthesia consult. Standard operating procedures should be crafted in cooperation with the department of anesthesia and rendered to written form, including:

- Preparative issues (e.g., patient selection criteria, *nil per os* status, and presedation evaluation parameters)
- Resuscitation equipment to be immediately available
- Which physicians are credentialed to perform sedation and how that credentialing is to occur (Murphy 2006a)
  - The numbers, roles, and responsibilities of ancillary personnel to be present during the procedure
  - Medications and dosages to be employed
  - Monitoring to be employed
  - Discharge criteria
  - Incident recognition and reporting
  - Quality assurance program

5.3.2.2 Setup of Sedation

Every patient should have an intravenous infusion established with crystalloid solution. Monitoring leads and oxygen delivery tubing should be secured to the table outside the scanner and tested for adequacy in the final scanning position.

5.3.2.3 Sedation

The choice of drug depends on availability and the preference and experience of the sedating physician.

Of note, some drugs may take some time following intravenous administration to reach their peak effect, rendering them difficult to use in situations where titration to a physiological or psychological end point is desirable. Premature administration of subsequent doses of medication before the peak effect of the initial dose has had its effect runs the risk of "stacking doses" and a potentially dangerous accumulation of drug!

A short-acting benzodiazepine (e.g., midazolam) may be administered at the start of the procedure to relieve procedure-related anxiety. For deeper sedation or for anticipated painful interventions, such medications may be combined with a medium-length-acting opioid (morphine, hydromorphone, piritramide). However, it must be emphasized that these classes of medications are synergistic in effect and may produce hypoventilation and apnea. Vigilance and monitoring are essential. Fentanyl is a short-acting opioid that may be used in small doses (1 μg/kg i.v.) before the actual puncture or in lieu of longer-acting medications such as morphine for shorter procedures (up to 30 min). The final dose of fentanyl should be titrated to the effect, remembering that the context-sensitive half-time lengthens with repeat doses (danger of accumulation).

Repeat doses of midazolam are seldom necessary in procedures shorter than 30 min. If more sedation is needed during the procedure, small repeat doses of propofol (0.1–0.2 mg/kg i.v.) can be given alternatively without risk of accumulation but with the risk of transient apnea. Each dose will calm the patient for approximately 3–10 min and should be administered under close respiration monitoring only. For a standard sedation regimen, see Fig. 5.2.

Supplemental Oxygen

Oxygen should always be administered during sedation to prevent alveolar hypercarbia in occult hypoventilation. Be aware that even with maximum flow, no fraction of inspired oxygen concentration higher than 60 % can be achieved using nasal prongs. Patients requiring higher fractions of inspired oxygen should be managed by anesthesia consult.

New Concepts

Special solutions are possible in collaboration with anesthesia and acute pain services. For example, a patient-controlled analgesia can be used for focused interventions (embolization, radiofrequency ablation) at distal sites without severe pain stimulus, e.g., bone or uterus.

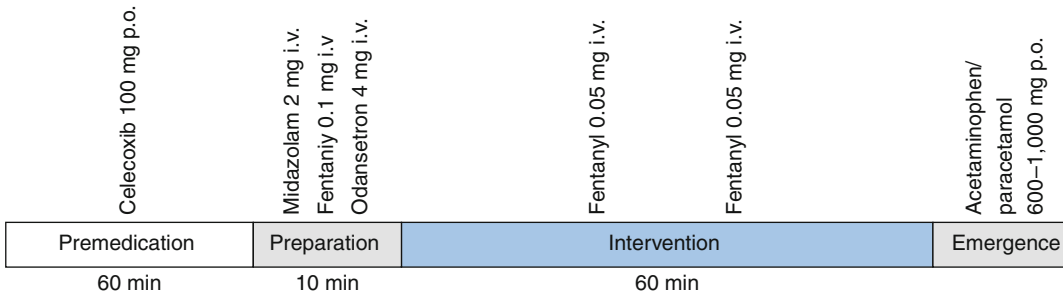

Fig. 5.2 Standard sedation regimen. For a 40-year-old, 75-kg adult without significant comorbidities, the regimen represents an example of how sedation might occur for a radiofrequency ablation of a tibial tumor. It is contemplated that local anesthetic agents are infiltrated for needle punctures. One ought to administer lower doses in older patients and young children, at least initially until a dose–response characteristic is identified (e.g., how much sedation did the initial dose of midazolam deliver, and how long did it take to produce a peak effect following intravenous administration). For sedation of children, refer to the text

5.3.3 Adjunctive Treatment

Ordinarily, less medication is required if the patient is reassured and informed of what to expect. Continuing reassuring verbal contact is crucial, particularly in children, the elderly, and those who are mentally challenged.

Preemptive analgesia may be of benefit when administered before a painful intervention to attenuate the perception of pain. This is generally felt to be more effective than a reactive strategy. Agents such as ibuprofen (400–800 mg p.o.), naproxen (500 mg p.o.), or COX-II inhibitors (celecoxib 100–200 mg p.o., etoricoxib 60–90 mg p.o.) should be considered, recognizing their risk profiles (platelet function, nephrotoxicity).

In the event that significant hypertension related to sympathetic activation due to stress or insufficient pain control occurs, adjunctive treatment is best with small doses of β-blockers (e.g., 5–20 mg labetalol intravenously titrated, 1–5 mg metoprolol intravenously titrated).

In very anxious patients or in patients with a history of nausea after sedation/anesthesia, a prophylactic dose of antiemetics is indicated.

5.3.4 Postsedation Care

Standards have been set by the American Society of Anesthesiologists (American Society of Anesthesiologists 2009b) for postanesthesia care, and these should be applied accordingly. These mandate inter alia that:

- All patients who have received […] monitored anesthesia care shall receive appropriate postanesthesia management.
- The patient's condition shall be evaluated continually […] postsedation.
- A physician is responsible for the discharge of the patient.

Monitoring of blood pressure, heart rate, oxygen saturation, and CO_2 must be continued until the effects of sedation have dissipated.

A health-care professional must be in continuous attendance to respond to alarms, assist the patient, and call for medical assistance if required. The patient can be transferred to an unmonitored but supervised area if:

- Hemodynamics and respiration are stable at preprocedural levels.
- The patient is awake and orientated.
- There is no acute pain.

Postprocedural pain management must take into account the fact that sedative and opioid medications employed during the sedation will be present at some level for days after discharge. The doses of oral and parenteral agents should be adjusted accordingly. All patients in the recovery phase should be monitored for at least 30 min following a dose of opioid medication. After the procedure, acetaminophen/paracetamol

(500–1,000 mg i.v./p.o.), ketorolac (30 mg i.v.), parecoxib (40 mg i.v.), or metamizole sodium (1,000 mg slowly i.v. or p.o.) are usually effective to provide sufficient analgesia. For patients suffering from chronic pain, the hospital's chronic pain service should be consulted prior to the procedure. Additional analgesic medication should be given if pain cannot be controlled by nonopioid substances. Medium-length-acting opioids are preferred (repeat doses of piritramide 1.5–3 mg i.v., hydromorphone 0.2–0.4 mg i.v., or morphine 0.5–1 mg i.v.). If pain cannot be controlled with usual doses, other reasons have to be excluded, e.g., liver capsule hematoma after radiofrequency ablation of liver tumors.

5.3.4.1 Respiratory and Cardiovascular Issues

Postprocedural bronchospasm in known asthmatics or COPD patients should be managed with head elevation, supplemental oxygen, and effective pain control. Bronchodilators such as salbutamol (two puffs, repeated every 2 min until relief is obtained) are indicated as are intravenously administered prednisolone (250 mg) or methylprednisolone (20 mg) for resistant or severe cases.

In the event that these symptoms do not improve with treatment, one ought to consider other disorders, such as:

- Congestive heart failure, pulmonary edema, or hypervolemia
- Pulmonary embolism
- Upper-airway obstruction, aspiration, atelectasis, or pneumothorax

The most frequent causes of postprocedural hypertension are unrecognized pain and inadvertent withholding of chronic antihypertensive medication. After effective treatment of pain, which is often denied by the patient, the patient's usual medication should be given by mouth. If viewed to be dangerous, hypertension may be managed (i.e., to avoid postinterventional bleeding) with the following medication:

- Nitro spray: two puffs (0.8 mg) sublingually, repeat after 2 min if there is no effect
- Ca channel blockers: nifedipine or nitrendipine (10 mg) sublingually
- Vasodilators: urapidil (10–50 mg) intravenously titrated
- β-Blockers: labetalol (5–20 mg) intravenously titrated or metoprolol (1–5 mg) intravenously titrated

The most frequent cause of postprocedural hypotension is unrecognized hypovolemia due to insufficient fluid resuscitation or occult blood loss. If after a fluid bolus of 10 ml/kg (in adults) hypotension persists, occult bleeding from the intervention site has to be ruled out by ultrasound or repeat CT scan.

5.3.4.2 Nausea and Vomiting

Nausea can result from opioid medication, accumulation of gastric secretions or air in the stomach, vestibular irritation, or visceral nerve irritation, e.g., peritoneal or liver capsule tension. The treatments of choice are intravenous serotonin antagonists (owing to their minor sedating side effects) such as:

- Tropisetron, 2.5–5 mg i.v.
- Ondansetron, 4–8 mg i.v., repeated after 12 h if needed

In children, dimenhydrinate is a good alternative, because it has mild sedating and antianxiety effects.

5.3.4.3 Patient Discharge

The patient can be discharged if:

- Consciousness, hemodynamics, and respiration remain stable at preprocedural levels for 30 min.
- The patient had tolerated some clear fluids and a light snack.
- The patient can sit unaided.
- The patient had voided.
- The patient's pain is controlled.

Under no circumstances should the patient be permitted to operate a motor vehicle for 24 h after a procedure involving sedation. Cases of fatal car accidents after interventions employing only light sedation have been reported, leading to the conviction of the treating physician. Patients must be discharged with a responsible caretaker and never alone.

5.3.5 Special Considerations in Children

Children under the age of 3 years (under 6 years if preterm born) and/or examinations lasting more than 120 min should be managed by specially qualified staff or with anesthesia staff in attendance only. Several aspects have to be considered in general regarding the sedation of pediatric patients (Kretz 2006):

- There is no "safe" sedation recipe that obviates the need for close monitoring of the infant patient!
- Smaller children require deeper levels of sedation than adults if they are required to lie still completely.
- Children tolerate pain less well than adults.
- Children are physiologically more susceptible to laryngospasm than adults.
- Some of the medications used are not approved for use in children and have to be considered as off-label use.
- Venous access is more difficult to establish than in adults, leading to the single-dose by mouth, per rectum, or intramuscular strategies. These strategies are inherently more hazardous with respect to respiratory and cardiovascular compromise than intravenous titration methods.

The following dosing schemes (see also Table 5.5) should be considered as examples only and should not be taken as recommendations. The final plan should be developed depending on the availability of drugs, personal experience, and hospital policies.

5.3.5.1 Preparations

Special attention should be given to the preparation of children. A quiet and secluded environment will remove anxiety from the children and their parents. Infections of the upper respiratory tract are not uncommon and should be carefully evaluated.

New onset of cough, pulmonary wheeze or bronchospasm, thick nasal secretions, or fever should lead to postponement of the procedure, since they present an increased risk of respiratory complications. Minor nasal secretions or congestion may be treated with nasal spray (oxymetazoline, xylometazoline) before starting the sedation to improve nasal breathing.

Many congenital and acquired conditions may complicate procedural sedation in children, because they affect the reserve of vital organ systems (cardiovascular, respiratory, and neurological). Practitioners are urged to consult anesthesia or pediatrics personnel in such cases.

Intravenous access is not considered to be mandatory in otherwise healthy children for non-interventional sedation. Antimuscarinic agents (glycopyrrolate or atropine, 0.01 mg/kg) designed to reduce oral secretions may be administered at the discretion of the treating physician.

5.3.5.2 Implementation of Sedation

The following regimens have been demonstrated to be effective in pediatric patients though practitioners are urged to exercise extreme caution in the patient population mentioned in the previous section. The practice of administering large doses of sedative hypnotics prior to coming to the diagnostic facility is to be condemned. Immediate access to trained personnel, monitoring apparatus, and resuscitation equipment is crucial.

Deep sedation can be produced with:

- Chloral hydrate, 50–75 mg/kg orally or rectally (20 min prior to the procedure)
- Midazolam, 0.5 mg/kg orally (maximum 7–8 mg) (20–30 min before) or 0.1 mg/kg nasally (10 min prior to the procedure)
- Ketamine, 5–10 mg/kg orally or rectally (20–30 min prior to the procedure)

Once the child has been sedated and accepts the monitoring modalities, they must be applied immediately, and blood pressure, heart rate, SpO_2, and CO_2 should be monitored. For painful procedures, acetaminophen/paracetamol or ketorolac may be administered in advance.

Table 5.4 gives an overview of commonly used medications and dosing.

Opioids should be administered with great caution to avoid respiratory depression. Repeat doses of sedation should involve short-acting substances only. Ketamine has the advantage of inducing deep sedation/analgesia without causing respiratory depression but is known to cause

Table 5.5 Pediatric medication

	Application	Initial dose	Repeat dose
Atropine	i.v.	10 μg/kg	NA
Midazolam	i.v.	30–50 μg/kg	10 μg/kg (maximum 10 mg)
	p.o.	0.5 mg/kg (maximum 8 mg)	NA
Atropine	i.v.	10 μg/kg	N/A
Propofol	i.v.	1 mg/kg	0.5–1 mg/kg
Ketamine (racemic)[a]	i.v.	1–2 mg/kg	0.5 mg/kg
	p.o., p.r.	2 mg/kg	NA
Chloral hydrate	p.o., p.r.	25–100 mg/kg	NA variable absorption
Pentobarbital	p.o., p.r.	2–6 mg/kg	NA
Acetaminophen/paracetamol	p.o., p.r.	30 mg/kg (maximum 1 g)	20 mg/kg 6 h
Ketorolac	i.v.	0.5 mg/kg (maximum 30 mg)	NA
Morphine	i.v.	50 μg/kg	NA
Fentanyl	i.v.	1.5 μg/kg	1.0 μg/kg
Piritramide	i.v.	0.05–0.1 mg/kg	0.05 mg/kg
Ondansetron	i.v.	0.1 mg/kg (maximum 4 mg)	0.1 mg/kg after 12 h
Tropisetron	i.v.	0.2 mg/kg (maximum 5 mg)	NA
Dimenhydrinate	i.v.	1.25 mg/kg (maximum 50 mg)	4 h

NA not applicable
[a]For (*S*)-ketamine, use half the dose

unpleasant hallucinations perhaps leading to fearful behavior and noncompliance in children subjected to repeated procedures. The addition of midazolam to ketamine to induce amnesia and prevent bad dreams has been suggested but has failed to prove its effectiveness in randomized studies.

The postprocedural care is as for the adult. Emergence reactions ranging from mild confusion to combative behavior and unremitting crying are seen not infrequently, especially after ketamine usage. Treatment options include small doses of dimenhydrinate, midazolam, or clonidine (1–2 μg/kg i.v.).

5.3.6 Emergency Care

During the procedure, multiple problems have to be anticipated, and one should be prepared to deal with them before patient harm supervenes. The most common life-threatening complications are hypoventilation/apnea and hypotension.

The recommendations given in the following sections cannot replace adequate emergency training but highlight common situations/treatments only. Reference to current specialty-specific guidelines is highly recommended.

5.3.6.1 Airway Obstruction and Respiratory Distress

The sedated patient is continuously at risk of losing control of the airway, resulting in upper-airway obstruction. Pharmacologic reversal agents such as naloxone (opioid antagonist) (0.2–0.4 mg i.v.) and flumazenil (benzodiazepine antagonist) (0.1–0.5 mg i.v.) may be effective in restoring spontaneous airway maintenance and ventilation. Otherwise, the practitioner is advised to call for help from those skilled in airway management and resuscitation and to proceed to manage the airway.

There are two maneuvers commonly used which have been shown in multiple studies to improve airway patency. Extension of the neck by head-tilt chin-lift is the primary maneuver used in any patient in whom cervical spine injury is not a concern. While the patient's forehead is pressed downward, the mentum is lifted with the fingertips of the other hand, which lifts the tongue from the posterior pharynx and opens the airway. The jaw-thrust also moves the tongue anteriorly

with the mandible, minimizing its obstructing potential. An even more effective jaw-thrust is achieved by forcibly and fully opening the mouth to "translate" the condyles of the mandible out of the temporomandibular joint, then pushing the mandible forward (Esmarch's maneuver) with both hands bilaterally (Fig. 5.3a).

To maintain the airway, oropharyngeal and nasopharyngeal (Fig. 5.3) airways will prevent the tongue from occluding the airway and provide an open conduit for air to pass. An oropharyngeal airway should be placed whenever bag mask ventilation is contemplated (i.e., gas exchange is not restored by airway opening maneuvers). Neither of these airway devices will protect the trachea from aspiration of secretions nor gastric contents.

In the event that the patient is apneic, endotracheal intubation should not be attempted by the inexperienced. Instead, securing appropriate ventilation and oxygenation utilizing bag mask ventilation is crucial. This rescue equipment must be immediately available in all sedating locations.

Once the airway has been opened, the resuscitation bag is connected to the mask and an optimal mask seal obtained. The standard adult resuscitation bag has a 1,500-ml capacity. This entire volume should not be delivered as it will lead to stomach insufflation. One ought to aim to deliver 500 ml/breath (one third of an adult bag) (Schneider and Murphy 2004). The goal is effective oxygenation and ventilation. To do so, one ought to deliver 10–12 breaths/min without exceeding the proximal and distal esophageal sphincter opening pressures of approximately 25 cm of water. High peak inspiratory pressures result from short inspiratory times, large tidal volumes, incomplete airway opening, increased airways resistance, and decreased compliance. To minimize the potential for gastric inflation, each breath ought to be delivered limiting the tidal volume to that which is sufficient to produce a visible chest rise. For the ventilation of children, pediatric resuscitation bags with smaller volumes should be used, delivering 14–20 breaths/min of 100–300 ml to produce a visible chest rise.

If ventilation cannot be facilitated via a face mask (difficult anatomy, sealing problems, i.e., in patients with a beard), a laryngeal mask is a viable alternative (Fig. 5.3d). With the patient's head tilted, the laryngeal mask is inserted, holding it like a pen, into the supraglottic space until it moves down no further and is inflated with 10–20 ml of air. Physicians planning to use this device in emergency situations should become familiar with the type and use of it beforehand.

Airway Management

1. Jaw-thrust (Esmarch's maneuver)
2. Oropharyngeal (Guedel's tube) and nasopharyngeal airway (Wendel's tube)
3. Facemask, sealed over mouth and nose utilizing the "C-grip" or two hands
4. Laryngeal mask airway (LMA)

5.3.6.2 Severe Hemodynamic Compromise

Hypotension is ordinarily easier to manage than hypoventilation. Intravenous bolus doses of balanced salt solutions (e.g., 10–20 ml/kg of Ringer's lactate or normal saline) or 5–10 ml/kg of synthetic colloidal solutions (e.g., pentastarch, tetrastarch) are the initial step in resuscitation. Small repeated doses of adrenergic agents such as ephedrine (5–10 mg i.v.), phenylephrine (0.1 mg i.v.), or cafedrine/theodrenaline (0.1 ml) are effective. In the event that higher doses are required, this should lead one to suspect other causes of hypotension, such as occult bleeding or cardiac disorders.

5.3.6.3 Anaphylaxis

Anaphylactic reactions to sedative hypnotic agents and opioids are decidedly uncommon. However, reactions might also be caused by local anesthetics or radiographic contrast media. Anaphylactoid reactions (dose-dependent drug-induced release of histamine from immune cells) will lead to urticaria, flushing, pruritis, and, rarely, hypotension. Anaphylaxis is defined as an immediate systemic reaction caused by immunoglobulin E-mediated rapid release of potent mediators from tissue mast cells and peripheral basophils.

Immediate management includes:

- Discontinuation of antigens
- Basic life support (ABC's)
- Start of volume expansion
- Epinephrine

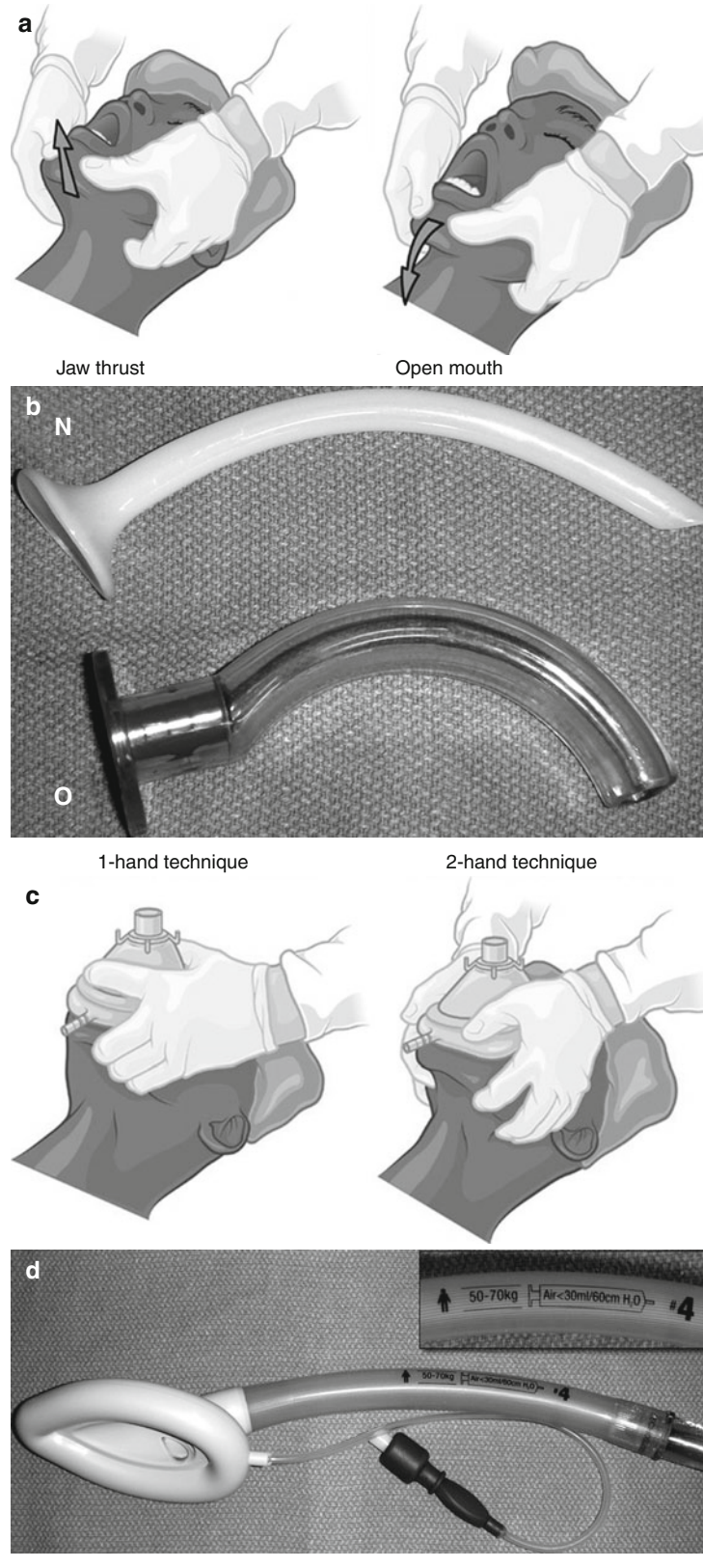

Fig. 5.3 Airway management: (**a**) jaw-thrust (Esmarch's maneuver); (**b**) oropharyngeal airway (Guedel's tube) and nasopharyngeal airway (Wendel's tube); (**c**) face mask, sealed over the mouth and nose utilizing the "C-grip" or two hands; (**d**) laryngeal mask airway

Epinephrine ought to be administered if the patient exhibits:

- Bronchospasm
- Significant gastrointestinal symptoms
- Laryngeal edema
- Hypotension
- Any rapidly progressive reaction

Administration should start at 5–10 μg/min intravenous infusion. Importantly, it must be appreciated that there is no benefit from the subcutaneous route of administration. Antihistamines should also be administered: diphenhydramine (0.5–1.0 mg/kg i.v.) or clemastine (2–4 mg i.v.) (H1-receptor blocker) and ranitidine (50 mg i.v.) (H2-receptor blocker). Bronchodilators such as 2.5 mg salbutamol in 5 ml of saline as an aerosol are employed continuously for bronchospasm. Corticosteroids (250–500 mg prednisolone, 0.25–1 g hydrocortisone, or 1 g methylprednisolone intravenously) are also indicated. Any patient suffering from an anaphylactic reaction should be admitted as an inpatient and monitored for 24 h.

Appraisal

Sedation can be performed by non-anesthesiologists safely if the administrative, technical, and medication administration requirements have been fulfilled, and the physician performing the sedation has adequate training in the application of sedation and emergency procedures. Patients and procedures eligible for non-anesthesiologist sedation should be determined in cooperation with the institution's anesthesia department, and standard operating procedures should be formulated for emergencies.

All patients undergoing more than minimal sedation (anxiolysis only) need to be monitored for respiratory and hemodynamic deterioration with continuous pulse oximetry, capnography, ECG, and blood pressure measurements.

After determining the desired level of sedation, one should asses each patient individually for risks considering there is no standard recipe suitable for all patients. Depending on the procedure (diagnostic vs. interventional) and the patient factors (e.g., age, comorbidities, level of anxiety), the sedation should be titrated with intravenous boluses of short-acting to medium-length-acting sedatives and analgesics. Small doses of midazolam for sedation and fentanyl for analgesia have been used frequently, with ketamine as an alternative.

Adjunctive treatment includes appropriate premedication, the management of hemodynamics, and postsedation nausea and pain. Special attention has to be given to airway patency and ventilation, particularly in the very young or the very old, particularly if the procedure requires deep sedation.

Sedating children mandates special caution and knowledge of pediatric physiology and pharmacology. The dosing of medication is usually done per kilogram of body weight. Chloral hydrate is an alternative agent for non-intravenous sedation.

All patients must be adequately monitored after sedation by a trained health-care professional with direct access to emergency care and medical assistance until the patient has returned to preprocedural levels of performance.

Key Points

- Respiratory and hemodynamic monitoring is necessary in every sedated patient.
- Indications for general anesthesia should be established in consultation with the department of anesthesia. For long-duration examinations, sedation is ordinarily sufficient; in painful interventions, an analgesic should be added.
- Special care has to be taken in sedating children and the elderly.
- Staff performing sedation should be familiar with emergency procedures.

References

American Society of Anesthesiologists (2009a) Continuum of depth of sedation definition of general anesthesia and levels of sedation/analgesia. http://www.asahq.org/publicationsAndServices/sgstoc.htm. Accessed 01 Dec 2012

American Society of Anesthesiologists (2009b) Standards for postanesthesia care. http://www.asahq.org/publicationsAndServices/sgstoc.htm. Accessed 01 Dec 2012

Heier T, Feiner JR, Lin J et al (2001) Hemoglobin desaturation after succinylcholine-induced apnea: a study of the recovery of spontaneous ventilation in healthy volunteers. Anesthesiology 94:754–759

Kretz FJ (2006) Anaesthesie und Intensivmedizin bei Kindern, 2nd edn. Thieme, Stuttgart

Murphy MF (2006a) Pain management and procedural sedation: definitions and clinical applications. In: Mace SE, Ducharme J, Murphy MF (eds) Pain management and sedation: emergency department management. McGraw Hill, New York, pp 7–14

Murphy MF (2006b) Preprocedural patient assessment and intraprocedural monitoring. In: Mace SE, Ducharme J, Murphy MF (eds) Pain management and sedation: emergency department management. McGraw Hill, New York, pp 47–53

Murphy MF, Thompson J (2002) Monitoring the emergency patient. In: Marx JA (ed) Rosen's emergency medicine. Mosby, Philadelphia, pp 28–32

Schneider RE, Murphy MF (2004) Bag mask ventilation and endotracheal intubation. In: Walls RM, Murphy MF, Luten RC (eds) Manual of emergency airway management, 2nd edn. Lippincott Williams & Wilkins, Philadelphia, pp 43–69

Tanoubi I (2006) Oxygenation before anesthesia (preoxygenation) in adults. Anesthesiol Rounds 5:1–6

Xue FS, Luo LK, Tong SY et al (1996) Study of the safe threshold of apneic period in children during anesthesia induction. J Clin Anesth 8:568–574

Ways to the Target

6

Andreas Lubienski

Contents

A. Lubienski
Radiology Health Care Centre Minden,
Ringstraße 44, Minden D-32427, Germany
e-mail: lubienski@rp-minden.de

6.1 Introduction

Cross-sectional imaging modalities such as ultrasound, computed tomography (CT), and magnetic resonance (MR) imaging are well-accepted guiding tools for interventional biopsies and therapies (Gupta and Madoff 2007). Especially CT combined with fluoroscopy is able to offer fast and safe ways to nearly any target in the human body, incorporating the major advantage of panoramic views compared with ultrasound, and therefore often represents the guiding modality of choice (Rogalla and Juran 2004). Even targets in bones and air-containing structures (e.g., lungs) can be addressed very easily and successfully with CT guidance. In contrast, MR imaging seems to be more complex and time-consuming and therefore is usually reserved for interventional procedures in very tricky areas with the necessity of high soft-tissue contrast and in situations where CT is contraindicated (Gupta 2004). The accuracy of the puncture and the complication rates depend on the target size and site, traversing and surrounding anatomical structures, the number of biopsies, the material and puncture technique selected, and patient's cooperation (Gupta and Madoff 2007).

A.H. Mahnken et al. (eds.), *CT- and MR-Guided Interventions in Radiology*,
DOI 10.1007/978-3-642-33581-5_6,

6.2 Materials and Techniques

6.2.1 Patient's Position

At the time of the assignment of the procedure, potential puncture routes have to be clarified on the basis of the preinterventional imaging in order to assess the risks and complexity of the procedure.

Depending on the access route, the position of the patient on the examination table is chosen (prone, supine, or angulated position). For all interventions, independent of their duration or complexity, it is crucial to select a stable and comfortable position of the patient. Upholstery should be considered when necessary. Especially when CT-guided punctures of the trunk are planned, one has to take into account streak artifacts caused by the arms and therefore has to adjust the position of the arms. In order to have enough room within the gantry, the table should be the lowest position possible (Gupta et al. 2004).

6.2.2 Planning of the Access Route

Depending on the diagnostics and/or expected complexity or level of risk, additional imaging is required. Usually a nonenhanced CT or MR scan is sufficient, but in special areas, such as head and neck or parenchymal organs contrast-enhanced imaging seems to be mandatory to delineate structures at risk and/or the target itself.

To get representative biopsies, one has to consider that in many cases soft-tissue tumors have necrotic tissue in the central parts, whereas viable tumor cells are located at the periphery. Owing to inflammatory changes in the vicinity of the targeted lesion, especially in lung tumors adjacent to the pleura, the needle tip should be placed preferably in the tumor part next to the hilum.

The way to the target should be as safe as possible. Traversing of sensible anatomical structures such as nerves, vessels, and/or pleural space and adjacent organs has to be avoided whenever possible. Adjusting the patient's position and additional respiratory maneuvers may be helpful to get an optimal and safe way to the target. Transparenchymal access (e.g., small bowel, stomach, liver) is possible (Figs. 6.1 and 6.2) (Iguchi et al. 2007).

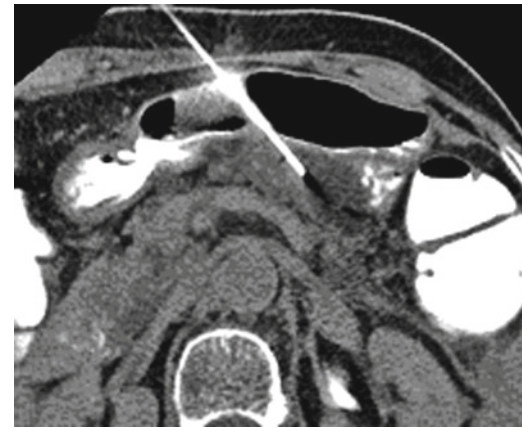

Fig. 6.1 Anterior transgastric biopsy approach to an unclear focal mass located in the pancreatic body. Biopsy revealed macro-cystic pancreatic adenoma (Courtesy of Andreas H. Mahnken, Philipps University, Marburg)

Fig. 6.2 Anterior transhepatic approach to an unclear focal mass located in the pancreatic body. Biopsy revealed a pancreatic carcinoma

Usually the easiest way to the target is chosen. Thus, complexity is increased when vertical and horizontal pathways are changed into angulated or doubled-angulated access routes. Planning of such pathways is realized with multiplanar imaging and should be restricted to specially trained physicians (Gupta et al. 2005; Ohno et al. 2004).

6.2.3 Local Anesthesia

Typically 5–20 ml of a local anesthetic drug (e.g., 1 % lidocaine) is administered subcutaneously at the puncture site (Maturen et al. 2007). On the

basis of reference scans, the infiltration depth of the local anesthesia, the minimal distance between the puncture site and the target, and the maximal depth of the puncture needle before traversing a critical anatomical structure are electronically assessed.

Sufficient anesthesia of pleura, peritoneum, and periosteum is mandatory. When lung punctures are planned, anesthesia should involve but not lacerate the pleura. Repositioning of the needle before administering the anesthetic drug is required when nerves have been punctured as indicated by a sharp and sudden pain.

6.2.4 Puncture Technique

Via a short intracutaneous incision, the needle is advanced along the previously planned route. Depending on traversing anatomical structures, the needle is advanced either directly into the target lesion without any interruption or step by step with control scans in-between.

Anatomical landmarks may help one navigate into the target. The majority of imaging-guided punctures are, of course, straightforward and can be easily performed using either a single needle pass or coaxial systems. Whenever possible the needle is placed as exactly as possible within the imaging plane. The latter allows one to visualize the entire needle shaft and ideally the target with a single image. This ensures the needle tip is in the correct position prior to biopsy or treatment. In CT, the exact needle tip position may be confirmed by looking for the needle artifact caused by beam hardening. In MR, the signal loss and susceptibility artifacts normally permit passive tracking of the puncture device. The majority of axial needle placements may be performed with the naked eye, particularly, if the patient and table are gently brought out of the gantry to remove problems of parallax which may otherwise occur if the operator works in a position oblique to the needle. Alternatively, the issue of parallax may be addressed using the laser alignment of the scanner, shining the laser through both skin puncture site, and needle hub to ensure correct axial needle alignment. In MR, the use of an open MR system provides almost unimpeded access to the patient, and multiplanar image acquisition eases the problem of the needle alignment.

There are different techniques to address the target. In CT, the so-called tilted-gantry technique uses a gantry angulation, which is set according to the planned angled approach. In reality, angles approaching 20 or 25° lead to problems of access to the patient and of effectively decreasing the gantry/patient distance, as well as being disconcerting for the patient. Following this, the CT laser alignment is then set such that the laser passes through the needle onto the skin surface, and if both the puncture site and the needle hub are confirmed to be in the line of the laser, then the needle placement is automatically aligned at the correct angle. By doing this, each scan performed during needle advancement will be in the plane of the entire needle.

In CT, as well as in MR-guided interventions, there are several tricks to avoid loops of overlying bowel:

1. The first and easiest approach to solve this problem is the so-called bowel displacement technique. The first step is to compress the abdomen to displace bowel loops from the potential needle track. This is done by placing a sterile drape or sheet in a ring- or nest-shaped configuration around the site for skin puncture. This is then taped and strapped firmly to the flanks and the examination table to push into the abdomen and displace bowel loops in a manner akin to the compression cone for small-bowel studies. This allows a needle to be placed in the center of the CT or MR gantry, thus maintaining the sterile field.
2. A second method that can be used in exceptional circumstances to displace the bowel is the needle angulation technique where an initial needle is placed adjacent to the bowel loop. The needle is passed beyond the bowel loop and levered across the skin surface to displace the bowel and free up a potential passage for the second biopsy needle to be placed.
3. A third way to displace a bowel loop is to create an artificial pneumoperitoneum via an initially placed first needle in order to free up a potential passage for the second needle.

Alternatively creation of an artificial ascites by injecting a fluid (e.g. 0.9 % saline) may be used to achieve a free passage to the target.

4. Finally, in cases of extreme obesity a coaxial needle technique can be used. In such cases it is important to begin the procedure with the table set as low as possible to maximize the space available between the patient's skin surface and the inner aspect of the CT or MR gantry. The latter helps one avoid being forced to pass the needle further than one initially feels comfortable to do, remember to use a coaxial system with a short outer needle. Alternatively, of course, a short biopsy needle may be used for this purpose. When imaging confirms the short needle is in a safe position, the second needle may be placed directly adjacent and parallel to it. This allows the needle to be placed sufficiently far enough to allow the patient to be scanned with the needle in situ. The short needle may then be removed and discarded, and the procedure continues as normal. After the entire procedure, a control scan of the target, including all adjacent structures, should follow in order to rule out immediate complications.

6.3 Special Techniques

6.3.1 Lung

Depending on the site of the target, one should consider the transbronchial approach (centrally located lesion) or the transpulmonal approach (peripherally located lesion) (Fig. 6.3). To prepare for diagnostic lung surgery, a percutaneously placed marking wire (Fig. 6.4) can be released. A sufficient pulmonary reserve (O_2 pressure greater than 60 mmHg) is an important prerequisite for percutaneous lung punctures especially because of the high risk for pneumothoraces (case-dependent up to 60 %). Interestingly, instillation of 0.9 % NaCl solution into the puncture access during extraction of the needle seems to reduce the incidence of pneumothoraces (Billich et al. 2008). Whenever a pneumothorax occurs during a transthoracic biopsy procedure one should always try to complete the biopsy samples – depending on the patients condition – in order to provide technical success (Fig. 6.5). Severe

Fig. 6.3 Lateral intercostal approach to a lung cancer nodule located adjacent to the pleura with the patient being in the lateral decubitus position

Fig. 6.4 Lateral intercostal approach to a very small lung cancer nodule located near the hilum with consecutive placement of a marking wire prior to surgery

Fig. 6.5 Successful CT-guided biopsy of a small lung cancer nodule despite consecutive pneumothorax via lateral intercostal approach in lateral decubitus position

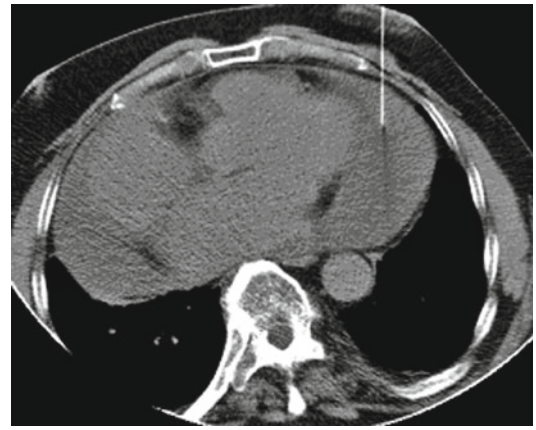

Fig. 6.6 Anterior intercostal approach to a pericardial fluid collection

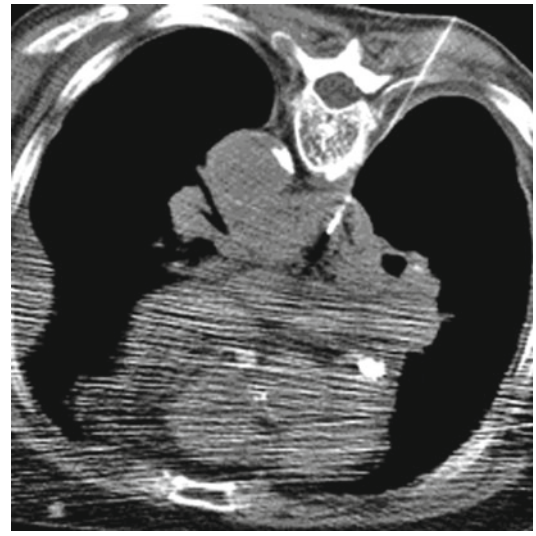

Fig. 6.7 Posterior paravertebral approach into the posterior compartment of the mediastinum in order to get tissue samples from an unclear paraesophageal mass. The needle is advanced close to the spine in order to avoid passage of the pleura and thereby reduce the risk of pneumothorax

lung emphysema and pulmonary hypertension are relative contraindications for the procedure. Perifocal hemorrhage and or hemorrhage along the needle path after the procedure can often be seen and are usually without any consequences. Hemoptysis is encountered in about 2–5 % of all cases. Air embolism is a very rare but sometimes fatal complication (Hiraki et al. 2007). Especially in small lesions, the needle tip should be advanced in the nodule in order to minimize the risk of secondary needle dislocation. The number of pleural passages needs to be kept as low as possible to reduce the risk of pneumothorax. Consequently, traversing two lobes on the way to the target should be avoided.

6.3.2 Mediastinum

Depending on the site of the target within the mediastinal compartment (anterior, middle, or posterior part) the access route – anterior (Fig. 6.6) or posterior (Fig. 6.7) – is chosen. Knowledge of the exact vascular routes is absolutely mandatory to prevent potentially fatal complications. Multiplanar imaging prior to the procedure may help one assess the exact mediastinal anatomy (Gupta et al. 2005). A direct mediastinal approach involves placement of the needle through an extrapleural space medial to the lung to avoid transgression of the lung and pleura. The needle can be advanced through (Gupta et al. 2002a) or lateral to the sternum (Fig. 6.8), through the posterior paravertebral space (Fig. 6.7),

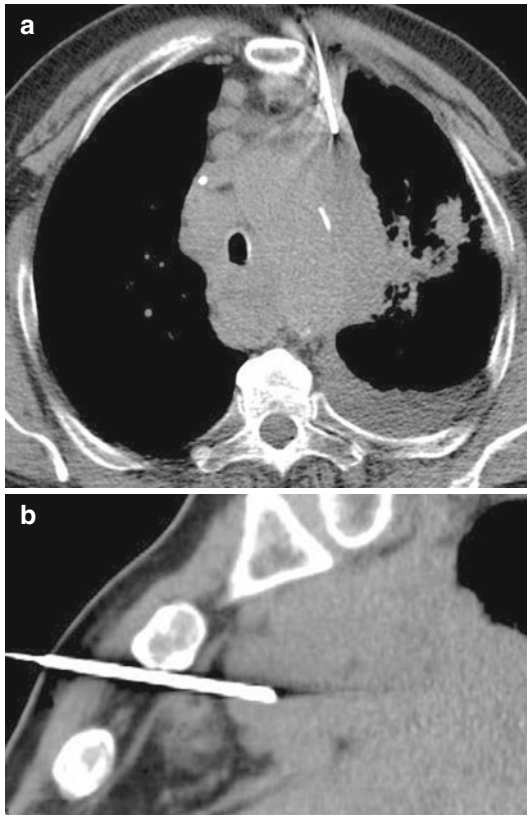

Fig. 6.8 Anterior parasternal approach to a mass located in the upper anterior mediastinal compartment. Biopsy revealed lymphoma. (**a**) The sagittal reformation shows the needle path to be outside any critical structures (**b**). Biopsy revealed metastatic tumor tissue from a neuroendocrine carcinoma of unknown origin

through the suprasternal notch, or through the subxiphoid space. To minimize the risk for a pneumothorax, the puncture should be performed in expiration in order to have a broader contact area at the anterior chest wall. To increase the space of the puncture channel injection of 10–50 ml, 0.9 % saline solution may be helpful. The latter widens the extrapleural space and creates space for the needle, permitting one to avoid passage of the pleura. Artificial pneumothorax is another safe method that provides access for CT-guided biopsy of mediastinal lesions without traversing aerated lung (Gupta et al. 2005). The transpulmonary approach to mediastinal biopsy allows access to targets in various anterior, middle, and posterior mediastinal locations. This approach is generally used for lesions that are not accessible with an extrapleural approach.

6.3.3 Liver

In general, there are two interventional ways to the liver, transjugularly and percutaneously. Like in other areas, the way to the target depends on its localization within the liver. Every intrahepatic target can be approached percutaneously in a safe way with image guidance; even targets located high in the liver dome do not need a transpleural approach (Figs. 6.9 and 6.10). In some situations, it is useful to navigate with the help of landmarks such as gallbladder, portal vein, etc. to reach the target. One should always have a transhepatic route long enough to realize a tamponade of a hemorrhage along the puncture channel by itself. Traversing the falciform ligament or Glisson's triad should always be avoided (Stattaus et al. 2007), as the passage of these structures is painful for the patient. If an intercostal approach is chosen, one should cross the rib at the top side to avoid damage to the intercostal nerve and vessels, which run underneath each rib.

6.3.4 Gallbladder and Spleen

Diagnostic or therapeutic interventional procedures for the gallbladder or the spleen are very rare. Whenever there is a process within the gallbladder exceeding the wall, the origin of the malignancy seems obvious, and a minimally invasive biopsy prior to surgery is not necessary. If there is an indication for gallbladder decompression by tube placement, a transhepatic pathway should be preferred.

Owing to the fact that intrasplenic lesions are often associated with malignant lymphoma, there are usually other anatomical sites where enlarged lymph nodes can be reached more easily and safely to assess the diagnosis by percutaneous biopsy. Despite a higher bleeding risk, biopsies or interventional treatments of the spleen can be performed in a safe way (Fig. 6.11). Sometimes postinterventional embolization of the puncture route is required (Lieberman et al. 2007). In most cases, targets within the spleen can be approached via a lateral intercostal access route (Kang et al. 2007).

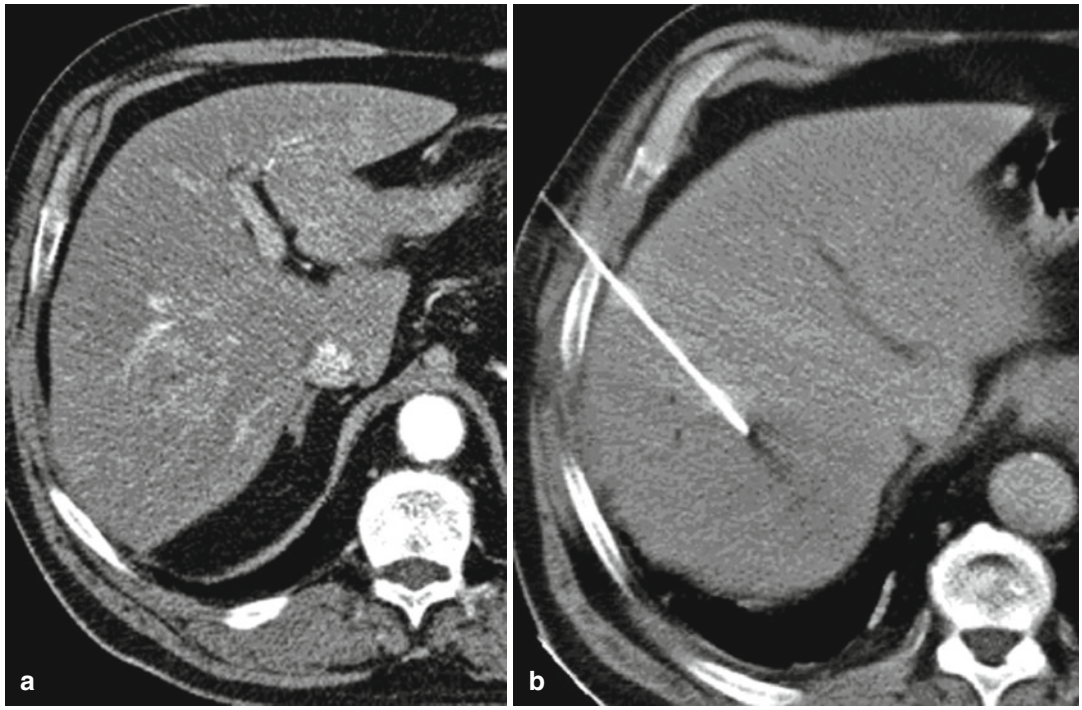

Fig. 6.9 Anterolateral intercostal approach to an unclear focal liver lesion enhanced slightly during arterial-phase computed tomography (CT) (**a**) in liver segment 5/8 in a patient suffering from prostate cancer. Biopsy revealed a well-differentiated hepatocellular carcinoma (**b**)

6.3.5 Pancreas

Pancreatic lesions are sometimes difficult to detect. Imaging protocols usually require contrast-enhanced scans or sequences to delineate focal intrapancreatic lesions. Because of this and because of the anatomical localization, punctures of the pancreas are somewhat challenging. Depending on the site of the target, several puncture routes can be chosen. Lesions in the pancreatic head or body are usually approached via an anterior pathway (Li et al. 2008). In some instances, a transgastric (Fig. 6.1) or a transhepatic (Fig. 6.2) route is necessary. Lesions located in the pancreatic tail can be reached either via a lateral or via a posterior route (Figs. 6.12 and 6.13). A transintestinal way to the target represents a further option. Fine-needle passage of the small bowel is usually safe. Owing to the gut flora and the subsequent risk of infection, passage of the colon should be avoided. Another option is a coaxial fine-needle aspiration biopsy with a posterior transcaval approach (Gupta et al. 2002b).

6.3.6 Kidney

The accuracy of percutaneous renal mass biopsy has been widely debated. Recent data have suggested that core needle biopsy is highly sensitive for the detection of renal malignancy, with relatively few nondiagnostic biopsies and very few procedure-related complications. Percutaneous renal mass biopsy significantly affects clinical management (Maturen et al. 2007). The kidneys are usually approached from a posterior route (Fig. 6.14) but can – depending on the site of the target – also be reached using a lateral approach (Fig. 6.15). In selected cases a transhepatic access to a renal target can be chosen (Iguchi et al. 2007) (Fig. 6.16). As renal tumors are commonly hypervascularized, puncture tract embolization may be required after renal punctures.

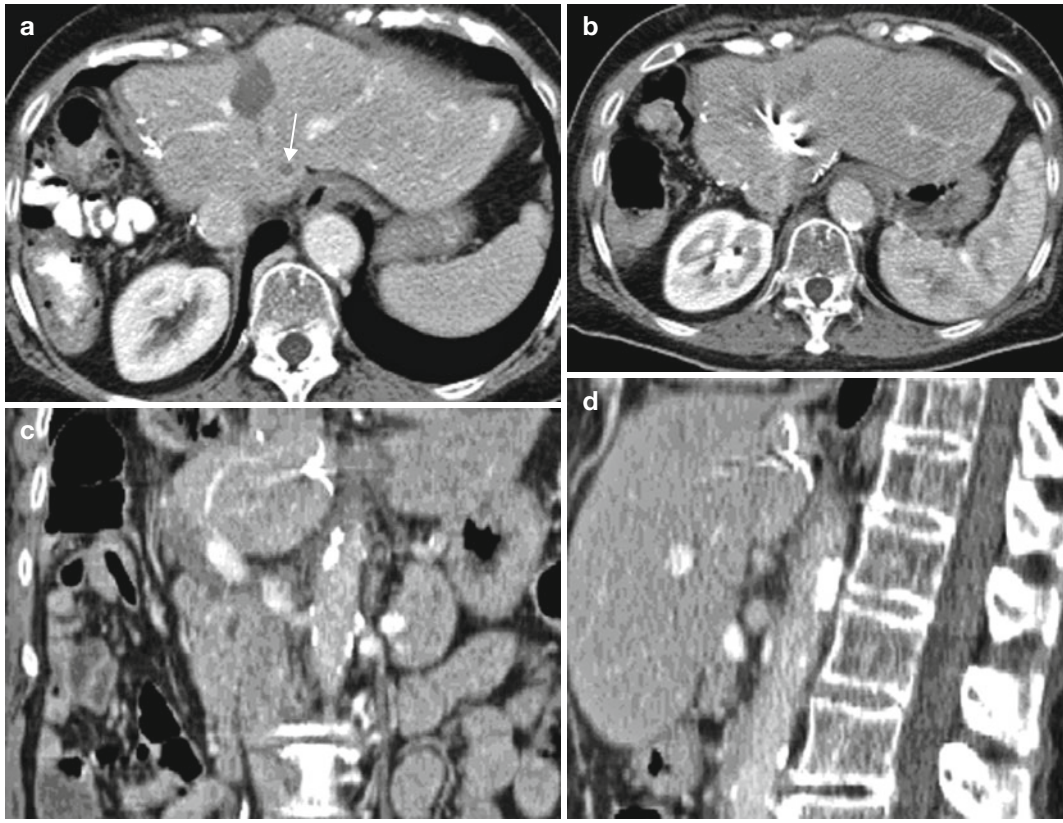

Fig. 6.10 Angulated outplane anterolateral approach to a suspected small focal liver lesion in segment 8. Biopsy revealed colorectal metastasis. Preinterventional enhanced CT (**a**) demonstrates a small focal hypodense lesion within liver segment 1 (*arrow*). (**b**–**d**) The way to the target in multiplanar views with a radiofrequency (*RF*) probe expanded in the lesion center

6.3.7 Adrenal Gland

Whenever there is an unclear focal lesion within the adrenal gland, noninvasive diagnostic tools such as MR imaging should be preferred to clarify the etiology of the lesion. If this is not possible, percutaneous image-guided biopsy is a well-accepted option. Special attention has to be paid when a pheochromocytoma cannot be ruled out prior to biopsy. In such situations, preparation with an increasing dose of a selective α1-adrenoceptor antagonist such as phenoxybenzamine (Dibenzyran®) over a 2–3 weeks period prior to the intervention is necessary to prevent a hypertensive crisis. Several ways to the target are possible, including posterior (Fig. 6.17), anterior, lateral, and transhepatic routes. Transrenal, transsplenic, or transpleural pathways should be avoided. In order to increase a paravertebral extrapleural puncture channel, physiological saline solution can be injected (Harisinghani et al. 2003).

6.3.8 Retroperitoneum and Peritoneal Cavity

The posterior approach is the standard route to lesions located within the retroperitoneum near to the aorta or the inferior vena cava (Fig. 6.18); the patient is positioned prone, and a needle path via the dorsal spinal and the psoas muscle is reasonable. With a strictly vertical needle path damage to the large vessels can be avoided, because the needle tends to end lateral to them. Special care must be taken regarding the ureter, which may be

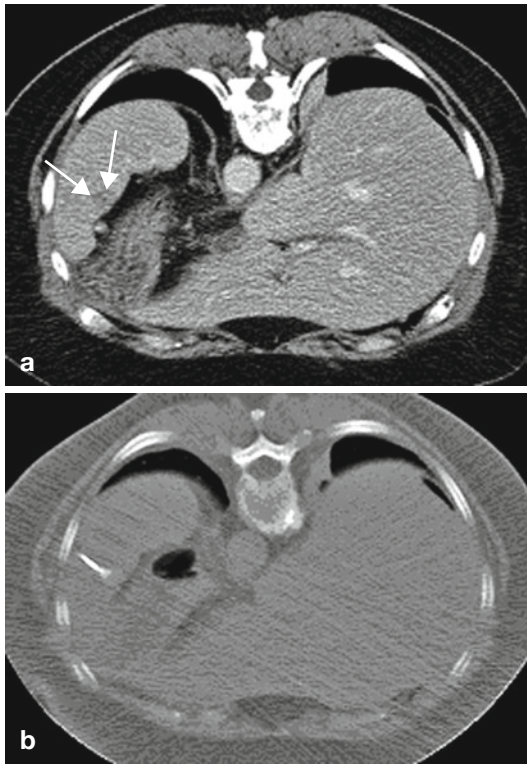

Fig. 6.11 Posterolateral approach to a small metastasis from colorectal cancer located near the splenic hilum with the patient being in the prone position. Preinterventional enhanced CT (**a**) demonstrates a small focal hypodense lesion within the spleen (*arrows*). (**b**) The way to the target in an axial plane with an RF probe opened in the lesion center

Fig. 6.12 Lateral approach to an unclear focal mass located in the pancreatic tail. Biopsy revealed metastasis from bronchial carcinoma

interposed between the target and psoas muscle. Therefore, if CT is chosen as the guiding method, the planning CT series should be acquired in the

Fig. 6.13 Posterior paravertebral approach to an unclear focal mass located in the pancreatic tail. Biopsy revealed a pancreatic carcinoma

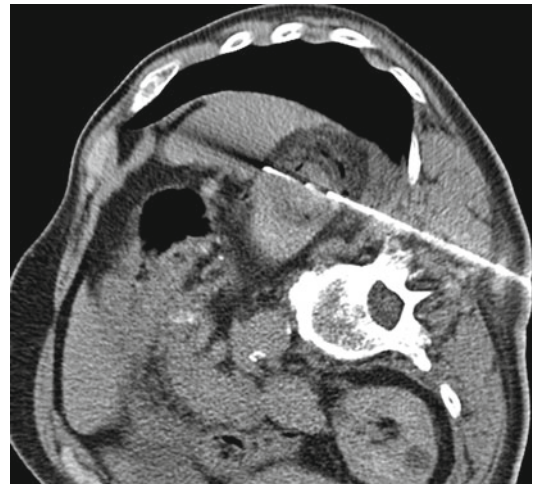

Fig. 6.14 Posterior approach to a renal cell carcinoma located in the left kidney for tissue sampling after CT-guided RF ablation.

venous phase after contrast medium injection, and thereafter the ureter will be delineated for the duration of the biopsy. Alternatively 20–30 ml of contrast agent can be injected intravenously about 3–5 min prior to the intervention to label the ureter. For the pararenal approach in patients with a pararenal mass, patient position (prone, supine, right-, or left-sided) and biopsy approach will be individually based on a safe access route avoiding major vascular structures as well as the pleural space. In most cases, this approach is noncritical and easy to perform. In the anterior–posterior approach in patients with a peripancreatic mass,

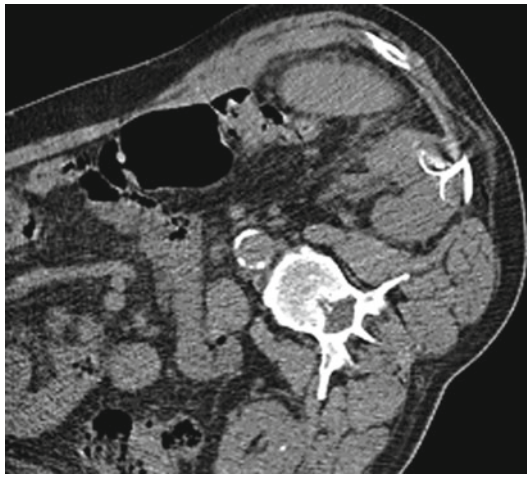

Fig. 6.15 Lateral approach to a recurrent renal cell carcinoma located in the contralateral left kidney 37 months after right-sided nephrectomy for renal cell carcinoma. Peri-interventional nonenhanced CT demonstrates an RF probe within the tumor

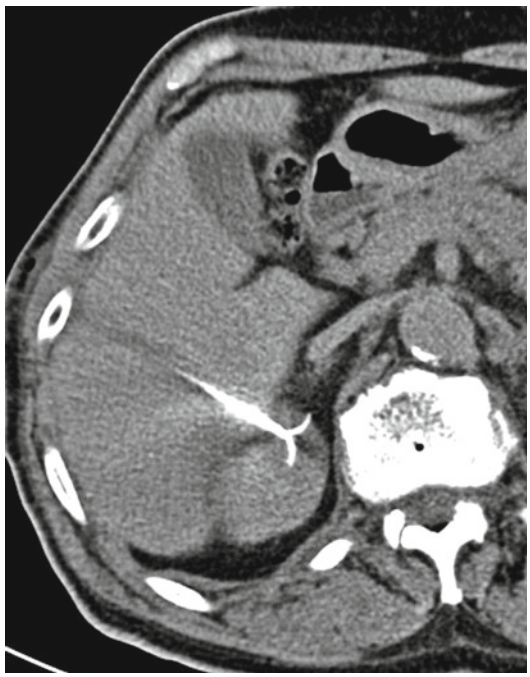

Fig. 6.16 Transhepatic approach to a small renal cell carcinoma for CT-guided RF ablation

Fig. 6.17 Posterior approach to an unclear focal mass located in the right adrenal gland. Biopsy revealed metastasis from bronchial carcinoma

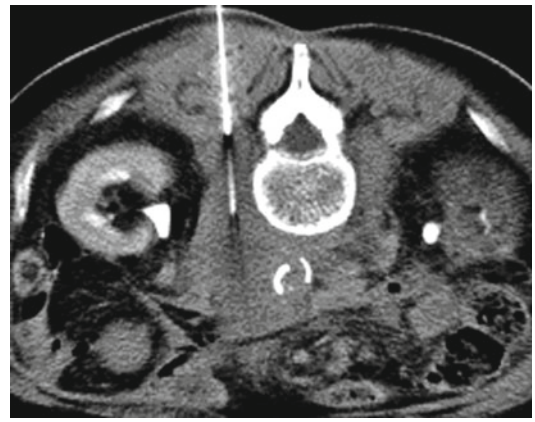

Fig. 6.18 Posterior approach via the dorsal spinal and psoas muscle to a malignant lymphoma located within the retroperitoneum near to the aorta

the patient is positioned supine, and the biopsy approach will be – if other ways are not available – via the left lobe of the liver. This transhepatic route requires administration of local anesthesia on both sides of the liver. In targets located near the aorta beneath the diaphragm (retrocrural), a posterior route is usually chosen (Fig. 6.19) in some cases with the necessity of angulated out-of-plane needle paths sometimes requiring injection of 0.9 % NaCl solution in order to increase the space of the puncture channel to prevent pleural laceration (Stattaus et al. 2008).

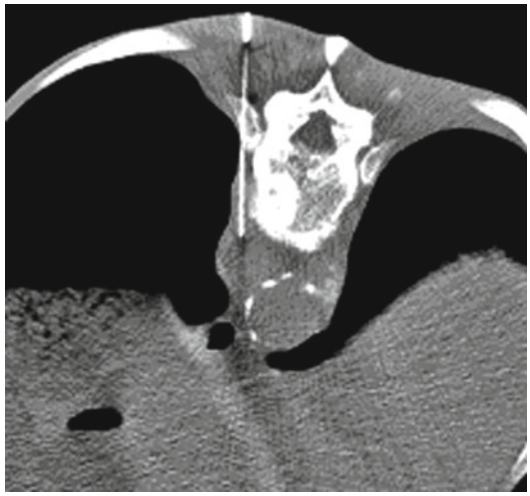

Fig. 6.19 Posterior paravertebral extrapleural approach to a malignant lymphoma located retrocrural near to the aorta

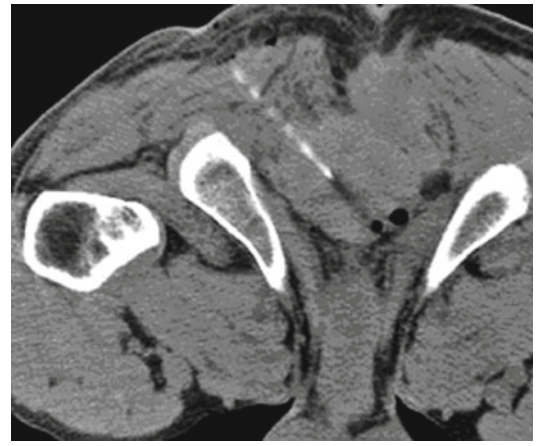

Fig. 6.21 Posterior transgluteal approach to an unclear perineal mass in a patient with a history of rectal cancer and extirpation of the rectum. Aspiration revealed hematoma

Fig. 6.20 Anterior approach to a fluid collection located in the mesenterium

Depending on the site of the target within the peritoneal cavity, the access route is chosen. Usually a transabdominal approach through the anterior or lateral abdominal wall is suitable for nearly all intra-abdominal targets (Fig. 6.20). Transintestinal pathways can be useful in some situations, but should be avoided whenever possible. The same holds true for the transaortic approach that is sometimes used for celiac plexus block. Anyhow, although these access routes are feasible options, they should be limited to fine needles (20–25 G); cutting within the bowel or vessel wall needs to be avoided under any circumstance.

6.3.9 Pelvis

Access route planning for image-guided punctures within the deep pelvic space remains challenging because vital structures such as overlying bowel, bladder, vessels, and bones, as well as the uterus and adnexa, in female patients, often obstruct the projected needle path. Therefore, a thorough understanding of the pelvic anatomy is mandatory. There are several potential pathways to reach an intrapelvic target. They usually depend on the site of the target within the pelvic space (Gupta et al. 2004). The transabdominal approach through the lower anterior or lateral abdominal wall is suitable for lesions located either cranial to the level of the urinary bladder or anterior or lateral to the bladder. The transgluteal approach is suitable for lesions located in the presacral and perirectal regions (Fig. 6.21). In addition, targets located posterior or posterolateral to the urinary bladder and adnexal lesions can be accessed with this approach. In general, this way is used for posterior pelvic lesions in the lower

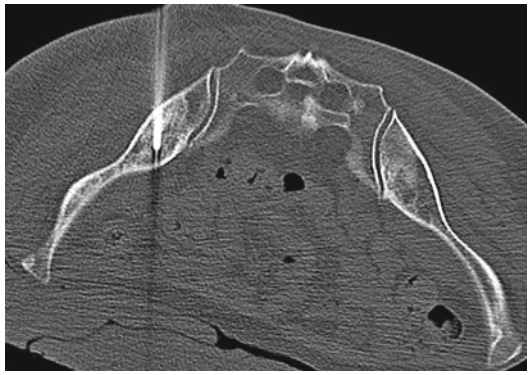

Fig. 6.22 Posterior transgluteal approach to an osteosclerotic bone lesion located in the left iliac wing. Biopsy revealed metastasis of breast cancer

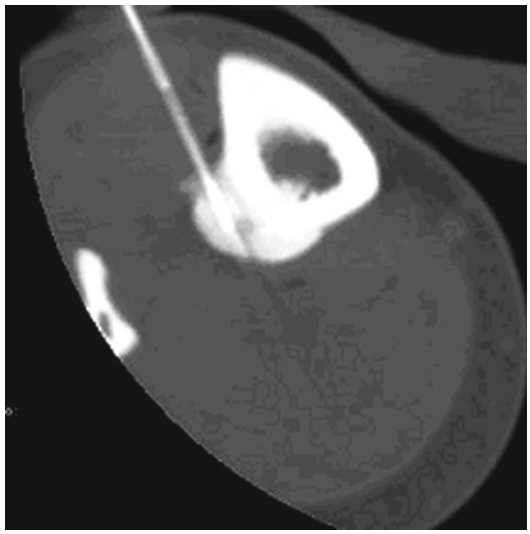

Fig. 6.23 Posterior approach for puncture of an osteoid osteoma prior to RF ablation

part of the pelvis at the level of the greater sciatic foramen that are not accessible with an anterior approach because of intervening bowel, bladder, uterus, and iliac vessels. To avoid damage to neurovascular structures, the posterior access route should be as close as possible to the sacral bone. The anterolateral extraperitoneal approach is ideally suited for percutaneous biopsy of lesions located along the medial aspect of the iliopsoas muscle. This approach provides safe access to obturator or deep external iliac, anterior external iliac, and internal iliac targets. For presacral and posterior pelvic lesions that are not accessible by means of the transgluteal approach because either they are located above the level of the greater sciatic foramen or intervening vascular structures are present, a transsacral approach might be an option. A transosseous approach through the iliac wing allows safe access to targets in close relation to the iliopsoas muscle that is not approachable by means of other routes (Schweiger et al. 2000; Yarram et al. 2007). However, puncture of infected fluid collections and particularly transosseous drainage needs to be avoided.

6.3.10 Bone

Each bone puncture is accompanied by an increased risk for infectious complications and therefore should be performed under sterile conditions. Because of this, transperitoneal approaches are contraindicated.

Prior to any bone puncture, the periosteum has to be well anesthetized, avoiding sedation and narcosis when the puncture route is next to nerve structures. In peripheral bones, the access route depends on the localization of the target and adjacent vascular and/ or nerve structures (Figs. 6.22, 6.23, 6.24, and 6.25). Targets in the spine are usually approached from posterior using a transpedicular (Fig. 6.26) or extrapedicular paraspinal (Fig. 6.27) route (Tehranzadeh et al. 2007). Lesions in the cervical spine are approached using an anterior–posterior parapharyngeal route, whereas targets located in the upper cervical spine (e.g., C_2) have to be accessed using a lateral (Fig. 6.28) and sometimes a transoral approach (Reddy et al. 2005).

6.3.11 Miscellaneous

There are many other target regions that can be safely approached by image guidance (Figs. 6.29, 6.30, 6.31, 6.32, 6.33, 6.34, 6.35, 6.36, 6.37, 6.38, 6.39, and 6.40). The way to the target depends on the site of the target and surrounding structures at risk. In the vast majority of cases,

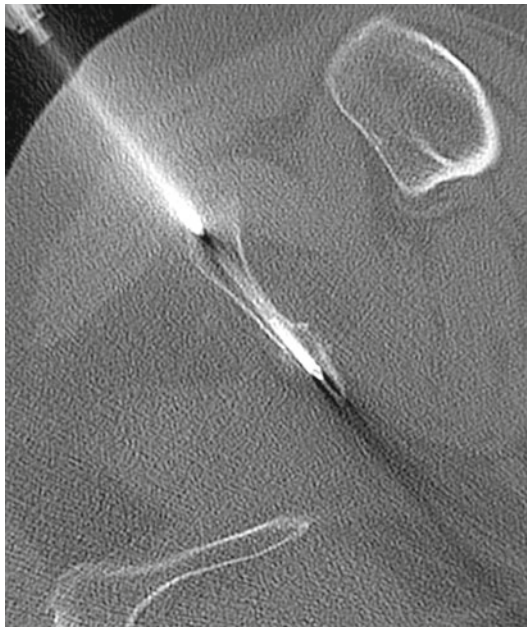

Fig. 6.24 Posterior approach to a pathologic fracture of the ischium prior to cementoplasty

Fig. 6.25 Anterior approach to an osteolytic lesion within the sternum. Biopsy revealed osteolytic metastasis of breast cancer

Fig. 6.26 Posterior transpedicular approach to an osteolytic lesion within lumbar vertebra 4. Biopsy revealed multiple myeloma

the shortest way seems to be the most appropriate and the safest. Adjusting the position of the patient according to the planned access route, including respiration maneuvers (e.g., Valsalva) (Fig. 6.36), represents a key point for successful punctures (Enoch et al. 2008; Akinci and Akhan 2005; Datta et al. 2007; Gupta et al. 2007; Boswell et al. 2007).

Fig. 6.27 Posterior extrapedicular approach to thoracic vertebra 5 prior to cementoplasty. The costovertebral joint can safely be passed to access thoracic vertebrae

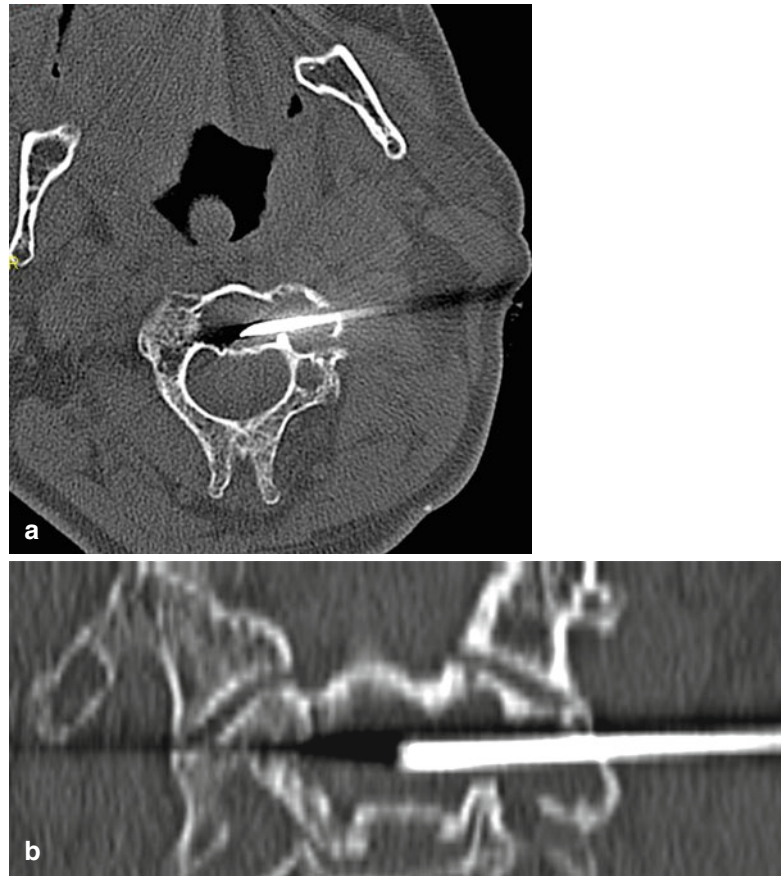

Fig. 6.28 Axial (**a**) and coronal (**b**) image of a lateral approach to an osteolytic lesion from multiple myeloma within cervical vertebra 2 prior to vertebroplasty

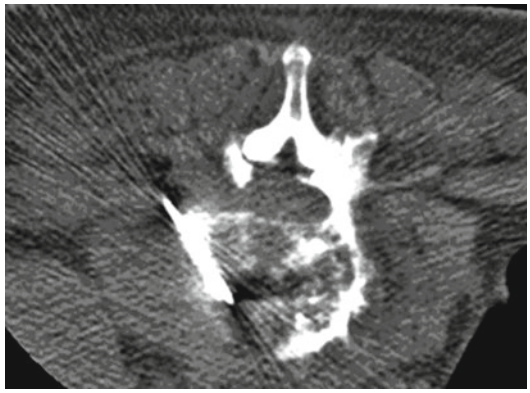

Fig. 6.29 Angulated posterior approach to the intervertebral space in septic discitis. Aspiration revealed intervertebral abscess with *Staphylococcus aureus*

Fig. 6.30 Right posterior approach for selective nerve block L5

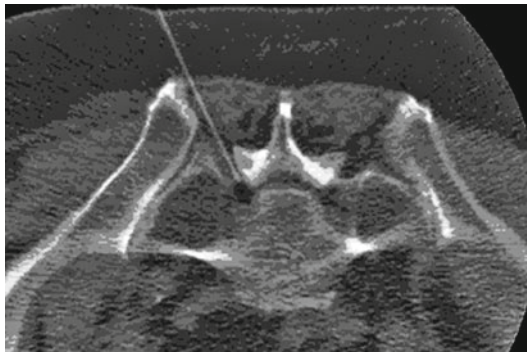

Fig. 6.31 Posterior approach to sacral vertebra 1 for selective nerve block

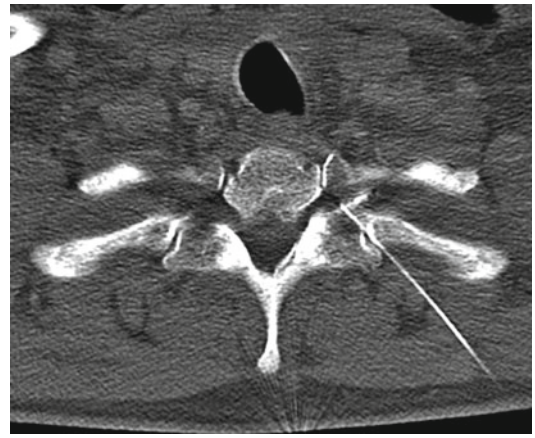

Fig. 6.32 Posterior approach via the costovertebral joint for selective block of Th 2

Fig. 6.33 Posterior interlaminar approach for epidural block of L 5

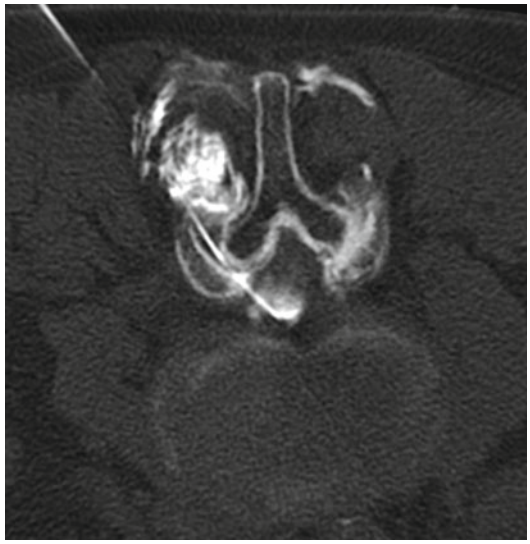

Fig. 6.34 Posterior approach to a synovial cyst of a lumbar facet joint via the facet joint itself. Consecutive contrast injection delineates the cyst which was located adjacent to L 4. Due to radicular pain the cyst was therapeutically punctured for decompression

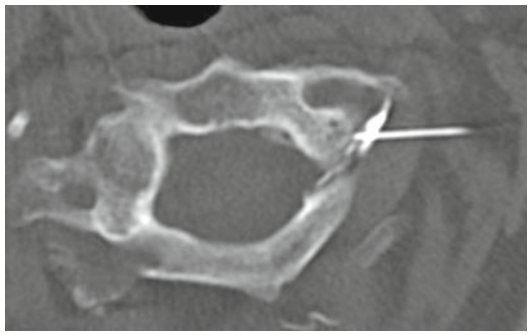

Fig. 6.35 Posterolateral approach for cervical facet joint block

Fig. 6.36 Anterolateral approach for selective stellate ganglion block

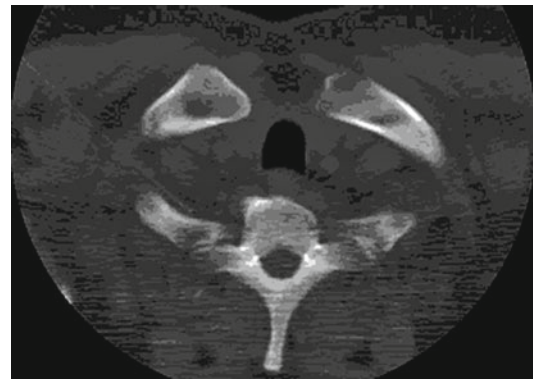

Fig. 6.37 Anterolateral approach for selective stellate ganglion block

Fig. 6.38 Posterior approach for bilateral lumbar facet joint block

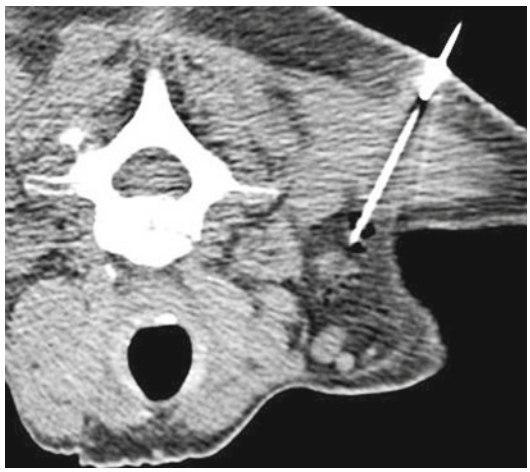

Fig. 6.39 Posterior approach for a suspected axillar lymph node in a lymphoma patient. Biopsy revealed inflamed lymphatic tissue with no evidence of malignant cells

Fig. 6.40 Posterolateral, transgluteal approach to an unclear iliac mass. Biopsy revealed metastasis from colorectal carcinoma

Appraisal

Virtually all regions of the body may be accessed by CT- or MR-guided puncture. Depending on the region that needs to be accessed for diagnostic or therapeutic purposes, a variety of more or less safe routes are available. Depending on the anticipated route, adequate patient position and material need to be selected, while the method for image guidance should depend on lesion visibility. The figures shown in this chapter only provide a glimpse at the potential access routes to different parts of the body, and depending on the individual patient, the access routes may vary widely. The general principle, however, is always the same: the shortest way with as little angulation as possible; avoid nerves, vessels, lung, and hollow organs; and select the least traumatic puncture device, that is, reasonable for the anticipated task. If these basic requirements are considered, safe and successful puncture will be achieved.

Key Points

- There is no inaccessible lesion!
- Use a stable and comfortable patient position.
- Avoid angulated trajectories if possible.
- Transgastric, transhepatic, transosseous, and transvascular access routes are feasible if needed. Balance the risk and the benefit of the different access routes.
- Consider surgical and endovascular approaches when deciding to perform a CT- or MR-guided puncture.

References

Akinci D, Akhan O (2005) Celiac ganglia block. Eur J Radiol 55:355–361

Billich C, Muche R, Brenner G et al (2008) CT-guided lung biopsy: incidence of pneumothorax after instillation of NaCl into the biopsy track. Eur Radiol 18:1146–1152

Boswell MV, Trescot AM, Datta S et al (2007) Interventional techniques: evidence-based practice guidelines in the management of chronic spinal pain. Pain Physician 10:7–111

Datta S, Everett CR, Trescot AM et al (2007) An updated systematic review of the diagnostic utility of selective nerve root blocks. Pain Physician 10:113–128

Enoch DA, Cragill JS, Laing R et al (2008) Value of CT-guided biopsy in the diagnosis of septic discitis. J Clin Pathol 16:750–753

Gupta S (2004) New techniques in image-guided percutaneous biopsy. Cardiovasc Intervent Radiol 27:91–104

Gupta S, Madoff DC (2007) Image-guided percutaneous needle biopsy in cancer diagnosis and staging. Tech Vasc Interv Radiol 10:88–101

Gupta S, Wallace MJ, Morello FA et al (2002a) CT-guided percutaneous needle biopsy of intrathoracic lesions by using the transsternal approach: experience in 37 patients. Radiology 222:57–62

Gupta S, Ahrar K, Morello FA Jr et al (2002b) Masses in or around the pancreatic head: CT-guided coaxial fine-needle aspiration biopsy with a posterior transcaval approach. Radiology 222:63–69

Gupta S, Nguyen HL, Morello FA et al (2004) Various approaches for CT-guided percutaneous biopsy of deep pelvic lesions: anatomic and technical considerations. Radiographics 24:175–189

Gupta S, Seaberg K, Wallace MF et al (2005) Imaging-guided percutaneous biopsy of mediastinal lesions: different approaches and anatomic considerations. Radiographics 25:763–786

Gupta S, Henningsen JA, Wallace MJ et al (2007) Percutaneous biopsy of head and neck lesions with CT guidance: various approaches and relevant anatomic and technical considerations. Radiographics 27:371–390

Harisinghani MG, Maher MM, Hahn PF et al (2003) Predictive value of benign percutaneous adrenal biopsies in oncology patients. Clin Radiol 57:898–901

Hiraki T, Fujiwara H, Sakurai J et al (2007) Nonfatal systemic air embolism complicating percutaneous CT-guided transthoracic needle biopsy: four cases from a single institution. Chest 132:684–690

Iguchi T, Hiraki T, Gobara H et al (2007) Transhepatic approach for percutaneous computed-tomography-guided radiofrequency ablation of renal cell carcinoma. Cardiovasc Intervent Radiol 30:765–769

Kang M, Kalra N, Gulati M et al (2007) Image guided percutaneous splenic interventions. Eur J Radiol 64:140–146

Li L, Liu LZ, Wu QL et al (2008) CT-guided core needle biopsy in the diagnosis of pancreatic diseases with an automated biopsy gun. J Vasc Interv Radiol 19: 89–94

Lieberman S, Libson E, Sella T et al (2007) Percutaneous image-guided splenic procedures: update on indications, technique, complications, and outcomes. Semin Ultrasound CT MR 28:57–63

Maturen KE, Nghiem HV, Caoili EM et al (2007) Renal mass core biopsy: accuracy and impact on clinical management. AJR Am J Roentgenol 188:563–570

Ohno Y, Hatabu H, Takenaka D et al (2004) Transthoracic CT-guided biopsy with multiplanar reconstruction image improves diagnostic accuracy of solitary pulmonary nodules. Eur J Radiol 51:160–168

Reddy AS, Hochman M, Loh S et al (2005) CT guided direct transoral approach to C2 for percutaneous vertebroplasty. Pain Physician 8:235–238

Rogalla P, Juran R (2004) CT fluoroscopy. Radiologe 44:671–675

Schweiger GD, Yip VY, Brown BP (2000) CT fluoroscopic guidance for percutaneous needle placement into abdominopelvic lesions with difficult access routes. Abdom Imaging 25:633–637

Stattaus J, Kühl H, Hauth EA et al (2007) Liver biopsy under guidance of multislice computed tomography: comparison of 16G and 18G biopsy needles. Radiologe 47:430–438

Stattaus J, Kalkmann J, Kuehl H et al (2008) Diagnostic yield of computed tomography-guided coaxial core biopsy of undetermined masses in the free retroperitoneal space: single-center experience. Cardiovasc Intervent Radiol 31(5):919–925. doi:10.1007/s00270-008-9317-5

Tehranzadeh J, Tao C, Browning CA (2007) Percutaneous needle biopsy of the spine. Acta Radiol 48:860–868

Yarram SG, Nghiem HV, Higgins E et al (2007) Evaluation of imaging-guided core biopsy of pelvic masses. AJR Am J Roentgenol 188:1208–1211

Navigated Interventions: Techniques and Indications

7

Gerlig Widmann and Reto Bale

Contents

7.1 Indications

Computer-assisted navigated interventions gain increasing importance in interventional radiology. Using frameless stereotactic navigation systems, the interventionalist can navigate a pointer and other instruments on multiplanar reconstructed images in real time. Sophisticated preoperative planning and simulation permits arbitrarily angulated guided puncturing through adjustable rigid aiming devices (Bale et al. 1997, 2000, 2001, 2006; Bale and Widmann 2007).

Indications for navigated interventions include several procedures:

- Interventions where both high-precision and double-angulated access routes are needed
- Radiofrequency ablation (RFA) of the Gasserian ganglion in patients with trigeminal neuralgia
- Percutaneous fixation of pelvic fractures
- Retrograde drilling of small osteochondral lesions in the ankle, knee, and hip
- Discography and vertebroplasty in difficult anatomical regions and conditions (e.g., scoliosis, extensive osteochondrosis etc.)
- RFA of large tumors/metastases requiring multiple probe positions in different locations to cover the large volume
- Surgical template production
- Fractionated interstitial brachytherapy

Depending on the precision needed for an interventional procedure, virtually all organs and body regions from head to toe can be the subject of navigated interventions. This includes brain, nerves, liver, kidney, adrenal gland, lung, bone,

G. Widmann (✉) • R. Bale
SIP – Department for Microinvasive Therapy/
Department of Radiology, Medical University Innsbruck,
Anichstr. 35, A-6020, Innsbruck, Austria
e-mail: gerlig.widmann@i-med.ac.at

A.H. Mahnken et al. (eds.), *CT- and MR-Guided Interventions in Radiology*,
DOI 10.1007/978-3-642-33581-5_7, © Springer-Verlag Berlin Heidelberg 2013

and soft tissue (Goldberg et al. 2000; Gazelle et al. 2000; Bale and Widmann 2007).

7.2 Materials and Techniques

7.2.1 Material Available/Needed

Navigated interventions are best performed in an interventional treatment center and require:

1. A cross-sectional imaging modality
2. A patient fixation system
3. A surgical navigation system
4. An image-to-patient registration technique
5. An aiming device
6. Puncture and treatment instruments

7.2.1.1 Imaging Modality

In computed tomography (CT), scanners with a large gantry bore are preferred. The availability of a sliding gantry is favorable. In magnetic resonance (MR) imaging, open systems are of particular value.

7.2.1.2 Patient Fixation

(Double) vacuum-based immobilization devices (e.g., BlueBAG® and BodyFIX®, Medical Intelligence, Schwabmünchen, Germany) allow for safe and easy patient fixation (Bale et al. 1999, 2002; Nagel et al. 2005). Such devices consist of a vacuum pump connected to different types of machine-washable pillows or plastic bags which are filled with tiny polystyrene balls.

For head fixation the noninvasive VBH head holder can be used (Bale et al. 1997; Widmann et al. 2010a; Ortler et al. 2010). The head holder consist of a VBH-vacuum mouthpiece, an adjustable, locking, adaptable mechanical arm, and a base plate (40 × 30 cm, with multiple fixing areas to hold the mechanical arms) with head rest. The mouthpiece is based on an individualized dental mould that is held against the upper palate by negative pressure and enables for rigid immobilization of the patient's head at the base plate.

7.2.1.3 Navigation System

Optical-based navigation systems (e.g., StealthStation® Treon™ plus, Medtronic, Louisville, USA; VectorVision® Colibri®, Brainlab, Feldkirchen, Germany; CAPPA® IRAD, Siemens, Erlangen, Germany) are routinely used for neurosurgery, ENT surgery, and orthopedic surgery (Caversaccio et al. 1999; Grunert et al. 2002; Bale and Widmann 2007). They offer the advantage of a high technical accuracy in the range 0.1–0.4 mm (Khadem et al. 2000), convenient handling, and easy sterilization. Disadvantages are the necessity of constant visual contact between the camera array, the dynamic reference frame, and instruments and the potential susceptibility to interference through reflection of light from metallic surfaces in the operating room environment.

Electromagnetic navigation systems (e.g., AxiEM™, Medtronic, Louisville, USA; CAPPA® IRAD, Siemens, Erlangen, Germany; Percunav, Traxtal, Toronto, Canada) can reach comparable accuracy (Mascott 2005; Penzkofer et al. 2011) and have the advantages of possible use of very small detector coils including angiographic catheters, navigation of flexible instruments, and no need for visual contact between the instrument and the sensor system (Schiemann et al. 2004; Wood et al. 2005; Banovac et al. 2005; Zhang et al. 2006a). However, these systems may be affected by external magnetic fields and metal objects (Wagner et al. 2002), leading to incorrect position sensing of up to 4 mm (Birkfellner et al. 1998; Marmulla et al. 1998; Hummel et al. 2005, 2006). They may also be considered a contraindication in patients with pacemakers and cochlear implants.

7.2.1.4 Registration Technique

Point-based registration using attachable skin markers (e.g., Beekley SPOTS®, Beekley, Bristol, CT, USA) is the most widely used registration technique (Maurer et al. 1998; Fitzpatrick et al. 1998). For the head, an external u-shaped Plexiglas frame equipped with eleven spherical CT markers (glass, diameter 5.8 mm) can be mounted to the VBH mouthpiece.

Point-based registration involves determining the coordinates of corresponding points (fiducials) in the image (manually or semiautomatically using the computer) and on the patient (with the probe of the navigation system) and computing

the geometrical transformation that best aligns these points.

Automatic registration can be achieved either by a stable camera position and a calibration of the CT system (i.e., modality-based navigation) (Jacob et al. 2000) or by using reflective markers that are automatically detected on the CT dataset and on the real patient (Jacob et al. 2000; Nagel et al. 2005).

7.2.1.5 Aiming Device

Most targeting devices are aligned to the preplanned virtual path by using the pointer (i.e., navigation probe) of the navigation system.

The EasyTaxis™ system (Philips Medical Systems, Best, The Netherlands) consists of a spherical alignment body (trapped ball) that rotates freely in a bearing and that can be locked by a screw (Dorward et al. 1997; Bale et al. 2001). It is connected to an adjustable mechanical arm with six degrees of freedom. The alignment body contains a large central cylindrical hole to accept a tube with an incomplete inner sleeve to place the navigation probe or other tubes for the guidance of different surgical instruments (e.g., biopsy needles and RF probes). The EasyTaxis™ system allows for separate positioning of the tip (which has to be in the virtual elongation of the pathway) and adjustment of the angulations of the probe (which has to be aligned with the virtual elongation of the path) via a trapped ball on the distal end of the mechanical arm.

The Vertek™ system (Medtronic, Louisville, USA) (Bale et al. 2006) consists of a mechanical device with two independent pivot joints. Thereby, the complex rotational movement is replaced by two degrees of freedom. Owing to the presence of a tracked needle with a light-emitting diode at the distal part of the needle, the tip can be continuously tracked in real time during the advancement. However, a possible bending of the needle would not be detected by the system.

The Atlas™ system (Medtronic, Louisville, USA) (Bale and Widmann 2007) is similar to the Vertek™ system but has the advantage of a freely adjustable mechanical guide accepting instruments with variable diameters and thus does not necessitate the use of reducing tubes.

7.2.2 Technique

7.2.2.1 (Double) Vacuum Patient Immobilization

To preserve the image-to-patient registration, the patient has to be immobilized in the intervention room, e.g., via a (double) vacuum system. The patient is positioned on a vacuum splint (plastic bags filled with polystyrene balls), and the air is evacuated, resulting in hardening of the plastic bag. If a rigid fixation is necessary (e.g., in interventions without general anesthesia), the double-vacuum fixation technique may be applied. In these cases the patient may be additionally covered with cushions filled with polystyrene balls, leaving an area for the surgical approach. Thereafter, the patient and the cushions are covered by a plastic foil. When the vacuum pump is turned on, the air is evacuated from the space between the covering foil and the patient/vacuum splint to a negative pressure of about 80 mbar, resulting in a hardening. Thus, the patient is rigidly sucked on the therapy couch (Bale et al. 1999, 2002; Nagel et al. 2005) (Fig. 7.1).

7.2.2.2 Imaging

Most navigation systems require a continuous (volumetric) CT dataset. Gaps or overlapping slices are usually not acceptable. Tilting of the CT gantry needs to be avoided. For most cases CT slices of 3 mm or less are recommended as there is a clear correlation between voxel size and accuracy (Bucholz et al. 1993; Dorward et al. 1999; Maciunas et al. 1994). In addition, multimodal fusion with previously obtained three-dimensional MR imaging/positron emission tomography (PET)/single photon emission CT (SPECT) data may improve the planning procedure especially in lesions that are poorly visible by CT.

7.2.2.3 Planning

According to the type of intervention, a single (e.g., biopsy) or multiple (e.g., RF ablation of large metastases) puncture paths are planned using the navigation software. The trajectory planning is based on various two-dimensional and three-dimensional reconstructions of the patient's CT data and superimposed MR imaging/PET/

Fig. 7.1 Set up for 3D-navigated radiofrequency (RF) ablation. The patient is immobilized by the double-vacuum immobilization. The vacuum pump can be seen in the *lower-right corner*, the camera of the navigation system in the *upper-right corner*, and the RF ablation system in the *lower-left corner*

SPECT data. By using the reconstructed longitudinal and orthogonal cuts along the planned path, one can prevent potential violation of vital structures (Fig. 7.2).

7.2.2.4 Registration

Registration markers should be broadly distributed around the volume of interest and have to be clearly indicated on the image data and the patient, respectively (West et al. 1999; Khan et al. 2006). Registration is performed by touching the real marker on the patient (Fig. 7.3) or on a reference frame and selecting the corresponding marker on the virtual three-dimensional dataset on the monitor. Automated registration technology may facilitate application (Jacob et al. 2000; Nagel et al. 2005). Respiratory motion decreases the accuracy and may require respiratory gating and affine transformation methods (Holzknecht et al. 2001; Zhang et al. 2006b). For stereotactic interventions in organs that are sensitive to respiratory motion (the liver or the bases of the lungs), the CT scans, the registration procedure, and the puncture must be performed in the same respiratory phase.

7.2.2.5 Navigation

After unsterile registration, the puncture area is disinfected and draped. The pointer of the navigation system is introduced into the aiming device, which is adjusted according to the preplanned path using the guidance view of the navigation software. The needle is advanced through the aiming device to the preplanned depth as indicated by the navigation system (Fig. 7.4).

7.2.2.6 Control Imaging of Needle Positioning

For verification of the accuracy of the needle position, a low-dose control CT scan (with the needles in place) is obtained and fused with the planning CT scan (with the planned paths). Blending between the two datasets allows the

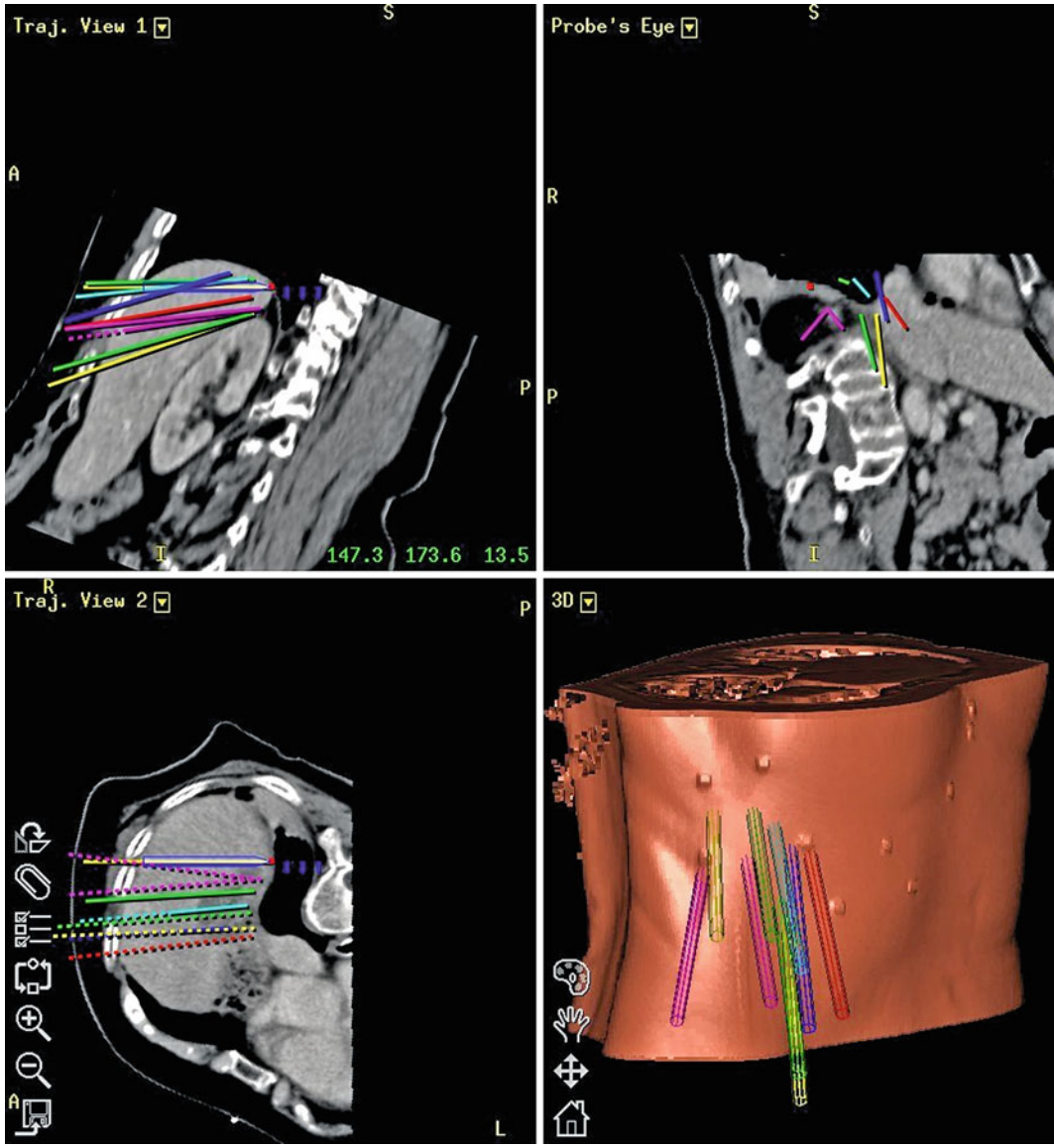

Fig. 7.2 Planning of multiple pathways on 2D reformatted and 3D computed tomography (CT) images (*lower-right quadrant*) for treating a large metastasis from colorectal carcinoma. The trajectory 0° (*upper-left quadrant*) and the trajectory 90° (*lower-left quadrant*) are planes along the needle trajectory, and the probe's eye view (*upper-right quadrant*) is perpendicular to the pathway

planned paths to be superimposed on the real needles in the patient (Fig. 7.5).

7.2.2.7 Intervention

After verification of the correct needle position, the actual intervention (e.g., biopsy, RF ablation, infiltration, osteoplasty, etc.) is performed (Fig. 7.6).

7.2.2.8 Control Imaging

Final control imaging may be performed to exclude intervention-related complications and to document the success of the intervention. Depending on the type of intervention, administration of contrast material or additional image registration may be needed (Fig. 7.7).

Fig. 7.3 Registration of the patient by touching the skin fiducials with the probe and selecting the corresponding markers on the screen (not shown)

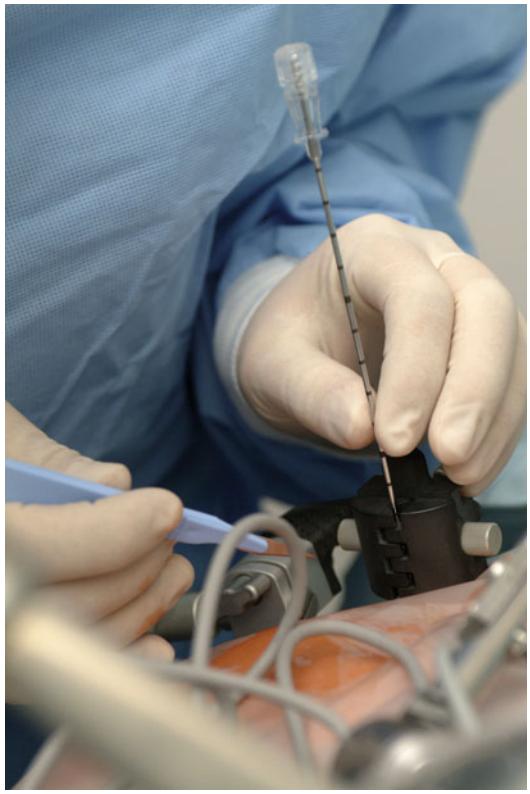

Fig. 7.4 Coaxial needle is advanced through the Atlas aiming device

7.3 Results

7.3.1 Cannulation of the Foramen Ovale

In patients with medically refractory trigeminal neuralgia, the foramen ovale is cannulated for RFA of the Gasserion ganglion. In a phantom study, the mean lateral error was 1.38 ± 0.65 mm (3 mm CT slices). The foramen ovale (3 × 5 mm) was successfully cannulated at the first attempt in all cadavers and patients, which indicates clinical localization accuracies better than 1.5 mm in anterior-posterior and 2.5 mm in medial-lateral direction (Bale et al. 2006; see Sect. 14.4).

7.3.2 Retrograde Drilling of Osteochondral Lesions

In human cadavers, ten talar drillings provided targeting errors of 2.1 ± 1.0 mm (range 1.0–3.5 mm), six tibial drillings 1.6 ± 0.8 mm (range 0.5–3.0 mm), and six femoral drillings 1.8 ± 0.9 mm (range 1.0–3.5 mm) (Bale et al. 2001) (Fig. 7.8).

7.3.3 Percutaneous Fixation of Pelvic Fractures

In human cadavers, a total of 16 stereotactic CT-guided wire placements simulating fixation of the iliosacral joint provided targeting errors of 1.84 ± 0.9 mm at the bone entrance point and 2.5 ± 1.2 mm at the target (Bale et al. 2008).

7.3.4 RFA of Bone Lesions

For treatment of osteoid osteoma, a benign painful bone lesion, percutaneous CT-guided RFA has become the method of choice. Precise targeting is essential in order to ablate the active nidus of the lesion that is usually only ≤ 1 cm in diameter and may include the spine in up to 10 %.

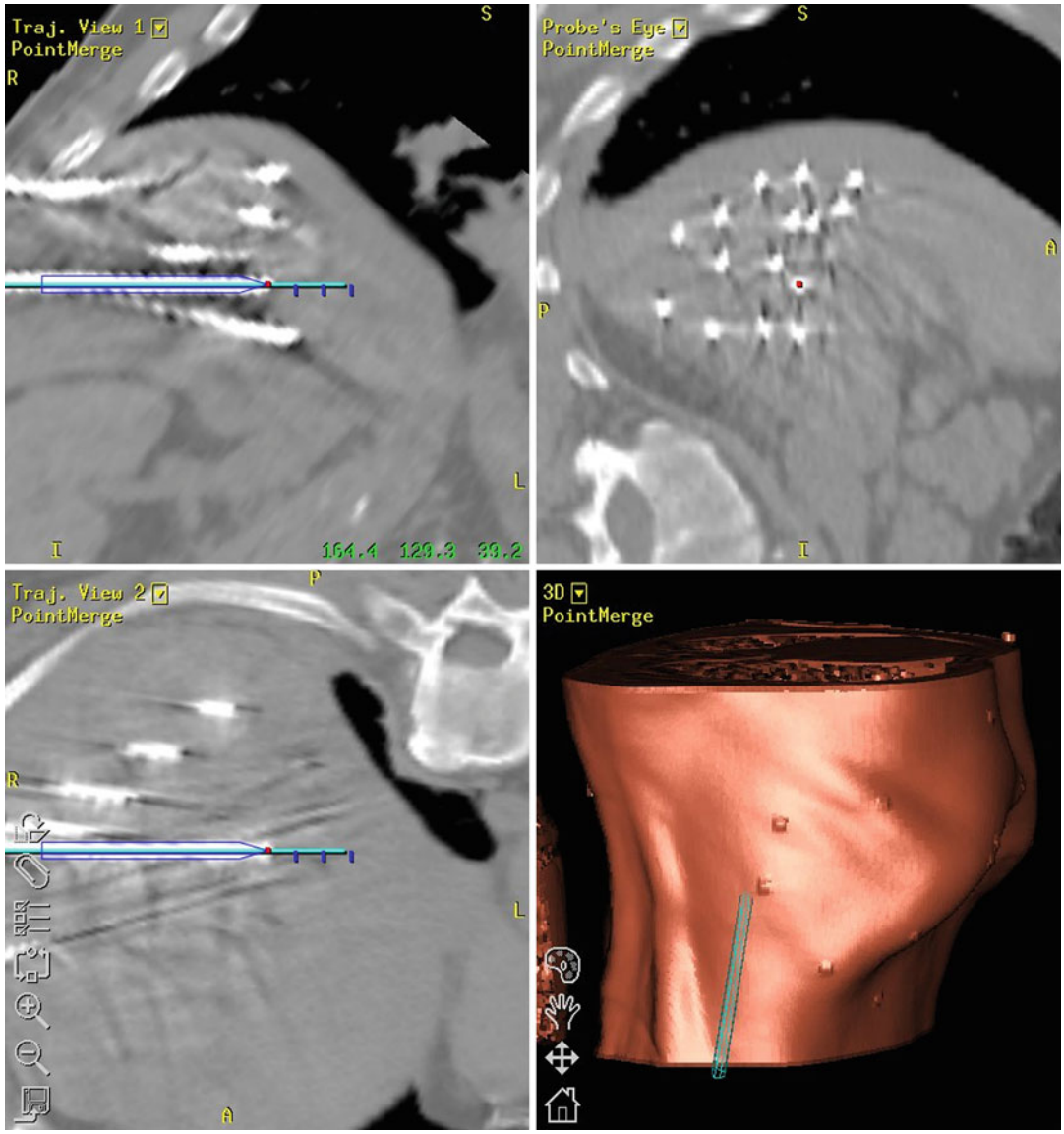

Fig. 7.5 The control CT scan is superimposed on the planning CT scan, with the pathway (*blue line*) showing precise placement

In a preliminary study of percutaneous stereotactic RFA (SRFA) of osteoid osteoma, all lesions could be successfully reached: the mean ± SD lateral targeting error was 2.6 ± 1.7 mm at the needle entry, 1.9 ± 1.2 mm at the needle tip, and the mean angular error was 2.0° ± 1.3° (work in progress) (Fig. 7.9). The same stereotactic approach can be used for placement of several probes for RFA of painful metastatic bone lesions.

7.3.5 RFA of Liver Lesions

For SRFA of primary or metastatic liver lesions, respiratory motion compensation can be successfully achieved when the interventional CT-scans, the registration procedure, and the targeting are performed in temporary disconnection of the endotracheal tube (ETT) in relaxed patients under general anesthesia as a modified standardized

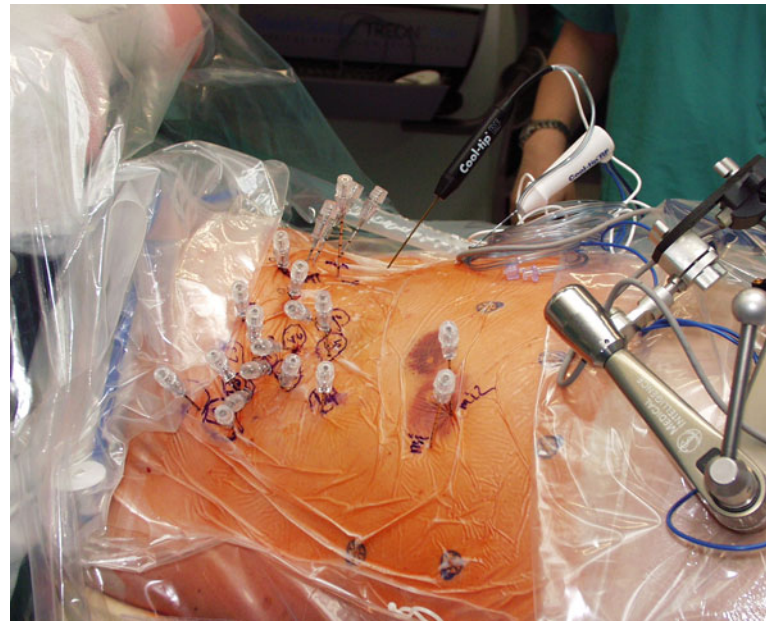

Fig. 7.6 Twenty-two coaxial needles have been introduced with 3D navigation

"end-expiratory breath-hold technique." Temporary ETT disconnections are safe and may control respiratory motion for liver interventions within 4 mm (Widmann et al. 2010b).

Multiple trajectories within and around the tumor(s) can be planned in 3D in order to treat the entire tumor volume and a sufficient intentional margin by creating overlapping necroses (Widmann et al. 2009a; Bale et al. 2010).

Navigation systems provide interactive visualization of the actual position of a probe or instrument in relation to the patient in real time with free angulations in the entire examination volume (Holzknecht et al. 2001). Usually, only a single planning CT scan and one low-dose control CT scan for confirmation of the correct needle position are required, which allows one to reduce the radiation exposure of the patient as well as of the interventionalist (Holzknecht et al. 2001). Multiple needles can be planned and placed under navigation using a single planning image dataset only (Banovac et al. 2005; Zhang et al. 2006b; Wood et al. 2007). This is especially helpful for ablation of large tumors where multiple overlapping ablation areas have to be achieved (Bale et al.; Fig. 7.7). Compared with the current free-hand movement of needles, adjustable aiming devices enable rigid trajectory alignment and instrument guidance in three-dimensional arbitrarily oriented tracks (Germano and Queenan 1998; Holloway et al. 2005; Dorward et al. 1997; Paleologos et al. 2001; Patel and Sandeman 1997; Bale et al. 1997; Nagel et al. 2005). In 20 patients with 35 liver lesions, a total of 145 needles were placed with mean (± SD) lateral errors of 3.6 ± 2.5 mm at the needle tip, angular errors of 1.3° ± 1.2°, and longitudinal errors at the needle tip of −7.4 ± 6.2 mm (Widmann et al. 2011) (Fig. 7.5). No puncture-related complications were noted. No significant differences of angular errors between segments, approach, and properties were recorded. This technique allows one to reduce needle misplacement and repeated puncture attempts and thereby helps in achieving a predictable and reproducible result. In that way image-guided interventions

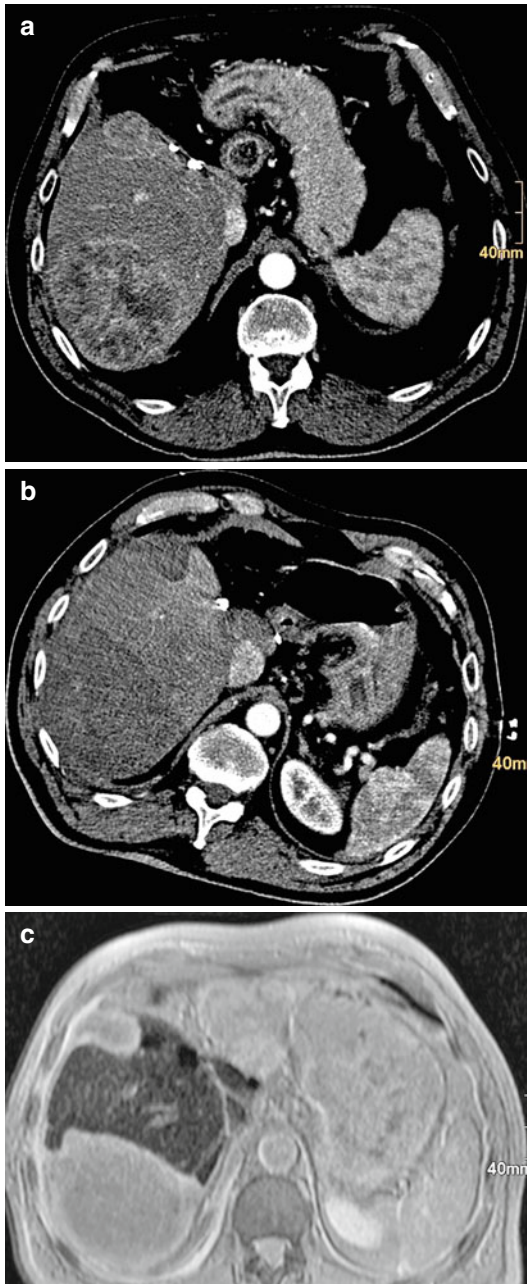

Fig. 7.7 RF ablation in a patient with two hepatocellular carcinomas (10 and 3 cm in diameter) and a history of left hemihepatectomy. The preinterventional CT scan shows two large contrast-enhanced tumors (**a**). Control CT after RF ablation shows the large areas of necrosis (**b**). MR imaging with iron nanoparticles 1 year after 3D-navigated RF ablation shows no evidence of tumor recurrence (**c**)

become less dependent on the individual interventionalist's experience (Banovac et al. 2005). Even large lesions, lesions close to vessels, and in subcapsular location may be successfully treated (Bale et al. 2010, 2011).

Despite of the apparent advantages over the conventional CT-guided puncture technique, such systems are currently only rarely used by interventional radiologists. The reasons for this are manifold and may depend on three basic requirements: knowledge about functionality of navigation systems, familiarity, and availability of such a system (Bale and Widmann 2007; Bale et al. 2010).

7.3.6 Surgical Template Production

The Innsbruck concept of computer-assisted oral implant surgery allows using a surgical navigation system for surgical template production (Widmann et al. 2005, 2007, 2009c, 2010c, d). After computerized implant planning using the navigation software, the stereotactic aiming device is used to drill the dental stone cast of the patient in the laboratory. Metal rods are placed in the drill holes of the stone cast in order to hold drill sleeves which are polymerized into a resin surgical template. Oral implants are placed using the surgical template (Widmann et al. 2009c). Stereotactic aiming device-guided drillings on dental stone casts based on paired-point registration using an external registration frame connected to a modified VBH mouthpiece provided mean lateral errors of 0.4 ± 0.3 mm (maximum, 1 mm) (Widmann et al. 2005). Five tooth-supported surgical templates provided lateral errors on duplicated dental stone casts of 0.6 ± 0.4 mm (range 0.1–1.4 mm) on the implant base, 0.7 ± 0.4 mm (range 0–1.4 mm) on the implant tip, and angular errors of 1.7° ± 0.6° (range 0.7°–2.8°) (Widmann et al. 2009c). In edentulous cadavers, eight surgical templates supported on three fixed oral reference points provided lateral errors of 0.7 ± 0.5 mm (range 0–2 mm) on the

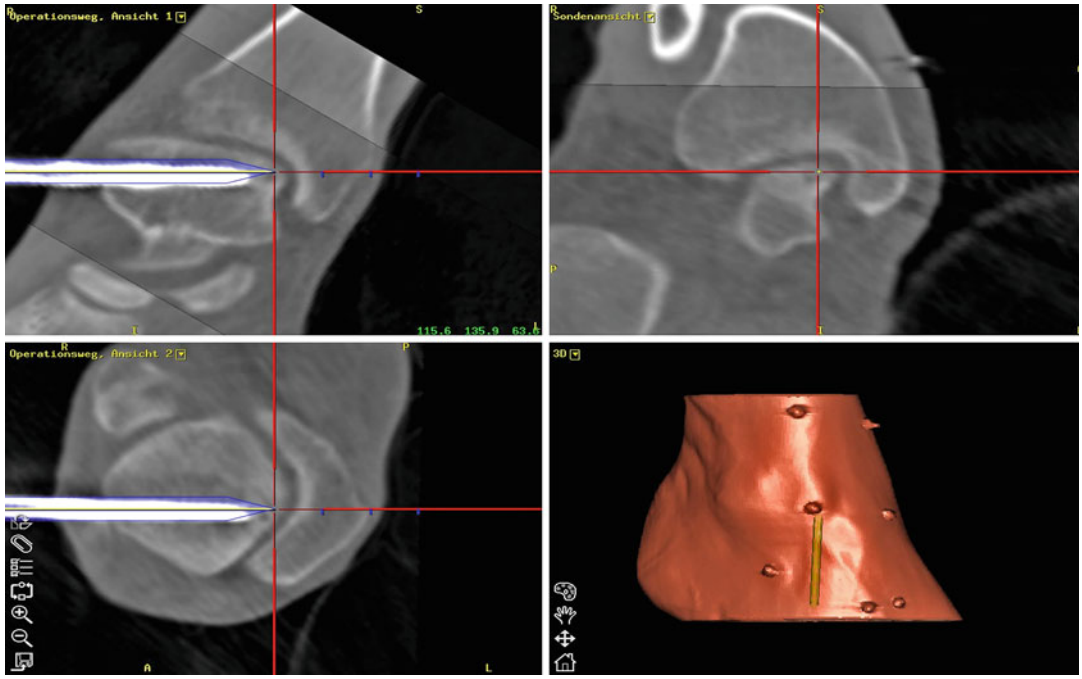

Fig. 7.8 Image fusion of surgical plan and the advanced bone needle 5 mm close to an osteochondral lesion of the medial talus dome. Trajectory 0° and 90° (*upper and lower left*), probe's eye view (*upper right*) and 3D view (*lower right*)

implant base, 0.9 ± 0.7 mm (range 0–3 mm) on the implant tip, and angular errors of 2.8° ± 2.2° (range 0.1°–9.2°) (Widmann et al. 2010d).

7.4 Complications

Navigated interventions include the following procedural errors (Grunert et al. 2002; Gralla et al. 2003; Mascott 2005; Mascott et al. 2006; Widmann et al. 2009b):

- *Patient fixation*: Movement in the time between image acquisition, registration, and puncture must be avoided. For interventions in the liver and lung respiratory gating may be necessary.
- *Planning*: The trajectories have to be planned in order to prevent violation of vital structures. For bone interventions, an orthogonal plan to the bone surface is favored to minimize the risk of needle/pin deviation.
- *Registration*: The registration process is one of the most crucial steps in three-dimensional navigation. It requires an optimal distribution and indication of the markers on the real patient as well as a precise definition of the markers on the virtual dataset. The registration accuracy has to be checked prior to navigation.
- *Navigation*: The aiming device has to be rigidly secured before advancement of the needle. The needle position has to be controlled prior to the actual intervention.

Interventional complications depend on the anatomical region and the type of procedure and are described in detail in each procedure-specific chapter.

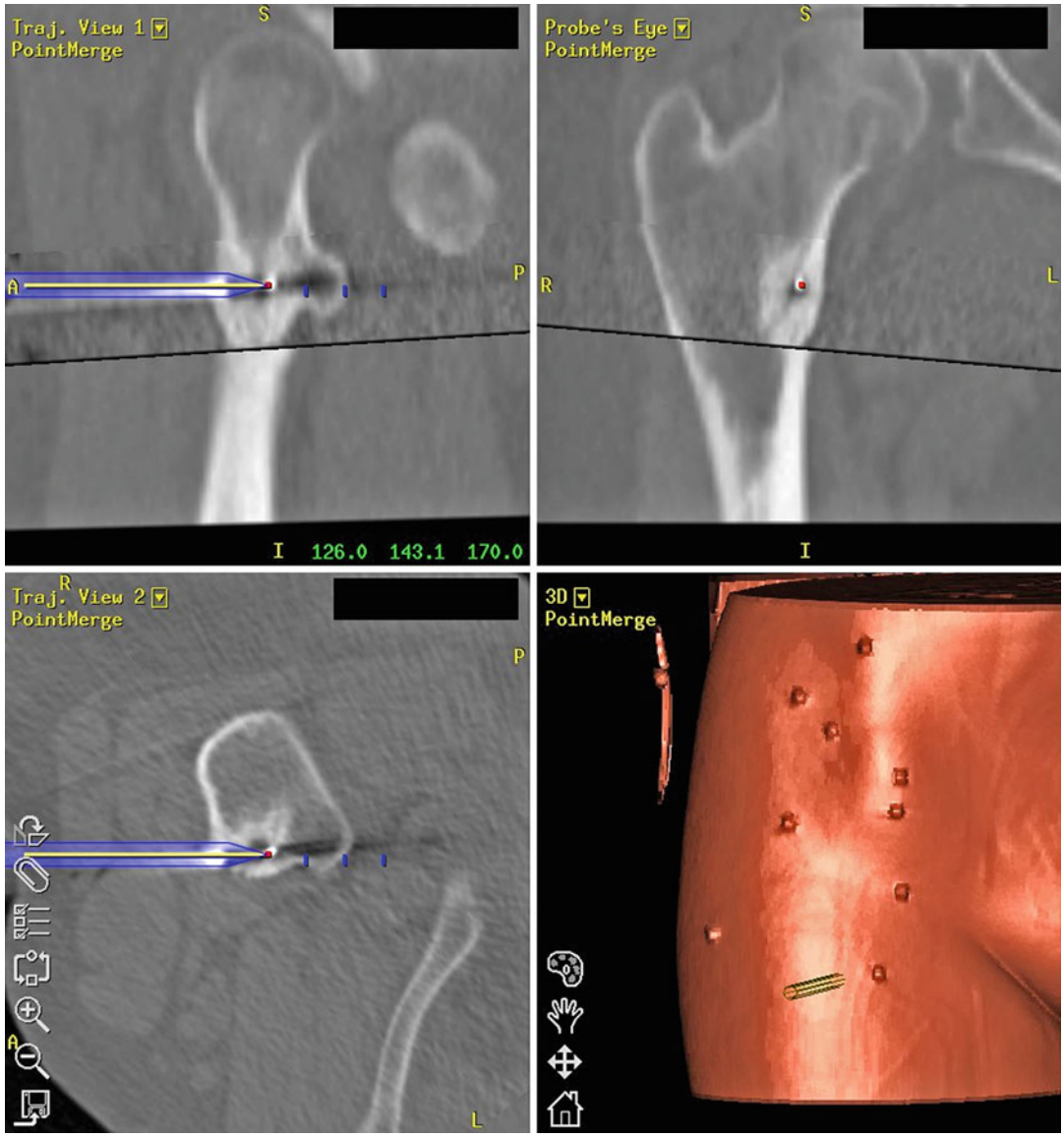

Fig. 7.9 Image fusion of surgical plan and the placed RF ablation probe in an osteoid osteoma of the femur. Trajectory 0° and 90° (*upper and lower left*), probe's eye view (*upper right*) and 3D view (*lower right*)

Summary

The spectrum of conventional CT- and MR-guided interventions is enlarged by navigated computer-assisted puncture techniques. Three-dimensionally guided puncture techniques provide a more sophisticated planning of the puncture path, because the puncture plane can be individually defined using a three-dimensional environment. Multimodal fusion imaging data for diagnostic and planning purposes in combination with fusion of postoperative data to the initial planning data improve the interventionalist's confidence. Rigid aiming devices enhance puncture accuracy and patient safety and reduce radiation dose and "room time." Based on the advantages of navigated interventions, including their multipurpose applicability, navigation systems may represent a valuable investment for an institution.

Key Points

- The interventionalist has to be aware of the relevant procedural steps:
  - Patient fixation
  - Imaging registration
  - Navigation
- The interventionalist also has to be aware of subsequent complications due to a three-dimensionally navigated approach.
- A check of the registration accuracy before navigation and a control CT scan to verify the correct needle placement are mandatory.

References

Bale R, Widmann G (2007) Navigated CT-guided interventions. Minim Invasive Ther Allied Technol 16: 16196–16204

Bale RJ, Vogele M, Martin A et al (1997) VBH head holder to improve frameless stereotactic brachytherapy of cranial tumors. Comput Aided Surg 2:286–291

Bale RJ, Vogele M, Rieger M et al (1999) A new vacuum device for extremity immobilization. AJR Am J Roentgenol 172:1093–1094

Bale RJ, Freysinger W, Gunkel AR et al (2000) Head and neck tumors: fractionated frameless stereotactic interstitial brachytherapy-initial experience. Radiology 214:591–595

Bale RJ, Hoser C, Rosenberger R et al (2001) Osteochondral lesions of the talus: computer-assisted retrograde drilling-feasibility and accuracy in initial experiences. Radiology 218:278–282

Bale RJ, Lottersberger C, Vogele M et al (2002) A novel vacuum device for extremity immobilisation during digital angiography: preliminary clinical experiences. Eur Radiol 12:2890–2894

Bale RJ, Laimer I, Martin A et al (2006) Frameless stereotactic cannulation of the foramen ovale for ablative treatment of trigeminal neuralgia. Neurosurgery 59:ONS394–ONS401

Bale RJ, Kovacs P, Dolati B, Hinterleithner C, Rosenberger RE (2008) Stereotactic CT-guided percutaneous stabilization of posterior pelvic ring fractures: a preclinical cadaver study. J Vasc Interv Radiol 19:1093–1098

Bale R, Widmann G, Stoffner DI (2010) Stereotaxy: breaking the limits of current radiofrequency ablation techniques. Eur J Radiol 75:32–36

Bale R, Widmann G, Haidu M (2011) Stereotactic radiofrequency ablation. Cardiovasc Intervent Radiol 34:852–856

Banovac F, Tang J, Xu S et al (2005) Precision targeting of liver lesions using a novel electromagnetic navigation device in physiologic phantom and swine. Med Phys 32:2698–2705

Birkfellner W, Watzinger F, Wanschitz F et al (1998) Systematic distortions in magnetic position digitizers. Med Phys 25:2242–2248

Bucholz RD, Ho HW, Rubin JP (1993) Variables affecting the accuracy of stereotactic localization using computerized tomography. J Neurosurg 79:667–673

Caversaccio M, Bachler R, Ladrach K et al (1999) The "Bernese" frameless optical computer aided surgery system. Comput Aided Surg 4:328–334

Dorward NL, Alberti O, Dijkstra A et al (1997) Clinical introduction of an adjustable rigid instrument holder for frameless stereotactic interventions. Comput Aided Surg 2:180–185

Dorward NL, Alberti O, Palmer JD et al (1999) Accuracy of true frameless stereotaxy: in vivo measurement and laboratory phantom studies. Technical note. J Neurosurg 90:160–168

Fitzpatrick JM, West JB, Maurer CR Jr (1998) Predicting error in rigid-body point-based registration. IEEE Trans Med Imaging 17:694–702

Gazelle GS, Goldberg SN, Solbiati L et al (2000) Tumor ablation with radio-frequency energy. Radiology 217:633–646

Germano IM, Queenan JV (1998) Clinical experience with intracranial brain needle biopsy using frameless surgical navigation. Comput Aided Surg 3:33–39

Goldberg SN, Gazelle GS, Compton CC et al (2000) Treatment of intrahepatic malignancy with radiofrequency ablation: radiologic-pathologic correlation. Cancer 88:2452–2463

Gralla J, Nimsky C, Buchfelder M et al (2003) Frameless stereotactic brain biopsy procedures using the Stealth Station: indications, accuracy and results. Zentralbl Neurochir 64:166–170

Grunert P, Espinosa J, Busert C et al (2002) Stereotactic biopsies guided by an optical navigation system: technique and clinical experience. Minim Invasive Neurosurg 45:11–15

Holloway KL, Gaede SE, Starr PA et al (2005) Frameless stereotaxy using bone fiducial markers for deep brain stimulation. J Neurosurg 103:404–413

Holzknecht N, Helmberger T, Schoepf UJ et al (2001) Evaluation of an electromagnetic virtual target system (CT-guide) for CT-guided interventions. Rofo 173: 12–618

Hummel JB, Bax MR, Figl ML et al (2005) Design and application of an assessment protocol for electromagnetic tracking systems. Med Phys 32:2371–2379

Hummel J, Figl M, Birkfellner W et al (2006) Evaluation of a new electromagnetic tracking system using a standardized assessment protocol. Phys Med Biol 51: N205–N210

Jacob AL, Messmer P, Kaim A et al (2000) A whole-body registration-free navigation system for image-guided surgery and interventional radiology. Invest Radiol 35:279–288

Khadem R, Yeh CC, Sadeghi-Tehrani M et al (2000) Comparative tracking error analysis of five different optical tracking systems. Comput Aided Surg 5: 98–107

Khan MF, Dogan S, Maataoui A et al (2006) Navigation-based needle puncture of a cadaver using a hybrid tracking navigational system. Invest Radiol 41:713–720

Maciunas RJ, Galloway RL Jr, Latimer JW (1994) The application accuracy of stereotactic frames. Neurosurgery 35:682–694

Marmulla R, Hilbert M, Niederdellmann H (1998) Intraoperative precision of mechanical, electromagnetic, infrared and laser-guided navigation systems in computer-assisted surgery. Mund Kiefer Gesichtschir 2(Suppl 1):S145–S148

Mascott CR (2005) Comparison of magnetic tracking and optical tracking by simultaneous use of two independent frameless stereotactic systems. Neurosurgery 57:295–301

Mascott CR, Sol JC, Bousquet P et al (2006) Quantification of true in vivo (application) accuracy in cranial image-guided surgery: influence of mode of patient registration. Neurosurgery 59:ONS146–ONS156

Maurer CR Jr, Maciunas RJ, Fitzpatrick JM (1998) Registration of head CT images to physical space using a weighted combination of points and surfaces. IEEE Trans Med Imaging 17:753–761

Nagel M, Schmidt G, Petzold R et al (2005) A navigation system for minimally invasive CT-guided interventions. Med Image Comput Comput Assist Interv 8:33–40

Ortler M, Trinka E, Dobesberger J et al (2010) Integration of multimodality imaging and surgical navigation in the management of patients with refractory epilepsy. A pilot study using a new minimally invasive reference and head-fixation system. Acta Neurochir (Wien) 152:365–378

Paleologos TS, Dorward NL, Wadley JP et al (2001) Clinical validation of true frameless stereotactic biopsy: analysis of the first 125 consecutive cases. Neurosurgery 49:830–835

Patel N, Sandeman D (1997) A simple trajectory guidance device that assists freehand and interactive image guided biopsy of small deep intracranial targets. Comput Aided Surg 2:186–192

Penzkofer T, Bruners P, Isfort P et al (2011) Free-hand CT-based electromagnetically guided interventions: accuracy, efficiency and dose usage. Minim Invasive Ther Allied Technol 20:226–233

Schiemann M, Killmann R, Kleen M et al (2004) Vascular guide wire navigation with a magnetic guidance system: experimental results in a phantom. Radiology 232:475–481

Wagner A, Schicho K, Birkfellner W et al (2002) Quantitative analysis of factors affecting intraoperative precision and stability of optoelectronic and electromagnetic tracking systems. Med Phys 29:905–912

West J, Fitzpatrick JM, Wang MY et al (1999) Retrospective intermodality registration techniques for images of the head: surface-based versus volume-based. IEEE Trans Med Imaging 18:144–150

Widmann G, Widmann R, Widmann E, Jaschke W, Bale RJ (2005) In vitro accuracy of a novel registration and targeting technique for image guided template production. Clin Oral Implants Res 16:502–508

Widmann G, Widmann R, Widmann E et al (2007) Use of surgical navigation systems for CT-guided template production. Int J Oral Maxillofac Implants 22:72–78

Widmann G, Bodner G, Bale R (2009a) Tumour ablation: technical aspects. Cancer Imaging 2(9 Spec No A): S63–S67

Widmann G, Stoffner R, Bale R (2009b) Errors and error management in image-guided craniomaxillofacial surgery. Oral Surg Oral Med Oral Pathol Oral Radiol Endod 107:701–715

Widmann G, Widmann R, Stoffner R et al (2009c) Multipurpose navigation system based concept for surgical template production. J Oral Maxillofac Surg 67:1113–1120

Widmann G, Pototschnig C, Bale R (2010a) Three-dimensionally navigated image-guided radiofrequency ablation in the head and neck. J Vasc Interv Radiol 21:165–166

Widmann G, Schullian P, Haidu M et al (2010b) Respiratory motion control for stereotactic and robotic liver interventions. Int J Med Robot 6:343–349

Widmann G, Keiler M, Zangerl A et al (2010c) Computer-assisted surgery in the edentulous jaw based on three

fixed intraoral reference points. J Oral Maxillofac Surg 68:1140–1147

Widmann G, Zangerl A, Keiler M et al (2010d) Flapless implant surgery in the edentulous jaw based on three fixed intraoral reference points and image-guided surgical templates: accuracy in human cadavers. Clin Oral Implants Res 21:835–841

Widmann G, Schullian P, Haidu M et al (2011) Targeting accuracy of CT-guided stereotaxy for radiofrequency ablation of liver tumours. Minim Invasive Ther Allied Technol 20:218–225

Wood BJ, Zhang H, Durrani A et al (2005) Navigation with electromagnetic tracking for interventional radiology procedures: a feasibility study. J Vasc Interv Radiol 16: 493–505

Wood BJ, Locklin JK, Viswanathan A et al (2007) Technologies for guidance of radiofrequency ablation in the multimodality interventional suite of the future. J Vasc Interv Radiol 18:9–24

Zhang H, Banovac F, Lin R et al (2006a) Electromagnetic tracking for abdominal interventions in computer aided surgery. Comput Aided Surg 11:127–136

Zhang X, Zheng G, Langlotz F et al (2006b) Assessment of spline-based 2D-3D registration for image-guided spine surgery. Minim Invasive Ther Allied Technol 15:193–199

Special Considerations for Image-Guided Interventions in Pediatric Patients

8

Dagmar Honnef

Contents

8.1 Introduction

Image-guided interventions are increasingly gaining importance in clinical routine practice. These include minimally invasive diagnostic procedures as well as percutaneous therapeutic interventions. Generally speaking, percutaneous interventions are less invasive than surgical procedures and should be considered whenever possible, particularly in patients in whom resection of the primary tumor is not intended or possible. Compared with interventional procedures in adults, several specific features have to be taken into account for image-guided interventions in pediatric patients. Children need special care, and they suffer from other diseases than grown-up patients. Proper physician training is imperative to provide the necessary confidence and expertise. In general, ultrasound and magnetic resonance (MR) imaging guidance should be preferred whenever possible, because unlike computed tomography (CT)-guided interventions, they are not associated with radiation exposure. In this chapter, special considerations for image-guided interventions in pediatric patients are presented.

8.2 Materials and Techniques

8.2.1 Preparation

Prior to any interventional procedure or a CT scan, clinical justification has to be ensured. Whenever possible the interventional radiologist

D. Honnef
Department of Diagnostic and Interventional Neuroradiology, University Hospital, RWTH Aachen University, Pauwelsstrasse 30, Aachen D-52074, Germany
e-mail: dhonnef@ukaachen.de

A.H. Mahnken et al. (eds.), *CT- and MR-Guided Interventions in Radiology*,
DOI 10.1007/978-3-642-33581-5_8,

who performs the procedure should talk to the parents and obtain parental consent. Antibiotics may be given prior to nephrostomy and abscess drainage or biliary procedures (Table 8.1). However, the findings of controlled studies dealing with preinterventional antibiotic treatment in children have not been published yet. The use of sedative protocols depends on the complexity of the intervention, the experience of the physician, as well as the capability of the patient to cooperate. Owing to the lack of cooperation or limited ability to cooperate, procedures are often performed with the patient under analgesic sedation or total intravenous anesthesia provided by an experienced physician (see Chap. 5). In addition, local anesthesia should be used to minimize depth of sedation during the procedure as well as postinterventional local pain.

It is recommended to perform lung biopsies in tracheal intubation and controlled ventilation because of potential complications (Bendon et al. 2005). The most common are pneumothorax and hemoptysis. Intubation helps to detect hemoptysis early and allows for effective suctioning. Furthermore, it aids in achieving a more reliable needle positioning and results in fewer complications and higher diagnostic accuracy (Bendon et al. 2005). In patients with hepatic or renal failure, general anesthesia should be preferred to analgesic sedation owing to the risk of drug toxicity, hypotension, respiratory depression, and prolonged sedation (Kaye et al. 2000). Compared with adults, the surface area to body volume ratio is higher in children, which causes the child to cool down more rapidly. To prevent hypothermia especially in small children, it is recommended to use blankets during the procedure. In thoracic and abdominal imaging, the arms should be elevated as they can cause artifacts. Furthermore, irradiation of the arms should be avoided as red bone marrow is located in the extremities. Therefore, in sedated patients it might be necessary to tape the arms in this position.

Oral contrast medium application is usually not necessary but may be helpful for detecting inter-enteric lesions. Diluted nonionic, low-osmolarity contrast media should be used to obviate electrolytes shift (1.5 % diluted: baby 100 ml, infant 200–300 ml, schoolchild 300–500 ml) (Honnef et al. 2004). Orally administered contrast medium also helps to avoid accidental bowel injury by mistaking the bowel for the target lesion. Depending on localization and tissue contrast, contrast medium may be applied intravenously (1–2.0 ml 300-mg/ml iodine/kg body weight).

8.2.2 Computed Tomography

Minimizing radiation exposure in CT examinations is crucial as children are more sensitive to X-rays than adults (Brenner et al. 2001). Regarding dose minimization, sequential scanning is superior to spiral data acquisition. A further tube voltage and/or tube current reduction compared with the levels used in pediatric diagnostic CT studies should be performed (Honnef et al. 2004, 2007; Siegel et al. 2004; Vock 2005). A standard CT protocol cannot be provided as the degree of radiation dose reduction depends on several factors, such as body region, tissue contrast, and lesion size. For large lesions, a lower image quality can be accepted with consequently increased dose reduction. A smaller dose decrease may be achieved in small lesions. Usually 80- or 100-kVp protocols should be used. The effective dose is determined by several factors, such as scan length, slice thickness, number of scans, collimation, pitch, and type of CT scanner. These factors have to be optimized for each procedure. Particularly slice thickness and collimation have to be adapted to needle and lesion size. Generally, submillimeter collimation should be avoided, as it is less dose-efficient than a thicker collimation. Additional gonad shielding is recommended in male patients (Hohl et al. 2005). Different computer software systems are available for estimating the radiation dose applied (Nagel et al. 2004).

8.2.3 Magnetic Resonance Imaging

There are only few publications dealing with MR-guided interventions in children (Schulz et al. 2003, 2005). At the moment, this technique is mainly used for neurosurgical procedures. MR imaging is in particular applicable to tumors,

Table 8.1 Suggestions for medication for interventional procedures

Indication	Pathogen	Antibiotics	Age	Dose in 24 h (mg/kg body weight)	Single dose
Spondylodiscitis	*Staphylococcus aureus*	Cefuroxime or cefotiam or flucloxacillin	<12 years 3–12 months 1–12 years	150–200 mg i.v. 40–100 mg i.v. 3–8 g i.v.	3 mg 3–4 mg 3–4 mg
Lung abscess	*S. aureus*	Cefuroxime or cefotiam			
Liver abscess	*Entamoeba histolytica*	Metronidazol Tinidazol	<12 years 6–12 years	30 mg i.v. or p.o.	3 mg
	Escherichia coli	Ampicillin + aminoglycoside + metronidazol		30 mg p.o.	
Abscess due to appendicitis	*E. coli*, *Streptococcus*	Cefuroxime or cefotiam and metronidazol	<12 years <12 years	75–150 mg i.v. 15–30 mg i.v.	3 mg 3 mg
Preinterventional					
Urologic system	*E. coli*, *Staphylococcus*	Cefuroxime or cefotiam or aminopenicillin + β-lactamase-inhibitor	<12 years	50 mg i.v.	1 mg
Biliary system	*E. coli*, *Streptococcus*	Cefuroxime or cefotiam or ampicillin + sulbactam	<12 years 1–12 years	50 mg i.v. 50 mg i.v.	1 mg 1 mg
Bone	*S. aureus*, *Staphylococcus epidermidis*	Clindamycin[a]	<12 years	10 mg i.v.	1 mg

Dosage and selection of antibiotics should be discussed with the referring pediatrician. Special considerations may be necessary in immunoincompetent children or patients with heart diseases. The data provided on medication have been adapted to body weight

[a]Clindamycin penetrates the bone

which are ill defined by ultrasound and CT as MR imaging provides an excellent soft-tissue contrast. It is especially useful in localizing bone marrow edema, for example, caused by medullar metastasis in Ewing's sarcoma (Schulz et al. 2003). Compared with CT, the major advantage is the lack of radiation exposure, but it is not known yet what effects exposure to the magnetic field in prolonged MR examinations may have on the pediatric body. Disadvantages of MR guidance include increased procedure duration with longer anesthesia time and higher costs as well as the limited number of open MR scanners with easy access to the patient. In general, better image quality due to fewer field inhomogeneities can be achieved with closed-bore MR-systems. These, however, hamper the access to the patient. At the moment, there are only a few MR-compatible biopsy instruments available (Schulz et al. 2003), and especially in small lesions (less than 1 cm), susceptibility artifacts may complicate the instrumentation (Lewin et al. 1998). The latter is more obvious with 1.5-T than with 0.5-T MR scanners. Spin-echo sequences should be preferred to minimize susceptibility artifacts. So far, MR guidance is not considered a reliable method in thoracic biopsies (Adam et al. 1999).

8.2.4 Biopsy

Percutaneous biopsy is suited to prove the structure of most lesions. It is mandatory prior to any radiation therapy or chemotherapy. The only exception in pediatric patients is suspected malignancy in large cartilaginous tumors, because malignant transformed large cartilaginous tumors typically contain large benign parts.

The choice of the biopsy needle depends on the access, further underlying diseases (e.g., coagulopathy, lung emphysema), and lesion size. Furthermore, the assumed tumor entity has to be considered because for differentiation of pediatric tumors (small, round, or blue cell), immunohistochemical, molecular pathological, and cytogenetic analysis have to be done apart from histologic analysis. These complex analyses require a certain amount of tissue, which results in the need for a core biopsy (Hoffer 2005). Many needles are available with selectable throw lengths. These should be adapted to the individual lesion size and localization.

Fine-needle biopsy is only justified in recurrent tumors, if there is malignancy or if a sample for microbiological analysis is obtained. For aspiration of fluid collections, 22 G needles are generally adequate in neonates (Coley and Hogan 2006). Particular care has to be taken in bone biopsy. In this case, sterility has to be guaranteed to avoid osteomyelitis.

8.2.5 Localization Techniques

Typical indications for preoperative lesion localization are unsuccessful pulmonary biopsies or very small, not palpable, or difficult-to-access lesions. It may also be used prior to resection of extrapulmonary lesions (Fig. 8.1). To minimize the surgical trauma, the puncture point of the needle should be agreed with the surgeon. The most common technique is the needle placement of a hookwire. An alternative method has been described by McConnell et al. (2002). They used a mixture containing 3-ml autologous blood stained with 0.3 ml methylene blue for CT-guided localization of pulmonary nodules prior to video-assisted thoracoscopic resection. Patrick et al. (2002) applied – also in children – methylene blue

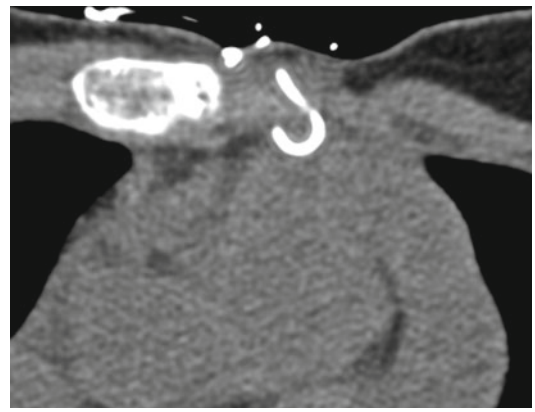

Fig. 8.1 Preoperative hookwire localization in a 17-year-old girl with Hodgkin's disease and positron emission tomography positive rest tumor in the anterior mediastinum (120 kVp, 110 mA $s_{eff.}$)

(0.2–0.5 ml) within the pulmonary parenchyma just beneath the pleura overlying the nodule.

8.2.6 Drainage

The choice of the drainage catheter size depends on the expected content of a fluid collection. A catheter size of 8.5 F is adequate for drainage of most fluid collections in pediatric patients (Cahill et al. 2005; Gobien et al. 1985) (Fig. 8.2). Even in pasty abscesses, clogging is virtually never observed with this catheter size. For drainage in neonates, 5- or 6-F catheters are recommended, because of the small body size (Coley and Hogan 2006). A small pigtail loop should be used in small fluid collections or neonatal kidneys. When compared with adults, tissue elasticity in children is much greater, and catheter insertion, especially at the abscess wall, may be difficult (Gervais et al. 2004). This problem can be overcome by use of a dilatator prior to final catheter placement. Thrombolytic substances such as streptokinase (120 000 IU) or tissue plasminogen activator (2–10 mg) may be used in addition to saline instillation (Gervais et al. 2004; Kilic et al. 2002). They should be kept for 20–30 min in the abscess and then be allowed to drain. To date, doses of thrombolytic substances have not been standardized. The volume of normal saline should be adjusted to the size of the abscess. The volume applied should be less than the amount of fluid removed. Otherwise, the abscess could be under pressure and cause sepsis. Aspiration may be sufficient only if the abscess is small (Hoffer et al. 1999) or if aspiration does not show any ichor (Cahill et al. 2005). Intravenous administration of antibiotics should always be done (Table 8.1).

Indications for nephrostomy include postoperative or congenital obstruction, massive vesicoureteral reflux, or congenital bladder problems as well as renal infection or postinterventional situations (Riccabona et al. 2002). This procedure is usually performed under ultrasound guidance (Riccabona et al. 2002), and CT or MR guidance should only be chosen if the procedure cannot be completed with ultrasound guidance.

Transgluteal as well as transabdominal and transrectal approaches have been described in pelvic drainages in infants (Cahill et al. 2005; Chung et al. 1996; Gervais et al. 2004; Jamieson et al. 1997; Pereira et al. 1996). Transrectal drainages should be performed only if it is certain that the fluid collection is infected as the approach will not be sterile. Catheter placement in interenteric abscesses should be done using the Seldinger technique with use of a 19–22 G needle, avoiding the colon (Gervais et al. 2004). Infected tumors may also be drained (Gervais et al. 2004).

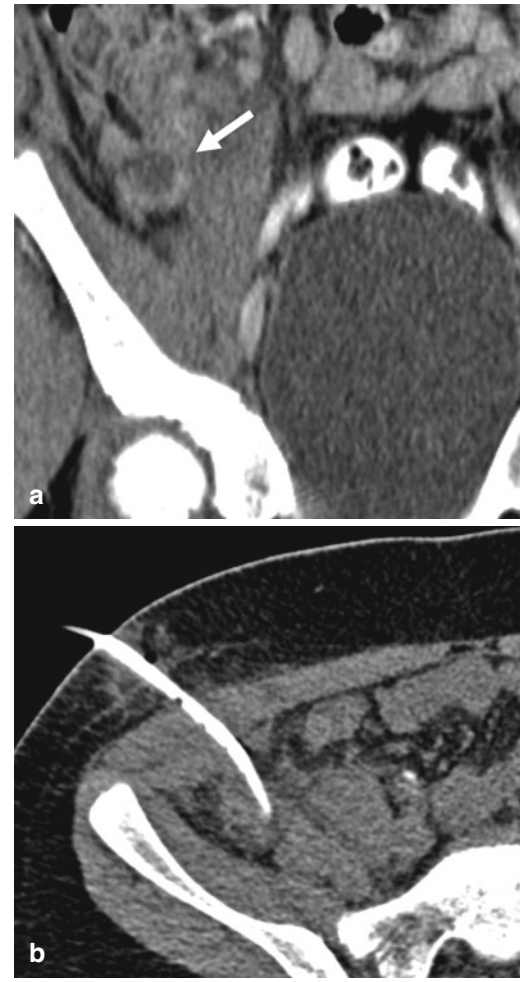

Fig. 8.2 Preinterventional computed tomography (CT; 100 kVp, 75 mA s_{eff}) in a 12-year-old boy after appendectomy. Coronal multiplanar reformation demonstrates an abscess in the right lower abdomen (**a**; *arrow*). After successful placement of an 8.5-F drainage catheter using the trocar technique (**b**), the abscess completely resolved within 8 days, proving the success of the interventional procedure

8.2.7 Other Therapeutic Procedures

Aneurysmal bone cysts can be treated with injection of Ethibloc (Ethnor Laboratories, Ethicon, Norderstedt, Germany). The cyst is localized with a fine needle (21–22 G) using CT guidance (Garg et al. 2000). Thereafter, a larger needle (16 G) is inserted into the cyst, and aspiration of blood proves the diagnosis. Before the injection of Ethibloc, contrast medium should be injected to ensure the intracavitary location of the needle and to exclude leakage into the soft tissues.

Finally 4–8 ml Ethibloc is injected, depending on the size of the cyst (Garg et al. 2000). Ethibloc prevents cyst growth and induces endosteal new bone formation. Particularly in septated cysts, it is important to reach all parts of the cyst to avoid local recurrence. Antibiotics should be prescribed (Table 8.1). It is recommended to perform a follow-up CT or MR scan after 6 months and a further reassessment after 12 months (Garg et al. 2000). Ethibloc should not be used in spinal lesions because of the possibility of leakage into the adjacent tissues or spinal vessels and potential paraplegia.

CT-guided intra-articular corticosteroid injection into inflammatory sacroiliac joints may be performed in patients with juvenile spondyloarthropathy who did not respond to oral nonsteroidal anti-inflammatory drugs. In these patients, intra-articular injection of 40-mg corticosteroid (e.g., triamcinolone) is a viable treatment option in children (Fischer et al. 2003).

Radiofrequency ablation is regularly performed in pediatric patients suffering from osteoid osteoma (Cioni et al. 2004; Mahnken et al. 2006). Successful radiofrequency ablation of a small number of benign cartilaginous tumors in children has also been reported (Erickson et al. 2001; Ramnath et al. 2002). Unfortunately, there is no dedicated material available for pediatric radiofrequency ablation. Particularly shorter radiofrequency probes, which may be more appropriate for smaller pediatric patients, are not available (Brown and van Sonnenberg 2007). Further application of radiofrequency in children in the future may be for incurable painful bone metastasis as in osteosarcoma or Ewing's sarcoma. Radiofrequency ablation is also a therapeutic option in selected patients suffering from nephroblastoma (Brown et al. 2005). Hypothetically, hyperthermia may occur in children, owing to a higher heat delivery relative to a smaller body volume when compared to adults (Brown et al. 2005). A combined CT-guided radiofrequency therapy and brachytherapy was used in a child with multiple recurrences of Wilms tumor (Ghandi et al. 2005). These strategies may be considered to obviate dialysis after nephrectomy. So far there exists no information on the long-term outcome of these therapeutic approaches.

Neurolysis is performed in the same technical way as in adults. Percutaneous celiac plexus block has been used in chronic pain refractory to medication due to chronic inflammatory bowel disease and several small-bowel resections (Tanelian and Cousins 1989) as well as upper abdominal malignancies (Berde et al. 1990; Staats and Kost-Byerly 1995).

Reflex sympathetic dystrophy or sympathetically maintained pain syndrome is another indication for image-guided neurolysis. It is a rare condition in children and differs from the adult form as it has a distinct female predilection; lower limb involvement is preferred and runs a relatively benign course. In these pediatric patients, CT- or MR-guided lumbar sympathetic block can also be applied successfully (Nordmann et al. 2006) (Fig. 8.3). In children, a permanent neurolysis

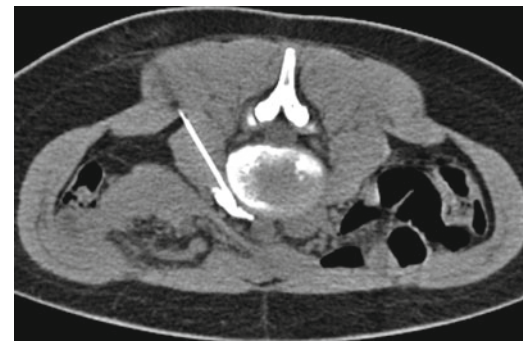

Fig. 8.3 A 16-year-old girl suffering from reflex sympathetic dystrophy of the left foot. For CT-guided (100 kVp, 50 mA $s_{eff.}$) left lumbar sympathicolysis 15-ml bupivacaine mixed with 0.5 ml contrast material for visualization of the fluid distribution was injected paraaortally at the level of lumbar vertebra 3. Immediately after the injection, the patient described a warm feeling in the foot, and the perfusion improved as could be seen by the change of the skin color of the foot. The procedure was repeated six times until the problems resolved permanently

should be avoided and never be used in the first place, even if this results in repeated interventions.

8.3 Results

8.3.1 Biopsy

Comparing fine-needle with cutting biopsies, the latter led to a significantly higher rate of specific diagnosis (83.7 vs. 38.9 %) with the same complication rate (Guimaraes et al. 2003). In 75 CT-guided lung biopsies in children, 56 coaxial core biopsies and 15 fine-needle aspiration biopsies or both ($n=4$) were performed with a major complication rate of 1.3 %. Of these biopsies, 85 % were diagnostic (Cahill et al. 2004). Even in small pulmonary nodules (0.5–2.0 cm), adequate cores could be obtained in 83 % of cases (Connolly et al. 1999). Open lung biopsy is still considered the gold standard in interstitial lung diseases, but core biopsies were also successfully applied in children (Heyer et al. 2005; Wilkinson et al. 1999). Specificity and sensitivity of 100 % was achieved in invasive aspergillosis with core biopsy; however, this was associated with a 46 % complication rate due to bleeding (Hoffer et al. 2001). In contrast to adults, hemoptysis as a complication of lung biopsies can be life-threatening in children, because it can lead to significant hypovolemia (Bendon et al. 2005).

Mediastinal biopsies, mainly spring-loaded core biopsies, showed 75 % sensitivity and 100 % specificity in children with suspected Hodgkin's disease or non-Hodgkin lymphoma (Garrett et al. 2002). Aspiration of fluid collections in non-Hodgkin lymphoma or leukemia is often sufficient for diagnosis and should be preferred as it is less invasive (Garrett et al. 2002).

In 90 pediatric abdominal biopsies, the results for the core biopsy were significantly better than for the fine-needle biopsy with a comparable complication rate (Hugosson et al. 1999). A sensitivity of 89.6 % and specificity of 100 % in 202 core biopsies (15 or 18 G) of solid pediatric tumors were reported (Garrett et al. 2005). Another study comparing fine-needle and core biopsy in solid tumors showed fewer differences regarding diagnostic accuracy (Sklair-Levy et al. 2001). However, in all studies fine-needle biopsy has been shown to limit the differentiation of nephroblastomatosis from nephroblastoma. Besides histologic information, percutaneous core biopsy provided additional genetic information (N-myc gene expression status, DNA Index) in up to 95 % of cases with advanced neuroblastomas (Hoffer et al. 1996). According to the United Kingdom Children's Cancer Study Group (UKCCSG) Wilms Tumor Study three, a needle biopsy of any renal mass prior to initiation of chemotherapy is recommended (Vujani et al. 2003). In 12 % of these patients with clinically and radiologically suspected Wilms tumor, cutting needle biopsy revealed a different tumor entity. In predominantly retroperitoneal punctures, 88 % of the diagnoses were correct after core biopsy (14 or 18 G) (Hussain et al. 2001). This result was confirmed in another series (Skoldenberg et al. 2002).

Diagnostic biopsies of solid tumors have resulted in a reported complication rate of 13.4 %, with bleeding as the most common complication (Garrett et al. 2005). In percutaneous renal core biopsies in children, subcapsular hematomas were observed in up to 16 % of the patients (Feneberg et al. 1998).

Percutaneous musculoskeletal biopsies are also feasible, accurate, and safe in children (Shin et al. 2007). The diagnostic success of biopsy in primary malignant tumors was significantly higher (92 %) than in primary benign tumors (65 %; $p=0.008$) (Shin et al. 2007). Biopsy could confirm osteosarcoma in up to 94 % of cases (Ahrar et al. 2004). In malignant bone tumors, passive dissemination of tumor cells from the bone biopsy site necessitates resection of the puncture tracts; therefore, the access course should be discussed with the surgeon in advance. If there is no doubt of malignancy prior to biopsy, open surgery may be appropriate. Shin et al. (2007) demonstrated that 76 % of core needle biopsies of musculoskeletal lesions were successful in children. The diagnostic success of biopsy in primary malignant tumors was 92 % compared with 65 % in primary benign tumors. Minor complications of 4.7 % occurred from the biopsies.

In children, spondylodiscitis is mainly due to hematogenous infection with *Staphylococcus*

aureus as the intervertebral discs are vascularized (Early et al. 2003). In spondylodiscitis either a fine-needle aspiration of an abscess formation or a core biopsy of the intervertebral disc or paravertebral granulation tissue is performed for microbiological analysis. Bacterial specimens can be found in up to 40 % of such pediatric cases (Ventura et al. 1996); therefore, samples should only be taken in patients with suspected tuberculosis or fungal disease or in children who do not respond to intravenous antibiotic therapy or who suffer from chronic inflammation (Early et al. 2003; Ventura et al. 1996).

8.3.2 Localization Techniques

Until now large series on pulmonary needle localization in children have not been reported in the literature (Hardaway et al. 2000; Waldhausen et al. 1997). Smith et al. (1996) found needle localization to be superior to intraoperative ultrasound during video-assisted thoracoscopic surgery because sonography may fail to detect superficially located lesions. As shown by Hardaway et al. (2000), one can also use hookwire localization in any other region of the body (Fig. 8.1). Successful MR-guided musculoskeletal tumor marking has been reported too (Schulz et al. 2005). Alternative techniques to preoperatively localize pulmonary nodules with methylene blue are also safe and effective especially in children with pulmonary nodules smaller than 1 cm (McConnell et al. 2002; Patrick et al. 2002).

McConnell et al. (2002) reported that 19 procedures performed in 17 children were diagnostic and 80 % demonstrated malignancy. In one patient, video-assisted thoracoscopic surgery had to be converted to open thoracotomy because of malfunction of the endoscopic stapler. In another study (Patrick et al. 2002) 13 procedures were completed successfully thoracoscopically. No thoracotomies were performed, and no complications occurred.

8.3.3 Drainage

The success rate of image-guided percutaneous thoracic drainage with catheters is superior to that of aspiration alone (Margau et al. 2006). In 58 children with parapneumonic effusion and empyema, complete resolution was achieved in 54 patients without mortality or 30-day recurrence after percutaneous intrapleural catheter placement with additional instillation of tissue plasminogen activator (Hawkins et al. 2004). Intrapleural fibrinolytic treatment with urokinase or streptokinase was effective in 80 % of infants with pleural empyema after insufficient tube thoracostomy and intravenous administration of antibiotics (Kilic et al. 2002). In one study with 60 children suffering from pleural empyema, the dose of urokinase used was 40,000 units in 40-ml saline for children aged 1 year and above; for children under age 1, 10,000 units in 10 ml were used. This dose was administered twice per day for 3 days (Thomson et al. 2002). An uncommon side effect of fibrinolysis is bleeding. A flow chart for treatment of childhood empyema based on current literature and local medical and surgical expertise is given by Proesmans and coworkers (Proesmans and De Boeck 2009).

It is reported that 80–90 % of small pulmonary abscesses can be cured with antibiotics alone (Klein and Zarka 2000). But aspiration of abscess fluid and microbiological analysis helps to perform targeted antibiotic therapy. Aspiration is only sufficient in lung abscesses with a volume below 15 ml (Hoffer et al. 1999). On the basis of the results of Hoffer et al. (1999), catheter drainage should be performed in lung abscesses with a volume of 20 ml or more or with an inner diameter of 3 cm. However, one has to consider the complication of a pleural empyema. Although interventional therapy provides diagnostic and therapeutic approaches toward lung abscesses, it is less effective in necrotizing pneumonia with complications such as bronchopleural fistula, pneumatocele, and persistent pneumothorax (Hoffer et al. 1999). Preoperative drainage of congenital cystic adenomatoid malformation may be considered in children with respiratory insufficiency (Margau et al. 2006).

The most common abdominal fluid collections requiring percutaneous aspiration and/or drainage are appendical and other abscesses (McCann et al. 2008) and cerebrospinal fluid collections in children with ventriculoperitoneal shunts (Coley et al. 2004).

Liver abscesses are relatively uncommon in developed countries (Mishra et al. 2010). *Staphylococcus aureus* is the most common pathogen worldwide. Percutaneous drainage along with antimicrobial drug therapy is widely accepted as adequate treatment in most cases.

Renal abscesses are often caused by vesicoureteral reflux. Small renal abscesses resolve with antibiotic treatment alone, whereas larger ones can be successfully drained (Wippermann et al. 1991). In xanthogranulomatous pyelonephritis, an uncommon chronic, inflammatory disease, percutaneous drainage of the abscess and adjunctive antibiotic therapy prior to nephrectomy is recommended to avoid complications (Bingöl-Kologlu et al. 2002).

The transgluteal approach to the drainage of pelvic fluid collections with image guidance has proven to be safe and effective (Cahill et al. 2005). Abscess recurrence is found in less than 5 % of pediatric patients after successful drainage (Gervais et al. 2004). Ninety-one percent of children suffering from appendiceal abscess could successfully be treated with an image-guided drainage and intravenous antibiotics (Jamieson et al. 1997) (Fig. 8.2). Other authors report a success rate of up to 93 % with a transrectal approach (Koral et al. 2010). Low-density tumors may be mistaken for an abscess. This should be considered in cases of minimal fluid drainage and little change in the appearance of the lesion (Gervais et al. 2004). Percutaneous abscess drainage is considered as a valuable procedure in pediatric patients with Crohn's disease presenting with pelvic and/or abdominal abscesses because it is less invasive and facilitates subsequent surgery (Rypens et al. 2007). Drainage is recommended prior to definitive treatment, and complications such as enterocutaneous fistulas are rare.

Intramuscular abscess is very rare in children. In a series of 18 children, drainage of a psoas abscess proved to be a valuable alternative to surgery (Belgith et al. 2003). This procedure is also feasible in obturator muscle abscess (Orlicek et al. 2001). Absolute recommendations to guide the duration of antibiotic treatment in childhood spondylodiscitis have not been published. Parenteral antibiotics should be given between 4 and 6 weeks, followed by oral antibiotics for 1–2 weeks (Early et al. 2003) (Table 8.1). Most children improve rapidly with a 4–6-week course of antibiotics (Kayser et al. 2005). Conservative treatment is usually sufficient in spondylodiscitis with paravertebral fluid collection; however, drainage may be necessary if clinical improvement cannot be assessed (Brown et al. 2001; Garron et al. 2002). An increase of complex, subcutaneous abscesses in the pediatric population is caused by methicillin-resistant *Staphylococcus aureus* (Ladd et al. 2010), which can be treated with image-guided procedures.

8.3.4 Other Therapeutic Interventions

Percutaneous Ethibloc injection in aneurysmal bone cysts, mainly localized at the extremities, showed complete resolution of the lesions in 70 % of patients (Garg et al. 2000); therefore, it can be an alternative to surgery (Cottalorda and Bourelle 2006). Pathologic fracture, local inflammation, and flulike illness are known complications of the procedure.

Intra-articular corticosteroid injection was effective in 87.5 % of patients with juvenile spondyloarthropathy who were not responding to nonsteroidal anti-inflammatory drugs. These patients showed a significant decrease in their subjective complaints (Fischer et al. 2003). Improvement was seen about 1–2 weeks later and lasted for a mean of 12 months.

Summary

In the last few years, there has been increasing interest in percutaneous image-guided interventions in children. Many interventions can be performed with ultrasound guidance, but CT- or MR-guided procedures may be needed in selected cases. Considering justified indications and correct performance of the procedures, CT- and MR-guided interventions in infants are feasible with limited risks. Apart from diagnostic procedures, therapeutic interventions (drainage, injection therapies, neurolysis, and radiofrequency ablation) are also successfully

applicable in children and may help to avoid surgery. However, the published data are very heterogeneous as different localizations (e.g., chest, abdomen), tumor entities, patient ages (adults and children), interventional instruments, and imaging modalities are used.

Key Points

- CT- or MR-guided interventional techniques used in adults can also be applied in children, but some special considerations have to be taken into account. Sedation or total intravenous anesthesia is more often necessary, because of limited cooperation. An additional local anesthesia is always recommended. Lung biopsies should be performed in tracheal intubation and controlled ventilation. Open lung biopsy is still considered the gold standard in interstitial lung diseases. In contrast to adults, hemoptysis as a complication of lung biopsies can be life-threatening in children because it can lead to significant hypovolemia. Aspiration of fluid collections in non-Hodgkin lymphoma or leukemia is often sufficient for diagnosis and should be preferred as it is less invasive. Depending on localization and tissue contrast, intravenous contrast media may be applied in CT examinations (1–1.5-mg iodine/kg body weight). Decrease of radiation exposure in CT examinations is essential (sequential scanning, tube voltage, and/or tube current reduction). Shielding may be applied. MR imaging is the preferred modality in biopsies of bone marrow abnormalities. However, small lesions (less than 1 cm) may not be visible owing to susceptibility artifacts. In pediatric small, round, or blue cell tumors, core biopsy is needed to gain additional genetic information.
- A drainage catheter size of 8.5 F is adequate for drainage of most fluid collections in pediatric patients. Thrombolytic substances may be used. Catheter drainage should be considered in lung abscesses with a volume of 20 ml or more or with an inner diameter of 3 cm. For neonatal drainages, 5- or 6-F catheters are recommended. Owing to high-tissue elasticity, insertion of a dilatator or catheter may be difficult.
- Conservative treatment is usually sufficient in spondylodiscitis with paravertebral fluid collection. Samples should only be taken in patients with suspected tuberculosis or fungal disease or in children who do not respond to intravenous antibiotic therapy or who suffer from a chronic course. Intraarticular corticosteroid injection is effective in juvenile spondyloarthropathy.
- Permanent neurolysis in children should not be used in the first place.

References

Adam G, Bücker A, Nolte-Ernsting C et al (1999) Interventional MR-imaging: percutaneous abdominal and skeletal biopsies and drainages of the abdomen. Eur Radiol 9:1471–1478

Ahrar K, Himmerich JU, Herzog CE et al (2004) Percutaneous ultrasound-guided biopsy in the definitive diagnosis of osteosarcoma. J Vasc Interv Radiol 15: 1329–1333

Belgith M, Ben Brahim M, Jouini R et al (2003) Psoas abscess in children based on a series of 18 cases. Prog Urol 13:1372–1375

Bendon AA, Krishnan BS, Korula G (2005) CT-guided lung biopsies in children: anesthesia management and complications. Paediatr Anaesth 15:321–324

Berde CB, Sethna NF, Fisher DE et al (1990) Celiac plexus blockade for a 3-year-old boy with hepatoblastoma and refractory pain. Pediatrics 86:779–781

Bingöl-Kologlu M, Ciftci AO, Senocak ME et al (2002) Xanthogranulomatous pyelonephritis in children: diagnostic and therapeutic aspects. Eur J Pediatr Surg 12:42–48

Brenner D, Elliston C, Hall E et al (2001) Estimated risks of radiation-induced fatal cancer from pediatric CT. AJR Am J Roentgenol 176:289–296

Brown SD, van Sonnenberg E (2007) Issues in imaging-guided tumor ablation in children versus adults. AJR Am J Roentgenol 189:626–632

Brown R, Hussain M, McHugh K et al (2001) Discitis in young children. J Bone Joint Surg Br 83:106–111

Brown SD, van Sonnenberg E, Morrison PR et al (2005) CT-guided radiofrequency ablation of pediatric Wilms tumor in a solitary kidney. Pediatr Radiol 35:923–928

Cahill AM, Baskin KM, Kaye RD et al (2004) CT-guided percutaneous lung biopsy in children. J Vasc Interv Radiol 15:955–960

Cahill AM, Baskin KM, Kaye RD et al (2005) Transgluteal approach for draining pelvic fluid collections in pediatric patients. Radiology 234:893–898

Chung T, Hoffer FA, Lund DP (1996) Transrectal drainage of deep pelvic abscesses in children using a combined transrectal sonographic and fluoroscopic guidance. Pediatr Radiol 26:874–878

Cioni R, Armillotta N, Bargellini I et al (2004) CT-guided radiofrequency ablation of osteoid osteoma: long-term results. Eur Radiol 14:1203–1208

Coley BD, Hogan MJ (2006) Image-guided interventions in neonates. Eur J Radiol 60:208–220

Coley BD, Shiels WE 2nd, Elton S et al (2004) Sonographically guided aspiration of cerebrospinal fluid pseudocysts in children and adolescents. AJR Am J Roentgenol 183:1507–1510

Connolly BL, Chait PG, Duncan DS et al (1999) CT-guided percutaneous needle biopsy of small lung nodules in children. Pediatr Radiol 29:342–346

Cottalorda J, Bourelle S (2006) Current treatments of primary aneurysmal bone cysts. J Pediatr Orthop B 15:155–167

Early SD, Kay RM, Tolo VT (2003) Childhood diskitis. J Am Acad Orthop Surg 11:413–420

Erickson JK, Rosenthal DI, Zaleske DJ et al (2001) Primary treatment of chondroblastoma with percutaneous radio-frequency heat ablation: report of three cases. Radiology 221:463–468

Feneberg R, Schaefer F, Zieger B et al (1998) Percutaneous renal biopsy in children: a 27-year experience. Nephron 79:438–446

Fischer T, Biedermann T, Hermann KG (2003) Sacroiliitis in children with spondyloarthropathy: therapeutic effect of CT-guided intra-articular corticosteroid injection. Rofo 175:814–821

Garg NK, Carty H, Walsh HP et al (2000) Percutaneous Ethibloc injection in aneurysmal bone cysts. Skeletal Radiol 29:211–216

Garrett KM, Hoffer FA, Behm FG et al (2002) Interventional techniques for the diagnosis of lymphoma and leukemia. Pediatr Radiol 32:653–662

Garrett KM, Fuller CE, Santana VM et al (2005) Percutaneous biopsy of pediatric solid tumors. Cancer 104:644–652

Garron E, Viehweger E, Launay F et al (2002) Nontuberculous-spondylodiscitis in children. J Pediatr Orthop 22:321–328

Gervais DA, Brown SD, Connolly SA et al (2004) Percutaneous imaging-guided abdominal and pelvic abscess drainage in children. Radiographics 24: 737–754

Ghandi S, Meech SJ, Puthawala MA et al (2005) Combined computed tomography-guided radiofrequency ablation and brachytherapy in a child with multiple recurrences of Wilms' tumor. J Pediatr Hematol Oncol 27:377–379

Gobien RP, Stanley JH, Schabel SI et al (1985) The effect of drainage tube size on adequacy of percutaneous abscess drainage. Cardiovasc Intervent Radiol 8: 100–102

Guimaraes AC, Chapchap P, de Camargo B et al (2003) Computed tomography-guided needle biopsies in pediatric oncology. J Pediatr Surg 38:1066–1068

Hardaway BW, Hoffer FA, Rao BN (2000) Needle localization of small pediatric tumors for surgical biopsy. Pediatr Radiol 30:318–322

Hawkins JA, Scaife ES, Hillman ND et al (2004) Current treatment of pediatric empyema. Semin Thorac Cardiovasc Surg 16:196–200

Heyer CM, Lemburg SP, Kagel T et al (2005) Evaluation of chronic infectious interstitial pulmonary disease in children by low-dose CT-guided transthoracic lung biopsy. Eur Radiol 15:1289–1295

Hoffer FA (2005) Interventional radiology in pediatric oncology. Eur J Radiol 53:3–13

Hoffer FA, Chung T, Diller L et al (1996) Percutaneous biopsy for prognostic testing of neuroblastoma. Radiology 200:213–216

Hoffer FA, Bloom DA, Colin AA et al (1999) Lung abscess versus necrotizing pneumonia: implications for interventional therapy. Pediatr Radiol 29:87–91

Hoffer FA, Gow K, Flynn PM et al (2001) Accuracy of percutaneous lung biopsy for invasive pulmonary aspergillosis. Pediatr Radiol 31:144–152

Hohl C, Mahnken AH, Klotz E et al (2005) Radiation dose reduction to the male gonads during MDCT: the effectiveness of a lead shield. AJR Am J Roentgenol 184:128–130

Honnef D, Wildberger JE, Stargardt A et al (2004) Multislice spiral CT (MSCT) in pediatric radiology: dose reduction for chest and abdomen examinations. Rofo 176:1021–1030

Honnef D, Wildberger JE, Schubert H et al (2007) CT-guided interventions in children. Rofo 179:605–612

Hugosson CO, Nyman RS, Cappelen-Smith JM et al (1999) Ultrasound-guided biopsy of abdominal and pelvic lesions in children. A comparison between fine-needle aspiration and 1.2 mm-needle core biopsy. Pediatr Radiol 29:31–36

Hussain HK, Kingston JE, Domizio P et al (2001) Imaging-guided core biopsy for the diagnosis of malignant tumors in pediatric patients. AJR Am J Roentgenol 176:43–47

Jamieson DH, Chait PG, Filler R (1997) Interventional drainage of appendiceal abscesses in children. AJR Am J Roentgenol 169:1619–1622

Kaye RD, Sane SS, Towbin RB (2000) Pediatric intervention: an update – part I. J Vasc Interv Radiol 11:683–697

Kayser R, Mahlfeld K, Greulich M et al (2005) Spondylodiscitis in childhood: results of a long-term study. Spine 30:318–323

Kilic N, Celebi S, Gurpinar A (2002) Management of thoracic empyema in children. Pediatr Surg Int 18:21–23

Klein JS, Zarka MA (2000) Transthoracic needle biopsy. Radiol Clin North Am 38:235–266

Koral K, Derinkuyu B, Gargan L et al (2010) Transrectal ultrasound and fluoroscopy-guided drainage of deep pelvic collections in children. J Pediatr Surg 45:513–518

Ladd AP, Levy MS, Quilty J (2010) Minimally invasive technique in treatment of complex, subcutaneous abscesses in children. J Pediatr Surg 45:1562–1566

Lewin JS, Petersilge CA, Hatem SF et al (1998) Interactive MR imaging-guided biopsy and aspiration with a modified clinical C-arm system. AJR Am J Roentgenol 170:1593–1601

Mahnken AH, Tacke JA, Wildberger JE et al (2006) Radiofrequency ablation of osteoid osteoma: initial results with a bipolar ablation device. J Vasc Interv Radiol 17:1465–1470

Margau R, Amaral JG, Chait PG et al (2006) Percutaneous thoracic drainage in neonates: catheter drainage versus treatment with aspiration alone. Radiology 241:223–237

McCann JW, Maroo S, Wales P et al (2008) Image-guided drainage of multiple intraabdominal abscesses in children with perforated appendicitis: an alternative to laparotomy. Pediatr Radiol 38:661–668

McConnell PI, Feola GP, Meyers RL (2002) Methylene blue-stained autologous blood for needle localization and thoracoscopic resection of deep pulmonary nodules. J Pediatr Surg 37:1729–1731

Mishra K, Basu S, Roychoudhury S et al (2010) Liver abscess in children: an overview. World J Pediatr 6:210–216

Nagel HD, Blobel J, Brix G et al (2004) 5 years of "concerted action dose reduction in CT" – what has been achieved and what remains done? Rofo 176:1683–1694

Nordmann GR, Lauder GR, Grier DJ (2006) Computed tomography guided lumbar sympathetic block for complex regional pain syndrome in a child: a case report and review. Eur J Pain 10:409–412

Orlicek SL, Abramson JS, Woods CR et al (2001) Obturator internus muscle abscess in children. J Pediatr Orthop 21:744–748

Patrick DA, Bensard DD, Teitelbaum DH et al (2002) Successful thoracoscopic lung biopsy in children utilizing preoperative CT-guided localization. J Pediatr Surg 37:970–973

Pereira JK, Chait PG, Miller SF (1996) Deep pelvic abscesses in children: transrectal drainage under radiologic guidance. Radiology 198:393–396

Proesmans M, De Boeck K (2009) Clinical practice: treatment of childhood empyema. Eur J Pediatr 168:639–645

Ramnath RR, Rosenthal DI, Cates J et al (2002) Intracortical chondroma simulating osteoid osteoma treated by radiofrequency. Skeletal Radiol 31:597–602

Riccabona M, Sorantin E, Hausegger K (2002) Imaging guided interventional procedures in paediatric uroradiology – a case based overview. Eur J Radiol 43:167–179

Rypens F, Dubois J, Garel L et al (2007) Percutaneous drainage of abdominal abscesses in pediatric Crohn's disease. AJR Am J Roentgenol 188:579–585

Schulz T, Bennek J, Schneider JP et al (2003) MR-guided pediatric interventions – a retrospective case study. Rofo 175:1673–1681

Schulz T, Tröbs RB, Schneider JP et al (2005) Pediatric MR-guided interventions. Eur J Radiol 53:57–66

Shin HJ, Amaral JG, Armstrong D et al (2007) Image-guided percutaneous biopsy of musculoskeletal lesions in children. Pediatr Radiol 37:362–369

Siegel MJ, Schmidt B, Bradly D et al (2004) Radiation dose and image quality in pediatric CT: effect of technical factors and phantom size and shape. Radiology 233:515–522

Sklair-Levy M, Lebensart PD, Applbaum YH et al (2001) Percutaneous image-guided needle biopsy in children – summary of our experience with 57 children. Pediatr Radiol 31:732–736

Skoldenberg EG, Jakobson AA, Elvin A et al (2002) Diagnosing childhood tumors: a review of 147 cutting needle biopsies in 110 children. J Pediatr Surg 37:50–56

Smith MB, Lobe TE, Schropp KP et al (1996) A prospective evaluation of an endoscopic ultrasonic probe to detect intraparenchymal malignancy at pediatric thoracoscopy. J Laparoendosc Surg 6:233–237

Staats PS, Kost-Byerly S (1995) Celiac plexus blockade in a 7-year-old child with neuroblastoma. J Pain Symptom Manage 10:321–324

Tanelian D, Cousins MJ (1989) Celiac plexus block following high-dose opiates for chronic noncancer pain in a four-year-old child. J Pain Symptom Manage 4:82–85

Thomson AH, Hull J, Kumar MR et al (2002) Randomised trial of intrapleural urokinase in the treatment of childhood empyema. Thorax 57:343–347

Ventura N, Gonzalez E, Terricabras L et al (1996) Intervertebral discitis in children: a review of 12 cases. Int Orthop 20:32–34

Vock P (2005) CT dose reduction in children. Eur Radiol 15:2330–2340

Vujanić GM, Kelsey A, Mitchell C et al (2003) The role of biopsy in the diagnosis of renal tumors of childhood: results of the UKCCSG Wilms tumor study 3. Med Pediatr Oncol 40:18–22

Waldhausen JH, Shaw DW, Hall DG et al (1997) Needle localization for thoracoscopic resection of small pulmonary nodules in children. J Pediatr Surg 32:1624–1625

Wilkinson AG, Paton JY, Gibson N et al (1999) CT-guided 14-G cutting needle lung biopsy in children: safe and effective. Pediatr Radiol 29:514–516

Wippermann CF, Schofer O, Beetz R et al (1991) Renal abscess in childhood: diagnostic and therapeutic progress. Pediatr Infect Dis J 10:446–450

Part II

Diagnostic Interventions

Biopsy

9

Christoph Gregor Trumm, Ralf-Thorsten Hoffmann, and Christoph Thomas

Contents

9.1 CT-Guided Biopsy

Christoph Gregor Trumm and Ralf-Thorsten Hoffmann

9.1.1 Introduction

Image-guided percutaneous biopsy using ultrasound (US) and computed tomography (CT) is widely established as a safe method for differentiation of benign and malignant masses while magnetic resonance (MR) imaging was only introduced as guidance method in the mid-1990s. Most of the procedures are performed in patients with a known primary tumor in order to rule out metastatic malignancy and to establish the final diagnosis or to differentiate between tumor necrosis and potential vital tumor tissue in residual lesions after therapy.

9.1.2 Patient Preparation and Aftercare

Most image-guided biopsies can be performed on an outpatient basis. Informed patient consent including possible conscious sedation after detailed explanation of potential complications should be obtained at least 24 h before the intervention. Coagulation disorders should be ruled out by taking platelet levels (more than 50,000/mm^3), partial thromboplastin time (PTT: less than 50 s), prothrombin time (PT: more than 50 %), and International Normalized Ratio (1.5 or less)

C.G. Trumm (✉) • R.-T. Hoffmann
Department of Clinical Radiology, Großhadern Campus, Ludwig-Maximilians-University Munich, Marchioninistrasse 15, D-81377, Munich, Germany
e-mail: christoph.trumm@med.uni-muenchen.de

C. Thomas
Department of Diagnostic and Interventional Radiology, Eberhard-Karls-University Tübingen, Hoppe-Seyler-Straße 3, D-72076, Tübingen, Germany

A.H. Mahnken et al. (eds.), *CT- and MR-Guided Interventions in Radiology*,
DOI 10.1007/978-3-642-33581-5_9,

in all patients, especially if the lesion is located in the depth of the chest and abdomen. In superficial lesions (e.g., in the neck), direct pressure is usually sufficient for hemostasis, and dedicated coagulation studies are not required. In case the patient has taken nonsteroidal anti-inflammatory drugs inhibiting platelet aggregation (e.g., acetylic salicylic acid), a core biopsy should be postponed by 7 days. In absence of any abnormalities regarding platelet levels, PTT, and PT, a fine-needle biopsy (20 G or smaller) may be performed because the risk of hemorrhage due to nonsteroidal anti-inflammatory drugs alone is low (Table 9.1) (Cardella et al. 2003).

The majority of CT-guided biopsies can be performed under local anesthesia. Children, incompliant adult patients, or biopsies of deep abdominal lesions (e.g., pancreatic masses) represent potential exceptions. In those selected cases, sufficient analgosedation can be reached by intravenous administration of benzodiazepines, for example, Midazolam (1 mg/dose; given in two to four doses) for anxiolysis and opioids, for example, Fentanyl (0.02 mg/dose; given in one to five doses) for analgesia (see Chap. 5). If analgosedation is used, the patient should be monitored during the whole procedure using pulse oximetry. The nurse or radiology technician is responsible for keeping the patient compliant while the radiologist can concentrate on the procedure. Before the intervention, the patient should be placed in a stable and comfortable position. Depending on the lesion location supine, prone, or lateral decubitus position are most commonly used.

Table 9.1 Contraindications for computed tomography (CT)-guided biopsy

Uncorrectable coagulation disorder
Platelets < 50,000/mm^3[a]
INR > 1.5[b]
Prothrombin time (quick) < 50 %[b]
Partial thromboplastin time > 50 s[c]
Intake of platelet inhibitors < 24 h before the intervention[d]
Massive ascites
Adipositas in combination with small cirrhotic liver (transjugular or surgical biopsy recommended)
Incompliant patients
Absence of a safe pathway from the skin to the target site

[a]A preprocedural platelet transfusion may be necessary
[b]Usually due to coumarins or liver disease; coumarin withdrawal takes a few days to reverse INR. INR can also be reversed by vitamin K or fresh frozen plasma
[c]Usually prolonged secondary to heparin or heparin-like drugs. These agents generally have short half-lives and can be quickly reversed
[d]Clinical assessment should be made as to whether to proceed or reschedule the biopsy

For correlation, pre-, peri- and post-interventional CT images should be obtained in the same position during the same respiratory cycle, preferably during expiration. In case of an anterior approach, the CT or MR table is set as low as possible in order to leave enough room for the needle insertion. Preparation of the skin area overlying the entry point of the biopsy needle includes shaving (if necessary), sterile draping, and skin disinfection.

Following CT guided biopsy, patients are kept in the ward with vital signs observed every 15 min for 1 h. In high-risk patients, observation can be continued beyond this time, for example, with checking of vital signs every 30 min for 3 h.

After lung biopsy, the patient should lie with the puncture site down for 2 h. The two pleural layers are compressed by the weight of the lung itself, and further air leakage through the pleural defect is minimized. Chest radiographs (p.a.) are obtained 2 and 4 h after the intervention in order to rule out delayed pneumothorax. If the chest radiograph in erect position after 2 h shows a small pneumothorax, a further chest X-ray should be obtained after 4 h. In case of pneumothorax and patient symptoms, air aspiration or a chest tube should be inserted for treatment (see Sect. 11.2.2).

At discharge, patients should be advised to take care of the puncture site. They are instructed to call their physician in the event of bleeding or marked swelling at the puncture site. Patients are advised not to bath for 24 h if no dedicated water proof bandage is used for sealing the puncture site.

9.1.3 CT and CT-Fluoroscopic Guidance

CT as guiding method is especially suitable for lesions located deep under the skin surface which

are not or not easily depictable via ultrasound (e.g., deep retroperitoneal, pelvic and thoracic lesions). With some exceptions such as liver lesions isodense to normal parenchyma at non-enhanced CT scans, CT usually provides excellent visualization of the target lesion and differentiation from adjacent organs. It is generally preferable not to schedule a biopsy procedure at the same time as the first diagnostic scan. If available, recent images not older than 2 weeks or a separate preceding diagnostic study should be used for selection of target lesions for biopsy and planning of the access pathway. Two different techniques of CT guidance can be utilized.

9.1.3.1 Sequential CT-Guidance

For planning of the access route, a CT scan of the region of interest is performed first. The preliminary scan can be performed without contrast if a recent diagnostic study is available and the lesion is easily visible. In the chest, a non-enhanced CT scan (slice thickness 3 mm or less) is also sufficient for detection of intrapulmonary lesions suitable for aspiration or punch biopsy. For suspect masses in the mediastinum and abdomen (intra- and retroperitoneal), a contrast-enhanced CT scan is necessary for clear differentiation of parenchymal organs, intestines, and blood vessels. Focal lesions within parenchymal organs are usually visualized during venous phase (scan delay 50–70 s). An additional arterial phase (scan delay approximately 30 s) may be beneficial if arteries are present along the access path (e.g., parasternal access, internal mammary artery) and in hypervascularized lesions (e.g., hepatocellular carcinoma, metastases of renal cell carcinoma).

For defining the skin entry point of the biopsy needle, a radiopaque grid is placed on the skin of the patient (Fig. 9.1a). The patient is positioned either in prone, supine, or lateral decubitus position, depending on the shortest distance from the skin surface to the lesion. Then, the CT scan is performed covering the region of interest. Grid systems are either commercially available, while also a homemade grid from several 4–5 F catheters that are cut into a length of 15–30 cm, and taped together at intervals of 1 cm, can be used. The use of barium paste instead of a radiopaque grid has also been described. After the planning CT scan (with the grid system taped on the skin of the patient) has been performed, the slice position showing both, the lesion and the potential in-plane access route, or the intended needle entry point only (double-oblique access), is chosen. The distance from the skin level of the needle entry point to the lesion is measured. The CT table is moved to the position of choice for biopsy, and the needle entry point can be marked with a felt pen using the grid as well as the centering laser light beam.

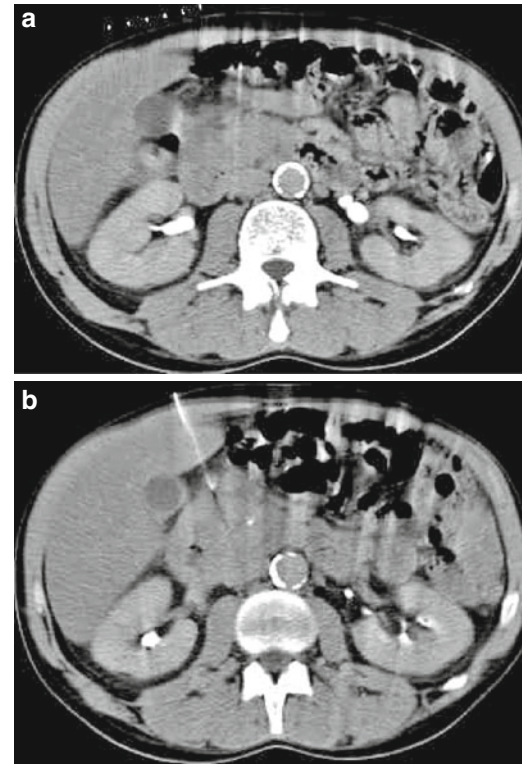

Fig. 9.1 Patient (supine position) with suspect mass of the pancreas head. A radiopaque grid made of 4-F catheters is taped on the patient's skin covering the intended region of needle entry before the planning computed tomography (CT) scan (**a**). An anterior transhepatic approach passing the left liver lobe was chosen for coaxial punch biopsy with an 18-G Tru-Cut needle under sequential CT guidance (**b**). Histopathology revealed a pancreatic adenocarcinoma

After skin disinfection, local anesthesia using 10–20 cc of 1–2 % lidocaine hydrochloride is applied in the subcutaneous fat and down to the capsule of parenchymal organs (e.g., the liver),

down to the pleura, or down to the periosteum of bones using a 22-G needle that additionally marks the entry point and intended angle of the biopsy needle. After a small skin incision with a scalpel and CT rescanning with the local anesthesia needle in the skin entry point to confirm the correct position, the biopsy needle is inserted parallel to the local anesthesia needle. Thereafter, repeated CT scans covering a short range above and below the needle entry point (e.g., 3–5 cm along the z-axis) are performed, and the angulation of the needle is adapted to interfering anatomical structures if necessary (Fig. 9.1b). The use of multislice spiral CT with its inherent ability to simultaneously acquire several sections is beneficial for this purpose, as it omits the need for multiple scans above and below the needle entry point. The direction of the needle in relation to the lesion can be easily detected using the streak artifact at the needle tip. Finally, the needle is inserted into the edge of the lesion for tissue sampling.

9.1.3.2 CT-Fluoroscopic Guidance

Since the introduction of CT-fluoroscopy (CTF) with faster image reconstruction on multislice CT scanners, real-time visualization nearly comparable to US is available. Cross-sectional CT images are reconstructed at reduced spatial resolution and updated continually at a rate of up to 10 frames/s by using a high-speed array processor (Carlson et al. 2001). In contrast to the sequential technique using repeated non-enhanced CT scans covering the volume of interest, the needle is visualized on an in-room monitor. The operator can dynamically adjust the needle position under single-shot or continuous CTF until the lesion is reached. The main advantages are a substantial reduction of in-room time for both, the patient and the operator, and real-time visualization of critical anatomical structures along the trajectory such as vessels during needle insertion. This technique is particularly helpful in case of incompliant patients who are unable to cooperate, for example, to hold their breath or in regions with persistent motion as it may be found close to the heart and diaphragm. In contrast to conventional CT guidance, the main disadvantage is the radiation exposure of the operator (Silverman et al. 1999). The use of a grab handle for holding the needle helps to avoid the direct exposure of the operator's hand to the radiation beam during CTF. As important advantages of this technique, patient-absorbed radiation dose and in-room time can be significantly reduced by 94 and 32 %, respectively (Carlson et al. 2001).

9.1.4 CT-Guided Aspiration Biopsy

Percutaneous fine-needle aspiration biopsy (FNAB) is a well established method to obtain an aspirate with a thin needle (20 G or greater) which usually provides enough material to confirm or rule out malignancy by cytologic analysis. In most cases, a histological diagnosis is not possible due to an insufficient amount of material.

9.1.4.1 Indication

FNAB is suitable for tissue sampling of pulmonary lesions as well as neck lesions (e.g., lymph nodes) and abdominal lesions given a known primary tumor in combination with suspected metastases of the liver, lymph nodes, etc. In abdominal lesions, FNAB is preferable where a direct access is precluded by surrounding organs. It is generally considered insufficient if the primary tumor is unknown.

9.1.4.2 Material

Fine-needle biopsies are performed with 20- to 25-G needles (small gauge) including various commercially available needle types and needle tip designs. The needle tip is either sharp-beveled (e.g., Chiba or spinal needle) or cutting (Turner needle, 45° bevel tip with cutting edge; Franseen needle, three-pronged needle tip; Westcott needle, slotted side-opening proximal to the needle tip; and E-Z-EM needle, trough cut in the needle tip) (Lee 2004) (Fig. 9.2). Coaxial biopsy sets consist of an outer guide needle in combination with a smaller aspiration needle. Typical needle combinations for coaxial FNAB are 23 G/20 G or 22 G/19 G sets (Table 9.2).

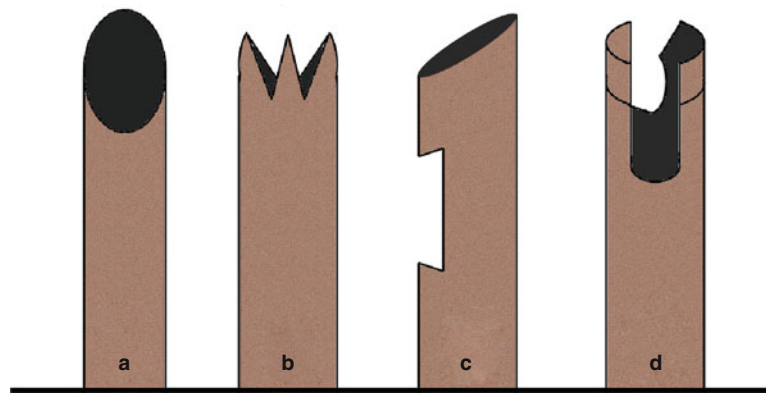

Fig. 9.2 The most common fine needle types: Turner (**a**), Franseen (**b**), Westcott (**c**), and E-Z-EM (**d**) needle. The Turner needle is characterized by a 45° bevel with a cutting edge. The Franseen needle has a three-pronged tip. The Westcott needle contains a side-cutting trough close to its tip. The E-Z-EM needle has a trough cut within the needle tip (schematic according to Lee (2004))

Table 9.2 Commercially available needles for CT-guided aspiration biopsy (exemplary selection of different manufacturers and needles)

Needle type (manufacturer)	Diameter (gauge)	Length (cm)[a]
Chiba (Boston Scientific, Natick, MA, USA)	22	6; 8
Franseen (Boston Scientific, Natick, MA, USA)	18; 20; 22	6; 8
Coaxial lung biopsy set Greene-type (Boston Scientific, Natick, MA, USA)	22	6
Chiba (Cook Medical, Bloomington, IN, USA)	18–23; 25	5; 10; 15; 20
Spinal needles (Cook Medical, Bloomington, IN, USA)	18; 20; 22	10; 15
Chiba-needle ultra (Somatex, Teltow, Germany)	19.5; 22	9; 12; 15; 22; 28
Chiba (E-Z-EM, Lake Success, NY, USA)	18; 20; 22	10; 15; 20
Percucut cut-biopsy needle with keyhole cutting edge (E-Z-EM, Lake Success, NY, USA)	18; 19.5; 21	5; 10; 15

[a]Not all diameter-length combinations may be available

9.1.4.3 Technique

General Considerations

FNAB can be performed either by solely using the fine needle, applying a coaxial approach, or using a tandem technique. The first technique is characterized by the straightforward puncture of the target lesion. This technique has some disadvantages including limited controllability. The coaxial technique is characterized by a combination of two needles. A thicker, shorter needle is inserted down to the anterior edge of the lesion. Then, a thinner, longer needle is introduced through the first needle. Multiple samples can be taken using the thinner needle without several punctures. If necessary, the larger needle can be pulled back and its angle changed in order to reach different areas of the lesion. With the tandem technique, first a single reference needle is introduced into the lesion. Then, further needles are introduced "in tandem," that is, parallel to the first needle without having to guide them separately.

After the appropriate needle length has been measured in the planning scan, preparation of the chosen entry site, and local anesthesia, the fine-needle is inserted to the lesion under image control, that is, repeated non-enhanced short CT scans or CTF sequences triggered by the operator. As soon as the needle has been introduced into the lesion, the trocar is removed, and a 10- or 20-ml Luer-Lok syringe is connected to the proximal end of the needle and suction is applied. The aspirated volume ranges between 3 and 5 ml for most biopsies and should be reduced (1–2 ml) in hypervascularized lesions in order to avoid

aspiration of larger amounts of blood. During application of suction, the needle is moved back and forth within the lesion for 10–15 s or until the hub of the syringe gets filled with blood. Before removing the needle from the lesion, the suction is stopped in order to avoid aspiration of further tissue potentially confusing cytologic evaluation of the sample.

In hypervascularized lesions like in the thyroid gland, non-aspiration fine-needle biopsy can be alternatively performed. The needle is introduced into the lesion without a syringe and moved back and forth several times.

If a cytopathologist is in the room during the biopsy procedure, he can give an initial statement if the tissue sample is sufficient for evaluation, or further samples have to be taken. Otherwise, the aspirated material is crossed out on a glass slide and immediately afterward fixated with alcohol. An additional blood clot should be obtained and fixated in formalin, as this will significantly increase sensitivity for malignancy (Wildberger et al. 2003).

Special Considerations

Lung

The advantage of CT-guided lung biopsy is that the lung parenchyma and not ventilated areas at the puncture site are visualized that can be used as access path to the lesion, substantially reducing the risk of pneumothorax. Local anesthesia is applied subcutaneously down to the pleura without touching the latter. Then, a coaxial needle can be inserted through the parietal pleura under suspended respiration. The operator can adjust the needle direction by withdrawing the coaxial needle to the periphery of the lung (without removing the needle outside the pleura). If the coaxial technique is used, the outer coaxial needle is inserted 2–3 mm into the edge of the lesion providing stability during coaxial biopsies. Then, the inner biopsy needle is introduced and at least two samples obtained (Fig. 9.3). The outer cannula should never be left inside the patient without the inner stylet in order to prevent air embolism. CT-guided biopsy of lung lesions can be done under stable pneumothorax if the lesion is close to the pleural surface. When pneumothorax occurs, the same position should be scanned 3 min later to see if the pneumothorax is progressing. If pneumothorax increases, a pigtail catheter should be inserted, and the procedure may be stopped (Tsai et al. 2009). In stable pneumothorax, the procedure should be completed and an end-expiratory chest radiograph should be obtained.

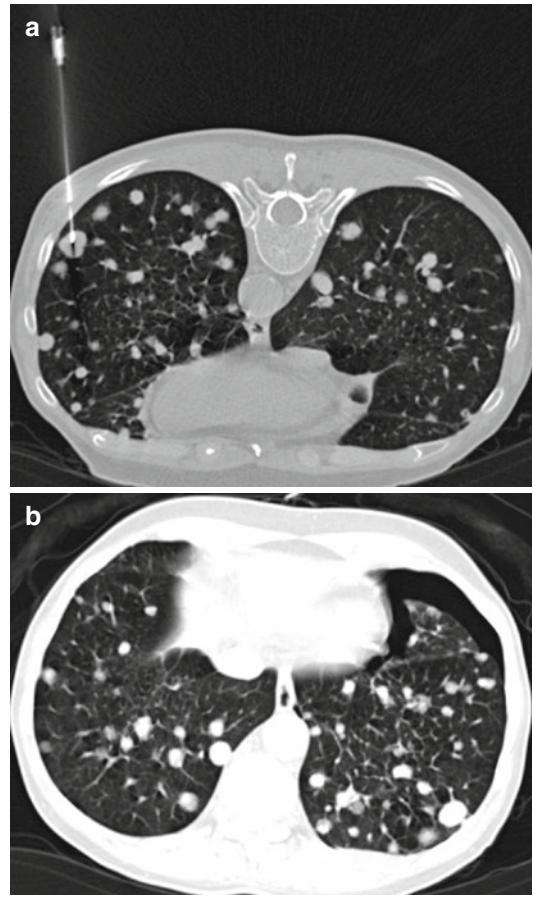

Fig. 9.3 Patient (prone position) with multiple lung metastases. A subpleural nodule in the left lower lobe was chosen for aspiration biopsy under CT-fluoroscopic guidance with a 19-G (10-cm) needle (**a**). Postinterventional CT (supine position) showed a small pneumothorax that did not require therapy after further follow-up with X-ray (**b**). Cytology revealed pulmonary metastases of an adenocarcinoma (sigmoid colon)

Mediastinum

Biopsies in the mediastinum have to be performed with special respect to vascular structures (Fig. 9.4). For planning of the biopsy procedure, a contrast-enhanced CT is performed in order to

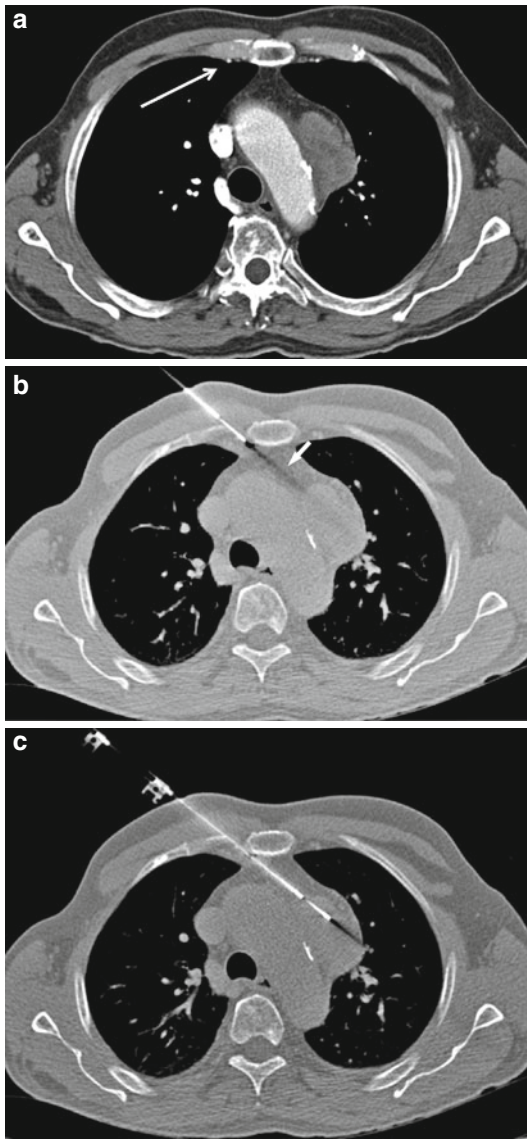

Fig. 9.4 Patient (supine position) with a paraaortal mass in the upper mediastinum. The preinterventional CT (arterial phase) showed the right internal mammary artery and vein (*arrow*) next to the sternum (**a**). First, sterile saline was injected with a 22 G needle for widening of the parasternal space. Then, an 18-G (13 cm) Tru-Cut biopsy needle was introduced under CTF-guidance. Note the typical black streak artifact (*arrow*) along the needle pathway (**b**, **c**). Histopathologic analysis revealed a mesenchymal tumor

rule out vascular abnormalities like aneurysms and to visualize the mediastinal vessels. For sampling lesions in the anterior mediastinum, an anterior parasternal approach is usually chosen. The internal mammary artery and vein that are located approximately 1 cm from the sternum have to be avoided (Fig. 9.4a). Additionally, the access path through the mediastinal fat can be widened by injection of sterile saline through a 22-G needle. After distension of the anterior mediastinum, the FNAB needle can be safely introduced without passing the paramediastinal lung parenchyma (Fig. 9.4b, c). In case the lesion is located in the posterior mediastinum, the paravertebral space can also be distended using sterile saline.

Liver

Depending on the experience of the operator and availability of an interventional CT unit, the majority of liver biopsies can also be performed under US guidance. If lesions in the dome of the liver cannot be visualized with US, a CT/CTF-guided (double) oblique approach may be preferable, while crossing the costophrenic sulcus should be avoided. Gantry angulation may help to access lesions in the liver dome. Before introducing the biopsy needle into the liver parenchyma, the capsule has to be infiltrated with local anesthetic. During penetration of the liver capsule, the patient should be asked not to breathe. Passing normal liver tissue before entering the lesion reduces the risk of relevant subcapsular or intraparenchymal bleeding occurring after the puncture due to self-tamponade. The biopsy may also be performed in a right decubitus position or under maximum expiration when the costophrenic sulcus is not inflated. The sample should normally be taken from the edge of the liver mass where the vital tumor tissue (in contrast to the central necrotic area) is located. In cases of liver lesions with large necrotic areas, a coaxial technique combining an outer cannula with the biopsy needle may be useful as the liver capsule is crossed only one time.

Pancreas

Typically, the pancreas is surrounded by various organs like the stomach, liver, transverse colon, kidney, or major vessels. Especially needle biopsy of small suspicious masses in the pancreatic head is therefore usually regarded as technically sophisticated, and CT-guidance preferred

over of ultrasound. For differentiation of the tumor from surrounding normal parenchyma or inflammation, an arterial phase contrast-enhanced CT scan should be performed prior to the intervention. The most common access route is from an anterior approach and often traverses gastrointestinal structures and the mesenteric vessels, increasing the general risk of the procedure. On the other hand, with CT-fluoroscopy, transgression of vital structures can be avoided in most cases. In difficult-to-access lesions, the stomach or the small intestines may be punctured with a 20–22-G needle. Given an immunocompetent patient, FNAB traversing the GI tract or the liver has been shown to be technically feasible and safe in many studies (Brandt et al. 1993; Elvin et al. 1990; Luning et al. 1985; Mueller 1993). Transhepatic, transsplenic, and paracaval/transcaval approaches have also been described (Brandt et al. 1993).

If the pancreatic tumor is too scirrhous to obtain a sufficient specimen in spite of several attempts, usually a switch to a large-gauge core biopsy system is necessary. The colon should generally not be penetrated even with a small gauge needle in order to avoid superinfection, especially if cystic pancreatic lesions containing fluid are sampled (Mueller 1993). In case of unintended penetration, metronidazole should be administered prophylactically.

Kidney

Biopsies of the kidney are rarely performed because they are often interpreted as hemorrhagic or inconclusive, and most solid renal masses are surgically removed. Exceptional indications for biopsy are suggested lymphoma and metastasis to the kidney from another primary tumor, since these conditions are usually not treated surgically. The usual access route under CT guidance is posterior or lateral while the renal hilum should be avoided (Fig. 9.5).

Adrenal Glands

Owing to the anatomic localization in the upper retroperitoneum, the access path for biopsy is relatively sophisticated while several approaches are possible:

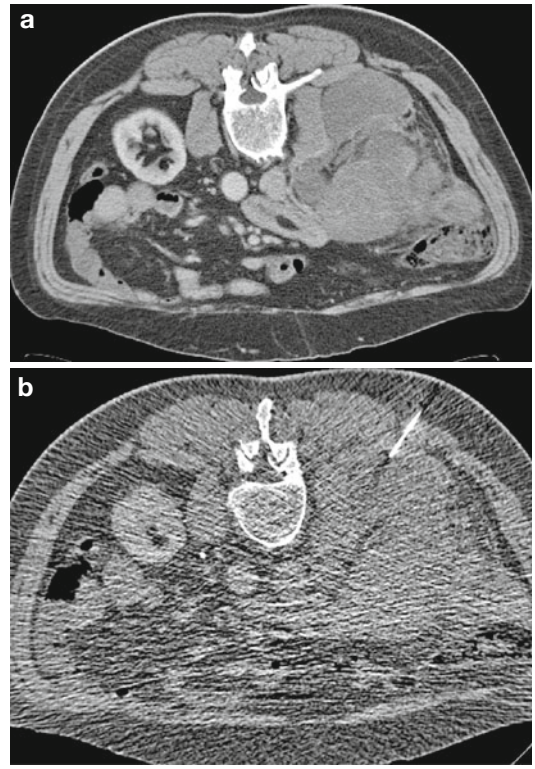

Fig. 9.5 Patient (prone position) with suspect retroperitoneal mass encasing the right kidney (**a**). A right posterior approach was chosen for aspiration biopsy with a 19-G (10-cm) needle under CT-fluoroscopic guidance (**b**). Cytology revealed a lymphoma

- The right lateral transhepatic approach (right adrenal gland: through right liver lobe, supine position)
- The left anterior transhepatic approach (left adrenal gland: through left liver lobe, supine position)
- The angled prone approach (both adrenals: subcostal approach in a 45° angle, prone position; Fig. 9.6)
- The lateral decubitus approach (the patient side with the adrenal lesion is placed next to the table, preventing full expansion of the ipsilateral pulmonary recessus while the overlying lung is fully expanded)

Retroperitoneum

Biopsies of retroperitoneal lesions are usually performed under CT-guidance. With the most common posterior approach, the needle passes

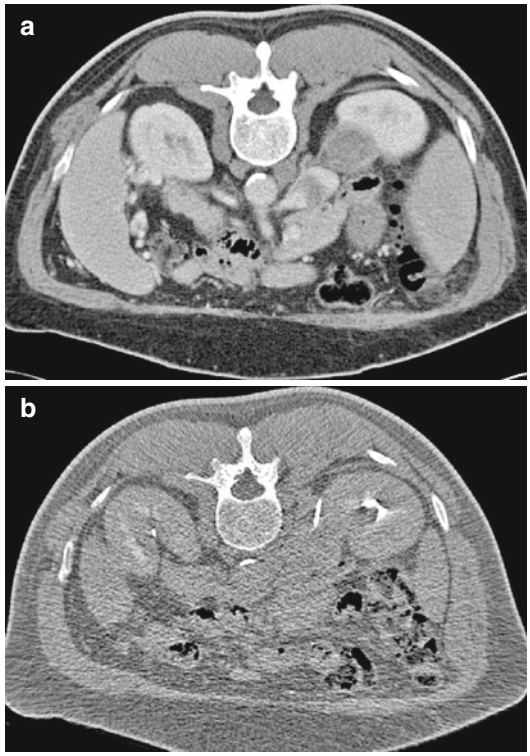

Fig. 9.6 Patient (prone position) with a known hepatocellular carcinoma (HCC). The preinterventional CT showed a suspect mass of the right adrenal gland (**a**). A posterior right paravertebral approach was chosen for aspiration biopsy with a 19-G (13-cm) needle under CT-fluoroscopic guidance (**b**). Cytology revealed an adrenal metastasis of HCC

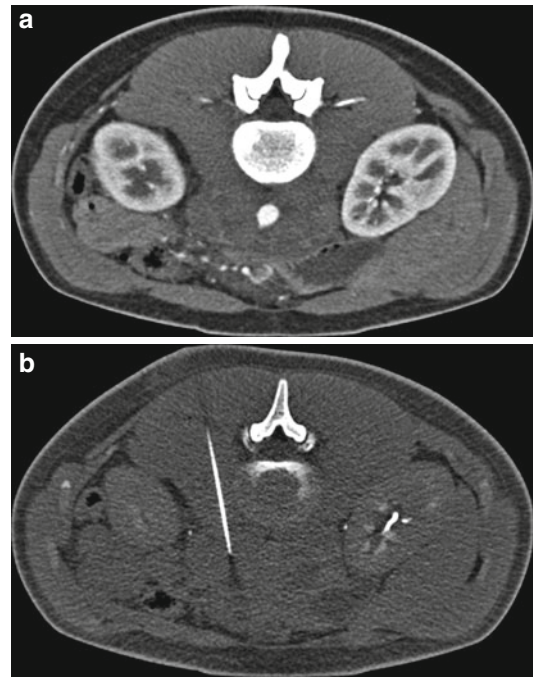

Fig. 9.7 Patient (prone position) with extensive paraaortal lymph node bulking (**a**). A left posterior paravertebral approach was chosen for aspiration biopsy with a 19-G (15-cm) needle under CT-fluoroscopic guidance (**b**). Cytology revealed lymph node metastases of an adenocarcinoma

through or parallel to the psoas muscle (Figs. 9.7 and 9.8). This approach permits the safe use of large needles, while small-gauge needles are recommendable in an anterior approach.

Pelvic Lesions

While transrectal and transvaginal biopsies are routinely guided using ultrasound, the access routes for CT-guided biopsy in the pelvis include:

- The transgluteal approach through the greater sciatic foramen
- The presacral approach through the gluteal cleft
- The anterior approach (Fig. 9.9)

For the transgluteal approach, the patient is placed in prone position. The needle is introduced from the buttock through the greater sciatic foramen into the deep pelvis as close to the coccygeal bone as possible in order to avoid puncture of the sciatic nerve.

9.1.4.4 Results

Lung

In pulmonary lesions, FNAB has been reported to have diagnostic accuracy and sensitivity rates of more than 93 % (Swischuk et al. 1998) and 95 % (Klein et al. 1996; Laurent et al. 2000), respectively. Kothary et al. recently performed a study to compare the diagnostic accuracy and complication rate of CT-guided biopsy of lung nodules of 1.5 cm or smaller versus nodules of more than 1.5 cm in diameter. Though not statistically significant, diagnostic accuracy for malignancy was higher in larger nodules than in lesions of 1.5 cm or smaller (81.3 % vs. 69.6 %), whereas there was no correlation between nodule size and the incidence of complications (Kothary et al. 2009). While other authors have also reported accuracy rates of less than 75 % for lesions 1 cm or smaller (Li et al. 1996; Tsukada et al. 2000;

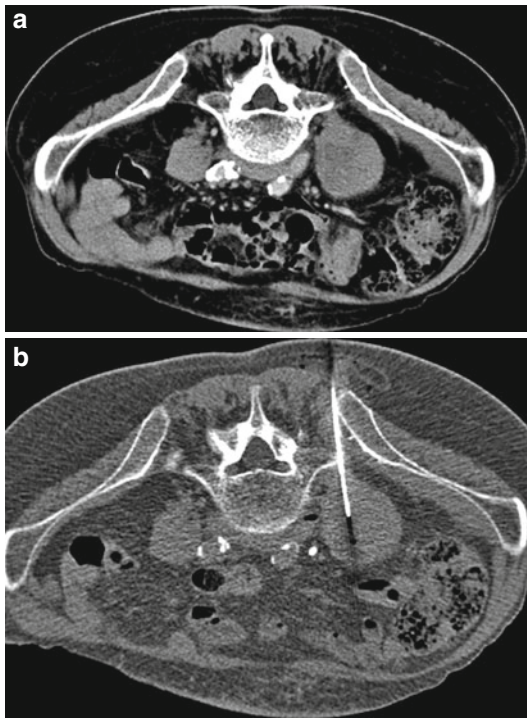

Fig. 9.8 Patient (prone position) with suspect mass of the right psoas muscle (**a**). A posterior paravertebral (fifth lumbar vertebra) access was chosen for Tru-Cut biopsy with an 18-G (13-cm) needle under CT-fluoroscopic guidance (**b**). Histopathology revealed metastasis of ovarial carcinoma

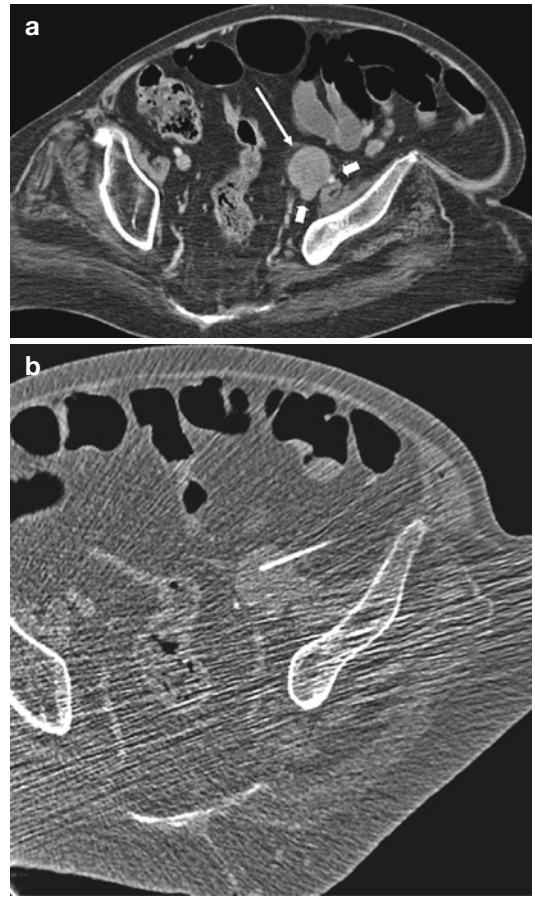

Fig. 9.9 Patient (supine position) with a history of diffuse large B-cell lymphoma (DLCL). Preinterventional CT showed a moderately enhancing nodule (*large arrow*) next to the iliac vessels (*small arrows*) (**a**). The 18-G (13-cm) Tru-Cut biopsy needle was introduced under CT-fluoroscopic guidance next to the left iliac crest through the peritoneal fat (**b**). Histopathology revealed recurrence of DLCL

van Sonnenberg et al. 1988), respiratory gating (Tomiyama et al. 2000) and CTF (Irie et al. 2001) have contributed to improve success rates. In patients with peripheral intrapulmonary nodules larger than 1 cm, an interactive breath-hold control system (IBC) including a strain detector belt indicating the respiratory position of the patient on a LED array could significantly reduce the number of imaging steps, as well as the intervention time (Schoth et al. 2010). The work by Kim et al. showed a significantly lower complication rate (pneumothorax, hemoptysis) when comparing percutaneous CT-guided pulmonary aspiration biopsy with (Group I: 13.4 %) and without (Group II: 31.4 %) CTF. Mean estimated effective dose to the interventionalist was 0.054 mSv in Group I and 0.029 mSv in Group II (Kim et al. 2011). Subpleural pulmonary nodules are often more challenging than deep lesions. Especially the ribs or scapula may potentially hinder the direct access to a nodule. In the comparison of an oblique-versus a right-angle access path ($n=61$ subpleural lesions) by Tanaka et al. (1996), success rates were significantly better for the oblique path (81.2 %) compared to the right-angle access (43.3 %). With a direct access, the parenchymal distance to the subpleural nodule may be less than 1 cm, not allowing to correct the needle direction without another pleural passage. Once a pneumothorax has occurred, usually a retraction of the lung is observed making further sampling difficult if not impossible. A longer, tangential

transparenchymal access route implies an improved needle stability (Wallace et al. 2002).

Mediastinum

In 89 patients undergoing CT-guided mediastinal FNAB for lung cancer staging (50 with and 39 without core biopsy of lymph nodes with short axis diameter greater than 1.5 cm) before mediastinoscopy, Zwischenberger et al. reported diagnostic success (cancer cell type, sarcoidosis, or caseating granulomas) in 78 % of the cases, while only in 9 patients, lymph nodes (paraesophageal, pulmonary ligament, parasternal and paraaortic) could not be accessed (Zwischenberger et al. 2002). In the study by Assaad et al. (157 mediastinal FNAB), adequate diagnostic cytological material could be obtained in 82 % of the cases, with concordance of subsequent histological and FNAB diagnosis in 78 % (53 of 68) of the corresponding cases (Assaad et al. 2007).

Liver

FNAB in the abdomen with both ultrasound and CT-guidance has been described as safe and technically successful procedure by several authors (Ferrucci et al. 1980; Memel et al. 1996; Smith 1991; Welch et al. 1989). CT-guided FNAB of liver lesions has been reported to have sensitivity rates of 92 % and specificity rates of 96 % (Luning et al. 1984). Tatli et al. described a technique of CT-guided fine needle biopsy of abdominal lesions using the nonenhanced intraprocedural CT scan registered to PET/CT images acquired earlier. The authors recommended the technique especially for biopsy of masses with heterogeneous metabolic activity (Tatli et al. 2010).

Kidney

Most renal masses can be characterized with high accuracy by noninvasive imaging alone, and a solid nonfat-containing or complex renal mass should be considered a renal cell carcinoma until proven otherwise. Metastases to the kidney are usually small and multifocal or perinephric. Lymphomatous involvement of the kidneys usually occurs in the setting of disseminated disease and is characterized by typical CT patterns with multiple small masses, spread from retroperitoneal disease, diffuse infiltration, and perinephric encasement.

In a study by Brierly et al. with 49 patients undergoing FNAB for various renal masses, the sensitivity of CT-guided biopsy for the diagnosis of malignancy ranged from 89 % in large solid masses to only 50 % in complex cysts. Inadequate specimens were obtained in 16 % of the patients (Brierly et al. 2000). In another study by Lechevallier et al., CT-guided renal biopsy of 63 patients had an overall accuracy of 89 %. Biopsy material was not sufficient for analysis in 15 patients (21 %). Unsuccessful biopsy was related to lesion size: Biopsy was unsuccessful in 11 of 30 tumors (37 %) of 3 cm or less versus 4 of 43 (9 %) of tumors greater than 3 cm (Lechevallier et al. 2000).

Adrenal Glands

Incidentally, discovered adrenal masses (incidentalomas) are relatively frequent. Adrenal incidentalomas (AI) exceeding 1 cm in size are found in 1–5 % of the patients undergoing chest or abdominal CT for unrelated reasons. The risk of malignancy in patients with nonfunctioning adrenal masses is between 3.5 and 34 % (Lumachi et al. 2001). Since the development of dedicated MR-imaging techniques for differentiation of adrenal masses, adrenal biopsy is performed only in exceptional cases, and benign adrenocortical nodules are the most common lesion to be found with FNAB (more than 40 %).

Lumachi et al. performed a study in order to compare the usefulness of FNAB cytology, CT and MR imaging in patients with nonfunctioning adrenal masses. Including 34 patients with adrenal masses incidentally discovered in a CT scan, the authors found a sensitivity and specificity of 100 % for the combination of both, MR imaging and FNAB. The authors recommended performing image-guided FNAB in all patients with nonfunctioning adrenal masses of 2 cm or more in size. Morbidity rate of the study was 2.9 % (Lumachi et al. 2003).

Retroperitoneum and Pelvis

Nahar Saikia et al. performed 242 aspiration biopsies of deep-seated thoracic, abdominal, and

retroperitoneal lymph nodes under ultrasound ($n=216$) and CT ($n=26$) guidance, respectively. The diagnostic accuracy rate was 86 % (Nahar Saikia et al. 2002). In 23 patients with 26 suspect abdominal, pelvic ($n=6$), or retroperitoneal ($n=12$) lymph nodes, Memel et al. reported technical success, that is, sampling of adequate tissue for cytologic or histologic evaluation, in 21 of 23 ultrasound-guided biopsies (91 %). Three of 26 lymph nodes (11.5 %) could not be sampled due to poor visualization under ultrasound (Memel et al. 1996).

9.1.4.5 Complications

In the lung, apart from pneumothorax (16–44.6 %) and consecutive thoracostomy tube insertion, complication rates for image-guided FNAB are low (Laurent et al. 2000; Swischuk et al. 1998; van Sonnenberg et al. 1988). Factors increasing the risk of pneumothorax are small lesion size (Cox et al. 1999; Fish et al. 1988; Kazerooni et al. 1996), increasing depth of the lesion, several passes through the pleura, and underlying pulmonary disease (Poe et al. 1984; Quon et al. 1988). Zaetta et al. evaluated an expanding hydrogel biopsy tract plug deployed through the coaxial needle to reduce rates of pneumothoraces. Compared with control subjects (31 %), treatment subjects developed fewer pneumothoraces (18 %). Rates of chest tube placement and postprocedure hospital admission were also reduced (Zaetta et al. 2010). Pulmonary hemorrhage and hemoptysis are observed in up to 1.4 and 1.7 % of the procedures, respectively (Arslan et al. 2002). In case of hemoptysis, the patient should lie in a lateral decubitus position on the punctured side, preventing aspiration of blood into the contralateral lung. Air embolism is also a rare complication of thoracic FNAB resulting from a direct communication between a pulmonary vein and atmospheric air. Reasons for the entry of air are the operator leaving the proximal end of the biopsy needle open after insertion into the chest and the patient breathing deeply during the intervention. The patient should receive 100 % oxygen and lie in the left lateral decubitus position with the head down in order to prevent cerebral embolism.

Complication rates of FNAB in the abdomen are very low. In the meta-analysis including literature data and results of questionnaires distributed in North American and European hospitals in the 1980s, Smith found mortality rates between 0.006 % (63,108 biopsies) and 0.031 % (16,381 biopsies) in the USA and between 0.008 and 0.018 % in European hospitals (Smith 1991). Leading causes of death reported in Europe ($n=33$) were hemorrhage after liver biopsy (17 of 21) and pancreatitis after pancreas biopsy (five of six). Frequency of needle tract seeding was in a range between 0.003 and 0.009 % in the four questionnaires.

In hepatocellular carcinoma, given a high positive predictive value of suspicious imaging findings alone (Torzilli et al. 1999), percutaneous biopsy has a limited role. Common risks include intraperitoneal bleeding and needle tract tumor implantation. In the study of Bret et al., 2.5 % of 159 patients ($n=4$) with HCC who underwent fine-needle aspiration biopsy developed serious bleeding after the procedure, and one died (Bret et al. 1988). Factors that may contribute to hemorrhage include tumor hypervascularization, failure of cirrhotic liver tissue to seal the needle track, free bleeding into perihepatic ascites, and coagulopathy secondary to liver dysfunction (Grant and Neuberger 1999). Needle tract implantation has a reported incidence of up to 5 % (Takamori et al. 2000).

Acute pancreatitis has been described as rare but potentially fatal complication of needle biopsy of the pancreas (Mueller et al. 1988; Smith 1991). In their series of 184 pancreatic biopsies in 178 patients, Mueller et al. reported severe postprocedure pancreatitis in 5 patients (3 %) (Mueller et al. 1988).

As far as vascular structures are concerned, many studies have shown that the transgression of vessels, especially low-pressure veins, does not significantly elevate the complication rate (Ferrucci et al. 1980; Smith 1991; Welch et al. 1989).

Key Points

- Histopathologic analysis is not possible in FNAB
- FNAB is a suitable technique in patients with a known primary tumor
- Needle diameter for FNAB range from 20 to 25 G with standard needle lengths of 5–20 cm
- Needle should be introduced in coaxial or tandem technique
- Cytologic samples are obtained through back-and-forth movement of needle within lesion under manual aspiration
- Sampling of hypervascularized lesions should be performed without aspiration
- Transgression of bowels is possible if direct access to lesion is precluded

9.1.5 CT-Guided Punch Biopsy

In comparison to aspiration biopsy, the punch biopsy (synonym: core biopsy) technique is either performed with (semi-)automatic spring-activated cutting needles (Tru-Cut) in combination with a biopsy gun or with manually activated cutting needles. This technique allows for obtaining cores of tissue with an intact histological structure that facilitates a precise histological diagnosis or immunohistochemical analysis.

9.1.5.1 Indication

Large-gauge automated needle biopsies (12–19 G) are traditionally performed in patients without a known primary tumor, in cases of potential lymphoma, and after inconclusive fine-needle aspiration biopsy. Owing to the varying availability of a cytopathologist and results that are comparable to FNAB (or even better), punch biopsy has meanwhile been established as the primary technique of choice in most radiological departments. Moreover 18–19 G needles are almost as thin as fine needles but provide specimen for histology instead of mere cytological specimen.

9.1.5.2 Material

In comparison to the aspiration technique, core biopsy needles are defined by diameters of 12–19 G (large gauge) and usually by the combination with a spring-activated Tru-Cut system. The Tru-Cut biopsy needle is characterized by a trough at the distal end. First, the biopsy gun fires the inner needle into the lesion where a core of tissue falls into the trough. Then, the outer needle cuts the sample lying in the trough out of the surrounding tissue and captures the sample which can be safely removed through the outer needle or with the whole system (Fig. 9.10). When an automated

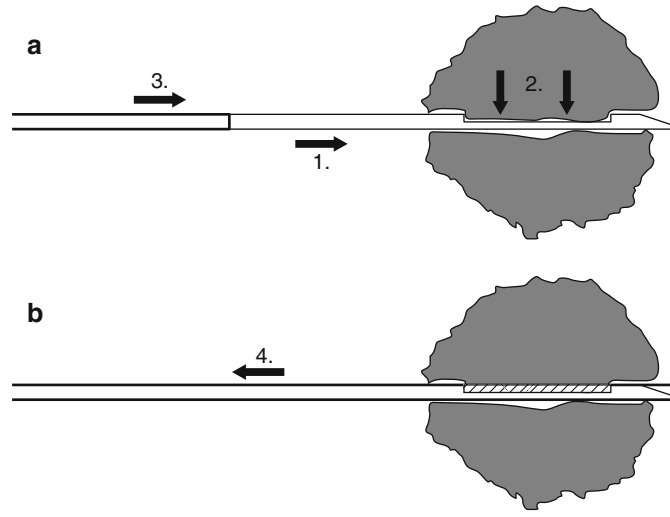

Fig. 9.10 The automated Tru-Cut biopsy technique: (**a**) The inner needle (characterized by a trough at its end) is fired into the target lesion by the biopsy gun (*1*). A core of tissue falls into the trough (*2*). The outer needle slides across the trough and thereby cuts out the specimen (*3*). (**b**) Finally, the specimen can be safely removed with the inner needle or with the whole system (*4*)

Table 9.3 Commercially available needles for CT-guided punch biopsy (exemplary selection of different manufacturers and needles)

Needle type (manufacturer)	Diameter (gauge)	Length (cm)[a]
Tru-Cut manual biopsy needle (Allegiance, McGaw Park, IL, USA)	14; 18	7; 11; 15
Temno semiautomated biopsy system, adjustable cutting length (Allegiance, McGaw Park, IL, USA)[b]	14–22	6; 9; 11; 15; 20; 48
Percucut self-aspirating type cut needle (E-Z-EM, Lake Success, NY, USA)	18; 19.5; 21	5; 10; 15
Easy Core automated biopsy system (Boston Scientific, Natick, MA, USA)	15; 18; 20	10; 15; 21; 25
Magnum reusable core biopsy gun with disposable biopsy needles (Bard Biopsy, Tempe, AZ, USA)[b]	12–20	10; 13; 16; 20; 25; 30
Max Core disposable automated biopsy needle (Bard Biopsy, Tempe, AZ, USA)	14; 16; 18; 20	10; 16; 20; 25
Monopty disposable core biopsy system (Bard Biopsy, Tempe, AZ, USA)	12; 14; 16; 18; 20	10; 16; 20
Quick Core automated biopsy needle with spring (Cook, Medical, Bloomington, IN, USA)[b]	14; 16; 18; 19; 20	6; 9; 15; 20
Biopsy-Handy (Somatex, Teltow, Germany)[b]	14–20	10; 15; 20
Semiautomated biopsy device SABD (Pflugbeil, Zorneding, Germany)	14–21	11.5; 15; 20

[a]Not all diameter-length combinations may be available
[b]Coaxial needles available

Tru-Cut system is used for biopsy, the localization of the needle tip next to the lesion should be documented before taking the sample. Usually, at least two samples are taken for histological evaluation and instantly put into 10 % formalin. Different manufacturers offer either disposable all-in-one systems or the combination of disposable biopsy needles of various diameters and lengths (up to 30 cm) with a standard multi-use gun (Table 9.3). The main advantage is cost reduction. With respect to histopathological evaluation, the advantages of the core biopsy system are that the amount of obtained tissue is more or less constant while the sample keeps its histological structure. In contrast to manually handled large-gauge biopsy systems, the automated mechanism ensures a quick procedure with the biopsy needle in the patient only for a short period of time.

9.1.5.3 Technique

Before introduction of the biopsy needle, local anesthesia is applied with a 22 G needle. In children, elderly, and anxious patients, IV anxiolysis and sedation may be used. During the intervention, cardiorespiratory monitoring is needed in case of conscious sedation. After local anesthesia, a small skin incision is made at the intended needle entry point. The rest of the puncture procedure is performed in an identical manner as described in chap. 2 and Sect. 9.1.4.3.

9.1.5.4 Results

Lung

Anderson et al. performed a study to determine diagnostic accuracy comparing fine-needle aspiration with core biopsies of 195 pulmonary lesions in 182 patients and found a significantly higher diagnostic yield of the core biopsy technique (93 %) compared to FNAB (78 %) (Anderson et al. 2003). The authors concluded that core biopsy should be the method of choice especially if a dedicated cytopathologist is not available (Fig. 9.11). Charig et al. reported their results of 185 core lung biopsies in 183 patients with predominantly 18 and 20 G needles. Diagnostic accuracy (93.5 %) and complication rates were comparable to the published figures for FNAB (Charig and Phillips 2000).

Fig. 9.11 Patient (right lateral decubitus position) with a history of asbestos exposure. Preinterventional CT showed pleural wall thickening of the left lung. An 18-G (10-cm) Tru-Cut biopsy needle was introduced under CT-fluoroscopic guidance parallel to the posterior thoracic wall through an intercostal access. Histopathology revealed pleural mesothelioma

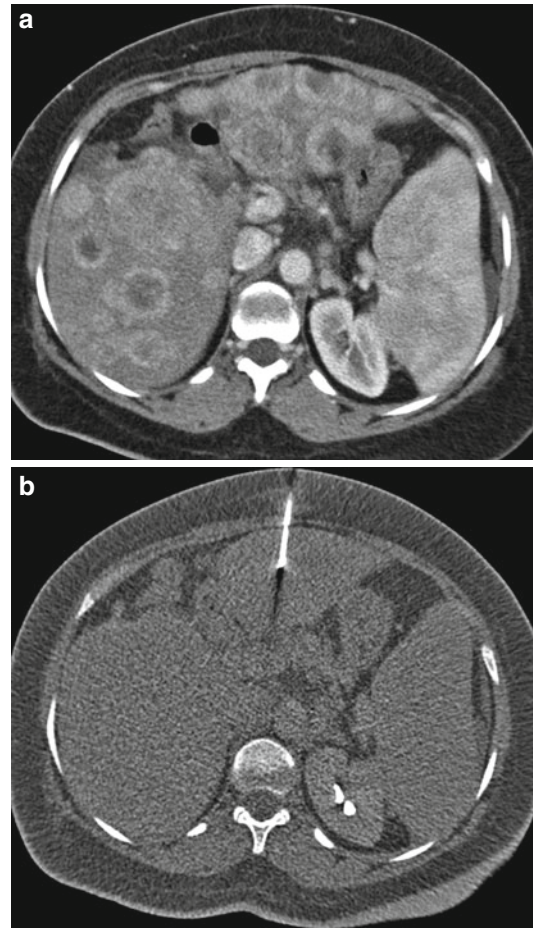

Fig. 9.12 Patient (supine position) with multiple hepatic rim-enhancing lesions in both liver lobes (preinterventional CT; venous phase) (**a**). An easy-to-access lesion in segment 3 was chosen for Tru-Cut biopsy with a 16-G (10-cm) needle under CT-fluoroscopic guidance (**b**). Histopathology revealed hepatic metastases of gall bladder carcinoma

Abdomen

In contrast to FNAB, histological classification of liver masses is only possible with larger core biopsy systems in most cases, as true-positive findings increase from 84 to 98 % (Pagani 1983) (Fig. 9.12). Regarding the ability to differentiate samples obtained with either 14 or 18 G needles, no significant difference was found between both large-gauge needle types (Haage et al. 1999). Automated cutting needles have additionally contributed to increase the accuracy of the histological sample (Hopper et al. 1993). Stattaus et al. conducted a study to determine the visibility of small liver lesions in 50 patients during CT-guided biopsy with 16 and 18 G semiautomated biopsy needles and the influence on biopsy results. 38 patients underwent biopsy guided by non-enhanced CT (89.5 % accuracy), and 12 patients received contrast media at different time points during the biopsy for better visualization leading to a reduced accuracy (75 %). Overall accuracy was 86 %. The authors concluded that in case of poor visualization of liver lesions in non-enhanced CT scans, correlation between the liver lesion and anatomical landmarks can be used for verifying the correct position of the biopsy needle. In addition, interventional MR imaging has the potential to reveal lesions that are poorly visible in CT and US, providing results comparable to CT-guidance: 87–94 % sensitivity, 90–100 % specificity, and 85–93 % accuracy (Salomonowitz 2001; Zangos et al. 2003).

Numerous studies evaluated fine-needle aspiration of pancreatic masses (Gupta et al. 2002; Luning et al. 1985; Sofocleous et al. 2004), while only few authors focused on core biopsy in the pancreas (Elvin et al. 1990; Tseng et al. 2009; Wutke et al. 2001). Tseng et al. published 34 CT-guided biopsies of the pancreas including 9 successful transgastric procedures with a 17-gauge coaxial introducer needle and an 18-gauge biopsy needle, without any complications of peritonitis or bleeding (Tseng et al. 2009). For CT-guided core biopsies conducted in intraabdominal organs (liver, pancreas) the study by Wutke et al. showed sensitivity, specificity, and accuracy values of 88.4, 100, and 90.4 %, respectively. CTF can furthermore help avoid penetration of vital structures with the core biopsy needle along its pathway (Fig. 9.13).

Retroperitoneum and Pelvis

In their analysis of 180 CT-guided coaxial core biopsies, Wutke et al. reported markedly higher diagnostic utility rates for non-organ-related retroperitoneal (88 %) than liver and pancreatic lesions (66 %). Overall sensitivity, specificity, and accuracy rates were 91.1, 100, and 93.3 %, respectively (Wutke et al. 2001). The study of Hau et al. focused on the diagnostic accuracy of both, CT-guided fine-needle and core biopsy of musculoskeletal lesions. The authors found an accuracy rate of 74 % for the subset of core biopsies (258 procedures) in comparison to 63 % for CT-guided fine-needle aspiration (101 procedures). Diagnostic accuracy rates for pelvic and non-pelvic musculoskeletal lesions were 81 and 68 %, respectively (Hau et al. 2002). Stattaus et al. examined 49 cases of coaxial core biopsies performed in the retroperitoneal space. Diagnostic accuracy was 95.9 %, while a specific histological diagnosis could be established in 92.9 % of malignant lesions (Stattaus et al. 2008).

Complications

The study by Anderson et al. (see Sect. 9.1.5.4) showed an initial pneumothorax rate after the biopsy of 30 % which was reduced to 18 % after 4-h follow-up. Only 2 % of the patients developed clinical symptoms requiring further therapy with a chest tube. Separated pneumothorax rates according to the biopsy technique were 35 % (FNAB) and 16 % (core biopsy), respectively (Anderson et al. 2003). Charig and Phillips reported pneumothoraces in 25.9 % (4 of 48 patients (8.3 %) requiring an intercostal drain) and small hemoptyses without pneumothorax in 7 % of their patients (Charig and Phillips 2000).

In a large retrospective multicenter study by Piccinino et al. including 68,276 liver biopsies with a Tru-Cut system, a complication rate of only 0.4 % was found (Piccinino et al. 1986). Deaths after liver biopsy were rarely observed, usually due to hemoperitoneum in patients with

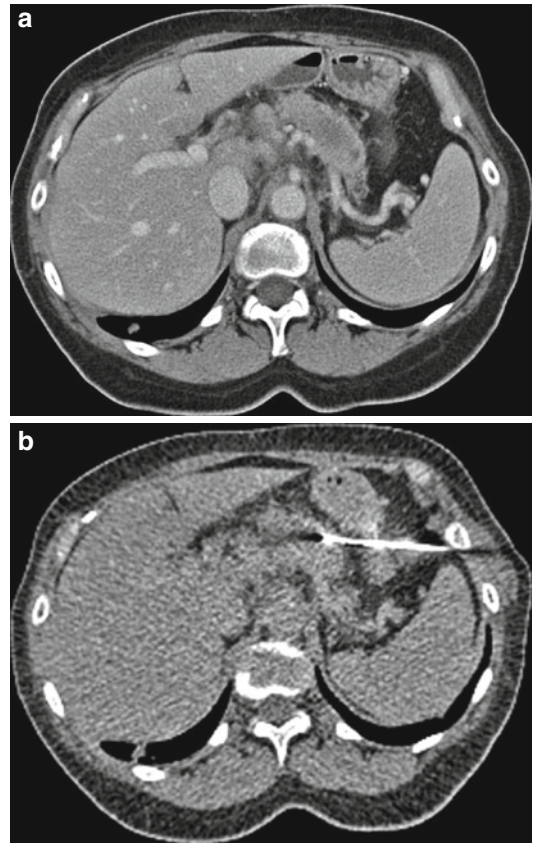

Fig. 9.13 Patient (supine position) with suspect pancreatic mass and pulmonary metastases. Preinterventional CT (venous phase) showed a hypodense area in the pancreatic body and tail (**a**). An intercostal left lateral access path between the spleen and the smaller gastric curvature was chosen for Tru-Cut biopsy with an 18-G (13-cm) needle under CT-fluoroscopic guidance (**b**). Histopathology revealed a pancreatic adenocarcinoma

malignant disease or cirrhosis. The authors reported a higher rate of deaths, serious hemorrhagic complications, pneumothorax, and biliary peritonitis in biopsies performed with the Tru-Cut needle (0.003 %) than with the Menghini needle (0.001 %). In contrast to the analysis by Smith, revealing values between 0.003 and 0.009 % (Smith 1991), the rate of tumor cell seeding after percutaneous tumor puncture of HCC has been reported to be in the range between 1 % (Llovet et al. 2001) and 5 % (Takamori et al. 2000). In biopsy of subcapsular lesions, the rate may even increase up to 12 % (Llovet et al. 2001).

Appraisal

CT-guided percutaneous aspiration and punch biopsy may be performed in essentially every organ system while overall complication rates are low. Success rates depend on the number of samples obtained, the size of the lesion, the organ in which the biopsy is performed, the experience of the local pathology staff, the available imaging equipment, and – first and foremost – the skills of the operator. More complex situations include biopsies of lesions that are protected by overlying bone structures or that require transgression of vital organs to reach the target lesion. Fine-needle aspiration biopsy requires availability of an on-site cytopathologist. The major advantage of fine needle aspiration biopsy is the possibility of bowel transgression without an increased complication rate. In comparison, punch biopsy – especially if performed with a Tru-Cut needle and an automated biopsy gun – facilitates quick histopathological sampling in most cases with comparable complication rates.

Key Points

- Needle diameters range from 12 to 19 G with needle lengths of 5–20 cm
- A spring-activated Tru-Cut needle is common standard
- The samples are usually sufficient for histopathological analysis
- The needle must not transgress the colon

9.1.6 CT-Guided Drill Biopsy

During the past few decades, surgical (open) biopsy of muskuloskeletal tumors could be gradually replaced by image-guided (closed) biopsy techniques (Bickels et al. 1999). Main advantages of image-guided percutaneous biopsy in the muskuloskeletal system are reduced morbidity and costs. Fine-needle aspiration biopsy is often limited in bone tumors given an inadequate ability to sample the tissue matrix while core biopsy reaches accuracy rates of 68–100 % (Pramesh et al. 2001). On the other hand, in young patients with deep subcortical lesions or suspect lesions with a sclerotic rim, the core biopsy needle alone may not be sufficient to penetrate the cortical bone.

9.1.6.1 Indications

Indications for image-guided percutaneous bone biopsy are bone metastases and primary bone tumors and sometimes infectious disease. The biopsy is performed to verify that a suspicious bone lesion is indeed a metastasis in order to detect the primary tumor or to further investigate the diagnosis of osteomyelitis. In patients with breast cancer, hormone sensitivity of a metastatic bone lesion can be important for adequate therapy. In suspected primary bone tumors, biopsy is only exceptionally performed for histological evaluation with respect to the intended therapy. Special attention should be given to potential tumor seeding and the access path for biopsy carefully planned together with the surgeon responsible for resection (Schweitzer et al. 1996). Another indication for percutaneous bone biopsy is suspected osseous infection with microorganisms that have to be identified before antibiotic therapy. In infectious disease, it is sometimes difficult to distinguish osteomyelitis from other diseases such as Charcot osteoarthropathy. Common contraindications are an uncorrectable coagulopathy and potential soft tissue infection with the danger of superinfection of the bone.

9.1.6.2 Material

A variety of bone biopsy needles are available, ranging from sharp-threaded, drilling-type 17-G needles to large-bore 8-G needles (Table 9.4).

For sclerotic or osteoplastic bone lesions of the spine, it is advantageous to collect as much material as possible, because these lesions are often difficult to adequately decalcify for diagnostic workup. Therefore, for sclerotic bone lesions, bone biopsy needles of 11 G or larger are usually best.

When a spinal lesion is in a location that is difficult to access (e.g., a tight passage between the carotid sheath and vertebral artery in the upper cervical spine), lightweight short drilling needles may be advantageous in setting and keeping trajectories in shallow soft tissues, in contrast to larger 11-G needles with heavy handles, which often throw the trajectory of the needle off course when used under CT-guidance. Because the small 17-G E-Z-EM needles are short and very lightweight, they can be set in shallow soft tissues during targeting and still hold their trajectory without hand support. Because they are also very sharp and threaded, they can thus be drilled deeply into the bone to obtain core samples very effectively in most cases.

9.1.6.3 Technique

In comparison to MR imaging, CT is inexpensive and readily available in most institutions. Therefore, most bone biopsies are performed under CT-guidance. First, a CT scan is performed in order to visualize the bone lesion, and the needle entry point and access path are chosen. In case of superficial bone biopsies without potential interference with vascular and nerve structures along the access path, a non-enhanced CT scan is usually sufficient for planning of the access route. Vessels, nerves, visceral, and articular structures should be avoided. Depending on the localization of the bone lesion, different approaches are available:

- Vertebral body: Depending on the vertebral level, the access path is anterior (cervical spine), transpedicular (Fig. 9.14) or intercostovertebral (thoracic spine) (Fig. 9.15), and transpedicular or posterolateral (lumbar spine).
- Pelvis: An anterior, lateral, or posterior approach (avoiding the femoral and sacral nerve plexus and the sacral canal) are used (Fig. 9.16).

Table 9.4 Commercially available needles for CT-guided drill biopsy (exemplary selection of different manufacturers and needles)

Needle type (manufacturer)	Diameter (gauge)	Length (cm)[a]
Ackermann biopsy needle set (Cook, Medical, Bloomington, IN, USA)	14	9.6; 10.8
	14	17.1; 18.3
Elson biopsy needle set (Cook, Medical, Bloomington, IN, USA)	14 (with 22 G introducer and 12 G coaxial needle)	17.1; 18.3
Geremia vertebral biopsy set (Cook, Medical, Bloomington, IN, USA)	16 (with 22 G introducer needle)	15
Myers biopsy needle set (Cook, Medical, Bloomington, IN, USA)	14	10
Spi-Cut biopsy needle (Somatex, Teltow, Germany)[b]	12.5; 14	5; 10; 15; 20
Ostycut Bone biopsy needle (Bard Biopsy, Tempe, AZ, USA)[b]	13–17	5; 7.5; 10; 12.5; 15
Bonopty coaxial biopsy system eccentric drill penetration set (Radi Medical Systems, Uppsala, Sweden)	14	
Percucut bone biopsy needle (E-Z-EM, Lake Success, NY, USA)	17	5; 7.5; 10; 12.5; 15
Percucut coaxial sheath cut-biopsy needle with keyhole cutting edge (E-Z-EM, Lake Success, NY, USA)	19.5	15
Laredo trephine needle	8	

[a]Not all diameter-length combinations may be available
[b]Removal of sample under aspiration

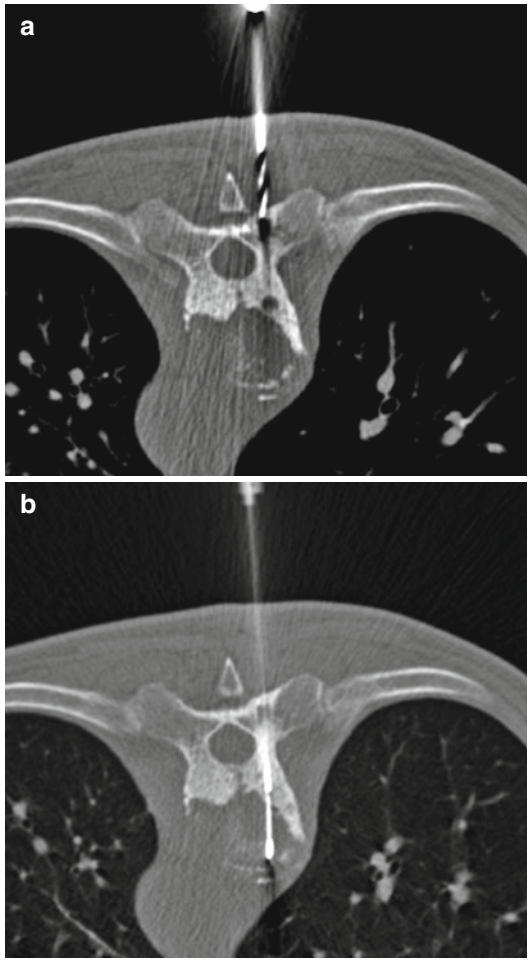

Fig. 9.14 Patient (prone position) with major osteolysis (anterior 2/3) of lower thoracic vertebra showing osteosclerosis of the posterior 1/3 and both pedicles. First, transpedicular access was obtained with a surgical manual drill (**a**). Then, the soft tissue sample was taken with an 18-G (13-cm) Tru-Cut biopsy needle under CT-fluoroscopic guidance (**b**). Histopathology revealed a spinal metastasis of prostate carcinoma

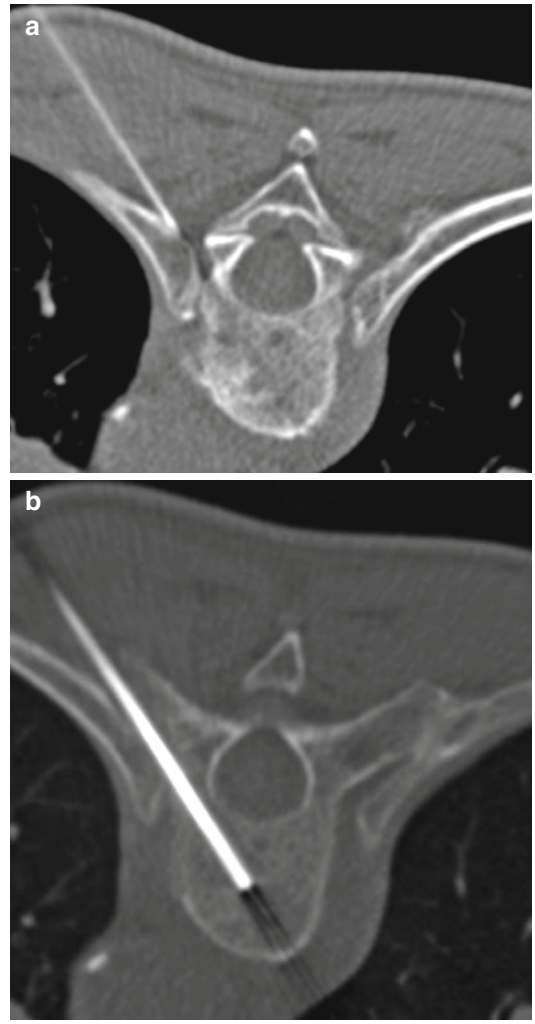

Fig. 9.15 Patient (prone position) with suspicion of spondylodiscitis in the Th°7/8 spinal segment. Preinterventional CT showed small osteolytic defects close to the upper end plate of thoracic vertebra 8. After local anesthesia with a 22-G needle (**a**), a 12.5-G bone biopsy needle was introduced through the left costovertebral joint (**b**). Microbiological analysis revealed spondylodiscitis due to a *Staphylococcus aureus* infection

- Peripheral long tubular bones: an approach orthogonal to the cortical bone is used. This reduces the risk of the biopsy needle gliding off the cortex. The shortest possible access path should be chosen in order to avoid critical structures like vessels and nerves (Fig. 9.17).
- Flat bones (ribs, sternum, scapula): An oblique approach angle of 30–60° is chosen that provides more material for biopsy and helps to protect the underlying structures behind the flat bone (Fig. 9.18).

The whole procedure has to be carried out under strictly sterile conditions to avoid osseous infection with subsequent osteomyelitis. Percutaneous drill biopsy is usually performed under local anesthesia or analgosedation (in incompliant patients), while pediatric bone biopsy represents an exception requiring general

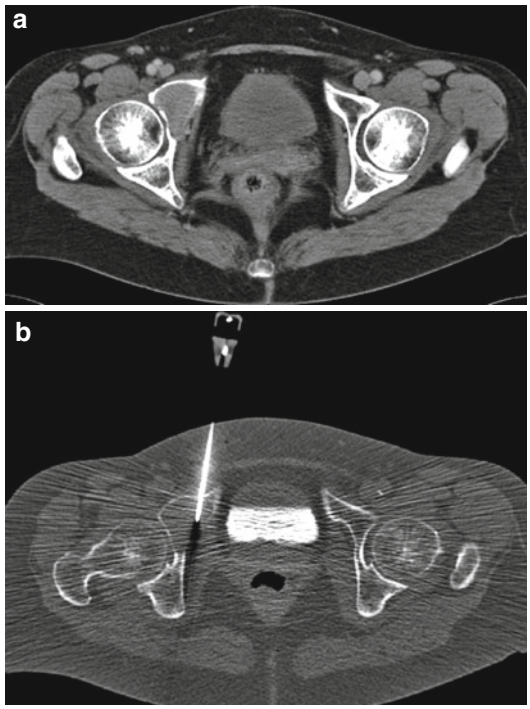

Fig. 9.16 Patient (supine position) with osteolysis of the anterior column of the right acetabulum (**a**). A 14-G bone biopsy needle was introduced with a sterile surgical hammer avoiding the right common femoral artery and vein (**b**). Histopathology revealed multiple myeloma

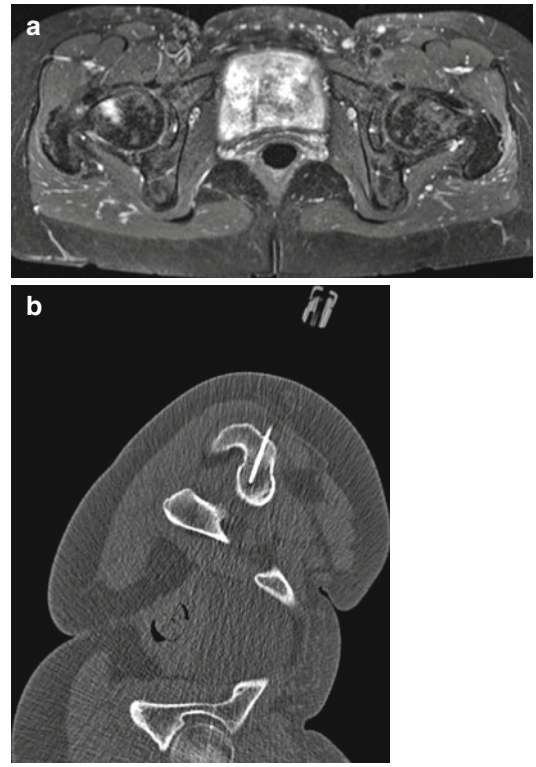

Fig. 9.17 Patient with history of breast cancer and hip pain. Fat-suppressed MR imaging (Short Tau Inversion Recovery (STIR) sequence) of the pelvis showed a hyperintense lesion of the right proximal femoral neck (**a**). A 14-G bone biopsy needle was introduced in a left lateral decubitus position providing stability during insertion with a surgical hammer (**b**). Histopathology revealed bone metastasis of breast cancer

anesthesia. Local anesthesia is applied from the skin level down to the periosteum of the intended entry point of the biopsy needle with a 22-G needle. Leaving the anesthetic needle in the skin by detaching the syringe from the needle with the needle along the intended trajectory course saves time in subsequent needle placements. The initial anesthetic needle serves as a relative directional marker on both the images and the skin, and longer needles can subsequently be placed with positional readjustments as necessary, so that the final needle can be placed in tandem (or coaxial) fashion relative to the target zone. The biopsy needle is introduced through the cortical bone under intermittent CT/CTF control verifying the correct needle direction. The needle containing the sample is completely removed, and the sample fixed in 10 % formalin. In case of suspected infection, the specimen is not fixed but directly put into a sterile container for microbiological analysis. Osteolyses characterized by a soft tissue core are directly sampled using a 16- or 18-G Tru-Cut biopsy needle (Fig. 9.14b). Depending on the thickness of the cortical bone and the degree of sclerosis surrounding the bone lesion, either a surgical hammer in combination with the bone biopsy needle (e.g., 14 G Somatex Spi-Cut, Teltow, Germany), an 8-G trephine needle (e.g., Laredo type), a dedicated bone penetration set (e.g., Bonopty; AprioMed, Uppsala, Sweden), or a manual drill can be used in order to penetrate the cortex (Fig. 9.14a).

9.1.6.4 Results

In their study including 359 CT-guided bone biopsies of muskuloskeletal lesions with the FNAB and core biopsy technique, Hau et al.

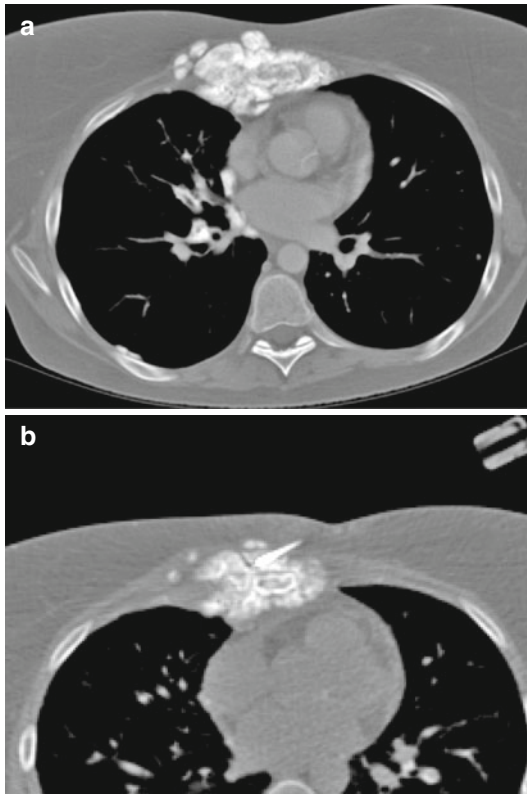

Fig. 9.18 Patient (supine position) with a history of Hodgkin's lymphoma and complete remission after radiochemotherapy who developed a painful swelling around the sternum. The preinterventional CT showed an osteoblastic tumor of the sternum and calcifications in the right pulmonary hilum and pleura (**a**). A slightly oblique approach with a 12-G needle was chosen for CT-guided biopsy of the sternum (**b**). Histopathology revealed an osteosarcoma

reported accuracy rates of 63 % ($n=101$) and 74 % ($n=258$), respectively (Hau et al. 2002). Especially sarcomas have been shown to be undergraded with FNAB sampling only. Therefore core biopsy is the technique of choice. Jelinek et al. reported their results in 110 primary bone tumors that were sampled under CT and fluoroscopic guidance, respectively. Correct final diagnosis could be obtained by biopsy in 88 % of the patients, while the only minor complication was a small hematoma (0.9 % complication rate) (Jelinek et al. 2002). Dupuy et al. performed 176 CT-guided core needle biopsies and 45 fine-needle biopsies with accuracy rates of 93 and 80 %, respectively, and a complication rate below 1 % (Dupuy et al. 1998). In a recently published large retrospective analysis including 2027 cases of CT-guided core needle biopsies of musculoskeletal lesions, the correct diagnosis was possible in 77.3 %, while the remaining patients underwent a second biopsy within 30 days, finally allowing a diagnostic accuracy of 94 %. Most false negative results were found in cervical lesions and in benign, pseudotumoral, inflammatory, and systemic pathologies. The complication rate was low (22 minor adverse events; 1 %), predominantly including transient pareses and hematomas (Rimondi et al. 2011).

In comparison with conventional CT guidance, the advantage of CT-fluoroscopy is the online visualization, the excellent resolution of bone, and the surrounding soft tissue and the possibility to even target small lesions (Daly and Templeton 1999). The very good resolution of bone and soft tissue helps to reduce the amount of complications due to misplacement of the needle. Another major advantage is the possibility to perform biopsies in an off-plane direction enabling the physician to easily target spinal lesions of lumbar vertebra 5 or the sacrum. In the upper lumbar and thoracic regions, CTF provides a means of real-time, visualizing the adjacent lung and other posteriorly located visceral organs, such as the kidneys, in the case of a high lumbar target. In the cervical region, CTF may also be the preferred method of image guidance for biopsies because it can be used to define the positions of the jugular vein, carotid artery, vertebral artery, and pharyngeal and esophageal structures.

9.1.6.5 Complications

In bone lesions that are assumed to be extremely hypervascularized such as suspected metastases of renal cell carcinoma, a digital subtraction angiography may have to be obtained prior to biopsy. Transarterial embolization or direct puncture of the lesion with injection of absorbable gelatin sponge or polyvinyl alcohol particles helps to prevent serious hemorrhage when samples of the lesion are taken.

When biopsies are performed in thoracic lesions, the operator should always be cautious of

a possible pneumothorax; at the end of the procedure, either a follow-up CT scan or an expiratory chest radiograph should be obtained to rule out a pneumothorax. A chest tube kit should be available before biopsy of the thoracic spine.

When pushing or drilling a needle through very dense bone, and when vital structures such as the aorta, the carotid artery, or the vertebral artery are located just beyond the target zone along the trajectory path, the operator may want to use a détente technique with one hand pushing the needle toward the target and the other hand grasping the needle shaft to provide a counteraction force in order to prevent piercing beyond the target area into vital structures if resistance to the needle should suddenly give way.

When delivering a bone core that is impacted within the bone biopsy needle, it is prudent to avoid pushing the core out of the needle with such force that it suddenly flies off and becomes lost. To remove a bone core from the biopsy needle, the operator should use the appropriate trocar design that is intended for such removal.

Appraisal

The growing availability and inexpensiveness, as well as the ability to safely access muskuloskeletal structures have substantially increased the role of computed tomography for guidance of percutaneous biopsies in comparison to other imaging modalities like ultrasound and conventional fluoroscopy. Adjacent major vessels, nerves, and visceral structures can be avoided, and the biopsy needle precisely positioned within the target lesion for histopathologic sampling. CT provides an excellent visualization of bone with the exception of some bone marrow lesions only detectable on MR imaging. Though CTF is necessary only in selected cases, given an experienced operator using repeated single-shot CT-fluoroscopy for needle positioning – CTF can markedly reduce both, the in-room time and radiation dose for the patient.

Key Points

- Needle diameter 8–19 G
- Needle lengths 5–20 cm
- Strictly sterile conditions mandatory during the whole biopsy procedure
- For primary bone tumors, the needle pathway should lie within the surgical resection area
- The access angle should be chosen according to type of bone (tangential access in flat bones, orthogonal access in tubular bones)
- Access to the spine should be anterior/anterolateral in the cervical, intercostovertebral/transpedicular in the thoracic, and transpedicular/ posterolateral in the lumbar spine
- Needle insertion should be with a handgrip or a surgical hammer
- A hand drill preferable for access to lesions with a sclerotic rim/thickened cortical bone

9.2 MR-Guided Biopsies

Christoph Thomas

9.2.1 Indications

In comparison to computed tomography (CT) or ultrasound guided procedures, magnetic resonance (MR)-guided biopsies require a higher degree of training and experience and the use of MR-compatible materials. In addition, they tend to be more time consuming and expensive (Alanen et al. 2004). Furthermore, in most institutions magnet-time is limited. Thus, this technique is currently reserved to cases where MR imaging can unfold its advantages over other modalities:

- Multiplanar MR-fluoroscopy
- Excellent soft tissue contrast
- The lack of radiation exposure

Multiplanar fluoroscopy enables image guidance of extremely angulated trajectories which might be necessary to reach liver lesions in the liver dome and can also be advantageous in the biopsy of other intraabdominal lesions with otherwise limited access. The inherently high soft tissue contrast of MR imaging facilitates the biopsy of lesions which are isodense to their surrounding tissue and therefore invisible in CT imaging. This might be the case in certain liver lesions but also in bone marrow lesions and in inflammatory disease such as acute myositis, where the muscular edema can be targeted. MR imaging can also be used to target breast lesions which cannot be visualized clearly in ultrasound or mammography (Chap. 10). In children and young patients, the lack of radiation exposure using MR imaging is a major advantage.

9.2.2 Materials

9.2.2.1 MRI System

Basically, MR-guided interventions are possible using standard closed bore magnets (Fischbach et al. 2011). In an analogous matter to CT-guided interventions, the patient has to be moved in and out of the magnet for needle manipulation and imaging. Due to the spatial restrictions in a closed magnet, the maximal length of the biopsy devices is limited. Concepts like robotic assistance devices or augmented reality systems to support MR-guided biopsies in closed bore magnets are currently under development (Moche et al. 2008; Wacker et al. 2006). In contrast, an open magnet system allows patient access during imaging and facilitates real-time imaging during needle insertion. Furthermore, it offers more space for the use of longer biopsy devices within the magnet. Currently, two different open magnet designs are available: (1) Sandwich-like magnet designs with field strengths of up to 1.0 T (e.g., Panorama, Philips, Netherlands) with a vertical main magnetic field have been introduced; (2) short and wide bore magnets with a horizontal main magnetic field with field strengths of up to 3.0 T (e.g., MAGNETOM Espree, Siemens, Germany) also offer sufficient patient access. The newer high-field systems provide an improved image quality and imaging speed compared to open low-field systems (Stattaus et al. 2008; Streitparth et al. 2009).

Different surface coils can be used for interventional imaging. Typically, flexible loop coils and multipurpose body array coils are sufficient.

In addition to standard diagnostic setups, further materials are necessary to perform interventions in an MR-imaging suite: An RF-shielded in-room monitor or a beamer to project the acquired images against the wall is needed for image guidance. For communication of the interventionalist and the technician who normally works outside the magnet room, either the standard patient intercom system or a dedicated MR-compatible wireless communication system can be used (Guttler et al. 2011). If an MR-compatible wireless computer mouse or trackball are available in addition to the in-room monitor, the interventionalist can control the scanner and does not depend on the technician and communication, especially in the noisy environment of the MR-imaging suite. Especially in open bore scanners, an MR-compatible stool can facilitate patient access for the interventionalist, and an MR-compatible table is necessary to serve as a tray for the biopsy materials.

9.2.2.2 Instruments

For MR-guided biopsies, dedicated MR-compatible instruments have to be used in order to avoid an interaction of the needle with the magnetic field. Typical materials for MR-compatible biopsy systems are alloys of titanium, nickel, chromium, and molybdenum. MR-compatible materials tend to be softer than surgical steel, leading to a slightly decreased sharpness and stiffness in comparison to non-MR-compatible instruments. However, in recent years, technical advances

have been made regarding the alloys, continuously improving instrument sharpness. As nowadays, mainly core biopsies are requested and performed; this chapter omits fine-needle aspiration. MR-compatible biopsy instruments are available from different manufacturers (Table 9.5). MR-compatible bone biopsy sets and a piezoelectric drill can be purchased from Daum-InVivo (Schwerin, Germany). Basically, off-label use of non-MR-compatible biopsy instruments is possible, if an MR-compatible introducer sheath has been positioned under image guidance and if the device is strictly kept outside the 0.5 T line. However, due to the security hazards connected to the presence of ferromagnetic materials in an MR-imaging suite and the resignation to verify the correct needle position using non-MR-compatible instruments, an off-label use of non-MR-compatible instruments is not recommended.

9.2.2.3 Pulse Sequences

In interventional MR imaging, instruments are visualized by the signal void which is a result of the susceptibility differences of the instruments in comparison to the surrounding tissue. The sizes of the artifacts depend on the material itself (alloy and size), the magnetic field strength, the angle of the needle versus the main magnetic field, the sequence type, and certain sequence parameters (Chap. 3). Large artifacts are generated by a perpendicular needle orientation in relation to the main magnetic field (B_0), use of gradient echo sequences, phase-encoding direction parallel to the needle shaft, low bandwidth settings, and a high echo time, whereas needle orientations parallel to the magnetic field, spin echo or turbo spin echo sequences, phase-encoding direction perpendicular to the needle shaft, a high bandwidth, and low echo time cause smaller artifacts (Lewin et al. 1996). The true needle tip is not necessarily located at the end of the artifact; there can be a deviation of several millimeters. Two classes of sequences are used for MR-guided biopsies: MR-fluoroscopy sequences which repeatedly image one section with an acquisition time of less than 1 s/slice are applied to monitor the insertion of a device, and fast static 2D-sequences are employed for planning and for the verification of the correct needle position. Typically, gradient echo sequences are applied for MR fluoroscopy (e.g., T1w fast low-angle shot (FLASH) and T2w true fast imaging with steady state precession (TrueFISP)). For verification of the needle position, gradient echo, spin echo or turbo spin echo sequences are used. Modern biplanar MR-fluoroscopy sequences can image the needle in perpendicular slices which allows for the verification of the correct angulation in three dimensions. Due to the complex nature of the artifact generation, interventionalists planning to begin MR-guided interventions should perform in vitro experiments with their biopsy devices prior to clinical use in order to familiarize with sequences and artifacts.

Table 9.5 Examples for manufacturers of MR-compatible core biopsy systems

Manufacturer	Model	Size (gauge)	Length (mm)
Daum InVivo (Schwerin, Germany)	Fully automatic BiopsyGun	14–18	100–175
Daum InVivo (Schwerin, Germany)	Semi automatic BiopsyGun	14–18	100–150
EZ-E-M (Lake Success, NY, USA)	Bio-Gun	14; 18	150
EZ-E-M (Lake Success, NY, USA)	Biopsy needles	18; 20	100–200
Somatex (Teltow, Germany)	MR Biopsy Handy	14–18	100–200

9.2.3 Technique

9.2.3.1 Pre-interventional Diagnostics + Informed Consent

Sufficient recent cross-sectional imaging studies (CT or MR imaging) should be available prior to the intervention to enable the planning of the trajectory and to preselect biopsy materials of the correct size and length. Pre-interventional CT imaging can depict osseous structures and calcifications which are only visualized indirectly in MR images and should be requested when in doubt.

Informed consent and pre-interventional screening of the coagulation status have to be obtained in the same way as for CT-guided biopsies. Contraindications for MR-guided biopsies include contraindications for CT-guided biopsies and contraindications for MR examinations, which include the presence of non-MR-compatible ferromagnetic implants and foreign bodies. Most electronic implants such as pacemakers, cochlea implants, and implanted pumps are not MR-compatible. Pregnancy is regarded as a relative contraindication.

9.2.3.2 Pre-interventional Preparation

The patient position on the examination table is determined by the intended access trajectory. For planning of the trajectory, physical factors have to be considered, since the size and contrast of the artifact which depicts the device depend on the angle of the device to B_0. The artifact is most pronounced if the needle is placed in a 90° angle versus B_0. In open sandwich-style magnets, B_0 is oriented vertically, which leads to optimal artifact characteristics in a horizontal direction, while in open bore scanners, B_0 is oriented horizontally, enabling a radial approach. The patient should be placed in a comfortable position to improve his compliance. Then, the surface coils are placed appropriately. A flexible loop coil with a diameter of approximately 10 cm can be placed around the intended skin incision site, allowing later skin disinfection and sterile draping. An additional multipurpose body array coil can be placed adjacently to the flexible loop coil to improve image quality especially in deeper body regions. The coils can be draped to avoid staining with disinfectant.

9.2.3.3 Intervention

Figure 9.19 illustrates the strategy for MR-guided biopsies in a step-by-step-approach. At first, planning images are acquired. In order to shorten the intervention time, only sequences which are necessary for planning should be selected, and it should be refrained from performing a complete diagnostic examination. For liver lesions, coronal and axial fast single shot-sequences can be recommended to gain to a good overview. Furthermore, the available fast needle verification and fluoroscopy sequences should be tested to determine which sequence leads to the best depiction of the anatomy and pathology and offers the highest background signal for an optimal depiction of the needle. After selection of the optimal sequences and determination of the trajectory, the designated needle path should be imaged in two orthogonal planes.

For the determination of the skin access site, the "finger pointing technique" can be used: Two orthogonal MR fluoroscopy planes are placed on the planned trajectory, and the interventionalist uses his index finger or a water-filled plastic syringe to find the correct position on the skin. Alternatively, the skin access site can be determined by placing a capsule (e.g., Nifedipine, Adalat®, Bayer Healthcare, Berlin) onto the estimated skin entry site, followed by repeated imaging and replacing of the capsule, until the correct position is found (Figs. 9.20, 9.21, 9.22, and 9.23). Furthermore, MR-compatible localization grids are available. The struts of these grids typically contain water or diluted gadolinium, leading to high-signal intensity in T1w and T2w sequences. After marking of the entry site, skin disinfection, sterile draping, and local anesthesia are performed in an analogous manner to CT-guided biopsies. Local anesthesia and skin incision can be performed using standard ferromagnetic equipment; however, special attention

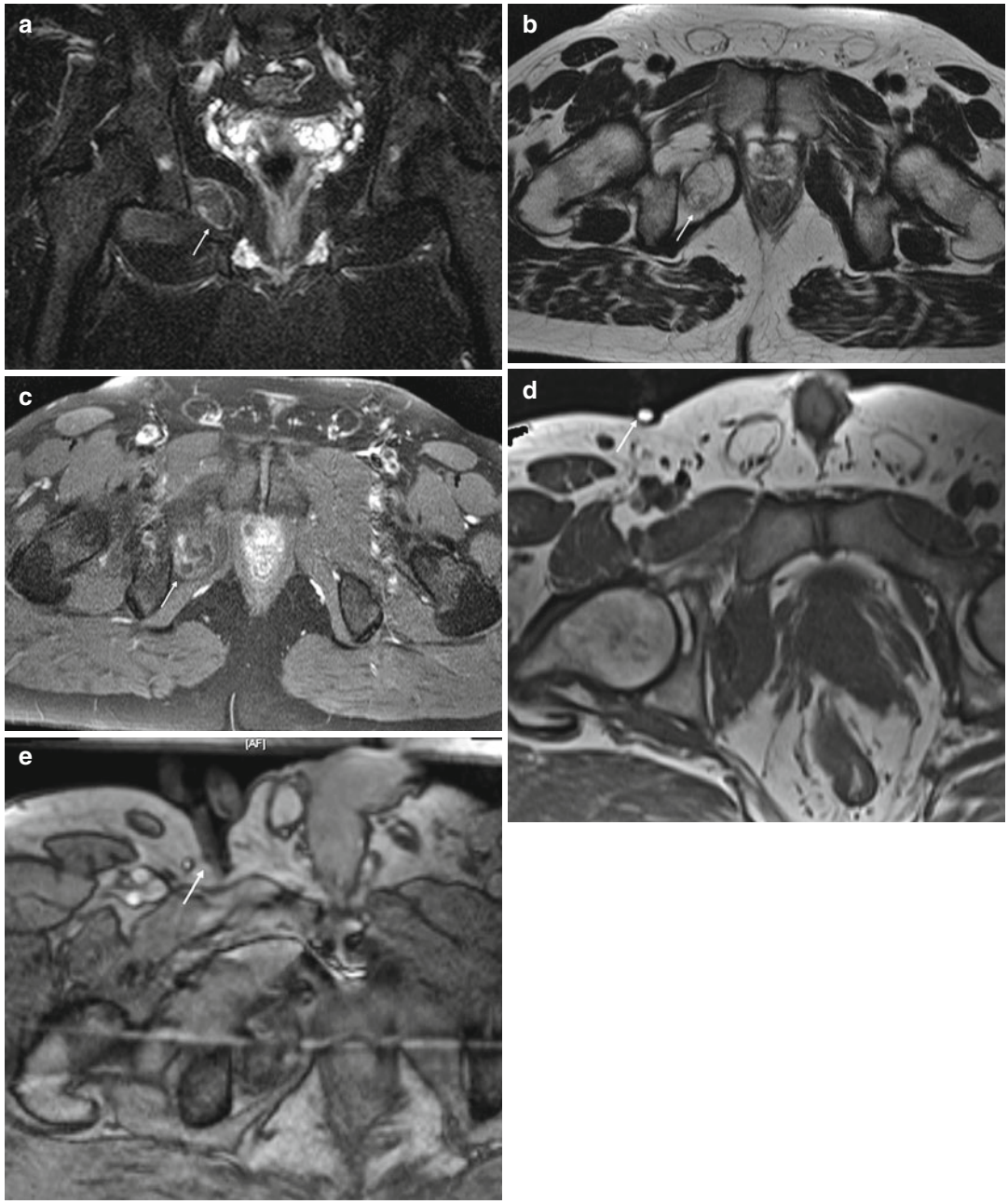

Fig. 9.19 Step-by-step illustration of the strategy for MR-guided biopsies. A 37-year-old man with partly fat-equivalent, partly contrast-enhancing mass in the right obturator foramen (*arrows*). (**a**–**c**) Planning images (**a**: coronal fat-saturated T2w, **b**: axial T1w, **c**: Axial fat-saturated T1w after intravenous contrast administration). (**d**) Verification sequence after placement of an Adalat® capsule (*arrow*), revealing insufficient placement of the capsule (T1w FLASH-2D). (**e**) Identification of the skin entry site using the finger-pointing technique with a plastic syringe (*arrow*, T1w FLASH-2D) after removal of the capsule. (**f**) Biplanar real-time MR fluoroscopy for monitoring the introduction of the biopsy needle (T1w FLASH-2D). (**g**, **h**) Biplanar verification of needle position (T1w FLASH-2D). (**i**, **j**) Biplanar verification of the correct position of the biopsy chamber. Histology: Chondroid lipoma

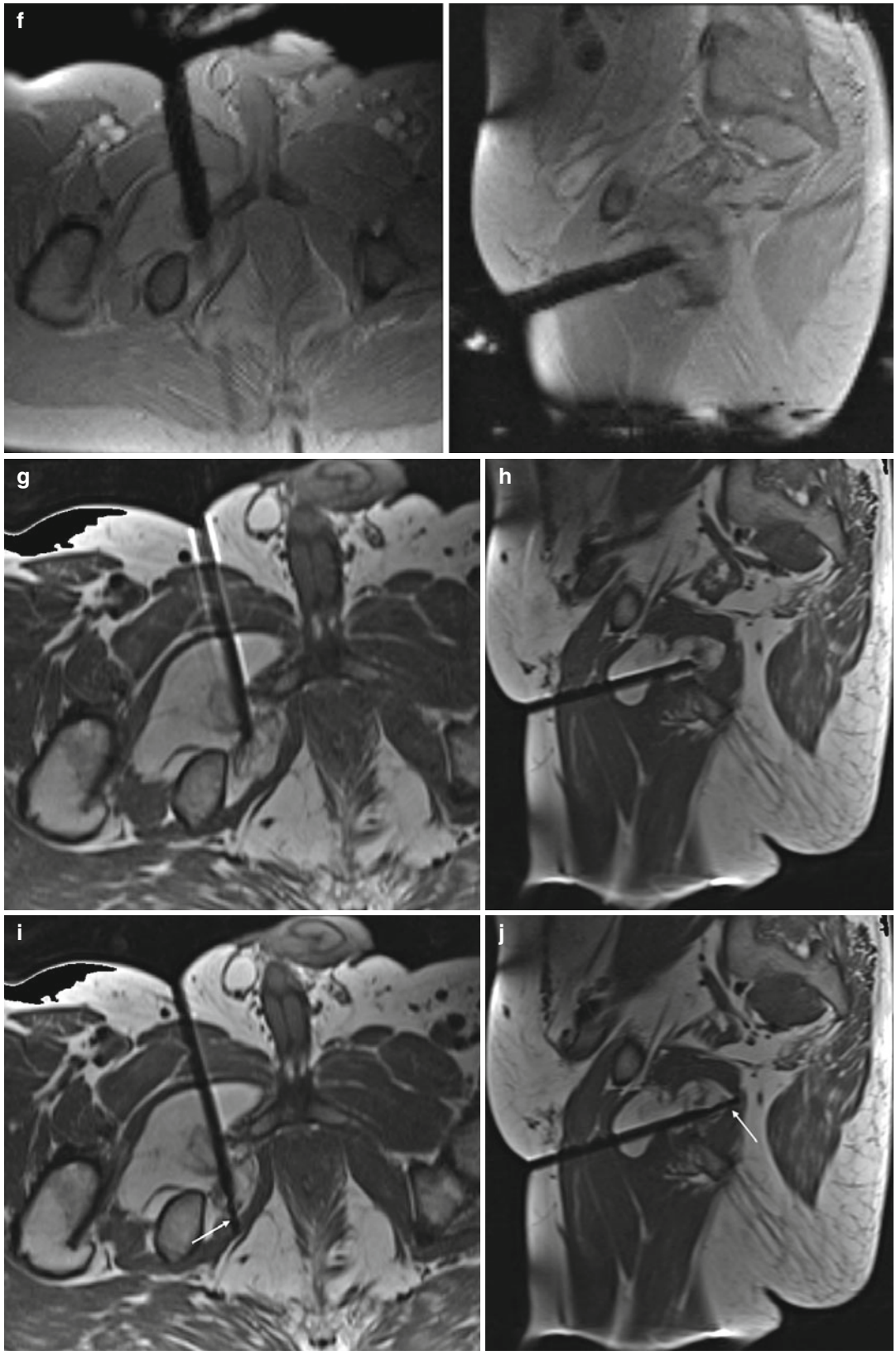

Fig. 9.19 (continued)

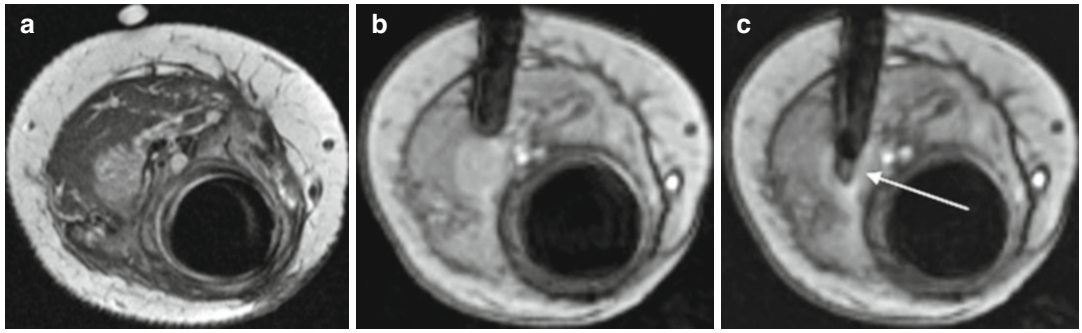

Fig. 9.20 A 14-year-old girl with tumor-prosthesis of the tibia due to osteosarcoma and a new lesion adjacent to the tibia, which was invisible in CT due to metal artefacts. (**a**) Definition of the skin access site using an Adalat® capsule. (**b**) MR fluoroscopy-guided introduction of the biopsy sheath. (**c**) Introduction of the biopsy chamber (*arrow*) under MR fluoroscopy. Histology: Osteosarcoma

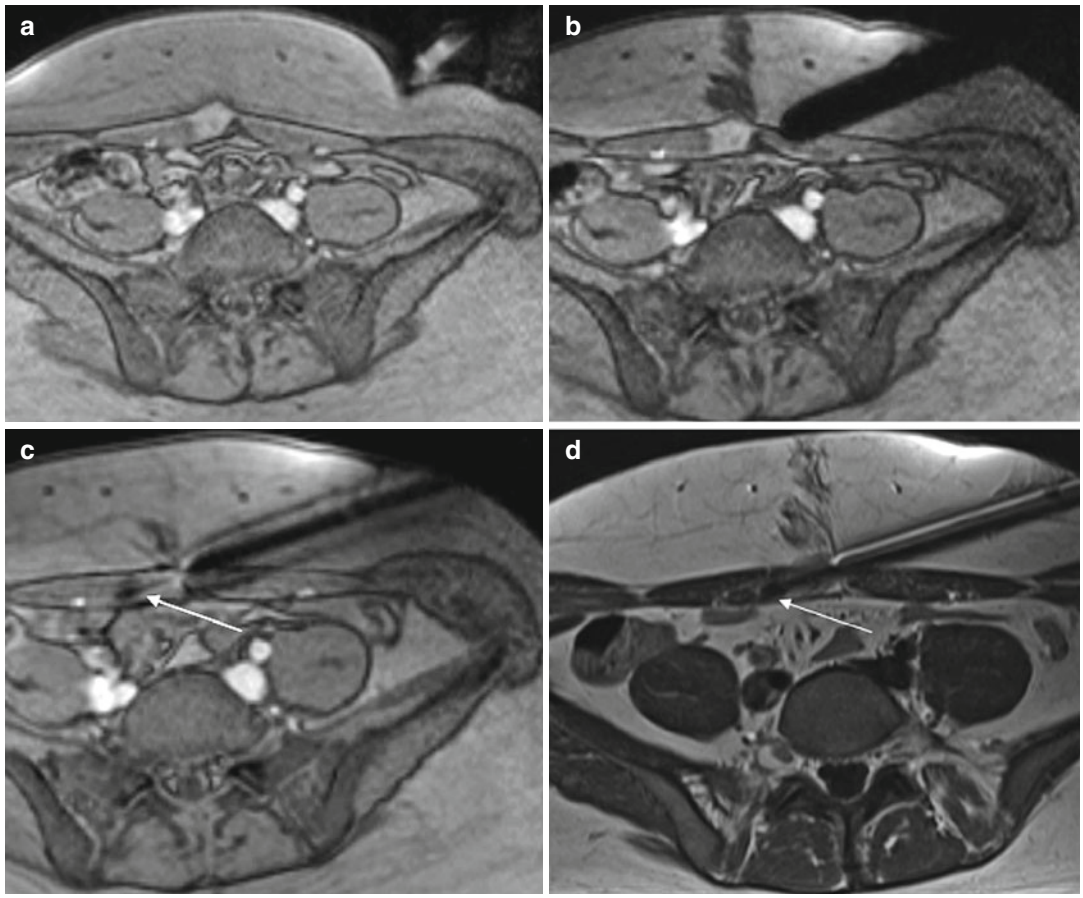

Fig. 9.21 A 35-year-old women with intramuscular lesion of the right rectus abdominis muscle. An oblique trajectory was chosen in order to spare the peritoneum. (**a**) Finger-pointing technique to determine the skin access site. (**b**) MR fluoroscopy-guided introduction of the biopsy sheath. (**c**) Introduction of the biopsy chamber (*arrow*) under MR-fluoroscopic control. (**d**) Documentation of the correct position of the biopsy chamber (*arrow*; Turbo spin echo sequence). Histology: Endometriosis

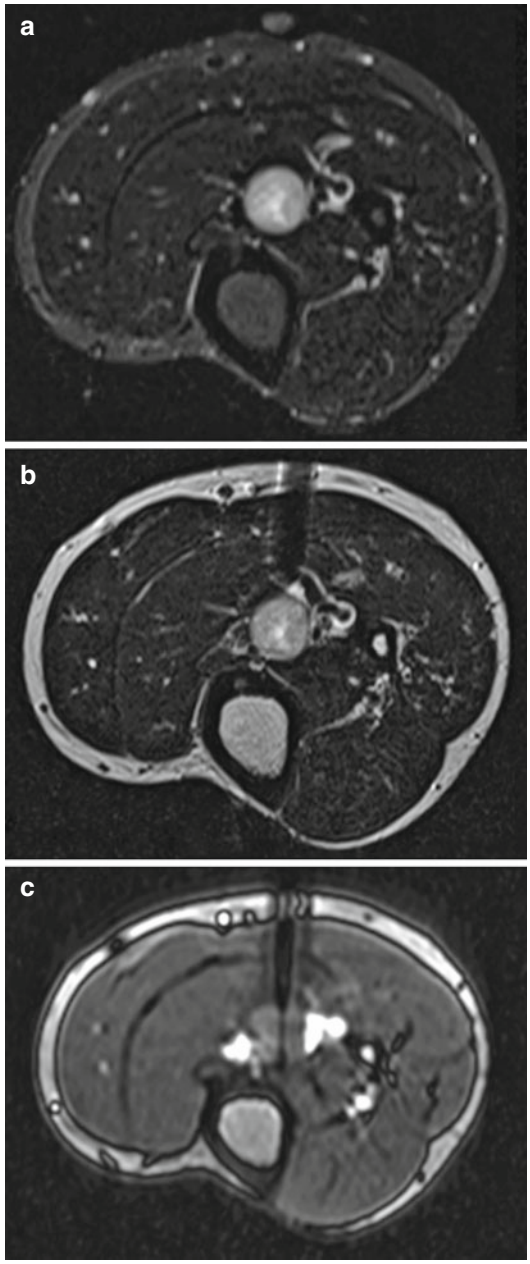

Fig. 9.22 A 32-year-old woman with painful lesion in proximity of the tibial nerve and vessels. The biopsy was performed under regional nerve block anesthesia. (**a**) Planning images with Adalat® capsule. (**b**) Documentation of the correct position of the introducer sheath. (**c**) Introduction of the biopsy chamber under MR fluoroscopy. Histology: Neurinoma

has to be paid to the magnetic forces which act onto ferromagnetic material inside the 0.5 T line. Then, the biopsy sheath is introduced until it penetrates the subcutaneous fat and the superficial fascia. At this point, two fast orthogonal control sequences should be performed to ensure the correct position and orientation of the needle in relation to the planned trajectory. If the position and angulation are correct, the needle can be advanced toward the target. For monitoring, either continuous MR-fluoroscopy or a sequential scanning approach with alternating imaging and advancement of the needle as in sequential CT-guided biopsies can be used. In open bore MR-imaging systems with patient access, the use of MR fluoroscopy is encouraged. If conventional closed bore scanners are used, the sequential strategy has to be applied. Unlike in CT imaging, it is difficult to detect a diversion of the needle from the imaging plane early enough if only one plane is used, thus, it is important to always acquire perpendicular image planes to verify the correct needle position. After the target is reached, biopsy can be performed. Especially in small lesions or in close proximity to relevant anatomic structures, the introduction of the biopsy chamber can be monitored using MR fluoroscopy, and the correct position within the lesion should be documented. The specimen are obtained and fixed in formalin as described for CT-guided biopsy. In case of bleeding out of the sheath which does not resolve spontaneously, gelatin sponge material (e.g., Gelfoam, Pfizer, New York) may be introduced for a more efficient hemostasis.

To rule out postinterventional hematoma, fat-saturated T2w images should be acquired after withdrawal of the cannula. After the intervention, patients are managed according to the rules described for CT-guided biopsies.

Unless the interventionalist controls the scanner himself, sufficient communication between interventionalist and technician is crucial, as the technician

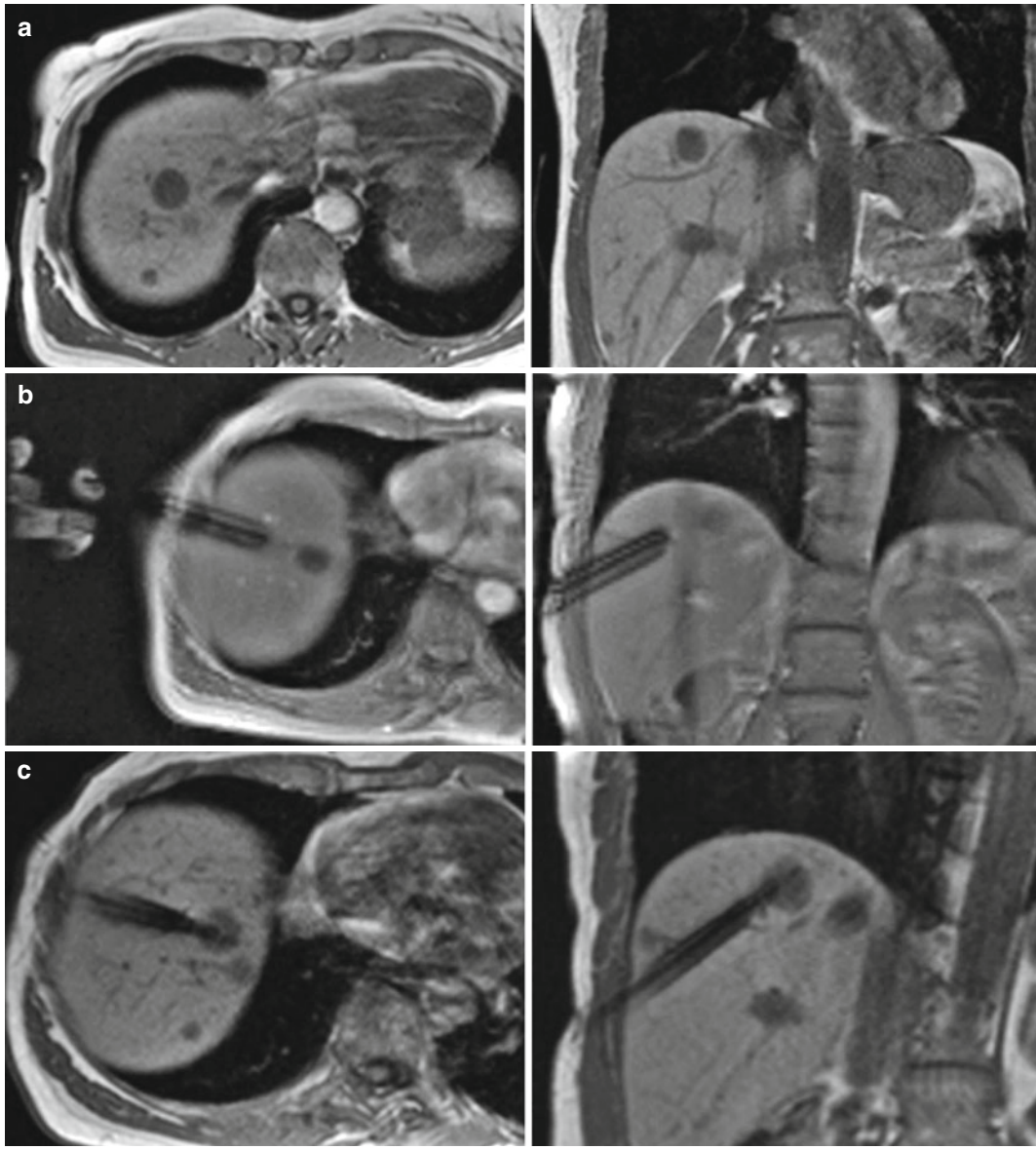

Fig. 9.23 A 55-year-old woman with liver lesions. (**a**) Perpendicular planning sequences. (**b**) Biplanar MR fluoroscopy. (**c**) Biplanar documentation of correct position of the biopsy chamber in the lesion. Histology: Metastasis of breast cancer

normally works outside the scanner room. Verbal communication through the standard patient intercom system can be difficult due to the distance of the interventionalist from the microphone and is impossible during MR fluoroscopy. To improve communication, previously practiced gestures can be used. Alternatively, the use of a MR-compatible communication systems with suppression of background noise is recommended (Guttler et al. 2011).

9.2.4 Results

Regarding sensitivity, specificity, and complications, reported results for MR-guided biopsies are widely comparable to CT-guided biopsies. Zangos et al. reported the largest retrospective study with 322 patients who received MR-guided biopsies of the liver, the prostate, other abdominal, retroperitoneal, musculoskeletal, and thoracic lesions and

lesions in the neck using an open 0.23-T device (Zangos et al. 2009). Combined sensitivity and specificity were 86 and 87 %, respectively. Only two major complications (retroperitoneal and rectal bleeding) occurred, leading to a prolonged hospital stay. Other smaller studies reported comparable results using open low-field devices for abdominal lesions (Kariniemi et al. 2005; Zangos et al. 2006). Regarding the biopsy of musculoskeletal lesions, initial results have been published by Koenig et al. (2001). Carrino et al. have reported good overall results for bone- and soft-tissue biopsies (diagnostic accuracy of 91 %) (Carrino et al. 2007). For the use of open high-field MR-imaging systems (1.0–1.5 T and even 3.0 T), recent publications show excellent results for 1.0-T sandwich magnets (Fischbach et al. 2011), open bore 1.5-T systems (Stattaus et al. 2008), and open bore 3.0-T systems (Kuhn et al. 2010), although for field strengths above 1.5 T, it might be necessary to specifically redesign instruments due to the dependence of the artifact size on the magnetic field.

9.2.5 Complications

As in CT-guided biopsies, possible complications include hemorrhage, infection, organ injury, and implantation of metastases. In the literature, only two major complications leading to a prolonged hospital stay are reported (Zangos et al. 2009). No fatal complications have been reported so far.

Appraisal

After more than a decade of development, MR imaging has matured toward a valuable alternative to other guidance modalities like CT or ultrasound for image-guided biopsies. Due to the higher complexity and intervention costs, MR-guided biopsies are currently not a "first line" option in most institutions but are performed in difficult cases where lesions are not visible using other imaging modalities, where extreme needle angulations are necessary and in pediatric patients. In experienced hands, MR-guided biopsies yield results comparable to CT-guided interventions. For the future, a growing demand and a drop in procedure-related costs for MR-guided biopsies can be expected.

Key Points for the Successful Intervention

- Sufficient pre-interventional imaging is necessary for planning the intervention thoroughly beforehand and to shorten intervention time.
- Communication between interventionalist and technician should be simple and clear and be ideally practiced beforehand; alternatively, the interventionalist should control the scanner by himself from the magnet room.
- The use of MR fluoroscopy can facilitate and accelerate the procedure.
- For needle verification and for MR fluoroscopy, two perpendicular images should be acquired.

References

CT-Guided Biopsy

Anderson JM, Murchison J, Patel D (2003) CT-guided lung biopsy: factors influencing diagnostic yield and complication rate. Clin Radiol 58:791–797

Arslan S, Yilmaz A, Bayramgürler B et al (2002) CT-guided transthoracic fine needle aspiration of pulmonary lesions: accuracy and complications in 294 patients. Med Sci Monit 8:CR493–CR497

Assaad MW, Pantanowitz L, Otis CN (2007) Diagnostic accuracy of image-guided percutaneous fine needle aspiration biopsy of the mediastinum. Diagn Cytopathol 35:705–709

Bickels J, Jelinek JS, Shmookler BM et al (1999) Biopsy of musculoskeletal tumors. Current concepts. Clin Orthop Relat Res 368:212–219

Brandt KR, Charboneau JW, Stephens DH et al (1993) CT- and US-guided biopsy of the pancreas. Radiology 187:99–104

Bret PM, Labadie M, Bretagnolle M et al (1988) Hepatocellular carcinoma: diagnosis by percutaneous fine needle biopsy. Gastrointest Radiol 13:253–255

Brierly RD, Thomas PJ, Harrison NW et al (2000) Evaluation of fine-needle aspiration cytology for renal masses. BJU Int 85:14–18

Cardella JF, Bakal CW, Bertino RE et al (2003) Quality improvement guidelines for image-guided percutaneous biopsy in adults. J Vasc Interv Radiol 14: S227–S230

Carlson SK, Bender CE, Classic KL et al (2001) Benefits and safety of CT fluoroscopy in interventional radiologic procedures. Radiology 219:515–520

Charig MJ, Phillips AJ (2000) CT-guided cutting needle biopsy of lung lesions – safety and efficacy of an outpatient service. Clin Radiol 55:964–969

Cox JE, Chiles C, McManus CM et al (1999) Transthoracic needle aspiration biopsy: variables that affect risk of pneumothorax. Radiology 212:165–168

Daly B, Templeton PA (1999) Real-time CT fluoroscopy: evolution of an interventional tool. Radiology 211: 309–315

Dupuy DE, Rosenberg AE, Punyaratabandhu T et al (1998) Accuracy of CT-guided needle biopsy of musculoskeletal neoplasms. AJR Am J Roentgenol 171: 759–762

Elvin A, Andersson T, Scheibenpflug L et al (1990) Biopsy of the pancreas with a biopsy gun. Radiology 176:677–679

Ferrucci JT Jr, Wittenberg J, Mueller PR et al (1980) Diagnosis of abdominal malignancy by radiologic fine-needle aspiration biopsy. AJR Am J Roentgenol 134:323–330

Fish GD et al (1988) Postbiopsy pneumothorax: estimating the risk by chest radiography and pulmonary function tests. AJR Am J Roentgenol 150:71–74

Grant A, Neuberger J (1999) Guidelines on the use of liver biopsy in clinical practice. British Society of Gastroenterology. Gut 45(Suppl 4):IV1–IV11

Gupta S et al (2002) Masses in or around the pancreatic head: CT-guided coaxial fine-needle aspiration biopsy with a posterior transcaval approach. Radiology 222:63–69

Haage P, Piroth W, Staatz G et al (1999) CT-guided percutaneous biopsies for the classification of focal liver lesions: a comparison between 14 G and 18 G puncture biopsy needles. Rofo 171:44–48 [German]

Hau A et al (2002) Accuracy of CT-guided biopsies in 359 patients with musculoskeletal lesions. Skeletal Radiol 31:349–353

Hopper KD et al (1993) Automated biopsy devices: a blinded evaluation. Radiology 187:653–660

Irie T et al (2001) Biopsy of lung nodules with use of I-I device under intermittent CT fluoroscopic guidance: preliminary clinical study. J Vasc Interv Radiol 12:215–219

Jelinek JS et al (2002) Diagnosis of primary bone tumors with image-guided percutaneous biopsy: experience with 110 tumors. Radiology 223:731–737

Kazerooni EA et al (1996) Risk of pneumothorax in CT-guided transthoracic needle aspiration biopsy of the lung. Radiology 198:371–375

Kim GR et al (2011) CT fluoroscopy-guided lung biopsy versus conventional CT-guided lung biopsy: a prospective controlled study to assess radiation doses and diagnostic performance. Eur Radiol 21:232–239

Klein JS, Salomon G, Stewart EA (1996) Transthoracic needle biopsy with a coaxially placed 20-gauge automated cutting needle: results in 122 patients. Radiology 198:715–720

Kothary N et al (2009) Computed tomography-guided percutaneous needle biopsy of pulmonary nodules: impact of nodule size on diagnostic accuracy. Clin Lung Cancer 10:360–363

Laurent F et al (2000) CT-guided transthoracic needle biopsy of pulmonary nodules smaller than 20 mm: results with an automated 20-gauge coaxial cutting needle. Clin Radiol 55:281–287

Lechevallier E et al (2000) Fine-needle percutaneous biopsy of renal masses with helical CT guidance. Radiology 216:506–510

Lee M (2004) Image-guided percutaneous biopsy. In: Kaufman J, Lee M (eds) Vascular and interventional radiology: the requisites. Mosby, Philadelphia, pp 469–488

Li H et al (1996) Diagnostic accuracy and safety of CT-guided percutaneous needle aspiration biopsy of the lung: comparison of small and large pulmonary nodules. AJR Am J Roentgenol 167:105–109

Llovet JM et al (2001) Increased risk of tumor seeding after percutaneous radiofrequency ablation for single hepatocellular carcinoma. Hepatology 33:1124–1129

Lumachi F et al (2001) Fine-needle aspiration cytology of adrenal masses in noncancer patients: clinicoradiologic and histologic correlations in functioning and nonfunctioning tumors. Cancer 93:323–329

Lumachi F et al (2003) CT-scan, MRI and image-guided FNA cytology of incidental adrenal masses. Eur J Surg Oncol 29:689–692

Luning M, Schmeisser B, Wolff H et al (1984) Analysis of the results of 96 CT-guided fine needle biopsies of liver masses. Rofo 141:267–275 [German]

Luning M et al (1985) CT guided percutaneous fine-needle biopsy of the pancreas. Eur J Radiol 5:104–108

Memel DS, Dodd GD, Esola CC (1996) Efficacy of sonography as a guidance technique for biopsy of abdominal, pelvic, and retroperitoneal lymph nodes. AJR Am J Roentgenol 167:957–962

Mueller PR (1993) Pancreatic biopsy: striving for excellence. Radiology 187:15–16

Mueller PR et al (1988) Severe acute pancreatitis after percutaneous biopsy of the pancreas. AJR Am J Roentgenol 151:493–494

Nahar Saikia U, Khirdwadkar N, Saikia B et al (2002) Image-guided fine-needle aspiration cytology of deep-seated enlarged lymph nodes. Acta Radiol 43: 230–234

Pagani JJ (1983) Biopsy of focal hepatic lesions. Comparison of 18 and 22 gauge needles. Radiology 147:673–675

Piccinino F et al (1986) Complications following percutaneous liver biopsy. A multicentre retrospective study on 68,276 biopsies. J Hepatol 2:165–173

Poe RH et al (1984) Predicting risk of pneumothorax in needle biopsy of the lung. Chest 85:232–235

Pramesh CS et al (2001) Core needle biopsy for bone tumours. Eur J Surg Oncol 27:668–671

Quon D et al (1988) Pulmonary function testing in predicting complications from percutaneous lung biopsy. Can Assoc Radiol J 39:267–269

Rimondi E et al (2011) Percutaneous CT-guided biopsy of the musculoskeletal system: results of 2027 cases. Eur J Radiol 77:34–42

Salomonowitz E (2001) MR imaging-guided biopsy and therapeutic intervention in a closed-configuration

magnet: single-center series of 361 punctures. AJR Am J Roentgenol 177:159–163
Schoth F, Plumhans C, Kraemer N et al (2010) Evaluation of an interactive breath-hold control system in CT-guided lung biopsy. Rofo 182:507–511
Schweitzer ME et al (1996) Percutaneous skeletal aspiration and core biopsy: complementary techniques. AJR Am J Roentgenol 166:415–418
Silverman SG et al (1999) CT fluoroscopy-guided abdominal interventions: techniques, results, and radiation exposure. Radiology 212:673–681
Smith EH (1991) Complications of percutaneous abdominal fine-needle biopsy. Review. Radiology 178: 253–258
Sofocleous CT et al (2004) CT-guided transvenous or transcaval needle biopsy of pancreatic and peripancreatic lesions. J Vasc Interv Radiol 15:1099–1104
Swischuk JL et al (1998) Percutaneous transthoracic needle biopsy of the lung: review of 612 lesions. J Vasc Interv Radiol 9:347–352
Takamori R et al (2000) Needle-tract implantation from hepatocellular cancer: is needle biopsy of the liver always necessary? Liver Transpl 6(1):67–72
Tanaka J, Sonomura T, Shioyama Y et al (1996) "Oblique path"–the optimal needle path for computed tomography-guided biopsy of small subpleural lesions. Cardiovasc Intervent Radiol 19:332–334
Tatli S, Gerbaudo VH, Mamede M, Tuncali K, Shyn PB, Silverman SG (2010) Abdominal masses sampled at PET/CT-guided percutaneous biopsy: initial experience with registration of prior PET/CT images. Radiology 256:305–311
Tomiyama N et al (2000) CT-guided needle biopsy of small pulmonary nodules: value of respiratory gating. Radiology 217:907–910
Torzilli G et al (1999) Accurate preoperative evaluation of liver mass lesions without fine-needle biopsy. Hepatology 30:889–893
Tsai IC et al (2009) CT-guided core biopsy of lung lesions: a primer. AJR Am J Roentgenol 193:1228–1235
Tseng HS et al (2009) Percutaneous transgastric computed tomography-guided biopsy of the pancreas using large needles. World J Gastroenterol 15: 5972–5975
Tsukada H et al (2000) Diagnostic accuracy of CT-guided automated needle biopsy of lung nodules. AJR Am J Roentgenol 175:239–243
van Sonnenberg E, Casola G (1988) Interventional radiology 1988. Invest Radiol 23:75–92
van Sonnenberg E et al (1988) Difficult thoracic lesions: CT-guided biopsy experience in 150 cases. Radiology 167:457–461
Wallace MJ et al (2002) CT-guided percutaneous fine-needle aspiration biopsy of small (< or =1-cm) pulmonary lesions. Radiology 225:823–828
Welch TJ et al (1989) CT-guided biopsy: prospective analysis of 1,000 procedures. Radiology 171:493–496
Wildberger JE, Biesterfeld S, Adam GB et al (2003) Refinement of cytopathology of CT-guided fine needle aspiration biopsies with additional histologic examination of formalin-fixed blood-clots. Rofo 175:1532–1538 [German]
Wutke R, Schmid A, Fellner F et al (2001) CT-guided percutaneous core biopsy: effective accuracy, diagnostic utility and effective costs]. Rofo 173:1025–1033 [German]
Zaetta JM, Licht MO, Fisher JS et al (2010) A lung biopsy tract plug for reduction of postbiopsy pneumothorax and other complications: results of a prospective, multicenter, randomized, controlled clinical study. J Vasc Interv Radiol 21:1235–1243
Zangos S, Kiefl D, Eichler K et al (2003) MR-guided biopsies of undetermined liver lesions: technique and results. Rofo 175:688–694 [German]
Zwischenberger JB et al (2002) Mediastinal transthoracic needle and core lymph node biopsy: should it replace mediastinoscopy? Chest 121(4):1165–1170

MR-Guided Biopsies

Alanen J, Keski-Nisula L, Blanco-Sequeiros R, Tervonen O (2004) Cost comparison analysis of low-field (0.23 T) MRI- and CT-guided bone biopsies. Eur Radiol 14:123–128
Carrino JA, Khurana B, Ready JE, Silverman SG, Winalski CS (2007) Magnetic resonance imaging-guided percutaneous biopsy of musculoskeletal lesions. J Bone Joint Surg Am 89:2179–2187
Fischbach F, Bunke J, Thormann M et al (2011) MR-guided freehand biopsy of liver lesions with fast continuous imaging using a 1.0-T open MRI scanner: experience in 50 patients. Cardiovasc Intervent Radiol 34:188–192
Guttler FV, Rump J, Seebauer C, Teichgraber U (2011) A wireless communication system for interventional MRI. Rofo 183:68–70 [German]
Kariniemi J, Blanco Sequeiros R, Ojala R, Tervonen O (2005) MRI-guided abdominal biopsy in a 0.23-T open-configuration MRI system. Eur Radiol 15:1256–1262
Koenig CW, Duda SH, Truebenbach J et al (2001) MR-guided biopsy of musculoskeletal lesions in a low-field system. J Magn Reson Imaging 13:761–768
Kuhn JP, Langner S, Hegenscheid K et al (2010) Magnetic resonance-guided upper abdominal biopsies in a high-field wide-bore 3-T MRI system: feasibility, handling, and needle artefacts. Eur Radiol 20:2414–2421
Lewin JS, Duerk JL, Jain VR, Petersilge CA, Chao CP, Haaga JR (1996) Needle localization in MR-guided biopsy and aspiration: effects of field strength, sequence design, and magnetic field orientation. AJR Am J Roentgenol 166:1337–1345
Moche M, Trampel R, Kahn T, Busse H (2008) Navigation concepts for MR image-guided interventions. J Magn Reson Imaging 27:276–291
Stattaus J, Maderwald S, Baba HA et al (2008) MR-guided liver biopsy within a short, wide-bore 1.5 Tesla MR system. Eur Radiol 18:2865–2873
Streitparth F, Gebauer B, Melcher I et al (2009) MR-guided laser ablation of osteoid osteoma in an open high-field

system (1.0 T). Cardiovasc Intervent Radiol 32: 320–325

Wacker FK, Vogt S, Khamene A et al (2006) An augmented reality system for MR image-guided needle biopsy: initial results in a swine model. Radiology 238:497–504

Zangos S, Eichler K, Wetter A et al (2006) MR-guided biopsies of lesions in the retroperitoneal space: technique and results. Eur Radiol 16:307–312

Zangos S, Muller C, Mayer F et al (2009) Retrospective 5-year analysis of MR-guided biopsies in a low-field MR system. Rofo 181:658–663 [German]

MR-Guided Breast Intervention

10

Simone Schrading

Contents

S. Schrading
Department of Diagnostic and Interventional Radiology, University Hospital, RWTH Aachen University, Pauwelsstrasse 30, D-52074 Aachen, Germany
e-mail: sschrading@ukaachen.de

10.1 Introduction

The role of magnetic resonance (MR) imaging for diagnosing and staging of breast cancer is ever increasing. It has been shown that MR imaging can detect breast cancer that is occult on mammography, ultrasound, and clinical examination. With the increasing use of breast MR imaging, there is an increasing number of women who require an MR-guided intervention for lesions that are visible with breast MR imaging alone, i.e., that are occult on mammography and on second-look ultrasound. Until recently, MR-guided needle localization with subsequent surgical biopsy has been the standard technique to deal with this situation. During the last years, MR-guided breast biopsy is available and is gaining more and more importance in the management of only MR visible lesions. But MR-guided breast biopsy is a challenging endeavor for many reasons, including the requirement for equipment that will work in the MR imaging environment, need to remove the patient from the magnet to perform biopsy in closed systems, limited access to the medial and posterior part of the breast, decreasing lesion conspicuity with time after contrast injection (vanishing phenomenon), and difficulties confirming lesion retrieval. Semiautomatic core biopsy under MR guidance has been successfully performed, but for a variety of reasons did not gain broad clinical acceptance. MR-guided vacuum biopsy, however, is a technique that allows a more accurate and successful tissue sampling of

A.H. Mahnken et al. (eds.), *CT- and MR-Guided Interventions in Radiology*,
DOI 10.1007/978-3-642-33581-5_10, © Springer-Verlag Berlin Heidelberg 2013

lesions seen only on MR imaging. This chapter gives an overview about procedures and results of MR-guided breast needle localization and MR-guided breast biopsy using semiautomatic core needles and vacuum-assisted biopsy probes.

10.2 Indication

Before a breast MR-guided intervention of a suspicious lesion is performed, all patients should undergo an extensive workup in order to find out whether the questionable MR imaging detected lesion is visible, in retrospect, by conventional imaging studies. The workup should consist of a targeted ultrasound of the area of the MR-identified abnormality ("second-look ultrasound") and a review of the respective mammograms. The diagnostic mammogram should be amended by additional mammographic views and spot compression over the area of the MR-detected abnormality. Only in case this workup does not reveal a clear correlate for the MR imaging finding, patients should proceeded to an MR-guided intervention.

10.3 Patient Preparation

Prior to MR-guided interventions, the procedure and all risks involved as well as the benefits should be explained to the patient. Written informed consent needs to be obtained from the patient.

Although the intervention is quite fast and is well tolerated, the procedure can cause patient anxiety. At our institution, patients receive intravenous sedation with 5–10 mg diazepam i.v. just before starting the intervention. MR-guided vacuum biopsy is not performed under the medication with anticoagulants. Any medication with aspirin or anticoagulants should be paused for at least 5 days. Blood values should be checked for thrombocytes, INR (international normalized ratio), and partial thromboplastin time (PTT).

The patient is positioned prone with both breasts in a dedicated surface breast in the magnet. Then the skin is cleansed with alcohol or povidone-iodine (Fig. 10.1a). The breast undergoing the intervention is fixated with a breast immobilization system. Breast immobilization is important in MR-guided interventions for several reasons. Often the lesion becomes less evident during the procedure due to the transient nature of contrast enhancement; it is therefore essential to identify the lesion at the outset of the procedure and then to ensure that the lesion remains fixed in position. Furthermore, breast immobilization is necessary to help minimize lesion motion during needle placement. Immobilization of the breast can be achieved by immobilizing the breast between two compression plates. Compression plates are usually oriented in the mediolateral plane. Compression plates have been manufactured with perforated holes, four flexible horizontal bands, or fixed grid lines (Fig. 10.1b, c). Only gentle breast fixation should be used in order to avoid nonenhancement of the lesion, due to a too strong compression of vessels.

10.4 Imaging Protocol

To identify the target lesion, a diagnostic breast MR imaging study needs to be performed. For example, the following imaging protocol can be used: axial 2D T1-weighted gradient echo, contrast-enhanced, and dynamic series (290/4.6 (repetition time msec/echo time msec), 90° flip angle, slice thickness 3 mm (no gap), matrix 512×512) before and four times after bolus injection of gadolinium dimeglumine. In addition, a T2-weighted turbo spin echo images (3,000/120 (repetition time msec/echo time msec), slice thickness 3 mm, matrix 512×512) with the same anatomic parameters as the gradient echo sequence should be obtained. As in most cases only on breast will be biopsied, the field of view should be adjusted to the single breast setting (e.g. 220 mm).

Fig. 10.1 Compression device for MR-guided intervention. (**a**) For interventional MR imaging examinations as for diagnostic studies, the patient lies prone with the breast having biopsy in the dedicated breast coil. The breast is cleansed with alcohol. (**b**) Breast MR coil with compression grid (Biopsy Device Model MR-BI-160, MRI devices) in place. The patient is positioned that way that the expected lesion is located under the grid system. (**c**) Breast MR coil with compression post and pillar system (Biopsy Device Model MR-BI-160, MRI devices). The immobilization system housed a perforated compression plate and a striated hole structure consisting of four 2 cm wide and 10 cm long openings. The pillar needle holder consisted of detachable pillar on a rail. This pillar has housing for needle holder collars of different sizes from 9 to 18 gauges. The pillar can be repositioned and fixed to certain position both horizontally and vertically. The system enables an oblique approach. Therefore, the needle guide can be angulated up to 15° which allows to biopsy or the mark lesions which are very close to the chest wall

10.5 Calculation of the Target's Coordinates

The target's coordinates and an appropriate needle trajectory can be calculated by using dedicated software tools (e.g., DynaCAD, MRI devices/Invivo, Orlando USA). The software automatically calculates based on the coil, the immobilization system and the biopsy device, the coordinates of the lesion location, and the desired depth of probe insertion. With these coordinates, the location of the lesion and the corresponding needle trajectory can be directly established on the breast compression device.

If such software is not available, prior to the diagnostic imaging, a marker (e.g., a vitamin E capsule) is placed on the skin overlying the expected lesion localization. For sagittal images (Fig. 10.2a), after reviewing the images at the console, a cursor is placed over the lesion on the monitor; the horizontal (x) and vertical (y) coordinates of the lesion are measured in cm on the basis of the spatial relationship between the lesion, vitamin E marker, and grid lines. The depth (z) coordinate of the lesion is determined on the basis of the relationship between the lesion and the skin surface. The skin surface is at the slice where the indentations from the grid are evident as low signal intensity lines. The depth of the lesion from the skin surface in millimeters (z) is calculated by determining the number of sagittal slices between the skin and the lesion and multiplying by the slice thickness (e.g., 3 mm).

For axial images (Fig. 10.2b), the horizontal (x) coordinate is determined on the basis of the difference in cm between the vitamin E marker and the lesion. The vertical (y) coordinate is calculated by determining the number of axial slices between the slice of which the marker is visible and the slice of which the lesion is visible and multiplying by the slice thickness (e.g., 3 mm). The depth (z) is determined by measuring the distance between the skin surface and the lesion.

After calculating the lesion coordinates and establishing these on the compression device, the breast is anesthetized in the area of the calculated lesion position with 10 ml or more of local anesthetics.

10.6 Procedure MR-Guided Needle Localization and MR-Guided Biopsy

10.6.1 MR-Guided Needle Localization

Magnetic resonance imaging-guided interventions can be performed free hand or by using guidance methods, such as a compression grid system (Fig. 10.1b). The freehand method has the advantage of allowing the needle to be angled, but the potential disadvantage of a long examination time because of repeated imaging to confirm needle placement. Because of these disadvantages, the standard method is needle localization by using compression systems that allow more accurate initial needle placement.

10.6.1.1 Material

A variety of needles are now commercially available for MR-guided needle localization. Conventional ferromagnetic needles cannot be used for MR-guided localization procedures due to the high magnetic field. Nonferromagnetic materials such as stainless steel produce severe artifacts. Materials with increased nickel content such as iconel and other high nickel and low susceptibility alloys generate fewer artifacts. Titanium wires and needles also have fewer artifacts and are used widely at present. Usually needles with a size of 18 or 20 G are usually used. Table 10.1a gives an overview over available MR compatible wires.

10.6.1.2 Performing Needle Localization

A needle guide that is provided with the grid compression system is inserted into the grid at the calculated position overlaying the target lesion (Fig. 10.3a). The needle guides are manufactured to have 18- or 20-gauge holes to accommodate various needle sizes. The needle guide is used to enable insertion of the needle in a straight approach, without angulation. The MR compatible needle/hook wire is then placed in the calculated hole of the needle guide. The needle is inserted to the desired depth. After needle insertion, a T1-weighted spin echo sequence is obtained to document the location of the needle.

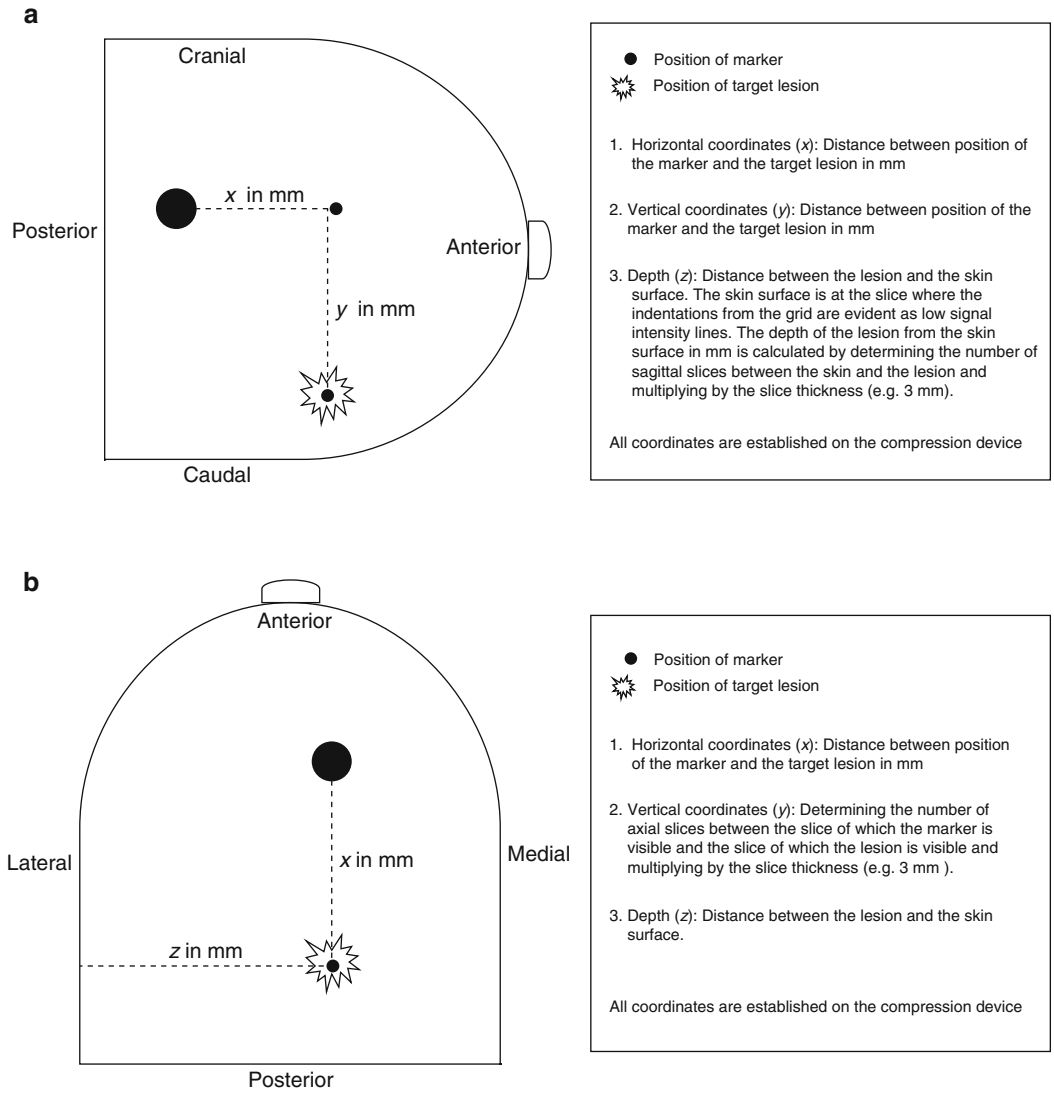

Fig. 10.2 Calculation of the target's coordinates. (**a**) Sagittal imaging. (**b**) Axial imaging

The needle is evident as a low signal intensity structure with adjacent susceptibility artifact (Fig. 10.3e). If the needle is too deep or too superficial, adjustments are made. When the needle tip is in good position, the wire is deployed by advancing the wire to the mark, indicating that the tip had emerged from the needle. The needle is then removed, leaving the wire in place, and a final series of T1-weighted spin echo sequence images are obtained to document the final wire position (Fig. 10.3f).

After localization, a two-view mammogram can be obtained so that the surgeon can see the location of the wire with respect to the nipple, the chest wall, and the remainder of the breast tissue.

10.6.2 MR-Guided Core Biopsy

MR-guided semiautomatic core biopsy can be performed with MR compatible, single-use,

Table 10.1 Material: MR-guided breast intervention

(a) MR-guided needles/hook wires		
Hook wire	Gauge (G)	Repositionable
SOMATEX, MR Tuloc	20	Yes
SOMATEX, MR Duo system	20	Yes
Cook, Kopans breast lesion localization needles	20	No
Invivo, hook wire localization needle	18	No
E-Z-EM Inc., Lesion marking system	20	No

(b) MR-guided vacuum biopsy systems				
Vacuum biopsy system	Gauge	Flashing of biopsy cavity with NaCl	Continuous tissue collection	Clip placement through biopsy system
Suros, ATEC	9G	Yes	Yes	Yes
Bard, VACORA	10G	No	No	Yes
Devicor Medical Systems, Mammotome Biopsy System	8G and 11G	No	Yes	Yes
SenoRx, EnCor MRI	7G and 10G	Yes	Yes	Yes

semiautomatic core guns with 14–20 gauge. After determining the lesion coordinates and local anesthetics, a skin nick is made with a scalpel, and the coaxial needle is placed until the calculated depth. Then the position of the needle is verified with a T1-weighted spin echo sequence. If necessary, the needle position is adjusted. Then 5–10 core biopsies should be obtained with rotating the biopsy notch in a clockwise direction. After the biopsy, a second contrast-enhanced series (T1-weighted turbo SE before and after contrast injection) can be obtained to control whether the biopsy was sufficient or not. Alternatively a contrast-enhanced T1-weighted turbo SE with spectral-selective fat suppression can be performed. If the lesion has not been sufficiently biopsied, another 5–10 core biopsies should be obtained.

10.6.3 MR-Guided Vacuum Biopsy

10.6.3.1 Material

Different vacuum biopsy devices are commercially available with 11–7G probes (Table 10.1b). With all available systems, a quick and accurate MR-guided vacuum biopsy is possible, and differences exist only regarding handling of the biopsy device.

10.6.3.2 Performing Vacuum Biopsy

The appropriate hole of the needle guide is selected. A stylet and an introducer sheath are then placed through the needle guide and advanced to the calculated depth (Fig. 10.4a). Then the stylet is removed, and an obturator is placed inside the introducer sheath to assist in MR imaging confirmation of location (Fig. 10.4b). A fast T1-weighted gradient echo sequence is performed to document the location of the obturator, with the ideal location of the tip being at the site of the lesion. A distance of 5 mm between the tip of the obturator and the lesion is still acceptable because the lesion will still be sampled due to the strong vacuum of the system. If positioning is appropriate, the biopsy device is inserted (Fig. 10.4c). The direction of tissue acquisition is chosen based on location of the introducer with respect to the lesion. The radiologist performing the biopsy controls the direction of tissue acquisition, by turning the biopsy probe in the desired direction. Most of the biopsy systems allow a continuous sampling of tissue without removing the biopsy needle. Each specimen is then automatically transported into a container. Only one system (VACORA System) does not allow continuous tissue sampling. With this system after each needle pass, the needle needs to be removed

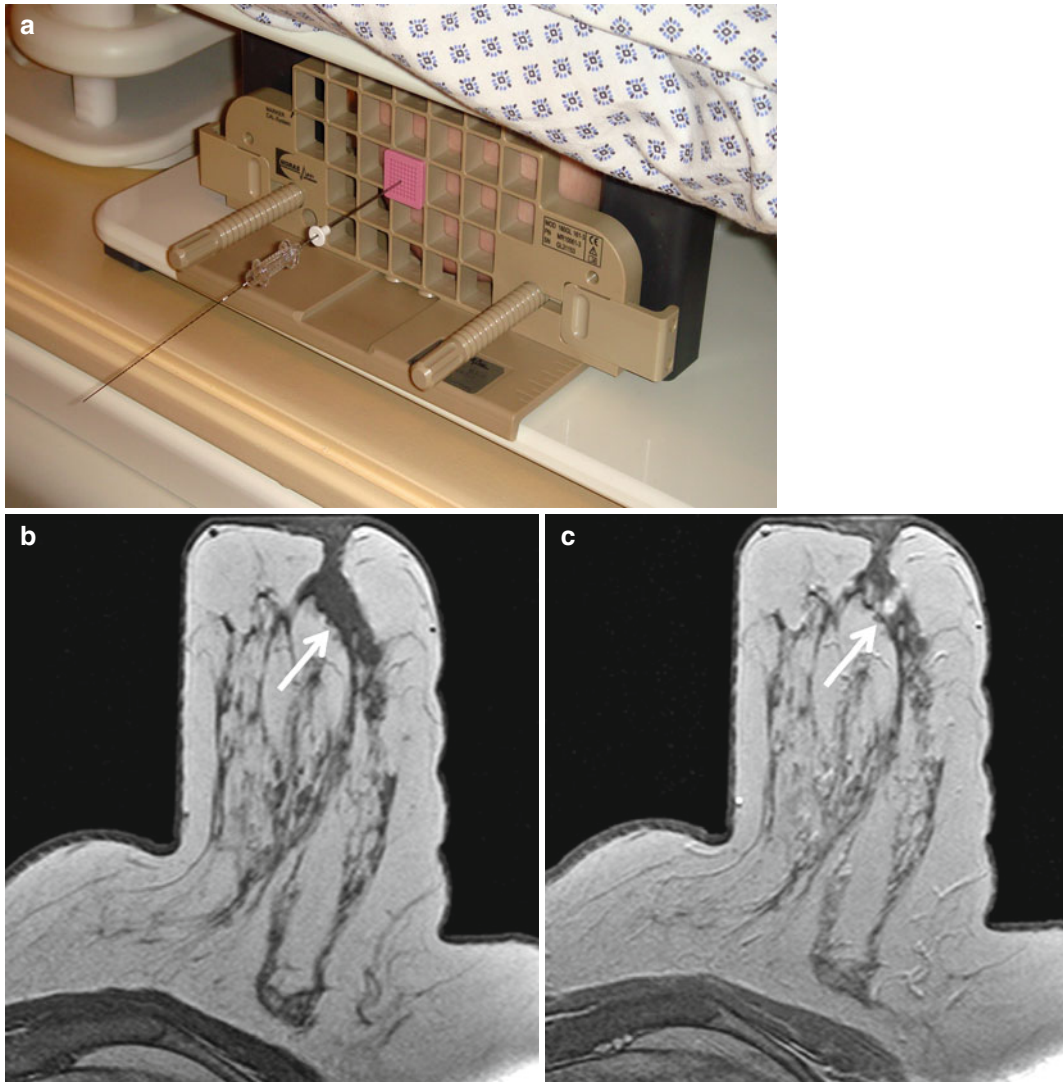

Fig. 10.3 MR-guided needle localization. (**a**) Picture of needle guide and needle in place. (**b–f**) 56-year-old patient with biopsy proven breast cancer on the right breast. Preoperative breast MR imaging showed a suspicious focal (<5 mm) retromamillary lesion in the left breast. (**b**) T1-weighted gradient echo (TR/TE, 290/4.6; flip angle, 90°) before contrast and (**b**) first contrast enhanced, (**d**) subtraction. (**e**) T1-weighted spin echo sequence after placing the needle to control the correct position of the needle. The needle is evident as a low signal intensity structure with adjacent susceptibility artifact (*arrow*). Needle tip is in good position. (**f**) T1-weighted spin echo sequence after deploying the hook wire from the needle. Needle tip is in a good final position (*arrow*)

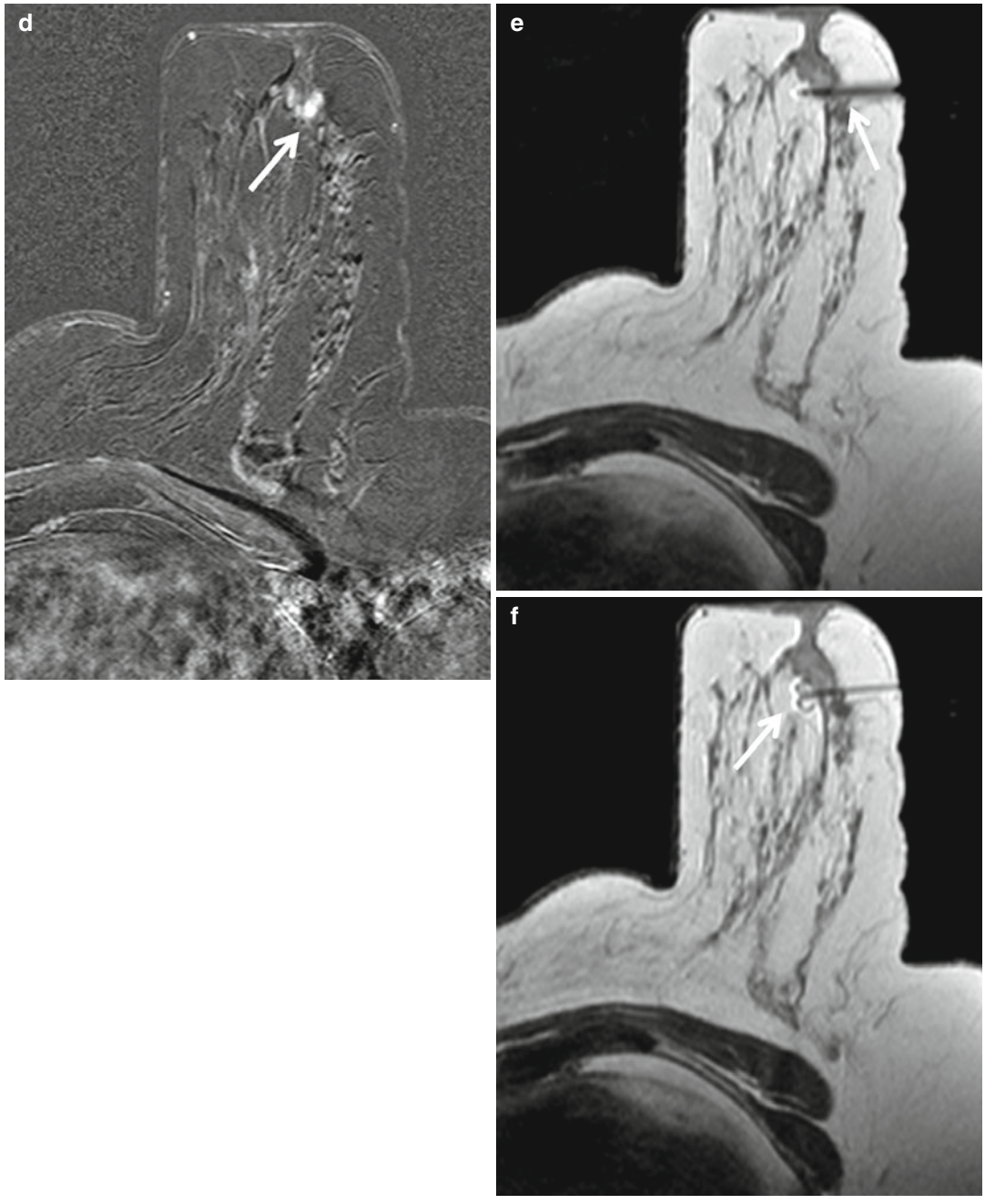

Fig. 10.3 (continued)

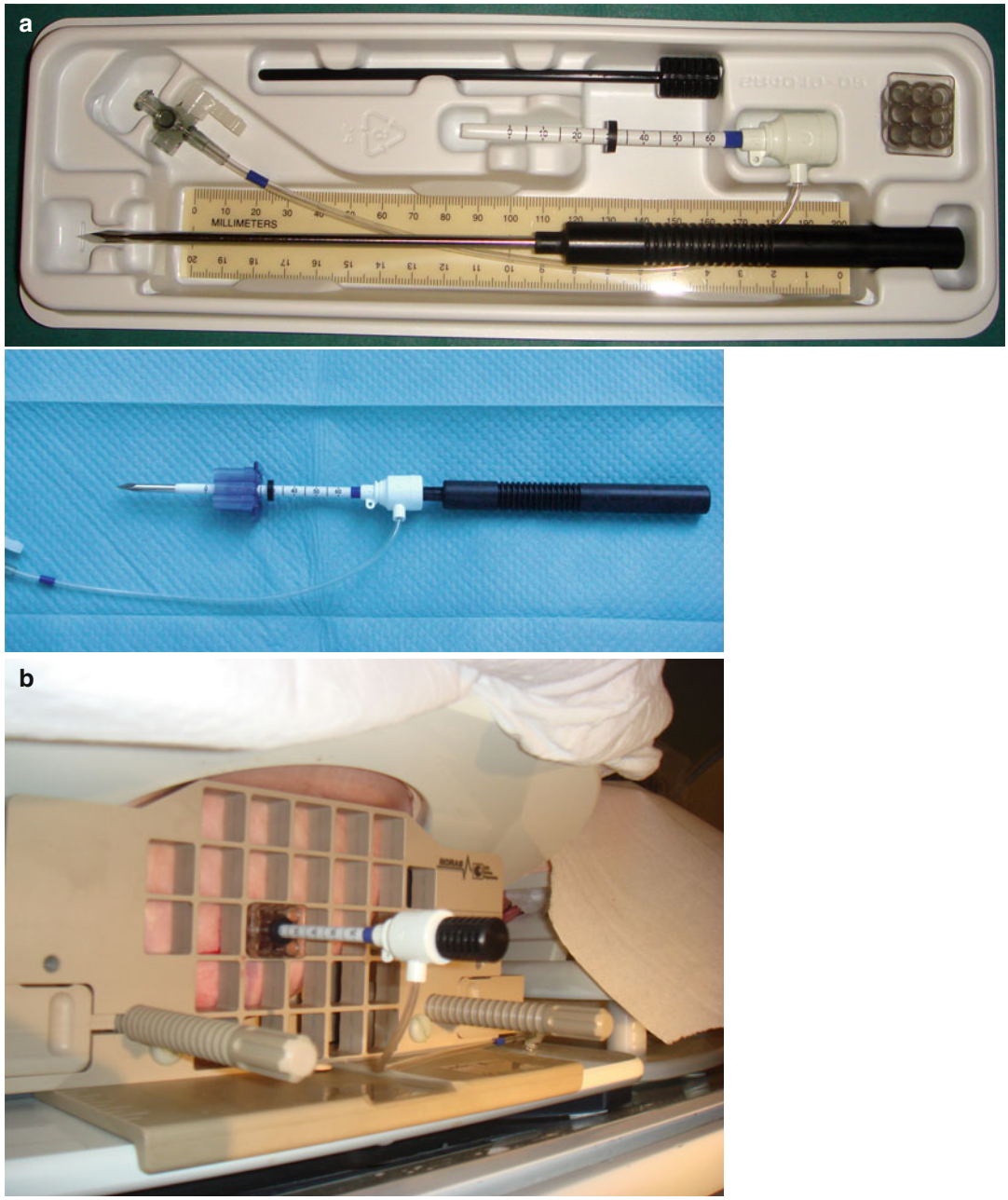

Fig. 10.4 MR-guided vacuum biopsy (with Suros, ATEC system). (**a**) Equipment for MR-guided vacuum-assisted biopsy includes the needle guide; the white introducer sheath, which is scored with marks; the plastic obturator, which serves as a placeholder for MR imaging; the sharp stylet, which creates the tract. (**b**) Introducer sheath with the obturator positioned in the breast at the calculated lesion position. (**c**) Biopsy device inserted through the introducer sheath. The direction of tissue acquisition can be controlled by turning the arrow on the biopsy probe in the desired direction. The specimens are collected in a specimen collecting chamber at the end of the biopsy handpiece, which can be retrieved after tissue acquisition is complete. (**d**) Due to the strong vacuum, a high volume of tissue can be obtained with a high specimen quality

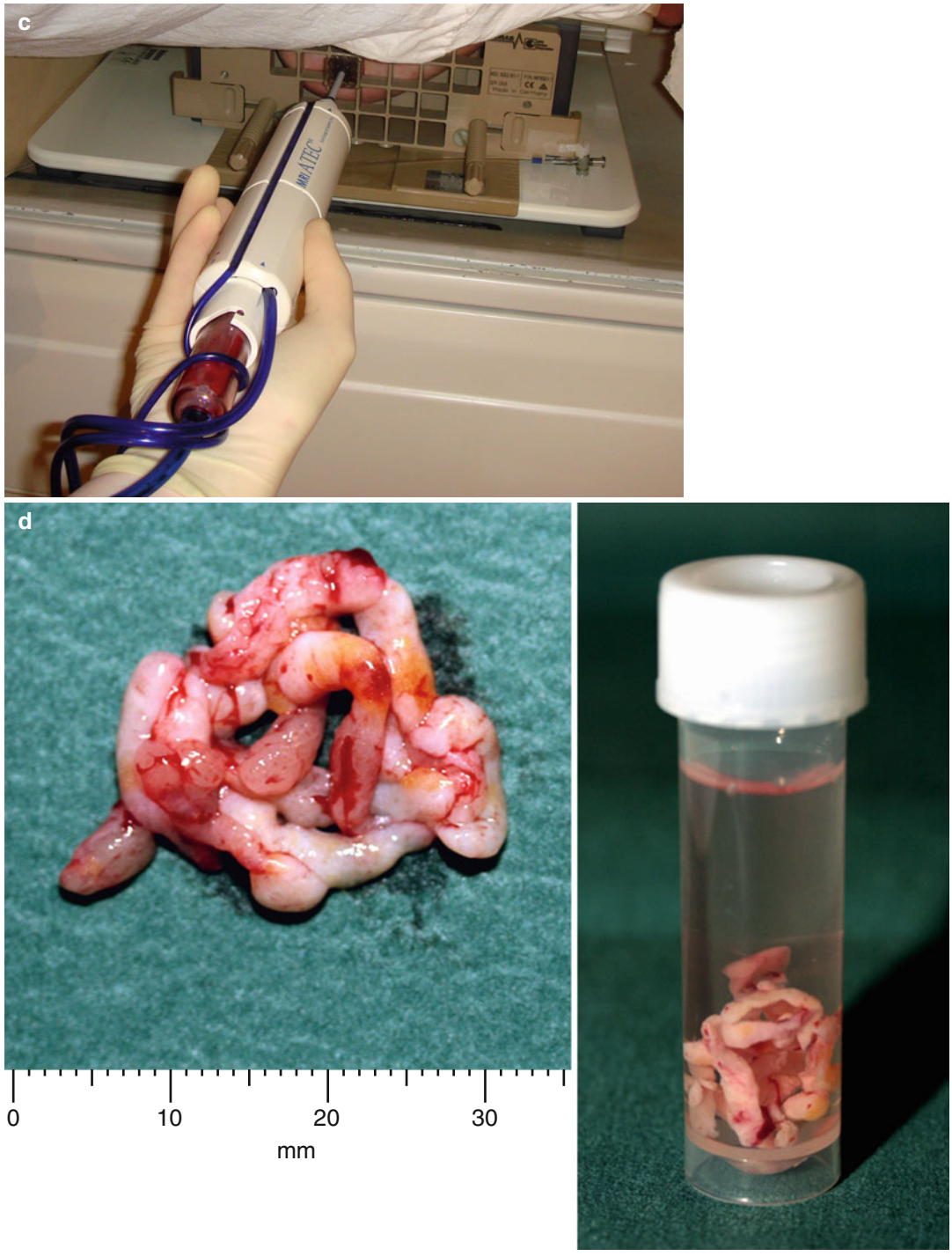

Fig. 10.4 (continued)

to retain the specimen from the biopsy notch. Then the biopsy device needs to be reinserted into the introducer sheath again to obtain the next specimen. In general, 15–30 specimens should be obtained.

After tissue acquisition is complete, the biopsy device is removed. Then an axial T2-weighted turbo SE sequence is performed to show the biopsy cavity and to assess whether the biopsy site did include the target lesion. Due to the progressive enhancement in the surrounding fibroglandular tissue ("vanishing target"), it is impossible to directly image the target lesion in the late phase of an MR-guided intervention. Therefore, the location of the biopsy site must be carefully compared with the preinterventional images in order to find out whether the biopsy site should have included the target lesion. If any doubt persists, additional biopsy passes should be performed. Additional contrast-enhanced images can be obtained in case the lesion had a strong washout to help to decide whether the lesion has been removed or sampled or not (Figs. 10.5 and 10.6).

10.6.4 Clip Placing

A MR compatible clip should be placed immediately subsequent to the vacuum biopsy. This clip can serve as target for mammography-guided localization prior to definitive oncologic surgery. The clips are titanium clips. The clip is placed through the introducer sheath. Postclip MR imaging examination (T1-weighted gradient echo) is performed to assess clip deployment and to document clip position (Fig. 10.6f). Subsequently, a two-view mammogram can be obtained to determine the location of the clip with respect to the remainder of the breast parenchyma.

10.6.5 Postbiopsy Care

After biopsy, manual compression is held approximately 20 min to achieve hemostasis. The biopsy site is cleansed with alcohol and dried with sterile gauze. Sterile strips are placed over the biopsy site. A gauze bandage and a pressure dressing are

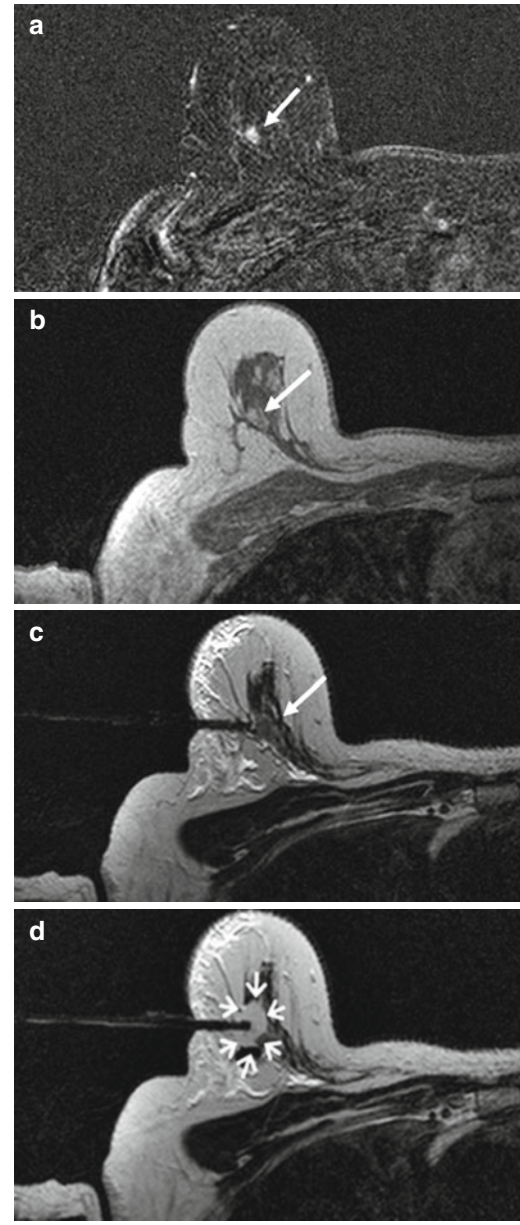

Fig. 10.5 41-year-old patient with a history of a lobular carcinoma in situ of the left breast. Breast MR imaging showed a 6-mm mass-like lesion in the upper outer quadrant of the right breast (*white arrow*). Mammography and a second-look ultrasound did not reveal a correlate for the MR imaging finding. Vacuum biopsy with a 9-G system (ATEC, Suros) revealed an invasive ductal cancer, pT1b, pN0, G3. 5a-b: dynamic breast MR imaging of the right breast, axial orientation, T1-weighted 2D gradient echo TR/TE/FA 290/4.6/90°; (**a**) subtracted image, (**b**) first post-contrast image; (**c**): T2-weighted image (TR 3000/TE120) before vacuum biopsy, after placing an obturator, (**d**): T2-weighted image after vacuum biopsy and flushing the biopsy cavity with saline. The biopsy cavity can accurately be delineated on the T2-weighted TSE image (*white arrows*)

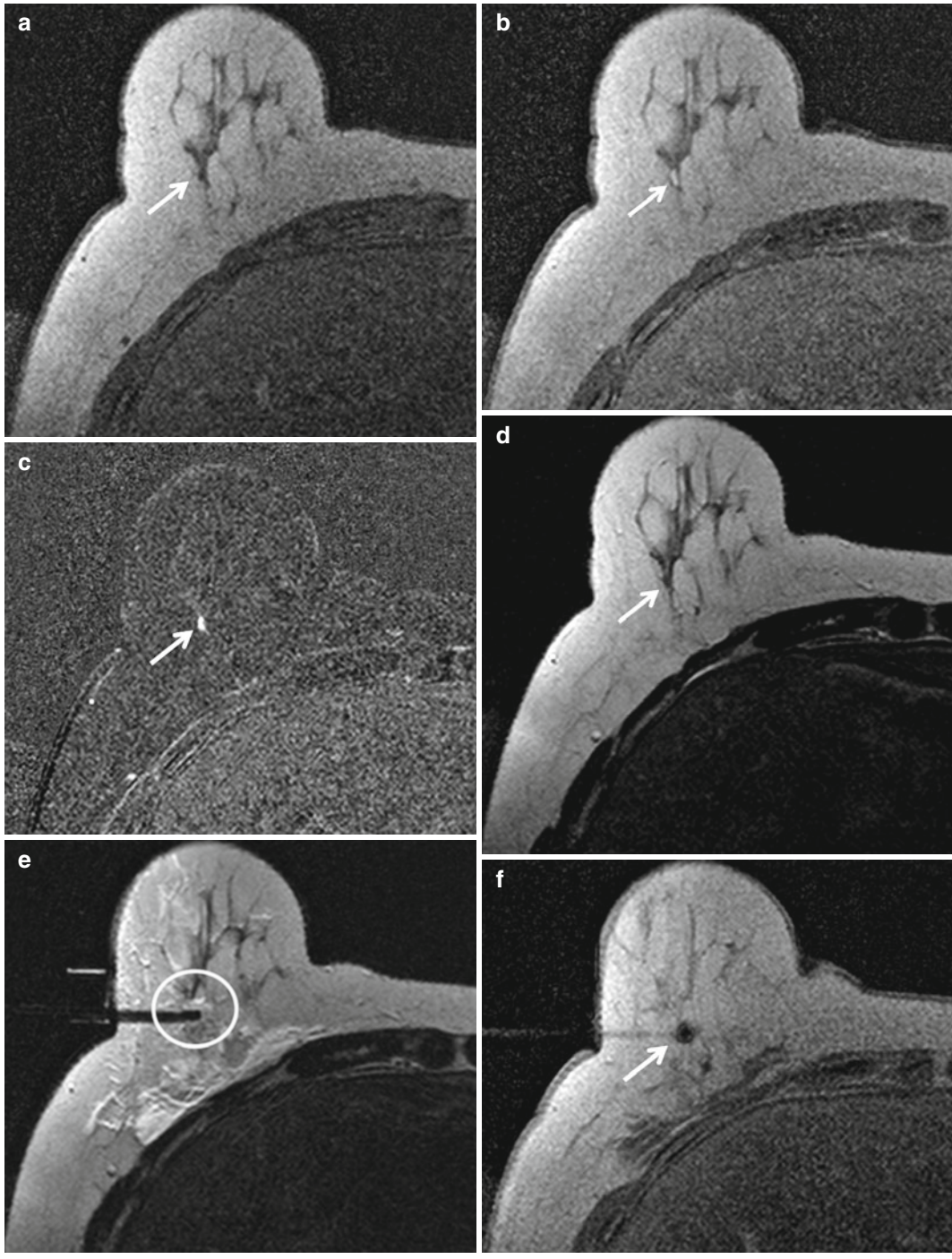

Fig. 10.6 37-year-old woman. Prior history of an invasive breast cancer on the left. Breast MR imaging showed a 3-mm mass-like lesion in the upper outer quadrant of the right breast (*white arrow*). Mammography and a second-look ultrasound did not reveal a correlate for the MR imaging finding. Vacuum biopsy with a 9-G system (ATEC, Suros) revealed an invasive ductal cancer, pT1a, pN0, G3. (**a**) T1-weighted 2D gradient echo (TR/TE, 290/4.6; flip angle, 90°) before contrast and (**b**) first contrast enhanced, (**c**) subtraction, (**d**) T2-weighted (3,000/120) MR images obtained before vacuum biopsy, (**e**) T2-weighted image after vacuum biopsy and flushing the biopsy cavity (*circle*) with saline and (**f**) after placing a clip (*arrow*)

placed over the sterile strips for 24 h. The patient should come back the next day for wound control and ultrasound at the biopsy site.

10.7 Results

10.7.1 Results: Needle Localization

Magnetic resonance imaging-guided needle localization can be readily performed with commercially available equipment. In published series of MR-guided needle localization, the technical success rate was 98–100 %; histological analysis revealed cancer in 31–73 % [of which up to half were ductal carcinoma in situ (DCIS)] and high-risk lesions such as atypical ductal hyperplasia (ADH) or lobular carcinoma in situ (LCIS) in up to 29 %. Table 10.2 gives an overview over the results of MR-guided needle localizations.

10.7.2 Results: Core Biopsy

The use of magnetic resonance imaging-guided semiautomatic core biopsy is reported in different studies using 14–20-gauge needles (Table 10.3). In these studies, technical success rate ranged from 33 to 100 %. No major complications occurred in these studies. Although these studies indicate that MR-guided 14-gauge automated core biopsy can have high diagnostic yield, this method has potential limitations. A high proportion of lesions detected by breast MR imaging contain ductal carcinoma in situ (DCIS) or atypical ductal hyperplasia (ADH); a 14-gauge automated needle often underestimates the pathology of these complex lesions (Liberman 2002). In addition, MR-guided biopsy has the problem of the vanishing target—during the biopsy procedure, the lesion often becomes less conspicuous, due to washout of contrast material from the lesion and progressive enhancement of the surrounding breast parenchyma. For such lesions, it would be helpful to be able to acquire a larger volume of tissue than is possible with the 14-gauge automated needle. Finally, 14-gauge automated needles do not readily provide a mechanism for placement of an MR compatible localizing clip, which may be helpful for the small lesions that undergo MR-guided biopsy.

10.7.3 Results: MR-Guided Vacuum Biopsy

Vacuum-assisted biopsy has a higher technical success rate than semiautomatic biopsy, with fewer inadequate specimens. Compared with automated core biopsy, MR-guided vacuum biopsy enables retrieval of a larger volume of tissue, with each specimen weighing 200 mg (Fig. 10.4d) as compared with approximately 17 mg per specimen for 14-gauge automated needles (Schnall 2000). The larger volume of tissue can help compensate for decreasing lesion conspicuity during the MR-guided biopsy procedure and provides better characterization of complex lesions containing ADH and DCIS (Liberman et al. 2003). Table 10.4 gives an overview over the results of the use of MR-guided vacuum biopsy. In all studies, a very high success rate ranging from 96 to 100 % could be achieved. Another advantage of MR-guided vacuum biopsy is that significantly smaller lesions can be biopsied. In all published studies lesions also <5 mm could be sufficient biopsied. All studies confirm that MR-guided vacuum-assisted biopsy is a fast and safe method and an accurate alternative to surgical excision for MR-detected lesions that are suspicious or highly suggestive of malignancy.

10.8 Complications

In all published studies, major complications occurred neither for MR-guided needle localizations, MR-guided semiautomatic core biopsies, nor for MR-guided vacuum biopsies. Minor complications as larger hematoma or vasovagal reactions occurred in these studies in less than <1 %. Major complications such as hemodynamic relevant bleeding or hematoma, which needed surgical revision, occurred in under 0.01 % of all published cases. All published studies confirm that MR-guided semiautomatic and especially vacuum-assisted biopsy is a safe technique.

Table 10.2 Results: MR-guided needle localization

Study	No.	Needle gauge	Size cm (mean/range)	Technical success rate (%)	No. cancer (%)	Invasive (%)	DCIS (%)	Time min (mean/range)
Heywang-Kobrunner et al. (1994)	11	NS	1.4 (0.6–1.5)	100 %	73 % (8/11)	55 % (6/11)	18 % (2/11)	<1 h
Kuhl et al. (1997)	97	10G	NS	95 %	55 % (53/97)	43 % (42/97)	11 % (11/97)	40/30–60
Fischer et al. (1998)	130	NS	NS	98	49 % (64/130)	45 % (58/130)	5 % (6/130)	42/30–60
Orel et al. (1999)	137	20G	1.2 (0.3–7.0)	98 %	42 % (57/137)	29 % (40/137)	12 % (17/137)	NS
Morris et al. (2002)	101	18G	1.1 (0.2–8.0)	100 %	31 % (31/101)	16 % (16/101)	15 % (15/101)	31/15–59
Taourel et al. (2002)	264	NS	NS	98 %	36 % (95/264)	29 % (76/264)	7 % (19/264)	NS

Table 10.3 Results: MR-guided core breast biopsy

Study	No.	Needle gauge	Size cm (mean/range)	Technical success rate (%)	No. cancer (%)	Invasive (%)	DCIS (%)	Time min (mean/range)
Orel et al. (1994)	3	20	NS	33 %	33 % (1/3)	33 % (1/3)	0 %	NS
Doler et al. (1996)	2	14	NS	100 %	50 % (1/2)	50 % (1/2)	0 %	NS
Kuhl et al. (1997)	5	16	NS	80 %	80 % (4/5)	80 % (4/5)	0 %	40/30–60
Fischer et al. (1998)	4	NS	NS	100 %	25 % (1/4)	25 % (1/4)	0 %	NS/30–60
Kuhl et al. (2001)	78	14	1.5 (0.6–3.0)	99 %	36 % (28/78)	29 % (23/78)	6 % (5/78)	60/45–100
Schneider et al. (2002)	21	14	NS	95 %	38 % (8/21)	38 % (8/21)	0 %	45/40–65
Chen et al. (2004)	35	14	1.5 (0.3–7.0)	34 (97 %)	23 % (8/35)	20 % (7/35)	3 % (1/35)	NS

NS not stated

Table 10.4 Results: MR-guided vacuum breast biopsy

Study	No.	Needle gauge	Size cm (mean/range)	Technical success rate (%)	No. cancer (%)	Invasive (%)	DCIS (%)	Time min (mean/range)	Complications
Heywang-Kobrunner et al. (1999)	55	11	0.8/NS	98 % (54/55)	25 % (14/55)	16 % (9/55)	9 % (5/55)	60 min/NS	–
Viehweg et al. (2002)	280	11	NS	99 % (277/280)	26 % (72/280)	10 % (27/280)	16 % (45/280)	60 min/NS	–
Perlet et al. (2002)	341	11	NS	98 % (334/341)	11 % (37/341)	11 % (37/341)	14 % (47/341)	70 min/NS	5 % (16/341)
Liberman et al. (2003)	28	9	1.0/0.4–0.6	96 % (27/28)	22 % (6/28)	18 % (5/28)	4 % (1/28)	35/24–48	4 % (1/28)
Lehman et al. (2005)	38	9	0.3–7.0	100 % (38/38)	48 % (14/38)	24 % (9/38)	13 % (5/38)	38/23–57	–
Liberman et al. (2005)	98	9	1.0/0.4–8.5	97 % (95/98)	24 % (24/98)	11 % (11/98)	13 % (13/98)	33/17–60	–
Orel et al. (2006)	85	9	1.7/0.5–10.0	96 % (83/85)	61 % (52/85)	40 % (34/85)	20 % (17/85)	NS	–
Schrading et al. (2010)	316	9/10	9G: 9.0/0.3–8.5	9G: 100 %	9G: 43 % (116/267)	9G: 29 % (78/267)	14 % (38/267)	9G: 35/23–64	–
			10G: 17.0/11.0–6.2	10G: 98 % (45/47)	10G: 29 % (14/49)	10G: 16 % (8/49)	12 % (6/49)	10G: 67/35–95	–

Appraisal

Magnetic resonance imaging-guided percutaneous biopsy can be accomplished with a variety of automated core needles and vacuum-assisted biopsy probes. MR-guided vacuum biopsy allows histological verification of "MR only" visible lesions with adequate reliability and reaches a diagnostic accuracy equivalent or even higher to that of MR-guided needle localization. Vacuum-assisted biopsy is advantageous over MR-guided automatic core biopsy for MR-guided percutaneous breast biopsy, because vacuum-assisted biopsy can be performed quickly, removes a large volume of tissue, provides more accurate characterization of lesions containing ADH and DCIS, and enables placement of a localizing clip.

Key Points

- MR-guided needle localization using a needle guided followed by open surgery is a quick and accurate technique for histological verification of "MR-only" visible lesions. Freehand needle localizations should not be performed anymore.
- As not all MR suspicious lesions are malignant, MR-guided biopsy should be performed to avoid unnecessary surgery of "MR only" visible lesions.
- MR-guided vacuum biopsy has advantages over MR-guided core biopsy, e.g., higher technical success rate; higher tissue volume and smaller lesions can be biopsied. Therefore, if available, MR-guided vacuum biopsy should be used instead of MR-guided core biopsy.
- MR-guided vacuum-assisted biopsy is a fast, safe, and accurate alternative to surgical excision for the diagnosis of lesions detected on MR imaging.

References

Chen X, Lehman CD, Dee KE (2004) MRI-guided breast biopsy: clinical experience with 14 gauge stainless steel core biopsy needle. AJR Am J Roentgenol 182:1075–1080

Doler W, Fischer U, Metzger I et al (1996) Stereotaxic add-on device for MR-guided biopsy of breast lesions. Radiology 200:863–864

Fischer U, Kopka L, Grabbe E (1998) Magnetic resonance guided localization and biopsy of suspicious breast lesions. Top Magn Reson Imaging 9:44–59

Heywang-Kobrunner SH, Huynh AT, Viehweg P et al (1994) Prototype breast coil for MR-guided needle localization. J Comput Assist Tomogr 18:876–881

Heywang-Kobrunner SH, Heinig A, Schaumloeffel-Schulze U et al (1999) MR-guided percutaneous excisional and incisional biopsy of breast lesions. Eur Radiol 9:1656–1665

Kuhl CK, Elevelt A, Leutner CC et al (1997) Interventional breast MR imaging: clinical use of a stereotactic localization and biopsy device. Radiology 204:667–675

Kuhl CK, Morakkabati N, Leutner CC et al (2001) MR imaging-guided large-core (14-gauge) needle biopsy of small lesions visible at breast MR imaging alone. Radiology 220:31–39

Lehman CD, Deperi E, Peacock S, McDonough M, DeMartini W, Shook J (2005) Clinical experience with MRI-guided vacuum-assisted breast biopsy. AJR Am J Roentgenol 184:1782–1787

Liberman L (2002) Percutaneous image-guided core breast biopsy. Radiol Clin North Am 40:483–500

Liberman L, Morris EA, Dershaw DD et al (2003) Fast MRI-guided vacuum-assisted breast biopsy: initial experience. AJR Am J Roentgenol 181:1283–1293

Liberman L, Bracero N, Morris E, Thornton C, Dershaw D (2005) MRI-guided 9-gauge vacuum-assisted breast biopsy: initial clinical experiences. AJR 185:183–193

Morris EA, Liberman L, Dershaw DD et al (2002) Preoperative MR imaging-guided needle localization of breast lesions. AJR Am J Roentgenol 178:1211–1220

Orel SG, Schnall MD, Newman RW et al (1994) MR imaging-guided localization and biopsy of breast lesions: initial experience. Radiology 193:97–102

Orel SG, Schnall MD, Czerniecki B et al (1999) MRI-guided needle localization: indications and clinical efficacy. Radiology 213:454 [Abstract]

Orel SG, Rosen M, Mies C, Schnall MD (2006) MR imaging-guided 9-gauge vacuum-assisted core-needle breast biopsy: initial experience. Radiology 238:54–61

Perlet C, Heinig A, Prat X et al (2002) Multicenter study for the evaluation of a dedicated biopsy device for MR-guided vacuum biopsy of the breast. Eur Radiol 12:1463–1470

Schnall MD (2000) MR-guided breast biopsy. In: Lufkin RB (ed) Interventional MRI. Mosby, St. Louis, pp 315–319

Schneider JP, Schulz T, Horn LC et al (2002) MR-guided percutaneous core biopsy of small breast lesions: first experience with a vertically open 0.5 T scanner. J Magn Reson Imaging 15:374–385

Schrading S, Simon B, Braun M, Wardelmann E, Schild HH, Kuhl CK (2010) MRI-guided breast biopsy: influence of choice of vacuum biopsy system on the mode of biopsy of MRI-only suspicious breast lesions. AJR Am J Roentgenol 194:1650–1657

Taourel PH, Sittek H, Boetes C et al (2002) MR-guided localization and surgery: results of a European multicenter study. Radiology 225:556

Viehweg P, Heinig A, Amaya B, Alberich T, Laniado M, Heywang-Kobrunner SH (2002) MR-guided interventional breast procedures considering vacuum biopsy in particular. Eur J Radiol 42:32–39

Drainage

11

Roman Fischbach and Christian Hohl

Contents

R. Fischbach (✉)
Department of Radiology, Asklepios Klinik Altona,
Paul-Ehrlich-Straße 1, Hamburg D-22763, Germany
e-mail: r.fischbach@asklepios.com

C. Hohl
Department of Diagnostic and Interventional Radiology,
HELIOS Hospital Siegburg,
Ringstrasse 49, Siegburg D-53721, Germany
e-mail: christian.hohl@helios-kliniken.de

11.1 Drainage in Abscess

Roman Fischbach

11.1.1 Introduction

Abscess formation is associated with significant morbidity and mortality, despite the availability of potent antibiotics. Undrained abscess results in a mortality rate of 50–80 %. Therefore, early diagnosis and subsequent open surgical or percutaneous drainage are the most important factors influencing successful abscess treatment. Since the introduction of imaging-guided drainage procedures in the late 1970s, percutaneous abscess drainage has become the standard care for treatment of abdominal and thoracic fluid collections, replacing invasive surgical procedures in most cases (Rivera-Sanfeliz 2008). Percutaneous drainage provides a rapid means of therapy with relatively simple devices and techniques and yields a high success rate with few complications. Drainage may be either the only therapy necessary to effectively treat an abscess or will delay and downstage a necessary surgical procedure subsequently decreasing surgery's risks (van Santvoort et al. 2010; van Sonnenberg et al. 2001).

The main goal in drainage procedures is to decompress and drain as much pus as possible so that antibiotics will be (more) effective. The major benefit of the procedure occurs at the time of intervention when the collection is evacuated (Mueller et al. 1984). This can lead to recovery of

A.H. Mahnken et al. (eds.), *CT- and MR-Guided Interventions in Radiology*,
DOI 10.1007/978-3-642-33581-5_11, © Springer-Verlag Berlin Heidelberg 2013

an unstable, critically ill patient within a matter of hours. Continued external drainage adds to the initial therapeutic effect.

Especially in deep locations or complicated anatomic relations like in the pelvis, introduction of cross-sectional imaging has facilitated diagnosis of abscess and access planning. Today, image-guided percutaneous aspiration and drainage are among the most frequent interventional procedures performed. Close follow-up of catheter drainage, adjunctive antibiotic therapy, controlled irrigation, and sometimes application of lytic agents to facilitate drainage of viscous fluid collections are necessary to assure treatment success (Beland et al. 2008). Follow-up imaging is important to document successful resolution of a fluid collection. Minimal tube drainage alone does not necessarily equate with resolution of a fluid collection as the tube may be blocked, dislodged, or simply too small to drain the abscess content. Imaging remains crucial to identify an underlying cause for abscess development. If, for example, an enteric fistula is diagnosed, the fistula must heal before the drainage tube can be successfully removed.

11.1.2 Diagnosing Abscess

Prior to making a treatment decision, the proper diagnosis of an abscess has to be established. This may be difficult especially in the postoperative patient in whom clinical symptoms of infection are common and oftentimes nonspecific. Ultrasound (US) and computed tomography (CT) are commonly used to diagnose or rule out abscess formations with CT being the preferred diagnostic method in most institutions. US is readily available and is very reliable in diagnosing fluid collections. However, extensive surgical wounds or dressings, obesity, or air-filled bowel may impair US but do not hamper CT. In addition, CT is ideal for image guidance in percutaneous drainage procedures or diagnostic needle aspiration. On the other hand, CT carries a significant radiation exposure, which has to be kept in mind when frequent follow-up imaging is necessary, as in patients suffering from enteric fistulae. MRI can serve as an alternative to diagnose fluid collections, but in most clinical settings, access to CT is quicker and easier. Coronal or sagittal reformations from thin-slice imaging are helpful in exactly describing the location of a fluid collection and neighboring structures. Delineating bowel anatomy in additional planes significantly helps differentiation of fluid-filled bowel loops from extraluminal fluid. In order to further improve the diagnostic quality of CT in questionable cases, delayed scans after additional oral or rectal contrast administration may help to distinguish bowel from extraluminal fluid collections especially in the pelvis. Delayed images 60–80 s after i.v. contrast help to differentiate a contrast-filled urinary bladder from suspicious fluid in the pouch of Douglas.

Strong signs of an abscess are a well-circumscribed fluid collection, thickened membranes or septations, gas bubbles, rim enhancement, and debris. Extraluminal air-fluid levels or air detected in an intrahepatic fluid collection renders an imaging diagnosis of an abscess very likely, but less than 20 % of hepatic abscesses reveal air inclusions. Weaker signs are non-loculated or thin-walled nonenhancing collections that may have alternative explanations, such as peritoneal or pleural fluid. The differential diagnosis of potential abscess formations is substantial. Differential diagnosis of hepatic abscesses includes simple and complicated cysts, echinococcal cysts, hematoma, cystadenocarcinoma, and necrotic malignancies (Fig. 11.1). An abdominal fluid collection may represent primary and secondary malignancy as well as benign processes like hematoma, bilioma, pancreatic pseudocyst, or distended bowel loops. The classic US appearance of an abscess as a well-circumscribed round anechoic lesion with posterior acoustic enhancement is found in less than 50 % of abdominal abscesses. As specific signs are rare and appearance of a fluid collection is quite variable depending on location, age, and composition, image interpretation remains a difficult task by magnetic resonance (MR) imaging, CT, or US. In conclusion, any extraluminal fluid collection in the proper clinical setting is potentially an abscess and warrants further workup.

Fig. 11.1 Patient with fever. Computed tomography (*CT*) shows a hypodense mass in the right liver lobe. An abscess was included in the differential diagnosis, but needle aspiration revealed no fluid. Biopsy was performed and non-Hodgkin lymphoma was diagnosed

11.1.3 Indications and Contraindications

Indications for percutaneous abscess aspiration and drainage are straightforward, serving therapeutic and diagnostic purposes. In patients with fever, weight loss, and malaise, any suspicious fluid collection confirmed by ultrasound, CT, or MRI could represent an abscess, and a reliable diagnosis must be reached without significant delay. Needle aspiration is the method of choice to clarify the nature of a fluid collection, as it can quickly confirm its infectious nature and will provide information on the viscosity as well as the composition of a fluid collection (Fig. 11.2). This in turn will help to determine whether the abscess is amenable to catheter drainage and which type of catheter to choose. Further diagnostic information will be obtained from aspiration material. It should therefore be preserved for chemical and microbiologic assessment to determine the microorganism causing the infection, for antibiotic testing, and for analysis of fluid composition.

If the diagnosis of an abscess is made, the decision to proceed to drainage depends on:

- A safe access route
- Acceptable coagulation parameters
- Informed consent from the patient or appropriate others

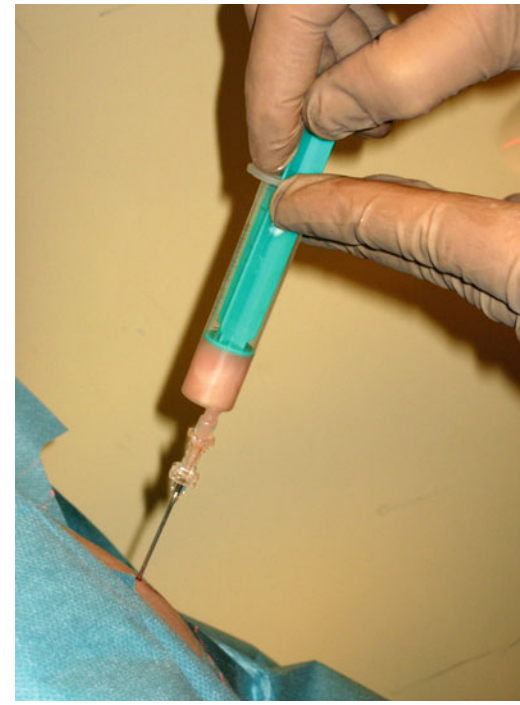

Fig. 11.2 CT-guided aspiration of a suspicious fluid collection. Abscess is confirmed as pus is aspirated

Absolute contraindications to percutaneous drainage are rare as treatment alternatives with smaller risk usually do not exist. Only in cases where no safe access for drainage can be determined, open surgical drainage may be preferred. Relative contraindications for percutaneous drainage are small collections less than 3 cm in diameter as these may be successfully treated by aspiration and irrigation alone (Wroblicka and Kuligowska 1998). If multi-septate and interloop abscesses are present or if a high-flow enteric fistula is suspected, surgery should be considered. Bleeding diatheses (INR >1.5/PT>18) which cannot be corrected are another rare contraindication. Other relative contraindications include infected necrotic tumor, complicated Crohn's disease, and solid necrosis in acute pancreatitis.

11.1.4 Material

All required materials have to be prepared prior to the intervention and should be readily available

to avoid interruptions of the procedure. The different procedure steps (access planning, needle aspiration, drainage) determine the material needed.

The access site is usually determined from axial CT images. To identify the skin entry site, a radiopaque marker attached to the patient's skin in the vicinity of the intended entry site is helpful. A wire or needle may serve as marker; however, a grid made of an angiographic catheter (Fig. 11.3) or commercially available grids are recommended, as the distance from a specific marker to the planned entry site is easier to gauge. A felt-tip pen to mark the skin site and a ruler to measure the distance between marker and entry site should be available. Alcohol spray or povidone-iodine is used for skin disinfection.

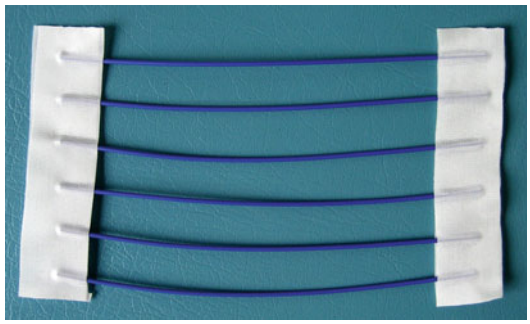

Fig. 11.3 Grid for marking the skin entry site made of angiographic catheter segments taped at the ends

The procedure tray should be large enough that all needed materials can be placed on the tray and are within reach. The basic tray should contain sterile draping material; a long 21 G needle for deep anesthesia infiltration; two 10-ml syringes, one for local anesthesia (1 % mepavicaine, lidocaine, or prilocaine) and another one for fluid aspiration; and a scalpel for skin incision (Fig. 11.4). Other material needed should be at hand but is not put on the procedure tray until the diagnosis of an abscess is confirmed by aspiration. At that point, a sterile microbiology vial for fluid aspirate, a three-way stopcock, drainage bag, skin fixation material, and wound dressing will be required.

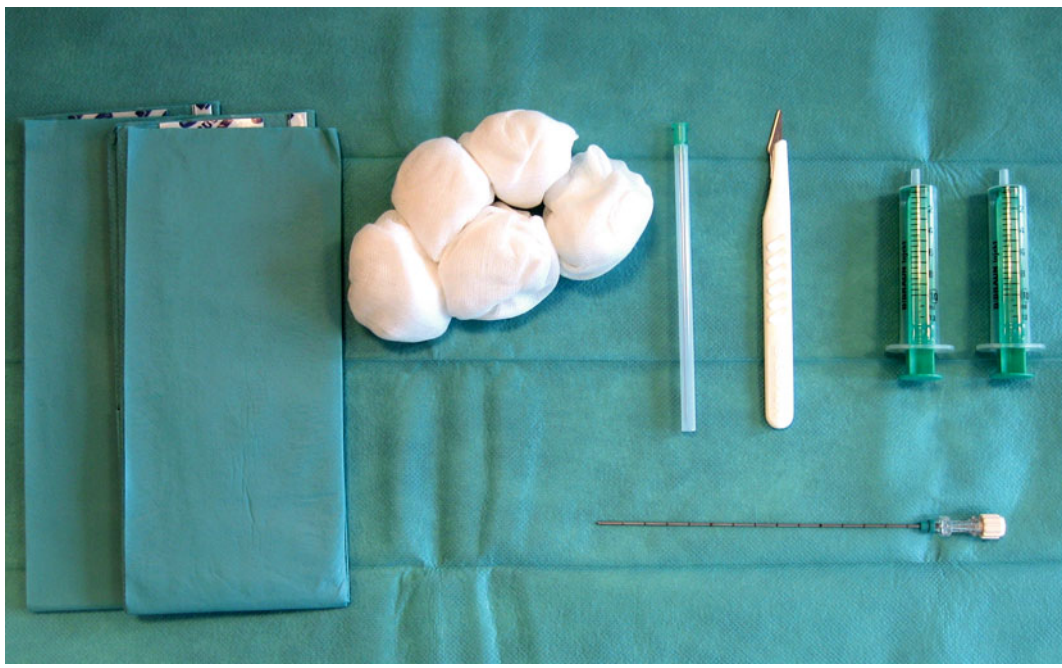

Fig. 11.4 Procedure tray for CT-guided puncture and aspiration. The initial tray has sterile draping material, a 21 G needle for local anesthesia, a scalpel for skin incision, an 18 G puncture needle, and two syringes for local anesthetics and aspiration

11.1.4.1 Needle

In most cases, a 15- or 20-cm trocar-type 18 G needle is used for diagnostic puncture and aspiration of fluid. The 18 G needle is easy to control especially when a 20-cm long device is needed, and it accepts a standard 0.035-in. guidewire for placement of drains using the Seldinger technique. A smaller size needle may be preferred for a challenging localization to minimize puncture risk but at the expense of a significantly higher resistance to fluid flow. Therefore, a small-size needle carries the risk of false-negative aspirate as only clear supernatant may return through the needle. Furthermore, a 0.018-in. wire has to be followed by a coaxial dilator, which increases the necessary steps to complete the procedure and therefore carries higher cost. Moreover, a 0.018-in. guidewire is less stable than a heavy-duty wire and may dislodge when a coaxial dilator is introduced. Superficial collections may be reached with an angiographic puncture needle, and very deep collections may even require a long Colapinto needle.

11.1.4.2 Guidewire and Dilator

For the Seldinger technique, supplies include a 0.035-in.-diameter, 80–90 cm extrastiff guidewire and a set of hydrophilic dilators (e.g., 8, 10, 12 F) matching the intended drainage catheter. A variety of guidewires are available for percutaneous abscess drainage with different properties and prices. Guidewires should be short to make their use convenient with short drainage catheters. The wire stiffness is crucial to guide dilator and catheter into the abscess and macerate septae within the abscess; however, the wire tip needs to be floppy and several centimeters long to let the wire coil within the abscess without perforation of the abscess wall. Stainless steel is cheaper and stiffer than nitinol but does not have its kink resistance. As the drainage catheter tends to be rather soft and flexible, sometimes dilation of the drainage tract is necessary before a tube is advanced into an abscess cavity over the wire. Dilators are well-known from vascular procedures, and most products now have a hydrophilic coating. Coated dilators greatly ease dilator passage compared to standard dilators without coating. The effect is similar to a hydrophilic guidewire; therefore, the dilator should be moistened with saline to make them wet and slippery.

11.1.4.3 Drainage Catheter

Commercial drainage catheters come in a wide variety of sizes and materials. Most catheters have a curved-tip or pigtail configuration and come with a stiff inner metallic cannula and/or a more flexible plastic cannula. Many drainage catheters can be deployed as a trocar. In this case, a stylet is placed inside the cannula. Effective drainage is usually accomplished by 8- or 10-F catheters in small nonviscous collections. If the fluid can be easily aspirated by a 10-ml syringe through an 18 G needle, then the abscess viscosity will allow drainage with a single lumen 8-F or 10-F catheter system (Gobien et al. 1985). The drainage catheters have multiple side holes and a curved tip (Fig. 11.5).

Larger tubes, such as 12–16-F drainage catheters, are used when the contents are viscous or debris-laden. These larger size catheters are usually available as double-lumen sump catheters. The sump catheter has a bigger lumen for drainage and a smaller lumen, which allows for circulation of room air into the abscess to avoid adherence of the abscess wall to the side holes of the catheter. Many double-lumen catheters come with an air filter that can be attached to the small lumen. The small lumen also serves for irrigation of the abscess. Sump drainage has a demonstrated higher efficiency than closed drainage and is the most common approach to infected fluids (van Sonnenberg et al. 2001). For complex abscesses containing necrotic tissue as in pancreatic necrosis or some empyemas, a catheter lumen of 24–30 F might be necessary. Initial catheter placement can almost always be performed using a 12-F system. In cases with complicated clinical course or debris detected on follow-up imaging, a small-lumen catheter is easily exchanged by a larger lumen catheter later.

11.1.5 Technique

11.1.5.1 Patient Preparation

In order to ensure an efficient workflow, all possible scenarios need to be considered and

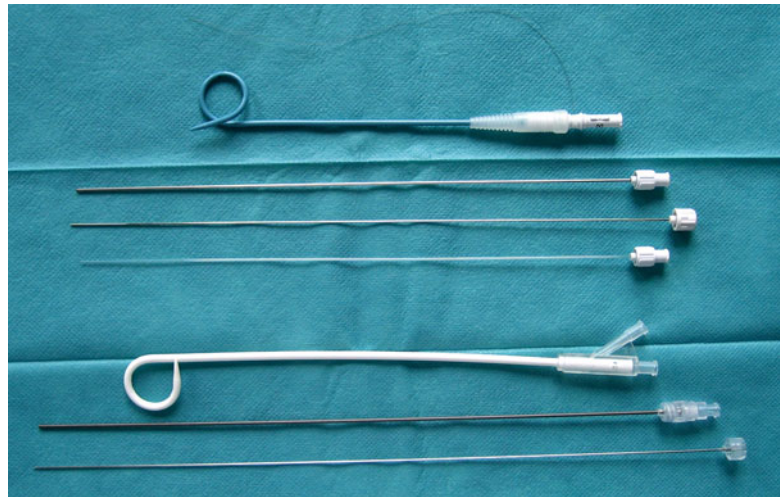

Fig. 11.5 An 8-F pigtail-shaped drainage catheter with an inner metallic cannula, an optional plastic cannula, and a trocar-type stylet in the *upper half* and a 12-F double-lumen sump catheter in the *lower half* (note the side port). The double-lumen catheter comes with an inner metallic cannula and a stylet

should be planned for and discussed with patient and the referring physician prior to the diagnostic examination. A patient suspected of suffering from abscess may reveal a normal or unremarkable examination with no indication for percutaneous treatment or may show an unspecific or suspicious fluid collection. In this case, diagnostic needle aspiration or placement of a drainage catheter may follow the diagnostic study. Depending on the location and composition of the fluid collection, the access route may be technically demanding and can carry specific risks. The patient therefore should be informed about the suspected diagnosis and about the possible necessity of a diagnostic needle aspiration or drainage as well as alternative treatment options.

Since obtaining informed consent with the patient on the CT table or even inside the examination room may not be accepted as legally correct in many countries, the informed consent statement should be signed before the examination begins. If the likelihood of infected fluid is low, the diagnostic scan can be completed first, and the drainage is planned as a two-step procedure with separate discussion of potential risks of a drainage procedure. If intervention carries significant risks due to complexity of the abscess or intervening or adjacent vital structures, the patient should be informed accordingly, and obtaining a detailed signed consent statement is advised. In these complex cases, the clinical situation and the procedure as well as alternatives should be explained to the patient and need to be discussed with the referring clinicians.

Since percutaneous drainage is performed using standard aseptic technique and local anesthesia, the patient should have a well-functioning intravenous access line and needs to be on antibiotics prior to the procedure. Intravenous broad-spectrum antibiotics covering multiple organisms should be initiated shortly before the procedure to address bacteremia resulting from catheter manipulation. If this is started not earlier than 1 h before the procedure, it will not affect microbiological analysis. Postinterventionally, antibiotics are continued until a more appropriate agent is selected according to the result of microbiological testing.

Usually, generous administration of local anesthesia is sufficient to perform the procedure without significant patient discomfort. One has to consider that the efficacy of local anesthetics is reduced in acidic milieu, as it is present in infection. Particularly, anesthesia of the abscess wall may not be possible with local anesthetics. In challenging access routes or uncompliant patients, sedation improves the safety of the procedure by reducing patient motion. However, there is a trade-off with patient cooperation. If sedation is necessary, adequate monitoring of the patient's vital signs (pulse oximetry, ECG) and specially trained personnel are required (see Chap. 5).

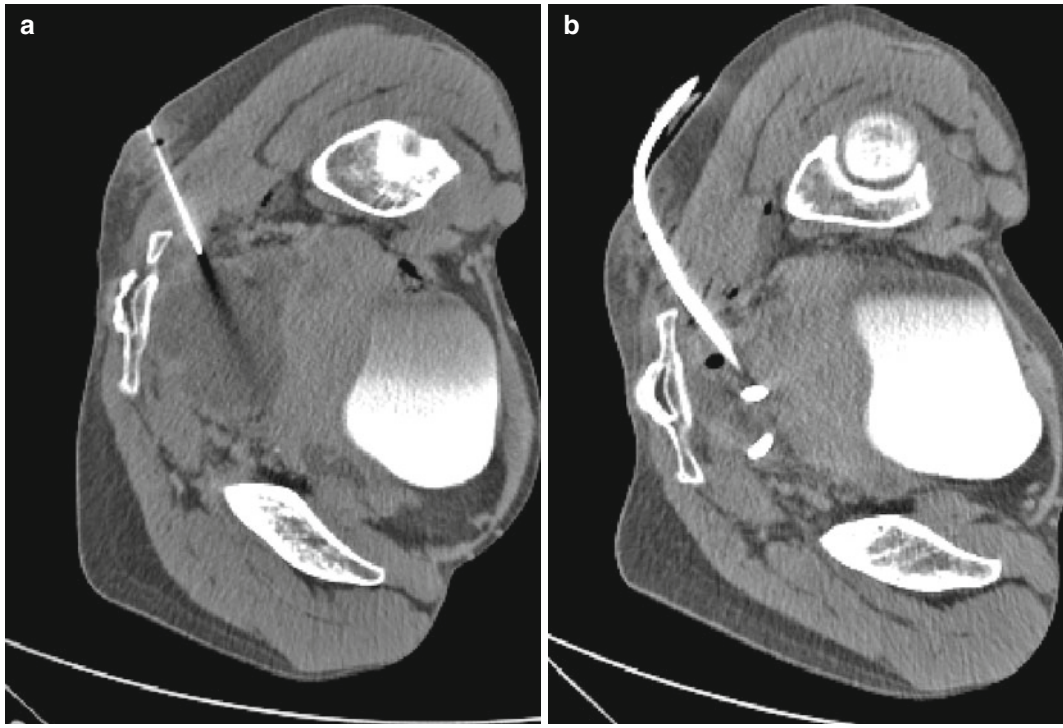

Fig. 11.6 Patient with recurrent abscess formation in the presacral and perirectal space suffering from Crohn's disease. The patient is positioned in a left lateral position, and a transgluteal access is chosen. The needle is advanced into the fluid collection (**a**). Pus was confirmed, and a 12-F sump catheter was introduced using the Seldinger technique (**b**). After evacuation, the abscess cavity has markedly decreased in size

11.1.5.2 Abscess Drainage

Common locations for abscess formations are subphrenic, perihepatic, perisplenic, iliopsoas, abdominal wall, and pelvis. If a suspicious fluid collection is identified on a diagnostic CT exam, potential access routes have to be identified.

Subtle planning and selection of a safe access route is the most crucial aspect of a drainage procedure. The catheter should be placed in a way that allows dependant drainage whenever possible. After defining the approach, optimal positioning of the patient to allow easy handling and guiding of the drainage catheter combined with a comfortable patient position helps to perform a quick and successful procedure. The optimum access route is determined by the following:

- Shortest pathway
- Easiest angulation or localization
- Avoidance of intervening or adjacent structures
- Most convenient catheter location for the patient

Patient positioning largely depends on the location of the suspicious fluid collection and possible access routes. In peripancreatic or perihepatic locations, a slight lateral elevation may move critical structures out of the way or can improve catheter handling. The patient is placed in a prone or lateral decubitus position in retroperitoneal abscess as well as paraspinal collections or for transgluteal drainage (Fig. 11.6). In this case, the prone position is more stable but is less well tolerated by the patient as positioning of the patient's arms is difficult in the CT gantry or breathing is impaired from chest compression or neck stiffness in elderly or ill patients. In our experience, a lateral decubitus position is better tolerated than the prone position by most patients facilitating comfortable positioning and access to the patient. The patient will, however, move more freely, and anatomic landmarks may be obscured, rendering route planning more difficult.

For a solid organ abscess (e.g., liver), the access route should traverse a small amount of normal

organ parenchyma to reduce the risk of peritoneal spillage and bleeding. Superficial abscesses of the left or right liver lobes may be easily approached through a simple route in the axial plane on CT. Collections in the cranial part of the liver or spleen as well as subdiaphragmatic abscesses may be accessed using cranial angulation to avoid the pleural space. If cephalocranial angulation is necessary, gantry tilt might improve access planning. Real-time US guidance may be superior to sequential CT in such cases. CT fluoroscopy is an ideal imaging technique providing real-time images and therefore providing excellent guidance and online monitoring of a puncture.

Multiplanar magnetic resonance (MR) imaging may be an alternative modality for image-guided drainage procedures (Buecker et al. 2001; Kariniemi et al. 2006). Using fast sequences and MR compatible material, percutaneous drainage can be successfully completed using MR guidance. Still, MR guidance is rarely applied as patient access, patient monitoring in critically ill patients, and visualization of the puncture needle and guidewire are inferior to CT or fluoroscopy. Prolonged procedure times and limited access to MR systems further hamper widespread use of MR for percutaneous drainage procedures.

Avoiding bowel is of utmost importance to preclude contamination of a sterile fluid collection and the aspirated sample and to avoid bowel perforation due to its high risk of peritonitis. Bowel transgression is of concern, particularly if the colon is affected. The (small) bowel might be traversed when all alternative access routes have a less favorable risk-benefit ratio. One should pass up aspiration of "low-probability" collections, such as hematoma through the colon. If vital organs cannot be excluded from the access path, bleeding risk, especially in splenic puncture, has to be considered. A transpleural passage needs to be avoided especially in subphrenic abscess to prevent infectious spread to sterile pleural effusions.

Once the access route is planned, the patient is positioned accordingly. The abscess is located using a short spiral scan or stepwise axial scans with a radiopaque grid attached to the skin at the estimated level of the lesion (Fig. 11.7). Once the patient is at the desired table position, the external

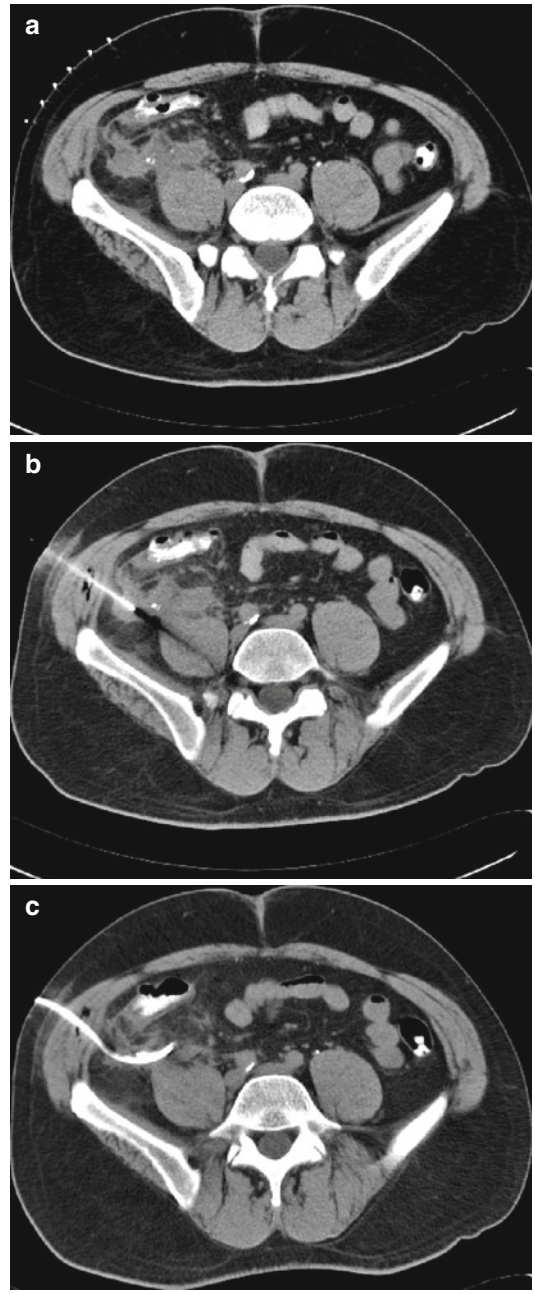

Fig. 11.7 Patient suffering from fever and groin pain after laparoscopic appendectomy. A fluid collection is identified in the cecal region. A radiopaque grid marker is positioned over the planned skin entry site (**a**). After local infiltration with an anesthetic, an 18 G needle is advanced (**b**). After aspiration of pus, a guidewire is introduced, and a 10-F drainage catheter is positioned in the abscess cavity. The cavity is irrigated with saline, and as much fluid as possible is evacuated (**c**)

marker is used to determine the exact skin entry site, the length, and the angulation of the access path to reach the abscess formation. The entry point is marked on the skin with a felt-tip pen using the laser light of the CT as guide. Thereafter, the patient can be moved out of the gantry for skin disinfection and appropriate draping. Then local anesthesia is applied. In difficult access routes, the small-caliber needle used for anesthesia may be left in place to correlate entry point and angulation. Careful skin infiltration and infiltration of the entire access path should be performed. In deep locations, the puncture tract can be infiltrated through the 18 G puncture needle as the needle is advanced. The peritoneum or pleura is very sensitive, and sufficient local anesthesia improves patient compliance when dilating the puncture tract or advancing the drainage catheter.

In general, there are two basic puncture techniques:

1. Seldinger technique (over the wire)
2. Trocar technique (direct puncture)

Seldinger Technique

If the Seldinger technique is used, an 18 G needle is advanced into the lesion. Needle advancement can be controlled by repetitive single scans or CT fluoroscopy. Especially in complex access routes, CT fluoroscopy greatly improves puncture safety and speed as the advancement of the initial puncture needle can be monitored online (Daly et al. 1999). The abscess wall is usually felt as a tender resistance. The needle should be advance with a short, firm motion into the collection. Once the intended puncture depth has been reached or passage through the abscess capsule is felt, diagnostic aspiration is performed. If the aspirated fluid is purulent, catheter placement follows. It should be emphasized that if the initial puncture and aspiration are negative, a drain should still be placed if the fluid collection is confirmed by imaging.

A guidewire is advanced into the abscess through the needle. Care has to be taken to avoid perforation of the abscess wall. Usually, a resistance is felt when advancing the guidewire, and the wire starts to coil in the collection. If the position of the guidewire tip is uncertain, an axial control scan or a short scout view should be obtained. Once the guidewire has reached the desired position, it is critical not to lose guidewire access during the procedure. When access is lost, reentry may be difficult because of spontaneous decompression of the abscess or difficulties in imaging due to access tract manipulation especially in challenging anatomic situations.

The puncture needle is carefully withdrawn, keeping the guidewire in place. Then, the puncture tract is dilated using hydrophilic coated dilators. The dilator should be securely advanced into the abscess without perforating it. The initial puncture needle will show the distance covered and can be used as a depth gauge before introducing the dilator. Depending on the push resistance, it can be advisable to slightly overdilate the tract to the next dilator size to facilitate catheter passage. When encountering difficulties passing the dilator or drainage tube, make sure that the skin incision is large enough and that no strands of subcutaneous connective tissue have remained. If the skin tents up with gentle backward pull on the dilator or catheter, the incision should be enlarged.

When resistance to passing the dilator or catheter persists, the wire may kink under the skin. In these cases, it may be helpful to slightly withdraw the wire and advance the dilator over the kink and then slowly readvance the unit. The guidewire needs to be held straight. In bigger patients, the procedure is facilitated by compressing the skin and holding the catheter close to the skin. If this fails, either a bigger dilator is needed or the catheter has to be exchanged for a smaller or more rigid system. A hydrophilic 5-F dilator can almost always be advanced. Once the dilator has reached the abscess, a kinked or soft guidewire can be exchanged for a stiffer wire. Therefore, it is crucial to continuously maintain guidewire access to the lesion.

Once the access tract has been secured and dilated, the drainage catheter is placed over the guidewire. In most cases, a drainage catheter will be placed with an inner-stiffening cannula using an over-the-wire technique. When the metal cannula is used, the catheter-cannula combination is straightened and can be advanced as a unit into

the fluid collection. It is helpful to measure the distance from the skin to the central abscess using the CT caliper to better estimate how far the catheter needs to be advanced. Once the catheter tip has reached the lesion, the inner-stiffening cannula is unlocked from the catheter. The catheter is then deployed like an intravenous catheter. The guidewire and inner cannula are held steady while the catheter is further advanced into the abscess. All catheter side holes need to be within the abscess cavity to prevent contamination of intervening spaces. Once the catheter is in place, the cannula can be removed. Depending on the individual situation, the guidewire may remain in place when obtaining control images to check for the catheter position. If the catheter is documented well within the abscess, the guidewire is removed, and the fluid is evacuated.

Trocar Technique

Easily accessible abscesses may be drained with the trocar technique where a stylet is placed in the inner cannula. In experienced hands, the trocar technique is quick and safe, as guidewire insertion and puncture tract dilation are omitted. If an initial aspiration has been performed, the aspiration needle can be left in place to serve as a guide for the drainage catheter. After the tip of the stylet and the inner cannula have reached the abscess, the stylet is removed, and fluid is aspirated. If aspiration proves the correct catheter position, the catheter is advanced over the cannula, which is held in place until all side holes are inside the fluid collection. Thereafter, the cannula is removed. Inherent problems of the trocar technique are difficulties traversing multiple tissue planes with a large-diameter object and malpositioning of the catheter either too deep or too superficial. Especially if a large (12 F and bigger) drainage catheter is employed, placement may fail due to friction and deformation of the plastic catheter over the metallic stylet.

Initial Drainage and Catheter Fixation

In order to drain as much pus as possible, the catheter should be flushed with 10–20 ml of saline. The fluid is aspirated, and irrigation can be repeated several times to facilitate initial removal of debris and viscous fluids. If clear fluid returns, a CT scan should be obtained to document the size and residual filling of the abscess cavity. In abdominal or pelvic abscesses, opacification of the cavity with a solution of iodinated contrast material and saline (1:30) (Fig. 11.8) is performed to diagnose enteric fistula (Harisinghani et al. 2002) and to prove drainage of the entire fluid collection. This is particularly useful in septated abscess formations. Additional catheter manipulation or placement of an additional catheter is based on these results.

Finally, the catheter is fixed to the skin. Careful attention must be paid to securing the drainage catheter, as the most common postdrainage problem is catheter dislodgment. No ideal fixation device or technique is available, and a catheter fixator can only be seen as a catheter position reminder. A patient rolling over in bed will overcome any catheter fixation system. Debilitated, confused, and uncooperative patients are at high risk of catheter dislodgment. The classic approach in surgery is skin fixation of the drainage tube, which still is the most reliable fixation method. Various adhesive-type fixation devices are available and can be used if skin suture has to be avoided or if short-term drainage is planned. If adhesive securing devices are used, two devices placed in tandem may prevent premature dislodgment. Catheter dislodgment is reflected in a change in the length of the catheter visible outside the patient. Therefore, it is helpful for the nursing staff to have an adhesive marker attached to the catheter at the skin exit site to identify catheter dislodgment early. When dislodgment is suspected, radiographs for comparison with the baseline study should be obtained. Catheter dislodgment may be noticed only when the catheter is leaking. Replacement catheters may be placed along the existing tract using an over-the-wire technique if catheter dislodgment is detected early.

11.1.5.3 Special Considerations

Spleen

In splenic abscess, drainage is preferred over surgery with splenectomy, as percutaneous drainages preserve the spleen and reduce the risk of sepsis. Successful drainage in splenic abscess is reported in more than 70 % of treatments. Factors

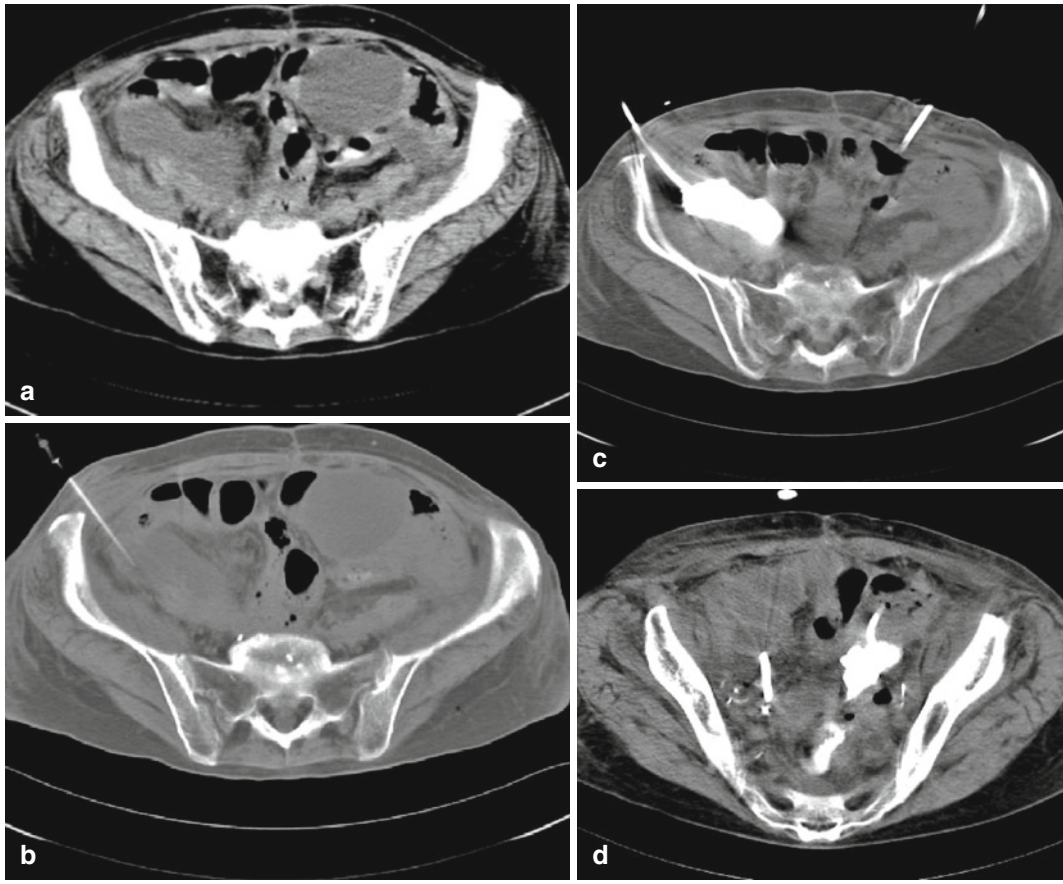

Fig. 11.8 Patient with multiple pelvic fluid collections after surgery for ovarian cancer (**a**). Needle aspiration revealed pus, and a drainage catheter was placed in the right iliac abscess and the paramedian fluid collection (**b**). After evacuation and irrigation follow-up, imaging was performed after 2 days. The *right* cavity shows no communication with the intestine (**c**). When the left abscess cavity is filled, contrast is seen in the sigmoid and rectum, establishing the diagnosis of an enteric fistula (**d**)

impairing successful drainage are multiloculated abscess formations and phlegmonous infections (Quinn et al. 1986). Because of the vascularity of the spleen, coagulation parameters should be checked carefully, and the catheter tract should traverse as little uninvolved spleen parenchyma as possible. In planning the access to a splenic abscess, structures such as colon, kidney, or pleura have to be avoided. Especially transpleural passage is of concern, as this would result in spread of the infection to another body compartment. Therefore, access route planning should be done in deep inspiration to improve visualization of the pleural recess. However, even if transpleural passage is discouraged, it may occur inadvertently (McNicholas et al. 1995). The access route typically is steeply angulated in the caudocranial direction. CT fluoroscopy with close online control of the needle passage has greatly improved successful access to this difficult location. Multislice CT scanners with simultaneous display of four or more sections are very helpful to control angulations that cannot be followed by tilting the gantry.

Pancreas

Pancreatic abscesses are more difficult to treat, as infected collections in pancreatitis. They are frequently septated, often associated with fistulas, and contain necrotic debris (Fig. 11.9).

Percutaneous treatment in pancreatitis has to consider the spread of pancreatic fluid into the lesser sac, pararenal space, and pericolic areas. Combination of multiple drainage procedures with surgery may be necessary to successfully treat this type of abscess (Ferrucci and Mueller 2003). Interventional treatment in infected pancreatic fluid collections requires aggressive therapy with large-lumen catheters to allow evacuation of viscous fluid and necrotic tissue. Close follow-up with imaging and clinical evaluation to identify complications or an unfavorable clinical course early are necessary. When compared to traditional open necrosectomy, percutaneous drainage and minimally invasive retroperitoneal debridement if necessary were shown to significantly reduce major complications and death in a randomized trial (van Santvoort et al. 2010). In this trial, 35 % of the patients in the minimally invasive group were treated with percutaneous drainage alone.

Psoas and Iliacus Muscle

Psoas abscess typically occurs secondary to disc infection or spondylodiscitis (Mückley et al. 2003). Other causes are retroperitoneal spread of diverticulitis or appendicitis or direct involvement from renal or pancreatic infections. Pain is frequently referred to the flank, hip, or knee, which makes clinical diagnosis difficult. With CT or MR, psoas enlargement and fluid accumulation in the muscle are easily depicted. In lumbar locations, drainage is performed from a posterior approach (Fig. 11.10). In pelvic spread, an anterior approach from the iliac rim into the iliacus or psoas muscle avoiding the bowels is used. If safe access to deep retroperitoneal collection is precluded due to surrounding structures, retroperitoneal injection of saline may create an access window by displacing bowel (Arellano et al. 2011).

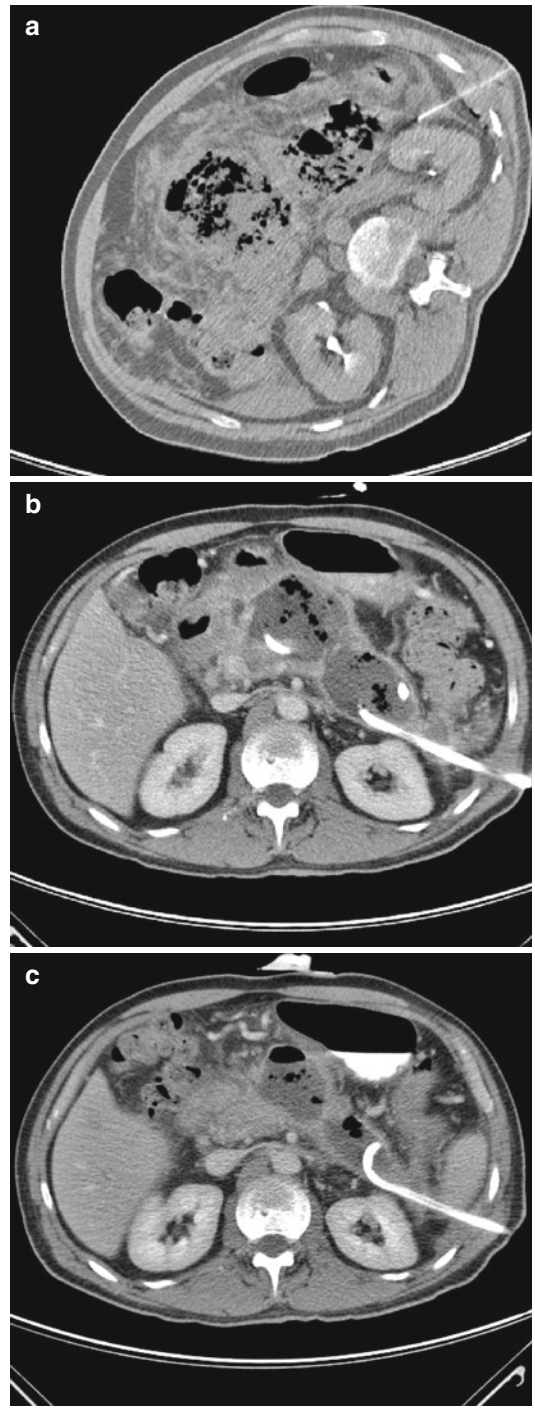

Fig. 11.9 Left lateral access to the pancreas in severe necrotizing pancreatitis. The puncture was performed with CT fluoroscopy guidance to access the pancreatic tail region, avoiding bowel injury by passing close to Gerota's fascia (**a**). A second drainage catheter was placed from a ventral access. The follow-up scan after 4 days with continuous irrigation and significant clinical improvement depicts the two catheters in place (**b**). The pancreatic bed is fluid-filled and contains air bubbles as well as necrotic tissue. Follow-up CT after 2 weeks with both catheters still in place shows a further decrease of the abscess cavity (**c**)

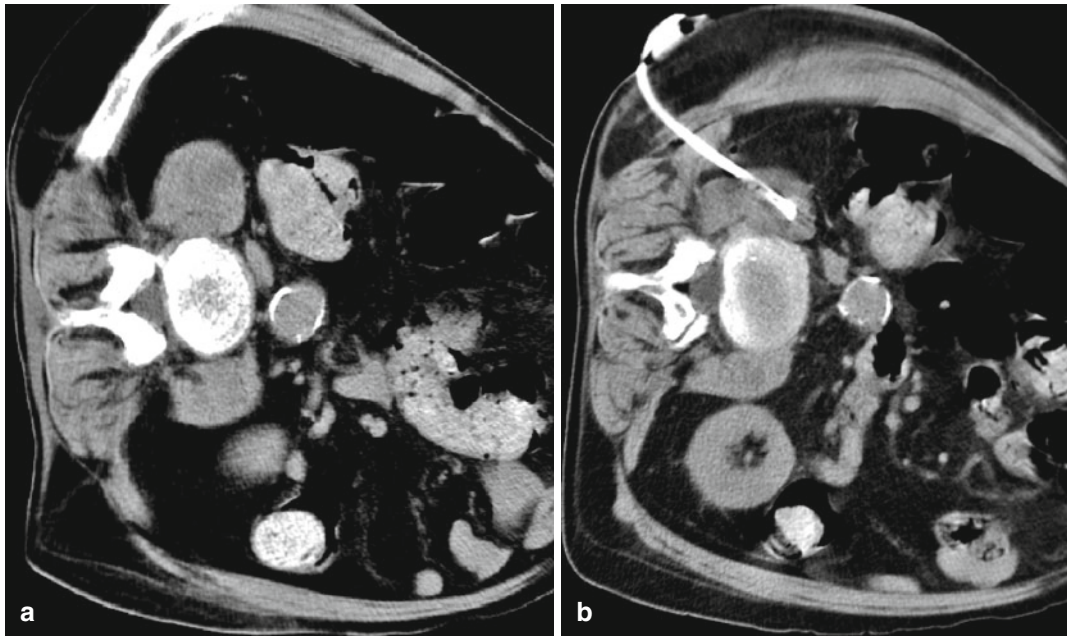

Fig. 11.10 Patient with right-sided psoas abscess. The psoas muscle is enlarged, and a hypodense area representing the abscess formation is depicted (**a**). After puncture and aspiration, a sump catheter is placed within the abscess via a dorsal approach (**b**)

Pelvis

Periappendiceal abscess may complicate acute appendicitis or appendectomy. CT with intravenous contrast administration can reliably stage complicated appendicitis and postappendectomy inflammation. CT-guided aspiration may still be beneficial for antibiotic sensitivity testing. Patients with larger, well-defined abscess responded well to percutaneous drainage. Drainage has to be maintained for several weeks to allow the fistula that is usually present to heal.

Sigmoid diverticulitis is a common condition occasionally complicated by abscess formation. Abscesses less than 3 cm in size may be managed by antibiotic therapy alone, but larger collections require drainage. Percutaneous drainage in sufficiently large collections is safe and can either be a definitive treatment or is used as a bridging procedure to delay surgery (Fig. 11.11). Delayed surgery has a better clinical outcome and a significantly lower stoma rate (Mueller et al. 1987; Singh et al. 2008).

Crohn's disease is complicated by abscess formation in more than 20 % of patients. MR imaging or CT is invaluable in early detection of abscess or fistula and in differentiation of abscess and phlegmon in these patients as clinical signs of infection and abscess formation may be masked by concurrent steroid therapy and diffuse complaints of the patient. In patients without enteric communication, percutaneous drainage is an effective treatment alternative to surgical drainage or may be used in conjunction with surgery. If enteric fistula is established, long-term drainage is often required to allow resolution of infection and closure of an enteric fistula (Casola et al. 1987; Sahai et al. 1997).

The transgluteal approach is chosen when a transabdominal route is not possible. This approach is probably underutilized due to overestimation of associated complications. Published results show that this access can be used safely avoiding critical structures like the sciatic nerve or gluteal vessels using CT guidance and proper planning.

If the catheter is inserted medially close to the sacrum at the level of the sacrospinous ligament,

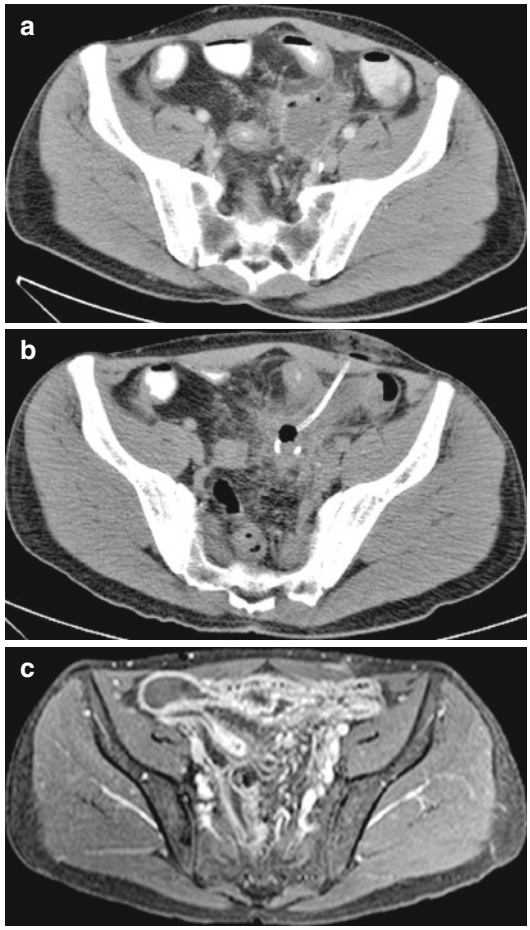

Fig. 11.11 Sigmoid diverticulitis with 5-cm abscess formation (note air bubbles) (**a**). A 12-F drainage catheter was placed using a ventral transabdominal approach. Bowel loops are identified after oral contrast administration. The documentation after fluid evacuation showed significant size reduction (**b**). Follow-up MR imaging 3 weeks after drainage shows complete resolution (**c**)

critical structures can be avoided, as vessels and sciatic nerve have a more lateral position. Pain is common due to the close proximity of the sacral plexus, and generous local anesthesia should be applied. If possible, an infrapiriformis puncture should be planned since the transpiriformis route is associated with increased pain (Harisinghani et al. 2003). Prone patient position and caudocephalic gantry tilt may be helpful to choose an entry point below the piriformis muscle and guide the cranially directed puncture to reach a presacral or retrovesical collection.

11.1.5.4 Postinterventional Care

Postinterventionally, 4–6 h of bed rest is recommended depending on the complexity of the procedure. Blood pressure, pulse, and pain should be monitored shortly after the procedure at 30 and 60 min and then at hourly intervals for at least 4 h after the procedure.

The catheter is repeatedly flushed with 10–20 ml of sterile 0.9 % saline solution at least three times a day. The quality and quantity of drainage is monitored along with signs of patient recovery. Clinical follow-up care may be augmented with CT, ultrasound, fluoroscopy, and plain film contrast studies if the infection is not resolving. In viscous or debris-laden fluids, continuous irrigation using 500–1,000 ml of saline per day may help to clear the abscess. Continuous irrigation via a sump drainage offers an effective alternative to repeated saline flushing of the drainage catheter.

White blood cell counts, fever, and pain have to be monitored. Normalization of white blood cell count and temperatures indicates improvement. Persistent fever or pain after 2 days indicates undrained pus, and a repeat CT scan is warranted. Repeat imaging should be routinely performed after 3–4 days to assess drainage success and to rule out catheter dislodgment. This can be easily achieved using fluoroscopy and contrast injection to obtain a cavernogram. Depending on the case, treatment is complete within a matter of days to weeks. Simple abscess treatment is usually completed within 1–2 weeks. A complex abscess or enteric fistula may require weeks to months to heal. The drainage catheter should be kept in place until the abscess cavity begins to close, and the drainage diminishes to a few milliliters per day of clear fluid. The patient has to be kept on antibiotic therapy as long as a drainage catheter is in place.

11.1.5.5 Management of Complicated Abscesses

Despite a high initial success rate of percutaneous drainage, some cases will not show adequate improvement with persisting fluid, fever, and leukocytosis. In these cases, catheter exchange over

a wire should be performed first, as this may be a useful salvage avoiding open surgery in up to 76 % of primary failures (Gee et al. 2010).

Complex fluid collections of high viscosity as in empyemas or infected hematoma may fail to drain despite correct catheter placement. In these cases, fibrinolytics can be used to dissolve viscous material. Haaga showed that intracavitary urokinase was safe and tended to have an improved clinical outcome in a phase II trial including 38 patients with undergoing percutaneous abscess drainage (Haaga et al. 2000). Patients underwent urokinase or saline injection at 8-h intervals during 4 days after catheter placement. The dose of urokinase depended on the abscess size and ranged from 25,000 U for abscess 3–5 cm to 100,000 U for collections larger than 10 cm in diameter. In a recent study, rtPA was applied in cases with viscous contents yielding minimal drainage or significant undrained fluid on follow-up imaging despite correct catheter position. Intracavitary injection of 4–6 mg rtPA in 25 ml of saline twice daily for 1–3 days resulted in completed drainage in 89 % of 46 abscesses (Beland et al. 2008). No hemorrhagic complications were observed, even in patients on anticoagulant therapy. It has to be noted that intracavitary rtPA instillation was performed in less than 3 % of all cases treated during the observation period.

11.1.6 Results

Comparison of percutaneous drainage and open surgical drainage in large published series revealed that the percutaneous approach is associated with a better overall outcome with fewer complications, more effective drainage, and shorter treatment duration. Percutaneous drainage can frequently be performed using a short, direct approach and very little intervention-related trauma. Open midline incision can be avoided therefore limiting the potential for spreading contamination and postsurgical hernia. With percutaneous drainage, a shorter hospital stay is anticipated, as general anesthesia is not necessary and patients can be discharged early with small catheters in place, which can be managed on an outpatient basis.

Numerous studies have documented the efficacy of catheter drainage in many anatomic locations with cure rates of 80 % and greater (Akinci et al. 2005; Gee et al. 2010; Harisinghani et al. 2003; van Sonnenberg et al. 2001). Even in multiloculated abscesses, catheter drainage is effective, as most locules will communicate. Mortality is reported to be 3–4 % in solitary abscess, which is better than results from surgery showing 9 % mortality (Gerzof et al. 1985). In postsurgical patients, anastomotic leak is a frequent complication occurring in 10–15 % of patients. These postoperative complications are well addressed with percutaneous drainage and have a success rate close to 80 % (Gervais et al. 2004).

11.1.7 Complications

Complications of percutaneous puncture and drainage largely depend on the location of the collection, which determine the access route and underlying pathology influencing clinical success of a drainage procedure. The drainage route should avoid unnecessary contamination of uninvolved areas thus should be short and simple. Spread of infection is possible as well as injury to organs, blood vessels, or intestine (Thomas et al. 2006). Specific complications related to access route include bowel perforation, fistula, spread of infection, pneumothorax, and catheter dislocation. As with all punctures, local bleeding and discomfort are common. The most important complication is catheter dislodgment resulting in insufficient drainage or even spread of infection in the area of the puncture tract.

Appraisal

Percutaneous abscess drainage is a minimally invasive intervention performed under local anesthesia with success rates, morbidity, and mortality as good as or better than those of surgery. Complications are

rare and mostly refer to pain and catheter dislodgment. In combination with surgery, the extent of subsequent surgery is reduced, and one-stage procedures become possible. Owing to the minimally invasive nature and the availability of CT guidance, percutaneous drainage procedures have become an indispensable tool in successful management of the patient with infected fluid collections. Using CT fluoroscopy, one can reach almost any location safely, making percutaneous drainage the first choice. Even in recurrent abscess, a repeated attempt using a percutaneous approach is warranted before open surgery is considered. Close follow-up of the patient with ongoing communication and consultation with the clinicians is necessary to ensure satisfactory outcome. Imaging follow-up is required to control or adjust catheter position, to prove resolution of abscess formation, or to make an early decision on whether to convert to surgery in unsuccessful cases.

Key Points

- Percutaneous abscess drainage has a better risk-success ratio, when compared with surgery.
- There are virtually no absolute contraindications to percutaneous abscess drainage.
- Needle aspiration is the best way to determine the nature of a fluid collection and to access its drainability.
- The catheter size needs to be selected in adaption to the fluid's viscosity.
- Proper catheter fixation is crucial as catheter dislodgment is the most important complication in percutaneous abscess drainage.
- Consequent irrigation and postinterventional care are vital for treatment success.

11.2 Drainage in Pneumothorax

Christian Hohl

The use of small-caliber chest tubes to treat postinterventional pneumothorax was first described by Sargent and Turner (1970). They used a 9-F drainage catheter with a flutter valve as described by Heimlich (1968). Since then, numerous reports proved the percutaneous radiological treatment to be a well-established and safe technique to handle postinterventional pneumothoraces.

11.2.1 Indications

Pneumothorax is the most common complication in CT-guided biopsy of pulmonary and pleural masses, with a frequency of 8.2–54.3 % (Yamagami et al. 2005). It is more frequent in patients with emphysema or obstructive airway disease. Cox et al. noted that evidence of emphysema and smaller lung lesions (≤2 cm) correlated with the incidence of pneumothorax after lung biopsy (Cox et al. 1999). Furthermore, pneumothorax can occur in punctures for central vein catheters (subclavian or jugular vein) or biopsies of the upper abdomen. Thus, the ability to treat pneumothorax is as important as to perform the primary intervention itself. Anybody participating in an intervention with the potential risk of pneumothorax must be familiar with the correct handling of chest tube and Heimlich valve.

If pneumothorax is recognized during a CT-guided intervention, there are three different therapeutic options:

1. Observation
2. Aspiration or
3. Placement of pleural drainage (Fig. 11.12)

Ad 1: In patients in which pneumothorax is only evident on the CT scan but who have no clinical symptoms such as dyspnea, tachypnea, or tachycardia, observation and control radiographs are a good option. If the pneumothorax is stable or decreasing under observation, no further action is necessary.

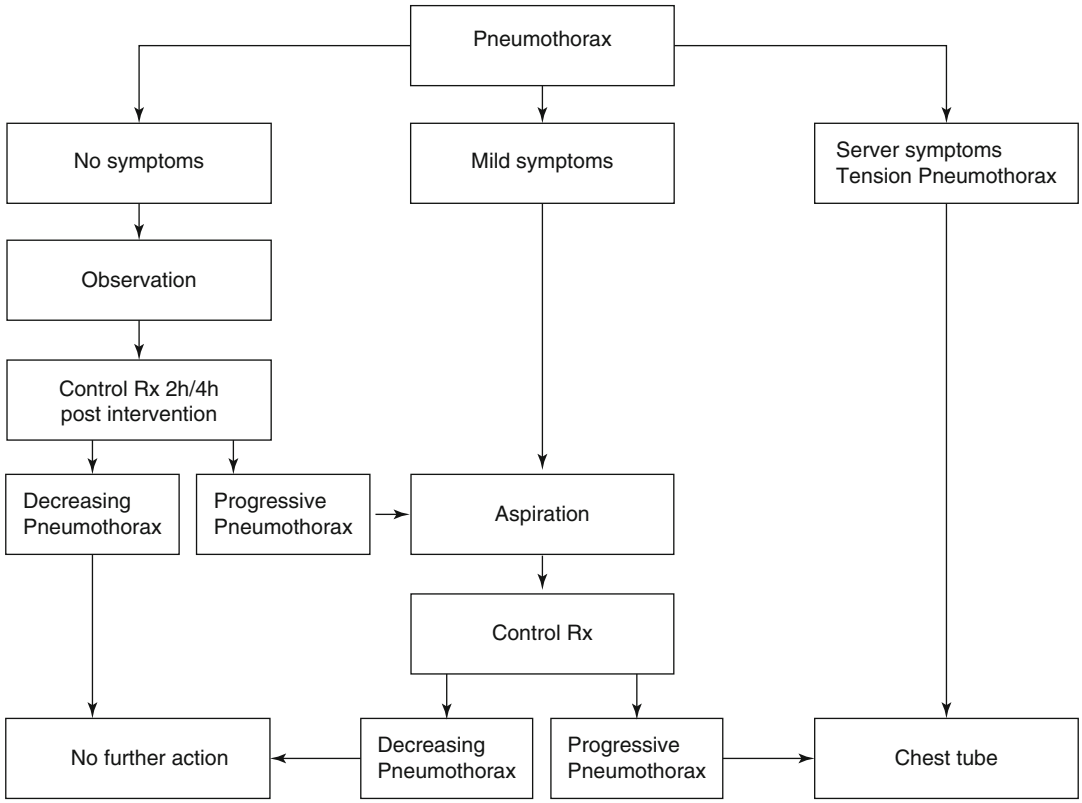

Fig. 11.12 Flow chart for the adequate procedure after postinterventional pneumothorax

Ad 2: In patients with progressive pneumothorax in the control radiograph or in patients with mild symptoms, manual aspiration of air from the pleural space can help to stabilize the situation and reduce the need for subsequent chest tube placement.

Ad 3: When the pneumothorax recurs after aspiration, no second attempt should be made, and immediately chest tube placement is recommended. Furthermore, Yamagami et al. (Yamagami et al. 2005) recommend placing a chest tube if the aspirated volume is larger than 500 cc.

In all patients with severe complaints such as heavy dyspnea, symptoms of circulatory shock, or tension pneumothorax, instantaneous placement of a chest tube is essential. Also, any patient with an iatrogenic pneumothorax on mechanical ventilation should strongly be considered for placement of a chest tube (Baumann et al. 2004).

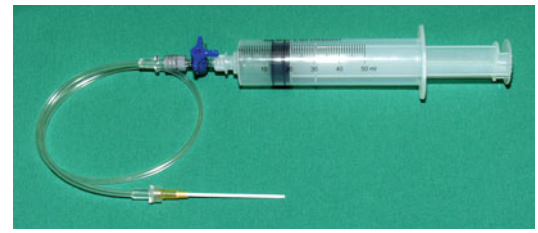

Fig. 11.13 Self-assembled set for thoracocentesis consisting of a 14 G puncture needle, a connecting tube, a three-way stopcock, and a 50-ml syringe

11.2.2 Material

For thoracocentesis, which means the aspiration of air from the pleural space, no special equipment is needed. It can be performed with the use of a 14–18 G puncture needle, a connecting tube, a three-way stopcock, and a 50-ml syringe (Fig. 11.13).

For the placement of a chest tube with Heimlich valve, prepacked sets are available

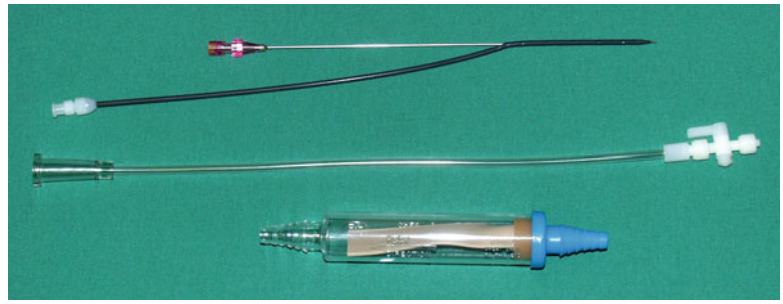

Fig. 11.14 Prepacked chest tube set (C-TPT-100, Cook Europe, Bjaeverskov, Denmark) consisting of an 18 G needle (20 cm length) with a premounted 9-F catheter (29 cm length) with four side holes near to the tip, a connecting tube with one-way stopcock, and a Heimlich valve

(Fig. 11.14). To treat a postinterventional pneumothorax, a 9-F tube as described by Sargent and Turner is sufficient (Sargent and Turner 1970).

11.2.3 Technique

11.2.3.1 Aspiration

The aspiration of air from the pleural space can be performed in different locations; the appropriate site with the largest aspect of the pneumothorax is chosen from the computed tomography (CT) scan. In most cases, the second or third intercostal space in the midclavicular line is a good choice in supine patient position. A 14–18 G intravenous catheter is inserted. Particular attention should be given to the puncture angle. With a slanted puncture in the craniocaudal direction, the puncture holes in the different layers of the thoracic wall are displaced a little to each other which helps to prevent recurrent pneumothorax after catheter removal. To avoid the neurovascular bundle beneath the inferior aspect of the adjacent rib, the catheter should be placed close to the superior aspect of the rib. The catheter is advanced into the pleural space, and the stylet is removed. The connection tube with the three-way stopcock is connected to the intravenous catheter, and the air from the pneumothorax is drawn in the 50-ml syringe and expelled by alternately opening and closing the stopcock. Whenever resistance is encountered, the catheter is slightly withdrawn, and aspiration is resumed. After complete or almost complete re-expansion of the lung is documented on a control CT scan, the catheter is completely withdrawn. During catheter withdrawal, suction is maintained, and the skin entry point should be manually compressed after catheter removal.

11.2.3.2 Chest Tube

For the insertion of a chest tube, two different entry sites can be recommended, the fifth intercostal space in the anterior axillary line or the second intercostal space in the midclavicular line (Choi et al. 2007). After the entry site is determined, the skin is prepared with antibacterial wash and draped in a sterile fashion. The catheter is preassembled, connecting Heimlich valve and tube. It is important that the Heimlich valve is attached in the direction indicated by the arrow on the valve. Local anesthesia is injected liberally along the intended tube tract through skin, subcutaneous tissue, muscle, and fascia down to the parietal pleura. A small incision is made with a no. 11 blade at the entrance site, taking care to avoid the neurovascular bundle beneath the inferior aspect of the adjacent rib. Now the needle tip is inserted, with the catheter as its sheath, into the pleural cavity. Again it is advantageous to choose a slanted puncture angle to avoid an air leak after tube removal. Needle and catheter are advanced with one hand while the other hand maintains pressure upon the stylet within the needle. In patients with a large pneumothorax, when it is certain that stylet and catheter are well within the pleural cavity, the catheter is pushed forward by sliding it over the stylet into the pleural space (Fig. 11.15). If there is uncertainty if needle and catheter tip are well within the pleural space, a control scan is performed before the catheter is pushed forward. The catheter must be advanced so that all side holes are within the pleural space. While advancing the catheter, the needle is slowly

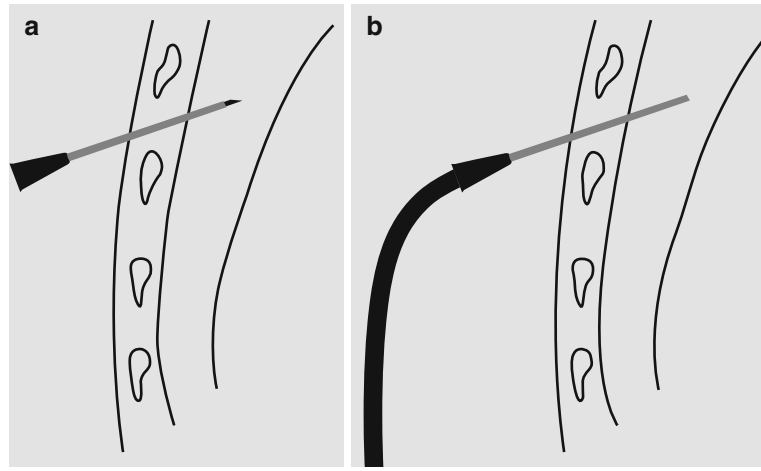

Fig. 11.15 Thoracocentesis with an intravenous catheter. The pleural space is punctured with a 14 G puncture needle until air can be aspirated (**a**). Then the stainless steel needle is removed and the Teflon catheter is pushed up against the thoracic wall (**b**). In this position, the air in the pleural space can be aspirated with the syringe and removed via the three-way stopcock

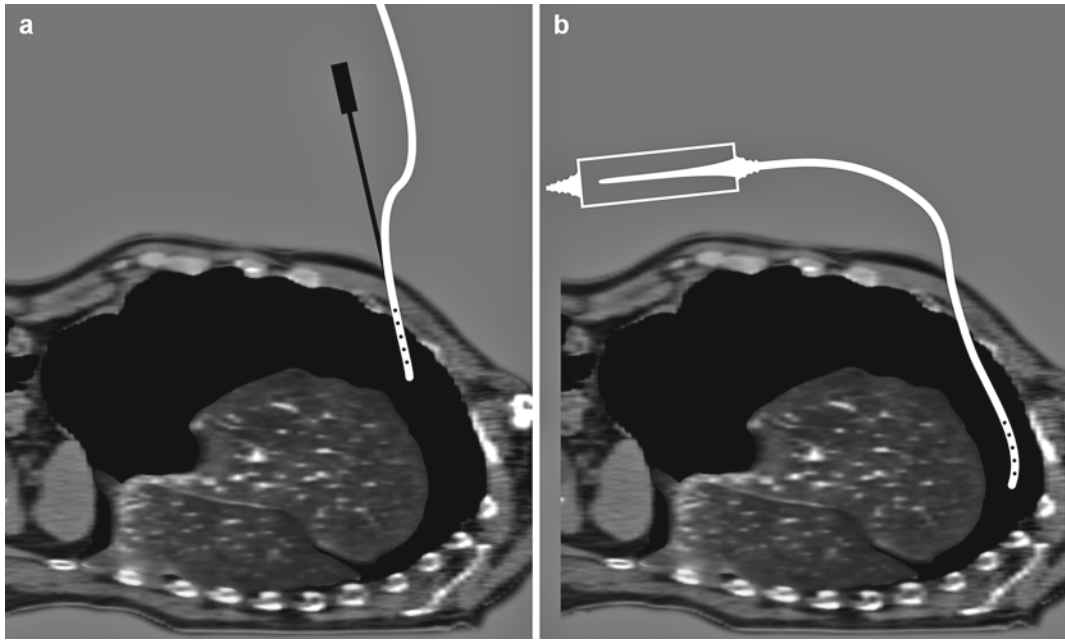

Fig. 11.16 Insertion of a 9-F catheter in trocar technique. The pleural space is punctured with an 18 G stylet with the premounted 9-F catheter. When catheter and stylet are well within the pleural cavity, the catheter is pushed forward by sliding it over the stylet into the pleural space (**a**). The distal tip of the catheter should be positioned in the apex of the pleural space whereas all side holes must be within the pleural space (**b**)

withdrawn. The distal tip of the catheter should be positioned with the tip pointing toward the apex of the pleural space. When the catheter is in place and the needle is completely withdrawn, the connection tube with the Heimlich valve is connected with the catheter, and the stopcock is unblocked. To avoid displacement, the catheter is attached to the chest wall with skin suture and adhesive tape. A U-shaped suture around the skin entry point may be helpful. It can be pulled together during chest tube withdrawal and thereby help to avoid a recurrent pneumothorax due to a puncture site fistula.

In most patients, the symptoms will improve within minutes after tube insertion (Fig. 11.16). In few patients who do not improve noticeably,

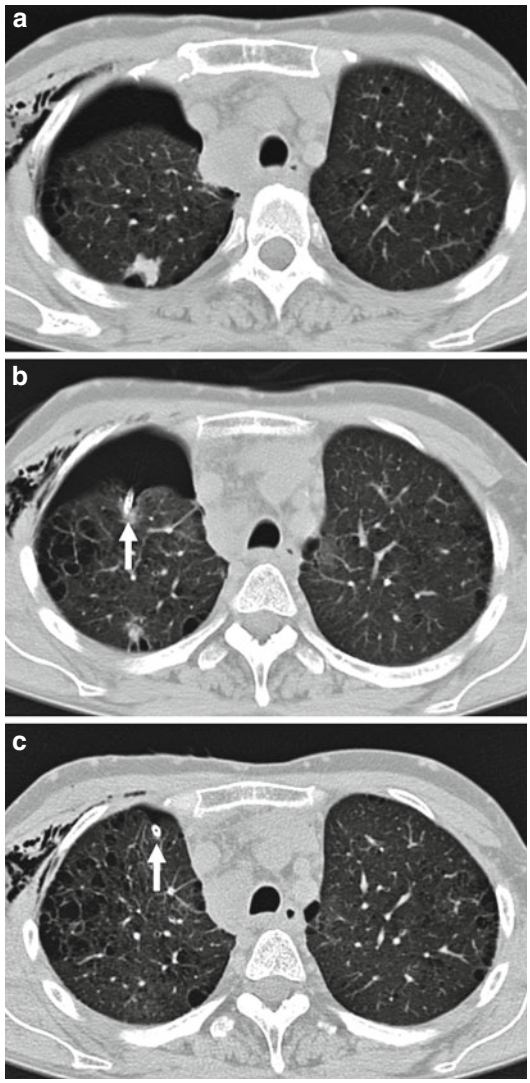

Fig. 11.17 Patient with severe emphysema and coin lesion in the right upper lobe developed pneumothorax after biopsy (**a**). Due to dyspnea, a catheter (*arrow*) with Heimlich valve was inserted on the CT table (**b**). Five minutes after insertion of the catheter, the pneumothorax was completely resolved (**c**)

additional wall suction can be attached to the Heimlich valve (Fig. 11.17).

Directly after placement of the drainage catheter, a p.a. chest radiograph is obtained to confirm the catheter position and to examine for residual pneumothorax. The following morning and subsequently as indicated, chest x-rays were obtained. If the lung remains expanded, the stopcock is turned off, and a chest x-ray is obtained 4 h later. If the lung still remains expanded, the catheter can be removed (Conces et al. 1988). If pneumothorax recurs, the stopcock is opened again, and the process is repeated at a later time.

Removal of the drainage catheter is performed in expiration under continuous suction on the catheter. After drainage with small-bore catheters (9 F), inflow of air into the pleural space can be avoided by short-term manual compression and adhesive bandage. After removal of the catheter, a final chest x-ray is obtained to document the success.

11.2.4 Results

The success rate of chest tubes with Heimlich valve in the treatment of pneumothoraces ranges between 87 and 95 % (Conces et al. 1988). Typical reasons for malfunction of chest tubes with Heimlich valve are kinking, malpositioning in major fissure, inadvertently removement by the patient, or clogging of tube or valve. Another very rare reason for malfunction of the catheter is an air leak that exceeds the catheters ability to remove air. The mean duration of drainage with small-bore catheters with Heimlich valve reported in the literature ranges between 1.6 and 5.1 days (Yamagami et al. 2005; Conces et al. 1988; Martin et al. 1996; Laronga et al. 2000; Niemi et al. 1999).

11.2.5 Complications

Unlike large tube thoracostomy, no significant complications are observed in 9-F catheters with Heimlich valve. Misplacement of catheters into lung parenchyma, liver, or spleen, as seen in surgical chest tubes, is under CT guidance nearly impossible. Hematoma of the chest wall can occur if the neurovascular bundle under the adjacent rib is punctured.

The presence of pleural fluid can result in clogging of the 9-F tube or the Heimlich valve. In the latter case, the problem can be solved by replacing the valve with a new one or by removing

the valve and attaching the tube directly to suction (Conces et al. 1988). If the catheter becomes clogged, placement of a second catheter may be required.

Summary

Using the trocar technique, the 9-F catheter is a safe and quick method to resolve postinterventional pneumothoraces. Following placement, little nursing care is required, and patients with a Heimlich valve can even be treated as outpatients. When a patient is to be sent home with a catheter in place, one must ensure that the catheter is secured in such a fashion as to prevent it from being dislodged (Conces et al. 1988).

Key Points

- Successful management of pneumothorax depends on the correct indication (Fig. 11.12).
- The described trocar technique with a preassembled 9-F pneumothorax set and a flutter is a quick and safe method for treating postinterventional pneumothoraces.
- Sufficient catheter fixation is crucial to prevent catheter dislocation with subsequent treatment failure.

11.3 Nephrostomy

Christian Hohl

11.3.1 Indications

Percutaneous nephrostomy (PCN) is one of the most common interventional procedures since its first description in 1955 (Goodwin et al. 1955). A dilated collecting system is not a priori an indication for PCN, the more so as the kidney function is not necessarily compromised by the obstruction and can maintain normal for a length of time. In cases of superinfected obstruction, the parenchyma will quickly perish if PCN is not immediately performed. In most cases, nephrostomy is performed as an elective procedure in patients with:

- Ureteric obstruction
- Obstructing tumors
- Urinary fistulas

Urgent drainage is needed in cases with:

- Infected postrenal obstruction
- Pyonephrosis
- Septicemia
- Hemorrhagic cystitis
- Uremia in which a rapid renal loss threatens the patient
- Infected postoperative urinomas

Further indications for PCN can be the access-creation for endo-urologic interventions such as percutaneous nephrostolithotomy or antegrade ureteric dilation or stent insertion (Matlaga et al. 2003). PCN is also performed prior to RF-ablation of renal tumors to cool the renal pelvis and the calyces. In rare cases, it may be used as access route for local drug delivery (e.g., bacilli Calmette-Guerin (BCG)).

PCN is typically performed under ultrasound (US) or fluoroscopic guidance, but sometimes computed tomography (CT) or magnetic resonance (MR) guidance can be advantageous. Especially in patients with an unfavorable anatomy (e.g., retrorenal colon) or a non-dilated collecting system, it can sometimes be really difficult to find an appropriate access. In this chapter, only the techniques of CT- and MR-guided nephrostomy are discussed; for detailed descriptions of fluoroscopic or ultrasound guidance, please refer to the corresponding literature (Osman et al. 2005; Miller et al. 2007).

The minimal patient preparation includes besides the informed consent an up-to-date blood testing (blood count, coagulation, renal function) and US of the kidneys. In elective interventions, the international standardized ratio (INR) should be ≤2, and the platelet count should be above 80,000/mm^3. If the platelet count is less than this level, platelet transfusion should be performed just before the intervention.

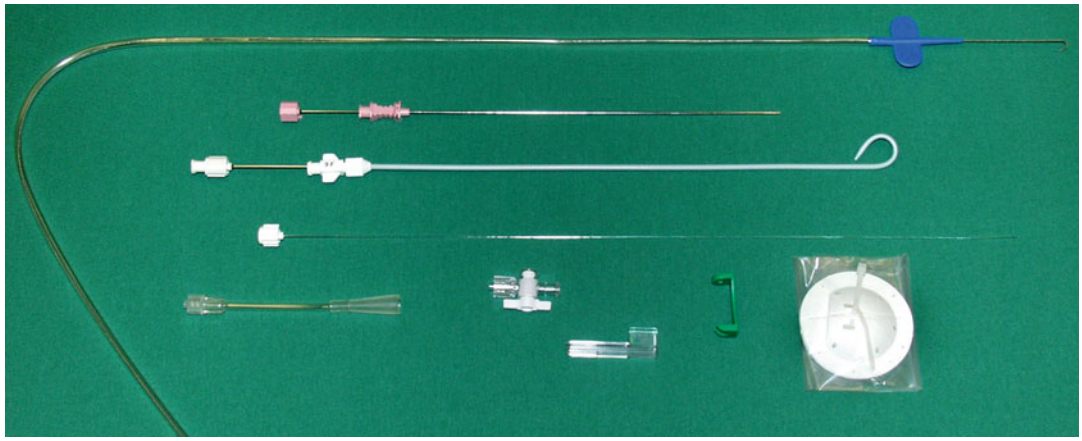

Fig. 11.18 Prepacked nephrostomy set for Seldinger technique (Soft-Drain, Bard-Angiomed, Karlsruhe, G) containing a 17.5 G puncture needle (200 mm length), a 0.038 guidewire, and a 9-F drainage catheter (285 mm length) in pigtail configuration

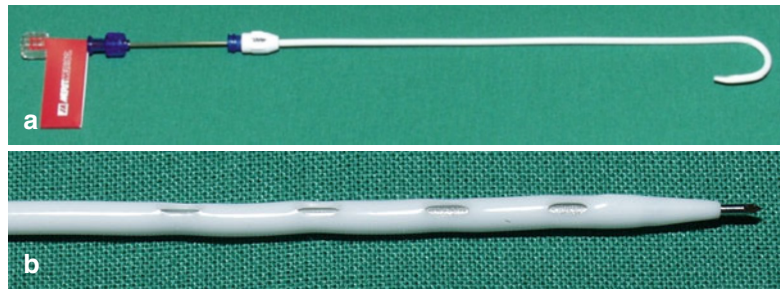

Fig. 11.19 Drainage catheter system for the trocar technique (Resolve, Merit Medical, South Jordan, UT, USA) composed of a 8.5-F J-tip catheter with hydrophilic coating, a metal stiffening cannula, and 0.038 trocar stylet (**a**). Before puncture, the stiffening cannula and the stylet must be inserted completely into the catheter so that the J-tip is straightened (**b**). The catheter tip is tapered to provide a smooth transition. The four side holes are located at the inner circle of the J-tip to prevent sealing

11.3.2 Material

In general, there are two different techniques to perform percutaneous nephrostomy: Seldinger technique and the one-step or trocar technique. For both techniques, a variety of different prepacked sets, needles, and catheters are available. Exemplary prepacked nephrostomy set (Soft-Drain, BARD-Angiomed, Karlsruhe, G) for the Seldinger technique is shown in Fig. 11.18. Seldinger sets comprise, for example, a 17.5 G puncture needle, a 0.038" stiff guidewire with floppy tip, and a 9-F drainage catheter in pigtail configuration. For selected patients, the use of an atraumatic 22 G puncture needle and a 0.018" guidewire may be needed.

For the trocar technique, the drainage catheter is premounted on the puncture needle as shown in Fig. 11.19. Tubes of 8–10 F are usually sufficient for drainage of noninfected urine. Larger tubes (12–14 F) may be necessary for drainage of infected urine or to ensure appropriate urine flow in procedures complicated by gross hematuria. Additional required material includes suture, drainavge bag, connecting tube, and drainage bag connector.

11.3.3 Technique

Normally, PCN can be performed under local anesthesia; only in children, a deep sedation or general anesthesia is required. To prevent septicemia, single-shot antibiotic prophylaxis (e.g., 1,500-mg cefuroxime) is recommended 1 h prior to the intervention (Lewis and Patel 2004).

Percutaneous nephrostomy can be performed in two different techniques. The one-step or trocar technique is principally used in patients with dilated collecting system and has the advantage that the renal parenchyma is only passed once and no guidewire maneuvers are necessary. The main drawback of the one-step technique is that the kidney is punctured with a relatively chunky instrument with the risk of hemorrhage if the catheter is not positioned correctly in the first attempt. This can be problematic in patients with a non-dilated pelvicalyceal system.

The Seldinger technique on the other hand is more subtle and a little more complicated. Using the Seldinger technique, the collecting system is punctured with a small puncture needle through which a guidewire is inserted and placed in the proximal ureter. Then the drainage catheter is placed in the renal pelvis over the guidewire.

For both techniques, the patient positioning is pivotal for a successful intervention. The patient is positioned either in a prone or prone/oblique position on the examination table. It is important to obtain a position which is as comfortable as possible for the patient to assure good compliance, especially if the intervention takes its time.

A contrast-enhanced CT is not necessary to plan the intervention, but especially in patients with non-dilated collecting system, an i.v. injection of 20–40-ml iodinated contrast medium about 3–5 min prior to the procedure can be very helpful to identify the calyces. If the intervention is performed under MR guidance, the collecting system can easily be depicted on T2-weighted images.

To minimize the risk of hemorrhage, puncture site selection should be performed with care. Brödel described the water shed between the anterior and the posterior vascularization of the kidney (Brodel 1901). This "avascular line" is located approximately 1–2 cm behind the lateral convex margin of the kidney. To avoid injury of interlobar arteries, which are situated in the renal columns between the renal papillae, the collecting system should be punctured through the papillae and the calyces. In this respect, a posterior calyx of the mid or lower pole should be chosen (Fig. 11.20). Puncture of upper pole calyces is only necessary for nephrolithotomy. Direct puncture of the renal pelvis or anterior puncture should be avoided for the risk of hemorrhage and extravasation due to lacking parenchymal cover.

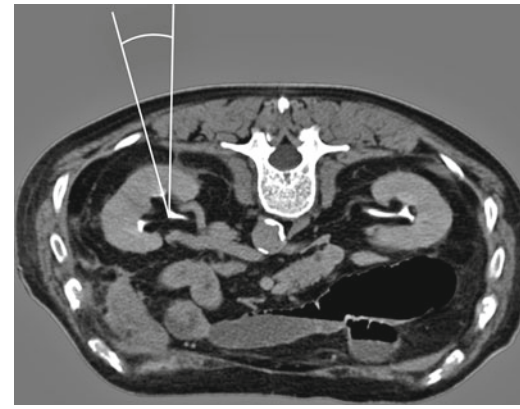

Fig. 11.20 Optimal approach for nephrostomy in non-dilated collecting systems. The patient is positioned in a prone position. The posterior calyx of the lower pole is targeted via a posterolateral approach below the 12th rib

When the patient is positioned in a comfortable position (prone or prone/oblique), the back and flank are sterilely cleansed and draped. Thereafter, a planning scan is performed, and an appropriate calyx has to be chosen. Once the target has been identified, the angle between the puncture path and the vertical center line is measured (Fig. 11.20). The puncture path should avoid ribs by several centimeters to allow for unobstructed breathing once the PCN is in place. The needle entry point is marked in usual technique with the help of the positioning laser and a planning grid. There are sophisticated instruments to guide the puncture needle along the exact path, but we prefer a straightforward method in which a colleague at the table top is checking the correct angle with a simple goniometer. After infiltration of the skin and subcutaneous tissues with 1 % lidocaine over the selected

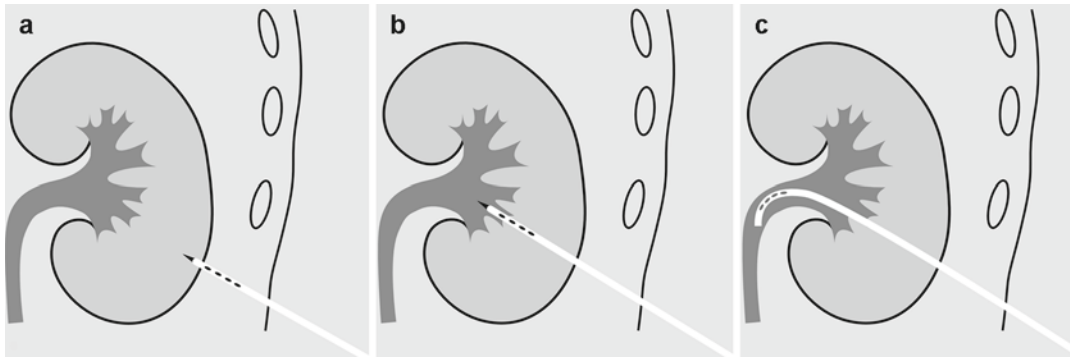

Fig. 11.21 Trocar technique for percutaneous nephrostomy. With a drainage catheter already mounted on a trocar stylet, the calyx is targeted (**a**). When the needle has entered the collecting system (**b**) and urine can be aspirated, the drainage catheter is advanced while the stylet is kept in place (**c**)

site, a skin incision appropriate to the anticipated nephrostomy tube size is made with a no. 11 blade, taking care to avoid the neurovascular bundle beneath the inferior aspect of the adjacent rib. Then respiration is suspended, and the puncture needle is inserted. When the needle is advanced a few centimeters, the correct path is checked by a single sequential control CT scan or a fast T2-weighted gradient echo sequence. In this manner, the needle is advanced step by step until the correct needle placement is documented, and hopefully, urine can be aspirated. There may be a sudden "give" when the calyx is entered. A urine sample is obtained on entry into the collecting system and sent for culture. Do not decompress the system completely, as this makes subsequent manipulation more difficult.

In patients with dilated collecting system using the one-step (trocar) technique, the needle is advanced a little more until the tip is securely within the collecting system. Thereafter, the stainless steel trocar is retained while the premounted drainage catheter is advanced with caution until all side holes are within the collecting system (Fig. 11.21).

Using the Seldinger technique, a 0.035 or 0.038 guidewire is inserted over the puncture needle and should be advanced without resistance down the ureter. If it is difficult to find the way in the ureter, a 4-F multipurpose catheter can be helpful to negotiate the guidewire into the ureter. Once the guidewire is in position, the drainage catheter is inserted over the wire. If there is too much resistance advancing the catheter, dilators can be inserted to widen the tract (Fig. 11.22). It may be necessary to overdilate a track by 1–2 F for tubes made of materials with high friction coefficients (e.g., silicone) or when there is significant perirenal scarring. Tubes coated with hydrophilic material are usually easily placed through tracks dilated to an identical French size. When the catheter is in place, a small amount of diluted contrast medium is injected to document the correct position. In order to minimize the risk of septicemia, an infected system should never be overdistended. In difficult patients with completely collapsed collecting system, the use of an atraumatic 22 G puncture needle and a 0.018" guidewire is recommended.

If the aspirated urine is clear or only slightly hemorrhagic (rosé), the drainage bag is connected. If the urine is dark red, a lavage with 0.9 % saline solution should be performed until it becomes rosé. If pus can be aspirated, the system should be decompressed without lavage. Finally, the catheter should be secured in position by a suture and adhesive dressing to prevent dislocation with the need for subsequent reinterventions. A nephrostogram should be performed not earlier than 24 h following tube placement.

Some CT scanners are equipped for CT fluoroscopy (CTF) which provides real-time reconstruction and display of CT images during interventional procedures. CT fluoroscopy guidance can increase target accuracy and reduce the

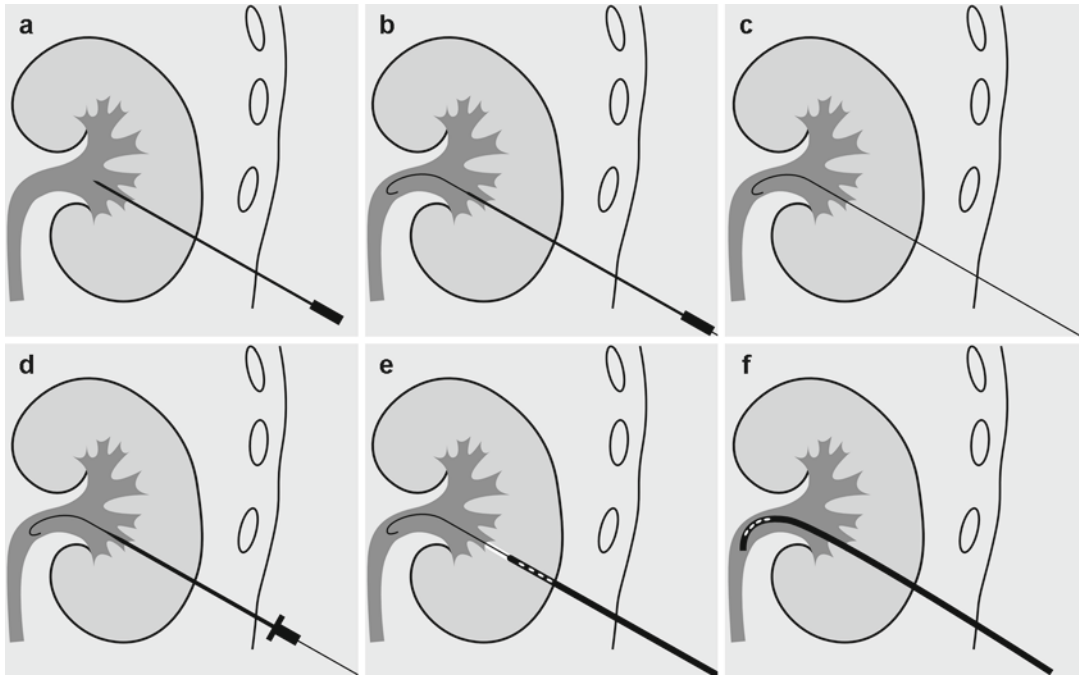

Fig. 11.22 Seldinger technique for percutaneous nephrostomy. A calyx is punctured with a 17.5 G needle (**a**). A 0.038" guidewire is inserted over the needle and placed with the tip in the proximal ureter (**b**). Then the puncture needle is removed (**c**), and the tract is widened with a dilator if necessary (**d**). Finally, the drainage catheter is inserted (**e**), and the guidewire is retracted (**f**)

intervention time (Silverman et al. 1999). When CTF is used, special attention has to be paid to radiation exposure as especially the interventionalist's hand is near the x-ray beam during the intervention. Therefore, the use of angular beam modulation, which turns off the x-ray beam in a 120° sector without impairing the image quality, is recommended during CTF-guided nephrostomy (Hohl et al. 2008). During MR-guided nephrostomy (Fig. 11.23), the same effect can be achieved with real-time imaging (Fritz and Pereira 2007).

11.3.4 Results

The technical success rate for PCN under fluoroscopic und US guidance varies between 95 and 98.5 % (Gupta et al. 1997; Lang and Price 1983). With CT guidance, the technical success rate can be improved up to 100 % (Egilmez et al. 2007). The same has been reported in the only small patient series on MR-guided nephrostomy (Fischbach et al. 2011). In cases with failed US guidance, CT-guided nephrostomy has still a success rate of 91 % (Sommer et al. 2011). CT guidance has its particular strength in difficult patients without dilation of the collecting system. The clinical impact of PCN as an emergency intervention can be demonstrated by the decrease of gram-negative septicemia from 40 % down to 8 % (Lang and Price 1983).

11.3.5 Complications

Major complications may be seen in 4–6 % of patients who undergo fluoroscopy- or US-guided percutaneous nephrostomy procedure (Stables 1982; Zagoria and Dyer 1999). Using CT or MR imaging as guiding modality, the rate for major complications can be reduced to 0 % (Egilmez et al. 2007; Thanos et al. 2006; Fischbach et al. 2011). Minor complications such as pain or transient

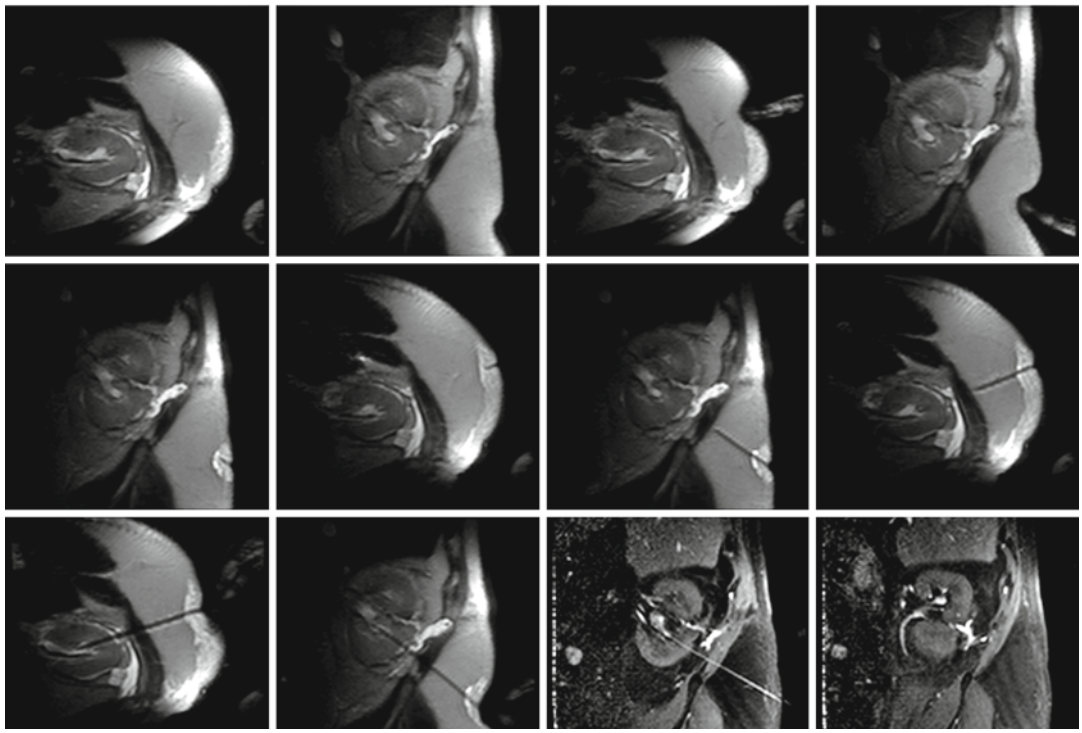

Fig. 11.23 MR-fluoroscopically guided nephrostomy for urinoma after partial renal resection. The first 10 images show the fluoroscopically guided puncture using an ultrafast spin echo sequence (TR/TE 1,000/100). The control MR scan (*image 11 and 12*) was performed after direct injection of diluted contrast material using a T1 FFE sequence (TR/TE 90/7/80°). The control MR images illustrate the successful placement of the 7.6-F drainage catheter (courtesy of Frank Fischbach, University of Magdeburg, G)

macroscopic hematuria occur in 4.9–30.9 %, depending on the number of punctures (Egilmez et al. 2007; Thanos et al. 2006). The formation of clots in the renal pelvis is unproblematic due to the endogenous thrombolytic activity of urokinase.

In most instances, significant bleeding noted at the time of nephrostomy can be controlled by tamponade of the track with a nephrostomy catheter for a small-bore track or with a balloon dilation catheter for large tracks. When this fails or when significant blood loss develops several days after nephrostomy tube placement or removal, angiographic evaluation for identification of a renal arteriovenous fistula, pseudoaneurysm, or vessel laceration is indicated (Dyer et al. 2002). If a persistent bleeding from vascular injury is confirmed, it can be embolized during angiography in most cases. Surgical intervention is rarely necessary (Kessaris et al. 1995).

Sometimes, a disruption of the renal pelvis with extravasation of contrast can be observed. If an adequate drainage of the urinary system can be established, this extravasation will settle on its own. The same goes for extravasation of contrast along the drainage catheter (Fig. 11.24).

An inadvertent puncture of adjacent structures such as colon, liver, spleen, or lung is a typical complication of fluoroscopy or ultrasound guidance and can be avoided by CT guidance. If inadvertent puncture occurs nevertheless, no severe consequences should be expected if a small puncture needle is used.

Especially in patients with an infected urinary system, incrustation of the catheter can obstruct the lumen if the nephrostomy catheter stays in place too long. Therefore, the catheter should be replaced approximately every 6 weeks if a long-term nephrostomy is indispensable.

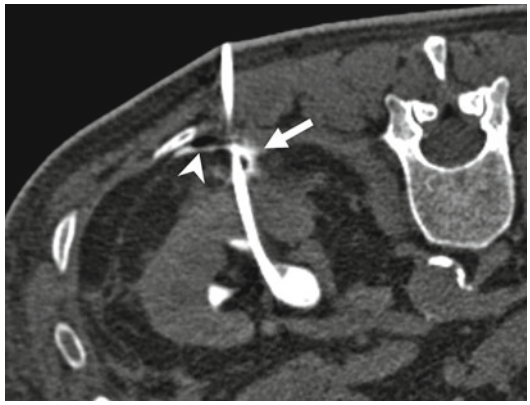

Fig. 11.24 Control CT scan after successful placement of the drainage catheter. Some contrast media (*arrow*) and a little air (*arrowhead*) are visible in the perirenal fatty tissue. This extravasation along the drainage catheter is self-limiting and need no further action as long as adequate drainage is provided

Summary

PCN is a distinguished method for temporary urine drainage. Furthermore, it enables minimally invasive alternatives for therapy of a number of urologic conditions. Also primarily inoperable patients can be converted in an operable condition. CT-guided PCN has the lowest complication rate of all methods and is especially indicated in patients with a non-dilated collecting system or after unsuccessful drainage attempts under fluoroscopy or ultrasound guidance. MR-guided PCN is restricted to special cases such as allergic patients in which CT- or US-guided is contraindicated or not possible.

Key Points

- CT- or MR-guided nephrostomy is a powerful alternative to US-guided nephrostomy and particularly effective in patients with non-dilated calyces or after failure of US-guided procedures.
- An appropriate puncture site has to be selected (preferably a posterolateral calyx of the lower pole) to minimize the risk of hemorrhage.
- A massively dilated collecting system can be punctured in trocar technique, whereas a non-dilated system should be approached in Seldinger technique.
- Proper fixation of the catheter is needed to prevent dislocation with subsequent re-interventions.

References

Drainage in Abscess

Akinci D, Akhan O, Ozmen MN et al (2005) Percutaneous drainage of 300 intraperitoneal abscesses with long-term follow-up. Cardiovasc Intervent Radiol 28:744–750

Arellano RS, Gervais DA, Mueller PR (2011) CT-guided drainage of abdominal abscesses: hydrodissection to create access routes for percutaneous drainage. Am J Roentgenol 196:189–191

Beland MD, Gervais DA, Levis DA et al (2008) Complex abdominal and pelvic abscesses: efficacy of adjunctive tissue-type plasminogen activator for drainage. Radiology 247:567–573

Buecker A, Neuerburg JM, Adam GB et al (2001) MR-guided percutaneous drainage of abdominal fluid collections in combination with X-ray fluoroscopy: initial clinical experience. Eur Radiol 11:670–674

Casola G, vanSonnenberg E, Neff CC et al (1987) Abscesses in Crohn disease: percutaneous drainage. Radiology 163:19–22

Daly B, Krebs TL, Wong-You-Cheong JJ, Wang SS (1999) Percutaneous abdominal and pelvic interventional procedures using CT fluoroscopy guidance. Am J Roentgenol 173:637–644

Ferrucci JT 3rd, Mueller PR (2003) Interventional approach to pancreatic fluid collections. Radiol Clin North Am 41:1217–1226

Gee MS, Kim JY, Gervais DA et al (2010) Management of abdominal and pelvic abscesses that persist despite satisfactory percutaneous drainage catheter placement. Am J Roentgenol 194:815–820

Gervais DA, Ho CH, O'Neill MJ et al (2004) Recurrent abdominal and pelvic abscesses: incidence, results of repeated percutaneous drainage, and underlying causes in 956 drainages. Am J Roentgenol 182: 463–466

Gerzof SG, Johnson WC, Robbins AH, Nabseth DC (1985) Intrahepatic pyogenic abscesses: treatment by percutaneous drainage. Am J Surg 149: 487–494

Gobien RP, Stanley JH, Schabel SI et al (1985) The effect of drainage tube size on adequacy of percutaneous abscess drainage. Cardiovasc Intervent Radiol 8:100–102
Haaga JR, Nakamoto D, Stellato T et al (2000) Intracavitary urokinase for enhancement of percutaneous abscess drainage: phase II trial. Am J Roentgenol 174:1681–1685
Harisinghani MG, Gervais DA, Hahn PF et al (2002) CT-guided transgluteal drainage of deep pelvic abscesses: indications, technique, procedure-related complications, and clinical outcome. Radiographics 22:1353–1367
Harisinghani MG, Gervais DA, Maher MM et al (2003) Transgluteal approach for percutaneous drainage of deep pelvic abscesses: 154 cases. Radiology 228:701–705
Kariniemi J, Sequeiros RB, Ojala R, Tervonen O (2006) Feasibility of MR imaging-guided percutaneous drainage of pancreatic fluid collections. J Vasc Interv Radiol 17:1321–1326
McNicholas MM, Mueller PR, Lee MJ et al (1995) Percutaneous drainage of subphrenic fluid collections that occur after splenectomy: efficacy and safety of transpleural versus extrapleural approach. Am J Roentgenol 165:355–359
Mückley T, Schütz T, Kirschner M et al (2003) Psoas abscess: the spine as a primary source of infection. Spine 28:E106–E113
Mueller PR, Saini S, Wittenburg J et al (1987) Sigmoid diverticular abscesses: percutaneous drainage as an adjunct to surgical resection in 24 cases. Radiology 164:321–325
Mueller PR, vanSonnenberg E, Ferrucci JT Jr (1984) Percutaneous drainage of 250 abdominal abscesses and fluid collections. Part II: current procedural concepts. Radiology 151:343–347
Quinn SF, vanSonnenberg E, Casola G et al (1986) Interventional radiology in the spleen. Radiology 161:289–291
Rivera-Sanfeliz G (2008) Percutaneous abdominal abscess drainage: a historical perspective. Am J Roentgenol 191:642–643
Sahai A, Belair M, Gianfelice D et al (1997) Percutaneous drainage of intra-abdominal abscesses in Crohn's disease: short and long-term outcome. Am J Gastroenterol 92:275–278
Singh B, May K, Coltart I et al (2008) The long-term results of percutaneous drainage of diverticular abscess. Ann R Coll Surg Engl 90:297–301
Thomas J, Turner SR, Nelson RC, Paulson EK (2006) Postprocedure sepsis in imaging-guided percutaneous hepatic abscess drainage: how often does it occur? AJR Am J Roentgenol 186:1419–1422
van Santvoort HC, Besselink MG, Bakker OJ et al (2010) A step-up approach or open necrosectomy for necrotizing pancreatitis. N Engl J Med 362:1491–1502
van Sonnenberg E, Wittich GR, Goodacre BW et al (2001) Percutaneous abscess drainage: update. World J Surg 25:362–369; discussion 70–72
Wroblicka JT, Kuligowska E (1998) One-step needle aspiration and lavage for the treatment of abdominal and pelvic abscesses. Am J Roentgenol 170:1197–1203

Drainage in Pneumothorax

Baumann MH, Noppen M (2004) Pneumothorax. Respirology 9:157–164
Choi SH, Lee SW, Hong YS et al (2007) Can spontaneous pneumothorax patients be treated by ambulatory care management? Eur J Cardiothorac Surg 31:491–495
Conces D Jr, Tarver R, Gray W et al (1988) Treatment of pneumothoraces utilizing small caliber chest tubes. Chest 94:55–57
Cox JE, Chiles C, McManus CM et al (1999) Transthoracic needle aspiration biopsy: variables that affect risk of pneumothorax. Radiology 212:165–168
Heimlich HJ (1968) Valve drainage of the pleural cavity. Dis Chest 53:282–287
Laronga C, Meric F, Truong MT et al (2000) A treatment algorithm for pneumothoraces complicating central venous catheter insertion. Am J Surg 180:523–527
Martin T, Fontana G, Olak J et al (1996) Use of pleural catheter for the management of simple pneumothorax. Chest 110:1169–1172
Niemi T, Hannukainen J, Aarnio P (1999) Use of the Heimlich valve for treating pneumothorax. Ann Chir Gynaecol 88:36–37
Sargent EN, Turner AF (1970) Emergency treatment of pneumothorax: a simple catheter technique for use in the radiology department. Am J Roentgenol 109: 531–535
Yamagami T, Kato T, Iida S et al (2005) Efficacy of manual aspiration immediately after complicated pneumothorax in CT-guided lung biopsy. J Vasc Interv Radiol 16:477–483

Nephostromy

Brodel M (1901) The intrinsic blood-vessels of the kidney and their significance in nephrostomy. Johns Hopkins Hosp Bull 12:10–13
Dyer RB, Regan JD, Kavanagh PV et al (2002) Percutaneous nephrostomy with extensions of the technique: step by step. Radiographics 22:503–525
Egilmez H, Oztoprak I, Atalar M et al (2007) The place of computed tomography as a guidance modality in percutaneous nephrostomy: analysis of a 10-year single-center experience. Acta Radiol 48:806–813
Fischbach F, Porsch M, Krenzien F et al (2011) MR imaging guided percutaneous nephrostomy using a 1.0 Tesla open MR scanner. Cardiovasc Intervent Radiol 34:857–863

Fritz J, Pereira PL (2007) MR-gesteuerte Schmerztherapie: Prinzipien und klinische Applikationen. Rofo 179: 914–924

Goodwin WE, Casey WC, Woolf W (1955) Percutaneous trocar (needle) nephrostomy in hydronephrosis. J Am Med Assoc 157:891–894

Gupta S, Gulati M, Uday Shankar K et al (1997) Percutaneous nephrostomy with real-time sonographic guidance. Acta Radiol 38:454–457

Hohl C, Suess C, Wildberger JE et al (2008) Dose reduction during CT fluoroscopy: phantom study of angular beam modulation. Radiology 246:519–525

Kessaris DN, Bellman GC, Pardalidis NP et al (1995) Management of hemorrhage after percutaneous renal surgery. J Urol 153:604–608

Lang E, Price E (1983) Redefinitions of indications for percutaneous nephrostomy. Radiology 147:419–426

Lewis S, Patel U (2004) Major complications after percutaneous nephrostomy–lessons from a department audit. Clin Radiol 59:171–179

Matlaga BR, Shah OD, Zagoria RJ et al (2003) Computerized tomography guided access for percutaneous nephrostolithotomy. J Urol 170:45–47

Miller NL, Matlaga BR, Lingeman JE (2007) Techniques for fluoroscopic percutaneous renal access. J Urol 178:15–23

Osman M, Wendt-Nordahl G, Heger K et al (2005) Percutaneous nephrolithotomy with ultrasonography-guided renal access: experience from over 300 cases. BJU Int 96:875–878

Silverman SG, Tuncali K, Adams DF et al (1999) CT fluoroscopy-guided abdominal interventions: techniques, results, and radiation exposure. Radiology 212:673–681

Sommer CM, Huber J, Radeleff BA et al (2011) Combined CT- and fluoroscopy-guided nephrostomy in patients with non-obstructive uropathy due to urine leaks in cases of failed ultrasound-guided procedures. Eur J Radiol 80:686–691

Stables DP (1982) Percutaneous nephrostomy: techniques, indications, and results. Urol Clin North Am 9:15–29

Thanos L, Mylona S, Stroumpouli E et al (2006) Percutaneous CT-guided nephrostomy: a safe and quick alternative method in management of obstructive and nonobstructive uropathy. J Endourol 20:486–490

Zagoria RJ, Dyer RB (1999) Do's and don't's of percutaneous nephrostomy. Acad Radiol 6:370–377

Localization Techniques

12

Ulf Redlich

Contents

12.1 Indications

In diagnostic imaging, the detection of mostly singular, isolated tumors is a frequent problem since they often cannot be qualified. In risk populations such as smokers, 65 % of patients present noncalcified lung nodules, with <5 % of lesions <1 cm being malignant. However, the incidence of malignancy increases dramatically above 1-cm lesion diameter (Diederich 2003). Even though lesion calcification helps to identify benign processes, lesion characterization by computed tomography (CT) or thorax radiography is unreliable. In unclear lesions with no previously known underlying malignancy, either follow-up imaging or percutaneous biopsy will usually be performed for further workup. In cases were either a primary lung cancer or limited metastastic disease is suspected, thoracic surgery will be considered. In recent years, thoracic surgery has adopted lesser invasive approaches for confined lesions such as video-assisted thoracoscopic surgery (VATS). A problem often encountered during VATS is localizing the tumor, depending on its position relative to the lung surface. Pulmonary lesions located ≥5 mm from the visceral pleura with a diameter ≤10 mm are hard to find during VATS, and two-thirds of these cases need to be converted to open surgery (Suzuki et al. 1999). In these cases, preoperative marker placement is extremely helpful and significantly improves the surgeon's technical success.

In 1991, wire marking has first been described to mark small targets such as lymph nodes, neurofibromas, or foreign objects at various

U. Redlich
Department of Radiology and Nuclear Medicine,
University Hospital Magdeburg,
Leipzigerstrasse 44, Magdeburg D-39120, Germany
e-mail: ulf.redlich@med.ovgu.de

A.H. Mahnken et al. (eds.), *CT- and MR-Guided Interventions in Radiology*,
DOI 10.1007/978-3-642-33581-5_12, © Springer-Verlag Berlin Heidelberg 2013

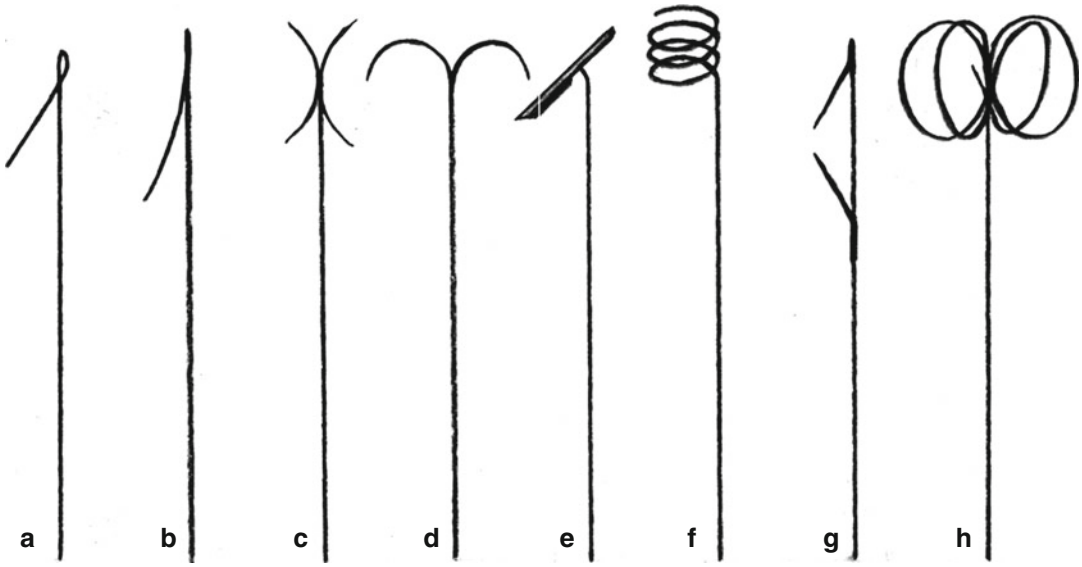

Fig 12.1 Various designs of marker wires: (**a**) Kopans hook [Mamma, Pulmo], (**b**) Hawkins II hook [Mamma], (**c**) X-hook [Mamma], (**d**) double hook [Mamma], (**e**) tumor loc [Mamma, Pulmo], (**f**) Miller Corkscrew [Pulmo], (**g**) double hook [Mamma], (**h**) Mullan Cloverleaf [Pulmo]

locations of the body (Finch 1991). Preoperative localization of musculoskeletal lesions, prolapsed discs, or even appendicoliths as an inflammatory focus in difficult-to-access peritoneal recesses has also been described (Morrison et al. 2001; Endres et al. 2005; Lossef 2005). To assist implantation of a transjugular intrahepatic portosystemic shunt (TIPSS), wire marking of the portal vein has also been published (Fontaine et al. 1997).

Preoperative localizations are most often done in lung and breast tumors. Mammography-, magnetic resonance (MR)-, and CT-guided localization of breast lesions is performed routinely today. MR-assisted wire marking is a much more involved procedure but helpful specifically in the breast or, not frequently adopted, in the liver if a lesion is hard to identify with standard imaging procedures. In MR mammography, 10–39 % of tumors detected are visible with MR only, making MR marking or guidance inevitable (Schneider et al. 2002; LaTrenta et al. 2003; Heywang-Köbrunner et al. 2000).

12.2 Material

Localization material such as a wire marker is inserted via a cannulated puncture needle. The needle should be as thin as possible but still well-detectable by the imaging technique being used without applying to many artifacts to the image. For lung puncture, nothing larger than an 18-gauge needle should be used. The risk of pneumothorax or other less common adverse events in lung puncture most likely is related to the diameter of the puncture needle. The choice of materials for fluoroscopic or CT-assisted marking is simple; however, for MR-compatible materials, the range is wide, and the optimal choice depends on several variables.

The marker material, from a variety of compositions, should ideally make the target region visible or palpable. However, some markers available are detectable only under fluoroscopy. Currently in use are wire systems (x, spiral, and hook), platinum coils, tantalum beads, methylene blue, lipiodol, barium suspension, or agar. *Wire markers* (Fig. 12.1) are composed of variable materials (stainless steel, nitinol, etc.). The designs of the wires varies greatly (i.e., classic Kopans hookwire or the Miller corkscrew wire) and should be chosen according to the type of tissue to be marked. Dislocation in diligent tissue such as pulmonary parenchyma can, for example, best be avoided by using a four-leaf clover design (Mullan et al. 1999).

Metal spirals or platinum coils, usually used for interventional occlusion of blood vessels, can

also be used as marker material. The advantage is that after the marker has been placed, no parts are left outside the body, therefore minimizing the risk of a pneumothorax or marker dislocation (Powell et al. 2004). However, just following a marker wire disappearing in a human body may ease the surgeon's job significantly.

Tantalum beads and contrast medium are visible under fluoroscopy only. During surgical removal of the target area, it is thus necessary to use a C-arm for orientation. Liquid markers are injected via the cannulated puncture needle. A limitation is the diffusion of the material into the adjacent tissue and lymph drainage, making early surgery following marker placement necessary. An exception is barium which usually remains stable in tissue. Fluoroscopy-assisted resection can be performed up to 1 week after injection (Kobayashi et al. 1997).

Agar is used only in pulmonary lesions. It provides a palpable area within the parenchyma but requires an open surgical resection (Tsuchida et al. 1999).

12.3 Technique

The technique of localization of the target volume, for example, for potential tumors, follows a uniform process, regardless of which imaging modality is used:

- Lesion documentation (ultrasound, CT, MR imaging)
- Planning of the lowest-risk access
- Sedation
- Sterile covering, local anesthesia
- Localization intervention (e.g., by CT/MR-fluoroscopy)
- Documentation of the proper marker location
- Ruling out complications (e.g., bleeding, pneumothorax)
- Prevention of dislocation of the marker (if necessary)
- Transportation of the patient to the operating room and resection

For wire marking, the access point should be planned – if possible – together with the surgeon. It is best to place the wire marker using the same access and course as the surgeon will use, then the preparation along the wire into the depth and finding the region to be removed is simple. The wire should ideally be placed through the tumor, but a deviation of up to10 mm is generally considered tolerable.

If the peritoneal or pleural cavity has been crossed, the point of entry will be recognizable on the visceral side and will guide to the target location even in case the wire marker has dislocated. A wire dislocation must be preserved by diligent fixation of the extracorporeal wire-part to the patient skin, for example, by using sterile tape. In pulmonary nodules, it is recommendable to cut the wire at skin level (Fig 12.2). Metal spirals or platinum coils should be placed with one end at the tumor and the other end at the surface of the organ – the according length has to be determined preinterventionally. To mark a pulmonary tumor before VATS, for example, an 80-mm coil via a 22-gauge needle can be used. Because of a possible marker dislocation, the injection of liquid marker material is of advantage when the targeted tissue is loosely structured, for example, fatty tissue or preformed cavities. In order to keep the diffusion of the marker liquid to a minimum, surgery should be performed early afterwards.

12.4 Results

The data available on CT- and MR-guided localization procedures is scarce and nonuniform. Localization of lung lesions with wire markers has technical success rates of up to 100 % (Hänninen et al. 2004; Kastl et al. 2006), most likely depending on the degree of experience of the interventionalist. Hence, such procedures, for example, in the lung usually have a good acceptance rate once established, and they offer safe navigation at a short procedural time and very few complications. 100 % success rate has also been reported for needle localization of breast lesions (Kuhl 2002; Fischer et al. 1998).

The duration of the procedure depends on experience and the imaging modality which has been chosen. On average, wire marking of a pulmonary

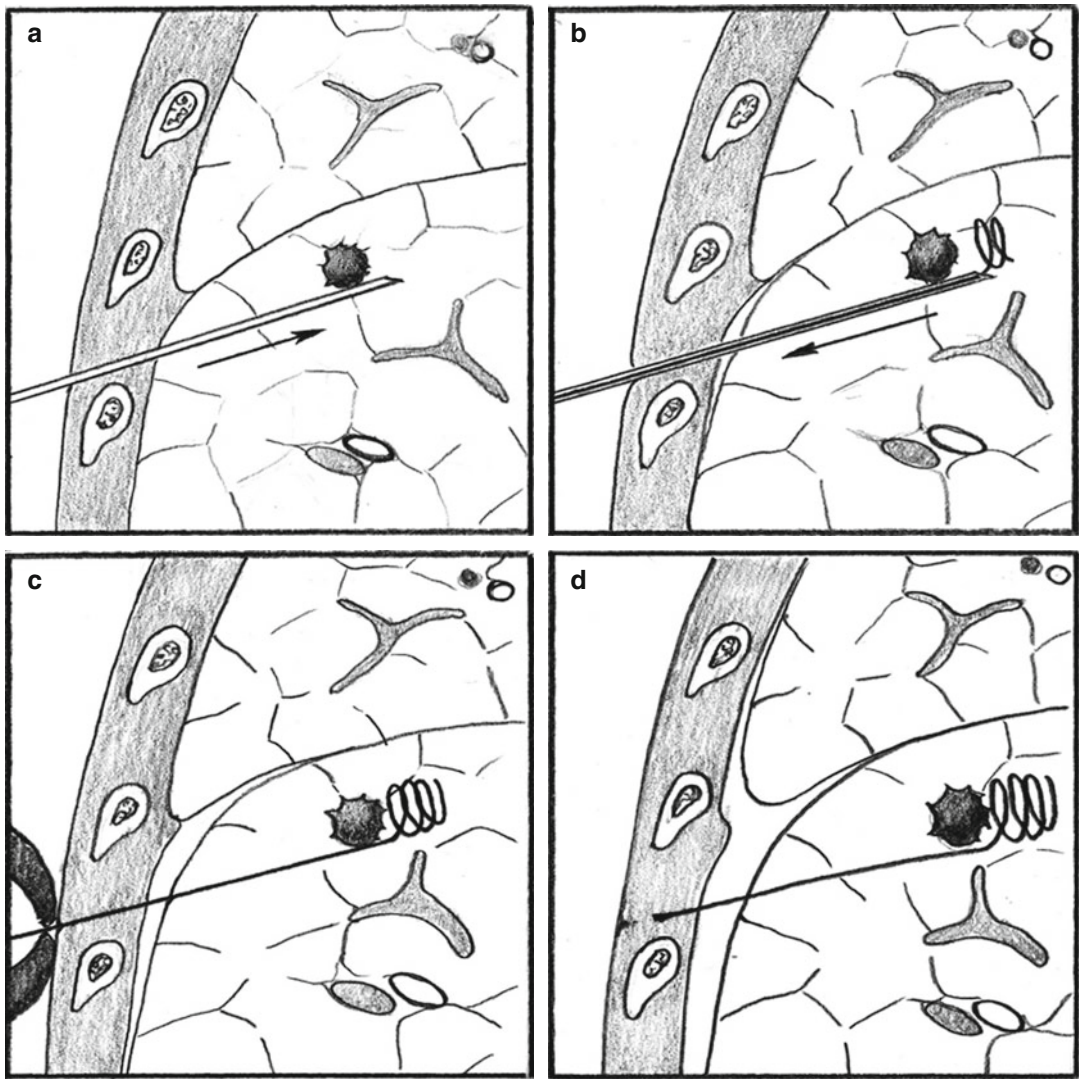

Fig 12.2 Deposition of a marker wire near a pulmonary lesion. First a hollow needle is placed through or close by the target lesion (**a**). Shortly distal of the target the wire marker is pushed out of the needle while slowly retracting the needle (**b**). After correct marker placement the wire may be cut at the skin level or fixed with sterile tape (**c**). The final control confirms the position of the marker in the vicinity of the target lesion (**d**)

nodule will add up to a time range from 7.5 to 25 min (Hänninen et al. 2004; Kastl et al. 2006).

12.5 Complications

Wire dislocation mostly occurs when dealing with relatively soft tissue such as lung or breast. Between 2 and 5 % of wire-marked breast tumors could not be removed because the wire had been displaced during surgery (Heywang-Köbrunner 2000). In case of dislocation of lung wire markers, pneumothorax is a frequent event (10–35 %) (Shah et al. 1993; Poretti et al. 2002). However, since thoracoscopic or open surgery is usually done early after, usually no clinical consequences are faced. Serious complications are extremely rare and may include symptomatic bleeding or infections. A very rare complication in thoracic puncture is air embolism, which may potentially even require resuscitation of the patient (Horan et al. 2002).

Summary

Marking a surgical target previous to the operation usually is a simple procedure with a very low complication rate. It may provide faster and safer performance during subsequent minimally invasive or open surgery specifically in lung and breast lesions. In most regions of the human body, localization of tumors can be done quickly and with very little strain for the patient, and should therefore be considered more often.

Key Points

- Localization techniques can be applied to virtually all regions of the body.
- Wire markers offer perfect guidance for the surgeon and can be placed with minimal risk and discomfort for the patient.
- Specifically in lung and breast lesions, surgical results may improve significantly with a reduction in procedural time.

References

Diederich S (2003) Screening for early lung cancer with low-dose spiral computed tomography. Lancet 362: 588–589

Endres S, Riegel T, Wilke A (2005) Präoperative Markierung thorakaler Bandscheibenvorfälle. Orthopade 34:791–793 [German]

Finch IJ (1991) Preoperative CT-guided percutaneous localization of small masses with a Kopans needle. AJR Am J Roentgenol 157:179–180

Fischer U, Kopka L, Grabbe E (1998) Magnetic resonance guided localization and biopsy of suspicious breast lesions. Top Magn Reson Imaging 9:44–59

Fontaine AB, Verschyl A, Hoffer E et al (1997) Use of CT-guided marking of the portal vein in creation of 150 transjugular intrahepatic portosystemic shunts. J Vasc Interv Radiol 8:1073–1077

Hänninen EL, Langrehr J, Raakow R et al (2004) Computed tomography-guided pulmonary nodule localization before thoracoscopic resection. Acta Radiol 45:284–288

Heywang-Köbrunner SH, Heinig A, Pickuth D et al (2000) Interventional MRI of the breast: lesion localization and biopsy. Eur Radiol 10:36–45

Horan TA, Pinheiro PM, Araujo LM et al (2002) Massive gas embolism during pulmonary nodule hook wire localization. Ann Thorac Surg 73:1647–1649

Kastl S, Langwieler TE, Krupski-Berdien G et al (2006) Percutaneous localization of pulmonary nodules prior to thoracoscopic surgery by CT-guided hook-wire. Anticancer Res 26:3123–3126

Kobayashi T, Kaneko M, Kondo H et al (1997) CT-guided bronchoscopic barium marking for resection of a fluoroscopically invisible peripheral pulmonary lesion. Jpn J Clin Oncol 27:204–205

Kuhl CK (2002) Interventional breast MRI: needle localisation and core biopsies. J Exp Clin Cancer Res 21(3 Suppl):65–68

LaTrenta LR, Menell JH, Morris EA et al (2003) Breast lesions detected with MR imaging: utility and histopathologic importance of identification with US. Radiology 227:856–861

Lossef SV (2005) CT-guided Kopans hookwire placement for preoperative localization of an appendicolith. AJR Am J Roentgenol 185:81–83

Morrison WB, Sanders TG, Parsons TW et al (2001) Preoperative CT-guided hookwire needle localization of musculoskeletal lesions. AJR Am J Roentgenol 176:1531–1533

Mullan BF, Stanford W, Barnhart W et al (1999) Lung nodules: improved wire for CT-guided localization. Radiology 211:561–565

Poretti FP, Brunner E, Vorwerk D (2002) Einfache Lokalisation von intrapulmonalen Rundherden - CT-gesteuerte perkutane Hakenmarkierung. Rofo 174:202–207 [German]

Powell TI, Jangra D, Clifton JC et al (2004) Peripheral lung nodules: fluoroscopically guided video-assisted thoracoscopic resection after computed tomography-guided localization using platinum microcoils. Ann Surg 240:481–489

Schneider JP, Schulz T, Rüger S et al (2002) MRT-gestützte Markierung und Stanzbiopsie suspekter Mammaläsionen Möglichkeiten und Erfahrungen an einem vertikal offenen 0,5-T-System. Radiologe 42:33–41 [German]

Shah RM, Spirn PW, Salazar AM et al (1993) Localization of peripheral pulmonary nodules for thoracoscopic excision: value of CT-guided wire placement. AJR Am J Roentgenol 161:279–283

Suzuki K, Nagai K, Yoshida J et al (1999) Video-assisted thoracoscopic surgery for small indeterminate pulmonary nodules: indications for preoperative marking. Chest 115:563–568

Tsuchida M, Yamato Y, Aoki T et al (1999) CT-guided agar marking for localization of nonpalpable peripheral pulmonary lesions. Chest 116:139–143

Part III

Therapeutic Interventions

Interventional Oncology

13

Stephan Clasen, Philippe L. Pereira, Andreas Lubienski, Arnd-Oliver Schäfer, Andreas H. Mahnken, Thomas Helmberger, Martin G. Mack, Katrin Eichler, Thomas J. Vogl, Christian Rosenberg, Suzanne C. Schiffman, Robert C.G. Martin, Thierry de Baère, Philipp Bruners, Markus Düx, Konrad Mohnike, Jens Ricke, Philip Ditter, Kai E. Wilhelm, Holger Strunk, Alexander Beck, Susanne Hengst, Joseph P. Erinjeri, and Thomas Gast

Contents

S. Clasen (✉)
Department of Diagnostic and Interventional Radiology, Eberhard-Karls-University Tübingen, Hoppe-Seyler-Straße 3, D-72076 Tübingen, Germany
e-mail: stephan-clasen@gmx.de

J. Ricke
Department of Radiology and Nuclear Medicine, University Hospital Magdeburg, Magdeburg, Germany
e-mail: jens.ricke@med.ovgu.de

P.L. Pereira
Department of Radiology and Nuclear Medicine, Klinikum am Gesundbrunnen, Am Gesundbrunnen 20-26, D-74078 Heilbronn, Germany
e-mail: philippe.pereira@slk-kliniken.de

A. Lubienski
Radiology Health Care Centre Minden, Ringstraße 44, D-32427 Minden, Germany
e-mail: lubienski@rp-minden.de

A.-O. Schäfer
Department of Diagnostic Radiology, University Hospital Freiburg, Hugstetter Straße 55, D-79106 Freiburg, Germany
e-mail: arnd-oliver.schaefer@uniklinik-freiburg.de

A.H. Mahnken
Department of Diagnostic and Interventional Radiology, University Hospital, Marburg, Germany

Philipps University of Marburg, Marburg, Germany
e-mail: mahnken@med.uni-marburg.de

T. Helmberger
Department of Diagnostic and Interventional Radiology and Nuclearmedicine, Klinikum Bogenhausen, Englschalkinger Str. 77, D-81925 Munich, Germany
e-mail: thomas.helmberger@kh-bogenhausen.de

M.G. Mack • K. Eichler • T.J. Vogl
Department of Diagnostic and Interventional Radiology, University of Frankfurt/Main, Theodor-Stern-Kai 7, D-60590 Frankfurt am Main, Germany
e-mail: martinmack@arcor.de

C. Rosenberg
Department of Diagnostic Radiology and Neuroradiology, Ernst Moritz Arndt University, Ferdinand-Sauerbruch-Straße, 17475 Greifswald, Germany
e-mail: christian.rosenberg@uni-greifswald.de

A.H. Mahnken et al. (eds.), *CT- and MR-Guided Interventions in Radiology*,
DOI 10.1007/978-3-642-33581-5_13, © Springer-Verlag Berlin Heidelberg 2013

S.C. Schiffman • R.C.G. Martin
Division of Surgical Oncology,
University of Louisville School of Medicine,
315 East Broadway-Rm 311,
40292 Louisville, KY, USA
e-mail: robert.martin@louisville.edu

T. de Baère
Department of Interventional Radiology,
Institut Gustave Roussy, 39 rue Camille Desmoulins,
94805 Villejuif, France

P. Bruners
Department of Diagnostic and
Interventional Radiology, University Hospital,
RWTH Aachen University, Pauwelsstrasse 30,
D-52074 Aachen, Germany
e-mail: pbruners@ukaachen.de

M. Düx
Department of Radiology and Neuroradiology,
Krankenhaus Nordwest, Steinbacher Hohl 2-26,
D-60488 Frankfurt am Main, Germany
e-mail: duex.markus@khnw.de

K. Mohnike
Klinik für Radiologie und Nuklearmedizin,
Universitätsklinikum Magdeburg,
Leipzigerstrasse 44,
D-39120 Magdeburg, Germany
e-mail: konrad.mohnike@med.ovgu.de

P. Ditter
Department of Radiology, University Hospital Bonn,
Sigmund-Freud-Stra9e 25, D-53127 Bonn, Germany
e-mail: philip.ditter@ukb.uni-bonn.de

K.E. Wilhelm
Department of Radiology, University Hospital Bonn,
Sigmund-Freud-Str. 25, D-53127 Bonn, Germany
e-mail: kai.wilhelm@ukb.uni-bonn.de

H. Strunk
Department of Radiology, University Hospital Bonn,
Sigmund-Freud-Stra9e 25, D-53127 Bonn, Germany
e-mail: holger.strunk@ukb.uni-bonn.de

A. Beck • S. Hengst
Klinik für Strahlenheilkunde, Charité Campus-Virchow-Klinikum, Augustenburger Platz 1, D-13353 Berlin, Germany
e-mail: alexander.beck@charite.de;
susanne.hengst@charite.de

J.P. Erinjeri
Department of Radiology, Interventional Radiology Service, Memorial Sloan-Kettering Cancer Center,
1275 York Avenue – H118, 10065 New York, NY, USA
e-mail: erinjerj@mskcc.org

T. Gast
Interventional Radiology Service,
Memorial Sloan-Kettering Cancer Center,
New York, NY, USA

13.1 Radiofrequency Ablation

13.1.1 Technical Basics

Stephan Clasen and Philippe L. Pereira

13.1.1.1 Introduction

Percutaneous thermal ablation therapy represents a local tumor treatment. Hyperthermal ablation procedures eradicate tumor tissue with heat in a circumscribed area. Applied techniques are radiofrequency (RF) ablation, laser interstitial thermotherapy, microwave ablation, and high-intensity focused ultrasound. Image guidance enables a minimally invasive application of thermal ablation therapy. Among these techniques, percutaneous RF ablation has attained widespread consideration. Image-guided local ablation therapy has gained importance predominantly in the therapy of primary and metastatic liver tumors (Solbiati et al. 2001; Livraghi et al. 2000). Beside the hepatic application, RF ablation is an established treatment for osteoid osteoma (Rosenthal et al. 2003). Furthermore, potential indications for image-guided RF ablation include primary and secondary pulmonary malignancies (Dupuy et al. 2000), renal cell carcinoma (Gervais et al. 2003), and treatment of symptomatic osseous and soft tissue tumors (Goetz et al. 2004).

The application of heat for coagulation of vital tissue was mentioned in about 3000 B.C. in the Edwin Smith papyrus (Siperstein and Gitomirski 2000). In the Egyptian and Greek literature, it is reported that the probes were heated by a flame. In the nineteenth-century direct current became available and was used for cauterization to surgically control bleeding, thereby the current induced a resistive heating within the tip of the surgical probes. The discovery of direct heating within living tissue by using an RF current was made by d'Arsonval in 1891. He described that an alternating current at high frequency (10 kHz) does not cause pain or muscular contractions, but causes elevation in temperature while passing through the living tissue (d'Arsonval 1891). This transformation of electric energy into thermal energy within living tissue represents the basis for RF ablation. In 1900, Riviere demonstrated that by increasing

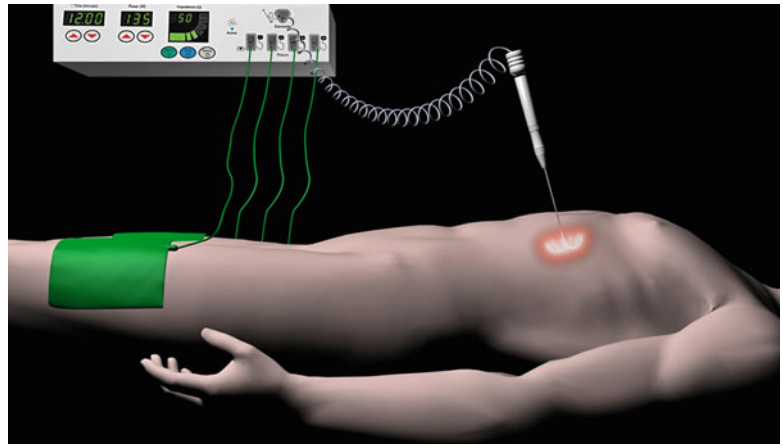

Fig. 13.1 The electric circuit of a monopolar RF system comprises the RF generator, the cables, a needlelike "active" electrode placed within the target tissue, the dispersive electrodes ("grounding pads") placed on the body surface, and the patient's body

the density of the electric current with a small electrode, higher tissue temperatures with destructive effects are obtained (Siperstein and Gitomirski 2000). At the beginning of the nineteenth century, electrocauterization was characterized by a limited extent of thermally induced coagulation. In 1926, Cushing introduced RF energy to neurosurgery for ablation of intracranial tumors (Siperstein and Gitomirski 2000). In 1990, two independent groups of researchers introduced hepatic RF ablation (Rossi et al. 1990; McGahan et al. 1990). The clinical application of percutaneous RF ablation for the treatment of hepatic tumors was subsequently described by these two groups at the beginning of the 1990s. Since that time, ongoing technical development of RF ablation has focused on the improvement of RF systems to induce predictable and larger zones of coagulation.

13.1.1.2 Principle of RF Ablation

RF ablation is a local tumor treatment by inducing thermal injury within the target tissue. The principle of RF ablation is a transformation of electromagnetic energy into thermal energy. For that reason an alternating electric current that oscillates at a high frequency (200–1,200 kHz) is applied (Rhim et al. 2001). Commercially available RF systems operate at a frequency in the range of 375–480 kHz (Pereira et al. 2004; Clasen et al. 2006). High-frequency electric current causes the tissue ions to become agitated owing to the ions attempting to follow the changes in the direction of the alternating electric current (Rhim et al. 2001). The ion agitation causes frictional heat within the tissue. For local tumor ablation, a focal induction of heat is essential to avoid thermal injury to critical anatomic structures in the surroundings of the target tissue. In monopolar RF systems, one electrical pole is placed inside the target tissue, and the second electrical pole is placed on the body surface; in bipolar RF systems, both electrical poles are placed inside the target tissue. The most widely used RF devices are monopolar systems, and the electric circuit comprises the RF generator, the cables, a needlelike "active" electrode placed within the target tissue, the dispersive electrodes ("grounding pads") placed on the body surface, and the patient's body (Rhim et al. 2001; Fig. 13.1). The tissue between the "active" electrode and the grounding pads acts as a resistor. Given the relatively high electrical resistance of tissue in comparison with that of the metal electrodes, there is a marked agitation of tissue ions (Rhim et al. 2001). Consequently, the tissue represents the source of heating and not a heated applicator placed in the target tissue. Due to the marked discrepancy between the surface area of the small needle electrode within the target tissue and the large dispersive electrode on the body surface, the density of the electric field is focused on the immediate surroundings of the needle electrode; therefore, the heating is concentrated on the target tissue adjacent to the needle electrode. The use of multiple large grounding pads ensures an optimal dispersion of the electric current within the patient's body and minimizes the risk of unintended heating at a distance from the needle electrode. In addition, the grounding pads should be equidistant from the target tissue and should be oriented with the longest surface edge facing the needle electrode to avoid skin burns at the site of the grounding pads

(Goldberg et al. 2000c). Modifications of the RF technique will be discussed in conjunction with the different RF systems.

13.1.1.3 Thermal Bioeffects

Interaction of Heat and Cell Function

Thermal effects depend on both the tissue temperature and the duration of heating. Cell homeostasis can be maintained if the normal body temperature is slightly increased in the region of up to 40 °C. An increased temperature in the range 42–45 °C results in the cells being more susceptible to damage (Seegenschmiedt et al. 1990). Exposure to 45 °C for several hours causes irreversible cellular damage (Rhim et al. 2001). A further increase in temperature to 50–55 °C reduces the duration necessary to irreversibly damage cells to 4–6 min (Rhim et al. 2001). With temperatures between 60 and 100 °C, nearly immediate thermal damage occurs, being characterized by irreversible protein denaturation, damage to cytosolic and mitochondrial enzymes, as well as destruction of the important protein structure of the DNA (Zervas and Kuwayama 1972; Goldberg et al. 2000a). Histopathologically, these high temperatures result in a coagulation necrosis. When the temperature is increased to more than 100–110 °C, the tissue vaporizes and carbonizes. Vaporization and carbonization result in a marked increase of tissue resistance and subsequently in a reduced effectiveness of the RF energy applied; therefore, an increase in temperature to more than 100 °C should be avoided during RF ablation. Consequently, achievement and maintenance of a temperature in the range 60–100 °C within the entire target volume is considered optimal for RF ablation (Fig. 13.2).

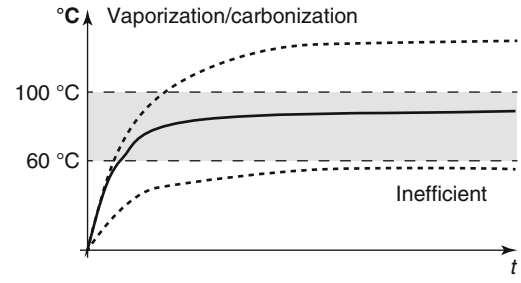

Fig. 13.2 Graphical display of the target temperature in RF ablation. Ablation is effective between 60 and 100 °C. Below 60 °C, there is no instant tissue coagulation and therefore a high risk of remaining vital tumor, while above 100 °C, tissue vaporization and carbonization limit heat delivery

Interaction of RF Ablation and Tissue Characteristics

The physical parameters of tumor tissue and the surrounding tissue have a significant impact on the application of RF energy. Thermal and electrical conductivity influences the alternating electric current and the distribution of heat. The focus of generated heat by the alternating electric field is in the immediate surroundings of the non-insulated tip of the RF electrode. Since high thermal gradients occur during RF ablation, thermal conduction contributes significantly toward tissue heating in the periphery of the ablation zone (Schramm et al. 2006). High thermal conductivity may contribute to heat loss at the periphery of the ablation zone. On the other hand, increased thermal conductivity allows heat to diffuse more quickly and deeper into the tissue; consequently, increased thermal conductivity enables an increased input of energy and greater volumes of coagulation (Liu et al. 2005). Tissues with low thermal conductivity in the surrounding of the tumor tissue increase heating within the central tumor, particularly in long-lasting application of RF energy and in smaller tumors (Liu et al. 2006). For example, heating of hepatocellular carcinoma within a cirrhotic liver, having a low thermal conductivity, may be augmented (Liu et al. 2006). Electrical conductivity of the tumor and background tissue influences the electric field. Modulation of electrical conductivity in the surrounding of the RF electrode by injection of a conductive fluid such as saline is feasible. The effect of this modulation depends on the generator capabilities, the type of fluid, as well as the volume and concentration of the injected fluid (Lobo et al. 2004; Bruners et al. 2007). Application of small amounts of saline or other fluids with high concentration of ions increases the efficiency of energy application by increasing the electrical conductivity in the surrounding of the RF electrode (Lobo et al. 2004). In contrast, there is an inverse relationship for the coagulation volume and the overall impedance of the electric circuit. High impedance, corresponding to a low electrical conductivity, correlates to larger volumes of coagulation (Ahmed et al. 2004); therefore, a low electrical conductivity of the tissue surrounding

the tumor may increase the effectiveness of RF ablation. For example, RF ablation in lung tissue is characterized by a low electrical conductivity of the normal lung parenchyma, leading to pronounced resistive heating at the interface of tumor tissue, having a high electrical conductivity, and the lung tissue, having a low electrical conductivity (Ahmed et al. 2004). Therefore, beside the focus of heating adjacent to the RF electrode, there is a second focus of heating at the tumor periphery, leading to larger volumes of coagulation. On the other hand, a low electrical conductivity at the tumor boundaries can restrict current flow into peripheral tissue; consequently, induction of a safety margin might be hindered (Ahmed et al. 2004).

Interaction of RF Ablation and Blood Flow

Convection by means of blood flow leads to removal of heat; therefore, vascularization of tumor tissue and the surrounding tissue does significantly determine the efficiency of the energy applied. Macroscopic vessels with a diameter of more than 1 mm lead to the so-called heat-sink effect (Goldberg et al. 2005). In effect, the shape of coagulation is altered away from the blood vessel, and the overall volume of coagulation is reduced (Goldberg et al. 2005). This cooling effect of blood flow may protect macroscopic vessels from thermal injury and reduces the risk of bleeding and thrombosis. On the other hand, the probability of an incomplete ablation is increased owing to the possibility of persistent vital tumor cells adjacent to the vessels. The term "perfusion-mediated tissue cooling" encompasses the effects of larger heat-sink vessels and the effects of capillary microperfusion (Goldberg et al. 1998a). Computer modeling has demonstrated that increased perfusion exponentially decreases the ablation zone and the time to achieve thermal equilibrium (Liu et al. 2007). For smaller tumors (2–3 cm), the tumor ablation is supposed to be mainly determined by the perfusion of the outer tissue. For larger tumors (4–5 cm), the inner tumor perfusion is supposed to be predominant (Liu et al. 2007). Owing to the significant impact of blood flow on the effectiveness of RF ablation, several strategies have been developed to overcome this limitation. These techniques include a pharmacologically decrease of the blood flow, a temporary vascular balloon occlusion of specific vessels (e.g., in hepatic RF ablation—hepatic artery, hepatic vein, portal vein), an intra-arterial embolization or chemoembolization, and a Pringle maneuver in the case of intraoperative hepatic RF ablation (Goldberg et al. 2005). General anesthesia also increases the effectiveness of thermal ablation as it reduces the visceral blood flow.

13.1.1.4 RF Systems

The initial RF systems were developed for neurosurgical and cardiac applications, such as the treatment of hyperactive neurological foci or aberrant cardiac conductive pathways (Gazelle et al. 2000); therefore, precise and small zones of coagulation were required. The use of conventional monopolar RF electrodes enabled a maximum diameter of induced coagulation no greater than 1.6 cm (Rhim et al. 2001). For the treatment of malignant tumors, larger zones of coagulation are required to enable complete coagulation of tumor tissue, including a safety margin. The numerous parameters influencing the volume of thermally induced coagulation necrosis were previously explained by Pennes (1948) using a complicated formula (Goldberg et al. 2000b; Liu et al. 2005):

$$\rho_t c_t \partial T(r,t)/\partial t = \nabla(k_t \nabla T) - c_b \rho_b m \rho_t (T - T_b) + Q_p(r,t) + Q_m(r,t),$$

where ρ_t and ρ_b are the density of tissue and of blood (kg/m^3), c_t and c_b are the specific heat of tissue and of blood (W s/kg °C), k_t is the thermal conductivity of tissue, T = temperature, r corresponds to the applicator distance, t = time, m is the perfusion (blood flow rate per unit mass of tissue) (m^3/kg), Q_p is the power absorbed per unit volume of tissue, and Q_m is the metabolic heating per unit volume of tissue (Goldberg et al. 2000b). In addition, one also has the electrostatic equation: $Q_p = j^2/\sigma$, where j is the current density and σ is the electrical conductivity (Liu et al. 2005).

This so-called bio-heat equation can be simplified by the formula extent of coagulation = applied energy × local tissue interactions – heat loss (Goldberg et al. 2000b). In accordance with the bio-heat equation, a strategy to extend the volume of coagulation is to increase the amount of energy applied. Therefore, investigators and

Table 13.1 Technical data and characteristics of the most widely used radiofrequency (RF) systems

RF system	CC (Covidien)	HiTT 106 (Integra)	Model 1500X (AngioDynamics)	RF 3000 (Boston Scientific)	CelonLab Power (Olympus)
Principle	Monopolar	Monopolar	Monopolar	Monopolar	Bi- and multipolar
Maximum power output	200 W	60 W	250 W	200 W	250 W
Frequency	480 kHz	375 kHz	460 kHz	480 kHz	470 kHz
Applicator type	Internally cooled	Perfusion	Multi-tined expandable	Multi-tined expandable	Internally cooled
Applicator tip configuration	Straight	Straight	Christmas tree	Umbrella	Straight
Applicator shaft diameter	1.6 mm (single); 3 × 1.6 mm (cluster)	1.7 mm	2.2 mm	2.5 mm	1.8 mm (1–6 applicators)
Monitoring of ablation	Tissue impedance	Tissue impedance	Tissue impedance and temperature	Tissue impedance	Tissue impedance

manufacturers have made several technical developments to improve the RF systems to optimize the energy application. These strategies include:

- Internally cooled electrodes (Goldberg et al. 1998b)
- Perfusion ("wet") electrodes (Schmidt et al. 2003)
- Multi-probe arrays such as clusters (Goldberg et al. 1995)
- Multi-tined expandable electrodes (de Baere et al. 2001)
- Bipolar and multipolar electrodes (Clasen et al. 2006)
- Modification of the algorithm of energy deposition (Goldberg et al. 1999)

In addition, the local tissue interaction may be modified by increasing the electrical conductivity within the target tissue, by improving the heat conduction into the tissue, or by increasing the vulnerability of the tumor tissue for thermal injury (Rhim et al. 2001). Moreover, the heat loss may be minimized by adjunct techniques to reduce perfusion-mediated tissue cooling (Rossi et al. 2000). The characteristics of different commercially available RF systems are summarized in Table 13.1.

Monopolar RF Systems

Monopolar RF systems apply the energy between an active electrode placed in the target tissue and one or more large dispersive electrodes (grounding pads) placed on the body surface. The alternating electric current is generated by an RF generator. The monopolar RF generators use a power output of 60 W (HiTT 106®, Integra, Plainsboro, NJ), 200 W (RF 3000®, Boston Scientific, Mountain View, CA, and CC®, Valleylab, Boulder, CO), or 250 W (1500X®, RITA Medical Systems, Mountain View, CA). The function of these RF generators is to generate a predefined alternating current and to control the amount of electric current applied to the tissue. The control of energy deposition is based on the tissue impedance (Integra, Boston Scientific, Valleylab), whereas the RITA systems additionally use the temperature at the electrode tip. The electrode design differs among the manufactures and has an important impact on the size and shape of the coagulation (Pereira et al. 2004).

Multi-tined Expandable Electrodes

The amount of energy applied can be increased by increasing the surface area of the non-insulated tip of the RF electrode placed within the target tissue (Goldberg et al. 1995; de Baere et al. 2001). Two manufacturers have designed multi-tined expandable electrodes. An array of multiple thin electrodes expands from a larger needle cannula. The array may have the configuration of an umbrella (Boston Scientific) or a Christmas tree (RITA Medical Systems). Usually the larger needle cannula is placed centrally within the target tissue and, thereafter, the smaller electrodes are expanded. Variable deployment lengths and diameters of the array are available. For larger arrays a stepwise deployment may be necessary.

Internally Cooled Electrodes

Internal cooling of the RF electrode is a strategy to increase energy application. Internal lumina enable a perfusion of the electrode shaft with saline or water. Only recently a gas-cooled electrode was introduced. The fluid or gas does not

get in contact with the tissue surrounding the RF electrode. By cooling the electrode tip during the application of RF energy, one can increase the generator output and prevent vaporization and carbonization adjacent to the RF electrode. Subsequently, internal cooling prevents or delays a deleterious increase in circuit impedance (Gazelle et al. 2000). To ensure complete coagulation adjacent to the RF electrode, the internal cooling has to be switched off at the end of energy application. Application of an additional energy pulsing further increases the mean intensity of energy deposition (Goldberg et al. 2000b). When pulsing is used, periods of higher power output are rapidly alternated with periods of low power output (Goldberg et al. 1999). The periods of low power output enable preferential tissue cooling adjacent to the RF electrode without significantly decreasing heating deeper in the tissue (Goldberg et al. 2000b). The combination of pulsed energy application and internal cooling leads to a synergistic increase of induced coagulation (Goldberg et al. 2000b). Internally cooled electrodes are available as a straight single electrode and as the so-called cluster electrode with three straight electrodes combined in one applicator (Covidien). The intention of these cluster electrodes is to increase the surface area of the RF electrode and, subsequently, to increase the energy deposition within the target tissue (Goldberg et al. 1995).

Perfusion Electrodes

This principle of perfusion electrodes is based on continuous infusion of fluid into the target tissue. The fluid is infused into the tissue through two to four micropores at the tip of the RF electrode (Integra, RITA). Usually normal or hypertonic saline is used to increase the electrical conductivity of the target tissue by application of ions. Other fluids, such as contrast ionic agents or ethanol, may be used alternatively (Bruners et al. 2007). Subsequently, the tissue resistance is reduced, and the amount of energy applied can be increased. Perfusion electrodes enable the induction of large zones of coagulation (de Baere et al. 2001; Pereira et al. 2004). Disadvantages of a saline infusion may be an unpredictable distribution of fluid in the tissue (Gillams and Lees 2005) and the possibility of irregularly shaped zones of coagulation (Pereira et al. 2004).

Multi-probe Arrays

The combination of multiple monopolar RF electrodes can increase the volume of coagulation (Goldberg et al. 1995). The presence of multiple independent heat sources is supposed to lead to less heat dissipation (Haemmerich et al. 2001) and a synergistic effect of additive heat diffusion (Goldberg et al. 1995). A commercially available switching controller (Valleylab) enables rapid switching between three internally cooled single electrodes. If an impedance spike occurs during activation of one of these three electrodes, the application of energy is switched to the next electrode (Laeseke et al. 2006). This multiple-electrode ablation induces larger volumes of coagulation compared with an internally cooled single or cluster electrode (Laeseke et al. 2006). In addition, the simultaneous production of separate zones of coagulation might be possible by switching the application of energy between different monopolar RF electrodes (Laeseke et al. 2005). For multi-probe arrays an accurate placement of all electrodes is necessary. This may lead to a prolonged electrode positioning compared with the application of a single RF electrode.

Bipolar and Multipolar RF Systems

A different strategy compared with that for monopolar RF systems is to apply the RF energy exclusively in the target tissue by using bipolar or multipolar RF devices. In monopolar RF systems, the electric current passes through tissue between the monopolar electrode and the grounding pads, and only a reduced amount of applied energy is used for RF ablation in the surrounding of the "active" electrode. The intention of bipolar and multipolar RF devices is to apply the RF energy exclusively within target tissue (Clasen et al. 2007). Therefore, in bipolar RF ablation the electric circuit is closed between two electrodes placed in proximity inside the target tissue, and no grounding pads are required. A design with two electrodes located on different applicator shafts (McGahan et al. 1996) or on the same applicator shaft (Tacke et al. 2004; Clasen et al. 2007) is possible for bipolar RF ablation (Fig. 13.3). As opposed to the monopolar system, the tissue is heated around both poles of the electric circuit. In multipolar RF ablation, more than two electrodes are placed within the target tissue, and the electric field can be switched between

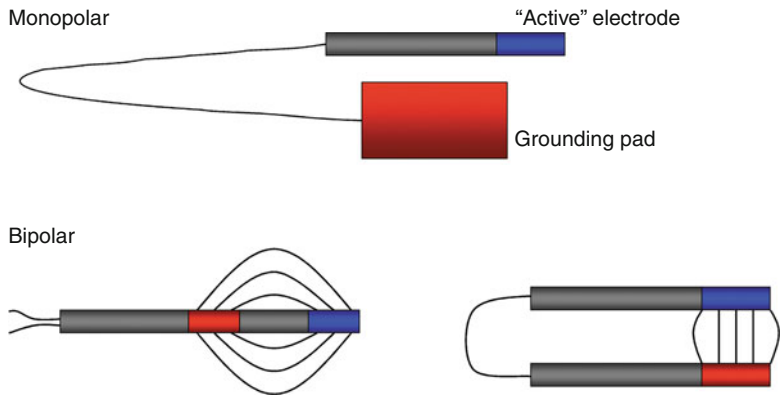

Fig. 13.3 Schematic drawing of the electric circuit in monopolar and bipolar RF ablation. In monopolar RF ablation the electric circuit is closed between an "active" electrode placed within the target tissue and grounding pads placed on the body surface. In bipolar RF ablation, the electric circuit is closed between two electrodes placed within the target tissue, omitting the need for grounding pads. A design of two electrodes located on the same (*left*) or on different applicator shafts (*right*) is possible

every possible pair of electrodes. A commercially available RF generator (CelonLab Power, Olympus, Teltow, Germany) providing a maximum power output of 250 W enables energy application in a bipolar and a multipolar mode. In the bipolar mode, RF energy is applied by an internally cooled applicator containing two non-insulated electrodes separated by insulation. The electric field is orientated parallel to the bipolar applicator shaft. When more than one bipolar applicator is connected to the RF generator, the electric current is automatically applied in a multipolar mode. In this multipolar mode, every possible pair of electrodes is activated one after the other for a short period of time like a bipolar electrode, whereas the pairs of electrodes are not necessarily located on the same applicator shaft (Clasen et al. 2006). Therefore, the electric fields are orientated parallel to the bipolar applicators and cross the tissue between the applicators. Thus, when three bipolar applicators are used with six electrodes, there are 15 possible combinations of electrode pairs. Modification of applicator connection with the RF generator enables the simultaneous use of up to six bipolar applicators (Bruners et al. 2008). The tissue resistance between the electrodes is used to control bipolar and multipolar RF ablation.

Summary

Percutaneous RF ablation represents a technique for hyperthermal tumor ablation. Understanding the underlying mechanism and technical basics of RF ablation is essential to ensure safe and effective coagulation of the tumor tissue. The technical development of RF devices enables reproducible energy application and coagulation of tumor tissue. Several RF devices and protocols for energy application are available; however, clinical experience has shown that the standard protocols provided by the different manufacturers may have to be adapted to the individual situation because of the variable underlying tissue and tumor biology. Therefore, the interventional radiologist has to be familiar with the relationship between the parameters of RF ablation and the RF devices applied. Beside the technical aspects of RF ablation, the determination of appropriate indications for ablation therapy represents a key aspect for a reasonable and an effective clinical application of RF ablation. Considerations regarding the indication of RF ablation in relation to different tumor types and organ sites are discussed in subsequent sections.

Key Points

- RF ablation is influenced by multiple parameters, including tissue and tumor conductivity.
- The material has to be selected carefully for each ablation procedure.
- Additional measures such as fluid injection, pre-interventional tumor embolization, pharmacological reduction of blood flow, or mechanical vessel occlusion may be used to modify the size and the shape of coagulation necrosis.

13.1.2 RF Ablation of Liver Tumors

Andreas Lubienski

13.1.2.1 Indications

RF ablation of primary and secondary hepatic tumors has been used for nearly 20 years. Rapid technological developments have led to good and reproducible results. However, given the limitations of currently available RF systems in addition to oncological considerations, the size and the site of a liver tumor play a crucial role in the achievement of complete ablation (Kuvshinoff and Ota 2002). Therefore, based upon adequate assessment of the overall tumor situation, including a precise hepatic tumor staging, a dedicated oncology team (e.g., tumor board) has to balance advantages and disadvantages of a minimally invasive approach and has to incorporate interventional therapy into a comprehensive treatment concept. Especially for liver metastases, no generally accepted recommendation for the use of RF ablation exists worldwide, resulting in a broad spectrum of individual indications for RF ablation in the liver. Since RF ablation is not yet a generally accepted first- or second-line treatment for liver metastases, it has to be considered as a palliative intention-to-treat therapy option. Given the unique biology of metastatic neuroendocrine disease, surgical experience has shown that debulking of tumors can considerably improve patient survival and symptoms. However, there is no proven evidence of this concept in other tumor entities, even though one can argue that aggressive ablation of hepatic metastases with destruction of more than 90 % of the tumor burden could result in a benefit (Atwell et al. 2005). Treatment strategies for hepatocellular carcinoma (HCC) also vary throughout the world, in particular owing to geographical differences in the incidence and presentation of the disease and the treatment options available. In contrast to secondary liver malignancies, several treatment guidelines for HCC have been published by the European Association for the Study of the Liver (Bruix et al. 2001), with the Barcelona Clinic Liver Cancer (BCLC) staging recommendation being the most accepted one (Table 13.2) (Rhim et al. 2010; Vauthey et al. 2010; Llovet and Bruix 2008; Sala et al. 2004; Mor et al. 1998; Forner et al. 2012). It links tumor stage with treatment strategy and is aimed at incorporating an estimation of the prognosis and potential treatment advancements in a single unified proposal (Sala et al. 2004). According to these guidelines, RF ablation has replaced ethanol injection therapy and has a place in the treatment strategy of HCC. While local ablation has been as second choice and was only recommended when resection was not considered feasible, it now emerged as first-line treatment (Forner et al. 2012).

To destroy any given hepatic tumor completely, the ablation volume should encompass the entire tumor burden with an additional safety margin of 5–10 mm according to the experience from liver surgery. The pathophysiological rationale for the safety margin is the high likelihood of scattered tumor cells (invisible to imaging) immediately around the tumor itself (visible by imaging). Tumors of 2-cm diameter present local metastases less than 10-mm distance from the primary tumor in about 10 % of cases and microscopic portal invasion in up to 25 % of cases (Kojiro 2004). If only the visible tumor is ablated, local recurrence can easily emerge from tumor cells remaining around the visible tumor. Since the available probe designs allow more or less spherical ablation volumes with a maximum diameter of about 4–5 cm

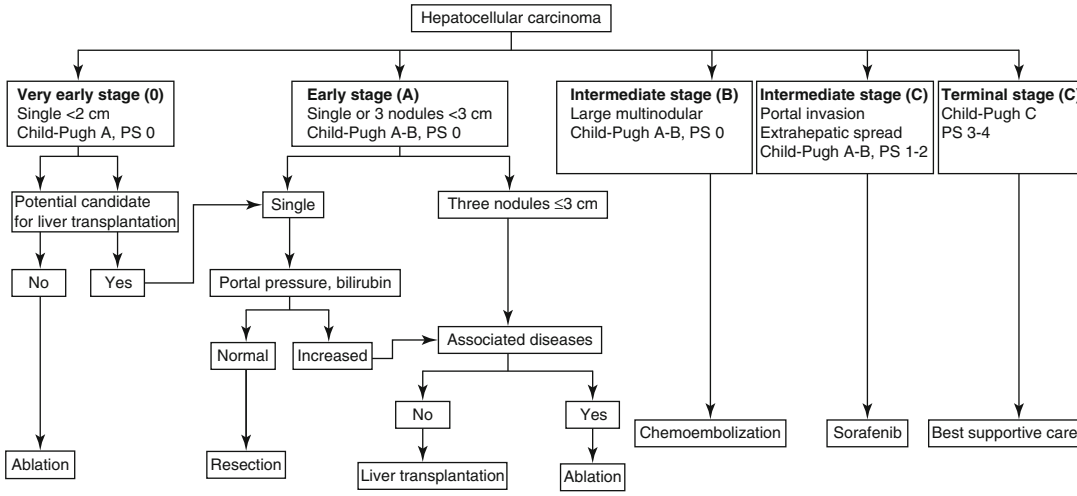

Table 13.2 Barcelona Clinic Liver Cancer: stage-dependent treatment of hepatocellular carcinoma (HCC) (Forner et al. 2012)

in a single ablation session, tumors presenting with a diameter of 3–4 cm can safely be treated with an adequate safety margin. A possible reason for failures in the treatment of larger tumors is the inability to determine the optimal number of ablations and the exact location of probe placement needed to completely destroy tumors larger than the size of a single ablation zone. To treat even larger tumors, multiple overlapping ablations need to be performed to build a composite thermal injury of sufficient size to kill the tumor and provide an adequate tumor-free margin (McGahan and Dodd 2001; Chen et al. 2004). Dodd and coworkers reported their results of computer analysis of the thermal injury sizes created by overlapping ablations and proposed 6- and 14-ablation models for diameters of 4.25 and 6.3 cm, respectively (Dodd et al. 2001). Their results demonstrated the importance of performing these types of calculations to develop tumor ablation strategies. These considerations are approved by the recent literature, in which local recurrence rates of primary and secondary liver tumors are reported to rise with tumor size after a single ablation, or several ablation sessions are needed to achieve complete ablation (Poon et al. 2002, 2004a, b; Lencioni et al. 2005; Lu et al. 2005; Choi et al. 2007a). According to these current data, the cutoff tumor diameter for a primary successful RF ablation in the liver is about 3 cm using current RF systems—independent of the anatomical tumor site and histopathological tumor type. An innovative strategy for treating large liver tumors with overlapping ablations is the use of multiple electrodes in a stereotactic ablation approach (Bale et al. 2012). Applying this technique, lesions of more than 10 cm can be treated with favorable outcome.

Another independent predictor of successful ablation is the so-called heat-sink effect caused by heat dissipation when tumors are located adjacent to major vessels. Lu et al. (2003) showed that, in 105 tumors with a mean diameter of 2.4 cm treated with two different multi-tined and one clustered RF system (no difference regarding the RF system used or whether it was open or percutaneous access), tumors at least 3 mm from major vessels presented a primarily incomplete ablation or recurrence only in 7 % of cases, while this was true in 48 % of tumors that were located directly adjacent to major vessels. As a consequence, both these independent predictors of success—tumor size and vascular proximity—have to be incorporated into treatment planning. Some of these limitations are thought to be overcome by addition of endovascular procedures such as pre-ablation transarterial tumor embolization. Although no general consensus concerning the indication of RF ablation in liver malignancies exists, basic inclusion and exclusion criteria, as shown in Table 13.3, are recommended and should be taken into account when RF ablation in liver tumors is discussed.

Table 13.3 Inclusion and exclusion criteria for RF ablation in liver tumors

Prerequisites	Adequate assessment of the overall tumor situation Incorporation of RF ablation into a comprehensive treatment concept Balance of advantages and disadvantages of a minimally invasive therapy by an interdisciplinary oncology team
Indications	Exclusion of resectability Bilobar hepatic tumors Medical reasons Fewer than 4–5 tumors Tumor diameter < 3.5–5 cm
Contraindications	Progressive systemic disease More than 5 tumors Tumor diameter >5 cm Colorectal metastases >3.5 cm Septicemia, coagulopathy Tumor volume >50 % liver volume
Relative contraindications	Biliodigestive anastomosis Pacemaker Vicinity to critical structures Portal vein thrombosis

13.1.2.2 Material

RF Generators

Several commercially available RF generators are FDA and CE approved and can be used in the clinical setting. These may be separated in monopolar, bipolar, and multipolar RF systems.

The monopolar RF generators work with a power ranging from 60 W (HiTT Elektrotom 106, Berchtold-Integra, Plainsboro, NJ) to 200 W (RF 3000, Boston Scientific, Mountain View, CA, and Cool Tip, Valleylab, Boulder, CO) and 250 W (1500×, RITA Medical Systems, Mountain View, CA). The different vendors pursue slightly different strategies in terms of generator control and therefore the ablation process. On the one hand ablation is controlled on the basis of tissue resistance (Berchtold-Integra, Boston Scientific, Valleylab), and on the other hand it is controlled on the basis of temperature (RITA) (see Sect. 13.1.1). Each device comes with a standard protocol for liver ablation which, from clinical experience, has to be adapted to each individual tumor. Thus, a successful tumor ablation depends on the experience of the interventionalist who has to decide on the ablation parameters, such as the ablation length, probe, power output, and number of applicator repositioning procedures required to treat the entire tumor, including a safety margin (Poon et al. 2004b). Recently a commercially available RF device (Celon Lab Power, Olympus-Celon, Teltow, Germany) providing a maximum power output of 250 W has enabled application of RF energy in bipolar and multipolar modes.

Monopolar Systems

Monopolar RF systems consist of an RF generator, large dispersive electrodes (grounding pads usually placed on the thighs of a patient), and a needle electrode. This setting turns the patient into a resistor within a closed-loop circuit. Thus, an alternating electric field is created within the tissue of the patient. The electrical energy is concentrated around the non-insulated tip of the needlelike electrode, resulting in marked agitation of the ions in the surrounding tissue (Ni et al. 2000; Goldberg and Gazelle 2001; Pereira et al. 2003).

Bipolar Systems

In contrast to monopolar systems, bipolar systems consist of two non-insulated electrodes (positive and negative) integrated into one applicator. Owing to the fact that the electrical circuit is closed between these two electrodes, grounding pads are not necessary. The tissue is heated either around the positive or the negative electrode, which in fact is different from monopolar

systems. So far only one bi-/multipolar RF system is commercially available (Celon Lab Power, Olympus, Teltow, Germany). With this device, two electrodes are located on the same shaft of the applicator for bipolar RF ablation. The electric field is orientated parallel to the bipolar applicator shaft. Several of these bipolar probes can be placed cluster-like in situ, allowing multipolar ablation controlled by a specific switch box. The combination of three bipolar probes leads to a more spherical ablation zone when compared with two bipolar arrays (Burdio et al. 2003; Tacke et al. 2004; Clasen et al. 2006, 2007).

RF Probes

Currently several different probe designs are available for clinical use. In principle, an RF electrode consists of an insulated metallic shaft and a non-insulated, active tip of variable length and/or design. The active tip is in contact with the target tissue to close the electric circuit including the RF generator, the probe, and the patient. As described already, the electrical energy provided by the RF generator is concentrated around the non-insulated tip of the probe, resulting in a certain ablation area which in fact is dependent on the design of the RF probe. To increase the ablation volume, several modifications to the probe design have been developed, for example, extending the length of the antenna (cluster needle, umbrella-like/inverted-umbrella-like design) or internal cooling of the probe to avoid premature carbonization around the needle tip followed by insulation and energy decay. At present, the available probes provide ablation volumes with more or less spherical diameters of between 2 and 5 cm. Although comparisons of different probe designs concerning efficacy have been made (Pereira et al. 2004b), it seems that a more important role regarding the proper use of a device is the experience of its user (Poon et al. 2004b; Lu et al. 2005). The rate of complete ablation significantly increased during the learning period in a prospective analysis regardless of the RF probe chosen (single or cluster electrode) (Poon et al. 2004b). Lu et al. (2005) confirmed these results, since in their work the most important factor influencing the primary success rate was tumor size, independent of electrode design (cluster vs. multi-tined).

13.1.2.3 Technique

Patient Preparation

Preprocedural evaluation should include adequate laboratory tests to rule out severe coagulopathy, acute inflammation, poor liver function (Child class B and C cirrhosis), and/or other severe comorbidities. A screening for viral hepatitis should follow. Baseline serum tumor markers—α-fetoprotein (AFP) in patients with HCC and carcinoembryonic antigen in metastatic patients—are helpful for monitoring the therapeutic success during follow-up. Recently, several studies suggested that circulating VEGF level may be an independent prognostic marker in highly vascular tumors such as HCC, therefore supporting plasma VEGF in the monitoring of treatment outcomes (Kaseb et al. 2009). For therapy planning, assessment of the tumor extent at baseline and subsequent follow-up studies, contrast-enhanced dynamic computed tomography (CT), and magnetic resonance (MR) imaging still play the major role, while ultrasound is hampered by its reproducibility (Vilana et al. 2006). If there is a history of bone pain and/or the serum alkaline phosphatase is disproportionately elevated, a bone scan or whole-body MR imaging is necessary to rule out bone metastases (Nakanishi et al. 2005). Informed consent is necessary 24 h prior to the procedure at the latest.

RF ablation can usually be performed as a minimally invasive, percutaneous procedure under conscious sedation. General anesthesia is usually not required. For image guidance, ultrasound, CT, or MR imaging can be used (Lencioni et al. 2001). Since ultrasound is widely available and is a real-time, multiplanar technique which allows in many cases for easy in-plane and off-plane access to the target and visualization of the RF probe, it is reported to be the most often used guiding method for RF ablation (Solbiati et al. 2004a). However, depending on the given individual's anatomical and pathological characteristics, ultrasound is not able to tag the target or to follow the probe in all cases. Owing to the fact that during the ablation process, the target is masked by a cloud of micro gas bubbles, it is difficult to identify the probe and the target during RF ablation and to assess the success of the ablation. Recent data suggest that contrast-enhanced ultrasound and new innovative hybrid systems merging the freedom of ultrasound

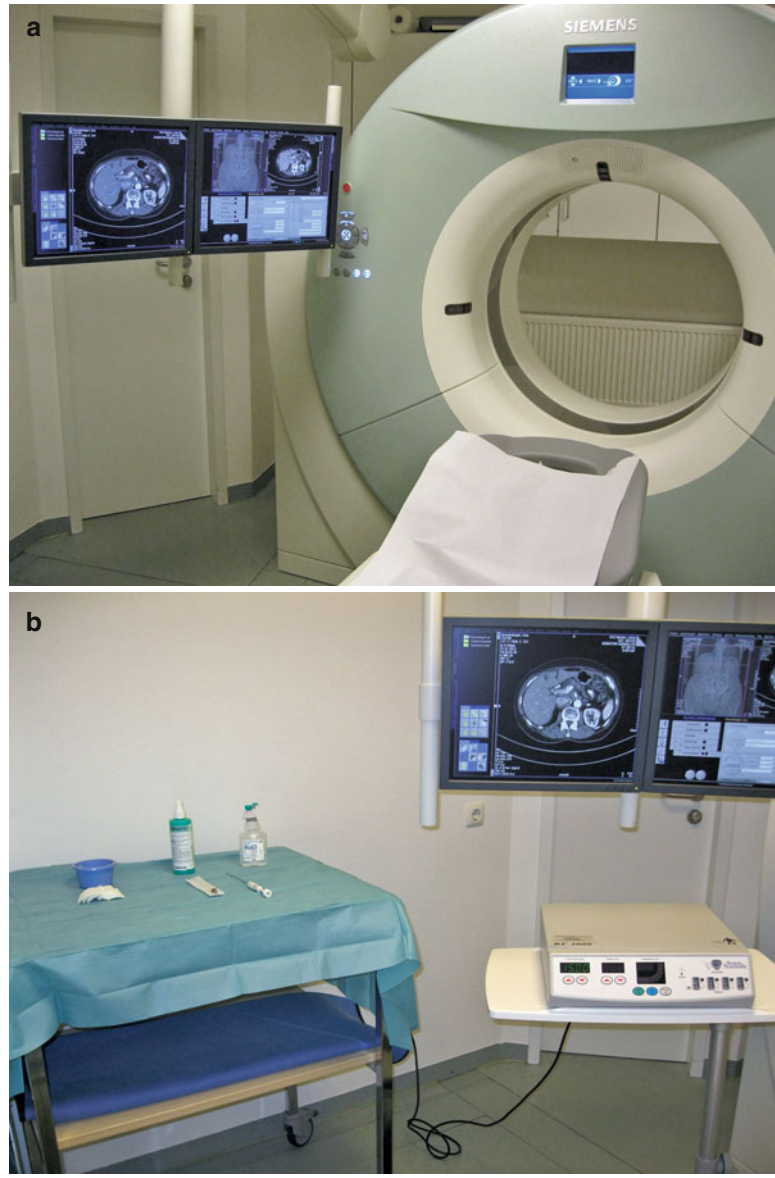

Fig. 13.4 Typical setting for RF ablation using CT-guidance: CT scanner with CT fluoroscopy and additional external guiding support (**a**). RF ablation rack and special equipments for CT-guided interventions (e.g., apron for X-ray protection) (**b**)

guidance with the superior image information of CT or MR imaging may help to overcome the known ultrasound obstacles (Solbiati et al. 2004b; Nicolau et al. 2004). In contrast, CT guidance is mostly used by interventional radiologists (Fig. 13.4). It offers a significantly more "panoramic" view than ultrasound, and especially when implemented with fluoroscopy, it allows for optimal targeting of almost all hepatic tumors in all anatomical localizations. Major disadvantages are the lack of elbowroom within the scanner gantry, the exposure of the patient and the interventionalist to the radiation, and the use of a contrast agent for visualization of the target. In addition no significant immediate changes in the treated tissue can be appreciated by CT in contrast to ultrasound. The full extent of the ablation can be identified only 12–18 h after RF ablation. Compared with ultrasound and CT, MR imaging offers the advantage of displaying heat-related intrinsic tissue alterations directly and online. In particular, MR-guided RF ablation is advantageous in locations unfavorable for CT guidance or in patients in whom iodized contrast media are contraindicated.

Procedure

To start the RF procedure for all guiding modalities, the patient is usually placed in a supine position and an intravenous access line for sedation, analgesia, and emergent medication is established using an intravenous cannula placed in a cubital vein. Prophylactic antibiotics are usually not necessary. During the entire RF procedure, the vital parameters of the patient are consequently monitored. After localization of the tumor using the preferred guidance method, the skin is prepped and draped. Then local anesthesia from the skin entry point of the needle down to the liver capsule is administered. For local anesthesia, common local anesthetics such as mepivacaine, for sedation midazolam, and for analgesia piritramide or fentanyl can be used. Subsequently, the probe is either placed within the tumor, or multiple probes are placed around the tumor ("no touch technique"). Then the probe and, in monopolar systems, also the grounding pads have to be connected to the RF generator. Depending on the RF system used, the ablation process is started with different RF protocols. The control of the ablation itself is also device dependent. Most RF systems use the relative increase of impedance as a parameter for controlling the ablation process, while increasing impedance regulates the delivered power down. At present only one system is equipped with multiple thermostats at the tips of the tines, thus offering online monitoring of the temperature. In general, to provide complete tissue necrosis, the RF procedure takes 10–30 min per probe placement. Depending on the size of the target tumor, repositioning of the probe may be required.

Post-interventional Follow-Up

Monitoring of therapy effectiveness is deemed to be a major issue in interventional tumor therapy. CT and MR imaging is, although widely used, of limited sensitivity, specificity, and accuracy when assessing the liver for residual tumor following RF ablation (Gillams and Lees 2000; Gillams 2001, 2003). This limitation relates to their predominantly morphologic character, which can only partly be compensated for by administration of contrast agents. The accuracy is limited by both spatial and contrast resolution to approximately 2–3 mm (depending on the imaging modality) (Gillams and Lees 2004). Post-procedural imaging findings are only a rough guide to the success of ablation therapy, since microscopic foci of residual disease, by definition, cannot be expected to be identified. Based on these facts, advanced MR imaging methods including diffusion-weighted imaging (DWI), perfusion-weighted imaging (PWI), and magnetic resonance elastography (MRE) are more and more integrated in the routine post-procedural MR imaging protocols in order to improve sensitivity and specificity of

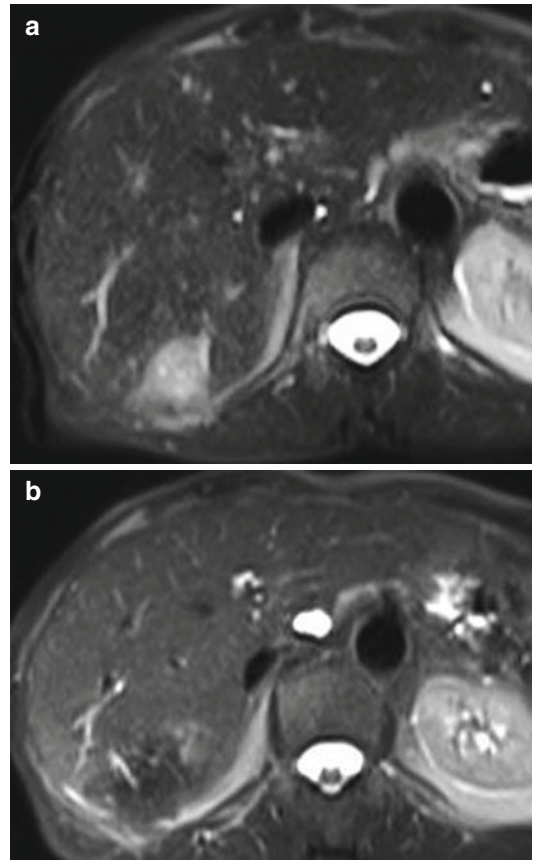

Fig. 13.5 T2-weighted MR-imaging using fat-suppressed HASTE-Sequence demonstrates clearly a hyperintense metastatic nodule in segment 6 of the liver (**a**). Follow-up imaging 6 months after percutaneous RF ablation revealed no evidence of residual tumor (**b**)

residual tumor detection following RF ablation (Willat et al. 2008). But in daily routine work, dynamic contrast-enhanced CT and MR imaging still plays the major role in follow-up imaging after RF ablation (Fig. 13.5). A very interesting approach to predict tumor recurrence after RFA of liver metastases was recently presented by Mahnken et al. (2011). The authors could demonstrate that the mean arterial enhancement fraction of segments that developed metastases was significantly higher when compared to segments that did not develop new lesions.

There are two types of imaging findings that can be identified after an ablation procedure: those related to zones of decreased or absent perfusion and those in which the signal intensity (MR imaging) or attenuation (CT) is altered (Dupuy and Goldberg 2001). Owing to the characteristics of some metastatic liver lesions (e.g., colorectal cancer), which are relatively hypovascular compared with the normal liver tissue, interpretation of follow-up scans is sometimes difficult since contrast enhancement of viable tumor foci may not be present or only minor. In addition, a peri-ablational enhancement may be seen in early follow-up scans (Fig. 13.6). Especially in tumors with distinct contrast enhancement in pre-interventional studies, rim enhancement after treatment might be confused with residual enhanced tumor tissue. Depending on the protocol used for contrast-enhanced imaging (injection rate and scanning delay), this transient finding can be seen immediately after ablation and can last for up to 6 months after ablation (Choi et al. 2001). It usually manifests itself as a penumbra, or a thin rim peripheral to the zone of ablation, that can typically measure up to 5 mm (in the immediate post-interventional phase), but most often measures 1–2 mm. It is characterized by a relatively concentric, symmetric, and uniform enhancement with smooth inner margins, which needs to be differentiated from irregular peripheral enhancement suspicious of recurrent or new tumor (Fig. 13.7). The finding is most readily appreciated on arterial phase CT scans, with persistent enhancement that is often seen on late phase contrast-enhanced MR images. Histopathologically, it represents a benign

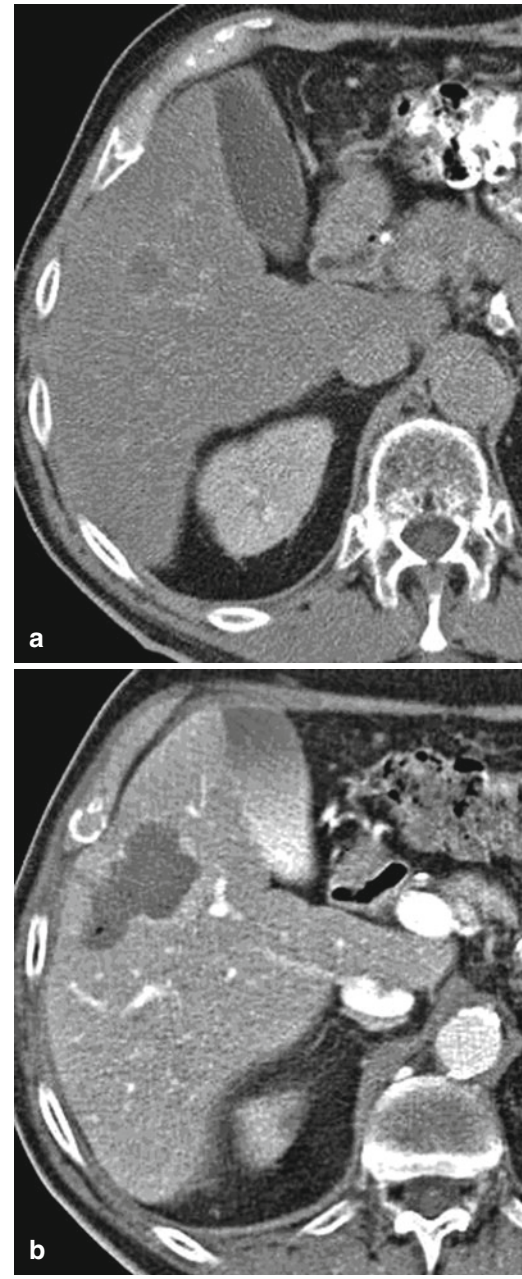

Fig. 13.6 CT scan prior and 24 h post-RF ablation of a recurrent unifocal liver metastasis of colorectal cancer. Contrast-enhanced portovenous CT scan delineates unifocal recurrent liver metastasis in segment 5 of the liver (**a**; *arrow*). Contrast-enhanced portovenous CT scan 24 h post-RF ablation shows a clear demarcation of the RF ablation zone (**b**; *short arrows*) including the probe track (*long arrow*) with typical small hyperdense rim encompassing the former tumor nodule

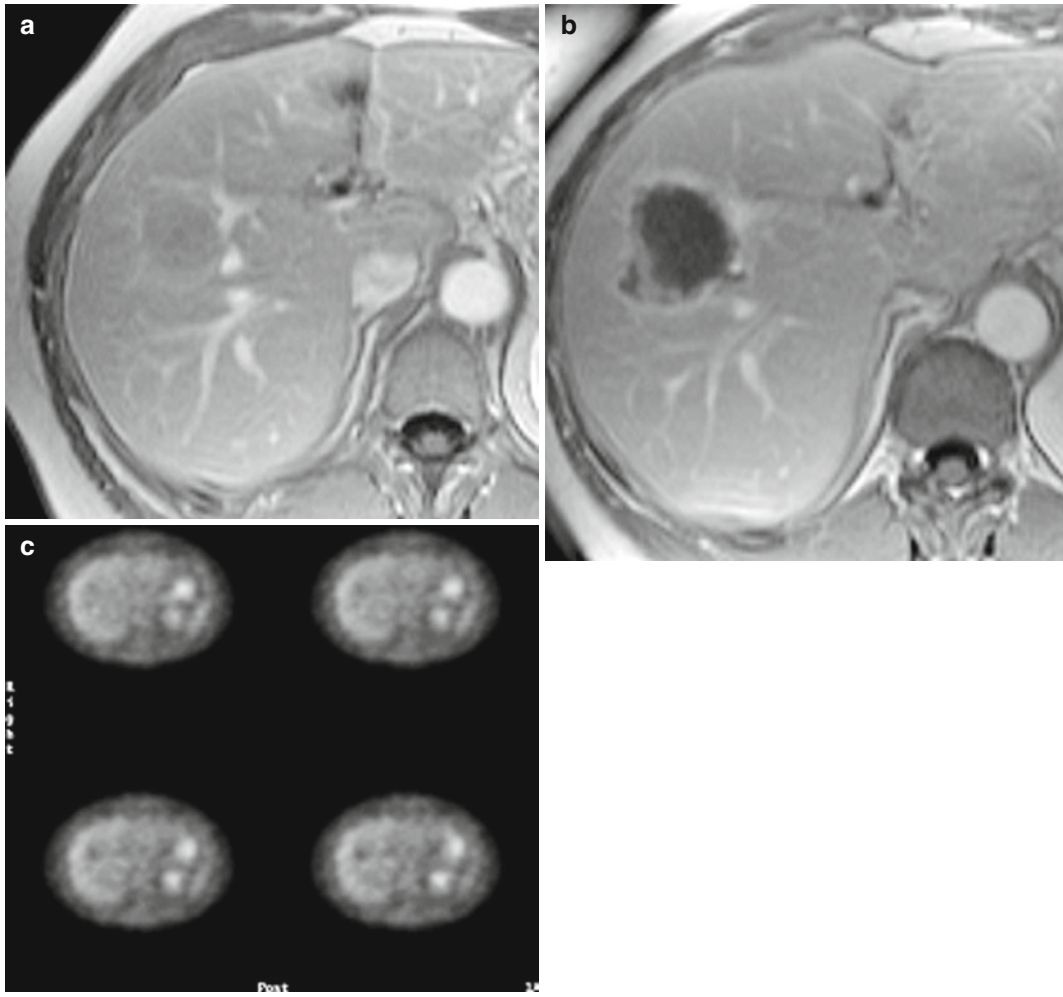

Fig. 13.7 CT scan prior and 6 weeks post-RF ablation and additional PET scan of a recurrent unifocal liver metastasis of colorectal cancer: contrast-enhanced portovenous CT scan delineates unifocal recurrent liver metastasis in segment 8 of the liver (**a**; *arrow*). Contrast-enhanced portovenous CT scan 6 weeks post-RF ablation shows a clear demarcation of the RF ablation zone with some eccentric nodular irregularities at the posterolateral part of the ablation zone (**b**; *arrow*). PET scan 8 weeks post-RF ablation demonstrates no evidence of pathological glucose metabolism within or around the ablation zone (*arrows*) representing complete RF ablation (**c**)

physiological response to thermal injury (initially, reactive hyperemia; subsequently, fibrosis and giant cell reaction) (Goldberg et al. 2000). In contrast, irregular peripheral enhancement represents residual tumor at the treatment margin. It often appears in scattered, nodular, or eccentric patterns indicating incomplete local treatment (Figs. 13.7 and 13.8). Given the delayed enhancement characteristics of many hypovascular tumors, this finding is often best appreciated in a side-by-side comparison of portal venous or delayed images (3 min or more after contrast material injection) with baseline images. Complete coagulation necrosis corresponds to hypoattenuating areas and fails to be enhanced after contrast injection. On MR imaging, the treated tumor is characterized by low signal intensity on T2-weighted images, whereas viable tumor is shown to be hyperintense on T2-weighted images (Sironi et al. 1999).

Biopsies of ablated areas in order to prove complete necrosis are generally unreliable and therefore not recommended (Solbiati et al. 2001). The ablation of appropriate margins (0.5–1.0 cm) beyond the borders of the tumor is necessary to

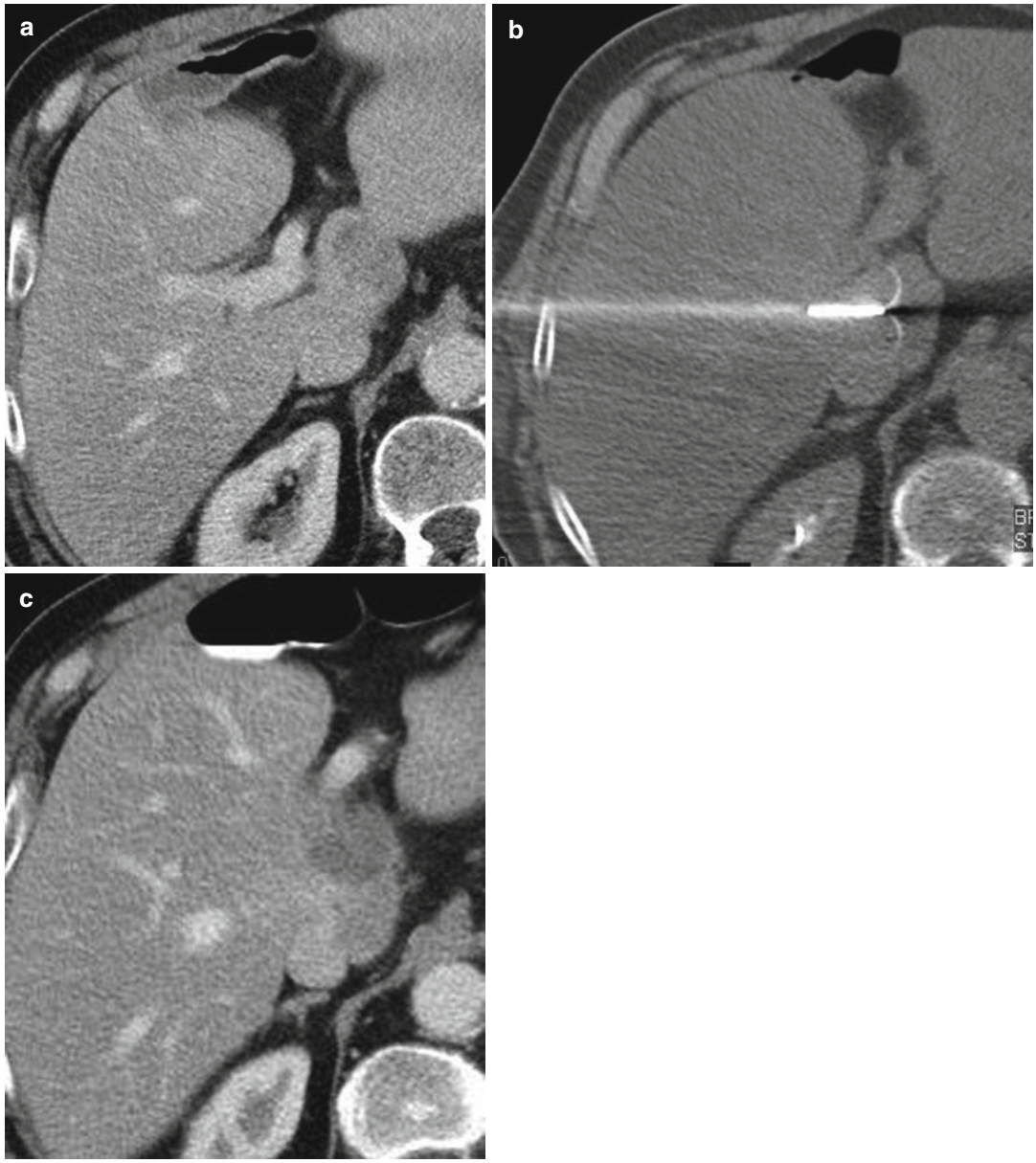

Fig. 13.8 CT scan prior, during and 3 months post RF-ablation of a colorectal liver metastasis: Contrast-enhanced portovenous CT scan delineates unifocal recurrent liver metastasis in segment 1 of the liver (**a**). Unenhanced CT scan during RF-ablation shows the RF-probe within the metastatic lesion (**b**). Contrast-enhanced portovenous CT scan 3 months post RF-ablation clearly depicts residual tumor foci posterior to the ablation zone in segment 1 (**c**)

achieve complete tumor destruction (Dodd et al. 2001). Therefore, an ablation zone that equals the tumor before ablation should be followed up closely. Long-term follow-up imaging may show a gradual decrease in the volume of the ablation zone considered to represent only residual necrotic or fibrotic tissue that is present during the absorption process (Lim et al. 2001). It is important to note that no or minimal involution does not imply treatment failure. Many other imaging findings, such as inflammatory stranding in the acute period after ablation, and more

chronic findings, such as fibrosis, scarring, and architectural distortion, that represent both host reaction to ablation and repair mechanisms will be seen.

When imaging and clinical findings at short-term follow-up are inconclusive and the suspected lesion is small, follow-up at 1–3-month intervals should be considered before performing an invasive diagnostic procedure such as percutaneous biopsy or repeated treatment (Lim and Han 2002). In most centers, follow-up scans are performed in 3-month intervals and are often combined with serum tumor markers such as carcinoembryonic antigen (Tacke 2003; Pereira et al. 2004a). Any increase in lesion size or irregularity or residual enhancement should be carefully interpreted in terms of residual tumor foci or recurrent metastases (Fig. 13.7). It is mandatory to look for evidence of both intrahepatic and extrahepatic tumor spread.

Initial results indicate that positron emission tomography (PET)/CT imaging may prove to be more accurate when evaluating the ablative zone for residual tumor than image analysis based on morphologic data alone. PET/CT may be expected to play a distinctive role in follow-up of patients undergoing RF ablation of liver lesions for the detection of residual tumor. The advantages of fused PET/CT data sets over PET alone and CT alone, respectively, are related to accurate localization of focally increased glucose metabolism in terms of therapeutic planning in an area of residual tumor, offering guidance for subsequent interventional procedures to these areas of viable tumor cells (Veit et al. 2006; Barker et al. 2005).

13.1.2.4 Results

The early clinical studies of RF ablation were performed to assess feasibility, aiming at safety, tolerability, and local therapeutic effect of the treatment. In recent years, RF ablation has evolved significantly concerning technical developments and procedure-related improvements, and even in the so-called difficult localization of hepatic tumors, RF ablation can nowadays be performed safely and effectively (Figs. 13.9 and 13.10). Therefore, the data collected in early studies may not be comparable with those of recent series. Although the findings of many studies on hepatic RF ablation as well as recommendations for the standardization and reporting criteria in RF ablation have been published, the analysis of clinical results of percutaneous RF ablation in liver tumors is still hampered by several problems (Goldberg et al. 2005). Many reports presented data which involve different tumor entities, including primary and metastatic liver tumors with different tumor sizes. Treatment was performed with different types of RF generators and probe designs, and additional therapies such as resection, regional or systemic chemotherapy, and other local ablative techniques were used in combination with RF ablation. Finally, the studies had different end points and follow-up durations, as well as criteria for evaluating results.

Liver Metastases

Although RF ablation has been used increasingly in the treatment of liver metastases, especially of colorectal origin, the definitive role of RF ablation in the treatment strategy of liver metastases has not been established yet. To date there is still no generally accepted recommendation for the use of RF ablation in metastatic liver disease, and no randomized controlled trial evaluating RF ablation in the treatment of liver metastases has been published (Wong et al. 2010; Stang et al. 2009). In early clinical series, Solbiati et al. (1997a) and Lencioni et al. (1998) performed RF ablation in patients with limited hepatic metastatic disease, who were excluded from surgery. In the first series, 29 patients with 44 hepatic metastases ranging from 1.3 to 5.1 cm in diameter were treated. Each tumor was treated in one or two sessions, and technical success, defined as the lack of residual unablated tumor at CT or MR imaging obtained 7–14 days after completion of treatment, was achieved in 40 of 44 lesions. However, follow-up imaging studies confirmed complete necrosis of the entire metastasis in only 66 % of the cases, whereas local tumor progression was observed in the remaining 34 %. Only one complication, self-limited hemorrhage, was seen. One-year survival was 94 %. In the study by Lencioni et al. (1998), 29 patients with 53 hepatic metastases ranging from 1.1 to 4.8 cm in diameter were enrolled. A total of 127 insertions were performed (mean, 2.4 insertions per lesion) during 84 treatment sessions (mean, 1.6 sessions per lesion) in the absence of

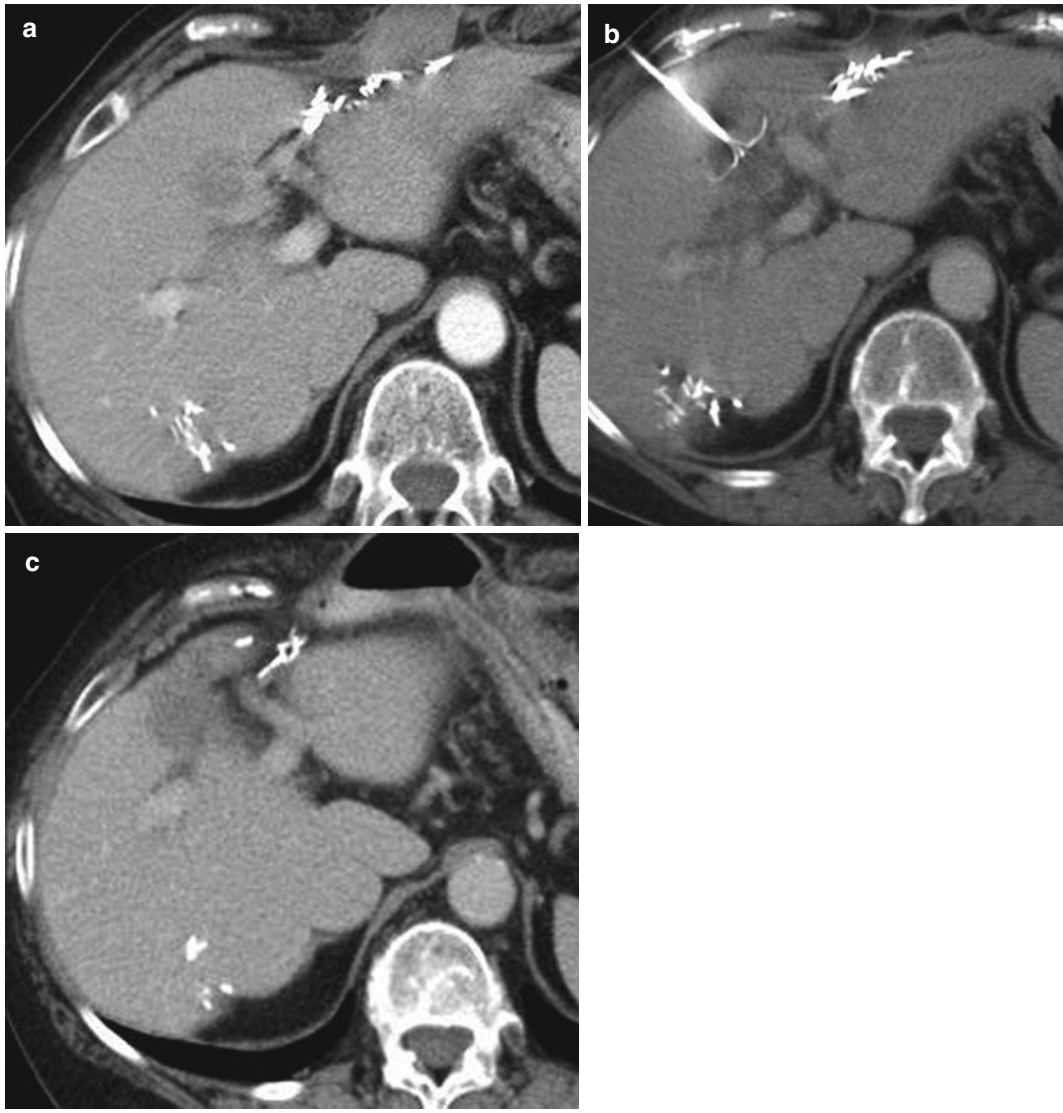

Fig. 13.9 CT scan prior, during and 2 years post RF-ablation of a recurrent colorectal liver metastasis 15 months after metastasectomy: Contrast-enhanced portovenous CT delineates unifocal recurrent liver metastasis in segment 4 of the liver (**a**). Unenhanced CT scan during RF-ablation shows the RF-probe within the metastatic lesion (**b**). Contrast-enhanced portovenous CT scan 2 years post RF-ablation shows a clear demarcation of the ablation zone with no evidence of residual tumor (**c**)

complications. Complete tumor response, defined as the presence of a non-enhanced ablation zone larger than the treated tumor on posttreatment spiral CT, was seen in 41 (77 %) of 53 lesions. After a mean follow-up period of 6.5 months (range, 3–9 months), local tumor progression was seen in 12 % of cases. One-year survival was 93 %.

A systematic review on the outcomes of RF ablation for unresectable hepatic metastases in 2002 revealed a dearth of long-term follow-up data. Seidenfeld et al. (2002) found only seven articles that provided data on disease-free or recurrence-free survival, rates of hepatic relapse, and median or percentage survival at 1–5 years after treatment. Five studies reported 86–94 % survival at 1 year, but only one study reported survival at 2 years or longer (Solbiati et al. 1997b). In a recent study by Solbiati et al.(2001), the

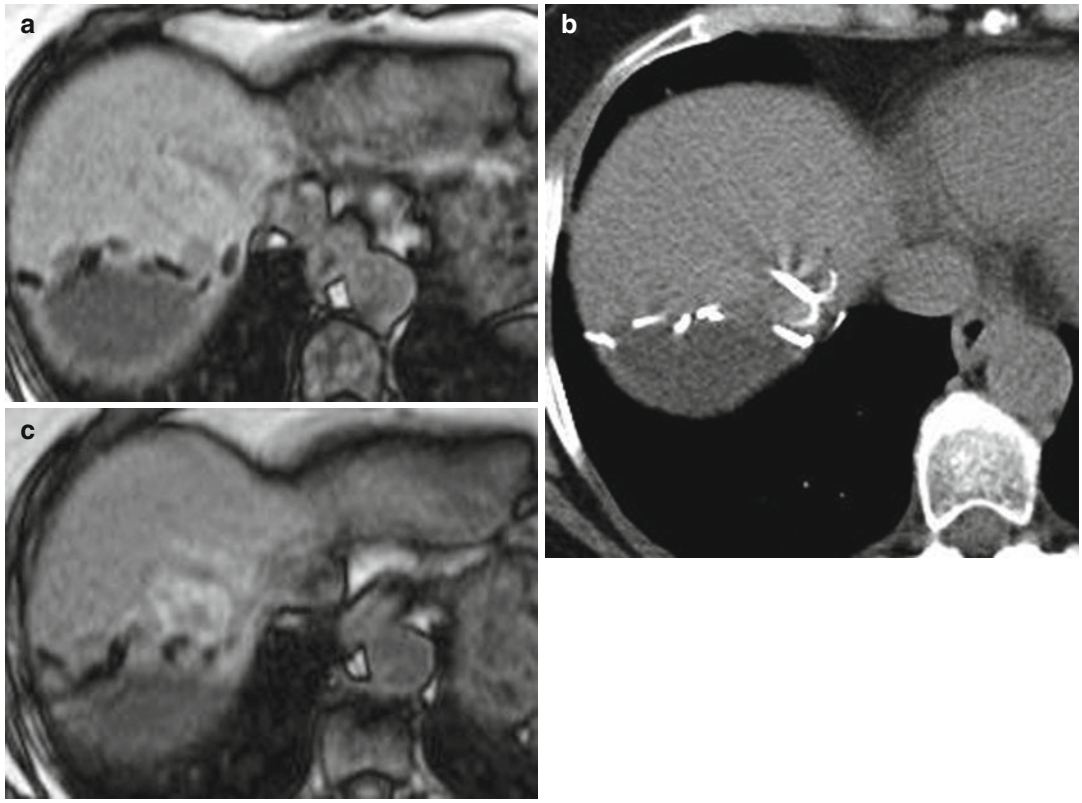

Fig. 13.10 MR imaging prior and post RF-ablation of residual metastatic tumor 9 months after metastasectomy: T1-weighted opposed phase image demonstrates residual tumor adjacent to the resected area (**a**). Unenhanced CT scan during RF-ablation shows the RF-probe within the metastatic lesion (**b**). T1-weighted opposed phase image 3 months post RF-ablation delineates the hemorrhagic ablation zone encompassing the former metastasis (**c**)

results from 109 patients with 172 metastatic lesions who underwent RF ablation under ultrasound guidance were analyzed. The median follow-up was 3 years, and local tumor control was achieved in 70 % of the lesions. Local recurrence—including residual tumor foci—occurred in 30 % of the lesions, and these were treated again by RF ablation, and the entire rate of local tumor control reached 78 %. New metastases developed in 50.4 % of the patients at a median time to recurrence of 12 months after RF ablation. The overall 2- and 3-year survival rates were 67 and 33 % and the median survival was 30 months. This compares favorably with data reported by Gillams (2001) with a median survival of 34 months and a 3-year survival of 36 %. Survival of 36 % at 3 years for inoperable patients is similar to that for patients undergoing resection for operable metastatic disease, showing a 3-year survival of 42–44 % (Jaeck et al. 1997; Jenkins et al. 1997). In another large series, 328 hepatic metastases in 76 patients were treated with RF ablation. At a mean follow-up of 15 months, local recurrence was noted in 9 % of patients (Bowles et al. 2001). Data from the Tumor Radiofrequency Ablation Italian Network (TRAIN) study by Lencioni et al. (2004) demonstrated long-term data on colorectal and breast cancer metastases to the liver treated by RF ablation. In colorectal metastases, 423 patients were evaluated presenting unifocal liver metastases (mean size, 2.7 cm). The overall survival after 1, 3, and 5 years was 86, 47, and 24 %, respectively. Interestingly, the TRAIN study revealed very good 5-year survival of 56 % in a subgroup of patients having one tumor nodule 2.5 cm or smaller. Patients with tumors bigger than 2.5 cm and multifocal tumors showed a significant decrease in the 5-year

Table 13.4 Survival after RF ablation, selected references

Authors	No. of patients	Tumor	Survival (%)		
			1 year	3 years	5 years
Solbiati et al. (1997b)	29	CRC (22 patients)	94	–	–
Lencioni et al. (1998)	29	CRC (24 patients)	93	–	–
Gillams and Lees (2000)	69	CRC	90	34	22[a]
Solbiati et al. (2001)	109	CRC	–	33	–
Oshowo et al. (2003)	25	CRC	–	52	–
Abdalla et al. (2004)	57	CRC	–	–	22[a]
Gillams and Lees (2004)	167	CRC	–	–	30
Lencioni et al. (2004)	423	CRC	86	47	24
		CRC <2.5 cm	–	–	56
		CRC >2.5 cm	–	–	13
		CRC multifocal	–	–	11
	102	Breast cancer	95	50	30
	96	HCC ≤2 cm	99	88	65
		Child class A, unifocal	46[b]		
Livraghi et al. (2004)	210	Early HCC	90	83	43
	164	Late HCC	68	49	28
Tateishi et al. (2005)	319	HCC first line	95	78	54
	345	Recurrent HCC	92	62	38
Chen et al. (2006a)	205	HCC	90	60	
Machi et al. (2006)	100	CRC	90	42	31
Choi et al. (2007b)	570	Early HCC	95	70	58
Choi et al. (2007a)	102	Recurrent HCC after resection ~2 cm Naïve HCC	94	66	52
Takahashi et al. (2007)	171		99	91	77
Sorensen et al. (2007)	102	CRC	96	64	44
Livraghi et al. (2008)	216	HCC	–	76	55
Gillams and Lees (2009)	123	CRC ≤5 and ≤5 cm	–	–	24
		CRC ≤3 and ≤3.5 cm	–	–	33
N'Kontchou et al. (2009)	235	HCC	–	60	40

CRC colorectal cancer metastases
[a]Four years
[b]Seven years

survival of 13 and 11 %. The data of the 102 patients suffering from breast cancer metastases confirmed that in selected breast cancer patients where the metastases are unifocal with a mean diameter of 2.4 cm with no further extrahepatic spread, RF ablation plays an interesting role in the treatment strategy, with overall survival rates after 1, 3, and 5 years being 95, 50, and 30 % (Lencioni et al. 2004) (Table 13.4). These long-term data go very well with the data published by Gillams and Lees (2009). For 123 patients with five or less metastases of 5 cm or less maximum diameter and no extrahepatic disease, median survival was 36 months from ablation, and corresponding 5-year survival rate was 24 %. Sixty-nine patients had three or less tumors below 3.5 cm in diameter, and their 5-year survival from ablation was 33 %. In comparison to chemotherapy, 5-year survival of 24–33 % post-ablation in selected patients is superior to any published chemotherapy data and approaches the results of liver resection. To evaluate effectiveness of RF ablation for unresectable colorectal liver metastases in first- and second-line management, Machi et al. (2006) conducted a study in 100 patients with 507 colorectal hepatic tumors. After a median follow-up of 24.5 months, 1-, 3-, and 5-year survival was 90, 42, and 30.5 %. Median survival was 48

months among 55 patients who received RFA (first line) before initiation of chemotherapy versus 22 months among 45 patients who received RFA (second line) for residual or progressive metastatic disease after chemotherapy, demonstrating a potential survival benefit of RF ablation over systemic chemotherapy alone, particularly when offered as part of first-line therapy.

Recent studies analyzed the role of RF ablation with respect to surgical resection. Abdalla et al. (2004) evaluated the survival of 418 patients with colorectal metastases isolated to the liver, who were treated with hepatic resection ($n=190$), RF ablation plus resection ($n=101$), RF ablation only ($n=57$), or chemotherapy only ($n=70$). Overall survival for patients treated with RF ablation plus resection or RF ablation only was significantly greater than for those who received chemotherapy only. However, overall survival was highest after resection: 4-year survival rates after resection, RF ablation plus resection, and RF ablation only were 65, 36, and 22 %, respectively ($p<0.0001$). However, RF ablation only had been used in patients ineligible for surgery; thus, the results of this study are not comparable. In contrast, Oshowo et al. (2003) found no difference in survival outcome of patients with solitary colorectal liver metastases treated by surgery ($n=20$) or by RF ablation ($n=25$). In this study, the survival rate at 3 years was 55 % for patients treated with surgery and 52 % for those treated with RF ablation, suggesting that the survival after resection and RF ablation is the same. Elias et al. (2002) demonstrated that RF ablation instead of repeated resections for the treatment of liver tumor recurrence after partial hepatectomy has the potential to increase the percentage of curative local treatments for liver recurrence after hepatectomy from 17 to 26 % and to decrease the proportion of repeated hepatectomies from 100 to 39 %. Despite the promising results of RF ablation in metastatic liver disease, recently several studies demonstrated better progression-free and overall survival and lesser local tumor recurrence after liver resection compared to RF ablation in metastatic liver disease. Thus, resection is still the standard of reference in colorectal liver metastases, and to date, RF ablation cannot be considered an equivalent procedure to hepatic resection (Park et al. 2008; Mulier et al. 2008; McKay et al. 2009). An interesting aspect concerning resection versus RF ablation of colorectal liver metastases could be emphasized in the paper by Berber et al. (2008). The authors performed RF ablation ($n=68$) and liver resection ($n=90$) in 158 patients suffering from solitary liver metastasis from colorectal cancer. RF ablation patients tended to have a higher ASA score and presence of extrahepatic disease at the time of treatment. Main indications for referral to RFA were technical reasons, patient comorbidities, extrahepatic disease, and patient decision. Complication rate was 2.9 % for RFA and 31.1 % for resection. Overall survival was 24 months for RFA with and 34 months without extrahepatic disease. Five-year survival was 30 % for RFA and 40 % for resection. The authors concluded that with a simultaneous ablation program, higher risk patients have been channeled to RFA, leaving a highly selected group of patients for resection with a very favorable survival, whereas RFA still achieved long-term survival in patients who were otherwise not candidates for resection.

A completely different approach was taken by Livraghi et al. (2003a). They evaluated 88 patients with 134 colorectal liver metastases, who were potential candidates for surgery concerning the potential role of performing RF ablation during the interval between diagnosis and resection as part of a "test-of-time" management approach. Among the 53 patients in whom complete tumor ablation was achieved after RF treatment, 98 % were excluded from surgical resection: 44 % because they remained free of disease and 56 % because they developed additional metastases leading to unresectability. No patient in whom RF treatment did not achieve complete tumor ablation became unresectable owing to the growth of the treated metastases.

Hepatocellular Carcinoma

Various minimally invasive interventions have been introduced and tested for the treatment of HCC over recent years. Among them, RF ablation has been the most widely assessed percutaneous therapy option after percutaneous ethanol injection (PEI) for local ablation of HCC (Gillams 2003, 2005; Goldberg and Ahmed 2002; Raut et al. 2005).

Compared with PEI, which is the recommended treatment of choice in unresectable early-stage HCC, presenting with up to three tumors of 3 cm or less and underlying liver cirrhosis of Child class A and B according to the BCLC staging system (Llovet et al. 2003), RF ablation has proven more effective with fewer complications and therefore should replace PEI for those tumors (Table 13.5) (Lencioni et al. 2003; Lin et al. 2004, 2005; Shiina et al. 2005; Brunello et al. 2008).

Treatment success, in terms of initial technical performance and long-term survival, is strongly influenced by tumor size and surrounding tissue. Lu et al. (2005) demonstrated complete tumor necrosis in 83 % of tumors smaller than 3 cm and 88 % of tumors in non-perivascular location. Poon et al. (2002) reported on studies where complete tumor necrosis could be achieved in a single treatment session in 80–90 % of tumors smaller than 3–5 cm, whereas tumors exceeding 5 cm (mean diameter, 5.4 cm) seem to result in significantly less tumor necrosis (48 %) after RF ablation as evaluated in 126 patients with medium and large HCC (Livraghi et al. 2000). To date, the findings of eight randomized controlled trials evaluating the efficacy of RF ablation in HCC have been published (Table 13.5). Two studies recently reported the long-term outcome of RF ablation in HCC. In the first study, by Lencioni et al. (2005), RF ablation was used as first-line treatment for early-stage HCC in 187 patients not eligible for surgery in an intention-to-treat prospective trial. Overall survival was 97 % at 1 year, 67 % at 3 years, and 41 % at 5 years in 187 patients. Median survival was 49 months. Survival of patients treated with RF ablation was dependent on the Child class ($p=0.0006$) and tumor multiplicity ($p=0.0133$). Patients who had Child class A cirrhosis with solitary HCC ($n=116$) had 1-, 3-, and 5-year survival rates of 100, 89, and 61 %. Median survival was 65 months. The 1-, 3-, and 5-year recurrence rates were 14, 49, and 81 for the emergence of new tumors and 4, 10, and 10 % for local tumor progression. In the second study, 319 patients received RF ablation as primary treatment, and 345 patients received it for recurrent tumor after previous local treatment (Tateishi et al. 2005). In this particular study the cumulative survival rates at 3 and 5 years were 78 and 54 % for primary treatment and 62 and 38 % for recurrent tumor (Table 13.4).

The prognosis after RF ablation of HCC is significantly affected by the initial treatment response. Sala et al. (2004) reported 282 cirrhotic patients with early nonsurgical HCC, who were treated with percutaneous RF ablation. Initial complete response was achieved in 192 patients and was independently related to the size of the main tumor and the tumor stage (2 cm or less, 96 %; 2.1–3 cm, 78 %; 3 cm or more, 56 %; two to three nodules, 46 %). Patients with Child class A cirrhosis with an initial complete response achieved 42 % survival at 5 years, and for tumors 2 cm or less, the survival was 63 %. These results were confirmed by two recent studies (Takahashi et al. 2007; Guglielmi et al. 2007). Takahashi et al. (2007) retrospectively analyzed 171 cirrhotic Child class A patients who received RF ablation for naïve HCC within the Milan criteria. Overall cumulative survival was 98.8, 91.1, and 76.8 % at 1, 3, and 5 years. Cumulative survival in patients with no local recurrence was 96.6, 94.6, and 84.4 % compared with 96.6, 74.8, and 42.1 % in patients with local tumor recurrence.

A recent study by Livraghi et al. (2008) questioned resection still being the treatment of choice in very early HCC and claimed a paradigm shift in the treatment of such patients. The authors evaluated 218 patients with single HCC of 2 cm or less (very early or T1 stage), concerning the rate of sustained, local, complete response, the rate of treatment-related complications, and the secondary 5-year survival in the 100 patients whose tumors had been considered potentially operable. After a median follow-up of 31 months, sustained complete response was observed in 216 patients (97.2 %), with a perioperative mortality of 0 %, a major complication rate of 1.8 %, and a 5-year survival rate of 68.5 %. On the basis of these results, they concluded that percutaneous RF ablation in very early HCC is less invasive and associated with lower complications than resection, ensuring similar local control and survival, and therefore should be considered the treatment of choice in single HCC of 2 cm or less, even when surgical resection is possible. There are two randomized trials comparing RFA

Table 13.5 Randomized trials including RF ablation for the treatment of HCC

Authors	Therapy	No. of patients	No. of tumors ≤2 cm/>2 cm	Complete necrosis (%)	Survival (%)			Local recurrence (%)
					1 year	2 years	3 years	
Shibata et al. (2002)	RFA	36	23/32	96		NE		12[c]
	PMC	36	19/31	89		NE		24[c]
Lencioni et al. (2003)	RFA	52		91	100	98		4[d]
	PEI	50		82	96	88		38[d]
Lin et al. (2004)	RFA	52	47/110	96	90	82		18[c]
	PEI	52		88	85	61		45[c]
	High-dose PEI	53		92	88	63		33[c]
Akamatsu et al. (2004)	PTA (PEI/RFA)	20 (14/6)	NE	NE	96	96	82	41[d]
	TAE–PTA (PEI/RFA)	22 (12/10)	NE	NE	100	82	82	68[d]
Shiina et al. (2005)	RFA	118	102/130	100	97	91	74[b]	2[c]
	PEI	114		100	92	81	57[b]	11[c]
Lin et al. (2005)	RFA	62	111/76	96	93	81		14[c]
	PEI	62		88	88	66		34[c]
	PAI	63		92	90	67		31[c]
Shibata et al. (2006)	RFA (internally cooled probe)	38	41[a]	95	100	94	94	20[c]
	RFA (umbrella probe)	36	42[a]	93	94	92	77	22[c]
Brunello et al. (2008)	RFA	70	NE	96			63	
	PEI	69	NE	66			59	

PAI percutaneous acetic acid injection, *PTA* percutaneous tumor ablation, *PMC* percutaneous microwave coagulation, *TAE* transarterial embolization, *NE* not evaluated

[a]Three centimeters or less

[b]Four years

[c]Two years

[d]Two-year local recurrence-free survival

and surgery in the treatment of HCC. While Chen et al. did not find differences in overall survival, Huang and coworkers come to the conclusion that surgery is superior to RFA (Chen et al. 2006b; Huang et al. 2010). However, this topic is discussed highly controversially, and only recently RFA was accepted as a first-line treatment in early-stage HCC (Forner et al. 2012).

13.1.2.5 Complications

The overall complication rate for RF ablation seems low in comparison with that of other more or less minimally invasive procedures. Nevertheless a significant number of major complications (2.4 %) were reported by an Italian multicenter trial including 3,554 lesions in 2,320 patients (Livraghi et al. 2003b). The latter was confirmed by Rhim et al. (2003, 2004), who presented a survey of 11 Korean institutions, including 1,663 lesions in 1,139 patients, with the rate of major complications being 2.43 %. Mortality was 0.3 and 0.09 %, respectively, which is similar to the findings of a meta-analysis by Mulier et al. (2002), who recently reviewed a total of 3,670 patients after RF ablation with a mortality rate of 0.5 %. The authors could also demonstrate the lowest total complication rate of 7.2 % for percutaneous RF ablation, compared with laparoscopic (9.5 %), intraoperative (9.5 %), and combined procedures with resection and open RF ablation (31.8 %).

The total minor complication rate including common side effects ranges between 4.6 % and 36 (Mulier et al. 2002; Livraghi et al. 2003b; Rhim et al. 2003, 2004). This wide range depends on the fact that minor complications according to the Society of Interventional Radiology guidelines are usually not listed in the published data, so the true (whenever clinically not relevant) minor complication rate is difficult to assess. Common side effects in RF ablation are pain in the area of the puncture site, peritoneal irritation, nausea, vomiting, moderate fever, tiredness, and headache. The so-called post-ablation syndrome including fever, nausea, vomiting, and tiredness can last for up to several weeks and can be found in up to two-thirds of patients. Symptomatic supportive care is sufficient in such cases.

Complications may occur immediately or with a delay after RF ablation and may be related to the puncture, the entire procedure, or the patient's underlying disease and individual situation (de Baere et al. 2003). Immediate complications can be due to vascular, nonvascular, and metabolic reasons, whereas delayed complications usually derive from complex metabolic reactions, infections, biliary obstruction, and tumor seeding.

Concerning vascular complications, there are several factors which influence the risk of bleeding: the patient's coagulation status, tumor type and site, surrounding tissue properties, way to the target, and interpositioned anatomical structures. To avoid bleeding, especially from the access route in coagulopathies, special measures have to be taken to correct coagulation abnormalities by additional infusion of platelets or fresh frozen plasma and stopping anticoagulative regimens if justifiable.

Vascular complications such as arterial bleeding (Fig. 13.11), pseudoaneurysm, arteriovenous/arterioportovenous fistulae, and hepatic and portal vein thrombosis, with subsequent hepatic infarction in extremely rare cases (Fig. 13.12), may occur from mechanical injuries caused by the RF probe traversing a vessel or from sustained ablation. Real-time imaging such as ultrasound or CT fluoroscopy during the procedure might help to minimize the rate of such complications. Nevertheless self-limiting hemorrhagic diapedesis usually representing hemorrhage due to thermal damage to the capillary bed of the tumor can be appreciated during the ablation process. In cases of intra-procedural bleeding and significant, ongoing pain, a baseline follow-up study has to be performed within the first 3 h after the ablation. In cases of vascular injuries, early angiography with interventional standby is mandatory (Fig. 13.11). To avoid needle track bleeding, it is recommended to perform "hot" probe repositioning and removal ("track ablation"). Therefore, regarding the present literature, bleeding in total is a rare, in most cases self-limiting, complication with an overall frequency of no more than 2 %. Mulier et al. (2002) recently found in a total of 3,670 patients after RF ablation intraperitoneal bleeding in 0.8 %, subcapsular hematoma in 0.6 %, and hepatic vascular damage in 0.4 %.

Nonvascular complications include infection, tumor seeding, and nontarget thermal damage. Predisposing factors such as an underlying inflammatory focus, a compromised immune

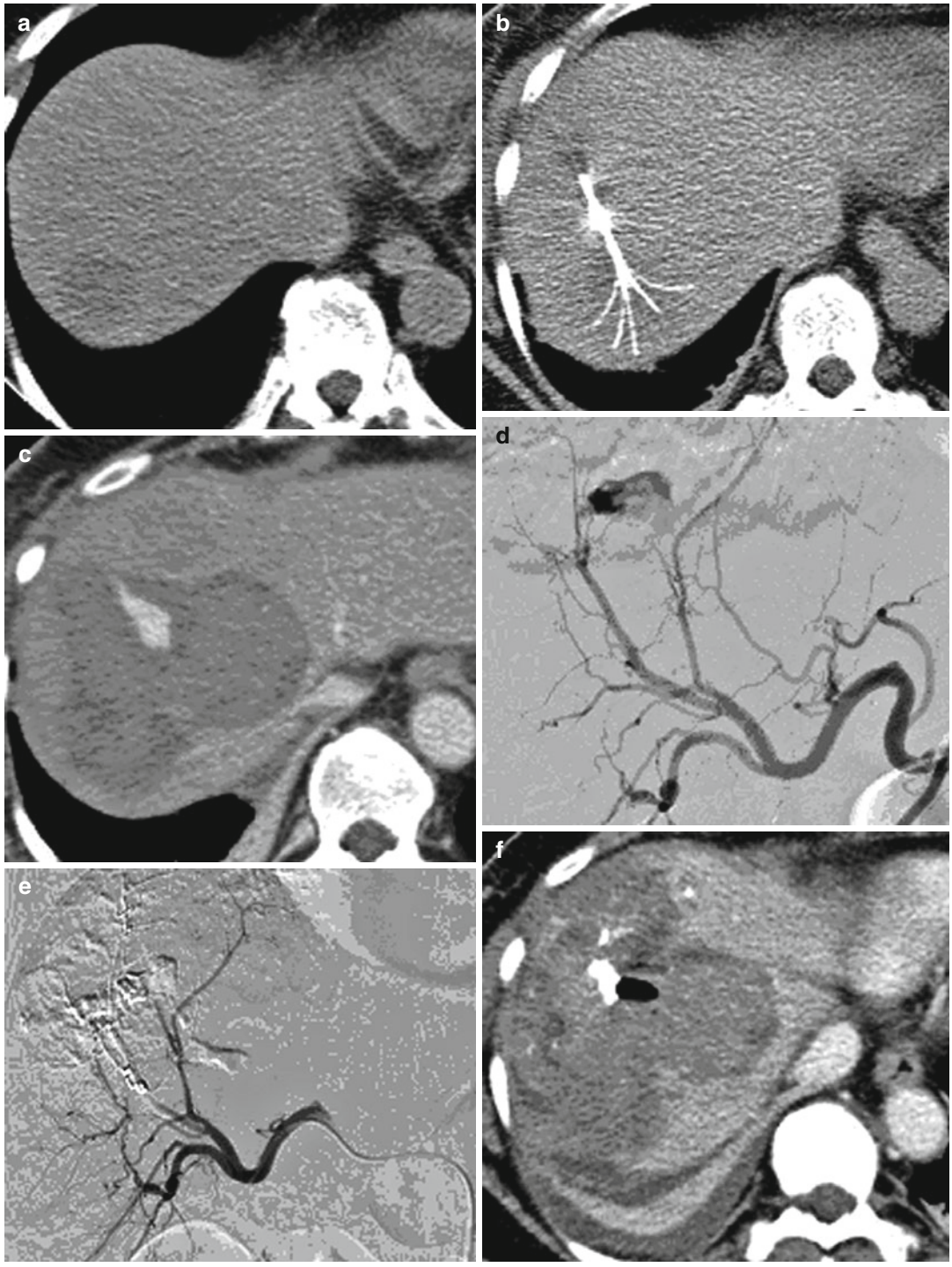
a
b
c
d
e
f

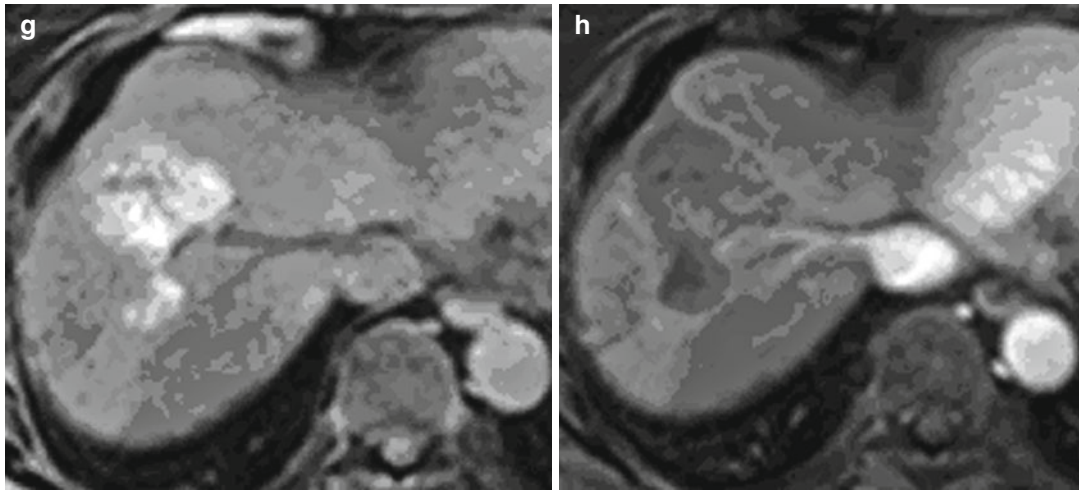

Fig. 13.11 (continued)

system, or a bilioenteric anastomosis usually promote infectious complications. Although infectious complications in total seem to be rare (about 1.5 %), de Baere et al. (2003) found a significantly higher incidence of liver abscesses in patients with a bilioenteric anastomosis. Patients who underwent a Whipple procedure, for example, were jeopardized by colonization of the biliary tract by ascending infections and consecutive abscess formation within the ablation volume. Any persistent or recurrent fever in the 2–3 weeks after RF ablation should increase awareness concerning infectious complications such as abscess formation. In fact, such patients can be treated interventionally by placing a drainage under image guidance. Additionally, there seems to be an increased risk for infection also in patients who previously underwent lipiodol embolization for HCC.

Neoplastic seeding along the needle tract usually manifests 3–12 months after RF ablation and is due to the carrying of tumor cells on the probe itself. It was reported in 0.3 % of ablation in the analysis of Mulier et al. (2002), whereas a rate of 12.5 % was found in the study population of Llovet et al. (2001). De Baere et al. (2003) reported seeding also to be rare with 0.5 %. The reason for this significant difference was most likely due to lack of track ablation in study by Llovet and coworkers. In a very recent multicenter study including 1,314 patients with 2,542 HCC nodules by Livraghi et al. (2005), neoplastic seeding was identified in 12 patients (0.9 %); the rates were comparable at the three centers (0.9, 0.7, and 1.4 %). Only previous biopsy was significantly associated with tumor seeding ($p=0.004$). Jaskolka et al. (2005) found three statistically significant risk factors for needle tract seeding in 200 patients treated 298 times with RF ablation for different hepatic tumors: treatment of a subcapsular lesion (odds ratio, 11.57; $p=0.007$), multiple treatment sessions (odds ratio, 2.0; $p=0.037$), and multiple-electrode placements (odds ratio, 1.4; $p=0.006$). The risk can be almost eliminated if the RF probe is properly positioned on the first pass and does

Fig. 13.11 CT demonstrates a hypodense focal lesion in liver segment 7 (*arrow*), representing the breast cancer liver metastasis (**a**). CT-guided RF ablation was performed. CT shows the RF probe at the posterior rim of the tumor (**b**). Contrast-enhanced CT scan showed an active arterial bleeding (*arrow*) with a consecutive huge intrahepatic hematoma (**c**). The subsequently obtained selective diagnostic angiogram demonstrates a laceration of the segment 8 artery with pathological extravasation of contrast media (**d**; *arrow*). The vessel was selectively embolized with coils and a histoacryl-lipiodol mixture. The control angiogram shows no evidence of further active arterial bleeding (**e**). The corresponding contrast-enhanced CT-scan post-bleeding embolization shows the hematoma without evidence of an active bleeding site (**f**). Follow-up MR imaging (native and contrast-enhanced T1-weighted images) 8 months after embolization shows a marked decrease of the intrahepatic hematoma and no viable tumor (**g**, **h**)

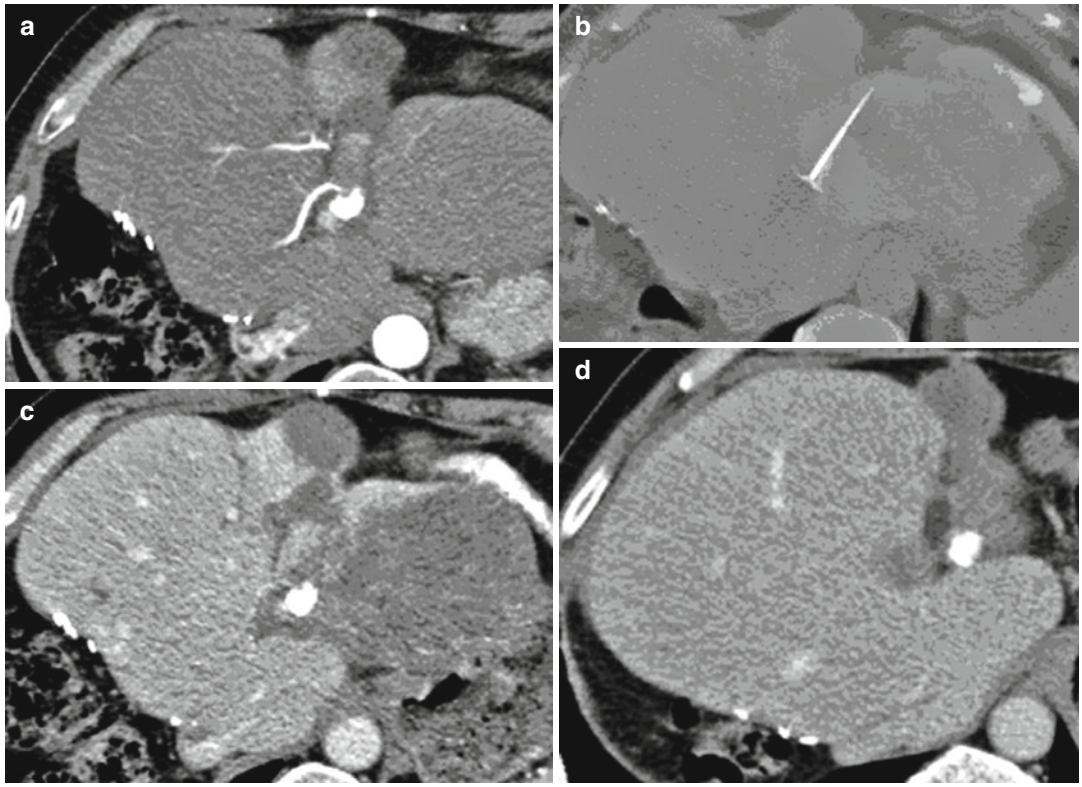

Fig. 13.12 Hepatic infarction of liver segments 2 and 3 after RF ablation for a recurrent HCC nodule adjacent to the falciforme ligament. CT demonstrating a recurrent HCC nodule in liver segment 3 adjacent to the falciforme ligament after transarterial chemoembolization with nodular contrast enhancement during arterial phase scan (**a**; *arrow*). Note the formerly treated HCC presents still with some Lipiodol uptake. CT with the RF probe exactly within the recurrent HCC nodule (**b**). 24 h after the procedure, CT reveals a complete necrosis of liver segments 2 and 3 (**c**). 18 months post-RF ablation, CT demonstrates nearly complete shrinkage of liver segments 2 and 3 with no evidence of tumor recurrence (**d**)

not cross the tumor. A sufficient safety margin around the tumor and removing the probe by additional ablation of the needle tract will further lower the risk of tumor cell spread (Fig. 13.6).

Complications related to the thermal ablation itself include unintentional thermal harm to nontargeted areas, burns at the dispersive electrodes, and interference with metallic implants such as pacemaker wires and cardioverter defibrillators. Therefore, exact selection and consecutive placement of the dispersive electrodes are crucial to minimize the risk for pad skin burns. There is an increased risk of pad burns which closely correlates with the amount of energy delivered if the grounding pads are too small or not equidistant from the active electrode in monopolar systems. In consequence, more or larger grounding pads should be used if more power is applied. If the contact of the dispersive electrodes with the skin surface is not sufficient (e.g., by sweat or hairs under the pad), the RF power is not dispersed efficiently and "spots" of high current flow may be generated, resulting in burns. Defects in the electrode's insulation or metallic coaxial introducers, which may act as secondary antenna by induction, can also create burns at the skin entry site.

To prevent unintentional burns to anatomical structures within the vicinity of the targeted

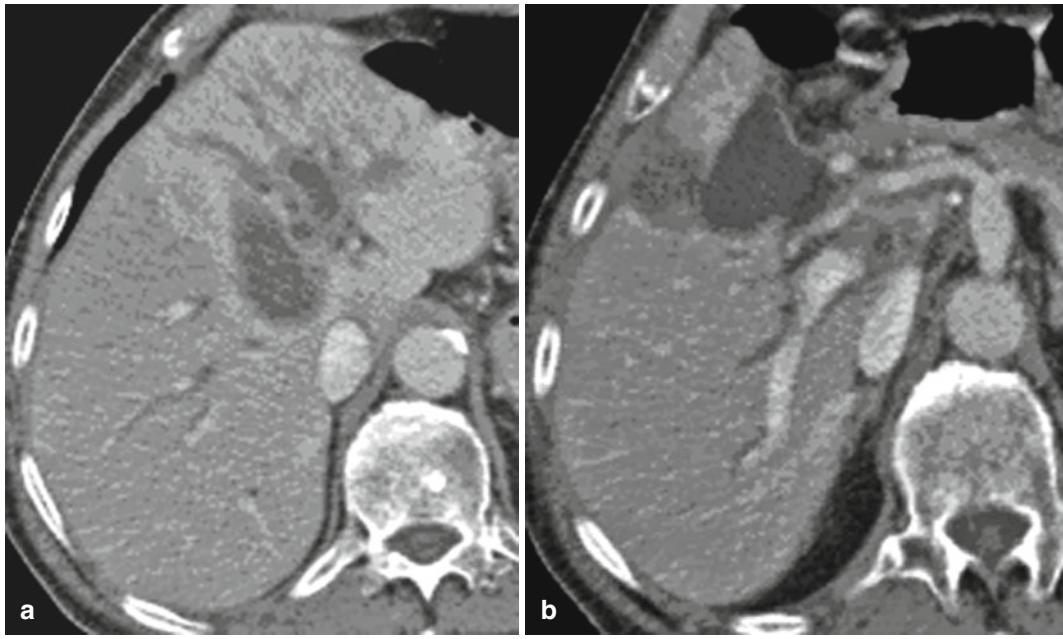

Fig. 13.13 Biliary leakage with consecutive biloma and cholestasis of the right hepatic lobe and bile duct necrosis of the left main duct with consecutive, massive cholestasis of the left liver lobe after laparoscopic RF ablation in a patient with multifocal colorectal liver metastases: contrast-enhanced CT scan 3 weeks post-laparoscopic RF ablation demonstrates cholestasis of the left and right liver lobe (**a**) accompanied by a biloma (**b**; *arrow*) adjacent to two RF ablation zones (**a**, **b**)

ablation area, a thorough planning of the access route and final probe placement may help to avoid damage of such structures, for example, the gallbladder, the bile ducts (Fig. 13.13), or the renal calices. In clinical reality, the vascular heat-sink effects, the peritoneal surfaces, and the motility/mobility of some organs such as stomach and large bowel may also have some protective properties. Nevertheless, there are some reports documenting the fatal outcome of secondary thermal damage to the stomach or bowel (Choi et al. 2001; Meloni et al. 2002; Livraghi et al. 2003b; Rhim et al. 2003). Particularly after previous surgery, where intra-abdominal adhesions may fix the stomach or bowel to the surface of the liver surface, there is an increased risk of thermal damage to these organs. Dislodgement by air insufflation or glucose injection will protect these structures at risk. A recent report by Song et al. (2009) documented the feasibility and efficacy of artificial ascites in 143 patients with HCC abutting the diaphragm or bowel. Additionally, cooling of adjacent structures such as bile ducts via interventionally placed tubes may also prevent secondary thermal damage (Fig. 13.14). Therefore, collateral damage to vital structures can be generally avoided if organ-specific anatomical peculiarities are considered.

There is clear evidence that the patient's condition during the procedure can be affected by changes of the metabolic status of the patient such as changes in blood pressure, heart rhythm, hormonal reactions, or sensations of pain. The so-called metabolic complications are mainly dependent on the underlying or accompanying disease; therefore, it is mandatory to know the patient's medical condition prior to RF ablation to address any necessary additional medication ahead of a potential complication.

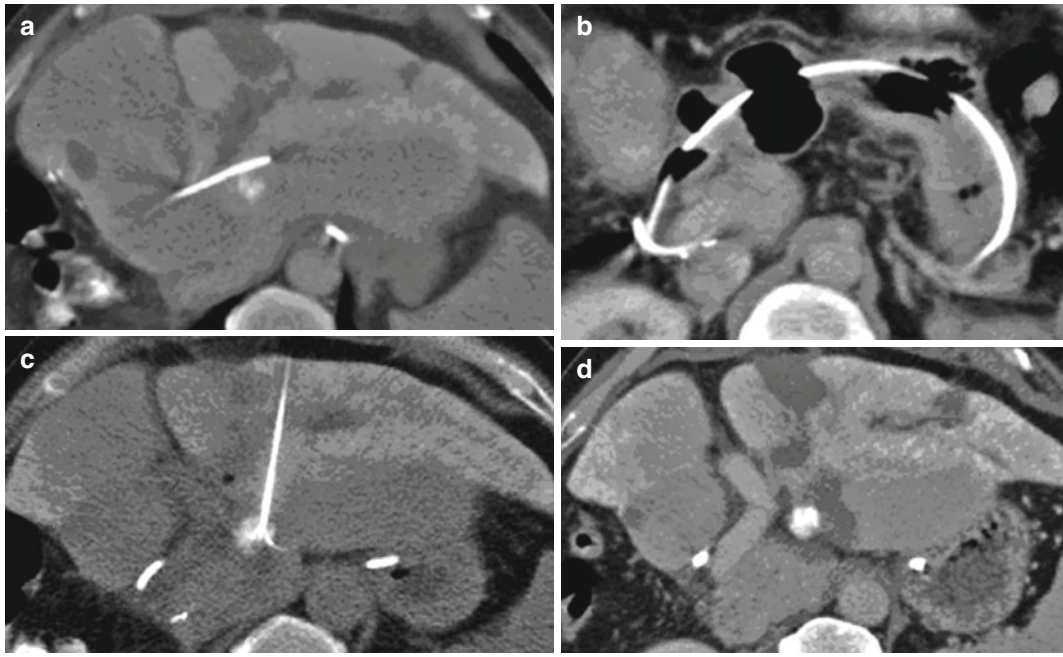

Fig. 13.14 CT shows a recurrent HCC nodule in liver segment 3 after transarterial chemoembolization (**a**; *arrow*). Note the nasobiliary tube adjacent to the tumor. CT scan demonstrating the endoscopically placed nasobiliary tube that was used for continuous cooling of the adjacent bile ducts (**b**). CT scan with the RF probe already placed within the center of the tumor (**c**; *arrow*). 24 h post-RF ablation, the ablation zone entirely encompasses the tumor nodule without any collateral damage (**d**; *arrow*)

Summary

The liver is frequently affected by metastases of different tumor entities. Surgical resection provides the greatest potential for cure in patients with secondary liver tumors; however, surgery can be offered only to a small number of patients (5–20 %). In selected patients, image-guided, minimally invasive treatment such as percutaneous RF ablation takes the role as a palliative treatment option with a potential curative intention, especially in patients who are technically and/or medically not eligible for surgery. According to the BCLC guidelines, RF ablation has a clear indication in patients not eligible for surgery and suffering from early-stage HCC with one to three nodules of 3 cm or less. In selected patients with very early HCC, it seems that RF ablation might be the treatment of choice despite operability. The effective and reproducible tumor destruction of RF ablation is accompanied by an acceptable mortality and morbidity. Although usually "unfavorable" patients in a highly palliative situation are treated with RF ablation, local tumor control by RF ablation is often as good as or even better than systemic chemotherapy. Combination of RF ablation with other treatments is an area of ongoing active research. It is highly desirable to implement local ablative therapies such as RF ablation in the treatment algorithm for non-resectable liver tumors not only as third-line but also as second- or first-line treatment in early HCC probably, in metastatic disease, in combination with systemic chemotherapy. RF ablation should always be embedded in a multidisciplinary treatment strategy tailored to the individual patient and to the features of the disease ("customized therapy"). Patient selection is very crucial for successful treatment with RF ablation. It should be based upon the tumor site and size, proximity of large vessels, bleeding risk, respiratory motion, probe pathway, and last but not least physician's experience. The technique is operator dependent with a steep learning curve. Until the role of RF ablation within a multimodal treatment strategy for liver tumors is completely defined, RF ablation should be restricted to centers with highly experienced interventionalists incorporated into an interdisciplinary oncology team.

Because follow-up imaging is crucial in determining therapy success, imaging of ablation should only be performed by physicians experienced with RF ablation. To further assess the role of RF ablation in tumor patients, multicenter trials, more long-term follow-up data, further refinements in technique and procedure-related features, and studies of combined treatments, including all therapies available for liver tumors, must be evaluated with respect to the current therapeutical reference standard to date.

Key Points

- Tumors with a size of 3.5 cm or less are ideal candidates for ablation.
- Tumor characteristics such as vascularity need to be considered for treatment planning with embolization and multiple probe positions being suited measures to enhance treatment efficacy.
- Thorough planning of the access route to prevent complications. "Hot" probe repositioning and removal to prevent tumor seeding and bleeding.
- Intention of "complete" tumor ablation is a significant prognostic factor.
- Close follow-up is needed as "post-ablation is pre-ablation."
- Close cooperation with surgeons and oncologists is needed as tumor treatment is always a multidisciplinary issue.

13.1.3 RF Ablation of Lung Tumors

Arnd-Oliver Schäfer

13.1.3.1 Introduction

Lung cancer is among the most commonly occurring malignancies and continues to be the leading cause of cancer death worldwide (Jemal et al. 2010). Non-small-cell lung cancer (NSCLC) comprises approximately 80 % of primary malignant tumors of the lung. Surgical resection is the treatment of choice for early-stage NSCLC. Patients with NSCLC are frequently poor surgical candidates owing to coexistent chronic obstructive bronchopneumopathy or other underlying diseases. However, when lung cancer is detected at an early stage, the outcome of patients is significantly improved, with 5-year survival rates ranging from 43 to 77 %. Unfortunately, NSCLC tends to recur even after successful resection (Asamura et al. 2008; Mountain 1997; Van Rens et al. 2000). Conventional treatment of inoperable or unresectable patients with systemic chemotherapy and external-beam radiation therapy has not been satisfactory in terms of survival. The median survival has been reported to be less than 1 year after chemotherapy alone (7.1–9.9 months) or radiation therapy alone (9.7–10.3 months). Despite combined use of both treatments, the survival rates have not been greatly improved (10.4–13.8 months) (Akeboshi et al. 2004). However, substantial technical improvements such as three-dimensional conformal radiation therapy and stereotactic ablative radiotherapy are promising regarding improvements in outcome (Das et al. 2010).

Lung parenchyma represents the second most frequent site of metastatic spread from various malignancies, for example, in patients with colorectal carcinoma. And although lung resection can achieve a 5-year survival rate of 20–40 % (Yan et al. 2007), it is limited to only a small proportion of patients. Furthermore, surgery is often precluded by the number and the location of metastatic lesions. The high risk of recurrence in patients with metastatic disease and the need to remove the healthy lung call for alternative therapeutic procedures. Attention has therefore been focused on interventional treatment options such RF ablation, which achieves tumor destruction in patients with unresectable primary or secondary lung malignancies. Although RF ablation cannot realistically be expected to reach the same degree of tumor eradication as complete lobar resection, patients may experience survival benefit and relief of symptoms. RF ablation can also be used as an adjunct to chemotherapy and radiation therapy.

13.1.3.2 Indications

In the light of the current literature, there are two groups of patients who have to be considered suitable candidates for lung RF ablation: patients suffering from stages I and IIA NSCLC (Table 13.6) and patients with pulmonary metastases (with a focus on metastases from colorectal cancer) who

Table 13.6 Staging of NSCLC including TNM stages

Stage	TNM	Description
I	T1–T2 N0 M0	Tumor less than 5 cm *and* no metastases to lymph node (N0) *and* no known distant metastases (M0)
IIa	T1–T2 N1 M0	Tumor of 5–7 cm *and* no lymph node metastases (N0) *or* tumor less than 5 cm with lymph node metastases in bronchopulmonary or ipsilateral hilar lymph nodes (N1) *and* no known distant metastases
IIb	T1–T2 N1 M0	Tumor of 5–7 cm *and* with lymph node metastases in bronchopulmonary or ipsilateral hilar lymph nodes (N1) *or* tumor larger than 7 cm, but there are no cancer cells in any lymph nodes *or* no lymph node metastases, but tumor has spread into the chest wall, the diaphragm, the phrenic nerve, or the mediastinal pleura and parietal pericardium or tumor less than 2 cm from the bifurcation *or* any tumor size but more than one tumor in the same lobe of the lung *and* no known distant metastases
IIIA	T3 N0–1 M0, T1–3 N2 M0	Tumor extends into pleura, chest wall, diaphragm, *or* pericardium (T3) *or* lymph node metastases in the ipsilateral mediastinum *or* underneath the carina (N2)
IIIB	Any T4 *or* any N3 M0	Tumor invades mediastinum (i.e., heart, great vessels, trachea, esophagus, bone) (T4) *or* lymph node metastases in lymph nodes at the top of the lung *or* the opposite side of the chest *or* above either collar bone
IV	T1–4, N0–N3, *or* any M1	Any metastatic tumor (M1) *or* tumor in both lungs *or* malignant pleural effusion or pericardial effusion

were considered to be inoperable as a result of the number of tumors and the distribution of tumor spread or poor performance status, especially concomitant cardiovascular disease and chronic lung disease. Therefore, the indications for lung RF ablation are for either definitive tumor therapy (NSCLC) or palliation (metastases). The rationales for palliative therapy are tumor reduction (cytoreductive therapy) prior to systemic chemotherapy and relief of symptoms such as chest pain, dyspnea, hemoptysis, and cough.

Inclusion criteria for lung RF ablation are as follows:

- Patient age 18 years or more.
- Patients who were considered nonsurgical candidates.
- Refusal of surgery.
- Stages I or IIa NSCLC.
- Target tumor not exceeding 3.5 cm in greatest diameter, bigger tumors only in studies.
- Lesions farther than 1 cm from heart, major blood vessels, or airways.
- No invasion of the hilum or mediastinum.
- Number of lesions between one and five per hemithorax.
- Complete resection of the primary tumor in the case of lung metastasis.
- Extrapulmonary metastases are acceptable if they are stable during systemic chemotherapy or if they are not expected to limit life expectancy.
- In patients without a history of extrapulmonary cancer, malignancy of the target lesion has to be proven on histology.

Exclusion criteria for lung RF ablation comprise:

- Lesions adjacent to the major pulmonary vessels, the heart, and the major bronchi
- Bleeding diathesis not responding to medical therapy with an International Normalized Ratio greater than 1.5 and/or a platelet count of 100×10^9 g/l or less
- Significantly compromised lung function, with an expiratory volume in 1 s of less than 0.8–1 l
- Active infection
- Concomitant disease with restricted life expectancy of less than 6 months

The final decision for RF ablation, particularly the exclusion from surgery, needs to be determined by a multidisciplinary team (tumor board) including thoracic surgeons, radiation therapists, oncologists, and interventional radiologists. Written informed consent has to be obtained from the patient prior to treatment.

13.1.3.3 Materials and Techniques

Pre-interventional Patient Management

All patients should undergo an extensive pre-interventional workup including routine physical examination, spirometry, cardiovascular assessment, and imaging-based tumor staging including abdominal and chest CT 2–4 weeks prior to

RF ablation. Staging may be completed by a bone scan. To exclude mediastinal lymph node involvement, PET (or PET/CT) is recommended. Baseline chest CT plays the key role in the diagnostic workup of RF ablation candidates since it determines the number, size, and exact location of the target lesions and provides the terms of reference for all post-interventional follow-up imaging studies. Blood tests focus on the exclusion of renal function impairment and coagulopathy.

Antiplatelet and anticoagulation medications are recommended to be discontinued for at least 2 days prior to the intervention. Routine antibiotic treatment is not required, although some centers prophylactically administer antibiotics, especially in patients with underlying lung disease as well as in elderly or immunocompromised patients with subsequently increased risk of infection. In those cases, a second-generation cephalosporin can be administered intravenously for 2 days starting on the day of the procedure. It should be continued orally for 1 week.

Anesthesiology Care

To date, no consensus has been reached on the optimal anesthesiology care for lung RF ablation. Patients who are considered candidates for the procedure normally have a medium to high risk of undergoing anesthesia, while local anesthesia may not provide adequate pain relief for thermal ablation. To keep the hospitalization short, RF ablation is most frequently performed with the patient in conscious sedation. The combination of a hypnotic drug and a short-half-life analgesic drug enables mild sedation and allows for bearing of pain induced by the ablation procedure and the often uncomfortable position and for cooperation with the operator. Typically recommended agents are fentanyl and midazolam hydrochloride. Conscious sedation requires continuous electrocardiography and pulse oximetry with blood pressure monitoring throughout the entire ablation process. Only a few centers propose epidural block or general anesthesia.

The puncture of the target lesion is performed with the patient under local anesthesia, while sedation is started immediately before the current is turned on. Keeping this order is helpful, as the patients may cooperate and not hold their breath under sedation as needed for the safe puncture of a lung lesion.

RF Ablation Procedure

Percutaneous lung RF ablation is routinely performed under CT guidance, ideally with the use of CT fluoroscopy following standard rules for CT-guided lung biopsy.

First the patient is placed in the appropriate position: supine, prone, or lateral decubitus according to the location of the target lesion. A radiopaque grid is fixed on the patient's skin, and this is followed by a non-enhanced CT scan of the anticipated region with 3-mm section thickness. The shortest path that thoroughly avoids bullae, interlobar fissures, vessels, and bronchi is chosen. Thereafter the skin entry point is marked with a permanent ink marker. Depending on whether a monopolar or a (bipolar) multipolar RF ablation system is used, none or up to four grounding pads are applied to the patient's abdomen, back, or shaved thighs. Using the opposite chest wall for placing the grounding pads is discouraged, as it results in a high electrical field density in the chest, which is particularly cumbersome in the presence of metallic implants or pacemakers. Standard surgical prepping and draping is mandatory. The skin at the needle entry point is cleaned with a 10 % solution of povidone-iodine. Subsequently, 10–30 ml of a local anesthetic such as lidocaine (1–2 %) is instilled using a 22 G needle. Local anesthesia should include the skin and the deep subcutaneous tissue and should reach down to the pleura. To facilitate insertion of the RF probe, a small incision of the skin is performed.

Following accurate preparation, the needle electrode is advanced to the lesion. Needle advancement requires careful planning since minor degrees of misalignment can cause the tip of the needle to miss the target, particularly in small deep lesions. Special attention must be paid to verify the correct placement of the active part of the electrode inside the tumor. Usually it should be placed centrally inside the tumor. If expandable electrodes are used, the prongs should exceed beyond the tumor margin. Care has to be taken to avoid placement of tines into vessels or bronchi. Needle electrodes should exceed the opposite tumor margin by only a few millimeters.

Multiple or cluster electrodes may be used to increase the ablation volume. Owing to multiple passages of the pleura, this approach increases the risk of pneumothorax and should therefore be avoided whenever possible. To prove the correct position of the RF probe, it is strongly recommended to assess the relationship between the needle electrode and the target lesion by assessing axial slices as well as multiplanar reformations (De Baère 2011).

Once the needle electrode has been correctly positioned and connected to the RF generator, the ablation is started. During the ablation, either impedance or temperature or both are continuously monitored and recorded. Treatment algorithms are based on incremental power delivery. The different steps of the procedure should follow the protocols provided by the manufacturers. If expandable RF probes are used, the tines should be withdrawn after one treatment cycle and the electrode rotated about 30–60°. Subsequently, the tines should be redeployed and the ablation repeated, thereby the presence of viable tumor cells beyond the initial area of ablation is minimized (Gillams and Lees 2008). Generally lung ablation requires less energy than hepatic or renal RF ablation because the tumor is insulated by the surrounding air, resulting in heat being trapped inside the lesion.

For lesions that exceed a diameter of 3 cm, overlapping ablations have to be performed to ensure complete ablation. To minimize the risk of pneumothorax, the position of the electrode within the tumor is changed by withdrawing it into superficial lung tissue along its major axis, changing its angle, and then reinserting the probe into the target without an additional passage of the pleura. When technically feasible, the ablation zone should encompass the tumor by at least 1 cm. After the ablation has been completed, the needle electrodes are retracted, and the device is removed. Track ablation is routinely performed with cautery of the access tract on the way out after completion of lesion ablation.

A control CT scan is obtained within 30 min after completion of the procedure. The total duration of the RF procedure varies widely owing to the lesion geometry, lesion size, and RF system used. Ablation times may range from 7 to 100 min (Suh et al. 2003; Lee et al. 2004).

Post-interventional Patient Management

Following lung ablation, the patients should be instructed to stay in bed for 4 h. Chest radiographs are obtained within the first 4 h after the procedure and before discharge to exclude pneumothorax. The hospital observation period can be limited to 24 h in the majority of cases. Patients with a small, asymptomatic pneumothorax are observed in hospital without any specific therapy. In symptomatic patients or large pneumothorax, needle aspiration or a chest tube may be needed. To evacuate small intra-procedural pneumothoraces, needle aspiration can be used, as well as pigtail catheter insertion combined with a Heimlich valve.

Post-interventional Imaging

There has been a lively discussion about the value of different imaging modalities for follow-up. Thin section pre- and post-contrast multi-detector spiral CT is currently most commonly used for follow-up after pulmonary RF ablation, although some authors suggest PET scanning to be superior to CT for the detection of residual or recurrent tumors (Akeboshi et al. 2004; Dupuy et al. 2006; Kang et al. 2004). Others are of the opinion that high-quality CT scans interpreted by an experienced radiologist will be more sensitive to subtle recurrence (Bojarski et al. 2005; Jin et al. 2004; Rossi et al. 2006; Suh et al. 2003).

Post-interventional contrast-enhanced CT scans are acquired on the day following the procedure in order to detect delayed complications. After that, the patients should be reviewed at 1, 3, and 6 months following RF ablation and every 6 months thereafter with dual-phase (including the venous phase) chest CT.

Lesion size is measured and reported as the largest bidimensional diameters. Non-enhanced CT scans are obtained before, during, and immediately after RF ablation. Follow-up CT examinations have to be compared with pre-interventional CT imaging. Decisive findings include:

- Presence and extent of ground-glass opacification
- Patterns of contrast enhancement of the lesion
- Attenuation of the lesion on non-contrast scans
- Peripheral rim enhancement
- Complications

Immediately after RF ablation, non-enhanced CT scans show a decreased attenuation of the tumor and ground-glass opacification enveloping

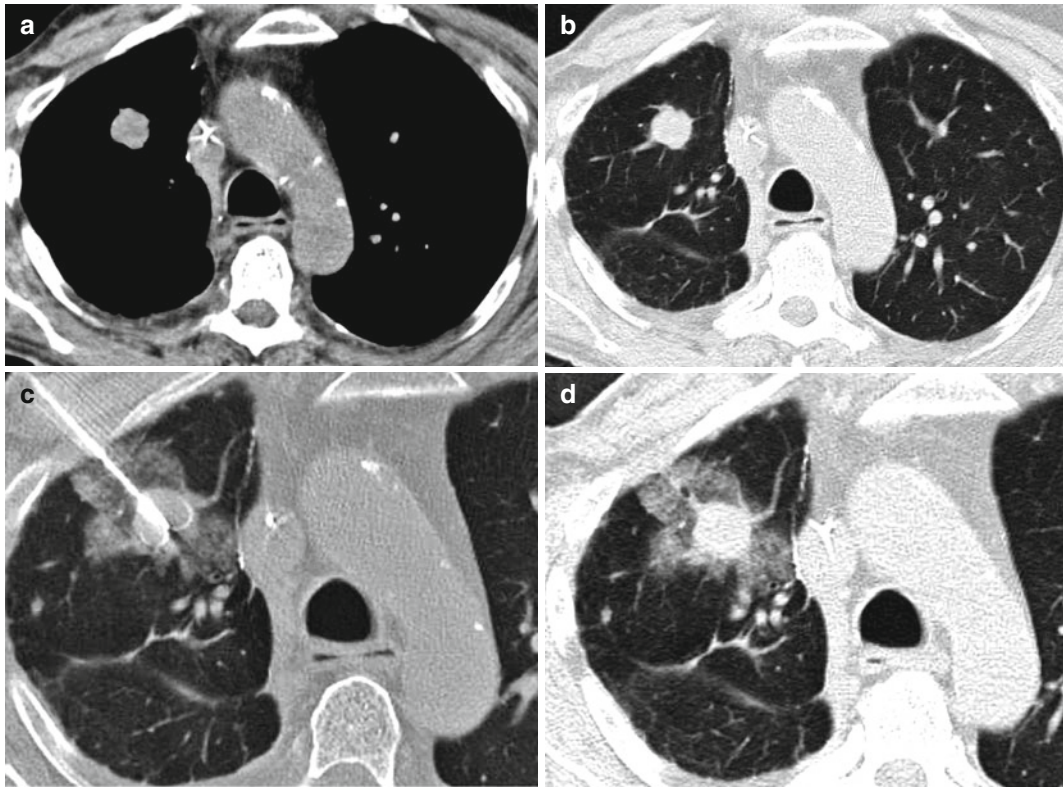

Fig. 13.15 (**a**–**d**) CT-guided RF ablation of a colorectal pulmonary metastasis of the right upper lobe (**a**, **b**). During insertion of the needle electrode, self-limiting, parenchymal hemorrhage occurred (**c**). The CT scan immediately after RF ablation displays enlargement of the treated metastasis surrounded by ground-glass opacity of the lung parenchyma in the vicinity of the lesion, indicating successful treatment (**d**)

the treated zone. The thickness and pattern of ground-glass opacity is one of the most reliable predictors of treatment success (Fig. 13.15). Ground-glass opacifications should extend more than 5 mm beyond the margins of the treated tumor. They likely represent localized edema and hemorrhage. If the tumor is only incompletely surrounded by ground-glass opacifications immediately after the procedure, the intervention should be continued.

On initial contrast-enhanced CT, a well-demarcated non-enhanced zone is visible. Tumor necrosis is considered complete if the non-enhanced area at the treatment site has a diameter greater than or equal to that of the treated tumor. All contrast-enhancement profiles within the ablation zone should remain lower than those prior to the procedure. Any portion of the treated lesion that is enhanced by more than 15 HU when compared with the initial post-interventional images after contrast material administration is highly suspicious of local tumor recurrence. Within 6 months after ablation, a circumferential rim of enhancement no larger than 5 mm around the ablation zone is considered to be reactive.

Local tumor progression is defined as tumor growth from the zone of ablation, whereas local treatment success is defined as involution of the ablation zone over time. However, owing to intratumoral hemorrhage, the treated lesion may increase in size, but will start shrinking after a few months (Fig. 13.16). If the size of the ablation zone does not decrease by at least 25 % between 6 and 9 months after ablation, PET is recommended to assess metabolic activity. Two characteristic types of local recurrence are described following RF ablation of the lung. The most common type is seen as enlargement of parts of the ablation zone with or without contrast enhancement. A different type of local relapse is represented by the development of tumor nodules adjacent to the ablation zone.

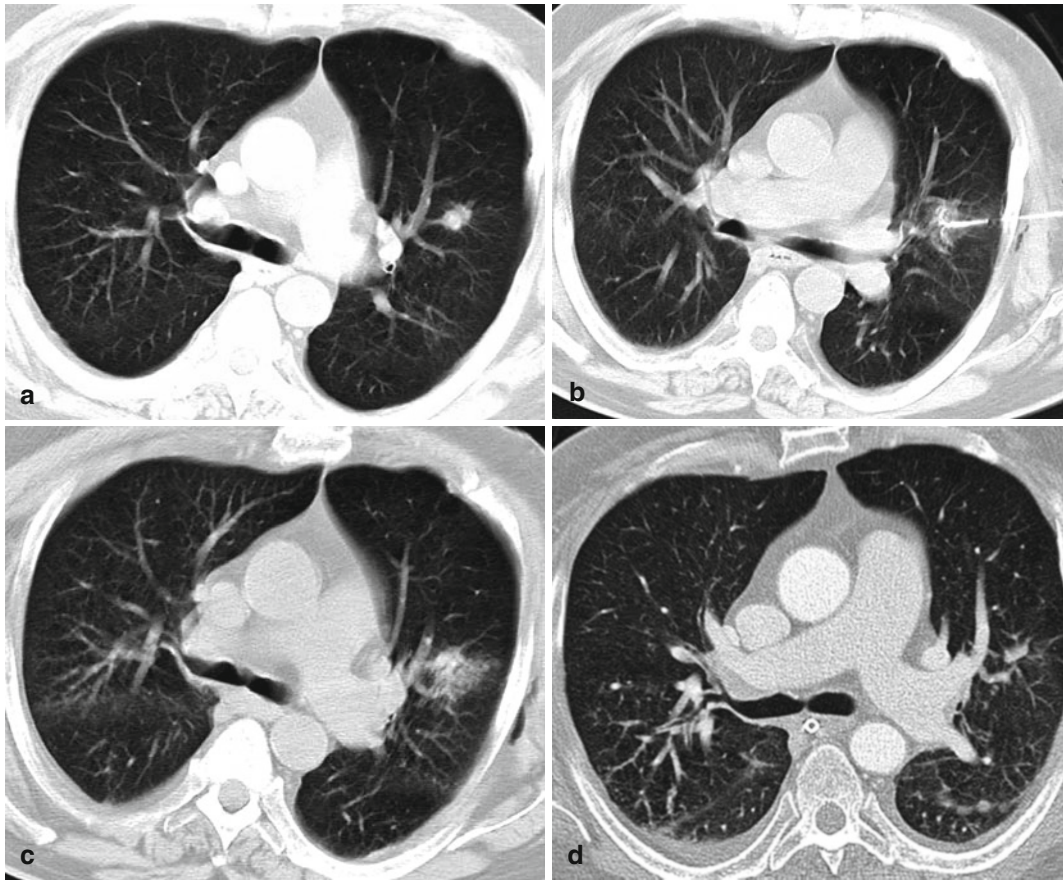

Fig. 13.16 (**a**–**d**) CT-guided RF ablation procedure of an early-stage non-small-cell lung cancer (NSCLC) in the left upper lobe adjacent to a major pulmonary artery (**a**). Enfolded jack hooks of an expandable needle electrode within the tumor (**b**). The control scan reveals ground-glass opacification encompassing the treated tumor nodule (**c**). Follow-up CT after 6 months demonstrates considerable shrinkage of the coagulation necrosis indicative of successful tumor treatment (**d**)

As neither change in tumor shape and size nor enhancement pattern unequivocally predicts complete ablation, CT-guided biopsy and histological analysis in combination with the CT findings may be used for follow-up (Belfiore et al. 2004). Indeed, biopsy of the ablation zone has been recommended, but sampling error is inevitable as only parts of the treated tumor can be targeted. Thus, the combination of tumor morphology and contrast enhancement seems to be the most practical approach for predicting incomplete treatment and local tumor recurrence.

13.1.3.4 Results

In early clinical experience with lung RF ablation, patients were treated within a framework of feasibility studies to investigate safety, tolerability, and local therapeutic effects of the procedure. The first percutaneous RF ablation of a lung tumor was reported by Dupuy and coworkers in 2000 (Dupuy et al. 2000). However, regardless of the great amount of data on the clinical and radiological response of RF ablation in lung tumors published so far, its efficacy in the mid- and long term still remains poorly understood. Rationales for the existence of residual tumor may be intrinsic heat-resistant properties of a tumor, residual vascular flow, or reperfusion of the ablation zone.

Technical Success and Local Tumor Control

Lung RF ablation was used in a study of 31 patients with 54 tumors, and the initial therapeutic response has been evaluated with both ^{18}F-fluorodeoxyglucose PET and contrast-enhanced CT (Akeboshi et al. 2004). Complete necrosis could be achieved in 32 of the 54 treated

nodules. A significant difference in the rate of complete tumor necrosis was found for tumors 3 cm or less and tumors more than 3 cm in diameter (69 % vs. 39 %). Tumor type did not influence complete necrosis rates. Of note, a recurrence rate of 100 % for tumors exceeding 3.5 cm was reported (Gillams and Lees 2008). Therefore, either more than one ablation procedure or additional therapy is needed when treating tumors exceeding 3.5 cm. Considering current evidence, acceptable results of lung ablation are expected in peripheral, less than 3.5-cm diameter tumors which are not in direct contact with vessels larger than 3 mm. Another interesting finding refers to viable tumor cells beyond the periphery of the ablation zone resulting in tumor recurrence (Gillams and Lees 2008). The cause of this special nodular pattern of recurrence is still unknown and may be based on satellites that were not recognized at the time of initial treatment or cells carried into the parenchyma by the tines of expandable RF electrodes (Fig. 13.17).

In a study conducted on 26 patients with 27 NSCLC and four patients with five lung metastases, complete tumor necrosis could be established in 12 of 32 lesions (38 %) and partial necrosis in 20 of 32 (62 %) confirmed by contrast-enhanced CT during follow-up (Lee et al. 2004). The mean survival time in patients with complete necrosis was 19.7 months, in contrast to 8.7 months for those patients in which only partial necrosis was obtained by RF ablation. Additionally, the results of the study demonstrate excellent palliation of mild hemoptysis (80 %) but a less satisfactory palliation of chest pain (36 %), and cough (25 %).

Twenty-one RF-ablated lung lesions were evaluated with helical CT during follow-up by comparing two groups of patients (complete ablation vs. partial necrosis) (Jin et al. 2004). CT scans obtained after the ablation revealed an increase in mean lesion diameters. In the complete-ablation group, the diameters of the treated lesions decreased at 3, 6, 9, 12, and 15 months when compared with the diameters measured on the immediate post-interventional CT. In contrast, lesion diameters in the partial-necrosis group increased gradually on follow-up CT scans at 9 and 11 months after initial shrinkage.

In a review, Beland et al. investigated recurrence patterns of 79 non-small-cell lung cancers in 79 patients treated with percutaneous RF ablation (Beland et al. 2010). Mean tumor size was 2.5 cm. 15 (19 %) tumors were centrally, and 64 (81 %) tumors were peripherally located. 45 (57 %) patients demonstrated no evidence of recurrence at follow-up imaging (range: 1–72 months). Recurrence was seen in 34 (43 %) patients (range: 2–48 months). Recurrence after RF ablation was local in 13 (38 %), intrapulmonary in six (18 %), nodal in six (18 %), mixed in two (6 %), and distant metastases in seven (21 %) patients. Median disease-free survival was 23 months. Lesion size and tumor stage were predictors of tumor recurrence.

Patient Survival

RF ablation has provided good results for local tumor control in the short-term follow-up; however, reliable data confirming its mid- and long-term efficacy are scarce. De Baère and coworkers treated 97 lung tumors with RF ablation. The authors found 18-month overall survival rates of 76 % for primary tumors and of 71 % for metastases (De Baère et al. 2006). The 18-month lung disease-free survival rates were 44 % for primary tumors and 32 % for metastases.

In another study of 153 patients with 189 consecutive lesions, 602 RF ablations were accomplished in 183 sessions (Simon et al. 2007). Technical success was achieved in 159 (98.1 %) of 162 tumors ablated for local control. Observed residual tumor enhancement immediately after RF ablation was attributed to the close proximity to major pulmonary arteries or veins 3 mm or more in diameter and the subsequent subcytotoxic temperatures recorded at the end of ablation. The Kaplan–Meier median time to death for all patients with stage I NSCLC was 29 months, with estimated 1-, 2-, 3-, 4-, and 5-year survival rates of 78, 57, 36, 27, and 27 %, respectively. For patients with colorectal metastases, the estimated 1-, 2-, 3-, 4-, and 5-year survival rates were 87, 78, 57, 57, and 57 %, respectively. Local tumor progression rates over time turned out to be significantly lower in patients with smaller index tumors (smaller than 3 cm vs. larger than 3 cm). The calculated Kaplan–Meier median time to progression for tumors 3 cm or smaller was 45 months, with estimated 1-, 2-, 3-, 4-, and 5-year progression-free rates of 83, 64, 57, 47, and 47 %, respectively, while the median time to progression for tumors larger than 3 cm was 12 months, with

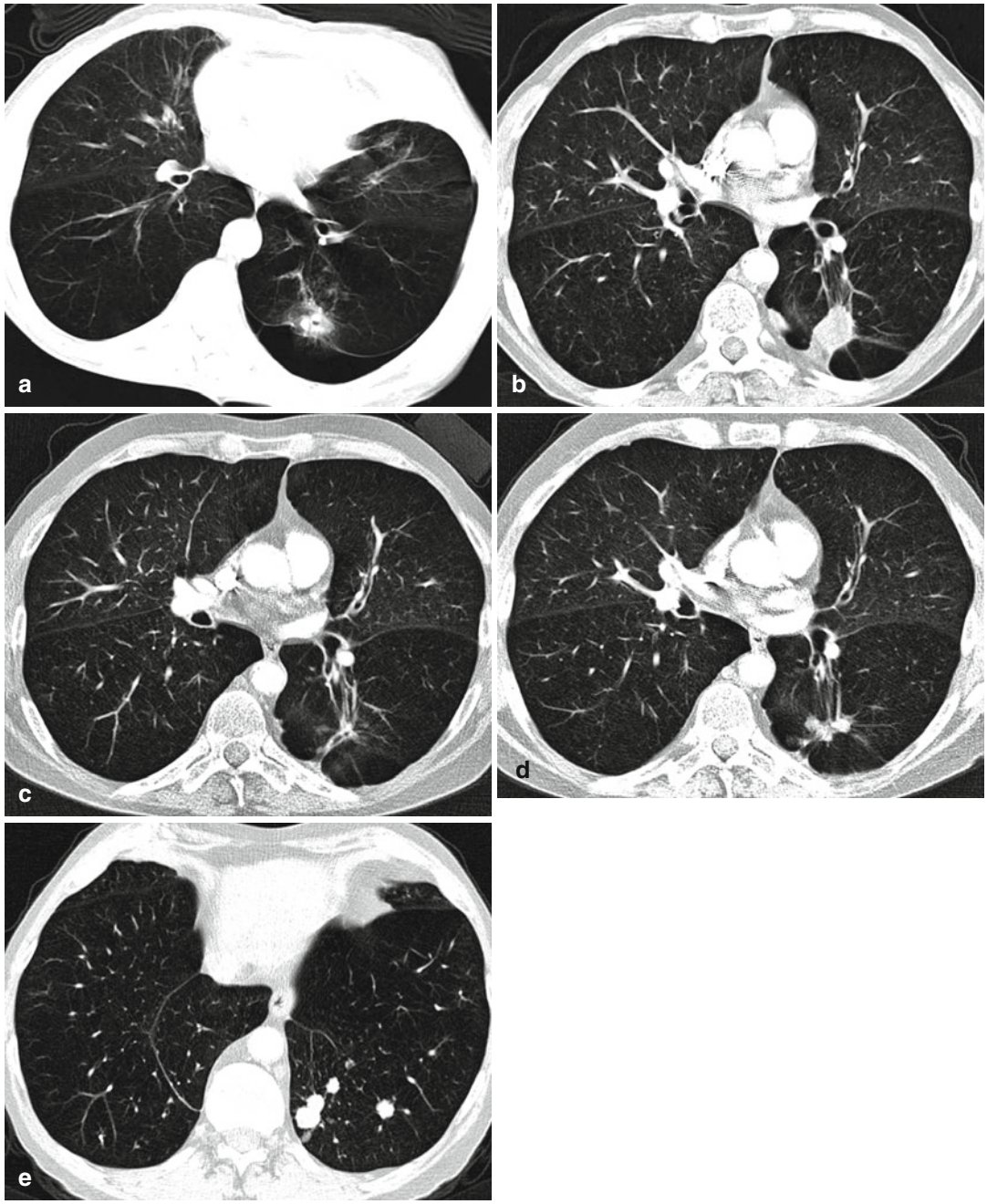

Fig. 13.17 (**a**–**e**) Small intra-procedural pneumothorax occurred during percutaneous RF ablation of an early-stage NSCLC of the left lower lobe (**a**). Note the underlying lung emphysema. On the follow-up CT scan after 3 months, the treated tumor increased in size, exhibiting pleural contact in the region of the needle entry (**b**). The CT scan 6 months after the procedure reveals shrinkage of the ablation zone with scar formation (**c**). On the CT scan 12 months following RF ablation, local recurrence is visible, arising from both the ablation zone and the surrounding lung parenchyma, where a number of newly diagnosed satellites can be detected (**d**, **e**)

estimated 1-, 2-, 3-, 4-, and 5-year progression-free rates of 45, 25, 25, 25, and 25 %, respectively.

Yamakado et al. reported an intrapulmonary total recurrence rate of 47 % after RF ablation within a mean follow-up of 19 months (Yamakado et al. 2007). Not surprisingly, the local tumor progression rate was 11 % in patients with tumors 3 cm or smaller and 50 % in those with tumors larger than 3 cm. Of the 33 patients with pulmonary recurrence, 19 patients underwent repeat lung RF ablation. The 1-, 2-, and 3-year survival rates were 84, 62, and 46 %, respectively. The median survival time was 31 months. Tumor size and extrapulmonary metastases represented significant independent factors affecting prognosis in the study.

Furthermore, a follow-up study of RF ablation for pulmonary colorectal metastases demonstrated a median survival of 32 months with 1-, 2-, and 3-year survival rates of 75, 63, and 45 %, respectively (Yan et al. 2007). The size of the largest pulmonary metastasis, proximity of metastases to major pulmonary vessels, pre-lung-RF-ablation carcinoembryonic antigen level, and post-lung-RF-ablation carcinoembryonic antigen level were found to be predictors of survival.

Recently the results of a study on long-term outcome of RF ablation of lung metastases were reported (Chua et al. 2010). Of 148 patients treated, 66 patients (46 %) had a complete response, 38 patents (26 %) had a partial response, 57 patients (39 %) had stable disease, and 23 patients (16 %) had progressive disease. The median progression-free survival was 11 months. The median overall survival was 51 months with and 3- and 5-year survival rates of 60 and 45 %, respectively. Disease-free interval and response to treatment were found to be independent predictors for overall survival.

13.1.3.5 Complications

Mortality

So far, no intra-procedural deaths have been reported for lung RF ablation. However, in a large series, the overall 30-day mortality rate was 3.9 % (six of 153 patients), with four deaths (2.6 %) being believed to be procedure related (Simon et al. 2007). In another study, a procedure-related mortality rate of 0.9 % was reported (Sano et al. 2007).

Morbidity

From the preliminary experiences, lung RF ablation seems to be associated with an acceptable rate of adverse events that can be divided into three groups according to the criteria of the Society of Interventional Radiology Technology Assessment Committee and the International Working Group on Image-Guided Tumor Ablation (Goldberg et al. 2005):

1. Major complications
2. Minor complications
3. Side effects

A major complication is defined as an event that leads to substantial morbidity and disability and increased level of care, or results in hospital admission or substantially lengthened hospital stay. This includes any case in which a blood transfusion or interventional drainage procedure is required. All other complications are considered minor. Side effects were considered undesired consequences of the procedure that, although occurring frequently, rarely result in substantial morbidity.

Reported overall morbidity rates vary widely in the range from 15.2 to 64.9 % (Ambrogi et al. 2006; Fernando et al. 2005; Huang et al. 2011; Sano et al. 2007). Mostly minor complications were reported; however, Sano et al. (2007) noted a major complication rate of 17.1 %. Pneumothorax is one of the most common complications of lung RF ablation, occurring in 30–51.2 % of procedures (Steinke et al. 2004; Sano et al. 2007). It may be associated with central location of the tumor, obstructive airway disease, emphysema, and multiple electrode insertions. Aspiration may be needed in up to 9 % of cases and chest tube placement in 11.8 % of cases (Sano et al. 2007). The number of ablated lung lesions and the duration of the ablation procedure are two important risk factors closely associated with overall morbidity, pneumothorax, and chest drain requirement.

The majority of patients treated with RF ablation experience mild to moderate pain during the procedure. Asymptomatic pleural effusion and development of post-ablation syndrome consisting of mild fever and fatigue for several days are other common side effects after lung ablation. Acute hemorrhage can occur after probe insertion, which is demonstrated on control CT scans

as sudden opacification surrounding the electrode. As it is self-limiting in the vast majority of cases, it rarely requires additional treatment. Cavitation can also be observed as a result of the RF ablation. In most cases cavitation resolves spontaneously within 3 months after the procedure. Sometimes it may persist for up to 1 year. Only a few patients develop infection at the site of cavitation requiring hospitalization and antibiotic treatment. Malignant seeding along the needle tract is another extremely rare complication. The track ablation procedure at the end of procedure should render this serious adverse event unlikely.

In summary, major procedure-related complications include:

- Pneumothorax requiring chest tube placement
- Pleural effusion requiring intercostal drainage
- Massive hemorrhage
- Pneumonia
- Lung abscess
- Empyema
- Bronchopleural fistula
- Acute respiratory distress syndrome

Minor complications following lung RF ablation comprise:

- Intraparenchymal, self-limiting hemorrhage
- Hemosputum lasting 1–2 weeks after ablation
- Nausea and/or vomiting
- Subcutaneous emphysema
- Dyspnea
- Cough
- Skin burn
- Atelectasis
- Subileus
- Myalgia

Summary

CT-guided percutaneous lung RF ablation is a promising minimally invasive technique for the treatment of inoperable early-stage NSCLC and pulmonary metastases. So far, it is difficult to determine the true clinical efficacy of RF ablation, especially since the reported follow-up periods tend to be short and some recurrences may remain undetected. However, all recent clinical trials have reported a good local response and an acceptable rate of complications. Nevertheless, its role in the treatment of lung malignancies is promising, and the clinical acceptance is evolving.

Lung ablation can be used as an adjuvant therapy to systemic anticancer treatment, including chemotherapy or radiation therapy, to decrease the tumor cell volume with reasonably low morbidity and mortality in the otherwise severely ill patient. Furthermore, it could be a powerful alternative to surgical treatment or chemotherapy, particularly in selected patients with tumors smaller than 3 cm in diameter, who have combined medical illnesses or limited functional lung reserve (Fig. 13.18). Since lung tumors cause debilitating symptoms such as cough, hemoptysis, and pain, percutaneous lung RF ablation may also have a role in improving the quality of life even in this patient group with a palliative intent.

Key Points

- Select patients carefully, taking into account selection factors such as expected survival, size, number, and location of pulmonary lesions.
- The final decision to perform RF ablation is made in an interdisciplinary consensus with the referring physicians and the individual patient.
- Adequate local anesthesia of the puncture site and an appropriate dose of intravenous sedation are imperative to minimize the irritation to the pleura and to facilitate the procedure.
- Whenever possible, treat lesions of one hemithorax in a single session; at the beginning, select patients with a maximum of two lesions per hemithorax and a diameter of 3 cm or less.
- Avoid multiple needle insertions.
- Control the RF ablation process by using repeated CT scans. Close patient monitoring during the course of the intervention is mandatory.

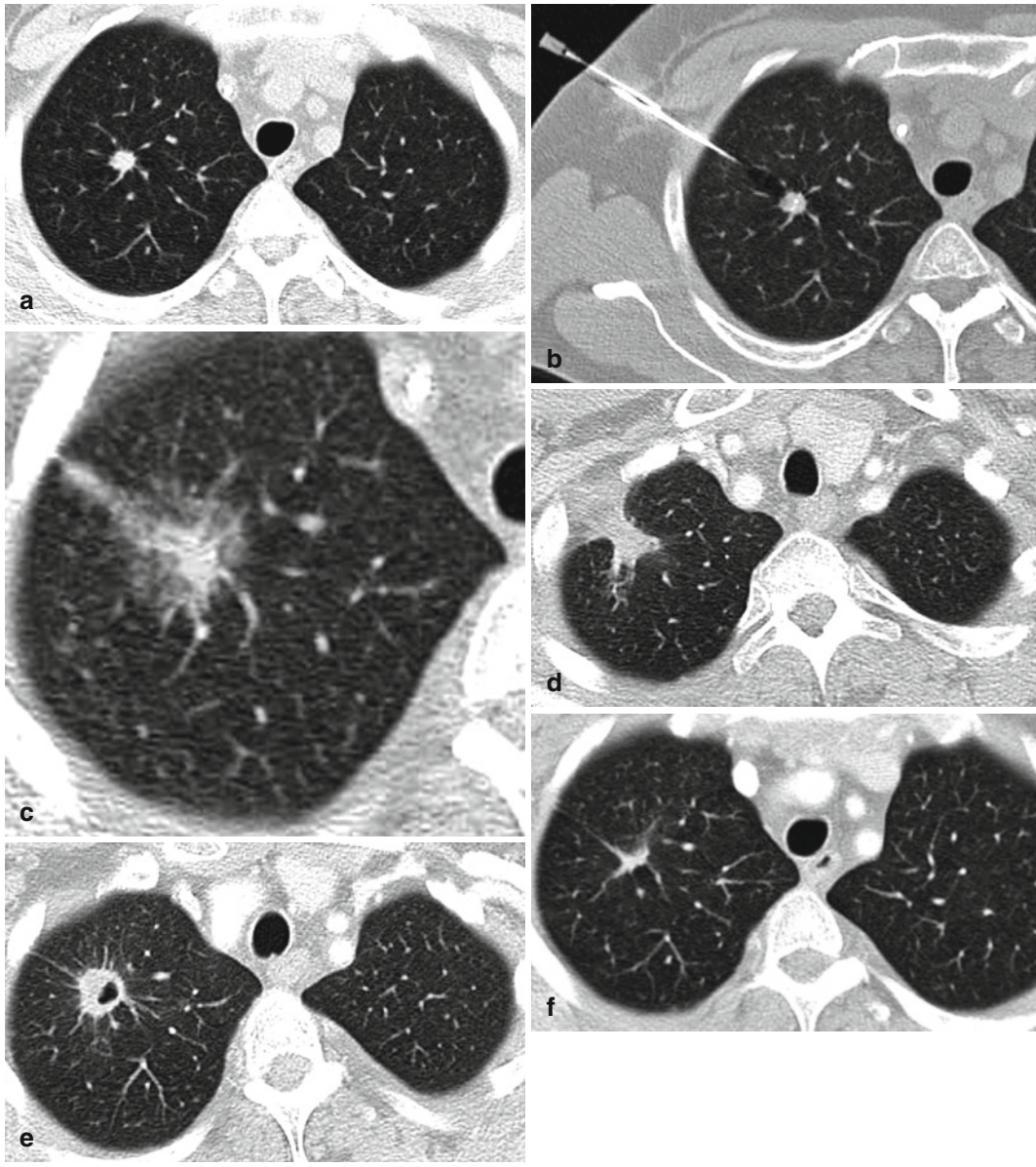

Fig. 13.18 (**a**–**f**) RF ablation of a small NSCLC in the right upper lobe (**a**). Needle electrode placement using a tandem technique with a second needle for guiding the RF probe resulting in a central position of the enfolded tines (**b**). Post-ablation needle track hemorrhage and typical ground-glass opacification indicating a successful procedure (**c**). The control scan after 3 months shows enlargement of the treated tumor and thickening of the pleura in the region of the former needle entry site (**d**). On follow-up CT after 6 months, central cavitation can be differentiated (**e**). Follow-up CT 2 years after the ablation procedure reveals scar formation with no signs of local recurrence (**f**)

- Management of major complications is a cornerstone of the procedure.
- Record and report all adverse events precisely.
- Propose a structured clinical and imaging follow-up protocol, including dual-phase CT scans in the close post-procedural period, after 4 weeks, 3 months, and 6 months, and in intervals of 3–6 months thereafter.

13.1.4 Renal Radiofrequency Ablation

Andreas H. Mahnken

13.1.4.1 Introduction

In 2012 the American Cancer Society estimated 64,770 new cases of cancer of the kidney and the renal pelvis, accounting for 12,890 deaths (Siegel et al. 2012). Beside sporadic tumor occurrence, several hereditary syndromes are associated with an increased risk of renal cell carcinoma (RCC), of which von Hippel–Lindau disease is the most recognized with up to 45 % of affected patients developing one or more RCC during their lifetime (Herring et al. 2001). Historically RCC was detected by flank pain and hematuria, but with introduction of cross-sectional imaging techniques like ultrasound (US) and computed tomography (CT), renal tumors are increasingly detected at earlier asymptomatic stages (Pantuck et al. 2001). Nowadays about two-thirds of all RCCs are discovered incidentally (Homma et al. 1995). Tumor stage and histological tumor type are most relevant prognostic factors. As small tumors (≤4 cm) rarely metastasize, there is a rationale for local therapy of small RCCs. This knowledge was used when nephron-sparing surgical techniques like partial nephrectomy via an open or laparoscopic approach were established in clinical routine (Uzzo and Novick 2001). The 10-year tumor-free survival rates are greater than 85 %, equaling the result of open surgical nephrectomy (Fergany et al. 2000). These findings gave way for the introduction of new therapeutic concepts including minimal-invasive, energy-based treatment options of which radiofrequency (RF) ablation has evolved as the most commonly used technique.

13.1.4.2 Indications

First of all, even before considering RF ablation as a treatment option in suspected RCC, a recent (not older than 2 weeks) contrast-enhanced cross-sectional imaging study (CT or MR) needs to be obtained. Thoracic and abdominal imaging is needed to perform pre-interventional staging because the number of lesions, tumor size, location, and extrarenal tumor manifestations may influence the choice of treatment.

From a technical point, RF ablation may be performed open surgically, laparoscopically, or percutaneously. From animal experiments the results of the different approaches toward the kidney are known to be comparable (Crowley et al. 2000). Using the percutaneous approach, RF ablation does not necessarily require general anesthesia. Eventually it can be applied on an outpatient basis. It is technically feasible to treat multiple tumors in both the kidneys. In exophytic tumors ≤3 cm, complete tumor ablation is consistently achieved, while larger tumors may require repeated treatment (Gervais et al. 2005). Generally RF ablation preserves larger amounts of healthy renal parenchyma when compared with surgery. Centrally located tumors are associated with a higher risk of incomplete ablation and thermal damage to the urinary system than exophytic tumors.

From a clinical perspective the treatment strategy has to be adapted to the individual patient. The overall clinical situation including age and life expectancy, physical and laboratory parameters, as well as patient compliance needs to be considered. So far, radical nephrectomy is the gold standard for treatment of RCC against which all other forms of treatment have to be measured. Only recently a retrospective comparison with this standard of reference has been performed indicating no differences in cancer-specific survival between RF ablation and surgery (Takaki et al. 2010). In addition, there is an increasing amount of long-term follow-up data available on renal RF ablation (McDougal et al. 2005;

Table 13.7 Indications and contraindications for renal RF ablation, with the ideal candidate being a patient with an exophytic tumor with a diameter of ≤5 cm

Indication	Contraindication
Exophytic tumor ≤4 cm[1]	Sepsis
Unfit for surgery	Vascular invasion
Solitary kidney	Uncorrected coagulopathy
Multiple renal tumors	
von Hippel–Lindau disease	
(Refractory hematuria)	(Life expectancy < 1y or > 10ys)
(Tumor debulking)	(Severe debilitation)
(Extrarenal tumor manifestation)	(Central tumor location)
(Bosniak III and IV lesions)	

Extended indications and relative contraindications are given in brackets

[1]Larger or more centrally located tumors may be suited for ablation, depending on the expertise of the interventional radiologist

Tracy et al. 2010; Zagoria et al. 2011). Nevertheless, the indication for renal RF ablation is still an individual therapeutic decision that limits renal RF ablation to selected patients. An interdisciplinary consensus between urologists, oncologist, and interventional radiologist is recommended in order to provide the optimal therapy to the patient and to select the right patients for RF ablation.

Considering the above-mentioned basics, RF ablation has to be considered as a treatment option for patients with contraindications for surgery, predominantly patients with comorbid conditions or those who refuse open surgery (Table 13.7). RF ablation is particularly suited for elderly patients with risks for anesthesia. In patients with impaired renal function, solitary kidney, and von Hippel–Lindau disease or in the presence of multiple tumors, it is a viable alternative to nephron-sparing surgery. In these patients, thermal ablation helps to avoid dialysis, as local ablation of renal masses does not negatively affect renal function. Potential palliative indications include the treatment of refractory hematuria (Neeman et al. 2005) or tumor debulking prior to immunotherapy in patients with advanced stage of disease or local tumor recurrence after nephrectomy. RF ablation should be considered the method of choice for local tumor treatment in patients with extrarenal metastases. Due to its minimally invasive character, it can also be considered a therapeutic option in patients suffering from Bosniak III and IV lesions, which have to be considered potentially malignant (Bosniak 1986). However, one has to be aware that salvage surgery may be complicated due to perirenal fibrosis in the area of ablation.

In strictly selected patients, RF ablation may be thought of as an innovative, experimental therapeutic option. Thus, successful RF ablation has been reported from of a Wilms tumor refractory to chemotherapy in a multimorbid child with a solitary kidney (Brown et al. 2005).

Besides treating tumors of the renal parenchyma, this technique might be also applied to transitional cell carcinomas (Schultze et al. 2003). However, transitional cell carcinoma may grow inside the urothelium, unnoticed by current imaging techniques, and may metastasize early. In these patients, RF ablation is restricted as a salvage option.

To achieve local tumor control, it is mandatory to completely coagulate the entire lesion. In centrally located tumors, thermal damaging of the calices and renal pelvis is feared. Therefore, these tumors are considered a relative contraindication, while exophytic tumors are ideal candidates for RF ablation (Gervais et al. 2003) (Fig. 13.19). Some authors also consider tumors at the anterior aspect of the kidney not suited for ablation as this region may not be visualized appropriately using ultrasound and the risk for bowel injury is increased. These limitations, however, can easily be overcome by use of CT guidance and application of additional measures such as hydrodissection. The decision of treating anterior or central lesions depends on the interventionalist's expertise and the availability of protective measures (see below). With adequate precautions, even centrally located renal tumors can be treated successfully.

Currently sepsis, severe debilitation, and uncorrectable coagulopathies and the presence

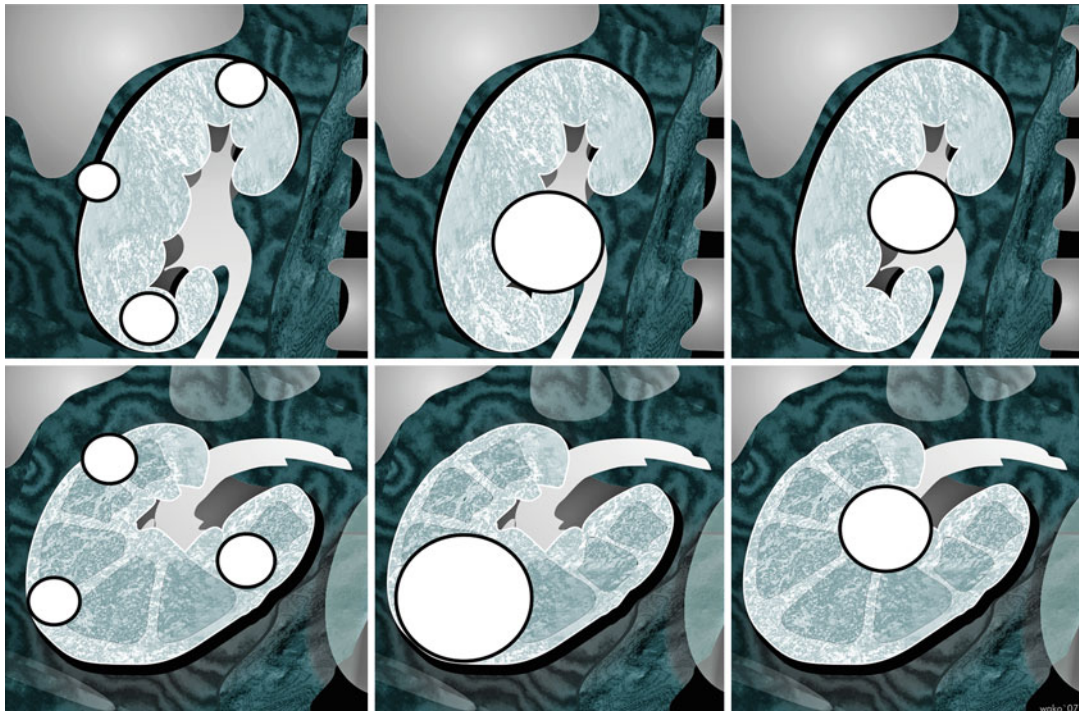

Fig. 13.19 Exophytic and cortical tumors (*left row*) are ideal candidates for percutaneous renal RF ablation. Parenchymal tumor location with contact to the renal hilum (*middle row*) might be considered for RF ablation. Central tumor location (*right row*) is generally considered a contraindication for RF ablation

of a tumor thrombus in the renal vein are rated as absolute contraindications to renal RF ablation. Some centers limit treatment with curative intent to patients with greater than 1-year life expectancy (McDougal et al. 2005). As RCCs normally grow slowly with an increase in tumor diameter of 0.2–1.2 cm/year, a wait-and-see strategy may be justified in patients with a life expectance of less than 1 year (Sowery and Siemens 2004). In the reverse case, patients without comorbid conditions and with life expectancies longer than 5–10 years are often excluded from RF ablation.

13.1.4.3 Material

Probe and Generator

For renal RF ablation, monopolar as well as bipolar ablation systems may be used. No RF system has specifically been designed for renal application. Needle electrodes as well as hooked or umbrella-shaped arrays are suited for renal tumor ablation as long as the shape of the active needle tip fits to the shape and the size of the tumor. Besides these general thoughts, there are some particular considerations for selecting the appropriate RF device for renal ablation:

1. In order to completely destroy the tumor, heat must exceed the tumor margin into healthy renal parenchyma. This concern greatly affects the choice of the applicator:
   (a) When an expandable device is chosen, the size of the RF probe should exactly fit or better slightly exceed (≤3 mm in each direction) the circumference of the tumor. If no adequate probe is available, the probe has to repositioned during the intervention.
   (b) In case a needle electrode—or in bigger tumors a needle array—has been chosen, the length of the needle (array) should exceed the diameter of the tumor by approximately 3 mm. If this is not achievable, repeated ablations using the pull-back technique are recommended.

2. If a biopsy will be obtained during the same intervention, the use of a coaxial ablation device is recommended in order to avoid tumor seeding.

13.1.4.3.2 Further Mandatory Equipment

For all ablation procedures, sterile drape and disinfectant (e.g., povidone-iodine) need to be available for preparation of a sterile working place. To avoid unintentional traction on the RF probe, additional sterile tape should be on hand for fixation of the cables.

20–22 G fine needles should be available, as they are sometimes needed for bowel displacement by injecting a fluid (hydrodissection) or gas. For this purpose, either up to 1.5 l of glucose 5 % (for fluid injection) or a sterile air filter with a Luer-lock connection (for air insufflation) needs to be on hand. Instead of air, medical grade carbon dioxide is equally effective.

In case centrally located tumors are treated, a nephrostomy kit may be required to provide external–external cooling via a double-lumen nephrostomy catheter or an external–internal cooling via a single-lumen nephrostomy catheter (Mahnken et al. 2009).

13.1.4.4 Technique

Preparation

Renal RF ablation can either be performed with i.v. analgo-sedation or under general anesthesia. The latter ensures optimal patient compliance and comfort. A single-shot pre-interventional antibiotic prophylaxis is recommended using a cephalosporin (e.g., 1.5 g cefuroxime) if:

1. Nephrostomy is performed for the intervention.
2. Repositioning maneuvers have to be performed.
3. Additional injection of air or fluid is needed for bowel displacement.
4. The procedure is expected to take longer than 2 h.

For renal RF ablation the patient needs to be positioned comfortably in the prone or lateral position. The optimal patient position is derived from pre-interventional imaging. It is mandatory to achieve a comfortable position, particularly if analgo-sedation is used. The use of dedicated positioning and fixation devices is strongly recommended to firstly guarantee the same position during the entire position and secondly avoid damage to the skin. If needed, body fixation devices like a vacuum mattress, bandages, or soft tape are helpful. Thereafter, imaging for planning the access route can be obtained.

Procedure

In case expandable probes are used, a small incision following the tension lines of the skin is made after analgesia. For sharpened needle-shaped probes, a direct puncture technique is preferable. Ideally the lesion is punctured centrally with the ablation device covering the entire lesion at once. To achieve this target, the RF probe is advanced just before the lesion. After controlling the position of the probe and the tumor, the needle is inserted to the center of the tumor. As the renal capsule presents an elastic resistance to the probe, it is helpful to rapidly advance the probe for passing the renal capsule. Repeated passages of the renal capsule should be avoided to reduce the risk of bleeding and local tumor seeding. Needle electrodes are advanced through the lesion so that the tip of the probe passes the lesion by approximately 3 mm. Expandable probes are positioned to extend their tines exactly to the tumor margin, better about 1–3 mm beyond the tumor margin (Fig. 13.20). This technique preserves most of the healthy renal parenchyma, as it results in a scanty safety margin. Nevertheless, this approach is sufficient to ensure local tumor control because renal tumors do not show an infiltrative growth pattern.

If the tumor geometry and the expected shape and/or size of the ablation zone do not match perfectly, overlapping ablations may be needed. Depending on the deviation between expected volume of necrosis and tumor size and shape, repositioning the RF probe may involve a simple pull-back maneuver to cover the length of the tumor along the puncture path, or it may require withdrawal from the lesion and reinsertion at a different angle. As lesion size and shape depend on the selected RF system as well as on the parameters used for ablation, detailed knowledge of the specific characteristics of the used RF system is helpful to assure complete and reliable

ablation. For renal ablation the same energy settings as for hepatic ablation can be used.

At the end of the procedure, the needle is removed. To avoid bleeding and tumor seeding along the puncture track, the so-called track ablation is performed. For this purpose, the needle is slowly retracted while a reduced amount of energy in the range of 10–25 W is applied. If internally cooled electrodes are used, the cooling has to be ceased by switching off the pump. In case an expandable probe is used, the tines need to be pulled back, and it has to be ensured that there is an uninsulated part at the tip of the probe after the prongs have been retracted. Otherwise, track ablation will be insufficient. Energy deposition has to be ended as soon as the active tip of the probe gets into the subcutaneous fat.

Special Considerations

With approximately 4 ml/min/g, the kidneys are much better perfused than liver (hepatic artery: 0.3 ml/min/g, portal vein: 0.7 ml/min/g) or muscle

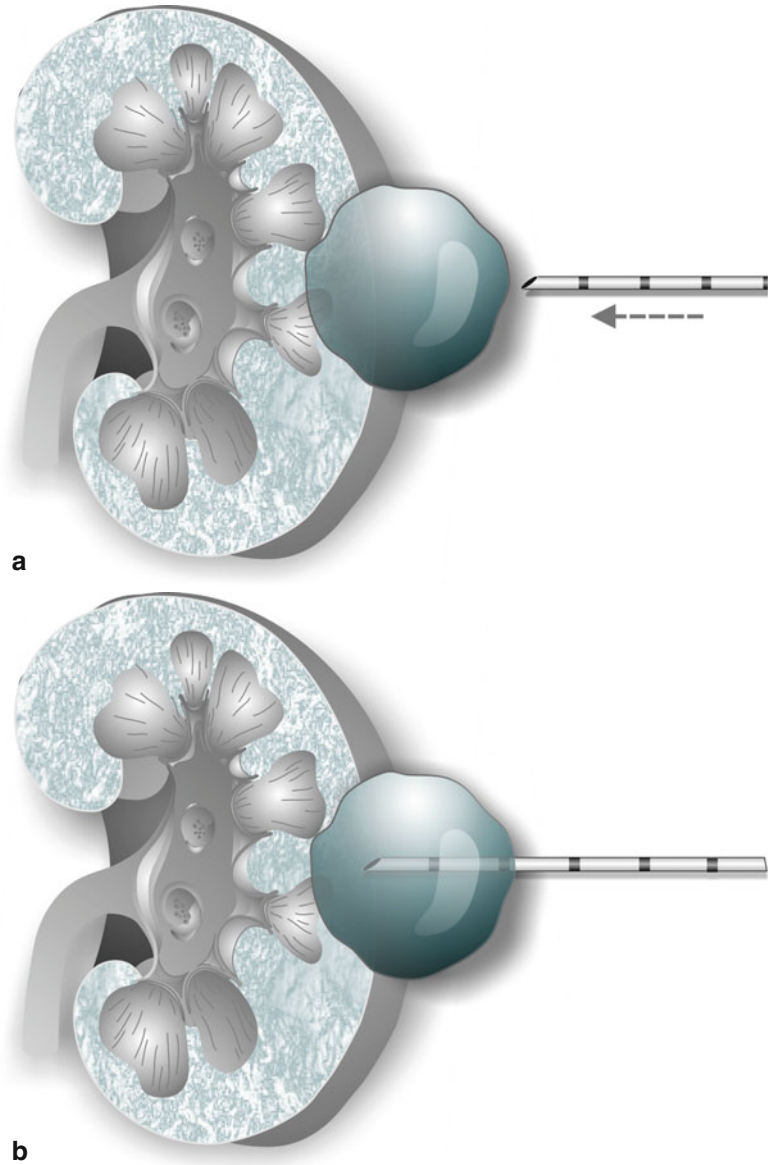

Fig. 13.20 For renal RF ablation, the RF probe is advanced just before the lesion (**a**). After controlling the position of the probe and the tumor, the needle is rapidly inserted to the center of the tumor (**b**). If a needle probe is used, the tip of the needle is advanced through the lesion (**c**). In case an expandable RF probe is used, the probe is expanded so that the tines of the probe extend 1–3 mm beyond the tumor margin (**d**)

Fig. 13.20 (continued)

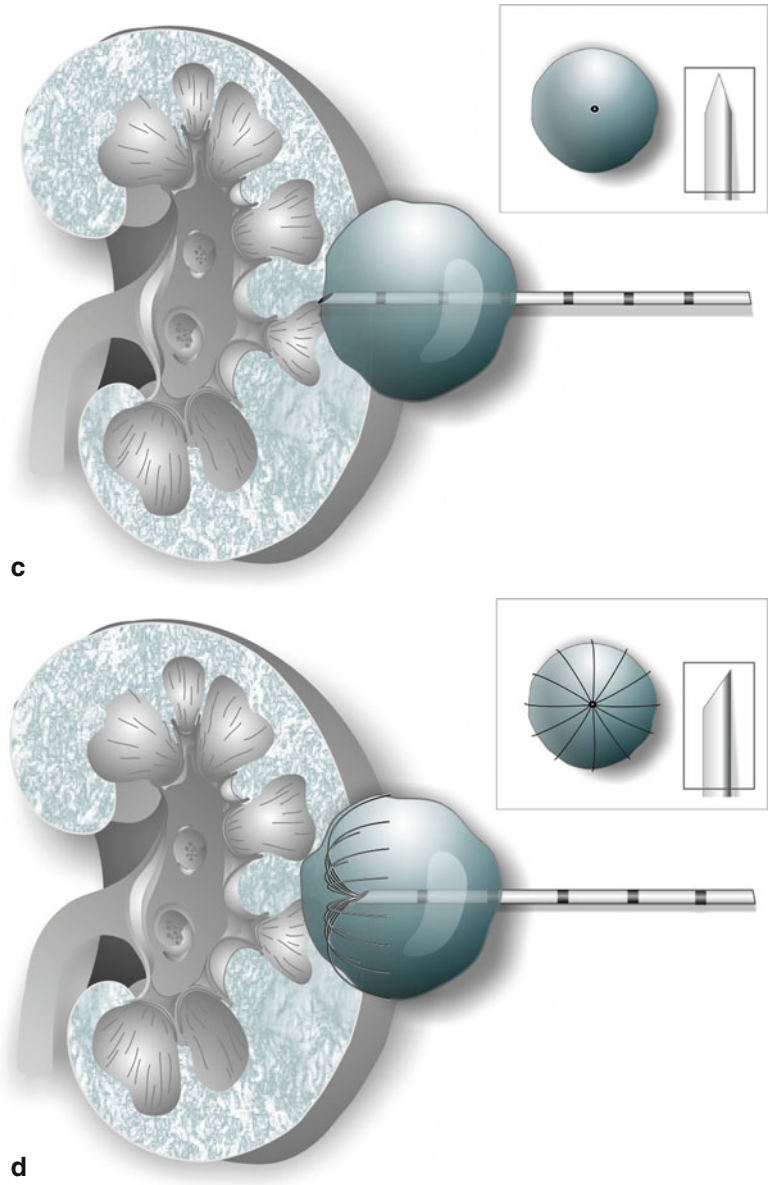

(0.04 ml/min/g) (Klinke and Silbernagel 2003). Moreover, renal tumors are typically hypervascularized, resulting in an even higher intratumoral perfusion. Increased perfusion requires to either apply more energy over a longer time or to accept smaller volumes of necrosis. This is the basis for the marked efficacy of local blood flow modulation in renal RF ablation. Selective transarterial tumor embolization with microparticles (300–700 μ) or micro-coils prior to RF ablation reduces the blood flow in the embolized tissue and therefore results in more homogeneous heat distribution (Fig. 13.21). Alternatively lipiodol may be used for pre-ablative embolization. It does not only embolize the tumor but also mark the lesion for CT guidance (Mahnken et al. 2009). As a noteworthy limitation, lipiodol masks contrast enhancement during CT follow-up. In these patients, MR imaging is better suited for post-interventional imaging. Ablation of previously embolized tumors

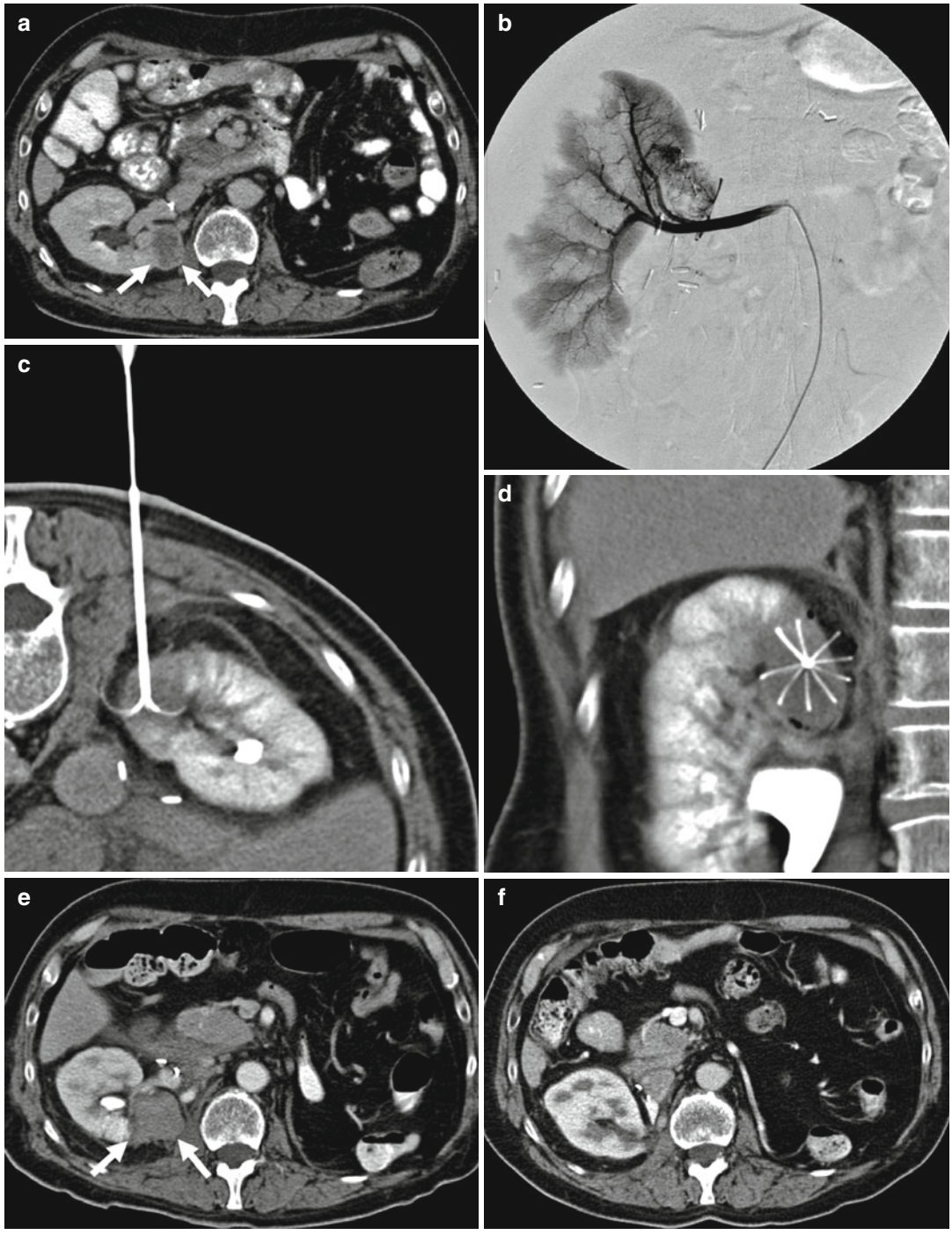

Fig. 13.21 A 64-year-old patient with recurrent renal cell carcinoma in the right kidney (*arrows*) after previous nephrectomy on the left (**a**). With a diameter of 3.5 cm, pre-interventional embolization of the hypervascularized tumor was performed (**b**) to achieve a more homogeneous heat distribution. The day after the embolization procedure, RF ablation was performed with an expandable, umbrella-shaped LeVeen probe (**c**). The probe was placed inside the tumor with the tines exceeding the tumor margin (**d**). To avoid damage to the renal pelvis, a slightly eccentrically probe position was chosen. Applying the pull-back technique, the tumor was completely ablated, resulting in a homogeneous coagulation necrosis (**e**, *arrows*). Over time the lesion decreased in size, and 4 years after ablation, the lesion has almost completely been resolved (**f**)

requires much less energy to achieve the same size of necrosis, when compared with normally perfused tissue. Furthermore, embolization adds a therapeutic effect on its own. Consequently, preablative embolization of hypervascularized renal tumors with a diameter of more than 3 cm is recommended (Mahnken et al. 2005).

In case the tumor is located directly beside a major artery with a diameter ≥0.5 mm or close to the renal vein, the so-called "heat-sink" effect will occur, where heat is removed from the ablation area by using the blood vessels as heat exchanger. This effect is particularly strong in the renal hilum. Instead of a local heating of the tumor, it may result in a systemic hyperthermia and even more importantly may leave viable tumor cells close to the vessel wall, where the temperature fails to rise above 60 °C, which is needed to guarantee coagulation necrosis. This effect is either addressed by pre-interventional transarterial tumor embolization or by placing the probe directly beside the vessel.

In central lesions there is increased risk of damaging the collecting system. This may result in hematuria with or without obstructive coagulation, development of strictures, or perforation. The latter may result in external fistulas. In these patients the heat-sink effects can be used to protect the collecting system from thermal damage by either external–external cooling via a double-lumen nephrostomy catheter or an external–internal cooling using a single-lumen nephrostomy with or without an additional drainage via a transureteral catheter. Normally infusion of saline at room temperature is sufficient to avoid thermal damage. If only small amounts of fluid can be injected into the collecting system, the use of cooled saline should be considered (Margulis et al. 2005).

As imaging-based differentiation of renal tumors (benign vs. malignant, classification of RCC)—particularly in small tumors ≤4 cm—remains difficult, a biopsy should be obtained prior to ablation. The results of the biopsy will affect subsequent patient management, particularly if biopsy proves the lesion to be nonmalignant. Biopsy should be performed in combination with RF ablation using a coaxial needle system. This approach firstly secures the tract during the biopsy procedure and seals the access route by the so-called tract ablation at the end of the procedure, thereby tumor seeding along the puncture tract can be avoided. The sole use of the track ablation technique after a renal biopsy may not be sufficient, as the paths of the biopsy needle and of the ablation device may differ if separate needles are used.

To avoid thermal damage to neighboring structures, particularly to the colon, pararenal injection of fluid or gas might be useful to displace endangered organs. It is recommended to use an isolating substance. From various experiments, glucose and air are known to be suited best for this purpose. In case air is used, it should be filtered prior to insufflation. The gas or fluid is injected via 18–20 G fine needles with end holes. The different distribution volumes of fluids and gas need to be considered when planning to displace neighboring structures. In some patients it might be necessary to use multiple needles and large amounts of fluids, exceeding 1 l. This technique, however, may be limited by adhesions after previous surgery. In very rare cases, optimal access to the tumor can also include induction of an iatrogenic pneumothorax.

13.1.4.5 Results

Imaging Findings

For the assessment of technical success and further imaging surveillance, contrast-enhanced CT or MR imaging is recommended. After successful RF ablation of renal tumors a wedge-shaped defect with a lack of contrast enhancement, shrinkage and occasional retraction from normal parenchyma by fat infiltration are seen on cross-sectional imaging (Matsumoto et al. 2004). Typical MR imaging characteristics in successfully treated lesions include a hypointense lesion surrounded by a bright rim on T2-weighted images. On T1-weighted images these lesions appear hyperintense. After administration of contrast material, a thin-rim enhancement may be seen (Merkle et al. 2005). Consequently, unenhanced and contrast-enhanced studies are needed to reliably assess treatment success. If no viable tumor is demonstrated, subsequent scans are recommended at 3 months, 6 months, and every 1 year. If there is residual tumor on post-interventional imaging, repeated RF ablation is needed. In several studies a re-intervention rate of 8–9 % has been reported (Joniau et al. 2011).

Table 13.8 Results of percutaneous renal RF ablation. Only case series including 100 or more tumors were included in this summary

Author/year	Technique	Patients/tumors	Mean size (cm)	Local tumor control (%)[1]	Follow-up (months)
Matsumoto et al. 2005	Perc. CT, lap.	91/109	2.4	100	–
Gervais et al. 2005	Perc. CT/US	85/100	3.2	89	28
Breen et al. 2007	Perc. CT/US	97/105	3.2	90.5	16.7
Tracy et al. 2010	Perc. CT, lap.	208/243	2.4	97	27
All/mean		481/557	2.8	94 %	23.9

Perc. percutaneous, *Lap*. laparoscopic, *US* ultrasound, *CT* computed tomography,
[1]Incl. re-interventions

Histology

From histopathologically controlled animal studies, the zone of RF ablation is known as sharply delineated area (Hsu et al. 2000). Immediately after the procedure, microscopy reveals increased cytoplasmic eosinophilia, loss of cell border integrity, blurring of nuclear chromatin, and interstitial hemorrhage. Typical coagulative necrosis develops by day 3. Until then the tumor may appear viable on simple HE staining. Thus, dedicated staining techniques, for example, for NADHase or apoptosis, are needed to avoid misjudging of the histological finding as it has happened in early studies on renal RF ablation (Rendon et al. 2002). From day 3 to day 14, inflammatory and fibroblastic changes separate ablated renal tissue from the adjacent healthy renal parenchyma. This process is followed by necrosis without features of renal parenchyma. From the center to the periphery, four different zones can be distinguished from histology: complete necrosis, inflammatory infiltrate, hemorrhage, fibrosis, and regeneration (Crowley et al. 2000).

Therapy Outcome

The first successful clinical case of renal RF ablation was reported in 1997 (Zlotta et al. 1997). In 2003 the first relevant series with 34 patients (42 RCC; 1.1 to 8.9 cm) with a mean follow-up period of 13.2 months was published (Gervais et al. 2003). Most importantly, this study firstly identified relevant factors for success of the ablation procedure. While parenchymal and central tumors recur more frequently if the diameter exceeds 3 cm, exophytic tumors can be treated effectively, even if they are bigger than 3 cm in diameter. Effectiveness of RF treatment was proven by a histologically controlled case series with tumor resection secondary to laparoscopic RF ablation in 5 of 17 RCCs (Jacomides et al. 2003). The short-term effectiveness of renal RF ablation has been shown by several studies (Table 13.8). There is only little, but steadily growing, data on long-term effectiveness, with very promising results. In several studies a more than 4-year cancer-specific survival of almost 100 % has been reported (McDougal et al. 2005; Tracy et al. 2010; Zagoria et al. 2011).

Only recently a retrospective study directly compared the outcome after RF ablation and surgery in T1a tumors. While the 5-year overall survival was worse after RF ablation, the cancer-specific survival was identical surgery. The differences in overall survival were considered to be due to the significantly higher rate of comorbid conditions in the local ablation group (Takaki et al. 2010).

Cost-Effectiveness

Considering the increasing economic pressure on the worldwide healthcare market, several authors conducted studies regarding the cost-effectiveness of renal ablation. Percutaneous RF abaltion proved to be the most cost-effective technique when compared with laparoscopic ablation and open nephrectomy (Lotan and Cadeddu 2005). The most

important cost-reducing factors were shorter hospital stay and less operating room costs. This finding was confirmed by later studies including decision analytic models (Pandharipande et al. 2008).

13.1.4.6 Complications

In general, complications are less common in percutaneous RF ablation when compared with the laparoscopic approach (Park et al. 2006). The most common complication is self-limiting hematuria. More severe complications include bleeding, hematoma, urinoma, renal infarction, ureteral obstruction, cutaneous fistulas, skin burns, or nerval damage (Rhim et al. 2004). Tumor seeding along the puncture tract was reported, but can be avoided by using a proper ablation technique (Mayo-Smith et al. 2003). Animal experiments indicate that central tumors are more prone to major complications than exophytic tumors (Lee et al. 2003). In a recent systematic review, a complication rate of 13.2 % was reported with major complications occurring in 3.2 % of patients (Joniau et al. 2011). Most of these complications can be treated conservatively.

Summary

Experimental as well as clinical studies proved percutaneous renal RF ablation to be an accurate and safe alternative to open or laparoscopic surgery in the treatment of small renal tumors. It is well tolerated in patients with percutaneously accessible lesions. Moreover, it is known to be less costly than open or laparoscopic partial nephrectomy. Considering recent data comparing RF ablation and surgery as well as the increasing volume of long-term data, it holds the potential to replace surgery as first-line therapy in small RCCs.

Key Points

- Pre-interventional patient evaluation including a physical examination (renal function, coagulation, platelet count, comorbidity) combined with a thorough imaging workup is the basis for correct patient selection.
- Availability of adequate material for the intervention has to be ensured to be prepared for unexpected peri-interventional developments.
- Hypervascular tumors with a diameter of 3 cm or more should be embolized prior to ablation. In all patients a biopsy should be obtained.
- To ensure long-term success, a stringent post-interventional imaging surveillance is mandatory.

13.1.5 RF Ablation Miscellaneous

Thomas Helmberger and Andreas H. Mahnken

13.1.5.1 Introduction

Radiofrequency (RF) ablation of hepatic, renal, and pulmonary malignancies as well as of benign bone tumors, particularly osteoid osteoma, is already widely accepted as a very effective therapeutic option—given the specific inclusion and exclusion criteria as outlined in the corresponding chapter of this book. Based on the rather long-standing experience in these areas in many centers, RF ablation came into operation also in other tumor entities. These entities encompass malignant bone tumors and various soft tissue tumors. Although—secondary much more than primary—osseous, lymphatic, and soft tissue tumors are very commonly valid, study-proven data on RF ablation of these tumor types are still limited. Nevertheless, there is a rapid growth of publications on this issue. However, most of the presented papers are anecdotal case reports or case collections. The reason for that is mainly related to the tumors pathology, as a specific tumor manifestation of more widespread tumor disease rarely needs local treatment. Therefore, RF-ablation treatment in many of the tumors of the bones and soft tissue follows the concept of local, symptomatic therapy. This approach represents a major difference to the commonly applied systemic treatment concepts in these tumor entities.

Table 13.9 Indications and contraindications of RF ablation in bone and soft tissue tumors

	Benign bone TU	Malignant bone TU	Lymph node	Soft tissue
Potential indications				
Tumor treatment	Definitive	Symptomatic	Symptomatic	Symptomatic
Pain relief	Very effective	Effective	NA	Effective
Contraindications	Impending fracture			
	Direct contact of tumor with neurovascular and other structures susceptible to thermal damage			
	Impending secondary burns due to metallic internal fixations			
	Acute infection			
	Coagulopathy			
	Extent to large			

13.1.5.2 Indications

In general, local ablative tumor therapy – as RF ablation – follows the rule of treatment of a locally limited disease where the intended lesion to treat is the leading, survival or life quality determining manifestations of the specific disease. Up to now there is no proof that in hepatic, pulmonary, or renal tumors, debulking in terms of partial or incomplete ablation may affect the patients' outcome effectively. If these procedures positively influence subsequent chemo- or radiation therapies, is discussed controversially. In consequence, local ablation of these tumor entities should strictly be subject to indications where:

1. It is likely to achieve complete local tumor control or even complete tumor eradication.
2. It is likely to achieve secondary targets such as pain relief (e.g., bone tumors).
3. It is likely to achieve symptom control (e.g., endocrine tumors).

Anyway, the indications of local ablative therapy in malignant bone and soft tissue tumors are not yet well-defined and are based on personal experience in many centers (Table 13.9). In most cases, pain palliation or decompression of space-occupying masses will be the predominant therapeutic goal (Simon et al. 2006).

In benign lesions, RF ablation is less commonly used when compared to surgery. However, in osteoid osteomas, minimal-invasive thermal ablation is considered as the most effective therapy and is widely accepted as method of primary treatment (Rosenthal 2006). Only recently RF ablation became an alternative treatment in endocrine tumors of the pancreas or the adrenal glands. While this approach may more or less liberally be applied in the adrenals, it should only be a reserve measure in pancreatic lesions.

In general, the contraindications for RF ablation of any tumor are similar as in RF ablation of, for instance, hepatic tumors:

- Acute infection
- Uncorrectable coagulopathy
- Tumor size
- Number not suitable for ablation by the available RF systems (Coldwell and Sewell 2005; Simon and Dupuy 2006)

13.1.5.3 Material and Technique

RF generators and probes used for thermal ablation in bone and soft tissue tumors are generally not different as in other tumor entities and are discussed extensively within the preceding technical chapter. Nevertheless, some "adjustments" might be necessary to take specific pathoanatomical conditions into consideration. The potentially close vicinity of heat-sensitive structures as in spinal or intra-abdominal lesions demands special attention to anatomical conditions and the choice of the appropriate RF probe. For instance, in osteoid osteomas with a small nidus, a single-needle probe with a short active tip is much more appropriate than a multi-tined expandable probe. Regarding the anatomical localization of the tumor, close proximity to neurovascular structures—which is often the reason for the clinical

symptoms—may prohibit local thermal therapy. Otherwise, severe, permanent damage might happen to these structures. In these lesions, injections of a cooling fluid or an insulating gas like carbon dioxide via a second needle may prevent adverse events and warrant a safe and successful ablation procedure. Application of a dedicated neuromonitoring may also be suited to avoid damage to nerve structures. Moreover, often less energy is needed to achieve a sufficient result in terms of pain control or decompression of a space-occupying mass.

For probe placement, imaging guidance by ultrasound, computed tomography (CT), and magnetic resonance (MR) tomography is necessary. Adequate guidance is mandatory to provide proper probe placement into the target and to avoid collateral damage along the pathway to the target. For RF ablation of osseous and nearby lesions, CT will be the imaging method of choice, while ultrasound might be suitable and easy to use in superficial soft tissue tumors as, for example, breast lesions, and MR imaging will be reserved to tumors that can only be displayed by MR imaging.

Adrenal tumors require some special pre-interventional preparations, whereas a standard patient preparation is sufficient in bone, breast, and pancreatic lesions. In suspected hormonally active adrenal (or pancreatic) tumors, plasma assays for catecholamines, aldosterone, or cortisol should be pursued. This may even include selective venous blood sampling. As puncture and ablation has the potential to result in the release of large amount of hormones from the target lesion, there is a need for pre- and intra-procedural antiadrenergic and corticosteroid therapy. In pheochromocytoma, premedication with phenoxybenzamine (α-adrenergic inhibition) and atenolol (β-adrenergic inhibition) is recommended starting at least a week before the procedure in order to avoid intra-procedural hypertensive crisis. The additional use of α-methyl-paratyrosine (inhibition of catecholamine synthesis) has also been described (Venkatesan et al. 2009). In Cushing adenoma, hydrocortisone should be administered during and after the procedure with a gradual taper after the intervention.

Independent from the lesions location, the procedure itself follows the general principles of CT and MR-guided punctures as described in the previous chapters. Energy should be delivered following the recommendations of the vendor of the specific RF generator. For most lesions the same protocols as for liver ablation may be used, while in bone tumors energy delivery should be reduced markedly. In breast ablation, either external cooling or internal distension of the skin from the lesion by injection of glucose between the target lesion and the skin should be performed in order to minimize the risk of thermal skin injury.

13.1.5.4 Results

Malignant Bone Tumors

Bone metastases are very frequent and can be found in 70–90 % of all patients with an underlying malignant disease, predominantly in patients with breast, lung, kidney, and prostate cancer. Due to the distribution of the red bone marrow, the most common localization of bone metastases is the spine, followed by pelvis, femur, skull, and other long bones. More than 50 % of all patients will develop severe pain during their remaining lifetime caused by osteolyses affecting soft tissue and periosteal nerve endings. Ongoing osteolytic destruction will destabilize the bone, causing occult micro- and macro-fractures. Standard therapies in those patients include surgery, chemotherapy, radiation therapy, and adjuvant administration of analgesics. An increasing number of patients are encountering a rather wide variety of sequential therapies, where tumors might lose their sensitivity for chemotherapy and will have been already irradiated and an additional radiation therapy would exceed the maximum suitable radiation dose, and where supportive analgesic therapy is no longer tolerable because of increasing side effects. Nevertheless, these "prolonged" therapies will result in "prolonged" survival times in many cases, where intensified supportive care is often necessary. Especially with regard to supportive care, local ablative therapies such as radiofrequency and laser ablation as well as osteoplasty with local cement injection (Hoffmann et al. 2008) will support the concept for palliation in pain of soft tissue and osseous tumors (Goetz et al. 2004; Gangi et al.

Table 13.10 Primary and secondary success rate of RF ablation in malignant bone tumors in comparison to various ablation therapies in terms of pain relief

Author	Pat/proced.	Method	Primary success (%)	Long-term succ.	Complications	F-up (months)
Weill et al. 1996	37/52	OP	94	73 %	Neurologic ($n=3$)	13
Alvarez et al. 2003	21	OP+R (15), surgery (3)	81	–	Neuritis ($n=1$)	5.6 (1–18)
Fourney et al. 2003	56/97	OP/KP	84	–	0	4.5 (1–19.7)
Goetz et al. 2004	43	*RFA*	95	–	Burns ($n=1$) Transient incontinence ($n=1$) Fracture ($n=1$)	16
Jagas et al. 2005	21/21	OP+R	100		0	1–8
Jang and Lee 2005	28/72	OP+R	89	–	0	1–9
Kelekis et al. 2005	14/23	OP	92	–	Leakage ($n=1$)	9 (1–24)
Mont'Alverne et al. 2005	12/12 (axis)	OP	80		Neurologic ($n=2$)	6.9
Toyota et al. 2005	17/23	*RFA + OP*	100	82.4 %	Hematoma ($n=1$)	1–30
Callstrom et al. 2006	14/22	Cryo	67	86 %	0	3–24
Calmels et al. 2007	52/59	OP	86	92 %	Neurologic ($n=4$) Hematothorax ($n=1$) Pulmonary embolism ($n=2$)	17
Hoffmann et al. 2008	22/28	*RFA + OP*	90.9	100 %	0	7.7 (3–15)
Lane et al. 2011	36/53	*RFA + OP*	97.2	NA	Neurologic ($n=1$) Transient pain ($n=2$)	NA

OP osteoplasty, *KP* kyphoplasty, *Cryo* cryoplasty, *RFA* Radiofrequency ablation, *R* radiation therapy

2005; Callstrom et al. 2006). The pathophysiological process causing the pain relief by RF ablation is not yet completely understood. Most likely, periosteal nociceptors might be destroyed by the direct impact of heat. Nevertheless, the success rate of RF ablation of 67–100 % of immediate post-procedural pain relief seems to be equivalent to the above-mentioned other therapies and combination methods (Table 13.10).

It is still under debate if the combination therapy of thermal ablation together with, for example, cementoplasty is superior to a single therapy (Fig. 13.22). Furthermore, there are a few cases of painful bone tumors with a dense stroma that hinders a cement injection. In these cases, thermal ablation may soften the tumor stroma, allowing subsequent cement instillation (Hoffmann et al. 2008).

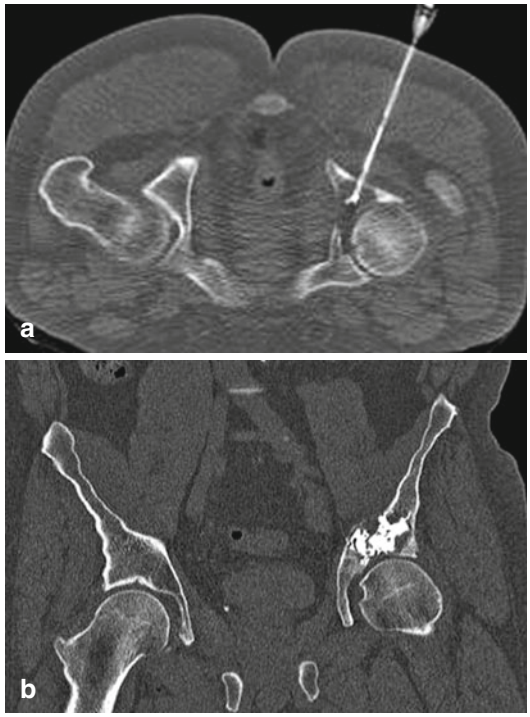

Fig. 13.22 This osteolytic metastasis of a follicular thyroid cancer in the weight-baring parts of the left acetabulum was first treated by RF ablation with a multi-tined probe (**a**) followed by percutaneous cement injection for stabilization (**b**). A significant pain relief could be achieved; nevertheless, the patient died 4 months later due to rapid progress of the underlying disease

Breast

In the industrialized countries, breast cancer is a major health problem with almost 230,000 new cases alone in the USA. More than a quarter of all cancer occurring in women will be breast cancer, and 40 % of all patients will be younger than 60 years. Even if breast-conserving therapy with or without postoperative radio- and chemotherapy—dependent on the stage of the disease—is considered the therapy of first choice, the advent of screening programs and the increasing number of detected tumors of small size (<2 cm) also enforce the trend to more minimal-invasive therapies. Consequently, the concepts of local thermal ablation therapy can be also translated into the field of minimal-invasive therapy of breast tumors.

Up to now RF ablation of breast carcinoma is still work in progress. Nevertheless, this field is continuously evolving, and there is a relevant body of studies on RF ablation followed by early or delayed resection (Table 13.11). After first intraoperative attempts to treat larger tumors up to 7 cm in diameter (Jeffrey et al. 1999), recent studies incorporate smaller tumors up to 3 cm (Izzo et al. 2001; Hayashi et al. 2003; Fornage et al. 2004). Complete coagulation necroses could be achieved between 80 and 100 %, with higher degrees of necroses in small lesions.

Based on these data, several pilot studies addressed the clinical effectiveness of RF ablation in elderly patients. The biggest of these studies included 52 patients with a mean tumor diameter of 1.3 cm (0.5–2.0 cm). All patients underwent RF ablation and adjuvant chemo- and/or endocrine therapy and radiotherapy (50 Gy) with no recurrence after 15 months (6–30 months). The cosmetic aspect after RF ablation was considered excellent in 43 patients (83 %), good in 6 (12 %), and fair in 3 (6 %). One patient experienced skin burn at the entry site of the RF ablation probe (Oura et al. 2007). These data are encouraging, but follow-up periods are too short to validly judge the clinical efficacy of RF ablation in breast cancer.

So far, RF ablation seems to be a very promising new tool for minimal-invasive therapy for small breast carcinomas. Intensive further investigation is needed to identify the best candidates and best comprehensive concepts for this therapy.

Adrenal Gland

Adrenal neoplasms comprise a broad spectrum of diseases. Common pathology includes cortisol-producing adenomas, aldosteronoma, pheochromocytoma, adrenocortical carcinoma, and metastatic disease. There is a growing body of evidence that RF ablation is effective in treating adrenal tumors. Arima et al. reported the successful RF ablation in four patients with Cushing adenoma, with a mean follow-up of 33 months. One patient had to undergo repeated ablation 3 years after the initial procedure (Arima et al. 2007). Venkatesan and coworkers reported the successful treatment of adrenal pheochromocytoma, with complete ablation in six out of seven tumors and a follow-up of 12.3 months (Venkatesan et al. 2009). A very recent series included 23 tumors including adrenal metastases

Table 13.11 Summary of studies on RF ablation followed by surgery in patients with breast cancer

Author	Patients (*n*)	Tumor size (cm)	Complete ablation (%)	Complications	Time to resection
Jeffrey et al. 1999	5	4–7	80	0	Immediate
Izzo et al. 2001	26	1.8 (0.7–3.0)	96	4 % skin burn	Immediate
Burak et al. 2003	10	1.2 (0.8–1.6)	90	0	1–3 weeks
Hayashi et al. 2003	22	0.9 (0.5–2.6)	86	5 % skin burn	1–2 weeks
Fornage et al. 2004	21	1.2 (0.6–2.0)	95	0	Immediate
Earashi et al. 2007	24	1.1 (0.5–2.4)	100	0	Immediate ($n=17$); 1–7 months ($n=7$)
Khatri et al. 2007	15	1.28 (0.8–1.5)	93	6 % infection	Immediate
Medina-Franco et al. 2008	25	2.08 (0.9–3.8)	76	0	Immediate
Imoto et al. 2009	30	1.7 (0.9–2.4)	92	30 % (skin burn, muscle burn)	Immediate
Manenti et al. 2009	34	1.89 (1.65–1.96)	97	3 % skin burn	4 weeks
Kinoshita et al. 2011	49	1.7 (0.5–3.0)	77	10 % (skin burn, muscle burn)	Immediate
Hung et al. 2011	29	1.4	90	0	Immediate

($n=20$), pheochromocytoma ($n=2$), and aldosteronoma ($n=1$). Despite a relative large lesion size of 4.2 cm (range: 2–8 cm) of the metastatic lesions, a technical success rate of 100 % was achieved with a local tumor control in 83 % in metastatic disease (Wolf et al. 2012).

Pancreas

Adenocarcinoma of the pancreas is a highly aggressive cancer with 5-year overall survival of only 5 %. Complete resection is the only potentially curative measure in these patients with less than 25 % of patients being eligible for surgery. More than a decade ago, Matsui et al. described their results with intraoperative RF ablation in 20 patients with stage IV pancreatic adenocarcinoma (Matsui et al. 2000). While the procedure was feasible, there was a high complication rate with two fatal complications. Moreover there was no survival benefit when compared with a control group that underwent palliative care. Since this initial series, there were several case series with a total of more than 100 patients. The results regarding complications and survival are contradictory. The only prospective study covers only three patients treated with RF ablation. While the authors consider RF ablation feasible, they also comment on the poor quality of life (Casadei et al. 2010). In contrast, the largest patient series covering 50 patients considers pancreatic RF ablation as well tolerated (Girelli et al. 2010). There is only scarce data on survival, with only two studies with survival as primary end point (Matsui et al. 2000; Spiliotis et al. 2007). In contrast to Matsui et al., Spiliotis and coworkers also included stage III tumors. Interestingly there was a significant survival benefit in stage III lesions treated with RF ablation, while there was no difference in stage IV lesions, when compared with a control group. These findings are consistent with the previous report (Matsui et al. 2000).

Only recently several authors reported on the successful ablation of endocrine tumors of the pancreas such as gastrinoma and insulinoma (Limmer et al. 2009; Wu et al. 2010).

Other

In most malignancies, metastatic spread to the lymphatic system or to soft tissue by more or less direct invasion is common. Since such a tumor manifestation represents a systemic tumor burden, commonly local ablative therapy has no influence on the patient's outcome. Nevertheless, secondary symptoms such as pain and compression may require medical intervention. Based on anecdotal reports on RF ablation in lymph node metastases (Hiraki et al. 2005; Hanazaki et al. 2006), recurrent pelvic cancer (Lefevre et al. 2008; Belfiore et al. 2009), or secondary (metastatic) and primary soft tissue tumors like liposarcoma

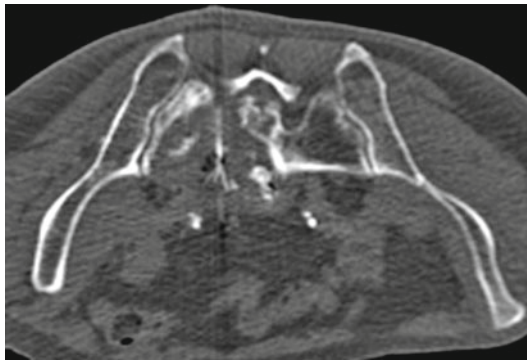

Fig. 13.23 In this local recurrence of a colorectal carcinoma with a large osteolytic bone metastasis of the sacral bone with an extensive soft tissue component, RF ablation using a multi-tined RF probe could achieve significant pain relief for 6 months until the patient died due to massive multi-organ metastasis of the underlying malignancy

or rhabdomyosarcoma (Locklin et al. 2004; Nashida et al. 2007; Keil et al. 2008), it seems that RF ablation can play a role in adjuvant palliative treatment—in most of the cases without intention of cure but of preservation of the quality of life (Figs. 13.23, 13.24).

13.1.5.5 Complications

The overall complication rate of RF ablation in bone and soft tissue tumors is not different to complications of RF ablation in other anatomical areas and tumor entities. According to the SIR (Society of Interventional Radiology) classification, the reported complication rates are below 4 % without reports on major complications (Table 13.10). Adverse events may be puncture related such as hemorrhage at the entry site or technically procedure related such as skin burns, and neurological symptoms due to secondary thermal damage to nontarget ablation (e.g., close vicinity to nerve or joint structures), and are usually self-limiting (Fig. 13.24).

Incomplete treatment with residual or recurrent tumor tissue particularly in bone tumors is accepted with acquiescence since clinically, pain is the leading symptom triggering the therapy indication (Lencioni et al. 2004; Marchal et al. 2006; Gangi et al. 2005; Thanos et al. 2008). In hormonally active tumors, for example, in the adrenal gland, excess release of hormones may cause problems. Correspondingly hypertensive crisis up to cardiac

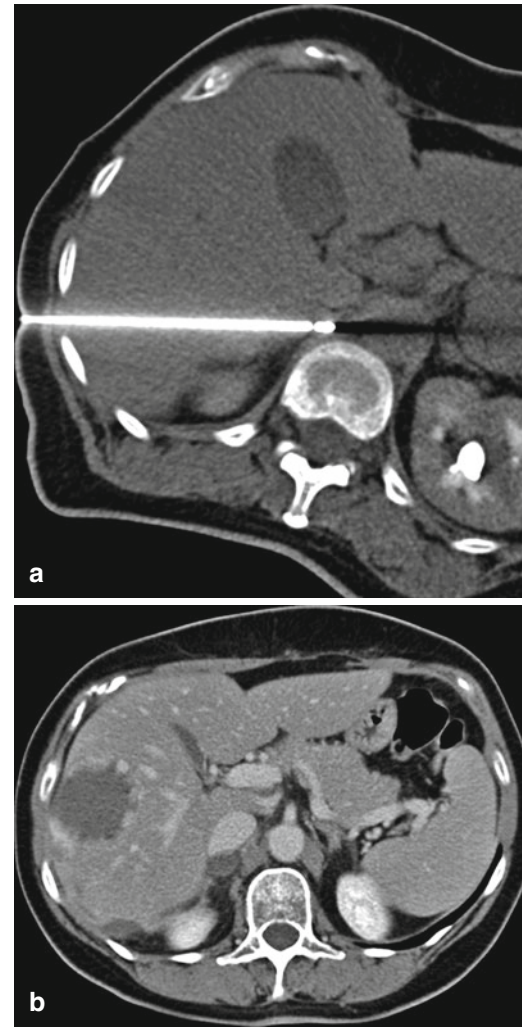

Fig. 13.24 A 56-year-old woman suffering from metastatic melanoma with a history of locally controlled liver and lung metastases. In order to reduce the total tumor burden, the right adrenal gland was treated by RF ablation. Ablation was performed under CT guidance via a transhepatic approach (**a**). The contrast-enhanced post-procedural CT scan shows the lack of contrast enhancement as indicator of successful treatment. CT also depicts a liver hemangioma (**b**)

arrest has been reported after ablation of pheochromocytoma or adrenal metastases (Chini et al. 2004; Tsoumakidou et al. 2010).

A particular problem of RF ablation in breast lesions is skin burns (6.5 %) or burns to the pectoralis muscle (23 %), as both structures are close to the site of ablation (Imoto et al. 2009). However, these are minor complications which can usually be treated conservatively.

In pancreatic RF ablation, the reported complication rates vary from 0 to 100 %. On average a rate of 25 % of relevant complications has to be assumed (Girelli et al. 2010). Several studies reported fatal complications including hemorrhagic pancreatitis, septic shock, and gastrointestinal bleeding. Tumor location in the pancreatic head appears to be a risk factor for fatal complications. Other complications are due to the complex anatomy of the pancreas including biliary leaks and fistulas, pseudocysts, and ascites.

Summary

Even though the present database is somewhat limited and lacks large studies, RF ablation of bone and soft tissue tumors is already producing evidence of its high efficacy in pain treatment and consequently in improving the quality of life in patients with primary and secondary bone tumors and with space-occupying soft tissue masses. In osteoid osteoma the results of RF ablation with a very high success rate, a very low complication rate, and—socioeconomically also important—a very short recovery time represent the standard of care. In other tumor entities as in bone metastases, breast carcinomas, and other so far rare cases of locally symptomatic soft tissue tumors, local thermal ablation could prove its efficacy mainly in terms of pain relief as well. Therefore, it can be anticipated that RF ablation will play an even further growing valuable role also in the adjuvant, minimal-invasive therapy of bone and soft tissue tumors.

Key Points

- RF ablation in bone and soft tissue tumors is a powerful minimal-invasive tool to control lesion-related symptoms such as pain on the one hand and may also prove to be efficient in tumor control.
- Although there are no large-scale studies on RF ablation in malignant bone tumors or non-organ-related soft tissue tumors, it should be considered a valuable treatment option in nonsurgical candidates.

13.2 Laser-Induced Thermotherapy

13.2.1 Laser Ablation: Liver and Beyond

Martin G. Mack, Katrin Eichler, and Thomas J. Vogl

13.2.1.1 Introduction

Interstitial laser-induced thermotherapy (LITT) is a minimally invasive technique suitable for local tumor destruction within solid organs, using optical fibers to deliver high-energy laser radiation to the target lesion(Mack et al. 2004; Vogl et al. 1997a, 2004a). Due to light absorption, temperatures of up to 120 °C are reached within the tumor, leading to substantial coagulation necrosis. Magnetic resonance (MR) imaging is used both for placement of the laser applicator in the tumor and for monitoring progress of thermocoagulation. The thermosensitivity of certain MR sequences is the key to real-time monitoring, allowing accurate estimation of the actual extent of thermal damage (Castren Persons et al. 1992; Jolesz et al. 1988; Le Bihan et al. 1989).

Thus, laser can destroy tumor by direct heating while greatly limiting damage to surrounding structures. Experimental work has shown that a well-defined area of coagulative necrosis is obtained around the fiber tip, with minimal damage to surrounding structures. Pilot clinical studies have demonstrated that this technique is practical for the palliation of hepatic tumors (Amin et al. 1993; Masters et al. 1992; Matsumoto et al. 1992). The success of LITT is dependent on delivering the optical fibers to the target area, real-time monitoring of the effects of the treatment, and subsequent evaluation of the extent of thermal damage (Vogl et al. 1996). The key to achieving these objectives is the imaging methods used.

MR-guided laser-induced thermotherapy offers a number of potential treatment benefits. First, MR imaging provides excellent topographic accuracy due to its excellent soft tissue contrast and high spatial resolution. Secondly, the temperature sensitivity of specially designed MR sequences can be used to monitor the

temperature elevation in the tumor and surrounding normal tissues (Meister et al. 2007). This enables the exact visualization of the growing coagulative necrosis. Online MR imaging during LITT is helpful for avoiding local complications due to laser treatment. Thirdly, recovery times, lengths of hospital stay, and risk of infection and other complications can be reduced when compared with palliative open surgery. Finally, successful implementation of such minimal-invasive procedures has the potential to significantly reduce costs in comparison to surgical procedures. A further, indirect advantage is the psychological effect due to avoidance of cosmetic deformities that can result from major reconstructive surgery.

To generate an MR image, a radiofrequency pulse is used. If there is any RF source in the MR room, there is always interference between the radiofrequencies from the RF generator and the radiofrequencies from the MR scanner, resulting in a complete destruction of the MR image. Even with MR-compatible RF probe, it is necessary to disconnect the probes for every MR scan which is quite uncomfortable. Another advantage of the laser is that multiple laser applicators can be used in completely different parts of the liver simultaneously because the different laser applicators do not interact. Therefore, two or three metastases can be ablated simultaneously with the laser, permitting short overall intervention times. This may be done under local anesthesia on an outpatient basis.

MR-guided minimally invasive LITT has become a well-established procedure for local treatment of liver metastases and primary liver tumors in some European centers. Several studies using this technique have shown that local minimally invasive destruction of liver tumors improves the survival rate of patients with liver metastases (Mack et al. 2004; Vogl et al. 2004b). For recurrent extrahepatic tumors the value of minimally invasive treatment modalities has not yet been demonstrated. Initial clinical data obtained from laser therapy of lung cancer (Vogl et al. 2004b) and head and neck tumors (Mack and Vogl 2004) suggest that there are indications for minimal treatment of tumors in other regions of the body.

13.2.1.2 Indications

The primary therapy goal is defined as the local tumor control in patients with limited hepatic malignant tumor involvement. The majority of patients suffer from liver metastases of colorectal cancer. Generally accepted indications for LITT of liver tumors are as follows:

- The maximum diameter of the lesion should not exceed 5 cm.
- The maximum number of lesions should be 5.
- Patients with tumor recurrence after surgery, radiation, or chemotherapy.
- New metastases after liver resection.
- No response to chemotherapy.
- Metastases in both liver lobes.
- Lesions in high-risk locations, for example, near the bile duct.
- LITT as a replacement for the oncological therapy in case of patient refusal.

More than five lesions or patients with extrahepatic disease (e.g., lung or bone metastases) can be treated under certain circumstances based on an individual decision.

Contraindications for MR-guided LITT are as follows:

- Extensive extrahepatic tumor spread
- Contraindications for MRI (pacemaker)
- Ascites
- Apparent infections
- Diffuse and multiple patterns of metastasis
- Insufficient coagulation parameter

Written informed consent has to be obtained from the patient, including the information of the patients about possible complications and side effects as well as alternative treatment options at least 24 h before the treatment.

Before LITT, a plain and contrast-enhanced MR imaging of the liver or the region of interest is performed. The imaging protocol included a T2-weighted breath-hold TSE sequence in transverse slice orientation, a HASTE sequence, and a T1-weighted unenhanced and contrast-enhanced gradient (GRE) sequence in transverse and sagittal slice orientation followed by a dynamic

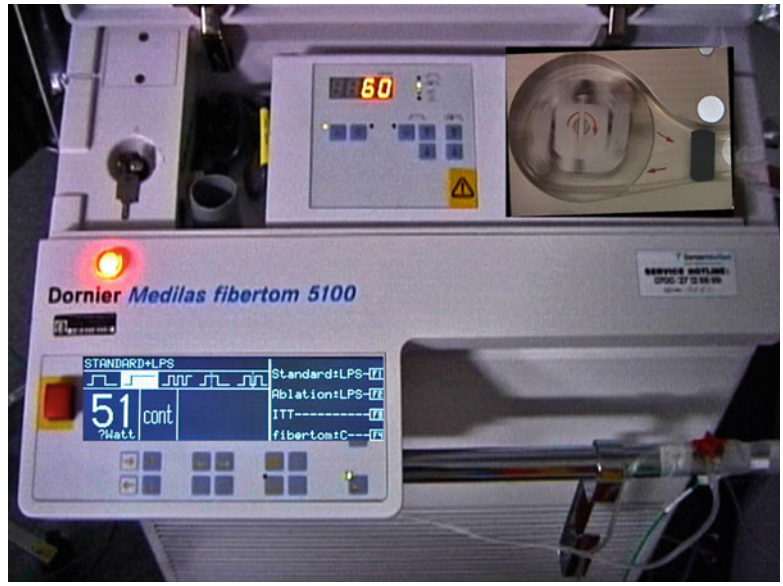

Fig. 13.25 The figure is showing one Nd:YAG laser with a maximum output power of 100 W. Note the roller pump which is included for the irrigated laser application system. The laser is equipped with a light guide protection system (LPS) which is switching the laser off immediately in case of any damage to the laser fiber

evaluation during contrast administration. After contrast administration the T1-weighted GRE sequences are repeated.

LITT can be also performed without MR guidance using ultrasound (US) or CT guidance. MR monitoring, particularly MR temperature mapping, allows an exact guidance of the treatment and avoids over- or undertreatment, potentially resulting in better local tumor control.

The following indications for extrahepatic LITT can be claimed. However, all treatment decisions of extrahepatic tumors have to be made on an individual basis, preferable within an interdisciplinary tumor board. The discussion should focus on therapeutic alternatives and on the individual situation of the patient.

(a) *LITT of lung metastases and lung tumors*
(b) *LITT of soft tissue tumors*
- Residual tumors
- Head and neck region
- Upper abdomen
- Retroperitoneum
- Lymph node metastases
- Head and neck region
- Upper abdomen
- Retroperitoneum

(c) *Rare indications*
- Kidney tumors
- Prostate tumors

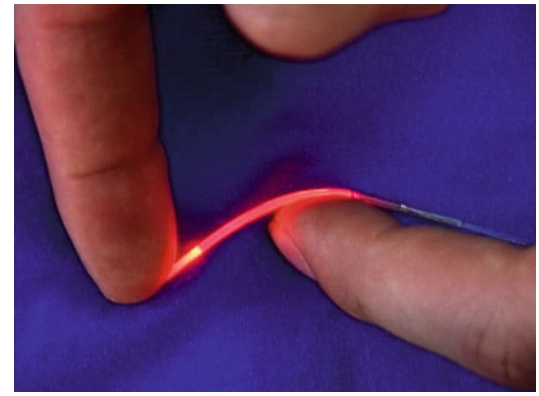

Fig. 13.26 The figure is showing a laser applicator with a flexible diffuser tip and an active length of 3 cm

13.2.1.3 Material

Laser System

Laser coagulation is accomplished using a neodymium-YAG laser light with a wavelength of 1,064 nm (MediLas 5060, MediLas 5100, Dornier Germering, Germany) (Fig. 13.25), delivered through optic fibers terminated by a flexible diffuser tip with a diameter of 1.0 mm. The flexible tip reduces the risk of damage to the diffuser tip to almost zero (Fig. 13.26). The diffuser tip is mounted at the end of a 10-m-long silica fiber (diameter 400 μm). The active length of the diffusor tip ranges from 20 to 40 mm. The laser power is adjusted to 10–12 W/cm active length of

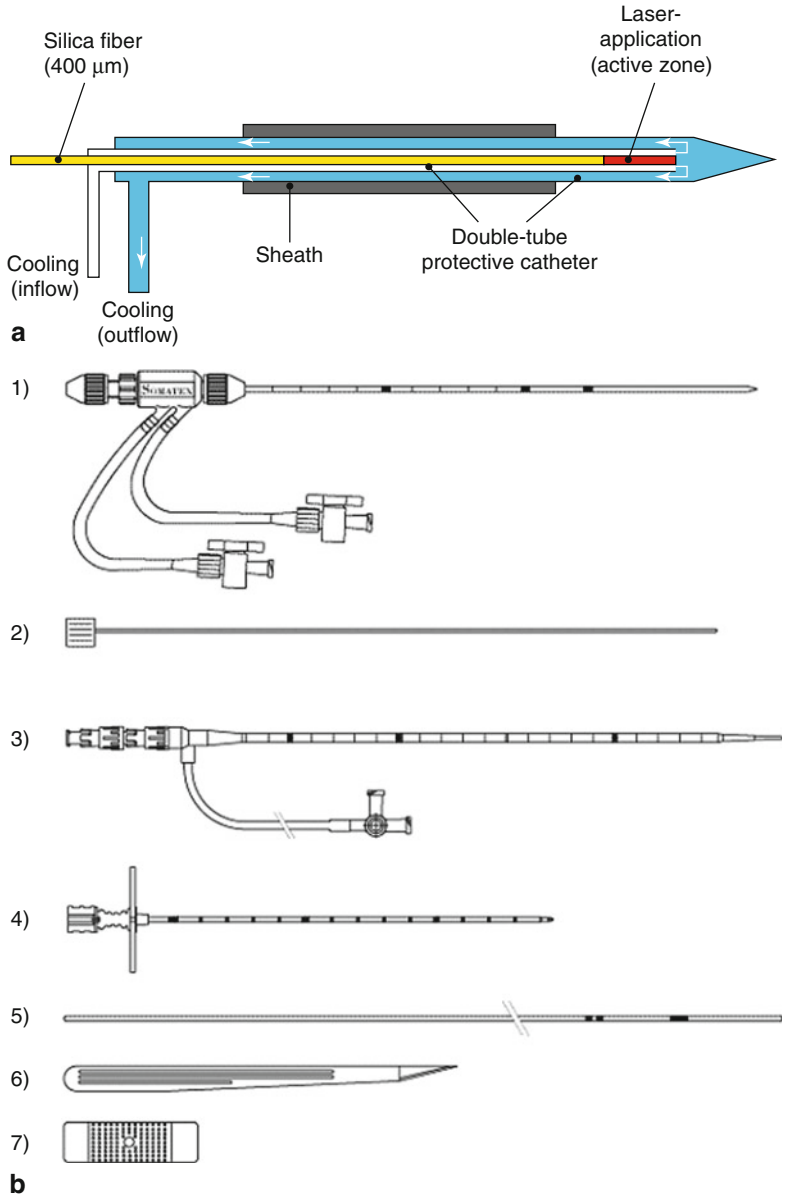

Fig. 13.27 (**a**) Illustration of the internally cooled power laser system. (**b**) Schematic drawing of all components of the laser application system. *1*) Protective catheter, *2*) Mandrin for protective catheter, *3*) Sheath with dilatator, *4*) Puncture needle, *5*) guide wire, *6*) scalpel, *7*) fixation plaster

the laser applicator. The effective laser power at the diffuser tip should be verified with a power meter. The laser system is equipped with a roller pump, which allows internal cooling of the protective catheter.

Laser Application Set

The power laser application system (Fig. 13.27) (SOMATEX, Teltow, Germany) for MR-guided minimally invasive percutaneous laser-induced thermotherapy of soft tissue tumors consists of an MR-compatible cannulation needle (length 20 cm, diameter 1.3 mm) with a tetragonally beveled tip and stylet, a guide wire (length 100 cm), a 9 French sheath with stylet, and a 7 French double-tube thermostable (up to 400 °C) protective catheter (length 40 cm) also with a stylet which enables internal cooling with saline solution and prevents direct contact of the laser applicator with the treated tissues (Vogl et al. 1997b).

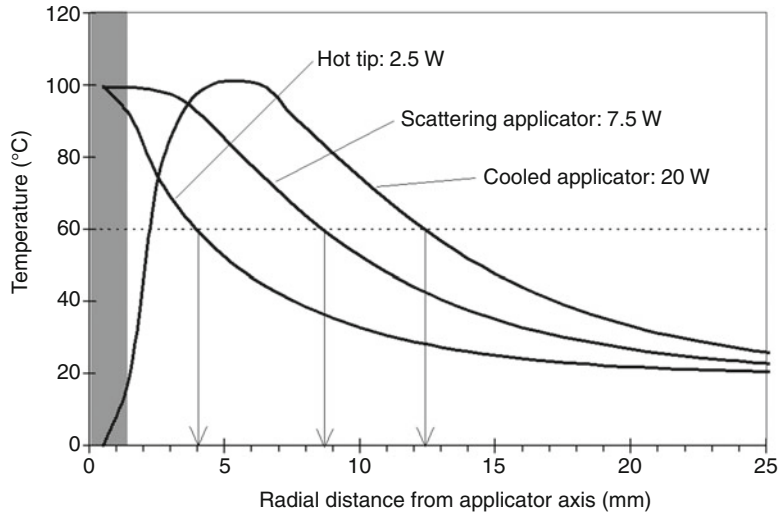

Fig. 13.28 The drawing is showing the influence of internal cooling of the laser application system. The cooling allows to ablate with higher power settings and is resulting in larger ablation volumes

Cooling of the surface of the laser applicator modifies the radial temperature distribution so that the maximum temperature shifts into deeper tissue layers (Fig. 13.28). This was evaluated by computer simulations calculating the temperature distribution of different types of applicators in pig liver by defining the input power to achieve a maximum tissue temperature of 100 °C. The temperature distribution at the cooled applicator is a combined effect of deep optical penetration of neodymium-YAG laser and cooling of the applicator surface. Hence, the cooled applicator can be used at higher laser powers than non-cooled systems without exceeding critical temperatures. The protective catheter is flexible, transparent, or near-infrared radiation and made of teflon. Marks on the sheath and the protective catheter allow exact positioning of the sheath and the protective catheter in the patient. The protective catheter has a sharpened tip, which —in combination with an adapted mandrin—allows repositioning of the system.

The system is fully compatible with MR imaging systems. Magnetite markers on the laser applicator allow an easier visualizing and positioning procedure.

The laser itself is installed outside of the examination unit; the light is transmitted via a 10-m-long optical fiber. The complete clinical setup used for LITT is shown in Fig. 13.29a. Up to two laser fibers can be connected to one laser system via a beam splitter (Fig. 13.29b).

13.2.1.4 Technique

The success of LITT depends on delivering the optical fibers to the target area, real-time monitoring of the effects of the treatment, and subsequent evaluation of the extent of thermal damage. The key to achieve these objectives is the imaging methods used.

The metastasis is localized on computed tomographic scans, and the access to the lesion is planned. The entrance and destination points are marked at the skin, followed by a skin disinfection and sterile covering (Fig. 13.30). After that the injection site is infiltrated with 10–40 ml of 1 % Scandicain. The laser application system is inserted under CT guidance using the Seldinger technique. Initially a puncture needle (18 G) will be advanced to the tumor. The position of the tip of the needle will be verified by a CT scan. Afterward the mandarin of the needle will be removed, and a guide wire will be inserted until the end of the needle. In the following step, the needle will be removed, and the guide wire is hold in place. After that, the sheath with the mandarin will be advanced over the guide wire with the tip of the sheath to the end of the guide wire. Afterward the mandarin of the sheath will be removed, and the protective catheter will be

Fig. 13.29 (**a**) The photograph is showing the setup of five laser systems (Dornier MediLas 5100) in the control room for simultaneous treatment of multiple lesions. To each of the five laser systems, up to two laser fibers can be connected via a beam splitter (see also Fig. 13.29b). (**b**) The picture is showing a beam splitter, connected to the laser, which allows the simultaneous use of two laser fibers at one laser system

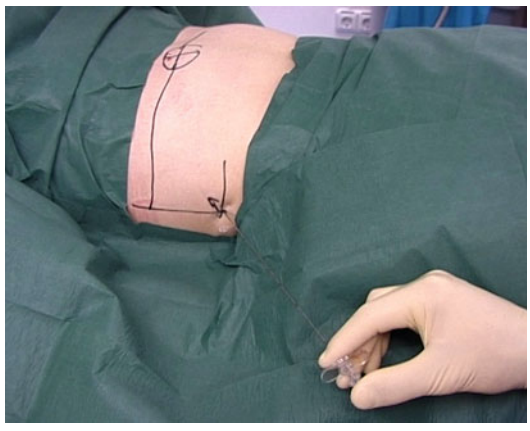

placed through the sheath. The tip of the protective catheter should be advanced until the distal end of the sheath system. Afterward the sheath will be pulled back 5 cm, while the protective catheter will be hold in place. This allows afterward penetration of the laser light through the protective catheter into the tissue without hitting the sheath system, which is not transparent for

Fig. 13.30 The picture is showing the access planning to a lesion in segment 7. Skin entrance and location of the target are marked with a waterproof pen

the laser light. Reference markers on all devices are helping to position the system in the right way. After that the sheath will be fixed at the skin with a special plaster.

Depending on the size of the lesion, up to five laser applicators are used simultaneously. Based on the fact that always a safety margin of about 5–10 mm at least should be ablated, surrounding the lesion, the following rough rule can be used to calculate the number of laser applicators, which should be inserted. Per centimeter metastases, one laser applicator should be used (Fig. 13.31). Based on the size of the lesion and the active length of the laser applicator, it can be necessary to use the pull-back technique in addition either alone or in combination with multiple applicators (Fig. 13.32a–c). The pull-back technique was used to enlarge the coagulation necrosis in the longitudinal axis and is always used if the active length of the laser applicator is shorter than the required length of the coagulation area. In these cases we start with an ablation at the distal end of the lesion or even behind the lesion. If the MR thermometry is showing complete ablation in this area, we are pulling back the laser fiber within the protective catheter between 1 and 2.5 cm and continue the ablation in the proximal part of the lesion.

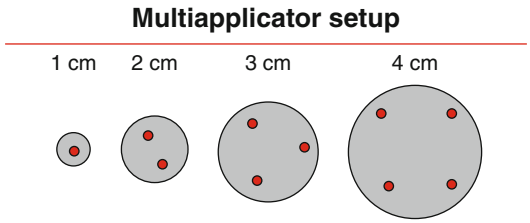

Fig. 13.31 The figure is showing the principal use of the multi-applicator technique. Depending on the size of the lesion, one or more laser application systems should be inserted to get a complete ablation of the lesion and a reliable safety margin

The LITT treatment itself should be performed under MR monitoring. For this purpose, we use a 0.5 T scanner (Privilig, Escint, Israel) and

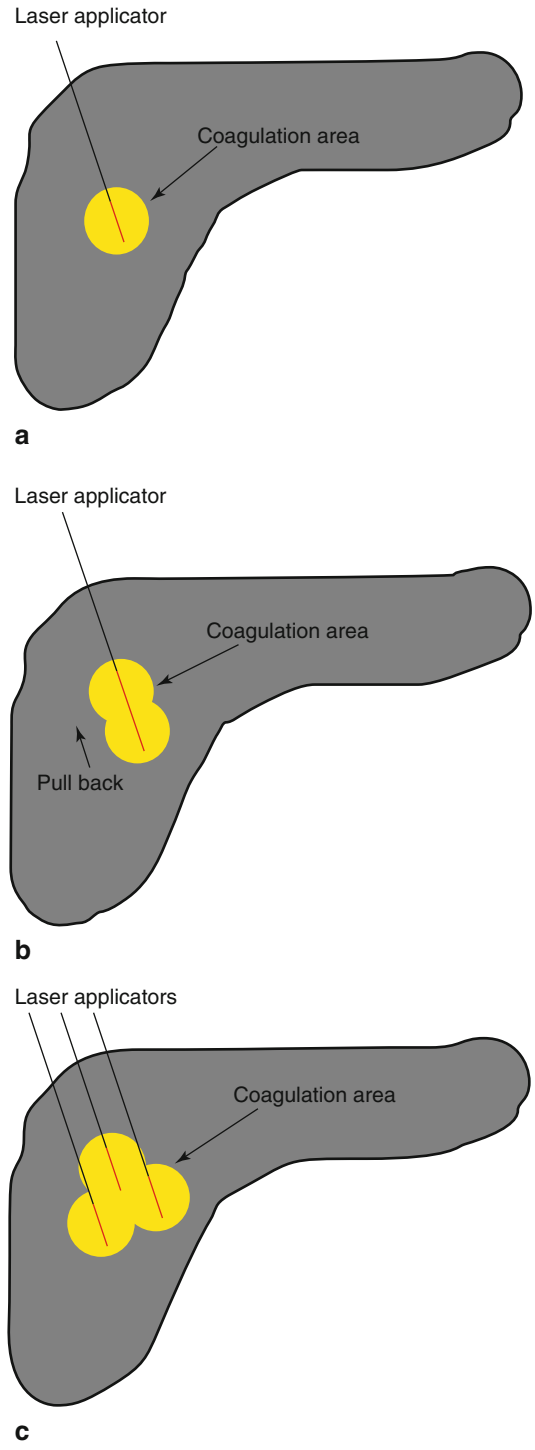

Fig. 13.32 (**a**) Demonstration of a single applicator with a single ablation zone. (**b**) Demonstration of a single applicator in combination with a pull-back technique. This technique permits increasing the volume of ablation along the needle path. (**c**) Demonstration of the multi-applicator technique. Overlapping ablation with multiple laser probes allows to treat large liver lesions up to a diameter of 5 cm

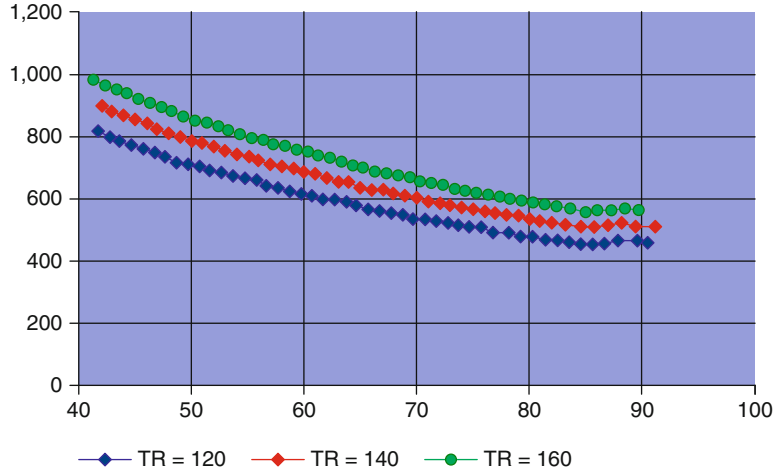

Fig. 13.33 Relationship between signal intensity and temperature using T1-weighted gradient echo sequences with variable TR

T1-weighted GRE sequences (TR/TE = 140/12, flip angle = 80°, matrix 128 × 256, 5 slices, slice thickness 8 mm, interslice gap 30 %, acquisition time 15 s) in axial slice orientation and parallel to the laser applicators. These two sequences were repeated every minute. However, every other MR unit can be used for peri-interventional monitoring. From our experience we recommend the use of T1-weighted gradient echo sequences for thermal monitoring. These sequences are very robust and generally result in acceptable images even in case of by motion or pulsation artifacts. With increasing tissue temperature there is an increase in T1 relaxation time of the tissue, which results in a decrease of signal intensity. There is an almost linear correlation between decreasing signal intensity and increasing tissue temperature in the temperature range, which is relevant for LITT treatment (Fig. 13.33).

The entire LITT treatment can be performed using local anesthesia and intravenously injected analgesics (e.g., pethidine 10–80 mg and/or piritramide 5–15 mg) and sedation (2–10 mg midazolam). Local anesthesia can be achieved with 20–30 ml of 1 % mepivacaine (see Chap. 5).

After the procedure the needle track is closed with fibrin glue. For this procedure the sheaths are pushed forward to the end of the protective catheter, and the protective catheter will be removed. After that a two-lumen catheter will be inserted through the sheath system (Fig. 13.34a), and the fibrin glue will be connected (Fig. 13.34b). The double-lumen catheter results in a mixing of the two components of the fibrin glue at the distal end. Afterward the complete system will be removed slowly under continuous injection of fibrin glue (Fig. 13.34c). After complete removal of the system, only a small skin lesion is visible (Fig. 13.34d), which should be covered with a small plaster.

The first follow-up MR imaging study should be performed on the day after the procedure in order to verify the obtained coagulation area (Figs. 13.35, 13.36, and 13.37). Further follow-up studies are recommended every 3 months after the intervention.

13.2.1.5 Results

Most experience exists with colorectal and breast cancer metastases to the liver. A large-scale, 14-year study has found that laser ablation with MR guidance is very effective in the treatment of liver tumors. In the meantime we ablated a total of 4,887 liver lesions in a total of 1,833 patients. The two largest patient groups are patients suffering

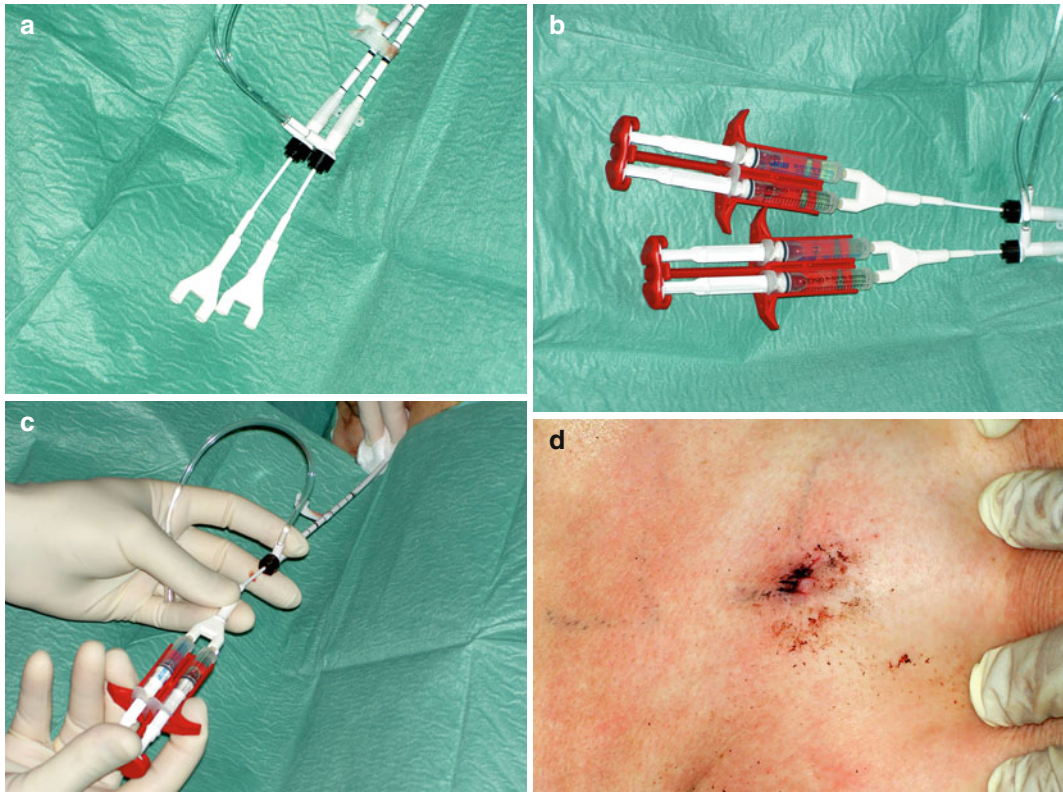

Fig. 13.34 (**a**) Two double-lumen catheters were inserted into the sheaths. (**b**) The fibrin glue is connected to the double-lumen catheter. (**c**) The picture is showing the continuous removal of the complete system under injection of fibrin glue. (**d**) After complete removal of the system, only a small wound is visible, which should be covered with a small plaster

from colorectal liver metastases and breast cancer liver metastases.

Colorectal Liver Metastases

In our institution, MR-guided LITT was performed in 980 patients with 2,874 liver metastases of colorectal cancer between 1993 and 2007. 31.1 % of the patients had recurrent metastases after surgery, 37.8 % had metastases in both liver lobes, 14.8 % refused surgical resection, 3.5 % had contraindications for surgery, and 12.8 % had metastases at difficult localization for surgery. Seven thousand thirty-four patients were treated in curative intention; 246 patients were treated in palliative intention.

The mean survival rate (SR) for all patients with curative intention, starting the calculation at the date of diagnosis of the metastases which were treated with LITT, was 3.6 years (95 % confidence interval (CI): 3.4–3.9 years). In the palliative group, mean survival was 2.7 years (95 % CI: 2.4–3.0 years). Patients who have refused surgical resection of resectable liver metastases ($n = 135$) had a mean survival of 4.3 years.

Prognostic factors are the primary lymph node status, the number of initial metastases, the synchronous metastases versus metachronous, the complete ablation of all visible metastases, the indication for LITT, the size of the treated metastases, and the time between the primary metastases and the development of the first liver metastases.

Breast Cancer Liver Metastases

Also in patients suffering from breast cancer liver metastases, LITT is an effective treatment option.

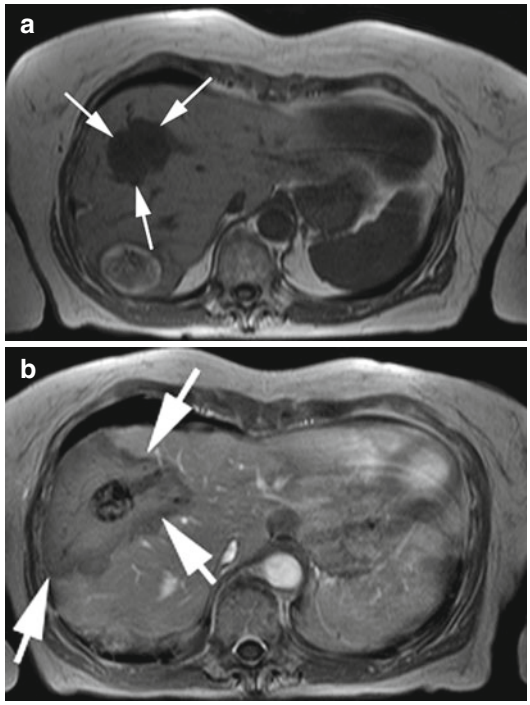

Fig. 13.35 (**a**) The T1-weighted plain image shows a liver metastasis (*arrows*) with a diameter of 4.9 cm. (**b**) The contrast-enhanced MR image 24 h after LITT is showing the obtained coagulation area (*arrows*), significantly exceeding the initial tumor volume

Between 1993 and 2007, we treated 965 metastases in 421 patients. The influence of prognostic factors such as the number of treated metastases, presence of bone metastases, and hormone receptor status was evaluated. 73.4 % of patients were treated in curative intention (≤5 metastases, no extrahepatic disease except controlled bone metastases); 26.6 % of patients were treated in palliative intention (>5 metastases and/or extrahepatic disease).

The mean overall SR was 4.6 years (95 % CI: 4.2–5.0 years, 1-year SR 95 %, 2-year SR 77 %, 3-year SR 58 %, 5-year SR 35 %) after diagnosis of treated metastases. In the curative patient group, the mean SR was 5.0 years (95 % CI: 4.5–5.4 years) and significantly superior to the palliative group with a mean survival of 3.2 years (95 % CI: 2.7–3.7 years).

Hepatocellular Carcinoma (HCC)

A total of 156 lesions were treated in 99 patients. The mean survival was 4.3 years (95 % CI: 3.6–4.9 years, 1-year SR 95 %, 2-year SR 72 %, 3-year SR 54 %, 5-year SR 32 %).

Extrahepatic LITT

There is only scarce data on extrahepatic LITT. The following tumors were treated: paravertebral

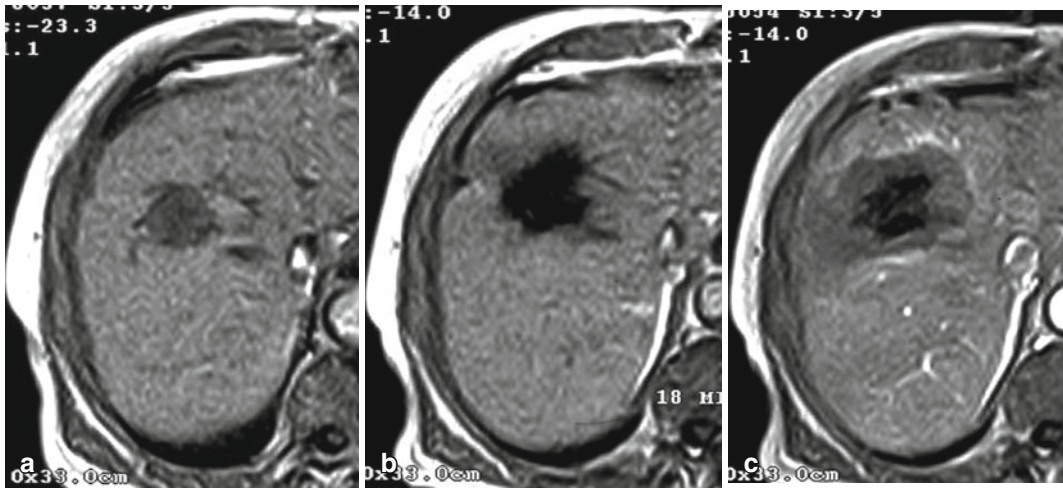

Fig. 13.36 (**a**) The FLASH 2D image is showing the metastases in segment 8 before starting the laser ablation. (**b**) The FLASH 2D image is showing the decrease of signal intensity 18 min after starting the laser ablation. (**c**) The contrast-enhanced FLASH 2D image immediately after stopping laser ablation is showing coagulation area, which is exactly corresponding with the area of decreased signal intensity during ablation (compare Fig. 13.36b)

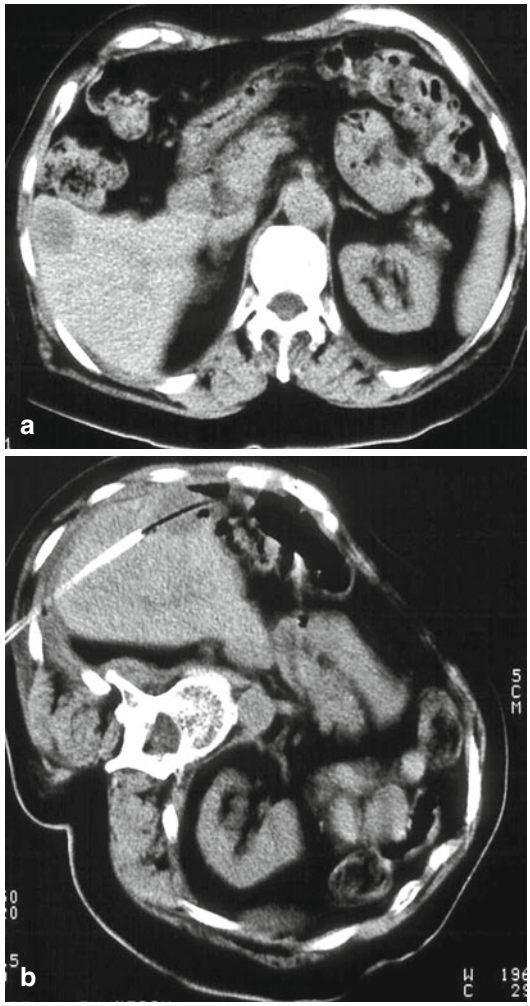

Fig. 13.37 (**a**) The CT image is showing a metastasis at the anterior border of the liver. (**b**) The CT image is showing a positioned laser applicator

recurrence of hypernephroma (Fig. 13.38), recurrence of uterus carcinoma, recurrence of chondrosarcoma of the pubic bone, presacral recurrence of rectal carcinoma and anal cancer, metastases in the abdominal wall, and lymph node metastases of colorectal carcinoma close to the aorta or inferior vena cava. The maximum diameter of the lymph node metastases was 3.5 cm. Other indications for LITT were malignant kidney tumors and recurrent tumors in the head and neck region. LITT of lung tumor is described in detail in Chap. 13.3.3.

Especially in the head and neck area, which contains a multitude of small, complexly arranged anatomic structures, intimate knowledge of normal spatial relationships and variations is necessary to plan and implement appropriate therapy. Lesions often lie near vital structures, complicating diagnostic and therapeutic procedures. Improved visualization during such procedures can therefore provide the physician with critical information, permitting innovative procedures. For the treatment of tumors of the nasopharynx and parapharyngeal space, a subzygomatic approach is used (Fig. 13.39). Tumors of the maxillary sinus are directly punctured from anterior or lateral; lesion of the neck and the floor of the mouth is punctured using either an anterior or lateral approach.

13.2.1.6 Complications

Typical complications of LITT include pleural effusion and subcapsular hematoma. Common side effects are short-term fever and fatigue as well as local pain, in case the lesions were close to the capsule. Most of these complications are minor and do not cause hospitalization.

In our experience the most common side effect of LITT treatment is reactive pleural effusion. In detail, typical complications are as follows:

- Pleural effusion (9.2 %) requiring puncture in 1.0 %
- Small, self-limiting subcapsular hematoma (4.3 %)
- Intrahepatic abscess (1.1 %)
- Intrahepatic bleeding (0.6 %) requiring treatment in 0.1 %
- Intra-abdominal bleeding (0.2 %) requiring treatment in 0.1 %
- Pleural empyema (0.1 %)
- Local infection (0.1 %)
- Injury to the bile duct (0.1 %)

Four patients (0.2 % on patient basis, 0.1 % on treatment session basis) died within 30 days. Interestingly patients who were treated for pancreatic metastases have a higher risk to develop a liver abscess, which was observed in 12.5 % compared to 0.6 % in the other patients.

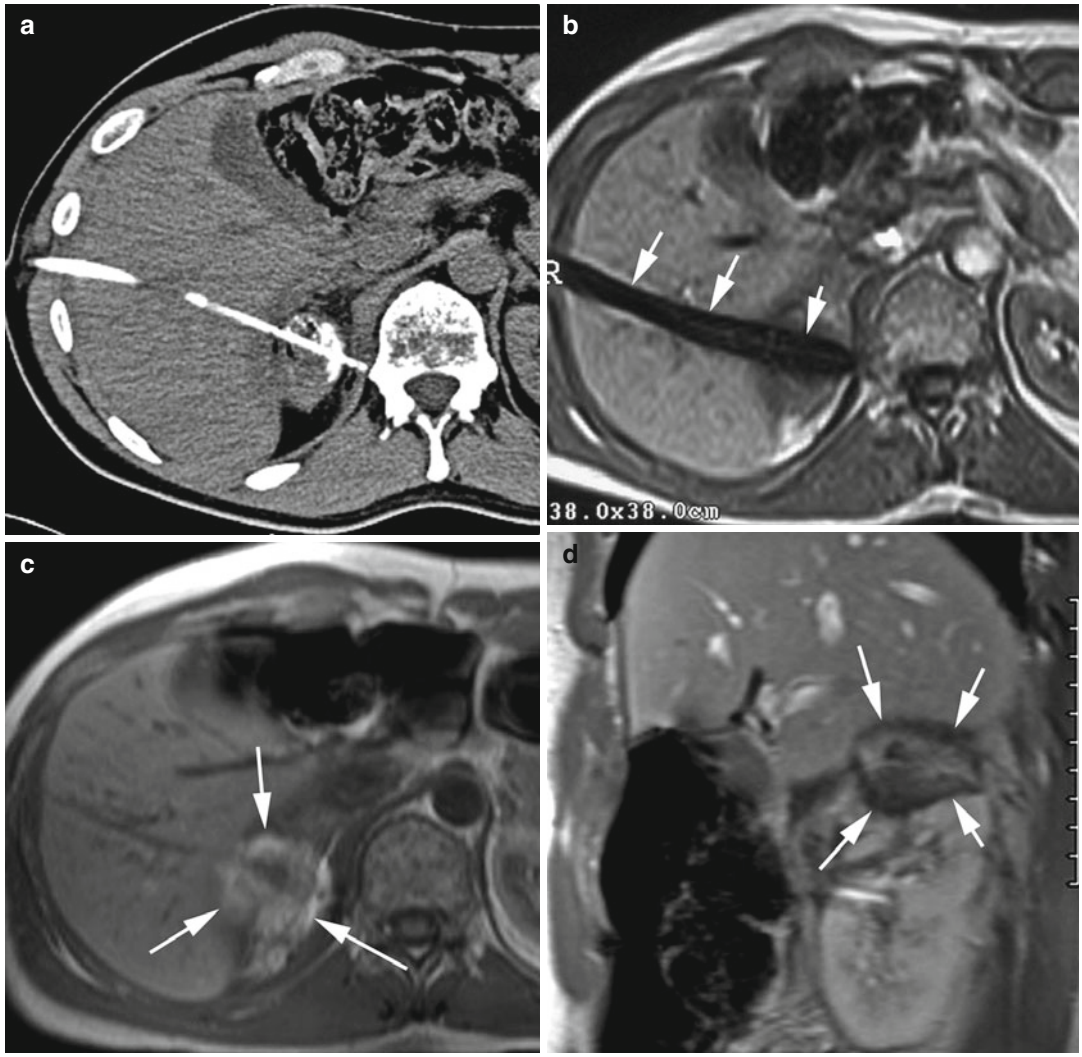

Fig. 13.38 (**a**) CT-guided transhepatic placement of a laser application system in an embolized kidney carcinoma. (**b**) The gradient echo image is showing the susceptibility artifact of the laser application system due to the inserted magnetite marker (*arrows*) in order to verify the positioning on MR imaging. (**c**) The non-enhanced FLASH 2D image (sagittal view) 24 h after the ablation is showing the induced coagulation area. Please note the typical hyperintense signal of the coagulation area due to hemorrhagic diffusion into the coagulation area. (**d**) The contrast-enhanced FLASH 2D image (0.1 mmol Gd/kg b.w.) 24 h after the ablation is showing the induced coagulation area (*arrows*)

Summary

Up to 70 % of patients with colorectal cancer—which is among the most common cancers—eventually develop liver metastases. In 30 to 40 % of those patients with metastases, their metastases are confined to the liver at the time of diagnosis (Harned et al. 1994; Hughes et al. 1988; Nordlinger et al. 1996; Scheele et al. 1991, 1996).

Until recently, the traditional treatment for primary or metastatic liver tumors has been surgical resection. However, only 25 % of

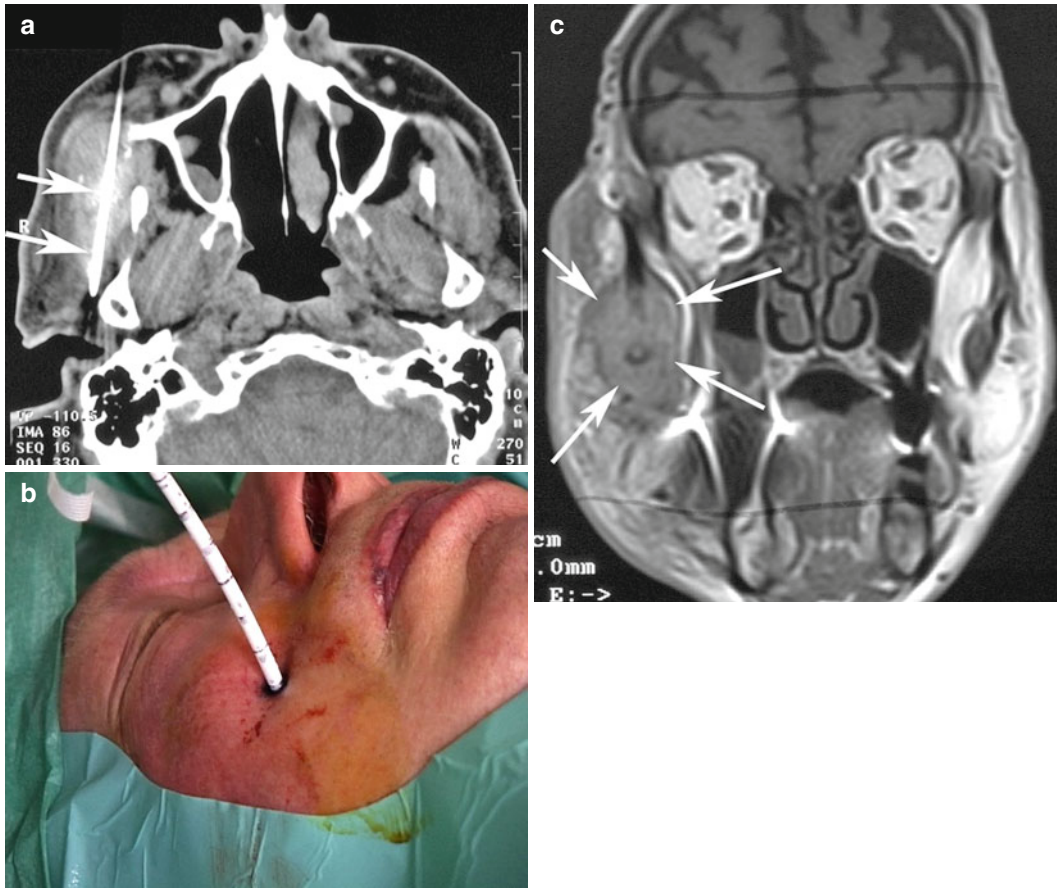

Fig. 13.39 Metastases of a hepatocellular carcinoma in the masticator space. (**a**) CT-guided puncture of the lesion. Note the positioning of the needle (*arrows*). (**b**) The clinical image shows the laser application system in situ using a subzygomatic approach. (**c**) This contrast-enhanced T1-weighted sequence after LITT (12 min, 22.8 W) shows a significant amount of necrosis (*arrows*)

those with liver metastases are candidates for surgery because of the size, distribution, or accessibility of their tumors. Also, the morbidity rate for surgery is high. Therapeutic alternatives are also needed because the incidence of new liver metastases following successful resection of metastases is high—with 60 to 80 %. Many studies have shown that large liver resections stimulate many growth factors, including growths of micro-metastases, which are potentially somewhere else in the liver. This is probably the reason why many patients are developing new metastases already in the first year after surgical resection. There also are indicators that the stimulation of the growth factors after surgical resection is stimulating the development of new metastases not only within the liver but also outside of the liver, such as in the lung or lymph nodes. Chemotherapy is still widely used to treat liver metastases. However, the survival is still limited, and many patients are suffering from relevant side effects (Gallagher et al. 2007; Mehta et al. 2008; Mentha et al. 2007; Min et al. 2007; Tan et al. 2007; Ychou et al. 2008; Zorzi et al. 2007).

Therefore, we believe that minimal-invasive tumor ablation using the LITT technique

is resulting in improved survival and should be routinely used in an adapted oncologic concept including surgery, chemotherapy, and ablation.

Key Points

- Select your patients carefully.
- Discuss all therapeutic alternatives with the patients.
- Do an optimal treatment planning, including high-resolution cross-sectional imaging and access planning.
- Know the possible complications, and stick to the thesis that the best way to avoid complications is to know the potential complications.
- Integrate the patients into a well-adapted oncologic concept.
- Follow your patients regularly.

13.2.2 Laser Ablation: Lung

Christian Rosenberg

13.2.2.1 Introduction

Imaging-guided percutaneous laser ablation (LA), also known as laser-induced thermal therapy (LITT), is a local treatment option for primary and secondary malignant lung tumors, primarily in patients not amenable to surgical resection.

Local treatment of distant tumor metastases as part of a multimodal cancer therapy has been reported to deliver a proven survival advantage for selective patients, as known from the surgical patient collective (Goya et al. 1989; McCormack et al. 1992; Martini et al. 1995; Shirouzu et al. 1995; Okumura et al. 1996; Baron et al. 1998; Pastorino et al. 1998; Friedel et al. 1999; Inoue et al. 2000; Pages Navarrete et al. 2000; Davidson et al. 2001; Hendriks et al. 2001; Rena et al. 2002; Vogelsang et al. 2004). Despite recent successes in developing systemic therapy regimens and new drugs, surgical resection is the only known curative therapy option in stage IV colorectal carcinoma patients with pulmonary metastases as sole residual disease (Pfannschmidt et al. 2002; Watanabe et al. 2003). Eventhough, a huge number of patients with metastatic disease confined to the lungs are not amenable to surgery for different reasons (Penna and Nordlinger 2002).

Non-small-cell lung cancer (NSCLC) is one of the most common cancer diseases worldwide. Only 20 % of the patients with primary diagnosis of NSCLC are suitable for potentially curative resection, usually the treatment of choice for localized cancers (Simon et al. 2007).

The possibility of reoperation in case of recurrent tumor, metastatic or primary, is limited due to the repeat loss of parenchyma. Other local therapies less tissue consumptive and with less morbidity have become more important during the last few years. Video-assisted thoracoscopic surgery (VATS) accounts for respectable therapy results, even though it comprises technical limitations due to a high dependance on lesion localization (Landreneau 1996; McCormack et al. 1996). In this context, minimally invasive procedures, such as percutaneous thermal ablation, have gained influence. Selective heating of tumor tissue to temperatures of over 60 °C leads to irreversible protein denaturation and cell death. A variety of different thermal ablation modalities—radiofrequency, laser, cryo-, or microwave ablation—seem to have comparable parenchymal impact and side effects. Nevertheless lung-specific conduction characteristics for laser light are proposed to improve therapeutic success and control (Knappe and Mols 2004).

13.2.2.2 Indications

From our experience performing laser ablation in lungs, several criteria as stated below have been found to be crucial for treatment eligibility.

Inclusion Criteria:

1. Histologic proof of malignancy of the lung lesion or newly found lung nodule in a patient suffering from a previously treated primary tumor known to metastasize to the lung.
2. Interdisciplinary stating of inoperability.

3. In case of metastatic disease and at the time of presentation the patient has been staged locally "R0" and received adequate therapy for his primary tumor.
4. If the patient suffers from primary NSCLC it is critical to exclude metastatic disease to mediastinal lymph nodes. PET–CT is appreciated.

Exclusion Criteria:

1. Constitutional or medically induced coagulopathies:
   - Platelet count <50,000/mm^3
   - PTT >50 s
   - Quick value <50 %
2. A Karnowsky index below 60 % or a body weight of more than 30 % below ideal weight, a FEV1 below 800 ml, or earlier pneumonectomy are considered contraindications.
3. A lesion size beyond 4 cm both for primary cancer and metastatic disease, a lesion count of at least 10 for both lungs, infiltration of the pleura, or central necrosis with drainage into bronchi are considered relative contraindications. Such constellations demand case-specific decisions.

A technically complete therapy may include several ablational procedures. It comprises an adequate therapeutical impact per lesion and treatment of all known tumor correlate. Therapy goals may therefore be either "technically complete" or "cytoreductive," the latter aiming at symptom palliation or systemic therapy support. The therapy goal should be initially determined and communicated to both patient and referring physician.

13.2.2.3 Material

Different laser generating systems are designed for specific medical use. For interstitial ablation, the neodymium yttrium aluminum garnet (Nd:YAG) laser with a near-infrared wavelength of 1,064 nm is suited best. The specific wavelength utilizes deeper light penetration into tissue (Roggan et al. 1997). In our own setting we use three Nd:YAG laser generators, fitted with facultative 2- and 4-time beam splitters providing a variety of setting designs if it comes to simultaneous use of multiple fibers.

Different commercially available applicator systems are being used for LA. All systems safely provide transmission of light through an optical fiber and into the target zone, energy transformation into heat, and fiber cooling to prevent carbonization. Whereas an established 9 French system with a closed cooling circuit is widely used in hepatic tumor ablation (Vogl et al. 2000) and occasionally in lungs (Vogl et al. 2010), only one system has been designed especially for the use in lungs (RoweCath, RoweMed, Parchim, Germany, formerly: Monocath, Trumpf Medizinsysteme, Umkirch, Germany) (Hosten et al. 2003; Rosenberg et al. 2009). It consits of the optical laser fiber with a flexible diffusor tip and a surrounding 5.5 French teflon tube (Fig. 13.40). The major advantage is its comparably small diameter, mostly due to invention of a one-way open cooling solution. Cooling of the heat-releasing fiber tip is provided by continuous instillation of saline (sterile isotone sodium chloride, 40 ml/h, regular perfusor) through a capillary gap between the tube and fiber. A y-shaped connection piece comprises an axial adjustment capability, hemostatic valve, and connection of the cooling line. Below operating temperatures, residual fluid may evaporate into the surrounding lung parenchyma at the terminal tube opening. For applicator placement a sharpend titanium mandrin carries the flexible tube and is later replaced by the laser fiber. Different lenghts of diffusor tips (1, 2, 2.5, or 3 cm) are available, as well as different applicator lengths of 12, 14, 16, and 18 cm.

CT fluoroscopy is the preferred imaging technique for imaging guidance and therapy monitoring. Sterile draping is performed analogously to any surgical procedure. Material and skills for implementation of a thoracic drainage must be in place to treat peri-procedural pneumothoraces (see Sect. 11.2). Instrumentation for synchronous air aspiration from the pleural space through a small-lumen cannula should be prepared. Capabilities to monitor oxygen saturation and heart rate and to apply oxygen are demanded. Skills and instrumentation to intubate the patient should be within range.

13.2.2.4 Technique

Pre-interventional Workup

Pre-interventional imaging involves a contrast-enhanced computed tomography (CT) scan of the

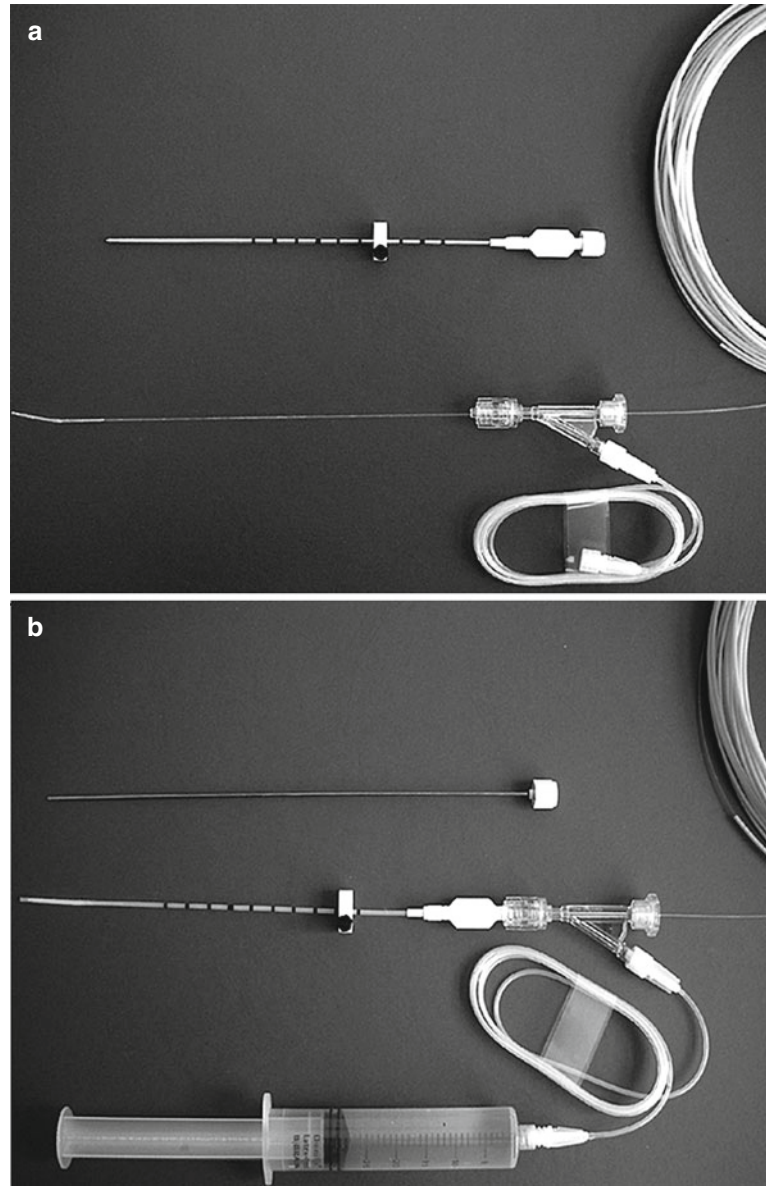

Fig. 13.40 Applicator: miniaturized applicator system consisting of 5.5 F teflon tube with titanium mandrin (**a**). In the second picture the mandrin is removed and replaced by the laser fiber with a 3-cm flexible diffusor tip (**b**)

chest with a standardized intravenous contrast injection protocol (tube voltage 120 kVp, 5-mm slice thickness with overlapping increment, tube current 80–120 mA, 27–35 g iodine, injected with a flow rate of 0.9–1.3 mg iodine/s, injection delay 25 s). If the patient underwent CT within 1 month prior to presentation, a plain spiral CT at the day of the intervention is usually sufficient for procedure planning.

Preprocedural measures include:

- Patient anamnesis
- Cinical examination
- Spirometry
- Blood sampling (small blood count, coagulation parameters, serum creatinine, TSH)

Informed consent has to be obtained at least 24 h before each procedure. It is critical and has to be achieved in analogy to any elective surgical procedure. At that state the patient has signed a written document stating that he or she is informed

about treatment options and risks and willing to undergo the treatment. He or she has explicitly been informed about laser ablation being a local treatment in contrast to a systemic cancer therapy.

Procedure

At the day of ablation, patients are transferred to the CT suite. The lung ablational procedure is performed in the CT suite with the patient positioned on the CT table during the entire procedure. The easiest approach to the target lesion determines the patient position, which is supine in most cases, prone or lateral to access, for example, dorsal or pericardial tumors. Dedicated technical or nursing radiology staff performs sterile draping and assists the procedure.

Cooperation of the conscious patient, who is supposed to follow breathing commands, will be appreciated in most cases, even though it is not critical. The patient receives local anesthesia (e.g., lidocaine 1 %) at the puncture site, infiltrating subcutis, costal periosteum, and parietal pleura. Accessing the thoracic space, intercostal and internal thoracic arteries have to be avoided. The patient is asked to suppress coughing, in case it is triggered passing the pleural space. A wide enough angle to the pleura, a fast puncture, and a minimum of pleural penetrations are most important to prevent pneumothorax. The duplicated visceral pleura of the interlobar spaces has to be taken into account, when planning the procedural approach. A translobar access should be avoided whenever possible.

CT fluoroscopy with 5-mm slice thickness, 120 kV, and approximately 60 mAs is the preferred imaging technique. The patient is conscious and under intravenous analgo-sedation, for example, 10 mg haloperidol and 100 mg pethidine slowly infused together with 20 mg of metoclopramide in 500 ml sodium chloride (see Chap. 6). Oximetry, breathing frequency, and electrocardiography are monitored continuously throughout the procedure.

Ablation parameters, including count and type of applicators and number and length of treatments, are to be determined according to target size, location, and primary treatment goal. Lung tumors are treated using single or multiple applicators synchronously (Fig. 13.41), tumors larger than 2 cm with at least two applicators in parallel or crossed position. Two applicators are also used to flank nodules that are too small to be speared. If a single applicator is used, it is positioned in the middle of the target, piercing both opposite tumor margins. In most cases, 3-cm active tips will be used; only small nodules located close to vulnerable structures, such as pericardium or pleura, sometimes indicate the use of shorter tips (1, 2, or 2.5 cm). The preprocedural measurement of the puncture depth determines the choice of applicator length (12, 14, 16, or 18 cm). If multiple applicators are used simultaneously, positioning is planned in a way to create overlapping areas of ablation. For procedure planning, an ellipsoid zone of sufficient impact with the length of the active tip that is used and a maximum width of 2.5 cm is estimated. Overlapping of at least 0.5 cm is mandatory. Depending on tumor size, tumor shape, or number of lesions, repeated treatment may be needed to achieve local tumor control. Duration of therapy, meaning continuous application of laser light, and maximum energy are standardized according to earlier ex vivo and in vivo experiments (Hosten et al. 2003; Knappe and Mols 2004). In these experiments the extent of therapy impact had been saturated after 15 min and a maximum energy of 14 W. In our own treatment regimen, we stepwise elevate the watt count (2 W/min) and maintain the maximum energy of 14 W for at least 15 min.

Once all applicators are in place, the titanium mandrins are removed one by one and immediately replaced by the prepared laser fibers. CT fluoroscopy in repeated sequences is used to monitor therapeutic effects within the impact zone (intratumoral lytic changes and a hemorrhagic external rim) and to exclude progressive pneumothoraces or parenchymal bleeding.

After the therapy is completed, fibers and tubes are removed. Performing laser ablation in the lungs, puncture tract coagulation is not necessary. A final regional CT scan should be done to document absence of pneumothorax and bleeding. Small and locally defined air inclusions within the pleural space can be tolerated if not progressive. If a pneumothorax develops on table, during or after the

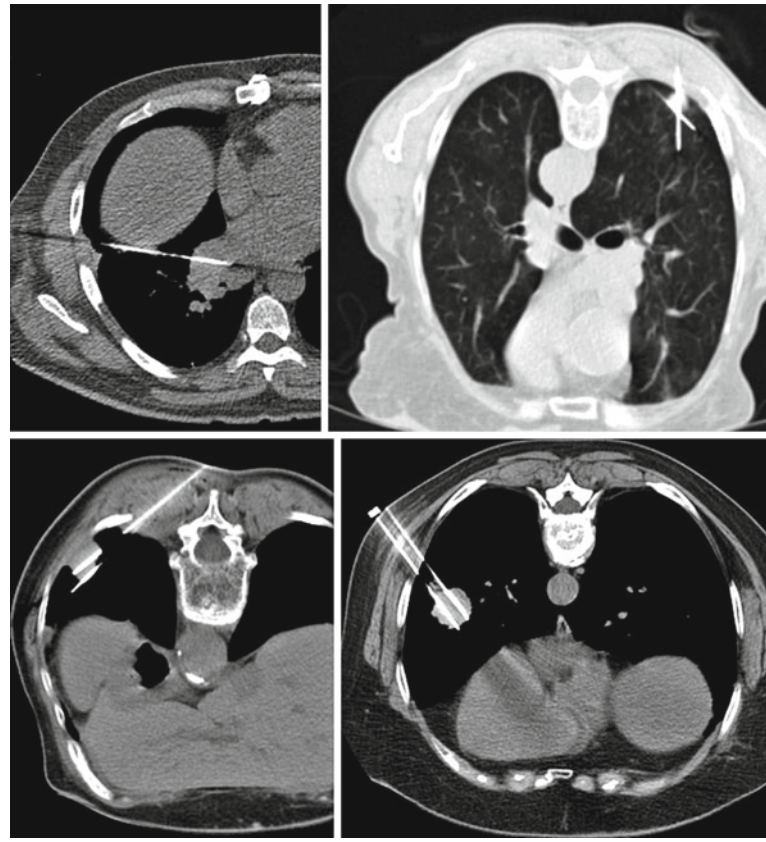

Fig. 13.41 Four different lung lesions being punctured for laser ablative therapy in single or multiple applicator technique. Depending on lesion size and location (pericardial, peripheral, and subpleural), different puncture techniques are used

procedure, a small-lumen cannula can be applied at the highest point of the widened pleural space to manually and simultaneously extract air without disturbing the setting. If larger or progressive pneumothoraces are detected, drain implementation and connection to a suction machine is mandatory, preferably done still on table (see Sect. 11.2). Most patients can immediately be transferred to the standard care unit and regularly dismissed the day after, after two nights in case of drainage, respectively. All patients receive a control chest radiograph 2–4 h after the procedure in order to rule out delayed or progressive pneumothorax. Post-procedural oral analgetics (e.g., 3×40 novaminsulfonium drops) should be given depending on the patients' symptoms (see Chap. 6).

Follow-Up

Post-interventional imaging is performed using a multislice spiral CT scanner. Non-enhanced and contrast-enhanced images of the entire chest are acquired. For the contrast-enhanced CT scan, the same scan protocol as for pre-interventional imaging is used. A contrast-enhanced CT, acquired the first post-procedural day, is used for definitive treatment evaluation. A coagulative zone fully covering the target lesion and comprising a safety margin (aimed 5 mm) of altered regular tissue in all three dimensions on the one hand and absence of contrast enhancement within the treated tumor on the other hand is read as technical ablative success. In few cases of nonreactive (as far as imaging is concerned) and primarily or secondarily very dense targets, a complete defect of earlier shown contrast enhancement is the only therapy-related alteration and read as technically successful ablation. Immediately after therapy, tumors may slightly increase in size due to necrosis and interstitial fluid uptake. Others, mainly small sized, will

significantly decrease in size and leave an amorphous residuum of fat- or air-isodense signal. If the first day control exam shows residual vital tumor due to insufficient extent of the ablative zone or due to intralesional contrast enhancement, a re-intervention within the actual hospital stay is the treatment of choice.

Follow-up CT exams are performed within 6 weeks after the procedure; then 3, 6, 9, and 12 months after the ablation; and every 6 months thereafter. Newly found contrast enhancement within the treated tumor or residuum, respectively, or within the ablative zone, if at least 3 months from the date of procedure, is read as recurrent tumor. Also progression in size—of the residuum in toto or marginal and eccentric—compared with the initial post-ablative exam is read as recurrent tumor growth if not inflammatory. Typically the diagnosis of recurrent or residual tumor initiates a re-ablation. In consultation with the patient and referring physician, the achievement of local tumor control, patient's overall condition, and state of disease are reevaluated.

Morphologically the vast majority of treated tumors show a peritumoral diffuse hyperdensity consistent with reactive edema after heat injury. Regularly a thin hyperdense line, representing hyperemic tissue, demarcates the zone of coagulation necrosis (Figs. 13.42 and 13.43). In a minority of cases, therapy will cause cavitation.

Retraction and significant size reduction can be seen after 12 weeks at the earliest. Scar formation as residual finding will be observed in about half of the cases. For all tumors in common, post-procedural absence of contrast enhancement within the treated targets is critical (Weigel et al. 2006).

In general, tumor tissue reaction—imaging wise—can be diverse and depends on tumor entity and pretreatment (Rosenberg et al. 2009). A hypervascular metastasis of a renal cell carcinoma without pretreatment may disappear soon after ablative therapy, leaving a flurry scar, whereas metastases of a hepatocellular carcinoma in another case, representing a stable disease after radiation therapy, may show no correlate for therapy success but loss of contrast enhancement.

13.2.2.5 Results

In our institution, 235 interventional procedures have been performed in 114 patients with an overall tumor count of 206, which up to now is the biggest single center study cohort. In ten cases, two seperate lung lesions were targeted in one same session; consecutive total count of targets was 245. Of these 245 targets, 41 were treated repetetively. Two sessions to complete treatment of a single tumor were necessary in eight cases; in two other cases, three sessions were needed.

At the stage of 64 patients and 108 treated metastases (excluding primary lung cancer), our data showed achievement of initial technical success—according to the criteria described in Sect.. 13.2.2.2—in 85/108 (78 %) tumors (Rosenberg et al. 2009). The per-lesion-based tumor progression rate after therapy was 30 % ($n=32$) for all 108 treated lesions. Local recurrence after initially complete therapy was diagnosed in 24 of 85 (28 %) tumors. Tumor recurrence was seen as late as 25 months after initial procedure (1.1–24.5 months, median 7.1 months). The overall recurrence-free interval was median 4.4 months (0.0–52.9 months). If the lesion size was beyond 4.0 cm, the tumor progression rate was 33 % (4/12) for these lesions; in lesions smaller than 1.5 cm, it was 19 % (7/36) with progression-free intervals of median 1.9 months (0.1–52.9 months) and 5.0 months (0.0–52.5 months), respectively.

Thirty-three patients suffering from metastatic disease did not receive technically complete therapy of their initially diagnosed disease; therefore, they were primarily or secondarily treated with cytoreductive intent. For these patients the Kaplan–Meier median time to death was 12.2 months (95 % CI 0.8–23.6 months) with 1-, 2-, and 3-year survival rates of 57, 37, and 7 %. For 31 patients who were technically completely treated, median survival was 32.1 months (95 % confidence interval (CI) 17.5–47.3 months) with 1-, 2-, 3-, 4-, and 5-year survival rates of 81, 59, 44, 44, and 27 %. The survival benefit for the group of patients with initially complete ablation was statistically significant ($p=0.008$). Median time to death in the subgroups with renal cell carcinoma ($n=10$) and

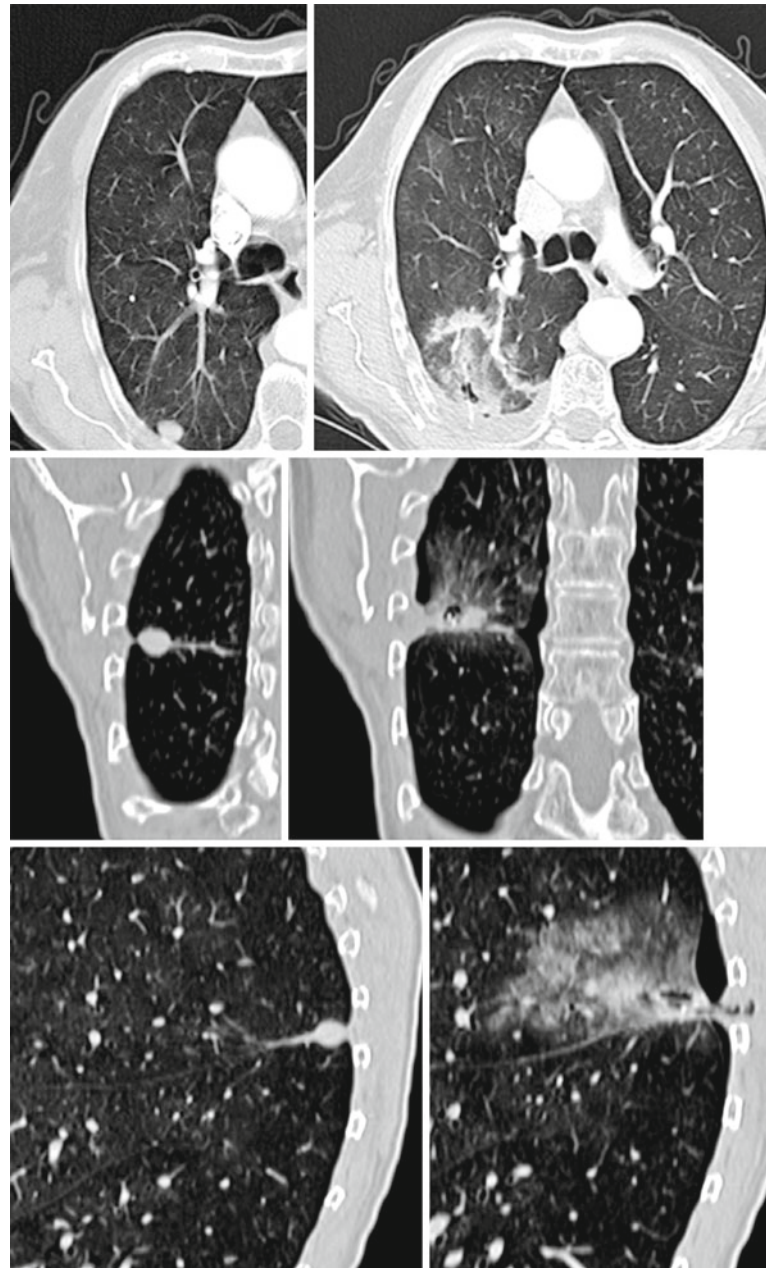

Fig. 13.42 The same right upper lobe (segment 3) peripheral metastasis before and after therapy in three different planes. CT thin-slice reconstruction helped to correlate lesion and ablation zone for therapy evaluation. Notice the small air-isodense body in the center of the ablation zone, consistent with the coagulated residual target tumor

colorectal carcinoma metastasis ($n=20$) were 24.3 and 33.6 months, respectively.

The rate of local tumor recurrence in a per-patient-based calculation was 30 % for all treated patients. Later progressive pulmonary disease was seen in 25/64 (39 %) cases, the latest after 24.5 months (0.5–24.5 months, median 2.8 months). Patients who received complete treatment of their initial disease showed later pulmonary progression in only 32 % (10/31) of the cases. Extrapulmonary metastasis occurred in 32/64 (50 %) patients, after 0.5–52.9 months (median 4.5 months). In the Kaplan–Meier analysis, the median recurrence-free interval was 7.4 months (95 % CI 2.5–12.4 months) for patients who received technically complete treatment.

Fig. 13.43 A 83-year-old female patient with subpleural metastasis of a renal cell carcinoma in the right lower lobe segment 6. Scans are taken before and immediately after laser ablation, 4 weeks, 3 months, and 6 months thereafter. The coagulation zone is nicely demarcated and retracts over weeks. The latest scan shows a residual scar

Recurrence-free intervals of median 10.9 months (95 % CI 3.9–11.8 months) for colorectal metastasis patients were the longest within the treated patient group.

Only one study group described a 1-year local tumor control of 91 % after laser ablation (Vogl et al. 2004) but did not follow its patients thereafter. Data on long-term follow-up after thermal ablation other than the ones described above are all derived from radiofrequency (RF)-induced therapies. The Morris group from Sydney reported local recurrence in 38 % and systemic progression in 66 % of their 55 patients having undergone radiofrequency ablation of colorectal metastatic disease (Yan et al. 2006). They achieved a progression-free interval of median 15 months. The Osaka group (Yamakado et al. 2007) presented variable disease-free survival times in the range of 11–50 months, depending on lesion size. Colorectal metastases with a diameter of more than 3 cm showed a worse outcome, when compared to smaller lesions. Similar results were reported by the Dupuy group from Providence (Simon et al. 2007) (Table 13.12).

13.2.2.6 Complications

Major and minor complications should always be differentiated in accordance with the guidelines of the Society of Cardiovascular & Interventional Radiology (SCVIR), with major complications being defined as an unexpected demand of treatment or a prolonged hospitalization period (Omary et al. 2003).

In 129 procedures, three cases of major complications lead to delayed dismissal, unexpected escalation of treatment measures, or readmission. Two of these patients were transferred to the intensive care unit for overnight monitoring after coincidence of parenchymal bleeding and dyspnea. Both of them were retransferred to the standard care unit the day after. In one case, late onset pneumonia with the diagnosis of empyema leads to readmission 6 weeks after therapy. The patient received abscess drainage and demanded intensive care treatment for two nights. There were no therapy-related deaths. Pneumothorax appeared in 38 % (49/129) of the cases, with the need of peri-procedural drainage in 7/129 (5 %) cases. Parenchymal bleeding (13 %, 17/129) was always self-limited and led to temporary hemoptysis in 9/129 (7 %) cases. Small reactive effusion in 24/129 (19 %) cases never required drainage (Table 13.13). Simon et al. reported four procedure-related deaths after radiofrequency-induced thermal ablation in 153 patients (Simon et al. 2007). Compared with other groups performing percutaneous thermal ablation, the necessity of chest tube application to treat pneumothorax was very low in our patient population. Other authors report indications for tube drainage in up to 22 %

Table 13.12 Therapy outcome and survival rates for local cancer treatment in the lung as reported in the literature

Year	Author	Modality	Entity	Patients	1-year survival (%)	3-year survival (%)	5-year survival (%)
1992	McCormack	Thoracotomy	CRM	144	–	–	40
1999	Friedel	Thoracotomy	Diverse M	5,206	84	46	33–45
2000	Inoue	Thoracotomy	CRM	25	–	–	39
1996	Landreneau	VATS	CRM	80	–	–	31
2002	Pfannschmidt	Thoracotomy	CRM	167	–	–	32
2006	Yan	RFA	CRM	55	85	46	–
2007	Yamakado	RFA	CRM	71	84	46	–
2008	Lencioni	RFA	RFA	53	89	–	–
2009	Rosenberg	LA	Diverse M	64	81	44	27
2006	Thanos	RFA	DiverseNSCLC	14	78	18	–
2007	Hiraki	RFA	St.I-NSCLC	20	90	74	–
2007	Simon	RFA	DiverseNSCLC	75	78	36	27

VATS video-assisted thoracoscopy, *M* metastases, *CRM* colorectal metastases, *NSCLC* non-small-cell lung cancer, *RFA* radiofrequency ablation, *LA* laser ablation

of the procedures. Variable data on incidence of pneumothorax (between 17 and 43 %) should mainly be due to different measuring criteria (Grieco et al. 2006; Yan et al. 2006; Simon et al. 2007; Yamakado et al. 2007). Data on procedure-related complications after different local ablative therapies is summarized in Table 13.12.

Appraisal

Percutaneous laser ablation in the lung is an effective and safe procedure. Our results show 1-, 3-, and 5-year survivals of 81, 44, and 27 % for patients after definite ablative therapy of their pulmonary metastatic disease. These data correlate not only with recently published survival rates after radiofrequency ablation (Yan et al. 2007; Yamakado et al. 2007; Lencioni et al. 2008; Chua et al. 2010) but also with findings in surgical patients who underwent local resection to treat their lung metastases (McCormack et al. 1992; Landreneau 1996; Baron et al. 1998; Friedel et al. 1999; Inoue et al. 2000; Pfannschmidt et al. 2002) (Table 13.13).

Our own results showed no significant increase in incidence of peri-procedural complications compared with daily routine diagnostic lung biopsies (Weigel et al. 2004; Rosenberg et al. 2009). Mortality is negligible compared with thoracotomy, eventhough one has to be aware of reported cases of central embolism in patients who underwent radiofrequency ablation of pulmonary metastases (Yamamoto et al. 2004; Ghaye et al. 2006; Hiraki et al. 2007a, b). Aberrant currents or uncontrolled heat proliferation in contrast to radiofrequency-based ablational concepts has never been a challenge in laser-induced thermal therapy.

To date, published data on thermal ablation in the lung has become disease specific. Other than a decade ago and leaving the feasibility stage, it is strictly differentiated between study cohorts suffering from primary or secondary malignancies. Outcome evaluation for metastatic disease is getting more and more entity specific. Unfortunately there is a lack of prospectively randomized studies comparing ablation and surgery. By now there is no evidence showing a superiority of any invasive thermal ablative modality over another by means of outcome.

In conclusion, LA of primary and secondary malignant tumors in the lung is a promising option in multimodal cancer therapy. Procedure safety and efficacy have been proven. First clinical outcome data strongly support the therapy´s potential to improve survival and recurrence-free intervals for selected patients.

Table 13.13 Procedure-related complications reported for different local lung ablation techniques

Year	Author	Modality	Pneumothorax (%)	Chest tube (%)	Hemoptysis	Infection
2004	Steinke	RFA	43	7	9 %	NA
2004	Yamakado	RFA	17	20	NA	1 % severe 20 % mild
2005	VanSonnenberg	RFA	22	3	11 %	NA
2006	Weigel	LA	40	7	9 %	1 %
2007	Simon	RFA	18.6	9.8	2.7 %	2.2 %
2009	Rosenberg	LA	38	5	7 %	2 %

RFA radiofrequency ablation, *LA* laser ablation

Key Points

- Definition of eligibility criteria and patient selection are crucial.
- Interdisciplinary approach, best in institutional tumor board.
- Initial determination of the therapy goal.
- Take your time for procedure planning.
- Have your patient feel comfortable.
- Pneumothorax can always be controlled without therapy break off.

13.3 Microwave Ablation

13.3.1 Introduction to Microwave Ablation

Suzanne C. Schiffman and Robert C.G. Martin

13.3.1.1 Introduction

Tumor ablation is the application of chemical or thermal therapies to a tumor to achieve eradication or substantial destruction. Ablative techniques have been developed to enable local control of tumors and cytoreduction while limiting damage to surrounding healthy parenchyma (Goldberg et al. 2009). Ablative therapies may be useful in patients who are not amenable to surgical resection. Ablative therapies have reduced morbidity and mortality, and cost and length of hospital stay as compared to traditional cancer treatments. Additionally, these therapies can be performed in conjunction with other cancer treatments and may be repeated if necessary (Goldberg et al. 2000; Dupuy and Goldberg 2001).

Ablation has been performed using multiple modalities including ethanol ablation, laser ablation, cryoablation, and radiofrequency ablation (RFA). Microwave ablation (MWA) is a thermal ablation technique which uses electromagnetic waves to induce tumoral necrosis. As with other techniques, MWA can be performed via a percutaneous, laparoscopic, or open surgical technique. The percutaneous approach can be performed with ultrasound or computerized tomography guidance, according to the site of the lesion and preference of the physician. Additionally, the procedure may be performed in an outpatient setting with sedation and local anesthesia.

MWA was first developed in the early 1980s as a hemostatic adjunct to parenchymal transection during hepatic resection (Tabuse et al. 1985). Microwave coagulation of tissue surfaces was slower than electrocautery and produced deeper areas of tissue necrosis (Izzo 2003). The extended areas of tissue necrosis led to investigation of the use of MWA in unresectable hepatic malignancies. MWA initially gained popularity in Japan for the treatment of hepatocellular carcinoma (Seki et al. 2000a). Recent approval for MWA devices has led to increased use within the United States and Europe. MWA has been utilized in the treatment

- MW Spectrum
  - Approved microwave frequency bands are at 915 and 2,450 MHz (regulated by FCC)
  - Cell phones, cordless phones

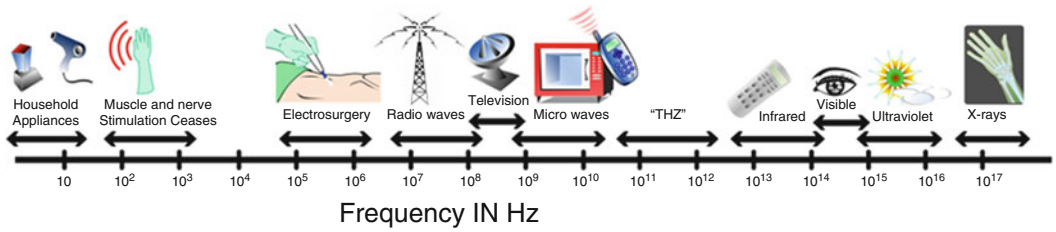

Fig. 13.44 Current frequencies of the two types of microwave ablation devices (915 and 2,450 MHz) as well as corresponding frequencies of other types of instruments

of unresectable tumors in the liver, kidney, lung, adrenal gland, pancreas, and bone. MWA can be used in curative intent or as a palliative measure to reduce symptoms of pain or recurrent bleeding.

13.3.1.2 Technical Basics of Microwave Ablation

MWA utilizes electromagnetic methods for inducing tumor destruction by using devices with frequencies from 915 to 2,450 MHz (Seki et al. 2000b; Lu et al. 2001; Shibata et al. 2002) (Fig. 13.44). Electromagnetic microwaves heat matter by agitating water molecules in the surrounding tissue, which produces friction and heat and thus induces cellular death via coagulation necrosis (Simon et al. 2005). Water molecules have an asymmetric electrical charge (polar molecules). The hydrogen side of the molecule has a positive charge, whereas the oxygen side has a negative charge. Microwaves have an oscillating electrical charge that changes charge very rapidly. Microwaves interact with a water molecule and cause charge on the water molecule to flip back and forth 2–5 billion times per second to produce heat and friction (Fig. 13.45). This process is known as dielectric hysteresis—polar molecules try to continuously realign with an applied electromagnetic field which causes them to rapidly alternate polarity.

Microwave energy is absorbed by materials and converted to heat when polar molecules (i.e., water) fail to realign with the alternating field. The rate of heat generation (Q_h) is proportional to the square of the applied electric field (E) multiplied by the effective conductivity (σ) (Fig. 13.46):

$$Q_h = \sigma |E|^2$$

Microwave energy is coupled into the tissue using an antenna. Microwave antenna(e) ranges in size from 12 to 17 gauge. They are selected for use based on the size of the lesion. The antenna(e) is placed directly either into the tumor, if using a single probe for small lesions or in a bracketed approach for larger lesions, or under direct visualization or localization by a cross-sectional imaging modality. MWA probes can be single or multiple antenna arrays, as well as loop antennae for expanded ablation zones. Most interstitial antennae create a teardrop or elliptical-shaped pattern. The change in tissue properties that occurs during ablation tends to alter the impedance matching of the antenna and the way in which the electromagnetic fields propagate through the tissue. The reflection coefficient determined the efficiency in which the antenna transfers power to the tissues—the lower the reflection coefficient, the more efficient the transfer.

The antenna is attached to the microwave generator with a coaxial cable. Coaxial cables

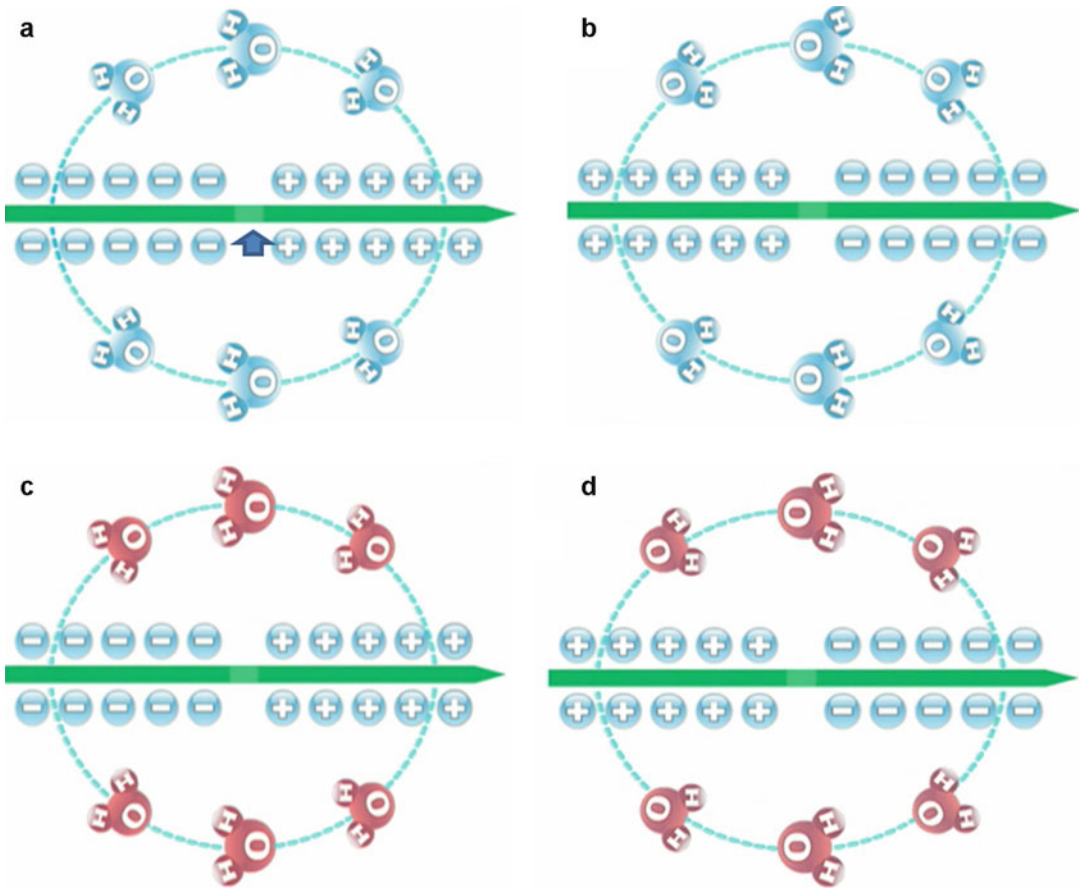

Fig. 13.45 Microwaves interact with polar molecules and cause the charge on the molecule to flip back and forth which produces heat and friction. The energy is delivered from a feed point (*large arrow head*), which induces the water molecules (**a**) to then flip (**b**). This action of flipping back and forth creates heat (**c**), to temperatures as high as 150 °C (**d**)

consist of an inner conductor, a dielectric material, and an outer conductor. The ability to carry large amounts of power is limited by cable (and antenna) diameter. Generators are capable of producing 60–110 W of power at frequencies of 915–2,450 MHz (Fig. 13.47; Table 13.14).

Electromagnetic microwaves are emitted from the exposed, non-insulated portion of the antenna (Fig. 13.46). The antennae radiate electromagnetic fields which are responsible for heat generation. Microwave antennae radiate electromagnetic fields which are not inhibited by tissue desiccation; thus, microwave heating is not limited by impedance which allows for a larger volume of active heating. The device does not need to be grounded, thus eliminating the potential for grounding pad burns as they were reported after RFA.

Microwave energy produces a larger zone of active heating (up to 2 cm surrounding the antenna), thus allowing for more uniform cell kill in the target area depending on the type of generator and the power that is utilized (Izzo 2003). Simon et al. measured the size of the ablation zone and evaluated the histological changes in patients with hepatic masses following MWA. Large blood vessels in the resection specimens did not create typical ablation zone distortion because of the minimal heat-sink effect observed. Additionally, on histology HE staining demonstrated marked thermal effect with greatest intensity closest to the antenna. There was a uniform absence of viable tumor cells in the ablation zone (Simon et al. 2005). Clark et al. demonstrated no viable

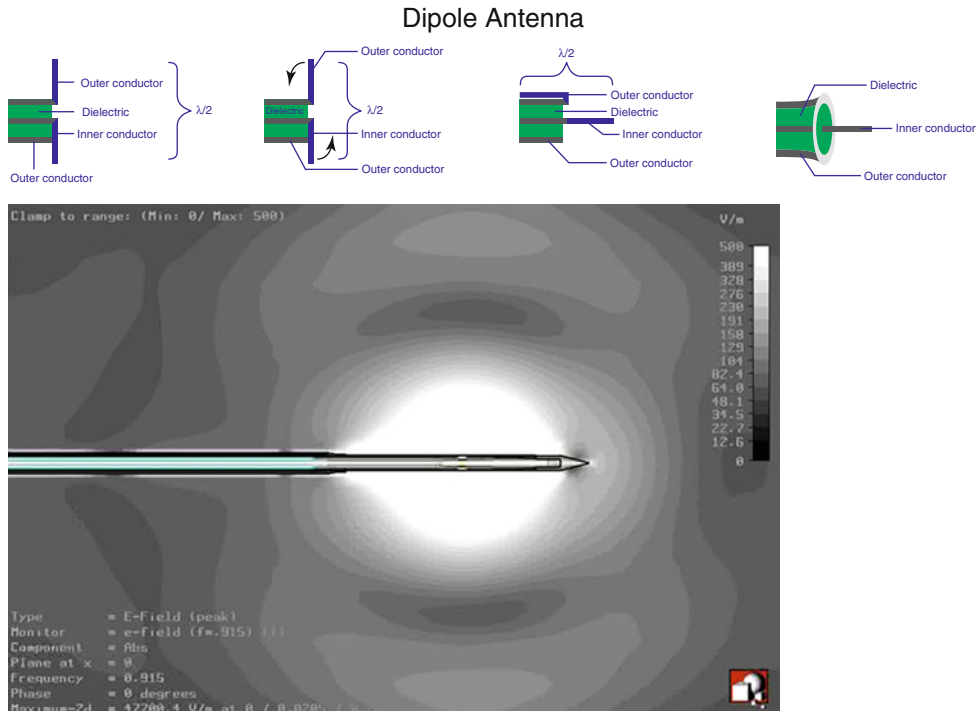

Fig. 13.46 Dielectric properties of the antenna design and the feed point of energy deposition. The single probes are made up of a dipole antenna with an inner conductor and an outer conductor. The goal is to make the antenna a smooth streamlined shape that will radiate a field (has lines of force or field lines) that is relevant to an efficient ablation defect and thus the outer conductor it turned onto itself, and then the inner conductor is extended straight through. There are the two poles, side by side in the antenna and separated by a feed point. The feed point is the dispersion point for the energy and the origination of the heat (i.e., the hottest point) and thus creating the wavelengths (λ). *Lower figure* is an MW antenna with a half-wavelength dipole

tumor cells within the ablation zone on histopathologic examination after MWA of renal tumors (Clark et al. 2007).

Moreover, MWA produces consistently higher intratumoral temperatures, larger tumor ablation volumes, faster ablation times, and improved convection profile (Skinner et al. 1998; Stauffer et al. 2003; Wright et al. 2003). Thermal conduction from the active heating zone and changes in tissue properties during heating alter the ablation zone. Additionally, the blood vessels, cystic structures, bowel, and other nearby structures alter antenna performance. However, these effects appear to be less pronounced when compared with RFA. With any given antenna design, increasing power can increase the size of the ablation zone. However, as power is increased, unwanted ablation of the puncture track may occur, potentially resulting in severe skin burns.

MWA produces 10- to 25-mm zones of coagulation necrosis after 30–60 s. The treatment areas can be spherical or elliptical. The rapid development of coagulation necrosis around the antenna produces a tissue coagulum which further prevents further heat dissipation into the tissues (Izzo 2003). For tumors larger than 2 cm, multiple probes must be utilized to produce overlapping zones of coagulation necrosis.

Appraisal

MWA is a technique with properties challenging RFA. MWA has the potential to create larger zones of active heating due to improved convection profile. It has a broader field of power density up to 2 cm surrounding a single probe, with a corresponding larger zone of active heating. The active zone leads to more

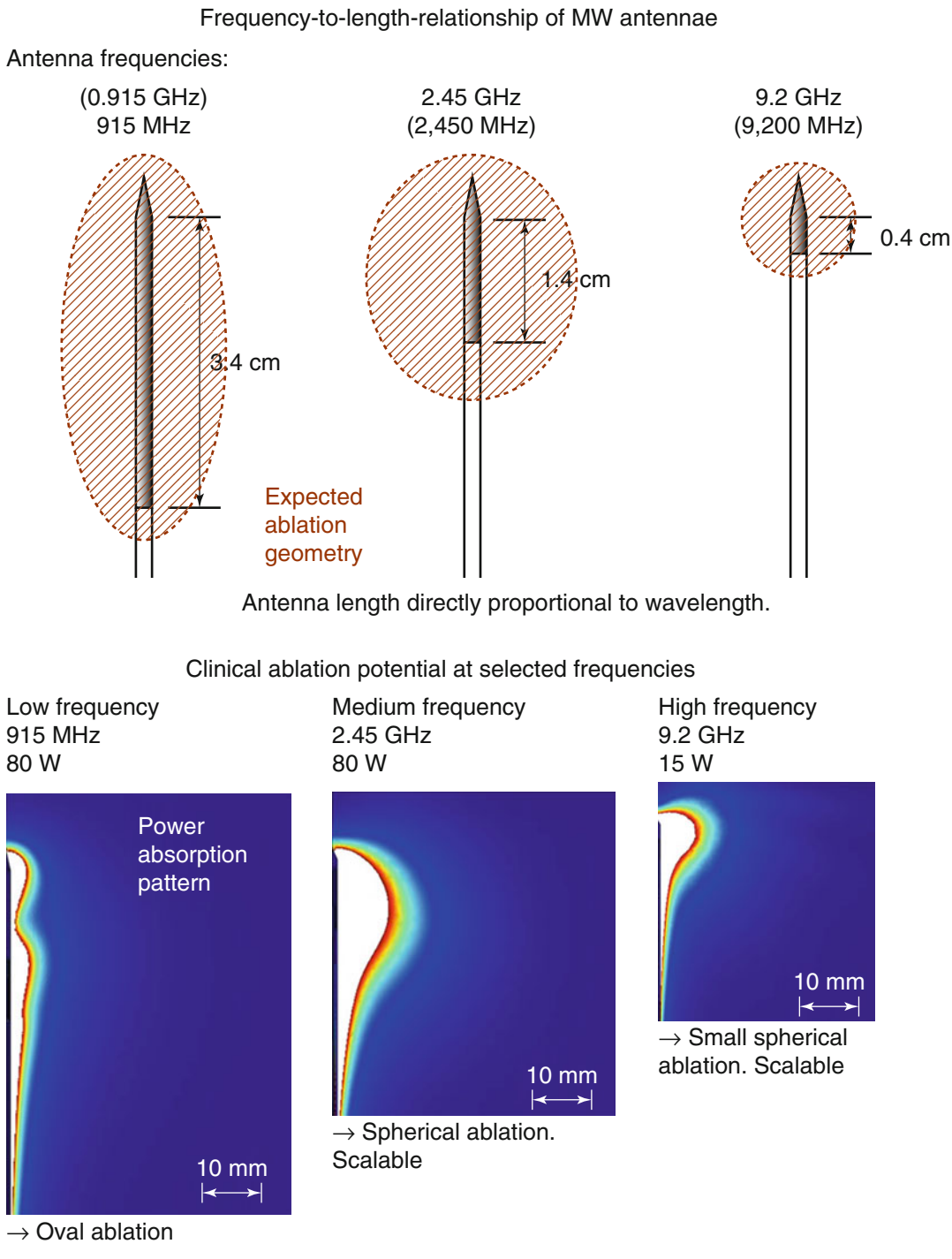

Fig. 13.47 Reported instructions for use liver ablation estimates from in vivo non-tumor-bearing pig liver of the three types of microwave generators that have been reported in the liver (**a**). Energy deposition at similar wattage (80 W) of two of the most common frequencies (915 and 2,450 MHz) demonstrating the loss of efficiency of the 915 MHz at high wattage and why a lower wattage of 45 W or less is recommended (**b**)

Table 13.14 Current available microwave generators

Company name	Clearance	Generator	Antenna gauge
Product name	FDA/CE	Frequency/power	Antenna cooling
Alfresa Pharma (JP)	No/no	2,450 MHz/110 W	18/14/12
Microtaze			No
Covidien (USA)	Yes/yes	915 MHz/45 W	14
Evident			Water
MedWaves (USA)	Yes/yes	915 MHz/45 W	14
–			No
Microsulis (UK)	Yes/yes	2,450 MHz/100 W	16
			Water
BSD Medical (USA)	In progress	915 MHz/60 W	14
Microtherm		3 antennae at 60 W	Water
NeuWave (USA)	In progress	2,450 MHz/140 W	17
Certus 140		3 antennae at 60 W	CO_2
Hospital Service (Italy)	Yes/yes	2,450 MHz/100 W	11/14/16
Amica			Water

uniform tumor ablation and subsequent tumor kill both within the targeted zone and next to blood vessel. While RFA is limited by increase in impedance with tissue boiling and charring because water vapor and char act as electrical insulators, MWA is not subject to this limitation.

Key Points

- MWA is a thermal ablation technique which uses electromagnetic waves to induce tumoral necrosis.
- Microwaves heat matter by agitating water molecules in the surrounding tissue to induce cellular death via coagulation necrosis.
- The potential benefits of MWA include consistently higher intratumoral temperatures, larger ablation volumes, faster ablation times, ability to use multiple probes, improved convection profile, and optimal heating of cystic masses.

13.3.2 Microwave Ablation of Liver Tumors

Thierry de Baère

13.3.2.1 Introduction

Microwave ablation (MWA) represents one of the most recent additions to the growing armamentarium of thermal ablation techniques. MWA is used for thermal destruction of tissue obtained with energy delivered through antennae previously inserted in the targeted tissues. MWA like any other thermal ablative therapy has to deal with the following three different phenomena:

- *Heat production* which is proportional to the energy delivered into the tissue and interaction of this energy with the tissue. It diminishes rapidly with the distance to the applicator which delivers the energy because most of the energy is absorbed in the vicinity of the applicator.
- *Heat conduction* which is the means by which heat obtained via energy deposition spreads to neighboring tissues, and conduction properties differ from one tissue to another.
- *Heat convection* which causes decay in tissue heating by transporting heat via fluid traversing

heated tissue. In the liver, convection is mostly due to calorific dispersion due to vascularization, but in the lung, airways are responsible for convective heat loss. Convection is responsible for a slightly different phenomenon when dealing with the macrocirculation and microcirculation. Indeed for macrocirculation, the so-called heat-sink effect has been clearly reported and identified as difficulties in achieving thermal destruction close to large vessels (large is usually understood in most of the reports as larger than 2–3 mm). Microcirculation is also responsible for convection and explains why volume of thermal ablation obtained ex vivo (in non vascularized tissues) is usually larger that what obtained in vivo (in vascularized tissues). In vivo, there is a competition between heat conduction and convection, and consequently the temperature drops faster with increasing distance from the applicator than ex vivo.

These three factors are responsible for a thermal equilibrium which is dependent on the distance from the electrode, the type and quantity of energy delivered, the duration of treatment, and the type of tissue and its vascularization.

The next sections summarize experimental data and results of hepatic MWA. Finally potential applications for hepatic MWA will be discussed, knowing that most of the results are recent, from small series in a rapidly evolving field, driven by new technological developments.

13.3.2.2 Basics and Experimental Data

MWA induces thermal destruction of tissues and does not have any specificity for tumor cells. The goal of MWA is to destroy tumors by heating cells above 60 °C in order to obtain immediate nonreversible cellular death. Exposure to temperatures below 60 °C can be lethal but needs longer exposure time, which extends with decreasing temperature.

The frequency of MWA used in medical applications is either 915 or 2,450 MHz, which is much higher than the frequency of radiofrequency ablation (RFA), which is in the range of 400–500 kHz. Consequently, RFA is considered an electrosurgery device, while MWA is a wave-emitting device. The wavelength of MWA is in the range of 30 cm (1 GHz) when used in liver tissue. The physical parameter that describes the effect of microwaves, and, namely, penetration of the waves in tissue, is permittivity. The permittivity varies from one tissue to another with large differences between different organs (Stuchly et al. 1981) and is even different in tumor and normal tissue of the same organ (Joines et al. 1994). In general, at frequencies used in clinical practice, permittivity was greater in malignant tissue than in normal tissue of the same type (Joines et al. 1994). Such differences favor propagation of MWA in tumor. The differences in electrical properties from normal to malignant tissue were lowest for the kidney (about 6 %) and greatest for the lung and breast (over 150 %) due to the differences between permittivity of tumors and surrounding breast fat or air-filled lung parenchyma. In the liver the microwave length is 4–5 cm in healthy liver and 7–8 cm in liver tumor (Stuchly et al. 1981). These differences might explain the slightly different results in the volume of ablation using the same setting in healthy liver and liver tumor as reported by Kuang et al. (2007). Indeed for the power and time setting of 70 W during 20 min, the long axes of ablation were 5.8 ± 0.2 cm in vivo healthy liver and 4.5 ± 0.6 cm in liver tumor, while short axes were 3.3 ± 0.3 and 3.2 ± 0.6 cm, respectively. In the same study, no difference was demonstrated in the volume of ablation between hepatocellular carcinoma (HCC) and liver metastases when the same power and time settings were used.

When applied to tissue, MWA excites the water molecules' electric dipoles, which try to align themselves with the alternating electric field, resulting in frictional heating. Unlike in RFA, microwaves are emitted, omitting the need for current conduction. Consequently boiling, charring, and vaporization in the vicinity of the needle are no more an obstacle to energy delivery. In MWA temperatures around 160–180 °C are achieved at the antennae. In contrast, in RFA the energy deposition needs to be limited to maintain a temperature below the boiling point of tissue, as charring and vaporization, which occur beyond this point, limit energy deposition (Brace et al. 2009). With MWA a faster rise in tempera-

Table 13.15 Severity of heat-sink effect depending to vessel size after liver MWA ablation at 45 W during 10 min

	Severity of heat-sink effect			
Vessel diameter (mm)	None (%)	Mild (%)	Moderate	Marked (%)
<3	78.4	10.8	10.8	0
3–6	56.3	31.3	12.5	0
>6	38.9	33.3	27.8	0

According to Yi-u et al. (2008)

ture is obtained, and consequently treatment times are usually shorter. Indeed a target temperature of 54 °C at 5 mm from the electrode is obtained in less than 40 s using microwaves, while 60 s is needed in bipolar RFA (Yu et al. 2010). Due to the better thermal profile the principle of microwave-induced heating and less conductive dispersion, there are preclinical data that argue for less heat-sink effect, namely, in the vicinity of large vessels. Indeed it has been demonstrated in healthy liver that deflection of the ablation was 3.5 ± 5.3 % for MWA with a single antenna (915 MHz, 40 W, 10 min) and 26.2 ± 27.9 % for RFA (150 W, 15 min, 3-cm array). Deflection was defined as the percentage difference between the diameter of the zone of ablation at a blood vessel and the diameter of the same zone of ablation next to the same blood vessel. This deflection was considered by the authors as a quantification of the heat-sink effect (Wright et al. 2003). More recently, Yu et al. evaluated the heat-sink effect in normal pig liver after MWA with a 915-MHz generator activated at 45 W during 10 min. In 61 % of the ablation zone, the thermal injury extended to the vein wall around the entire circumference of the coagulation front without distortion of the ablation margin. Vessels were classified as small (≤3 mm), medium (3–6 mm), and large (>6 mm), and heat-sink effect was graded as none, mild, moderate, or marked, and results are given in percent in Table 13.15 according to vessel size. It is however noticeable that no heat-sink effect was found in 78 % of small-size vessels, 56 % of medium-size vessels, and only 39 % of large-size vessels (Yu et al. 2008). It is also noticeable that the results suggest that both RFA and MWA are susceptible to thermal/heat-sink effect of large vasculature (Brannan and Ladtkow 2009). Moreover, a mathematical model of RFA ablation during 12 min and MWA during 6 min demonstrated that maximum tissue temperature was 100 °C for RF ablation and 177 °C for MWA. In this model, MWA was less affected by tissue perfusion mainly due to the shorter ablation time and higher tissue temperature, but not due to MWA providing deeper heating than RFA. Both MW and RF applicators only produce significant direct heating within few mm around the applicator, with most of the ablation zone being created by thermal conduction (Schramm et al. 2007). In conclusion, MWA is likely to perform better close to large vessels, but remains susceptible to heat-sink effect, and so far, no real benefit of MWA over RFA regarding local recurrence close to large vessels has been proven in clinical practice.

An unexpected finding of Wright et al. was the presence of selective tracking of coagulation necrosis up to 1 cm away from the main body outward along blood vessels up to 5 mm in diameter, after simultaneous ablation with 3 probes (Wright et al. 2003). This preferential tracking of the ablation zone along vascular pathways can be due to the creation of high-temperature water vapor that follows blood vessels as the path of least resistance. Such damage along vessels has been described with perfused RFA and was attributed to water vapor as in MWA (Denys et al. 2002). Alternatively, MW energy may selectively affect perivascular tissue according to differences in permittivity between perivascular liver and tissue more distant from blood vessels, but it is not known whether there is a difference in permittivity. A potential third explanation could come from ex vivo data showing that circulating blood exhibited higher electrical conductivity than surrounding liver tissue and provided a significant means for transport of thermal energy effect

(Brannan and Ladtkow 2009). The selective tracking of the microwave lesions along blood vessels may decrease the tumor recurrence near blood vessels, but it may also present the risk of thrombosis of major vessels. The latter, however, has not yet been reported in clinical practice.

The temperature of the antenna shaft rises quickly when delivering the high power of microwaves, and consequently, the application of microwave energy is usually limited to 60 W with non-cooled antennae and can result in severe skin burns when higher power is used (Seki et al. 1994). For this reason, most of the ablation systems available today have a cooled-shaft antennae. In addition, some systems have a choke placed between the shaft and the active part, aiming at lowering reflected energy from the active tip. Most of the cooling system uses liquid perfused around the antenna with a peristaltic pump, but CO_2 cooling is also used by some vendors. Cooling has been shown to avoid charring around the shaft, permitting larger diameters of destruction transverse to the probe, thereby providing a more spherical lesion shape, mostly due to the possibility of delivering higher power. Indeed for He et al., non-cooled antennae failed to deliver 60 W for longer than 10 min, while 60 W could be delivered during 20 min with cooled-shaft antennae. In addition, volumes of ablation were more spherical with cooled antennae (He et al. 2010).

The volume of ablation obtained with a single treatment with MWA has been greatly improved during recent years, namely, by improvement in the antenna's ability to deliver higher power to tissue as discussed above. Some differences have been reported according to the two most common MWA frequencies used for medical devices. 915 MHz seems to provide larger ablation volumes than 2,450 MHz for (Sun et al. 2009; Yu et al. 2010). On the other hand, for both Yu et al. and Sun et al., the ablation zone is more spherical with the 2,450-MHz system. Very few results have been reported today with higher power up to 100 W that can be delivered with the most recent devices.

Whatever the volume of ablation obtained with a single MWA application, one advantage of MWA is the possibility of activating several antennae at the same time. Indeed such synergy has been clearly demonstrated by comparing the volumes of ablation obtained with a single probe or three antennae activated subsequently or three probes activated at the same time. Simultaneous multiple-probe ablations were nearly six times larger in volume than single-probe lesions and almost three times larger than sequential ablations (Wright et al. 2003). Sequential activation of the probe induces more cleft and needs closer probe placement when compared to simultaneous activation. When using multiple antennae, spacing is a key parameter in order to achieve the largest possible ablation zone. While too short spacing will be a waste of energy, spacing the antennae to broadly will produce a nonspherical ablation zone with deflection. Using 3 probes activated at 45 W during 10 min, there was a significant difference between MWA ablation zones obtained with probe separation of 1.7 cm or less, which were round and confluent, whereas clefts were present with distances of more than 1.7 cm between the probes (Wright et al. 2003). At higher power, using 2 probes at 70 W for 10 min, a distance of 20–25 mm allowed round shape ablation with a length of 6.95 ± 0.32 cm and transverse diameter of 5.3 ± 0.22 cm (Shi et al. 2011). The excellent reproducibility is highlighted by the low standard deviation, but these data were obtained in ex vivo liver and need in vivo validation in tumors.

13.3.2.3 Indications

Today, indications for liver MWA ablation are similar to RFA, but should probably try to target larger tumors than RFA. Since liver RFA is recommended to target HCC up to 4 cm and metastases up to 3 cm (Crocetti et al. 2010), it might be beneficial to treat larger tumors with MWA because of the synergy of multi-probe application. Due to the uncertainty of the results, these patients should be enrolled in a clinical evaluation. It is very likely that the possibility to create larger ablation volumes by the use of multiple applicators working at much higher temperature than RFA may cause more complications. Superiority of MWA over RFA for tumors close to large vessels remains to be demonstrated, and clinical evaluations are needed. MWA treatment

of small tumors distant from large vessels that are candidates for RFA is questionable because there is less data on MWA results, while MWA is more expensive. The potential decrease in heat-sink effect demonstrated in preclinical studies could favor the choice of MWA over RFA for tumors close to large vessels even this benefit has not yet been demonstrated in clinical practice.

13.3.2.4 Technique

MWA ablation technique is very similar to RFA in terms of image guidance for the treatment. Ultrasound and CT guidance have been used according to visibility, accessibility of the tumor, and operator preference. So far there are no reports on MR-guided MWA. As the target lesions are often larger than in RFA, there typically is a need for the insertion of multiple antennae. When using multiple antennae for ablation, there is a need for a predefined spacing between the antennae (usually 1.5 to 2 cm). For accurate treatment planning, CT with multiplanar reconstructions is useful to check for the distance between the antennae and the fact that they are in parallel position. This setting is much more difficult to obtain in clinical practice due to tumor configuration, location of the tumor, presence of ribs, and other structures one needs to avoid along the puncture tract. Anyhow, efforts should be undertaken to place the probe as parallel as possible because the volume and shape of ablation obtained with nonparallel antennae are unknown. Antenna tips are usually more fragile than RF probes, and operators must make a large and deep enough cut to the skin and be gentle by avoiding forced angulations of the antennae.

An advantage of MWA over RFA is that the emission of the MWA does not interact with ultrasound or CT imaging as reported for RFA. However, during MWA the increase in temperature is responsible for out-gazing from the tissue, causing the same hyperechoic pattern on ultrasound as it is known from RFA impairing further visualization with ultrasound. MWA seems less painful at the onset of the power on the generator, but pain generated by thermal increase is very similar to RFA. We recommend general anesthesia when possible in all patients in order to render the procedure more tolerable to the patient and make the physician comfortable and avoid incomplete treatment by rushing the end of the procedure due to pain or discomfort.

Physicians must keep their hands off the probe during MWA delivery because there might be some backscattered energy from the probe. Cables are usually insulated or cooled to avoid excessive increase in temperature because some energy is dissipated in the cable and responsible for heating these cables. It is noteworthy that the use of shorter cables might be helpful to deliver higher energies to the antennae.

In the same manner as in RFA, tumors close to the liver hilum are a relative contraindication due to the risk of biliary complications. When tumors are at the periphery of the liver, thermal diffusion to the neighboring organ should be avoided. Aerodissection (preferably with CO_2) is most adequate for shielding, while liquids should not be used in MWA.

Coagulation parameters need to be assessed prior to percutaneous access to the liver, and tract coagulation must be used to decrease the risk of bleeding as well as the risks of tumor seeding. The recommendations regarding blood tests including coagulation parameters are identical to the ones recommended for RFA.

13.3.2.5 Follow-Up

Contrast-enhanced CT or MR imaging are the most commonly used modalities for assessing treatment outcome. CT and MR imaging results obtained 4–6 weeks after treatment show successful ablation as a non-enhancing area with or without a peripheral enhancing rim (Figs. 13.48 and 13.49). The enhancing rim that may be observed along the periphery of the ablation zone appears to be a relatively concentric and uniform process with smooth inner margins. This transient finding represents a benign physiological response to thermal injury consisting of initial reactive hyperemia and subsequent fibrosis and giant cell reaction. Benign peri-ablational enhancement must be differentiated from irregular peripheral enhancement due to residual tumor that eventually occurs at the treatment margin. Compared with

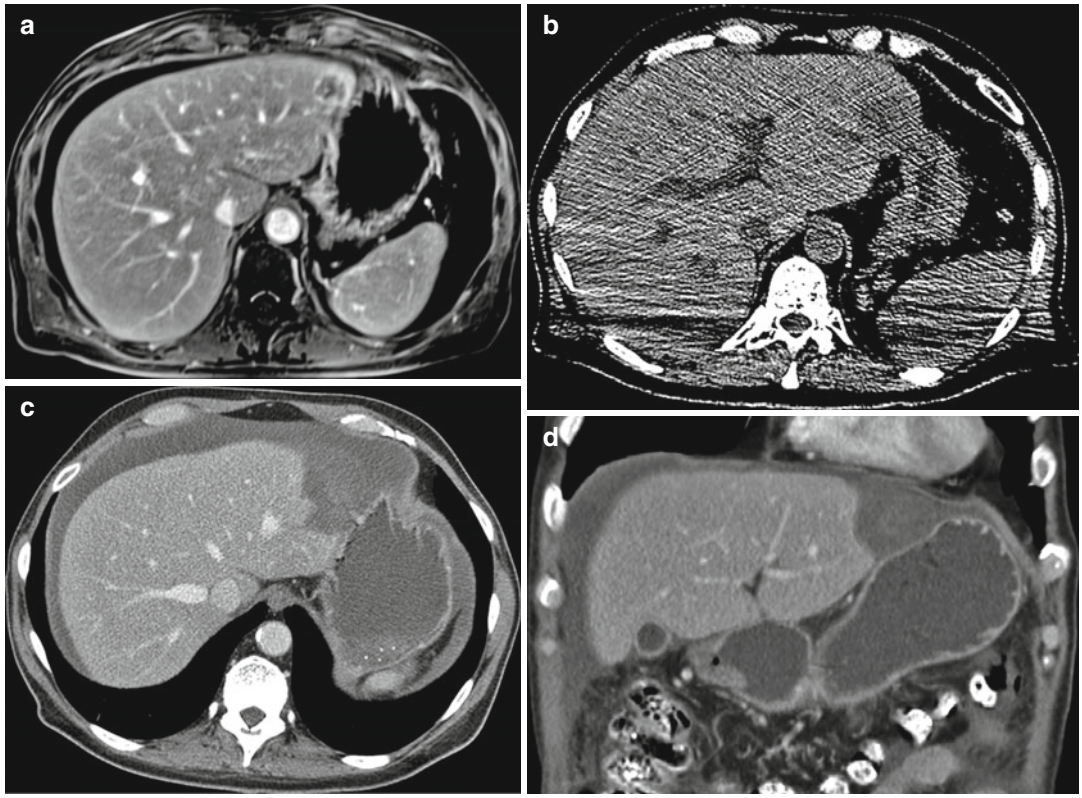

Fig. 13.48 Axial contrast-enhanced T1-weighted MR image shows a metastasis in liver segment III in a patient treated with peritoneal dialysis for renal insufficiency (**a**). CT immediately before percutaneous placement of the microwave antenna depicts a slight increase in size of the target tumor, which is now in contact with the stomach wall (**b**). MWA was performed at 80 W during 12 min using a single internally cooled antenna. CT obtained 1 month after the procedure shows a large volume of ablation without viable tumor (**c**, **d**). Of note, ascites due to peritoneal dialysis

benign peri-ablational enhancement, residual tumor often grows in scattered, nodular, or eccentric patterns. Contrast-enhanced ultrasound can be performed after the end of the procedure and may allow initial evaluation of treatment effects mostly for hypervascular tumors such as HCC. Later follow-up imaging studies should be aimed at detecting local tumor progression, development of new hepatic lesions, or emergence of extrahepatic disease. A recommended follow-up protocol includes CT or MR imaging at 3, 6, 9, and 12 months after treatment and at 6-month intervals thereafter for the next 3–5 years.

13.3.2.6 Results

Medical application of MWA has initially been reported in the early 1980s with external probes which achieved mild hyperthermia in combination with intra-arterial or systemic 5-FU. Most of the reports remained experimental (Hugander et al. 1985) with few clinical studies being performed (Miura et al. 1985). The use of MWA for liver tissue destruction was initially reported in Japan, using the MWA energy as a surgical coagulator to facilitate liver resection (Tabuse et al. 1985) and as a coagulator for biopsy tracts (Tabuse et al. 1986). Anecdotal destruction of a liver hemangioma was reported in 1983 (Oku et al. 1983), but the first reports of malignant tumors occurred 10 years later with the report of 21 HCC smaller than 5 cm treated with "microwave coagulo-necrotic therapy" (Saitsu et al. 1993).

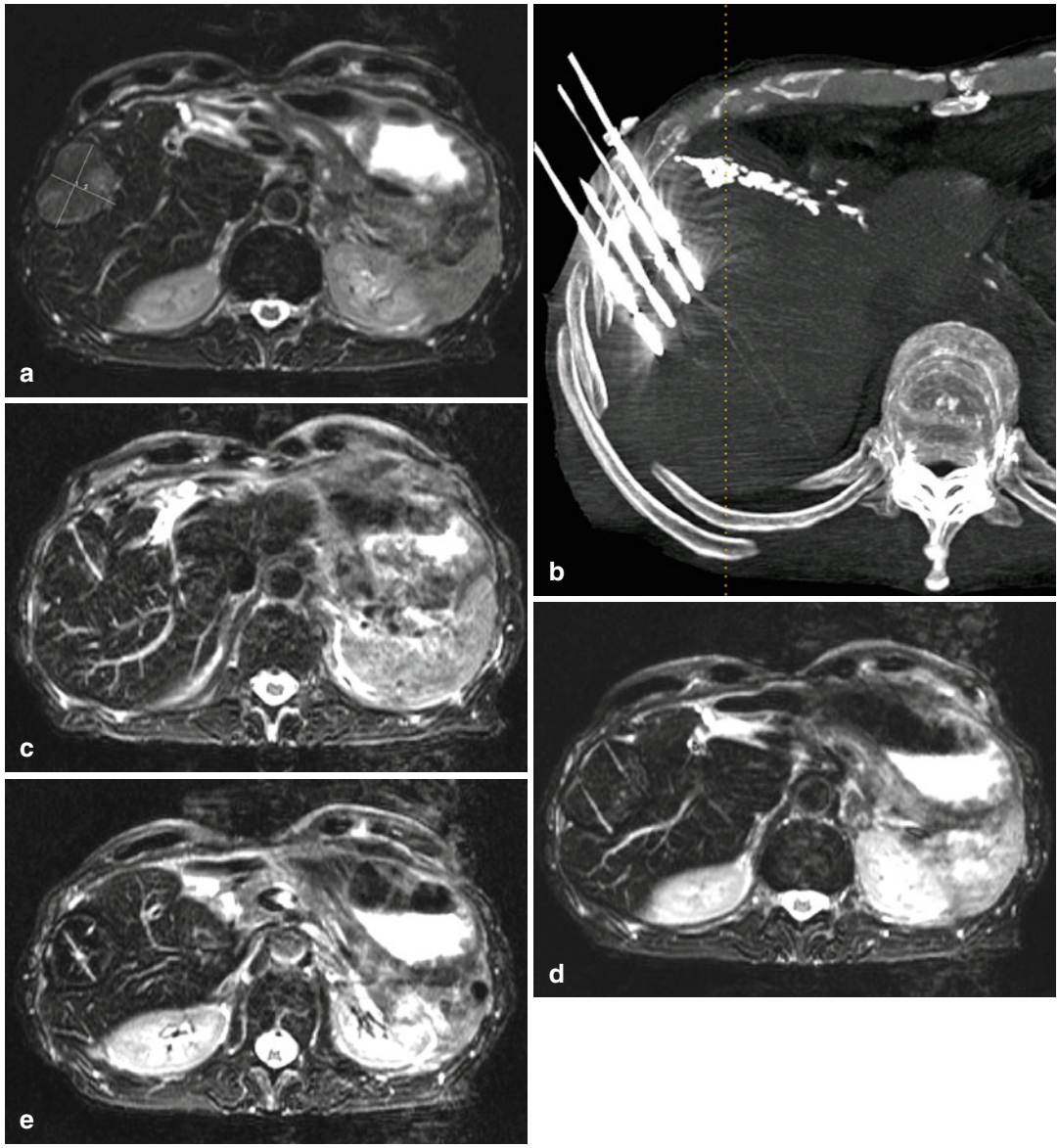

Fig. 13.49 T2-weighted MR image of a 47×37-mm HCC in the remaining right liver after previous left hepatectomy (**a**). Thick slab MIP of the CT obtained after placement of 4 microwave antennae (**b**). Axial T2-weighted MR images obtained one month after ablation show disappearance of the previously hyperintense HCC (**c**–**e**). Notably the previous locations of the antennae remained visible

It is noteworthy that improvement in MWA technology and in particular improvement in applicator design, rendering delivery of higher power possible, paved the way for a clinical breakthrough around 2005–2007. This development was driven by the release of cooled-shaft antennae that allowed application of higher power without overheating of the antenna shaft (Kuang et al. 2007; Liang et al. 2009). Consequently before 2005, treatment was performed with systems which provided small volumes of ablation, and the results of these treatments are hardly comparable with results obtained with modern cooled-shaft systems.

Hepatocellular Carcinoma

In 2002, when treating 99 HCC measuring 1–3.7 cm (mean = 2.2), early results of MWA with non-cooled-shaft systems demonstrated complete ablation in 96 % with RFA and in 89 % with MWA ($p = 0.26$). The complication rates did not differ, while less sessions were needed for RFA versus MWA (1.1 vs. 2.4; $P < 0.001$) (Shibata et al. 2002). Three years later, a series with slightly larger tumors measuring 1–7 cm (mean: 2.5 cm) showed again no difference in local control between RFA and MWA, although the overall recurrence rate was 11.8 % (11/93) using MWA ablation versus 20.9 % (14/67) using RFA (Lu et al. 2005). In this report, there was no difference in overall survival between patients treated with RFA or MWA. For HCC measuring 1.2–8 cm (mean = 3.75 ± 1.58; 83 tumors <2.5 cm, 127 tumors 2.5–4 cm, 78 tumors >4 cm) treated with MWA, reported prognostic factors of survival were the number of lesions, tumor size, Child–Pugh classification, tumor differentiation, and local recurrence or presence of new tumors at univariate analysis (Liang et al. 2005). At multivariate analysis, diameter of the largest tumor (Hazard Ratio (HR) = 2.32, 95 % CI, 1.66–3.25), number of tumors (HR = 1.92; 95 % CI, 1.22–3.02), and Child–Pugh classification (HR = 1.91; 95 % CI, 1.17–3.14) had the most relevant impact on survival. The authors conclude that "with the use of microwave ablation, there is a high probability of long-term survival of patients with a single lesion of 4.0 cm or less in maximum diameter and Child–Pugh class A cirrhosis". A recent study included 89 patients with an index HCC measuring 3.0–5.0 cm and 20 patients with an index HCC measuring 5.0–7.0 cm treated either with RFA or MWA. The rate of complete ablation was significantly higher in patients with tumors measuring 3.0–5.0 cm (95.4 %) than that in patients with tumors measuring 5.0–7.0 cm (80 %). The difference in the complete-ablation rate between RFA (89.8 %) and MWA (95.9 %) was not significant (Yin et al. 2009). In this report, complete tumor ablation, recurrent tumors, and pre-ablation AFP >8,200 ng/mL were independent unfavorable prognostic factors, with an HR of 4.158, 1.568, and 1.593, respectively.

Metastases

For liver metastases treated with MWA, prognostic factors of survival are number of metastases, tumor size, and local recurrence or new metastasis on univariate analysis and tumor grade (HR = 0.45; 95 % CI, 0.23–0.91), number of metastases (HR = 1.94; 95 %CI, 1.06–3.52), and local recurrence or new metastasis (HR = 3.57; 95 % CI, 1.02–12.64), on multivariate analysis (Liang et al. 2003).

Results obtained with the use of new-generation cooled-shaft antennae are scarce. A report of ten tumors with a mean maximal tumor diameter of 4.4 cm (range: 2.0–5.7 cm) receiving synchronous triple antenna MWA with 45 W during 10 min before elective hepatic resection demonstrated a mean maximal ablation diameter of 5.5 cm (range: 5.0–6.5 cm), corresponding to an ablation zone volume of 50.8 cm^3 (range: 30.3–65.5 cm^3) (Simon et al. 2006). In this report the three individual ablation zones had completely fused to create one large continuous ablated volume that encompassed the grossly visible tumor mass in its entirety confirmed by vital histochemical NADH stain to demonstrate no viable tumor tissue. The same system with the same settings (triple antennae, 45 W, 10 min) was used in phase II study in 87 patients who underwent 94 ablation procedures for 224 hepatic tumors (Iannitti et al. 2007). The average tumor size was 3.6 cm (range: 0.5–9.0 cm). Single antenna ablation volumes were 10.0 ml (range: 7.8–14.0 ml), and clustered antenna ablation volumes were 50.5 ml (range: 21.1–146.5 ml). Local recurrence at the ablation site occurred in 6 (2.7 %) tumors, and regional recurrence occurred in 37 (43 %) patients after a mean follow-up of 19 months. Using higher power up to 80 W for 25 min, complete-ablation rates in small (<3.0 cm), intermediate (3.1–5.0 cm), and large (5.1–8.0 cm) liver cancers were 94 % (81 of 86), 91 % (31 of 34), and 92 % (12 of 13), respectively. During a mean follow-up period of 17.4 months, local tumor progression occurred in seven tumors (5 %) (Kuang et al. 2007). It is noticeable that delivering 70 W during

20 min with a triple antennae achieved volume of destruction measuring 8.0 ± 0.9 cm in the long axis and 6.4 ± 1.5 cm in the short axis. The largest recent report of the Western world with MWA ablation concerns 100 patients with 270 tumors (metastatic colorectal cancer 50 %, HCC 17 %, metastatic carcinoid 11 %, and other metastatic disease 22 %). Median tumor size was 3.0 (range: 0.6–6.0) cm; median number of tumors was 2 (range: 1–18). Open surgery was used in 68 % and laparoscopic in 32 %, and median total ablation time was 13 (range: 5–45) min. Overall 90-day mortality was 0 %, and morbidity was 29 %. One patient developed a hepatic abscess, and no patients experienced bleeding complications. After a median follow-up of 36 months, 7 % of patient had incomplete ablation or local recurrence at the site of ablation, and 37 % developed distant intrahepatic recurrence (Martin et al. 2010).

Complications

MWA ablation is safe and well tolerated as underlined by the report of a large series of 1,136 patients with 1928 malignant liver tumors receiving MWA (Liang et al. 2009). This report includes cooled-shaft and non-cooled-shaft ablation because it extended over a 13-year period. Major complications occurred in 30 (2.6 %) patients and included liver abscess and empyema ($n=5$), bile duct injury ($n=2$), perforation of the colon ($n=2$), tumor seeding ($n=5$), pleural effusion requiring thoracentesis ($n=12$), hemorrhage requiring arterial embolization ($n=1$), and skin burn requiring resection ($n=3$). Minor complications included pain (80 %), asymptomatic pleural effusion (10.4 %), gallbladder wall thickening (2.8 %), skin burn requiring no treatment (1.8 %), and small stricture of the bile duct (0.4 %). Use of non-cooled-shaft versus cooled-shaft antennae was associated with a higher rate of major complications, 21/583 (3.6 %) versus 9/553 (1.6 %), respectively.

Appraisal

The introduction of cooled antennae significantly increased the efficacy of MWA as hyperthermal ablation technique and paved the way to clinical routine use. While indications for MWA are similar to RFA, MWA offers some theoretical advantages, including a higher efficacy. Currently new generators with higher wattage are introduced in clinical routine, thereby further improving MWA's efficacy. Therefore, future indications are likely to include larger lesions, which are not suited for RFA. The safety profile is excellent, with complication rates comparable to RFA. As the data on treating liver lesions with recent 915- or 2,450-MHz generator is scarce, patients should be included in clinical registries.

Key Points

- MWA may be used under US or CT guidance, as no MR-compatible antennae are available.
- MWA is safe and likely to be more efficient when compared to RFA.
- MWA does not require grounding pads, and the use of multiple applicators is recommended.
- It is particularly suited for lesions, which are poor candidates for RFA due to lesion size or proximity to larger vessels.

13.3.3 Microwave Ablation: Lung

Philipp Bruners and Andreas H. Mahnken

13.3.3.1 Introduction

Besides radiofrequency (RF) ablation (Lencioni et al. 2008) and laser-induced thermotherapy (Rosenberg et al. 2009), microwave ablation (MWA) represents a relatively new image-guided, minimal-invasive treatment modality for lung malignancies. Taking the underlying physical principle into account, MWA provides some potential benefits over RF ablation which is the most commonly used image-guided technique for the ablation of lung tumors, so far. MWA applies oscillating electromagnetic fields with frequencies between 915 and 2,450 MHz by a

percutaneously placed antenna, resulting in tissue heating due to continuously repeated realignments of polar water molecules. Because of the radiating nature of microwave energy, effective heating of tissue types with low electrical and thermal conductivity and high impedance such as the bone and lung is possible (Lubner et al. 2010) where RF ablation reaches its limits. In contrast to other energy sources, microwave energy even can pass through charred or desiccated tissue (Skinner et al. 1998). In a preclinical animal study, Brace et al. showed that MWA using a triaxial antenna with a diameter of 17 gauge creates larger and more circular ablation zones than does an RF applicator with a similar size in porcine lung tissue (Brace et al. 2009). Crocetti et al. found that after pulmonary MWA in a rabbit model, 90 % of vessels in the periphery of the ablation zone showed complete thrombosis whereas thrombosis was depicted only in 20 % of peripheral vessels after RF ablation (Crocetti et al. 2010). These findings support the assumption that MWA is less sensitive to the heat-sink effect when compared to RF ablation. Furthermore, the use of a conductive pad as it is needed in monopolar RF ablation is not necessary which might be beneficial in patients with implanted electrical devices like cardiac pacemakers (Skonieczki et al. 2011).

13.3.3.2 Indications

As surgical resection still represents the only proven curative treatment in patients suffering from primary and secondary lung malignancies, image-guided thermal ablation therapies are indicated in patients who are deemed to be at high risk for surgical resection or who refuse surgical therapy. Because image-guided MWA of pulmonary malignancies is a quite recent treatment modality, definitive indications have not yet been established, so far. According to indications for other local ablative therapies like RF ablation, MWA of lung malignancies can be offered to patients who meet the following criteria (Vogl et al. 2011):

- Patients with inoperable (e.g., due to inadequate pulmonary reserve) non-small-cell lung cancer (Stage I/II) or a limited number ($n \leq 5$) of pulmonary metastases per hemithorax from any primary cancer.
- The largest diameter of a single lesion should not exceed 5 cm, although best results are achieved in tumors <3.5 cm which are completely surrounded by lung tissue.
- Bilobar metastatic disease should be treated in two sessions in order to prevent potentially severe bilateral complications.
- Tumors with pleural contact can be treated, but this is associated with increased post-interventional pain.

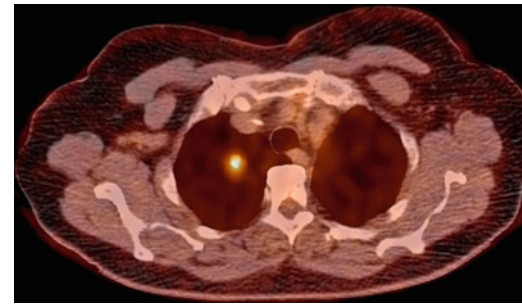

Fig. 13.50 The PET/CT scan reveals a single pulmonary metastasis in a female patient suffering from colorectal cancer. Due to previous partial lung resection on the left side, surgery was not considered an option in this patient

The decision to treat a patient with pulmonary MWA should be based on a recent (<2 weeks) diagnostic CT or PET/CT scan (Fig. 13.50).

Contraindications include the following criteria:

- Target lesion abutting main bronchi, main pulmonary artery, or esophagus
- Transgression of the target lesion into the chest wall
- Uncorrectable coagulopathy
- Active inflammatory disease as represented by fever, leucocytosis, and elevated serum level of C-reactive protein

Metastatic disease outside the lung is no absolute contraindication if there is a comprehensive treatment concept for these sites, for example, local resection of hepatic metastasis.

13.3.3.3 Material

MWA of pulmonary tumors has successfully been performed using different MWA systems (He et al. 2006; Wolf et al. 2008). As in RF ablation, single or multiple needle-shaped applicators

can be used as well as deployable multi-probe arrays depending on the employed MWA system. Some MWA systems feature peristaltic pumps to circulate saline solution through the antenna shaft in order prevent heating followed by thermal injury along the proximal antenna shaft. The length of the MWA applicator should be chosen long enough to allow precise placement even if the position of the target tumor changes for example due to pneumothorax occurring during the puncture. If different lengths of the active antenna tips are available for the used MWA system, the length should be adjusted to the size of the target lesion.

Most commonly CT guidance is used for applicator placement in the lung because of the excellent contrast between target and surrounding lung tissue even if low-dose scan protocols are used. In order to clearly visualize small target lesions, a slice thickness of ≤2 mm should be achievable with the used CT scanner. CT fluoroscopy might be helpful for a fast and precise applicator placement in uncooperative patients, but is not generally recommended due to the associated radiation exposure to the interventionalist.

As for diagnostic lung punctures, disinfectant and sterile drape sheets for the skin entry site are needed. A grid simply made of parallel fixed catheter pieces can be attached to the skin and works as a reference for planning of the puncture trajectory. The injection of a long-acting–local-acting anesthetic agent like bupivacaine 0.25 % along the puncture tract down to the parietal pleura is recommended in order to reduce post-procedural pain, especially when tumors with broad pleural contact are treated. In these cases a peripheral block of the supplying segmental nerve can also be helpful for post-interventional pain management. A sterile single-use scalpel is used for a stitch incision at the skin entry point.

13.3.3.4 Technique

Patient Preparation

Informed consent should be obtained from the patient at least 24 h prior to the intervention including a discussion of alternative treatment options. In addition, the patient should be informed about possible complications of the pulmonary MWA procedure including treatment failure due to incomplete tumor ablation or local recurrent disease, pneumothorax, hemoptysis, skin burn, infection, and local as well as pleuritic pain. Also potential fatal complications such as cerebral air embolism or severe hemorrhage for example due to injury of an intercostal artery need to be mentioned.

The authors prefer to perform pulmonary ablation procedures in general anesthesia with endotracheal intubation because it provides optimal patient comfort and compliance. In addition, special techniques like single-lung ventilation which might be beneficial due to larger achievable coagulation volumes can be implemented (Santos et al. 2010). Furthermore, general anesthesia provides optimal tagging of the target due to reproducible target positioning. Nevertheless, in compliant patients a pulmonary ablation procedure can safely be performed under conscious sedation (e.g., piritramide + midazolam). In this case continuous monitoring of the patient's ECG and blood oxygen level is strongly recommended.

Based on a current (<2 weeks) thoracic CT examination, the optimal trajectory for MWA applicator placement as well as the anticipated positioning of the patient (prone/supine/oblique) can be planned beforehand. As in diagnostic thoracic punctures, the repeated passage of the pleura should be avoided in order to minimize the risk for a pneumothorax. In case there is no recent CT examination available, an appropriate CT scan should be performed the day before the intervention.

Medication with inhibitors of platelet aggregation should be paused 5 days before the intervention in order to let the platelet function recover. Patients receiving anticoagulants like phenprocoumon should be switched to heparin. Prior to the MWA, a recent (<1 week) full blood cell count and coagulation test should be available to rule out any inflammation or hemorrhagic diathesis. International normalized ratio should be below 1.5 (Malloy et al. 2009).

Furthermore a chest X-ray and a pulmonary function test should be performed pre-interventionally, especially in patients who already underwent thoracic surgery.

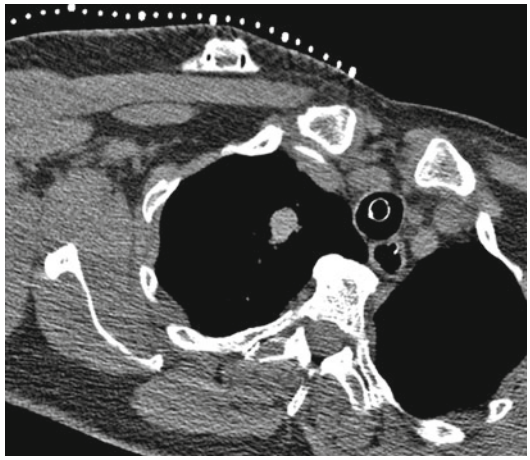

Fig. 13.51 A radiopaque grid is placed on the skin for planning of the MWA applicator placement

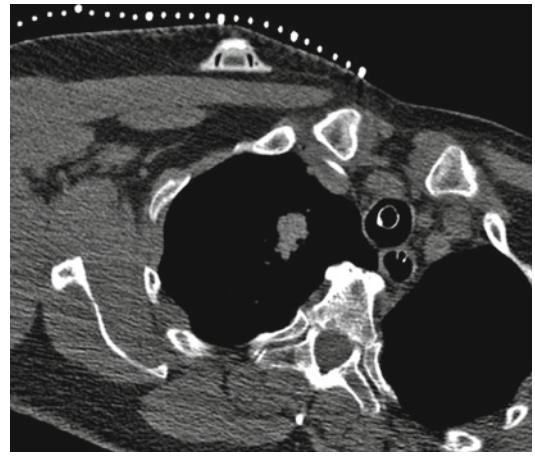

Fig. 13.52 The trajectory is planned for a central placement of the MWA applicator in the target lesion. Note the bronchus within the lesion; in such cases a prophylactic antibiotic treatment after MWA may be helpful to prevent superinfection of the induced coagulation volume

A prophylactic antibiotic treatment is not routinely recommended. At the authors' institution, patients receive a single shot 1.500-mg cefuroxime i.v. at the beginning of the intervention followed by an orally administration of 2×250-mg cefuroxime per day for 5 days. In special cases when the coagulation volume is in the direct contact with a bronchus, the oral administration of antibiotics may be prolonged for up to 4 weeks.

Procedure

As most thoracic interventions, pulmonary MWA is typically performed under CT guidance. During orotracheal intubation, patients usually lie in supine position on the CT table. Thereafter, the patient is positioned according to the planned puncture path to the target with special attention being paid to possible pressure sites, for example, elbows, knees, pelvic bones, or potential nerve compressions. An unenhanced full-dose CT examination including the estimated skin entry point and the target lesion is performed for definition of the actual trajectory for applicator placement (slice thickness ≤2 mm). After skin entry site has been defined, the CT table is moved to the corresponding slice position, and radiopaque markers (e.g., grid) are fixed on the skin followed by acquisition of a single sequential CT scan (Fig. 13.51). Then the skin entry site and the puncture path are defined using the grid as landmark (Fig. 13.52), and the entry site is marked on the skin with a water-resistant pen. Next the grid is removed, and the skin at the puncture site is cleaned and disinfected before sterile draping is applied. Sufficient local anesthesia of the puncture including the parietal pleura needs to be performed using a long-acting local anesthetic agent. Patients suffering from peripheral lung tumors with broad contact to the visceral pleura may benefit from a selective block of the supplying intercostal nerves resulting in less post-interventional pain. Then the MWA applicator is advanced along the planned trajectory under CT guidance using either CT fluoroscopy or sequential control scans. Due to the high contrast within the lung tissue, low-dose protocols for both techniques can be used. After successful placement of the MWA applicator (Fig. 13.53), energy is applied according to the vendor's recommendations. Depending on the size of the target lesion and the intended coagulation volume, the use of multiple MWA antennae or repositioning followed by repeated energy application might be considered (Wolf 2008). After removal of the antenna and closure of the skin entry site with a sterile adhesive bandage, another unenhanced CT scan of the target region is performed in order to rule out significant pneumothorax requiring aspiration or drainage and significant hemorrhage requiring embolization therapy. Similarly to the findings after pulmonary

Fig. 13.53 The MWA applicator is centrally placed in the target lesion along the previously planned puncture path

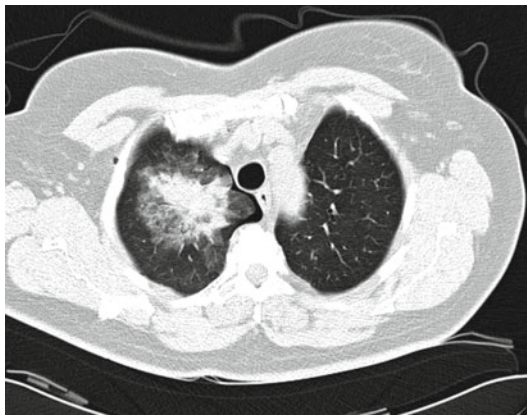

Fig. 13.54 The post-interventionally planned CT scan shows the coagulated target lesion which is surrounded by an area of ground-glass opacity. Note the small medial pneumothorax

RF ablation, an area of hazy ground-glass opacity should be present around the ablation area, representing thermal injury of the surrounding healthy lung tissue. In case the target lesion is not fully encircled by ground-glass opacity, incomplete ablation has to be assumed, and the procedure should be continued. Histological workup of specimens obtained from in vivo animal experiments in healthy lung tissue showed septal necrosis, edema, and hemorrhage (Crocetti et al. 2010). An area of at least 0.5 cm of this ground-glass opacity should surround the ablated target lesion, representing the safety margin (Fig. 13.54).

Post-interventional Management

After pulmonary MWA, patients should undergo conventional chest X-ray 2 h post-procedurally to rule out any pneumothorax requiring treatment (Fig. 13.55). If a clinically relevant pneumothorax is found on post-interventional imaging, thoracentesis followed by further X-ray controls after 2 and 4 h is recommended. In case of recurrent or persistent pneumothorax that results in clinical symptoms, insertion of a drainage catheter or a chest tube with a Heimlich valve should be placed. If no complication occurs, patients can be discharged from the hospital 24 h after the intervention. In some institutions, pulmonary MWA is even performed on an outpatient basis, although delayed pneumothoraces have been described after pulmonary ablation procedures. Therefore, patients should be informed to come back if any signs of dyspnea or acute thoracic pain occur.

For further follow-up, multiphasic contrast-enhanced CT examinations (unenhanced and venous phase)are recommended at 1-, 3-, 6-, 9-, and 12-month intervals. Afterward 6-month intervals can be recommended. There is some evidence that cavitation of the ablated area is associated with a lower cancer-specific mortality (Wolf et al. 2008). During follow-up, special attention should be paid to signs of infection of the ablation area as this delayed complication might lead to potential fatal side effects like sepsis or erosion of adjacent pulmonary blood vessels followed by severe hemorrhage (Wolf et al. 2008). PET/CT scans might be useful for the early detection of local recurrence in pre-interventionally PET-positive tumors, although this has not been shown by any clinical study, so far.

13.3.3.5 Results

As image-guided MWA is a relatively new method, there are only few studies available reporting clinical results. He et al. performed percutaneous MWA under ultrasound guidance

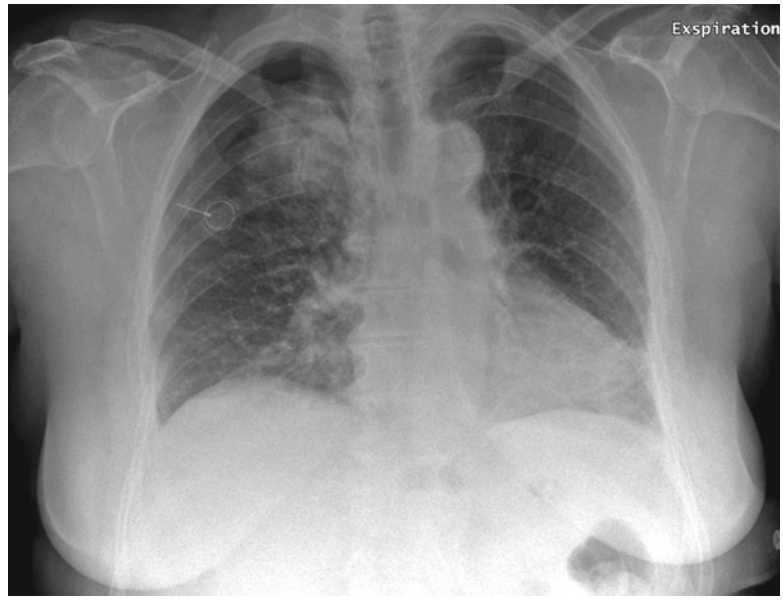

Fig. 13.55 The conventional chest X-ray shows the consolidation in the upper right lobe corresponding to the coagulation area. The depicted pneumothorax did not require any treatment

in 12 patients with 16 histologically proven lung malignancies and found the technique to be effective and safe. After an average follow-up of 20 months, 7 of 12 patients were alive (He et al. 2006). Wolf et al. treated 50 patients with 82 pulmonary masses using CT-guided MWA (Wolf et al. 2008). Technical success, as defined by a lack of contrast enhancement of the target lesion on post-ablation CT examination, was 95 %. An index tumor size >3 cm was found to be associated with a higher risk of residual disease but did not affect the cancer-specific or all-cause mortality. The 1-, 2-, and 3-year survival rates were 65 % ± 7, 55 % ± 9, and 45 % ± 11, respectively. A technical success rate of 100 % was reported by Carrafiello et al. after treatment of ten lesions in nine patients (Carrafiello et al. 2010).

13.3.3.6 Complications

In general, MWA of pulmonary malignancies was found to be a safe and effective treatment (Wolf et al. 2008). Pneumothoraces are the most common complications occurring during or after the intervention. In cases where it is associated with clinical symptoms and, therefore, requires additional therapy, it can be handled with simple aspiration or placement of a drainage catheter featuring a Heimlich valve. Wolf et al. described a rate of 39 % pneumothoraces (Wolf et al. 2008) which is similar to the rate found in other pulmonary ablation therapies (Vogl et al. 2011). Small amounts of pleural effusion are a common finding after pulmonary ablation procedures and rarely require any treatment. Typically these effusions are asymptomatic and resolve after a couple of days. Skin burns at the puncture site may occur due to heating of the applicator shaft. Other complications that were described include post-ablation syndrome featuring cough, fever, and residual soreness in the treated area. Severe side effects are acute respiratory distress syndrome and delayed infection of the ablated area as described above.

Appraisal

In summary, although pulmonary MWA is a relatively new technique, the published data shows promising results. From a technical point of view, MWA offers some potential

benefits in comparison to pulmonary RFA, but this was not shown in clinical studies, so far. The indications for image-guided MWA of malignant lung tumors cover the same patients as pulmonary RFA does. It has been shown that MWA of malignant tumors is safe and effective, although long-term follow-up is not available to date.

Key Points

- Indication: Nonsurgical patients suffering from stage I NSCLC or metastatic pulmonary disease with max. 5 lesions per hemithorax, none of them exceeding a diameter of 5 cm.
- Ablation procedure: Precise applicator placement should be performed avoiding repeated pleural passage; complete tumor ablation should be achieved including a safety margin which is recognized by an area of ground-glass opacity encasing the tumor.
- Pneumothoraces represent the most common complication, which can require aspiration or chest tube placement. Rare complications include ARDS and delayed infection of ablation area.

13.4 Percutaneous Ethanol Injection

Markus Düx

13.4.1 Introduction

Percutaneous ethanol injection (PEI) represents one of the most commonly performed techniques of local tumor ablation worldwide. Since it was performed first in 1983, PEI has been increasingly used for treating hepatocellular carcinoma (HCC). Nowadays, thermal ablation techniques tend to gradually replace PEI which is therefore no longer a first-line treatment of HCC. However, besides its unchallenged low-cost profile, PEI may still offer distinct advantages over other regional therapies in some situations (Lin et al. 2004, 2005).

Absolute alcohol works in two ways. First, it leads to coagulation necrosis at a cellular level as it diffuses into the neoplastic cells, causing immediate dehydration of the cytoplasm. Cellular necrosis finally results in a fibrous reaction. The second mechanism induces necrosis of endothelial cells and platelet aggregation with subsequent thrombosis of the small vessels. The thromboembolic effect of absolute alcohol leads to ischemia of the neoplastic tissue (Festi et al. 1990). Percutaneous acetic acid injection may be an alternative to ethanol injection, also causing dehydration of the cytoplasm, endothelial necrosis, as well as thrombosis of the small vessels (Tsai et al. 2008).

HCC in cirrhotic liver is best suited to be treated by PEI because in this case the tumor tissue is softer than the surrounding cirrhotic tissue of the liver. As a result, alcohol selectively diffuses within the HCC. Moreover, HCC with a size of 2 cm and more shows arterial hypervascularization that ensures an uniform distribution of alcohol within the rich network of the neoplastic sinusoids (Livraghi 1999).

On one hand, the combination of liver cirrhosis and arterial hypervascularization of HCC results in a tremendous local effect of alcohol to the tumor tissue as it is not able to disrupt the intratumoral septa and the surrounding tumor capsule. On the other hand, increasing size of HCC reduces the antitumoral effect of PEI because it does not reach all parts of the tumor and may not destroy all neoplastic cells (Llovet and Sala 2005). In addition, tumors that are not surrounded by cirrhotic liver tissue are not a target of PEI because diffusion of the alcohol is not limited to the tumor and a sufficient antitumoral effect cannot be achieved. Thus, PEI is a technique that is linked together with the treatment of HCC and only some rare oncologic indications other than HCC.

Table 13.16 Calculation of the Child–Pugh score uses five parameters, each scored 1–3, with three indicating most severe derangement

Measure	1 point	2 points	3 points	Units
Bilirubin (total)	<34 (<2)	34–50 (2–3)	>50 (>3)	μmol/l (mg/dL)
Serum albumin	>35	28–35	<28	g/L
INR	<1.7	1.71–2.20	>2.20	–
Ascites	None	Suppressed with medication	Refractory	–
Hepatic encephalopathy	None	Grades I–II (or suppressed with medication)	Grades III–IV (or refractory)	–

Table 13.17 By adding the scores from the Table 13.16 chronic liver disease can be classified in Child–Pugh stages A–C, indicating the patients' prognosis

Points	Class	1-year survival (%)	2-year survival (%)
5–6	A	100	85
7–9	B	81	57
10–15	C	45	35

13.4.2 Indications

Patient selection is very crucial for successful local treatment of HCC. It should be based upon tumor localization, size, proximity to large vessels, bleeding risk, respiratory motion, pathway of probe, and last but not least physician's experience. The most important question is whether the tumor is accessible under image guidance without putting the patient at increased risk for bleeding complications, injury of bile ducts, or bowel loops. Thermal ablation of HCC nodules may often be difficult or impossible due to one of the reasons mentioned before. In those cases, PEI is a welcome alternative to perform local tumor ablation as there is hardly any reason not to be able to reach a tumor nodule with a fine needle.

The best candidates for PEI are those with Child A cirrhosis (Tables 13.16 and 13.17) and small tumors (≤3 cm). The cancer should be confined to the liver, and the number of hepatic tumors to be treated by PEI should not exceed four to five lesions. In addition, the patient should be classified unresectable because of the distribution of disease or due to the severity of underlying cirrhosis (Ebara et al. 2005). HCC ≤3 cm treated by PEI are expected to achieve complete responses (Lin et al. 2004; Livraghi et al. 1999). Treatment of patients with larger tumors (3–5 cm) or advanced liver failure (Child B) has to be decided on a patient's individual basis. According to the Barcelona Clinic Liver cancer staging classification (Table 13.18), patients classified as stage A, who do not fulfill the criteria for tumor resection or liver transplantation, qualify best for percutaneous ablation (Bruix et al. 2001).

Limitations for PEI are rare including:

Systemic tumor progression

Severe coagulopathy (Quick <35 %, platelets <40,000/mcl)

Child C cirrhosis with refractory ascites

Limited life expectancy (Ebara et al. 2005; Lencioni et al. 2003)

In order to reduce the risk for recurrent tumor and to enhance overall survival, combined-treatment options including PEI have been evaluated for HCC. It has been demonstrated that transluminal arterial chemoembolization (TACE) combined with alcohol injection has the potential to prolong survival compared to TACE alone in small HCC (Koda et al. 2001; Wang et al. 2011) and even in nodules with a mean size of 8 cm (Lubienski et al. 2004; Wang et al. 2010). Thus, stage B and C patients according to the Barcelona Clinic Liver cancer staging classification may also profit from PEI as far as they are candidates for TACE.

According to recent reports (Tsai et al. 2008; Germani et al. 2010), alcohol injection may be replaced by percutaneous acetic acid injection, especially in HCC, resulting in fewer treatment sessions and providing better survival of patients. Basically, indications as well as technical considerations are the same for PEI and acetic acid injection.

Table 13.18 Barcelona Clinic Liver cancer staging classification (BCLC): stage-dependent treatment of HCC

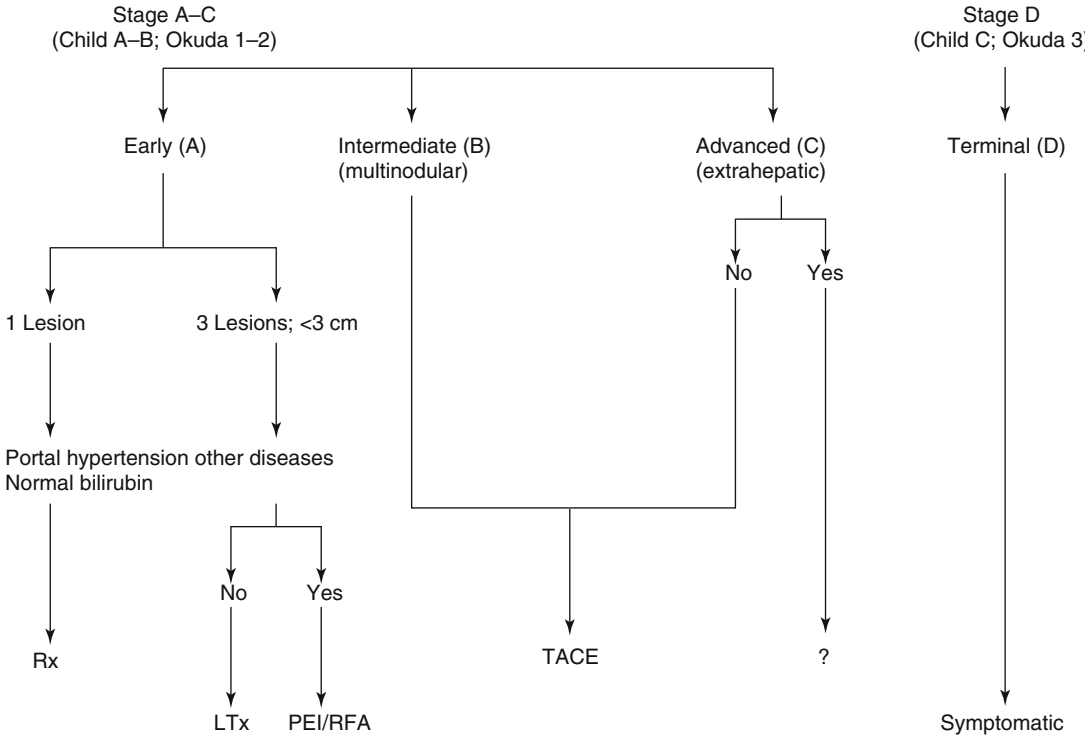

Rx liver resection, *LTx* liver transplantation

13.4.3 Material and Technique

13.4.3.1 Preprocedural Rests

Preprocedural evaluation should include adequate laboratory tests to rule out severe coagulopathy, acute inflammation, poor liver function (Child B and C cirrhosis), and/ or other severe comorbidities. A screening for viral hepatitis is mandatory, and baseline serum tumor markers—alpha-fetoprotein (AFP) in patients with HCC—are helpful to monitor the therapeutic success during follow-up.

Assessment of the tumor extent and staging for metastatic disease are the baseline for subsequent follow-up studies. To decide on the size, location, and number of liver lesions, contrast-enhanced computed tomography (CT) and magnetic resonance (MR) imaging play a major role, while ultrasound (US) is hampered by its reproducibility (Vilana et al. 2006; Mahnken et al. 2009). As HCC is characterized by arterial hypervascularization, any imaging test needs to be obtained during the arterial phase of contrast enhancement followed by image acquisitions during the portal and venous phase of liver perfusion. Thus, multiphase liver imaging is necessary to allow an appropriate diagnosis of HCC, the number and size of tumor nodules, and their location to correctly plan local ablation treatments. If there is a history of bone pain and/or the serum alkaline phosphatase is disproportionately elevated, a bone scan or whole-body MR imaging is necessary to rule out bone metastases (Nakanishi et al. 2005). Informed consent has to be obtained 24 h prior to the procedure by the latest.

13.4.3.2 Imaging Considerations

PEI is most commonly performed under US guidance (see Sect. 13.3.3.3). When a single-session approach is used, CT is a regularly used technique for performing and monitoring the procedure. MR imaging can also be used to perform PEI (Adam et al. 1997; Kim et al. 2005).

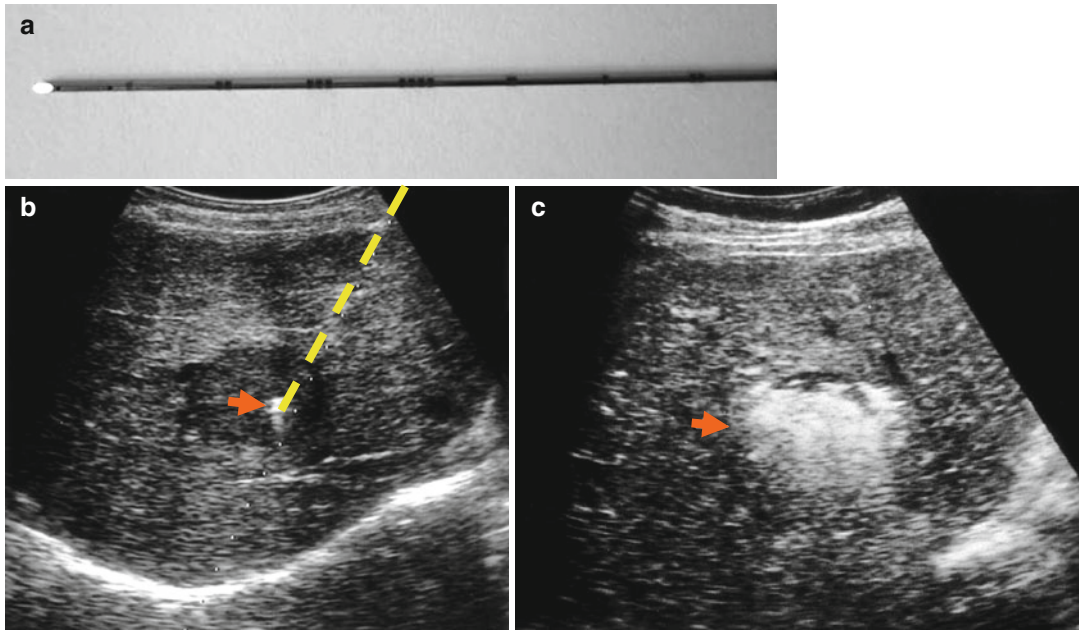

Fig. 13.56 (**a**) PEI needle: fine needle with a conical tip that is closed and releases the alcohol by side holes. (**b**) Encapsulated HCC that has been punctured by ultrasound guidance (*yellow line*). The bright echo within the tumor nodule indicates the needle tip (*arrow*). (**c**) During the course of alcohol injection, a dense echogenic cloud (*arrow*) forms with distal acoustic shadowing that makes it difficult to evaluate whether the alcohol has diffused through the entire tumor or not

Due to its physicochemical properties, alcohol injection/diffusion can reliably be visualized by MR imaging. In particular, MR-guided PEI is being advantageous in locations unfavorable for CT guidance or in patients in whom iodized contrast media are contraindicated. At MR imaging it is suggested to use an inversion-recovery spin-echo sequence using an inversion time of 250 ms and an echo time of 150 ms in combination with water saturation pulses which effectively suppresses the tissue water signal from human liver while obtaining a high signal from the alcohol (Alexander et al. 1996).

13.4.3.3 Ablation Technique

Puncture and Injection Technique

PEI does not differ much from fine-needle aspiration biopsy. An intravenous access line for sedation and analgesia is established using an intravenous cannula placed in a cubital vein. There is no need for prophylactic antibiotics. The patient's skin is prepped and draped. Then local anesthesia from the skin entry point of the needle down to the liver capsule is administered. For local anesthesia, common local anesthetics such as mepivacaine, for sedation midazolam or fentanyl, and for analgesia piritramide can be used. Subsequently, the tumor is punctured, using a fine needle (20–22 gauge) with a length of 10–20 cm. There are fine needles that are dedicated to the PEI procedure, whose tip is closed, conical, and equipped with several side holes that release the alcohol (Livraghi 1998). Those needles are preferred because they offer a more homogeneous release of alcohol into the tumor tissue. The needle is passed to the distal margin of the tumor, and absolute alcohol is injected slowly while rotating the needle. Ethanol usually spreads within a radius of 1–3 cm around the tip of the needle to the periphery of the tumor (Livraghi 1998). Alternatively, a normal fine needle may be used instead of the needle with the closed conical tip and side holes. In this case, the alcohol is injected via the end hole without rotating

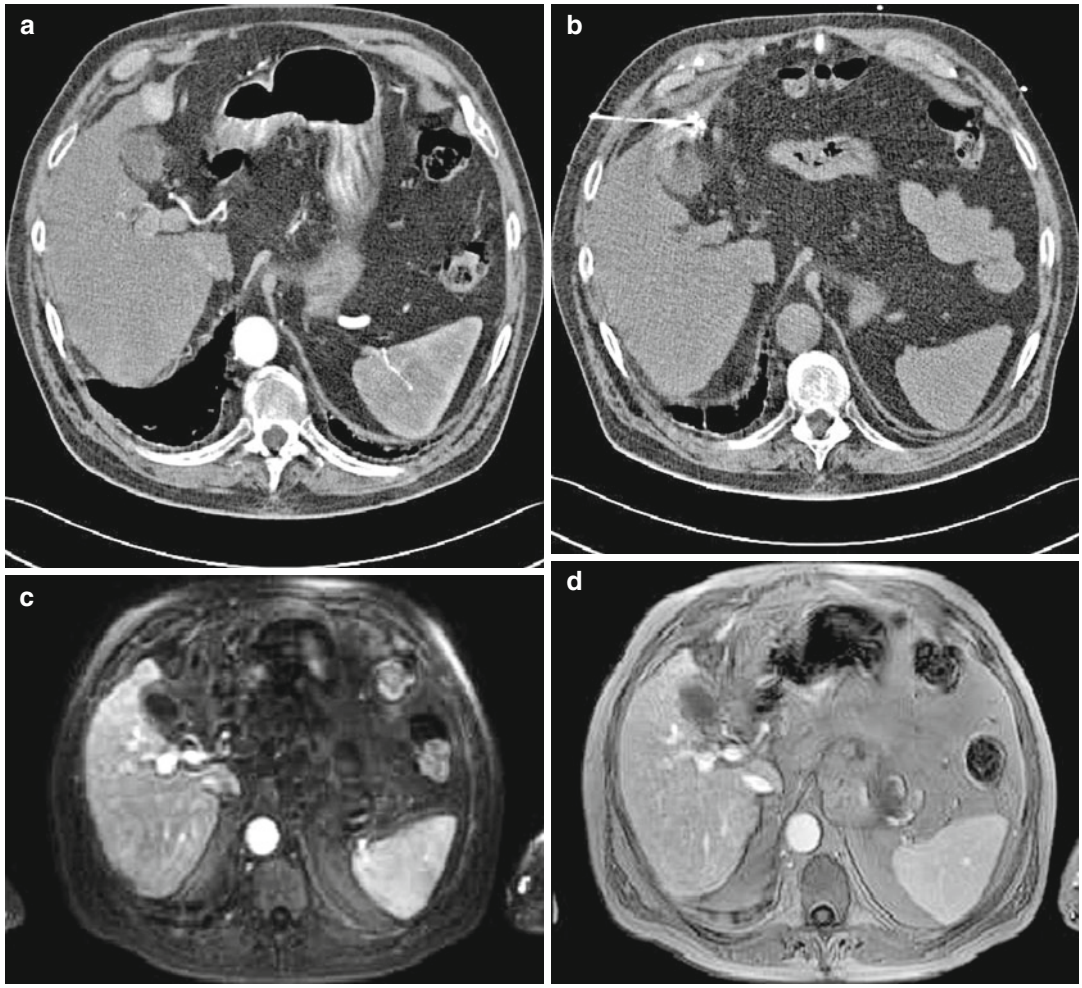

Fig. 13.57 (**a**) A small HCC is depicted hyperdense on CT during the arterial phase. (**b**) A PEI needle is positioned within the center of the tumor, and contrast material was injected through the needle to estimate the distribution of the alcohol. MR imaging control 24 h later indicates complete necrosis of the tumor without uptake of contrast media during the (**c**) arterial and (**d**) portal venous phase

the needle. It is gradually withdrawn toward the proximal edge of the tumor, and injection is stopped when the alcohol saturation of the tumor is considered to be total.

For monitoring alcohol distribution within the tumor, either CT or US may be used. On US, which is well suited for real-time imaging of the procedure, the entire tumor appears hyperechoic when it is completely filled with alcohol (Fig. 13.56). For CT monitoring of the alcohol distribution, it can be mixed with a little iodinated contrast material (Fig. 13.57). Alternatively the alcohol appears as hypodense area after injection (Fig. 13.58). If alcohol is observed to flow into a blood vessel, bile duct, or leaks outside the tumor into the liver, the needle is repositioned. Depending on the size and shape of the tumor, repositioning of the needle is mandatory to treat not only the center but also the edges of the tumor. This prevents tumor tissue to survive in parts isolated by a tumor capsule or intratumorous septa.

After completing the injection, the needle is left in place for 1–2 min to allow the alcohol to diffuse into the tumor and away from the needle tract. Then the needle is aspirated firmly during

Fig. 13.58 HCC of 5.5 cm in diameter that had been submitted to repeated TACE before. Homogeneous uptake of lipiodol that shows no metabolism over time indicates inactive tumor tissue. However, the CT scan also shows viable tumor next to the lipiodol deposition that therefore selectively was treated by PEI due to its neighborhood to the gallbladder. The control scan shows the distribution of the alcohol that is depicted hypodense at CT

withdrawal to minimize leakage since alcohol reflux may cause pain.

Multisession Approach

Most PEI procedures are performed under the US guidance, allowing one to control not only the puncture itself but also the release of the alcohol into the tumor tissue. Real-time visualization of the alcohol diffusion may be accomplished since microbubbles contained in the injected alcohol are markedly echogenic just after injection. However, in the late course of alcohol injection, a dense echogenic cloud forms with distal acoustic shadowing that makes it difficult to evaluate whether the alcohol has diffused through the entire tumor or not (Fig. 13.56). US-guided PEI is an outpatient procedure, and the injected volume per session/per tumor is varying between 2 and 10 ml. The toxic dose of ethanol is 0.8–1.0 cm^3/kg with a recommended maximum volume of 30–40 ml per session. Tumors smaller than 2 cm are treated by 3–4 sessions and tumors of 2–3.5 cm by 8–12 sessions (Lee et al. 1995). Usually two to four treatment sessions per week are performed using this US-guided multisession approach (Adam et al. 1997). The end point of the treatment is the arterial devascularization of the tumor depicted by color-coded duplex sonography.

Single-Session Approach

Multisession treatment of HCC needs the patient to come in regularly to receive PEI. Alternatively, a single-session procedure offers the advantage that the "treatment logistics" are more acceptable for the patient (Fig 13.57). However, depending on the tumor size, an appropriate volume of absolute alcohol is required to kill the tumor entirely. It is reported to use volumes of 40 ml up to more than 200 ml per session (Livraghi et al. 1998). In order to prevent serious side effects of a single-session treatment, the total volume of alcohol applied to the tumor should not exceed 70 ml. Injection volume may be calculated from the radius of the tumor, using the formula for the volume of a sphere, $4/3\pi \times (\text{radius} + 0.5\ \text{cm})^3$. Here, 0.5 cm is added to the radius to obtain a safety margin. That means a total volume of 32 ml is necessary to

cover a tumor of 3 cm in diameter ($V = 4/3\ \pi$ (1.5 + 0.5 cm)). According to the formula, a tumor 4 cm in size should be treated with 65 ml of alcohol, and a tumor of 5 cm in diameter needs 113 ml of alcohol to devascularize it entirely. However, it is well accepted to treat HCC ≤3 cm in diameter by percutaneous tumor ablation only (Wang et al. 2010; Germani et al. 2010).

To avoid pain sensations to the patient, single-session procedures are usually performed under general anesthesia that results in a better control of the procedure. In order to sufficiently cover the entire tumor volume with alcohol, CT guidance is preferred as it may be necessary to position a second, third, fourth, or even fifth needle within the tumor (Fig. 13.58). The total amount of alcohol is divided into portions and is injected slowly via the different needles into the tumor. During the injection, each needle is gently pulled back within the tumor in order to equally treat the edges and the center of the tumor equally. The treatment is ended when the entire tumor appears hypodense or if mixed with contrast material, hyperdense on CT, or the calculated total amount of alcohol is injected (Livraghi et al. 1995) (Fig. 13.58).

Single-session treatment offers the advantage that bigger tumors can be treated much faster and more complete, which may well be documented by a CT/MRI scan 24 h post-procedurally (Fig. 13.58). In case of incomplete ablation, a second treatment session should be scheduled instead of increasing the total amount of alcohol.

Combined-Treatment Approaches

By solely using PEI, complete necrosis can be achieved in 70–92 % of cases in tumors ≤3 cm (Ikeda et al. 2001; Lin et al. 2004; Livraghi et al. 1999). Efficacy of PEI decreases with increasing tumor size. Therefore, combined approaches were sought. HCC >3 cm in size should be treated by TACE first and then in a second step by percutaneous ablation (Wang et al. 2010, 2011). TACE significantly reduces arterial inflow into the tumor and breaks down intratumoral septa. Persistent/recurrent ischemia by repeated TACE improves the effect of PEI as the alcohol may diffuse more easily within the tumor and, on the other hand, its washout is minimized due to the reduced arterial in- and outflow. As a consequence, additional PEI may be performed with reduced amounts of alcohol to achieve devascularization of the entire tumor. Combined procedures to treat HCC >3 cm always start with repeated TACE. CT helps to judge the uptake of lipiodol into the tumor as well as its metabolism. Areas of the tumor that show a persistent uptake of lipiodol are supposed to be inactive for the moment as the tumor is not capable to metabolize it (Fig. 13.58). Thus, single-session PEI may be steered according to the uptake of lipiodol and the results obtained by multiphase contrast-enhanced CT or MR imaging of the liver. CT imaging enables, on the one hand, positioning of the needles into all parts of the tumor in order to cover it completely with alcohol. On the other hand, the total amount of alcohol injected into the tumor is divided in portions, aiming predominantly at the viable areas of the tumor (Fig. 13.58). As a result, parts of the tumor with persistent uptake of lipiodol receive less alcohol compared to those that show a marked contrast enhancement at CT/MR imaging. As mentioned before, single-session treatment should not exceed 70 ml of absolute alcohol. Due to repeated TACE prior to the PEI procedure in HCC >3 cm, it is recommended to consider the maximum diameter of the tumor to calculate the total amount of alcohol. Although this is only subject to personal experiences, a tumor of 3, 4, 5, 6, and 7 cm in diameter may sufficiently be treated by 30, 40, 50, 60, and 70 ml of alcohol, respectively.

13.4.4 Results

PEI is efficient in the treatment of HCC and may achieve a complete tumor necrosis in more than 80 % of tumors smaller than 3 cm in diameter. However, response rates decrease with growing size of HCC, and tumor necrosis is obtained in only 50 % of tumors measuring 3–5 cm in diameter (Lencioni and Crocetti 2005; Livraghi et al. 1995; Mahnken et al. 2009). Histopathology reveals complete coagulation necrosis after PEI in 70 % of tumors smaller than 3 cm in diameter

and no damage to healthy tissue surrounding the tumor. The 5-year survival of patients with an HCC<3 cm treated by PEI ranges between 48 and 78 % (Arii et al. 2000; Ebara et al. 2005; Lencioni et al. 1997; Livraghi et al. 1995, 2004; Omata et al. 2004; Sakamoto and Hirohashi 1998). Recent long-term data with 20 years of follow-up show that Child A patients with a solitary tumor smaller than or equal to 2 cm in diameter have better long-term outcomes compared to patients with a 2–3-cm HCC (Ebara et al. 2005). They do not only have the best overall survival, but also show significantly less tumor recurrences that usually develop from the treated nodule. Those results are confirmed by a recent study by Sala et al. (2004). Independent predictors of survival are:

- Initial complete response
- Child–Pugh score
- Number or size of nodules
- Baseline alpha-fetoprotein levels

The major limitation of PEI is the high local recurrence rate that may reach 33 % in tumors smaller than 3 cm and 43 % in tumors exceeding 3 cm (Khan et al. 2000; Koda et al. 2000).

When considering PEI as a treatment option in HCC, one has to keep in mind that radiofrequency (RF) ablation is superior to PEI with 80 % versus 90 % of complete response rates in tumors ≤3 cm. This has been achieved in a substantially lower number of treatment sessions (Livraghi et al. 1999). A similar study in 119 patients with solitary HCC less than 3 cm in diameter treated either by RF ablation or PEI shows complete tumor responses in 100 and 94 % of patients, respectively (Ikeda et al. 2001). RF ablation needed 1.5 versus 4 treatment sessions in the PEI group. Lencioni et al. (2003) performed a prospective randomized analysis of RF ablation versus PEI in small HCC and report an overall 1- and 2-year survival of 100 and 98 % compared to 96 and 88 % which has not been statistically significant. However, the 1- and 2-year local recurrence-free survival has been significantly higher using thermal ablation (98 and 96 % vs. 83 and 62 %). Other randomized controlled trials comparing RF ablation versus PEI in early-stage HCC confirm the superiority of RF ablation versus PEI treatment (Lin et al. 2004, 2005; Shiina et al. 2005). Lin et al. (2004, 2005) report survival advantages of RF ablation in a subgroup of tumors larger than 2 cm compared to either percutaneous ethanol or acetic acid injection. As a result, RF treatment is confirmed as an independent prognostic factor for local recurrence-free survival by multivariate analysis (Lencioni et al. 2003). Finally, a meta-analysis including 1,035 patients who had been treated within eight randomized clinical trials concludes that RF ablation is superior to PEI for survival, complete necrosis of tumor, and local recurrence (Germani et al. 2010).

Percutaneous acetic acid injection seems to be advantageous compared to ethanol injection too (Tsai et al. 2008). According to recent data, the local recurrence rate and new tumor recurrence rate are reported to be similar between alcohol and acetic acid injection. However, acetic acid injection resulted in a significantly better survival, and multivariate analysis revealed acetic acid to be the significant factor associated with overall survival. In addition, the treatment sessions required to achieve complete tumor necrosis were significantly fewer using acetic acid. Although RF ablation and acetic acid injection tend to be superior to alcohol with respect to local tumor control and patient survival, PEI is a safe and well-established technique for local tumor ablation. Worldwide it has been successfully used for decades, and because of its low cost and availability, PEI will remain a treatment option of HCC in the near future.

Most recent data suggest PEI to be an important modulator of tissue properties prior or directly during RF ablation. Tissue modulation with alcohol lowers the boiling point of the tissue, resulting in reduced ablation times. According to Kurokohchi et al. (2005), injection of alcohol prior to RF ablation may equally enhance the volume of coagulated necrosis in three dimensions regardless of types of RFA instruments. It has been demonstrated that the volumes of coagulated necrosis were significantly larger in the group of patients treated by PEI and RF ablation compared to HCC patients treated by RF ablation alone. The amount of total energy required was comparable between both groups, and it was concluded that the energy needed for coagulation

per unit volume is significantly lower in case of a combined treatment by PEI and RF ablation. Furthermore, the volume of coagulated necrosis showed a stronger correlation with the amount of alcohol injected than the total energy requirements, respectively. Obviously, less energy is required when combining PEI and RF ablation to induce ablation areas similar to those that may be obtained by RF ablation alone. In addition, antitumoral effects of PEI may lower recurrence rates when combined with RF ablation (Kurokohchi et al. 2005).

It has been demonstrated that TACE combined with alcohol injection has the potential to prolong survival compared to TACE alone in small HCC (Koda et al. 2001) and even in nodules with a mean size of 8 cm (Lubienski et al. 2004; Wang et al. 2010). A retrospective evaluation of patients suffering from large HCC with a medium size of 8.6 cm ± 4.5 cm and multifocal disease in 46 % of cases compared efficiacy of TACE alone and TACE combined with PEI (Lubienski et al. 2004). It reported an overall 1-, 2-, and 3-year survival of 21, 4, and 4 % compared to 55, 39, and 22 %, which has been statistically significant. There are several other studies (Cheng et al. 2008; Georgiades et al. 2008; Guan and Liu 2006; Kurokohchi et al. 2006) that forecast a better outcome of HCC patients if treated by a combination of arterial devascularization and percutaneous ablation such as PEI or RFA. Thus, quality of life, survival without local recurrence, and long-term survival are significantly improved by a combination therapy in HCC ≥3 cm.

13.4.5 Complications

Care has to be taken to avoid direct injection of ethanol into the hepatic veins because a sudden and high concentration of ethanol in terms of a bolus may lead to prolonged hypoxemia with cardiopulmonary arrest (Livraghi 1998). Livraghi et al. (1998) reported a significant higher rate of mortality (0.1 % vs. 4.6 %) while performing single-session treatment under general anesthesia. However, alcohol volumes of more than 200 ml had been used. This large amounts of ethanol should strictly be avoided.

A major concern of percutaneous tumor ablation is seeding along the needle tract. Because injected alcohol damages cancer cells immediately (Shiina et al. 1991), seeding of cancer cells is unlikely to occur. Nevertheless, it has been reported in <0.01–0.6 % of patients (Di Stasi et al. 1997; Livraghi et al. 1995). Altogether, PEI results in low complication rates (morbidity 1.7 %) and a negligible rate of treatment-related deaths (mortality 0.1 %).

13.4.6 Percutaneous Ethanol Injection in Thyroid and Parathyroid Disease

There are indications for PEI other than HCC. Some diseases of the neck region may be treated by PEI using ultrasonography for guidance. PEI may be an alternative to surgical parathyroidectomy in the management of parathyroid hyperplasia in patients with secondary hyperparathyroidism resistant to medical therapy (Solbiati et al. 1985; Harman et al. 1998). PEI is mostly used in dialyzed patients suffering from secondary hyperparathyroidism and gives best results when combined with vitamin D analogs if 1–2 parathyroid glands are enlarged or a residual parathyroid gland is identified after parathyroidectomy has taken place. In those cases, ultrasonography is able to guide the procedure, placing the needle tip into the region of interest. A maximum of 3–5 ml of ethanol or the volume of ethanol corresponding to half of the calculated volume of the affected gland is slowly injected using ultrasonographic guidance to control the procedure. Ethanol injection is usually administered in two or three sessions 24 h apart, looking carefully not to extravasate the alcohol. Success rates of 50–70 % have been reported, depending of the number of enlarged parathyroid glands. Criteria of success are a size reduction or complete fibrozation of the gland and a reduction or disappearance of vascularization, respectively. Normalization of serum calcium is often achieved after 36–120 h, and parathormone

levels usually decrease or normalize 6–78 h after ethanol injection (Karstrup et al. 1993; Verges et al. 1993). Approximately 65 % of patients experience a long-term effect of PEI, maintaining normal serum calcium and parathormone concentrations for at least 5 years (Verges et al. 2000). PEI is also successfully used in selected patients suffering from primary hyperparathyroidism (Iglesias and Diez 2009; Veldman et al. 2008). It is considered to be an alternative to surgery if there are contraindications to surgery because of high risk, advanced age, symptoms of acute severe hypercalcemia, and persistent primary hyperparathyroidism after parathyroidectomy (Ackmann and Janowitz 1997). Adverse effects are rare and include pain or discomfort when ethanol is extravasated, vocal cord paralysis due to damage to recurrent laryngeal nerves, and Horner's syndrome.

Cervical cysts (for example thyroid cysts, parathyroid cysts) may also be a well-accepted target of PEI replacing surgery. In most cases a single treatment with ethanol is sufficient to achieve a volume reduction between 50 and 95 %, depending on size and content of the cyst (clear, colloidal, or hemorrhagic) as well as the presence of solid tissue (Chu et al. 2003).

A further indication for PEI is toxic and autonomous thyroid adenoma and toxic nodular goiter. Especially, patients who refuse radiation therapy or surgery are candidates because complete cure may be achieved in more than 75 % of cases. The goals of successful PEI are nodal size reduction as well as normalization of thyroid hormones and TSH levels leading to an improved subjective condition of the patients (Chu et al. 2003).

Thyroid cancer is the most common malignant tumor of the endocrine system. More than 80 % of these cancers are papillary thyroid carcinomas (Sohn et al. 2009). While most well-differentiated thyroid carcinomas have a benign course with a 10-year survival rate of 93 %, there is a 20 % recurrence rate mostly involving cervical lymph nodes. Patients who have undergone previous neck dissection are considered to have a high risk of reoperation due to scar tissue formation. PEI is therefore a well-accepted method to treat patients with recurrent cervical lymph node metastases, who are not candidates for another operation or who refuse surgery. Reduction of nodal size or complete disappearance of thyroid cancer neck metastases may be achieved in approximately 70 % of patients with a decrease in serum thyroglobulin, except for patients suffering from additional distant metastases (Sohn et al. 2009). However, it has to be taken into account that the ethanol injection has to be repeated several times until the desired effect is obtained. On the other hand, the procedure is well tolerated and is therefore regarded as a minimally invasive alternative to surgery.

13.4.7 Percutaneous Ethanol Injection in Rare Indications

Other indications for PEI are tumors of the kidney as well as adrenocortical adenoma (Wang et al. 2003). Finally, PEI may be used as a percutaneous treatment of patients suffering from hydatid cysts in echinococcosis (Gabal et al. 2005) (see Chap. 16.1.2.6). Especially, patients who are at high risk for surgery or who suffer from symptomatic hydatid cysts are candidates. A combination of aspiration of the content of hydatid cysts and repeated injections of ethanol into the tumor leads to size reduction in nearly all treated cysts and a separation of endocyst from pericyst in approximately 41 % of tumors. Most cysts tend to become heterogeneous after the procedure, and in about 12 % of cases, a pseudotumor develops.

13.4.8 Absolute Ethanol Sclerotherapy of Venous Malformations

PEI may also be indicated in patients suffering from symptomatic venous malformations (Su et al. 2010). In case of low-flow vascular lesions that mostly occur in the head and neck but may

be found in any part of the body, PEI is a well-accepted treatment to sclerose the dilated venous sacs if the patient suffers from symptoms such as deformity, pain, or bleeding. External compression of draining veins keeps the alcohol in place that should not exceed 1 ml/kg of body weight in a single treatment session. The procedure is performed under guidance of venography. Within a series of 60 consecutive patients receiving PEI for venous malformations in the face and neck, 37 % of patients were treated once, while the treatment had to be repeated 2–18 times in the remaining patients (Su et al. 2010). Sixty-eight percent of the patients achieved a complete volume reduction, 25 % had a marked response, and 7 % showed a moderate success of PEI. Minor complications like local skin necrosis and transient facial nerve palsy are reported in 10 % of patients, while there was no procedure-related mortality. Therefore, percutaneous sclerotherapy of low-flow venous malformations is considered a safe and effective treatment.

Appraisal

In most centers, PEI has an accepted role in the treatment strategy of small HCC. When surgical techniques are precluded in patients with early-stage tumors, PEI is generally regarded as a second-choice treatment (Llovet et al. 2003). In those patients, RFA is the first-choice treatment since more complete tumor necrosis will be achieved using thermal ablation techniques. Combined treatments using TACE and PEI have the potential to prolong survival compared to TACE alone in small HCC. Even stage B and C patients, according to the Barcelona Clinic Liver cancer staging classification, may profit from additional PEI as far as they are candidates for TACE. The final role of PEI in combination with RFA is not established so far since there is no sufficient scientific evidence.

PEI may also be an effective treatment in primary and secondary hyperparathyroidism, in benign nodular thyroid disease used for sclerotherapy of solid nontoxic and autonomously functioning nodules, as well as in cystic nodules of the thyroid gland. Further indications are thyroid neck cancer metastases in patients who have undergone previous neck dissection. Patients suffering from symptomatic hydatid cysts may also be candidates for PEI. Finally, PEI is a first-line treatment of symptomatic low-flow venous malformations.

Key Points

- PEI is a cheap, easy, and safe procedure in the treatment of HCC.
- PEI may only be used in cirrhotic livers and has no effect in non-cirrhotic patients suffering from HCC.
- Single-session treatment appears advantageous when compared with multisession treatment.
- PEI is generally regarded as a second-choice treatment of HCC when compared to RF ablation.
- Small HCC may be treated by RF ablation or PEI alone.
- Combined therapies including TACE and RF ablation or PEI markedly increase efficacy of treatment of HCC ≥3 cm.
- Combining PEI and RF ablation reduces local recurrence rates; however, the final role of this combination is not definitely established due to the lack of scientific evidence.
- Indications for PEI other than HCC include primary and secondary hyperparathyroidism, benign nodular disease of the thyroid gland, recurrent cervical lymph node metastases of thyroid cancer after neck dissection, and symptomatic hydatid cysts.
- Percutaneous sclerotherapy of low-flow symptomatic venous malformations is considered a first-line treatment.

13.5 Interstitial HDR Brachytherapy: Technique

13.5.1 CT-Guided HDR Brachytherapy

Konrad Mohnike and Jens Ricke

13.5.1.1 Indications

Indications for computed tomography (CT)-guided brachytherapy comprise of unresectable liver and extrahepatic malignancies, unlimited by size or location near risk structures such as liver hilum, gallbladder, or large vessels which frequently limit the use of thermal techniques such as radiofrequency or laser ablation.

The majority of indications target large liver metastases of colorectal or other primary cancers as well as hepatocellular carcinoma (HCC) or cholangiocarcinoma. Patients should not be eligible to surgical resection with curative intent, and local ablation must be part of a multimodal therapeutic management. In most patients with metastatic disease, local ablation serves to enable a pause of chemotherapy or as a salvage approach if systemic therapies are not well tolerated. In any case, systemic therapy should be stopped 2 weeks before the procedure and should not be started earlier than 1 week after the intervention to avoid cumulative toxic effects, for example, from radiosensitizing agents. Almost any tumor location outside the central nervous system has been described to be eligible for brachytherapy. Outside the liver, specifically lung tumors at difficult locations close to the lung hilum, but also tumors with pleural or mediastinal infiltration, dominate the list of indications (Amthauer et al. 2006; Bergk et al. 2005; Ricke et al. 2004a; Wieners et al. 2006).

Eligibility criteria include a preserved hemostasis, but diminished liver function is a relative contraindication only because it may be the leading prognostic factor, and local tumor ablation may not help to improve the patient's prognosis. Interventions in patients with high bilirubin levels >3 mg/dl or liver cirrhosis Child–Pugh B or even C have been performed successfully in selected cases.

13.5.1.2 Material and Technique

Beside the typical material used for cross-sectional image-guided procedures like sterile drapings, povidone-iodine, or scalpel for skin incision, some dedicated material needs to be on hand:

- 18 G puncture needle of various length
- 6 F-introducer sheath (25 cm length)
- Stiff angiographic guide wire
- Brachytheraphy catheters
- Gelfoam

The placement of the applicators usually is performed using CT fluoroscopy. As the common 16 G brachytherapy catheters have a closed tip, a sheath needs to be used for application in the tumor volume. The sheath itself may be a regular 6 F vascular sheath of appropriate length (commonly up to 25 cm). A hydrophilic coating has proven to minimize patient discomfort when the sheath is pushed through the liver capsule. For sheath placement, an 18 G puncture needle is placed in the according position and exchanged against the sheath over a very stiff angiographic guide wire. In case the guide wire has a soft tip, it should be used with the stiff end going in first.

For treatment planning purposes, a spiral CT of the liver enhanced by i.v. application of iodinated contrast media is acquired after catheter placement in breath-hold technique and transferred to the treatment planning unit. Electronic data handling with DICOM data transferred directly from CT or magnetic resonance (MR) into the treatment planning system is helpful.

Definition of the catheter positions and tumor boundaries in the 3D-CT dataset is performed using a dedicated software system which in most cases will be integrated in the afterloading unit (Figs. 13.59 and 13.60). The high-dose-rate (HDR) afterloading system employs an ^{192}iridium source of 10 Ci. The source diameter usually is <1 mm. Dwell positions are located every 5 mm.

In the majority of patients, a reference dose between 15 and 25 Gy is prescribed, which is by definition identical with the minimum dose enclosing the lesion, and applied as a single dose. Even though no appropriate comparison is available, colorectal metastases will most likely need higher doses than breast cancer or hepatocellular

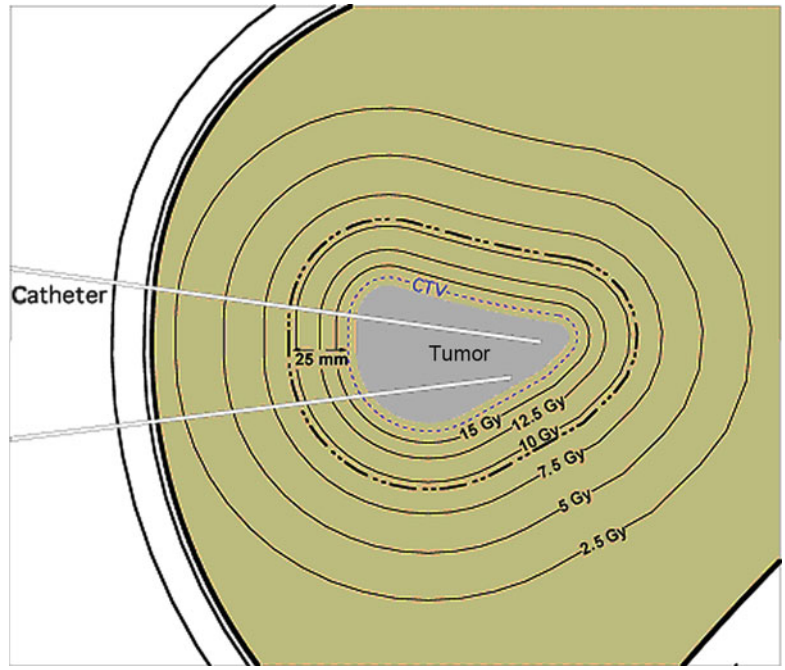

Fig. 13.59 Isodose distribution in CT-guided HDR brachytherapy of a liver lesion. Radiographic tumor volume (*gray*), clinical target volume (tumor volume and safety margin, *dotted line*), and dose distribution around the tumor (Courtesy of M. Seidensticker). Note the steep dose gradient outside the clinical target volume

carcinoma to achieve long-term local tumor control (see Sect. 13.5.1.3).

CT guidance for catheter placement has some drawbacks. In liver intervention, numerous lesions will be masked on non-enhanced imaging. During the intervention, non-enhanced fluoroscopy can be used to determine the target, often visually correlated with anatomic landmarks and corrected using previous MR imaging examinations. As a result, it may sometimes be necessary to reposition or add catheters after acquisition of the contrast-enhanced CT dataset. Furthermore, tumor volume is systematically underestimated in contrast-enhanced CT compared to MR imaging (Pech et al. 2008). For this reason, MR-guidance using open MR systems may in future become state of the art specifically for liver tumor ablation.

To prevent bleeding, Gelfoam embolization should be performed during step-by-step removal of the sheath.

13.5.1.3 Dose Considerations

CT-guided brachytherapy in some ways opposes the mainstream in radiotherapy today. The key issue in traditional electron beam percutaneous irradiation is to deliver a dose from an external source with optimal homogeneity in the target volume. In interstitial brachytherapy, things are very different, and its inherent character is that the dose is delivered with substantial heterogeneity since the radiation source is located at several widely distributed positions inside the tumor volume. It is quite obvious that a very dense catheter distribution will increase the degree of homogeneity—however, the primary goal of catheter positioning for therapy is not the dose homogeneity inside the tumor, but the minimal (and hopefully lethal) dose delivered in the clinical target volume (CTV, tumor plus safety margin) as well as the dose gradient outside the CTV. The dose gradient outside the CTV is decisive to spare adjacent risk organs as well as healthy tissue (e.g., functional liver parenchyma). As a rule of thumb, 1 catheter per 1–2 cm tumor diameter is used by our group, and preplanning of the catheter positions by a medical physicist previous to the intervention may prove helpful specifically in very large tumor volumes or if risk organs are close. However, the inherent advantage of the overall technique remains the ability to vary radiation time at each given dwell position following

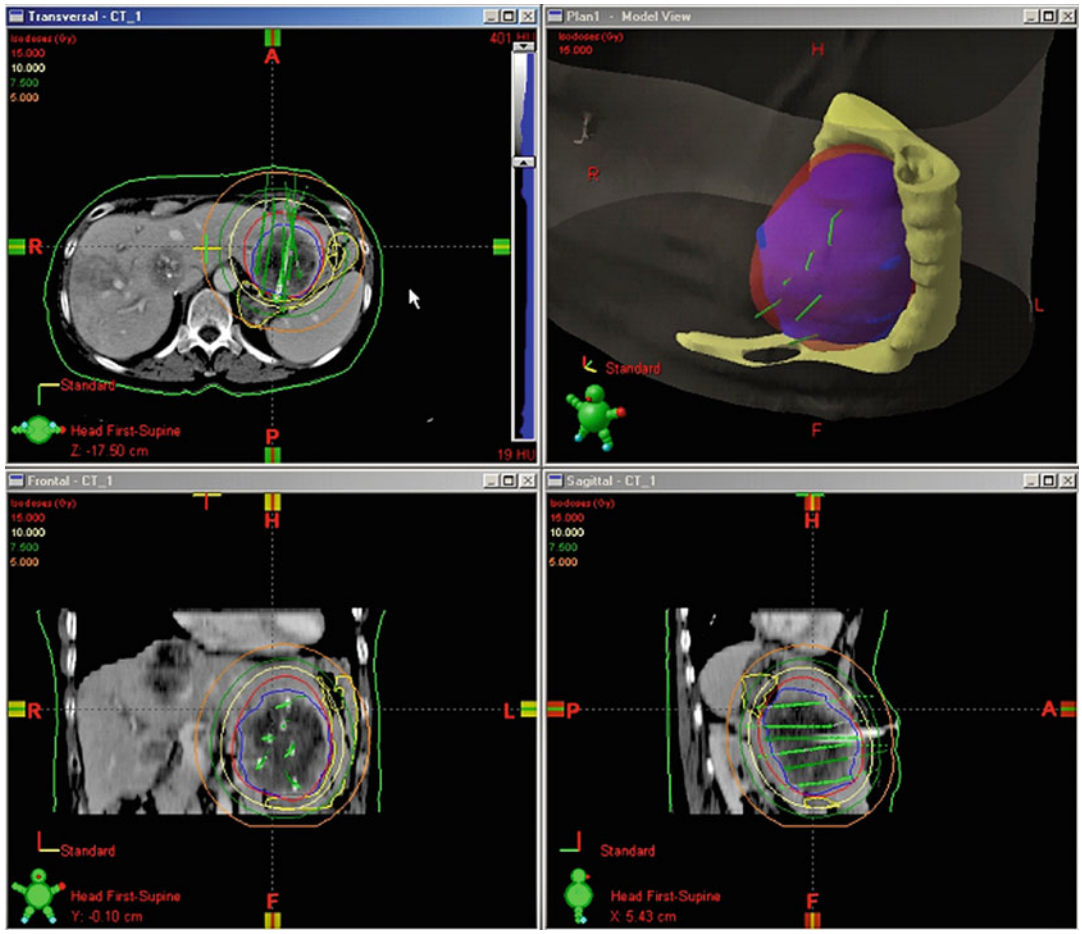

Fig. 13.60 Liver metastasis of colorectal carcinoma after application of six brachytherapy catheters. Isodose distribution as calculated by BrachyVision® (Varian, Palo Alto, CA). The two other lesions visible had been treated in previous sessions

diligent calculations of the optimal dosimetry after the catheters have been positioned in the tumor. Out of experience, even for senior interventionalists the final catheter positions will be somewhat different from any preplan.

No maximum dose constraints are given inside the tumor volume, but the total irradiation time has to be carefully considered. Iridium sources decay and have to be exchanged in regular intervals. A correction factor is applied to ensure that the dose prescribed is delivered irrespective of the source's age. However, if source exchange is undertaken every 8 or even every 12 weeks only, radiation time may be prolonged by a factor of greater than 2. No threshold radiation time can be given, but it is obvious that prolonged radiation bares the risk of increased rates of adverse events, starting with general symptoms of radiation toxicity such as nausea and vomiting up to 48 h after treatment. In our own patients, radiation time typically ranges between 20 and 40 min. However, we regard 60 min as the preferred maximum irradiation time that should be given, and we have not encountered unexpected toxicity in more than 1,000 applications. However, directly after extraction of the catheters, severe and uncontrolled post-procedural shivering may molest the patient in some cases, usually without accompanying fevers but sometimes associated with a vasovagal reaction. We hypothesize that

this event is not related to the total radiation time, but induced by extraction of the brachytherapy catheters triggering endotoxin release from lytic tumor cells into tumor blood vessels.

If a total irradiation time of 60 min is expected to be exceeded either due to a high iridium source factor or due to a very large tumor volume to be treated, the intervention may be divided in two or even three steps. In tumors or tumor conglomerates exceeding 8-cm diameter, it may be recommended to perform two interventions. In a first session, one-half of the tumor may be treated; preplanning of the catheter positions during the second session for the other half of the tumor is suggested to minimize radiation overlap.

The minimal single-fraction dose covering the CTV which is necessary to achieve long-term local tumor control varies considerably between tumor biologies. In addition, tumor volume influences the dose necessary—the higher the cell count, the higher the applied radiation dose should be. Randomized data is available for colorectal or breast cancer metastases as well as HCC (Ricke et al. 2010; Mohnike et al. 2008). HCC as well as breast cancer metastases may be treated with 15 Gy minimal dose inside the CTV, and local control rates after 12 months between 80 and 90 % can be expected for tumors with a median size of 4–5 cm. In colorectal cancer, minimal doses inside the CTV unfortunately need to be considerably higher, and local control rates of >80 % after 12 months are limited to tumors covered by 20 Gy at minimum. However, applying a minimal dose 20 Gy may often not be possible in large or multiple large tumor volumes since radiation time or overall patient distress due to potentially multiple treatments may be excessive. Lower doses such as 15 Gy may be applied in these patients in palliative intent, counting on the fact that cytoreduction will nevertheless be extensive and local control will still be around 70 % after 12 months in these patients. It is worth mentioning that at least in the liver, repeated treatments in case of local tumor progression may be performed without a significant increase of toxicity. In an owned, yet unpublished series of 30 patients with liver tumors receiving between 2 and 4 treatment repetitions at the same or nearby locations, no adverse events were recorded.

Since we established CT-guided brachytherapy as an application specifically in liver and lung tumors, we have almost always applied brachytherapy as a single fraction. In some patients, leaving the catheters inside the tumor for 2 or even 3 days for repeated irradiation with lower single doses may be an interesting option which has not been systematically followed yet. We have applied this approach in abdominal locations in selected patients with excellent results (e.g., lymphoma or symptomatic peritoneal carcinomatosis from rectal cancer). In these patients, the adjacent gut prohibited dose delivery in a single fraction; thus, dose might be delivered in 3 fractions of 5–8 Gy each within 2 days.

Data on dose tolerance of risk organs may be derived from experiences after percutaneous irradiation or intraoperative brachytherapy. Since percutaneous irradiation usually is applied in multiple fractions, according doses for HDR single-fraction brachytherapy must be calculated by applying the α,β-model. Organs at risk for liver intervention include the bile duct, gallbladder, spinal cord, stomach, duodenum, or colon. From intraoperative brachytherapy it is known that the bile duct or gallbladder may be exposed to 20 Gy without acute or late toxicity, an experience we share with our own patients, where we applied a threshold of 20 Gy per max.1-ml tissue surface without evident acute or late failures such as bile duct strictures. Applying 15 Gy per max.1-ml gastric surface will induce a 5 % risk of symptomatic stomach ulceration (Streitparth et al. 2006). Stomach protection (e.g., proton pump inhibitors) should be prescribed in all patients where a significant organ exposure cannot be avoided (such as when treating metastases of the left liver lobe).

13.5.1.4 Results

CT-guided brachytherapy is generally very well tolerated, and analgo-sedation during the intervention is sufficient in almost all patients.

As for most ablation techniques, data available focuses on technical aspects and local tumor control in phase II studies, even though prospective randomized data is now available for brachytherapy of liver metastases from colorectal

carcinoma. Local tumor control after brachytherapy of liver metastases or HCC is similar to thermal techniques, with control rates between 70 and 90 % after 12 months. However, in contrary to thermal ablation, size does not necessarily hamper local control when brachytherapy is employed, and local control specifically for large HCC may be >90 %. This is even more remarkable since thermal ablation of HCC is often limited by high tumor perfusion leading to adverse cooling effects and early local recurrence. In addition, repeated treatments in case of local failure are usually well tolerated specifically in the liver. Even though no reliable data is available, repeated brachytherapy of the identical tumor location in the lung must probably be handled with more caution due to the risk of local bronchial necrosis.

A phase III trial was performed in patients with surgically unresectable liver malignancies of colorectal cancer. All patients displayed failure of second-line chemotherapy or absolute or relative contraindications to chemotherapy (comorbidity, age, general condition). CT-guided brachytherapy was applied repeatedly if technically applicable in case of any tumor progression. In this study, repeated tumor ablation proved to be the dominant prognostic factor, dominating also salvage chemotherapies when applicable (Ricke et al. 2010). No upper size limit for the metastases was applied. Mean local recurrence-free survival for all lesions was 34 months (median not reached), and local tumor control demonstrated a strong dose dependency.

In a prospective study of 83 patients presenting 140 lesions of HCC, a matched pair analysis was performed indicating a significant survival benefit of patients compared to best supportive care. Patients presented with a median diameter of 5.1 cm of the largest lesion and a comparatively high proportion of Child B stages of 20 %. Median survival achieved was 17 months after the intervention and 36 months after first diagnosis, and survival was strongly associated with the CLIP score (Mohnike et al. 2008).

13.5.1.5 Complications

Typical side effects comprise moderate gastric and intestinal toxicity, prevented effectively by peri-interventional antiemetic drugs. These general symptoms of radiation exposure are usually limited to the day of treatment. Subfebrile temperatures up to 1 week after the intervention are frequently observed, as are moderate leucocytosis and elevated C-reactive protein as well as moderately elevated liver enzymes.

Local bleeding is the most common complication. Diligent Gelfoam embolization during sheath removal is extremely helpful to lower the bleeding risk of patients, and close post-interventional monitoring specifically of patients with underlying cirrhosis is mandatory. However, the rate of major bleeding complications requiring blood transfusion or embolization still is <5 % even in the high-risk group. It has to be noted though that specifically in HCC patients, additional major complications such as symptomatic pleural effusion or other conditions prolonging the hospital stay make up for a 10 % rate of major complications. Complications are associated with the high degree of comorbidity in cirrhotic patients and include transient diminished liver function treated symptomatically post-intervention. Close collaboration with the hepatologists is extremely valuable in these patients. We have never observed acute encephalopathy due to liver function failure after treatment. Clinically relevant radiation-induced liver disease (RILD) has yet not been observed due to the limited irradiation volumes even in cases of advanced cirrhosis. Liver abscesses are another important, but rare, complications with less than 0.5 %, and bleeding complications are usually limited to cirrhotic patients specifically when portal vein thrombosis is present.

Summary

Inherent advantage of brachytherapy as compared to thermal ablation is the lack of a technical size limit of the target as well as the fact that it may be applied even adjacent to risk structures due to its precise dose planning and distribution.

Even though CT-guided brachytherapy is more complex than, for example, radiofrequency (RF) ablation, its value lies in the broad range of indications it provides. Even very large tumor conglomerates may be treated in multiple steps at a very low risk of adverse events and with only minimal discomfort for the patient. Compared to percutaneous irradiation, again the lack of a size limit is advantageous, as well as the fact that the method is motion independent, which gives it superiority specifically in moving targets such as liver or lung tumors (Pech et al. 2008; Ricke et al. 2004a, b, c, 2005a, b; Streitparth et al. 2006; Wieners et al. 2006).

Key Points

- Local tumor ablation by CT-guided brachytherapy is valuable and may well improve prognosis if patients are selected appropriately.
- Successful application of local ablation depends on careful planning of the individual oncological concept of each patient.
- Brachytherapy bares no technical size limit of the target, it delivers a reliable prediction of the dose distribution unaffected by patient motion, and it may be applied almost anywhere in the body.

13.6 Irreversible Electroporation

Philip Ditter and Holger Strunk

13.6.1 Introduction

Irreversible electroporation (IRE) is a procedure that enables a targeted tumor therapy by using electrical fields. These fields induce a change of a cell's membrane potential and consecutively lead to a destruction of the membranous lipid bilayer (Edd et al. 2006).

IRE represents a technology that completes the spectrum of radiologic-interventional techniques used for the treatment of oncologic diseases. Unlike in currently well-established thermal ablative treatments, factors like protein denaturation, tissue perfusion, or proximity to blood vessels are irrelevant in IRE as IRE does not rely on coagulation necrosis and provides a precise control of tumor destruction with a distinct separation between targeted and surrounding normal tissue (Lee et al. 2010b). Experimental studies indicate that IRE induces a natural cell death in soft tissue lesions without damaging critical structures such as blood vessels, bile ducts, nerves, or connective tissue around. Thus—in an ideal case—rapid and scarless tissue regeneration appears to become possible (Rubinsky et al. 2007).

13.6.2 Principle of IRE

IRE treatment consists of electric fields altering a cell's transmembrane potential difference. Very brief electric impulses cause the formation of nanoscale pores in a cell's membrane, affecting the lipid bilayer's integrity and thereby increasing its permeability (Weaver 1995; Tieleman et al. 2003; Edd et al. 2006). This process can be either reversible or irreversible depending on the intensity of the electric pulses (Davalos et al. 2005; Edd and Davalos 2007) (Fig. 13.61).

Reversible electroporation is increasingly used as a minimal-invasive therapeutic method for intracellular application of non-membrane-permeable substances (e.g., drugs, genes, macromolecules). For this purpose, the substance is typically injected intravenously, and electrodes are placed in the target area. Subsequently, electric pulses are delivered choosing field strength and pulse length within a range that a transient, reversible formation of pores in the cell's membrane occurs (Davalos et al. 2005; Mir et al. 2005; Rubinsky 2007; Mir 2008). In a therapeutic context this technique represents the basis of electrochemotherapy, where cytostatic drugs

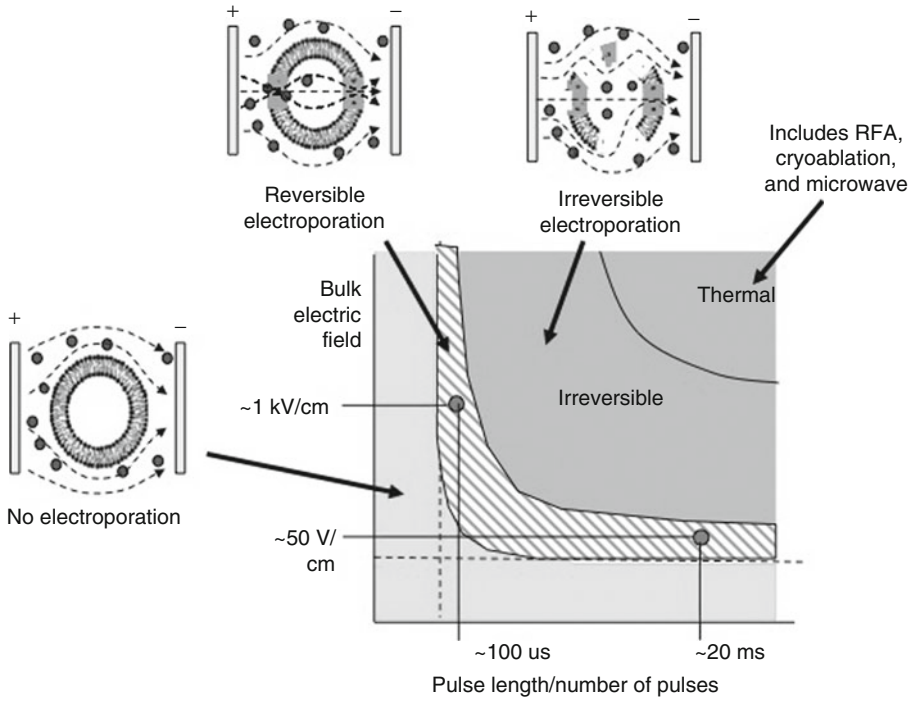

Fig. 13.61 Depending on the intensity and duration of the electric pulses, electroporation can either be reversible or irreversible

(e.g., bleomycin) are applied in cancer cells by means of reversible electroporation (Mir et al. 1991; Heller et al. 1999; Davalos et al. 2005; Linnert and Gehl 2009). Moreover, reversible electroporation is used for intracellular delivery of DNA in gene therapy (Jaroszeski et al. 1999; Miklavcic et al. 2000; Davalos et al. 2005).

By technically amplifying strength and/or length of the electric fields, impairment of a cell's membrane can become irreversible. Finally this will cause nonthermal apoptotic cell death (Davalos et al. 2005; Bertacchini et al. 2007; Lee et al. 2010a; Lencioni et al. 2010). As such IRE is applied in sterilization processes, for example, in order to sterilize bacteria- or amoeba-contaminated water (Rowan et al. 2000; Joshi and Schoenbach 2002; Vernhes et al. 2002; Davalos et al. 2005; Rubinsky 2007).

The irreversible effect of electroporation can also be used as a minimal-invasive tumor treatment without an additional application of drugs. However, increasing magnitude and duration of the electric pulses will heat tissue after a certain point. In this case the extent of tissue ablation due to irreversible electroporation alone compared to the extent of tissue ablation due to thermal effects cannot be estimated (Davalos et al. 2005). Therefore, Davalos and coworkers developed "a mathematical model for calculating the electrical potential and temperature field in tissue during electroporation" (Davalos et al. 2005). They came to the conclusion that the extent of nonthermal tissue ablation by IRE can theoretically be compared to the effect of other local ablative techniques (Davalos et al. 2005). This novel approach was practically taken up, and subsequent animal studies confirmed the feasibility of local tissue ablation by IRE without the influence of thermal effects (Al-Sakere et al. 2007; Onik et al. 2007; Deodhar et al. 2011a, b; Tracy et al. 2011).

Electroporation as such is not a recent discovery: for the first time, electroporation was reported

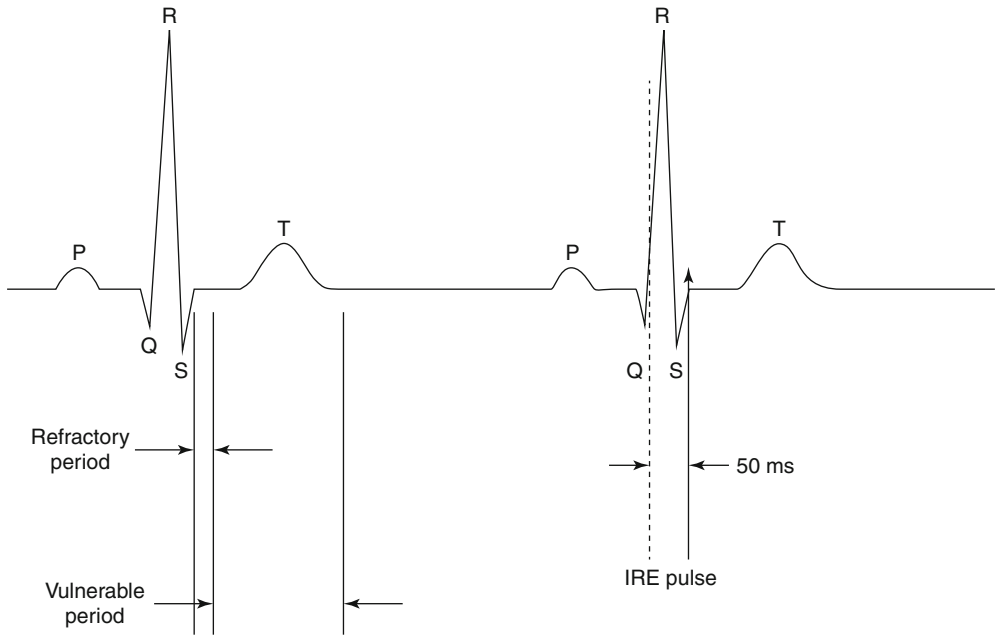

Fig. 13.62 ECG-synchronized IRE: In order to prevent the occurrence of arrhythmias, synchronization of the IRE pulses with the refractory period of the heart rhythm is essential. Therefore, the IRE generator waits 50 ms after the R-wave and then delivers a single IRE pulse

in experiments on electricity by Jean Antoine Nollet (1700–1770) and later by Fuller who investigated the bactericidal effect of high-voltage current (Rubinsky 2007).

Unlike all other thermal percutaneous methods (e.g., RFA, HIFU), IRE represents a different therapeutic approach that theoretically provides several advantages:

- IRE is a nonthermal ablation method. For this reasons, factors like protein denaturation, tissue perfusion, or proximity to major blood vessels are irrelevant (Lee et al. 2010a; Ahmed et al. 2011). This is supported by experimental studies where successful treatment of lesions neighbouring major blood vessels was feasible (Rubinsky et al. 2007; Lee et al. 2010a; Charpentier et al. 2011).
- IRE is not based on local drug application, and harmful side effects of chemotherapeutic substances do not occur (Davalos et al. 2005).
- IRE is minimally invasive, and the application of the electrical pulses is quick. After percutaneous placement of the electrodes, the actual treatment consists of extremely short electric impulses that last only for micro- or milliseconds (Edd and Davalos 2007; Esser et al. 2007; Lavee et al. 2007; Lee et al. 2010b). In comparison, energy application in thermal ablation techniques lasts from few minutes up to several hours (Lencioni et al. 2010).

However, the use of high-voltage current can lead to dangerous cardiac arrhythmias, especially during the "vulnerable" phase of the cardiac cycle (atrial and ventricular systole) (Lavee et al. 2007; Ball et al. 2010; Lee et al. 2010b). In order to prevent the occurrence of arrhythmias, synchronization of the IRE pulses with the refractory period of the cardiac rhythm is an essential prerequisite. For this reason, the IRE generator is connected with an ECG-triggering device, and each IRE pulse is delivered 50 ms after the R-wave during the so-called "absolute refractory period" (Fig. 13.62).

13.6.3 Indications and Contraindications

Thermal ablation is particularly limited in lesions bordering critical structures such as branches of the portal vein, bile ducts, or liver veins. There is a risk of damaging these critical structures as a precise distinction between target and nontarget tissue is not possible in thermal ablation. In addition there are cases in which a lesion's proximity to major blood vessels limits thermal ablation as the necessary rise of tissue temperature cannot be maintained due to a physical phenomenon known as "heat-sink effect." In these patients, IRE—which can be focused exactly and which is not based on thermal effects—is a promising alternative.

Although IRE is approved for medical use (FDA, CE certified), it remains an experimental local ablative tumor treatment because so far there are almost no human studies. However, there are many promising animal studies on several different tissues, for example, liver (Lee et al. 2007, 2010a; Choi et al. 2010; Guo et al. 2010), kidney (Deodhar et al. 2011a; Tracy et al. 2011), pancreas (Charpentier et al. 2010; Bower et al. 2011), lung (Deodhar et al. 2011b; Dupuy et al. 2011), prostate (Onik et al. 2007), breast (Neal et al. 2010), and brain (Garcia et al. 2009; Garcia et al. 2010; Ellis et al. 2011).

Hepatocellular carcinoma, colorectal liver metastases, renal masses, and bronchogenic tumors are the focus of IRE application (Lee et al. 2010b). Concerning human trials, only one "first-in-man phase I clinical study" on irreversible electroporation of renal cell carcinoma was published so far (Pech et al. 2011). It revealed that IRE represents a safe local ablative technique that might provide some benefits in treatment of renal cell carcinoma compared to more established thermal ablative methods (Pech et al. 2011). Another study in humans concentrated on the specific needs of anesthesia for IRE procedures (Ball et al. 2010).

Absolute contraindications include uncorrectable coagulopathy and presence of any type of pacemakers.

Relative contraindications are tumor size>2.5 cm, disseminated tumors with multifocal metastatic spread, and extensive ascites.

So far there is no sufficient data on how the distance of the electrodes to the heart promotes the occurrence of peri-procedural arrhythmias. However, Ball et al. observed that 25 % of the subjects developed transient ventricular tachycardia during an IRE procedure (Ball et al. 2010). The most severe peri-procedural arrhythmias occurred in patient with a large infradiaphragmatic liver lesion in close proximity to the inferior cardiac margin. This observation suggests that the incidence of arrhythmias caused by IRE is more likely in close proximity to the heart (Ball et al. 2010). Thus, the indication for the treatment of such lesions should be analyzed critically.

13.6.4 Material

Currently only one IRE system (NanoKnife; Angiodynamics, Queensbury, NY) is commercially available. It consists of two main components: (1) a generator and (2) "needlelike" electrodes. The IRE generator delivers high-voltage pulses (10–100 pulses) with an amplitude of 1,700–3,000 V, a pulse length of 20–100 μs, and a conduction current between 20 and 50 A. The IRE electrodes measure 19 G in diameter with an active tip length of up to 4 cm. For IRE treatment, two or more monopolar electrodes or one single bipolar electrode has to be placed in the target lesion (Edd and Davalos 2007). The number of necessary monopolar electrodes depends on the size and shape of a target lesion, whereupon not more than six electrodes can be plugged in the generator at the same time. The required energy depends on the distances between applied electrodes. In general, electrodes should be placed between 10 and 20 mm apart.

13.6.5 Technique

13.6.5.1 Preprocedural Evaluation

Informed patient consent with a detailed explanation of possible complications has to be obtained at least 24 h prior to the procedure. As IRE has to be performed under general anesthesia with muscle relaxation, a dedicated anesthesiological workup is needed. Taking a blood sample is

Fig. 13.63 Under general anesthesia the patient is placed on the CT table, and image-guided electrode placement is performed. CT images are necessary to estimate the exact needle position. Usually multiple electrodes are necessary

obligatory, especially in consideration of a possible coagulopathy. The following reference values are required: platelet level >50,000/mm^3, partial thromboplastin time >50 s, prothrombin time (quick) >50 % and INR <1.5. Platelet aggregation inhibitors (e.g., acetylic salicylic acid) should be discontinued 5–7 days before the procedure.

13.6.5.2 Procedure

General anesthesia and—due to the use of high-voltage electricity—additional muscle relaxation are mandatory in IRE procedures in order to avoid unwanted muscle contractions (Ball et al. 2010; Lencioni et al. 2010). Anesthetized patients are positioned on the CT-scanning table, and an initial CT scan is performed. After sterile coverage and distinctive skin disinfection isolated IRE needle, electrodes (15 or 25 cm long) are placed in the target area under cross-sectional image guidance (Fig. 13.63). Repetition of a CT scan after each electrode placement is recommended for position control. As mentioned above, depending on the lesion size, two or more monopolar electrodes or a single bipolar electrode (for more localized lesions) is needed (Lencioni 2010) (Figs. 13.63, 13.64, and 13.65).

Using six electrodes allows treatment of lesions up to a size of 3 cm. It is important to place monopolar electrodes no more than 20 mm apart to keep them parallel and to ensure equal penetration depth. Monopolar electrodes must be numbered, as each electrode must be plugged in an equivalent, numbered generator output. Furthermore, it is mandatory to measure all distances between the individual electrodes.

Practically the basic process of an IRE treatment is as follows:

- Activation of the unit
- Connection of the IRE unit and the patient with the ECG-triggering device
  - Entering patient parameters
  - Entering lesion parameters (size, location)
  - Placement of electrodes in target area under image guidance and control
  - Entering number of electrodes
  - Entering inter-electrode distances
  - Entering treatment parameters (voltage, pulse length, number of pulses)
  - Confirmation of all parameters
  - Activation of the system to start ablation
  - Perform ablation process
  - Remove electrodes or reposition of electrodes to start second ablation process

The generator's software leads through the whole treatment planning process and determines which parameters have to be entered. Treatment parameters (voltage, pulse length, number of pulses) are suggested by the generator's software following preset protocols provided by the manufacturer.

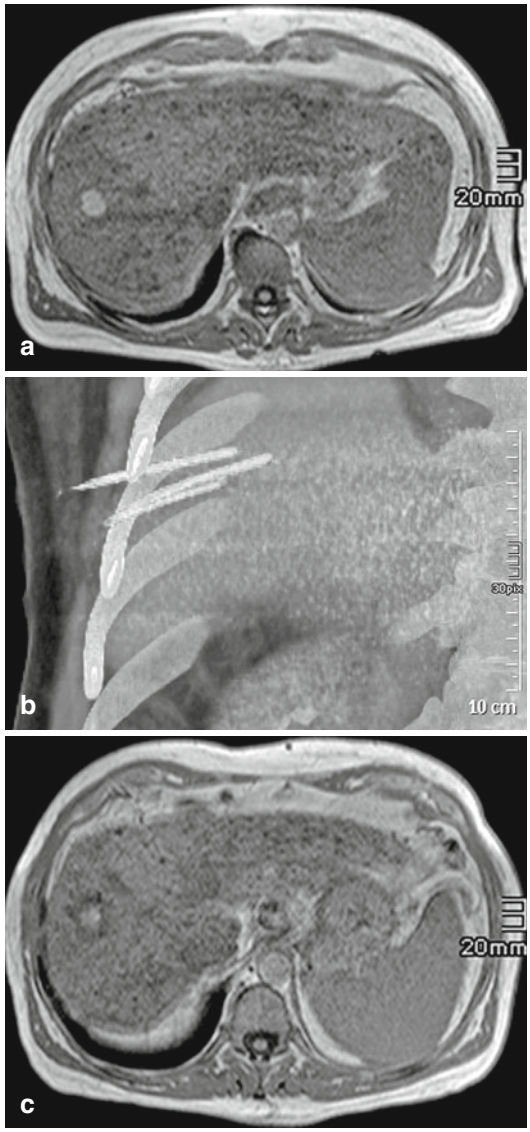

Fig. 13.64 IRE in a patient with liver cirrhosis and hepatocellular carcinoma (HCC): the initial MR imaging shows a hyperintense lesion in the in-phase FFE image (**a**). Volume-rendered image computed from CT data obtained during the procedure shows three electrodes in the tumor (**b**). The post-interventional MR imaging 3 weeks after IRE shows the IRE area as a hyperintense lesion in the in-phase FFE image (**c**). It already decreases in size. The lesion is surrounded by a hypointense rim of reactive changes

Using the maximum number of six electrodes, tumor size should not exceed 2.5 cm in order to sustain a sufficient "safety margin" of 0.9 cm (due to the recommendations of the IRE generator). However, repositioning of the electrodes, increasing the number of treatment cycles, increasing the number and length of the pulses, as well as increasing field strength may enable the treatment of lesions up to 6 cm. Nevertheless this is an even more experimental approach, and the ideal lesion size still should not exceed 2.5 cm.

Due to the anesthesiology procedure and the necessary exact placement of several electrodes, the average duration of the whole procedure is approximately 2–3 h, whereupon the actual IRE treatment takes only 10–20 min (Lencioni 2010). The main difficulty in the clinical application of IRE is the parallel placement of multiple electrodes in a defined distance to each other. For this reason, the correct electrode placement may take relatively long. Unlike thermal ablative techniques, the puncture tract is not adhered in IRE procedures.

13.6.5.3 Post-interventional Follow-Up

In our institution a first follow-up CT scan is performed instantaneously after the procedure. Immediate post-interventional monitoring has to be provided by the department of anesthesiology according to current guidelines concerning general anesthesia. Once the patient is transferred on a regular ward, vital signs should be checked every 30 min for 6 h. On the next day a blood sample has to be taken: platelet level, partial thromboplastin time, prothrombin time (quick), INR, erythrocytes, hemoglobin, hematocrit, leucocytes, electrolytes, creatinine, and liver enzymes.

An additional ultrasound examination of the abdomen with a special focus on the IRE site is recommended to exclude free fluid and other major complications. Depending on their clinical and subjective condition, patients can be discharged 24 h after IRE intervention at the earliest. Patients are instructed to call their physician in the event of any aggravation. Currently there is no general consensus on post-interventional imaging. First outpatient follow-up including CT or MR imaging should be provided 4 weeks after IRE treatment. Thereafter, imaging intervals should follow the recommendations regarding the underlying disease.

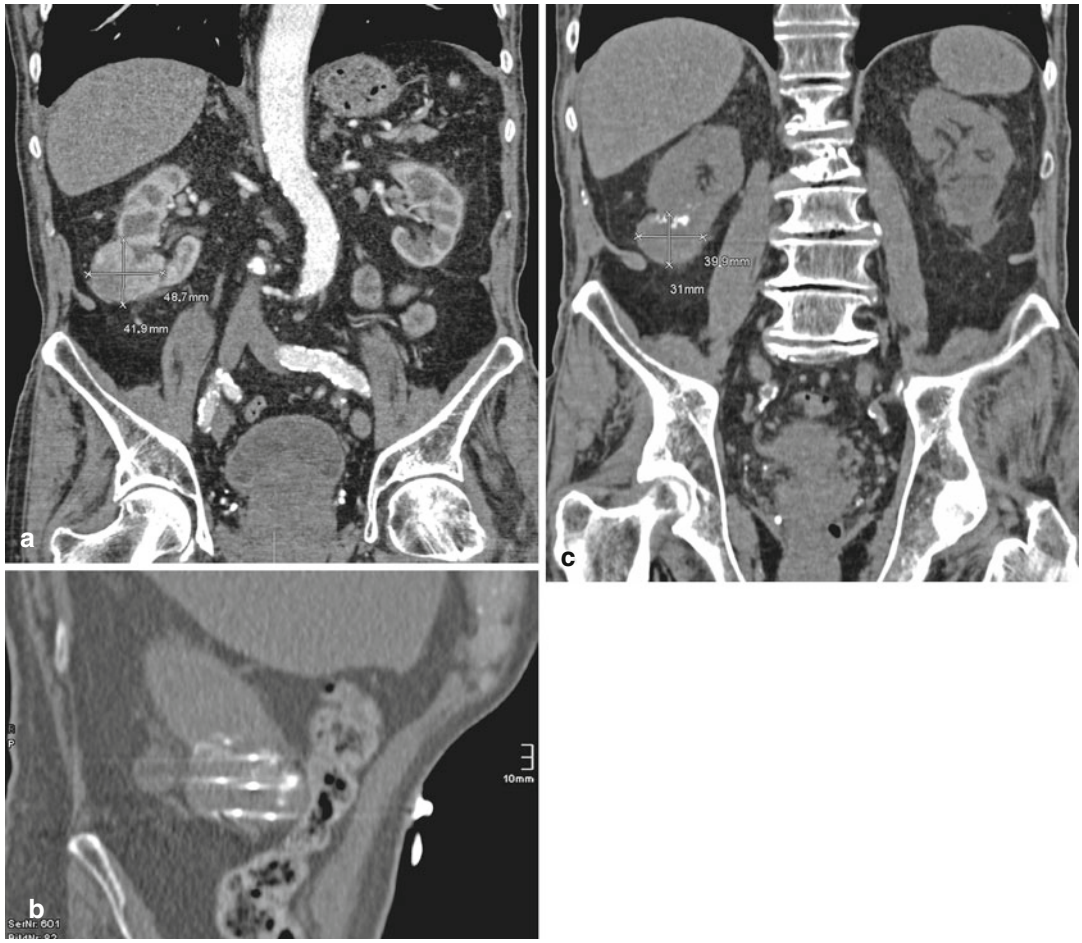

Fig. 13.65 IRE in a patient with right-sided renal cell carcinoma: the initial CT scan shows the almost 5-cm-measuring renal cell carcinoma in the lower third of the right kidney (**a**). An oblique reconstruction from a CT scan during the procedure shows the tips of six electrodes (*arrowheads*) in the tumor (*arrows*; **b**). A CT scan 2 months after the procedure shows a marked reduction of the tumor size (**c**)

13.6.6 Results

Up to now there is mainly experimental evidence for the efficacy of IRE as a local ablative treatment technique. Some of the several animal experiments are briefly summarized below.

Studies on rats in which liver tumors were experimentally generated revealed that IRE treatment each with eight 100 μs-/2,500 V-pulses leads to a considerable reduction of tumor size within 15 days (Guo et al. 2010). First there was heterogeneous necrosis after 1–3 days, followed by extensive tumor necrosis after 7–15 days, and finally entire ablation prevailed in nine of ten rats.

Blood vessels, nerves, bile ducts, connecting tissue, or renal pelvis are not affected. Several studies showed that IRE selectively destroys tumor cells whereas normal structures such as mentioned above are preserved (Al-Sakere et al. 2007; Maor et al. 2007; Onik et al. 2007; Rubinsky et al. 2007; Garcia et al. 2009). In ideal cases even scarless tissue regeneration has been reported (Phillips et al. 2010). Tumor ablation using IRE had no effect on renal pelvis (Tracy et al. 2011) or vessels and nerves around the IRE site (Rubinsky 2007). These findings differ from thermal ablation. Especially in central lesions like HCC or renal cell carcinoma, RFA bears a

relevant risk of necrosis in the surrounding area, for example, necrosis of blood vessels, renal pelvis, or renal calices. Onik et al. examined prostate glands in six dogs with percutaneously or rectally applied IRE electrodes (Onik et al. 2007). Structures like urethra, nerves, blood vessels, or rectum were not affected and stayed intact after IRE treatment. In other studies using IRE in animal experiments, bronchovascular architecture in pig lungs (Deodhar et al. 2011b), blood vessels and bile ducts in pig livers (Charpentier et al. 2011), as well as connecting tissue, blood vessels, and renal pelvis in pig kidneys (Deodhar et al. 2011a; Tracy et al. 2011) did not suffer any damage.

IRE is highly focused and enables a clear distinction between treated and not-treated tissue. Hence, tumor ablation can be precisely controlled (Lavee et al. 2007; Lee et al. 2007, 2010a; Guo et al. 2010). This was shown in experiments with pig livers which underwent IRE treatment (Lee et al. 2007). Different studies report epicardial atrial ablation in pigs (Lavee et al. 2007), percutaneous and transrectal treatment of prostate glands in dogs (Onik et al. 2007), and even first attempts in pancreatic applications (Charpentier et al. 2010). After pancreatic IRE in pigs, there was a rise of amylase and lipase for 3 days. However, no systemic side effects were observed. Histological examination revealed both tissue necrosis and integrity of vascular structures (Bower et al. 2011).

Concerning clinical trials, there is only one first phase study in which six patients suffering from renal cell carcinoma underwent IRE treatment (Pech et al. 2011). The focus was IRE's effects on ECG and laboratory parameters during 12-week post-intervention. Only one patient showed a single supraventricular extrasystole during the IRE procedure. After IRE, surgical tumor resection was performed. Subsequent histopathology showed cellular swelling. However, cell death had not (not yet) commenced (Pech et al. 2011).

In further studies on feasibility of IRE (8 kidney-, 17 liver-, 3 lung-procedures), self-limiting ventricular tachycardia and ventricular arrhythmias were observed in 25 % of the procedures (Ball et al. 2010). Hence, it was recommended to perform IRE under continuous ECG control.

13.6.7 Complications

In general IRE complications can be compared with those of other local ablative techniques such as RFA. However, as IRE is a very young method, there is little data on complications available up to now. Infection and bleeding are potential complications in all interventional procedures. Compared to thermal ablation techniques, however, some authors discuss that IRE might bear a higher risk of bleeding around the needle insertion site (Ahmed et al. 2011). Insertion of the IRE electrodes can also lead to pneumothorax, not only in lung treatment but also in treatment of abdominal lesions close to the diaphragm (Ball et al. 2010). Transient rise of blood pressure is observed in many patients during IRE treatment and can be easily controlled by anesthesiologists. Occurrence of extreme hypertension (>200/100 mmHg) during treatment of renal masses (especially upper pole tumors) can be an indicator of needle malposition in the adrenal gland (Ball et al. 2010).

Due to the use of electricity, cardiac arrhythmias (e.g., ventricular bigeminy or transient ventricular tachycardia) also belong to the spectrum of possible complications. Especially in lesions close to the heart (e.g., subdiaphragmatic liver lesions), occurrence of transient arrhythmias seems to be more likely (Ball et al. 2010). Pacemaker patients should be excluded from IRE treatment.

IRE furthermore induces muscle stimulation with possible contractions of the entire upper body (Ball et al. 2010). For this reason a sufficient peri-procedural muscle relaxation is obligatory. Slight disturbances in acid–base and electrolyte metabolism may be observed after IRE and should be checked in the post-procedural blood sample.

Summary

IRE is an emerging technique in the spectrum of local ablative tumor treatments. It is a non-thermal method using electric pulses to impair a cell's transmembrane potential and thereby leads to cell death by causing pores within the lipid bilayer. Compared to currently well-established thermal ablative treatments (e.g., RFA), IRE provides a set of advantages: IRE is

highly focused and enables a clear distinction between target and nontarget tissues. Proximity to critical structures such as major blood vessels, bile ducts, nerves, or renal pelvis is irrelevant as the "heat-sink effect" and thermal injury are no limiting factors in this nonthermal technique. Hence, IRE can be a promising alternative in lesions in which thermal ablative interventions are of limited efficacy or even considered impossible.

Key Points

- Promising nonthermal local ablation technique with only very limited clinical evidence so far.
- Procedures have to be performed under general anesthesia.
- Feasible in solid tumors up to 2.5 cm.

13.7 High Intensity Focussed Ultrasound

13.7.1 Technical Basics of MR-Guided Focused Ultrasound Surgery

Alexander Beck and Susanne Hengst

13.7.1.1 Introduction

The abbreviation HIFUS stands for "High-intensity focused ultrasound" and is a totally noninvasive thermoablation method. Usually it is combined with imaging equipment to control the ultrasound beam. The method of choice for imaging is magnetic resonance (MR) imaging because on one hand it can give good imaging for targeting as well as real-time thermometry to control thermoablation during ultrasound (US) application (McDannold et al. 2006). HIFUS combined with real-time imaging and thermometry by MR imaging has become the method of choice, and the technical aspects of this technique will be described in the following article. Combination of HIFUS with real-time MR imaging is usually abbreviated MRgFUS, which stands for magnetic resonance-guided focused ultrasound surgery and gives a pretty good short description of this technique.

Probably the first descriptions of US waves for thermal ablation of tissues date back to the first half of the last century and are made by Wood RW and Loomis AL in 1927 and Lynn et al. in 1942. Due to lack of adequate imaging equipment, the technique was not widely used and started to become of more clinical relevance with introduction of MR imaging into regular practice. Several authors describe the application of MRgFUS in humans—clinical indications now include several organ systems like the brain (Jääskeläinen 2003; Fry and Fry 1960); breast (Gombos et al. 2006); uterus, especially leiomyomas (Hengst et al. 2004); bone (Catane et al. 2007); liver (Hengst et al. 2004; Kopelman et al. 2006); or prostate (Murat et al. 2007).

Limitations for MRgFUS are organ systems that cannot be reached by US waves, especially systems that are anatomically behind structures of high acoustic impedance (for example lung) or patients that are not suitable for MR imaging (e.g., metal implants or cardiac pacemakers). In some cases like brain interventions, additional invasive measures may be necessary such as skull trepanation to enable access (Jääskeläinen 2003; Fry and Fry 1960).

13.7.1.2 Material

In order to perform MRgFUS treatment, a US application unit and an MR system are needed. In our practice we use a treatment unit (Exablate 2000, Insightec, Haifa, Israel) that is integrated in a regular MR scanner table for patient positioning (Signa, General Electric Medical Systems, Milwaukee, WI). Several other vendors provide very similar systems. Each different system is usually integrated into a dedicated MR system and can only be used with that specific hard- and software.

The treatment unit is integrated into the regular patient MR table. In a central position of this table, the US applicator is placed with a sliding positioning system. The whole system is enclosed in an $83 \times 34 \times 11$-cm basin filled with degassed water and covered by a membrane made of polyvinyl chloride. In order to

enable acoustic coupling with the patient on top of the membrane, a gel pad and additional degassed water are applied for each treatment—it is essential to perform this preparation carefully to avoid enclosing air bubbles as this might locally increase acoustic impedance and can be a reason for treatment failure or complications like serious skin burns (Hengst et al. 2004).

The ultrasound applicator can be moved in a longitudinal and horizontal axis. It can also be tilted up to 20° in two directions. In combination with a phased array transducer, the focus depth of each US application, in the following referred to as a "sonication," can be chosen in the range from 5 to 22 cm. The focus spot size can be switched from small sizes beginning at 2×2×4 mm up to 10×10×30 mm or 6×6×45 mm if larger volumes shall be treated. The maximum energy of the transducer is 1,300 W, applied at frequencies of 1–1.5 MHz. This setting in our experience is sufficient to reach temperatures >60 °C needed for treatment within even large sonication spots over an application time of 16–30 s for each spot (Gombos et al. 2006; Hengst et al. 2004; Hindley et al. 2004).

Sufficient temperatures are reached if the proteins within the volume of the sonication spot are denaturized—as a usual parameter, an equivalent time of 240 min exposure at 43 °C is quoted to be sufficient for denaturation (Meshorer et al. 1983; Damianou and Hynynen 1994). The equivalent time $t43$ is estimated by the formula of Sapareto and Dewey (1984). $t43$ is calculated by

$$t43 = \sum_{t=0}^{t=\text{final}} R^{(43-T)} \Delta t.$$

$t43$ equals the thermal equivalent dose at 43 °C, T is the mean temperature during time Δt, and R is a constant that equals 0.50 above 43 °C and 0.25 below 43 °C. The temperature profiles gathered from MR thermometry for each voxel are interpolated linearly with a time-step of $\Delta t = 0{,}1$ second (Sapareto and Dewey 1984; Nathan et al. 2000). Other authors postulate that even shorter $t43$ times are sufficient to completely denaturize proteins if a minimum temperature is reached. Nathan et al. (2000) showed that in a rabbit model, a $t43$ of 31.2 equivalent minutes and a minimum temperature of 50.4 °C induce enough thermal stress for protein destruction. In common MRgFUS systems the values of $t43$ are automatically calculated, color coded, and displayed for each sonication. This information is mandatory to evaluate the efficacy and progress of each treatment. Real-time imaging of temperature changes within the target volume is necessary to monitor treatment progress and to avoid thermal damage of nontarget tissues. On their way to their target, ultrasound waves have to pass through different tissue types. Specific absorption, dispersion, and reflection based on different acoustic impedance of tissue reflect differences in speed of sound in different tissue types (i.e., muscle 1,590 m/s, water 1,526 m/s, or fat 1,468 m/s). These differences may account for changes of spot position and varying focus characteristics (Hengst et al. 2004; Damianou and Hynynen 1994; Mahoney et al. 2001). Target volume temperature is also influenced by the absorption rate within the target volume and by external cooling effects such as tissue perfusion. These conditions may differ at each single sonication.

Real-time MR thermometry (Fig. 13.66) may be performed accurately by employing changes of the proton resonance frequency (PRF) (Mulkern et al. 1998). The shift in proton resonance frequency is nearly linear within the temperature range (40–90 °C) needed for MRgFUS treatments (Wlodarczyk et al. 1999). PRF changes are calculated as changes in phase divided by 2 times π multiplied by echo time. Subtraction images based on acquisitions before and during sonications allow a relatively reliable measurement of temperature changes in and around the target (Hengst et al. 2004; Damianou and Hynynen 1994; Nathan et al. 2000). Post-interventional imaging is commonly based on MR imaging, providing detailed information on treatment success (Fig. 13.67).

13.7.1.3 Complications

Complications are rare and in most cases easy to manage (Hengst et al. 2004). General complications refer to the inevitable use of MR imaging including the application of MR contrast agents. Specific risks of MRgFUS include:

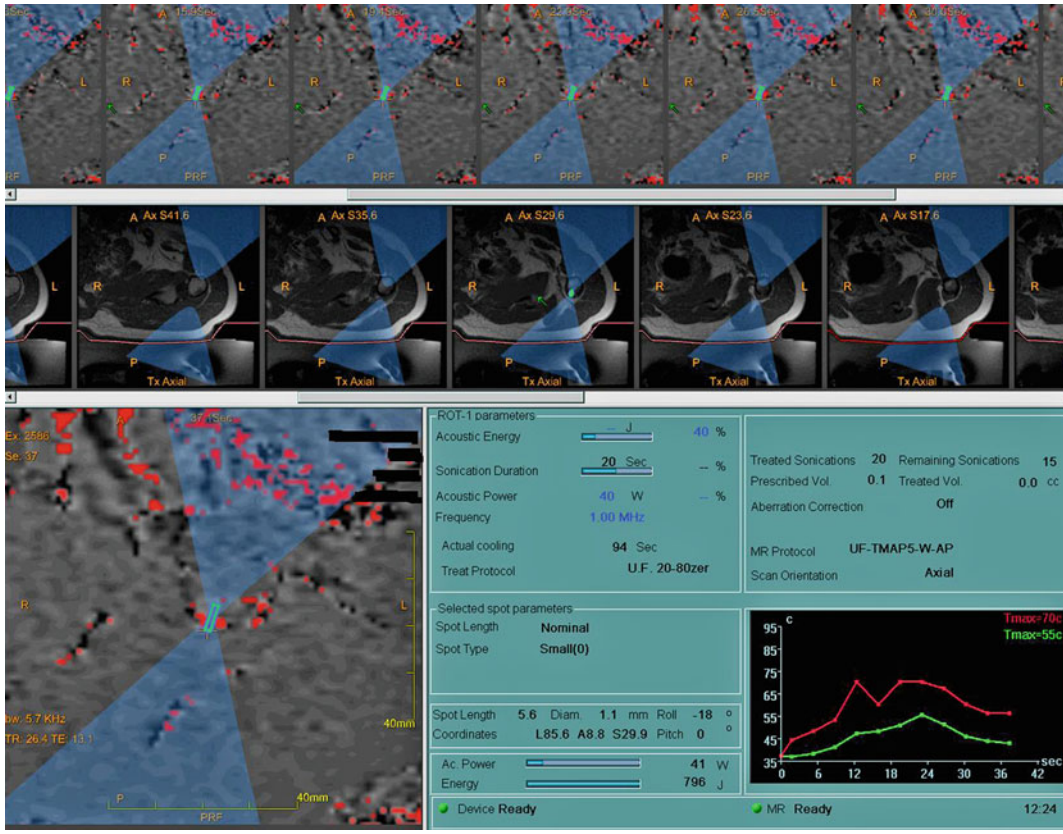

Fig. 13.66 User interface of the MRgFUS system during treatment. The location of one sonication spot is displayed as well as the MR thermometry over time. In this example, the according temperature has been reached depositing 41 W over 20 s duration of the sonication

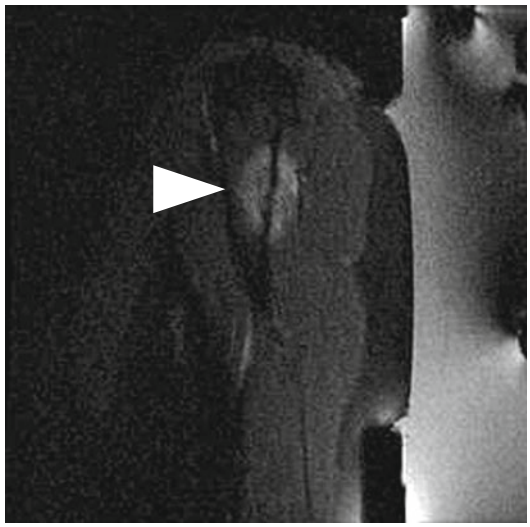

Fig. 13.67 Posttreatment T2-weighted image, bone metastasis of the humerus. Note the edema of the lesion in the upper humerus as well as the adjacent tissue (*arrowhead*)

1. Heat development outside the according target occurs in the path of the beam due to acoustic impedance changes: predominant organ at risk is the skin in case of scars, hair, gels, or air bubbles at the entry point of the beam. If the patient is awake, skin heating will lead to pain, and the energy deposition can be adjusted. However, skin burns are very limited in size as a function of the small sonication spots.
2. In abdominal MRgFUS, a rare complication is thermal injury to the bowel. To avoid such an event, sonication must not be performed through the bowel.
3. The "back beam" may reach other structures, which are apparently not in the path of the beam. This may include nerve roots along the sacral bone. However, energy deposited through the back beam most likely is not high enough to provoke serious injuries.

Summary

MRgFUS is a noninvasive and safe intervention. It offers a unique and noninvasive method for tissue ablation. In combination with MR imaging, it is also free from radiation. Unfortunately, access to target volume is a limiting factor.

Key Points

- Accessibility of target-tissue volume is the key to successful MRgFUS treatment (Fig. 13.68).
- Most careful treatment planning will ensure a safe and efficient intervention.
- Temperature mapping allows detailed treatment monitoring.
- If any doubt persists with respect to safety of the beam path, other methods should be considered.

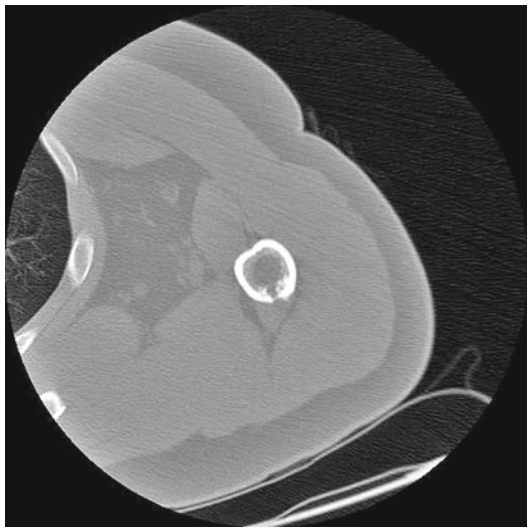

Fig. 13.68 Pre-interventional CT of a bone metastasis of the humerus from a cholangiocellular carcinoma (same patient as in Fig. 13.67). Free access from the posterior aspect without nerves or vessels within the expected ultrasound beam path

13.7.2 Clinical Application of MR-Guided Focused Ultrasound Surgery

Susanne Hengst and Alexander Beck

13.7.2.1 Introduction

Nowadays most invasive modalities are evaluated not only by their ability to cure but also by their side-effect profile including the cosmetic, physical, and psychological outcome. High-intensity focused ultrasound (HIFUS) is an important step on the way to noninvasive surgery. In fact ultrasound (US) was first researched due to its therapeutic possibilities before starting its victorious way into diagnostics. Today, specifically the combination of magnetic resonance (MR) guidance and MR thermometry with focused ultrasound therapy offers most promising perspective for noninvasive surgery.

13.7.2.2 Indications

Perhaps the most common application of MR-guided focused ultrasound surgery (MRgFUS) today is thermoablation of uterine fibroids. More than 5,000 patients have been treated to date with this method worldwide. Uterine fibroids are the most common benign tumors of the inner female genitals. Up to 25 % of all woman suffer from fibroid-related symptoms such as hypermenorrhea, dysmenorrhea, and bulk-related symptoms (Stewart 2001). A patient asking for an organ-preserving therapy is a suitable candidate for MRgFUS if the following criteria are met:

- The patient suffers from fibroid-related symptoms.
- Five or less fibroids with each single fibroid smaller than 8 cm are to be treated. In fibroids larger than 8 cm (approximately up to 12 cm), a pretreatment with GnRH-Analoga is suggested.
- The patient should have no scars, tattoos, or skin abnormalities of the abdominal wall within the treatment area.
- The woman must be able to tolerate the procedure in prone position for up to 3 h.
- All fibroids have to be accessible with no risk structures in the expected beam path. This

excludes fibroids with intestine loops wedged between the tumor and the abdominal wall and targets closer than 4 cm to the sacral bone.

Pedunculated fibroids should not be treated with MRgFUS. Although no standard recommendations concerning fibroid location and fibroid morphology exist, some authors recommend the treatment of low and medium signal intensity fibroids only, as may be determined on T2-weighted images (Funaki et al. 2007a, b).

Patients diagnosed with uterine fibroids who desire future pregnancy present a therapeutic dilemma. Considering the prevalence of uterine fibroids, many women conceive and experience an uneventful pregnancy despite having uterine fibroids. On the other hand uterine fibroids are associated with secondary infertility and several complications during the course of pregnancy, with lower birth weight, premature birth, placenta abnormalities, or severe pain related to fibroid infarction. However, the currently available surgical standard treatment options increase the complication rate during consecutive pregnancies due to traumatization of the uterus. Embolization suffers from the need for radiation exposure. Thus, MRgFUS might be a good alternative for these patients.

The bones absorb US particularly well. Primary indication for bone lesion treatment is pain management. In contrast to the point shape focus used for soft tissues, a wide-beam approach is the method of choice for the treatment of bone lesions. In combination with low-energy sonications, this method allows a fast yet effective heating of the bone and metastases, with a proposed denervation leading to symptom relief. Preliminary results of a multicenter trial with 13 patients suffering from painful bone metastases show a significant reduction in pain intensity and a reduction of pain medication in the weeks following treatment. However, extensive research still has to be performed to evaluate the long-term effectiveness and side-effect profile for this intervention (Catane et al. 2007).

In 1993 Madersbach et al. (1993) first published phase II results of the treatment of benign prostate hyperplasia with high-intensity focused ultrasound based also on US for treatment guidance. Since then the use of HIFUS became more widespread in urology including clinical trials for such a treatment option in prostate cancer. Most commonly endorectal probes are used. However, the clinical use of this technique is limited due to difficulties in real-time thermometry and in the definition of the target by ultrasound. MR-based systems with endorectal applicators are yet not available. Significant improvements of treatment outcomes can be expected.

First studies demonstrating the safety and effectiveness of MRgFUS for benign and malignant tumors of the breast were published 2001 and 2003 (Hynynen et al. 2001, Gianfelice et al. 2003a, b, c). Whereas treatment with MRgFUS is planned with plain T2-weighted or T1-weighted images, patients with breast carcinoma benefit greatly from contrast-enhanced imaging for treatment planning. Furusawa et al. (2007) treated 21 patients for primary breast cancer. Follow-up was performed by MR imaging. After a median follow-up period of 14 months (ranging from 6 to 26 months), one case of local recurrence was observed.

Focused ultrasound has proven to be effective for the treatment of hepatic lesions in early studies (Wu et al. 2004; Visioli et al. 1999; Rowland et al. 1997). For this research mostly US guidance or no optical guidance has been employed. Even worse, the interventionalist had no feedback regarding the target temperature. The combination of MR guidance and HIFUS most likely increases efficacy by providing excellent visibility of the target and real-time feedback by thermomapping. First animal studies have been published already. Fifteen pig livers were treated with MRgFUS. Complete destruction of the lesions was demonstrated by histopathology (Kopelman and Papa 2007; Kopelman et al. 2006). Jolesz published favorable results for the treatment of hepatocellular carcinoma in two patients (Jolesz et al. 2004). Several obstacles have to be overcome, though before MRgFUS may be established as a reasonable alternative for the treatment of liver lesions. With applicators available to date, the majority of the liver volume cannot be reached because of the limited acoustic windows between the ribs. To minimize

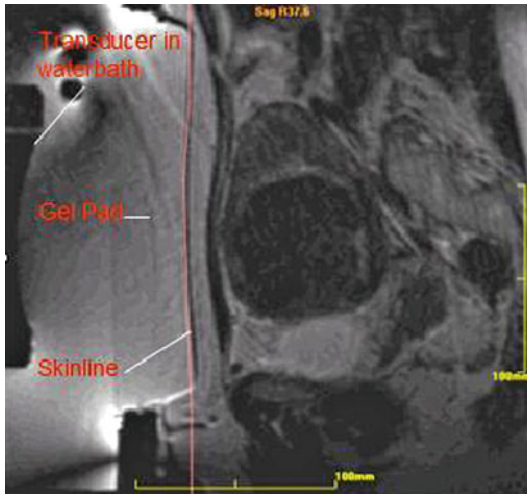

Fig. 13.69 Positioning for MRgFUS of uterine fibroids

movement of the target during ablation, this procedure has still to be performed in intermittent apnea under general anesthesia. Extensive research is to be done to overcome these problems.

13.7.2.3 Technique

Patient Preparation (Uterine Fibroids)

MRgFUS for uterine fibroids is commonly performed on an outpatient basis. To ensure a constant position of the uterus, a Foley catheter is inserted. The patient is positioned prone with her pelvis above a gel pad. Aim of a careful positioning maneuver is an air-free coupling between the transducer and the target volume (Fig. 13.69). For this purpose the transducer unit may be placed within a water bath of degassed water. The skin has to be shaved, and no additional gels should be applied to the skin. It is also essential to exclude scars as they have higher acoustic impedance. Patient motion has to be reduced to a minimum to ease targeting and real-time thermometry during the intervention. A stable i.v. access and continuous monitoring of vital signs are mandatory. MRgFUS is commonly performed under minimal analgo-sedation. The use 1–5 mg of midazolam i.v., and up to 15 mg of piritramide i.v. is usually sufficient for this purpose. The use of general anesthesia is normally not needed. Moreover, it contradicts the noninvasiveness of the method, complicates patient positioning, is expensive, and—most important—may mask symptoms of complications such as emerging pain from skin burns.

Procedure (Uterine Fibroids)

For treatment planning purposes, T2-weighted images are obtained in three different planes. In a 3D planning module, the target area and treatment protocol (diameter and length of spots, grid density, acoustic energy, wave frequency, sonication, and cooling duration) are defined. Landmarks and heat-sensitive structures at risk such as the bowel or the pubic bone are marked on the treatment planning images. The system calculates the sonications needed to treat the target volume identified in the planning MR images. Sonications that are close to or pass through sensitive structures are marked and can be edited by changing the angulation of the transducer in two planes to modify the direction of the beam path. As soon as geometrical planning is complete, a first low-dose test sonication is performed. After verification of the target spots with initial low-energy sonications, the fibroid is ablated in up to 100 single sonications. The MRgFUS system enslaves the MRI during this period, and real-time thermometry is obtained. The operator can manually adjust the power level for each sonication to optimize the target temperature and minimize the patient pain and discomfort level. Depending on the volume of the treated area, treatment time can be very variable—sonication time is about 20–30 s per spot; between each spot an individually calculated "cooling time" of up to 90 s is needed to prevent peripheral tissue damage from heat still within the beam path. Different techniques like an interleaved sonication with reduce cooling time or a wide-beam approach for bone treatment can shorten intervention time significantly. During this whole process the patient is able to stop a sonication at each time point with a "panic button." To ensure treatment success, the interventionalist should always aim for the highest volume that may be ablated safely. The treatment ends with T2-weighted and contrast-enhanced T1-weighted sequences to document treatment outcome (Fig. 13.70).

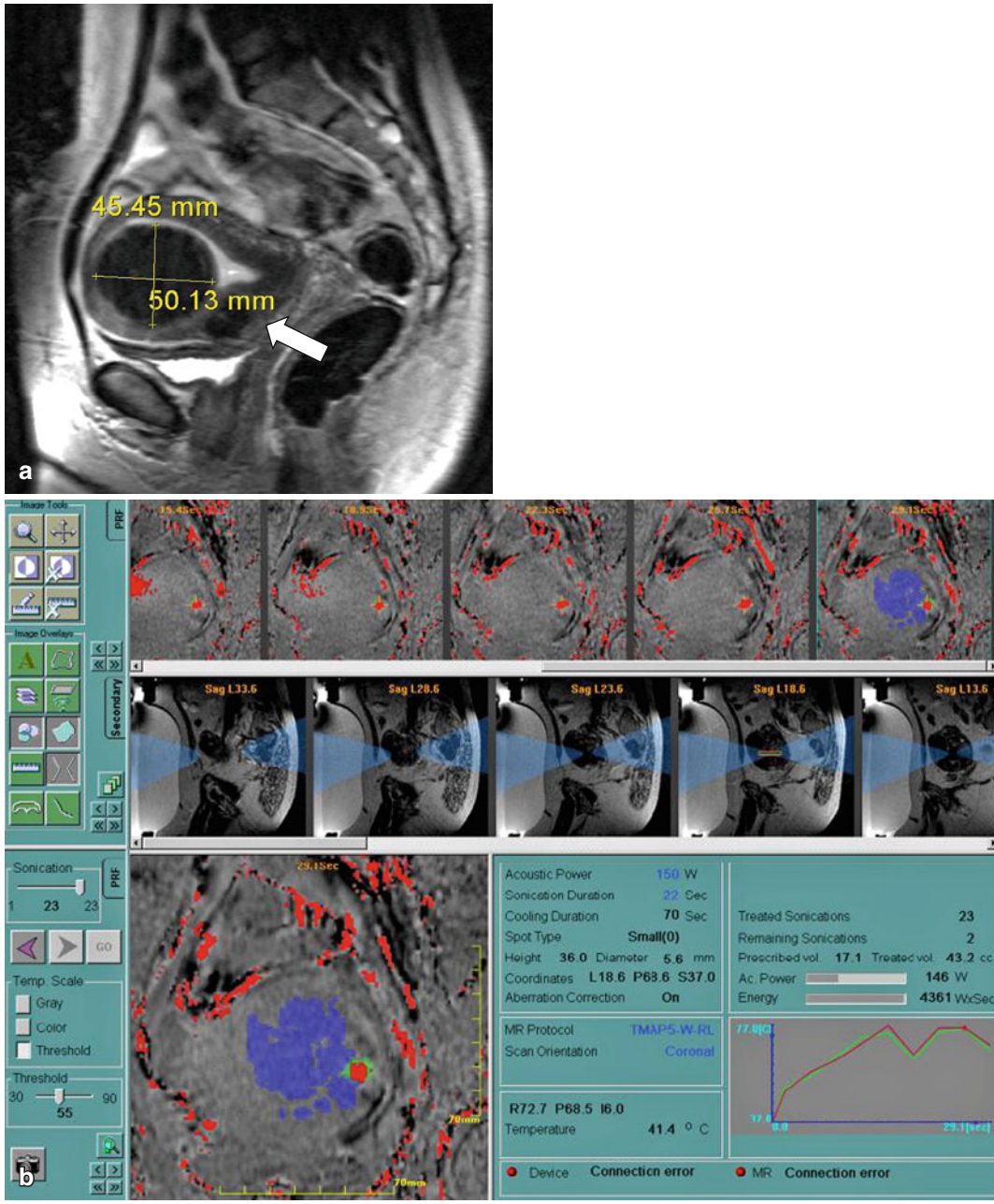

Fig. 13.70 (**a**) Pretreatment T2-weighted sagittal image shows a large submucous fibroid of the uterus. In addition, a small intramural fibroid can be seen (*white arrow*). (**b**) Thermomapping during MRgFUS. *Blue areas* indicate the volume that has already been treated. The *yellow and green dots* show the ongoing sonication. The curve on the *right side* indicates the temperature in the target area. (**c**) Immediately posttreatment, contrast-enhanced T1-weighted images are obtained to demonstrate the extent of the non-perfused volume in the fibroid. (**d**) T2-weigted image 6-month post-MRgFUS reveals a relevant decrease of lesion volume

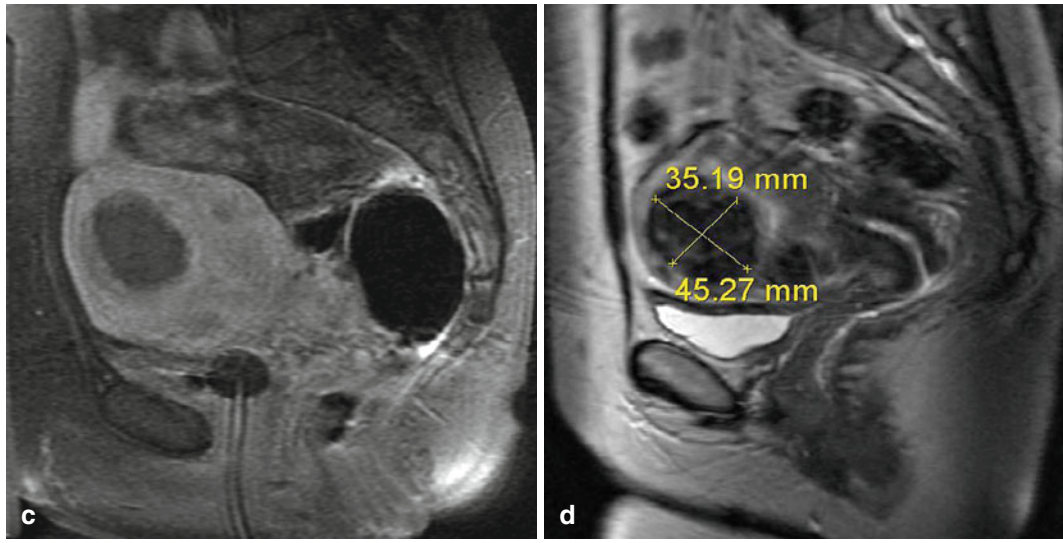

Fig. 13.70 (continued)

13.7.2.4 Results

MRgFUS has proven to be a safe and effective method for symptomatic uterine fibroids. A recent study by Rabinovici et al. (2007) shows a significant or partial symptom relief in 69 % of the treated patients after 12 months. Stewart et al. (2006) determine the amount of symptom relief on the uterine–fibroid symptom severity score (UF-SSS) by 39 %. In this study with 109 patients, 71 % reached the target symptom relief of ten points on the UF-SSS. Recent studies show favorable outcomes regarding the volume loss of the fibroids and better symptom relief for patients with larger ablated volumes. A minimum of 20 % non-perfused volume is the proposed threshold for symptomatic improvement (Stewart et al. 2007).

In patients with childbearing potential, there are currently extensive research activities investigating the possibility and safety of pregnancies following MRgFUS treatment. Latest reports indicate that safe pregnancies and vaginal deliveries are possible after treatment of uterine fibroids or adenomyosis with MRgFUS (Rabinovici et al. 2006; Hanstede et al. 2007).

13.7.2.5 Complications

All current studies show that MRgFUS may be applied safely for treatment of uterine fibroids (Stewart et al. 2003; Fennessy and Tempany 2005; Funaki et al. 2007a, b). Known adverse events result mostly from adverse heat refocusing outside the actual target area. Seldom the patients experience grade 1 or grade 2 skin burns. Grade 3 skin burns are very rarely encountered. These serious burns usually result from preexisting skin abnormalities such as scars. Cases of damage to the intestine have been reported as a rare complication. Additionally, heat absorption in the sacral bone may provoke temporary symptoms of lumbosacral nerve irritation as radiating pain or dysesthesia. No case of permanent nerve damage has been reported to date. However, minor discomfort and pain or increased menstrual bleeding in the first weeks following treatment are reported quite frequently.

Summary

MRgFUS is a new noninvasive thermoablative procedure. In several centers it has already become a routine procedure for uterine fibroids. The indication, however, has weighted against routine techniques like surgery and embolization. Moreover, long-term results still need to be assessed. Indications for MRgFUS are likely to expand dramatically following modifications and improvements of current technologies.

Key Points

- MRgFUS is a totally noninvasive therapy.
- It can be used for treating patients with symptomatic fibroids as well as in case of childbearing wish.
- For the treatment of uterine fibroids, it is a routine procedure in dedicated centers; other indications have currently to be considered experimental.

13.8 Percutaneous Cryoablation

Joseph P. Erinjeri and Thomas Gast

13.8.1 Introduction

Cryoablation refers to all methods of destroying the tissue by freezing. Cryoablation has been applied to the treatment of cancer since the mid-nineteenth century, when Dr. James Arnott chilled salt solutions with crushed ice to temperatures of −18 to −24 °C to freeze breast, cervical, and skin cancers (Arnott 1850). He observed resultant shrinkage of the tumors and a significant decrease in pain. Although cryoablation has been used to treat malignancies in a wide variety of organs, including the eye, brain, head/neck, and esophagus, in current practice it is most commonly used in the treatment of liver, kidney, lung, prostate, and breast malignancy. Cryoablation can be performed via surgical (open or laparoscopic) or percutaneous approaches (Hui et al. 2008). Improvements in imaging (which allow earlier detection of smaller cancers) and trends toward minimally invasive techniques in oncology have made image-guided oncologic interventions like cryoablation an attractive alternative to surgical treatments.

13.8.2 Mechanism of Action

13.8.2.1 Thermodynamics

Percutaneous cryoablation begins with the insertion of a specialized needle (cryoprobe) into malignant tissue under cross-sectional imaging guidance; the needle is then rapidly cooled to sub-zero temperatures, causing removal of heat from the tissue via conduction. Cooling of the cryoprobe takes place by means of the Joule–Thompson effect, whereby rapid, adiabatic expansion of a gas results in a change in the temperature of the gas (O'Rourke et al. 2007). Most gases, including oxygen, nitrogen, and argon, exhibit Joule–Thompson cooling when quickly expanded at room temperature. Notable exceptions are hydrogen and helium, which due to their unique physical characteristics, warm when rapidly expanded at room temperature.

The cryoprobe is essentially a closed loop, high-pressure gas-expansion system (Fig. 13.71).

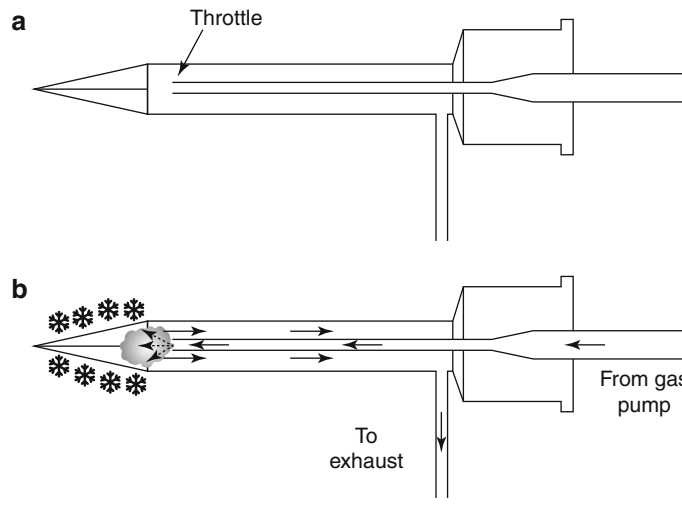

Fig. 13.71 Schematic drawing of the cryoprobe (explanation see text 13.8.2.1)

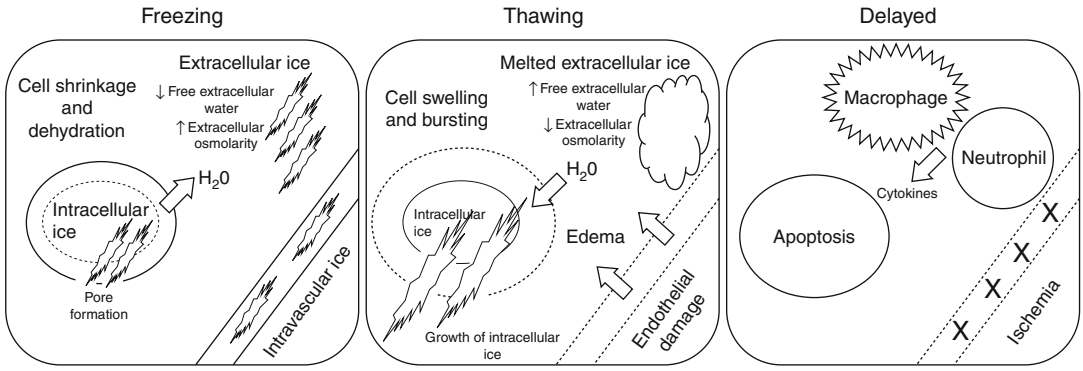

Fig. 13.72 Effects of Cryoablation causing cellular damage, and cell necrosis (explanation see text 13.8.2.2)

When the high-pressure room-temperature gas (typically argon) reaches the distal aspect of the cryoprobe, the argon is forced through a narrow opening (throttle). Within the tip of the needle, the argon expands rapidly to atmospheric pressure, causing a marked decrease in the temperature of the gas that is rapidly transferred by convection and conduction to the metallic walls of the cryoprobe. The depressurized gas is vented back out of the hub of the needle. Following ablation, thawing of the tissue is performed through the same system using high-pressure helium, which warms the cryoprobe during expansion to atmospheric pressure.

13.8.2.2 Direct and Indirect Cellular Injury

Cryoablation causes cellular damage, death, and necrosis of tissues (Fig. 13.72) by direct mechanisms (which cause cold-induced injury to cells) and indirect mechanisms (which cause impaired tissue viability by changing the cellular microenvironment). The cryoprobe absorbs heat from the tissue, eventually causing ice crystals to form in the extracellular space. The ice crystals sequester free water, increasing the tonicity of the extracellular space. Osmotic tension draws free intracellular water from cells, resulting in dehydration (Mazur 1984). The concomitant increase in intracellular solute concentration results in damage to cytoplasmic enzymes and the destabilization of the cell membrane. The cooling and dehydration of the tissue cause cold denaturation of proteins, whereby the three-dimensional conformation of proteins is altered, leading to enzymatic dysfunction (Privalov 1990). Because peptide bonds are not disrupted in the process, cold denaturation of proteins can be reversible with warming and rehydration.

When the cooling of tissues occurs rapidly, there is not enough time for intracellular dehydration. Free water is trapped within cells during the freezing process. Rapid intracellular cooling results in intracellular ice crystal formation, a harbinger of lethal cellular injury causing immediate death (Mazur et al. 1984). Although the exact mechanism of cellular damage from intracellular ice formation is unknown, injury is thought to be mediated by physical damage to intracellular organelle membranes and the plasma membrane (Bryant 1995). Crystal-induced pore formation in the plasma membrane initiates a loss of electrochemical gradients which prevents transport after the cell has thawed. If the pores are large enough, cellular components can diffuse into the extracellular space. During thawing, melting ice within the extracellular space results in its hypotonicity with respect to the intracellular compartment. This osmotic gradient can trigger a fluid shift, leading to cell swelling and/or bursting. In addition, an influx of free water into the intracellular space provides substrate for the growth of intracellular ice crystals, exacerbating their biocidal effects (Baust and Gage 2005). Interestingly, the growth of intracellular ice crystals during thawing can occur even when the temperature is below 0 °C (as high solute concentrations lower the freezing point of water) and is maximized at −20 to −25 °C.

Cells that are not immediately killed by direct cryoablation-induced injury may subsequently die by apoptosis, or programmed cell death (Hanai et al. 2001). Despite preservation of the integrity of plasma membranes and continued cellular active transport, intracellular damage to mitochondria can signal activation of a family of cysteine–aspartate proteases (caspases) that cleave various proteins, resulting in morphological and biochemical changes characterized by cell shrinkage, membrane blebbing, chromatin condensation, and genomic fragmentation (Yang et al. 2003). Apoptotic cell death following cryoablation is typically seen in the periphery of ablation zones, where exposure to temperatures which are not immediately lethal results in irrecoverable cellular injury without immediate cell death.

Indirect cellular injury is the result of cold-induced changes to tissues, causing an unfavorable microenvironment for cellular survival. Intravascular and extravascular ice crystal formation causes damage to the vascular endothelial cells. In the post-thaw period, reperfusion brings in platelets which contact the damaged endothelium, resulting in thrombus formation followed by ischemia. The resultant release of inflammatory cytokines begins a cascade of molecular events that increases vascular permeability and produces tissue edema (Baust and Gage 2005). Ischemia also results in the production of vasoactive substances causing regional hyperemia. An influx of inflammatory cells (neutrophils and macrophages) ensues, which aid in the cleanup of cellular debris. This process can continue for weeks to months after the ablation, culminating with a zone of coagulation necrosis in the ablation zone, surrounded by a band of neutrophil in its periphery.

Cellular injury, both indirect and direct, is thus influenced by four factors: cooling rate, target temperature, time at target temperature, and thawing rate. The influence of each factor stems from the biology of cold-induced injury described above. A faster rate of cooling results in a higher intracellular water content prior to freezing, maximizing intracellular ice crystal formation. The rate of cooling will be most rapid adjacent to the cryoprobe, and lower in the periphery of the ice ball, where the greater surface area lowers the flux of heat removal. Concomitantly, the target temperature will be lowest adjacent to the cryoprobe and highest in the periphery of the ice ball. Based on this fact, increasing the time at target temperature will increase the likelihood that there will be adequate time, and sufficiently low temperature, for intracellular ice crystals to form in the peripheral portion of the ice ball (Baust et al. 2009). Another challenge to intracellular ice formation in the periphery of the cryolesion is a lowered intracellular freezing point due to intracellular dehydration and increased solute concentration that occurs during slow peripheral cooling. In addition, cells from different organs, as well as different tumor types, display differing thresholds for cold-induced cell death (Klossner et al. 2007). However, almost all tissues exhibit subsequent cell death when cooled rapidly below –40 °C. Finally, the rate of thawing plays a role in the degree of cellular injury with cryoablation. Rapid thawing can increase the chance of cell survival by limiting the size of intracellular ice crystals. This idea is supported by studies which show a greater degree of cell death with passive thawing than with active thawing (Klossner et al. 2007) and by studies where repeated freeze-thaw cycles lead to a higher degree of liquefactive necrosis (Woolley et al. 2002).

13.8.3 Technique

13.8.3.1 Cryoablation Advantages

The primary advantage of cryoablation over other thermal ablation techniques is the ability to easily monitor the ablation zone during the procedure in real time (Uppot et al. 2009). During freezing, the water of the tissue undergoes a phase transition from liquid to solid, forming an ice ball which is visible under ultrasound, computed tomography, and magnetic resonance imaging guidance. Ice has a slightly lower density than water due to a slight expansion during the phase transition from liquid to solid because of the crystalline structure of the ice. During CT, the ablation zone (Fig. 13.73) appears as a sharply demarcated hypoattenuating zone around the cryoprobe (Silverman et al. 1999). The edge of the ice ball where the phase

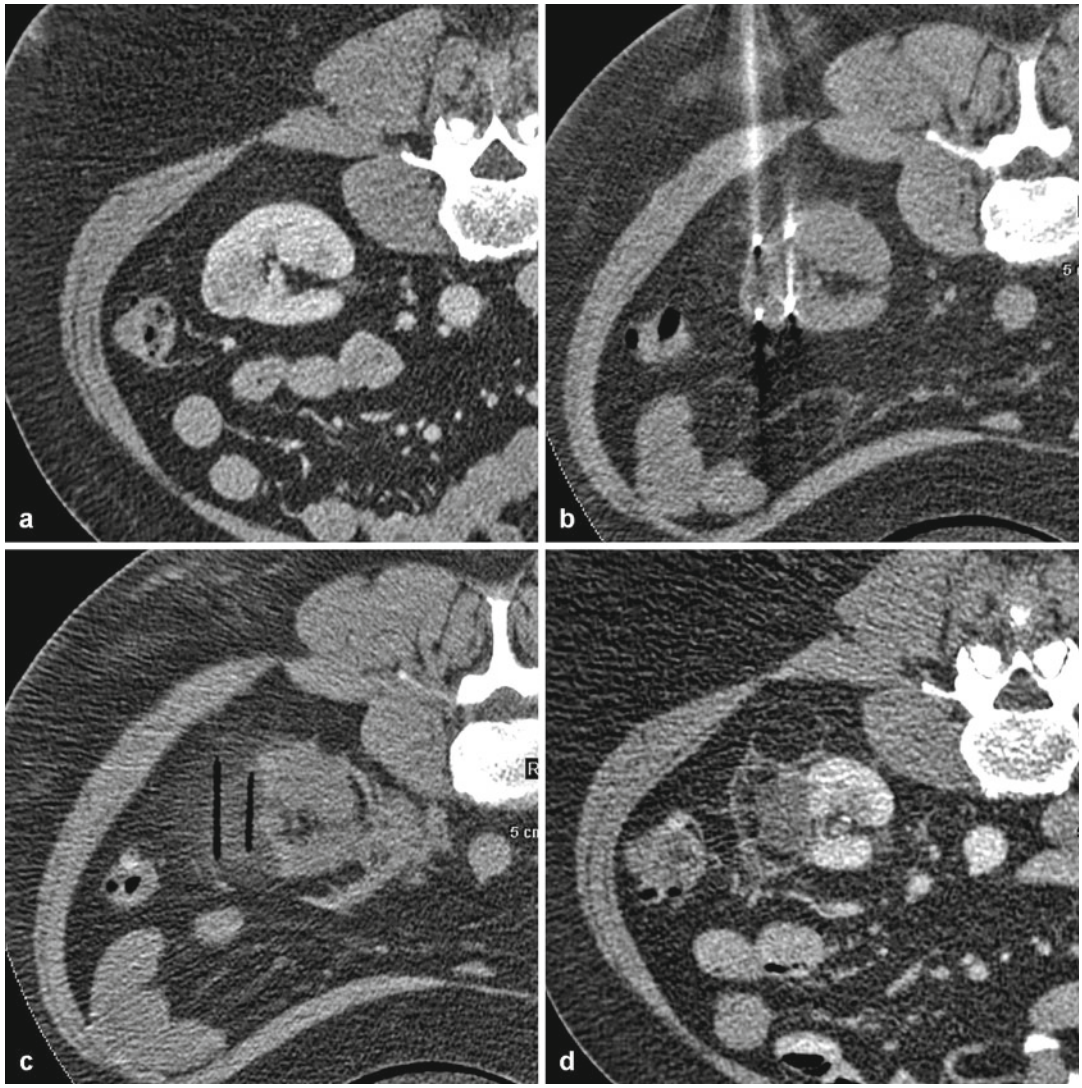

Fig. 13.73 Cryoablation in a patient with renal cell carcinoma (prone position): initial CT scan shows the renal cell carcinoma in the lower third of the left kidney (**a**). axial CT performed during cyroablation therapy (**b**). Follow-up CT performed immediately after (**c**) and 3 months after cryoablation (**d**) demonstrate total devascularized of the tumor without tumor recurrence

transition occurs marks the 0 °C isotherm. By ultrasound, the superficial surface of the ice ball appears as a hyperechoic rim, with intense acoustic shadowing that limits the ability to directly determine the depth of ice formation (Tacke et al. 1999). Magnetic resonance monitoring of cryoablation (Morrison et al. 2008) can be performed with either T1- or T2-weighted sequences; the ice ball appears as a dark signal void. Interestingly, due to the small amount of free water present in frozen tissue and the temperature sensitivity of its relaxation properties, magnetic resonance thermography can be used to assess temperature gradients within the ice ball (Butts et al. 2001).

Because the cooling of tissues and nerves provides an anesthetic effect, cryoablation tends to be less painful than heat-based thermal ablation techniques such as microwave or radiofrequency ablation. As such, it typically does not require general anesthesia and is performed in the outpatient setting with moderate sedation. Because the cooling mechanism is primarily mechanical

rather than electronic, operation of cryoablation devices typically does not cause interference with computed tomography or magnetic resonance imaging machines. In addition, each cryoablation probe acts independently of others, allowing multiple probes to be used simultaneously to ablate a zone which conforms to the tumor being treated. Radiofrequency probes require a closed-loop electric circuit, and although multiple probes can be placed in a single tumor, they must each be used sequentially rather than simultaneously.

Given the novelty of cryoablation and the lack of randomized trials comparing cryoablation to other thermal ablation techniques, it has yet to be determined how cryoablation compares with other image-guided therapies with regard to clinical efficacy. However, a lower complication rate has been seen with cryoablation than with radiofrequency ablation in the treatment of renal cell cancer (Goel and Kaouk 2008). One hypothesis to explain this finding is that freeze-induced cellular injury may be less destructive to structural components of tissue than radiofrequency thermal ablation, preserving the integrity of basement membranes. This observation is supported by the porcine model of collecting system injury following both radiofrequency and cryoablation (Janzen et al. 2005). However, collecting system injuries have been seen with renal cryoablation.

In contrast to radiofrequency ablation, cryoablation results in a robust inflammatory response. This may be due to the fact that tumor proteins remain in situ after cryoablation, whereas coagulative denaturation of proteins occurs with radiofrequency ablation. Not surprisingly, tumor antigens in the presence of inflammatory and immunomodulatory mediators initiate immunologic responses to tumor-specific antigens in ablated tissue (Sabel 2009), which have the potential to target and kill tumor cells that are not in the vicinity of the ablation zone. In fact, cryoablation has been shown to produce antibodies to the ablated tumor antigen in both animals (Shulman et al. 1967) and humans (Ablin et al. 1973). In addition to potential humoral responses mediated by cryoablation, animal studies suggest that a more tumoricidal cell-mediated immune response may be stimulated to a greater degree with cryoablation than with radiofrequency ablation (den Brok et al. 2006). A possible explanation is that the combination of the increased inflammation and the larger degree of in situ tumor antigen with cryoablation results in greater antigen presentation by dendritic cells, eliciting a more robust T cell-mediated antitumoral response. Research directed toward adjuvant immunomodulatory therapies given concurrently or after cryoablation may prove beneficial in maximizing the efficacy of cryoablation.

13.8.3.2 Cryoablation Disadvantages

The robust inflammatory response following cryoablation can lead to a systemic inflammatory response syndrome termed cryoshock (Washington et al. 2001). This constellation of findings, which can include hypotension, respiratory compromise, multi-organ failure, and disseminated intravascular coagulation, is mediated by cytokine production. It is typically seen with large-volume cryoablation, particularly in the liver. This syndrome is not seen with other thermal ablation modalities. Because cryoablation does not use heat, cautery effects and coagulation of injured vessels do not occur, and bleeding complications can therefore be exacerbated. Frozen tissues are more brittle than heated tissues, and excessive torque or displacement of cryoprobes while in the tissue can result in organ fracture, which can lead to significant hemorrhage. Aside from the ablation needle and machinery required of all ablation modalities, cryoablation also requires purchase and storage of sufficient quantities of argon and helium gas, which can cost up to US $200 per case.

13.8.3.3 Cryoablation Systems

Currently, there are two commercially available cryoablation devices in the United States, both of which cool tissue using the Joule–Thompson effect. The size and shape of the resulting ice balls are a function of cryoprobe size and Joule–Thompson chamber configuration. Healthronix, formerly Endocare, produces the Percryo system, which allows placement of up to eight individually controlled cryoprobes. Needle sizes range from 17 to 24 mm in diameter. Galil Medical's cryoablation system relies on 14.7-mm probes that have the

added advantage of being MR compatible. Up to 25 probes can be used simultaneously. Both systems enable real-time monitoring of cryoprobe temperature, as well as monitoring of tissue temperature using available thermocouples.

New cryoablation devices under development seek to overcome some of the difficulties that arise when cooling tissue using the Joule–Thompson effect. Rare noble gases like argon and helium are expensive, and attempts have been made in the past to create systems that cool needles by simply circulating a cold liquid cryogen. The challenge of this type of system is that as the cryogen chills tissue at the tip of the cryoprobe, absorption of heat from the tissue causes a phase transition from liquid to gas in the cryogen. This rapid expansion of gas results in the ability to circulate the liquid cryogen through the needle, an effect termed "vapor lock." However, by circulating pressurized nitrogen near its critical point, which refers to the point where there is no distinct phase transition between liquid and gas, vapor lock can be avoided. In this way, large amounts of expanding gases are not lost, as is seen with devices which utilize the Joule–Thompson effect, creating the potential for significant cost and space savings.

13.8.3.4 Indications

Indications for cryoablation include primary or metastatic tumors <5 cm which are amenable to locoregional therapy in patients that:

- Have comorbidities that preclude surgery
- Have comorbidities that preclude general endotracheal anesthesia
- Require conservation of organ parenchyma (solitary kidney, renal insufficiency)
- Have multiple tumors in the same organ (von Hippel Lindau) where surgical extirpation would make viability of the residual organ difficult
- Have complex tumors where surgical resection would require an extended ischemia time
- Prefer minimally invasive techniques over open or laparoscopic surgery

13.8.3.5 Procedure

Cryoablation can be performed with moderate sedation or general anesthesia. Thermal injury due to cold is associated with minimal pain, while thermal injury with heat can be considerably painful. Patients undergoing cryoablation generally tolerate the procedure with moderate sedation (fentanyl and midazolam). Scout imaging is obtained to localize the target. If necessary, contrast can be given to increase conspicuity of the target. The CT gantry can be angled on scout imaging to maintain longitudinal needle visualization during subcostal needle placement. The point of skin entry is determined based on the planned needle trajectory. The skin entry site is prepped and draped. The site is anesthetized with 2 % lidocaine.

A small dermatotomy is made to facilitate needle placement. Multiple probes may be placed simultaneously to insure that the ice ball will encompass the lesion. After confirming needle placement(s), ablation is usually conducted with two freeze-thaw cycles (e.g., a 10-min freeze, 8-min thaw, and 10-min refreeze). The diameter of the ice ball initially increases rapidly; cross-sectional imaging during the procedure may be performed at 3–5 min intervals to minimize nontarget ablation. Ice ball temperature readings are usually in the −80 to −150 °C range. Cytotoxic intracellular ice formation in renal cells occurs best with rapid cooling below −20 °C. Ice ball formation can be monitored in real time via CT (hypodense ice ball), MRI (hypointense ice ball), and ultrasound (shadowing ice ball). It should be noted that the edge of the ice ball marks the 0 °C isotherm, and the −20 °C is deep to the ice ball margin. Therefore, to insure cytotoxic target temperature within the lesion, an ice ball margin should exceed the margin of the lesion by at least 5 mm. Some operators utilize a thermocouple at the tumor margin to ensure that the target temperature at the margin of the lesion reaches −20 °C. If the cryoablation zone is in close proximity to the skin, saline can be injected under the skin to prevent thermal injury to the dermis. Alternatively, the skin can be warmed with heating packs. Some protocols recommend double freeze-thaw cycles to enhance efficacy.

Following the freeze-thaw-freeze cycle, the cryoprobe can be removed with a twisting motion; the probe should not be removed forcefully if it remains frozen to the lesion, as renal fracture can occur. Instead, active thawing to 15 °C with gentle twisting traction can facilitate removal of the

probe. Immediate post-procedure imaging should be performed following removal of the ablation probe to assess for immediate complications (see below). Finally, sterile dressing is applied.

13.8.4 Results

13.8.4.1 Kidney

While open partial nephrectomy is still the standard of therapy, its associated morbidity has encouraged researchers and practicing clinicians toward less radical approaches. Cryoablation offers the potential advantage of combining a nephron-sparing therapy together with a minimally invasive approach. In addition, anesthetic requirements, postoperative analgesia, and hospital stay are significantly reduced, with a rapid return to normal activity and work (Dominguez-Escrig et al. 2008).

No randomized controlled trials have been performed to compare thermal ablation (radiofrequency ablation or cryoablation) to partial nephrectomy, the reference standard for treatment of T1 renal cancer. Local recurrence is seen in 2.6 % of patients following nephron-sparing surgery, 4.6 % following cryoablation, and 11.7 % following radiofrequency ablation (as determined by a meta-analysis of 99 case series of 6,471 tumors treated with partial nephrectomy, cryoablation, radiofrequency ablation, or active surveillance) (Kunkle et al. 2008). Local recurrence was higher in patients with larger tumors. Primary effectiveness (defined as the percentage of tumors successfully treated by a single ablation procedure) is 87 % for percutaneous ablation versus 94 % for surgical ablation (as determined by a meta-analysis of 46 case series of percutaneous and surgical ablations of 1,180 renal tumors in 1,055 patients) (Hui et al. 2008). There was no significant difference in secondary effectiveness (defined as the percentage of tumors treated successfully overall, including repeat ablations following identification of residual or recurrent tumors) when comparing percutaneous ablations to surgical ablations (92 % vs. 95 %, respectively, $p < 0.05$). However, comparing percutaneous ablations to surgical ablations, percutaneous ablation had a significantly lower major complication rate (3 % vs. 7 %, respectively, $p < 0.05$) and a significantly lower length of hospital stay (1.4 vs. 3.0 days, respectively, $p < 0.05$).

Bleeding complication following renal cryoablation is usually self-limited and is seen in 20–40 % of cases (Georgiades et al. 2006). Gross hematuria, with passage of clots, is rare. In the event of subcapsular or extracapsular hematoma, drainage is rarely helpful, as bleeding will be tamponaded by the capsule. If severe, worsened renal function or hypertension can be seen (Page kidney). Capsular disruption with urine leak can range from a small amount of urine seen outside the kidney on follow-up imaging to frank urinoma. Animal studies and human case series suggest that the risk of collecting system injury may be less with cryoablation than with radiofrequency ablation (Warlick et al. 2006). Nerve injury occurs in less than <1 % of cases. Thermal damage to the intercostal nerve can result in trunk numbness. The ilioinguinal, iliohypogastric, or genitofemoral nerves run along the anterior aspect of the psoas muscle and can be injured during ablation of posteromedial renal lesion, resulting in groin/leg numbness and/or hip flexion weakness. These effects can be transient or permanent, depending on the degree of nerve injury. Track seeding is rare 0.6–2.5 %, and track ablation may minimize risk.

13.8.4.2 Bone and Soft Tissue Tumors

Cryoablation can be used effectively for local tumor control in patients with primary and metastatic soft tissue and bone tumors, and it is particularly useful in pain palliation for these patients (Rybak 2009). Several studies have shown a promising role for cryoablation in patients who have failed conventional therapies. Callstrom et al. showed that percutaneous cryoablation of metastatic bone lesions is both a safe and effective method for palliation of pain (Callstrom et al. 2006). A significant advantage is that cryoablation causes mild or insignificant intra-procedural pain compared with other ablation techniques.

13.8.4.3 Lung

The majority of NSCLC patients presenting with early-stage disease (I/II) are not surgical candidates due to comorbid disease. RFA of lung neoplasms has found widespread use in the treatment of primary and metastatic lung malignancy. Some preliminary studies suggest that cryoablation has potential for lung malignancy as well (Kawamura et al. 2006; Wang et al. 2005). Cryoablation may be preferable to RF ablation for tumors adjacent to mediastinal structures since with cryoablation the ablation zone can be monitored close to mediastinal and hilar vessels.

13.8.4.4 Prostate

The optimal strategy for managing localized prostate cancer has not been established and currently includes several potential options: active surveillance, radical prostatectomy, external-beam radiation, brachytherapy, and cryoablation. Unfortunately, randomized, multicenter clinical trials comparing cryoablation to other minimally invasive techniques are lacking. Prospective, randomized trials are needed to control for the many known and unknown confounding factors that can affect long-term outcomes.

Several retrospective studies suggest that cryoablation can result in long-term progression-free survival in a subset of carefully selected, high-risk men who have been adequately staged to confirm localized disease (Cheetham et al. 2010; Cytron et al. 2009). However, since no single treatment modality has demonstrated superiority with respect to survival, differences in quality of life and complication rate are important considerations in treatment selection. Short-term complications of prostate cryoablation include urinary retention due to gland swelling, usually persisting for 1 or 2 weeks. Penile and/or scrotal swelling is also common in the first few weeks post-procedure, but is self-limited and usually resolves within 2 months. Long-term complications include fistula formation, incontinence, urethral sloughing, and erectile dysfunction. During whole-gland cryoablation, both neurovascular bundles can be included within the ice ball, resulting in erectile dysfunction rates that are universally high. As a result, cryosurgery is generally considered suitable as a treatment option when retaining sexual function is not an issue or the relationship of the tumor to the neurovascular bundle creates a minimal risk of erectile dysfunction. One study comparing cryoablation to external-beam radiation found that men who wish to increase their odds of retaining sexual function might be counseled to choose EBRT over cryoablation (Robinson et al. 2009).

13.8.4.5 Other Tumors

A significant advantage of cryoablation is that virtually any local solid tumor that is not responding to local therapy can be treated with percutaneous cryoablation. Cryoablation can provide excellent oncologic and cosmetic results in unifocal subclinical breast cancer (Manenti et al. 2011). Even MR-guided percutaneous cryoablation of uterine fibroids has shown to be an effective treatment (Sakuhara et al. 2006). Cryoablation of liver tumors has also been performed (Hinshaw and Lee 2007). A syndrome of multi-organ failure, severe coagulopathy, and disseminated intravascular coagulation, known as cryoshock, can be seen following hepatic cryotherapy. In a study of 2,173 patients, the phenomenon of cryoshock was observed in approximately 1 % of cases (Seifert and Morris 1999). It should be noted that when cryoshock is present, it is associated with a high risk of death, being responsible for 18.2 % of deaths in this study. Though infrequent, the cryoshock phenomenon likely accounts for decreased use of hepatic cryoablation in some institutions.

Appraisal

Cryoablation refers to all methods of destroying tissue by freezing. Cryoablation causes cellular damage, death, and necrosis of tissues by direct mechanisms (which cause cold-induced injury to cells) and indirect mechanisms (which cause changes to the cellular microenvironment, impairing tissue viability). Understanding the relationships between these factors and tumor injury will be critical in applying future adjuvant therapies to maximize the efficacy of cryoablation and minimize procedural morbidity. Although it is

certain that the technologies to perform cryoablation have great potential for evolution, cryoablation of malignancy has already become established as an important modality in image-guided interventional oncology.

Key Points

- Cryoablation systems create rapid cooling of the cryoprobe by the rapid Joule–Thompson expansion of argon.
- The cold-induced tumor injury sustained through image-guided cryoablation is affected by four factors: cooling rate, target temperature, time at target temperature, and thawing rate.
- The major advantage of cryoablation over other thermal ablative modalities is the ability to directly visualize the ablation zone "ice ball" under radiologic (MR, CT, U/S) guidance.

References

Technical Basics

Ahmed M, Liu Z, Afzal KS et al (2004) Radiofrequency ablation: effect of surrounding tissue composition on coagulation necrosis in a canine tumor model. Radiology 230:761–767

Bruners P, Hodenius M, Gunther RW et al (2007) Flüssigkeitsmodulierte RF-ablation: in-vitro-experimente. Rofo 179:380–386 [German]

Bruners P, Schmitz-Rode T, Günther RW et al (2008) Multipolar hepatic radiofrequency ablation using up to six applicators: preliminary results. Rofo 180:216–222

Clasen S, Schmidt D, Boss A et al (2006) Multipolar radiofrequency ablation with internally cooled electrodes: experimental study in ex vivo bovine liver with mathematic modeling. Radiology 238:881–890

Clasen S, Schmidt D, Dietz K et al (2007) Bipolar radiofrequency ablation using internally cooled electrodes in ex vivo bovine liver: prediction of coagulation volume from applied energy. Invest Radiol 42:29–36

d'Arsonval MA (1891) Action physiologique des courants alternatifs. C R Soc Biol 43:283–286

de Baere T, Denys A, Wood BJ et al (2001) Radiofrequency liver ablation: experimental comparative study of water-cooled versus expandable systems. Am J Roentgenol 176:187–192

Dupuy DE, Zagoria RJ, Akerley W et al (2000) Percutaneous radiofrequency ablation of malignancies in the lung. Am J Roentgenol 174:57–59

Gazelle GS, Goldberg SN, Solbiati L et al (2000) Tumor ablation with radiofrequency energy. Radiology 217:633–646

Gervais DA, McGovern FJ, Arellano RS et al (2003) Renal cell carcinoma: clinical experience and technical success with radiofrequency ablation of 42 tumors. Radiology 226:417–424

Gillams AR, Lees WR (2005) CT mapping of the distribution of saline during radiofrequency ablation with perfusion electrodes. Cardiovasc Intervent Radiol 28:476–480

Goetz MP, Callstrom MR, Charboneau JW et al (2004) Percutaneous image-guided radiofrequency ablation of painful metastases involving bone: a multicenter study. J Clin Oncol 22:300–306

Goldberg SN, Gazelle GS, Dawson SL et al (1995) Tissue ablation with radiofrequency using multiprobe arrays. Acad Radiol 2:670–674

Goldberg SN, Hahn PF, Tanabe KK et al (1998a) Percutaneous radiofrequency tissue ablation: does perfusion mediated tissue cooling limit coagulation necrosis? J Vasc Interv Radiol 9:101–111

Goldberg SN, Solbiati L, Hahn PF et al (1998b) Large-volume tissue ablation with radio frequency by using a clustered, internally cooled electrode technique: laboratory and clinical experience in liver metastases. Radiology 209:371–379

Goldberg SN, Stein MC, Gazelle GS et al (1999) Percutaneous radiofrequency tissue ablation: optimization of pulsed-radiofrequency technique to increase coagulation necrosis. J Vasc Interv Radiol 10: 907–916

Goldberg SN, Gazelle GS, Compton CC et al (2000a) Treatment of intrahepatic malignancy with radiofrequency ablation: radiologic-pathologic correlation. Cancer 88:2452–2463

Goldberg SN, Gazelle GS, Mueller PR (2000b) Thermal ablation therapy for focal malignancy: a unified approach to underlying principles, techniques, and diagnostic imaging guidance. Am J Roentgenol 174: 323–331

Goldberg SN, Solbiati L, Halpern EF et al (2000c) Variables affecting proper system grounding for radiofrequency ablation in an animal model. J Vasc Interv Radiol 11:1069–1075

Goldberg SN, Grassi CJ, Cardella JF et al (2005) Image-guided tumor ablation: standardization of terminology and reporting criteria. Radiology 235:728–739

Haemmerich D, Staelin ST, Tungjitkusolmun S et al (2001) Hepatic bipolar radiofrequency ablation between separated multiprong electrodes. IEEE Trans Biomed Eng 48:1145–1152

Laeseke PF, Sampson LA, Haemmerich D et al (2005) Multiple-electrode radiofrequency ablation: simultaneous production of separate zones of coagulation in an in vivo porcine liver model. J Vasc Interv Radiol 16:1727–1735

Laeseke PF, Sampson LA, Haemmerich D et al (2006) Multiple-electrode radiofrequency ablation creates confluent areas of necrosis: in vivo porcine liver results. Radiology 241:116–124
Liu Z, Lobo SM, Humphries S et al (2005) Radiofrequency tumor ablation: insight into improved efficacy using computer modeling. Am J Roentgenol 184:1347–1352
Liu Z, Ahmed M, Weinstein Y et al (2006) Characterization of the RF ablation-induced 'oven effect': the importance of background tissue thermal conductivity on tissue heating. Int J Hyperthermia 22:327–342
Liu Z, Ahmed M, Sabir A et al (2007) Computer modeling of the effect of perfusion on heating patterns in radiofrequency tumor ablation. Int J Hyperthermia 23:49–58
Livraghi T, Goldberg SN, Lazzaroni S et al (2000) Hepatocellular carcinoma: radiofrequency ablation of medium and large lesions. Radiology 214:761–768
Lobo SM, Afzal KS, Ahmed M et al (2004) Radiofrequency ablation: modeling the enhanced temperature response to adjuvant NaCl pretreatment. Radiology 230:175–182
McGahan JP, Browning PD, Brock JM et al (1990) Hepatic ablation using radiofrequency electrocautery. Invest Radiol 25:267–270
McGahan JP, Gu WZ, Brock JM et al (1996) Hepatic ablation using bipolar radiofrequency electrocautery. Acad Radiol 3:418–422
Pennes HH (1948) Analysis of tissue and arterial blood temperatures in the resting human forearm. J Appl Physiol 1:93–122
Pereira PL, Trubenbach J, Schenk M et al (2004) Radiofrequency ablation: in vivo comparison of four commercially available devices in pig livers. Radiology 232:482–490
Rhim H, Goldberg SN, Dodd GD 3rd et al (2001) Essential techniques for successful radiofrequency thermal ablation of malignant hepatic tumors. Radiographics 21: 17–39
Rosenthal DI, Hornicek FJ, Torriani M et al (2003) Osteoid osteoma: percutaneous treatment with radiofrequency energy. Radiology 229:171–175
Rossi S, Fornari F, Pathies C et al (1990) Thermal lesions induced by 480 KHz localized current field in guinea pig and pig liver. Tumori 76:54–57
Rossi S, Garbagnati F, Lencioni R et al (2000) Percutaneous radiofrequency thermal ablation of nonresectable hepato-cellular carcinoma after occlusion of tumor blood supply. Radiology 217:119–126
Schmidt D, Trubenbach J, Brieger J et al (2003) Automated saline-enhanced radiofrequency thermal ablation: initial results in ex vivo bovine livers. Am J Roentgenol 180:163–165
Schramm W, Yang D, Haemmerich D (2006) Contribution of direct heating, thermal conduction and perfusion during radiofrequency and microwave ablation. Conf Proc IEEE Eng Med Biol Soc 1:5013–5016
Seegenschmiedt MH, Brady LW, Sauer R (1990) Interstitial thermoradiotherapy: review on technical and clinical aspects. Am J Clin Oncol 13:352–363
Siperstein AE, Gitomirski A (2000) History and technological aspects of radiofrequency thermal ablation. Cancer J 6(Suppl 4):5293–5303
Solbiati L, Livraghi T, Goldberg SN et al (2001) Percutaneous radiofrequency ablation of hepatic metastases from colorectal cancer: long-term results in 117 patients. Radiology 221:159–166
Tacke J, Mahnken A, Roggan A et al (2004) Multipolar radiofrequency ablation: first clinical results. Rofo 176:324–329
Zervas NT, Kuwayama A (1972) Pathological characteristics of experimental thermal lesions: comparison of induction heating and radiofrequency electrocoagulation. J Neurosurg 37:418–422

RF Ablation of Liver Tumors

Abdalla EK, Vauthey JN, Ellis LM, Ellis V et al (2004) Recurrence and outcomes following hepatic resection, radiofrequency ablation, and combined resection/ablation for colorectal liver metastases. Ann Surg 239:818–825; discussion 825–827
Akamatsu M, Yoshida H, Obi S et al (2004) Evaluation of transcatheter arterial embolization prior to percutaneous tumor ablation in patients with hepatocellular carcinoma: a randomized controlled trial. Liver Int 24:625–630
Atwell TD, Charboneau JW, Que FG, Rubin J et al (2005) Treatment of neuroendocrine cancer metastatic to the liver: the role of ablative techniques. Cardiovasc Intervent Radiol 28:409–421
Bale R, Widmann G, Schullian P et al (2012) Percutaneous stereotactic radiofrequency ablation of colorectal liver metastases. Eur Radiol 22:930–937
Barker DW, Zagoria RJ, Morton KA, Kavanagh PV, Shen P (2005) Evaluation of liver metastases after radiofrequency ablation: utility of 18 F-FDG PET and PET/CT. Am J Roentgenol 184:1096–1102
Berber E, Tsinberg M, Tellioglu G et al (2008) Resection versus laparoscopic radiofrequency thermal ablation of solitary colorectal liver metastasis. J Gastrointest Surg 12:1967–1972
Bowles BJ, Machi J, Limm WM et al (2001) Safety and efficacy of radiofrequency thermal ablation in advanced liver tumors. Arch Surg 136:864–869
Bruix J, Sherman M, Llovet JM et al (2001) Clinical management of hepatocellular carcinoma. Conclusions of the Barcelona-2000 EASL conference. J Hepatol 35:421–430
Brunello F, Veltri A, Carucci P et al (2008) Radiofrequency ablation versus ethanol injection for early hepatocellular carcinoma: a randomized controlled trial. Scand J Gastroenterol 43:727–735
Burdio F, Guemes A, Burdio JM et al (2003) Bipolar saline-enhanced electrode for radiofrequency ablation: results of experimental study of in vivo porcine liver. Radiology 229:447–456
Chen MH, Yang W, Yan K et al (2004) Large liver tumors: protocol for radiofrequency ablation and its clinical

application in 110 patients – mathematic model, overlapping mode, and electrode placement process. Radiology 232:260–271
Chen MH, Wei Y, Yan K et al (2006a) Treatment strategy to optimize radiofrequency ablation for liver malignancies. J Vasc Interv Radiol 17:671–683
Chen MS, Li JQ, Zheng Y et al (2006b) A prospective randomized trial comparing percutaneous local ablative therapy and partial hepatectomy for small hepatocellular carcinoma. Ann Surg 243:321–328
Choi H, Loyer EM, DuBrow RA et al (2001) Radiofrequency ablation of liver tumors: assessment of therapeutic response and complications. Radiographics 21:S41–S54
Choi D, Lim HK, Rhim H et al (2007a) Percutaneous radiofrequency ablation for recurrent hepatocellular carcinoma after hepatectomy: long-term results and prognostic factors. Ann Surg Oncol 14:2319–2329
Choi D, Lim HK, Rhim H et al (2007b) Percutaneous radiofrequency ablation for early-stage hepatocellular carcinoma as a first line treatment: long-term results and prognostic factors in a large single-institution series. Eur Radiol 17:684–692
Clasen S, Schmidt D, Boss A et al (2006) Multipolar radiofrequency ablation with internally cooled electrodes: experimental study in ex vivo bovine liver with mathematic modeling. Radiology 238:881–890
Clasen S, Schmidt D, Dietz K et al (2007) Bipolar radiofrequency ablation using internally cooled electrodes in ex vivo bovine liver: prediction of coagulation volume from applied energy. Invest Radiol 42:29–36
de Baere T, Risse O, Kuoch V et al (2003) Adverse events during radiofrequency treatment of 582 hepatic tumors. Am J Roentgenol 181:695–700
Dodd GD III, Frank MS, Aribandi M, Chopra S et al (2001) Radiofrequency thermal ablation: computer analysis of the size of the thermal injury created by overlapping ablations. Am J Roentgenol 177: 777–782
Dupuy DE, Goldberg SN (2001) Image-guided radiofrequency tumor ablation: challenges and opportunities – part II. J Vasc Interv Radiol 12:1135–1148
Elias D, De Baere T, Smayra T et al (2002) Percutaneous radiofrequency thermoablation as an alternative to surgery for treatment of liver tumour recurrence after hepatectomy. Br J Surg 89:752–756
Forner A, Llovet JM, Bruix J (2012) Hepatocellular carcinoma. Lancet 379(9822):1245–1255
Gillams A (2001) Thermal ablation of liver metastases. Abdom Imaging 26:361–368
Gillams AR (2003) Radiofrequency ablation in the management of liver tumours. Eur J Surg Oncol 29:9–16
Gillams AR (2005) The use of radiofrequency in cancer. Br J Cancer 92:1825–1829
Gillams AR, Lees WR (2000) Survival after percutaneous, image-guided, thermal ablation of hepatic metastases from colorectal cancer. Dis Colon Rectum 43:656–661
Gillams AR, Lees WR (2004) Radiofrequency ablation of colorectal liver metastases in 167 patients. Eur Radiol 14:2261–2267
Gillams AR, Lees WR (2009) Five-year survival in 309 patients with colorectal liver metastases treated with radiofrequency ablation. Eur Radiol 19:1206–1213
Goldberg SN, Ahmed M (2002) Minimally invasive image-guided therapies for hepatocellular carcinoma. J Clin Gastroenterol 35:S115–S129
Goldberg SN, Gazelle GS (2001) Radiofrequency tissue ablation: physical principles and techniques for increasing coagulation necrosis. Hepatogastroenterology 48:359–367
Goldberg SN, Gazelle GS, Compton CC et al (2000) Treatment of intrahepatic malignancy with radiofrequency ablation: radiologic-pathologic correlation. Cancer 88:2452–2463
Goldberg SN, Grassi CJ, Cardella JF et al (2005) Image-guided tumor ablation: standardization of terminology and reporting criteria. Radiology 235:728–739
Guglielmi A, Ruzzenente A, Sandri M et al (2007) Radiofrequency ablation for hepatocellular carcinoma in cirrhotic patients: prognostic factors for survival. J Gastrointest Surg 11:143–149
Huang J, Yan L, Cheng Z et al (2010) A randomized trial comparing radiofrequency ablation and surgical resection for HCC conforming to the Milan criteria. Ann Surg 252:903–912
Jaeck D, Bachellier PGM, Boudjema K et al (1997) Long-term survival following resection of colorectal hepatic metastases. Association Francaise de Chirurgie. Br J Surg 84:977–980
Jaskolka JD, Asch MR, Kachura JR et al (2005) Needle tract seeding after radiofrequency ablation of hepatic tumors. J Vasc Interv Radiol 16:485–491
Jenkins LT, Millikan KW, Bines SD et al (1997) Hepatic resection for metastatic colorectal cancer. Am Surg 63:605–610
Kaseb AO, Hanbali A, Cotant M et al (2009) Vascular endothelial growth factor in the management of hepatocellular carcinoma. Cancer 115:4895–4906
Kojiro M (2004) Focus on dysplastic nodules and early hepato-cellular carcinoma: an eastern point of view. Liver Transpl 10:S3–S8
Kuvshinoff BW, Ota DM (2002) Radiofrequency ablation of liver tumors: influence of technique and tumor size. Sugery 132:605–611; discussion 611–612
Lencioni R, Goletti O, Armillotta N et al (1998) Radiofrequency thermal ablation of liver metastases with a cooled tip electrode needle: results of a pilot clinical trial. Eur Radiol 8:1205–1211
Lencioni R, Cioni D, Bartolozzi C (2001) Percutaneous radiofrequency thermal ablation of liver malignancies: techniques, indications, imaging findings, and clinical results. Abdom Imaging 26:345–360
Lencioni RA, Allgaier HP, Cioni D et al (2003) Small hepatocellular carcinoma in cirrhosis: randomized comparison of radiofrequency thermalablation versus percutaneous ethanol injection. Radiology 228:235–240
Lencioni R, Crocetti L, Cioni D et al (2004) Percutaneous radiofrequency ablation of hepatic colorectal metastases: technique, indications, results, and new promises. Invest Radiol 39:689–697

Lencioni R, Cioni D, Crocetti L et al (2005) Early-stage hepatocellular carcinoma in patients with cirrhosis: long-term results of percutaneous image-guided radiofrequency ablation. Radiology 234:961–967

Lim HK, Han JK (2002) Hepatocellular carcinoma: evaluation of therapeutic response to interventional procedures. Abdom Imaging 27:168–179

Lim HK, Choi D, Lee WJ et al (2001) Hepatocellular carcinoma treated with percutaneous radiofrequency ablation: evaluation with follow-up multiphase helical CT. Radiology 221:447–454

Lin SM, Lin CJ, Lin CC et al (2004) Radiofrequency ablation improves prognosis compared with ethanol injection for hepatocellular carcinoma≤4 cm. Gastroenterology 127:1714–1723

Lin SM, Lin CJ, Lin CC et al (2005) Randomised controlled trial comparing percutaneous radiofrequency thermal ablation, percutaneous ethanol injection, and percutaneous acetic acid injection to treat hepatocellular carcinoma of 3 cm or less. Gut 54:1151–1156

Livraghi T, Goldberg SN, Lazzaroni S et al (2000) Hepatocellular carcinoma: radiofrequency ablation of medium and large lesions. Radiology 214:761–768

Livraghi T, Solbiati L, Meloni F et al (2003a) Percutaneous radiofrequency ablation of liver metastases in potential candidates for resection: the "test-of-time approach". Cancer 97:3027–3035

Livraghi T, Solbiati L, Meloni MF et al (2003b) Treatment of focal liver tumors with percutaneous radiofrequency ablation: complications encountered in a multicenter study. Radiology 226:441–451

Livraghi T, Meloni F, Morabito A, Vettori C (2004) Multimodal image-guided tailored therapy of early and intermediate hepatocellular carcinoma: long-term survival in the experience of a single radiologic referral center. Liver Transpl 10(Suppl 1):S98–S106

Livraghi T, Lazzaroni S, Meloni F et al (2005) Risk of tumour seeding after percutaneous radiofrequency ablation for hepatocellular carcinoma. Br J Surg 92:856–858

Livraghi T, Meloni F, Di Stasi M et al (2008) Sustained complete response and complication rates after radiofrequency ablation of very early hepatocellular carcinoma in cirrhosis: is resection still the treatment of choice? Hepatology 47:82–89

Llovet JM, Bruix J (2008) Novel advancements in the management of hepatocellular carcinoma in 2008. J Hepatol 48(Suppl 1):S20–S37

Llovet JM, Vilana R, Bru C et al (2001) Increased risk of tumor seeding after percutaneous radiofrequency ablation for single hepatocellular carcinoma. Hepatology 33:1124–1129

Llovet JM, Burroughs A, Bruix J (2003) Hepatocellular carcinoma. Lancet 362:1907–1917

Lu DS, Raman SS, Limanond P et al (2003) Influence of large peritumoral vessels on outcome of radiofrequency ablation of liver tumors. J Vasc Interv Radiol 14:1267–1274

Lu DS, Yu NC, Raman SS et al (2005) Radiofrequency ablation of hepatocellular carcinoma: treatment success as defined by histologic examination of the explanted liver. Radiology 234:954–960

Machi J, Oishi AJ, Sumioda K et al (2006) Long-term outcome of radiofrequency ablation for unresectable liver metastases from colorectal cancer: evaluation of prognostic factors and effectiveness in first- and second-line management. Cancer J 12:318–326

Mahnken AH, Klotz E, Schreiber S et al (2011) Volumetric arterial enhancement fraction predicts tumor recurrence after hepatic radiofrequency ablation of liver metastases: initial results. Am J Roentgenol 196:W573–W579

McGahan JP, Dodd GD III (2001) Radiofrequency ablation of the liver: current status. Am J Roentgenol 176:3–16

McKay A, Fradette K, Lipschitz J (2009) Long-term outcomes following hepatic resection and radiofrequency ablation of colorectal liver metastases. HPB Surg 2009:346863

Meloni MF, Goldberg SN, Moser V et al (2002) Colonic perforation and abscess following radiofrequency ablation treatment of hepatoma. Eur J Ultrasound 15:73–76

Mor E, Kaspa RT, Sheiner P, Schwartz M (1998) Treatment of hepatocellular carcinoma associated with cirrhosis in the era of liver transplantation. Ann Intern Med 129:643–653

Mulier S, Mulier P, Ni Y et al (2002) Complications of radiofrequency coagulation of liver tumours. Br J Surg 89:1206–1222

Mulier S, Ni Y, Jamart J et al (2008) Radiofrequency ablation versus resection for resectable colorectal liver metastases: time for a randomized trial? Ann Surg Oncol 15:144–157

N'Kontchou G, Mahamoudi A, Aout M et al (2009) Radiofrequency ablation of hepatocellular carcinoma: long-term results and prognostic factors in 235 Western patients with cirrhosis. Hepatology 50:1475–1483

Nakanishi K, Kobayashi M, Takahashi S et al (2005) Whole body MRI for detecting metastatic bone tumor: comparison with bone scintigrams. Magn Reson Med Sci 4:11–17

Ni Y, Miao Y, Mulier S et al (2000) A novel cooled-wet electrode for radiofrequency ablation. Eur Radiol 10:852–854

Nicolau C, Català V, Vilana R et al (2004) Evaluation of hepatocellular carcinoma using SonoVue, a second generation ultrasound contrast agent: correlation with cellular differentiation. Eur Radiol 14:1092–1099

Oshowo A, Gillams A, Harrison E et al (2003) Comparison of resection and radiofrequency ablation for treatment of solitary colorectal liver metastases. Br J Surg 90:1240–1243

Park IJ, Kim HC, Yu CS et al (2008) Radiofrequency ablation for metachronous liver metastasis from colorectal cancer after curative surgery. Ann Surg Oncol 15:227–232

Pereira PL, Truebenbach J, Schmidt D (2003) Radiofrequency ablation: basic principles, techniques and challenges. Rofo 175:20–27

Pereira PL, Clasen S, Boss A et al (2004a) Radiofrequency ablation of liver metastases. Radiologe 44:347–357

Pereira PL, Truebenbach J, Schenk M et al (2004b) Radiofrequency ablation: in vivo comparison of four

commercially available devices in pig livers. Radiology 232:482–490
Poon RT, Fan ST, Tsang FH et al (2002) Locoregional therapies for hepatocellular carcinoma: a critical review from the surgeon's perspective. Ann Surg 235: 466–486
Poon RT, Ng KK, Lam CM et al (2004a) Effectiveness of radiofrequency ablation for hepatocellular carcinomas larger than 3 cm in diameter. Arch Surg 139:281–287
Poon RT, Ng KK, Lam CM et al (2004b) Learning curve for radiofrequency ablation of liver tumors: prospective analysis of initial 100 patients in a tertiary institution. Ann Surg 239:441–449
Raut CP, Izzo F, Marra P et al (2005) Significant long-term survival after radiofrequency ablation for hepatocellular carcinoma in patients with cirrhosis. Ann Surg Oncol 12:616–628
Rhim H, Yoon KH, Lee JM et al (2003) Major complications after radiofrequency thermal ablation of hepatic tumors: spectrum of imaging findings. Radiographics 23:123–134; discussion 134–136
Rhim H, Dodd GD 3rd, Chintapalli KN et al (2004) Radiofrequency thermal ablation of abdominal tumors: lessons learned from complications. Radiographics 24:41–52
Rhim H, Lim HK, Choi D (2010) Current status of radiofrequency ablation of hepatocellular carcinoma. World J Gastrointest Surg 2:128–136
Sala M, Llovet JM, Vilana R et al (2004) Initial response to percutaneous ablation predicts survival in patients with hepatocellular carcinoma. Hepatology 40:1352–1360
Seidenfeld J, Korn A, Aronson N (2002) Radiofrequency ablation of unresectable liver metastases. J Am Coll Surg 195:378–386
Shibata T, Iimuro Y, Yamamoto Y et al (2002) Small hepatocellular carcinoma: comparison of radiofrequency ablation and percutaneous microwave coagulation therapy. Radiology 223:331–337
Shibata T, Shibata T, Metani Y et al (2006) Radiofrequency ablation for small hepatocellular carcinoma: prospective comparison of internally cooled electrode and expandable electrode. Radiology 238:346–353
Shiina S, Teratani T, Obi S et al (2005) A randomized controlled trial of radiofrequency ablation with ethanol injection for small hepatocellular carcinoma. Gastroenterology 129:122–130
Sironi S, Livraghi T, Meloni F et al (1999) Small hepatocellular carcinoma treated with percutaneous RF ablation: MR imaging follow-up. Am J Roentgenol 173: 1225–1229
Solbiati L, Goldberg SN, Ierace T et al (1997a) Hepatic metastases: percutaneous radiofrequency ablation with cooled-tip electrodes. Radiology 205:367–373
Solbiati L, Ierace T, Goldberg SN et al (1997b) Percutaneous US-guided radiofrequency tissue ablation of liver metastases: treatment and follow-up in 16 patients. Radiology 202:195–203
Solbiati L, Ierace T, Tonolini M et al (2001) Radiofrequency thermal ablation of hepatic metastases. Eur J Ultrasound 13:149–158
Solbiati L, Tonolini M, Cova L (2004a) Monitoring RF ablation. Eur Radiol 14(Suppl 8):P34–P42
Solbiati L, Ierace T, Tonolini M, Cova L (2004b) Guidance and monitoring of radiofrequency liver tumor ablation with contrast-enhanced ultrasound. Eur J Radiol 51:S19–S23
Song I, Rhim H, Lim HK et al (2009) Percutaneous radiofrequency ablation of hepatocellular carcinoma abutting the diaphragm and gastrointestinal tracts with the use of artificial ascites: safety and technical efficacy in 143 patients. Eur Radiol 19:2630–2640
Sorensen SM, Mortensen FV, Nielsen DT (2007) Radiofrequency ablation of colorectal liver metastases: long-term survival. Acta Radiol 48:253–258
Stang A, Fischbach R, Teichmann W et al (2009) A systematic review on the clinical benefit and role of radiofrequency ablation as treatment of colorectal liver metastases. Eur J Cancer 45:1748–1756
Tacke J (2003) Percutaneous radiofrequency ablation – clinical indications and results. Rofo 175:156–168
Tacke J, Mahnken A, Roggan A et al (2004) Multipolar radiofrequency ablation: first clinical results. Rofo 176:324–329
Takahashi S, Kudo M, Chung H et al (2007) Initial treatment response is essential to improve survival in patients with hepatocellular carcinoma who underwent curative radiofrequency ablation therapy. Oncology 72(Suppl 1):98–103
Tateishi R, Shiina S, Teratani T et al (2005) Percutaneous radiofrequency ablation for hepatocellular carcinoma. Cancer 103:1201–1209
Vauthey JN, Dixon E, Abdalla EK et al (2010) Pretreatment assessment of hepatocellular carcinoma: expert consensus statement. HPB 12:289–299
Veit P, Antoch G, Stergar H et al (2006) Detection of residual tumor after radiofrequency ablation of liver metastasis with dual-modality PET/CT: initial results. Eur Radiol 16:80–87
Vilana R, Bianchi L, Varela M et al (2006) Is microbubble-enhanced ultrasonography sufficient for assessment of response to percutaneous treatment in patients with early hepatocellular carcinoma? Eur Radiol 16:2454–2462
Willat JM, Hussain HK, Adusumilli S et al (2008) MR imaging of hepatocellular carcinoma in the cirrhotic liver: challenges and controversies. Radiology 247:311–330
Wong SL, Mangu PB, Choti MA et al (2010) American Society of Clinical Oncology 2009 evidence review on radiofrequency ablation of hepatic metastases from colorectal cancer. J Clin Oncol 28:493–508

RF Ablation of Lung Tumors

Akeboshi M, Yamakado K, Nakatsuka A et al (2004) Percutaneous radiofrequency ablation of lung neoplasms: initial therapeutic response. J Vasc Interv Radiol 15:463–470

Ambrogi MC, Lucchi M, Dini P et al (2006) Percutaneous radiofrequency of lung tumors: results in the mid-term. Eur J Cardiothorac Surg 30:177–183

Asamura H, Goya T, Koshiishi Y et al (2008) A Japanese Lung Cancer Registry study: prognosis of 13,010 resected lung cancers. J Thorac Oncol 3:46–52

Beland MD, Wasser EJ, Mayo-Smith WW et al (2010) Primary non – small cell lung cancer: review of frequency, location, and time of recurrence after radiofrequency ablation. Radiology 254:301–307

Belfiore G, Moggio G, Tedeschi E et al (2004) CT-guided radiofrequency ablation: a potential complementary therapy for patients with unresectable primary lung cancer – a preliminary report of 33 patients. Am J Roentgenol 183:1003–1011

Bojarski JD, Dupuy DE, Mayo-Smith WW (2005) CT imaging findings of pulmonary neoplasms after treatment with radiofrequency ablation: results in 32 tumors. Am J Roentgenol 185:466–471

Chua TC, Sarkar A, Saxena A et al (2010) Long-term outcome of image-guided percutaneous radiofrequency ablation of lung metastases: an open-labeled prospective trial of 148 patients. Ann Oncol 21:2017–2022

Das M, Abdelmaksoud MH, Loo BW Jr et al (2010) Alternatives to surgery for early stage non-small cell lung cancer-ready for prime time? Curr Treat Options Oncol 11:24–35

De Baère T (2011) Lung tumor radiofrequency ablation: where do we stand? Cardiovasc Intervent Radiol 34:241–251

De Baère T, Palussière J, Aupérin A et al (2006) Midterm local efficacy and survival after radiofrequency ablation of lung tumors with minimum follow-up of 1 year: prospective evaluation. Radiology 240:587–596

Dupuy DE, Zagoria RJ, Akerley W et al (2000) Percutaneous radiofrequency ablation of malignancies in the lung. Am J Roentgenol 175:1263–1266

Dupuy DE, DiPetrillo T, Gandhi S et al (2006) Radiofrequency ablation followed by conventional radiotherapy for medically inoperable stage I non-small cell lung cancer. Chest 129:738–745

Fernando HC, De Hoyos A, Landreneau RJ et al (2005) Radiofrequency ablation for the treatment of non-small cell lung cancer in marginal surgical candidates. J Thorac Cardiovasc Surg 129:639–644

Gillams AR, Lees WR (2008) Radiofrequency ablation of lung metastases: factors influencing success. Eur Radiol 16:672–677

Goldberg SN, Grassi CJ, Cardella JF et al (2005) Image-guided tumor ablation: standardization of terminology and reporting criteria. Radiology 235:728–739

Huang L, Han Y, Zhao J et al (2011) Is radiofrequency thermal ablation a safe and effective procedure in the treatment of pulmonary malignancies? Eur J Cardiothorac Surg 39:348–351

Jemal A, Siegel R, Ward E et al (2010) Cancer statistics 2010. CA Cancer J Clin 60:277–300

Jin GY, Lee JM, Lee YC et al (2004) Primary and secondary lung malignancies treated with percutaneous radiofrequency ablation: evaluation with follow-up helical CT. Am J Roentgenol 183:1013–1020

Kang S, Luo R, Liao W et al (2004) Single group study to evaluate the feasibility and complications of radiofrequency ablation and usefulness of post treatment positron emission tomography in lung tumours. World J Surg Oncol 2:30

Lee JM, Jin GY, Goldberg SN et al (2004) Percutaneous radiofrequency ablation for inoperable non-small cell lung cancer and metastases: preliminary report. Radiology 230:125–134

Mountain CF (1997) Revisions in the international system for staging lung cancer. Chest 111:1710–1717

Rossi S, Dore R, Cascina A et al (2006) Percutaneous computed tomography-guided radiofrequency thermal ablation of small unresectable lung tumours. Eur Respir J 27:556–563

Sano Y, Kanazawa S, Gobara H et al (2007) Feasibility of percutaneous radiofrequency ablation for intrathoracic malignancies: a large single-center experience. Cancer 109:1397–1405

Simon CJ, Dupuy DE, DiPetrillo TA et al (2007) Pulmonary radiofrequency ablation: long-term safety and efficacy in 153 patients. Radiology 243:268–275

Steinke K, King J, Glenn D et al (2003) Pulmonary hemorrhage during percutaneous radiofrequency ablation: a more frequent complication than assumed? Interact Cardiovasc Thorac Surg 2:462–465

Suh RD, Wallace AB, Sheehan RE et al (2003) Unresectable pulmonary malignancies: CT-guided percutaneous radiofrequency ablation – preliminary results. Radiology 229:821–829

Van Rens M, de la Riviere AB, Elbers HJR et al (2000) Prognostic assessment of 2,361 patients who underwent pulmonary resection for non-small cell lung cancer, stage I, II, and IIIA. Chest 117:374–379

Van Sonnenberg E, Shankar S, Morrison PR et al (2005) Radiofrequency ablation of thoracic lesions: part 2, initial clinical experience – technical and multidisciplinary considerations in 30 patients. Am J Roentgenol 184:381–390

Yamakado K, Hase S, Matsuoka T et al (2007) Radiofrequency ablation for the treatment of unresectable lung metastases in patients with colorectal cancer: a multicenter study in Japan. J Vasc Interv Radiol 18:393–398

Yan TD, King J, Ebrahimi A et al (2007) Hepatectomy and lung radiofrequency ablation for hepatic and subsequent pulmonary metastases from colorectal carcinoma. J Surg Oncol 96:367–373

Further Reading

Kelekis AD, Thanos L, Mylona S et al (2006) Percutaneous radiofrequency ablation of lung tumors with expandable needle electrodes: current status. Eur Radiol 16:2471–2482

Lencioni R, Crocetti L, Cioni R et al (2004) Radiofrequency ablation of lung malignancies: where do we stand? Cardiovasc Intervent Radiol 27:581–590

Morrison PR, van Sonnenberg E, Shankar S et al (2005) Radiofrequency ablation of thoracic lesions: part 1, experiments in the normal porcine thorax. Am J Roentgenol 184:375–380

Nguyen CL, Scott WJ, Young NA et al (2005) Radiofrequency ablation of primary lung cancer: results from an ablate and resect pilot study. Chest 128:3507–3511

Okuma T, Matsuoka T, Yamamoto A et al (2007) Factors contributing to cavitation after CT-guided percutaneous radiofrequency ablation of lung tumors. J Vasc Interv Radiol 18:399–404

Steinke K, Sewell PE, Dupuy D et al (2004) Pulmonary radiofrequency ablation – an international study survey. Anticancer Res 24:339–343

Tominaga J, Miyachi H, Takase K et al (2005) Time-related changes in computed tomographic appearance and pathologic findings after radiofrequency ablation of the rabbit lung: preliminary experimental study. J Vasc Interv Radiol 16:1719–1726

Yamakado K, Akeboshi M, Nakatsuka A et al (2005) Tumor seeding following lung radiofrequency ablation: a case report. Cardiovasc Intervent Radiol 28:530–532

Yan TD, King J, Sjarif A et al (2006a) Percutaneous radiofrequency ablation of pulmonary metastases from colorectal carcinoma: prognostic determinants for survival. Ann Surg Oncol 13:1529–1537

Yan TD, King J, Sjarif A et al (2006b) Learning curve for percutaneous radiofrequency ablation of pulmonary metastases from colorectal carcinoma: a prospective study of 70 consecutive cases. Ann Surg Oncol 13:1588–1595

Renal Radiofrequency Ablation

Bosniak MA (1986) The current radiological approach to renal cysts. Radiology 158:1–10

Breen DJ, Rutherford EE, Stedman B et al (2007) Management of renal tumors by image-guided radiofrequency ablation: experience in 105 tumors. Cardiovasc Intervent Radiol 30:936–942

Brown SD, Vansonnenberg E, Morrison PR et al (2005) CT-guided radiofrequency ablation of pediatric Wilms tumor in a solitary kidney. Pediatr Radiol 35:923–928

Crowley JD, Shelton J, Iverson AJ et al (2000) Laparoscopic and computed tomography-guided percutaneous radiofrequency ablation of renal tissue: acute and chronic effects in an animal model. Urology 57:976–980

Fergany AF, Hafez KS, Novick AC (2000) Long-term results of nephron-sparing surgery for localized renal cell carcinoma: 10-year follow up. J Urol 163: 442–445

Gervais DA, McGovern FJ, Arellano RS et al (2003) Renal cell carcinoma: clinical experience and technical success with radio-frequency ablation of 42 tumors. Radiology 226:417–424

Gervais DA, McGovern FJ, Arellano RS et al (2005) Radiofrequency ablation of renal cell carcinoma: part 1, indications, results, and role in patient management over a 6-year period and ablation of 100 tumors. Am J Roentgenol 185:64–71

Herring JC, Enquist EG, Chernoff A et al (2001) Parenchymal sparing surgery in patients with hereditary renal cell carcinoma: 10–year experience. J Urol 165:777–781

Homma Y, Kawabe K, Kitamura T et al (1995) Increased incidental detection and reduced mortality in renal cancer – recent retrospective analysis at eight institutions. Int J Urol 2:77–80

Hsu TH, Fidler ME, Gill IS (2000) Radiofrequency ablation of the kidney: acute and chronic histology in porcine model. Urology 56:872–875

Jacomides L, Ogan K, Watumull L et al (2003) Laparoscopic application of radio frequency energy enables in situ renal tumor ablation and partial nephrectomy. J Urol 169:49–53

Joniau S, Tsivian M, Gontero P (2011) Radiofrequency ablation for the treatment of small renal masses: safety and oncologic efficacy. Minerva Urol Nefrol 63:227–236

Klinke R, Silbernagel S (2003) Lehrbuch der Physiologie. Thieme, Stuttgart

Lee JM, Kim SW, Chung GH et al (2003) Open radiofrequency thermal ablation of renal VX2 tumors in a rabbit model using a cooled-tip electrode: feasibility, safety, and effectiveness. Eur Radiol 13:1324–1332

Lotan Y, Cadeddu JA (2005) A cost comparison of nephron-sparing surgical techniques for renal tumour. BJU Int 95:1039–1042

Mahnken A, Rohde D, Brkovic D et al (2005) Percutaneous radiofrequency ablation of renal cell carcinoma: preliminary results. Acta Radiol 46:208–214

Mahnken AH, Penzkofer T, Bruners P et al (2009) Interventional management of a renal cell carcinoma by radiofrequency ablation with tagging and cooling. Korean J Radiol 10:523–526

Margulis V, Matsumoto ED, Taylor G et al (2005) Retrograde renal cooling during radiofrequency ablation to protect from renal collecting system injury. J Urol 174:350–352

Matsumoto ED, Watumull L, Johnson DB et al (2004) The radiographic evolution of radio frequency ablated renal tumors. J Urol 172:45–48

Matsumoto ED, Johnson DB, Ogan K et al (2005) Short-term efficacy of temperature-based radiofrequency ablation of small renal tumors. Urology 65:877–881

Mayo-Smith WW, Dupuy DE, Parikh PM et al (2003) Imaging-guided percutaneous radiofrequency ablation of solid renal masses: techniques and outcomes of 38 treatment sessions in 32 consecutive patients. Am J Roentgenol 180:1503–1508

McDougal WS, Gervais DA, McGovern FJ et al (2005) Long-term follow-up of patients with renal cell carcinoma treated with radiofrequency ablation with curative intent. J Urol 174:61–63

Merkle EM, Nour SG, Lewin JS (2005) MR imaging follow-up after percutaneous radiofrequency ablation of

renal cell carcinoma: findings in 18 patients during first 6 months. Radiology 235:1065–1071
Neeman Z, Sarin S, Coleman J, Fojo T et al (2005) Radiofrequency ablation for tumor-related massive hematuria. J Vasc Interv Radiol 16:417–421
Pandharipande PV, Gervais DA, Mueller PR et al (2008) Radiofrequency ablation versus nephron-sparing surgery for small unilateral renal cell carcinoma: cost-effectiveness analysis. Radiology 248:169–178
Pantuck AJ, Zisman A, Belldegrun AS (2001) The changing natural history of renal cell carcinoma. J Urol 166:297–301
Park S, Anderson JK, Matsumoto ED et al (2006) Radiofrequency ablation of renal tumors: intermediate-term results. J Endourol 20:569–573
Rendon RA, Kachura JR, Sweet JM et al (2002) The uncertainty of radiofrequency treatment of renal cell carcinoma: findings at immediate and delayed nephrectomy. J Urol 167:1587–1592
Rhim H, Dodd GD, Chintapalli KN et al (2004) Radiofrequency thermal ablation of abdominal tumors: lessons learned from complications. Radiographics 24:41–52
Siegel R, Naishadham D, Jemal A (2012) Cancer statistics, 2012. CA Cancer J Clin 62:10–29
Schultze D, Morris CS, Bhave AD et al (2003) Radiofrequency ablation of renal transitional cell carcinoma with protective cold saline infusion. J Vasc Interv Radiol 14:489–492
Sowery RD, Siemens DR (2004) Growth characteristics of renal cortical tumors in patients managed by watchful waiting. Can J Urol 11:2407–2410
Takaki H, Yamakado K, Soga N et al (2010) Midterm results of radiofrequency ablation versus nephrectomy for T1a renal cell carcinoma. Jpn J Radiol 28: 460–468
Tracy CR, Raman JD, Donnally C et al (2010) Durable oncologic outcomes after radiofrequency ablation: experience from treating 243 small renal masses over 7.5 years. Cancer 116:3135–3142
Uzzo RG, Novick AC (2001) Nephron sparing surgery for renal tumors: indications techniques and outcomes. J Urol 166:6–18
Zagoria RJ, Pettus JA, Rogers M et al (2011) Long-term outcomes after percutaneous radiofrequency ablation for renal cell carcinoma. Urology 77:1393–1397
Zlotta AR, Wildschutz T, Raviv G et al (1997) Radiofrequency interstitial tumor ablation (RITA) is a possible new modality for treatment of renal cancer: ex vivo and in vivo experience. J Endourol 11:251–258

RF Ablation Miscellaneous

Alvarez L, Perez-Higueras A, Quinones D et al (2003) Vertebroplasty in the treatment of vertebral tumors: postprocedural outcome and quality of life. Eur Spine J 12:356–360
Arima K, Yamakado K, Suzuki R et al (2007) Image-guided radiofrequency ablation for adrenocortical adenoma with Cushing syndrome: outcomes after mean follow-up of 33 months. Urology 70:407–411
Belfiore G, Tedeschi E, Ronza FM et al (2009) CT-guided radiofrequency ablation in the treatment of recurrent rectal cancer. Am J Roentgenol 192:137–141
Burak WE Jr, Agnese DM, Povoski SP et al (2003) Radiofrequency ablation of invasive breast carcinoma followed by delayed surgical excision. Cancer 98:1369–1376
Callstrom MR, Charboneau JW, Goetz MP et al (2006) Image-guided ablation of painful metastatic bone tumors: a new and effective approach to a difficult problem. Skeletal Radiol 35:1–15
Calmels V, Vallee JN, Rose M et al (2007) Osteoblastic and mixed spinal metastases: evaluation of the analgesic efficacy of percutaneous vertebroplasty. AJNR Am J Neuroradiol 28:570–574
Casadei R, Ricci C, Pezzilli R et al (2010) A prospective study on radiofrequency ablation locally advanced pancreatic cancer. Hepatobiliary Pancreat Dis Int 9:306–311
Chini E, Brown M, Farrell M et al (2004) Hypertensive crisis in a patient undergoing percutaneous radiofrequency ablation of an adrenal mass under general anesthesia. Anesth Analg 99:1867–1869
Coldwell DM, Sewell PE (2005) The expanding role of interventional radiology in the supportive care of the oncology patient: from diagnosis to therapy. Semin Oncol 32:169–173
Earashi M, Noguchi M, Motoyoshi A et al (2007) Radiofrequency ablation therapy for small breast cancer followed by immediate surgical resection or delayed mammotome excision. Breast Cancer 14:39–47
Fornage BD, Sneige N, Ross MI et al (2004) Small (< or = 2-cm) breast cancer treated with US-guided radiofrequency ablation: feasibility study. Radiology 231:215–224
Fourney DR, Schomer DF, Nader R et al (2003) Percutaneous vertebroplasty and kyphoplasty for painful vertebral body fractures in cancer patients. J Neurosurg 98(1 Suppl):21–30
Gangi A, Basile A, Buy X et al (2005) Radiofrequency and laser ablation of spinal lesions. Semin Ultrasound CT MR 26:89–97
Girelli R, Frigerio I, Salvia R et al (2010) Feasibility and safety of radiofrequency ablation for locally advanced pancreatic cancer. Br J Surg 97:220–225
Goetz MP, Callstrom MR, Charboneau JW et al (2004) Percutaneous image-guided radiofrequency ablation of painful metastases involving bone: a multicenter study. J Clin Oncol 22:300–306
Hanazaki M, Taga N, Nakatsuka H et al (2006) Anesthetic management of radiofrequency ablation of mediastinal metastatic lymph nodes adjacent to the trachea. Anesth Analg 103:1041–1042
Hayashi AH, Silver SF, van der Westhuizen NG et al (2003) Treatment of invasive breast carcinoma with

ultrasound-guided radiofrequency ablation. Am J Surg 185:429–435
Hiraki T, Yasui K, Mimura H et al (2005) Radiofrequency ablation of metastatic mediastinal lymph nodes during cooling and temperature monitoring of the tracheal mucosa to prevent thermal tracheal damage: initial experience. Radiology 237:1068–1074
Hoffmann RT, Jakobs TF, Trumm C et al (2008) Radiofrequency ablation in combination with osteoplasty for the treatment of bone malignancies. J Vasc Interv Radiol 19:419–425
Hung WK, Mak KL, Ying M et al (2011) Radiofrequency ablation of breast cancer: a comparative study of two needle designs. Breast Cancer 18:124–128
Imoto S, Wada N, Sakemura N et al (2009) Feasibility study on radiofrequency ablation followed by partial mastectomy for stage I breast cancer patients. Breast 18:130–134
Izzo F, Thomas R, Delrio P et al (2001) Radiofrequency ablation in patients with primary breast carcinoma: a pilot study in 26 patients. Cancer 92:2036–2044
Jagas M, Patrzyk R, Zwolinski J et al (2005) Vertebroplasty with methacrylate bone cement and radiotherapy in the treatment of spinal metastases with epidural spinal cord compression. Preliminary report. Ortop Traumatol Rehabil 7:491–498
Jang JS, Lee SH (2005) Efficacy of percutaneous vertebroplasty combined with radiotherapy in osteolytic metastatic spinal tumors. J Neurosurg Spine 2:243–248
Jeffrey SS, Birdwell RL, Ikeda DM et al (1999) Radiofrequency ablation of breast cancer: first report of an emerging technology. Arch Surg 134:1064–1068
Khatri VP, McGahan JP, Ramsamooj R et al (2007) A phase II trial of image-guided radiofrequency ablation of small invasive breast carcinomas: use of saline-cooled tip electrode. Ann Surg Oncol 14:1644–1652
Keil S, Bruners P, Brehmer B et al (2008) Percutaneous radiofrequency ablation for treatment of recurrent retroperitoneal liposarcoma. Cardiovasc Intervent Radiol 31(Suppl 2):S213–S216
Kelekis A, Lovblad KO, Mehdizade A et al (2005) Pelvic osteoplasty in osteolytic metastases: technical approach under fluoroscopic guidance and early clinical results. J Vasc Interv Radiol 16:81–88
Kinoshita T, Iwamoto E, Tsuda H et al (2011) Radiofrequency ablation as local therapy for early breast carcinomas. Breast Cancer 18:10–17
Lane MD, Le HB, Lee S et al (2011) Combination radiofrequency ablation and cementoplasty for palliative treatment of painful neoplastic bone metastasis: experience with 53 treated lesions in 36 patients. Skeletal Radiol 40:25–32
Lefevre JH, Parc Y, Lewin M et al (2008) Radiofrequency ablation for recurrent pelvic cancer. Colorectal Dis 2008(10):781–784
Limmer S, Huppert PE, Juette V et al (2009) Radiofrequency ablation of solitary pancreatic insulinoma in a patient with episodes of severe hypoglycemia. Eur J Gastroenterol Hepatol 21:1097–1101
Locklin JK, Mannes A, Berger A et al (2004) Palliation of soft tissue cancer pain with radiofrequency ablation. J Support Oncol 2:439–445
Manenti G, Bolacchi F, Perretta T et al (2009) Small breast cancers: in vivo percutaneous US-guided radiofrequency ablation with dedicated cool-tip radiofrequency system. Radiology 251:339–346
Marchal F, Brunaud L, Bazin C et al (2006) Radiofrequency ablation in palliative supportive care: early clinical experience. Oncol Rep 15:495–499
Matsui Y, Nakagawa A, Kamiyama Y et al (2000) Selective thermocoagulation of unresectable pancreatic cancers by using radiofrequency capacitive heating. Pancreas 20:14–20
Medina-Franco H, Soto-Germes S, Ulloa-Gómez JL et al (2008) Radiofrequency ablation of invasive breast carcinomas: a phase II trial. Ann Surg Oncol 15: 1689–1695
Mont'Alverne F, Vallee JN, Cormier E et al (2005) Percutaneous vertebroplasty for metastatic involvement of the axis. AJNR Am J Neuroradiol 26:1641–1645
Nashida Y, Yamakado K, Kumamoto T et al (2007) Radiofrequency ablation used for the treatment of frequently recurrent rhabdomyosarcoma in the masticator space in a 10-year-old girl. J Pediatr Hematol Oncol 29:640–642
Noguchi M, Earashi M, Fujii H et al (2006) Radiofrequency ablation of small breast cancer followed by surgical resection. J Surg Oncol 93:120–128
Oura S, Tamaki T, Hirai I et al (2007) Radiofrequency ablation therapy in patients with breast cancers two centimeters or less in size. Breast Cancer 14:48–54
Rosenthal DI (2006) Radiofrequency treatment. Orthop Clin North Am 37:475–484
Simon CJ, Dupuy DE (2006) Percutaneous minimally invasive therapies in the treatment of bone tumors: thermal ablation. Semin Musculoskelet Radiol 10:137–144
Spiliotis JD, Datsis AC, Michalopoulos NV et al (2007) Radiofrequency ablation combined with palliative surgery may prolong survival of patients with advanced cancer of the pancreas. Langenbecks Arch Surg 392:55–60
Susini T, Nori J, Olivieri S et al (2007) Radiofrequency ablation for minimally invasive treatment of breast carcinoma. A pilot study in elderly inoperable patients. Gynecol Oncol 104:304–310
Thanos L, Mylona S, Galani P et al (2008) Radiofrequency ablation of osseous metastases for the palliation of pain. Skeletal Radiol 37:189–194
Toyota N, Naito A, Kakizawa H et al (2005) Radiofrequency ablation therapy combined with cementoplasty for painful bone metastases: initial experience. Cardiovasc Intervent Radiol 28:578–583
Tsoumakidou G, Buy X, Zickler P et al (2010) Life-threatening complication during percutaneous ablation of adrenal gland metastasis: takotsubo syndrome. Cardiovasc Intervent Radiol 33:646–649
Venkatesan A, Locklin J, Lai E et al (2009) Radiofrequency ablation of metastatic pheochromocytoma. J Vasc Interv Radiol 20:1483–1490

Weill A, Chiras J, Simon JM et al (1996) Spinal metastases: indications for and results of percutaneous injection of acrylic surgical cement. Radiology 199:241–247
Wolf FJ, Dupuy DE, Machan JT et al (2012) Adrenal neoplasms: effectiveness and safety of CT-guided ablation of 23 tumors in 22 patients. Eur J Radiol 81:1717–1723
Wu PH, Pan CC, Huang ZL et al (2010) Percutaneous radiofrequency ablation approach through the spleen: initial case report for pancreatic tail gastrinoma. Chin J Cancer 29:836–841

Laser Ablation: Liver and Beyond

Amin Z, Bown SG, Lees WR (1993) Local treatment of colorectal liver metastases: a comparison of interstitial laser photocoagulation (ILP) and percutaneous alcohol injection (PAI). Clin Radiol 48:166–171
Castren Persons M, Lipasti J, Puolakkainen P et al (1992) Laser-induced hyperthermia: comparison of two different methods. Lasers Surg Med 12:665–668
Gallagher DJ, Capanu M, Raggio G et al (2007) Hepatic arterial infusion plus systemic irinotecan in patients with unresectable hepatic metastases from colorectal cancer previously treated with systemic oxaliplatin: a retrospective analysis. Ann Oncol 18:1995–1999
Harned RK 2nd, Chezmar JL, Nelson RC (1994) Recurrent tumor after resection of hepatic metastases from colorectal carcinoma: location and time of discovery as determined by CT. Am J Roentgenol 163:93–97
Hughes KS, Rosenstein RB, Songhorabodi S et al (1988) Resection of the liver for colorectal carcinoma metastases. A multi-institutional study of long-term survivors. Dis Colon Rectum 31:1–4
Jolesz FA, Bleier AR, Jakab P et al (1988) MR imaging of laser-tissue interactions. Radiology 168:249–253
Le Bihan D, Delannoy J, Levin RL (1989) Temperature mapping with MR imaging of molecular diffusion: application to hyperthermia. Radiology 171:853–857
Mack M, Vogl T (2004) MR-guided ablation of head and neck tumors. Neuroimaging Clin N Am 14:853–859
Mack M, Straub R, Eichler K et al (2004) Breast cancer metastases in liver: laser-induced interstitial thermotherapy – local tumor control rate and survival data. Radiology 233:400–409
Masters A, Steger AC, Lees WR et al (1992) Interstitial laser hyperthermia: a new approach for treating liver metastases. Br J Cancer 66:518–522
Matsumoto R, Selig AM, Colucci VM et al (1992) Interstitial Nd:YAG laser ablation in normal rabbit liver: trial to maximize the size of laser-induced lesions. Lasers Surg Med 12:650–658
Mehta NN, Ravikumar R, Coldham CA et al (2008) Effect of preoperative chemotherapy on liver resection for colorectal liver metastases. Eur J Surg Oncol 34:782–786
Meister D, Hubner F, Mack M et al (2007) MR-Thermometrie bei 1,5 Tesla zur thermischen Ablation mittels laserinduzierter Thermotherapie. Rofo 179:497–505
Mentha G, Majno P, Terraz S et al (2007) Treatment strategies for the management of advanced colorectal liver metastases detected synchronously with the primary tumour. Eur J Surg Oncol 33(Suppl 2):S76–S83
Min BS, Kim NK, Ahn JB et al (2007) Cetuximab in combination with 5-fluorouracil, leucovorin and irinotecan as a neoadjuvant chemotherapy in patients with initially unresectable colorectal liver metastases. Onkologie 30:637–643
Nordlinger B, Guiguet M, Vaillant JC et al (1996) Surgical resection of colorectal carcinoma metastases to the liver. A prognostic scoring system to improve case selection, based on 1568 patients. Association Francaise de Chirurgie. Cancer 77:1254–1262
Scheele J, Stangl R, Altendorf-Hofmann A et al (1991) Indicators of prognosis after hepatic resection for colorectal secondaries. Surgery 110:13–29
Scheele J, Altendorf-Hofmann A, Stangl R et al (1996) Surgical resection of colorectal liver metastases: gold standard for solitary and completely resectable lesions. Swiss Surg Suppl 4:4–17
Tan MC, Linehan DC, Hawkins WG et al (2007) Chemotherapy-induced normalization of FDG uptake by colorectal liver metastases does not usually indicate complete pathologic response. J Gastrointest Surg 11:1112–1119
Vogl TJ, Mack MG, Scholz WR et al (1996) MR imaging guided laser-induced thermotherapy. Min Invas Ther & Allied Technol 5:243–248
Vogl TJ, Mack MG, Hirsch HH et al (1997a) In-vitro evaluation of MR-thermometry for laser-induced thermotherapy. Rofo 167:638–644
Vogl TJ, Mack MG, Staub R et al (1997b) Internallly cooled laser applicator system for MR-guided laser induced thermotherapy. Radiology 205(P):177
Vogl T, Fieguth H, Eichler K et al (2004a) Laserinduzierte Thermotherapie von Lungenmetastasen und primären Lungentumoren. Radiologe 44:693–699
Vogl T, Straub R, Eichler K et al (2004b) Colorectal carcinoma metastases in liver: laser-induced interstitial thermotherapy – local tumor control rate and survival data. Radiology 230:450–458
Ychou M, Viret F, Kramar A et al (2008) Tritherapy with fluorouracil/leucovorin, irinotecan and oxaliplatin (FOLFIRINOX): a phase II study in colorectal cancer patients with non-resectable liver metastases. Cancer Chemother Pharmacol 62:195–201
Zorzi D, Laurent A, Pawlik TM et al (2007) Chemotherapy-associated hepatotoxicity and surgery for colorectal liver metastases. Br J Surg 94:274–286

Laser Ablation: Lung

Baron O, Hamy A et al (1998) Surgical treatment of pulmonary metastasis of colorectal cancer. Prognostic survival factors. Presse Med 27(18):885–888
Davidson RS, Nwogu CE et al (2001) The surgical management of pulmonary metastasis: current concepts. Surg Oncol 10(1–2):35–42

Friedel G, Pastorino U et al (1999) Resection of lung metastases: long-term results and prognostic analysis based on 5206 cases – the international registry of lung metastases. Zentralbl Chir 124(2):96–103

Ghaye B, Bruyere PJ et al (2006) Nonfatal systemic air embolism during percutaneous radiofrequency ablation of a pulmonary metastasis. Am J Roentgenol 187(3):W327–W328

Goya T, Miyazawa N et al (1989) Surgical resection of pulmonary metastases from colorectal cancer. 10-year follow-up. Cancer 64(7):1418–1421

Grieco CA, Simon CJ et al (2006) Percutaneous image-guided thermal ablation and radiation therapy: outcomes of combined treatment for 41 patients with inoperable stage I/II non-small-cell lung cancer. J Vasc Interv Radiol 17(7):1117–1124

Hendriks JM, Romijn S et al (2001) Long-term results of surgical resection of lung metastases. Acta Chir Belg 101(6):267–272

Hiraki T, Gobara H et al (2007a) Percutaneous radiofrequency ablation for clinical stage I non-small cell lung cancer: results in 20 nonsurgical candidates. J Thorac Cardiovasc Surg 134(5):1306–1312

Hiraki T, Fujiwara H et al (2007b) Nonfatal systemic air embolism complicating percutaneous ct-guided transthoracic needle biopsy: four cases from a single institution. Chest 132(2):684–690

Hosten N, Stier A et al (2003) Laser-induced thermotherapy (litt) of lung metastases: description of a miniaturized applicator, optimization, and initial treatment of patients. Rofo 175(3):393–400

Inoue M, Kotake Y et al (2000) Surgery for pulmonary metastases from colorectal carcinoma. Ann Thorac Surg 70(2):380–383

Knappe V, Mols A (2004) Laser therapy of the lung: biophysical background. Radiologe 44(7):677–683

Landreneau RJ (1996) Vats anatomic lung resections. The Hong Kong experience. Chest 109(1):1–2

Lencioni R, Crocetti L et al (2008) Response to radiofrequency ablation of pulmonary tumours: a prospective, intention-to-treat, multicentre clinical trial (the RAPTURE study). Lancet Oncol 9(7):621–628

Martini N, Bains MS et al (1995) Incidence of local recurrence and second primary tumors in resected stage I lung cancer. J Thorac Cardiovasc Surg 109(1): 120–129

McCormack PM, Burt ME et al (1992) Lung resection for colorectal metastases. 10-year results. Arch Surg 127(12):1403–1406

McCormack PM, Bains MS et al (1996) Role of video-assisted thoracic surgery in the treatment of pulmonary metastases: results of a prospective trial. Ann Thorac Surg 62(1):213–216

Okumura S, Kondo H et al (1996) Pulmonary resection for metastatic colorectal cancer: experiences with 159 patients. J Thorac Cardiovasc Surg 112(4):867–874

Omary RA, Bettmann MA et al (2003) Quality improvement guidelines for the reporting and archiving of interventional radiology procedures. J Vasc Interv Radiol 14(9 Pt 2):S293–S295

Pages Navarrete C, Ruiz Zafra J et al (2000) Surgical treatment of pulmonary metastasis: survival study. Arch Bronconeumol 36(10):569–573

Pastorino U, McCormack PM et al (1998) A new staging proposal for pulmonary metastases. The results of analysis of 5206 cases of resected pulmonary metastases. Chest Surg Clin N Am 8(1):197–202

Penna C, Nordlinger B (2002) Colorectal metastasis (liver and lung). Surg Clin North Am 82(5):1075–1090

Pfannschmidt J, Hoffmann H et al (2002) Prognostic factors for survival after pulmonary resection of metastatic renal cell carcinoma. Ann Thorac Surg 74(5):1653–1657

Rena O, Casadio C et al (2002) Pulmonary resection for metastases from colorectal cancer: factors influencing prognosis. Twenty-year experience. Eur J Cardiothorac Surg 21(5):906–912

Roggan A, Mesecke-von Rheinbaben I et al (1997) Applicator development and irradiation planning in laser-induced thermotherapy (LITT). Biomed Tech (Berl) 42(Suppl):332–333

Rosenberg C, Puls R et al (2009) Laser ablation of metastatic lesions of the lung: long-term outcome. Am J Roentgenol 92(3):785–792

Shirouzu K, Isomoto H et al (1995) Surgical treatment for patients with pulmonary metastases after resection of primary colorectal carcinoma. Cancer 76(3):393–398

Simon CJ, Dupuy DE et al (2007) Pulmonary radiofrequency ablation: long-term safety and efficacy in 153 patients. Radiology 243(1):268–275

Steinke K, Sewell PE et al (2004) Pulmonary radiofrequency ablation – an international study survey. Anticancer Res 24(1):339–343

Thanos L, Mylona S et al (2006) Percutaneous radiofrequency thermal ablation of primary and metastatic lung tumors. Eur J Cardiothorac Surg 30(5):797–800

VanSonnenberg E, Shankar S et al (2005) Radiofrequency ablation of thoracic lesions: part 2, initial clinical experience – technical and multidisciplinary considerations in 30 patients. Am J Roentgenol 184(2):381–390

Vogelsang H, Haas S et al (2004) Factors influencing survival after resection of pulmonary metastases from colorectal cancer. Br J Surg 91(8):1066–1071

Vogl TJ, Mack M et al (2000) Percutaneous interstitial thermotherapy of malignant liver tumors. Rofo 172(1):12–22

Vogl TJ, Straub R et al (2004) Percutaneous thermoablation of pulmonary metastases. Experience with the application of laser-induced thermotherapy (LITT) and radiofrequency ablation (RFA), and a literature review. Rofo 176(11):1658–1666

Vogl TJ, Naguib NN et al (2010) Radiofrequency, microwave and laser ablation of pulmonary neoplasms: clinical studies and technical considerations – review article. Eur J Radiol 77(2):346–357

Watanabe I, Arai T et al (2003) Prognostic factors in resection of pulmonary metastasis from colorectal cancer. Br J Surg 90(11):1436–1440

Weigel C, Kirsch M et al (2004) Percutaneous laser-induced thermotherapy of lung metastases: experience gained during 4 years. Radiologe 44(7):700–707

Weigel C, Rosenberg C et al (2006) Laser ablation of lung metastases: results according to diameter and location. Eur Radiol 16(8):1769–1778
Yamakado K, Nakatsuka A et al (2004) Combination therapy with radiofrequency ablation and transcatheter chemoembolization for the treatment of hepatocellular carcinoma: short-term recurrences and survival. Oncol Rep 11(1):105–109
Yamakado K, Hase S et al (2007) Radiofrequency ablation for the treatment of unresectable lung metastases in patients with colorectal cancer: a multicenter study in Japan. J Vasc Interv Radiol 18(3):393–398
Yamamoto A, Matsuoka T et al (2004) Assessment of cerebral microembolism during percutaneous radiofrequency ablation of lung tumors using diffusion-weighted imaging. Am J Roentgenol 183(6):1785–1789
Yan TD, King J et al (2006) Percutaneous radiofrequency ablation of pulmonary metastases from colorectal carcinoma: prognostic determinants for survival. Ann Surg Oncol 13(11):1529–1537

Introduction to Microwave Ablation

Clark PE, Woodruff RD, Zagoria RJ et al (2007) Microwave ablation of renal parenchymal tumors before nephrectomy: phase I study. Am J Roentgenol 188:1212–1214
Dupuy DE, Goldberg SN (2001) Image-guided radiofrequency tumor ablation: challenges and opportunities – part II. J Vasc Interv Radiol 12:1135–1148
Goldberg SN, Gazelle GS, Mueller PR (2000) Thermal ablation therapy for focal malignancy: a unified approach to underlying principles, techniques, and diagnostic imaging guidance. Am J Roentgenol 174:323–331
Goldberg SN, Grassi CJ, Cardella JF et al (2009) Image-guided tumor ablation: standardization of terminology and reporting criteria. J Vasc Interv Radiol 20:S377–S390
Izzo F (2003) Other thermal ablation techniques: microwave and interstitial laser ablation of liver tumors. Ann Surg Oncol 10:491–497
Lu MD, Chen JW, Xie XY et al (2001) Hepatocellular carcinoma: US-guided percutaneous microwave coagulation therapy. Radiology 221:167–172
Seki S, Sakaguchi H, Kadoya H et al (2000a) Laparoscopic microwave coagulation therapy for hepatocellular carcinoma. Endoscopy 32:591–597
Seki T, Tamai T, Nakagawa T et al (2000b) Combination therapy with transcatheter arterial chemoembolization and percutaneous microwave coagulation therapy for hepatocellular carcinoma. Cancer 89: 1245–1251
Shibata T, Iimuro Y, Yamamoto Y et al (2002) Small hepatocellular carcinoma: comparison of radio-frequency ablation and percutaneous microwave coagulation therapy. Radiology 223:331–337
Simon CJ, Dupuy DE, Mayo-Smith WW (2005) Microwave ablation: principles and applications. Radiographics 25(Suppl 1):S69–S83
Skinner MG, Iizuka MN, Kolios MC et al (1998) A theoretical comparison of energy sources – microwave, ultrasound and laser – for interstitial thermal therapy. Phys Med Biol 43:3535–3547
Stauffer PR, Rossetto F, Prakash M et al (2003) Phantom and animal tissues for modelling the electrical properties of human liver. Int J Hyperthermia 19:89–101
Tabuse K, Katsumi M, Kobayashi Y et al (1985) Microwave surgery: hepatectomy using a microwave tissue coagulator. World J Surg 9:136–143
Wright AS, Lee FT Jr, Mahvi DM (2003) Hepatic microwave ablation with multiple antennae results in synergistically larger zones of coagulation necrosis. Ann Surg Oncol 10:275–283

Microwave Ablation of Liver Tumors

Brace CL, Hinshaw JL, Laeseke PF et al (2009) Pulmonary thermal ablation: comparison of radiofrequency and microwave devices by using gross pathologic and CT findings in a swine model. Radiology 25:705–711
Brannan JD, Ladtkow CM (2009) Modeling bimodal vessel effects on radio and microwave frequency ablation zones. Conf Proc IEEE Eng Med Biol Soc 2009:5989–5992
Crocetti L, de Baere T, Lencioni R (2010) Quality improvement guidelines for radiofrequency ablation of liver tumours. Cardiovasc Intervent Radiol 33:11–17
Denys A, de Baere T, Kuoch V et al (2002) Radiofrequency of liver lesion: comparison of 4 devices. J Vasc Interv Radiol 13(sup):S94, Abstract
He N, Wang W, Ji Z et al (2010) Microwave ablation: an experimental comparative study on internally cooled antenna versus non-internally cooled antenna in liver models. Acad Radiol 17:894–899
Hugander A, Bolmsjo M, Hafstrom L et al (1985) Effects of local microwave hyperthermia and 5-fluorouracil in treatment of experimental liver cancer. Anticancer Res 5:281–285
Iannitti DA, Martin RC, Simon CJ et al (2007) Hepatic tumor ablation with clustered microwave antennae: the US phase II trial. HPB (Oxford) 9:120–124
Joines WT, Zhang Y, Li C et al (1994) The measured electrical properties of normal and malignant human tissues from 50 to 900 MHz. Med Phys 21:547–550
Kuang M, Lu MD, Xie XY et al (2007) Liver cancer: increased microwave delivery to ablation zone with cooled-shaft antenna – experimental and clinical studies. Radiology 242:914–924
Liang P, Dong B, Yu X et al (2003) Prognostic factors for percutaneous microwave coagulation therapy of hepatic metastases. Am J Roentgenol 181: 1319–1325
Liang P, Dong B, Yu X et al (2005) Prognostic factors for survival in patients with hepatocellular carcinoma after percutaneous microwave ablation. Radiology 235:299–307

Liang P, Wang Y, Yu X et al (2009) Malignant liver tumors: treatment with percutaneous microwave ablation – complications among cohort of 1136 patients. Radiology 251:933–940

Lu MD, Xu HX, Xie XY et al (2005) Percutaneous microwave and radiofrequency ablation for hepatocellular carcinoma: a retrospective comparative study. J Gastroenterol 40:1054–1060

Martin RC, Scoggins CR, McMasters KM (2010) Safety and efficacy of microwave ablation of hepatic tumors: a prospective review of a 5-year experience. Ann Surg Oncol 17:171–178

Miura T, Hatta Y, Endo Y et al (1985) Hyperthermia: microwave hyperthermia in combination with intra-arterial infusion chemotherapy of cancer of the pancreas. Gan No Rinsho 31:704–711, Japanese

Oku A, Nishioka S, Yokoya Y et al (1983) Microwave coagulation under ultrasound guidance in liver hemangioma. Nippon Shokakibyo Gakkai Zasshi 80:1504, Japanese

Saitsu H, Mada Y, Taniwaki S et al (1993) Investigation of microwave coagulo-necrotic therapy for 21 patients with small hepatocellular carcinoma less than 5 cm in diameter. Nippon Geka Gakkai Zasshi 94:359–365, Japanese

Schramm W, Yang D, Wood BJ et al (2007) Contribution of direct heating, thermal conduction and perfusion during radiofrequency and microwave ablation. Open Biomed Eng J 1:47–52

Seki T, Wakabayashi M, Nakagawa T et al (1994) Ultrasonically guided percutaneous microwave coagulation therapy for small hepatocellular carcinoma. Cancer 74:817–825

Shibata T, Iimuro Y, Yamamoto Y et al (2002) Small hepatocellular carcinoma: comparison of radio-frequency ablation and percutaneous microwave coagulation therapy. Radiology 223:331–337

Simon CJ, Dupuy DE, Iannitti DA et al (2006) Intraoperative triple antenna hepatic microwave ablation. Am J Roentgenol 187:W333–W340

Stuchly MA, Athey TW, Stuchly SS et al (1981) Dielectric properties of animal tissues in vivo at frequencies 10 MHz–1 GHz. Bioelectromagnetics 2:93–103

Sun Y, Wang Y, Ni X et al (2009) Comparison of ablation zone between 915- and 2,450-MHz cooled-shaft microwave antenna: results in in vivo porcine livers. Am J Roentgenol 192:511–514

Tabuse K, Katsumi M, Kobayashi Y et al (1985) Microwave surgery: hepatectomy using a microwave tissue coagulator. World J Surg 9:136–143

Tabuse Y, Tabuse K, Mori K et al (1986) Percutaneous microwave tissue coagulation in liver biopsy: experimental and clinical studies. Nippon Geka Hokan 55:381–392

Wright AS, Lee FT Jr, Mahvi DM (2003) Hepatic microwave ablation with multiple antennae results in synergistically larger zones of coagulation necrosis. Ann Surg Oncol 10:275–283

Yin XY, Xie XY, Lu MD et al (2009) Percutaneous thermal ablation of medium and large hepatocellular carcinoma: long-term outcome and prognostic factors. Cancer 115:1914–1923

Yu NC, Raman SS, Kim YJ et al (2008) Microwave liver ablation: influence of hepatic vein size on heat-sink effect in a porcine model. J Vasc Interv Radiol 19:1087–1092

Yu J, Liang P, Yu X et al (2010) A comparison of microwave ablation and bipolar radiofrequency ablation both with an internally cooled probe: results in ex vivo and in vivo porcine livers. Eur J Radiol 2:2

Microwave Ablation: Lung

Brace CL, Hinshaw JL, Laeseke PF et al (2009) Pulmonary thermal ablation: comparison of radiofrequency and microwave devices by using gross pathologic and CT findings in a swine model. Radiology 25:705–711

Carrafiello G, Mangini M, De Bernardi I et al (2010) Microwave ablation therapy for treating primary and secondary lung tumours: technical note. Radiol Med 115:962–974

Crocetti L, Bozzi E, Faviana P et al (2010) Thermal ablation of lung tissue: in vivo experimental comparison of microwave and radiofrequency. Cardiovasc Intervent Radiol 33:818–827

He W, Hu XD, Wu DF et al (2006) Ultrasonography-guided percutaneous microwave ablation of peripheral lung cancer. Clin Imaging 30:234–241

Lencioni R, Crocetti L, Cioni R et al (2008) Response to radiofrequency ablation of pulmonary tumours: a prospective, intention-to-treat, multicentre clinical trial (the RAPTURE study). Lancet Oncol 9:621–628

Lubner MG, Brace CL, Hinshaw JL et al (2010) Microwave tumor ablation: mechanism of action, clinical results, and devices. J Vasc Interv Radiol 21(8 Suppl):S192–S203

Malloy PC, Grassi CJ, Kundu S et al (2009) Consensus guidelines for periprocedural management of coagulation status and hemostasis risk in percutaneous image-guided interventions. J Vasc Interv Radiol 20(7 Suppl): S240–S249

Rosenberg C, Puls R et al (2009) Laser ablation of metastatic lesions of the lung: long-term outcome. Am J Roentgenol 92(3):785–792

Santos RS, Gan J, Ohara CJ, Daly B et al (2010) Microwave ablation of lung tissue: impact of single-lung ventilation on ablation size. Ann Thorac Surg 90:1116–1119

Shi W, Liang P, Zhu Q et al. (2011) Microwave ablation. Results with double 915MHz antennae in ex vivo bovine Livers. Eur J Radiol 79(2):4

Skinner MG, Iizuka MN, Kolios MC et al (1998) A theoretical comparison of energy sources – microwave, ultrasound and laser – for interstitial thermal therapy. Phys Med Biol 43:3535–3547

Skonieczki BD, Wells C, Wasser EJ et al (2011) Radiofrequency and microwave tumor ablation in patients with implanted cardiac devices: is it safe? Eur J Radiol 79:343–346

Vogl TJ, Naguib NN, Lehnert T et al (2011) Radiofrequency, microwave and laser ablation of pulmonary neoplasms: clinical studies and technical considerations—review article. Eur J Radiol 77:346–357

Wolf FJ, Grand DJ, Machan JT et al (2008) Microwave ablation of lung malignancies: effectiveness, CT findings, and safety in 50 patients. Radiology 247:871–879

Percutaneous Ethanol Injection

Ackmann S, Janowitz P (1997) The curative therapy of primary hyperparathyroidism by percutaneous ethanol injections. Dtsch Med Wochenschr 122:648–652

Adam G, Neuerburg J, Bucker A, Glowinski A, Vorwerk D, Stargardt A, Van Vaals JJ, Guenther RW (1997) Interventional magnetic resonance. Initial clinical experience with a 1.5-tesla magnetic resonance system combined with c-arm fluoroscopy. Invest Radiol 32:191–197

Alexander AL, Barrette TR, Unger EC (1996) Magnetic resonance guidance of percutaneous ethanol injection in liver. Acad Radiol 3:18–25

Arii S, Yamaoka Y, Futugawa S, Inoue K, Kobayashi K, Kojiro M, Makuuchi M, Nakamura Y, Okita K, Yamada R (2000) Results of surgical and nonsurgical treatment for small-sized hepatocellular carcinomas: a retrospective and nationwide survey in Japan. Hepatology 32:1224–1229

Bruix J, Sherman M, Llovet JM et al (2001) Clinical management of hepatocellular carcinoma. Conclusions of the Barcelona-2000 EASL conference. J Hepatol 35:421–430

Cheng BQ, Jia CQ, Liu CT, Fan W, Wang QL, Zhang ZL, Yi CH (2008) Chemoembolization combined with radiofrequency ablation for patients with hepatocellular carcinoma larger than 3 cm: a randomized controlled trial. JAMA 299:1669–1677

Chu CH, Chuang MJ, Wang MC, Lam HC, Lu CC, Lee JK (2003) Sclerotherapy of thyroid cystic nodules. J Formos Med Assoc 102:625–630

Di Stasi M, Buscarini L, Livraghi T, Giorgio A, Salmi A, De Sio I, Brunello F, Solmi L, Caturelli E, Magnolfi F, Caremani M, Filice C (1997) Percutaneous ethanol injection in the treatment of hepatocellular carcinoma. A multicenter survey of evaluation practices and complication rates. Scand J Gastroenterol 32:1168–1173

Ebara M, Okabe S, Kita K, Sugiura N, Fukuda H, Yoshikawa M, Kondo F, Saisho H (2005) Percutaneous ethanol injection for small hepatocellular carcinoma: therapeutic efficacy based on 20-year observation. J Hepatol 43:458–464

Festi D, Monti F, Casanova S, Livraghi T, Frabboni R, Roversi CA, Bertoli D, Borelli G, Mazzella G, Bazzoli F et al (1990) Morphological and biochemical effects of intrahepatic alcohol injection in the rabbit. J Gastroenterol Hepatol 5:402–406

Gabal AM, Khawaja FI, Mohammad GA (2005) Modified PAIR technique for percutaneous treatment of high-risk hydatid cysts. Cardiovasc Intervent Radiol 28: 200–208

Georgiades CS, Hong K, Geschwind JF (2008) Radiofrequency ablation and chemoembolization for hepatocellular carcinoma. Cancer J 14:117–122

Germani G, Pleguezuelo M, Gurusamy K, Meyer T, Isgro G, Burroughs AK (2010) Clinical outcomes of radiofrequency ablation, percutaneous alcohol and acetic acid injection for hepatocellular carcinoma: a meta-analysis. J Hepatol 52:380–388

Guan YS, Liu Y (2006) Interventional treatments for hepatocellular carcinoma. Hepatobiliary Pancreat Dis Int 5:495–500

Harman CR, Grant CS, Hay ID, Hurley DL, van Heerden JA, Thompson GB, Reading CC, Charboneau JW (1998) Indications, technique, and efficacy of alcohol injection of enlarged parathyroid glands in patients with primary hyperparathyroidism. Surgery 124:1011–1019

Iglesias P, Diez JJ (2009) Current treatments in the management of patients with primary hyperparathyroidism. Postgrad Med J 85:15–23

Ikeda M, Okada S, Ueno H, Okusaka T, Kuriyama H (2001) Radiofrequency ablation and percutaneous ethanol injection in patients with small hepatocellular carcinoma: a comparative study. Jpn J Clin Oncol 31:322–326

Karstrup S, Hegedüs L, Holm HH (1993) Acute change in parathyroid function in primary hyperparathyroidism following ultrasonically guided ethanol injection into solitary parathyroid adenomas. Acta Endocrinol (Copenh) 129:377–380

Khan KN, Yatsuhashi H, Yamasaki K, Yamasaki M, Inoue O, Koga M, Yano M (2000) Prospective analysis of risk factors for early intrahepatic recurrence of hepatocellular carcinoma following ethanol injection. J Hepatol 32:269–278

Kim YJ, Raman SS, Yu NC, Lu DS (2005) MR-guided percutaneous ethanol injection for hepatocellular carcinoma in a 0.2 T open MR system. J Magn Reson Imaging 22:566–571

Koda M, Murawaki Y, Mitsuda A, Ohyama K, Horie Y, Suou T, Kawasaki H, Ikawa S (2000) Predictive factors for intrahepatic recurrence after percutaneous ethanol injection therapy for small hepatocellular carcinoma. Cancer 88:529–537

Koda M, Murawaki Y, Mitsuda A, Oyama K, Okamoto K, Idobe Y, Suou T, Kawasaki H (2001) Combination therapy with transcatheter arterial chemoembolization and percutaneous ethanol injection compared with percutaneous ethanol injection alone for patients with small hepatocellular carcinoma: a randomized control study. Cancer 92:1516–1524

Kurokohchi K, Watanabe S, Masaki T, Hosomi N, Miyauchi Y, Himoto T, Kimura Y, Nakai S, Deguchi A, Yoneyama H, Yoshida S, Kuriyama S (2005) Comparison between combination therapy of percutaneous ethanol injection and radiofrequency ablation and radiofrequency ablation alone for patients with hepatocellular carcinoma. World J Gastroenterol 11:1426–1432

Kurokohchi K, Hosomi N, Yoshitake A, Ohgi T, Ono M, Maeta T, Kiuchi T, Matsumoto I, Masaki T, Yoneyama H, Kohi F, Kuriyama S (2006) Successful treatment of large-size advanced hepatocellular carcinoma by transarterial chemoembolization followed by the combination therapy of percutaneous ethanol-lipiodol injection and radiofrequency ablation. Oncol Rep 16: 1067–1070

Lee MJ, Mueller PR, Dawson SL, Gazelle SG, Hahn PF, Goldberg MA, Boland GW (1995) Percutaneous ethanol injection for the treatment of hepatic tumors: indications, mechanism of action, technique, and efficacy. Am J Roentgenol 164:215–220

Lencioni R, Crocetti L (2005) A critical appraisal of the literature on local ablative therapies for hepatocellular carcinoma. Clin Liver Dis 9:301–314

Lencioni R, Pinto F, Armillotta N, Bassi AM, Moretti M, Di Giulio M, Marchi S, Uliana M, Della Capanna S, Lencioni M, Bartolozzi C (1997) Long-term results of percutaneous ethanol injection therapy for hepatocellular carcinoma in cirrhosis: a European experience. Eur Radiol 7:514–519

Lencioni RA, Allgaier HP, Cioni D, Olschewski M, Deibert P, Crocetti L, Frings H, Laubenberger J, Zuber I, Blum HE, Bartolozzi C (2003) Small hepatocellular carcinoma in cirrhosis: randomized comparison of radiofrequency thermal ablation versus percutaneous ethanol injection. Radiology 228:235–240

Lin SM, Lin CJ, Lin CC, Hsu CW, Chen YC (2004) Radiofrequency ablation improves prognosis compared with ethanol injection for hepatocellular carcinoma ≤4 cm. Gastroenterology 127:1714–1723

Lin SM, Lin CJ, Lin CC, Hsu CW, Chen YC (2005) Randomised controlled trial comparing percutaneous radiofrequency thermal ablation, percutaneous ethanol injection, and percutaneous acetic acid injection to treat hepatocellular carcinoma of 3 cm or less. Gut 54:1151–1156

Livraghi T (1998) Percutaneous ethanol injection in the treatment of hepatocellular carcinoma in cirrhosis. Hepatogastroenterology 45:1248–1253

Livraghi T, Giorgio A, Marin G, Salmi A, de Sio I, Bolondi L, Pompili M, Brunello F, Lazzaroni S, Torzilli G, Zucchi A (1995) Hepatocellular carcinoma and cirrhosis in 746 patients: long-term results of percutaneous ethanol injection. Radiology 197:101–108

Livraghi T, Benedini V, Lazzaroni S, Meloni F, Torzilli G, Vettori C (1998) Long term results of single session percutaneous ethanol injection in patients with large hepatocellular carcinoma. Cancer 83:48–57

Livraghi T, Goldberg SN, Lazzaroni S, Meloni F, Solbiati L, Gazelle GS (1999) Small hepatocellular carcinoma: treatment with radio-frequency ablation versus ethanol injection. Radiology 210:655–661

Livraghi T, Meloni F, Morabito A, Vettori C (2004) Multimodal image-guided tailored therapy of early and intermediate hepatocellular carcinoma: long-term survival in the experience of a single radiologic referral center. Liver Transpl 10:98–106

Llovet JM, Sala M (2005) Non-surgical therapies of hepatocellular carcinoma. Eur J Gastroenterol Hepatol 17:505–513

Llovet JM, Burroughs A, Bruix J (2003) Hepatocellular carcinoma. Lancet 362:1907–1917

Lubienski A, Bitsch RG, Schemmer P, Grenacher L, Düx M, Kauffmann GW (2004) Long-term results of interventional treatment of large unresectable hepatocellular carcinoma (HCC): significant survival benefit from combined transcatheter arterial chemoembolization (TACE) and percutaneous ethanol injection (PEI) compared to TACE monotherapy. Fortschr Röntgenstr 176:1794–1802

Mahnken AH, Bruners P, Günther RW (2009) Local ablative therapies in HCC: percutaneous ethanol injection and radiofrequency ablation. Dig Dis 27:148–156

Nakanishi K, Kobayashi M, Takahashi S, Nakata S, Kyakuno M, Nakaguchi K, Nakamura H (2005) Whole body MRI for detecting metastatic bone tumor: comparison with bone scintigrams. Magn Reson Med Sci 4:11–17

Omata M, Tateishi R, Yoshida H, Shiina S (2004) Treatment of hepatocellular carcinoma by percutaneous tumor ablation methods: ethanol injection therapy and radiofrequency ablation. Gastroenterology 127:159–166

Sakamoto M, Hirohashi S (1998) Natural history and prognosis of adenomatous hyperplasia and early hepatocellular carcinoma: multi-institutional analysis of 53 nodules followed up for more than 6 months and 141 patients with single early hepatocellular carcinoma treated by surgical resection or percutaneous ethanol injection. Jpn J Clin Oncol 28:604–608

Sala M, Llovet JM, Vilana R, Bianchi L, Sole M, Ayuso C, Brú C, Bruix J, Barcelona Clinic Liver Cancer Group (2004) Initial response to percutaneous ablation predicts survival in patients with hepatocellular carcinoma. Hepatology 40:1352–1360

Shiina S, Tagawa K, Unuma T, Takanashi R, Yoshiura K, Komatsu Y, Hata Y, Niwa Y, Shiratori Y, Terano A, Sugimoto T (1991) Percutaneous ethanol injection therapy for hepatocellular carcinoma: a histopathologic study. Cancer 68:1524–1530

Shiina S, Teratani T, Obi S, Sato S, Tateishi R, Fujishima T, Ishikawa T, Koike Y, Yoshida H, Kawabe T, Omata M (2005) A randomized controlled trial of radiofrequency ablation with ethanol injection for small hepatocellular carcinoma. Gastroenterology 129:122–130

Sohn Y-M, Hong SW, Kim E-K, Kim MJ, Moon HJ, Kim SJ, Son EJ, Kwak JY (2009) Complete eradication of metastatic lymph node after percutaneous ethanol injection therapy: pathologic correlation. Thyroid 19:317–319

Solbiati L, Giangrande A, De Pra L, Bellotti E, Cantù P, Ravetto C (1985) Percutaneous ethanol injection of parathyroid tumors under US guidance: treatment for secondary hyperparathyroidism. Radiology 155:607–610

Su L, Fan X, Zheng L, Zheng J (2010) Absolute ethanol sclerotherapy for venous malformations in the face and neck. J Oral Maxillofac Surg 68:1622–1627

Tsai WL, Cheng JS, Lai KH, Lin CP, Lo GH, Hsu PI, Yu HC, Lin CK, Chan HH, Chen WC, Chen TA, Li WL, Liang HL (2008) Clinical trial: percutaneous acetic acid injection versus percutaneous ethanol injection for small hepatocellular carcinoma – a long-term follow-up study. Aliment Pharmacol Ther 28: 304–311

Veldman MW, Reading CC, Farrell MA, Mullan BP, Wermers RA, Grant CS, Thompson GB (2008) Percutaneous parathyroid ethanol ablation in patients with multiple endocrine neoplasia type 1. Am J Roentgenol 191:1740–1744

Verges BL, Cercueil JP, Jacob D, Vaillant G, Brun JM, Putelat R (1993) Results of ultrasonically guided percutaneous ethanol injection into parathyroid adenomas in primary hyperparathyroidism. Acta Endocrinol (Copenh) 129:381–387

Verges BL, Cercueil JP, Jacob D, Vaillant G, Brun JM (2000) Treatment of parathyroid adenomas with ethanol injection under ultrasonographic guidance. Ann Chir 125:457–460

Vilana R, Bianchi L, Varela M, Nicolau C, Sanchez M, Ayuso C, Garcia M, Sala M, Llovet JM, Bruix J, Brú C, BCLC Group (2006) Is microbubble-enhanced ultrasonography sufficient for assessment of response to percutaneous treatment in patients with early hepatocellular carcinoma? Eur Radiol 16:2454–2462

Wang P, Zuo C, Qian Z, Tian J, Ren F, Zhou D (2003) Computerized tomography guided percutaneous ethanol injection for the treatment of hyperfunctioning pheochromocytoma. J Urol 170:1132–1134

Wang W, Shi J, Xie WF (2010) Transarterial chemoembolization in combination with percutaneous ablation therapy in unresectable hepatocellular carcinoma: a meta-analysis. Liver Int 30:741–749

Wang N, Guan Q, Wang K, Zhu B, Yuan W, Zhao P, Wang X, Zhao Y (2011) TACE combined with PEI versus TACE alone in the treatment of HCC: a meta-analysis. Med Oncol 28:1038–1043

CT-Guided HDR Brachytherapy

Amthauer H, Denecke T, Hildebrandt B et al (2006) Evaluation of patients with liver metastases from colorectal cancer for locally ablative treatment with laser induced thermotherapy – impact of PET with F-18-fluorodeoxyglucose on therapeutic decisions. Nuklearmedizin 45:177–184

Bergk A, Wieners G, Weich V et al (2005) CT-guided brachytherapy of hepatocellular carcinoma in liver cirrhosis – a novel therapeutic approach. J Hepatol 42:89 [Abstract]

Mohnike K, Pech M, Seidensticker M et al (2008) A matched pair analysis comparing local ablation of HCC by CT-guided HDR brachytherapy with best supportive care. Submitted

Pech M, Mohnike K, Wieners G et al (2008) Radiotherapy of liver metastases – comparison of target volumes and dose-volume histograms employing CT- or MRI-based treatment planning. Strahlenther Onkol 184:256–261

Ricke J, Wust P, Wieners G et al (2004a) Liver malignancies: CT-guided interstitial brachytherapy in patients with unfavorable lesions for thermal ablation. J Vasc Interv Radiol 15:1279–1286

Ricke J, Wust P, Stohlmann A et al (2004b) CT-guided interstitial brachytherapy of liver malignancies alone or in combination with thermal ablation: phase I-II results of a novel technique. Int J Radiat Oncol Biol Phys 58:1496–1505

Ricke J, Wust P, Stohlmann A et al (2004c) CT-gesteuerte Brachytherapie. Eine neue perkutane Technik zur interstitiellen Ablation von Lebermetastasen. Strahlenther Onkol 180:274–280 [German]

Ricke J, Seidensticker M, Ludemann L, Hengst S et al (2005a) In vivo assessment of the tolerance dose of small liver volumes after single-fraction HDR irradiation. Int J Radiat Oncol Biol Phys 62:776–784

Ricke J, Wust P, Wieners G et al (2005b) CT-guided interstitial single-fraction brachytherapy of lung tumors: phase I results of a novel technique. Chest 127: 2237–2242

Ricke J, Mohnike K, Pech M et al. (2010) Local response and impact on survival after local ablation of liver malignancies from colorectal carcinoma by CT-guided HDR-brachytherapy. Int J Radiat Oncol Biol Phys. 2010;78(2):479–485

Streitparth F, Pech M, Bohmig M et al (2006) In vivo assessment of the gastric mucosal tolerance dose after single fraction, small volume irradiation of liver malignancies by computed tomography-guided, high-dose-rate brachytherapy. Int J Radiat Oncol Biol Phys 65:1479–1486

Wieners G, Pech M, Rudzinska M et al (2006) CT-guided interstitial brachytherapy in the local treatment of extrahepatic, extrapulmonary secondary malignancies. Eur Radiol 16:2586–2593

Irreversible Electroporation

Ahmed M, Brace CL, Lee FT Jr, Goldberg SN (2011) Principles of and advances in percutaneous ablation. Radiology 258:351–369

Al-Sakere B, Andre F, Bernat C, Connault E, Opolon P, Davalos RV, Rubinsky B, Mir LM (2007) Tumor ablation with irreversible electroporation. PLoS One 2:e1135

Ball C, Thomson KR, Kavnoudias H (2010) Irreversible electroporation: a new challenge in "out of operating theater" anesthesia. Anesth Analg 110:1305–1309

Bertacchini C, Margotti PM, Bergamini E, Lodi A, Ronchetti M, Cadossi R (2007) Design of an irreversible electroporation system for clinical use. Technol Cancer Res Treat 6:313–320

Bower M, Sherwood L, Li Y, Martin R (2011) Irreversible electroporation of the pancreas: definitive local therapy without systemic effects. J Surg Oncol 104:22–28

Charpentier KP, Wolf F, Noble L, Winn B, Resnick M, Dupuy DE (2010) Irreversible electroporation of the pancreas in swine: a pilot study. HPB (Oxford) 12:348–351

Charpentier KP, Wolf F, Noble L, Winn B, Resnick M, Dupuy DE (2011) Irreversible electroporation of the liver and liver hilum in swine. HPB (Oxford) 13: 168–173

Choi YS, Kim HB, Chung J, Kim HS, Yi JH, Park JK (2010) Preclinical analysis of irreversible electroporation on rat liver tissues using a microfabricated electroporator. Tissue Eng Part C Methods 16:1245–1253

Davalos RV, Mir IL, Rubinsky B (2005) Tissue ablation with irreversible electroporation. Ann Biomed Eng 33:223–231

Deodhar A, Monette S, Single GW Jr, Hamilton WC Jr, Thornton R, Maybody M, Coleman JA, Solomon SB (2011a) Renal tissue ablation with irreversible electroporation: preliminary results in a porcine model. Urology 77:754–760

Deodhar A, Monette S, Single GW Jr, Hamilton WC Jr, Thornton RH, Sofocleous CT, Maybody M, Solomon SB (2011b) Percutaneous irreversible electroporation lung ablation: preliminary results in a porcine model. Cardiovasc Intervent Radiol 34:1278–1287

Dupuy DE, Aswad B, Ng T (2011) Irreversible electroporation in a Swine lung model. Cardiovasc Intervent Radiol 34:391–395

Edd JF, Davalos RV (2007) Mathematical modeling of irreversible electroporation for treatment planning. Technol Cancer Res Treat 6:275–286

Edd JF, Horowitz L, Davalos RV, Mir LM, Rubinsky B (2006) In vivo results of a new focal tissue ablation technique: irreversible electroporation. IEEE Trans Biomed Eng 53:1409–1415

Ellis TL, Garcia PA, Rossmeisl JH Jr, Henao-Guerrero N, Robertson J, Davalos RV (2011) Nonthermal irreversible electroporation for intracranial surgical applications. Laboratory investigation. J Neurosurg 114:681–688

Esser AT, Smith KC, Gowrishankar TR, Weaver JC (2007) Towards solid tumor treatment by irreversible electroporation: intrinsic redistribution of fields and currents in tissue. Technol Cancer Res Treat 6:261–274

Garcia PA, Rossmeisl JH Jr, Robertson J, Ellis TL, Davalos RV (2009) Pilot study of irreversible electroporation for intracranial surgery. Conf Proc IEEE Eng Med Biol Soc 2009:6513–6516

Garcia PA, Rossmeisl JH Jr, Neal RE 2nd, Ellis TL, Olson JD, Henao-Guerrero N, Robertson J, Davalos RV (2010) Intracranial nonthermal irreversible electroporation: in vivo analysis. J Membr Biol 236:127–136

Guo Y, Zhang Y, Klein R, Nijm GM, Sahakian AV, Omary RA, Yang GY, Larson AC (2010) Irreversible electroporation therapy in the liver: longitudinal efficacy studies in a rat model of hepatocellular carcinoma. Cancer Res 70:1555–1563

Heller R, Gilbert R, Jaroszeski MJ (1999) Clinical applications of electrochemotherapy. Adv Drug Deliv Rev 35:119–129

Jaroszeski MJ, Gilbert R, Nicolau C, Heller R (1999) In vivo gene delivery by electroporation. Adv Drug Deliv Rev 35:131–137

Joshi RP, Schoenbach KH (2002) Mechanism for membrane electroporation irreversibility under high-intensity, ultrashort electrical pulse conditions. Phys Rev E Stat Nonlin Soft Matter Phys 66:052901

Lavee J, Onik G, Mikus P, Rubinsky B (2007) A novel nonthermal energy source for surgical epicardial atrial ablation: irreversible electroporation. Heart Surg Forum 10:E162–E167

Lee EW, Loh CT, Kee ST (2007) Imaging guided percutaneous irreversible electroporation: ultrasound and immunohistological correlation. Technol Cancer Res Treat 6:287–294

Lee EW, Chen C, Prieto VE, Dry SM, Loh CT, Kee ST (2010a) Advanced hepatic ablation technique for creating complete cell death: irreversible electroporation. Radiology 255:426–433

Lee EW, Thai S, Kee ST (2010b) Irreversible electroporation: a novel image-guided cancer therapy. Gut Liver 4(Suppl 1):S99–S104

Lencioni R (2010) Loco-regional treatment of hepatocellular carcinoma. Hepatology 52:762–773

Lencioni R, Cioni D, Della Pina C, Crocetti L (2010) Hepatocellular carcinoma: new options for image-guided ablation. J Hepatobiliary Pancreat Sci 17:399–403

Linnert M, Gehl J (2009) Bleomycin treatment of brain tumors: an evaluation. Anticancer Drugs 20:157–164

Maor E, Ivorra A, Leor J, Rubinsky B (2007) The effect of irreversible electroporation on blood vessels. Technol Cancer Res Treat 6:307–312

Miklavcic D, Semrov D, Mekid H, Mir LM (2000) A validated model of in vivo electric field distribution in tissues for electrochemotherapy and for DNA electrotransfer for gene therapy. Biochim Biophys Acta 1523:73–83

Mir LM (2008) Application of electroporation gene therapy: past, current, and future. Methods Mol Biol 423:3–17

Mir LM, Orlowski S, Belehradek J Jr, Paoletti C (1991) Electrochemotherapy potentiation of antitumour effect of bleomycin by local electric pulses. Eur J Cancer 27:68–72

Mir LM, Moller PH, Andre F, Gehl J (2005) Electric pulse-mediated gene delivery to various animal tissues. Adv Genet 54:83–114

Neal RE 2nd, Singh R, Hatcher HC, Kock ND, Torti SV, Davalos RV (2010) Treatment of breast cancer through the application of irreversible electroporation using a novel minimally invasive single needle electrode. Breast Cancer Res Treat 123:295–301

Onik G, Mikus P, Rubinsky B (2007) Irreversible electroporation: implications for prostate ablation. Technol Cancer Res Treat 6:295–300

Pech M, Janitzky A, Wendler JJ, Strang C, Blaschke S, Dudeck O, Ricke J, Liehr UB (2011) Irreversible electroporation of renal cell carcinoma: a first-in-man phase I clinical study. Cardiovasc Intervent Radiol 34:132–138

Phillips M, Maor E, Rubinsky B (2010) Nonthermal irreversible electroporation for tissue decellularization. J Biomech Eng 132:091003
Rowan NJ, MacGregor SJ, Anderson JG, Fouracre RA, Farish O (2000) Pulsed electric field inactivation of diarrhoeagenic Bacillus cereus through irreversible electroporation. Lett Appl Microbiol 31:110–114
Rubinsky B (2007) Irreversible electroporation in medicine. Technol Cancer Res Treat 6:255–260
Rubinsky B, Onik G, Mikus P (2007) Irreversible electroporation: a new ablation modality – clinical implications. Technol Cancer Res Treat 6:37–48
Tieleman DP, Leontiadou H, Mark AE, Marrink SJ (2003) Simulation of pore formation in lipid bilayers by mechanical stress and electric fields. J Am Chem Soc 125:6382–6383
Tracy CR, Kabbani W, Cadeddu JA (2011) Irreversible electroporation (IRE): a novel method for renal tissue ablation. BJU Int 107:1982–1987
Vernhes MC, Benichou A, Pernin P, Cabanes PA, Teissie J (2002) Elimination of free-living amoebae in fresh water with pulsed electric fields. Water Res 36:3429–3438
Weaver JC (1995) Electroporation theory. Concepts and mechanisms. Methods Mol Biol 55:3–28

Technical Basics of MR-Guided Focused Ultrasound Surgery

Catane R, Beck A, Inbar Y et al (2007) MR-guided focused ultrasound surgery (MRgFUS) for the palliation of pain in patients with bone metastases – preliminary clinical experience. Ann Oncol 18: 163–167
Damianou C, Hynynen K (1994) The effect of various physical parameters on the size and shape of necrosed tissue volume during ultrasound surgery. J Acoust Soc Am 95:1641–1649
Fry WJ, Fry FJ (1960) Fundamental neurological research and human neurosurgery using intense ultrasound. Trans Med Electron ME-7:166–181
Gombos EC, Kacher DF, Furusawa H et al (2006) Breast focused ultrasound surgery with magnetic resonance guidance. Top Magn Reson Imaging 17:181–188
Hengst SA, Ehrenstein T, Herzog H et al (2004) Magnetresonanztomographiegesteuerter fokussierter Ultraschall (MRgFUS) in der Tumortherapie – eine neuartige nichtinvasive Therapieoption. Radiologe 44:339–346 [German]
Hindley J, Gedroyc WM, Regan L et al (2004) MRI guidance of focused ultrasound therapy of uterine fibroids: early results. Am J Roentgenol 183:1713–1719
Jääskeläinen J (2003) Non-invasive transcranial high intensity focused ultrasound (HIFUS) under MRI thermometry and guidance in the treatment of brain lesions. Acta Neurochir Suppl 88:57–60
Kopelman D, Inbar Y, Hanannel A et al (2006) Magnetic resonance-guided focused ultrasound surgery (MRgFUS): ablation of liver tissue in a porcine model. Eur J Radiol 59:157–162
Lynn JG, Zwemer RL, Chick AJ et al (1942) A new method for the generation and use of focused ultrasound in experimental biology. J Gen Physiol 26:179–193
Mahoney K, Fjield T, Mcdannold N et al (2001) Comparison of modelled and observed in vivo temperature elevations induced by focused ultrasound: implications for treatment planning. Phys Med Biol 46:1785–1798
Meshorer A, Prionas SD, Fajardo LF et al (1983) The effects of hyperthermia on normal mesenchymal tissues. Application of a histologic grading system. Arch Pathol Lab Med 107:328–334
McDannold N, Tempany CM, Fennessy FM et al (2006) Uterine leiomyomas: MR imaging-based thermometry and thermal dosimetry during focused ultrasound thermal ablation. Radiology 240:263–272
Mulkern RV, Panych LP, McDannold NJ et al (1998) Tissue temperature monitoring with multiple gradient-echo imaging sequences. J Magn Reson Imaging 8:493–502
Murat FJ, Poissonnier L, Pasticier G et al (2007) High-intensity focused ultrasound (HIFU) for prostate cancer. Cancer Control 14:244–249
Nathan J, McDannold BS, Randy L et al (2000) Usefulness of MR imaging–derived thermometry and dosimetry in determining the threshold for tissue damage induced by thermal surgery in rabbits. Radiology 216:517–523
Sapareto SA, Dewey WC (1984) Thermal dose determination in cancer therapy. Int J Radiat Oncol Biol Phys 10:787–800
Wlodarczyk W, Hentschel M, Wust P et al (1999) Comparison of four magnetic resonance methods for mapping small temperature changes. Phys Med Biol 44:607–624
Wood RW, Loomis AL (1927) The physical and biological effects of high-frequency sound waves of great intensity. London Edinburgh Dublin Phil Mag J Sci 4:417–436

Clinical Application of MR-Guided Focused Ultrasound Surgery

Catane R, Beck A, Inbar Y et al (2007) MR-guided focused ultrasound surgery (MRgFUS) for the palliation of pain in patients with bone metastases – preliminary clinical experience. Ann Oncol 18:163–167
Fennessy FM, Tempany CM (2005) MRI-guided focused ultrasound surgery of uterine leiomyomas. Acad Radiol 12:1158–1166
Fennessy FM, Tempany CM, McDannold NJ et al (2007) Uterine leiomyomas: MR imaging-guided focused ultrasound surgery – results of different treatment protocols. Radiology 243:885–893
Funaki K, Sawada K, Maeda F et al (2007a) Subjective effect of magnetic resonance-guided focused ultrasound surgery for uterine fibroids. J Obstet Gynaecol Res 33:834–839

Funaki K, Fukunishi H, Funaki T et al (2007b) Mid-term outcome of magnetic resonance-guided focused ultrasound surgery for uterine myomas: from six to twelve months after volume reduction. J Minim Invasive Gynecol 14:616–621

Furusawa H, Namba K, Nakahara H et al (2007) The evolving non-surgical ablation of breast cancer: MR guided focused ultrasound (MRgFUS). Breast Cancer 14:55–58

Gianfelice D, Khiat A, Amara M et al (2003a) MR imaging-guided focused ultrasound surgery of breast cancer: correlation of dynamic contrast-enhanced MRI with histopathologic findings. Breast Cancer Res Treat 82:93–101

Gianfelice D, Khiat A, Amara M et al (2003b) MR imaging-guided focused US ablation of breast cancer: histopathologic assessment of effectiveness – initial experience. Radiology 227:849–855

Gianfelice D, Khiat A, Boulanger Y et al (2003c) Feasibility of magnetic resonance imaging-guided focused ultrasound surgery as an adjunct to tamoxifen therapy in high-risk surgical patients with breast carcinoma. J Vasc Interv Radiol 14:1275–1282

Hanstede MM, Tempany CM, Stewart EA (2007) Focused ultrasound surgery of intramural leiomyomas may facilitate fertility: a case report. Fertil Steril 88(497):e495–e497

Hynynen K, Pomeroy O, Smith DN et al (2001) MR imaging-guided focused ultrasound surgery of fibroadenomas in the breast: a feasibility study. Radiology 219:176–185

Jolesz FA, Hynynen K, McDannold N et al (2004) Noninvasive thermal ablation of hepatocellular carcinoma by using magnetic resonance imaging-guided focused ultrasound. Gastroenterology 127:S242–S247

Kopelman D, Papa M (2007) Magnetic resonance-guided focused ultrasound surgery for the noninvasive curative ablation of tumors and palliative treatments: a review. Ann Surg Oncol 14:1540–1550

Kopelman D, Inbar Y, Hanannel A et al (2006) Magnetic resonance-guided focused ultrasound surgery (MRgFUS): ablation of liver tissue in a porcine model. Eur J Radiol 59:157–162

Madersbacher S, Kratzik C, Szabo N et al (1993) Tissue ablation in benign prostatic hyperplasia with high-intensity focused ultrasound. Eur Urol 23(Suppl 1):39–43

Rabinovici J, Inbar Y, Eylon SC et al (2006) Pregnancy and live birth after focused ultrasound surgery for symptomatic focal adenomyosis: a case report. Hum Reprod 21:1255–1259

Rabinovici J, Inbar Y, Revel A et al (2007) Clinical improvement and shrinkage of uterine fibroids after thermal ablation by magnetic resonance-guided focused ultrasound surgery. Ultrasound Obstet Gynecol 30:771–777

Rowland IJ, Rivens I, Chen L et al (1997) MRI study of hepatic tumours following high intensity focused ultrasound surgery. Br J Radiol 70:144–153

Stewart EA (2001) Uterine fibroids. Lancet 357:293–298

Stewart EA, Gedroyc WM, Tempany CM et al (2003) Focused ultrasound treatment of uterine fibroid tumors: safety and feasibility of a noninvasive thermoablative technique. Am J Obstet Gynecol 189:48–54

Stewart EA, Rabinovici J, Tempany CM et al (2006) Clinical outcomes of focused ultrasound surgery for the treatment of uterine fibroids. Fertil Steril 85: 22–29

Stewart EA, Gostout B, Rabinovici J et al (2007) Sustained relief of leiomyoma symptoms by using focused ultrasound surgery. Obstet Gynecol 110:279–287

Visioli AG, Rivens IH, ter Haar GR et al (1999) Preliminary results of a phase I dose escalation clinical trial using focused ultrasound in the treatment of localised tumours. Eur J Ultrasound 9:11–18

Wu F, Wang ZB, Chen WZ et al (2004) Extracorporeal high intensity focused ultrasound ablation in the treatment of patients with large hepatocellular carcinoma. Ann Surg Oncol 11:1061–1069

Percutaneous Cryoablation

Ablin RJ, Soanes WA, Gonder MJ (1973) Elution of in vivo bound antiprostatic epithelial antibodies following multiple cryotherapy of carcinoma of prostate. Urology 2:276–279

Arnott J (1850) Practical illustrations of the remedial efficacy of a very low or anesthetic temperature in cancer. Lancet 2:257–259

Baust JG, Gage AA (2005) The molecular basis of cryosurgery. BJU Int 95:1187–1191

Baust JG, Gage AA, Robilottto AT, Baust JM (2009) The pathophysiology of thermoablation: optimizing cryoablation. Curr Opin Urol 19:127–132

Bryant G (1995) DSC measurement of cell suspensions during successive freezing runs: implications for the mechanisms of intracellular Ice formation. Cryobiology 32:114–128

Butts K, Sinclair J, Daniel BL, Wansapura J, Pauly JM (2001) Temperature quantitation and mapping of frozen tissue. J Magn Reson Imaging 13: 99–104

Callstrom MR, Atwell TD, Charboneau JW et al (2006) Painful metastases involving bone: percutaneous image-guided cryoablation – prospective trial interim analysis. Radiology 241:572–580

Cheetham P, Truesdale M, Chaudhury S, Wenske S, Hruby GW, Katz A (2010) Long-term cancer-specific and overall survival for men followed more than 10 years after primary and salvage cryoablation of the prostate. J Endourol 24:1123–1129

Cytron S, Greene D, Witzsch U, Nylund P, Bjerklund Johansen TE (2009) Cryoablation of the prostate: technical recommendations. Prostate Cancer Prostatic Dis 12:339–346

den Brok MH, Sutmuller RP, Nierkens S et al (2006) Efficient loading of dendritic cells following cryo and radiofrequency ablation in combination with immune modulation induces anti-tumour immunity. Br J Cancer 95:896–905

Dominguez-Escrig JL, Sahadevan K, Johnson P (2008) Cryoablation for small renal masses. Adv Urol: 479495

Georgiades CS, Hong K, Geschwind JF (2006) Pre- and postoperative clinical care of patients undergoing interventional oncology procedures: a comprehensive approach to preventing and mitigating complications. Tech Vasc Interv Radiol 9:113–124

Goel RK, Kaouk JH (2008) Probe ablative treatment for small renal masses: cryoablation vs. radio frequency ablation. Curr Opin Urol 18:467–473

Hanai A, Yang W-L, Ravikumar TS (2001) Induction of apoptosis in human colon carcinoma cells HT29 by sublethal cryo-injury: mediation by cytochrome c release. Int J Cancer 93:526–533

Hinshaw JL, Lee FT Jr (2007) Cryoablation for liver cancer. Tech Vasc Interv Radiol 10:47–57

Hui GC, Tuncali K, Tatli S, Morrison PR, Silverman SG (2008) Comparison of percutaneous and surgical approaches to renal tumor ablation: metaanalysis of effectiveness and complication rates. J Vasc Interv Radiol 19:1311–1320

Janzen NK, Perry KT, Han KR et al (2005) The effects of intentional cryoablation and radio frequency ablation of renal tissue involving the collecting system in a porcine model. J Urol 173:1368–1374

Kawamura M, Izumi Y, Tsukada N et al (2006) Percutaneous cryoablation of small pulmonary malignant tumors under computed tomographic guidance with local anesthesia for nonsurgical candidates. J Thorac Cardiovasc Surg 131:1007–1013

Klossner DP, Robilotto AT, Clarke DM et al (2007) Cryosurgical technique: assessment of the fundamental variables using human prostate cancer model systems. Cryobiology 55:189–199

Kunkle DA, Egleston BL, Uzzo RG (2008) Excise, ablate or observe: the small renal mass dilemma – a meta-analysis and review. J Urol 179:1227–1234

Manenti G, Perretta T, Gaspari E et al (2011) Percutaneous local ablation of unifocal subclinical breast cancer: clinical experience and preliminary results of cryotherapy. Eur Radiol 21:2344–2353

Mazur P (1984) Freezing of living cells: mechanisms and implications. Am J Physiol 247:C125–C142

Mazur P, Rall WF, Leibo SP (1984) Kinetics of water loss and the likelihood of intracellular freezing in mouse ova. Influence of the method of calculating the temperature dependence of water permeability. Cell Biophys 6:197–213

Morrison PR, Silverman SG, Tuncali K, Tatli S (2008) MRI-guided cryotherapy. J Magn Reson Imaging 27:410–420

O'Rourke AP, Haemmerich D, Prakash P, Converse MC, Mahvi DM, Webster JG (2007) Current status of liver tumor ablation devices. Expert Rev Med Devices 4:523–537

Privalov PL (1990) Cold denaturation of proteins. Crit Rev Biochem Mol Biol 25:281–305

Robinson JW, Donnelly BJ, Siever JE et al (2009) A randomized trial of external beam radiotherapy versus cryoablation in patients with localized prostate cancer: quality of life outcomes. Cancer 115:4695–4704

Rybak LD (2009) Fire and ice: thermal ablation of musculoskeletal tumors. Radiol Clin North Am 47: 455–469

Sabel MS (2009) Cryo-immunology: a review of the literature and proposed mechanisms for stimulatory versus suppressive immune responses. Cryobiology 58:1–11

Sakuhara Y, Shimizu T, Kodama Y et al (2006) Magnetic resonance-guided percutaneous cryoablation of uterine fibroids: early clinical experiences. Cardiovasc Intervent Radiol 29:552–558

Seifert JK, Morris DL (1999) World survey on the complications of hepatic and prostate cryotherapy. World J Surg 23:109–114

Shulman S, Yantorno C, Bronson P (1967) Cryoimmunology: a method of immunization to autologous tissue. Proc Soc Exp Biol Med 124:658–661

Silverman SG, Tuncali K, Adams DF, Nawfel RD, Zou KH, Judy PF (1999) CT fluoroscopy-guided abdominal interventions: techniques, results, and radiation exposure. Radiology 212:673–681

Tacke J, Speetzen R, Heschel I, Hunter DW, Rau G, Günther RW (1999) Imaging of interstitial cryotherapy – an in vitro comparison of ultrasound, computed tomography, and magnetic resonance imaging. Cryobiology 38:250–259

Uppot RN, Silverman SG, Zagoria RJ, Tuncali K, Childs DD, Gervais DA (2009) Imaging-guided percutaneous ablation of renal cell carcinoma: a primer of how we do it. Am J Roentgenol 192:1558–1570

Wang H, Littrup PJ, Duan Y, Zhang Y, Feng H, Nie Z (2005) Thoracic masses treated with percutaneous cryotherapy: initial experience with more than 200 procedures. Radiology 235:289–298

Warlick CA, Lima GC, Allaf ME et al (2006) Clinical sequelae of radiographic iceball involvement of collecting system during computed tomography-guided percutaneous renal tumor cryoablation. Urology 67:918–922

Washington K, Debelak JP, Gobbell C et al (2001) Hepatic cryoablation-induced acute lung injury: histopathologic findings. J Surg Res 95:1–7

Woolley ML, Schulsinger DA, Durand DB, Zeltser IS, Waltzer WC (2002) Effect of freezing parameters (freeze cycle and thaw process) on tissue destruction following renal cryoablation. J Endourol 16:519–522

Yang W-L, Addona T, Nair DG, Qi L, Ravikumar TS (2003) Apoptosis induced by cryo-injury in human colorectal cancer cells is associated with mitochondrial dysfunction. Int J Cancer 103:360–369

Interventional Pain Managment

14

Jan Hoeltje, Roland Bruening, Bruno Kastler, Reto Bale, Gerlig Widmann, Bernd Turowski, Gero Wieners, Oliver Beuing, Alexis Kelekis, Dimitris Filippiadis, Kai E. Wilhelm, and Jean-Baptiste Martin

Contents

J. Hoeltje (✉) • R. Bruening
Roentgeninstitut Asklepios Klinik Barmbek, Ruebenkamp 220, D-22999 Hamburg, Germany
e-mail: j.hoeltje@asklepios.com

B. Kastler
Department of Radiology and Laboratoire d'Imagerie et d'Ingenierie, University of Besançon, CHU Minjoz, F-25030 Besançon, France
e-mail: bruno.kastler@univ-fcomte.fr

R. Bale • G. Widmann
SIP – Department for Microinvasive Therapy/ Department of Radiology, Medical University Innsbruck, Anichstr. 35, A-6020 Innsbruck, Austria
e-mail: reto.bale@i-med.ac.at

B. Turowski
Department of Neuroradiology, Heinrich-Heine-University, Moorenstr. 5, D-40225 Düsseldorf, Germany
e-mail: bernd.turowski@uni-duesseldorf.de

G. Wieners
Department of Radiology and Nuclear Medicine, University Hospital Magdeburg, Leipzigerstraße 44, D-39120 Magdeburg, Germany

O. Beuing
Department of Neuroradiology, University Hospital Magdeburg, Leipzigerstraße 44, D-39120 Magdeburg, Germany

A. Kelekis • D. Filippiadis
2nd Department of Radiology, National and Kapodistrian University of Athens Medical School, University General Hospital « Attikon», 124 64 Haidari, Athens, Greece
e-mail: akelekis@hotmail.com; dfilippiadis@yahoo.gr

K.E. Wilhelm
Department of Radiology, University Hospital Bonn, Sigmund-Freud-Str. 25, D-53127 Bonn, Germany
e-mail: kai.wilhelm@ukb.uni-bonn.de

J.-B. Martin
GIC-Geneva Imaging Center Sàrl, 21, Rue Chantepoulet, 1201, Genève, Switzerland
e-mail: jbmartin@beaulieu.ch

A.H. Mahnken et al. (eds.), *CT- and MR-Guided Interventions in Radiology*,
DOI 10.1007/978-3-642-33581-5_14, © Springer-Verlag Berlin Heidelberg 2013

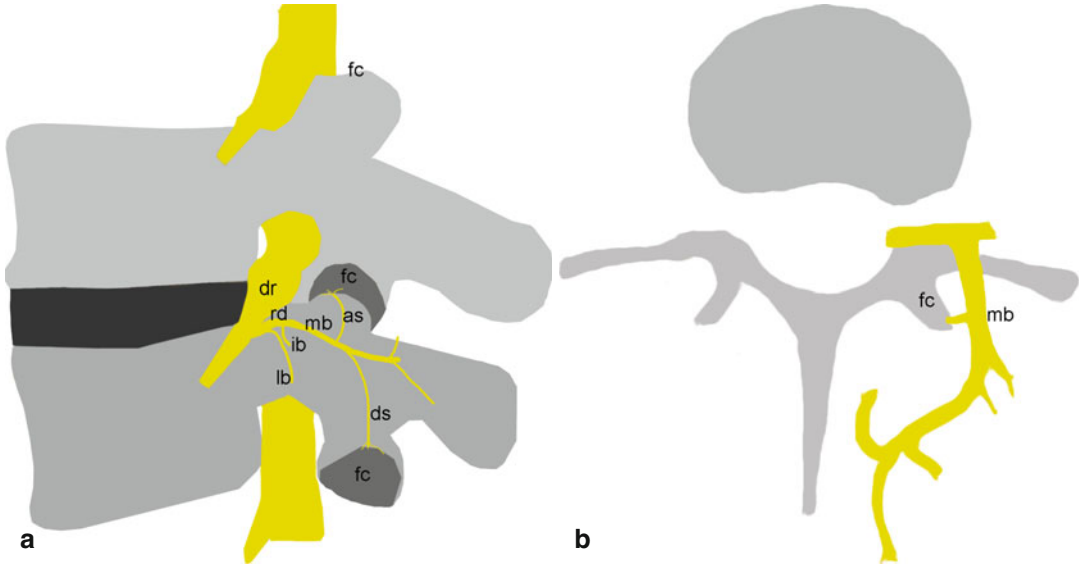

Fig. 14.1 Schematic image of the facet joint innervation. (**a**) Sagittal view: The ramus dorsalis (rd) arises from dorsal root (dr) and branching into lateral (lb), intermediate (ib), and medial branch (mb); From medial branch arises an ascending branch (as) to the level above and a descending branch (ds) to the nerve root level. (**b**) axial view

14.1 Neurolysis of the Facet Joint

Jan Hoeltje and Roland Bruening

14.1.1 Introduction

Chronic back pain is a widespread disease (Manchikanti et al. 2004; Neuhauser et al. 2005; Schwarzer et al. 1995). Due to the anatomy of the intervertebral joints and the increasing static load toward the lumbar spine, the lumbar facet syndrome is definitely more frequently observed than the cervical or thoracic one (Masharawi et al. 2004; Yoganandan et al. 2003). In many cases, the origin of pain may not be attributed to a focus, e.g., disc damage, neither by clinical examination nor by imaging methods.

A sufficiently reliable clinical definition of pain as caused by facet joint arthrosis is not possible (Helbig and Lee 1988; Jackson et al. 1988; Laslett et al. 2004, 2006; Lilius et al. 1990; Manchikanti et al. 2000; Revel et al. 1998; Schwarzer et al. 1994b, 1995). It may become manifest as unilateral or bilateral, exclusively lumbar or cervical pain whereby irradiation into the legs or arms does not exclude the spectrum of facet pain.

Clinically, an increased sensitivity to pressure is found above the concerned facet joint. In some cases, certain movements may increase pain. In contrast to disc prolapses, lumbar pain is not intensified by increasing intraabdominal pressure by maneuvers such as coughing. Cases of painful facet joint arthrosis are found increasingly in persons older than 65 years. Another clinical criterion is the absence of pain in rotation, in extension, or in flexion and absence of pain when straightening up from flexion. In a prone position and when walking, pain often decreases. There are controversial positions whether the pain does not occur in hyperextension or is even increased by this situation (Hildebrandt 2001; Revel et al. 1998; Schwarzer et al. 1994b). The most sufficient and reliable way to verify that the source of pain is the facet joint are nerve blocks of the medial branch or an anesthetic injection in the joint itself; it is the diagnostic approach (Cohen et al. 2010). Anatomically, the facet joints are supplied by the dorsal spinal root through the median branch (Fig. 14.1). The inferior part of the joint receives fibers of the same level (L 2/3 by L 3); the superior part from the nerve root placed the level above it (Bogduk et al. 1982; Cohen and Raja 2007; Suseki et al. 1997).

Due to this anatomy, it is either possible to apply a nerve block lateral of the facet joint (more common) or to inject directly in the capsule of the facet joint. For RF ablation, the probe should be placed nearby the capsule to affect all innervating fibers or to perform a neurolysis of the medial branch at the transverse process and facet joint in two levels (Kaplan et al. 1998; Marks et al. 1992; van Kleef et al. 1999).

The preferred imaging modality in most centers is the CT-guided approach, as it is the most exact procedure and allows reliable positioning of the probe and exact documentation of it. Alternatively, conventional two-dimensional fluoroscopy can be used (Gofeld et al. 2007), which is known to be less accurate than CT.

There are different techniques available for temporary or permanent facet joint neurolysis. The sole use of anesthetics, e.g., 1 % xylocaine or bupivacaine, is recommended for diagnostic reasons because of its very fast onset of only few minutes, very little side effects, and reversibility. Crystalloid long-acting steroids such as triamcinolone are most commonly used to achieve a longer-lasting therapeutic effect. Permanent neurolysis after two or more effective treatment with anesthetics became more common over the last years. The most common way of permanent neurolysis is radiofrequency ablation of the medial branch. An alternative approach for permanent neurolysis is cryotherapy. The injection of ethanol or phenol for permanent neurolysis of the medial branch has been described by some authors; none of these is based on a controlled study; because of this very sparse evidence, this therapeutic approach will not be dealt with within this chapter.

To guarantee a precise injection or the correct placement of the RF probe at the medial branch, a CT or MR must be performed. With conventional fluoroscopy or "blind" injections, it is only possible to position the needle tip near the target in the body. Moreover, monitoring of the distribution of injected liquids is much more precise with CT or MR (Meleka et al. 2005; Murtagh 1988). When compared to MRI, the availability of CT scanners is better, the space in the gantry is larger, the treatment time is shorter, and the material is cheaper, but in some cases, i.e., low back pain of pregnant women, it is necessary to perform the nerve block under MR guidance. Radiofrequency-based neurolysis using MR guidance is limited to experimental studies so far.

14.1.2 Indications

Facet joint neurolysis is indicated in patients with chronic back pain that arises from the facet joints as described above. However, it is not always possible to identify the facet joint pain as unique focus or at least as an important one for the genesis of pain by physical examination and morphological imaging. In these cases, temporary facet joint neurolysis has to be performed above all for diagnostic purposes. For this purpose, it has to be limited to one (or two levels) only. Periarticular infiltration with local anesthetics on a large area has to be avoided. At the beginning of such a diagnostic infiltration, pain should have been present for 2–4 weeks and treatment with, e.g., nonsteroidal antirheumatics should have been proven ineffective.

There are no absolute contraindications to facet joint neurolysis. Prior to the intervention, coagulation disorders or known intolerance to the substances used should be excluded. Infectious cutaneous lesions along the access route have to be treated previously. In case of a planned cortisone injection, diabetes has to be considered as a relative contraindication, particularly for diagnostic infiltrations.

The patient should be informed about general risks, such as hemorrhage, infection (Okada et al. 2005; Park et al. 2007), and drug intolerance. Possible treatment failure as well as conservative and operative treatment alternatives should be explained to the patient.

14.1.3 Material

For diagnostic injection, the following materials are needed:

- 22–26 G needle with 7–15 cm length with atraumatic cut, possibly with short-guiding needle, endhole or sidehole depends on personal preferences, with low artifacts in MRI (see Sect. 3.2)

- 10 ml local anesthetic (e.g., 1 % xylocaine) (10-ml syringe)
- 1 ml of diluted contrast material (1:1 contrast medium and saline)(2-ml syringe)
- Sterile table
- Sterile draping, sterile gloves, skin disinfection For therapeutic procedure, also:
- 40 mg (1 ml) triamcinolone (2-ml syringe) or RF probe with a short active tip of 0.5–1.0 cm

14.1.4 Technique

CT- or MR-guided intraarticular injection of the facet joint or neurolysis of the medial branch can be performed as follows:

- Level identification on the basis of a lateral scout image (for MRI, see Sect. 3.2).
- Acquisition of an axial scan for planning of the access route in order to reach the joint cavity (Fig. 14.2). For medial branch neurolysis, aim at the junction between the superior articular process and the superior transverse process; for L5 neurolysis, aim for the ala sacralis instead.
- Skin markers such as barium paste, radiopaque, gadolinium-filled, or metal marker grids may optionally be used.
- Skin disinfection and sterile draping.
- Puncture with the infiltration needle according to the planning until a slightly elastic or osseous resistance is registered. Local anesthesia may be used at this position.
- Acquisition of a control scan, possibly with subsequent correction of the needle position.
- If the patient reports to experience his known pain by provocation with the needle point, this has to be considered as an additional confirmation of the correct needle position. During injection of a very small quantity of contrast medium (ca. 0.3–0.5 ml), in case of pain, cease injection and ask for the pain irradiation area and whether this pain is identical with the known one. Perform a control tomography. If the contrast medium distributes in the joint cavity, the needle position is correct.
- Injection of 0.5 ml 1 % xylocaine for diagnostic purposes. In case of a therapeutic injection, possibly 0.5 ml (20 mg) triamcinolone can be injected afterward.

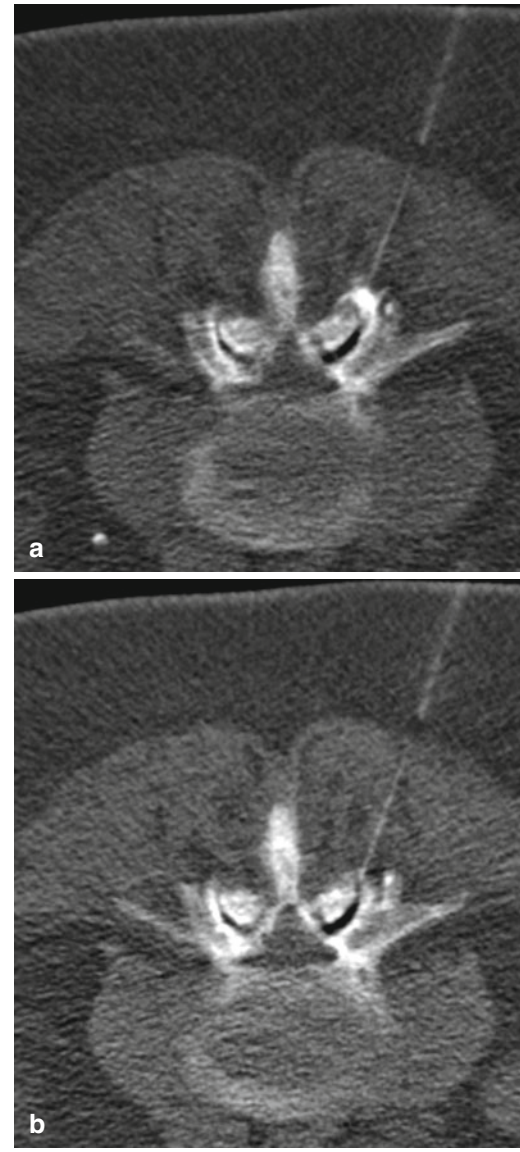

Fig. 14.2 CT-guided fact joint neurolysis. For injection therapy, a 25-G needle was placed in the arthrotic facet joint (**a**). After injection of approximately 0.1 ml of a contrast medium/NaCl mixture, CT shows a homogenous intraarticular distribution of the contrast medium (**b**)

- Injection of no more than a total of 1.5 ml of fluid for there is danger of rupture of the joint capsule.
- In case of a diagnostic infiltration, withdraw the needle. For diagnostic injections, it is crucial to avoid periarticular infiltration on a large extent as this will limit the diagnostic significance of the procedure.

- In case of a therapeutic procedure, slow withdrawal of the needle under aspiration and infiltration of the surrounding facet joint with local anesthetics.
- In case of RF ablation of the facet joint, the nerves are ablated outside the capsule. To achieve an optimal contact between RF probe and the nerve, the probe is inserted with an approximately 15° caudo-cranial angulation directly beneath the joint. For RF ablation, a 90–120 s heating (>80 °C) per position is considered sufficient (Hooten et al. 2005).

If the patient has tolerated this procedure well, subjective pain relief is key following application of analgesics. A few minutes after the end of intervention, the patient should report a clear relief or absence of pain. Since, in a lot of patients, spondylarthrosis is not the only painful degenerative change and after subsidence of this kind of pain another one, e.g., coxarthrotic pain, will dominate, such a patient has to be asked sometimes explicitly for changes of the treated pain syndrome in order to evaluate the result. According to the galenic properties of the local anesthetic, pain relief may persist only a few hours, and the beginning of the action of cortisone may delay pain recurrence up to 12 h. It is not unusual that the pain will occur again during the following days. A longer pain-free period will be achieved after at least a twofold repetition of the infiltration with a 1-week interval between the procedures.

14.1.5 Results

The therapeutic value of facet joint neurolysis is still in discussion (Aguirre et al. 2005; Cohen et al. 2008; Kaplan et al. 1998; Levin 2007; Lilius et al. 1990; Manchikanti et al. 2004; Marks et al. 1992; Nelemans et al. 2001; Schwarzer et al. 1994a). In 2007, a randomized, double-blind study was published comparing long-term success of facet blockages with and without steroids (Manchikanti et al. 2007). Although the number of patients involved was relatively small with 30 per study arm, a long-term success of the infiltrations could be shown for an average of four infiltrations per year. A superiority of infiltration with an addition of cortisone was not found so that there is no evidence for using steroids. However, these results will have to be confirmed by a larger study.

A multicenter study including 262 patients performed RF ablation; after 6 months, 54 % of patients report a pain relief of 50 % or greater was observed and 66 % perceived a positive global effect (Cohen et al. 2008); another trial reported about 68.4 % with good to excellent outcome (Gofeld et al. 2007).

Because other measurements such as physiotherapy have not been evaluated systematically together with a facet infiltration, their combined benefit remains unclear. Possibly, if these approaches were used in an optimized manner, opiates as well as their side effects may be avoided in some cases (Cohen et al. 2008).

Some authors contest the facet syndrome as an own entity. However, at current, its involvement in chronic back pain has to be taken as a basis (Helbig and Lee 1988; Hildebrandt 2001; Jackson et al. 1988; Laslett et al. 2006; Revel et al. 1998; Schwarzer et al. 1994b). A pathognomonic symptom on physical examination cannot be found, but there is evidence that many patients experienced repeated absence or relief of pain after two injections of local anesthetics with a variable duration of the effects. To guarantee a reliable diagnostic procedure, protagonists of this point of view require a blockage with different anesthetics twice in order to exclude false-positive infiltrations (Dreyfuss et al. 2003; Schwarzer et al. 1994a). Remarkably, only sparse evidence exists on the use of facet joint infiltration in relation to the outcome of a subsequent surgical intervention, e.g., arthrodesis (Cohen and Hurley 2007; Esses and Moro 1993).

14.1.6 Complications

Complications are rare with only few case reports. In controlled studies, no complications were observed. Paraspinal abscesses (Park et al. 2007) and cases of facet joint arthritis after infiltration are sporadically described in the literature; a transmission toward the epidural space or with resulting meningitis (Alcock et al. 2003; Gaul et al. 2005; Okada et al. 2005) was detected in

few cases only and is estimated to occur in less than 1 % of patients. In case of a suspected abscess, an MR scan and, after possible confirmation, relieving drainage or surgery should be performed. The danger of a paraspinal abscess has to be considered as extremely low if the procedure is performed under sterile conditions. The reports of abscess extension toward the epidural space, however, underline the necessity of working under absolute sterile conditions even if very small needles are used.

Summary

Facet joint neurolysis is indicated in patients with chronic back pain that arises from the facet joints. Pain should be present for 2–4 weeks, and treatment with nonsteroidal antirheumatics should have proven ineffective.

There are no absolute contraindications to facet joint neurolysis. Prior to the intervention, coagulation disorders or known intolerance to the substances used should be excluded. Complications are rare with only few case reports describing local infection and very rarely meningitis.

Key Points

- Percutaneous image-guided facet joint nerve block is a safe procedure with an extremely low complication rate. In many cases, diagnostic facet infiltration is the only procedure to clarify whether the facet joints causes the pain.
- In most of the cases, a quick relieve of pain is achieved and may last for several months.
- If needed, facet joint nerve block can be repeated several times.
- Repeated injections usually increase the length of the asymptomatic interval.
- A neurolysis of the medial branch with RFA after at least two successful infiltrations is a good alternative to achieve permanent neurolysis.
- In selected patients, nerve blocks may be performed with MR guidance.

14.2 Image-Guided Nerve Blocs and Infiltrations in Pain Management

Bruno Kastler

14.2.1 Introduction

Cross-sectional imaging namely computed tomography (CT) and magnetic resonance (MR) imaging offer an excellent and safe mean of guiding procedures by displaying a very good contrast between soft tissues, bone, and vessels. CT guidance in contrary to fluoroscopic guidance allows safe needle progression and precise positioning at target which reduces complications and optimizes procedure results (Kastler et al. 1999). We will demonstrate step by step our routinely used technique under cross-sectional imaging guidance (patient positioning, gantry tilting, saline injection, needle steering, etc.). Examples at different anatomic sites are here presented which can be used either in addition to or as an alternative to other conventional methods in pain management. To perform cross-sectional imaging-guided interventional procedures, one must first have a good understanding of the anatomical relationship of the target and the surrounding structures which determine the possible safe percutaneous pathways.

14.2.2 Materials and Technique: General Considerations

14.2.2.1 Radiofrequency Ablation

Radiofrequency (RF) ablation of nerves involves the placement of an insulated electrode needle with uninsulated small tip precisely targeted beneath or into nervous tissue. Heat is generated by the interaction between tissue and high-frequency current (see Chap. 13.1.1). In order to control thermal lesion size, a constant electrode tip temperature of ≥90 °C has to be maintained for 1–2 min. Tissue charring and boiling should be avoided in RF for pain management. Ideally, small needle electrodes (20 gauge) with active tip length in the range of 0.5–2 cm are available for

pain treatment. When compared with other techniques, RF ablation offers numerous advantages for interventional pain management:

- Adequate control of lesion size
- Control of needle placement by electrical stimulation with testing of possible pain reduction
- Selective sensory lesion (with no motor damage)
- Lower incidence of complications
- Ability to safely repeat treatment if the neural pathway regenerates

It however requires an initial investment (RF generator), and RF electrodes are more costly than simple spinal needles needed for injection therapy. Moreover, RF ablation is also more time consuming.

14.2.2.2 Alcohol Ablation

Percutaneous injection of alcohol (95 %) or phenol (6 %) can be used to perform neurolysis in analogy to its use as a destructive agent in tumor therapy.

For interventional pain management with alcohol, the correct position of the needle tip at target is determined by a test injection of diluted contrast media with local anesthetics (Kastler et al. 1999), which allows to anticipate possible diffusion of the alcohol and also to perform a block test.

In the estimation of the diffusion of alcohol, it needs to be noticed that alcohol is simultaneously hydrosoluble and liposoluble. The diffusion of absolute alcohol is thus not completely controllable and not strictly consistent with the diffusion of the preliminarily injected anesthetic-contrast mixture, which is hydrosoluble only.

To realize an adequate neurolytic effect, an intramural alcohol concentration of 66–75 % is required. The calculation for the concentration follows a simple rule: The injected total quantity of absolute (96 %) alcohol (A), which follows the injection of lidocaine-contrast mixture (X), must be at least twice or better three times the quantity of X ($A = 2 \cdot X$ or $A = 3 \cdot X$). With the injection of high concentrated alcohol, smaller total ablation volumes can be achieved when compared with the anesthetic effect of the test injection.

Alcohol must be instilled slowly, and aspiration is performed before injection to avoid accidental intravascular injection. Rare complications can be minimized by injecting small volumes of alcohol and by correctly positioning the needle tip. After injection, alcohol can be seen as hypodense area diluting the contrast media. An appropriate local anesthesia is needed to reduce the painful alcohol instillation. Before the needle is removed, it is flushed with a small amount of saline or anesthetic. An important advantage of alcohol ablation is its low costs and the longer-lasting effects when compared with RF ablation. Relevant drawbacks include the possible spread on distant motor nerves.

14.2.2.3 Steroid Infiltration

The injection of steroids can be used in local pain management because of its analgesic and anti-inflammatory effects. The procedure equals alcohol injection therapy, but unlike alcohol injection, steroid injection per se is not painful.

Short-acting steroids are used for spinal epidural or periganglionic foraminal infiltration because of steroid-induced arachnoiditis risk. Prednisolone (1 ml/5 ml volume which is equivalent as 25/125 mg of prednisone) is typically used for this indication. For peripherical infiltration long-acting glucocorticoids should be used (e.g., cortivasol 1, 5 ml which is equivalent to 75 mg prednisone).

14.2.2.4 Patient Preparation

All interventional procedures should be preceded by a consultant a few days prior to the procedure (at least 24 h). Obtaining a detailed patient history is necessary to rule out contraindications to the procedure. It also helps to establish patient's confidence through individual, clear, and simple explanation of the course of the procedure. The patient is informed on the possible rare complications of the procedure, and given consent should be obtained depending on federal and national country regulations.

Prior to the intervention, a review of the patient's complete blood count and blood chemistry by the interventionalist is necessary. Special attention is given to the hemostasis parameters including thromboplastin time, partial thromboplastin time, and platelet count in order to rule out

bleeding disorders. Contraindications for percutaneous procedures are represented by a platelet count lower than 100,000/mm^3, a thromboplastin time below 60 %, and an international normalized ratio ≥2. To ensure sufficient renal function, blood creatinine is assessed. In case of known hypersensitivity, antiallergic premedication may be appropriate. It is important that the patient does not eat for a minimum of 4 h prior to the intervention. In our experience, a preliminary empathic conversation makes an important contribution to an optimal cooperation of the patient. Particularly anxious patients require prescription of anxiolytic medication prior to the procedure.

14.2.2.5 Intervention Room Preparation

Prior to each intervention, cleaning and disinfection of all surfaces such as the CT-scan table and gantry, as well as the room floor, is routinely performed. The mobile stainless steel instrument table is covered with sterile sheets. The following items should be available:

- Syringes (5, 10, and 20 ml)
- Hypodermic needle for local anesthesia
- Saline solution, anesthetics, and different volumes of ionized contrast medium. In addition to clear labeling, it is advised to use a fixed arrangement in order to avoid confusion.
- Sterile pads
- A set of sterile sheet for interventional purposes
- Flexible or rigid 20-gauge therapy needles (22-gauge for neurolysis)
- Absolute (dehydrated) alcohol, steroids… (depending on the procedure)

14.2.2.6 Image Guidance: How I Do It

For procedure planning, images of recent examination can be used. To increase the precision of navigation, we prefer to acquire an additional set of contrast-enhanced cross-sectional images of the anatomical area of interest at the beginning of the intervention.

In detail, the procedure runs as follows:

1. The patient is placed in a supine or prone position depending on the entry point.
2. Contiguous axial CT sections with 3- to 5-mm slice thickness covering the entire region of interest are obtained.
3. A safe pathway is chosen carefully avoiding inadvertent puncture of vessels or hollow organs. Injection of contrast material may be needed to identify vessels.
4. The optimal skin entry point is determined and marked on the skin with a waterproof felt-tip pen.
5. The skin is scrubbed and sterilized, and the patient is draped in a sterile fashion. Local anesthesia is instilled at the skin entry point.
6. The hypodermic needle used for local anesthesia should first be left in place and used to visualize the actual skin entry point on CT to estimate and verify relevant information regarding the optimal puncture angle, the direction, and the distance to the target of the therapy needle.
7. The therapy needle is slowly moved forward toward the target. This can either be done step by step under image guidance or continuously using CT fluoroscopy. On CT images, the needle direction can be estimated from its hypodense shadow. This phenomenon is due to hardening of the x-ray beam. Correct positioning of the needle tip on the target can be verified by injecting contrast media. When using RF, the stimulation mode of the generator may be switched on. Reaction of the targeted nerve proves correct needle placement.

A control CT scan at the end of the procedure ensures the absence of complications. Most pain management procedures can easily be performed under CT guidance on an outpatient basis. Local anesthesia is normally sufficient for intervention-related pain.

14.2.3 Materials and Technique: Detailed Considerations

14.2.3.1 Pterygopalatine Ganglion Neurolysis

Indication

Neurolysis or blockade of the pterygopalatine ganglion (PPG) is an efficient method in the management of pain in patients suffering from (Devoghel 1981):

- Cluster headaches
- Atypical facial pain
- Trigeminal neuralgia
- PPG neuritis
- Postherpetic neuralgia
- Severe intractable cancer-related pain

Anatomy

The pterygopalatine fossa (Hardebo and Elner 1987; de Kersaint-Gilly et al. 1991) is located directly posterior to the maxillary sinus (Fig. 14.3). It houses the internal maxillary artery, the pterygopalatine ganglion, and the maxillary nerve. In general, the arterial component of the fossa lies anteriorly and the neural component, posteriorly.

Image Guidance for Alcoholization and RF Procedure (Clair et al. 1998)

The patient is placed in a supine position on the CT table with his head turned opposite to the side of puncture. Axial CT sections with a slice thickness of 3–5 mm are acquired from the upper part of the zygomatic arch to the lower part of the maxillary bone. The pterygopalatine fossa is seen dorsal to the maxillary sinus and anterior to the lateral pterygopalatine plate. The PPG is located at the level of the sphenopalatine foramen.

The skin entry point is located just above zygomatic arch. A safe pathway is chosen in order to avoid damage to the internal maxillary artery (Fig. 14.3). The needle is slowly and advanced forward using step-by-step CT guidance until the needle tip is safely placed within the pterygopalatine fossa.

The correct position of the needle tip (disposable 22.5-gauge – 12.70-cm spinal needle at target is determined by an injection of 0.5-ml) local anesthetic diluted (10 %) with contrast media (Fig. 14.3). Before the injection, the mounted syringe is maintained in aspiration (under vacuum) for 5 s in order to detect blood (vascular puncture). Neurolysis is performed with 1 ml of absolute alcohol which should be instilled slowly. Alternatively, RF ablation may be used. The procedure is carried out on an outpatient basis, and the patient is kept under observation for 1 h.

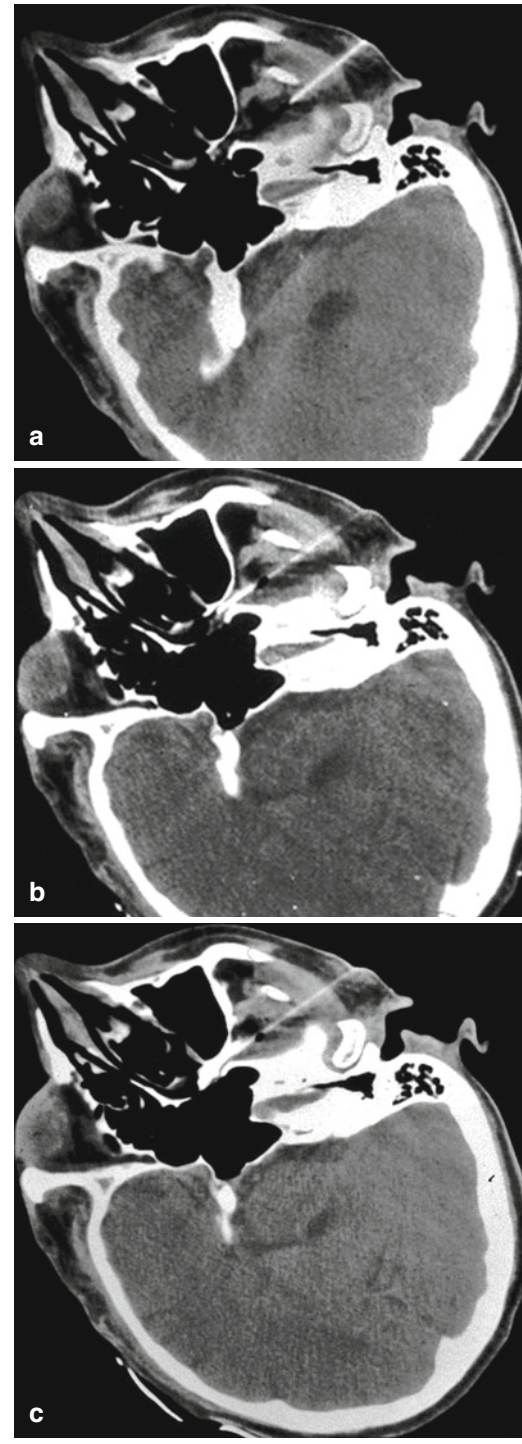

Fig. 14.3 Pterygopalatine ganglion neurolysis: The needle is placed under step-by-step CT guidance (**a**, **b**), and contrast media with a local anesthetic is injected to assure correct needle tip position on the target. Finally, 1 ml of absolute alcohol is slowly instilled (**c**)

Complications

Complications are rare. Control CT imaging at the end of the procedure ensures the absence of complications, particularly hematoma. It also shows the distribution of the neurolytic agent. Some patients experience epistaxis following this procedure. They should not be discharged until this condition has fully disappeared. The number of complications can be minimized by keeping the volume of injected alcohol within 1 ml and by correctly positioning the needle tip.

14.2.3.2 Arnold's Nerve Infiltration

Indication

Neurolysis or blockade of the nerve of Arnold is an efficient method in the management of Arnold's neuralgia. The symptoms have been well described. The typically unilateral (rarely bilateral) pain mostly starts in the suboccipital region and radiates over the posterior scalp to the top of the head. Retro-orbital pain may be present in severe attacks. Two forms have been described: a paroxysmal form and a continuous form.

Anatomy (Bogduk 1980)

The greater occipital nerve (GON) or nerve of Arnold corresponds to the posterior branch (sensory) of the second cervical nerve. It originates between the posterior arch of the atlas (C1) and the lamina of the axis (C2). The GON has a complex winding comprising a series of segments and angles. This complex course exposes the nerve to possible compression and/or stretching, particularly during movement of the head (Vital et al. 1989). Two zones where the nerve is anatomically vulnerable and where infiltrations can be of benefit can be outlined (Bogduk 1981; Bovim et al. 1992; Bovim and Sand 1992):

- Proximally at its origin ("or," "first site") and at its first bend ("b1," "second site") where the GON curves around the inferior oblique capitis muscle
- Distally at its emergence at the narrow and rigid aperture when perforating the tendinous area of the trapezius muscle ("em," "third site"; (pain trigger zone))

Image Guidance for Infiltration Procedure

Infiltration of the GON at Its Origin ("*or*," "*first site*"). The approach is posterior or posterolateral, and the patient is placed in a comfortable prone position with a pillow under his or her chest. The patient's head is turned opposite to the puncture site for a unilateral infiltration (Fig. 14.4) and face down on a padded surgical ring for a bilateral infiltration (Fig. 14.5). After bolus contrast injection, an initial series of axial 3–5-mm slices covering the occipital bone to C3 is obtained in order to visualize vascular structures particularly the vertebral artery and to ensure that it lies outside the chosen pathway).

The target "or" is at an intermediate level between the two arches, slightly below the posterior margin of the posterior arch of C1, directly behind the C1–C2 joint capsule (Fig. 14.4). Before the injection, the mounted syringe is maintained in aspiration (under vacuum) for 5 s in order to detect blood (vascular puncture) or cerebrospinal fluid (dural effraction). First, a mixture of 1 ml of saline and contrast medium (90 %/10 %) is injected. If the needle tip is safely positioned (outside of vascular structures and the foramen magnum), the spread of saline-contrast mixture molds the dura mater (and ideally the spinal C2 ganglion). Thereafter, the steroid is administered: slow depot steroid instillation of prednisolone 2 ml (50-mg prednisone equivalent).

If a radiofrequency generator is available, initially a test is performed in the stimulation mode at the C1 ganglion level; the patient should feel a tingling effect in the territory of the GON. Subsequently, thermal ablation can be performed.

Infiltration of the GON at the Second Proximal Site ("*b1*"). We advocate when retrieving the needle (or, alternatively, when aiming at the target) that a second infiltration be given behind the inferior oblique capitis muscle around which the GON describes its first bend (Fig. 14.4). The needle tip visualized by the tip artifact should be located in the fatty compartment between the dorsal aspect of the inferior oblique capitis muscle and the deep aspect of the semispinalis capitis muscle. The infiltration starts with a block comprising a 3-ml mixture of short- and long-acting anesthetics (lidocaine 1/3 and ropivacaine 2/3)

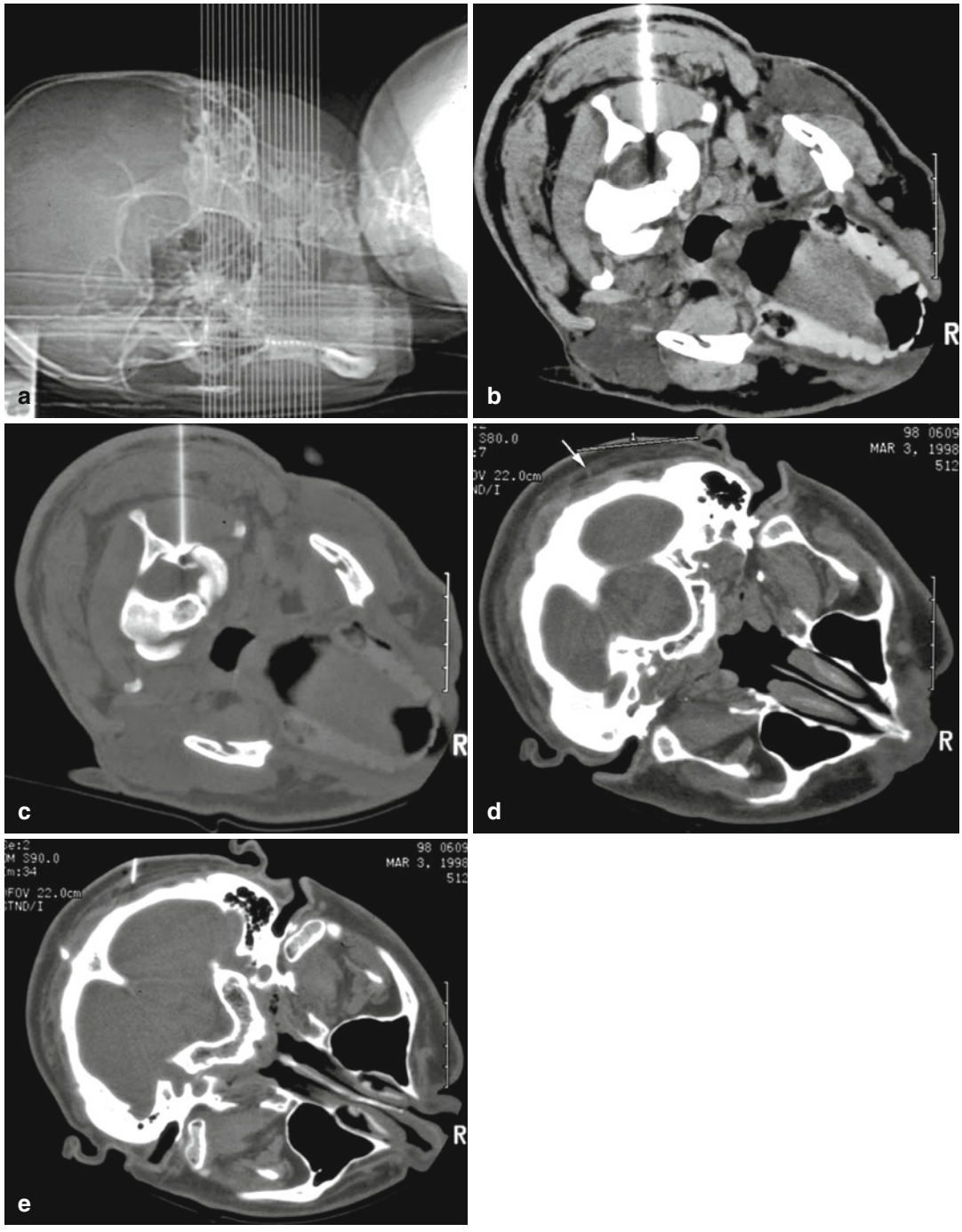

Fig. 14.4 Unilateral infiltration of the greater occipital nerve at its emergence origin ("or") and emergence ("em"); the scout view displays the scan range from the occipital bone to C3 (**a**). Infiltration at the origin: Needle tip is on target slightly under the posterior arch of the atlas directly behind the C1–C2 joints (close to the nerve origin) (**b**). Proper spread of the saline-contrast mixture molding the dura mater before the depot steroid injection is made (**c**). Optimal entry point (facing the occipital artery *arrow*) is determined on line with the nuchal ridge (**d**). The needle tip is placed in proximity and medial to the artery (**e**). The infiltration consists of a block with local anesthetic and depot steroid

and contrast media (10 %). The proper diffusion of this hyperdense mixture between the two muscles confirms that the needle tip is safely positioned (Fig. 14.5). The injection of prednisolone (2 ml; 50-mg prednisone equivalent) or cortivazol (1 ml; 50-mg prednisone equivalent) can then safely be performed.

Infiltration of the GON at Its Emergence ("*em*," "*third site*"). The infiltration is usually conducted using bony and palpable landmarks. The infiltration can also be performed under CT guidance by finding the occipital artery on the slice where the occipital artery becomes subcutaneous (accompanying the GON), usually close to the superior nuchal line (pain trigger zone).

Complications

At the origin of the nerve, the most frequent complication is the inadvertent puncture of the vertebral artery. This is avoided by CT guidance, which is far more precise than fluoroscopic guidance (Bogduk 1981; Bovim et al. 1992). The same applies for piercing the dura matter or infiltration of the neck muscle on the pathway. Pain at the puncture site, transitory torticollis, nausea, and dizziness are rare adverse reactions.

14.2.3.3 Stellate Ganglion Neurolysis

Indications

Neurolysis or stellate ganglion block is an efficient and accepted method in the diagnosis and treatment of acute and chronic sympathetically maintained pain syndrome of the upper limb, thoracic viscera, and head and neck (Forouzanfar et al. 2000; Kastler et al. 2001). Indications including:

- Algodystrophy or reflex sympathetic dystrophy syndrome, currently referred to as type I complex regional pain syndrome (CRPS). It is a combination of a nonsystematic pain syndrome, tenderness and swelling, changes in cutaneous blood flow, abnormal sweating, and stiff joints. CRPS, although benign, is highly invalidating because it resists specific medication.
- Causalgia or type 2 chronic regional pain syndrome.
- Postherpetic neuralgia.

It is also an effective treatment option in cases of severe intractable cancer-related pain arising from regional neoplasms invading the stellate ganglion (Pancoast and cervical tumors) (Gangi et al. 1996).

Anatomy

The stellate ganglion is a rather large oval-shaped structure. It typically measures $2.5 \times 1 \times 0.5$ cm. It is formed by the fusion of the inferior cervical and first thoracic sympathetic ganglia and is oriented along the axis of the spine. It is located anterior to the neck of the first rib, the transverse process of the seventh cervical vertebra, and posterior to the vertebral artery at the origin from the subclavian artery (Hogan and Erickson 1992; Hogan et al. 1992).

Image Guidance for Acoholization and RF Procedure

The patient is placed in a supine position on the CT table with his head turned opposite the side of puncture and his arms at his sides. Axial CT contiguous slices of ≤5 mm in thickness are obtained from the superior aspect of the sixth cervical vertebra through the superior level of the second thoracic vertebra as determined from the scout view. The stellate ganglion lies immediately in front of the transverse process of the seventh cervical vertebra and the neck of the first rib. It is targeted on these slice levels. A bolus injection of contrast media is given to display possible intervening vascular structures, particularly the vertebral artery. An anterolateral pathway is chosen. Inadvertent puncture of the external and internal jugular veins as well as the carotid and vertebral arteries need to be avoided meticulously. The needle is slowly moved forward using either sequential or real-time fluoroscopic CT images until its tip is correctly positioned within the target (Kastler et al 2001; Scott et al. 1993).

a. The ablation may be done by RF neurolysis (Fig. 14.6) or by the injection of ethanol (Fig. 14.7). For RF neurolysis, the 20-gauge RF electrode is used. The thermal lesion is created at a temperature of 60–80° which has to be maintained for 60–120 s. This procedure can be repeated up to three times moving the

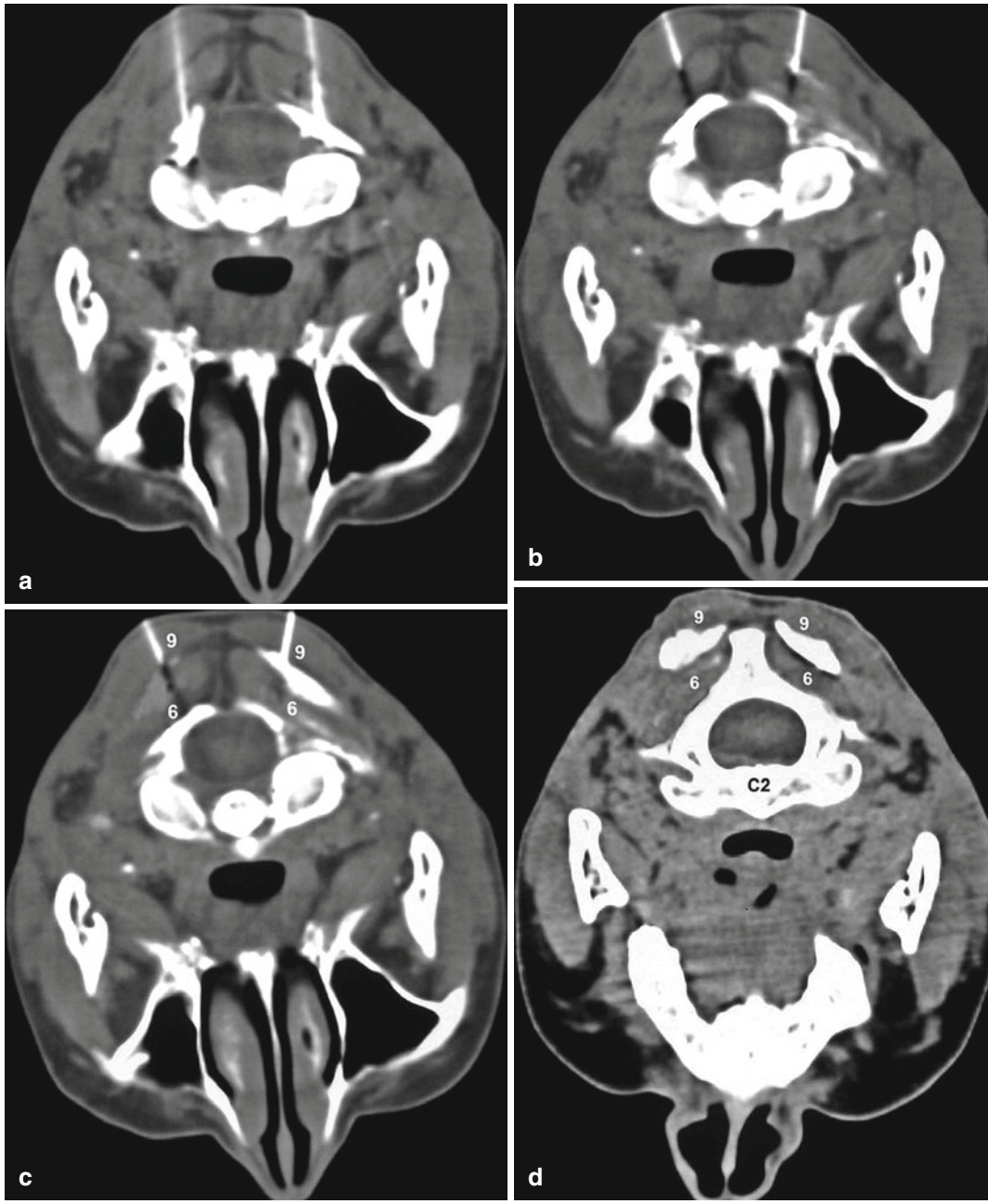

Fig. 14.5 Bilateral infiltration of the greater occipital nerve at its origin ("or") and on the second proximal site, first bend ("b1"): Left needle and right needle are on target slightly under the posterior arch of the atlas directly behind the C1–C2 joints (close to the nerve origin) (**a**). Proper spread of saline-contrast mixture molding the dura matter before the depot steroid injection is made. A second infiltration is performed by pulling back on the needles to arrive at the first bend (around the inferior oblique capitis muscle) with the needle tips being placed in the fatty compartment between the dorsal aspect of the inferior oblique capitis muscle (*6*) and the deep aspect of the semispinalis capitis muscle (*9*; **b**). The proper spread of this hyperdense mixture between the two muscles (especially toward the "b1" bend) can be verified on control CT slices (**c**, **d**)

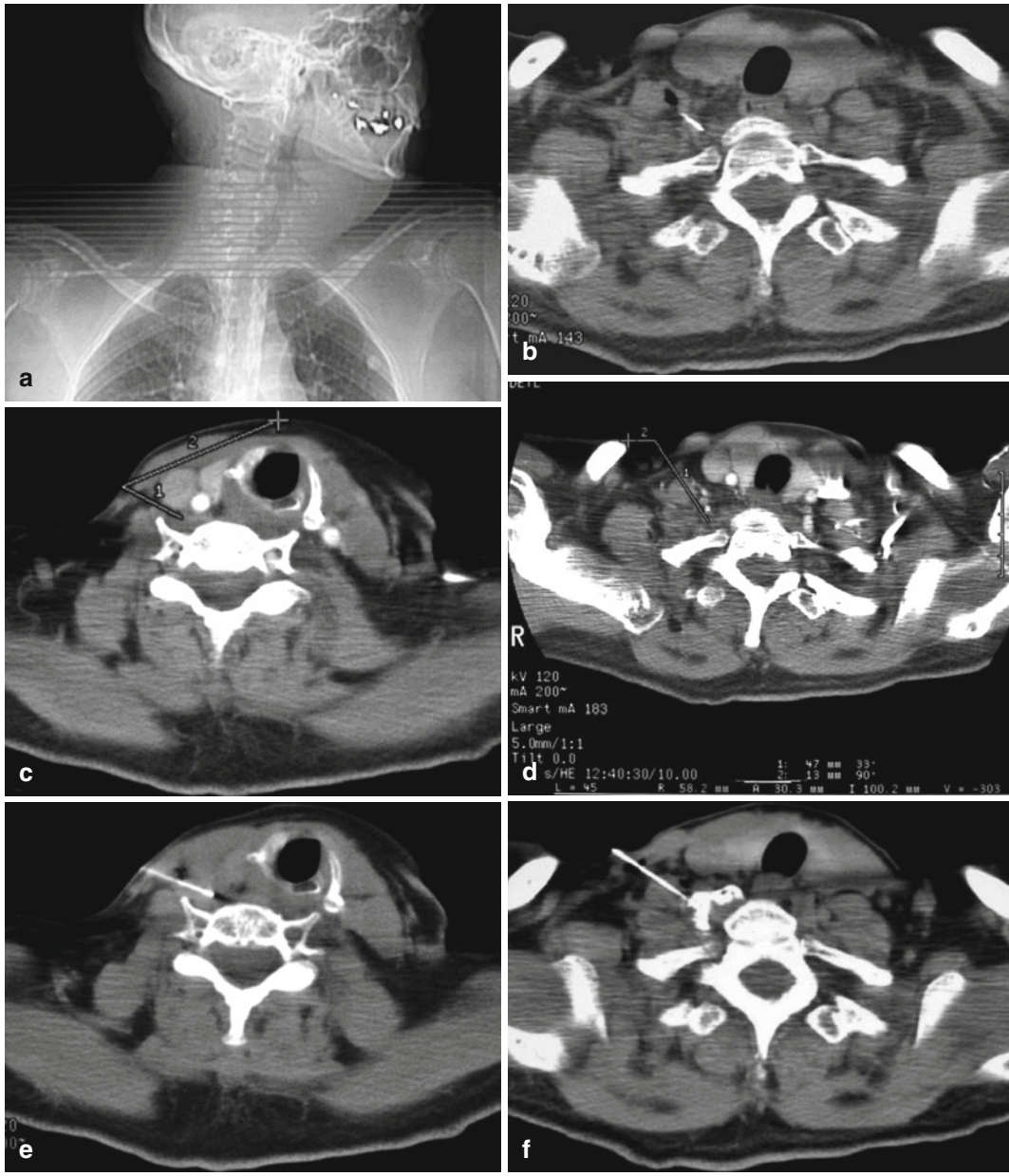

Fig. 14.6 Radiofrequency (RF) neurolysis of the stellate ganglion: 49-year-old man suffering CRPS type 1 syndrome after wrist trauma. Scan range is displayed on scout view (**a**). Entry points and trans-scalenic pathway are displayed at C7 and T1 levels (**b**, **c**). RF needle tips on targets at C7 and T1 levels (**d**, **e**). After RF thermolysis, additional blockade with local anesthetics was performed at the end of the procedure. Control CT scan shows the contrast-anesthetic mixture diffusing around the needle tip (**f**). Clinically, a good long-term result was obtained after the procedure

cannula forward and backward 1 mm each time. The level of the seventh vertebra and the neck of the first rib both should be targeted for RF ablation. As described above, RF thermal neurolysis creates a discreet lesion which provides good pain relief, but which does not interrupt the entire ganglion function and does not tend to produce a Horner's syndrome.

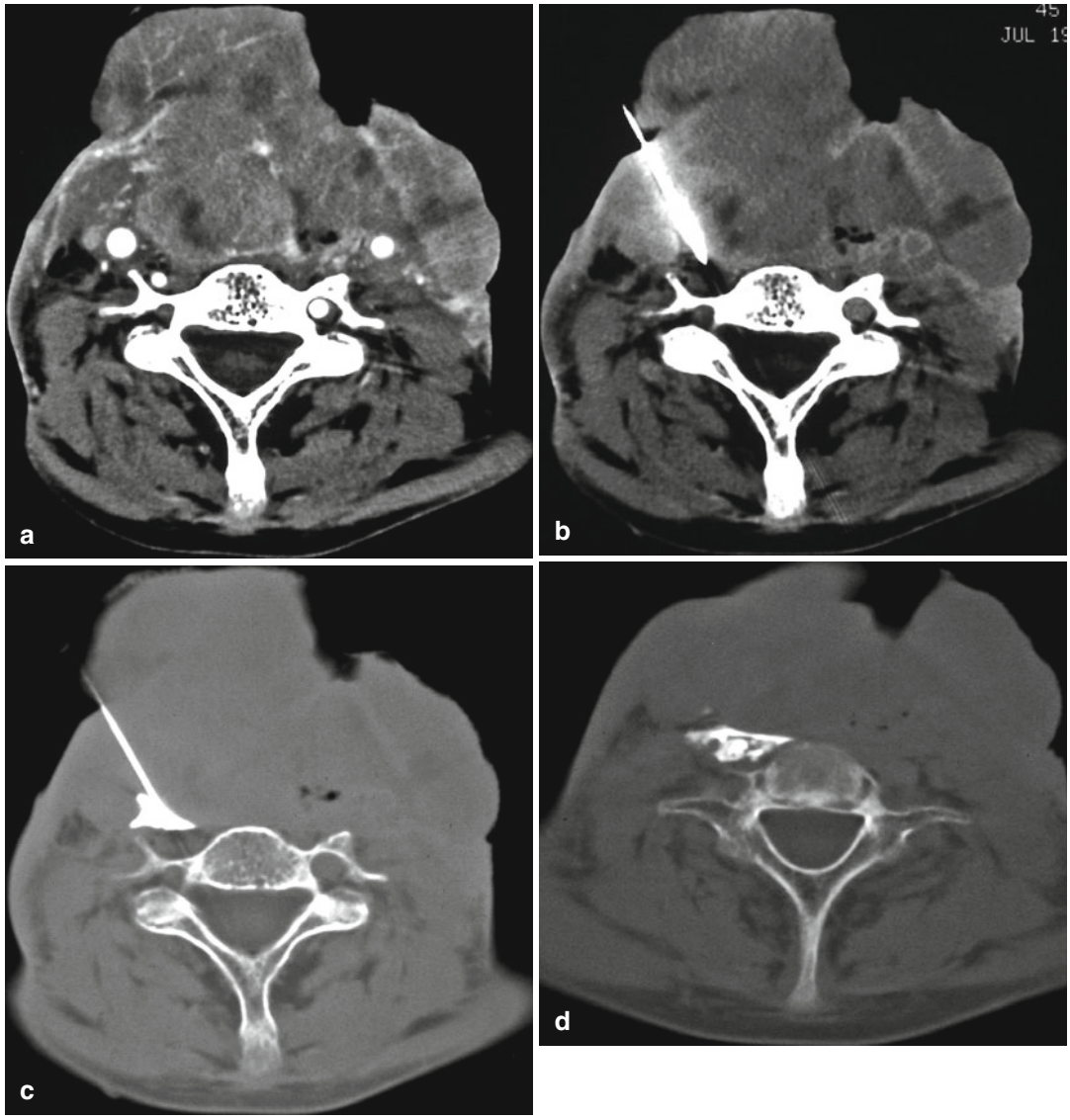

Fig. 14.7 Alcohol neurolysis of the stellate ganglion: 45-year-old male patient with locally advanced throat cancer suffering severe intractable cervical pain (**a**). Excellent pain relief was observed immediately following ethanol neurolysis. This effect lasted until the patient died 5 months later. An anterolateral approach at the posterolateral aspect of the mass at the level of C7 was chosen to avoid the hypervascularized tumor (**b**). Correct positioning of the needle tip at target is attested by the diffusion of a local anesthetic diluted with contrast medium showing good diffusion around and particularly behind the vertebral artery (**c**). Injection of 1 ml of absolute alcohol appearing as hypodensities within the contrast medium (**d**)

For alcohol ablation, the correct position of the needle tip at target (seventh cervical vertebra) is determined by an injection of 1 ml contrast medium 10 % diluted in a mixture of lidocaine 1/3 and ropivacaine 2/3. Before the injection, the mounted syringe is maintained in aspiration (under vacuum) for 5 s in order to detect blood (vascular puncture). The injected volume should be kept below 1 ml. The procedure is carried out on an outpatient basis, and the patient is kept under observation for 1 h.

Complications

A CT control covering the third cervical to second thoracic vertebra at the end of the procedure ensures the absence of complications. Using RF ablation, complications are less common when compared with alcohol ablation. Alcohol neurolysis usually produces a Horner's syndrome and should be limited to patients with a low life expectancy (intractable cancer-related pain). Alcohol may diffuse to surrounding motor nerves: The C8 and T1 roots of the brachial plexus are particularly exposed as they are located posterior to the stellate ganglion.

14.2.3.4 Celiac Plexus Neurolysis

Indications

Neurolysis of the celiac plexus (Buy et al. 1982) is an efficient method to treat pain secondary to malignancies of the retroperitoneum and the upper abdomen or secondary to pancreatitis.

Anatomy

The greater, lesser, and least splanchnic nerves provide the major preganglionic contribution to the celiac plexus. The celiac plexus is located anterior to the crus of the diaphragm and extends in front of and around the aorta. The ganglia usually lie approximately at the level of the first lumbar vertebra and at the level of the celiac arterial trunk (Ward et al. 1979).

Image Guidance and Alcoholization Procedure

The posterior transcrural approach with two needles and a transaortic approach are our techniques of choice (Ischia et al. 1983, 1992). Therefore, the patient is placed in the prone position with a pillow placed under the abdomen. Axial CT sections of ≤5 mm in thickness with injection of contrast media are obtained from the level of the eleventh thoracic vertebra to the second lumbar vertebra. The target level is chosen between the celiac arterial trunk and superior mesenteric artery. The 20–22 gauge needles are advanced under repeated sequential or fluoroscopic real-time CT guidance until their tips are positioned at the splanchnic nerves anterior and lateral to the first lumbar vertebral body. The left needle crosses the aorta to the region of the celiac ganglia. Adequate positioning is attested by a test injection of contrast medium 10 % diluted in a mixture of lidocaine 1/3 and ropivacaine 2/3 (3 ml celiac, 1 ml splanchnic). Before the injection, the mounted syringe is maintained in aspiration (under vacuum) for 5 s in order to detect blood (vascular puncture). The contrast media should be seen in the pre-aortic area and surrounding the aorta and celiac trunk (Fig. 14.8). Finally, a 10–15-ml volume of absolute alcohol is injected (Haaga et al 1984; Lee et al. 1993).

A transaortic path is excluded in aortic aneurysm, voluminous calcified parietal plaque, or mural thrombus and should be avoided with patients suffering from chronic respiratory insufficiency.

Alternatively, a posterior approach may be used using two needles with a lateral aortic approach. The material however rarely spreads as it should bilaterally in front of the aorta and/or on the right for the contralateral injection; the inferior vena cava or another obstacle often hinders the needle's trajectory.

The anterior approach to the celiac plexus involves the passage of a fine needle through the liver, stomach, and pancreas (Fig. 14.9). It is most useful in patients who are unable to lie prone. An anterior approach should be avoided when there is significant gastric stasis with distension.

Complications

Complications include local pain and orthostatic hypotension. Thus, the patient is observed for hemodynamic changes because of profound sympathetic blockade. Pleural effusion has been described (Fujita and Takaori 1987). Post-block diarrhea occurs in approximately 50 % of patients (Gafanovich et al. 1988). The latter in fact often alleviates the frequent cases of chronic constipation in these patients under opiates.

14.2.3.5 Pudental Nerve Infiltration

Indications

Pudental neuralgia is rare and very painful and invalidating (Amarenco et al. 1988). Infiltration

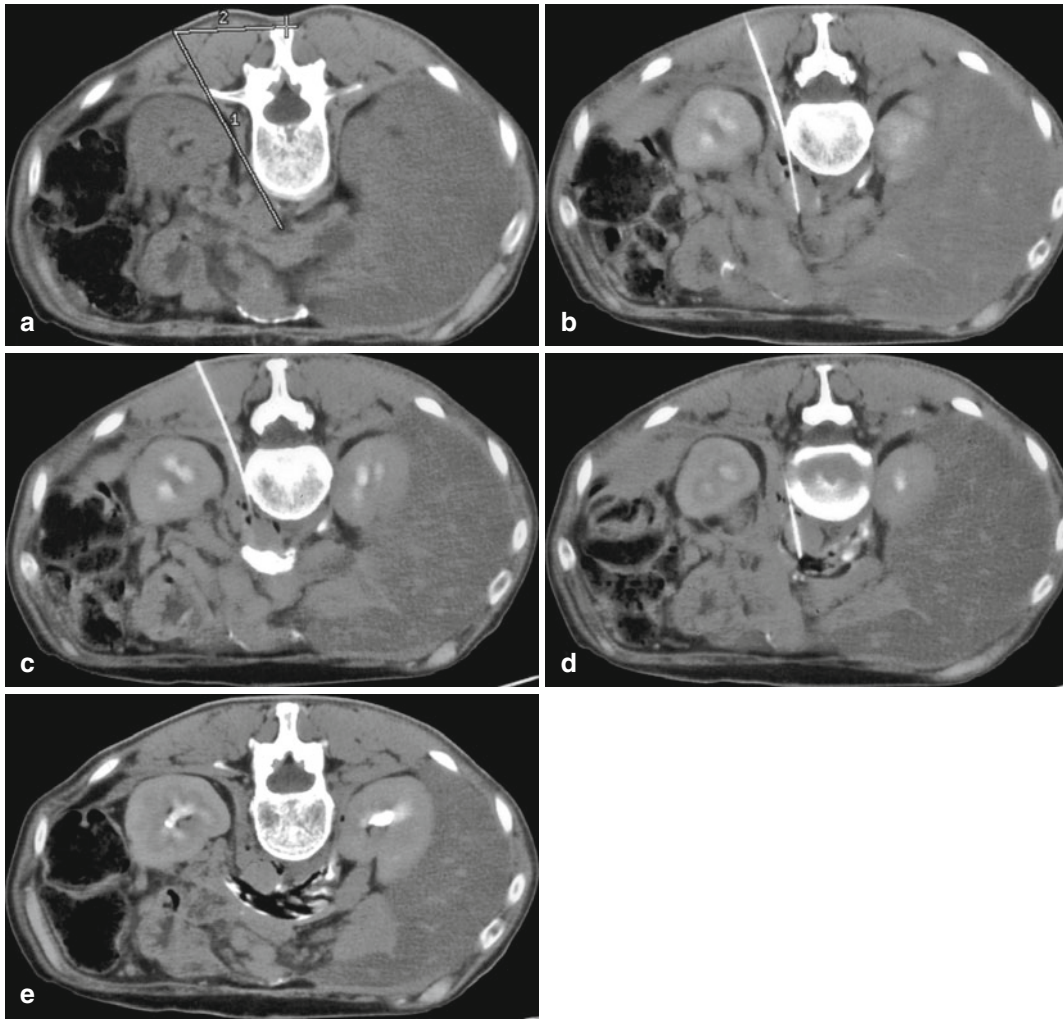

Fig. 14.8 Celiac plexus neurolysis: direct access using transaortic passage. Trajectory (*line*) for transaortic celiac neurolysis (**a**). Transaortic passage of the needle to the celiac site (**b**). After injection of a lidocaine/contrast mixture, there is a good symmetrical diffusion (**c**). Control after injection of 5 ml absolute alcohol seen as hypodensity within the contrast agent (**d**). Control scan after end of injection of 15 ml of absolute alcohol shows an excellent alcohol diffusion (**e**)

(Corréas et al. 1988) has been found helpful in managing the pain and to predict efficacy of surgical decompression.

Anatomy

The pudendal nerve is formed from the fusion of the second, third, and fourth sacral nerves which merge posterior to the ischiatic spine. Anatomical studies suggest that there are two possible conflicting sites: (1) entrapment of the pudendal nerve during its course at the ischial spine as the nerve can be entrapped under the sacrospinous ligament and/or (2) the Alcock's canal, a non-stretchable aponeurotic tunnel.

Image Guidance and Infiltration Procedure

The patient is placed in a prone position. Axial slices of ≤5 mm thickness are obtained covering the region of the obturator foramen. Both possible conflict sites are targeted (Figs. 14.10 and 14.11). Optimal skin entry points are determined choosing

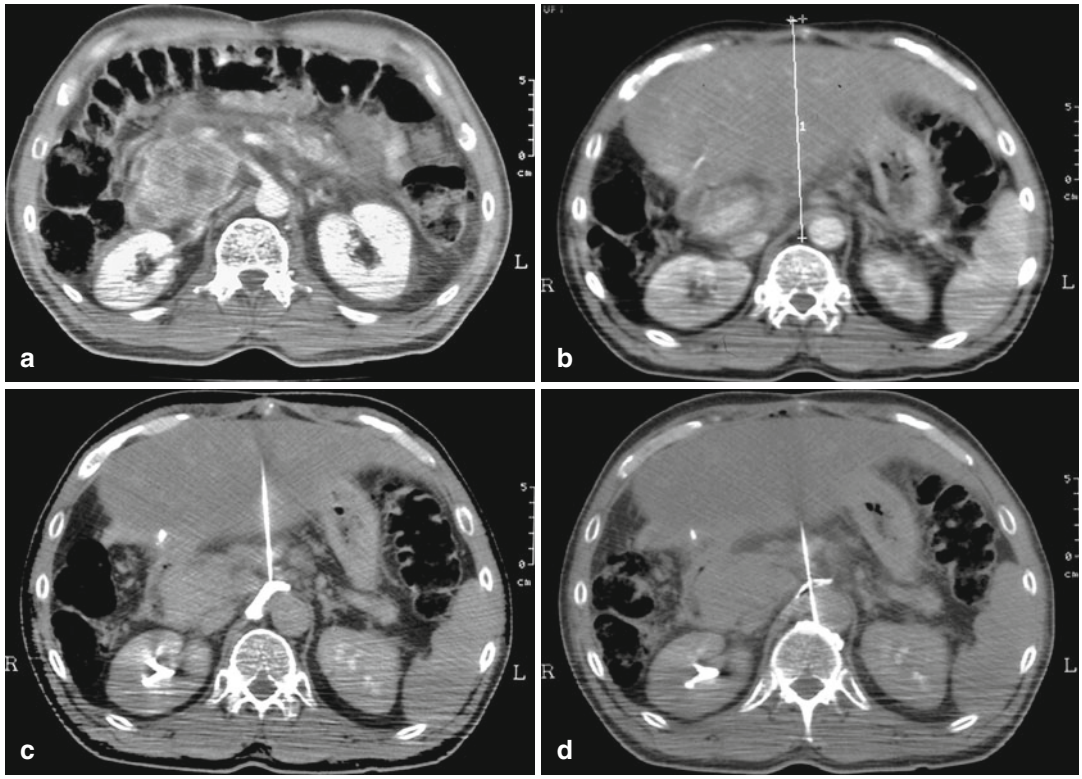

Fig. 14.9 Splanchnic and celiac neurolysis via an anterior approach: cancer of the pancreas (**a**). Trajectory indicated (*line*) for celiac and splanchnic neurolysis (**b**). Celiac neurolysis is performed (**c**), followed by splanchnic neurolysis via an approach lateral to the aorta (**d**). A transaortic approach is also possible for the splanchnic neurolysis

a grossly vertical course. The needles are slowly advanced transglutally under imaging guidance. Following the anesthetic block test, the patient should note a decrease in his pain. Before the injection, the mounted syringe is maintained in aspiration (under vacuum) for 5 s in order to detect blood (vascular puncture). Thereafter, the infiltration is performed with 1 ml of long-release-glucocorticoid (e.g., cortivazol 3.75 mg) which should be slowly instilled at both levels. After the infiltration, the solution is seen within pudental canal along the internal obturator muscle and between the sacrotuberal and sacrospinal ligaments.

A CT control at the end of the procedure ensures the absence of complications, namely hematoma. The procedure is carried out on an outpatient basis, and the patient is kept under observation for 1 h. Controlateral treatment (if justified) can be carried out around 2 weeks afterward.

14.2.3.6 Interiliac Sympathetic Plexus and Ganglion Impar Neurolysis

Indications

These techniques are generally recommended in the case of pelvic pain caused by a tumoral invasion of colorectal or gynecological cancers and also of radiation rectitis. The treatment of chronic pain related to endometriosis can also benefit from this procedure (Wechsler et al. 1996).

Anatomy

The interiliac plexus (corresponding to the presacral nerve) is located in an anterolateral position at L5-S1 beneath the aortic bifurcation between the common iliac arteries. It extends into the pelvis and divides into two streams, which integrate the hypogastric plexus. A section of the presacral nerve causes hypoesthesia of the pelvic organs, vasomotor changes in women, and ejaculatory problems in men.

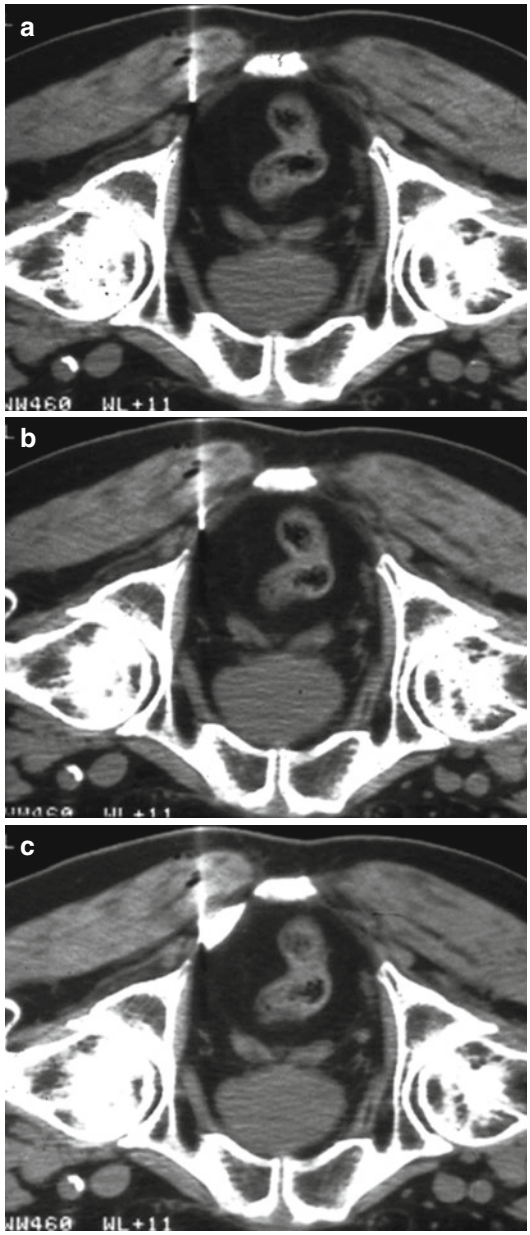

Fig. 14.10 Pudental nerve infiltration first site: sequential CT monitoring the needle tip progressing on the right to the ischial spine between the sacrospinous and sacrotuberal ligaments (**a**, **b**). Here, the added contrast media (not mandatory) diffuse between the sacrospinous and sacrotuberal ligaments (**c**; first site)

The ganglion impar, also known as the Walther ganglion, corresponds to anastomosis of the caudal tip of the laterovertebral chains. It is medially located at the anterior side of the coccyx.

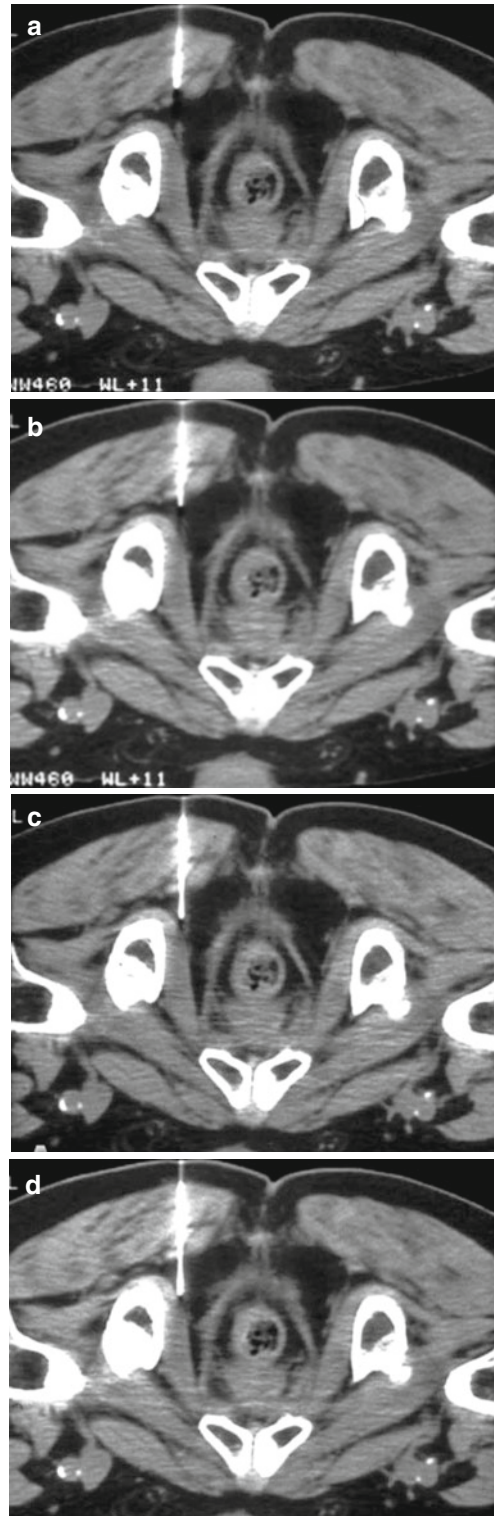

Fig. 14.11 Pudental nerve infiltration second site: CT shows the progress of the needle tip on the right to Alcock's canal (**a**–**c**) abutting the pudendal nerve (**d**; second site)

Image Guidance for Acoholization and RF Procedure. In the case of the presacral nerve, a posterolateral approach is taken, the patient positioned in a procubitus position (Fig. 14.12). The tip of a 22-G needle is positioned in front of L5-S1, dorsal to the iliac vessels. An anesthetic block test (e.g., 5 ml ropivacain 0.25) is performed, as is contrast medium to ascertain diffusion between the vessels, followed by an injection of delayed corticoid. Before the injection, the mounted syringe is maintained in aspiration (under vacuum) for 5 s in order to detect blood (vascular puncture). If a more definitive neurolysis is recommended, 3–5 ml of absolute alcohol is injected slowly. Full neurolysis generally requires several sessions carried out every 3 weeks.

In the case of neurolysis of the ganglion impar, the approach is lateral and the tip of the needle is positioned in front and median to the coccyx, behind the rectum (Fig. 14.13). In the case of coccygodynia, the infiltration of anesthetics and corticoids in the pericoccygeal can be completed by RF neurolysis of the ganglion impar (unpaired).

Summary

CT-guided procedure can be used either in addition to or as an alternative to the conventional methods of pain therapy. They are usually performed on an outpatient basis. CT guidance allows a step-by-step control of the procedure and is much safer and reliable than fluoroscopy guidance. Radiologist should get skilled in this field of interventional radiology aimed at pain therapy.

Key Points

- There are image-guided procedures for pain management for many otherwise untreatable pain syndromes including cancer pain, cluster headache, atypical facial pain, pudendal pain, or Arnold's neuralgia.
- Interventional pain management is safe and effective.
- Detailed knowledge of anatomy is mandatory for the interventionalist.

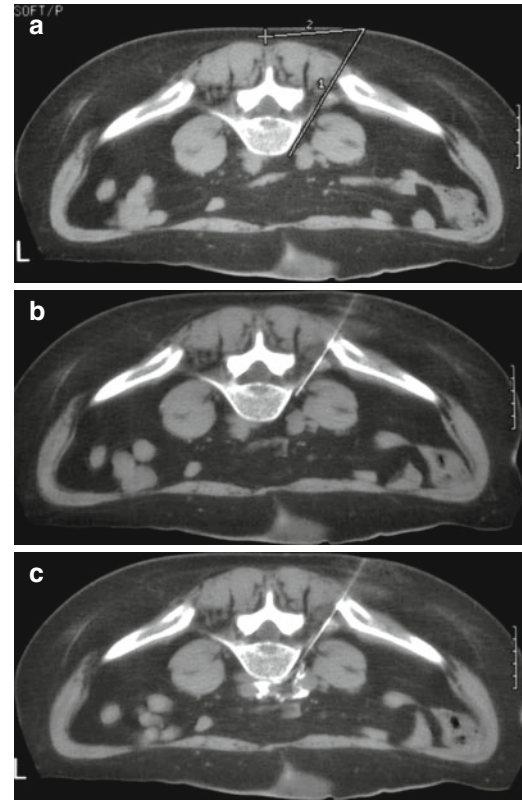

Fig. 14.12 Neurolysis of the interiliac plexus (presacral nerves): locating the trajectory with the patient in prone position (**a**). Progressive introduction of the needle behind the iliac vessels at the L5–S1 level (**b**). Injection of a contrast-anesthetic mixture (5 ml) followed by a slow-release corticoid (**c**)

14.3 Thoracic and Lumbar Sympathicolysis

Jan Hoeltje, Bruno Kastler, and Roland Bruening

14.3.1 Introduction

The sympathetic trunk is an extension of the cervical sympathetic chain. It is made up of nervous filaments with ganglion relays located on either side of the vertebra. As a doubled nerval network with segmental aired ganglia, it mimics a ladder-like appearance. In the chest, these paired ganglia are bilateral, situated latero-ventrally to the vertebral body in front of the capitulum of the rib. The second thoracic ganglion lies at the second rib neck, the first thoracic ganglion is fused with eighth

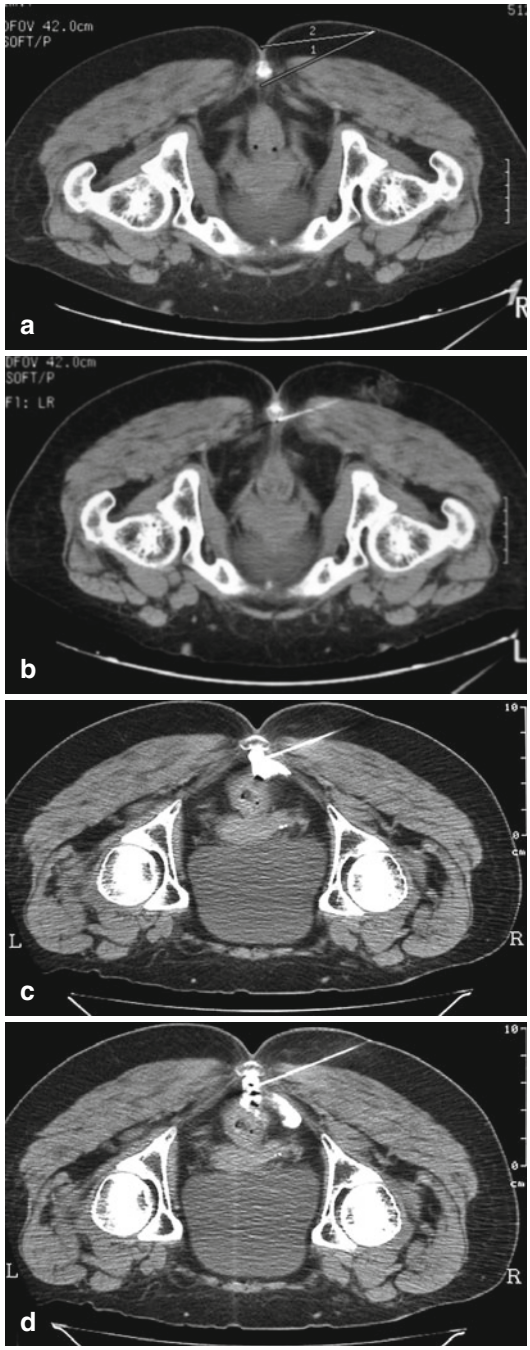

Fig. 14.13 Neurolysis of the ganglion impar in a patient suffering from acute coccygodynia. Locating the trajectory (**a**). Positioning the needle in front of the coccyx (**b**). An anesthetic block with an additional slow-release corticoid resulted in pain relief for 3 weeks. A second session with injection of a contrast-anesthetic mixture was performed (**c**). Radiofrequency ablation was performed resulting in definitive pain relief. Note the formation of bubbles due to vaporization (**d**)

cervical nerve root forming the stellate ganglion; ganglia T3–T6 lie at the rib heads, and T7–T10 ganglia are located at the costovertebral joints (in front of the costovertebral ligaments); T1 and T12 are more anterior in a lateral position in relation to the vertebra. Lumbar ganglia are located more anterior than the sympathetic thoracic sympathetic chain. On the left side, they are located dorsolaterally of the aorta, on the right side behind the inferior vena cava. In the upper abdomen, some fibers form the sympathetic ganglia branches to the celiac plexus. Lateral the lumbar sympathetic ganglia are bordered by the iliopsoas muscle, in which the lumbar plexus branches. The skin branches of the extremities are nearly completely innervated by the parasympathetic trunk. The sympathetic trunk also influences the regulation of the tonus of the peripheral arteries and thus to the perfusion of the limbs. It is also part of the regulation of peripheral hidrosis and plays a role in chronic pain syndromes.

Its anatomical location leading from the cervical ganglia to the thoracic paravertebral and finally to the lumbar prevertebral space is easily assessable for percutaneous CT- or MR-controlled treatment.

14.3.2 Indications and Contraindications

In 1899, Jaboulay (1899) described the first surgical sympathectomy for pain therapy in peripheral arterial occlusive disease. Currently, the most common indication for sympathicolysis is treatment of chronic limb ischemia in otherwise untreatable peripheral arterial occlusive disease (PAOD) with a PAOD grade III or IV according to Fontaine (Lee et al. 1983; Rosen et al. 1983; Duda et al. 1994; Heindel et al. 1998; Finkenzeller et al. 2001; Huttner et al. 2002; Pieri et al. 2005; Schmid et al. 2006). In other words, sympathicolysis is considered an indication if the patients are strongly affected, if their chronic pain syndrome exists for years, and the available therapies had failed or have had only a short-term effect.

Clinical severe limb ischemia caused by Raynaud's disease (Janoff et al. 1985; Di Lorenzo et al. 1998; Thune et al. 2006; Maga et al. 2007),

or thromboangiitis obliterans (M. Buerger), may also be an indication for sympaticolysis (Lau and Cheng 1997; Arkkila 2006).

Further indications for image-guided sympathicolysis include:

- Palmar or axillary hyperhydrosis
- Distal arthritis
- Distal arterial embolism
- Frostbite
- Posttraumatic dystrophy and causalgia (sympathetically maintained pain syndrome)
- Neoplasm of paravertebral gutters with vertebral invasion
- Phantom limb

In suspected sympathetically maintained pain syndrome (SMP), a detailed history of the patient, cross-sectional imaging, and laboratory examinations are mandatory to exclude other causes of pain.

There are no absolute contraindications to sympathicolysis; however, a sufficient thrombocytic platelet count (>60,000/mm^2) and absence of antiplatelet medication or coagulation disorders should be ensured. Prior to the intervention, known intolerance to the substances used should be excluded. Infectious cutaneous lesions along the access route have to be treated previously.

14.3.3 Material

- 20–22 G trocar with mandrin with a length of 10–25 cm depending on puncture site and patient constitution
- 10 ml local anesthetic (e.g., prilocaine 2 %)
- 96 % ethanol (or phenol)

In case of radiofrequency (RF) sympathectomy, disposable RF electrodes with 5–10 mm active tip length and a RF generator are needed.

- Iodinated contrast medium
- Physiologic saline solution
- Sterile bowl
- 10-ml syringe (A Luer lock syringe is recommended particularly in combination with alcohol. It is easier to guide than a standard syringe and improves safety during injection.)
- 2×5-ml syringe
- Short extension line
- Sterile table
- Sterile draping, sterile gloves, sterile gowns, and skin disinfection

14.3.4 Technique

Prior to any percutaneous sympathectomy, an intravenous access line should be applied. If bilateral treatment is intended, the more affected side should be treated first, and after successful therapy, the contralateral treatment should be performed after an interval of at least 24 h.

14.3.4.1 Thoracic Sympathicolysis

In our experience, the prone position with the needle advanced via a dorsal approach is preferable (Fig. 14.14). In principle, a ventral approach is also feasible for both thoracic and abdominal sites but will not be described. The intervention is performed as follows:

- Patient in comfortable prone position or later position.
- CT or MR scan from thoracic vertebral body 2–4, if possible in the arterial contrast phase with a slice thickness of approximately 3 mm.
- Planning of the access route from dorsolateral as the sympathetic trunk is located ventrolaterally to the vertebral body in front of the head of the corresponding rib.
- The level of the intervention depends on the indication: palmar hyperhidrosis = T4, axillary hyperhidrosis = T2/3, ischemic pain = T2/3, tumor-associated pain, or SMP (according to the pain location). Alternatively, a two-level therapy at T2 and T3 may be performed to improve success rates.
- Thorough skin surface disinfection and coverage with a sterile draping.
- Careful needle advancement to the target point under cross-sectional imaging control with either repeated sequential images or under CT- or MR fluoroscopy in order to follow the needle position and to avoid critical structures.

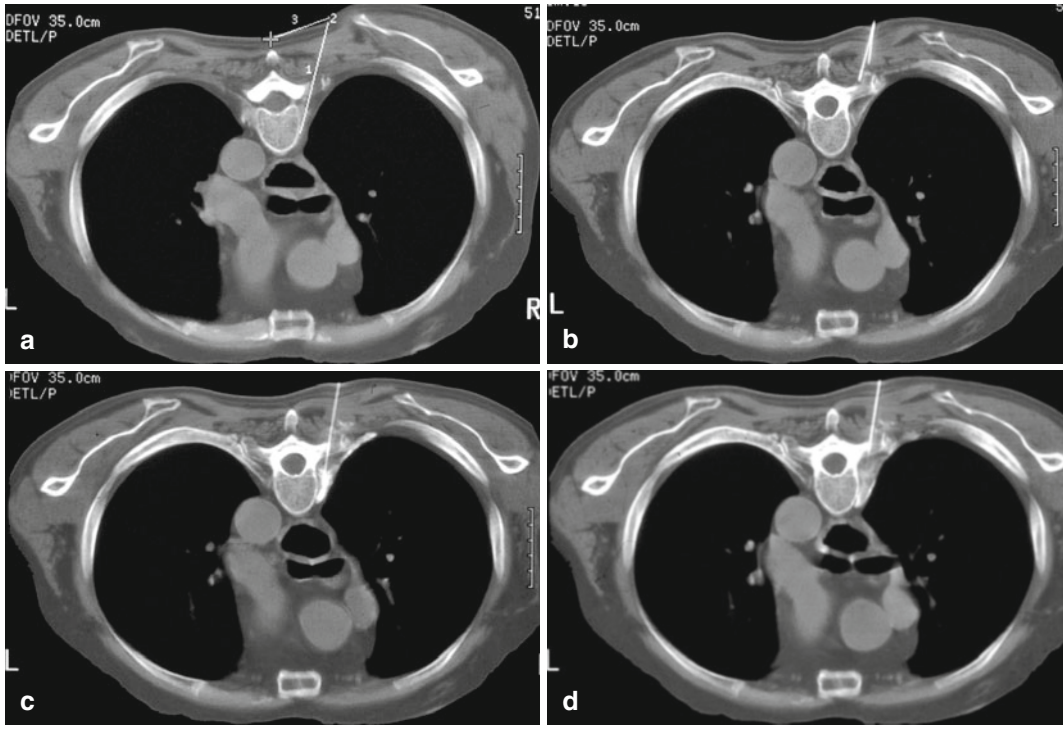

Fig. 14.14 Patient with thrombosis of the right subclavian artery following a stent emplacement. Sympathicolysis is planned at the level T3. (**a**) The space between pleura and the lateral aspect of the vertebral body is almost non-existent, too narrow for an adequate pathway. Guidance by the anesthesia needle left in position (**b**). Widening of the channel by injection of physiological saline and contrast, thus pushing away the pleuropulmonary parenchyma (**c**). Injection of absolute alcohol, resulting in a dilution of the contrast medium by the hypodense alcohol (**d**)

- If the puncture is hampered by a close relationship to the pleura, the pleura may be displaced laterally by a saline depot of 20 ml or more if needed.
- After correct needle placement ventral to the head of the rib, the extension line is fixed to the cannula. After aspiration to exclude intravascular needle position, it is irrigated with a contrast/prilocaine solution.
- Subsequently 2 ml of a 1:4 contrast medium/prilocaine solution are injected and a control scan is performed.
- The position of the needle is correct when the sympathetic ganglion is irrigated and no clinical symptoms of Horner´s syndrome or other neurological disorder occur. There must not be any intraspinal contrast distribution.
- Mixing of 9 ml ethanol, 4.5 ml prilocain, and 1.5 ml contrast medium (6:3:1) in the bowl to be drawn up in the 10-ml syringe.
- Slow injection of a total of 2–3 ml ethanol solution. Injection is stopped in case of pain. Alternatively, 3–5 ml of 7 % phenol diluted in 1 ml of contrast medium may also be used.
- Irrigation of the cannula with a very small amount of saline and withdrawal.
- Control scan according to the initial one to document the diffusion of the contrast medium and to exclude a pneumothorax.

Patients unwilling to run the risk of Horner's syndrome or surgery are treated by RF. The very localized character of thermal lesion ablation removes the risk of this complication. For RF ablation, a disposable RF probe without internal cooling and an active tip length of 5–10 mm is

used in order to restrict the ablation volume. First, a stimulation mode test is carried out. The patient should describe a posterior thoracic pain. There must be no intercostal fasciculation. Thereafter, 1 ml of local anesthetics is injected followed by 80 °C thermolysis for 90 s. The needle is inserted 2 mm further and a second thermolysis carried out. For thermolysis, low energy settings in the range of 2–5 W are usually sufficient.

Independent if alcohol, phenol, or RF ablation are used for the procedure, the patient should experience heat in the upper limb treated in particular of the hand. Effectivity of the procedure can objectively be assessed by comparing the temperature of both hands.

14.3.4.2 Lumbar Sympathicolysis

- Patient in comfortable prone position.
- Imaging from lumbar vertebra 2 to lumbar vertebra 4. If CT is used, imaging might be performed during the urographic contrast phase after injection of 30–60 ml of iodinated contrast material in order to clearly delineate the ureter.
- Planning of the access route. The sympathetic trunk takes its course dorsal to the aorta and the inferior caval vein. The target ganglia are located at the level L3 and L4. Injection may be performed at a single or at two levels simultaneously, with the latter improving treatment success. Most often, a single level injection between L2/L3 is performed. The L2 level should be left out because of the potential of intestinal motility disorders. The cutaneous entry point and trajectory are chosen to avoid the kidney, transverse process, colon, vertebral body, and intervertebral disc.
- Careful advancement of the puncture needle with repeated control scans if needed or use of CT/MR fluoroscopy.
- When the needle point is in correct position, in front of the psoas and dorsal to the aorta or inferior vena cava, an extension line irrigated with contrast medium/prilocaine solution is fixed to the needle. After aspiration, about 3 ml of a 1:4 contrast medium/prilocaine solution are injected, and a control scan is performed.
- The needle position is correct when the contrast medium spreads semicircularly around the dorsal aspect of the inferior caval vein and/or the aorta, excepting the ureter.
- Mixing of 9 ml ethanol, 4.5 ml prilocaine, and 1.5 ml contrast medium (6:3:1) to be drawn up in the 10-ml syringe. Alternatively, 7 % phenol may be used.
- Slow injection of up to 15 ml ethanol solution under repeated imaging control. Injection needs to be interrupted in case of significant diffusion toward the ureter, rear at the level of the second lumbar vertebra, because of the origin of the inguinofemoral nerves. Between L1 and L3, the femoral and obturator nerves originate while L4–L5 is important because of the sciatic nerve origin. Injection needs also to be stopped in case of pain.
- An alternative technique is to inject 15 ml of local anesthesia mixed with iodinated contrast material. If proper distribution of the contrast material has been proven, ethanol or phenol without additional contrast are injected utilizing the “negative” contrast of the second fluid to assess correct distribution of the chemical.
- Final control scan according to documentation of the spreading (Fig. 14.15).

For RF ablation, the same needle position as for ethanol injection may be used. For local ablation, disposable RF probes without internal cooling are used. The active tip length is in the range of 5–10 mm. After needle placement, a stimulation mode test is carried out: The patient should describe a posterior lumbar pain. Thereafter, local anesthesia is applied, followed by 80° thermolysis for 90 s. The needle is inserted 2 mm further and a second thermolysis carried out.

Independently of the puncture site, all patients should be supervised for at least 4–6 h after the procedure for pulse and blood pressure. Taking in consideration a possible orthostatic pressure drop, monitoring is advised, and the patient should get up at first slowly under supervision.

In pain therapy, repeated blockages with local anesthetics are often sufficient so that a definitive destruction with alcohol of nerve fibers may be avoided.

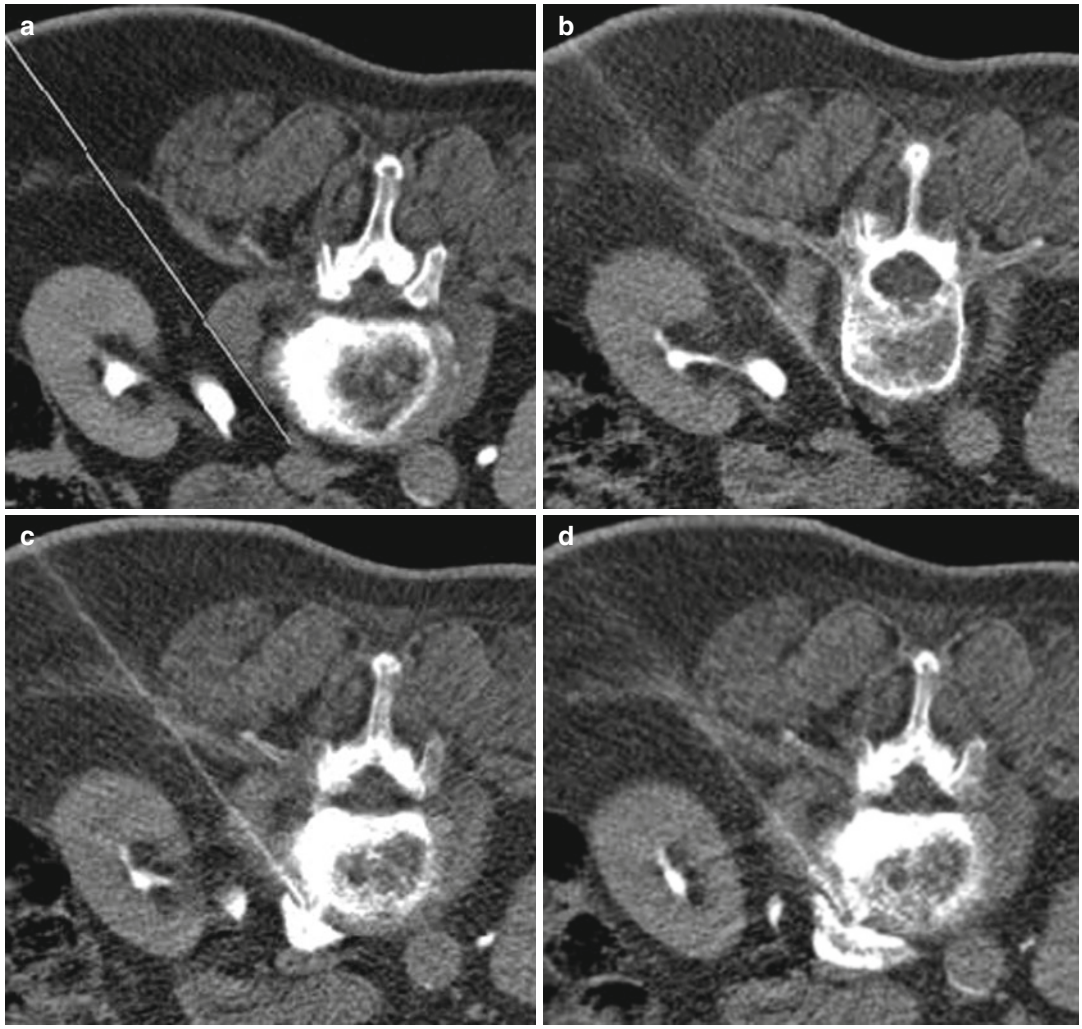

Fig. 14.15 79-year-old female patient suffering from PAOD grade IV with moist gangrene of the right foot and PAOD III on the left side. On the level of lumbar vertebra 3 (L III), the sympathetic trunk is situated ventral of the vertebral body. In this patient, it was reached best from the right side. After planning of the access route (**a**), the needle was advanced step by step and the final needle position documented on CT (**b**). After a test injection of local anesthetics mixed with contrast media, CT scan shows regular contrast distribution preserving the ureter (**c**). Final CT control after ethanol injection shows the same contrast distribution without spread to critical structures (**d**). The patient reported a sensation of heat on discharge after 4 h and pain relief at the control consultation 2 weeks later. The gangrene had become dry meanwhile, so the clinical staging improved from Fontaine Stage IV to IIb

14.3.5 Results

In case of ischemic pain in PAOD, pain relief or healing of an open wound has to be considered as treatment success. Clinically, regaining of a heat sensation in the dependent vascular areas is observed first. Typically, after 1–3 months, improvement is seen in 39–79 % of cases (Duda et al. 1994; Huttner et al. 2002). In PAOD, long-term improvement of the Fontaine grade or avoidance of amputation is described in more than 35 % of patients (Lee et al. 1983; Schild et al. 1984; Di Lorenzo et al. 1998; Huttner et al. 2002).

In case of other states of pain, Zoster's neuralgia, SMP, or tumor-associated pain, the

aim of therapy is achieved when the patient reports absence or marked relief of pain. There are only few small studies and case on this problem indicating a sometimes only temporary pain relief in SMP of 44 % and in Zoster´s neuralgia ($n=3$) of 100 % (Furlan et al. 2001; Price et al. 1998; Vranken et al. 2002). There is no advantage of RF neurolysis of chemolysis (Manjunath et al. 2008).

If thoracic or lumbar sympathicolysis was performed for treatment of hyperhidrosis, therapy may be considered successful if hyperhidrosis is reduced to a tolerable degree. The latter will be reached in more than 98 % and a long-term success in more than 80 % of patients (Adler et al. 1990; Romano et al. 2002). However, repeated treatments may be required.

14.3.6 Complications

Complications are rare, but there are several side effects of interventional sympathicolysis. Deep abdominal or genital (N. genitofemoralis) pain is not uncommon during the injection. It usually ends when the injection is terminated. Orthostatic dysregulation, which typically normalizes within 24 h, may be observed. Bed rest and a blood pressure monitoring is recommended to prevent complications. In most of the cases, accidental vessel puncture does not cause relevant hemorrhage because of the very small needle diameters.

Compensatory sweating (Baumgartner and Toh 2003; Katara et al. 2007; Montessi et al. 2007) should be mentioned particularly if hyperhidrosis is the indication for treatment. Furthermore, temporary or persisting hypoesthesia in the corresponding skin region may develop subsequently to a sympathicolysis. The patient has to be informed about the side effects referring to the substances used and the possibly resulting allergy.

For the thoracic level, the danger of a pneumothorax has to be mentioned. A possible, but unlikely danger of infection may cause pleuritis or peritonitis, at the thoracic or lumbar level, respectively. If a thoracic sympathicolysis has to be performed, Horner's syndrome may occur. In case T1 is affected up to 20 %, complete or incomplete Horner's syndrome may be observed. A theoretical complication results from accidental intraspinal injection.

Lumbar sympathicolysis involves the risk of renal puncture and intestinal perforation. The most relevant problem, however, is a possible stricture or necrosis of the ureter with consecutive hydronephrosis. In case of affection of the ureter, renal function needs to be monitored, and sonographic evaluation of the affected kidney is needed 2 weeks after the intervention. In case of renal engorgement, insertion of a DJ catheter has to be discussed with an urologist. Bilateral lumbar treatment at the level of L2 may cause disorders of voiding the bladder, as well as disorders of the intestinal motility and of ejaculation.

Summary

The benefit of sympathectomy had been introduced 100 years ago by Jaboulay (1899) for the treatment of PAOD in connection with ischemic pain. It is still applied in patients with otherwise and untreatable or unresponsive PAOD. Surgical sympathectomy is often and successfully used for this indication. In comparison to it, the radiological interventional procedure offers several advantages including the minimal invasive approach, the option of an outpatient treatment, lack of anesthesia, and a lower complication rate (Adler et al. 1990; Schneider et al. 1996; Chen et al. 2001; Baumgartner and Toh 2003; Moya et al. 2006; Katara et al. 2007; Montessi et al. 2007). In case of recurrent symptoms, repeated percutaneous sympathicolysis is possible.

One has to bear in mind that all procedures described above represent ultima ratio decisions and that the patients concerned often have suffered a long history of chronic disease and consider this kind of therapy as final option. Thus, indication should be liberal. As landmark structures neighboring the sympathetic trunk such as the pleura, the superior or inferior vena cava, aorta, or ureter are best visualized using cross-sectional imaging, this technique is very safe, and conventional fluoroscopy-controlled sympathicolysis should not be used any more.

Although the successful use of MR guidance has been reported in the literature, the vast majority of procedures is performed under CT guidance (König et al. 2002).

Key Points

- Sympathicolysis is a safe procedure with a low complication rate.
- Sympathicolysis is very successful in over 70 % of cases of hyperhidrosis and in up to 80 % of ischemic pain treatment.
- In ischemia-induced pain treatment after failure of transarterial or surgical treatment, this procedure often provides an improvement in the quality of life and helps to delay or avoid amputations.
- For treatment of the SMP and neuralgia, temporary nerve blocks without destruction of the nerves are often sufficient.

14.4 Trigeminal Ablation

Reto Bale and Gerlig Widmann

14.4.1 Introduction

Trigeminal neuralgia (TN), or tic douloureux, is a syndrome characterized by paroxysms of lancinating, shock-like pain in the distribution of the trigeminal nerve. It usually begins as a relapsing disease with pain-free intervals that may last months or years. These intervals decrease and eventually disappear. Pain attacks are being triggered by touching the skin, intraoral mucosa, or the tongue, or they occur spontaneously. Many patients have difficulties maintaining facial hygiene, talking, and eating. TN is either idiopathic (primary) or due to structural lesions including multiple sclerosis, tumor, or aneurysm (secondary). It is more common in females, in the right side of the face and in people older than 40 years. If major pain lasts for a period of seconds or minutes, atypical trigeminal neuralgia is diagnosed. Atypical symptoms are a negative predictor of outcome.

Although many patients respond to drugs (e.g., carbamazepine, baclofen, gabapentin, phenytoin, clonazepam), about 50 % of the patients require invasive treatment because they cannot tolerate the medications or their symptoms are intractable (Katusic et al. 1991).

14.4.2 Indications

Ablative techniques include neurectomy of peripheral trigeminal nerve branches, radiofrequency (RF) thermocoagulation, injection of glycerol into the trigeminal cistern (glycerol rhizolysis – GR), trigeminal ganglion balloon microcompression (BC), or stereotactic radiosurgery (SRS), causing controlled injury to the trigeminal nerve, ganglion, or root (Barker et al. 1996). More invasive approaches intend to relieve compression of the nerve at some point along its course. The most popular surgical procedure is the posterior fossa exploration for microvascular decompression (MVD). However, open surgical techniques are associated with a small but significant morbidity (keratitis, hemiparesis, hemorrhage, etc.) and mortality (1–2 %).

Based on a literature review and analysis of patients, Taha and Tew recommend RF thermocoagulation as the method of choice for the first treatment of TN (Taha and Tew 1996).

This review included patients who underwent RF thermocoagulation (6,205 patients), GR (1,217 patients), BC (759 patients), MVD (1,417 patients), and partial trigeminal rhizotomy (250 patients). RF thermocoagulation and MVD had the highest rate of initial pain relief and the lowest rate of pain recurrence. MVD showed the lowest rate of technical success and the highest rate of permanent cranial nerve deficit, intracranial hemorrhage or infarction, and perioperative morbidity and mortality. However, MVD had the lowest rates of facial numbness, dysaesthesia, corneal dysaesthesia, and keratitis. Based on their own results and the review of the literature, Taha and Tew recommend RF rhizotomy as the procedure of choice for TN patients undergoing first treatment. MVD is recommended in patients who have

pain in the first ophthalmic trigeminal division and in patients who desire no sensory deficit.

14.4.3 Material

Beside the routine material like sterile draping, disinfectant, local anesthesia, syringes, and scalpel, a dedicated ablation device is needed. For RF thermocoagulation, a RF probe with a thermocouple sensor is strongly recommended in order to produce a precise lesion at the electrode tip by monitoring the temperature (e.g., Neurotherm RF generator NT 1000; Precision Medical Engineering, Inc., MA, USA). For navigated ablation of the Gasserian ganglion, a dedicated head holder (e.g., Vogele-Bale-Hohner (VBH) head holder; Medical Intelligence GmbH, Schwabmuenchen, Germany) and a three-dimensional surgical navigation system are needed.

14.4.4 Technique

14.4.4.1 Pre-interventional Diagnostics

Before therapy, the patient has to be evaluated with a comprehensive interview, history, and physical examination of the cranial nerves. According to Scrivani et al. (1999), the clinical diagnosis of TN should be based on the following findings:

- Paroxysmal, lancinating, electric-like pain
- Tactile trigger areas
- Unilateral symptoms
- No neurosensory deficit

In addition, magnetic resonance (MR) imaging of the brain and brainstem has to be performed in order to exclude tumor, vascular abnormality, or demyelization.

14.4.4.2 Patient Preparation

The patient is positioned supine with the head lying on a radiolucent headrest. Continuous assessment of blood oxygen saturation and cardiac function is demanded. A nasal tube for oxygen administration may be helpful while the patient is covered by sterile drapes. Percutaneous RF thermocoagulation of the Gasserian ganglion is typically performed under intravenous sedation (puncture) and short general anesthesia (ablation). The dose of anesthetic medication is gradually increased to provide a considerable level of anesthesia so that patients experience no or minimal pain. Anesthesia is administered at a level that gives comfort to both the patient and the interventionalist during the electrical test procedure; for the ablation procedure, a short general anesthesia is performed.

During penetration of the foramen ovale, vagal reflex may lead to bradycardia, which may be treated with atropine. Complete general anesthesia should only be used in selected cases since the electrical test procedure is an important part of the intervention.

14.4.4.3 Puncture Technique

The RF thermocoagulation needle may be placed under fluoroscopic-, computed tomography (CT)-(Liu et al. 2005), or three-dimensionally navigated image guidance (Bale et al. 2000; Xu et al. 2006; Yang et al. 2007).

Conventional Approach

The conventional fluoroscopy-guided approach has been extensively described by Gauci (2004). Brief fluoroscopy should be used in order to visualize the foramen ovale in an orthogonal view. Therefore, the x-ray beam has to make an angle of 45 ° to an imaginary vertical line stretching from the lower margin of the orbit to the external ear channel and about 40 ° between the sagittal and vertical planes. The foramen ovale can be clearly visualized medial to the upper parts of the mandible.

The skin entrance point is about one inch lateral to the angle of the mouth at the level of the upper sixth tooth. To reach the maxillary and mandibular division of the trigeminal nerve, the foramen ovale should be entered in the middle of the foramen ovale. If just the third branch has to be reached, the entrance point is only half an inch lateral to the angle of the mouth. The direction of the needle in the lateral view is the middle point of the zygomatic arch and in the antero-posterior plane the infraorbital foramen (Fig. 14.16).

Local anesthesia may be applied at the skin entrance point. The needle is advanced to the foramen ovale under tunnel vision. Just before

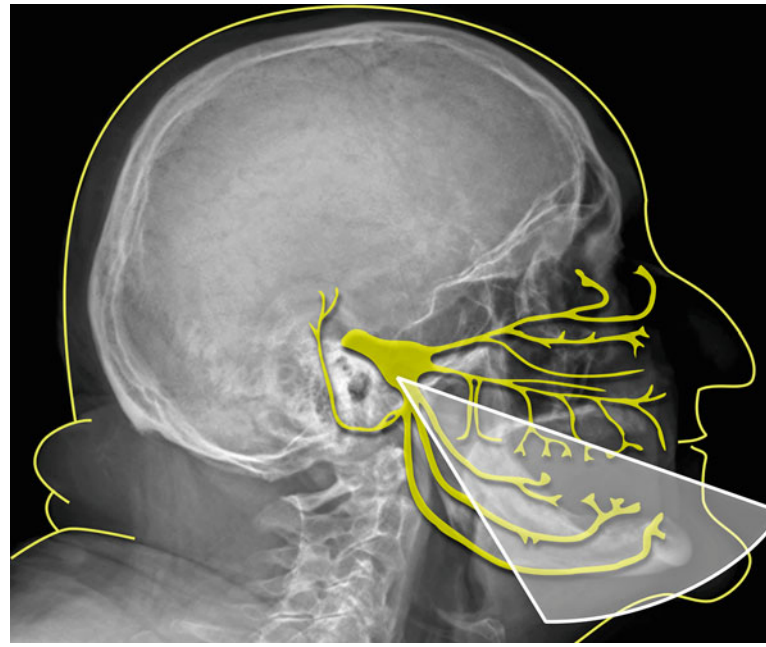

Fig. 14.16 Schematic draw of the puncture direction for reaching the third branch of the trigeminal nerve via the oval foramen

the foramen ovale is entered, a lateral view is obtained in order to advance the tip of the needle just above the bony skull base (the needle tip should be advanced about 1.5 cm further than the entrance into the foramen ovale). The cranial projection of the needle trajectory should lead directly into the angle formed by the clivus in the anterior and the petrous temporal bone in the posterior aspect. Cerebrospinal fluid should flow out as the trigeminal cistern is entered indicating correct placement.

Navigated CT-Guided Approach

The navigated CT-guided Innsbruck approach is based on the VBH head holder and a three-dimensional surgical navigation system. The head holder consists of the VBH vacuum mouthpiece, an adjustable, locking, adaptable mechanical arm and a base plate (40×30 cm, with multiple fixing areas to hold the mechanical arms) with head rest. The VBH mouthpiece is based on an individualized dental mold that is held against the upper palate by negative pressure (Bale et al. 1997a, b, 2000, 2006). Correct repositioning and precise fit on the patient are verified by successful generation of a negative pressure of 0.5–0.6 atm. The mechanical arm is connected to the two anterior extensions of the VBH mouthpiece for rigid immobilization of the patient's head at the base plate.

For image-to-patient registration, which is the essential step for navigated interventions, an external U-shaped Plexiglas frame equipped with eleven spherical CT markers (glass, diameter 5.8 mm), broadly distributed around the region of interest, is mounted to the mouthpiece (Fig. 14.17).

CT imaging with no more than 2 mm slice thickness is performed in the interventional CT unit. Thereafter, planning of the puncture path is performed on the navigation software. It includes trajectory planning as visualized on the two-dimensional and three-dimensional reconstructions of the patient's CT data. By using the longitudinal and orthogonal cuts along the planned path, potential penetration of the oral mucosa and damage of vital structures can be prevented (Fig. 14.18). For registration, the CT markers on the registration frame are replaced by registration markers that have a cone-shaped bur-hole in their geometric center. Thereby, the tip of the navigation systems probe can be precisely placed. After non-sterile registration and verification of registration accuracy, the interventional field is wrapped and prepared for the procedure.

Fig. 14.17 Fixation of patient in VBH head holder with SIP reference frame

The targeting device (e.g., Atlas™, Medtronic Inc., Louisville, KY, USA) is used for navigated adjustment of the planned trajectory. A coaxial needle is advanced through the aiming device to the calculated center of the foramen ovale. Finally, a low-dose CT scan is performed for verification of precise needle positioning (Fig. 14.19).

14.4.4.4 RF Thermocoagulation

After verification of precise needle position, the electrocoagulation needle is advanced through the coaxial guiding needle. For determination of the individual trigeminal branch, neurophysiologic testing should be performed which requires the cooperation of the patient throughout the procedure. To get the patient to cooperate and

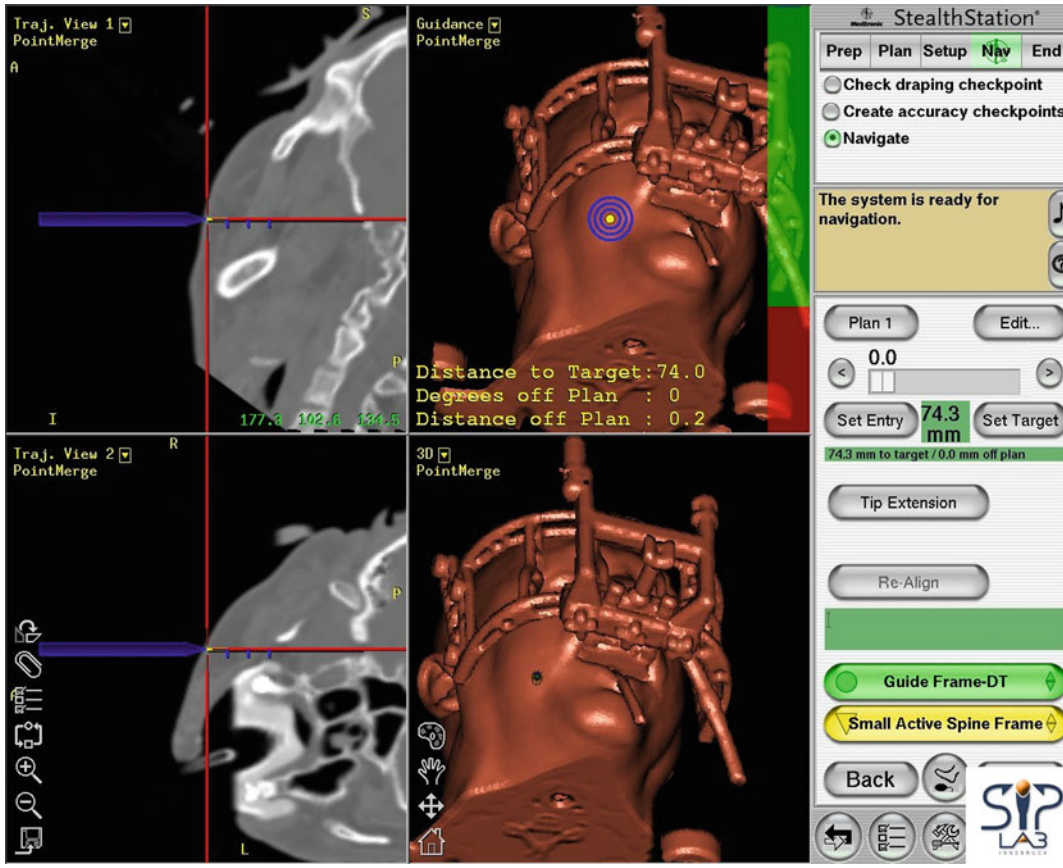

Fig. 14.18 Pathplanning on 2D- and 3D-reconstructed CT data. The *blue line* indicates the trajectory through the foramen ovale

Fig. 14.19 Axial control CT showing the needle in the right foramen ovale

respond, the VBH mouthpiece can be removed and disconnected from the head holder.

Thereafter, controlled thermocoagulation is performed which includes a first series of 60–90 s (73°), followed by a second series of 60 s (73°). During the coagulation procedure, the patients are usually anesthetized.

14.4.5 Results

In a systematic review of ablative neurosurgical techniques for the treatment of trigeminal neuralgia, Lopez et al. (2004) showed that RF thermocoagulation showed the highest rate of complete pain relief. RF thermocoagulation may safely be repeated if the pain recurs (Kanpolat et al. 2001). Satisfactory results and good long-term pain control can be obtained in patients having TN due to multiple sclerosis with percutaneous-controlled RF thermocoagulation (Kanpolat et al. 2000). Initial pain relief is about 98 %, but pain recurrence occurs in 20 % in 9 years and in 15 % in 5 years.

14.4.6 Complications

Correct puncture of the foramen ovale is a crucial step, and the incidence of complications due to incorrect puncture ranges from 5 to 7 % (Xu et al. 2006).

Typical adverse effects and complication include postoperative trigeminal nerve sensory loss (98 %), permanent trigeminal nerve sensory loss (30 %), masticatory weakness (12 %), corneal numbness (10 %), major dysesthesia (4 %), anesthesia dolorosa (2 %), and keratitis (1 %).

Rare complications (less than 1 %) include mortality (Egan et al. 2001), meningitis (Sweet 1986), temporal lobe hemorrhage, seizure, stroke, cranial nerve deficit, carotid-cavernous fistula, monocular blindness (Egan et al. 2001), brain stem injury (Berk and Honey 2004), diplopia, and rhinorrhea. However, these severe but rare complications are mostly due to severe puncture failure or hygienic deficiency. Introduction of navigated cross-sectional imaging-guided intervention techniques will help to reduce the number of puncture-related complications.

Summary

When compared to conventional two-dimensional image guidance (fluoroscopy), navigated, cross-sectional image-guided interventions require additional procedures including system setup, instrument calibration, registration, verification of accuracy, intraoperative application, and dismantling of the navigation system. Familiarity with these systems is important for routine and fast use. For the application of most navigation systems, an additional person (technician) is helpful, and the costs for the purchase of the guidance system (and the additional costs for the man power) are often hardly affordable for small hospitals. However, this technology will enhance patient security and puncture success independent from the interventionalist's experience (including complete forensic documentation) with acceptable duration and effort for routine clinical application and may be beneficial to all patients in whom trigeminal nerve ablation is recommended.

Key Points

- Before therapy, the patient has to be evaluated with a comprehensive interview, history, and physical examination of the cranial nerves.
- Tumor, vascular abnormality, or demyelination has to be excluded, and a clear diagnosis of trigeminal neuralgia has to be verified.
- Correct puncture of the foramen ovale is a crucial step of percutaneous RF thermocoagulation, and the needle position has to be controlled by CT scan before the ablation procedure.
- Navigated CT-guided approaches may provide significant benefit compared to non-guided approaches through cross-sectional imaging, virtual interventional planning, and intraoperative 3-dimensional guidance, which helps in improving puncture accuracy and reduction of complication rate.

14.5 Epidural Injection Therapy

Bernd Turowski

14.5.1 Introduction

Epidural therapy implies positioning of a therapeutic agent in the epidural space close to the spinal dura. This region becomes accessible for therapy as dura mater, and periosts are not fixed together in the spinal canal as they are intracranially. Instead, more or less fat is interposed between the bone and the spinal dura. Image guidance comprises techniques like fluoroscopy, ultrasound (US), computed tomography (CT), or magnetic resonance (MR) imaging. Fluoroscopy only displays bony structures while soft tissue is not shown. Thus, puncture planning has to be done by deducing this information from anatomical knowledge. Individual variation and particularly pathological changes may lead to inaccurate distribution of any therapeutic agent. The same holds true if the access route is oriented at anatomical landmarks without image guiding. US is limited by acoustical shadows due to bony structures. MR guidance requires much effort including MR-compatible instruments. In addition, small gantry-opening hampers access to the site of puncture. However, cross-sectional imaging guidance offers some relevant advantages:

- The injection can be accomplished close to the dura mater avoiding transdural puncture.
- The distribution of the injected substance can be monitored. Injection can be stopped as soon as the desired distribution is reached.
- The injection can be stopped in time if the injected agent causes compression of the dural sac.

Based on these considerations, CT guidance appears to be the most effective technique for spinal epidural injection techniques and is described in the following. The technique of epidural injection will be demonstrated on the example of the therapy of a cerebrospinal fluid leakage (Ishikawa et al. 2007). Moreover, the presented technical skills may be an instrument for epidural placement of any therapeutic agent.

14.5.2 Indications

Typical indications for epidural injection therapy include:

- Cerebrospinal fluid leakage
- Spontaneous intracranial hypotension (SIH)

The most important (relative) contraindications to epidural injection therapy are:

- Infection
- Immunosuppression
- Allergy to contrast media

Cerebrospinal fluid leakage may be acquired due to trauma (Huntoon and Watson 2007; Takagi et al. 2007) or diagnostic puncture. But recently, more and more publications address the clinical symptoms of spontaneous intracranial hypotension (SIH) in relationship to a spinal fluid leakage (Schaltenbrand 1938; Schwedt and Dodick 2007; Diener et al. 2010).

The pathophysiological mechanism of clinical symptoms is based on reduced cerebrospinal

fluid (CSF) volume (Gideon et al. 1994; Mokri and Low 2003; Thomke et al. 1999). Reduction of CSF volume results in a downwards movement of the brain. Due to constancy of intracranial volume defined by the skull (Monroe-Kellie-Doctrin), volume compensation is necessary.

The cardinal clinical symptom of SIH is orthostatic headache, which is characterized by aggravation within 15–30 min after rising from recumbency. Within 30 min after lying down, orthostatic headache disappears. Intracranial low pressure with venous volume compensation may even result in subdural hygroma or subdural hematoma. Downward placement of the brain mechanically irritates cranial nerves. This may result in symptomatic affection of cranial nerves. In descending frequency, the clinical symptoms are paresis of cranial nerves VI, IV, III (diplopic images), II (impaired vision), V, VII, VIII (tinnitus, vertigo), IX (dysphagia). Nausea, neck pain, neck rigidity, nystagmus, ataxia, and psychosyndrom may be observed too. Rarely, disturbance of the venous drainage (Chen et al. 1999) and venous thrombosis have been described (Savoiardo et al. 2006, 2007). The clinical course of the disease may be chronic or recurrent with symptom-free intervals.

14.5.3 Pre-procedural Imaging

In a patient presenting with typical symptoms of low CSF pressure, cranial MR imaging with contrast will be performed. Imaging should include coronal slices, which can easily depict meningeal contrast enhancement and subdural hygroma or hematoma. Spinal MR imaging with heavily T2-weighted axial images with fat suppression may help to find pathologic epidural fluid collections (Tsai et al. 2007). Alternatively, scintigraphy may be performed. If CSF leakage is confirmed, the localization of the leakage by CT myelography is important.

14.5.3.1 MR Imaging

Based on the typical clinical symptoms, the proof of *menigeal contrast enhancement* on MR images is evidentiary for leakage of CSF as long as there was no precedent lumbar puncture.

As direct localization of the leakage itself is difficult, one needs to look out for other imaging sings of low CSF pressure such as:

- Subdural hygroma or hematoma
- Narrowed ventricles, interpeduncular fossa, chiasmatic cistern
- Flattening of the pons
- Enlargement of intracranial veins
- Enlargement of epidural venous plexus
- Lowered cerebellar tonsils
- Venous congestion may mimic hypophyseal enlargement
- Detection of epidural fluid signal extending in paraspinal tissue

14.5.3.2 Scintigraphy

Scintigraphy after direct injection of a radionuclide into the cerebrospinal fluid is a highly sensitive method for proving the existence of a leakage. The complete neuro-axis can be displayed in a single examination. Sensitivity results from temporal sampling so that even small leaks may be found directly or indirectly by early renal excretion (Lay 2002). Due to limited spatial resolution, the direct localization of the leakage is difficult.

14.5.3.3 CT Myelography

CT myelography is sensitive for any leakage of contrast-enhanced CSF. High spatial resolution of CT mostly allows direct visualization of leakage. Technically perfect subarachnoid contrast application is the key requirement for the success of CT myelography. Puncture of the CSF space should be performed as distal as possible to the assumed location of leakage in order to avoid interference with iatrogenic epidural contrast. For leakages in the level of the upper spinal canal, a lumbar contrast application is recommended; for lower leakages, a cervical puncture is reasonable. Concerning cervical contrast application, lateral puncture in the C1/C2 level instead of suboccipital puncture should be considered.

A first CT scan of the suspected region will be obtained with the patient positioned supine 30 min after injection of about 20 ml of a dedicated myelographic contrast medium. If no

epidural contrast is seen, a second CT scan will be performed about 1 h later, with the patient positioned prone.

Epidural bloodpatch therapy must not be performed before complete absorption of intrathecal and epidural contrast applied for CT myelography. Otherwise, contrast-enhanced bloodpatch may not be visualized, and local compression of the dural sack may be overseen. This condition normally will be fulfilled 12–24 h after CT myelography.

14.5.4 Material

- Spinal needle (20 G)
- 20-ml syringe with Luer lock adapter
- 16–18 G peripheral venous access for taking fresh whole blood
- Dedicated contrast agent for myelography (e.g., Iotrolan)
- Sterile compresses
- Plaster
- Sterile draping
- Local anesthesia for skin infiltration

14.5.5 Technique

Prior to the intervention, informed consent needs to be obtained. Discussion of therapeutic options must include information about the spontaneous course of the disease with approximately 80 % of symptoms resolving within 6–12 months. Only in a small subgroup will there not be spontaneous healing within an acceptable period of time.

The affection of quality of life due to prolonged symptoms of intracranial hypotension justifies invasive therapy. Based on the assumed pathophysiologic background of either local dural disruption or regional increased penetrability along the nerve roots, it is the intention of any therapy to seal the peridural space. Induction of inflammation or any stimulation of scar tissue may help to reach this aim. Blood injection combined with contrast material alone or thrombin (500 IE in 9 ml blood + 1 ml contrast material) or even epidural saline infusion (20 ml/h during 36 h) has been reported to be effective (Rouaud et al. 2009). With saline infusion, side effects such as local compression are not be expected; however, one would stop infusion if the patient reports symptoms such as pain or sensible affections.

To avoid movement of the patient between localization of the site of injection and blood injection, a stable and comfortable positioning of the patient is important. Thereafter, thorough skin disinfection and sterile draping is performed. The use of sterile gloves is mandatory for hygiene. Under sterile conditions and CT guidance, the spinal needle will be positioned either using a step-by-step method or alternatively CT fluoroscopy. In order to avoid puncture of the dural sack, a trajectory tangentially to the dural sack is planned (Figs. 14.20 and 14.21). As soon as the target area has been reached, control aspiration may exclude subarachnoid or intravascular position of the needle tip. To confirm epidural position of the needle, 1 ml air or alternatively contrast material should be injected (Fig. 14.21).

If epidural distribution of air or contrast is proven without a doubt, about 15–20 ml whole blood will be sampled from a cubital vein. The blood is mixed with 1 ml of myelographic contrast agent contrast (e.g., Iotrolan) in order to be able to monitor the propagation of blood during injection. Injection should be started immediately after taking the blood. It will be impossible to inject if clotting has started. The speed of injection depends on individual conditions. One should avoid producing a locally space-occupying hematoma which may affect the cervical myelon. Slow injection at the level of the leakage allows the blood to spread around the dural sack and cranially as well as caudally. This may exclude local compression effects. Iatrogenic myelon compression by locally trapped blood must be avoided. The epidural bloodpatch typically distributes from the level of injection usually about three vertebral body heights cranially and caudally. Complete peridural cover normally only occurs close to the level of injection (Fig. 14.21).

After injection of 7–20 ml blood (depending on localization of the injection: less volume for cervical injections – more volume in lumbar injections), a range of four vertebral bodies above

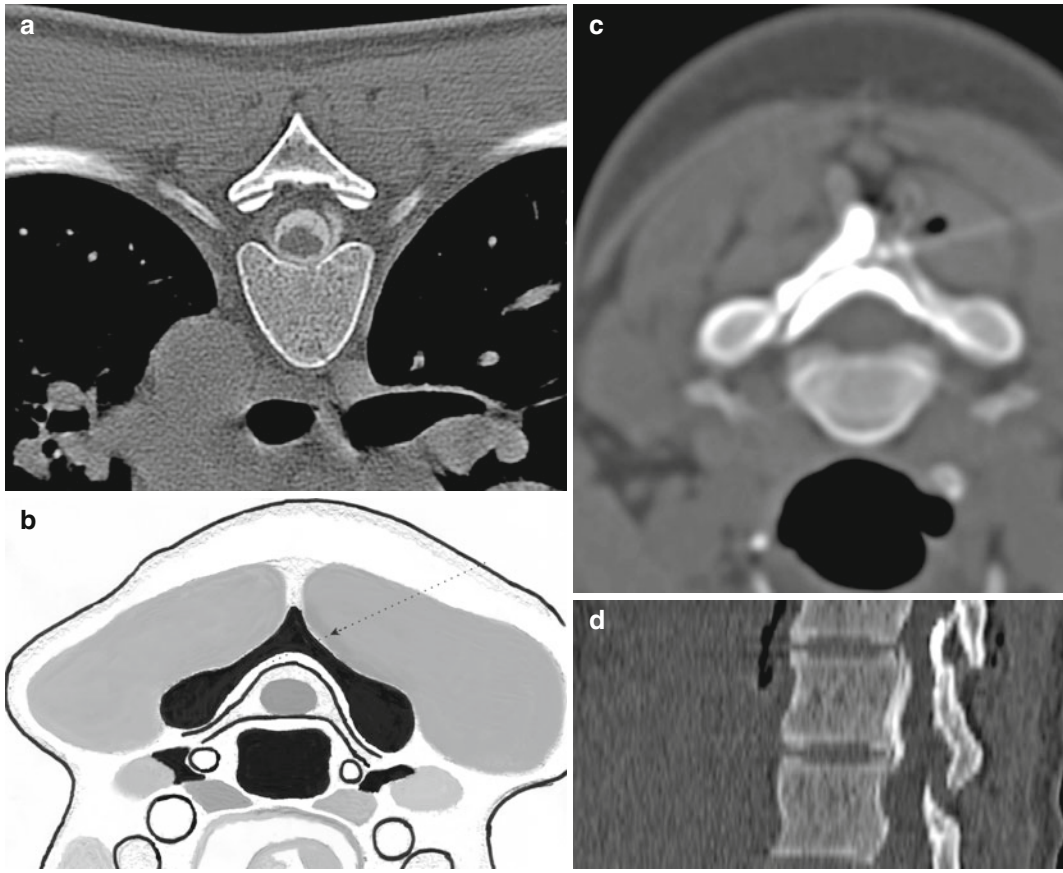

Fig. 14.20 Epidural extravasation of contrast material surrounding the contrast-filled dural sac is proven by CT myelography (**a**). The drawing illustrates the access route for epidural injection (**b**). In order to avoid contact to the nerve roots, the dorsal circumference of the dural sack should be targeted. Typically, a latero-dorsal approach with a caudo-cranial orientation is chosen because it permits excellent control of needle advancement and takes the roofing tile-like construction of the spinal processes into account (**c**). CT myelography after thoracic treatment is performed to confirm the epi- and peridural localization of the contrasted bloodpatch (**d**). The bloodpatch should extend over one vertebral body height corresponding to the site of the leakage

and below the level of injection is examined to show longitudinal and peridural dissemination of the bloodpatch.

In order to avoid displacement of the bloodpatch following gravity, rest in bed is recommended for 6–8 h after the injection.

14.5.6 Results

According to our experience in 50–60 % of all patients presenting with the clinical symptoms of orthostatic headache, the CSF leakage could be proven with imaging. In chronic whiplash disorder in which the pathophysiology may be comparable to intracranial hypotension 1 week after bloodpatch therapy as well as in a 6-month follow-up, Ishikawa et al. (2007) observed a significant percentage of patients with decreased symptoms compared to that before therapy. Headache as leading symptom in 100 % of patients could be found only in 17 % of all patients after therapy. Visual impairment could be resolved in two-thirds, nausea in 50 %.

In some cases, only repeated epidural bloodpatch therapy is successful, but in many cases, only one well-directed injection is sufficient. Symptoms should disappear within 72 h after successful therapy.

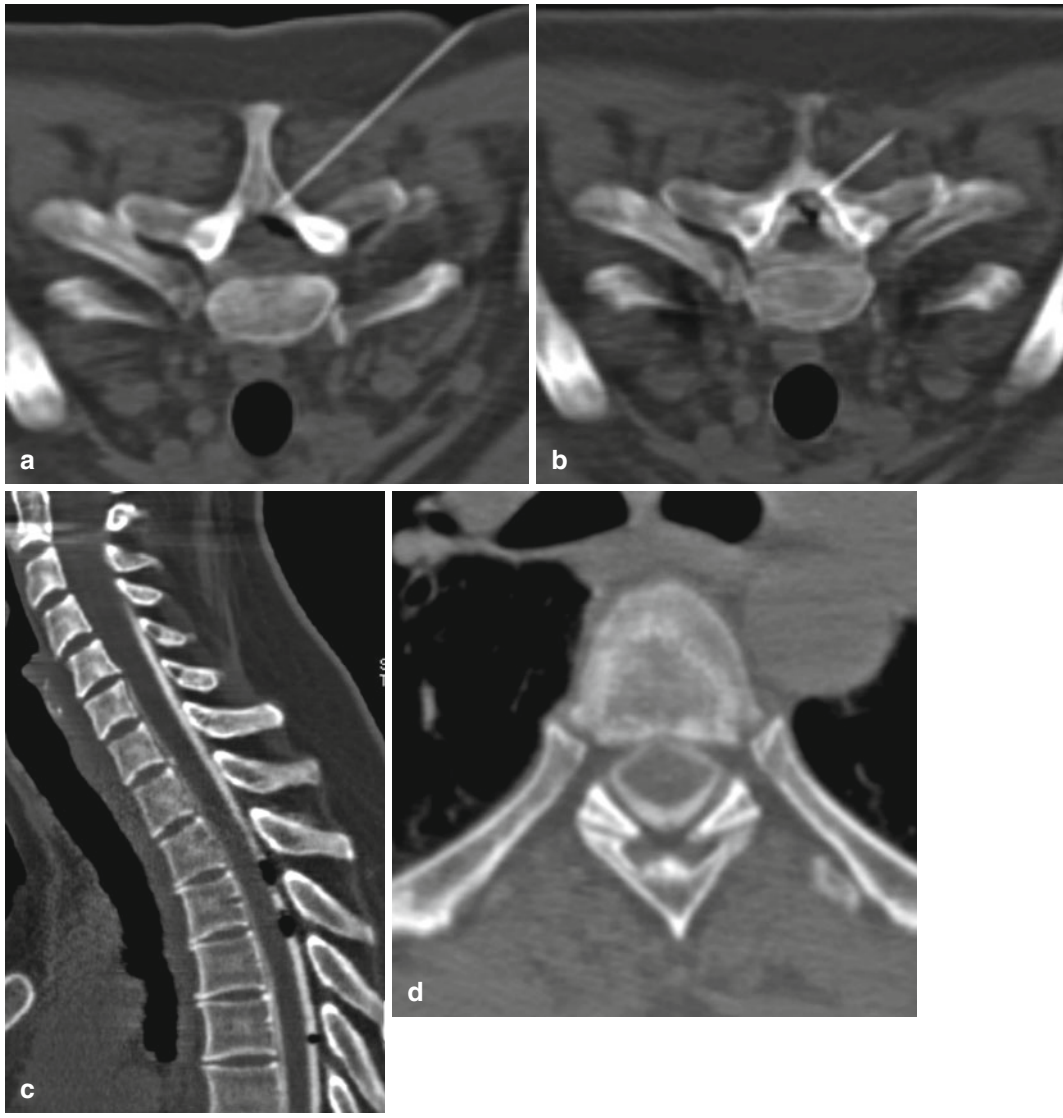

Fig. 14.21 Case study: epidural needle position showing epidural collection of injected air proving correct positioning of the needle (**a**). After injection, the epidural spread of contrast-enhanced bloodpatch is seen (**b**). The sagittaly reformatted images from the final control scan show the cranio-caudal extension of the bloodpatch (**c**). In addition, some initially injected air is still seen. The axial image of the same CT scan depicts the good circumferential extension of the blood patch (**d**)

14.5.7 Complications

Due to short diffusion distances, epidurally injected substances may affect spinal nerves and even the myelon. Therefore, all interventions close to the structures of the central nervous system may have an effect on neural function.

If performed by an experienced interventionalist, the technique is safe. Typical complications and their management is listed in (Table 14.1).

Table 14.1 Complications and their management

Infection	The risk will be minimized by sterile work and good skin disinfection (at the site of injection as well as at site of blood sampling)
Puncture of the dura mater	In case of accidental puncture of the duramater, the needle should be repositioned. Injection of a small amount of myelographic contrast agent may prove correct extradural position of the tip of the needle and exclude intradural injection
Puncture of the myelon	In the best case, hazard puncture of the myelon has no further consequences if there is no injection. However, a puncture may result in bleedings. Intramedullary injection of any fluid may be disastrous and lead to paraplegia
Injection into the subarachnoid space	Accidental injection of blood into the subarachnoid space may cause a space-occupying lesion that requires surgery. It may lead also to headaches and to subarachnoidal adhesions

Summary

In case of CSF leakage, pharmacological therapy with caffeine may help in some cases. Surgical occlusion of the leakage is an invasive option. In contrast, local application of blood is a very effective method to treat CSF leakage with peridural adhesions producing the designated result. Taking into account risks and complications, indication should be clearly defined. Therapy should be performed by an experienced interventionalist.

Key Points

- The correct indication is the key for a successful intervention, as only patients with CSF leakage will benefit from an epidural bloodpatch. Extensive experiences in image-guided interventions is recommended. Careful positioning and control of correct needle placement is the key for successful treatment without complications.

14.6 CT-Guided Periradicular Therapy (PRT)

Gero Wieners

14.6.1 Indications

Radicular or pseudoradicular pain is one of the most common painful spinal disorders. Most patients suffer from acute or chronic disc herniation, degenerative spinal disease, or postoperative epidural fibrosis. Next to paresthesia, pain is the leading symptom. Primary aim of therapy is pain control. Selective nerve root block by injecting lidocaine was first described by Macnab (1971). Several randomized studies on the effect of local application of corticosteroids have been performed since then (Narozny et al. 2001; Blankenbaker et al. 2005). In summary, best improvement of symptoms was gained by injecting a combination of local anesthetics and corticosteroids compared to an injection of just local anesthetics. The simple explanation for the benefit from corticosteroids is the fact that the nucleus pulposus tissue has inflammatory properties, leading to an intraneural edema, which is a very important factor in the pathogenesis of sciatic pain (Olmarker et al. 1995). The application of corticosteroids around the nerve root and epidural space reduces local edema and inflammation by reducing the release of inflammatoric enzymes such as phospholipase A2 in the degenerated and herniated disc (Nygaard et al. 1997; Blankenbaker et al. 2005).

Computed tomography (CT)-guided periradicular therapy was introduced in 1989 (Groenemeyer and Seibel 1989). At that time, periradicular therapy (PRT) was usually performed by orthopedic or neurosurgeons in a freehand technique or under fluoroscopic guidance. In recent years, CT-guided periradicular therapy performed by interventional radiologists gained

acceptance due to the accuracy of needle positioning right next to the nerve root under CT-image control. In addition, drug distribution around the nerve can be optimally controlled by adding a small amount of contrast agent (Silbergleit et al. 2001; Link et al. 1998). Studies of CT-guided periradicular pain therapy have shown very good short-term success with long-term duration in some cases (Zennaro et al. 1998; Lee et al. 2005; Riew et al. 2006). The use of MR-guided PRT has also been described but did not gain clinical acceptance (Ojala et al. 2000; Sequeiros et al. 2002).

14.6.2 Material

Materials needed for PRT include:

- Fenestrated sterile draping
- Local anesthetics (5 ml xylocitin 1 %)
- Compresses
- Spinal needle 20 or 22 G of about 10 or 15 cm depending on patient and target localization For cervical intervention, a 22-G spinal needle is usually appropriate.
- Drugs (may be varied according to individual preferences):
  - 1 ml bupivacaine 0.5 % plus 0.3 ml nonionic contrast agent in a 2-ml syringe
  - 1 ml triamcinolonacetonide (40 mg) in a 2-ml syringe
- Adhesive plaster

14.6.3 Technique

14.6.3.1 Preparation

The most important aspect in successful PRT is the accuracy of neurological pre-interventional evaluation. A precise correlation of the dermatoma and the nerve root to be targeted needs to be established. In this context, CT- or MR images are helpful in defining the appropriate level for PRT. In addition, these images may exclude further pathologies. Written informed consent has to be obtained prior to the intervention.

14.6.3.2 Intervention

A PRT cycle is normally best performed in three interventions with an interval of 3 weeks between each intervention. All procedures are best performed under CT or MR guidance. For lumbar PRT, the patient is placed head first in prone position on the CT or MR table with cushioning between table and pelvis. This improves the dorsal access to the nerve root and also patient comfort. For cervical PRT, the patient is placed in a supine position.

Under CT guidance, a lateral topogram has to be acquired to identify the right disc level and neuroforamen. Single CT sections serve to adjust the image plane according to the neuroforamen and nerve root. Section thickness may be 5 mm or less. The point of needle insertion should be marked on the skin, usually lumbar about 3–4 cm lateral of the midline and cervical on the dorsolateral neck. The skin should be disinfected and covered with a fenestrated sterile sheet.

An axial CT section guides the needle from the insertion point to the nerve root ganglion. The spinal needle should be advanced stepwise in the axial plane until access to the neuforamen close to the transverse process is gained. For reaching the S1 nerve root, the spinal needle has to be advanced through the dorsal neuroforamen of the sacral bone (foramen sacrale dorsale). In some patients, tilting the gantry is considered helpful.

The needle tip should be placed close to the nerve root, but direct contact should be avoided. In this position, retrograde distribution of the drug along the inserted needle is prevented by the cribriforme fascia, and most often, contrast will distribute along the axis of the nerve root and reach the epidural space.

Application of 0.5 ml of nonionic contrast agent and bupivacain should be controlled under fluoroscopy to confirm washout of the contrast agent from the area around the nerve (Fig. 14.22). After the correct distribution has been documented, the syringe is changed against another syringe containing 1 ml triamcinolonacetonide (40 mg). The corticosteroid is injected slowly, again followed by an exchange

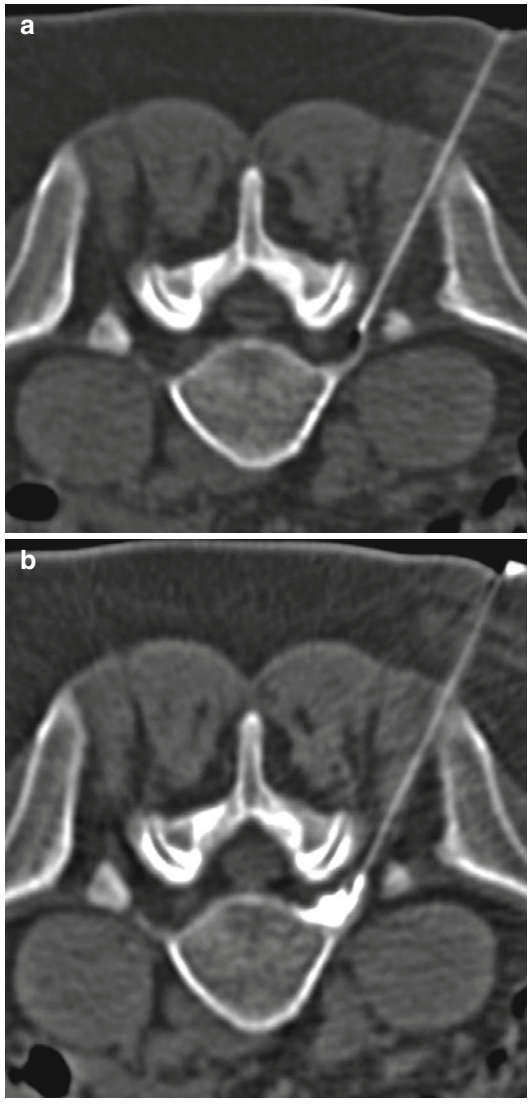

Fig. 14.22 CT-guided periradicular therapy of the lumbar spine. After CT-guided pararadicular needle placement (**a**), a steroid mixed with contrast medium was injected (**b**)

of the syringe to inject the remaining bupivacain. Doses from 1 ml triamcinolonacetonide (40 mg) and 1 ml bupivacaine up to 6 ml of this steroid-anesthetic combination have been described in the literature (Lee et al. 2005). However, most authors recommend an amount of just 1 ml triamcinolonacetonide (40 mg) and 1 ml bupivacaine.

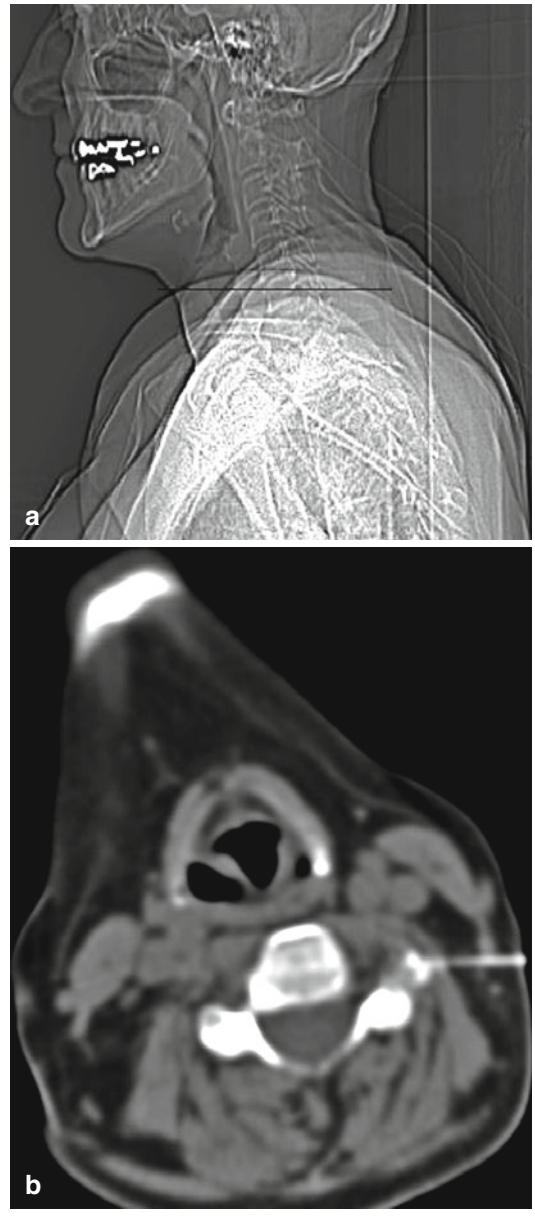

Fig. 14.23 CT-guided periradicular therapy (axial CT scan (**b**) of the cervical spine level C6 left (b, Sagittal CT-topogram)

For PRT of cervical nerve roots, the tip of the needle should be placed ventral to the vertebral transverse process (Fig. 14.23). The safest approach is puncture from the dorsolateral neck directly to the transverse process and after contact

to the bone stepwise progression into the final position. Among the direct approaches to a cervical nerve root, this technique provides greatest safety to avoid contact to the vertebral artery. For an indirect approach, the needle is positioned at the dorsal border of the facet joint for injection, and the drugs reach the target indirectly. This approach has recently been shown to be equally effective as direct approaches, while being considered more safe (Sutter et al. 2011).

The mean duration of this procedure is less than 20 min. It is generally performed as an outpatient treatment. Surveillance of the patient is usually limited to 30 min after treatment.

Sometimes, the correlation between dermatoma and nerve root is not clearly defined (Boos and Lander 1996). In this case, a stepwise therapy concept is recommended. This means that it is better to treat just the nerve root causing most severe symptoms at the first date of treatment. If there is only a response in the treated dermatoma and there is still pain or paresthesia, a combined therapy should be performed 3 weeks later on the same nerve root and following that on the nerve root above or below. This treatment should be repeated twice with an interval of 3 weeks to complete a treatment cycle.

After one cycle of treatment, an interval of 6 months at minimum is recommended. In exceptional cases, the interval can be reduced. However, adverse effects of systemic corticosteroid distribution have to be considered.

14.6.4 Results

Cervical and lumbar nerve root blocks have become more popular for treating patients with radiculopathy. CT- or MR-guided periradicular therapy is the safest and most accurate way for the application of drugs around spinal nerve roots. Of the patients, 60–80 % benefit significantly from the first treatment. However, a cycle of three injections should be completed to gain full and long-lasting therapeutic effects (Lee et al. 2005; Riew et al. 2006; Narozny et al. 2001). Several studies have shown excellent long-term results for patients who refused surgical intervention but who were considered to be candidates for surgical intervention because of symptoms and failure of nonoperative treatment (Peul et al. 2007; Riew et al. 2006). Five-year results of the study from Riew et al. (2006) were similar to the results of patients who underwent surgery, without the substantial risks of surgical interventions. The authors recommend CT-guided PRT of the nerve root as a first step prior to operative intervention in patients with radiculopathy due to a herniated nucleus pulposus or spinal stenosis. Surgery on patients presenting a radiculopathy with or without minor sensory/motor deficit is only required if pain cannot be controlled by nonoperative means (Saal and Saal 1989). This allows an effective reduction of costs, which would be necessary for surgical intervention (Karppinen et al. 2001).

Schmidt et al. (2006) evaluated dose exposure with a low-dose protocol during periradicular treatment under CT-fluoroscopy guidance. The effective dose was 0.22 and 0.43 mSv for four and ten CT scans, respectively. With pulsed fluoroscopy, the effective dose was reduced to 0.1 mSv. In this context, new open high-field MRI scanners offer the possibility of periradicular therapies without dose exposure and with superior tissue contrast. This is specifically of interest for young patients and patients who need repeated therapy cycles. Even low-field MR may deliver satisfying image quality for PRT (Sequeiros et al. 2002).

14.6.5 Complications

For informed consent, general and specific complications have to be considered. General complications such as bleeding, infection, or abscesses may occur. Specific complications to be considered include meningitis, liquor leakage, or nerve root trauma with paresthesia or even paralysis. In PRT of the cervical level, damage to the vertebral artery must be considered as well as misinjection of crystalline corticoids in spinal arteries leading to infarction. However, complications are extremely rare in PRT, and none of those incidences considered are even described in most

case series available in the literature. The most frequently seen minor complication may be a slight temporary weakness of the ipsilateral extremity or even a slight increase of pain caused by narrowing of the neuroforaminal space during drug administration. Allergic reactions to the nonionic CT-contrast agent, local anesthetics, and corticoid have to be considered.

Summary

CT-guided periradicular therapy in patients with lumbar or cervical radiculopathy is a safe and effective therapy while minimizing the need for surgical intervention. PRT of the nerve root is the first step prior to operative intervention in patients with radiculopathy due to a herniated nucleus pulposus or spinal stenosis. Surgery on patients suffering from radiculopathy with or without minor sensory or motor deficit is only required if pain cannot be controlled by nonoperative means.

Key Points

- The key to successful PRT is a careful pre-interventional neurological assessment!

14.7 Discography

Oliver Beuing

14.7.1 Introduction

Chronic back pain is one of the most common ailments in the industrialized nations (Milette et al. 1995). As various anatomic structures like facet joints, intervertebral discs, ligaments, and muscles may contribute to pain and innervation of these structures is complex and differs interindividually, it is crucial to identify the pain-generating structure for optimal interventional or surgical treatment planning.

Defiant of advances in imaging technology, findings of physical examination and noninvasive imaging are still inconclusive in a substantial number of patients, especially in those with multilevel changes or without frank nerve root compression. The intervertebral disc may cause radiating pain to the hip, groin, or even the leg, and distribution of pain does not necessarily correlate with the level of the affected disc. The mechanisms of pain development are not yet fully clarified, but probably, nerve roots are sensitive to chemical changes (inflammatory substances) in the direct surrounding of morphologically changed discs. However, there is also evidence that nociceptors sensitive to pressure and chemical changes may exist in the disc itself.

At current, the vast majority of discograms is performed using fluoroscopic guidance assessing the lower three lumbar segments. CT guidance is also applied. It particularly suited for assessing segments with markedly reduced intervertebral disc height. MR-guided discography has also been described but has no relevant role in clinical routine practice (Sequeiros et al. 2003).

14.7.2 Indications

The most common indications for discography are as follows (Resnick et al. 2002; Schellhas 2000):

- Chronic back pain with or without radicular pain and absence of documented nerve root compression in noninvasive tests.
- Disc or end plate changes are present, but clinical significance is unclear.
- Clinical findings suggest a specific level, but magnetic resonance (MR) imaging or computed tomography (CT) (-myelography) point to a different one.
- Disc protrusion in the suspected level is asymmetric and does not match the side where the patient indicates his pain.
- MR- and CT myelography already demonstrated instability in one segment, but the results concerning adjacent levels are equivocal.
- Percutaneous nucleotomy is planned.
- Exclusion of annular tears with potential epidural leakage in case chemonucleolysis is intended.
- Simulation of pain (exaggerated response may correlate with poor surgical outcome).
- Patients with previously fused segments develop pain after a symptom-free interval indicating affection of adjacent levels.

The contraindications for discography comprise of neurologic (motor) deficits, compression of the spinal cord with myelopathy, and if the patient has already undergone discectomy. Relative contraindications include coagulation disorders, allergies to substances used, and others.

14.7.3 Material

The list of materials and tools necessary comprises of:

- 22-G or 25-G needle (10 cm or longer), one for every level studied
- Nonionic contrast media (CT) or Gd-DTPA (MR imaging)
- Local anesthesia
- Sterile drapes
- Sterile latex gloves
- Disinfection (e.g., povidone iodine)
- Intravenous antibiotics (effective against Staphylococcus epidermis like cefazolin)
- Intravenous access

14.7.4 Technique

14.7.4.1 Pre-interventional Diagnostics

Prior to discography, clinical evaluation (history, physical examination), and noninvasive imaging (MR imaging, CT) with inconsistent results usually trigger the indication for the examination. In most patients, conservative pain management will already have failed. MR- or CT scans are reviewed for abnormalities helping to determine which discs should be studied in further detail. Facet joints should have been excluded as the symptoms origin.

Discography may be performed under fluoroscopy as well as by employing CT- or MR imaging.

14.7.4.2 Lumbar Discography

The patient is placed in prone position. A cushion placed under the patient's pelvis may help to reduce lordosis. If CT(fluoroscopy) or MR imaging are used, the intended access route is planned in the same manner as customary for percutaneous abscess puncture or biopsy. Sterile preparation is accomplished by thorough cleansing with iodinated solutions and, after drying, isopropyl, followed by fixing the sterile drapes.

Then, the solution for intradiscal injection is prepared. One mixes the antibiotic with the contrast material and, if desired, with local anesthesia. The entry point and the underlying tissue will then be anesthetized. Application of sedatives is rarely required. Using (CT-)fluoroscopy- or MR guidance, a 22–25-G needle is cautiously advanced to the disc space. Having placed the needle tip in the center of the disc nucleus (Fig. 14.24), injection of the solution (preferably under manometric control) begins (Fig. 14.25). Injection is terminated if a significantly increased pressure is needed for continuous application, after injecting a maximum of 6 ml of the solution, or if a concordant pain (>6/10 on a scale from 0 to 10) has been provoked. Some authors recommend discography of adjacent levels in the latter cases.

14.7.4.3 Thoracic Discography

As with lumbar discography, the patient is placed in prone position. In the thoracic levels starting approximately at the middle third, it is often impossible to gain an unobscured access to the disc by standard fluoroscopy due to costovertebral or vertebral body osteophytes, low disc height, or spinal deformity. Access is limited through the lung, which is anterior and lateral to the route, and the spinal cord, which is medial and posterior. In these cases, CT- or MR guidance is definitely advantageous.

14.7.4.4 Cervical Discography

The patient is placed in supine position with the shoulders slightly elevated. The cervical spine is palpated with two fingers, and after shifting the carotid artery and the esophagus away, the needle will be introduced from about 45° oblique and slightly below the disc.

Assessments reported should include (Sachs et al. 1987; Tomecek et al. 2002):

- Injected volume
- Intensity of pain (i.e., visual analog scale)
- Concordant pain during injection including its location
- Disc morphology using the Dallas discogram description

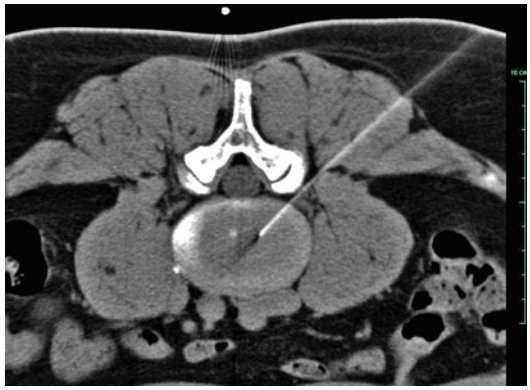

Fig. 14.24 CT-guided discography: positioning of the puncture needle

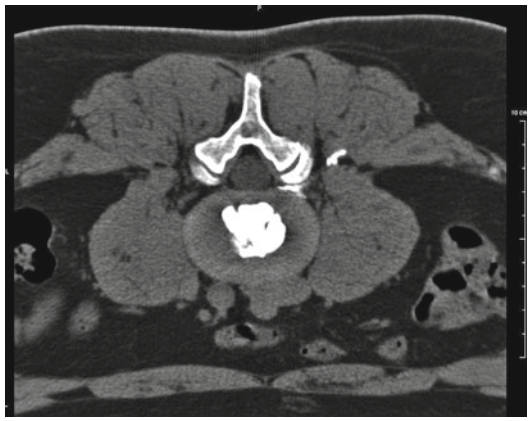

Fig. 14.25 Normal finding as obtained by CT-guided discography

- Pain in adjacent levels and, if present, has it been concordant
- If manometer has been used: opening pressure and pressure at pain onset

The Dallas discogram description has been established in 1987 for describing the CT appearance of the intervertebral disc (Sachs et al. 1987). Since its introduction, it has been modified several times. The most commonly used form defines grade 0–4 as follows:

- *Grade 0*: Contrast agent is confined within the normal nucleus pulposus.
- *Grade 1*: Contrast agent extends radially along fissure involving the inner one-third of the annulus fibrosis.
- *Grade 2*: Contrast agent extends into the middle one-third of the annulus fibrosis.
- *Grade 3*: Contrast agent extends into the outer one-third of the annulus fibrosis, either focally or radially, to an extent not greater than 30° of the disc circumference.
- *Grade 4*: Contrast agent extends into the outer one-third of the annulus fibrosis, dissecting radially to involve more than 30° of the disc circumference.

14.7.5 Results

Results of discography are discussed controversially in the literature. Whereas some authors claim a sensitivity of pain provocative discography around 80 %, others claim a best case positive predictive value of 50–60 % only. False-positive findings have been reported in up to 37 %.

14.7.6 Complications

Complication rates generally vary between 0 and 2.5 % (Pobiel et al. 2006; Guyer et al. 1997). The most serious complication is infection leading to discitis, spondylodiscitis, or epidural abscesses with an incidence well below 5 %. In case of discitis or spondylodiscitis, antibiotics must be administered intravenously. Microbiological assessments are often helpful. Epidural abscesses usually require instant surgical intervention.

Minor hematomas at the puncture site may appear; massive hemorrhage is extremely rare. Persistent pain should be managed with analgesics. However, repeat MR imaging is recommended particularly in cases of neurologic deficits indicating disc herniation.

Allergic reactions may occur. Pneumothoraces after thoracic discography are usually asymptomatic and only incidentally require treatment. Pulmonary embolism through disc material is a very uncommon complication with only a few cases reported.

Summary

Discography has been proven to be highly sensitive in isolating discogenic pain. However, specificity is low, and false-positive findings have been reported in up to 37 % (Carragee

et al. 1999). It has been shown that not only morphologic changes like internal disc disruption, disc degeneration, or annular rupture influence the patient's report on pain but also abnormal psychometric results. Improvement of specificity can only be achieved by selecting patients carefully and defining strict criteria for positive findings in discography. On the other hand, discography still remains the only diagnostic test potentially able to clearly identify disc pain and its origin.

Key Points

- Discography is an invasive but safe diagnostic procedure.
- It provides excellent morphologic detail of degenerative disc changes and, even more important, information on clinical significance.
- Especially in the work-up of patients with chronic lumbar pain, discography should be considered as a preinterventional or presurgical test for optimal treatment planning if clinical evaluation and noninvasive imaging do not conclusively explain the patient's pain.
- Strict criteria on the definition of a positive discogram must be used to avoid or lower false-positive results.

14.8 Interventional Therapy of the Intervertebral Disc

Alexis Kelekis, Dimitris Filippiadis, Kai E. Wilhelm and Jean-Baptiste Martin

14.8.1 Introduction

Low back pain and neuralgia are by far the common causes for acute and chronic pain syndromes. Approximately 80 % of the population worldwide will experience a minimum of one episode of back pain during their lifetime with intervertebral disc herniation accounting for 26–39 % of these cases (Aguirre et al. 2005; Alcock et al. 2003; Bogduk et al. 1982). Treatment options in intervertebral disc herniation include conservative therapy with a combination of 4–6 weeks of bed rest, analgesics, nonsteroidal anti-inflammatory drugs (NSAID) and physiotherapy, percutaneous image-guided steroid infiltrations, minimally invasive image-guided decompression techniques, and surgical therapies (Cohen and Hurley 2007; Cohen and Raja 2007). A variety of nonsurgical interventional procedures are used for treatment of low back pain. Percutaneous image-guided steroid infiltrations (either epidural or intradiscal) are palliative or curative measures for the symptoms of intervertebral disc herniation. They are performed either in combination with conservative therapy or as an intermediate treatment between conservative and minimally invasive percutaneous disc decompression (Cohen and Hurley 2007). The goal of this treatment is to achieve pain control during the acute phase until natural recovery occurs. Furthermore, percutaneous infiltrations can be used as a diagnostic test to identify a certain anatomic structure as source of pain by achieving temporary pain relief (Cohen and Hurley 2007).

Percutaneous disc decompression includes several image-guided treatments for intervertebral disc hernia, which can be performed on an outpatient basis. During therapy, a trocar is percutaneously inserted into the disc under imaging guidance. Through this trocar, a thermal, chemical, or mechanical decompression device is introduced into the nucleus pulposus, with the least possible disruption of surrounding tissues, in order to achieve its partial removal (Cohen and Raja 2007). Percutaneous decompression treatments are governed by the Hijikata theory (1975): "Reduction of intradiscal pressure reduces the irritation of the nerve root and the pain receptors in the annulus and peridiscal area" (Cohen and Hurley 2007; Cohen and Raja 2007). In other words, by removing a small nuclear volume, the result is a significant decrease of intradiscal pressure. Furthermore, space is created for the herniated fragment to retract, thereby reducing pain and improving mobility and quality of life.

14.8.1.1 Indications

Intradiscal Steroid Injection

- Contained disc herniation or focal protrusion at CT or MR imaging
- Discogenic pain due to degeneration or protrusion
- Dorsalgia without neurologic deficit
- Patients with equivocal neurologic examinations
- Symptomatic imaging abnormalities without herniated or free disc fragments, foraminal stenosis, spinal nerve root compression, or inflammation
- Decompression Techniques (Cohen and Hurley 2007; Cohen and Raja 2007; Cohen et al. 2008; Cohen and Williams 2010)
- Symptomatic-contained intervertebral disc herniation occupying less than 1/3 of the spinal canal as confirmed by CT or MR
- Back or neck pain attributed to the intervertebral disc herniation limiting normal activity for at least 6 weeks and being refractory to conservative therapy (leg/arm pain should be of greater intensity than back/neck pain)
- Single nerve root involvement (positive Laseque sign, decreased tendon reflex, sensation, and motor response) with specific dermatomal pain distribution

Discography and/or quantitative discomanometry should be performed as a diagnostic test prior to intervention. Discography should provoke memory pain in these patients.

14.8.1.2 Contraindications

Absolute

- Asymptomatic intervertebral disc herniation
- Local or systemic infection
- Allergy to any therapeutic agent
- Sequestered (free) disc fragment
- Segmental instability (e.g., spondylolisthesis) – in these patients, jellified ethanol is indicated
- Stenosis of either neural foramen or spinal canal
- Pregnancy – in these patients, MR guidance is recommended
- Uncorrectable hemorrhagic diathesis

Relative (Cohen and Hurley 2007; Cohen and Raja 2007; Cohen et al. 2008; Dreyfuss et al. 2003; Esses and Moro 1993; Gaul et al. 2005)

- Severe degenerative disc disease with more than 2/3 decrease in disc height (technical difficulty of introducing the trocar inside the disc)
- Medical record of intervertebral disc operation at the same level (at least 20 % less chances for success)

14.8.1.3 Material: Technique

Pre-procedural Care

All patients must be informed about the technique including possible benefits and complications and sign a written consent form. Clinical evaluation of the patient is mandatory in order to verify the discogenic origin of the pain and exclude other potential sources of pain (e.g., facet or sacroiliac joints). Pre-procedural imaging needs to include a MR scan while pre-procedural laboratory workup has to include a coagulation profile (Cohen and Hurley 2007; Cohen and Raja 2007). Discography should be performed before nucleoplasty in order to confirm annulus integrity. Moreover, diagnostic discography is helpful to determine the morphology of disc herniation (containment) and to prove discogenic pain provocation.

Intradiscal steroid injections and percutaneous decompression therapies for intervertebral disc herniation are performed under image guidance [fluoroscopy-, CT-, MR-, or hybrid (CT and fluoro) guidance]. Sterile conditions are mandatory, and pre-procedural antibiotic therapy is strongly recommended for percutaneous decompression therapy. Local anesthesia is limited to skin and subcutaneous tissues in order to avoid an accidental puncture of the nerve root without patient reaction during trocar positioning. The patient is positioned prone when thoracic or lumbar spine is concerned or supine when cervical spine is concerned. A posterolateral approach is used for treating the thoracic or lumbar spine while an anterolateral approach is used for treating the cervical spine (Cohen and Hurley 2007; Cohen and Raja 2007).

Once the trocar is inside the disc, with the target position as close to the center of the disc as possible, the stylet is removed. Through the trocar, intradiscal steroid injection is performed (recommend volume: ~1 ml triamcinolonacetonide (40 mg) and ~1 ml bupivacaine) or a

decompression device (thermal, mechanical, or chemical) is introduced to the center of the intervertebral disc. Mechanical decompression is achieved by means of mechanical high-speed rotation devices (with spiral tips or metallic wires/laminae which promote disc removal) or by a pneumatically driven, suction-cutting probe (Gofeld et al. 2007; Helbig and Lee 1988). There are several different thermal decompression techniques, e.g., applying via a laser fiber or a radiofrequency electrode (Table 14.2) (Dreyfuss et al. 2003; Gaul et al. 2005; Hildebrandt 2001). The latter is the only technique with the coil being deployed not at the nucleus pulposus but at the annulus fibrosus aiming at the destruction of nerve endings (Gaul et al. 2005). Chemical decompression is achieved by means of jellified ethanol (Discogel®, Gelscom, Hérouville-Saint-Clair, F) or ozone intradiscal injection which causes dehydration and subsequently breakdown of the nucleus pulposus (Hooten et al. 2005; Jackson et al. 1988) (Fig. 14.26).

Post-procedural Care

Intervertebral disc therapies can be performed on an outpatient basis. Patient have bed rest for 2–4 h and leave the hospital with detailed instructions including postoperative restrictions such as rest during the initial period, avoiding prolonged sitting, heavy lifting, twisting, or forward bending, and the use of NSAIDs and muscle relaxants. However, the application of these restrictions differs throughout the world (Cohen and Raja 2007; Cohen et al. 2008). Patient will only leave hospital if accompanied by a responsible person who will be in charge of his/her transfer.

14.8.1.4 Results: Complications

Intervertebral disc therapies are governed by an 85 % success rate and a mean clinically significant complication rate <0.5 % (Cohen and Hurley 2007; Cohen and Raja 2007; Cohen et al. 2008). When compared to conservative therapy, they seem to result in significantly better and longer-lasting outcome in terms of pain reduction and mobility improvement. Infection (spondylodiscitis) with or without epidural abscess is the most commonly encountered and fearsome complication (0.24 %/patient and 0.091 %/disc of patients) (Cohen and Hurley 2007; Cohen and Raja 2007; Cohen et al. 2008; Cohen and Williams 2010; Kaplan et al. 1998; Laslett et al. 2004, 2006). Specifically, thermal decompression techniques are governed by a 2.5 % complication ration including the possibility of thermal discitis (sterile inflammation of vertebral end plates due to iatrogenic damage). Less frequent complications include material failure, allergic reaction, reflex sympathetic dystrophy, accidental puncture of the thecal sac, hemorrhage and neurologic injury, pneumothorax, and vasovagal reactions (Cohen and Hurley 2007; Cohen and Raja 2007; Cohen et al. 2008; Cohen and Williams 2010; Laslett et al. 2006).

Intradiscal Steroid Injection

Six randomized trials evaluated intradiscal steroid injection (Manchikanti et al. 2000, 2004, 2007; Marks et al. 1992; Masharawi et al. 2004; Meleka et al. 2005; Murtagh 1988; Nelemans et al. 2001) .Two trials were included in a Cochrane review (Manchikanti et al. 2000). Three trials were placebo controlled (Manchikanti et al. 2004; Marks et al. 1992; Masharawi et al. 2004). All three placebo-controlled trials evaluated intradiscal steroid injection for degenerative disc disease. For chronic low back pain with magnetic resonance imaging evidence of degenerative disc disease and positive response to provocative discography, two trials found no significant difference between intradiscal steroid and control injections (saline or local anesthetic) for pain relief or improvement in functional status (Marks et al. 1992; Masharawi et al. 2004). A third, lower quality trial on patients with degenerative disc disease who did not respond to an epidural steroid injection found discography plus intradiscal steroid superior to discography alone only in the subgroup of patients with inflammatory endplate changes on magnetic resonance imaging (Manchikanti et al. 2004). Another, lower quality trial reported a trend favoring chemonucleolysis over intradiscal steroid injection after 2 years (Manchikanti et al. 2007; Nelemans et al. 2001). No trial reported on adverse events (such as discitis) following intradiscal steroid injection (Manchikanti et al. 2000).

Table 14.2 Summary of different techniques for intervertebral disc decompression

Decompression type	Method	Definition	Success rate (%)	Complication rate (%)
Mechanical Decompression	Automated percutaneous lumbar discectomy (APLD)	Pneumatically driven, suction-cutting probe	75	Technical failure rate 2.6
				Mild muscle spasm 9
				Functional lower limb paresis 0.4
	Percutaneous disc decompression (PDD)	Mechanical high rotation per minute device with spiral tips or metallic laminae	60–85	0.5
	Percutaneous laser decompression	Laser energy vaporizes a small volume of nucleus pulposus	63–89	Intraoperative 1.1
				Postoperative1.5
				General complication rate 0.5–1
	Intradiscal electrothermal therapy (IDET)	Flexible thermal resistive coil (electrode or catheter) coagulates the disc tissue with radiant heat	64–75	Transient and mild adverse events (radicular pain, paraesthesia numbness)
				0–15
				Serious adverse events (cerebrospinal fluid leak, cauda equine syndrome, vertebral osteonecrosis) <0.5
				General complication rate from meta-analysis 0.8
	Intervertebral disc nucleoplasty	Bipolar radiofrequency energy causes molecular dissociation and dissolves nuclear material	79	<0.5
	Discogel	Jellified ethanol causes dehydration of nucleus pulposus	91.4	<0.5
	Ozone therapy	Ozone's chemical properties and the reaction of hydroxyl radical with carbohydrates and amino acids lead to breakdown of nucleus pulposus	70–78	<0.5

Decompression Techniques

Intradiscal Electrothermal Therapy (IDET)

Two higher-quality, sham-controlled, randomized trials evaluated IDET (Neuhauser et al. 2005; Okada et al. 2005; Park et al. 2007).For chronic low back pain with positive response to provocative lumbar discography, 2 small (n=57 and n=64), sham-controlled trials of IDET reported inconsistent results (Okada et al. 2005; Park et al. 2007). In one trial, IDET was associated with moderately greater improvements in pain as measured on visual analog scale (VAS) (2.4 vs. 1.1 on a 0–10 scale, p=0.0045) and slightly greater improvements in mean *Oswestry disability index* (*ODI*) scores (11 vs. 4, p=0.050) compared with sham IDET, but was no better on the SF-36 bodily pain or physical functioning subscales (Park et al. 2007). In 1 controlled observational study, IDET was associated with substantially better VAS pain scores at 3 months (3.5 vs. 8.0 on a 0–10 scale, $p \geq 0.0005$) and 24 months (3.0 vs. 7.5, p=0.028), as well as a higher proportion pain-free at 24 months (20 % or 7 of 35 vs. 0 % or 0 of 17) (Revel et al. 1998).

Percutaneous Intradiscal Radiofrequency, Thermocoagulation (PIRFT), and Coblation Nucleoplasty

Two randomized trials evaluated PIRFT (Schwarzer et al. 1994a, b). A systematic review of coblation nucleoplasty identified no randomized trials and insufficient evidence from small case series to evaluate efficacy (Manchikanti et al. 2000). For chronic, presumed discogenic low back pain based on a positive response to analgesic discography, one higher-quality pla-

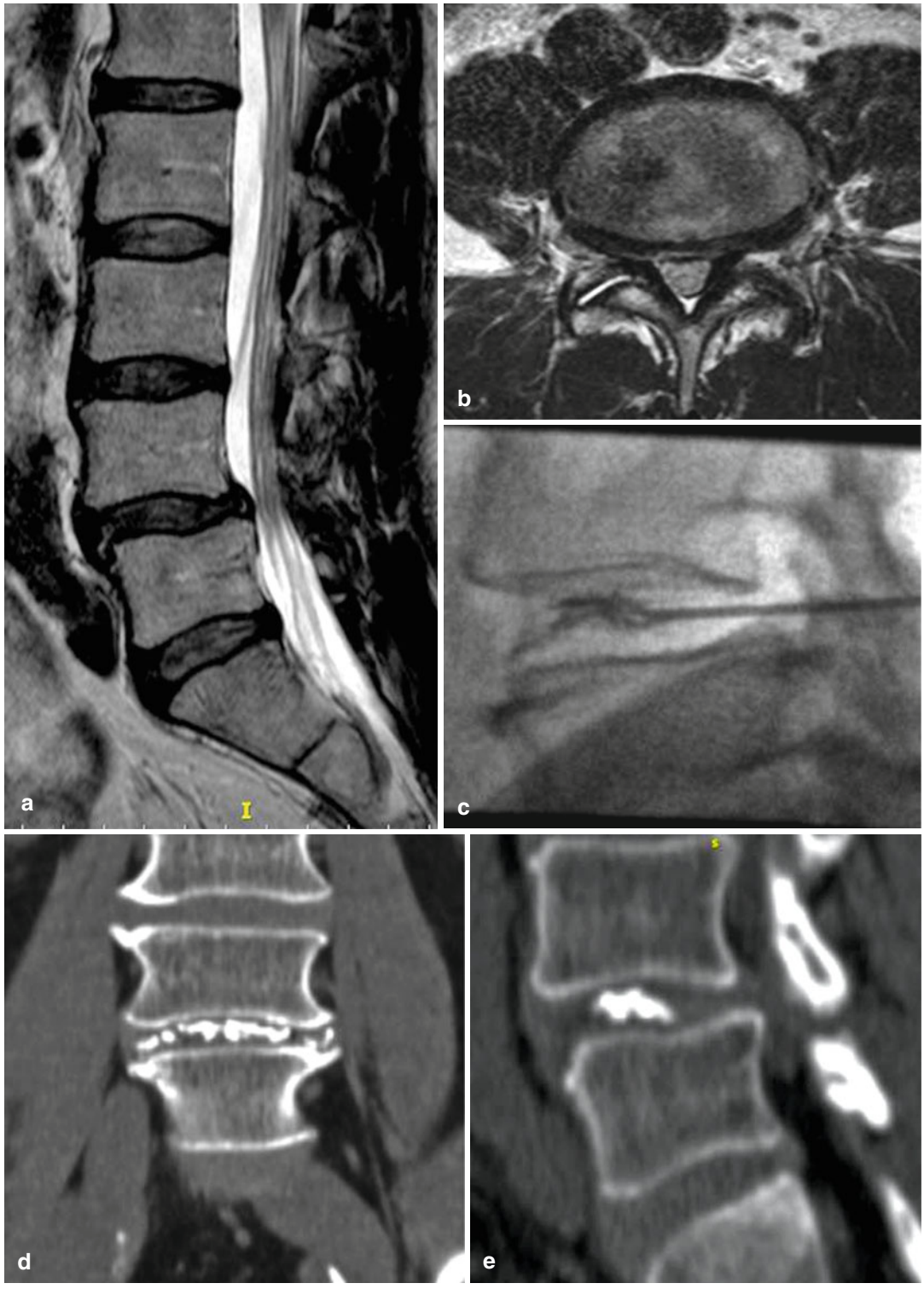

Fig. 14.26 L4–L5 intradiscal Discogel injection for the treatment of discogenic pain due to intervertebral disc degeneration and herniation. (**a**, **b**) Midsagittal T2-weighted MR image (**a**) shows degenerative disc changes with low signal intensity of the lower lumbar discs and central herniation at the level of L4–5 (**b**). (**c**) L4–L5 Intradiscal Discogel® injection is performed under lateral fluoroscopic guidance. (**d**, **e**) Computed tomography sagittal (**d**) and coronal (**e**) reconstruction: Discogel® is dispersed inside nucleus pulposus of L4–L5 intervertebral disc

cebo-controlled trial (Schwarzer et al. 1994a)found no significant differences between PIRFT and sham PIRFT in improvement in VAS pain scores, global effect, ODI, or a composite outcome of overall treatment success. A second trial was not sham-controlled but only found minimal improvement with either lower or higher intensity of PIRFT (Schwarzer et al. 1994b). Discitis was reported as a complication in one trial (Manchikanti et al. 2000).

14.8.2 Intervertebral Disc Biopsy

Biopsy of the intervertebral disc is performed in cases of suspected or proven spondylodiscitis for culture of the obtained sample in order to reveal the responsible microorganism and provide the proper therapy. Disc biopsy is performed under image guidance and under strict sterility conditions (Fig. 14.27). Prophylactic antibiotics are prohibited in order to achieve a significant result. However, some authors accept antibiotic therapy if started not longer than 1 h prior to biopsy because there will be no therapeutic level for that short time. Access to the intervertebral disc may either be direct or via a transpedicular access and through the vertebral endplate to reach the intervertebral disc. Vertebral biopsy is fundamental in determining whether a lesion is infectious or not. Accurate diagnosis is critical for proper medical and/or surgical treatment and consequently for the prognosis of the patient (Levin 2007).

14.8.2.1 Results: Complications

In a prospective series of 69 patients, Gassbarini et al. yielded a diagnosis in 81.8 % of cases after histological examination. Microbiologic culture and PCR for Mycobacterium tuberculosis were positive in 45.8 % (Levin 2007). To determine the role of CT-guided biopsy in the management of cases of infective discitis, Enoch et al. retrospectively analyzed a case series of 98 CT-guided biopsies over a 5-year period. Discitis and paravertebral abscess accounted for 27 cases (Lilius et al. 1990). Culture was positive in nine of 25 (36 %) samples received by the microbiology laboratory. *Staphylococcus aureus* and *Mycobacterium tuberculosis* were the most frequent organisms isolated. The main reason for a negative culture was prior antimicrobial therapy. Biopsy changed management in 9/25 (36 %) of cases. There were no reported complications or adverse events.

Summary

Minimally invasive, image-guided, percutaneous decompression techniques yield significant and long-lasting results upon pain reduction and mobility improvement in symptomatic patients with disc herniation. These decompression techniques include a variety of mechanical, thermal, or chemical instruments/agents used to extract/destroy a part of the nucleus pulposus thereby reducing intradiscal pressure and allowing the herniated part to retract. These techniques are nowadays considered either first-line therapies or attractive alternatives to surgical treatments due to their high success rates (~85 %) and the low complication rates (<0.5 %).

CT-guided biopsy is a useful tool if discal infection is considered. It is a safe and well-tolerated procedure, permitting a targeted antibiotic therapy.

Key Points

- Minimally invasive therapies for low back pain due to intervertebral disc herniation are safe (potential complication rate ~0.5 %) and effective (success rate ~85 %) techniques for pain reduction and mobility improvement.
- These techniques include intradiscal steroid injection as well as percutaneous disc decompression therapies.
- Disc decompression therapies include mechanical, chemical, and thermal techniques.
- Proper imaging guidance enhances safety and efficacy.
- CT-guided biopsy is a useful tool when discal/spinal infection is considered.

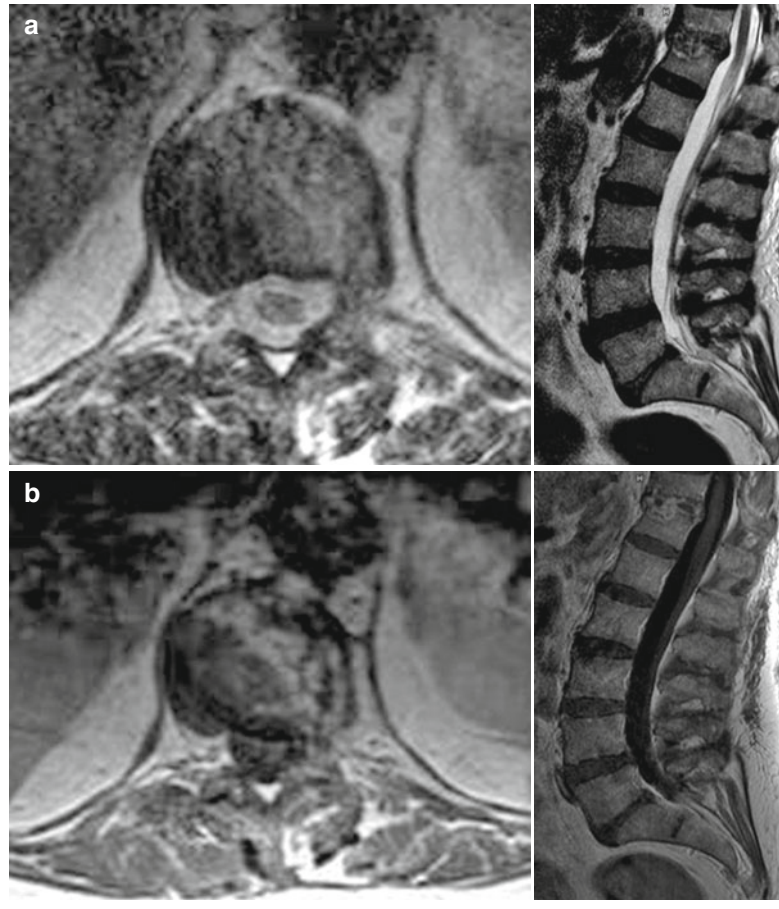

Fig. 14.27 Intervertebral disc biopsy performed in cases of suspected spondylodiscitis for microbiological examination. (**a**–**c**) MRI: sagittal and axial T2w (**a**) – and T1w post contrast (**b**) images demonstrating spondylodiscitis predominant in the left hemivertebra with beginning epidural and paravertebral abscess formation (coronal T2w-fat sat (**c**)). (**d**, **e**) CT-guided access to the intervertebral disc by direct access. The 11 gauge biopsy needle reaches the intervertebral disc

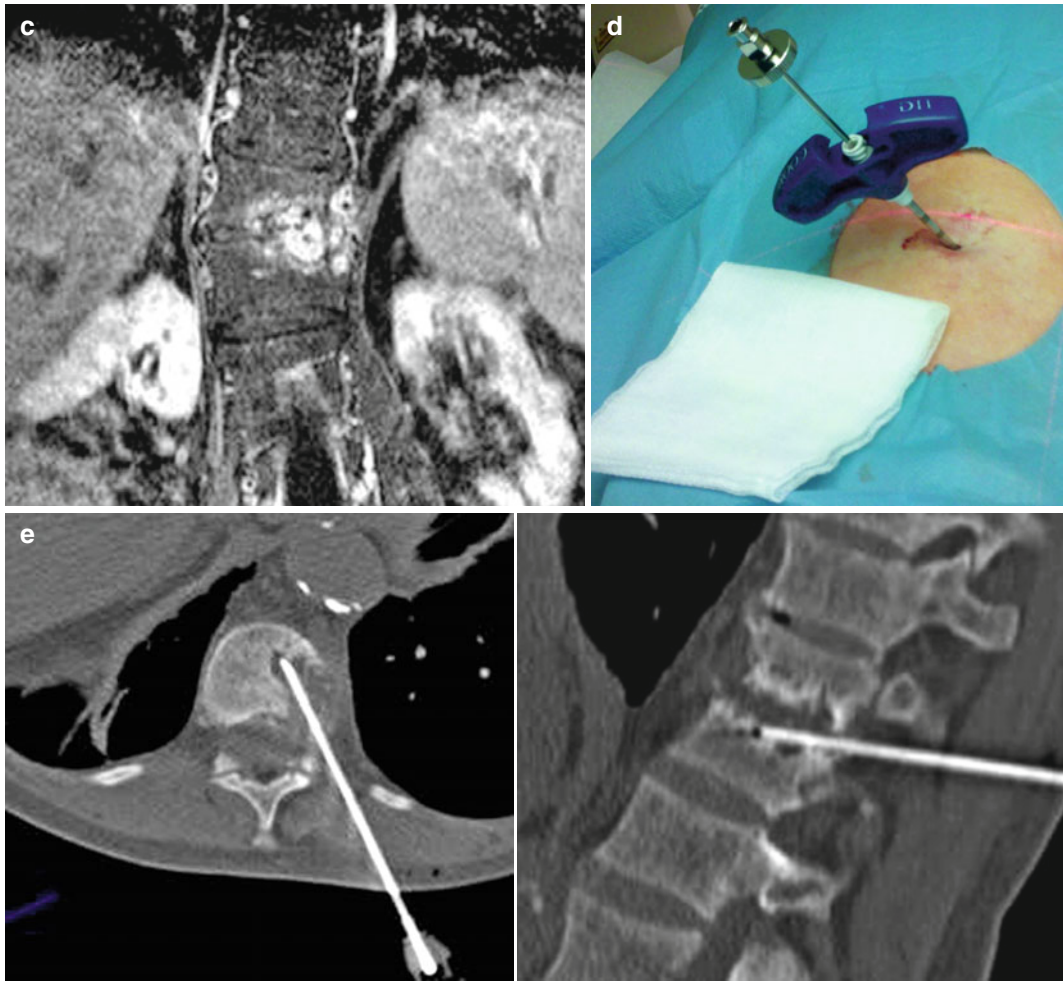

Fig. 14.27 (continued)

References

Neurolysis of the Facet Joint

Aguirre DA, Bermudez S, Diaz OM (2005) Spinal CT-guided interventional procedures for management of chronic back pain. J Vasc Interv Radiol 16(5):689–697

Alcock E, Regaard A, Browne J (2003) Facet joint injection: a rare form cause of epidural abscess formation. Pain 103(1/2):209–210

Bogduk N, Wilson AS, Tynan W (1982) The human lumbar dorsal rami. J Anat 134(2):383–397

Cohen SP, Hurley RW (2007) The ability of diagnostic spinal injections to predict surgical outcomes. Anesth Analg 105(6):1756–1775

Cohen SP, Raja SN (2007) Pathogenesis, diagnosis, and treatment of lumbar zygapophysial (facet) joint pain. Anesthesiology 106(3):591–614

Cohen SP, Stojanovic MP, Crooks M et al (2008) Lumbar zygapophysial (facet) joint radiofrequency denervation success as a function of pain relief during diagnostic medial branch blocks: a multicenter analysis. Spine J 8(3):498–504

Cohen SP, Williams KA, Kurihara C (2010) Multicenter, randomized, comparative cost-effectiveness study comparing 0, 1, and 2 diagnostic medial branch (facet joint nerve) block treatment paradigms before lumbar facet radiofrequency denervation. Anesthesiology 113(2):395–405

Dreyfuss PH, Dreyer SJ, Vaccaro A (2003) Lumbar zygapophysial (facet) joint injections. Spine J 3(Suppl 1): 50–59

Esses SI, Moro JK (1993) The value of facet joint blocks in patient selection for lumbar fusion. Spine 18(2): 185–190

Gaul C, Neundorfer B, Winterholler E (2005) Iatrogenic (para-) spinal abscesses and meningitis following

injection therapy for low back pain. Pain 116(3): 407–410
Gofeld M, Jitendra J, Faclier G (2007) Radiofrequency denervation of the lumbar zygapophysial joints: 10-year prospective clinical audit. Pain Physician 10(2):291–300
Helbig T, Lee CK (1988) The lumbar facet syndrome. Spine 13(1):61–64
Hildebrandt J (2001) Relevance of nerve blocks in treating and diagnosing low back pain – is the quality decisive? Schmerz 15(6):474–483
Hooten WM, Martin DP, Huntoon MA (2005) Radiofrequency neurotomy for low back pain: evidence-based procedural guidelines. Pain Med 6(2):139–142
Jackson RP, Jacobs RR, Montesano PX (1988) 1988 Volvo award in clinical sciences. Facet joint injection in low-back pain. A prospective statistical study. Spine 13(9):966–971
Kaplan M, Dreyfuss P, Halbrook B et al (1998) The ability of lumbar medial branch blocks to anesthetize the zygapophysial joint. A physiologic challenge. Spine 23(17):1847–1852
Laslett M, Oberg B, Aprill CN et al (2004) Zygapophysial joint blocks in chronic low back pain: a test of Revel's model as a screening test. BMC Musculoskelet Disord 5:43
Laslett M, McDonald B, Aprill CN et al (2006) Clinical predictors of screening lumbar zygapophyseal joint blocks: development of clinical prediction rules. Spine J 6(4):370–379
Levin KH (2007) Nonsurgical interventions for spine pain. Neurol Clin 25(2):495–505
Lilius G, Harilainen A, Laasonen EM et al (1990) Chronic unilateral low-back pain. Predictors of outcome of facet joint injections. Spine 15(8):780–782
Manchikanti L, Pampati V, Fellows B et al (2000) The inability of the clinical picture to characterize pain from facet joints. Pain Physician 3(2):158–166
Manchikanti L, Boswell MV, Singh V et al (2004) Prevalence of facet joint pain in chronic spinal pain of cervical, thoracic, and lumbar regions. BMC Musculoskelet Disord 5:15
Manchikanti L, Manchikanti KN, Manchukonda R et al (2007) Evaluation of lumbar facet joint nerve blocks in the management of chronic low back pain: preliminary report of a randomized, double-blind controlled trial: clinical trial NCT00355914. Pain Physician 10(3):425–440
Marks MJ, Pauly JR, Gross SD et al (1992) Nicotine binding and nicotinic receptor subunit RNA after chronic nicotine treatment. J Neurosci 12(7):2765–2784
Masharawi Y, Rothschild B, Dar G et al (2004) Facet orientation in the thoracolumbar spine: three-dimensional anatomic and biomechanical analysis. Spine 29(16): 1755–1763
Meleka S, Patra A, Minkoff E et al (2005) Value of CT fluoroscopy for lumbar facet blocks. AJNR Am J Neuroradiol 26(5):1001–1003
Murtagh FR (1988) Computed tomography and fluoroscopy guided anesthesia and steroid injection in facet syndrome. Spine 13(6):686–689
Nelemans PJ, deBie RA, deVet HC et al (2001) Injection therapy for subacute and chronic benign low back pain. Spine 26(5):501–515
Neuhauser H, Ellert U, Ziese T (2005) Chronic back pain in the general population in Germany 2002/2003: prevalence and highly affected population groups. Gesundheitswesen 67(10):685–693 [German]
Okada F, Takayama H, Doita M et al (2005) Lumbar facet joint infection associated with epidural and paraspinal abscess: a case report with review of the literature. J Spinal Disord Tech 18(5):458–461
Park MS, Moon SH, Hahn SB et al (2007) Paraspinal abscess communicated with epidural abscess after extra-articular facet joint injection. Yonsei Med J 48(4):711–714
Revel M, Poiraudeau S, Auleley GR et al (1998) Capacity of the clinical picture to characterize low back pain relieved by facet joint anesthesia. Proposed criteria to identify patients with painful facet joints. Spine 23(18):1972–1976; discussion 1977
Schwarzer AC, Aprill CN, Derby R et al (1994a) The false-positive rate of uncontrolled diagnostic blocks of the lumbar zygapophysial joints. Pain 58(2): 195–200
Schwarzer AC, Aprill CN, Derby R et al (1994b) Clinical features of patients with pain stemming from the lumbar zy-gapophysial joints. Is the lumbar facet syndrome a clinical entity? Spine 19(10):1132–1137
Schwarzer AC, Wang SC, Bogduk N et al. (1995) Prevalence and clinical features of lumbar zygapophysial joint pain: a study in an Australian population with chronic low back pain. Ann Rheum Dis 54(2):100–106
Suseki K, Takahashi Y, Takahashi K et al (1997) Innervation of the lumbar facet joints. Origins and functions. Spine 22(5):477–485
van Kleef M, Barendse GA, Kessels A et al (1999) Randomized trial of radiofrequency lumbar facet denervation for chronic low back pain. Spine 24(18): 1937–1942
Yoganandan N, Knowles SA, Maiman DJ et al (2003) Anatomic study of the morphology of human cervical facet joint. Spine 28(20):2317–2323

Image-Guided Nerve Blocks and Infiltrations in Pain Managment

Amarenco G, Lanoe Y, Ghnassia RT et al (1988) Syndrome du canal d'Alcock et névralgies périnéales. Rev Neurol (Paris) 144:523–526 [French]
Bogduk N (1980) The anatomy of occipital neuralgia. Clin Exp Neurol 17:167–184
Bogduk N (1981) Local anesthetic blocks of the second cervical ganglion: a technique with application in occipital headache. Cephalalgia 1:41–50
Bovim G, Sand T (1992) Cervicogenic headache, migraine without aura and tension-type headache. Diagnostic blockade of greater occipital and supra-orbital nerves. Pain 51:43–48

Bovim G, Fredriksen T, Stolt-Nielsen A et al (1992) Neurolysis of the greater occipital nerve in cervicogenic headache. A follow up study. Headache 32:175–179
Buy JN, Moss AA, Singler RC (1982) CT guided celiac plexus and splanchnic nerve neurolysis. J Comput Assist Tomogr 6:315–319
Clair C, Kastler B, Aubry R et al (1998) Neurolyse du ganglion sphénopalatin sous contrôle TDM. Radiol J CEPUR 18:405–411 [French]
Devoghel JC (1981) Cluster headache and sphenopalatine block. Acta Anaesthesiol Belg 32:101–107
Corréas JM, Belin X, Amarenco G et al (1990) Infiltration scano-guidée dans le syndrome du canal d'Alcock chronique. Rev Im Med 2:547–549 [French]
de Kersaint-Gilly A, Sonier CB, Legent F et al (1991) Radioanatomie de la fosse infratemporale. Région ptérygomaxillaire. Ann Otolaryngol Chir Cervicofac 108:77–81 [French]
Forouzanfar T, Van Kleef M, Weber WEJ (2000) Radiofrequency lesions of the stellate ganglion in chronic pain syndromes. Clin J Pain 16:164–168
Fujita Y, Takaori M (1987) Pleural effusion after CT guided alcohol celiac plexus block. Anesth Analg 66:911–912
Gafanovich I, Shir Y, Tsvang E et al (1988) Chronic diarrhoea induced by celiac plexus block. J Clin Gastroenterol 26:300–302
Gangi A, Dietemann JL, Schultz A et al (1996a) Interventional radiologic procedures with CT guidance in cancer pain management. Radiographics 16: 1289–1306
Haaga JR, Kori SH, Eastwood DW et al (1984) Improved technique for CT-guided celiac ganglia block. AJR Am J Roentgenol 142:1201–1204
Hardebo JE, Elner A (1987) Nerves and vessels in the pterygopalatine fossa and symptoms of cluster headache. Headache 27:528–532
Hogan QH, Erickson SJ (1992) MR imaging of the stellate ganglion: normal appearance. AJR Am J Roentgenol 158:655–659
Hogan QH, Erickson SJ, Abram SE (1992) Computerized tomography (CT) guided stellate ganglion blockade. Anesthesiology 77:596–599
Ischia S, Luzzani A, Ischia A et al (1983) A new approach to neurolytic block of the celiac plexus: the transaortic technique. Pain 16:333–341
Ischia S, Ischia A, Polati E et al (1992) Three posterior percutaneous celiac plexus block techniques. A prospective, randomized study in 61 patients with pancreatic cancer pain. Anesthesiology 76:534–540
Kastler B (2006) Interventional radiology in pain management. Springer, Berlin/Heidelberg/New York
Kastler B, Couvreur M, Clair C et al (1999) Tomodensitométrie interventionnelle: suivez le guide. Feuill Radiol 39:421–432 [French]
Kastler B, Narboux Y, Clair C (2001) Neurolyse par radiofréquence du ganglion stellaire. À propos d'un cas traité et suivi sur trois ans. J Radiol 82:76–78 [French]
Lee MJ, Mueller PR, Van Sonnenberg E (1993) CT-guided celiac ganglion block with alcohol. AJR Am J Roentgenol 161:633–636
Scott J, Erickson SJ, Quinn H et al (1993) CT guided injection of the stellate ganglion: description of technique and efficacy of sympathetic blockade. Radiology 188:707–709
Vital JM, Grenier F, Dautheribes M et al (1989) An anatomic and dynamic study of the greater occipital nerve (n. of Arnold). Applications to the treatment of Arnold's neuralgia. Surg Radiol Anat 11:205–210
Ward EM, Rorle DK, Nauss LA et al (1979) The celiac ganglia in man: normal anatomic variations. Anesth Analg 68:461–465
Wechsler RJ, Maurer PM, Halpern EJ et al (1996) Superior hypogastric plexus bloc for chronic pain in the presence of endometriosis: CT technique and results. Radiology 105:103–105

Thoracic and Lumbar Sympathicolysis

Adler OB, Engel A, Rosenberger A et al (1990) Palmar hyperhidrosis CT guided chemical percutaneous thoracic sympathectomy. Rofo 153:400–403
Arkkila PE (2006) Thromboangiitis obliterans (Buerger's disease). Orphanet J Rare Dis 1:14
Baumgartner FJ, Toh Y (2003) Severe hyperhidrosis: clinical features and current thoracoscopic surgical management. Ann Thorac Surg 76:1878–1883
Chen HJ, Liang CL, Lu K (2001) Associated change in plantar temperature and sweating after transthoracic endoscopic T2-3 sympathectomy for palmar hyperhidrosis. J Neurosurg 95(1 Suppl):58–63
Di Lorenzo N, Sica GS, Sileri P et al (1998) Thoracoscopic sympathectomy for vasospastic diseases. JSLS 2:249–253
Duda SH, Huppert PE, Heinzelmann B et al (1994) CT-gestützte perkutane lumbale Sympathikolyse bei peripherer Verschlusskrankheit. Rofo 160:132–136 [German]
Feinglass J, Brown JL, Aet LS et al (1999) Rates of lower-extremity amputation and arterial reconstruction in the United States, 1979 to 1996. Am J Public Health 89:1222–1227
Finkenzeller T, Techert J, Lenhart J et al (2001) CT-gesteuerte thorakale Sympathikolyse zur Behandlung der peripheren arteriellen Verschlusskrankheit und thorakaler Schmerzen in 6 Fällen. Rofo 173:920–923 [German]
Furlan AD, Ping-Wing L, Mailis A (2001) Chemical sympathectomy for neuropathic pain: does it work? Case report and systematic literature review. Clin J Pain 17:327–336
Heindel W, Ernst S, Manshausen G et al (1998) CT-guided lumbar sympathectomy: results and analysis of factors influencing the outcome. Cardiovasc Intervent Radiol 21:319–323
Huttner S, Huttner M, Neher M et al (2002) CT-gesteuerte Sympathikolyse bei peripherer arterieller Verschlusskrankheit – Indikationen, Patientenauswahl, Langzeitergebnisse. Rofo 174:480–484 [German]

Jaboulay M (1899) Le traitment de quelques troubles trophiques du pied et dela jambe par la dénudation de l`àterie fémorale et la distension des nerfs vasculaires. Lyon Med 91:467–468 [French]
Janoff KA, Phinney ES, Porter JM (1985) Lumbar sympathectomy for lower extremity vasospasm. Am J Surg 150:147–152
Katara AN, Domino JP, Cheah WK et al (2007) Comparing T2 and T2-T3 ablation in thoracoscopic sympathectomy for palmar hyperhidrosis: a randomized control trial. Surg Endosc 21:1768–1771
König CW, Schott UG, Pereira PL et al (2002) MR-guided lumbar sympathicolysis. Eur Radiol 12:1388–1393
Lau H, Cheng SW (1997) Buerger's disease in Hong Kong: a review of 89 cases. Aust N Z J Surg 67:264–269
Lee BY, Madden JL, Thoden WR et al (1983) Lumbar sympathectomy for toe gangrene: long-term follow-up. Am J Surg 145:398–401
Maga P, Kuzdzal J, Nizankowski R et al (2007) Long-term effects of thoracic sympathectomy on microcirculation in the hands of patients with primary Raynaud disease. J Thorac Cardiovasc Surg 133:1428–1433
Manjunath PS, Jayalakshmi TS, Dureja GP et al (2008) Management of lower limb complex regional pain syndrome type 1: an evaluation of percutaneous radiofrequency thermal lumbar sympathectomy versus phenol lumbar sympathetic neurolysis - a pilot study. Anesth Analg 106:647–649
Montessi J, de Almeida EP, Viera JP et al (2007) Video-assisted thoracic sympathectomy in the treatment of primary hyperhidrosis: a retrospective study of 521 cases comparing different levels of ablation. J Bras Pneumol 33:248–254
Moya J, Ramos R, Morera R et al (2006) Thoracic sympathicolysis for primary hyperhidrosis: a review of 918 procedures. Surg Endosc 20:598–602
Pieri S, Agresti P, Ialongo P et al (2005) Lumbar sympathectomy under CT guidance: therapeutic option in critical limb ischaemia. Radiol Med (Torino) 109: 430–437
Price DD, Long S, Wilsey B et al (1998) Analysis of peak magnitude and duration of analgesia produced by local anesthetics injected into sympathetic ganglia of complex regional pain syndrome patients. Clin J Pain 14:216–226
Romano M, Giojelli A, Mainenti PP et al (2002) Upper thoracic sympathetic chain neurolysis under CT guidance. A two year follow-up in patients with palmar and axillary hyperhidrosis. Radiol Med (Torino) 104: 421–425
Rosen RJ, Miller DL, Imparato AM et al (1983) Percutaneous phenol sympathectomy in advanced vascular disease. AJR Am J Roentgenol 141:597–600
Schild H, Grönniger J, Günther R et al (1984) Transabdominelle CT-gesteuerte Sympathektomie. Rofo 141:504–508 [German]
Schmid MR, Kissling RO, Curt A et al (2006) Sympathetic skin response: monitoring of CT-guided lumbar sympathetic blocks. Radiology 241:595–602
Schneider B, Richter GM, Roeren T et al (1996) CT-gesteuerte Neurolysen. Stand der Technik und aktuelle Ergebnisse. Radiologe 36:692–699 [German]
Thune TH, Ladegaard L, Licht PB (2006) Thoracoscopic sympathectomy for Raynaud's phenomenon – a long term follow-up study. Eur J Vasc Endovasc Surg 32:198–202
Vranken JH, Zuurmond WW, van Kemenade FJ et al (2002) Neurohistopathologic findings after a neurolytic celiac plexus block with alcohol in patients with pancreatic cancer pain. Acta Anaesthesiol Scand 46:827–830

Trigeminal Ablation

Bale RJ, Vogele M, Freysinger W et al (1997a) Minimally invasive head holder to improve the performance of frameless stereotactic surgery. Laryngoscope 107: 373–377
Bale RJ, Vogele M, Martin A et al (1997b) VBH head holder to improve frameless stereotactic brachytherapy of cranial tumors. Comput Aided Surg 2:286–291
Bale RJ, Freysinger W, Gunkel AR et al (2000) Head and neck tumors: fractionated frameless stereotactic interstitial brachytherapy-initial experience. Radiology 214:591–595
Bale R, Laimer I, Schlager A, Martin A, Rieger M, Mayr C, Czermak B, Kovacs P, Widmann G (2006) Frameless stereotactic cannulation of the foramen ovale for ablative treatment of trigeminal neuralgia. Neurosurgery 59:ONS394–ONS401
Barker FG, Jannetta PJ, Bissonette DJ et al (1996) The long-term outcome of microvascular decompression for trigeminal neuralgia. N Engl J Med 334: 1077–1083
Berk C, Honey CR (2004) Brain stem injury after radiofrequency trigeminal rhizotomy. Acta Neurochir (Wien) 146:635–636
Egan RA, Pless M, Shults WT (2001) Monocular blindness as a complication of trigeminal radiofrequency rhizotomy. Am J Ophthalmol 131:237–240
Gauci C (2004) Trigeminal ganglion RF. In: Gauci C (ed) Manual of RF techniques. Flivo Press SA, Meggen
Hajioff D, Dorward NL, Wadley JP et al (2000) Precise cannulation of the foramen ovale in trigeminal neuralgia complicating osteogenesis imperfecta with basilar invagination: technical case report. Neurosurgery 46:1005–1008
Kanpolat Y, Berk C, Savas A et al (2000) Percutaneous controlled radiofrequency rhizotomy in the management of patients with trigeminal neuralgia due to multiple sclerosis. Acta Neurochir (Wien) 142:685–689
Kanpolat Y, Savas A, Bekar A et al (2001) Percutaneous controlled radiofrequency trigeminal rhizotomy for the treatment of idiopathic trigeminal neuralgia: 25-year experience with 1,600 patients. Neurosurgery 48:524–532

Katusic S, Williams DB, Beard CM et al (1991) Incidence and clinical features of glossopharyngeal neuralgia, Rochester, Minnesota, 1945–1984. Neuroepidemiology 10:266–275
Liu M, Wu CY, Liu YG et al (2005) Three-dimensional computed tomography-guided radiofrequency trigeminal rhizotomy for treatment of idiopathic trigeminal neuralgia. Chin Med Sci J 20:206–209
Lopez BC, Hamlyn PJ, Zakrzewska JM (2004) Systematic review of ablative neurosurgical techniques for the treatment of trigeminal neuralgia. Neurosurgery 54: 973–982
Scrivani SJ, Keith DA, Mathews ES et al (1999) Percutaneous stereotactic differential radiofrequency thermal rhizotomy for the treatment of trigeminal neuralgia. J Oral Maxillofac Surg 57:104–111
Sweet WG (1986) The treatment of trigeminal neuralgia (tic douloureux). N Engl J Med 315:174–177
Taha JM, Tew JM Jr (1996) Comparison of surgical treatments for trigeminal neuralgia: reevaluation of radiofrequency rhizotomy. Neurosurgery 38:865–871
Xu SJ, Zhang WH, Chen T et al (2006) Neuronavigator-guided percutaneous radiofrequency thermocoagulation in the treatment of intractable trigeminal neuralgia. Chin Med J (Engl) 119:1528–1535
Yang Y, Shao Y, Wang H et al (2007) Neuronavigation-assisted percutaneous radiofrequency thermocoagulation therapy in trigeminal neuralgia. Clin J Pain 23:159–164

Epidural Injection Therapy

Chen CC, Luo CL, Wang SJ et al (1999) Colour Doppler imaging for diagnosis of intracranial hypotension. Lancet 354:826–829
Diener HC, Johansson U, Dodick DW (2010) Headache attributed to non-vascular intracranial disorder. Handb Clin Neurol 97:547–587
Gideon P, Thomsen C, Stahlberg F et al (1994) Cerebrospinal fluid production and dynamics in normal aging: a MRI phase-mapping study. Acta Neurol Scand 89:362–366
Huntoon MA, Watson JC (2007) Intracranial hypotension following motor vehicle accident: an overlooked cause of post-traumatic head and neck pain? Pain Pract 7: 47–52
Ishikawa S, Yokoyama M, Mizobuchi S et al (2007) Epidural blood patch therapy for chronic whiplash-associated disorder. Anesth Analg 105:809–814
Lay CM (2002) Low cerebrospinal fluid pressure headache. Curr Treat Options Neurol 4:357–363
Mokri B, Low PA (2003) Orthostatic headaches without CSF leak in postural tachycardia syndrome. Neurology 61:980–982
Rouaud T, Lallement F, Choui R et al (2009) Treatment of spontaneous intracranial hypotension by epidural saline infusion. Rev Neurol (Paris) 165:201–205
Savoiardo M, Armenise S, Spagnolo P et al (2006) Dural sinus thrombosis in spontaneous intracranial hypotension: hypotheses on possible mechanisms. J Neurol 253:1197–1202
Savoiardo M, Minati L, Farina L et al (2007) Spontaneous intracranial hypotension with deep brain swelling. Brain 130:1884–1893
Schaltenbrand G (1938) Neuere Anschauungen zur Pathophysiologie der Liquorzirkulation. Zentralbl Neurochir 3:290–299
Schwedt TJ, Dodick DW (2007) Spontaneous intracranial hypotension. Curr Pain Headache Rep 11:56–61
Takagi K, Bolke E, Peiper M et al (2007) Chronic headache after cranio-cervical trauma – hypothetical pathomechanism based upon neuroanatomical considerations. Eur J Med Res 12:249–254
Thomke F, Bredel-Geissler A, Mika-Gruttner A et al (1999) Spontaneous intracranial hypotension syndrome. Clinical, neuroradiological and cerebrospinal fluid findings. Nervenarzt 70:909–915 [German]
Tsai PH, Fuh JL, Lirng JF et al (2007) Heavily T2-weighted MR myelography in patients with spontaneous intracranial hypotension: a case-control study. Cephalalgia 27:929–934
Yuh EL, Dillon WP (2010) Intracranial hypotension and intracranial hypertension. Neuroimaging Clin N Am 20:597–617

CT-Guided Periradicular Therapy (PRT)

Blankenbaker D, De Smet A, Stanczak J et al (2005) Lumbar radiculopathy: treatment with selective lumbar nerve blocks – comparison of effectiveness of triamcinolone and betamethasone injectable suspensions. Radiology 237:738–741
Boos N, Lander P (1996) Clinical efficacy of imaging modalities in the diagnosis of low back pain disorders. Eur Spine J 5:2–22
Groenemeyer DHW, Seibel R (1989) Interventionelle Computertomographie. Ueberreuter Wissenschaft, Vienna/Berlin, pp 92–135 [German]
Karppinen J, Malmivaara A, Kurunlathi M et al (2001) Periradicular infiltration for sciatica – a randomized controlled trial. Spine 26:1059–1067
Lee K, Lin C, Hwang S et al (2005) Transforaminal periradicular infiltration guided by CT for unilateral sciatica – an outcome study. Clin Imaging 29:211–214
Link S, el-Khoury G, Guilord W (1998) Percutaneous lumbar sympatholysis. Radiol Clin North Am 36: 509–521
Macnab I (1971) Negative disc exploration. An analysis of the causes of nerve-root involvement in sixty-eight patients. J Bone Joint Surg Am 53(5):891–903
Narozny M, Zanetti M, Boos N (2001) Therapeutic efficacy of selective nerve root blocks in the treatment of lumbar radicular pain. Swiss Med Wkly 131: 75–80

Nygaard OP, Mellgren SI, Osterud B (1997) The inflammatory properties of contained and noncontained lumbar disc herniation. Spine 22:2484–2488
Ojala R, Vahala E, Karppinen J et al (2000) Nerve root infiltration of the first sacral root with MRI guidance. J Magn Reson Imaging 12:556–561
Olmarker K, Blomquist J, Strömberg J et al (1995) Inflammatogenic properties of nucleus pulposus. Spine 20:665–669
Peul W, Houwelingen H, Hout W et al (2007) Surgery versus prolonged conservative treatment for sciatica. N Engl J Med 356:2245–2256
Riew KD, Park JB, Cho YS et al (2006) Nerve root blocks in the treatment of lumbar radicular pain. A minimum five-year follow-up. J Bone Joint Surg Am 88: 1722–1725
Saal JA, Saal JS (1989) Nonoperative treatment of herniated lumbar intervertebral disc with radiculopathy. An outcome study. Spine 14:431–437
Schmidt G, Schmitz A, Borchardt D et al (2006) Effective dose of CT- and fluoroscopy-guided perineural/epidural injections of the lumbar spine: a comparative study. Cardiovasc Intervent Radiol 29:84–91
Sequeiros R, Ojala R, Klemola R et al (2002) MRI-guided periradicular nerve root infiltration therapy in low-field (0.23-T) MRI system using optical instrument tracking. Eur Radiol 12:1331–1337
Silbergleit R, Mehta B, Sanders W et al (2001) Imaging-guided injection techniques with fluoroscopy and CT for spinal pain management. Radiographics 21: 927–939
Sutter R, Pfirrmann CW, Zanetti M et al (2011) CT-guided cervical nerve root injections: comparing the immediate post-injection anesthetic-related effects of the transforaminal injection with a new indirect technique. Skeletal Radiol 40:1603–1608
Zennaro H, Dousset V, Viaud B et al (1998) Periganglionic foraminal steroid injections performed under CT-control. AJNR Am J Neuroradiol 19:349–352

Discography

Carragee EJ, Tanner CM, Yang B et al (1999) False-positive findings on lumbar discography. Reliability of subjective concordance assessment during provocative disc injection. Spine 24:2542–2547
Guyer RD, Ohnmeiss DD, Mason SL et al (1997) Complications of cervical discography: findings in a large series. J Spinal Disord 10:95–101
Milette PC, Fontaine S, Lepanto L et al (1995) Radiating pain to the lower extremities caused by lumbar disk rupture without spinal nerve root involvement. AJNR Am J Neuroradiol 16:1605–1615
Pobiel RS, Schellhas KP, Pollei SR et al (2006) Diskography: infectious complications from a series of 12,634 cases. AJNR Am J Neuroradiol 27: 1930–1932
Resnick DK, Malone DG, Ryken TC (2002) Guidelines for the use of discography for the diagnosis of painful degenerative lumbar disc disease. Neurosurg Focus 13:E12
Sachs BL, Vanharanta H, Spivey MA et al (1987) Dallas discogram description. A new classification of CT/discography in low-back disorders. Spine 12:287–294
Schellhas KP (2000) Diskography. Neuroimaging Clin N Am 10:579–596
Sequeiros RB, Klemola R, Ojala R et al (2003) Percutaneous MR-guided discography in a low-field system using optical instrument tracking: a feasibility study. J Magn Reson Imaging 17:214–219
Tomecek FJ, Anthony CS, Boxell C et al (2002) Discography interpretation and techniques in the lumbar spine. Neurosurg Focus 13:E13

Interventional Therapy of the Intervertebral Disc

Andersson GBJ (1999) Epidemiological features of chronic low-back pain. Lancet 354:581–585
Andreula CF, Simonetti L, de Santis F, Agati R, Ricci R, Leonardi M (2003) Minimally invasive Oxygen-Ozone therapy for lumbar disc herniation. AJNR Am J Neuroradiol 24:996–1000
Barendse GA, van Den Berg SG, Kessels AH et al (2001) Randomized controlled trial of percutaneous intradiscal radiofrequency thermocoagulation for chronic discogenic back pain. Spine 26:287–292
Bogduk N, Karasek M (2002) Two-year follow-up of a controlled trial of intradiscal electrothermal annuloplasty for chronic low back pain resulting from internal disc disruption. Spine J 2:343–350
Bontoux D, Alcalay M, Debiais F et al (1990) Treatment of lumbar disk hernia by intra-disk injection of chymopapain or triamcinolone hexacetonide. Comparative study of 80 cases. Rev Rhum Mal Osteoartic 57: 327–331
Boswell MV, Trescot AM et al (2007) Interventional techniques: evidence-based practical guidelines in the management of chronic spinal pain. Pain Physician 10:7–111
Bourgeois P, Benoist M, Palazzo E et al (1988) Multicenter randomized doubleblind study of triamcinolone hexacetonide versus chymopapain in the treatment of disc lumbosciatica. Initial results at 6 months. Rev Rhum Mal Osteoartic 55:767–769
Buttermann GR (2004) The effect of spinal steroid injections for degenerative disc disease. Spine J 4: 495–505
Cebrián Parra JL, Saez-Arenillas Martín A, Urda Martínez-Aedo AL, Soler Ivañez I, Agreda E, Lopez-Duran Stern L (2012) Management of infectious discitis. Outcome in one hundred and eight patients in a university hospital. Int Orthop 36: 239–244

Chou R, Loeser JD, Owens DK, Rosenquist RW, Atlas SJ, Baisden J, Carragee EJ, Grabois M, Murphy DR, Resnick DK, Stanos SP, Shaffer WO, Wall EM, American Pain Society Low Back Pain Guideline Panel (2009) Interventional therapies, surgery, and interdisciplinary rehabilitation for low back pain: an evidence-based clinical practice guideline from the American Pain Society. Spine (Phila Pa 1976) 34: 1066–1077

Choy DSJ, Ascher PW, Saddekni S (1992) Percutaneous laser disc decompressions: a new therapeutic modality. Spine 17:949–956

Eckel TS (2002) Intradiscal electrothermal therapy. In: Williams AL, Murtagh FR (eds) Handbook of diagnostic and therapeutic spine procedures. CV Mosby, St Louis, pp 229–244

Ercelen O, Bulutcu E, Oktenoglu T et al (2003) Radiofrequency lesioning using two different time modalities for the treatment of lumbar discogenic pain: a randomized trial. Spine 28:1922–1927

Erginousakis D, Filippiadis DK, Malagari A, Kostakos A, Brountzos E, Kelekis NL, Kelekis A (2011) Comparative prospective randomized study comparing conservative treatment and percutaneous disk decompression for treatment of intervertebral disk herniation. Radiology 260:487–493

Freeman BJ, Fraser RD, Cain CM et al (2005) A randomized, double-blind, controlled trial: intradiscal electrothermal therapy versus placebo for the treatment of chronic discogenic low back pain. Spine 30: 2369–2377

Gangi A, Guth S, Dietemann JL, Roy C (2001) Interventional musculoskeletal procedures. Radiographics 21:E1–e1

Gangi A, Dietemann JL, Ide C, Brunner P, Klinkert A, Warter JM (1996) Percutaneous laser disc decompression under CT and fluoroscopic guidance: indications, technique and clinical experience. Radiographics 16:89–96

Gasbarrini A, Boriani L, Salvadori C, Mobarec S, Kreshak J, Nanni C, Zamparini E, Alberghini M, Viale P, Albisinni U (2012) Biopsy for suspected spondylodiscitis. Eur Rev Med Pharmacol Sci 16(Suppl 2):26–34

Gibby W (2002) Automated percutaneous discectomy. In: Williams AL, Murtagh FR (eds) Handbook of diagnostic and therapeutic spine procedures. CV Mosby, St Louis, pp 203–225

Graham C (1975) Chemonucleolysis. A preliminary report on a double blind study comparing chemonucleolysis and intradiscal administration of hydrocortisone in the treatment of backache and sciatica. Orthop Clin North Am 6:259–263

Graham C (1976) Chemonucleolysis: a double blind study comparing chemonucleolysis with intra discal hydrocortisone: in the treatment of backache and sciatica. Clin Orthop 117:179–192

Kelekis AD, Somon T, Yilmaz H, Bize P, Brountzos EN, Lovblad K, Ruefenacht D, Martin JB (2005) Interventional spine procedures. Eur J Radiol 55: 362–383

Kelekis AD, Filippiadis DK, Martin JB, Brountzos E (2010) Standards of practice: quality assurance guidelines for percutaneous treatments of intervertebral discs. Cardiovasc Intervent Radiol 33:909–913

Khot A, Bowditch M, Powell J et al (2004) The use of intradiscal steroid therapy for lumbar spinal discogenic pain: a randomized controlled trial. Spine 29: 833–836

Manchikanti L, Singh V, Pampati V (2001) Evaluation of the relative contributions of various structures in chronic low back pain. Pain Physician 4:308–316

Ostelo RW, Deyo RA, Stratford P et al (2008) Interpreting change scores for pain and functional status in low back pain. Spine 33:90–94

Pauza KJ, Howell S, Dreyfuss P et al (2004) A randomized, placebo-controlled trial of intradiscal electrothermal therapy for the treatment of discogenic low back pain. Spine J 4:27–35

Schwarzer AC, April CN, Derby R (1995) The prevalence and clinical feature of internal disc disruption of patients with chronic low back pain. Spine 20: 1878–1883

Simmons JW, McMillin JN, Emery SF et al (1992) Intradiscal steroids. A prospective double-blind clinical trial. Spine 17(Suppl 6):S172–S175

Simopoulos TT, Kraemer JJ, Glazer P, Bajwa ZH (2008) Vertebral osteomyelitis: a potentially catastrophic outcome after lumbar epidural steroid injection. Pain Physician 11(5):693–697

Singh V, Derby R (2006) Percutaneous lumbar disc decompression. Pain Physician 9:139–146

Slipman CW, Bender FJ III, Menkin S, Garvan C, Salam A, Siegelman E (2006) PR_096: percutaneous lumbar disk decompression using the dekompressor: a pilot study. Arch Phys Med Rehabil 87:e21

Smuck M, Benny B, Han A, Levin J (2007) Epidural fibrosis following percutaneous disc decompression with coblation technology. Pain Physician 10:691–696

Theron J, Guimaraens L, Casasco A, Sola T, Cuellar H, Courtheoux P (2007) Percutaneous treatment of lumbar intervertebral disk hernias with radiopaque Gelified ethanol: a preliminary study. J Spinal Disord Tech 20:526–532

Muskulo-Skeletal Interventions

15

Philipp Bruners, Andreas H. Mahnken,
Kai E. Wilhelm, Sebastian Kos, Peter Messmer,
Deniz Bilecen, Augustinus L. Jacob,
Gabriele A. Krombach, and Oliver Wüsten

Contents

15.1 Radiofrequency Ablation of Benign Bone Tumors

Philipp Bruners and Andreas H. Mahnken

Radiofrequency (RF) ablation was shown to be an effective minimal invasive tool in the treatment of both malignant and benign bone lesions (Ruiz Santiago et al. 2011; Callstrom et al. 2002). Especially in the therapy of osteoid osteoma, image-guided RF ablation has emerged to be the gold standard. Osteoid osteoma is benign bone tumor which was first described by Jaffe in 1935 (Jaffe 1935). Histologically, it consists of a centrally located nidus composed of osteoblasts and osteoid which is surrounded by an area of reactive sclerosis and/or periosteal new bone formation. Prostaglandins which are produced by the tumor induce a chronic inflammatory reaction and vasodilatation which results in stimulation of unmyelinated nerve endings in the nidus causing pain. This leads to the clinical symptoms of this lesion with local pain often worsened during the night, which is typically relieved by aspirin or other related nonsteroidal anti-inflammatory drugs.

P. Bruners (✉)
Department of Diagnostic and Interventional Radiology, University Hospital, RWTH Aachen University, Pauwelsstrasse 30, D-52074 Aachen, Germany
e-mail: pbruners@ukaachen.de

A.H. Mahnken
Department of Diagnostic and Interventional Radiology, University Hospital, Marburg, Germany

Philipps University of Marburg, Marburg, Germany
e-mail: mahnken@med.uni-marburg.de

K.E. Wilhelm
Department of Radiology, University Hospital Bonn, Sigmund-Freud-Str. 25, D-53127 Bonn, Germany
e-mail: wilhelm@uni-bonn.de

S. Kos • P. Messmer • D. Bilecen • A.L. Jacob
Department of Interventional Radiology, University of Basel, Petersgraben 4, CH-4031 Basel, Switzerland

G.A. Krombach
Department of Radiology, University Hospital Gießen, Klinikstraße 33, D-35392 Gießen, Germany
e-mail: gabriele.krombach@radiol.med.uni-giessen.de

O. Wüsten
Radiologie im Liebig-Center, Bahnhofstraße 64, 35390 Gießen, Germany
e-mail: oliver.wuesten@radiologie-giessen.de

A.H. Mahnken et al. (eds.), *CT- and MR-Guided Interventions in Radiology*,
DOI 10.1007/978-3-642-33581-5_15,

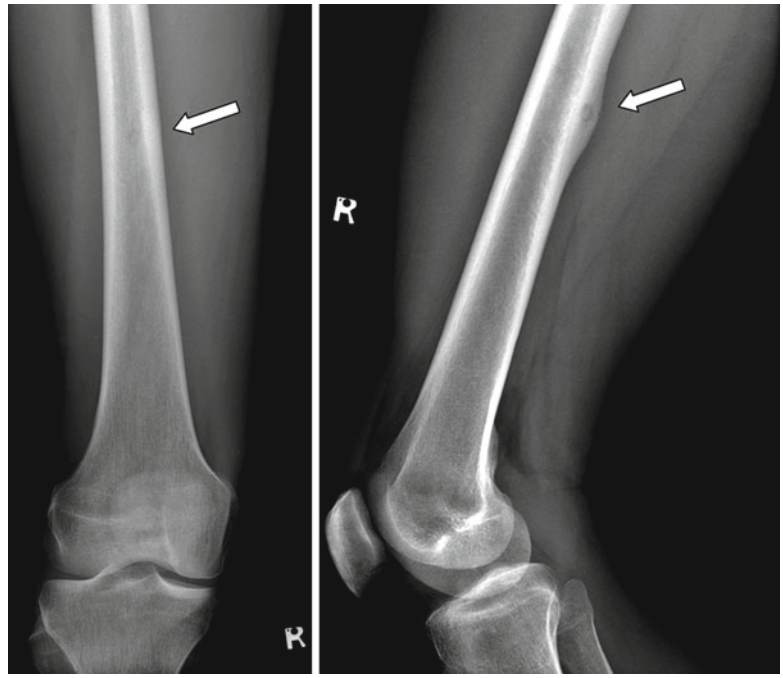

Fig. 15.1 Conventional x-ray of a 33-year-old male patient with pain in the right thigh. Thickening of the cortical bone with a round central radiolucent area in the femoral diaphysis is seen, corresponding to an osteoid osteoma

Osteoid osteomas occur more frequently in men than in women (2:1), and most patients, approximately 75 %, suffering from osteoid osteomas are between 5 and 25 years old. Most commonly, osteoid osteomas are found in the diaphysis of femur and tibia followed by humerus, radius, ulna, hand, and the vertebral spine. A malignant transformation of osteoid osteoma is not known.

The conventional x-ray typically shows a cortically located, sclerotic lesion with a central radiolucent area corresponding to the nidus (Fig. 15.1). In combination with the characteristic clinical symptoms, these findings usually lead to further cross-sectional imaging using computed tomography (CT) or magnetic resonance (MR) imaging. In MR imaging studies especially, the nonspecific edema of the surrounding bone marrow and collateral soft tissue alterations can be visualized which may result in a misleading aggressive appearance of the lesion, whereas the nidus is sometimes difficult to identify on MR imaging (Davies 2002). Native CT scans are more suitable to detect the central nidus and surrounding sclerotic bone (Fig. 15.2a).

Although the pain induced by osteoid osteomas often promptly reacts to anti-inflammatory drugs, a long-term conservative medical treatment may be unacceptable due to potentially severe side effects related to chronic use of nonsteroidal anti-inflammatory medication and sometimes refractory pain. Traditionally, osteoid osteomas have been treated using surgical resection or open curettage but because of the difficult intraoperative localization of the nidus, which needs to be completely removed, resection size sometimes is disproportional to the tumor size, necessitating the use of cortical bone matrix transfer or internal fixation (Marcove et al. 1991). Therefore, different minimally invasive techniques under image guidance have been developed to treat osteoid osteomas like drill trepanation with and without ethanol instillation, cryoablation, and laser photocoagulation (Sans et al. 1999; Adam et al. 1995; Skjedal et al. 2000; Gebauer et al. 2006). The most commonly used local ablation technique for the treatment of osteoid osteoma is radiofrequency (RF) ablation, which was introduced by Rosenthal in 1992 as an alternative minimal-invasive treatment (Rosenthal et al. 1992) and has evolved into a clinical routine procedure. Therefore, the following sections focus on the treatment of osteoid osteoma using RF-energy.

Besides osteoid osteoma, other benign bone pathologies may require a local treatment due to severe clinical symptoms, for example, pain- or

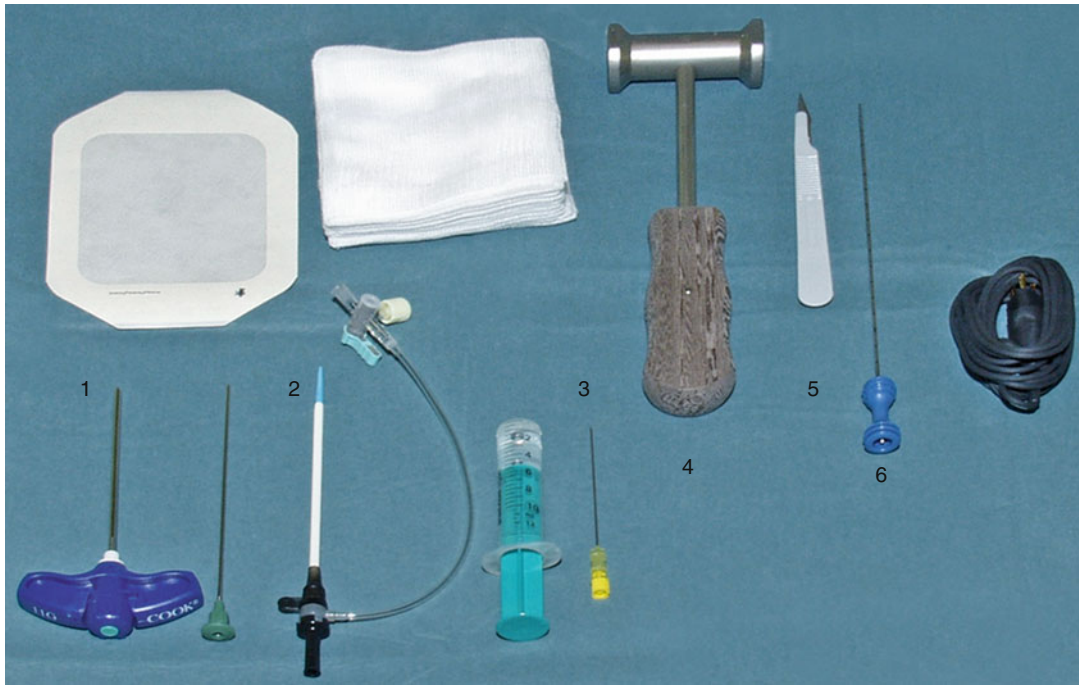

Fig. 15.2 Instruments recommended for CT-guided RF ablation of osteoid osteomas: *1*. 11-G hollow drill. *2*. Sterile angiographic introducer sheath. *3*. Spinal needle for injection of long-acting local anesthetic agent. *4*. Sterile hammer. *5*. Single-use scalpel. *6*. Needle-shaped RF probe

pressure-associated cortical bone atrophy. In cases large benign bone lesions carry the danger of local fracture, the combination of image-guided RF ablation and osteoplasty may be a helpful option. To date, there are only few case reports or small case series reporting about the successful treatment of benign bone lesions other than osteoid osteoma, including osteoblastoma, osteochondroma, enchondroma, hemangioma, eosinophilic granuloma, or giant cell tumors (Corby et al. 2008; Erickson et al. 2001; Ramnath et al. 2002; Rybak et al. 2009; Ruiz Santiago et al. 2011; Tins et al. 2006).

15.1.1 Indications

Minimally invasive local ablation of an osteoid osteoma is indicated if:

1. Typical clinical symptoms, particularly nocturnal pain, are present
2. Characteristic bone lesion with a clearly identified nidus is detected

Indications for the ablative therapy of other benign bone lesions cover local pain or risk of progressive weakening of the bone due to expansive growth.

There are no absolute contraindications for local ablation of benign bone tumors except for an uncorrectable coagulopathy or an active inflammation.

Relative contraindications for the local ablative therapy of osteoid osteoma include:

1. Impossibility to place the ablative device within the nidus at least 1 cm away from major nerves
2. Repeated (>3) ineffective local ablations

In these cases, surgical therapy should be considered if long-term medical treatment is not acceptable.

In all other patients suffering from a benign tumor or tumor-like lesion, decision for local RF ablation should be based on an interdisciplinary consensus with a musculoskeletal surgeon after discussion of alternative treatment options.

The use of RF ablation in patients with medical implants like cardiac pacemakers may lead to dysfunction, although this has not yet been described as a complication in the literature. On the contrary, only recently RF ablation in the presence of pacemakers has been shown to be safe (Skonieczki et al. 2011).

15.1.2 Material

As mentioned above, there are several local ablative therapies for the minimal-invasive treatment of osteoid osteoma. Most techniques use thermal energy either high (RF ablation, LITT) or low temperature (cryoablation) to destroy the nidus, and all of these therapies require the image-guided placement of an ablation probe. Because RF ablation is the most commonly used local ablative therapy, the following text describes this technique in detail. Different RF systems have been used for the successful ablation of osteoid osteomas commonly in combination with needle-shape RF probes. In most published studies, RF ablation of osteoid osteomas is performed with monopolar RF systems which need large grounding pads to draw current back to the radiofrequency system. Successful experience using a bipolar RF ablation device which obviates the need for a neutral electrode and thereby reduces the risk of skin burns at the site of the grounding pads has also been reported (Mahnken et al. 2006). With regard to the ablation protocol (generator output, energy delivery, time), the recommendations of the vendor for the used RF system should be carefully followed. Actually, there is some evidence that the use of a high-energy delivery technique leads to increased post-procedural pain and a prolonged interval to symptom resolution (Cantwell et al. 2006). Besides the RF generator, -probe, and grounding pads, also a bone drill is needed to penetrate the sclerotic cortical bone surrounding the nidus and thereby gain access for the placement of the RF probe. Typically, an 11–13-G hollow drill is used which allows performing biopsy of the bone lesion for histological confirmation of the diagnosis (Fig. 15.2). The use of a sterile angiographic introducer sheath is recommended to secure the puncture tract in the soft tissue. This technique provides an additional insulation of the RF probe and therefore helps to avoid skin burns, which are the most common complication of RF ablation in osteoid osteoma. A sterile single-use scalpel is needed for a stitch incision at the skin entry point. Furthermore, sterile drape sheets for the puncture site and disinfectant are required. Radiopaque markers, for example, a grid made of parallel catheter pieces, which are fixed on the patient's skin, can be used as references for the planning of the access path. A small tube filled with formalin is used to store the drilled bone specimen before histological analysis. A long-acting local anesthetic agent, for example, bupivacaine 0.25 %, can be applied into the nidus and along puncture tract after RF ablation for post-interventional pain management.

Treating larger benign bone lesions with RF ablation like, for example, epiphyseal chondroblastoma, a subsequent osteoplasty may be performed to stabilize the ablated area. In these cases, an additional cementoplasty needle and the equipment for the preparation of the cement are needed. Furthermore, some authors use an additional mobile C-arm to monitor cement injection under fluoroscopy. Alternatively, CT fluoroscopy may be used which provides real-time 3D information of cement distribution.

15.1.3 Technique

15.1.3.1 Patient Preparation

Informed consent should be obtained from the patient at least 24 h prior to the intervention after discussion of alternative treatment options and possible complications of the local ablation procedure. This should include general complications related to the puncture as bleeding, nerve injury, or infection but also statements about a possible reintervention in case of recurrent symptoms and a possible damage of articular cartilage for the treatment of bone lesions which are located near joints. The treatment of large tumors or tumor-like lesions may go along with a risk for a pathological fracture, especially when the cortical bone is thinned due to expansive growth patterns. Furthermore, patients should be advised that local pain may temporarily increase after the intervention. Because osteoid osteomas are often found in children and young underaged patients, informed consent of the patient's parents might be required.

In general, it is possible to perform local ablation therapy with spinal or general anesthesia.

Especially for the treatment of children, who might find the intervention frightening, the authors prefer general anesthesia which provides optimal analgesia and compliance. Instead of an endotracheal tube, a laryngeal airway mask can be used for anesthesia. An exception is the local ablation of vertebral osteoid osteomas where analgesic sedation should be considered for in order to be able to immediately recognize neural injury.

For the recovery of platelet function, pain medication with aspirin should be stopped one week prior to the intervention. The day before the intervention, full blood count and coagulation test should be obtained to identify inflammation or hemorrhagic diathesis. Due to the fact that most patients are young, a conventional chest radiograph is not routinely obtained.

A possible prophylactic antibiotic treatment would be the intravenous administration of 500 mg cefazolin during the procedure, followed by two oral doses after the intervention (Peyser et al. 2007). Alternatively, a single dose of clindamycin (600 mg) can be administered intravenously.

15.1.3.2 Procedure

In general, CT, MR imaging, and conventional x-ray fluoroscopy can be used for image-guided placement of the biopsy drill and the ablation probe, respectively. Due to the high spatial resolution and the mostly clear depiction of the nidus and the ablation probe, the authors prefer CT as modality for image guidance (Fig. 15.3). MR-guided local ablation requires the use of special MR-compatible tools.

In order to avoid pressure sites or damage of peripheral nerves during the procedure, the patient under anesthesia should be positioned carefully on the CT table. Most patients with limb lesions can be treated in prone position. If necessary, the limb can be internally or externally rotated and fixed with tape in order to achieve optimal access. Spinal lesions often require the placement of the patient in supine position to achieve a dorsal access to the tumor. After acquisition of a thin section (collimation ≤3 mm, slice thickness 1–3 mm), unenhanced spiral scan of the region of interest, the access path for the placement of the ablation probe is planned using the implemented software of the CT scanner. If an in-plane access to the target lesion, which should be preferred, is not feasible, the reconstruction of multiplanar reformations may be helpful. RF probe placement should be performed in a way that the risk for thermal damage of the skin or adjacent neural and vascular structures is avoided. Therefore, a safety distance of 1 cm should be kept between RF probe and critical structures, especially nerves. A contralateral access to the target lesion passing through the normal cortex may be chosen if vulnerable structures omit the direct path. Osteoid osteomas being located near joints should be ablated using an extraarticular access in order to reduce the risk of infection and damage of the articular cartilage. An access path perpendicular to the bone surface avoids slipping of the drill and the RF probe, respectively. Once the skin entry plane has been defined, the CT table is moved to the corresponding slice position and radiopaque markers are fixed on the skin around the puncture site using the light shield of the CT scanner as reference (Fig. 15.4). Thereafter, another unenhanced CT scan of the puncture site is performed, and the skin entry point is defined using the radiopaque

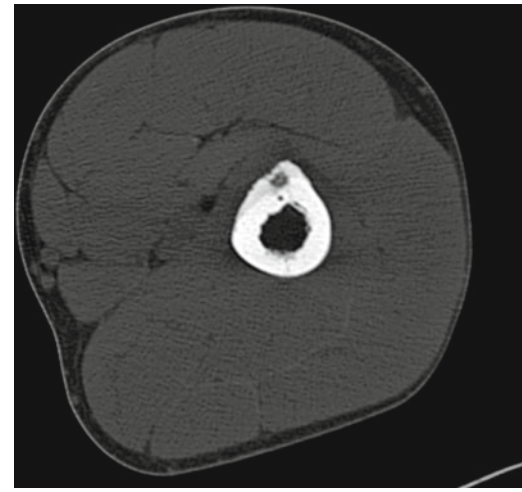

Fig. 15.3 CT-guided placement of an RF probe in a patient suffering from osteoid osteoma of the femur. Corresponding to conventional radiography, the unenhanced CT scan reveals the thickening of the cortical bone with the centrally located nidus

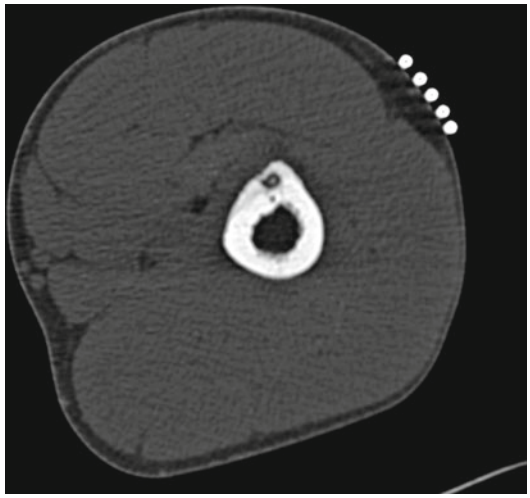

Fig. 15.4 For the planning of the access path and definition of the skin entry point, a grid made of radiopaque material is fixed on the skin

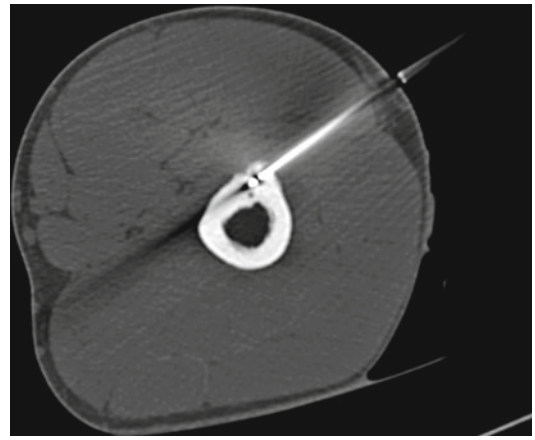

Fig. 15.5 After the skin entry point has been marked with a water-resistant pen, the grid was removed. After a specimen has been obtained using the hollow drill, the RF probe was placed centrally in the nidus

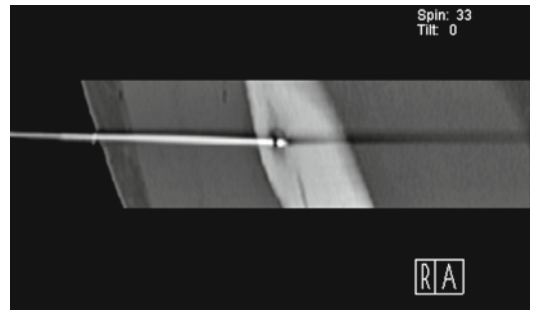

Fig. 15.6 The multiplanar reformation along the shaft of the RF probe shows the placement within the center of the nidus

markers as landmarks. To optimally meet the lesion and to achieve a central drill hole in the relatively small lesion, a slice thickness of 3 mm or less is recommended for the interventional CT imaging. After the skin entry point was marked with a water-resistant pen, radiopaque markers are removed and the skin is disinfected. Afterward, the puncture site is draped in sterile fashion. First, a stitch incision at the marked skin entry point is performed using a sterile single-use scalpel. In order to secure the puncture channel and to protect the surrounding soft tissue, the hollow drill can be put through an appropriately sized sterile introducer sheath. Then, the hollow drill is placed into the target lesion along the planned access path. Depending on the length of the access path, control scans should be performed to verify the position of the drill. Thereafter, the nidus of the osteoid osteoma is drilled out, and the obtained bone specimen can be used for histological analysis (Akhlaghpoor et al. 2010a). Therefore, it is put into a small tube containing formalin. The hollow drill is removed, whereas the sheath is left in place in order to secure the puncture tract. After that the RF probe is placed through the sheath into the target lesion. Another control scan should be obtained to verify the correct placement of the RF probe in the central area of the nidus with a maximum distance of 5 mm to edge of the nidus (Figs. 15.5 and 15.6). The RF ablation of lesions larger than 1 cm requires more than one probe position due to the limited size of the ablation zone (Pinto et al. 2002). Therefore, a second access tract may be necessary in order to create overlapping ablation zones which cover the entire nidus. Duration, output, and total energy deposition strongly depend on the used RF system and the vendor's recommendations. For commonly used monopolar RF systems, a tip temperature of 90 °C is maintained for 4–6 min. A second ablation cycle is recommended by some authors after rotation of the RF probe in order to improve heat conduction by removing carbonized

tissue from the RF probe (Mahnken et al. 2006). The injection of small volumes of 0.9 % saline solution into the ablation site can also be used to reduce impedance and avoid tissue carbonization especially in cortically located lesions (Rimondi et al. 2005). As heated saline may lead to thermal injuries along the puncture tracts, this approach should be limited to lesions with otherwise insufficient energy coupling. After the RF ablation procedure, the RF probe is removed and a long-acting local anesthetic agent can be applied into the lesion through the sheath to reduce post-interventional pain. Then, the introducer sheath is removed, and an adhesive sterile bandage is attached after the wound at the skin entry site is closed with elastic skin closures. Usually, sutures are not necessary. In our experience, between 90 and 120 min are required to perform the intervention including general anesthesia.

15.1.3.3 Post-interventional Management

Post-interventional imaging is not mandatory, although the induced thermal necrosis can be visualized using contrast-enhanced MR imaging (Aschoff et al. 2002). Usually, patients can be discharged from the hospital within 24 h after the ablation procedure so it is even possible to perform RF ablation of osteoid osteomas on an outpatient basis. Although there is no proven evidence, patients with osteoid osteomas in weight-bearing bones should avoid strenuous activities including sports for an interval of 2 weeks. After this period, a follow-up clinical assessment is helpful, especially to identify patients with persistent or recurrent pain. In these patients, follow-up MR imaging is recommended to identify contrast enhancement and therefore viable parts of the lesion. In these patients, up to two repeated interventions are recommended. Local ablation can be defined as successful if patients are free of pain without taking any pain medication. If follow-up imaging studies are performed, although this is not routinely recommended, a partial or complete replacement of the nidus by sclerotic bone can be expected over 2–27 months, although only less or no changes of the ablation site may be found (Pinto et al. 2002).

15.1.4 Results

During the last few years, multiple clinical studies investigated the benefit of RF ablation of osteoid osteomas showing a total success rate of ~95 % (Table 15.1). Cantwell et al. reported similar success rates for different surgical treatments varying between 88 and 100 % (Cantwell et al. 2004). Nevertheless, surgical treatment of osteoid osteomas using curettage or resection is associated with a more extensive bone and soft tissue trauma which is reflected by higher complication rates compared to RF ablation (Cantwell et al. 2004). The internal fixation rate after en bloc resection can reach up to 56 % (Cantwell et al. 2004). Using LITT as image-guided therapy for the treatment of osteoid osteoma, primary success rates range between 80 and 98 % (Gangi et al. 2007; Sequeiros et al. 2003; Witt et al. 2000).

In a retrospective analysis of a case series including 110 patients, Vanderschueren et al. investigated factors for increased risk of unsuccessful thermal coagulation (Vanderschueren et al. 2004). Besides advanced age, an increased number of RF probe positions during the ablation procedure were associated with a decreased risk of treatment failure. No evidence was found for an association between lesion location and increased risk for treatment failure.

In a case series of patients suffering from benign bone lesions including osteoblastoma ($n=2$), chondroblastoma ($n=2$), hemangioma ($n=1$), eosinophilic granuloma ($n=1$), and giant cell tumor ($n=1$), Santiago et al. reported successful treatment using RF ablation with/without additional cementation as reflected by resolution or significant reduction of pain assessed using a visual analogue scale (Table 15.2). Follow-up in this recent study was one year (Ruiz Santiago et al. 2011). In addition, Petsas and Erickson presented case series including two and three cases of chondroblastomas which were successfully treated with RF ablation in some cases in combination with bone grafting (Erickson et al. 2001; Petsas et al. 2007). Rybak et al. reported about a case series including 17 patients suffering from chondroblastomas. All patients were treated with RF ablation, and an initial pain relief was achieved

Table 15.1 Summary of percutaneous RF ablation in osteoid osteoma

Author	Patients/procedures	Primary success	Reablation/success	Total success	Complications	Follow-up (month)
Barei et al. (2000)	11/11	10/11 (91 %)	–	10/11 (91 %)	–	18.7
Lindner et al. (2001)	58/61	55/58 (95 %)	3/3	58/58 (100 %)	Skin burn ($n=1$)	23 (4–41)
Woertler et al. (2001)	47/50	44/47 (94 %)	3/3	47/47 (100 %)	–	22 (8–39)
Vanderschueren et al. (2002)	97/121	74/97 (76 %)	15/23	89/97 (92 %)	Skin burn ($n=1$); probe defect ($n=1$)	41 (5–81)
Ghanem et al. (2003)	23/24	21/23 (91 %)	1/1	22/23 (96 %)	Calf atrophy ($n=1$); asymmetry of joint mobility ($n=2$)	42 (13–62)
Venbrux et al. (2003)	9/13	5/9 (56 %)	3/4	8/9 (89 %)	Skin burn ($n=1$); transient paresthesia ($n=1$)	10,3 (1–26)
Rosenthal et al. (2003)	263/271	107/117 (91 %)	–	107/117 (91 %)	Cellulitis ($n=1$); vasomotor instability ($n=1$)	24
Cioni et al. (2004)	38/44	30/38 (79 %)	5/6	35/38 (92 %)	Skin burn ($n=1$); osteomyelitis ($n=1$)	35.5 (12–66)
Mastrantuono et al. (2005)	21/21	21/21 (100 %)	–	21/21 (100 %)	–	11.1 (0–24)
Martel et al. (2005)	38/39	37/38 (94 %)	1/1	38/38 (100 %)	Skin burn ($n=1$); tendinitis ($n=1$)	3–24
Rimondi et al. (2005)	97/114	82/97 (85 %)	13/15	95/97 (98 %)	Skin burn ($n=1$); phlebitis ($n=1$)	3–12
Mahnken et al. (2006)	14/16	12/14 (86 %)	1/1	13/14 (93 %)	–	15.1 (5–31)
Cantwell et al. (2006)	11/11	11/11 (100 %)	–	11/11 (100 %)	Muscle ablation ($n=1$)	14.4 (6–27)
Soong et al. (2006)	25/25	23/25 (92 %)	–	23/25 (92 %)	–	42 (12–136)
Kjar et al. (2006)	24/32	16/24 (67 %)	7/7	23/24 (96 %)	Broken drill ($n=1$)	26 (2–56)
Yip et al. (2006)	6/7	5/6 (83 %)	1/1	6/6 (100 %)	Skin burn ($n=1$)	40 (18–65)
Peyser et al. (2007)	51/52	50/51 (98 %)	1/1	51/51 (100 %)	Wound infection ($n=1$)	24 (5–91)
Donkol et al. (2008)	23/24	18/23 (78 %)	1/1	19/23 (83 %)	Wound infection ($n=1$); skin burn ($n=2$); hyperthermia ($n=2$)	30 (13–49)
Martel et al. (2005)	10/12	8/10 (80 %)	2/2	10/10 (100 %)	–	20 (6–24)
Vanderschueren et al. (2009)	24/28	19/24 (79 %)	4/4	23/24 (96 %)	–	72 (9–142)
Mylona et al. (2010)	23/25	21/23 (91 %)	2/2	23/23 (100 %)	–	12
Akhlaghpoor et al. (2010a, b)	21/21	21/21 (100 %)	–	–	Skin burn ($n=1$)	28 (12–37)
Hoffmann et al. (2010)	39/41	35/39 (92 %)	3/3	38/39 (97 %)	Broken drill ($n=1$); hematoma ($n=1$); infection ($n=1$); pain ($n=1$)	31 (1–61)
Mahnken et al. (2011)	17/20	14/17 (83 %)	3/3	17/17 (100 %)	–	30 (4–47)
Schmidt et al. (2011)	23/23	23/23 (100 %)	–	–	Broken drill ($n=2$)	76 (18–120)
Neumann et al. (2012)	33/34	32/33 (97 %)	1/1	33/33 (100 %)	Not reported	92 (60–121)
Omlor et al. (2012)	40/41	39/40 (98 %)	1/1	40/40 (100 %)	–	35 (8–74)
Total	*1,086/1,181*	*833/940 (89 %)*	*71/83 (86 %)*	*904/940 (96 %)*	*(n = 32)*	–

Table 15.2 Summary of percutaneous RF ablation in benign bone tumors other than osteoid osteoma

Author	Patients	Tumor	Success	Complications	Follow-up (months)
Erickson et al. (2001)	3	Chondroblastoma	3/3 (100 %)	None	36 (24–48)
Tins et al. (2006)	4	Chondroblastoma	4/4 (100 %)	Collapse of the tibial plateau; repeat recurrence; cartilage defects in the medial tibiofemoral joint	18.5 (12–22)
Petsas et al. (2007)	2	Chondroblastoma	2/2 (100 %)	None	12; 12
Christie-Large et al. (2008)	4	Chondroblastoma	4/4 (100 %)	Persistent local discomfort	12.25 (5–18)
Rybak et al. (2009)	17; three patients lost to follow-up	Chondroblastoma	12/14 (86 %)	Collapse of the articular surface of the tibia plateau; recurrent pain	41.3 (4–134)
Corby et al. (2008)	2	Eosinophilic Granuloma	2/2 (100 %)	None	11; 12
Ramnath et al. (2002)	2	Intracortical chondroma	1/2 (50 %)	Recurrence of pain after 6 months followed by resection	6 (recurrence); 24

in all cases (Rybak et al. 2009). Three patients were lost to follow-up. One local recurrence was histologically observed in one patient that had to be treated surgically due to collapse of the articular surface of the tibial head after RF ablation. A collapse of the tibial plateau following RFA of a chondroblastoma in the tibial head was also reported by Tins et al. who treated for patient with chondroblastoma using a multitined electrode (Tins et al. 2006). Corby et al. successfully treated two patients with eosinophilic granuloma using RFA (Corby et al. 2008).

15.1.5 Complications

In general, image-guided RF ablation of osteoid osteomas is a safe minimally invasive treatment associated with only few complications as described above. Nevertheless, potential complications may occur due to the passage of the RF probe and the hollow drill, respectively, including damage of neural and vascular structures or infection as it is known from other image-guided interventions.

Treatment-related complications were found in 25/700 cases reported in the literature of which skin burns were the most common ones (Table 15.1). Donkol and coworkers reported a slightly higher complication rate in children treated with RF ablation compared to adult patients (Donkol et al. 2008). In a case series of 23 patients, they described skin burns in two patients: a wound infection in one patient and generalized hyperthermia in another two patients. They stated that this finding might be due to the low body weight of the children resulting in higher applied energy per kilogram body weight.

Damage of neural structures can be avoided by the careful choice of an appropriate access path with at least 1 cm distance between neural structures and the active tip of the RF probe. More common procedure-related complications of RF ablation are skin burns which typically occur in patients with osteoid osteoma in superficially located bones due to contact of uninsulated parts of the RF probe to the skin (Cioni et al. 2004). A severe skin burn could also lead to a skin fistula, requiring surgical debridement or homologous skin transplant.

To minimize the risk of this complication, the insulation of the RF probe should be visually checked before probe placement. The use of an additional introducer sheath as described above helps to avoid skin burns at the entry point. Another typical site for skin burns is the grounding

pads, especially if high energy protocols are used.

Especially in large lesions being located near the articular surface, attention should be paid to potential reduced stability of the bone. In these cases, an additional cementoplasty may provide a helpful adjunct to the ablation procedure.

Appraisal

In summary, treatment local ablation of osteoid osteoma is a safe and effective minimal-invasive treatment modality. Compared to the surgical therapy, lower complication rates are described at comparable success rates. Furthermore, due to its minimal-invasive character, convalescence is quick after local ablation which leads to short hospitalization. Because stability of the treated bone is not essentially altered, no internal fixation or cast is needed and therefore patients can quickly return to normal daily activities including sports. In addition, with regard to the cost-effectiveness, RF ablation is beneficial when compared to surgical therapy (Rosenthal et al. 1998; Lindner et al. 1997). Therefore, percutaneous RF ablation nowadays has to be considered the method of choice for first- and second-line treatment of osteoid osteoma.

The treatment of other benign bone lesions can be indicated if they cause severe local symptoms. In these cases, image-guided RF ablation may represent a viable alternative to surgical treatment and can be combined with cementoplasty if larger lesions have to be treated.

Key Points

- Indication: Patients with typical symptoms of an osteoid osteoma and a clearly identified nidus in imaging studies
- Contraindications: Major neurovascular structures with less than 1 cm distance to the lesion intended to treat; repeated ($n > 3$) unsuccessful local ablation procedures.
- Needle placement: Careful RF probe placement in the central area of the nidus.
- Ablation technique: Multiple ablation-probe positions if nidus larger than 1 cm.
- Complications: ~2.6 % including skin burns, damage of neural and vascular structures adjacent to ablation zone, and wound infection.
- Total success rate: ~95 % (RF ablation); ablation of recurrence possible.
- RF ablation of other benign bone tumors is feasible but should be based on a multidisciplinary consensus.
- Treatment of larger lesions like chondroblastomas can be combined with image-guided cementoplasty especially if the lesion is located in a weight-bearing area.

15.2 Vertebroplasty, Osteoplasty, and Sacroplasty

Kai E. Wilhelm

15.2.1 Introduction

Percutaneous vertebroplasty (PV) using PMMA (polymethylmethacrylate) was first described in 1987 by Gallibert and Deramond for treating vertebral body instability in patients with aggressive forms of vertebral hemangioma (Galibert et al. 1987). Other types of painful osteolytic bone lesions, such as osteoporotic vertebral fractures and vertebral metastases, soon became more important in numbers (Weill et al. 1996; Deramond et al. 1998). Within the last few years, this technique has become widely accepted, and it was proposed for osteolytic bone lesions to regions difficult to approach surgically such as the pelvis and sacrum (Wetzel et al. 2002; Weill et al. 1998). Nowadays, there are different

cement augmentation procedures (vertebroplasty, balloon kyphoplasty, and shield kyphoplasty) performed via transpedicular approach either uni- or bipedicular (Bornemann et al. 2012; Shah 2012). Nevertheless, the recent standard procedure of central vertebral augmentation consists in a bipedicular approach to the vertebral body (Wetzel and Wilhelm 2006, Endres and Badura 2012). The rapidity of analgesia and resulting stability have conferred an important role upon osteoplasty, especially in palliative tumor treatment for patients with a shortened expected life span (Wetzel and Wilhelm 2006). Moreover, the combined treatment of spinal metastases with image-guided radiofrequency (RF) ablation and percutaneous cement injection has been shown to be a safe modality in the therapy of non-resectable tumors of spine (Grönemeyer et al. 2002; Georgy and Wong 2007; Toyota et al. 2005; Wilhelm 2009). Concerning pain reduction, the combination of thermal ablation and vertebroplasty shows high success rates of up to 100 % (Toyota et al. 2005).

15.2.2 Indications

The decision to perform PV, osteoplasty, or sacroplasty should be made as a multidisciplinary approach. Patient evaluation should consider all available clinical information, and clinical examination should identify the focal pain that correlates to the lesion considered. The patient's pain should be severe, altering activities of daily living or requiring substantial use of analgesics. This pain should be documented with measurement instruments such as a visual analog scale (VAS) and a quality-of-life questionnaire before PV and during follow-up (Mathis 2006; Helmberger et al. 2003).

The principal indications are:

- Painful osteoporotic vertebral compression fracture refractory to medical therapy
- Painful sacral insufficiency fracture refractory to medical therapy
- Painful vertebral fracture or relevant osteolysis with impending fracture related to benign or malignant tumor, such as hemangioma, myeloma, or metastasis
- Painful sacral fracture caused by osteolysis of a malignant tumor or metastasis refractory to radiation therapy

By now, osteoporotic compression fractures followed by osteolytic metastases represent the most frequent indications for vertebroplasty and osteoplasty. In addition, sacral insufficiency fractures that do not adequately respond to conservative therapy become a more frequent indication. The aim of cement injection is the consolidation of fractured or fragile vertebrae and pain treatment. The analgesic effect usually occurs within 24 h and permits the reduction of major analgesic agents in most cases. Additionally, vertebral stabilization due to the consolidation effect decreases the risk of fracture and shortens patient's immobilization period.

There are several absolute and relative contraindications to cement injection that need to be considered when PV is planned.

15.2.2.1 Absolute Contraindications

Asymptomatic stable fracture:

- Patients clearly improving from pain treatment
- Prophylaxis in osteopenic patients with no evidence of acute fracture
- Osteomyelitis of target vertebra/bone
- Acute traumatic fracture or non-osteoporotic vertebra
- Uncorrectable coagulopathy or hemorrhagic diathesis
- Allergy to any component required for the procedure

15.2.2.2 Relative Contraindications

- Severe vertebral body collapse (vertebra plana)
- Stable fracture without pain and known to be more than 2 years old
- Treatment of more than three levels performed at one time

Further relative contraindications in which PV may be indicated in combination with surgical spinal decompression procedure include:

- Radicular pain or radiculopathy and spinal compression significantly in excess of vertebral pain
- Rupture of the posterior wall, retropulsion of fracture fragments causing significant spinal canal compromise
- Tumor extension into the epidural space with severe spinal canal obstruction

Fig. 15.7 Combined CT and mobile C-arm fluoroscopy setup for percutaneous vertebroplasty: CT guidance is used to choose puncture site and for needle placement, while cement injection is performed under fluoroscopy control. This arrangement is preferred in the treatment of cervical or high thoracic vertebrae and sacroplasty where fluoroscopy alone is inadequate to visualize critical structures

15.2.3 Materials and Techniques

15.2.3.1 Imaging Guidance

Computed tomography (CT) is the established guidance technique for bone biopsies and collecting samples for histological evaluation. Since the first PV procedure, fluoroscopy has been the preferred method of imaging guidance for performing PV (Wetzel and Wilhelm 2006). Rotation C-arm fluoroscopy (C-arm CT) allows real-time visualization for needle placement and cement injection and permits rapid alteration between imaging planes without complex equipment or patient movement. However, CT guidance is especially valuable for osteoplasty and in deep-seated lesions and lesions that lie adjacent to vital structures. Although contrast resolution with CT is superior to that with fluoroscopy, the CT method does not include the ability to monitor cannula introduction, and it is certainly not optimal for monitoring the injection of cement, although CT fluoroscopy holds the potential to overcome these limitations. Therefore, the concept of using a combination of CT and single-plane C-arm fluoroscopy for PV is frequently used (Fig. 15.7) (Gangi et al. 1994). With the introduction of flat-panel detectors, it has also become possible to acquire CT-like images via a rotational C-arm fluoroscopy system in the angio suite. The feasibility of obtaining volumetric images immediately after or even during vertebroplasty procedures in the angio suite is clearly the key advantage over combined CT and single-plane C-arm fluoroscopy settings (Hodek-Wuerz et al. 2006). In addition, the use of flat-panel angiography systems provides the immediate possibility to perform cross-sectional imaging without any changing of patients position, resulting in an accelerated operational and organizational flow of bone augmentation procedures (Fig. 15.8) (Wilhelm and Babic 2006).

Magnetic resonance (MR) guidance for vertebroplasty is only at its beginning and is rarely used. Nevertheless, pre-interventional obtained MR images are very helpful to detect vertebral body bone marrow edema to reveal acute vertebral fracture in osteoporosis (Tanigawa et al. 2006) and to detect exact tumor expansion and presence of multiple spinal lesions in patients with known cancer and back pain related to spinal metastases (Voormolen et al. 2006; Koh et al. 2007). Therefore, pre-interventional MR imaging

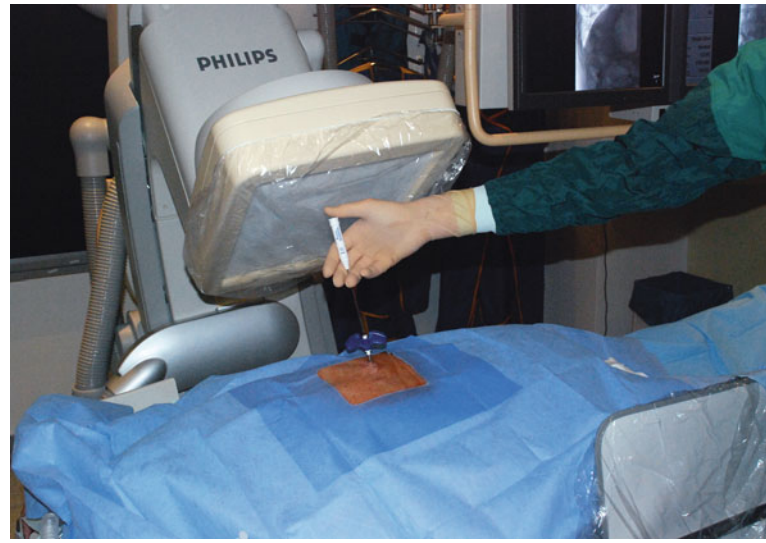

Fig. 15.8 Flat-panel detector angiography setup for vertebroplasty. The picture shows image-guided RF ablation prior to PV using a transpedicular access. Volumetric images can be obtained immediately after or even during fluoroscopically controlled intervention in the angio suite. Therefore, acquisition of CT-like images acquired by a rotational c-arm system (C-arm CT) is possible

should be available in all patients to assess vertebral fracture, the degree of collapse, osteolysis, extension of tumor into the epidural space, and potential compression of the neural tissue.

15.2.3.2 Informed Consent

Written permission for the procedure is recommended following patients instruction about potential risks and complications of the procedure. The clinical history and findings, including the indication for PV, must be reviewed and recorded in the patient's medical record (Mathis 2006; Helmberger et al. 2003). The potential need for immediate surgical intervention should be discussed. Additionally, the probability that the procedure may not result in significant pain relief should also be noted.

15.2.3.3 Procedure

Several excellent detailed technical descriptions of the technique of PV have been published (Mathis 2006). PV as well as any other cement injection procedure can be performed under local or general anesthesia. The choice of technique depends on the patient's general health status and the target region.

Using local anesthesia, the skin, subcutaneous tissue along the expected needle tract, and especially the periosteal tissue at the target side must be infiltrated completely. Once this is carried out, the patient will tolerate the procedure without further i.v. sedation. However, general anesthesia may be necessary for patients with extreme pain and those who cannot tolerate the position necessary for the procedure or those who have problems with ventilation lying in prone position.

Most PV procedures are performed at the lumbar and lower thoracic spine levels following standard access routes (Fig. 15.9). For lumbar, thoracic, and dorsal levels such as sacroplasty, the patient is positioned in prone position. For bone access, an 11-Gauge needle is placed using a transpedicular approach (Fig 15.10). Penetration of the medial border of the pedicle must be avoided to prevent nerve root or spinal canal injury. In cases of small pedicels or intended unilateral access, a parapedicular respectively posterolateral approach is feasible (Fig. 15.11) (Wetzel and Wilhelm 2006).

In AP projection, respectively, under CT guidance (Fig. 15.12), CT fluoroscopy, or MR guidance (Fig. 15.13), the needle is directed to the vertebral pedicle and entered through the cortical bone into the pedicle. Subsequently, alternating from AP in lateral fluoroscopic projection (or under CT or MRI guidance), the needle is pushed stepwise forward until the tip of the needle crosses the posterior wall of the vertebral body. Consecutively, lateral projection is used for needle progression to reach the anterior third of the vertebral body and finalized cement filling.

Osteoplasty of lytic and deep-seated bone lesions is performed using direct CT-guided access of the target region. Here, harming of the adjacent vital structures has to be avoided (Fig. 15.14). Sacral insufficiency fractures and fractures due to osteoporosis and trauma as well as metastatic lesions of the sacrum may be augmented percutaneously using a posterior-oblique and transiliac approach (Fig. 15.15).

For the cervical spine, the anterolateral approach is preferred. In these cases, patients are positioned in supine position. For C2

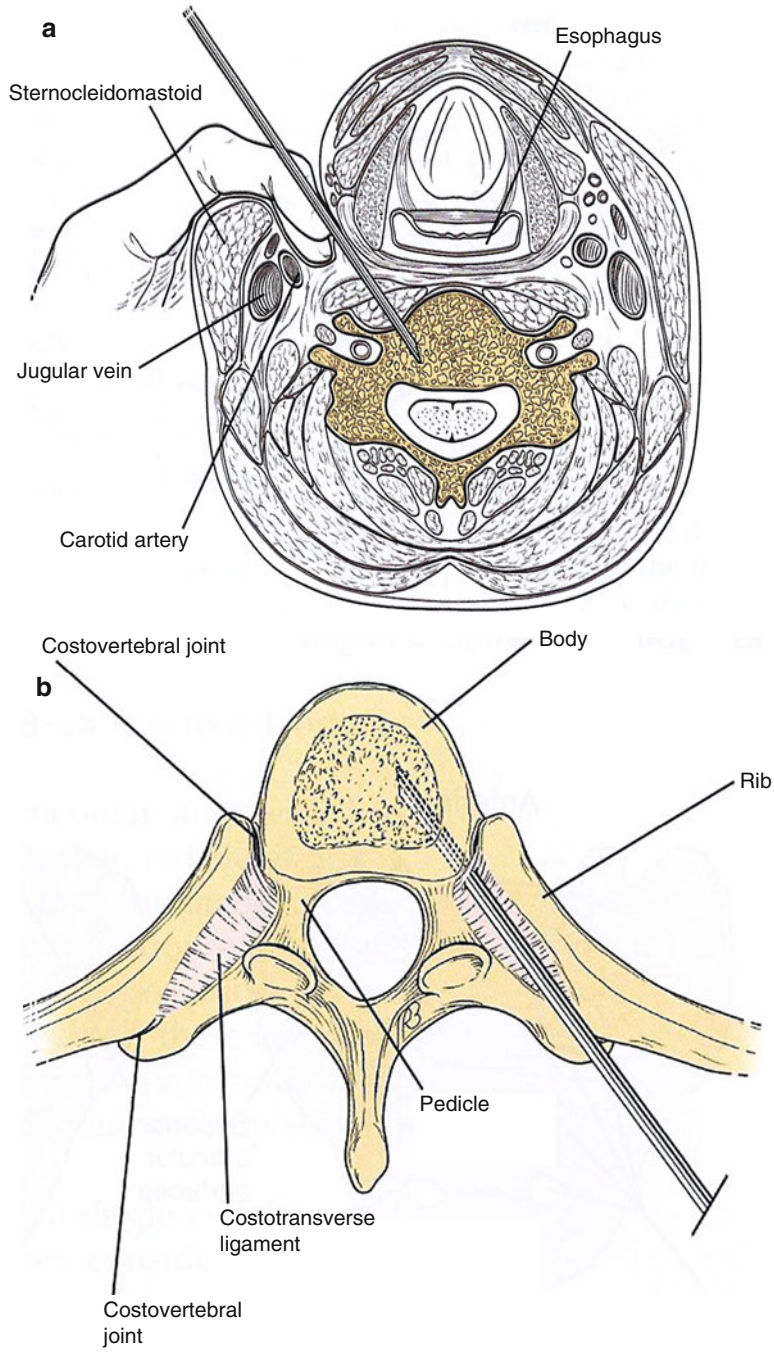

Fig. 15.9 (**a**–**d**) Depending on the anatomic level, there are different commonly used access routes to the spine. The anterolateral approach is the most common approach for the treatment of cervical spine levels. Axial drawing demonstrates manual displacement of the carotid-jugular complex and subluxation of the larynx. The anterolateral oblique access for cervical spine levels allows to reach the central part of a vertebral body (**a**). Due to the orientation and small size of the pedicles, the parapedicular (transcostovertebral) approach is used for vertebroplasty of thoracic spine levels in most cases. The needle is placed through the junction of the rib and transverse process (**b**). The pedicles of the lumbar spine are large and allow transpedicular needle placement in almost all cases. The transpedicular approach using both pedicles is the most common and safest access (**c**). Axial view of the sacrum (**d**) demonstrates the various angulations used for sacroplasty to access insufficiency fractures. The lateral posterior oblique approach is most frequently used. The needles have to be placed along the fracture lines, which are usually parallel to the sacroiliac joints. The needle tip location should be placed apart from the sacral foramina to avoid nerve laceration or cement leakage (Mathis 2006)

Fig. 15.9 (continued)

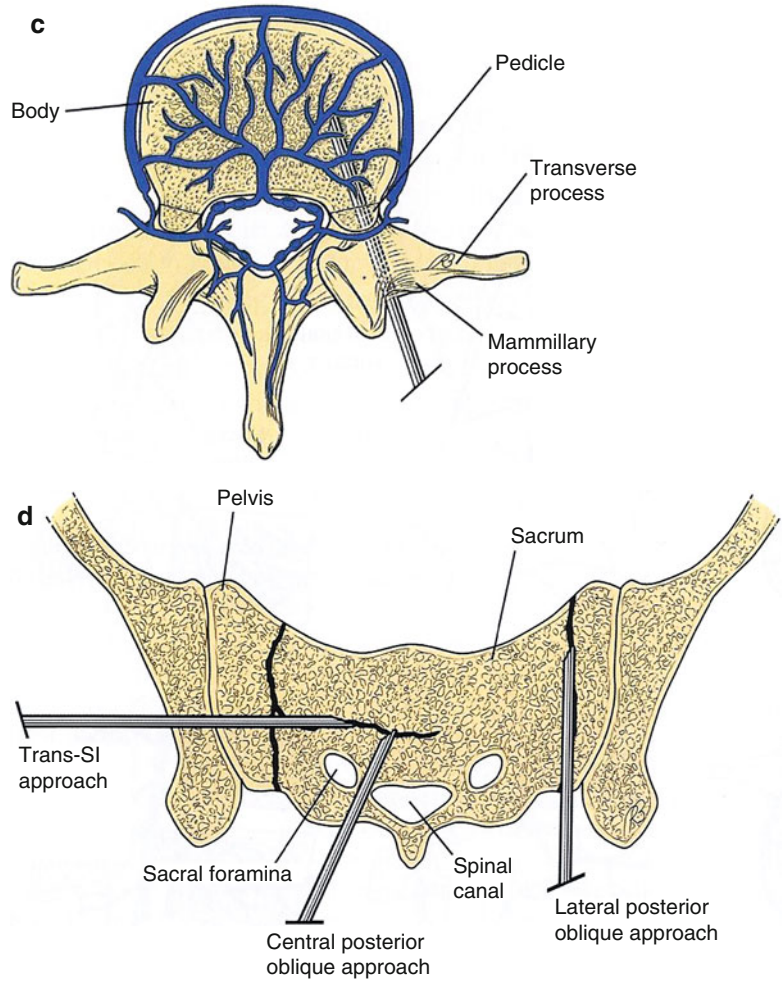

vertebrae, a posterolateral approach is possible if the vertebral body is affected (Wetzel et al. 2002). For the extremely rare treatment of the dens, a transoral approach is possible, too (Martin et al. 2002). In these cases, 13- or 15-Gauge bone biopsy needles are used (Huegli et al. 2005). The foremost concern for cervical vertebroplasty is to avoid damage of the carotid artery and jugular vein.

Depending on the preference of the operator, a direct intraosseous contrast injection under fluoroscopy in digital subtraction angiography (DSA) technique is performed (vertebrography). In most cases, this will be helpful to learn about potentially dangerous leakage and to adapt the cement viscosity to the given injection conditions (Wetzel and Wilhelm 2006).

In cases of suspected malignancy, a biopsy should precede cement injection (Mathis 2006). Appropriate biopsy devices are available. Using these devices, biopsy can be performed in one session without the necessity to create a secondary approach. Additionally, RF ablation may be performed prior to cement application in osteolytic bone metastases using suitable needle electrodes (Grönemeyer et al. 2002; Georgy and Wong 2007; Toyota et al. 2005). As the combination of PV and RF ablation is a palliative procedure that does jet not prevent tumor growth for certain, it should be used in combination with radiation therapy and/or chemotherapy (Mathis 2006).

If the needle position is considered correct within the anterior third of the vertebral body,

cement is injected under lateral fluoroscopic or CT fluoroscopic control. There are several dedicated bone cements and applicator systems usable for vertebroplasty that allow safe and easy control of the cement injection. During cement filling, particular attention is given to the epidural space and the posterior wall of the vertebral body (Mathis 2006). Usually 2–5 ml of cement per hemivertebra is adequate. Nevertheless, cement volume has to be adapted individually in order to avoid serious cement leakage, resulting in clinically significant complication. Any cement leakage outside the vertebral body gives a reason to interrupt the injection immediately. After about 1 min of waiting time, careful cement application may be continued under fluoroscopic control. Due to polymerization and

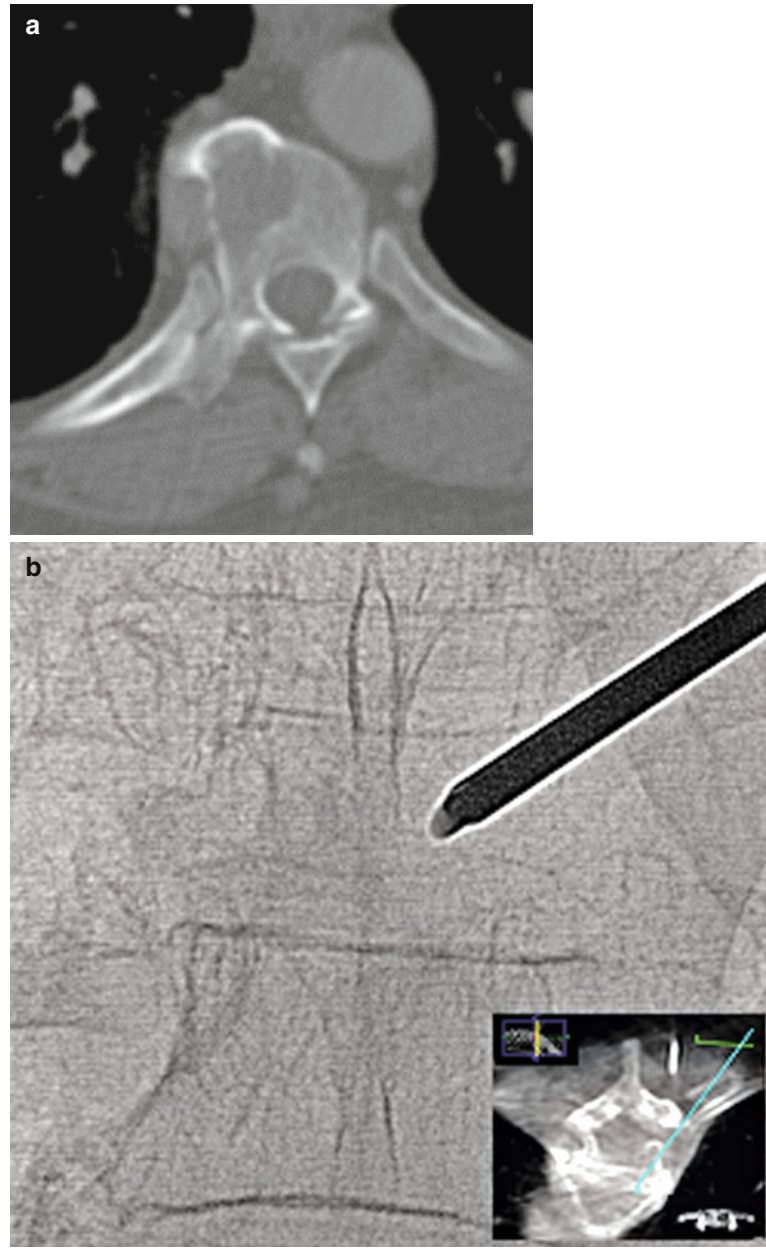

Fig. 15.10 (**a**–**d**) Flat-panel C-arm CT in percutaneous vertebroplasty in a 74-year-old female patient who presented with severe and focal back pain related to osteolytic metastases of TH 5. Unilateral transpedicular approach was used for PV. Pre-interventional axial CT image shows an osteolytic metastasis of the right hemivertebra (**a**). Fluoroscopy (pa projection) shows needle placement for unilateral transpedicular approach. *Insert image* demonstrates C-arm CT needle guidance (patient in prone position) for transpedicle access (**b**). The 11-Gauge bone biopsy needle in place (**c**). Prior to cement application, RF ablation is performed using a 2-cm LeVeen™ expandable needle electrode. *Insert image* shows correct positioning of the expandable needle electrode on C-arm CT obtained during RF ablation. Sagittal reformats from C-arm CT data obtained immediately after percutaneous vertebroplasty display the bony structures and cement filling without any cement extravasation (**d**)

Fig. 15.10 (continued)

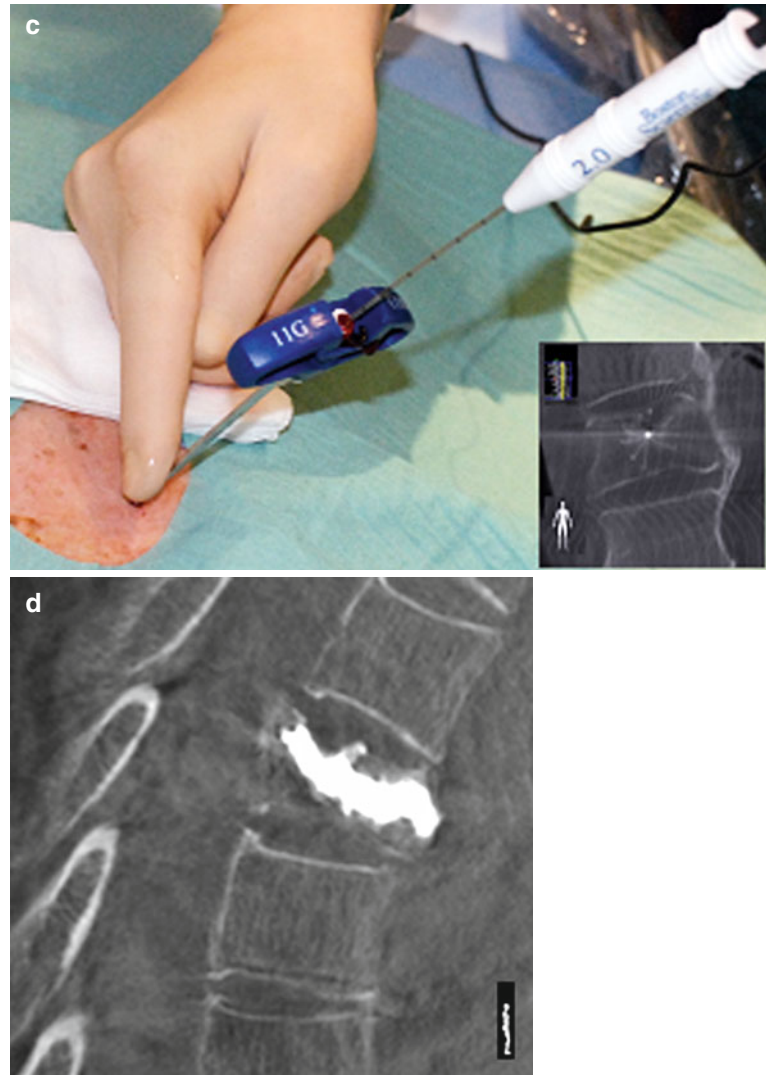

cement hardening, cement filling might be achieved into other areas of the vertebra. Nevertheless, if leakage is still visible or even becomes larger, cement application is terminated. The amount of cement needed for stabilization and pain relief is very small; therefore, filling of the entire vertebral body is not necessary at all. Finally, the trocars are withdrawn under fluoroscopic control to avoid cement tracking along the access site.

For PV, as for other surgical procedures that implant permanent devices, a single shot i.v. antibiotic prophylaxis is recommended (Mathis 2006). The most common antibiotic used is cefazolin (1–2 g), usually 30 min before starting the procedure. Working under strict aseptic conditions, infections should be avoidable. Nevertheless, there are some reports about serious infections, most likely with preexisting spondylodiscitis or in high-risk immunocompromised patients (Söyüncü et al. 2006; Lin et al. 2007).

Postinterventional assessment of cement distribution is best performed by CT; however, flat-panel detector CT and 3D reconstruction capabilities after rotational C-arm CT acquisition allow one to avoid an additional CT evaluation after vertebroplasty procedures and therefore accelerate proceedings (Fig. 15.11) (Hodek-Wuerz et al. 2006; Wilhelm and Babic 2006).

Clinical monitoring after cement injection is performed for 1–2 h for clinical changes in neurological function or for signs of any other change or side effects. During this time, complete hardening of the cement is achieved, and mobilization is possible. Appropriate to clinical follow-up discharge is conceded after 2–4 h if PV or osteoplasty is performed on an outpatient basis.

Fig 15.11 (**a**-**i**) CT-guided vertebroplasty in a patient with painful aneurysmal bone cyst of TH1. (**a**, **b**) pre-interventional obtained MRI: sagittal (**a**) and axial (**b**) T2-weighted images demonstrating high signal intensity of the aneurysmal bone cyst involving thoracic vertebra 1. Pre-interventional CT (**c**) sagittal reconstruction and (**d**) axial image clearly depict the extension of the cyst in the pedicle and transverse process of the right hemivertebra. The intervention is performed under CT guidance (**e**) via a transpedicular access (**f**) followed by repetitive fluoroscopic CT image control during the cement injection of small aliquots (usually 0.5 ml per injection); (**g**). Posttreatment CT control with sagittal reconstruction (**h**) and volume rendering (**i**) demonstrates cement filling of the bone cyst extending into the pedicle without epidural cement leakage and respecting the posterior wall and neuroforamina

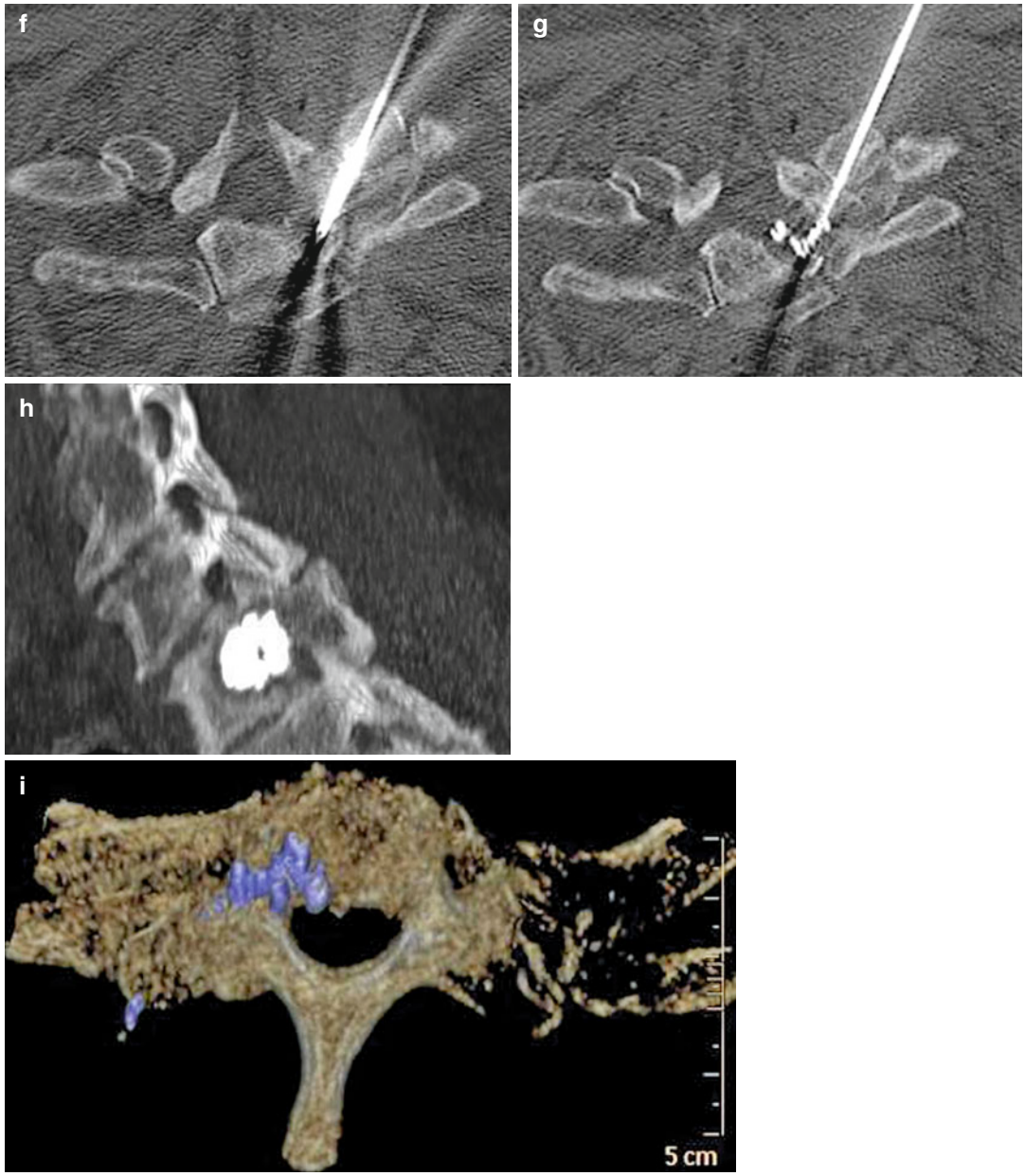

Fig. 15.11 (continued)

15.2.4 Results

Even though the vast majority of PV, osteoplasty, and sacroplasty cases concern osteoporotic compression fractures, patients with malignant disease are excellent candidates for these minimally invasive procedures (Murphy et al. 2008). The efficacy of PV and osteoplasty lies in its high potential in pain reduction and stabilization effect. Significant pain relief and improvement of mobility will be achieved in about 80–90 % of patients.

When PV is performed for osteoporosis, success is defined as an achievement of significant

Fig 15.12 (**a**-**c**) CT-guided vertebroplasty in a patient with painful spine metastases of L1. Sagittal T2-weighted SPIR MR image (**a**) shows vertebral compression fracture with bone marrow edema. Note the posterior wall involvement. The tumor has been extruded into the epidural space without deformity of the cauda or significant spinal canal compromise. Besides severe pain sensations, there were no neurologic symptoms. (**b**) Bone biopsy is performed using parapedicular access. (**c**) Cement injection is performed under fluoroscopic CT image control. Posttreatment CT control (**d**) demonstrates cement filling without epidural cement leakage or retropulsation of bone fragments

pain relief and/or improvement mobility as measured by validated measurement tools with a threshold of 80 %. For neoplastic involvement, success is classified as an achievement of significant pain relief and/or improvement mobility as measured by validated measurement tools with a threshold of 50–60 % (Mathis 2006). As an additional measure, sacroplasty is a safe and effective procedure in the treatment of sacral insufficiency fractures and osteolytic sacral metastases.

15.2.5 Complications

Clinical complication rates range from 1 to 10 % (Wetzel and Wilhelm 2006). However, the number of publications reporting from unusual or rare complications associated with PV has increased, as the method becomes more public and more procedures are being performed by less experienced physicians (Mathis 2006; Barragan-Campos et al. 2006).

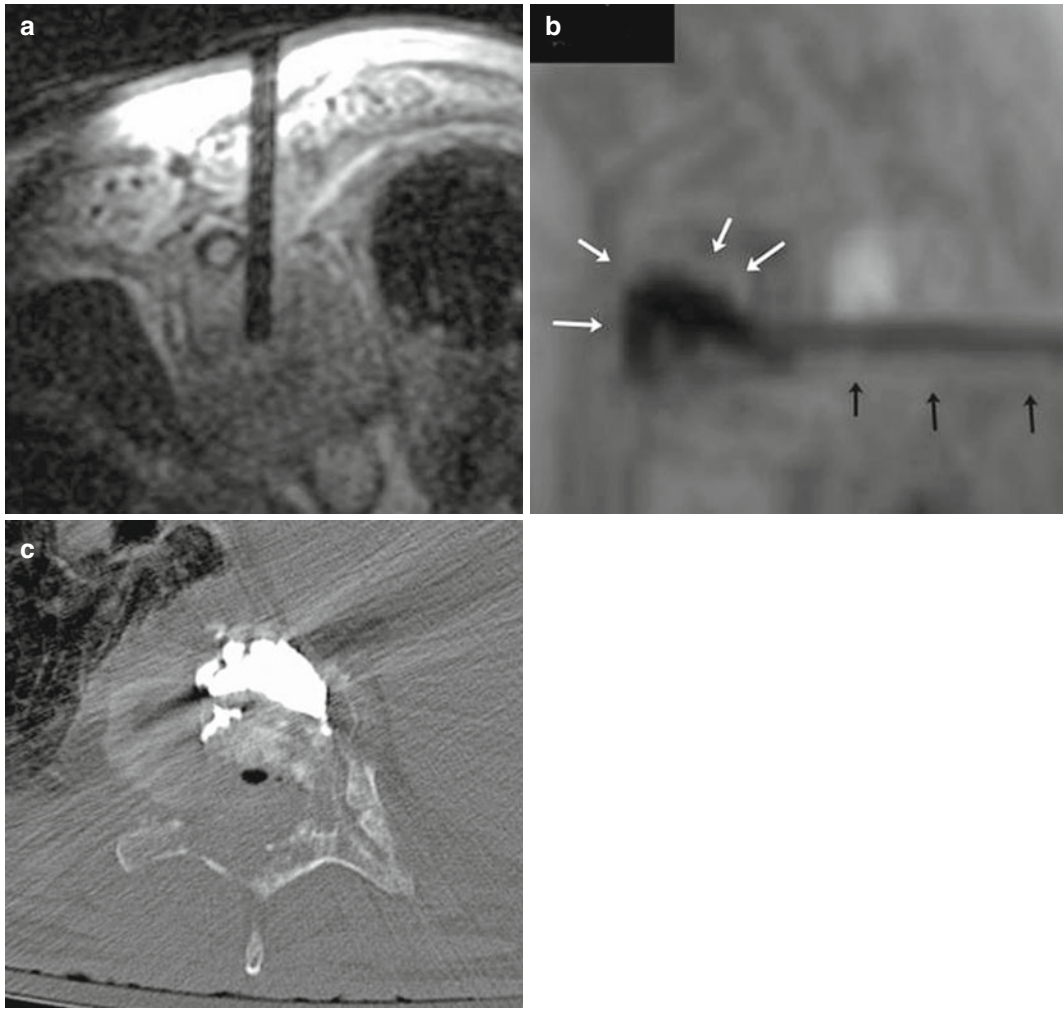

Fig 15.13 (**a**-**c**) MR-guided vertebroplasty using an open-bore low-field MR scanner. The transpedicular puncture path is clearly visible on the axial MR section (**a**). Tantalum opacified cement injection (*white arrows*) is performed under real time MR imaging using small aliquots of 0.5 ml per injection (**b**). MRI (sagittal T1 reconstruction) shows cement distribution. *Black arrows* show the actual needle position. Corresponding post-interventional CT control demonstrates cement filling of the target lesion (**c**) (Courtesy to Alexis Kelekis, MD, Ass. Professor of Interventional Radiology, National and Kapodistrian University of Athens Medical School, University General Hospital)

The most dangerous complication is cement leakage because of the risk of spinal cord or nerve root compression. The clinical symptoms resulting from cement extravasation range from temporary nerve root irritation to permanent paraplegia. In most cases, cement leakages are clinically asymptomatic.

Transient neurological deficit or radicular pain syndrome will occur in about 1 % of osteoporotic and up to 10 % of tumor patients. Although complications from vertebroplasty are uncommon, serious problems like death to pulmonary cement embolism, significant hemorrhage, or vascular injury are reported in the

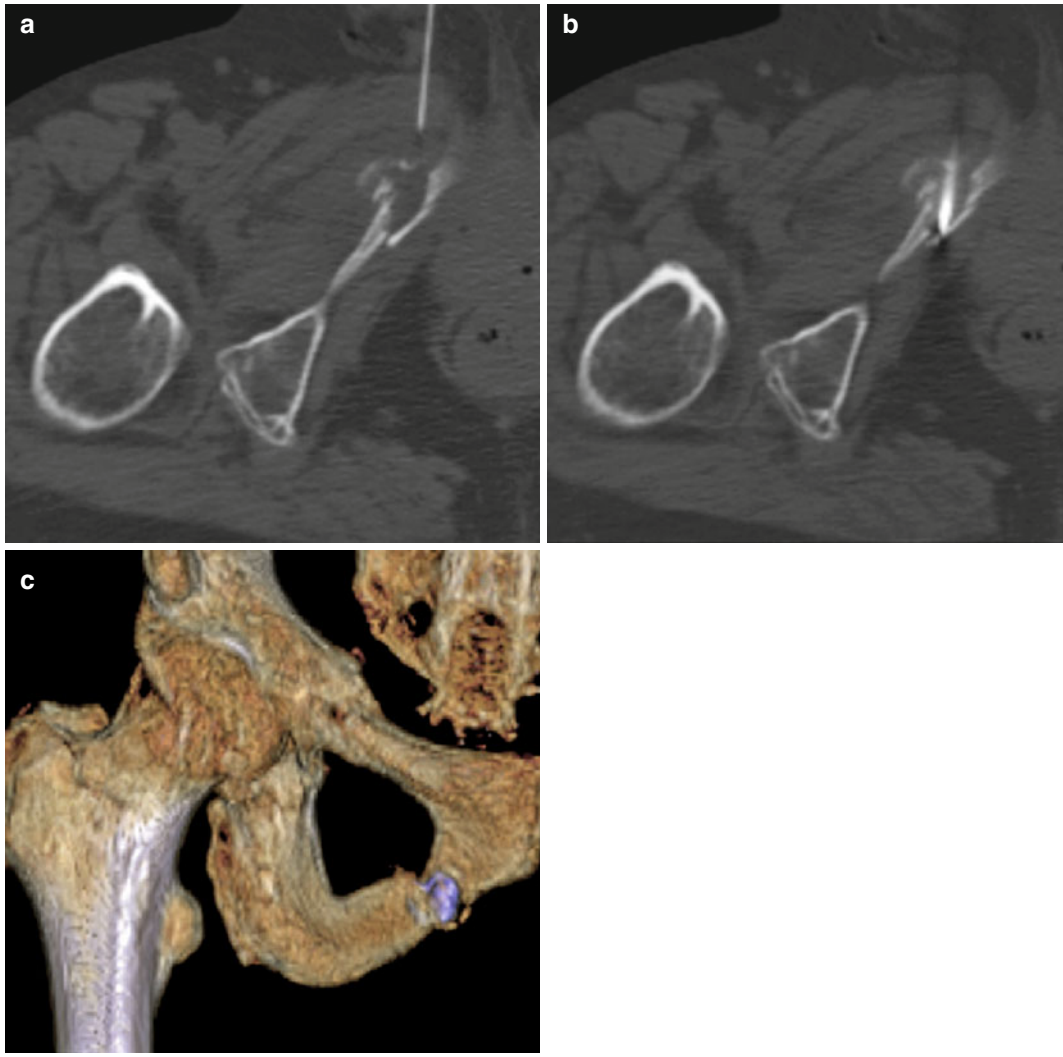

Fig. 15.14 (**a**–**c**) Osteoplasty: axial CT scan of the pelvis shows painful osteolytic lesion of the right pubic bone associated with pathologic fracture (**a**). A 22-Gauge needle for local anesthesia is placed under CT guidance (**b**). An 11-Gauge trocar bone biopsy needle is inserted. CT image shows correct position of the needle within the lesion. Additionally, biopsy is performed for histopathologic correlation of the lytic lesion. Three-dimensional reconstructed image (**c**) after osteoplasty reveals cement distribution

literature (McGraw et al. 2003). Overall, cement leakage is seen more frequently in the treatment of metastatic lesions.

In the majority of cases with epidural leakage or cement leakage into the foramina, the symptoms will be transient because they are caused by an inflammatory reaction due to increased cement temperature during hardening. In these cases, symptoms can be eased by administration of anti-inflammatory drugs or local steroid therapy (Mathis 2006; Kelekis and Martin 2005). On the other hand, spinal canal compression caused by a larger amount of cement extravasation resulting in paresis, paralysis, and bowel or bladder dysfunction will require immediate surgical decompression (Wetzel and Wilhelm 2006).

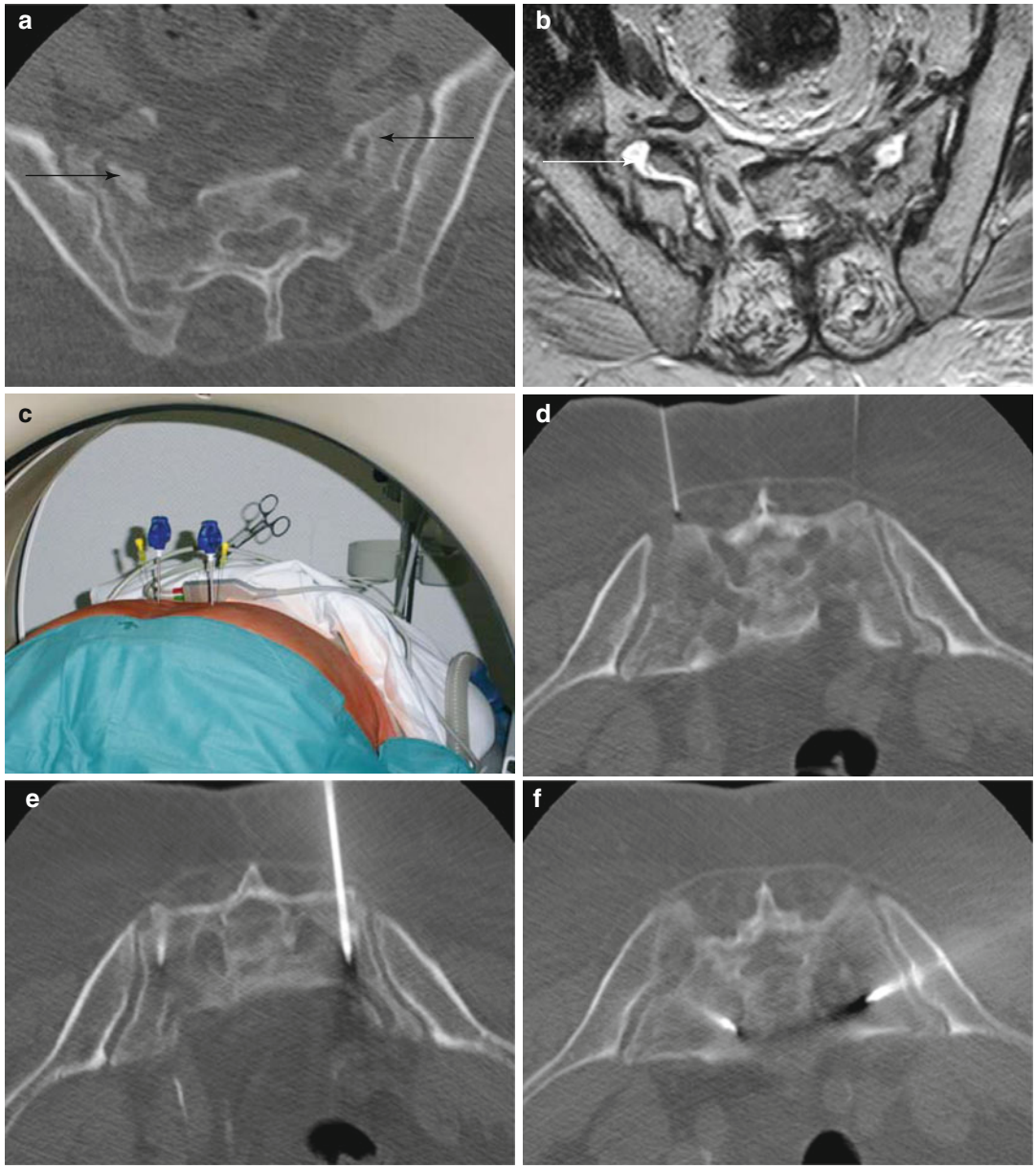

Fig. 15.15 (**a**–**f**) Sacroplasty: pretreatment axial CT (**a**) and MR images demonstrate the fractures in both sacral alae (*black arrows*). The fractures are parallel to the sacroiliac joints and show edema on T2-weighted MRI images (*white arrows*) (**b**). CT setup is used for needle placement (**c**, **d**). Bilateral sacroplasty is performed using a two-sided posterior (**e**) and transiliac approach (**f**). Cement injection is performed under fluoroscopic control for optimal visualization of cement distribution (**g**, **h**). The cement is injected simultaneously in small amounts via the four injection sites. Posttreatment CT (**i**, **j**) shows cement deposition within the fractures

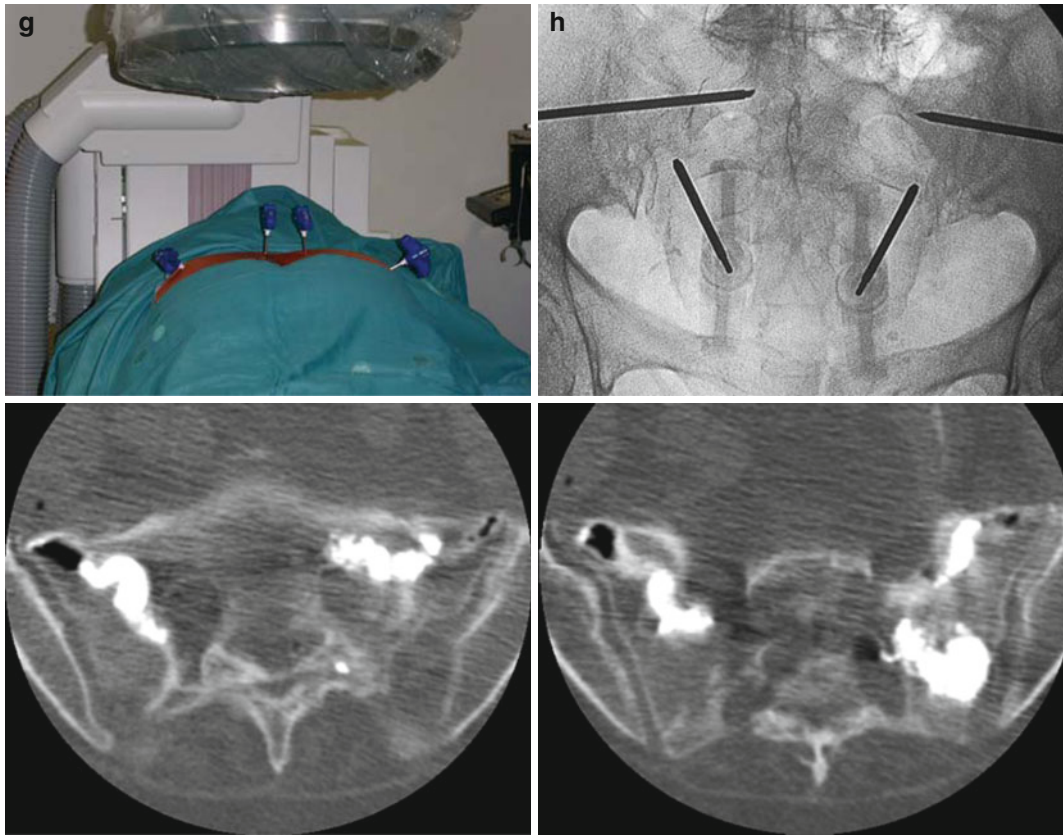

Fig. 15.15 (continued)

Summary

PV is a safe and very effective tool in vertebral pain management that permits pain reduction and instantaneously improved bone stability. Furthermore, in cancer patients, PV and osteoplasty are palliative therapy options supplementing other antineoplastic therapies that result in patients' comfort by giving them the possibility of reestablishing their daily activities in a short period of time. Both techniques may be combined with other tumor therapies, including radiation therapy or RF ablation. Sacroplasty has evolved as a safe and effective procedure in the treatment of sacral insufficiency fractures and osteolytic sacral metastases.

Key Points

- PV is safe and effective for managing a variety of painful bone lesions.
- Adequate image guidance for needle placement and during PMMA injection is the key to minimizing complications.
- Thorough peri-interventional patient surveillance is needed to detect and adequately deal in a timely fashion with potentially disabling complications.

15.3 Percutaneous Osteosynthesis of the Pelvis and the Acetabulum

Sebastian Kos, Peter Messmer, Deniz Bilecen, and Augustinus L. Jacob

15.3.1 Indications

Mostly caused by high-impact traumas, pelvic fracture account for about 0.3–8 % of all fractures (Gansslen et al. 1996; Senst and Bida 2000), but in cases with multiple traumas, a pelvic ring injury is more frequent (20 %). The trauma (Gansslen et al. 1996) may be lethal due to the injury itself (Kellam et al. 1987) or additional organ lesions (head, chest, abdomen, and limbs) (Poole and Ward 1994). This is reflected by mortality rates between 10 and 31 % (Pohlemann et al. 1994; Ben-Menachem et al. 1991; Hunter et al. 1997) and a high morbidity in survivors (Tile 2003). As a basic function, the pelvic ring transmits forces from the lower extremities to the spine (Isler and Ganz 1996). Any therapy has to restore and preserve this ability, not so much to offer a high-precision anatomical reconstruction. In addition, the acetabular joint enables movement of the femoral head, which means that those fractures need a minute reduction and fixation to minimize the risk of post-traumatic osteoarthritis or at least allow a consecutive joint replacement (Starr et al. 2001).

15.3.1.1 Pelvic Fractures

As the osseous pelvic ring is a rigid structure, an injury of, for example, the posterior ring (ilium, sacroiliac joint, sacrum), rarely occurs without a concomitant interruption of the anterior ring (symphysis, obturator rings, acetabular). The AO/ASIF classification groups pelvic fractures according to its severity (Fig. 15.16a–c) (Tile 1996, 2003; Isler and Ganz 1996).

The most common Type "A" injuries (50–60 %) are isolated fractures of the anterior pelvic ring with intact posterior stability. They are often treated conservatively with partial load bearing using crutches. Rare indications for open or percutaneous surgery may be muscle avulsion fractures, fragment dislocation, persistent pain, and a prolonged rehabilitation.

Type "B" fractures (20–30 %) preserve a partial posterior stability but are unstable toward rotational forces. This may occur in cases with complete anterior plus partial posterior disruptions. Those are usually treated conservatively (Tile 2003). Nevertheless, due to partial but clinically disabling functional pelvic ring instability, certain types of B fractures, for example, open book lesions with symphyseal disruption of more than 2–3 cm (AO B2.2), frequently undergo surgery. Other indications for surgery may be potentially unstable intermediate type B/C lesions to prevent secondary dislocation and malunion. In rotationally unstable fractures, an anterior stabilization, in combination with the preserved posterior sacroiliac ligament complex, provides sufficient stability. For simple cases with non-displaced fractures, either antegrade or retrograde superior pubic ramus screws or reconstruction plates can be used. Reconstruction plates may be used in displaced, comminuted, and/or complex cases (Simonian et al. 1994a).

Type "C" fractures (10–20 %) show a complete loss of posterior stability, are rotationally and vertically unstable, and should be treated surgically. An approach with initially anterior plating normally reduces the posterior pelvic ring sufficiently for a subsequent percutaneous iliosacral screw fixation.

15.3.1.2 Acetabular Fractures

The Letournel classification (Fig. 15.17) discriminates between simple fracture types of the posterior wall (1), posterior column (2), anterior wall (3), anterior column (4), and transverse fractures (5) and associated fracture types. The latter are a variety of combinations of the simple types (6–10). As mentioned, the main goal of treatment is the precise reconstruction of joint surface integrity. Insufficient reduction may lead to post-traumatic osteoarthritis in up to 1/3 of the cases, whereas this only occurs in about 10 % after a good reduction (Letournel 1993).

Accepted treatment is an open surgical reduction of the fracture itself and an internal fixation

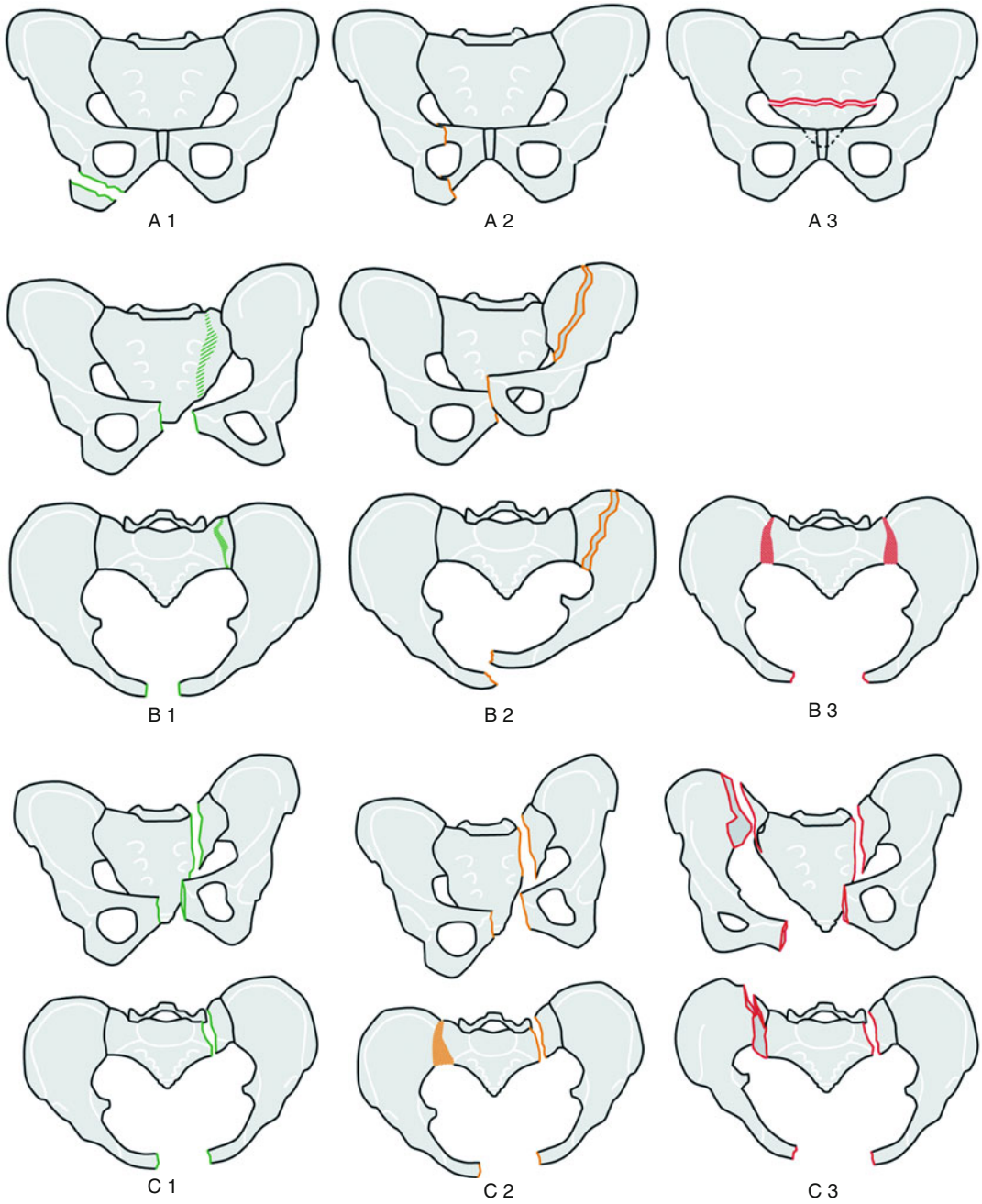

Fig. 15.16 AO/ASIF classification groups pelvic fractures according to its severity (See Sect. 15.3.1.1)

(ORIF) with screws and plates (Letournel 1993; Judet et al. 1964; Qureshi et al. 2004). In selected cases, a minimally invasive therapy is possible (Gay et al. 1992; Jacob et al. 2000a,b; Gross et al. 2004; Starr et al. 1998).

15.3.2 Material

15.3.2.1 Preinterventional Diagnostics

As both pelvic and acetabular fractures are usually complex, the exact fracture morphology is

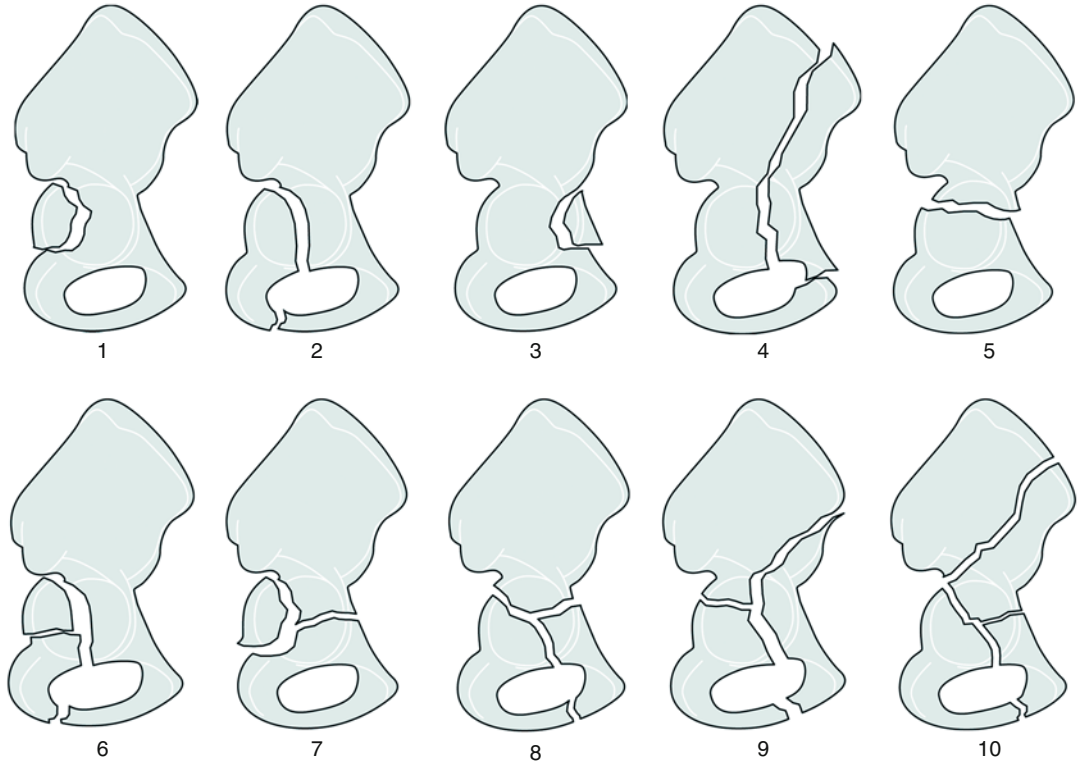

Fig. 15.17 Acetabular Fractures - Letournel classification (See Sect. 15.3.1.2)

hard to detect by routine radiographs alone (Falchi and Rollandi 2004). False negative rates regarding the detection of pelvic fractures in conventional a.p. views reach 32 %, and in up to 55 % of cases with a fracture detected on plain film, computed tomography (CT) reveals either additional fractures or an upgrade in fracture classification (Guillamondegui et al. 2002). In general, multi-slice spiral CT (MSCT) is superior regarding the depiction of the spatial fracture fragment arrangement and the fracture extent, particularly when using three-dimensional reformations and is therefore the actual gold standard for pelvic fracture assessment (Wedegartner et al. 2003). For the standard CT protocol, we use 3-mm slice thickness and 1.5-mm slice increment. Multiplanar reformations are obtained adapted to the individual fracture pattern.

15.3.2.2 Image Guidance Methods

The main task of percutaneous fixation is the safe placement of an implant well adapted to the fracture morphology. Such guidance is performed like in any standard CT or CT-fluoroscopy-guided procedure. As an advantage, by the end of the procedure, the postoperative control is already done. In strictly percutaneous procedures, a normal CT suite may be sufficient from a hygienic point of view, which nevertheless has to be approved by the local authorities. For any open or hybrid procedure, a sterile operating room is mandatory (Jacob et al. 2000c). Until today, MR guidance for percutaneous osteosynthesis is neither used for the preinterventional procedure planning nor for its guidance.

In recent years, newer generations of high-performance fluoroscopy/angiography suites have been introduced. These systems offer cone-beam CT as an additional functionality allowing for acquisition of CT datasets with acceptable resolution for skeletal interventions (Orth et al. 2008; Miyazawa et al. 2010). This in conjunction with newer navigational tools (e.g., iGuide, Siemens Medical Systems,

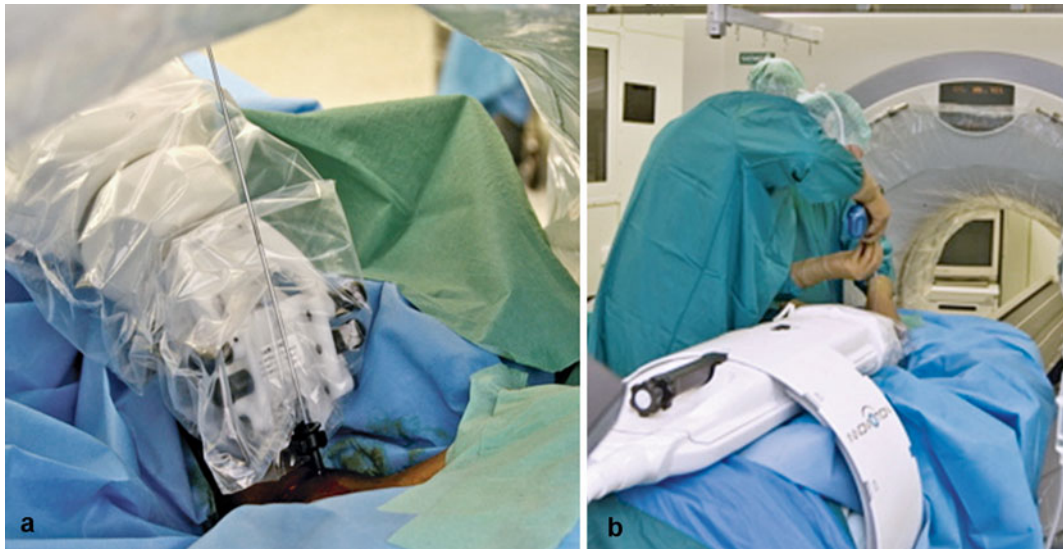

Fig. 15.18 Robotic assisted navigation (**a**) can be used for prcise screw insertion positioning (**b**)

Erlangen, Germany) of such systems may in the future allow for safe and precise treatment in those suites (Meyer et al. 2008).

15.3.2.3 Robotic Assistance

As ambitious robotic projects failed within the last decade (Glauser et al. 1995; Schrader 2005; Siebert et al. 2002), more conservative approaches were sought, such as robotic-assisted devices (e.g., Innomotion, Innomedic, Herxheim, Germany) (Fig. 15.18), that leave the medical act of introducing instruments and implants in the hand of the physician (Cleary et al. 2006) instead of an "active" robot performing the procedure. Of course, procedure guidance could be performed without robotic assistance either, but in our opinion, precise device positioning is facilitated by use of robotic assistance.

15.3.2.4 Hardware

To date, there is no dedicated hardware for closed reduction combined with percutaneous fixation (CRPF) available on the market. These procedures therefore rely on standard surgical tools (e.g., Schanz screws, external fixators, guide wires, cannulated screws, screwdriver, drill) (Fig. 15.19). From our experience, we want to emphasize some specific points for percutaneous osteosynthesis. We use 2.8-mm AO/ASIF guide wires (Synthes, Solothurn, Switzerland) which are both rigid and sharp (Fig. 15.20). Rigidity is needed for navigation where the near end of the instrument is guided and the tip is extrapolated, assuming linearity of the device. Acuity avoids the guide pin sliding off a bone entry site with an obtuse angle between device and cortex. We use self-cutting self-tapping AO/ASIF 7.3-mm set and lag screws (Synthes, Solothurn, Switzerland) without the need for additional drilling and tapping (Fig. 15.21). These are inserted immediately after correct placement of the guide wire is documented. Fully threaded set screws are needed in cases where additive compression is unwanted or dangerous (e.g., foraminal comminution) to fix the fragments in their current relative position. Those fully threaded set screws do not compress the fracture and therefore are biomechanically not as strong as lag screws. Lag screws are threaded in a defined region, from their tip backward, leading to fracture compression and are used in all other indications. The threaded portion is chosen by the interventionalist, in such a way that it lies entirely in the far fragment. In some cases, a lag screw may be inserted first to gain controlled compression, which is then held using a set screw.

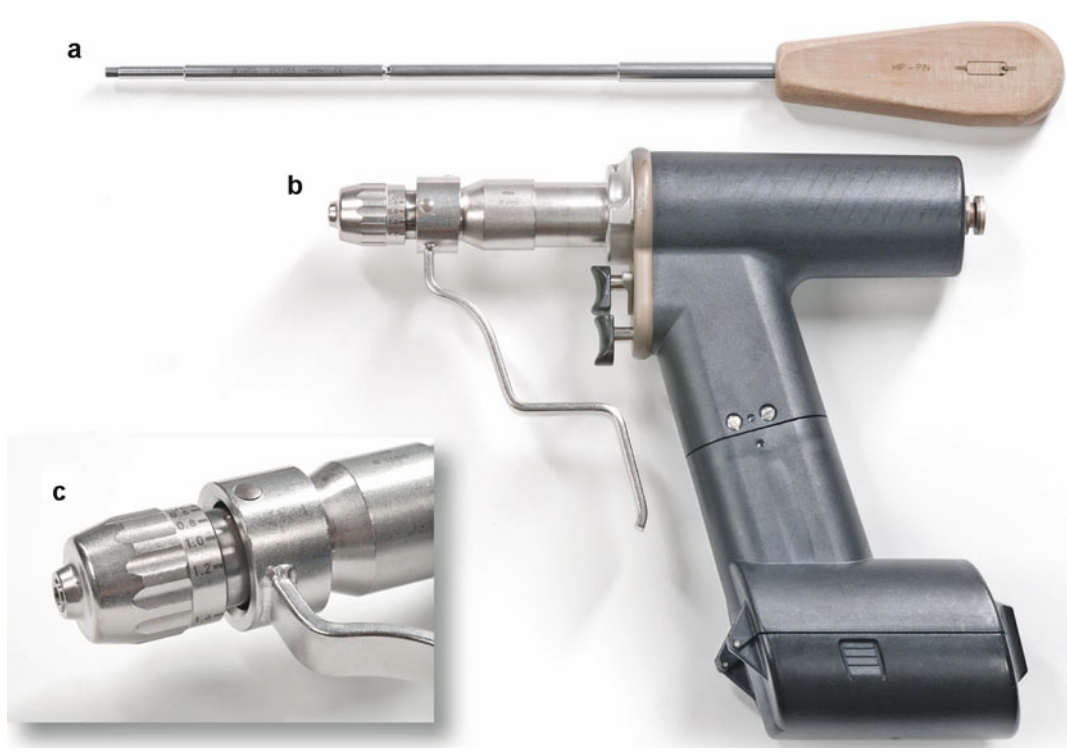

Fig. 15.19 Standard surgical tools: mechanical screwdriver (**a**) and drill (**b**, **c**) (See Sect. 15.3.2.4)

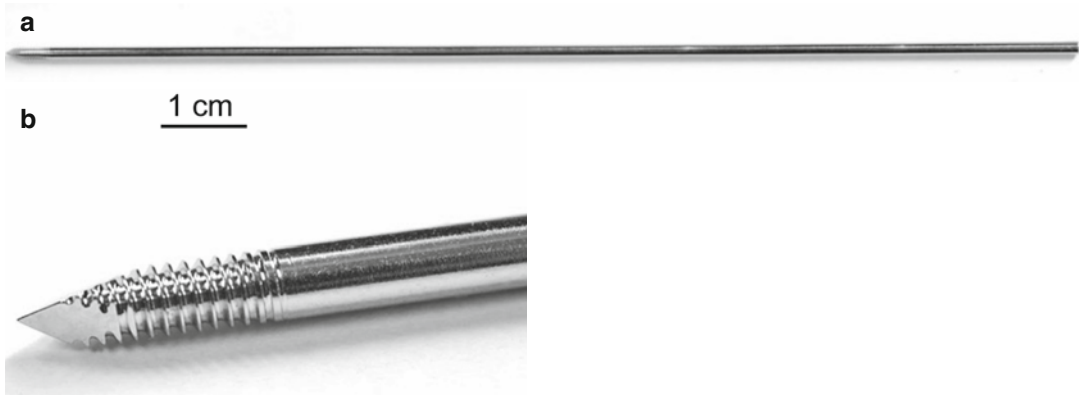

Fig. 15.20 AO/ASIF guide wires (Synthes, Solothurn, Switzerland) (**a**) with rigid and sharp screwtip (**b**) (See Sect. 15.3.2.4)

15.3.3 Technique

15.3.3.1 Placement, Immobilization, Patient Preparation

Procedures are performed with a written informed consent obtained at least 24 h prior to the procedure. All procedures are performed under general anesthesia and sterile conditions in an operation suite. In navigated procedures and using robotic assisted-devices, it is necessary to immobilize the patient. We routinely use a setup with a vacuum mattress and broad adhesive tape. The patient is fixed in a position where the screw trajectory envisioned runs either vertically or horizontally and "as

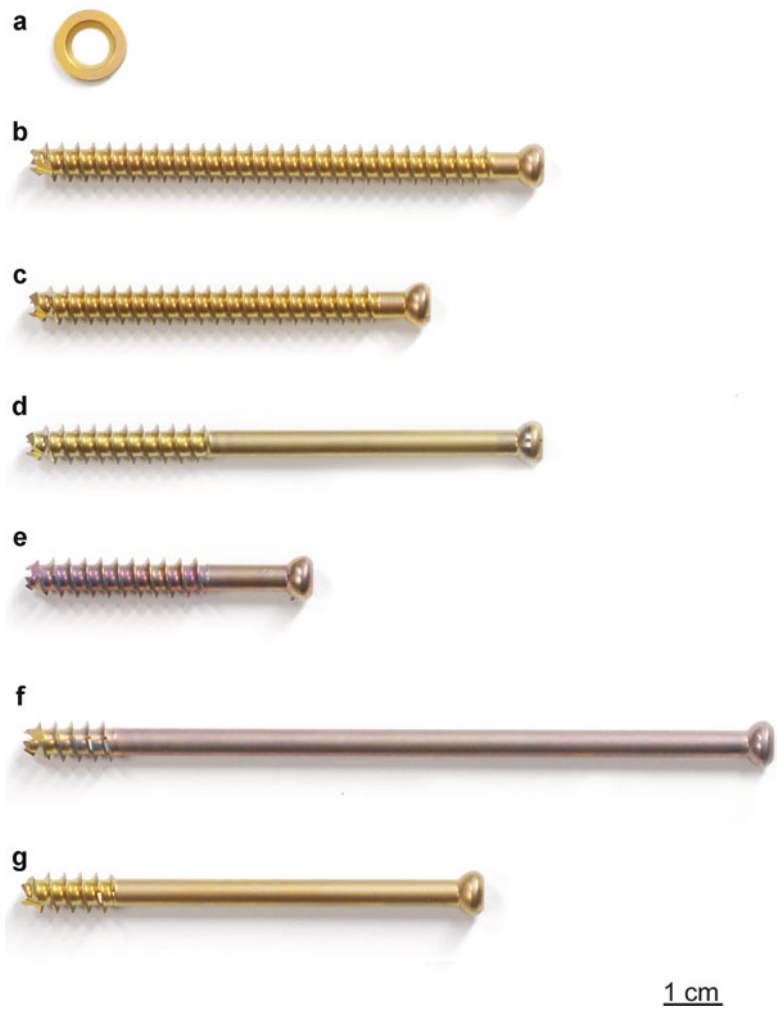

Fig. 15.21 Ring washer (**a**) and self-cutting self-tapping screws (**b**-**g**) (See Sect. 15.3.2.4)

orthogonal as possible," especially when a navigation or robotic assistance system is not used.

15.3.3.2 Minimally Invasive Reduction Methods

Imaging may identify different types of dislocation as, for example, seen in translation, joint step, gap, and rotation (Wedegartner et al. 2003). In cases with a fracture or luxation *gap*, ideally all points of the bone fragments have the same distance to their counterparts. The reduction may be achieved by a fixation, applied perpendicular to the gap plane. Fragment *translation* may be seen in all directions. In most cases, an external manipulation alone is sufficient, but in cases with a craniocaudal component, an additional fragment extension may be needed. *Rotated fragments* may be reduced with a percutaneously inserted guide pin or Schanz screw which is used as a handle. *Joint steps* (e.g., acetabular) are most difficult and least likely to be treatable by minimal invasive means alone.

A good reduction is an important prerequisite for further fixation, and a reduction in general should be attempted as early as possible to prevent complicating hematoma consolidation and soft tissue fibrosis which may occur within two days. Closed, percutaneous, and open or limited access types of reduction are feasible, each having its own limitations (Jacob et al. 1997, 2000a; Gross et al. 2004; Gansslen et al. 2006; Gay et al. 1992).

Open reduction (OR) or possibly *limited* access reduction (LAR) needing a posterior surgical exposure has been complicated by wound

problems. Regarding this, a *closed* reduction (CR) as the least invasive method is preferred whenever possible. CR may be applied by (1) gravity, (2) external manipulation, and (3) extension, depending on type and degree of dislocation, fracture age, involvement of joint surfaces, and/or adjacent (e.g., neural) structures. CR outcome is usually evaluated by control imaging.

Using *percutaneous* reduction (PR), handles, most often Schanz screws, are percutaneously attached to the fragments, which are then manipulated through the inserted devices. Examples are seen in the following:

1. Application of a pelvic clamp in cases with pelvic hemorrhage to close a gap in the posterior pelvic ring, reducing the internal pelvic volume and assisting spontaneous tamponade.
2. Schanz screws used in the pelvic girdle for force transmission safeguarding neurovascular structures. These are often inserted into the anterior superior iliac spine or the iliac crest, whereas screw insertion into deeper structures may necessitate image guidance.
3. The use of external fixators allows precise movements, and in addition the ability to retain the achieved osseous reduction (Kellam 1989).

15.3.3.3 Minimally Invasive Percutaneous Therapy

The fixation methods should be image-guided in cases where a planned and image-based linear trajectory is to be reproduced as precisely as possible to allow exact placement of compression and positioning screws. The linear trajectory is planned by the interventionalist according mainly to the individual fracture pattern, disregarding anything like surgical access, anatomy, or dissection plans. In a targeting step, a guide wire is placed, and within a fixation step, the active element, mostly a cannulated screw, is slid over the guide wire through the interjacent tissues (crossing, e.g., skin, fat, fascia, and muscles). The following indications for minimally invasive percutaneous therapy of pelvic injuries are given according to the literature and our own experience.

Superior Pubic Ramus Fracture

The superior pubic ramus screw, described in 1995, can be used in cases with non-displaced and non-comminuted fractures of the anterior acetabular pillar or the midportion of the superior pubic ramus (Routt et al. 1995a). It can replace an anterior reconstruction plate applied either through a formal or reduced ilioinguinal approach. It may be introduced in an antegrade (craniodorsal to caudoventral) fashion or in the retrograde direction with the insertion point near the pubic symphysis. The antegrade access requires a high targeting precision as it uses a long guiding trajectory while the retrograde approach may be made impossible through interference with the genitals. The cannulated screws used (7.3 mm) are big, providing a firm fixation, but may therefore interfere with the narrow isthmic portion above and in front of the hip joint. Indication can be seen in stabilization of the anterior compartment of an unstable pelvic ring fracture. For that, a straight and wide trajectory for the passage of the screw, distant from the hip joint, has to be found, as seen in cases with small primary displacement or a good primary reduction (Routt et al. 1995a).

Sacrum, Ilium, and Ilio-Sacral Joint

Ilio-sacral screws inserted from the lateral ilium, crossing the sacroiliac joint, reaching into the first sacral vertebral body, are broadly accepted for internal fixation of posterior pelvic ring and sacroiliac joint disruptions and sacral fractures (Fig. 15.22) (Nelson and Duwelius 1991; Routt et al. 1995b; Simonian et al. 1994b). Techniques for ilio-sacral screw insertion using fluoroscopy, CT, or even direct visual guidance have been described. Screws may be inserted with the patient in the supine, prone, or lateral position (Routt et al. 1995b; Ebraheim et al. 1987; Matta and Saucedo 1989). At our institution, we usually place and immobilize the patient on the side contralateral to the injury for a good reduction by gravity and an appropriate target path. This may necessitate two consecutive placements in cases with bilateral pathologies. In contrast, supine and prone positions both offer bilateral access. However, fixation in a supine position may be limited as the oblique trajectory may interfere with the OR table and draping as well as the scanner gantry. Prone placement may be associated with problems of mechanical ventilation and

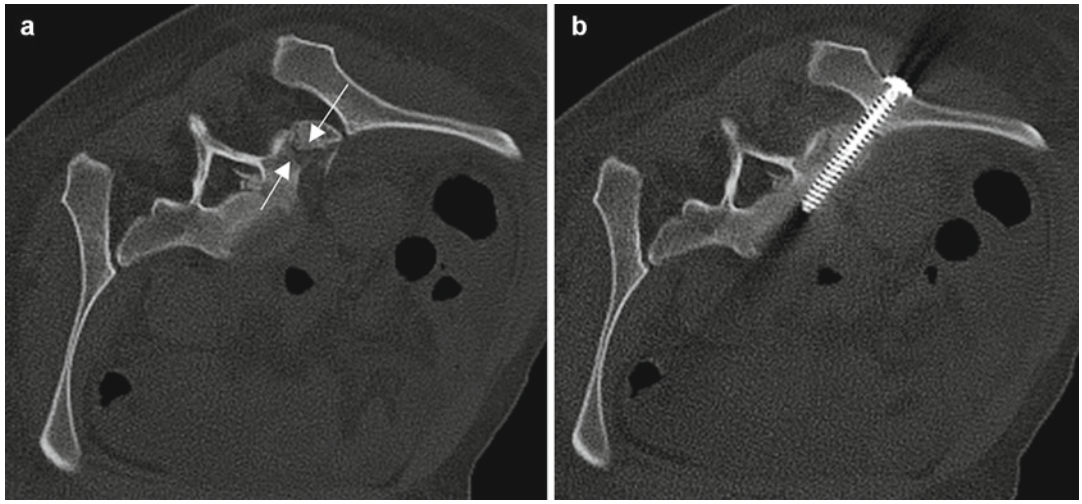

Fig. 15.22 Ilio-sacral screws insertion for sacral fractures (**a**). The scew is inserted from the lateral ilium, crossing the sacroiliac joint, reaching into the first sacral vertebral body (**b**)

rotation of the iliac wings if prior anterior fixation is not performed yet. Ilio-sacral screws are biomechanically at least equal to common sacral bars and open or local plating (Pohlemann et al. 1993), and with double ilio-sacral screw fixation, the strongest fixation of posterior pelvic ring disruptions is achieved (Yinger et al. 2003). Indications are the stabilization of the posterior component of unstable pelvic ring fractures, with either a small primary displacement or a good reduction achieved. For the treatment of comminuted fractures affecting the neural foramina or the spinal canal, set screws should be used either alone or after an initial controlled compression using lag screws. Position and complication control in such cases may be performed intraoperatively, either visually by CT or less commonly functionally by somatosensory evoked potentials (Moed et al. 1998). A few reports exist about the use of ilio-sacral screws in SI joint arthritis and even metastatic bone destruction (Ebraheim and Biyani 2003) as well as in cases with postpartum pelvic pain and sacral nonunion (van den Bosch et al. 2002; Huegli et al. 2003). These indications have to be considered experimental.

Acetabulum

In 1992, computed tomography was already used to guide the percutaneous placement of 6.5-mm cannulated screws (Gay et al. 1992). Starr et al. (1998, 2001) guided the placement of percutaneous screws in cases with non-displaced or minimally displaced acetabular fractures by fluoroscopy. This may also be used in terms of a supplemental fixation when combined with an open reduction and internal fixation of complex acetabular fractures. In cases of "simple" acetabular fractures lacking relevant steps or comminution, the acetabular roof screw alone may close the fracture gap and restore mechanical stability. We usually apply two screws: one adjacent to the joint and another a little more cranially. As the trajectory is dictated by the fracture course, sometimes a limited access to pull aside vital structures like the femoral nerve may be needed (Gross et al. 2004). Unlike others, we commonly use an anterior approach, as in a posterior access the sciatic nerve often disables the optimal screw trajectory (Jacob et al. 2000a). For the decision to treat percutaneously an acetabular fracture by osteosynthesis (Fig. 15.23), we apply the following criteria (Gay et al. 1992; Gross et al. 2004; Jacob et al. 2000a):

1. Two or very few fragments of the load bearing acetabulum portion.
2. The far fragment needs to be big enough to host the threaded portion of the inserted lag screw.
3. Intra-articular fragments not present.
4. At the most, a very small articular step-off or impression is present.

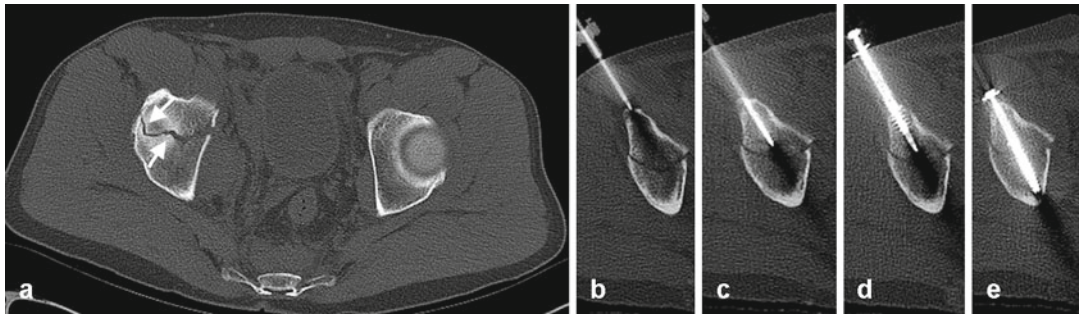

Fig. 15.23 Step-by-step illustration: osteosynthesis of acetabular fracture (See Sect. 15.3.3.3)

In selected cases, variant approaches, like a "bottom-up" screw in transverse fractures of the posterior acetabular pillar or an iliac wing screw to close a gaping iliac crest, may be applied. The paths are chosen at the discretion of the operator and according to the situation at hand. The reduction and fixation methods outlined above can of course well be used in combined approaches:

1. Open or limited access reduction and internal fixation (*ORIF/LARIF*) as a standard or less invasive surgery.
2. Open or limited access reduction and percutaneous fixation (*ORPF/LARPF*) if percutaneous fixation is possible after open reduction or an open release of neural compression combined with percutaneous fixation is wanted.
3. Closed or percutaneous reduction combined with percutaneous fixation (*CRPF/PRPF*) is a standard minimally invasive technique in non-displaced or externally reducible fractures.
4. Closed or percutaneous reduction and limited access fixation (CRLAF/PRLAF) may be used for guided insertion of an implant in cases with a limited surgical access due to vital structures disabling the optimal trajectory.

15.3.3.4 Follow-Up

Patients with surgically treated fractures of the pelvis and acetabulum at our institution undergo immediate postoperative CT control (Müller et al. 1991; Jacob et al. 1997). Further follow-up imaging should be performed according to the individual clinical symptoms, most often with conventional radiographies. Within clinical studies, for example, CT, controls were obtained up to 1 year after the operation (Jacob et al. 1997).

15.3.4 Results

The following quality criteria are presented according to the literature and our own experience. If these criteria are fulfilled, a decent morphological and clinical result as well as a minimum of complications can be expected.
Regarding clinical criteria:

1. Good indication adapted to the individual situation
2. Infection rate <1 %
3. Pain relief
4. Good functional outcome
5. Rehabilitation and return to work should be achieved and quality assured

Regarding imaging criteria we assess by CT:

1. Screws should lie as close as possible perpendicular to the fracture gap.
2. The thread of lag screws should completely lie in the distant fragment.
3. There should be no additional compression when compared with the preoperative images using set screws.
4. In posterior ring fractures, the maximum offset should be <10 mm.
5. Superior pubic ramus screws should splint both fragments centrally in the marrow canal through a sufficiently long distance.
6. Residual gaps in the articular surface of the hip joint should be <3 mm, steps <1 mm.
7. No hardware perforation into the hip joint itself should be visible.

Table 15.3 provides an overview of published results regarding ilio-sacral screw fixation. With 85–100 % of the screws being positioned adequately, the results are well acceptable. In

Table 15.3 Synopsis of literature on ilio-sacral screw fixation

Authors	Patients (*n*)	Screws (*n*)	Implant	Guidance method	Adequate positioning (%)	Malpositioned screws	Complications
van den Bosch et al. (2002)	88	285	7.3-mm cannulated screws	2-D fluoroscopy	93	7 % (15/220) @ CT	Neurologic complications in 8 % (7/88 pts) necessitating reoperation
						44 % (4/9) in pts with neurologic complaints	19 % (6/31 pts) with screw in second sacral body had neurologic complications
Peng et al. (2006)	18	n.k.	Cannulated screws	Single-plane vs. biplane 2-D fluoroscopy	100	0 % @ radiography	5 % (1/18) superficial wound infection
Arand et al. (2004)	10	10	22 cannulated screws	2D-fluoroscopy-based navigation	95	5 % (1/22) @ CT due to bending of guide wire	n.k.
			11: 7.5 mm				
			11: 6.5 mm				
Stöckle et al. (2004)	28	28	7.3-mm cannulated screws	2D-fluoroscopy based navigation	96	(4 %) 1/28 @ CT	1 malreduction of the posterior pelvic ring (4 %)
Grützner et al. (2002)	7	7	7.3-mm cannulated screws	Optoelectronic navigation	86	(14 %) 2/14 @ CT	None
Jacob et al. (1997)	13	27	7-mm cannulated screws	CT navigation	93	(7 %) 2/27	8 % (1/13) pulmonary embolism
							8 % (1/13) superficial wound infection
							8 % (1/13) broken screw after 1 year

Keating et al. (1999)	38	85	Cannulated screws	2D-fluoroscopy	87	13 % (5/38) pts @ radiography	Early complications 13 % (5/38) pulmonary embolism 14 % (3/22) deep infection in pts with ORIR 0 % (0/16) with CRPF Malunions 44 % (15/34) malunions 57 % (4/7) malunions in pts without anterior fixation Late complications 26 % (10/38) gradual loss of reduction @ 2 month 85 % (22/26) troublesome pain

essence, for acetabular fractures, excellent results have been published for 2D fluoroscopy guidance by Starr et al. (1998, 2001). Very precise (above 90 % adequate positioning) results have been obtained for CT guidance by several groups for ilio-sacral as well as acetabular screw fixation (Jacob et al. 1997, 2000a). Excellent results have been reported for both two-dimensional (2D) fluoroscopy and CT-based navigation systems (Jacob et al. 1997; Peng et al. 2006).

15.3.5 Complications

Considering the quality criteria mentioned above, and with appropriate procedure experience, the complication rate is extremely low with CT guidance and/or navigation. According to the literature, complications of ilio-sacral screw usage include fixation failures, misplaced screws, nerve injuries, infections, and poor posterior pelvic reduction, among others (Routt et al. 1995b; Keating et al. 1999). In reports on 2D fluoroscopy, guidance in type B fractures up to 8 % (7/88) of all patients and 19 % (6/31) of the subgroup with a screw into the second sacral body exhibited neurological complaints and needed reoperation in ilio-sacral screw fixation, making the latter a potential risk factor. In addition, 7 % (15/220) malpositioned screws were detected in all patients who underwent postoperative CT and even 44 % (4/9) in the subgroup with neurological complaints (van den Bosch et al. 2002). Although this is in contrast to better results reported earlier, it nevertheless emphasizes that patients with malpositioned screws are at higher risk to develop iatrogenic neurological injury. Keating et al. (1999) reported unusually high rates of pulmonary embolism, deep infection, late loss of reduction, and pain within a series, with 58 % (22/38) of the patients undergoing ORIF and not CRPF.

Summary

Minimally invasive percutaneous screw fixation of the pelvic ring in combination with closed, minimal access, or open reduction is safe and can be successfully applied to a variety of sacral, iliac, and pubic fractures and combinations thereof. The placement of sacroiliac and superior pubic ramus screws is the most widely used examples of this technique. Treatment of acetabular fractures is also feasible, with the restriction that a precise reduction of joint surfaces has to be achieved before percutaneous fixation is attempted to reduce the risk of developing secondary osteoarthritis. A critical and rational interdisciplinary selection of the best treatment modality for every patient is of extraordinary importance and may often be the most difficult part within the treatment process. An excellent quality of pre- and intraoperative imaging, image guidance, navigation, or robotic assistance is crucial for a good outcome.

Key Points

- Closed reduction and percutaneous osteosynthesis of the pelvic ring under image guidance is well feasible.
- Closed reduction and percutaneous osteosynthesis of the acetabulum is well feasible in selected cases.
- Radiologists performing percutaneous osteosynthesis of the pelvis need to know the capabilities and limitations of other open and minimal invasive operation techniques.
- A close cooperation between orthopedic surgeon and interventional radiologist is mandatory.

15.4 CT- and MR-Guided Arthrography

Gabriele A. Krombach and Oliver Wüsten

15.4.1 Introduction

Computed tomography (CT) and magnetic resonance (MR) arthrography are nowadays routinely used for evaluation of many joint disorders. MRI offers an inherent good contrast between skeletal muscle, cartilage, and ligaments. However, the subtle anomalies searched for in chronic joint disorders are difficult to assess on conventional MR images. It was soon recognized that the presence of intra-articular fluid improves visualization of the complex anatomical structures and subtle injuries, owing to the distension of the joint capsule. This finding has been termed the "arthrogram effect." Since intra-articular fluid is seldom present in subacute or chronic injury, direct injection of fluid has been introduced into clinical routine imaging to increase the sensitivity of the MR study in patients, in whom intra-articular pathologies are suspected. In order to allow for differentiation between leakage of fluid from the articular space and bursal effusion, diluted contrast medium is used instead of pure saline solution, which does not allow for this differentiation.

On CT, skeletal muscle has a density of approximately 50 Hounsfield units (HU), while cartilage, ligaments, and menisci have a slightly higher density, ranging from 79 to 90 HU. These small differences do not allow differentiation of these structures from each other. In CT arthrography, distension of the joint capsule as well as delineation of ligaments and cartilage due to enhanced contrast is obtained from injection of diluted iodinated contrast medium.

15.4.2 Indications

In general, CT or MR arthrography can be performed in any joint in which conventional arthrography is possible:

- In the shoulder, arthrography is commonly performed if a rotator cuff tear is suspected and in order to asses shoulder instability or injuries of the glenoid labrum.
- In the elbow, arthrography is carried out if collateral ligament tears are suspected.
- Arthrography of the wrist is applied for evaluation of the ligaments and triangular fibrocartilage.
- In the hip, arthrography can detect and differentiate CAM and PINCER femoroacetabular impingement.
- Arthrography of the knee is indicated if a residual or recurrent meniscal tear is suspected following meniscal surgery.
- In the ankle, arthrography can be used in patients in whom ligamentous damage is suspected but not assessable with conventional imaging.
- In all joints, direct arthrography can also be helpful in the assessment of loose bodies and cartilage lesions.

Arthrography is contraindicated if bacterial arthritis is suspected or if the periarticular soft tissue is infected. Some authors refuse to obtain arthrographies if conventional MR imaging has not been obtained. Written informed consent must be obtained at minimum 24 h prior to the intervention, and coagulation disorders need to be excluded.

15.4.3 Material

Usually, a standard 20-G puncture needle with an end hole (7–12-cm spinal needle for shoulder, hip, or knee; shorter needle for wrist and ankle) is used. In addition, a connecting tube, a stopcock, and a 10- or 20-ml syringe are required (Fig. 15.24). If double contrast is used, a bacterial filter is connected to the connecting tube before injection of air is started.

15.4.3.1 Contrast Medium

CT-Arthrography

For big joints, such as the shoulder and hip, either the double contrast or the monocontrast technique might be applied, while in small joints (wrist, elbow) only the monocontrast technique is possible. In order to obtain double contrast, intra-articular

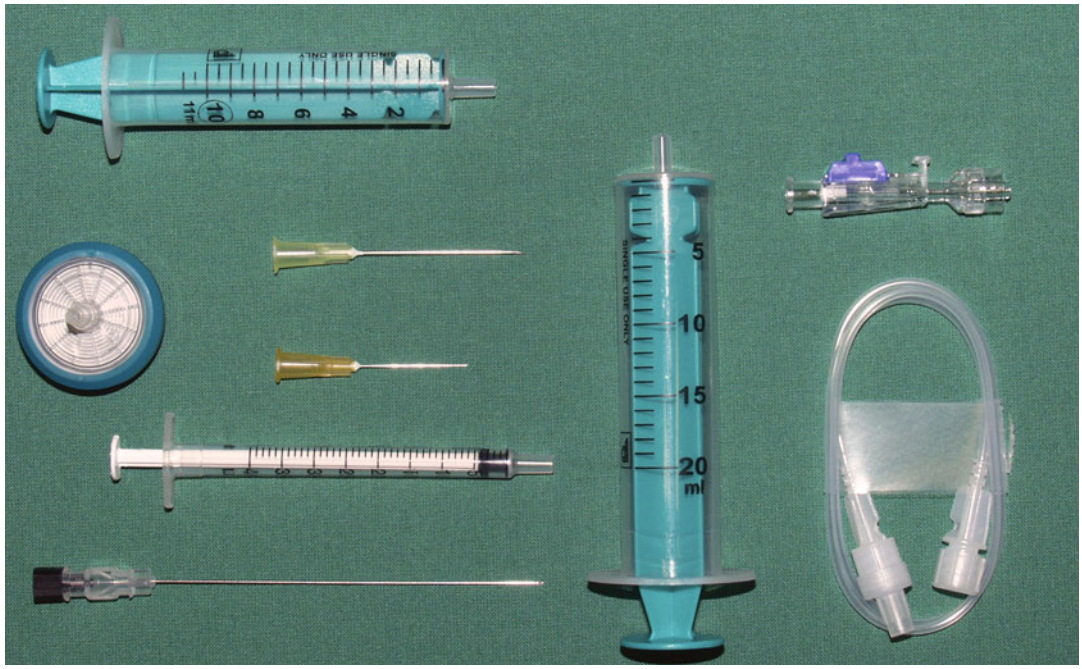

Fig. 15.24 Self-assembled sterile set for arthrography, containing syringes for local anesthesia (10-ml syringe), mixture of contrast medium (20 ml), and dosing of small amounts of MR contrast medium (1 ml), a connecting tube, a stopcock, a bacterial filter (used if air is injected), a 20-G spinal needle, a 22-G needle for local anesthesia, and an 18-G needle for filling the syringe with local anesthesia

injection of 2–3 ml contrast material is followed by injecting 12–15 ml air. Usually, a contrast medium containing 240 mg of iodine per ml is applied. If the concentration is higher, beam-hardening artifacts might occur. Nonionic iso-osmolar contrast material is preferred, since the osmotic effect and consecutive dilution of the contrast material as well as resorption from the articular space is less pronounced compared to hyperosmolar contrast medium. For the monocontrast technique, 10 ml contrast medium can be diluted with 5 ml saline solution and 5 ml lidocaine 1 %.

MR-Arthrography

Monocontrast is used for all joints since intra-articular air would cause susceptibility artifacts arising from the fluid air interface. The signal intensity, obtained from the injected diluted contrast medium, depends on the concentration of gadolinium and the field strength. At 1.5 T, concentrations ranging from 1:200 to 1:250 render optimal signal intensity on T1-weighted images. Several ways to obtain this concentration are possible. For example, 0.8 ml gadopentetate dimeglumine can be added to 100 ml of saline solution. Next, 10 ml of this solution can be mixed with 5 ml of iodinated contrast medium and 5 ml of lidocaine 1 %. The resulting solution has a dilution ratio of 1:250 gadolinium. In Europe and Australia, a precast preparation for intra-articular injection, containing 0.0025 mmol/ml Gd-DOTA (gadoterate meglumine), can be purchased (Artirem, Guerbet). The concentration of gadolinium of this solution is less than 1:200; however, it does not contain an anesthetic or iodinated contrast medium. Usually, an isovolumetric T1-weighted sequence with fat suppression is obtained.

15.4.4 Technique

15.4.4.1 Shoulder

Many investigators still prefer fluoroscopic guidance for needle placement (Fig. 15.25). However,

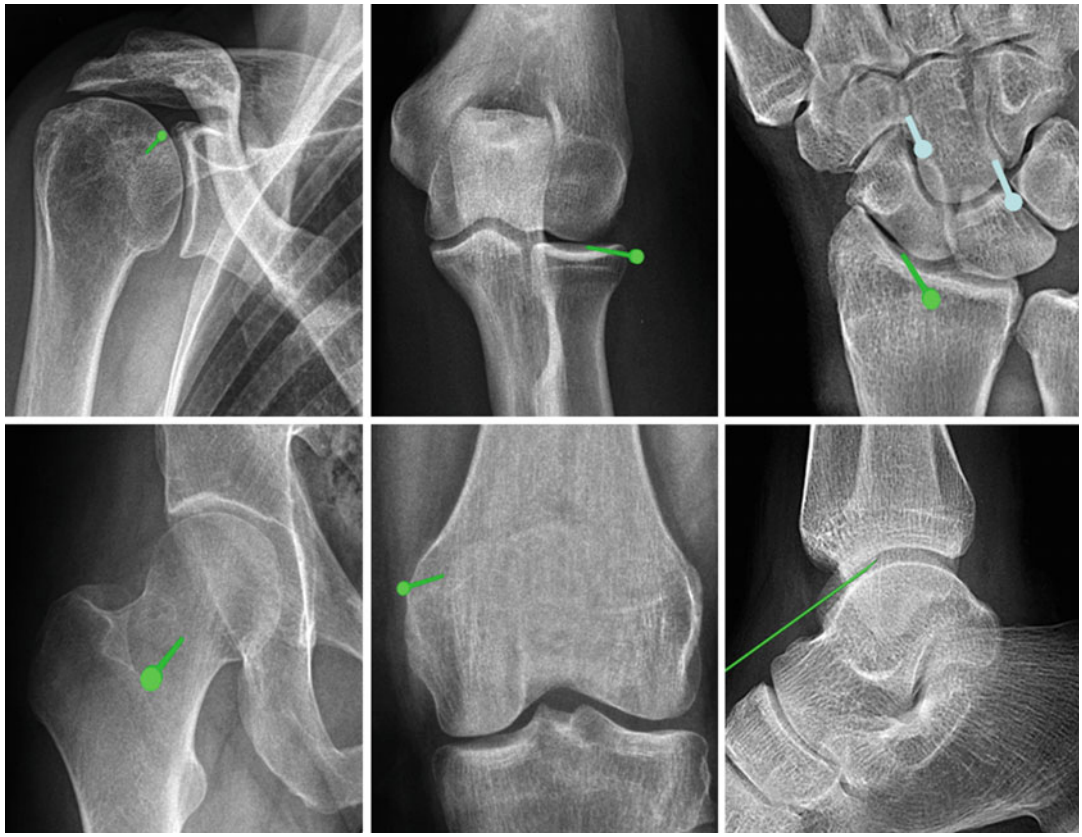

Fig. 15.25 Injection sites at the different joints for fluoroscopically guided puncture. With CT and MR guidance, identical approaches should be used. For the wrist, the *green needle* is located at the injection site for the radiocarpal compartment. The *blue needles* are located at the two alternative injection sites for injection into the midcarpal compartment

arthrography in general can be performed using solely MR or CT guidance. A clear advantage of applying only one modality for puncture and imaging is easier patient scheduling and workflow. For MR guidance, real-time imaging can be applied (Fig. 15.26). In this case, the needle can be advanced into the joint space under direct imaging control. This technique usually allows accessing of the joint space fast and reliably. Furthermore, the joints can be punctured using the widely established approach of stepwise CT or MR guidance. In this case, an external marker is placed over the possible entry site on the patient's, skin and a scan is obtained for planning the puncture. The target can then be chosen and the puncture path planned on the images. In the next step, the needle tip is placed on the selected entry point on the patient's skin and the angle of the needle adjusted according to the path obtained from the planning scan. Next, the needle can be advanced stepwise and the respective position of the needle tip repeatedly controlled. Alternatively, continuous CT or MR fluoroscopy may be used.

Regardless of which modality and technique has been chosen for the puncture, before arthrography of the shoulder is performed, anteroposterior radiographs in external and internal rotation of the shoulder should be obtained to assessing calcifications in the rotator cuff tendons. If calcifications have not been identified prior to CT arthrography, they can be misinterpreted as leakage of contrast medium on the CT images, suggestive of a tear. On MR arthrography, they are usually overlooked, owing to similar signal of tendons and

calcifications (Zubler et al. 2007). Supine positioning of the patient with the shoulder in external rotation allows for best access to the joint via the anterior approach. The optimal entry point is located at the upper inner quadrant of the humeral head or at the junction of the middle and inferior thirds of the humeral head just lateral to the medial cortex (Fig. 15.25). After this entry point has been marked on the skin, the region is prepped and draped with sterile cover sheds, and local anesthesia is administered. Puncture and injection of contrast medium solution must be performed under sterile conditions. The needle can then be inserted. If fluoroscopy is used, the needle hub is centered over the tip of the needle on the images in order to ensure that the path is perpendicular to the fluoroscopic beam. If MR or CT guidance has been chosen, the puncture is planned and performed as described above. The needle should be inserted and advanced together with the stylet so that injury of the tissue is minimized and clotting inside the needle avoided. However, it has to be kept in mind that the joint capsule is pain sensitive and small amounts of local anesthesia might repeatedly be injected as the needle is advanced if the patient complains about the pain. As soon as bone is reached, the needle can be pulled back slightly. Usually, a test injection of 2 ml of local

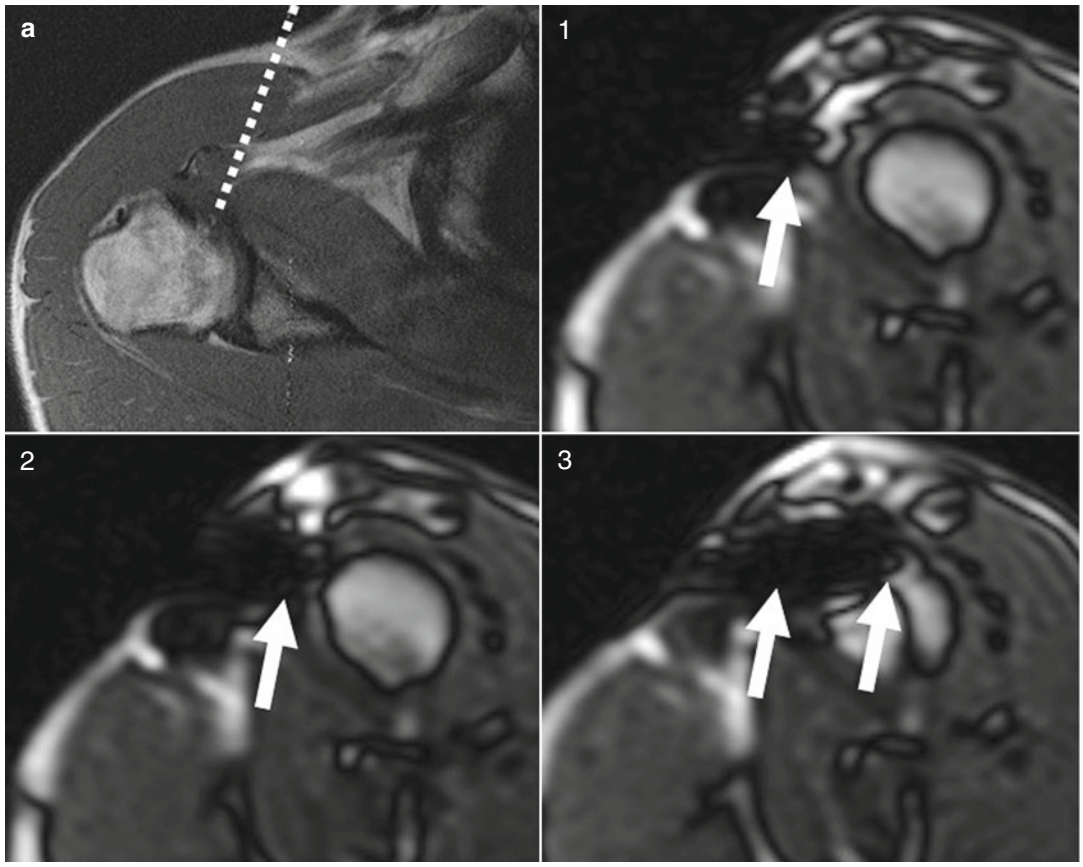

Fig. 15.26 (**a**) MR-guided arthrography. The puncture path can be planned on an axial slice (*top row left image*, *dotted line*). In the next step, a real-time sequence is planned in the course of the desired puncture path so that insertion of the needle can be visualized and guided with these images (*1–3*, the *arrows* mark needle artifact). (**b**) Injection of contrast-medium-doped solution, visualized on real-time true-FISP images. The increasing filling of the joint space is visible from *the top left to bottom right image* (*arrows*). (**c**) Axial true FISP prior (*left*) and after MR-guided injection of contrast solution into the articular space (*right*). The tear of the labrum cannot be visualized on the conventional MR image, but is clearly visible on MR arthrography (*arrow*)

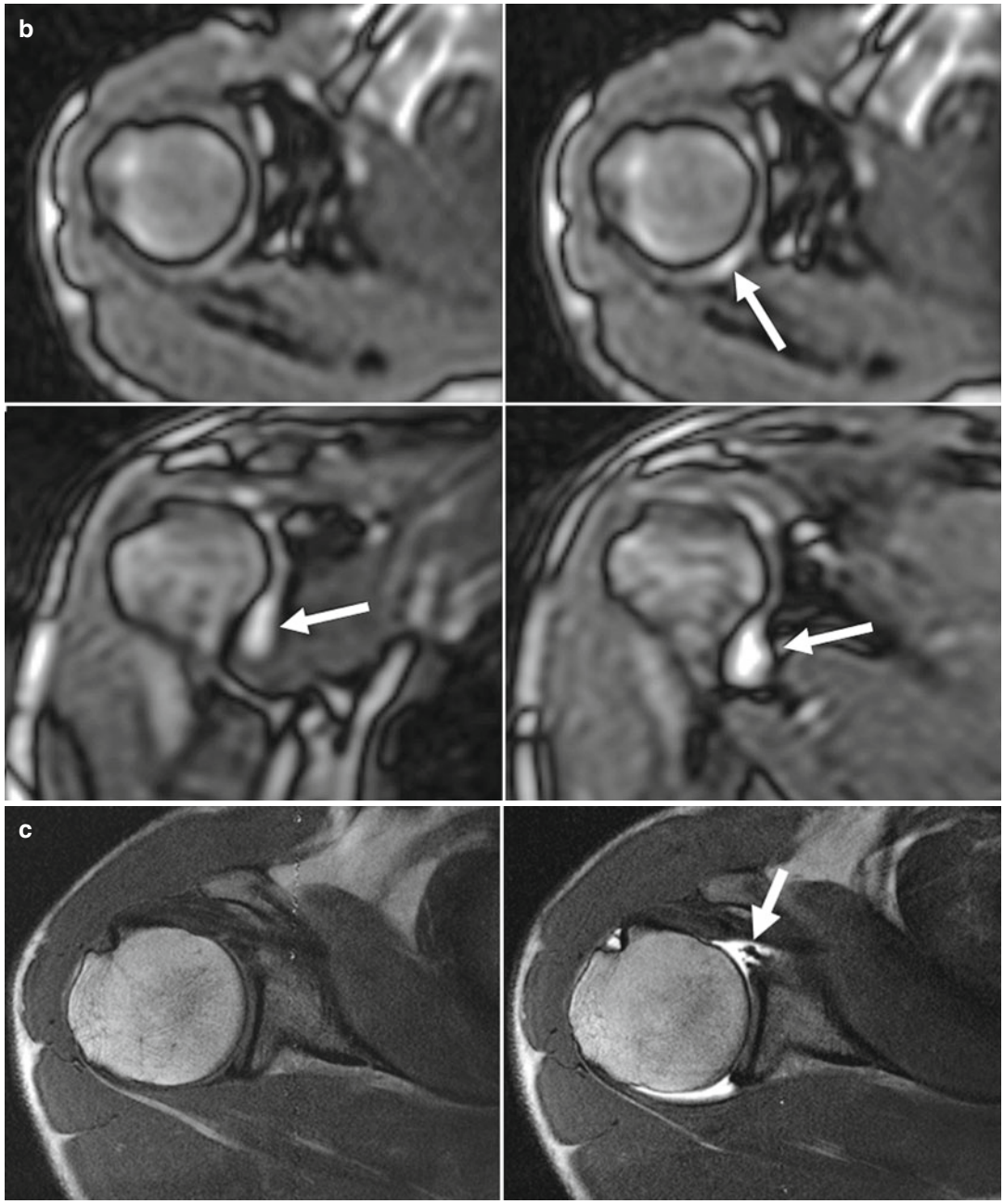

Fig. 15.26 (continued)

anesthetic confirms needle position in a compartment (low resistance) and further anesthetizes the joint. If joint effusion is present, the fluid should be aspirated. With injection, care must be taken to avoid air bubbles, and fluid should be dripped into the hub of the needle so that a wet-to-wet connection can be performed with the prefilled connecting tube and the syringe. By this means, injecting air bubbles can be avoided. One can inject up to 2 ml of the contrast medium solution in order to verify intra-articular position of the needle. If the puncture has been performed with fluoroscopy

guidance, distribution of contrast medium can directly be controlled using fluoroscopy. This is also feasible, using real-time MR imaging or CT fluoroscopy. If the intra-articular position has been verified, 12 ml of either the respective contrast medium solution are injected for monocontrast or air for CT arthrography with double contrast. Arthrography should be performed within a time frame of 40 min after injection of the contrast medium solution. Otherwise, resorption of contrast medium and air will result in inadequate distension of the joint capsule and insufficient image quality.

The shoulder is imaged with the arm placed in neutral position. If the anteroinferior labrum must be assessed, sensitivity of arthrography can be further increased by imaging in abduction and external rotation (ABER position) of the shoulder. The ABER position is achieved by elevating the patient's arm, flexing the elbow, and placing the patient's hand posterior to the contralateral aspect of the head.

In CT, submillimeter axial slices are obtained and multiplanar reconstructions performed. In MR imaging, preferably an isovolumetric 3D T1-weighted (gradient-echo) sequence with fat suppression should be obtained in an axial and paracoronal imaging plane, the later running perpendicular to the glenoid. A small field of view and a surface coil should be used for MR arthrography in order to obtain images with high resolution and increased signal-to-noise ratio. If isovolumetric voxel is obtained, multiplanar reformations can be computed from source data.

15.4.4.2 Elbow

The patient is placed prone, the arm elevated, and the elbow flexed. The joint can either be entered laterally over the radial head or posterolaterally between olecranon, humerus, and radial head (Fig. 15.27). The posterolateral approach has the advantage of avoiding the lateral collateral ligament complex on the puncture path. A total of up to 10 ml contrast medium solution can be injected into this joint. The ulnar and radial collateral ligaments are best visualized in a coronal plane tilted 20° posteriorly.

15.4.4.3 Wrist

Arthrography of the wrist can be performed with single- (radiocarpal), double- (midcarpal and radiocarpal), or triple-compartment (in addition distal radioulnar joint) injection. Usually, injection is started radiocarpal. The scapholunate and lunotriquetal ligaments merge with the articular capsule. They are horseshoe-like shaped and completely separate the radiocarpal and midcarpal compartments. Only if one of the ligaments has a full tear, fluids can transverse between the compartments. Accordingly, injection starts at the radiocarpal compartment. If the contrast medium does not spontaneously enter the midcarpal compartment, a complete tear is excluded (Fig. 15.28). Under this condition, contrast medium should be injected into the midcarpal compartment in order to allow assessment of a partial tear. For injections, the patient is in prone position, the arm elevated, and the palm pointing downward ("superman position"). The needle is introduced between the middle of the scaphoid and the radius for filling of the radiocarpal compartment. For carpal injection, the needle is inserted between lunate, capitate, hamate, and triquetrum or at the distal scaphoid. For injection into the radioulnar joint space, the distal part of the ulnar head just lateral of the medial cortical bone is targeted. Approximately 3–5 ml of fluid can be injected in each of the three compartments. Scanning of the wrist should also be performed in prone position, arm elevated, and palm pointing downward. To counteract radial or ulnar deviation, it might be helpful to fully extend the arm of the patient. For delineation of the ligaments, coronal and axial images should be obtained. For assessment of the cartilage, coronal and sagittal images should be acquired. The fibrocartilage complex is best visualized on sagittal images.

15.4.4.4 Hip

The patient is placed supine, a bolster placed under the knees, and the leg positioned in internal rotation. The symptomatic side can be elevated to 10–15°. This position increases the distance from the puncture path to the neurovascular bundle, which then decreases the probability

Fig. 15.27 Arthrography of the elbow: (**a**) *left image*: needle position, *middle image* ap view, *right image*: lateral view after injection of contrast medium. (**b**). *left image*, Normal elbow. The radial (*open arrow*) and ulnar collateral ligament (*arrow*) are visible. The contrast medium solution fills the space around the radial neck (*asterisk*). *Right images*: intra-articular loose body (*arrow*)

of infiltration of the femoral nerve. Anesthesia of the femoral nerve can cause fall of the patient when trying to get up after the procedure. To maintain internal rotation of the hips, the feet may be taped together. Mainly either the superior lateral quadrant of the femoral head or the middle of the femoral neck is used to enter the joint. The imaging plane should be axial and coronal (Fig. 15.29). If sports-related labral tears are suspected, oblique images, oriented parallel to the femoral neck on coronal images, should be acquired. The anterosuperior labrum is best visualized in this imaging plane.

15.4.4.5 Knee

In supine position of the patient, the joint is accessed medially between patella and femur. The injection can safely be performed without fluoroscopy guidance. Axial and sagittal images should be acquired or reconstructed from isovolumetric source data.

15.4.4.6 Ankle

The patient is in supine position and the x-ray tube angled laterally. The needle is introduced from anterior, medial to the extensor hallucis longus muscle and slightly tilted cranially. To avoid

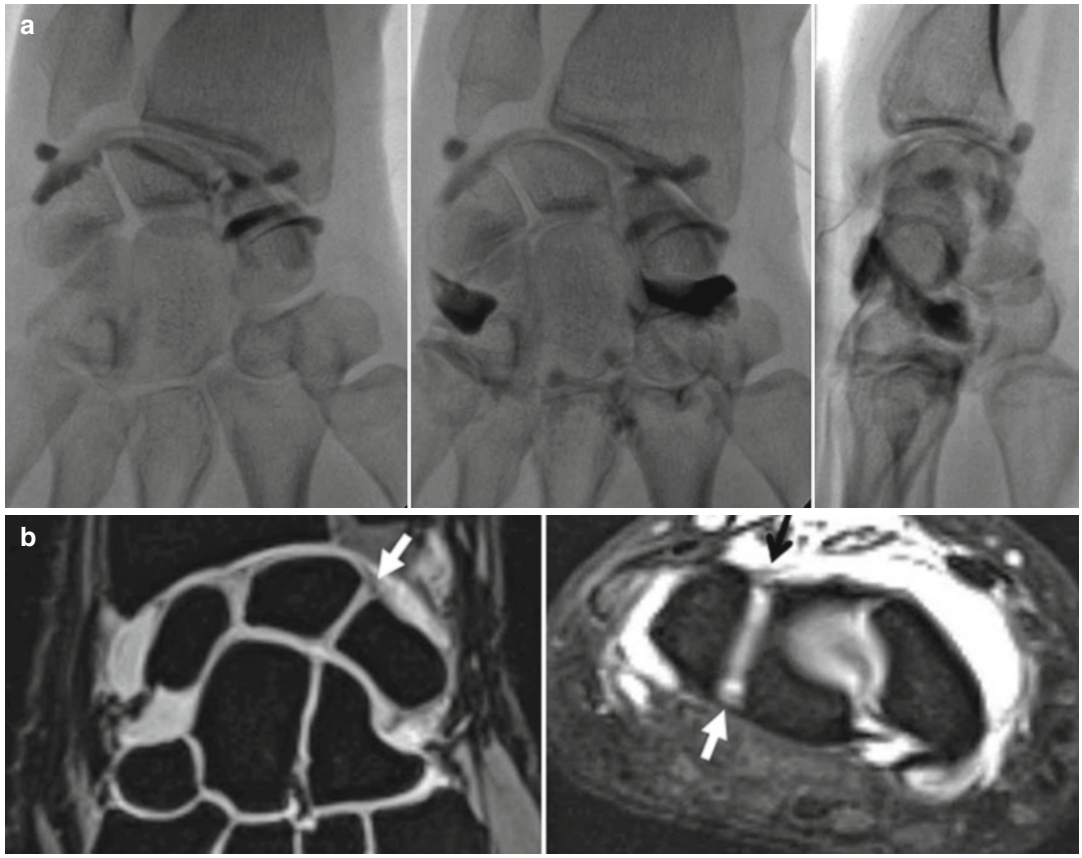

Fig. 15.28 (**a**) Arthrography of the normal wrist, after injection into the radiocarpal compartment; the contrast medium does not enter the midcarpal compartment. The midcarpal compartment was filled with a second injection of 3 ml contrast medium solution (*middle* and *right images*). (**b**) coronal and axial MR images: on coronal images, the proximal part of the scapholunate ligament is visible (*arrow*). Rupture of this ligament is present in over 50 % of people over 50 years and usually does not cause clinical symptoms. On axial images, the dorsal (*open black arrow*) and the volar (*white arrow*) parts of the scapholunate ligament are assessable

the dorsal pedal artery, it should be palpated prior to needle placement. Approximately 6 ml fluid can be injected into this joint. Images should be acquired in the sagittal and coronal plane.

15.4.5 Results

15.4.5.1 Shoulder

For the diagnosis of full thickness tears of the rotator cuff, both sensitivity and specificity approach 100 % for MR arthrography. For partial tears the corresponding values are 80 % and >95 %, respectively (Waldt et al. 2007). Sensitivity of CT arthrography is 73 % for full thickness tears of the rotator cuff (Bachmann et al. 1998). The characteristic imaging finding for a full thickness tear is presence of extra-articular contrast medium. Partial tears fill with contrast medium.

Labral tears present as defects within the labrum that fill with contrast medium. Anatomical variants represent possible pitfalls in assessing labral integrity. A small normal labrum can be difficult to differentiate from a blunted, deficient labrum. At two locations, a sublabral sulcus separates the normal labrum from the interface of the articular cartilage: anterosuperior between the origins of the inferior and middle glenohumeral ligament and superior at the junction of the

Fig. 15.29 Arthrography of a normal hip (*left*), *arrow pointing* to the sulcus along its junction with the cartilage. On the *right image*, a small lesion of the cartilage (*open arrow*) and PINCER impingement (*arrow*) is present

labrum with the bicipital tendon. Sulci can increase in size with age and then fill with contrast medium. This finding can be misinterpreted for a labral tear. A recent study evaluated interobserver agreement for evaluation of CT arthrography (Fogerty et al. 2011). These authors encountered a relatively low level of agreement and stress the high importance of exact knowledge of anatomical structures, variants, and imaging appearance of pathological findings. Different authors encountered a sensitivity for detecting labral tears of 96 % for MR- and 76 % for CT arthrography and specificity 96 % (MR-) and 92 % (CT arthrography), respectively (Blitzer et al. 2004). Lesions of the cartilage are more difficult to assess due to the concave shape of the articular facet. In a recent study, sensitivity for glenoidal cartilage lesions was 75 % and specificity 63 % on MR arthrography (Guntern et al. 2003) and 80 and 94 % on CT arthrography (Lecouvet et al. 2007).

15.4.5.2 Elbow

Although detailed description of all pathologic findings is beyond the scope of this chapter, tears of the ulnar collateral ligament present as defects that fill with contrast medium. Complete rupture causes extravasation of the contrast medium into the surrounding soft tissue. For tears of the ulnar collateral ligament, a comparative study using findings at surgery as the gold standard found a sensitivity of 86 % and a specificity of 100 % for CT arthrography (Timmerman et al. 1994). For MR arthrography, sensitivity is 86 % for partial and 95 % for complete tears of the ulnar collateral ligament, and specificity for both lesion types is 100 % (Schwartz et al. 1995). Lesions of the radial collateral ligament are extremely rare.

Cartilage lesions present as indentations, filling with contrast medium. For detection of cartilage lesions, CT arthrography had a sensitivity of 80 % and MR arthrography 78 % in a study conducted on cadaver specimen (Waldt et al. 2005). Specificity was 93 % for CT- and 95 % for MR arthrography.

Loose bodies become visible as round- to oval-shaped hypointense or hypodense regions within the contrast-medium-filled joint space (Fig. 15.28b). Care has to be taken to not misinterpret injected air bubbles for loose bodies on MR arthrography. Regarding the detection of loose bodies, a sensitivity of 88 and 100 % has been reported for MR- and CT arthrography, respectively (Dubberley et al. 2005). Specificity

was 20 % for MR- and 70 % for CT arthrography and did not exceed that of plain film radiography (specificity 71 %, sensitivity 84 %). Synovial plicae may cause locking of the elbow joint. However, plicae are a common finding in the elbow, and clinical correlation of such a finding is thus of utmost importance.

15.4.5.3 Wrist

A full tear of the triangular fibrocartilage becomes evident as presence of contrast medium in the distal radioulnar joint. Extrinsic ligament tears are not accessible on arthrography. In the interosseous ligaments, surface irregularity is a sign for partial tear. In the evaluation of CT arthrography, sensitivity and specificity of 94 and 86 % have been found for detecting tears of the scapholunate ligament, 85 and 79 % for detecting tears of the lunotriquetral ligament, and 30 and 94 % for diagnosing tears of the triangular fibrocartilage complex, compared to arthroscopy (Bille et al. 2007). In another study, a direct comparison of MR imaging, CT- and MR arthrography has been performed (Moser et al. 2007). Sensitivity and specificity were 59 and 70 % (MR imaging), 95 and 96 % (CT arthrography), and 68 and 87 % (MR arthrography) for tears of the scapholunate ligament; 30 and 94 % (MR imaging), 100 and 94 % (CT arthrography), and 60 and 97 % (MR arthrography) for tears of the lunotriquetral ligament; 27 and 100 % (MR imaging), 100 and 100 % (CT arthrography), and 82 and 100 % (MR arthrography) for tears of the triangular fibrocartilage complex; and 30 and 100 % (MR imaging), 100 and 100 % (CT arthrography), and 40 and 100 % (MR arthrography) for cartilage abnormalities. In this study, partial tears of the ligaments were better visualized with CT arthrography.

15.4.5.4 Hip

Femoroacetabular impingement is a cause for labral tears and cartilage lesions. CAM and PINCER impingement can be differentiated. In PINCER, acetabular overcoverage of the femur leads to restricted motion and consecutive labral tear. In CAM, a nonspherical shape of the femur in combination with a reduced depth of the femoral waist leads to labral tears (Pfirrmann et al. 2006). For treatment, the differentiation of cam and pincer is important, in addition to the diagnosis of a labral tear. Sensitivity and specificity of CT arthrography compared to arthroscopy are reported to approach 97–100 % and 87 % for labral tears and 88 and 82 % for acetabular cartilage lesions (Nishii et al. 2007; Christie-Large et al. 2010). Sensitivity and specificity were found to be 92 and 100 %, respectively, for detection of labral tears on MR arthrography compared to arthroscopy (Toomayan et al. 2006). The sensitivity and specificity in the diagnosis of cartilage lesions reach 79 and 77 % (Schmid et al. 2003). A recent meta-analysis demonstrated that MR arthrography has a higher sensitivity for labral tears compared to conventional magnetic resonance imaging (Smith et al. 2011); however, no direct comparison between both techniques in the same patients has been performed yet.

15.4.5.5 Knee

Recurrent meniscal tears might be difficult to differentiate from degenerative changes after partial resection of menisci. On direct arthrography, tears fill with contrast medium, while degenerative changes and scars do not. Sensitivity and specificity of MR arthrography were reported to be 90 and 78 %, and that of conventional MR imaging were 86 and 67 % (White et al. 2002). For CT arthrography sensitivity and specificity have been reported to approach 100 and 78 % for detection of meniscal tears (Mutschler et al. 2003). Arthrography has also been demonstrated being useful in the diagnosis of intra-articular bodies and cartilage lesions (Brossmann et al. 1996).

15.4.5.6 Ankle

MR arthrography has a sensitivity of 71 % and specificity of 96 % for detection of ligament tears (second- and third-degree sprains) (van Dijk et al. 1998). First-degree sprains are not associated with a tear and cannot be diagnosed on MR

arthrography. In this instance, a region of high signal intensity is visible within the ligament on T2-weighted images. Second-degree sprains present as a contrast-medium-filled defect of the ligament, and third-degree sprains are characterized by leakage of the contrast medium into the periarticular space.

In a current study, accuracy of MR arthrography for detection of cartilage lesions in the talus/tibia/fibula was 88 %/88 %/94 % and for CT arthrography 90 %/94 %/92 % (Schmid et al. 2003).

15.4.6 Complications

Complications following direct arthrography are rare. The most feared complication is infection (septic arthritis) of the joint, which has an incidence of 0.003–0.01 % (Schulte-Altedorneburg et al. 2003). The leading symptoms are increasing pain in the affected joint, especially when moving, and swelling and redness. Onset of symptoms is usually several days after the injection. This major complication must be immediately treated with antibiotics and eventually joint drainage in order to avoid destruction of the cartilage. Hematoma or hemarthros is also possible as a sequel of arthrography, especially in patients with coagulopathy.

In a case report, cerebral air embolism has been reported after injection of 20 ml air into the ankle (Müller et al. 2010). Neurologic symptoms were present; however, the patient fully recovered after hyperbaric oxygen therapy.

Summary

Direct arthrography extents the diagnostic capabilities of conventional imaging by far. It is the method of choice in patients with suspected partial tear of the rotator cuff, for the diagnosis of meniscal tears in the postoperative knee, and for assessment of the labrum in the hip. In the other indications, it increases the sensitivity and specificity of MR imaging and enables surveying ligaments and cartilage in CT. In the hand of an experienced radiologist, complications are extremely rare. However, it turns a noninvasive examination into a mildly invasive procedure. Accordingly, the indication for direct arthrography has to be critically reviewed in each patient. In general, MR arthrography should be preferred, if MR is available and contraindications for MR imaging are not present, in order to limit radiation exposure. Joint puncture with cross-sectional image guidance, particularly MR guidance, allows for a safe direct puncture of the joint and helps to reduce paravasation that might mimic pathology. Moreover, this technique permits online monitoring of intra-articular contrast injection, providing additional information on the joint.

Key Points

- Direct arthrography extends the diagnostic capabilities of CT and MR imaging.
- CT- and MR-guided joint puncture is safely feasible.
- Complications are extremely rare if the procedure is carried out under strictly sterile conditions.

References

Radiofrequency Ablation of Benign Bone Tumor

Adam G, Keulers P, Vorwerk D et al (1995) The percutaneous CT-guided treatment of osteoid osteomas: a combined procedure with a biopsy drill and subsequent ethanol injection. Rofo 162:232–235

Akhlaghpoor S, Ahari AA, Ahmadi SA et al (2010a) Histological evaluation of drill fragments obtained during osteoid osteoma radiofrequency ablation. Skeletal Radiol 39:451–455

Akhlaghpoor S, Aziz Ahari A, Arjmand Shabestari A et al (2010b) Radiofrequency ablation of osteoid osteoma

in atypical locations: a case series. Clin Orthop Relat Res 468:1963–1970
Aschoff AJ, Merkle EM, Emancipator SN et al (2002) Femur: MR imaging-guided radiofrequency-ablation in a porcine model – feasibility study. Radiology 225:471–478
Barei DP, Moreau G, Scarborough MT et al (2000) Percutaneous radiofrequency ablation of osteoid osteoma. Clin Orthop Relat Res 373:115–124
Callstrom MR, Charboneau JW, Goetz MP et al (2002) Painful metastases involving bone: feasibility of percutaneous CT- and US-guided radio-frequency ablation. Radiology 224:87–97
Cantwell CP, Obyrne J, Eustace S (2004) Current trends in treatment of osteoid osteoma with an emphasis on radiofrequency ablation. Eur Radiol 14:607–617
Cantwell CP, O'Byrne J, Eustace S (2006) Radiofrequency ablation of osteoid osteoma with cooled probes and impedance-control energy delivery. AJR Am J Roentgenol 186(5 Suppl):S244–S248
Christie-Large M, Evans N, Davies AM et al (2008) Radiofrequency ablation of chondroblastoma: procedure technique, clinical and MR imaging follow up of four cases. Skeletal Radiol 37:1011–1017
Cioni R, Armilotta N, Bargellini I et al (2004) CT-guided radiofrequency ablation of osteoid osteoma: long-term results. Eur Radiol 14:1203–1208
Corby RR, Stacy GS, Peabody TD et al (2008) Radiofrequency ablation of solitary eosinophilic granuloma of bone. AJR Am J Roentgenol 190:1492–1494
Erickson JK, Rosenthal DI, Zaleske DJ et al (2001) Primary treatment of chondroblastoma with percutaneous radio-frequency heat ablation: report of three cases. Radiology 221:463–468
Davies M (2002) The diagnostic accuracy of MR imaging in osteoid osteoma. Skeletal Radiol 31:559–569
Donkol RH, Al-Nammi A, Moghazi K (2008) Efficacy of percutaneous radiofrequency ablation of osteoid osteoma in children. Pediatr Radiol 38:180–185
Gangi A, Alizadeh H, Wong L et al (2007) Osteoid osteoma: percutaneous laser ablation and follow-up in 114 patients. Radiology 242:293–301
Gebauer B, Tunn PU, Gaffke G et al (2006) Osteoid osteoma: experience with laser- and radiofrequency-induced ablation. Cardiovasc Intervent Radiol 29:210–215
Ghanem I, Collet LM, Kharrat K et al (2003) Percutaneous radiofrequency coagulation of osteoid osteoma in children and adolescents. J Pediatr Orthop B 12:244–252
Hoffmann RT, Jakobs TF, Kubisch CH et al (2010) Radiofrequency ablation in the treatment of osteoid osteoma-5-year experience. Eur J Radiol 73:374–379
Jaffe HL (1935) "Osteoid osteoma", a benign osteoblastic tumor composed of osteoid and atypical bone. Arch Surg 31:709–728
Kjar RA, Powell GJ, Schilcht SM et al (2006) Percutaneous radiofrequency ablation for osteoid osteoma: experience with a new treatment. Med J Aust 184:563–565
Lindner NJ, Scarborough M, Ciccarelli JM et al (1997) CT-controlled thermocoagulation of osteoid osteoma in comparison with traditional methods. Z Orthop Ihre Grenzgeb 135:522–527
Lindner NJ, Ozaki T, Roedl R et al (2001) Percutaneous radiofrequency ablation in osteoid osteoma. J Bone Joint Surg Br 83:391–396
Mahnken AH, Tacke JA, Wildberger JE et al (2006) Radiofrequency ablation of osteoid osteoma: initial results with a bipolar ablation device. J Vasc Interv Radiol 17:1465–1470
Mahnken AH, Bruners P, Delbrück H et al (2011) Radiofrequency ablation of osteoid osteoma: initial experience with a new monopolar ablation device. Cardiovasc Intervent Radiol 34:579–584
Marcove RC, Heelan RT, Huvos AG et al (1991) Osteoid osteoma. Diagnosis, localization, and treatment. Clin Orthop Relat Res 267:197–201
Martel J, Bueno A, Ortiz E (2005) Percutaneous radiofrequency treatment of osteoid osteoma using cool-tip electrodes. Eur J Radiol 56:403–408
Mastrantuono D, Martorano D, Verna V et al (2005) Osteoid osteoma: our experience using radio-frequency (RF) treatment. Radiol Med (Torino) 109:220–228
Mylona S, Patsoura S, Galani P et al (2010) Osteoid osteomas in common and in technically challenging locations treated with computed tomography-guided percutaneous radiofrequency ablation. Skeletal Radiol 39:443–449
Neumann D, Berka H, Dorn U et al (2012) Follow-up of thirty-three computed-tomography-guided percutaneous radiofrequency thermoablations of osteoid osteoma. Int Orthop 36:811–815
Omlor G, Merle C, Lehner B et al (2012) CT-guided percutaneous radiofrequency ablation in osteoid osteoma: re-assessments of results with optimized technique and possible pain patterns in mid-term follow-up. Rofo 184:333–339
Petsas T, Megas P, Papathanassiou Z (2007) Radiofrequency ablation of two femoral head chondroblastomas. Eur J Radiol 63:63–67
Peyser A, Applbaum Y, Khoury A et al (2007) Osteoid osteoma: CT-guided radiofrequency ablation using a water-cooled probe. Ann Surg Oncol 14:591–596
Pinto CH, Taminiau AHM, Vanderschueren GM et al (2002) Technical considerations in CT-guided radiofrequency thermal ablation of osteoid osteoma: tricks of the trade. AJR Am J Roentgenol 179:1633–1642
Ramnath RR, Rosenthal DI, Cates J et al (2002) Intracortical chondroma simulating osteoid osteoma treated by radiofrequency. Skeletal Radiol 31:597–602
Rimondi E, Bianchi G, Malaguti MC et al (2005) Radiofrequency thermoablation of primary non-spinal osteoid osteoma: optimization of the procedure. Eur Radiol 15:1393–1399
Rosenthal DI, Alexander A, Rosenberg AE et al (1992) Ablation of osteoid osteomas with percutaneously placed electrode: a new procedure. Radiology 183:29–33
Rosenthal DI, Hornicek FJ, Wolfe MW et al (1998) Percutaneous radiofrequency coagulation of osteoid osteoma compared with operative treatment. J Bone Joint Surg Am 80:815–821

Rosenthal D, Hornicek FJ, Torriani M et al (2003) Osteoid osteoma: percutaneous treatment with radiofrequency energy. Radiology 229:171–175
Rybak LD, Rosenthal DI, Wittig JC (2009) Chondroblastoma: radiofrequency ablation – alternative to surgical resection in selected cases. Radiology 251:599–604
Sans N, Galy-Fourcade D, Assoun J et al (1999) Osteoid osteoma: CT-guided percutaneous resection and follow up in 38 patients. Radiology 212:687–692
Schmidt D, Clasen S, Schaefer JF et al (2011) CT-guided radiofrequency (RF) ablation of osteoid osteoma: clinical long-term results. Rofo 183:381–387
Ruiz Santiago F, Castellano García Mdel M, Guzmán Álvarez L et al (2011) Percutaneous treatment of bone tumors by radiofrequency thermal ablation. Eur J Radiol 77:156–163
Sequeiros RB, Hyvonen P, Sequeiros AB et al (2003) MR imaging guided laser ablation of osteoid osteomas with use of optical instrument guidance at 0.23 T. Eur Radiol 13:2309–2314
Skjedal S, Lilleås F, Follerås G et al (2000) Real-time MRI-guided excision and cry-treatment of osteoid osteoma in os ischii: a case report. Acta Orthop Scand 71:637–638
Skonieczki BD, Wells C, Wasser EJ et al (2011) Radiofrequency and microwave tumor ablation in patients with implanted cardiac devices: is it safe? Eur J Radiol 79:343–346
Soong M, Jupiter J, Rosenthal D (2006) Radiofrequency ablation of osteoid osteoma in the upper extremity. J Hand Surg [Am] 31:279–283
Tins B, Cassar-Pullicino V, McCall I et al (2006) Radiofrequency ablation of chondroblastoma using a multi-tined expandable electrode system: initial results. Eur Radiol 14:804–810
Vanderschueren GM, Taminiau AHM, Obermann WR et al (2002) Osteoid Osteoma: clinical results with thermocoagulation. Radiology 224:82–86
Vanderschueren GM, Taminiau AH, Obermann WR et al (2004) Osteoid osteoma: factors for increased risk of unsuccessful thermal coagulation. Radiology 233: 757–762
Vanderschueren GM, Obermann WR, Dijkstra SP et al (2009) Radiofrequency ablation of spinal osteoid osteoma: clinical outcome. Spine (Phila Pa 1976) 34:901–904
Venbrux AC, Montague BJ, Murphy KPJ et al (2003) Image-guided percutaneous radiofrequency ablation for osteoid osteomas. J Vasc Interv Radiol 14: 375–380
Witt JD, Hall-Craggs MA, Ripley P et al (2000) Interstitial laser photocoagulation for the treatment of osteoid osteoma. J Bone Joint Surg Br 82:1125–1128
Woertler K, Vestring T, Boettner F et al (2001) Osteoid osteoma: CT-guided percutaneous radiofrequency ablation and follow-up in 47 patients. J Vasc Interv Radiol 12:717–722
Yip PS, Lam YL, Chan MK et al (2006) Computed tomography-guided percutaneous radiofrequency ablation of osteoid osteoma: local experience. Hong Kong Med J 12:305–309

Vertebroplasty, Osteoplasty, and Sacroplasty

Barragan-Campos HM, Vallee JN, Lo D et al (2006) Percutaneous vertebroplasty for spinal metastases: complications. Radiology 238:354–362
Bornemann R, Deml M, Wilhelm KE et al (2012) Long-term efficacy and safety of balloon kyphoplasty for treatment of osteoporotic vertebral fractures. Z Orthop Unfall 150(4):381–388
Deramond H, Depriester C, Galibert P, Le Gars D (1998) Percutaneous vertebroplasty with polymethylmethacrylate. Technique, indications, and results. Radiol Clin North Am 36:533–546
Galibert P, Deramond H, Rosat P, Le Gars D (1987) Note préliminaire sur le traitement des angiomes vertébraux par vertébroplastie acrylique percutanée. Neurochirurgie 33:166–168
Endres S, Badura A (2012) Shield kyphoplasty through a unipedicular approach compared to vertebroplasty and balloon kyphoplasty in osteoporotic thoracolumbar fracture: a prospective randomized study. Orthop Traumatol Surg Res 98:334–340
Gangi A, Kastler BA, Dietemann JL (1994) Percutaneous vertebroplasty guided by a combination of CT and fluoroscopy. AJNR Am J Neuroradiol 15:83–86
Georgy BA, Wong W (2007) Plasma-mediated radiofrequency ablation assisted percutaneous cement injection for treating advanced malignant vertebral compression fractures. AJNR Am J Neuroradiol 28:700–705
Grönemeyer DH, Schirp S, Gevargez A (2002) Image-guided radiofrequency ablation of spinal tumors: preliminary experience with an expandable array electrode. Cancer J 8:33–39
Helmberger T, Bohndorf K, Hierholzer J, Noldge G, Vorwerk D (2003) Guidelines of the German Radiological Society for percutaneous vertebroplasty. Radiologe 43:703–708 [German]
Hodek-Wuerz R, Martin JB, Wilhelm K, Lovblad KO, Babic D, Rufenacht DA, Wetzel SG (2006) Percutaneous vertebroplasty: preliminary experiences with rotational acquisitions and 3D reconstructions for therapy control. Cardiovasc Intervent Radiol 29:862–865
Huegli RW, Schaeren S, Jacob AL, Martin JB, Wetzel SG (2005) Percutaneous cervical vertebroplasty in a multifunctional image-guided therapy suite: hybrid lateral approach to C1 and C4 under CT and fluoroscopic guidance. Cardiovasc Intervent Radiol 28:649–652
Kelekis AD, Martin JB (2005) Radicular pain after vertebroplasty: complication and prevention. Skeletal Radiol 34:816
Koh YH, Han D, Cha JH, Seong CK, Kim J, Choi YH (2007) Vertebroplasty: magnetic resonance findings related to cement leakage risk. Acta Radiol 48:315–320
Lin WC, Lee CH, Chen SH, Lui CC (2007) Unusual presentation of infected vertebroplasty with delayed cement dislodgment in an immunocompromised patient: case report and review of literature. Cardiovasc Intervent Radiol 31(Suppl 2):S231–S235

Martin JB, Gailloud P, Dietrich PY, Luciani ME, Somon T, Sappino PA, Rüfenach DA (2002) Direct transoral approach to C2 for percutaneous vertebroplasty. Cardiovasc Intervent Radiol 25:517–519

Mathis JM (2006) Percutaneous vertebroplasty: procedure technique. In: Mathis JM, Deramond H, Belkoff ST (eds) Percutaneous vertebroplasty and kyphoplasty, 2nd edn. Springer, Berlin/Heidelberg/New York

Murphy KJ, Kelekis DA, Rundback J et al (2008) Development of a research agenda for skeletal intervention: proceedings of a multidisciplinary consensus panel. Cardiovasc Intervent Radiol 31:678–686

McGraw JK, Cardella J, Barr JD et al (2003) Society of interventional radiology quality improvement guidelines for percutaneous vertebroplasty. J Vasc Interv Radiol 14:S311–S315

Shah RV (2012) Sacral kyphoplasty for the treatment of painful sacral insufficiency fractures and metastases. Spine J 12:113–120

Söyüncü Y, Ozdemir H, Söyüncü S, Bigat Z, Gür S (2006) Posterior spinal epidural abscess: an unusual complication of vertebroplasty. Joint Bone Spine 73: 753–755

Tanigawa N, Komemushi A, Kariya S, Kojima H, Shomura Y, Ikeda K, Omura N, Murakami T, Sawada S (2006) Percutaneous vertebroplasty: relationship between vertebral body bone marrow edema pattern on MR images and initial clinical response. Radiology 239:195–200

Toyota N, Naito A, Kakizawa H, Hieda M, Hirai N, Tachikake T, Kimura T, Fukuda H, Ito K (2005) Radiofrequency ablation therapy combined with cementoplasty for painful bone metastases: initial experience. Cardiovasc Intervent Radiol 28:578–583

Voormolen MH, van Rooij WJ, Sluzewski M, van der Graaf Y, Lampmann LE, Lohle PN, Juttmann JR (2006) Pain response in the first trimester after percutaneous vertebroplasty in patients with osteoporotic vertebral compression fractures with or without bone marrow edema. AJNR Am J Neuroradiol 27:1579–1585

Weill A, Chiras J, Simon JM, Rose M, Sola-Martinez T, Enkaoua E (1996) Spinal metastases: indications for and results of percutaneous injection of acrylic surgical cement. Radiology 199:241–247

Weill A, Kobaiter H, Chiras J (1998) Acetabulum malignancies: technique and impact on pain of percutaneous injection of acrylic surgical cement. Eur Radiol 8:123–129

Wetzel SG, Wilhelm KE (2006) Perkutane Vertebroplastie und Kyphoplastie. Radiol Up2 Date 3:255–272

Wetzel SG, Martin JB, Somon T, Wilhelm K, Rufenacht DA (2002) Painful osteolytic metastasis of the atlas: treatment with percutaneous vertebroplasty. Spine 27:E493–E495

Wilhelm K (2009) Osteoplastie in Kombination mit der Radiofrequenzablation zur palliativem Therapie schmerzhafter osteolytischer Knochenmetastasen. Deutsche Zeitschrift für Onkologie 41:183–186

Wilhelm K, Babic D (2006) 3D angiography in the interventional clinical routine. Medicamundi 12:24–31

Percutaneous Osteosynthesis of the Pelvis and the Acetabulum

Arand M, Kinzl L, Gebhard F (2004) Computer-guidance in percutaneous screw stabilization of the iliosacral joint. Clin Orthop Relat Res 422:201–207

Ben-Menachem Y, Coldwell DM, Young JW et al (1991) Hemorrhage associated with pelvic fractures: causes, diagnosis, and emergent management. AJR Am J Roentgenol 157:1005–1014

Cleary K, Melzer A, Watson V et al (2006) Interventional robotic systems: applications and technology state-of-the-art. Minim Invasiv Ther Allied Technol 15:101–113

Ebraheim NA, Biyani A (2003) Percutaneous computed tomographic stabilization of the pathologic sacroiliac joint. Clin Orthop Relat Res 408:252–255

Ebraheim NA, Rusin JJ, Coombs RJ et al (1987) Percutaneous computed-tomography-stabilization of pelvic fractures: preliminary report. J Orthop Trauma 1:197–204

Falchi M, Rollandi GA (2004) CT of pelvic fractures. Eur J Radiol 50:96–105

Gansslen A, Pohlemann T, Paul C et al (1996) Epidemiology of pelvic ring injuries. Injury 27(Suppl 1):S-A13–S-A20

Gansslen A, Hufner T, Krettek C (2006) Percutaneous iliosacral screw fixation of unstable pelvic injuries by conventional fluoroscopy. Oper Orthop Traumatol 18:225–244

Gay SB, Sistrom C, Wang GJ et al (1992) Percutaneous screw fixation of acetabular fractures with CT guidance: preliminary results of a new technique. AJR Am J Roentgenol 158:819–822

Glauser D, Fankhauser H, Epitaux M et al (1995) Neurosurgical robot Minerva: first results and current developments. J Image Guid Surg 1:266–272

Gross T, Jacob AL, Messmer P et al (2004) Transverse acetabular fracture: hybrid minimal access and percutaneous CT navigated fixation. AJR Am J Roentgenol 183:1000–1002

Grützner PA, Rose E, Vock B et al (2002) Computer assisted screw osteosynthesis of the posterior pelvic ring. Initial experiences with an image reconstruction based optoelectronic navigation system. Unfallchirurgie 105:254–260 [German]

Guillamondegui OD, Pryor JP, Gracias VH et al (2002) Pelvic radiography in blunt trauma resuscitation: a diminishing role. J Trauma 53:1043–1047

Huegli RW, Messmer P, Jacob AL et al (2003) Delayed union of a sacral fracture: percutaneous navigated autologous cancellous bone grafting and screw fixation. Cardiovasc Intervent Radiol 26:502–505

Hunter JC, Brandser EA, Tran KA (1997) Pelvic and acetabular trauma. Radiol Clin North Am 35:559–590

Isler B, Ganz R (1996) Classification of pelvic ring injuries. Injury 27(Suppl 1):S-A3–S-A12

Jacob AL, Messmer P, Stock KW et al (1997) Posterior pelvic ring fractures: closed reduction and percutaneous CT guided sacroiliac screw fixation. Cardiovasc Intervent Radiol 20:285–294

Jacob AL, Suhm N, Kaim A et al (2000a) Coronal acetabular fractures: the anterior approach in computed tomography-navigated minimally invasive percutaneous fixation. Cardiovasc Intervent Radiol 23:327–331

Jacob AL, Kaim A, Baumann B et al (2000b) A simple device for continuous leg extension during CT-guided interventions. AJR Am J Roentgenol 174:1687–1688

Jacob AL, Regazzoni P, Steinbrich W et al (2000c) The multifunctional therapy room of the future: image guidance, interdisciplinarity, integration and impact on patient pathways. Eur Radiol 10:1763–1769

Judet R, Judet J, Letournel E (1964) Fracture of the acetabulum: classification and surgical approaches for open reduction. Preliminary report. J Bone Joint Surg Am 46:1615–1646

Keating JF, Werier J, Blachut P et al (1999) Early fixation of the vertically unstable pelvis: the role of iliosacral screw fixation of the posterior lesion. J Orthop Trauma 13:107–113

Kellam JF (1989) The role of external fixation in pelvic disruptions. Clin Orthop Relat Res 241:66–82

Kellam JF, McMurtry RY, Paley D et al (1987) The unstable pelvic fracture. Operative treatment. Orthop Clin North Am 18:25–41

Letournel E (1993) The treatment of acetabular fractures through the ilioinguinal approach. Clin Orthop Relat Res 292:62–76

Matta JM, Saucedo T (1989) Internal fixation of pelvic ring fractures. Clin Orthop Relat Res 242:83–97

Meyer BC, Peter O, Nagel M et al (2008) Electromagnetic field-based navigation for percutaneous punctures on C-arm CT: experimental evaluation and clinical application. Eur Radiol 18:2855–2864

Miyazawa K, Kawaguchi M, Tabuchi M et al (2010) Accurate pre-surgical determination for self-drilling miniscrew implant placement using surgical guides and cone-beam computed tomography. Eur J Orthod 32:735–740

Moed BR, Ahmad BK, Craig JG et al (1998) Intraoperative monitoring with stimulus-evoked electromyography during placement of iliosacral screws. An initial clinical study. J Bone Joint Surg Am 80:537–546

Müller ME, Perren SM, Allgöwer M (1991) Manual of internal fixation: techniques recommended by the AO-ASIF Group, expanded and completely revised. Arbeitsgemeinschaft für Osteosynthesefragen, 3rd edn. Springer, Berlin/Heidelberg/New York

Nelson DW, Duwelius PJ (1991) CT-guided fixation of sacral fractures and sacroiliac joint disruptions. Radiology 180:527–532

Orth RC, Wallace MJ, Kuo MD (2008) C-arm cone-beam CT: general principles and technical considerations for use in interventional radiology. J Vasc Interv Radiol 19:814–820

Peng KT, Huang KC, Chen MC et al (2006) Percutaneous placement of iliosacral screws for unstable pelvic ring injuries: comparison between one and two C-arm fluoroscopic techniques. J Trauma 60:602–608

Pohlemann T, Angst M, Schneider E et al (1993) Fixation of transforaminal sacrum fractures: a biomechanical study. J Orthop Trauma 7:107–117

Pohlemann T, Bosch U, Gansslen A et al (1994) The Hannover experience in management of pelvic fractures. Clin Orthop Relat Res 305:69–80

Poole GV, Ward EF (1994) Causes of mortality in patients with pelvic fractures. Orthopedics 17:691–696

Qureshi AA, Archdeacon MT, Jenkins MA et al (2004) Infrapectineal plating for acetabular fractures: a technical adjunct to internal fixation. J Orthop Trauma 18:175–178

Routt ML Jr, Kregor PJ, Simonian PT et al (1995a) Early results of percutaneous iliosacral screws placed with the patient in the supine position. J Orthop Trauma 9:207–214

Routt ML Jr, Simonian PT, Grujic L (1995b) The retrograde medullary superior pubic ramus screw for the treatment of anterior pelvic ring disruptions: a new technique. J Orthop Trauma 9:35–44

Schrader P (2005) Technique evaluation for orthopedic use of Robodoc. Z Orthop Ihre Grenzgeb 143:329–336

Senst W, Bida B (2000) Expert assessment of pelvic injuries. Zentralbl Chir 125:737–743 [German]

Siebert W, Mai S, Kober R et al (2002) Technique and first clinical results of robot-assisted total knee replacement. Knee 9:173–180

Simonian PT, Routt ML Jr, Harrington RM et al (1994a) Biomechanical simulation of the anteroposterior compression injury of the pelvis. An understanding of instability and fixation. Clin Orthop Relat Res 309:245–256

Simonian PT, Routt ML Jr, Harrington RM et al (1994b) Internal fixation of the unstable anterior pelvic ring: a biomechanical comparison of standard plating techniques and the retrograde medullary superior pubic ramus screw. J Orthop Trauma 8:476–482

Starr AJ, Reinert CM, Jones AL (1998) Percutaneous fixation of the columns of the acetabulum: a new technique. J Orthop Trauma 12:51–58

Starr AJ, Jones AL, Reinert CM et al (2001) Preliminary results and complications following limited open reduction and percutaneous screw fixation of displaced fractures of the acetabulum. Injury 32(Suppl 1): SA45–SA50

Stöckle U, Krettek C, Pohlemann T et al (2004) Clinical applications – pelvis. Injury 35(Suppl 1):S-A46–S-A56

Tile M (1996) Acute pelvic fractures: I. Causation and classification. J Am Acad Orthop Surg 4:143–151

Tile M (2003) Fractures of the pelvis and acetabulum, 3rd edn. Williams and Wilkins, Baltimore

van den Bosch EW, van Zwienen CM, van Vugt AB (2002) Fluoroscopic positioning of sacroiliac screws in 88 patients. J Trauma 53:44–48

Wedegartner U, Gatzka C, Rueger JM et al (2003) Multislice CT (MSCT) in the detection and classification of pelvic and acetabular fractures. Rofo 175:105–111 [German]

Yinger K, Scalise J, Olson SA et al (2003) Biomechanical comparison of posterior pelvic ring fixation. J Orthop Trauma 17:481–487

CT- and MR-Guided Arthrography

Bachmann G, Bauer T, Jürgens I et al (1998) The diagnostic accuracy and therapeutic relevance of CT arthrography and MR arthrography of the shoulder. Rofo 168:149–156

Bille B, Harley B, Cohen H (2007) A comparison of CT arthrography of the wrist to findings during wrist arthroscopy. J Hand Surg Am 32:834–841

Blitzer M, Nasko M, Krackhardt T et al (2004) Direct CT-arthrography versus direct MR-arthrography in chronic shoulder instability: comparison of modalities after the introduction of multidetector-CT technology. Rofo 176:1770–1775

Brossmann J, Preidler KW, Daenen B et al (1996) Imaging of osseous and cartilaginous intraarticular bodies in the knee: comparison of MR imaging and MR arthrography with CT and CT arthrography in cadavers. Radiology 200:509–517

Christie-Large M, Tapp MJ, Theivendran K et al (2010) The role of multidetector CT arthrography in the investigation of suspected intra-articular hip pathology. Br J Radiol 83:861–867

Dubberley JH, Faber KJ, Patterson SD et al (2005) The detection of loose bodies in the elbow: the value of MRI and CT arthrography. J Bone Joint Surg Br 87:684–686

Fogerty S, King DG, Groves C et al (2011) Interobserver variation in reporting CT arthrograms of the shoulder. Eur J Radiol 80:811–813

Guntern DV, Pfirrmann CW, Schmid MR et al (2003) Articular cartilage lesions of the glenohumeral joint: diagnostic effectiveness of MR arthrography and prevalence in patients with subacromial impingement syndrome. Radiology 226:165–170

Lecouvet FE, Dorzee B, Dubuc JE et al (2007) Cartilage lesions of the glenohumeral joint: diagnostic effectiveness of multidetector spiral CT arthrography and comparison with arthroscopy. Eur Radiol 17: 1763–1771

Moser T, Dosch JC, Moussaoui A, Dietemann JL (2007) Wrist ligament tears: evaluation of MRI and combined MDCT and MR arthrography. AJR Am J Roentgenol 188:1278–1286

Müller MC, Lagarde SM, Germans MR et al (2010) Cerebral air embolism after arthrography of the ankle. Med Sci Monit 16:CS92–CS94

Mutschler C, Vande Berg BC, Lecouvet FE et al (2003) Postoperative meniscus: assessment of dual-detector row spiral CT arthrography of the knee. Radiology 228:635–641

Nishii T, Tanaka H, Sugano N et al (2007) Disorders of acetabular labrum and articular cartilage in hip dysplasia: evaluation using isotropic high-resolution CT arthrography with sequential radial reformation. Osteoarthritis Cartilage 15:251–257

Pfirrmann CWA, Mengiardi B, Dora C et al (2006) Cam and pincer femoroacetabular impingement. Radiology 240:778–785

Schmid MR, Nötzli HP, Zanetti M et al (2003) Cartilage lesions in the hip: diagnostic effectiveness of MR arthrography. Radiology 226:282–286

Schulte-Altedorneburg G, Gebhard M, Wohlgemuth WA et al (2003) MR arthrography: pharmacology, efficacy and safety in clinical trials. Skeletal Radiol 32:1–12

Schwartz ML, al-Zahrani S, Morwessel RM et al (1995) Ulnar collateral ligament injury in the throwing athlete: evaluation with saline-enhanced MR-arthrography. Radiology 197:297–299

Smith TO, Hilton G, Toms AP et al (2011) The diagnostic accuracy of acetabular labral tears using magnetic resonance imaging and magnetic resonance arthrography: a meta-analysis. Eur Radiol 21:863–874

Timmerman LA, Schwartz ML, Andrews JR (1994) Preoperative evaluation of the ulnar collateral ligament by magnetic resonance imaging and computed tomography arthrography. Am J Sports Med 22:26–31

Toomayan GA, Holman WR, Major NM et al (2006) Sensitivity of MR arthrography in the evaluation of acetabular labral tears. Am J Roentgenol 186: 449–453

van Dijk CN, Molenaar AH, Cohnen RH et al (1998) Value of arthrography after supinator trauma of the ankle. Skeletal Radiol 27:256–261

Waldt S, Bruegel M, Ganter K et al (2005) Comparison of multisclice CT arthrography and MR arthrography in the detection of articular cartilage lesions. Eur Radiol 15:784–791

Waldt S, Bruegel M, Mueller D et al (2007) Rotator cuff tears: assessment with MR arthrography in 275 patients with arthroscopic correlation. Eur Radiol 17:491–498

White LM, Schweitzer ME, Weishaupt D et al (2002) Diagnosis of recurrent meniscal tears: prospective evaluation of conventional MR imaging, indirect MR arthrography, and direct MR arthrography. Radiology 222:421–429

Zubler C, Mengiardi B, Hodler J et al (2007) MR arthrography in calcific tendinitis of the shoulder: diagnostic performance and pitfalls. Eur Radiol 17:1603–1610

Special Techniques

16

Jens-Peter Staub, Andreas H. Mahnken,
Markus Völk, Bernhard C. Meyer, Frank K. Wacker,
Toshihiro Tanaka, and Gabriele A. Krombach

Contents

16.1 Sclerosing Therapy in Cysts and Parasites

Jens-Peter Staub

16.1.1 Introduction

Due to the increasing utilization of cross-sectional imaging techniques like computed tomography (CT), magnetic resonance (MR) imaging, and ultrasound (US), cysts, in particular those of the abdominal organs like kidneys, liver, and spleen, are frequently diagnosed. Therapeutic consequences can only be driven if the cysts become symptomatic because of their position, increasing size, hemorrhage, or superinfection. The surgical excision, resection, or fenestration of the

J.-P. Staub (✉)
MVZ Schießstattweg,
Schießstattweg 60, D-94032 Passau, Germany
e-mail: jens-peter.staub@radio-log.de

A.H. Mahnken
Department of Diagnostic and
Interventional Radiology, University Hospital,
Marburg, Germany

Philipps University of Marburg, Marburg, Germany
e-mail: mahnken@med.uni-marburg.de

M. Völk
MVZ Theresientor,
Stadtgraben 10, 94315 D-Straubing, Germany
e-mail: markus.völk@radio-log.de

B.C. Meyer • F.K. Wacker
Department of Diagnostic and Interventional Radiology,
MH Hannover, Carl-Neuberg-Straße 1, D30265
Hannover, Germany
e-mail: meyer.bernhardmh-hannover.de;
wacker.frankmh-hannover.de

T. Tanaka
Department of Radiology, Nara Medical University,
840 Shijo-cho, Kashihara 634-8522, Japan
e-mail: toshihir@bf6.so-net.ne.jp

G.A. Krombach
Department of Radiology, University Hospital Gießen,
Klinikstraße 33, D-35392 Gießen, Germany
e-mail: gabriele.krombach@radiol.med.uni-giessen.de

A.H. Mahnken et al. (eds.), *CT- and MR-Guided Interventions in Radiology*,
DOI 10.1007/978-3-642-33581-5_16,

cyst by laparotomy or laparoscopic deroofing, with widest possible excision of the wall and coagulation, show high success rates and were regarded to be the standard procedure for a long time. However, during the last two decades, following the first description by Bean (1981), the percutaneous interventional therapy has gained more and more importance as a safe and low invasive procedure.

Cysts of the abdominal organs are histologically classified into true cysts or pseudocysts. While true cysts are surrounded by a single-layer epithelium wall and often congenital, pseudocysts originate from a trauma, an operation, or an infection. Hydatid cysts are acquired, true cysts which are surrounded by a multilayer membrane and thus require a different treatment.

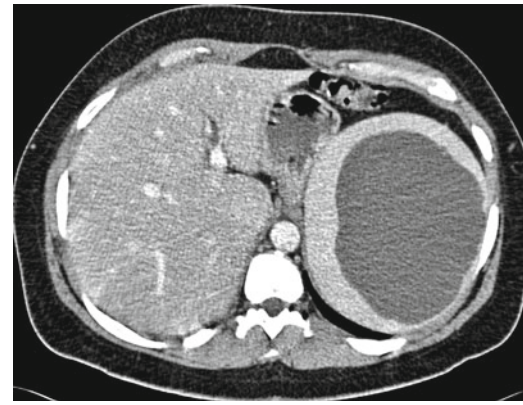

Fig. 16.1 Huge, asymptomatic cyst of the spleen: no indication for sclerotherapy

16.1.2 Indications

16.1.2.1 Renal Cysts

The most frequent form of the renal cyst is the cortical cyst which is surrounded by a single epithelial layer. It originates from dilatated tubules in the nephrons, detaches by increasing growth, and can reach enormous size. More than half of the adults over 50 years have renal cysts which are in general asymptomatic. Large cysts can cause flank pain by distension of the capsule, and a further complication is compression of the calices or the proximal ureter with the result of obstruction or renal hypertension. Infected renal cysts are treated like abscesses in other organs by percutaneous drainage and antibiotics.

16.1.2.2 Splenic Cysts

As many as 75 % of all splenic cysts are posttraumatic pseudocysts (Fig. 16.1), developed out of hematomas, whereas congenital splenic cysts are a rare finding (Klee et al. 1996). Splenic cysts can reach substantial sizes before they become symptomatic by their space-demanding effect on surrounding organs. Pain is the most often described complaint. Since the surgical standard therapy of splenectomy is associated with an increased risk of septic complications, especially the overwhelming postsplenectomy syndrome (OPSI syndrome), sclerotherapy is an alternative, safe option with high success rates (Akhan et al. 1997; Völk et al. 1999).

16.1.2.3 Hepatic Cysts

True hepatic cysts are often solitary and are found sonographically in 4.65 % of the normal population (Caremani et al. 1993). They originate in utero from a malformation of intrahepatic bile ducts and are lined by a cuboidal epithelium. Large cysts can cause hepatomegaly, pain, and sense of fullness; other possible complaints are feeling of sickness, nausea, and dyspnea. Compression of the biliary tree leads to intrahepatic cholestasis with jaundice. Cases of leg and scrotal edema by obstruction of the inferior vena cava were described (Frisell et al. 1979).

16.1.2.4 Pancreatic Cysts

Up to 85 % of the cystic lesions in the pancreas are pseudocysts. Sclerotherapy is contraindicated in half of all pseudocysts because of a communication with the pancreatic duct and a subsequent risk of pancreatitis. Noncommunicating pseudocysts have a low recurrence rate, so a simple drainage can be performed. Congenital cysts of the pancreas are rare and often occur in patients with polycystic diseases. They seldom become symptomatic due to large size or their position; in these cases, a percutaneous drainage and sclerotherapy can be indicated.

Table 16.1 The Gharbi classification of hydatid cysts based on ultrasound appearance (Gharbi et al. 1981)

Gharbi classification	Lesion features	Sclerosing therapy
Type I	Pure fluid collection	+
Type II	Fluid collection with a split wall	+
Type III	Fluid collection with septa	(+)
Type IV	Heterogeneous echo patterns	–
Type V	Reflecting thick walls	–

Table 16.2 Indications and contraindications for sclerosing therapy in cysts and hydatid disease

Indications	
Cysts	Symptomatic cysts (e.g., pain, nausea, vomiting, jaundice, shortness of breath, obstruction of collecting system)
Hydatid disease	Cyst types I and II according to Gharbi classification, type III if not of honeycomb appearance
Contraindications	
Cysts	No informed consent Uncorrected coagulation disorders Inaccessible location Communication with bile or pancreatic duct, blood vessels, renal collecting system, or free peritoneal cavity OK-432: penicillin allergy
Hydatid disease	Cyst types IV and V, type III with honeycomb appearance

16.1.2.5 Lymphoceles

In contrast to true cysts, lymphoceles are not surrounded by an epithelium but by fibromembranous tissue. They are a postoperative complication, following surgery in areas of lymphatic trajectories in the abdomen or pelvis. Often existing septations and locules complicate the entire drainage of many lymphoceles. If lymphocele recurrence appears after simple percutaneous aspiration, sclerotherapy can be an effective alternative to surgical treatment with a low complication risk (Sawhney et al. 1996).

16.1.2.6 Hydatid Cysts

Sclerosing therapy of hydatid cysts is performed percutaneously with the PAIR technique (puncture, aspiration (drainage), injection, and reaspiration of a scolicidal solution). Infections with Echinococcus granulosus occur worldwide, most especially in the Mediterranean region of Europe, the Middle East, Asia, South America, and North Africa as well as endemically in Australia in areas of intensive sheep breed. Ingested embryos from slipped eggs penetrate the intestinal mucosal wall and proceed to the capillary filters of the parenchymal organs via the venous system. The most frequently affected organ is the liver in about 80 % of cases, followed by the lungs (20 %). The peritoneum, kidney, and the spleen are affected less often (WHO Informal Working Group on Echinococcosis 1996).

Hydatid cysts are composed of three layers: the inner germinal layer with brood capsules and thousands of protoscolices, the ectocyst, a thin, chitin-like membrane, and the outer pericyst which consists of host cells and compressed fibrous tissue. Due to the multilayer structure and subsequent enhancement of cyst walls and septations, CT and MR imaging have a high sensitivity and specificity in detecting hydatid disease. The sonographic appearance of the cysts, according to the classification by Gharbi et al. (1981), has different therapeutic consequences: percutaneous therapy is only effective in cysts of type I and II, and in some cysts of type III (Table 16.1), that have only a small amount of daughter cysts (Kabaalioglu et al. 2006).

16.1.2.7 Summary of Indications and Contraindications

As emphasized above, sclerotherapy is only indicated in symptomatic cysts. The most frequent symptom is pain. Compression of the biliary tree by liver cysts can lead to cholestasis. Space-demanding cysts in the pancreas duct system may cause pancreatitis; if close to vascular structures, there is a risk of ischemia or impaired venous drainage. Renal cysts can lead to a compression of the renal collecting system, microhematuria, or renal hypertension (Table 16.2).

Hydatid cysts of type I and II according to Gharbi (pure fluid collection and fluid collection with a split wall) can be treated alternatively to

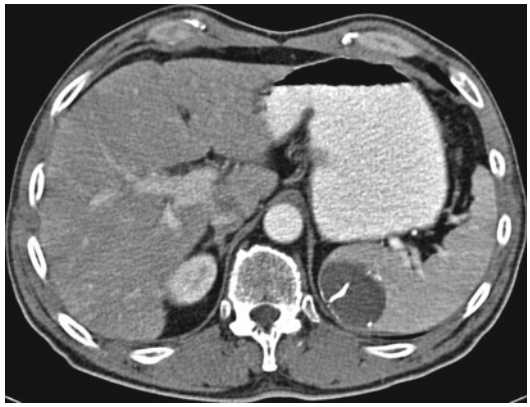

Fig. 16.2 Calcified, inactive hydatid cyst of the spleen type V according to Gharbi classification: no indication for sclerotherapy

the surgical procedure by sclerotherapy. Because every single subsidiary cyst must be treated, surgery should be preferred in multiseptated, honeycomb-like cysts of type III and in cysts of type IV. Calcified, inactive type V cysts (Fig. 16.2) are not treated (WHO Informal Working Group on Echinococcosis 1996).

Contraindications for sclerotherapy are the favoring of surgical procedures, absence of patients consent, or uncorrectable coagulation disorders. The platelet level should be at least 50,000/ml, the partial thromboplastin time (PTT) should be less than 50 s, and the international normalized ratio (INR) should be below 1.5. Lower values can be substituted by transfusion of thrombocytes or fresh frozen plasma (FFP). Difficult access routes with a high risk of vascular injury or injury of abdominal organs should be avoided as well as sclerotherapy of cysts, which communicate with the biliary tree, vascular system, or the free peritoneal space. A history of penicillin allergy or hypersensitivity should be ruled out before performing a sclerotherapy with OK-432.

16.1.3 Material

16.1.3.1 Sclerosing Agents

As secretion of the endocystic epithelium remains, sole puncture of a cyst shows a high recurrence rate and should only be performed for diagnostic reasons. A large number of different agents (glucose, formalin, phenol, povidone-iodine, Pantopaque, tetracycline, doxycycline, bleomycin) were used for sclerosing therapy of cysts and had either a high failure rate or were highly toxic.

Ethanol is also a highly toxic agent, but has been proven to be an effective agent in treatment of abdominal cysts. The injected solution leads within 1–3 min to a fixation of the epithelium cells so that secretion is interrupted. Cyst recurrences are related to an insufficient contact of alcohol with the epithelium. As a consequence, an adequate amount of ethanol (30–50 % of the cyst volume) has to be injected after complete evacuation of the cyst, and the patient has to be moved in supine, prone, and in both decubitus positions during sclerotherapy. With an injected ethanol amount of up to 200 ml and a maximum exposition time of 20 min, no side effects should occur by systemically absorbed alcohol. Therapy-related pain should be treated by intravenous injection of analgesics like fentanyl citrate.

OK-432 (picibanil) is a new promising substance that can be used for sclerosing therapy of renal cysts. It consists of a lyophilized mixture of a low-virulence strain of Streptococcus pyogenes incubated with benzylpenicillin and has shown high therapeutic effects in the treatment of malignant effusions, lymphangiomas, cystic hygromas, hemangiomas, and other benign cystic lesions. The injection of OK-432 leads to an inflammatory reaction with infiltration of natural killer and T cells. Raising activity of TNF- and IL-6 causes a higher endothelial permeability with increased lymph drainage and consequently shrinking of the cystic lesion (Ogita et al. 1996).

Since sclerosing agents can cause serious side effects, when injected intravasally, in the free peritoneal space, the biliary tree system, or the renal collecting system, such a communication must be excluded prior to treatment by fluoroscopy or CT after injection of diluted contrast medium.

Hypertonic saline (20–30 %) is the second most common scolicidal substance in hydatid cysts. The osmotic gradient of highly

concentrated saline results in a destruction of the infectious protoscolices and a delamination of the ecto- from the pericyst.

16.1.3.2 Needles, Wires, and Catheters

The required material is defined by the selected technique which depends on the size and location of the cyst, access route, and preferences of the performing radiologist. Larger cysts with a size of more than 5 cm should be drained with a pigtail catheter which guarantees a safe position in the cyst cavity, while evacuation, injection, and reaspiration can be performed even if the patient's position is changed during sclerotherapy. Due to the low viscosity of the serous cyst content, a catheter size of 5–8 gauge is usually sufficient. Pigtail catheters have multiple side holes along the distal shaft which permit drainage of large cysts with up to 1,000 ml content. They are mounted on a rigid trocar to allow direct puncture of a superficial-located cyst.

If there is a difficult access route, the less traumatic Seldinger technique should be used for puncturing with 20- to 22-gauge biopsy needles. A 0.018-in. guidewire is inserted through the biopsy needle and is finally replaced by a 5-French sheath. After coiling a rigid, 0.035-in. guidewire within the cyst, Teflon-coated dilatators of 6 and 8 French sizes are used to dilatate the access way of the final catheter.

Smaller cysts may be punctured directly by a long 18-gauge angiography or trocar needle; 0.035-in. guidewires can be inserted through the needle sheath for further dilatation maneuvers and final pigtail replacement (Figs. 16.3b, c and 16.4a, b).

16.1.4 Technique

16.1.4.1 Pre-Interventional Imaging

Before sclerotherapy is performed, true cysts must be differentiated from septated cysts, infected cysts, parasitic cysts, and cystic carcinomas. Communication with the biliary tree, the urinary tract, the vascular system, or the peritoneal cavity must be excluded. Contrast-enhanced CT and MR imaging are superior imaging modalities compared to US; besides, they permit the planning of difficult access routes by precise visualization of blood vessels and the bowel.

When compared with MR imaging and US, CT is the imaging modality of choice for guiding sclerotherapy in cysts due to its quick acquisition time, low movement artifacts, a high spatial resolution with better detection of blood vessels, available space, and the more precise visualization of the used puncture needles, guidewires, and catheters. The technique for puncture, aspiration, and sclerosis is the same for all parenchymal cysts, regardless of their etiology.

16.1.4.2 Sclerotherapy of Nonparasitic Cysts with Alcohol

Before intervention is performed, the whole procedure is explained in detail to the patient, who has to agree to the procedure by signing the consent papers. Coagulation parameters have to be determined and checked. Monitoring of oxygen saturation, ECG, and blood pressure should be available if the intervention is performed under conscious sedation of the patient.

The patient is placed comfortably in supine, prone, or lateral position, depending on the planned access route. In principle, the approach should be as little traumatic as possible. In order to avoid spilling of cyst content into peritoneal space, the puncture should reach through about 1–2 cm of healthy parenchyma.

In general, unenhanced CT scans are performed prior to the procedure (Fig. 16.3a). However, there may be cases that require intravenous contrast media to visualize the blood vessels. The access is planned on the CT console, the skin is disinfected, and a local anesthetic like 5–20 ml lidocaine 1 % is injected subcutaneously by a 25-gauge needle. The needle is left in situ to check its position on a CT control scan. Moderate conscious sedation may be achieved by intravenous injection of 1–5 mg midazolam in combination with opioid analgesics like fentanyl (0.025–0.05 mg) and piritramide (3.75–7.5 mg) or esketamine (6.25–12.5 mg). Standard initial doses of the listed agents have to be adapted to patients body mass, age, and disease and can be repeated every 3–5 min.

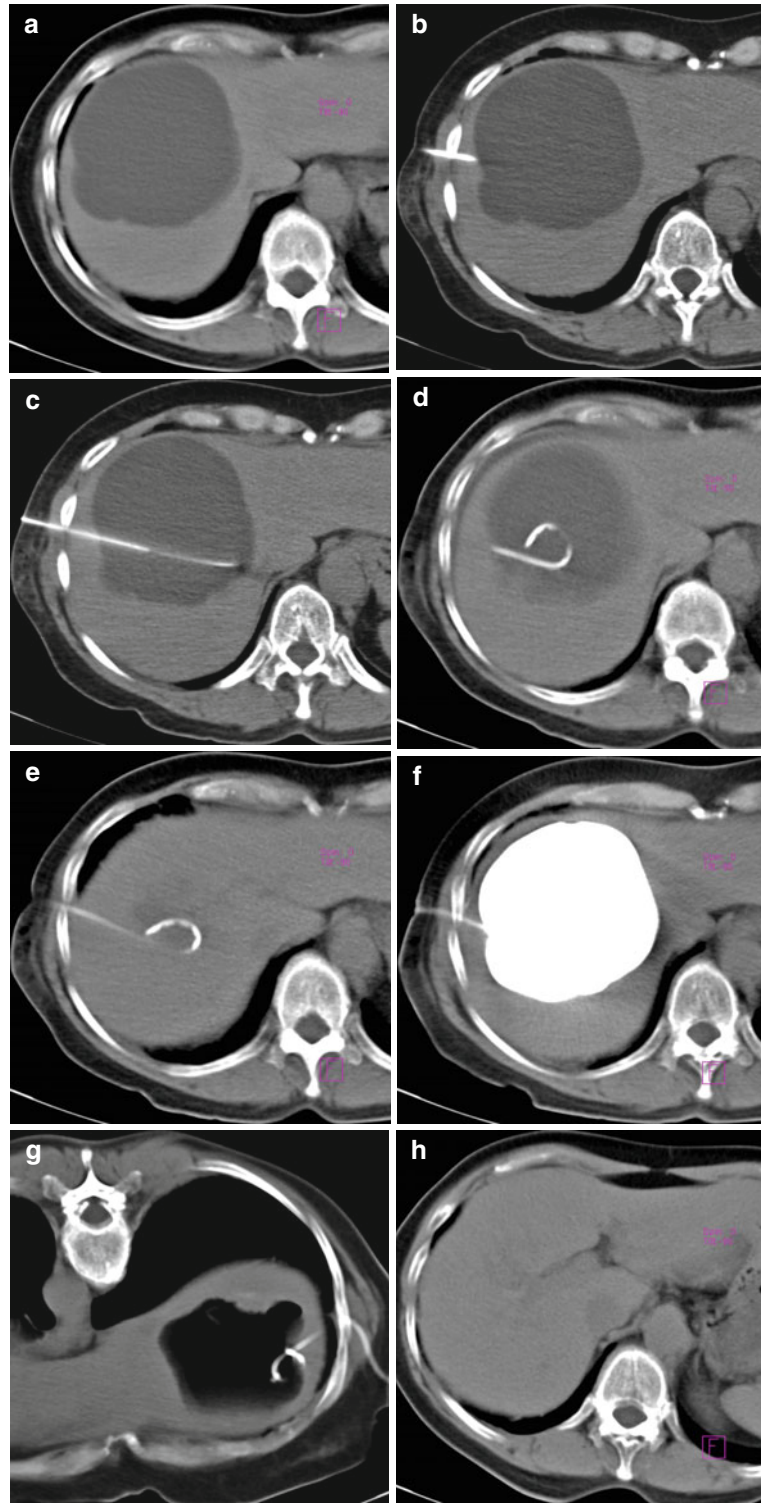

Fig. 16.3 Alcohol sclerotherapy of a 10-cm symptomatic hepatic cyst. Preprocedure scan to choose entry site shows the large fluid isodense lesion in *right* liver lobe (**a**). Puncture with 18-G angiography needle (**b**). Removal of the trocar and insertion of a 0.035-in. wire (*arrow*) through the needle sheath (**c**). Control scan of pigtail position (**d**). Complete evacuation of the cyst (**e**). No leakage after injection of diluted contrast media (**f**). Scan in prone position after injection of 160 ml ethanol 95 % (measured intracystic attenuation was 160 HU) (**g**). Postprocedure scan after reaspiration and removal of pigtail catheter (**h**)

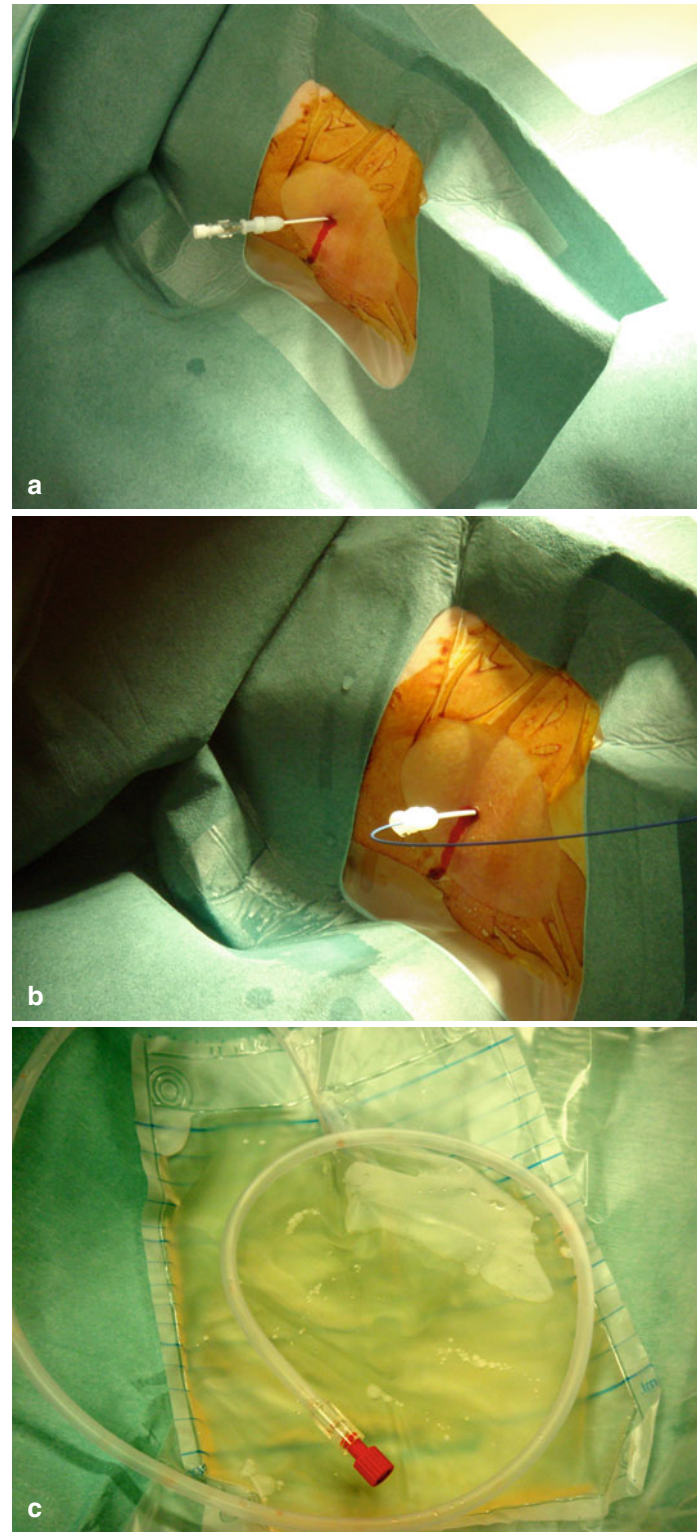

Fig. 16.4 Sclerotherapy of a benign hepatic cyst. A 10-cm 18-G angiography needle is placed in the cyst (**a**). A 0.035-in. guide wire is coiled in the cyst after removal of the trocar (**b**). Clear cyst fluid in the drainage bag (**c**) injection of 95 % ethanol, using a 60-ml syringe

The anesthesia needle is removed, and the skin carefully disinfected and draped. The further procedure depends on the location and size of the cyst, the access way, and experience of the performing radiologist. Small cysts with a size of <5 cm can be aspirated and sclerosed directly with an 18-gauge needle; large cysts should be drained with a pigtail catheter. Technically difficult access routes like a deep cyst position or adjacent vessels require the Seldinger technique instead of the direct puncture.

Small Cysts

Smaller (<5 cm) and superficially located cysts can be punctured directly with an 18-gauge angiography or trocar needle. After a small skin incision, the needle is directed into the cyst until the center of the cyst cavity is reached. Controlling CT scans can be necessary if the access route is long or very angulated. After checking the correct needle position, the trocar is removed, and the cyst content is sampled for laboratory analysis.

Trocar Technique

The trocar technique allows a quick and safe insertion of an indwelling catheter in superficially located cysts of more than 5 cm diameter. After straightening the catheter by inserting the trocar and stiffening cannula, the assembled drainage set is placed into the cyst cavity. The trocar stylet is removed, the stiffening cannula unlocked and held stationary, and the pigtail catheter is fully advanced into the cystic cavity. After removal of the cannula, the correct pigtail catheter position is checked by a control CT scan. The cyst content is sent to laboratory for analysis.

Seldinger Technique

Technically difficult approaches like a deep parenchymal location of the cyst or risk of injuring blood vessels or bowel require the Seldinger technique. A 22-gauge needle is positioned in the proximal cyst cavity under controlling CT scans. After aspiration of cyst fluid, a 0.018-in. guidewire is inserted via the sheath and coiled into the cyst. The puncture needle is replaced by an 18-gauge trocar-dilatator combination, and a stiff 0.035-in. guidewire is positioned. Teflon dilatators are passed over the guidewire, and the straightened pigtail catheter is advanced into the proximal cyst. The stiffening cannula is unlocked and held stationary, while the catheter is fully advanced into the cavity. Stiffening cannula and guidewire are removed; samples of the cyst fluid are obtained.

Sclerosing Therapy

Prior to sclerosing therapy, the correct position of the pigtail tip is checked by CT scanning. In order to avoid displacement of the sclerosing agent, it is important to ensure that all side holes of the catheter are located within the cyst. After checking the correct position of the needle or pigtail tip within the cyst cavity (Fig. 16.3d), samples of the cyst content are taken for cytological, microbiological, and biochemical analysis. The catheter is fixed, and a three-way stopcock is attached. The cyst is drained completely with a large syringe (e.g., 60 ml) and a drainage bag (Figs. 16.3e). The obtained volume should correspond to the CT calculation of the cystic content ($d_1 \times d_2 \times d_3 \times 0.5232$); if necessary, a control scan is performed to ensure complete evacuation of the cysts content. After complete evacuation, diluted contrast medium (300 mg iodine/ml mixed with 0.9 % NaCl 1:10) is injected, and a CT scan is performed to exclude leakage out of the cyst (Fig. 16.3f). If the contrast medium spreads into blood or lymphatic vessels, the biliary tree, the renal collecting system, or into peritoneum, sclerotherapy is contraindicated and the pigtail catheter has to be removed after complete reaspiration.

If there is no leakage, the contrast medium is aspirated completely and 95 % alcohol is injected (Fig. 16.4d). The amount of alcohol should be 30–50 % of the previous cyst content and not exceed 200 ml, even if the cyst size is larger than 600 ml. Because patients develop pain under injection of alcohol, additional application of analgesics is generally required. The alcohol remains for approximately 20 min in the cyst; during this time, the patient has to be moved into supine, prone, and left and right decubitus position in order to guarantee a sufficient alcohol

contact to the cystic epithelial layer (Fig. 16.3g). After sclerotherapy, the alcohol is removed completely, together with the catheter, and a postprocedure CT scan is performed to rule out possible complications (Fig. 16.3h).

Patients have to rest in bed for about 4 h, but can be dismissed on the same day if there are no suspicious clinical symptoms. After 3 months, a follow-up by US, CT, or MR imaging examination should be performed. US typically shows a small, irregular-shaped residual cyst with thick walls (Fig. 16.5a), CT normally depicts a higher density of the residual cyst than before the sclerotherapy, and can show an enhancement of the cyst wall (Fig. 16.5b). Recurrent symptomatic cysts require a repeated drainage or a surgical procedure.

16.1.4.3 Sclerotherapy of Renal Cysts with OK-432

The technique for draining is identical to the procedure described in the chapter above. Depending on the access route, the patient is placed comfortably in the proper position, and the preprocedure scan is performed. After planning the access route, the skin is disinfected and local anesthesia is administered subcutaneously. In contrast to sclerotherapy with alcohol, there is no need of a conscious sedation or preemptive analgesia; nevertheless, an intravenous access line is mandatory.

The procedure of draining depends on the size of the cyst and its location (see above). While smaller cysts can be punctured directly with an 18-G needle (Fig. 16.6a), cysts of more

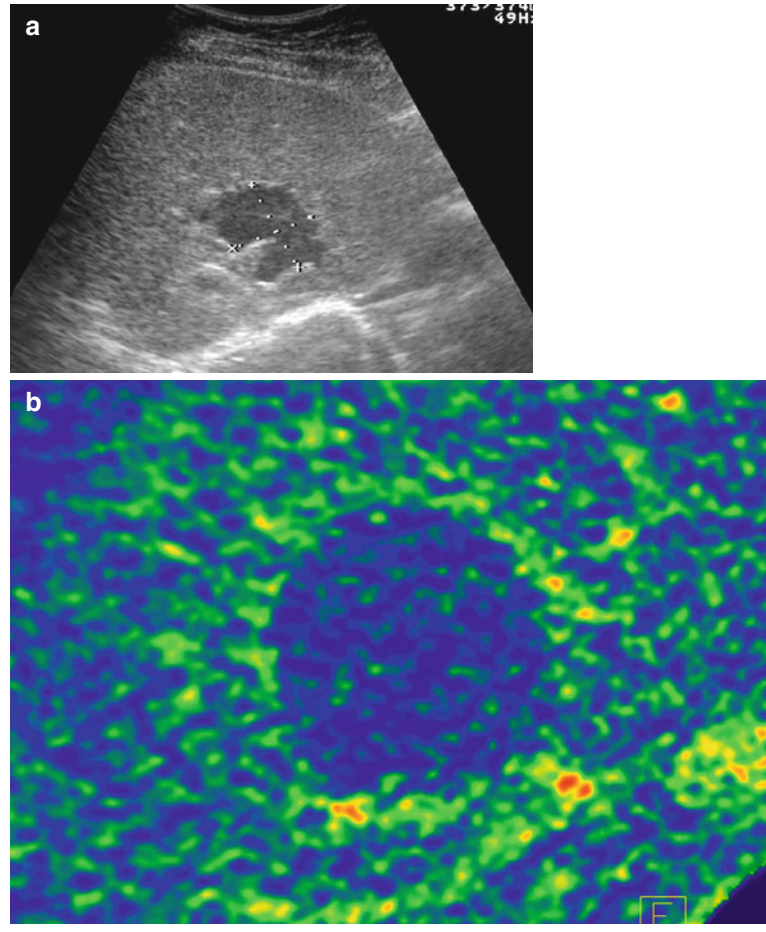

Fig. 16.5 Follow-up of hepatic cysts after sclerotherapy. Residual small cyst with thick, irregular walls at US (**a**). Slight enhancement of cyst wall in dual-energy CT scan, volume reduction was 98 % (**b**)

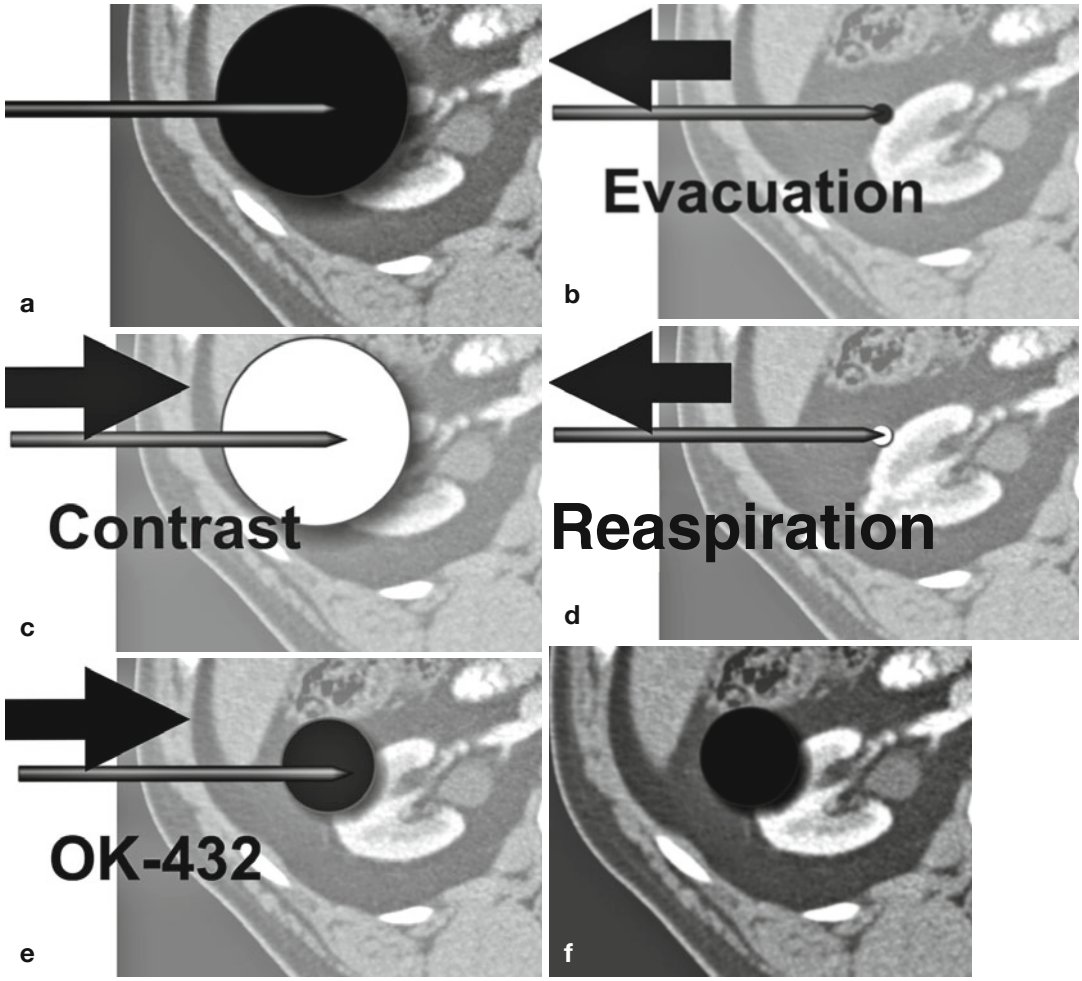

Fig. 16.6 Schematic drawing of a sclerotherapy with OK-432. Preprocedure scan and puncture with 18-G needle (**a**). Complete evacuation of the cyst (**b**). Injection of diluted contrast media on CT scan (**c**). Reaspiration (**d**). Injection of 0.1 mg OK-432 per 20 ml of cyst content (**e**). Removal of the needle without reaspiration (**f**)

than 5 cm should be drained by an indwelling catheter positioned either by trocar or by Seldinger technique. Once the needle or catheter is in correct intralesional position, the cyst is completely evacuated (Fig. 16.6b). Extravasation or communication with the renal collecting system has to be excluded by performing a CT scan after injection of diluted contrast media (300 mg iodine/ml mixed with 0.9 % NaCl 1:10, Fig. 16.6c). The contrast medium is aspirated completely (Fig. 16.6d), and the sclerotherapy with OK-432 can be performed. 0.1 mg OK-432, dissolved in 10 ml NaCl 0.9 %, is injected per 20 ml aspirated fluid (Fig. 16.6e). The maximum dose of OK-432 should not exceed 10 mg. The catheter is removed without reaspiration (Fig. 16.6f); follow-up examinations by ultrasound, CT, or MRI after intervention may show a marked shrinkage of the cyst within the first 3 months. Symptoms like pain at the injection site or fever can be controlled by orally administered nonsteroidal anti-inflammatory drugs.

16.1.4.4 Hydatid Cysts

Sclerosing therapy of hydatid cysts is performed applying the PAIR technique (percutaneous drainage consisting of puncture, aspiration, injection, and reaspiration of a scolicidal solution). Next to ethanol, hypertonic saline is the most common scolicidal substance. Because of the high density

of hypertonic saline on CT scans, the entire filling of the cyst and a communication with vessels or the biliary tree can be demonstrated. In contrast to ethanol, saline solution does not cause chemical cholangitis.

To minimize the risk of anaphylaxis and secondary echinococcosis, sclerotherapy of hydatid cysts must be accompanied by an antihelminthic chemotherapy with mebendazole or albendazole. Medical treatment begins 4–7 days before the planned intervention and should last for a minimum of 4 weeks. Because of the risk of anaphylaxis, the attendance of a radiologist experienced in emergency medicine or an anesthetist is advisable.

Sclerotherapy is only performed in liquid-filled cysts of type I and II according to Gharbi, and in type III cysts if there is no honeycomb appearance (Table 16.2). The technique of needle or catheter positioning is the same as described above in nonparasitic cysts. Hydatid cysts are evacuated completely after sampling 20 ml of cyst content for microbiological analysis; protoscolices and fragments of the membrane can be seen in the aspirated liquid (Fig. 16.7). The cyst is filled with hypertonic saline (20 %); the amount should be 50 % of the totally aspirated cystic volume. The saline remains 10–20 min within the cyst, and the delamination of the endocyst can be shown in a control CT scan. Particular cysts larger than 5 cm and septated cysts can be treated by injection of 95 % alcohol, after leakage is excluded. After sclerotherapy, the cyst is evacuated completely and the catheter is removed. Patients can be dismissed after resting for 4 h in bed if US control shows no hematoma. Follow-up should be performed closely including serology, immunology analysis, and US examinations every week during the first month, once a month during the first year, and once a year in the following 10 years.

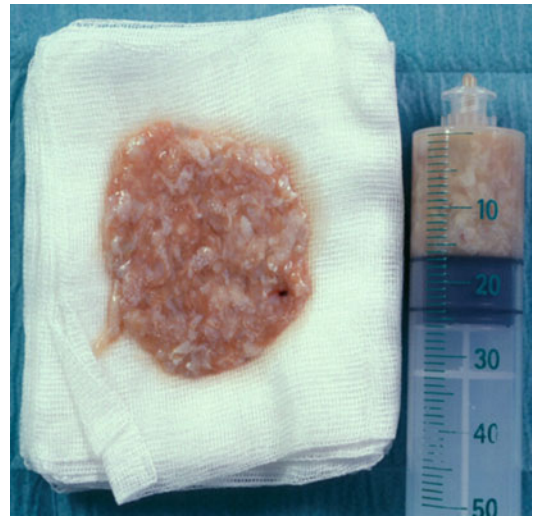

Fig. 16.7 Contents of a hydatid cyst (Courtesy of Prof. Feuerbach, Regensburg)

16.1.5 Results

16.1.5.1 Nonparasitic Cysts

While aspiration of the cyst content alone shows a high recurrence rate up to 100 % (Saini et al. 1983), the sclerotherapy of simple cysts with alcohol by percutaneous approach has been proven to be a safe and effective procedure shown by the first description by Bean (1981). Akinici et al. (2005) noted in 98 renal cysts treated with sclerotherapy a volume reduction of 93 % at the end of the first year of follow-up. Of the 74 patients with flank pain, 90 % reported a reduction or a complete disappearance of complaints. Hydronephrosis disappeared in 10 of 12 patients (83 %), and blood pressure values normalized in 7 of 8 patients (87.5 %). After an alcohol exposition time of only 10 min, Larssen and coworkers were able to achieve a volume reduction of 95 % in symptomatic liver cysts with a follow-up period of 12–47 months (Larssen et al. 2003). All of the seven treated patients experienced total relief of the clinical symptoms. Tikkakoski published a large study with 59 treated liver cysts and a technical success rate of 97 %, the follow-up time was up to 4 years (Tikkakoski et al. 1996). Interventional treatment of congenital liver cysts has similar results like laparoscopic fenestration and is associated with a lower mortality (Gigot et al. 1996).

There are only a few reports on the percutaneous sclerotherapy of splenic cysts using alcohol, describing a high technical success rate by a low risk of complications (Anon et al. 2006; Thanos et al. 2005; Akhan et al. 1997; Völk et al. 1999).

After sclerotherapy of renal cysts with OK-432, Choi et al. reported an overall success rate of 98.4 % at 1 year follow-up, defined as a reduction in size of more than 70 %. Complete

regression occurred in 75.4 % of the cysts; only one cyst (1.6 %) was regarded as a treatment failure. All patients improved in renal pain (Choi et al. 2009).

16.1.5.2 Hydatid Cysts

Since the first description of percutaneous drainage of a hydatid cyst (Mueller et al. 1985), the safety and efficacy of the method could be documented in more than 2,500 patients. Different procedures, primarily with hypertonic saline or with 90–96 % ethanol as a scolicidal substance achieved similar results. In a worldwide survey of the WHO Informal Group on Echinococcosis, the treatment of 765 hydatid cysts, primarily in the liver, with the PAIR method was evaluated (WHO Informal Working Group on Echinococcosis 2000). Positive response was achieved in 763 cases (99.7 %) with a reduction of size about at least 50 %. Recurrent cysts were observed in 12 cases (1.6 %); in 8 cases, recurrence was related to an insufficient amount of the injected scolicidal agent.

In a meta-analysis (Smego et al. 2003), 21 studies with 769 patients treated with PAIR and chemotherapy with mebendazole or albendazole were compared with a total amount of 962 patients from 14 studies undergoing surgical intervention (Table 16.3). The clinical and parasitological outcome was significantly better in 95.8 % of the patients undergoing PAIR compared with 89.8 % of the patients with surgical procedure alone. The recurrence rate was 1.6 % of patients in the PAIR group compared to 6.3 % ($P < 0.0001$) in the other group. The rate of complications was significantly higher in the surgical control objects.

Long time observations after percutaneous treatment of hydatid cysts for a period from up to 6 years confirmed the results that percutaneous aspiration, injection, and reaspiration is a safe and effective alternative to surgical procedures (Üstünsöz et al. 1999; Kabaalioglu et al. 2006).

16.1.6 Complications

16.1.6.1 Nonparasitic Cysts

The complication rate, regarding puncture and positioning of the pigtail catheter, ranges between 3 and 4 % of all cases and depends on the access way, position of the cyst, and utilized material. It includes infection, the risk of pneumothorax by penetrating the pleura, and in particular hemorrhage. The injection of alcohol does not seem to increase the risk of intracystic bleeding.

Table 16.3 Clinical outcomes and complications in patients undergoing PAIR plus chemotherapy ($n = 769$) or surgical intervention ($n = 952$) for hepatic echinococcosis appearance (Smego et al. 2003)

Clinical outcomes	PAIR + chemotherapy No. (%)	Surgical intervention no. (%)	*P* value
Cure	737 (95.8)	855 (89.8)	<0.0001
Died	1 (0.1)	7 (0.7)	<0.0827
Insufficient response	15 (2.0)	30 (3.2)	<0.1249
Recurrence	12 (1.6)	60 (6.3)	<0.0001
Major complications	61 (7.9)	239 (25.1)	<0.0001
Cyst infection	16 (2)	63 (6.6)	<0.0001
Abscess	3 (0.4)	34 (3.6)	<0.0001
Biliary fistula	34 (4.4)	140 (14.7)	<0.0001
Anaphylaxis	8 (1.0)	1 (0.1)	n.s.
Minor complications	101 (13.1)	314 (33.0)	<0.0001
Fever	42 (5.5)	24 (2.5)	<0.002
Allergic reactions	37 (4.8)	1 (0.1)	<0.0001
Wound infection/dehiscence	–	63 (6.6)	<0.0001
Pleural effusions	4 (0.5)	67 (7.0)	<0.0001
Hemorrhage	1 (0.1)	12 (1.3)	<0.008
Peritonitis	–	61 (6.4)	<0.0001
Intraperitoneal leakage	1 (0.1)	–	n.s.

As sclerosing agents are toxic substances, spilling along the catheter, via iatrogenic fistulas or through an existing communication with the biliary tree or the renal collecting system, must be excluded by cystography. Since the injection of alcohol into cysts may provoke severe pain, sufficient conscious sedation should be guaranteed in order not to interrupt or terminate the procedure. Pain immediately recedes after reaspiration of alcohol. If measured, the blood-alcohol level rises regularly, but does not reach values in the toxic range with amounts up to 200 ml and a maximum sclerosing time of 20 min, so that bed rest of 4 h and monitoring are sufficient after the procedure. Patients have to be advised not to drive for 24 h after intervention. Postprocedurally, the body temperature can rise up to 38.5 °C. However, if there are no further signs of infection, no therapy is required.

After intralesional injection, OK-432 can cause minor complications like flank pain, mild fever, and leukocytosis, probably caused by systemic leakage. The symptoms can be treated efficiently by orally administered nonsteroidal anti-inflammatory drugs.

16.1.6.2 Hydatid Cysts

Beside the general puncture-related complications such as infection, bleeding, and pneumothorax, the additional risk of an anaphylaxis and the peritoneal spilling of infectious cystic liquid exists in sclerotherapy of hydatid cysts. Periprocedural chemotherapy with mebendazole or albendazole is therefore necessary; the access to the cyst should lead through about 1–2 cm of normal parenchyma. Anaphylactic reactions appear in 0.5–1.0 % of cases (Smego et al. 2003); a lethal outcome due to anaphylaxis has been reported in 0.1–0.2 % (Akhan and Özmen 1999). Minor allergic reactions like urticaria, itching, and hypotension appear in up to 5 % of the cases and require a therapy with antihistaminics and infusion of volume. Fever up to 38.5 °C is another frequent symptom which is treated symptomatically in case of absent infection.

The rate of infected cysts and biliary fistulas is higher with hydatid cysts of the liver than with simple liver cysts. In comparison to surgical procedures, the rate of major (7.9 % compared with 25.1 %) as well as minor complications (13.1 % instead of 33.0 %) is significantly lower with PAIR, so the percutaneous treatment of hydatid cysts with hypertonic saline or alcohol is considered to be a safe procedure (Table 16.3).

Summary

Percutaneous sclerotherapy of nonparasitic cysts with alcohol or OK-432 is a technically simple and approved procedure. Only symptomatic cysts should be treated. Due to the quick acquisition time, the available space for intervention, and the precise visualization of the inserted puncture systems, CT is the imaging modality of choice for guiding the intervention. When indications and contraindications are properly considered, the technical and clinical success rate is high and comparable with the traditional surgical procedures. However, complications and mortality are clearly lower in comparison to surgical procedures. In addition, the method can be performed on an outpatient basis with considerably lower costs.

The risk of anaphylaxis or spreading of protoscolices into the peritoneum has been overestimated; however, it should not be neglected. Careful planning of the access route and periprocedural chemotherapy with mebendazole or albendazole is indispensable prior to percutaneous treatment of hydatid cysts. Considering the right indication (Table 16.2), sclerotherapy of hydatid cysts with hypertonic saline or alcohol has a high success rate of up to 95.8 % with a clearly lower morbidity (Smego et al. 2003) compared to surgical procedures.

Key Points

- A communication of the cyst with vessels, the biliary tree, the renal collecting system, or the peritoneal space must be excluded by cystography before sclerotherapy is applied. Patients often develop pain under the injection of alcohol, so

sufficient conscious sedation should be guaranteed. Therapy success depends on a sufficient intracystic concentration of ethanol, which must have contact to the whole cystic epithelial layer. Hence, after emptying the entire cyst content, an alcohol amount of 30–50 % (max. 200 ml) of the aspirated volume has to be injected, and the patient must subsequently be turned into different positions.

- Sclerotherapy of renal cysts with OK-432 is a simple and safe procedure with high success rates.
- In hydatid cysts, an adjuvant chemotherapy with mebendazole or albendazole must be carried out due to the risk of anaphylaxis and spilling of protoscolices. Because anaphylactic reactions appear with a rate of up to 1 % and the mortality ranges from 0.1 to 0.2 %, sufficient monitoring of the patient should be guaranteed and the attendance of a radiologist, competent in emergency medicine, or an anesthetist should be guaranteed.

16.2 Percutaneous Management of Endoleaks

Andreas H. Mahnken

16.2.1 Introduction

Endovascular treatment of aortic aneurysms (EVAR) is an increasingly used technique in patients with favorable vascular anatomy. A variety of complications have been reported after EVAR including endoleak, which is defined by persistent blood flow of the aneurysm sac. With an incidence in the range from 10 to 50 %, endoleak is the most common complication arising after endovascular treatment (Cuypers et al. 1999; Parent et al. 2002). Endoleaks are defined as persistent flow within the aneurysm sac but outside the graft. In case of persistent endoleakage, the aneurysm sac remains pressurized, and those aneurysms may rupture due to continued arterial pressure on the aneurysm wall.

Within the first 30 days after implantation, leaks are called "primary endoleak," while "secondary endoleaks" occur more than 30 days after the procedure. Leaks are classified as according to their origin (Table 16.4).

Computed tomography (CT) angiography with acquisition of a second delayed phase is considered the imaging technique of choice for the detection of endoleak (Görich et al. 1999; Rosenblit et al. 2003). Alternative techniques for diagnosing endoleaks include (Doppler) ultrasound (US) and magnetic resonance (MR) imaging. While various studies on US showed a variable sensitivity and specificity for the detection of endoleaks (Golzarian et al. 2002), contrast-enhanced MR imaging may yield a higher sensitivity to detect slow flow type II endoleaks (Ayuso et al. 2004). Unfortunately, there is no ideal imaging strategy, and a combination of US and CT is most often suggested.

Table 16.4 Classification of endoleaks

Type	Subtype	Location/details	Mechanism
I	A B C	Proximal Distal Iliac occluder	Separation from the arterial wall with insufficient seal at the fixation zones
II	A B	Single vessel Multiple vessels	Retrograde flow in the aneurysm sac from branching vessels
III	A B	Junctional separation Endograft fracture or holes	Tears, junctional leaks, or modular disconnection
IV			Graft porosity
V	A B	No detectable endoleak Sealed endoleak	Endotension—elevated pressure levels in the aneurysm sac without visible endoleak

16.2.2 Indications

Among the different types of leaks, type II endoleaks are the only group that is currently considered suited for percutaneous treatment. While there is a clear indication to treat types I and III endoleaks, management of type II endoleaks is discussed controversial. As type II endoleaks are associated with a lower risk of rupture than types I and III (0.5 vs. 3.4 %) and many of these endoleaks seal spontaneously, treatment might be limited to the point of aneurysm growth (Zarins et al. 2000; van Marrewijk et al. 2002). However, type II endoleaks also present with an elevated aneurysm sac pressure, and aggressive treatment may be advocated.

Considering currently published recommendations as well as our own experience, percutaneous management of endoleaks after endovascular aortic aneurysm repair is indicated in the following:

- Type II endoleak and aneurysm growth
- Persistent (>6 month) type II endoleak
- Type II endoleaks not suited for embolization

16.2.3 Material

For percutaneous embolization of type II endoleaks, all the materials needed for a CT-guided puncture have to be on hand, including the following:

- Sterile draping
- Povidone-iodine for skin disinfection
- Local anesthetics for skin infiltration
- Scalpel
- 5, 10, and 20 ml syringes with Luer-Lok adapter
- 18–20-G fine needle with end hole

For embolization, different materials may be used including the following:

- Coils as for endovascular treatment
- Onyx
- Ethibloc
- Thrombin (500 IU/ml)
- Cyanoacrylate

Depending on the choice of the embolic agent, additional materials are needed, for example, glucose for flushing lines and needle in order to avoid premature precipitation in cyanoacrylate.

Considering the different embolic agents, cyanoacrylate provides some advantages. Unlike thrombin, its effectiveness does not depend on the patient's coagulation system and is not affected by adding contrast agents for better visualization. Moreover, its radiopacity facilitates embolization and does not hamper future endoleak detection during the follow-up of patients as long as an unenhanced CT scan is performed before intravenous contrast is administered.

16.2.4 Technique

The patient is positioned in a way that allows reaching the feeding vessel. For most interventions, the patient will be put in the prone position for a translumbar approach. Alternatively a transabdominal route may be used. Ideally, the left-side access is used for the translumbar approach to avoid the inferior vena cava. For a transabdominal route, any bowel interposition needs to be avoided. After infiltration of the puncture site with local anesthetics, the tip of the fine needle is brought into the endoleak, either using CT fluoroscopy or a stepwise puncture technique as described in Chap. 2.2.2.

Once the needle is placed in the aneurysm sac, an angiogram of the sac might be performed via the puncture needle. It will show the extent of the endoleak including the draining vessels. Particularly in case of multiple vessels (type IIB), the endoleak can be compared with an arteriovenous malformation, with the sac forming the lesions nidus (Baum et al. 2002). To achieve good results in these complex lesions, it is crucial to disrupt the channel that connects the different feeding and draining vessels (Figs. 16.8 and 16.9). In addition, the feeding vessels should be occluded by injection of the embolic agent directly at the origin of these vessels.

Fig. 16.8 72-year-old patient with endovascular repair of an abdominal aortic aneurysm. Six months after the procedure, there was still a persistent endoleak (**a**, **b**, *arrows*) that was thought to be caused by retrograde filling of the aneurysm sac from the inferior mesenteric artery (type IIA). The aneurysm sac was punctured with a 20-G fine needle (**c**), and after aneurysm angiogram (not shown), 1.5 ml of a mixture of cyanoacrylate and Lipiodol was slowly injected. Control CT shows the cyanoacrylate distribution within the aneurysm sac following a preformed channel that connected the different vessels involved in the endoleak (**d**, *arrows*). Treatment was successful, and the aneurysm size gradually decreased after the procedure

Using cyanoacrylate, the viscosity of the embolic agent can be individually adapted by adding a variable amount of Lipiodol® (Guerbet, Aulnay-sous-Bois, France). As a contrast agent, it provides good visualization of the embolic agent during injection, and by adapting the viscosity, the spread of the agent within the aneurysm sac can be adapted to the size of the lesion. This is particularly helpful for occluding the feeding vessels. When using thrombin, not more than 1,000–1,500 IU

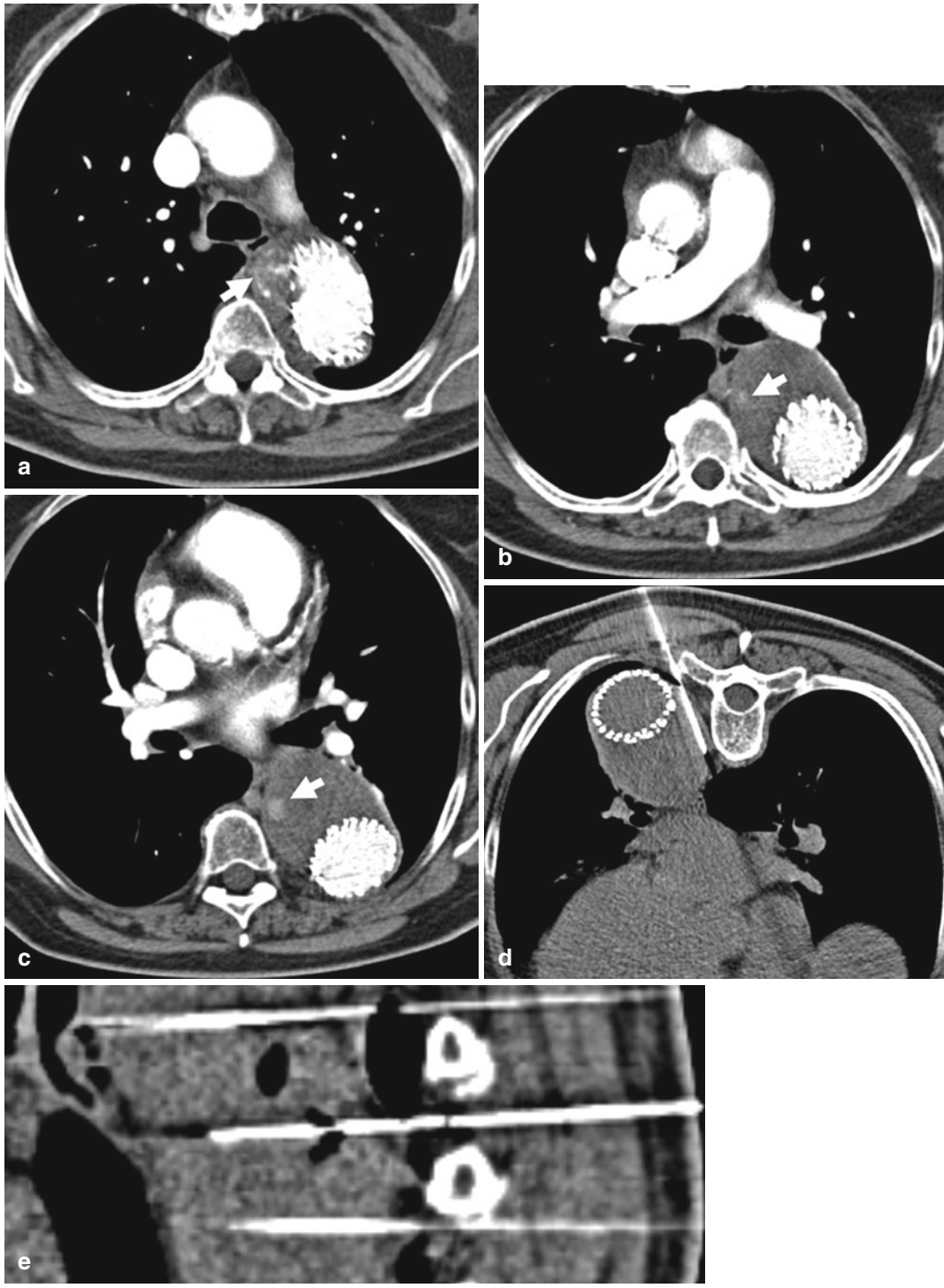

Fig. 16.9 62-year-old woman with endovascular repair of a thoracic aortic aneurysm. Six months after the procedure, there was still a persistent multilevel endoleak (**a**–**c** *arrows*) that was caused by multiple intercostal arteries (type IIB). The aneurysm sac was punctured at three levels with 18-G fine needle (**d**, **e**), and after aneurysm angiogram, (not shown) 2 ml of a mixture of cyanoacrylate and Lipiodol was slowly injected. Immediate control CT shows the cyanoacrylate distribution within the aneurysm sac (**f**, *arrows*). Treatment was successful, and at 9-month follow-up, no endoleak was seen, and the aneurysm size gradually decreased (**g**)

Fig.16.9 (continued)

should be injected for the initial treatment, as its local control is difficult and a high amount of thrombin has been reported to cause colonic ischemia (Gambaro et al. 2004). In general any embolizing agent should be injected slowly.

Additional pressure measurements are recommended before and after injection of the embolic agent. Reduction of the intrasac pressure proves efficacy of the procedure.

Repeat CT-guided injection therapy may be required in up to 20 % of patients. If repeated image-guided injection therapy is not successful, hybrid procedures utilizing CT-guided puncture of the aneurysm sack and fluoroscopic-guided endoleak embolization using standard angiographic techniques may be applied.

Although there is no published data, the same technique may also be applied in type II endoleaks after thoracic aneurysm repair (Fig. 16.9).

16.2.5 Results

There are several small case series on the use of percutaneous embolization of type II endoleaks (van den Berg et al. 2000; Schmid et al. 2002; Rial et al. 2004). There are two series comparing the transarterial and the translumbar approach for dealing with endoleaks after endovascular aneurysm repair. Baum et al. reported favorable results for the translumbar approach being effective in 92 % of patients versus 20 % in the transarterial approach (Baum et al. 2002). This was likely due to the fact that the network between the different feeding and draining vessels was disrupted using the percutaneous technique. Stavropoulos et al. did not find differences between the translumbar (72 %) and transarterial approach (78 %) with an 18.7-month follow-up (Stavropoulos et al. 2009). However, continuous growth of the aneurysm sac may require repeated interventions in about 20 % of patients, highlighting the need for a continuous surveillance after any embolization therapy (Sarac et al. 2012).

16.2.6 Complications

In general, percutaneous injection therapy for treating type II endoleaks has to be considered safe if properly performed and monitored. The risk of infection is considered minor when working under sterile conditions and if bowel passage is avoided in case of a transabdominal

route. Potential complications include thrombotic graft occlusion and peripheral embolism. Gambaro et al. reported a case of colonic ischemia which was considered to be due to embolization of the inferior mesenteric artery after thrombin injection in the aneurysm sac (Gambaro et al. 2004).

Summary

Endoleak is still an unsolved problem associated with endovascular repair of aortic aneurysms. Percutaneous treatment of type II endoleaks after endovascular repair of abdominal or thoracic aneurysms is feasible and effective. Although there is only very limited data available, this technique appears to be at least as effective as the endovascular approach. As this is a straightforward procedure, which is much less time-consuming when compared with the endovascular approach, the indication for using this technique may expand in the future.

Key Points

- CT angiography with additional delayed image acquisition is the first-line diagnostic modality for the detection of endoleaks.
- There are endovascular and percutaneous treatment options. Optimal therapy depends on the type of the endoleak.
- Thrombin and cyanoacrylate are most commonly used for percutaneous treatment of type II endoleaks.
- Disruption of the network between the involved vessels by embolizing the connecting channel is mandatory to ensure treatment success.
- Considering a 20 % rate of post-interventional aneurysm sac growth requiring reintervention, a continuous postprocedural imaging surveillance is needed.

16.3 Percutaneous Gastrostomy, Gastrojejunostomy, and Direct Jejunostomy

Markus Völk

16.3.1 Introduction

Pershaw (1981) reported the first percutaneous radiological gastrostomy (PRG) using fluoroscopy for image guidance. About 1 year before, the first percutaneous endoscopic gastrostomy (PEG) was performed (Gauderer et al. 1980). Percutaneous gastrojejunostomy (PRGJ) is a modified PRG where the catheter is placed distal to the ligament of Treitz. In 1987, Gray published the first direct percutaneous radiological jejunostomy (PRJ).

16.3.2 Indications

PRG, PRGJ, PGJ, or PEG are indicated in those patients who require nutritional support with an intact, functional gastrointestinal tract, but who are unable to process a sufficient amount of calories. Enteral feeding is generally preferred to parenteral feeding, due to preservation of gastrointestinal integrity, associated risks, and economical reasons. PRG, PRGJ, and PRJ are especially indicated when PEG is impossible or unavailable. Among others, this includes the following:

- Chilaiditi syndrome
- Previous gastrectomy
- Excessive hepatomegaly
- Inadequate transillumination in PEG
- High-grade upper digestive tract obstruction

For percutaneous radiological stomas, there are only a few contraindications. A normal coagulation screen and platelet count is necessary. Massive ascites has been described as a contraindication for the radiological methods; however, mild ascites is not a contraindication. In patients with markedly more ascites, preprocedural paracentesis is helpful. Gastric neoplasm is a contraindication for any kind of gastrostomy; here, a jejunostomy may be an alternative. For fluoroscopic-guided stomas and PEG relatively, contraindications are colonic interposition

(Chilaiditi syndrome), hepatomegaly, previous gastrectomy, and not-passable stenosis of the esophagus for a nasogastric tube; in these cases, CT-guided stomas are special techniques which allow an exact anatomical demonstration to avoid organ injury. A potential advantage of PRGJ compared with PRG is less gastric stimulation and, therefore, less gastric secretions, resulting in reduced incidence of aspiration pneumonia (Halkier et al. 1989). On the other hand, gastrojejunostomy catheters are longer and narrower than gastrostomy catheters, and this could result in more frequent tube blockage (Given et al. 2005).

16.3.3 Material

For percutaneous radiological stomas, a T-fastener set (e.g., Cope gastrointestinal T-fastener set of Cook, Bjaeverskov, Denmark) for gastropexy or jejunostomy and the stomy tray (e.g., Cook, William Cook Europe, Bjaeverskov, Denmark) are commonly used devices (Fig. 16.10). However, there are various gastro-, jejuno-, and gastrojejunostomy sets available for image-guided procedures (Table 16.5).

16.3.4 Technique

16.3.4.1 Patient Preparation and Aftercare

If possible, the patient should give his informed consent for the procedure at least 1 day before. The most important complications during the procedure are organ perforation and bleeding. That is why a recent coagulation screen must be performed. A nasogastric nasojejunal tube should be placed in the stomach the evening before. If a nasogastric tube cannot be placed, it should be tried under fluoroscopic guidance or direct puncture of the stomach or jejunum under CT guidance (Gottschalk et al. 2007; Seitz et al. 1997). Some authors recommend the oral application of 200 ml dilute barium 12 h before the procedure to identify the colon (Given et al. 2004).

The patient should fast from the night before. An intravenous access is necessary for the administration of sedative and analgesics (e.g., combination of midazolam hydrochloride and fentanyl citrate). All patients should be monitored for cardiac function (heart rate and rhythm, blood pressure) and oxygen saturation. The patient is placed in the CT scanner in supine position and draped with a sterile cover. Immediately before the localization, diagnostic 500–1,000 ml of compartment air should be applied over the nasogastric tube and 40 mg butylscopolamine and 1 mg glucagon, respectively, should be given intravenously for distention of the stomach. To localize the optimal access, only a few scans (10–15 cm) through the stomach are necessary. After selecting the slice for the puncture, the tract is anesthetized with 20 ml lidocaine (1 %). Routine antibiotic prophylaxis for percutaneous radiologically placed tubes is not necessary due to infrequent severe infectious complications following percutaneous radiological stomas (David et al. 1998; McDermott et al. 1997).

After the procedure, the patient remains fastening for 12–24 h, and then enteral feeding can be started beginning with tea. Normally, no further aftercare is needed. The catheter should be changed in case of blockage and leakage; a routine exchange is not necessary.

16.3.4.2 Procedure for Percutaneous Radiological Gastrostomy and Direct Jejunostomy

CT-guided PRG and PRJ consist of gastro- or jejunostomy using a T-fastener set for gastro- or jejunopexy and placement of the respective stoma catheter (Fig. 16.11). The principle of gastro- or jejunopexy is to accelerate tract formation. With the stomach or jejunum and abdominal walls closely apposed, the risk of peritoneal leakage is reduced. In addition, it is felt that gastro- and jejunopexy might reduce the risk of hemorrhage due to a tamponading effect (Given et al. 2005). That is why gastro- or jejunopexy is recommended for both methods by fixing the anterior gastric wall or the jejunum to the anterior

abdominal wall. This is performed with an 18-G hollow needle, containing a T-fastener which is inserted into the distended stomach or jejunum (Fig. 16.11a). An alternative method is to use four T-fasteners in a quadratic order, leave the T-fasteners for about 10 days before the nylon thread is cut. An intragastric or intrajejunal position can be confirmed by aspirating air into the syringe containing sterile water. After controlling the correct position, a stiff 0.035-in. guidewire is inserted through the needle into the stomach or jejunum (Fig. 16.11b). While the guidewire is pushed forward, the T-fastener in the stomach or jejunum has to be held by a nylon thread. Next, the needle is removed, and the anterior gastric wall or jejunum is temporary fixed to the anterior abdominal wall by gentle tension on the T-fastener fiber. The guidewire is kept in intragastric or intrajejunal position. Now the tract is dilatated over the lying guidewire up to the size of the chosen gastro- or jejunostomy catheter (Table 16.5). The Russell gastrostomy tray requires insertion

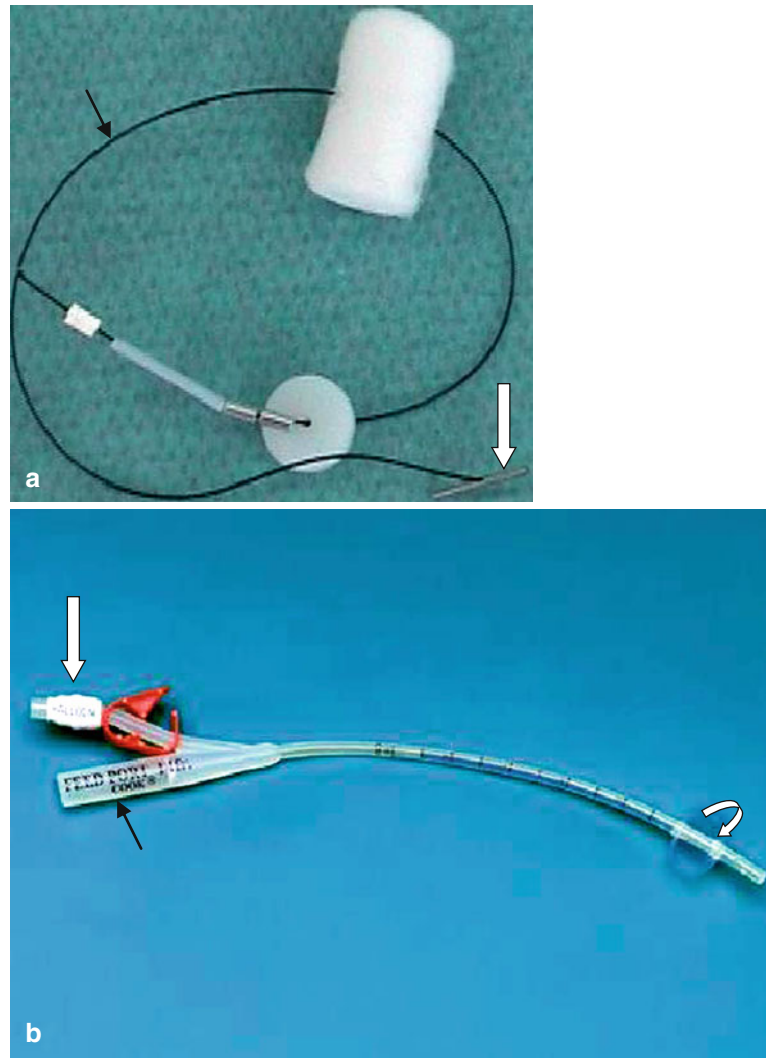

Fig. 16.10 (**a, b**) T-fastener with fiber (*white arrow*) and T-bar (*black arrow*) (**a**). Example for a gastrostomy set (Russell gastrostomy tray; copyright by Cook, William Cook Europe, Bjaeverskov, Denmark). Feeding lumen (*black arrow*), balloon inflation lumen (*white arrow*), and blocking balloon (*curved arrow*) (**b**). Part (**c**) shows an example of a jejunostomy set (www.radiographicceu.com/article24.html). Feeding lumen (*black arrow*) and balloon inflation lumen (*white arrow*). The *red* Robinson catheter needs to be sutured to the skin to maintain position. The clear silicon jejunal tube is held in position with a small saline-filled retention balloon (*curved arrow*). Fig. 16.10d shows an example of a gastrojejunostomy set (www.radiographicceu.com/article24.html). Gastric and jejunal feeding lumen (*black arrows*), balloon inflation lumen (*white arrow*), and blocking balloon (*curved arrow*)

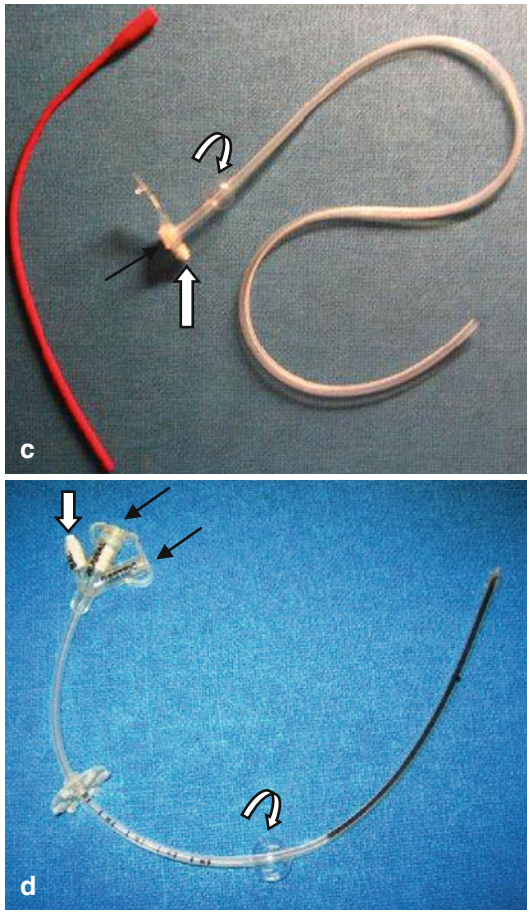

Fig.16.10 (continued)

Table 16.5 Available gastro-, jejuno-, and gastrojejunostomy sets. (This list is not exhaustive)

Type	Manufacturer
1. Russell gastrostomy tray 2. Carey-Alzate-Coons gastrojejunostomy set 3. C-GastryJ-1700-RFS 4. Marx-Cope gastrojejunostomy set 5. Shetty gastrojejunostomy set 6. Wills-Oglesby percutaneous gastrostomy set	Cook, William Cook Europe, A Cook Group Company, Sandet 6, 4632 Bjaeverskov, Denmark
1. Corflo Cubby 2. Corflo dual and triple G-tubes	CORPAK 100 Chaddick Dr., Wheeling IL 60090, USA
1. EndoVive standard PEG	Boston Scientific Corporate Headquarters, One Boston Scientific Place, Natick, MA, USA
1. Tri-funnel replacement gastrostomy tube 2. Button replacement gastrostomy devices	C.R. Bard Inc., 730 Central Avenue, Murray Hill, New Jersey, 07974, USA
1. MIC-KEY low-profile gastrostomy tube kit 2. MIC* gastrostomy	Kimberly-Clark, Belgicastraat 13, 1930 Zaventem, Belgium

through a peel-away sheath (Fig. 16.11c). After placement, the balloon is blocked with 5 ml of diluted contrast agent. The catheter is fixed by an extracorporeal fastening plate (Fig. 16.11d). After this, the T-fastener fiber is cut, and the T-fastener leaves the body through the intestinal tract. Correct intragastric or intrajejunal position must be documented (Fig. 16.11e).

16.3.4.3 Procedure for Percutaneous Radiological Gastrojejunostomy

The procedure itself is similar to that of PRG or PGJ. For this technique, the stomach puncture should be aimed toward the pylorus to aid cannulation of the pylorus. A torqueable 5-French catheter in combination with a guidewire is used to cannulate the pylorus and the proximal jejunum. When the catheter is in the proximal jejunum, the guidewire is exchanged for a stiff guidewire. The tract is then dilatated, and a gastrojejunal catheter (Table 16.5, Fig. 16.10d) is placed (Given et al. 2004).

16.3.5 Results

The reported technical success rates for percutaneous radiological stomas vary between 70 and 100 % (Gottschalk et al. 2007; Rieker et al. 2005; Neeff et al. 2003; Beaver et al. 1998; Cope et al. 1998; Wollmann et al. 1995). The largest series is a meta-analysis by Wollmann et al. (Table 16.6);

they compared PEG, fluoroscopic PRG, and surgical gastrostomy for technical success rate and found 99.2 % for PRG, 95.7 % for PEG, and 100 % for surgical gastrostomy. The technical success rate of 70 % for PRJ was founded by the lack of air insufflation over the transnasal tube (Rieker et al. 2005).

16.3.6 Complications

The mortality and major complications with PEG and PRG are significantly lower than in the surgical group (Table 16.6). The possible complications are almost equal for PRG, PRJ, and PRGJ. According to Gottschalk et al. (2007), complications with

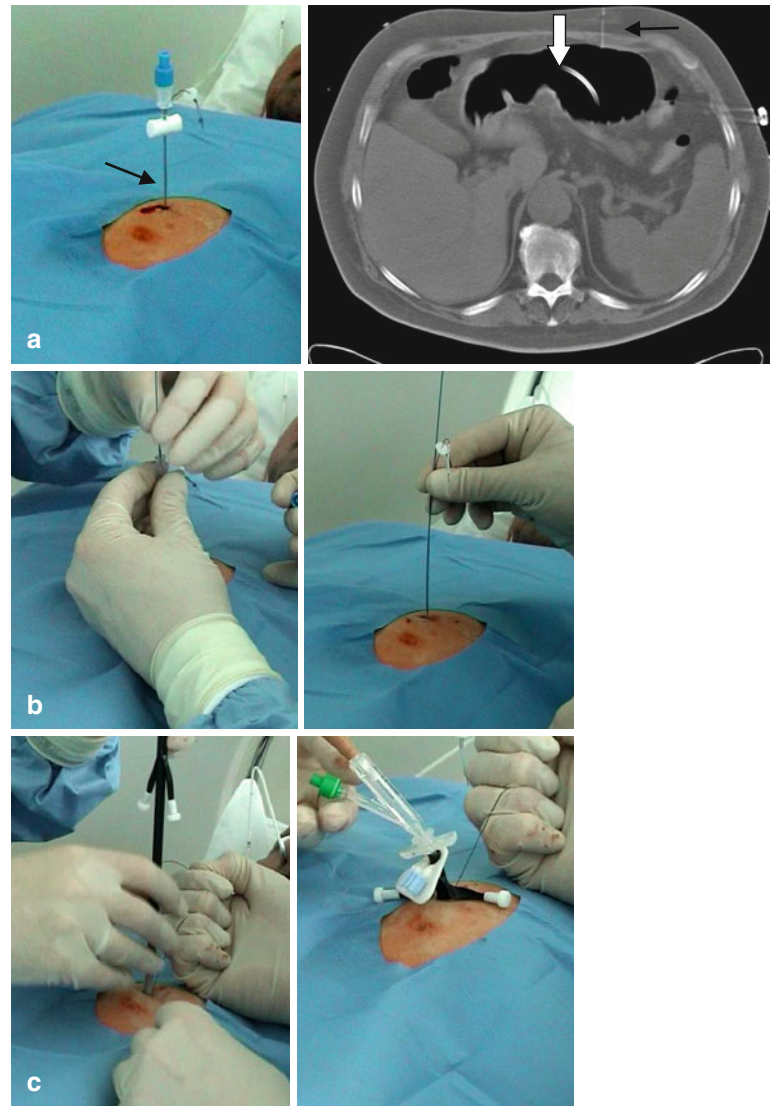

Fig. 16.11 Step-by-step illustration of a CT-guided gastrostomy: Percutaneous puncture with an 18-G hollow needle, containing a T-fastener. CT scan with the needle (*black arrow*) in the distended stomach with lying nasogastric tube (*white arrow*) (**a**). A 0.0035-in. guidewire is inserted through the 18-G hollow needle in the stomach. Afterward the 18-G hollow needle is removed. Then the fiber of the T-fastener is held under careful strain to fix the anterior gastric wall to the anterior abdominal wall (**b**). The tract is dilatated over the lying guidewire up to the size of the chosen gastrostomy catheter, and then the peel-away sheath is inserted. The gastrostomy set is inserted through a peel-away sheath (**c**). The peel-away sheath is removed. CT scan with the blocked balloon of the gastrostomy set (*black arrow*) and the nasogastric tube (*white arrow*). The T-fastener fiber is cut (**d**). The catheter is fixed by an extracorporeal fastening plate. CT scan to document the correct intragastric position of the catheter and the balloon (*white arrow*) (**e**)

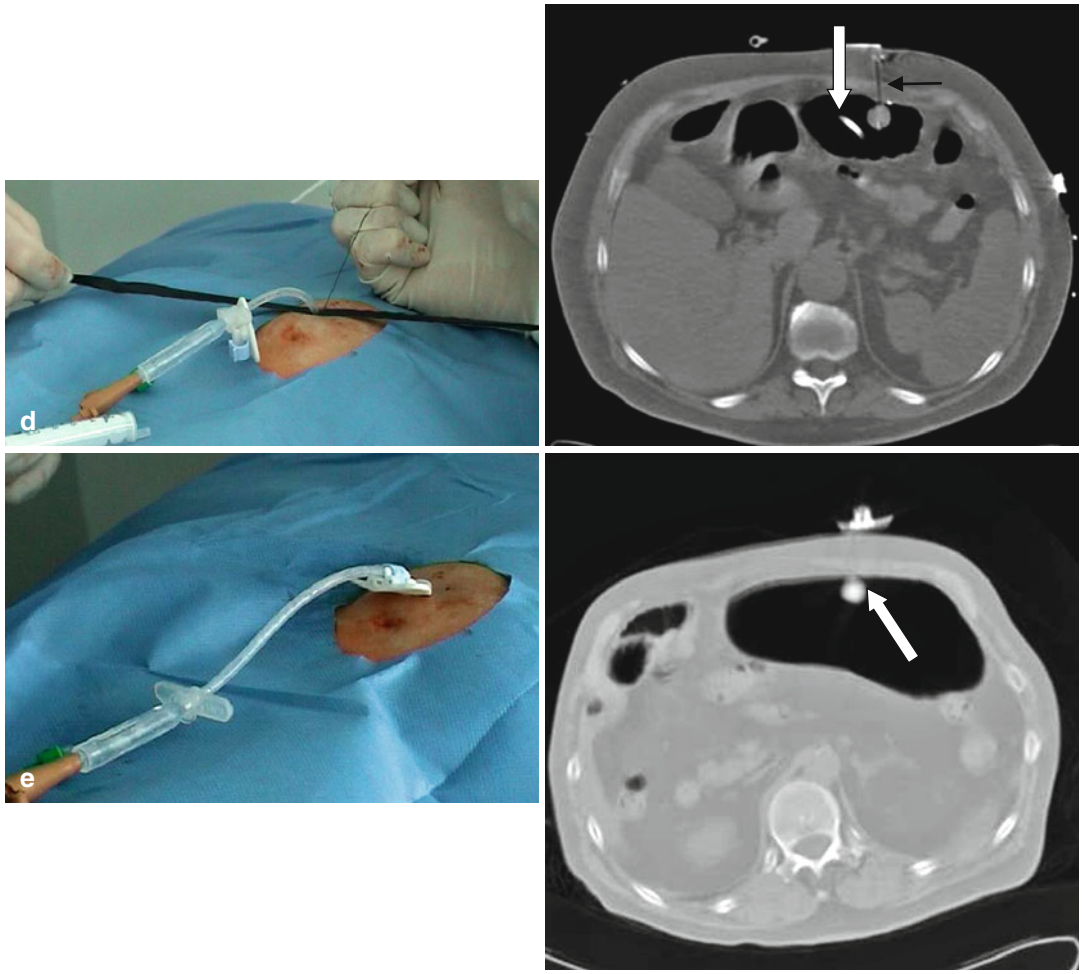

Fig. 16.11 (continued)

Table 16.6 Meta-analysis of complication rates according to Wollmann et al. (1995)

	Surgical gastrostomy	PEG	PRG
Number of patients	721	4,194	837
Technical success rate	100 %	95.7 %	99.2 %
Procedural mortality rate	2.5 %	0.5 %	0.3 %
Major complication rate	19.9 %	9.4 %	5.9 %
Minor complication rate	9.0 %	5.9 %	7.8 %

PRG can be classified in minor (early and late) and major (early and late) complications:

1. Early complications (within the first 3 days after intervention)
   (a) Major complications
      - Dislocation of the feeding tube or required surgical intervention
      - Peritonitis
      - Hemorrhage requiring blood transfusion
      - Perforation
      - Wound infection requiring systemic antibiosis
      - Death associated with complication

(b) Minor complications
- Wound infection requiring no systemic antibiosis
- Bellyache
- Peritubal leakages

2. Late complications (as from fourth day after intervention)
(a) Major complications
- Dislocation of the feeding tube or required surgical intervention
- Peritonitis
- Hemorrhage requiring blood transfusion
- Perforation
- Wound infection requiring systemic antibiosis
- Gastro- or jejunal paresis
- Death associated with complication

(b) Minor complications
- Dislocation of the feeding tube in case of granulated puncture canal
- Bellyache
- Peritubal leakages
- Local irritations and self-limiting wound infections

Summary

PEG is in most cases the method of choice. The technical success rate is almost the same for PEG and percutaneous radiologic methods, even the complication rates are comparable. CT-guided percutaneous stomas are safe and helpful methods when PEG is not possible due to anatomical reasons, for example, Chilaiditi syndrome, previous gastrectomy, and hepatomegaly or inadequate transillumination in PEG. Another special indication for CT-guided stomas is a high-grade obstruction of the upper digestive tract with an endoscopically not-passable stenosis, because direct gastric or jejunal punction is feasible with CT guidance.

Key Points
- Consider the correct indication and contraindications.
- Use adequate materials.
- Ensure adequate gastro- or jejunopexy.
- Thorough watch and treat early and late complications.

16.4 Interventions Using C-Arm Computed Tomography

Bernhard C. Meyer and Frank K. Wacker

16.4.1 Indications

Over the past 25 years, ultrasound (US)- and computed tomography (CT)-guided procedures and more recently magnetic resonance (MR)-guided interventions have proven to be safe, reliable, and provided accurate targeting of lesions for biopsy, drainage, and therapy. As outlined in the previous chapters, CT is often chosen as a guidance modality over the less expensive and more flexible ultrasound, if the loss of an acoustic window attributable to air, bone, or artifacts prevents a sonographically guided intervention. Known disadvantages of CT guidance include limited possible scan plane orientations for puncture guidance, small gantry diameter limiting the needle length, low soft tissue resolution without intravenous contrast, and lack of availability of a CT scanner dedicated for interventional procedures.

Another challenge in an economically driven hospital environment is that lengthy procedures might occupy the CT suite that could otherwise be used for diagnostic studies. On the other hand, angiography suites are no longer busy

with diagnostic angiograms as they are performed using CT angiography and MR angiography. Hence, in many interventional suites, there might be time slots that can be used for biopsies and drainage procedures. Since fluoroscopy alone does not provide sufficient soft tissue resolution, punctures had to be performed based on landmarks or in combination with ultrasound guidance.

With the recent advent of C-arm CT, three-dimensional (3D) image acquisition can be performed in the angiography suite using the C-arm. Performing such procedures in the angiography room has several advantages:

1. Angiography suites are usually well equipped and staffed for interventional procedures allowing for easy patient handling and management.
2. C-arms with free-floating tables facilitate easy patient movement in three directions and easy access to the patient without the need to bring the patient in and out of a scanner gantry for local anesthesia or needle advancement.
3. With a C-arm, 2D fluoroscopy is always at hand during the procedure for controlling needle position or guidewire and catheter placement, for example, for drainage procedures. In contrast to CT fluoroscopy, where coverage is limited by the detector width, 2D fluoroscopy provides a more flexible coverage in the craniocaudal direction.
4. C-arm CT permits one to switch immediately to endovascular procedures, for example, for managing complications of percutaneous interventions such as bleeding.

C-arm CT has evolved from 3D rotational angiography. Digital flat panel detector (FD) angiographic systems with high frame rates and high-contrast resolution facilitate 3D tomographic reconstructions, thereby resulting in a new class of hybrid C-arm systems capable of producing conventional, projectional fluoroscopy and angiography images as well as CT-like soft tissue images. As C-arm CT is a relatively new technique, the full range of indications is not jet defined and depends largely on the imaging properties of this new modality. When compared to multislice spiral CT (MSCT), C-arm CT provides higher spatial resolution, but encompasses a number of disadvantages, such as a lower contrast resolution in the range of 5–10HU, a limited field of view, and a lower temporal resolution. C-arm CT is therefore not aimed at challenging standard clinical CT with regard to the typical diagnostic studies. Nevertheless, it can be seamlessly used for peri-interventional imaging in those procedures in which current limitations are acceptable.

In percutaneous punctures, C-arm CT can act as a mere replacement for conventional CT as it also acquires axial slices similar to CT images. Furthermore, it provides the ability to use fluoroscopic controls, for example, for needle propagation or contrast injections in drainages, and therefore adds pertinent intraprocedural imaging options.

Another range of applications for C-arm CT are catheter-based endoluminal interventions, which are usually done in the angiography suite based on 2D images alone. In those interventions, C-arm CT bridges the gap between rotational 3D angiography and conventional CT and allows for imaging beyond blood vessels, visualizing soft tissue and thus alleviating complex procedures such as TIPSS placement, transarterial embolization, chemoembolization, radioembolization, and complication management in challenging neurointerventional cases.

16.4.2 Materials and Techniques

16.4.2.1 Technical Background of C-Arm CT

The idea to use a C-arm for acquisition of projection data over a partial circle-scan trajectory comprising at least 180° was first pursued in the early 1990s using C-arms equipped with image intensifier. That setup facilitated 3D imaging of high-contrast objects such as osseous structures and blood vessels during intra-arterial contrast injections. A few years ago, FD technology, initially developed for radiography, started replacing image intensifiers on angiography C-arm systems. FDs can dispense with image intensifiers distortion correction, provide a wider dynamic range, and high image quality at high frame rates. When mounted on C-arm gantries facilitating at least

200° partial circle scans, they provide a two-dimensional (2D) data acquisition setup for subsequent 3D reconstruction of CT-like images (Kalender 2006). Terms such as C-arm CT, FD-CT, cone beam CT, angiographic CT, DynaCT® (Siemens Medical Solutions), Innova CT® (GE Healthcare), or XperCT® (Philips Medical Systems) are used to describe this relatively new technology.

The current basic principle of FD still relies on the conversion of X-rays to light using a fluorescence scintillator screen. The light emitted is then recorded by an array of photodiodes. Direct-conversion detectors, for example, based on photon counting principles, are not yet commercially available. The standard detector frame rate for 2D clinical radiographic X-ray imaging on C-arm systems typically ranges between 1 and 6 frames per second but can be increased to 15 images per second if needed. For CT-like image acquisition in a C-arm system, higher readout rates of up to 60 images per second or more are desirable. This can be achieved with an FD using detector pixel binning that combines 2×2 or 4×4 pixels to be read out as one pixel. This enables faster readout rates up to 60 images per second by reducing the amount of data acquired. Noise and spatial resolution are also reduced. It is important to note that even with 2×2 binning, the spatial resolution of C-arm CT still exceeds that of most current MSCT scanners. The reduction of noise is also beneficial to the contrast resolution which is known to be inferior with C-arm CT in comparison to MSCT at any given dose level.

Since C-arm CT is an optional feature with angiography systems, the basic system design including X-ray source is still optimized for fluoroscopy and digital subtraction angiography applications. In contrast to MSCT, the X-ray source usually has a smaller focal spot, lower power limits, and it operates at voltage levels below 90 kV. As far as the mechanical properties of the C-arm are concerned, a circular scan range over 180–240° is needed together with a stable, reproducible gantry motion behavior. Thus, the system can be calibrated for 3D image acquisition facilitating 3D imaging.

Due to the special geometry of nonideal orbits based on the mechanic instability of a C-arm, accurate knowledge of the source and detector positions at each projection view and reproducibility of the positions is required for high-quality C-arm CT image reconstruction. Techniques for geometric calibration of C-arm CT systems have been previously reported (Fahrig and Holdsworth 2000). They usually provide removal of misalignment artifacts implicitly assuming a non-stable but reproducible imaging geometry (Wiesent et al. 2000). In addition to mechanical instabilities, C-arm CT is also characterized by smaller cone angles which result in artifacts due to data truncation and high scatter intensities. Truncation artifacts occur when the currently limited field of view of the C-arm CT scanner does not cover the volume of a patient. Tomographic reconstruction from truncated projections impacts the accuracy of the reconstructed CT values, and it disturbs the quantitative diagnostic quality of the images. Correction algorithms have been developed to restore image quality and improve the accuracy of the CT values in the field of view (Ohnesorge et al. 2000). The high scatter-to-primary ratios in the acquired input projections are due to its 2D character with 30 cm height and 40 cm width, for example, comprising around 1,000 rows in a typical 2×2 binning configuration. This can induce a drop in CT values toward the center of the patients. Scatter correction algorithms are available to improve CT value accuracy. The use of anti-scatter grids can also decrease the scatter artifact, but it results in a higher radiation dose due to its presence in front of the detector. In addition to C-arm CT specific artifacts, other well-known tomographic imaging artifacts also occur, including beam hardening, for example, due to metal within the scan range or detector element malfunction.

Due to the FD size, the scan range is limited to a cylindrical-shaped volume with a transversal coverage of up to 225 mm if a single rotation is used. To overcome this limitation and to reduce truncation artifacts, an angiographic system mounted on an industrial grade robotic arm (Zeego, Siemens Medical Solutions) has been introduced, which is able to perform a complex almost eight-shaped rotation to acquire the image information of two overlapping rotations. This leads to an improved image quality and a large

volume C-arm CT with an acquisition volume similar to MSCT but also to a doubling of the radiation dose. This can be beneficial in particular for punctures in bigger patients to include skin entry and target structure within the C-arm CT volume. Nevertheless, the transversal coverage of 225 mm of a single rotation C-arm CT should be sufficient to depict the region of interest in the majority of C-arm CT-guided interventions. Dose considerations for C-arm CT are largely the same as in MSCT. Traditional CT dose metrics such as the computed tomography dose index, CTDI, which represents a dose inside a standard phantom, are no longer applicable for both MSCT and C-arm CT, since the beam coverage in the *z* direction has increased to up to 30 cm in both techniques. As a result, standard CTDI phantoms and ionization chambers with a length of 150 and 100 mm, respectively, only measure a poor approximation of the true dose. Therefore, comparisons of modern MSCT and C-arm CT systems, including their dose characteristics, are challenging. Different approaches are currently being pursued, and a consensus on how to proceed exactly is yet to be found. The relationship between tube voltage, image noise, dose, and contrast perception are discussed in great detail by Fahrig et al. (2006) and Kalender and Kyriakou (2007).

16.4.2.2 Patient Bedding and Image Acquisition of C-Arm CT

Procedure-adapted patient bedding is a prerequisite for an optimal image quality and procedure guidance in C-arm CT. Image acquisition in the thorax and upper abdomen (which typically takes between 5 and 20s) should be performed in breath-hold technique. Patient movement should be minimized. In a prone or supine position, this is already secured by a standard viscoelastic mattress. If a more instable position, for example, a lateral patient position, is required, the standard mattress can be replaced by a vacuum mattress that provides stable patient bedding.

With MSCT, only the craniocaudal scan range has to be selected. In contrast, the imaging volume in C-arm CT is limited and has to be defined in all three directions on a lateral and frontal projectional image. This can be cumbersome due to the cylindrical shape of the imaging volume which has to be positioned in the center of the C-arm. A narrow patient table facilitates a more flexible patient positioning, since it may become necessary in the planning phase to move the patient toward the margin of the table to cover the area of interest and to avoid collision with the C-arm. In case of thoracoabdominal imaging, the patient's arms should be placed above his or her head if feasible. To ensure a proper image acquisition, a radiation-free test run is a mandatory prerequisite with all available C-arm systems. A potential collision with the patient or bedding material, sterile drapes, or infusion lines as well as other objects in the angio suite, such as power injectors or radiation protection devices, has to be ruled out during this test run, which can be stopped and repeated at any time.

16.4.2.3 Image Reconstruction and Postprocessing of C-Arm CT Images

Although it is beyond the scope of this chapter to provide exact details on how to perform a C-arm CT scan which is highly dependent on the angiographic system used, we want to provide typical guideline values for the acquisition of C-arm CT images of the abdomen or pelvis. The data are taken from an Axiom Artis angiography flat-detector C-arm (Siemens Medical Solutions, Forchheim, Germany). Usually an 8-s rotation with a total scan angle of 240°, a projection angle increment of 0.5°, and a system dose per pulse of 0.36 μGy is performed. The scan range has a cylindrical shape with a craniocaudal coverage of 185 mm and a transverse and sagittal scan range of 225 mm.

For image reconstruction, the raw data set is sent to a dedicated 3D image reconstruction workstation. The image reconstruction software on the workstation is used to transform the acquired projectional images (raw data) to a volumetric data set. The generation of a 3D data set takes usually less than 1 min when a fast network connection between the C-arm system and the reconstruction workstation is used. Dependent on the volume of interest and the purpose of the C-arm CT, the reconstruction kernel and the matrix of the cross-sectional C-arm CT images have to be chosen. For the purpose of soft tissue

Table 16.7 Image reconstruction parameters, image resolution, and postprocessing options dependent on the purpose of C-arm CT. The calculated image resolution assumes a maximum volume of interest (transversal image diameter of 225 mm)

Purpose (Target structure)	Contrast enhancement	Reconstruction, image resolution	Postprocessing options
Soft tissue visualization (e.g., puncture guidance)	None	Soft kernel, 256 × 256 matrix 0.9 × 0.9 mm	MPR (3–5 mm)
Bone visualization (e.g., spinal interventions)	None	Hard kernel, 512 × 512 matrix 0.4 × 0.4 mm	MPR (2–5 mm) VRT
Vessel visualization (e.g., endovascular interventions of the liver, embolization guidance)	Intra-arterial administration	Soft kernel, 512 × 512 matrix 0.4 × 0.4 mm	MPR (3–5 mm) MIP (5–100 mm) VRT

depiction using unenhanced C-arm CT images, for example, for puncture guidance, a suited soft tissue kernel and a smaller reconstruction matrix of 256 × 256 should be chosen to reduce the image noise. Contrast-enhanced C-arm CT images for the purpose of vessel depiction, for example, prior to chemoembolization, should be reconstructed with the highest matrix size of 512 × 512 to obtain a detailed vessel depiction.

General postprocessing strategies of MSCT can also be applied to C-arm CT images. A small slice thickness of below 1 mm and the slightly lower soft tissue contrast of C-arm CT results in a high image noise. To improve the soft tissue contrast of unenhanced C-arm CT images, multiplanar reformations (MPR) with a higher slice thickness (e.g., 3 or 5 mm, dependent on the target structure size) can be used. Maximum intensity projections (MIP) show an excellent image quality in contrast-enhanced C-arm CT images using intra-arterial contrast administration. Due to the very high intravascular contrast enhancement, even thick slab MIP can be used to depict the complete vascular territory. For the same reason, noise can be handled by selecting a high window center with a broad window width. Volume rendering technique (VRT) is typically used for vascular visualization and for spinal interventions (Table 16.7).

16.4.2.4 Percutaneous Puncture Technique Using C-Arm CT

C-arm CT-guided punctures in the angiography suite have several advantages: equipment and staff are dedicated to performing interventional procedures and easy patient access and fluoroscopic as well as US guidance are available if needed. On the other hand, the gold standard MSCT provides a contrast resolution of about 1 HU as the acquisition technique is optimized for soft tissue visualization. In contrast, the FD of an angiographic system is optimized for temporal and spatial resolution. Thus, contrast resolution of C-arm CT is slightly inferior to MSCT and ranges between 5 and 10 HU.

Under consideration of these pros and cons, feasibility and comfort of the intervention have to be validated before C-arm CT is chosen for puncture guidance. Percutaneous punctures with a high contrast of the target to the surrounding tissue can be well conducted under C-arm CT guidance. The use for spinal interventions, such as vertebroplasty, kyphoplasty, and periradicular infiltrations; biopsies or ablations of the bone; and lung biopsies are typical examples. In case of a lower contrast of the target structure, puncture planning is basically supported by contrast-enhanced preprocedural MSCT images, MRI, or PET images. To account for the limited conspicuity of the target with C-arm CT during the intervention, the images can either be reviewed side by side (Meyer et al. 2008b) or as an overlay after 3D image fusion with the C-arm CT data set (Becker et al. 2009). The availability of fluoroscopy and DSA also suggests the use of C-arm CT for percutaneous embolization of endoleaks after endovascular aortic repair (Fig. 16.12). For these cases, both preprocedural contrast-enhanced MSCT and contrast-enhanced C-arm CT during the procedure are beneficial to clearly identify the endoleak.

With the current C-arm systems, there are different techniques that facilitate percutaneous punctures in the angiography suite. Punctures can be performed using intermittent acquisition of C-arm CT images. This is similar to the traditional CT puncture technique that uses intermittent control scans, allowing for a stepwise propagation and control of the needle position. Since repeated confirmation of the needle path is necessary, this requires the acquisition of multiple C-arm CT volumes, resulting in relatively long procedure times and increasing radiation exposure. To reduce the radiation exposure of the individual patient, the volume of interest can be collimated from top and bottom, leaving open a slab that covers only the needle and the immediate surroundings (Fig. 16.12). Finding the entry point is more difficult in a C-arm than in MSCT, where the slice selection is usually done using the positioning laser in combination with an external marker grid. Dependent on the system configuration, more recent C-arm systems provide a laser sight which is usually part of a puncture guidance option. Without laser, the skin entry point has to be localized using markers, grids, or anatomical landmarks in the fluoroscopic image, which makes the definition of the needle entry point less intuitive.

To overcome boundaries that are associated with intermittent C-arm CT control scans during the puncture, fluoroscopy can be used to control the needle advancement. Since most targets are not visible under fluoroscopy and fluoroscopy offers only one projection image at a time, additional features are needed to facilitate safe and reliable puncture. One approach is to use a graphic overlay on top of the live fluoroscopic image that helps outlining the needle entry point and the needle path with different C-arm angulations. The initial planning of the needle path has to be performed prior to starting the puncture on C-arm CT images. Once the skin entry has been made, the C-arm can be brought in a position perpendicular to the needle and the depth can be determined based on live images, the graphic representation of the target, and a virtual needle path superimposed on the live fluoroscopic image. In addition to overlaying the live fluoroscopic image with graphic features representing the target and the virtual needle trajectory, the actual C-arm CT images (and any other information that can be fused with the C-arm CT mages) can be displayed as an overlay. With both methods, however, it is important to avoid any patient movement between acquisition of the planning C-arm CT and the actual procedure.

The need for both repeated C-arm CT as well as intermittent fluoroscopy can be overcome by using navigation systems for needle tracking. Such systems provide navigation information visualizing the puncture needle and road map information based on imaging obtained prior to the puncture. Careful trajectory planning within the 3D road map allows the physician to “see” nearby anatomy when planning the procedure as well as during needle advancement without any additional radiation exposure. Advantages are free needle angulations, use of additional image information such as MR imaging, CT, or positron emission tomography (PET) that can be co-registered with the 3D road map for virtual navigation, and, as mentioned before, reduction of radiation exposure to the patient and interventionalist. Disadvantages are need for co-registration of the patient’s body with the 3D space of the navigation system and respiratory, bowel, and patient motion error as well as organ shift during the needle advancement. There are optical as well as electromagnetic tracking systems available on the market. With optical needle tracking methods, known limitations are line-of-sight problems with the optical markers at the needle end and positioning errors due to needle bending. These problems have more recently been overcome with electromagnetic tracking. Here, an electromagnetic field generator (Fig. 16.13) is placed in proximity to the patient. The field generator produces an ultralow electromagnetic field that induces very weak currents in the sensor coils in the needle tip as well as the reference frame. The current strength in these coils is dependent on the location, the position, and the orientation of the detector and can thus be measured and localized within the electromagnetic space. The main advantage over optical navigation is that the actual needle tip position is electromagnetically tracked in real time, whereas with optical systems, the needle tip must be calculated from the

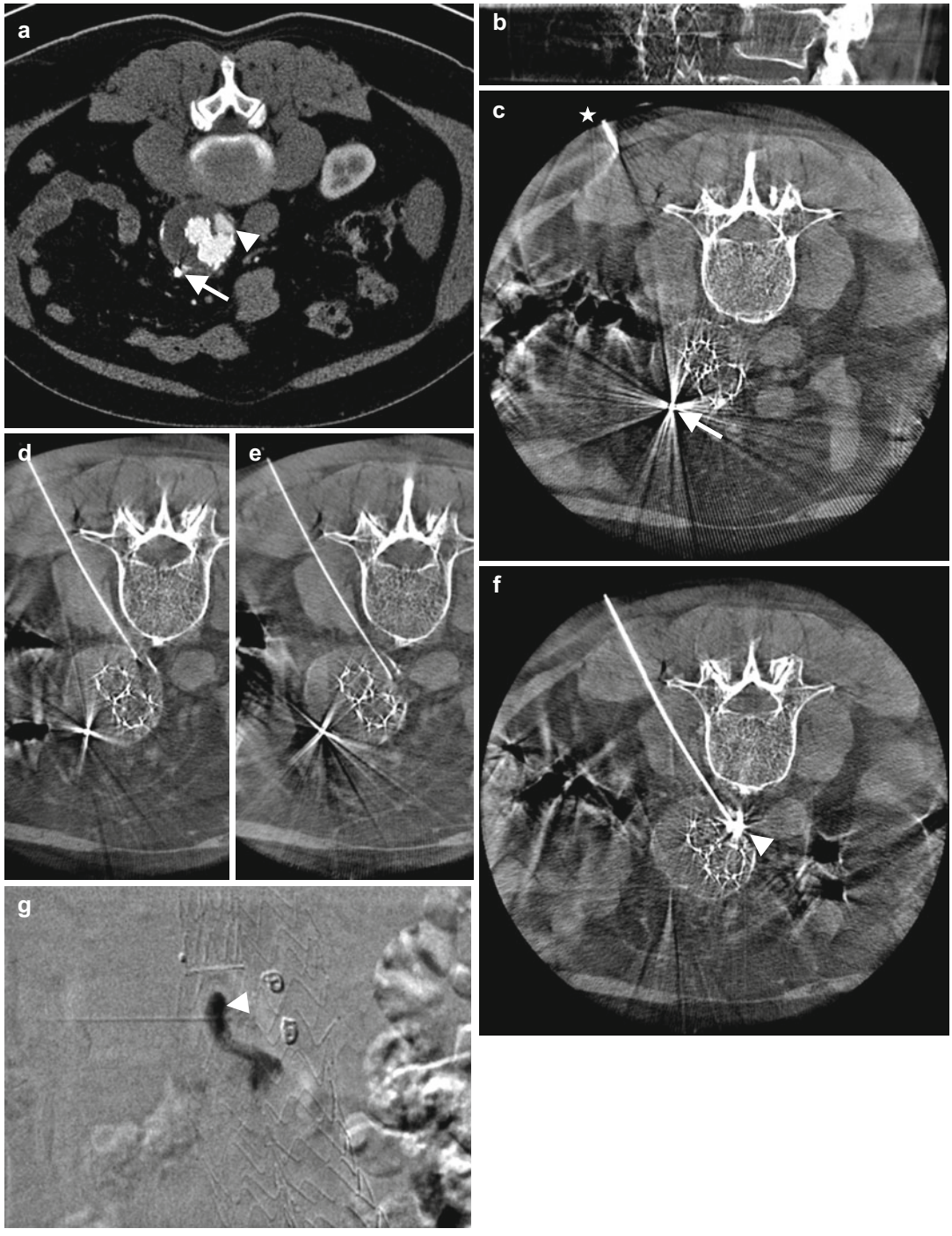

Fig. 16.12 Percutaneous puncture of a type II endoleak after EVAR. (**a**) 3-mm MPR of the lower abdomen MSCT shows the contrast-enhanced endoleak (*arrowhead*) at the level of the previously coil-embolized inferior mesenteric artery (IMA, *arrow*). (**b**, **c**) Sagittal and transversal 3-mm multiplanar reconstructions of the unenhanced C-arm CT using slab acquisition to cover only the needle (*asterisk*) and the immediate surroundings. The puncture site was fluoroscopically identified by the coils in the IMA. Note the hardening artifacts caused by the coil and the struts of the stent graft. (**d**, **e**) Control scans during the propagation of the needle toward the endoleak. (**f**, **g**) C-arm CT and DSA under contrast injection into the endoleak (*arrowhead*) to confirm the correct needle position prior to embolization

position and orientation of the needle end outside the body. The precision of electromagnetic navigation systems however may be limited if relevant amount of ferromagnetic metal such as a CT gantry is present in the proximity of the field generator.

Most needle tracking systems have been developed for use in CT. However, most CT-guided procedures are currently performed without a navigation system. Among other reasons, this is because ease of use of such navigation systems is often limited by lengthy software setups, tedious registration processes, and lack of seamless integration with the imaging system. With the advent of C-arm CT, however, navigation systems have gained increased interest. This is mainly because finding the optimal skin entry point in relation to the deeper laying target is more difficult with C-arm CT than with conventional CT. In addition, the acquisition of a C-arm CT takes longer than the acquisition of a CT scan, at least with the currently available C-arms. Therefore, a well-integrated navigation system could provide more time saving in percutaneous C-arm CT interventions when compared with conventionally CT-guided interventions.

Although the use of electromagnetic navigational systems with multiple other imaging

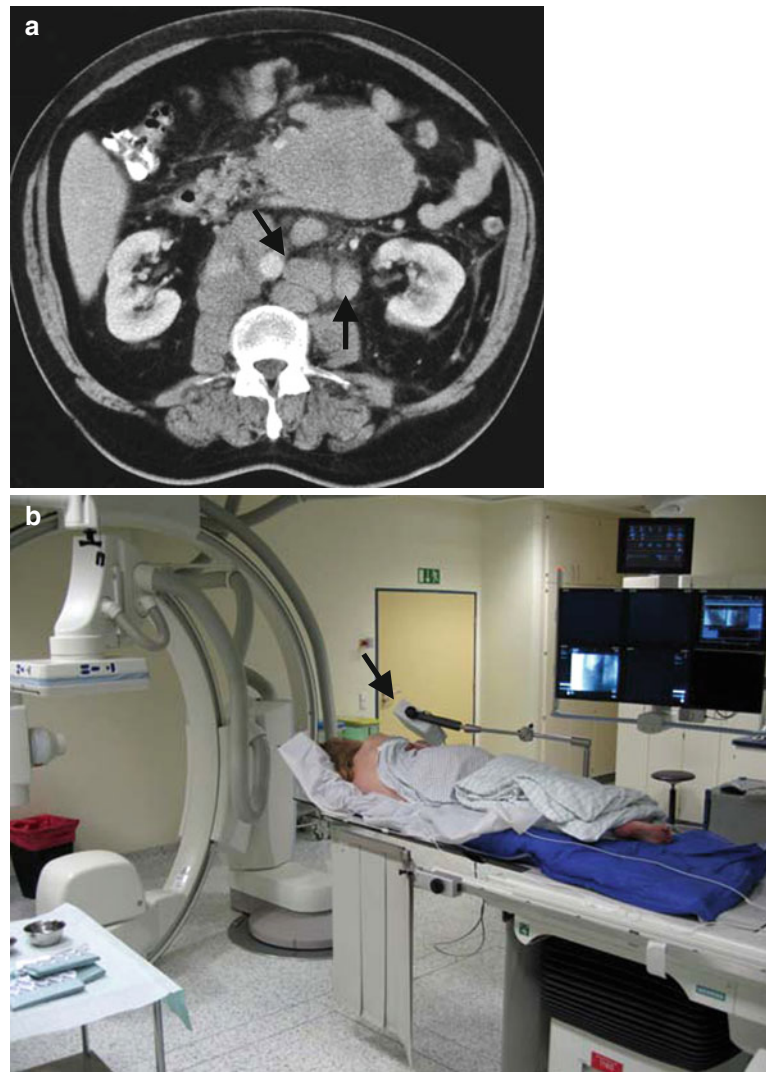

Fig. 16.13 (**a**–**e**) Biopsy of an enlarged retroperitoneal lymph node. a MPR of the upper abdomen MSCT shows multiple enlarged retroperitoneal lymph nodes (*arrow*). (**b**) Photograph of the setting of an electromagnetic field-based navigation device (ND). The patient is bedded on a vacuum mattress to avoid movements during baseline C-arm CT scan and intervention. (**c**) Initial phase of the puncture. Screenshot shows two preprocedural C-arm CT images that are displayed orthogonal to the needle (*red line*) in real time. The virtual needle extension (*yellow dotted line*) eases the correct angulation of the needle. The selected skin entry point (*yellow cross*) and the puncture target (*red cross*) are also superimposed on the MPR images. The schematic ring figure (*asterisk*) summarizes both the depth of the needle tip as well as the needle orientation. (**d**) The sterile, covered field generator (*arrow in* **b**) is attached to the patient table and connected to the ND (*dotted arrow*). (**e**) The transversal MPR image of the post-interventional C-arm CT scan confirms the correct needle placement

Fig. 16.13 (continued)

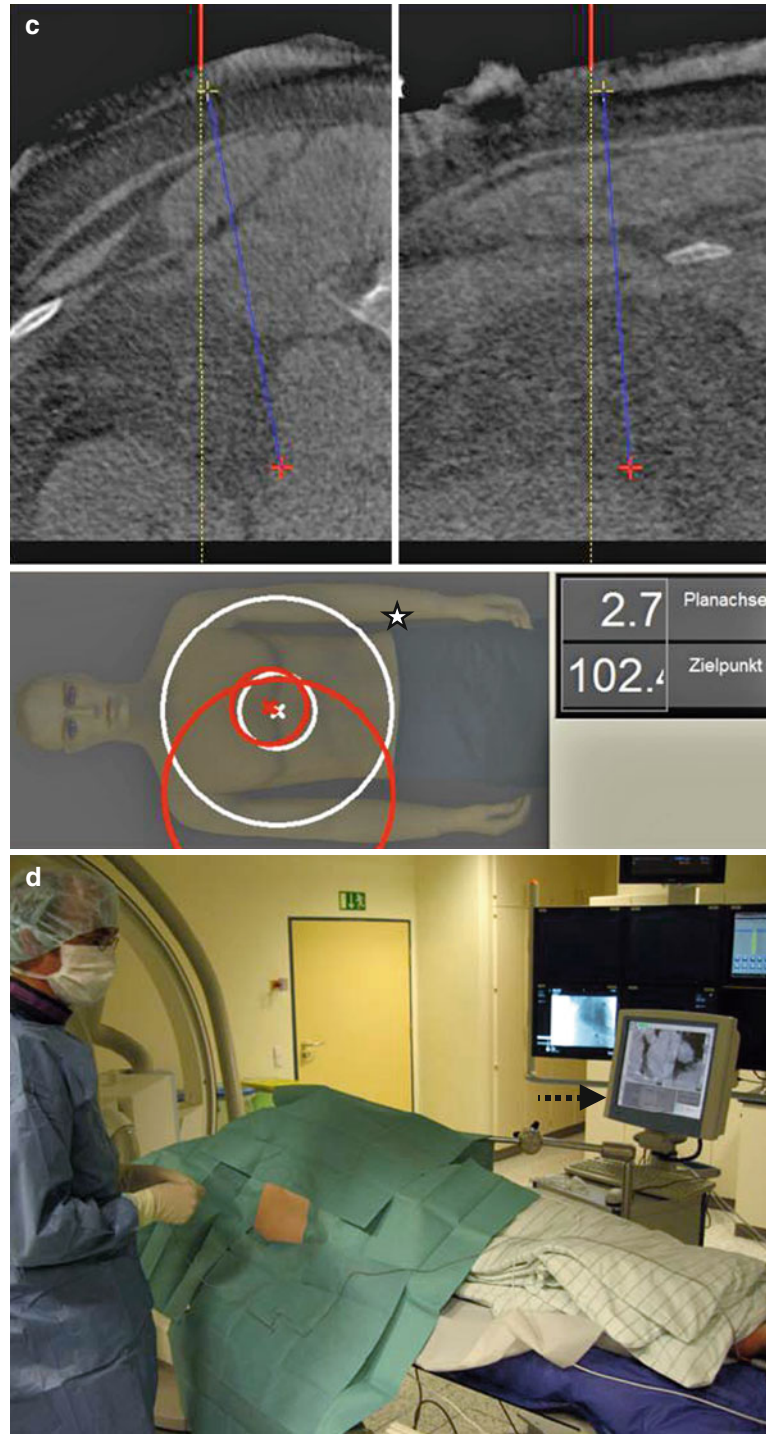

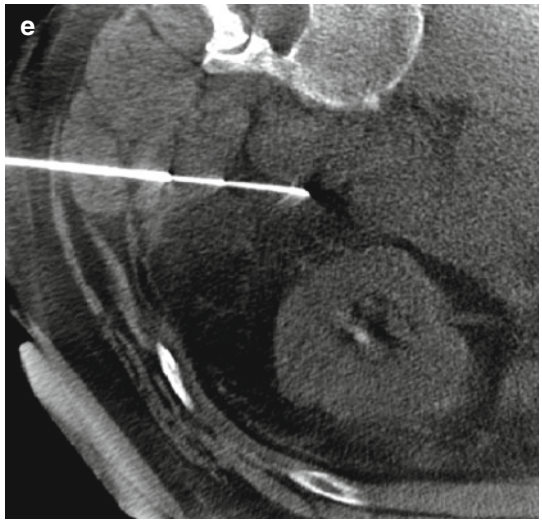

Fig. 16.13 (continued)

modalities has been reported previously, the use of such a system with C-arm CT is new. In general, preprocedural imaging has to be performed before the puncture. After data acquisition and image reconstruction, the 3D data set is sent to the navigation system using a local area network Ethernet connection. Co-registration of the tracking space and the C-arm CT image space can be performed using skin or anatomic fiducial markers. In one system, a reference frame inside the scan range with radiopaque markers and two sensor coils allow for automatic co-registration. After successful registration, real-time tracking of the needle within the electromagnetic space is performed. This is facilitated through a small coil embedded in the tip of the needle which is connected to the interface of the navigation system. Based on the current in the coil, the position of the needle tip is displayed in real time on the C-arm CT images.

16.4.2.5 Catheter-Based Interventions Using C-Arm CT

Vascular interventions are usually performed in an angiography suite relying on 2D real-time projection radiography with poor soft tissue contrast and no 3D information. This problem led to installation of the first combined suites or hybrid suites with both CT and digital subtraction angiography (DSA) units a decade ago (Capasso et al. 1996). These suites were used for various clinical indications, such as selective arterially enhanced CT examinations, organ and lesion perfusion studies before embolization and local chemotherapy, and combined CT- and fluoroscopy-guided interventions such as percutaneous biopsy and catheter drainage, bone interventions, and CT arthrography (Capasso et al. 1996; Vanderschelden et al. 1998; Froelich et al. 2000a, b). More recently, hybrid units combining DSA and MR imaging systems have been developed (Vogl et al. 2002; Dick et al. 2005). However, such suites require higher investment cost and spacious room for equipment installation in comparison to a single fluoroscopy C-arm angiography. In contrast to such hybrid suites, modern FD C-arms with C-arm CT capability offer unrestricted availability of both digital subtraction angiography and cone beam volume CT. Risky and time-consuming patient transfer from the angiography table to other imaging modalities such as MR or CT can be avoided.

The use of C-arm CT during endovascular interventions has two essential advantages compared to MSCT. First, contrast material can be administered intra-arterially as a compact bolus using a selective catheter position. Consecutively, a strong intravascular and parenchymal enhancement can be achieved. This at least compensates the limited contrast resolution of C-arm CT compared to MSCT. Second, C-arm CT provides a very high spatial resolution. In combination with the strong contrast enhancement, this results in a very detailed vessel depiction that has shown to be superior to that of MSCT (Fig. 16.14). For larger, well-defined targets, however, even unenhanced C-arm CT can be used to visualize the target, for example, the central portal vein, during TIPS placement.

Due to the higher contrast resolution of C-arm CT compared to DSA, contrast material administration has to be adapted for C-arm CT (Table 16.8). Since C-arm CT is very susceptible for beam-hardening artifacts with very strong contrast enhancement, the effective contrast material concentration in the vessel has to be reduced compared to DSA. This can be obtained

by a reduction of the flow rate, which bears the risk of inhomogeneous vascular opacification due to insufficient mixing of contrast material and blood especially in smaller vessels. A practicable way to avoid this phenomenon is to dilute the contrast material with normal saline and to use higher flow rates similar to those established for DSA. Table 16.8 provides exemplary contrast administration protocols of our institution dependent on the catheter position.

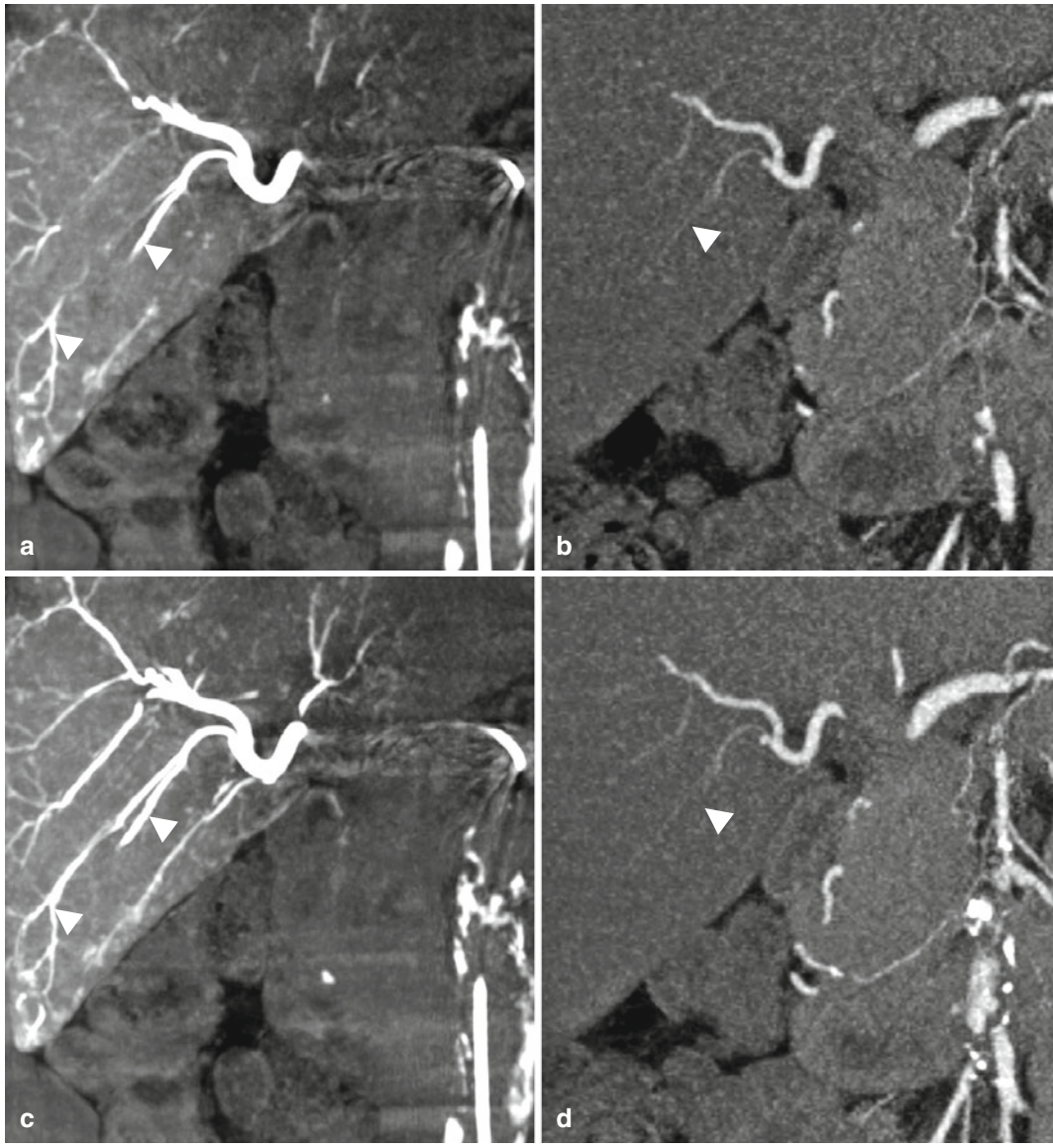

Fig. 16.14 (**a**, **c**, **e**) C-arm CT and (**b**, **d**, **f**) MSCT of the liver in the arterial phase prior to chemoembolization. Due to the different forms of contrast material administration (intravenously in MSCT, intra-arterially via the common hepatic artery in C-arm CT), a significant higher artery-to-liver contrast is obtained in C-arm CT. (**a, b**) 5-mm and (**c, d**) 10-mm coronal maximum intensity projections at corresponding positions of the liver in both modalities demonstrate the superior delineation of peripheral hepatic artery branches (*arrowhead*) in C-arm CT due to the stronger opacification and the superior spatial resolution of C-arm CT. (**e, f**) 3-mm multiplanar reconstructions demonstrate the excellent visualization of the gallbladder artery branches in C-arm CT (*arrows*)

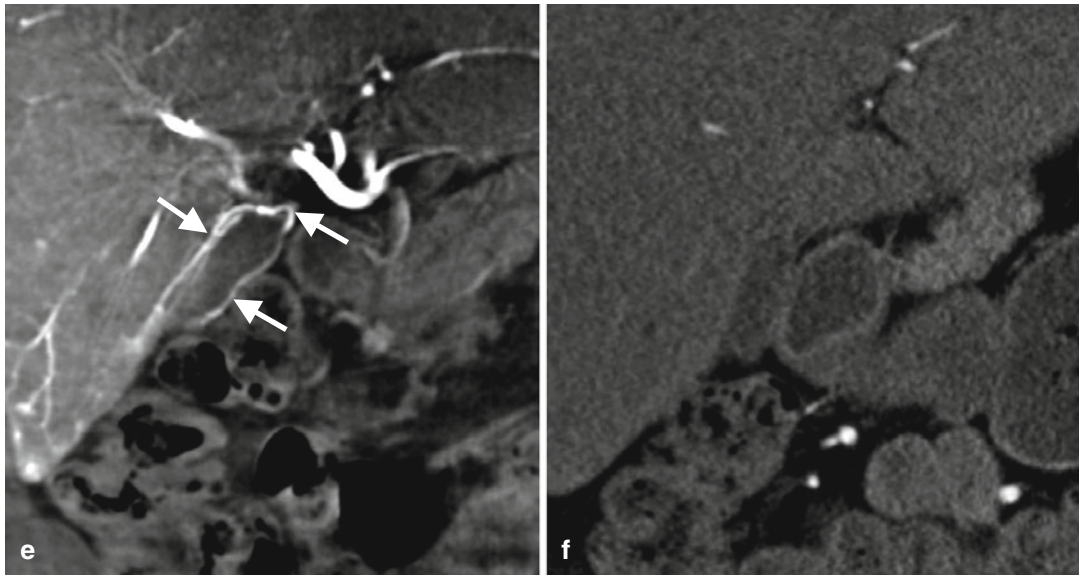

Fig. 16.14 (continued)

Table 16.8 Contrast material application in C-arm CT. The calculated total amount of contrast material assumes an injection time of 10s (acquisition time of 8 s, additional forerun of 2 s).

Vascular territory	Catheter type and position	Iodine concentration, flow rate, volume
Aorta, bilateral pelvic arteries	4-F/5-F pigtail catheter Aorta	150 mg iodine/ml 7–10 ml/s (70–100 ml)
Unilateral pelvic arteries	4-F/5-F pigtail catheter Common iliac artery	100 mg iodine/ml 4–8 ml/s (40–80 ml)
Abdominal aortic branches (e.g., celiac trunc, common hepatic artery, superior mesenteric artery, renal artery)	For example, 4-F cobra catheter Origin of the vessel	100 mg iodine/ml 2.5–5 ml/s[a] (25–50 ml)
Selective catheter position (e.g., hepatic segment arteries, small tumor-feeding arteries)	Microcatheter Selective position	100–150 mg iodine/ml 0.5–ml/s[a] (5–25 ml)

[a]Flow rate should be estimated in DSA

16.4.3 Results

16.4.3.1 Results of Percutaneous Punctures Using C-Arm CT

Currently, only few clinical papers are available on C-arm CT-guided percutaneous interventions. The successful use of C-arm CT for needle guidance has been recently reported for percutaneous vertebroplasty (Tam et al. 2010). C-arm CT was also used to assess the technical success of percutaneous vertebroplasty and sacroplasty (Pedicelli et al. 2009; Kang et al. 2010). For final postprocedure assessment, cement distribution was visualized equally well by C-arm CT compared to MSCT (Kang et al. 2010); reported sensitivity and specificity compared to MSCT for the detection of cement leakages was 95 and 100 %, respectively (Pedicelli et al. 2009).

Jin et al. performed percutaneous transthoracic biopsies of lung nodules under fluoroscopy and C-arm CT guidance in 71 patients with a technical success rate of 100 %(Jin et al. 2010) (Jin et al.). In this study, the skin entry point was either identified by fluoroscopy or by a radiopaque grid placed on the chest wall on C-arm CT.

In the majority of papers published on C-arm CT-guided percutaneous punctures in patients, puncture was performed using a fluoroscopic needle path overlay derived from the preprocedural C-arm CT (Braak et al. 2010; Mohlenbruch et al. 2010; Morimoto et al. 2010; Tam et al. 2010). The technical success rate was reported to be 100 % in all four studies. Beside the use for thoracic and abdominal therapeutic punctures and diagnostic biopsies (Braak et al. 2010), overlay guidance was also used for the translumbar placement of central venous catheters (Tam et al. 2009), for percutaneous gastrostomy (Mohlenbruch et al. 2010), and for hepatic tumor ablation (Morimoto et al. 2010). In the latter study, intra-arterial contrast administration was used to overcome the limited soft tissue resolution of C-arm CT.

Initial clinical applications of the electromagnetic tracking system are promising. In a pilot study, the needle deviation was less than 10 mm for targets as deep as 20 cm within the human body (Meyer et al. 2008b). So far, we have targeted only lesions that were not prone to breathing motion such as retroperitoneal lymph nodes or abscesses. Although electromagnetic tracking shows the advantage of radiation-free puncture guidance and real-time needle tip visualization, the clinical value of this approach seems to be diminished by the need for additional devices and dedicated needles.

Based on the experience in our own group and on the results in the literature, C-arm CT-guided punctures have the ability to expand the range of procedures that can be performed in an angiography suite. One of the main advantages is the seamless transition from a C-arm CT-guided to a fluoroscopy-guided intervention for procedures such as percutaneous biliary drainage (Fig. 16.15), percutaneous nephrostomy, abscess drainage, or percutaneous endoleak embolization (Fig. 16.12).

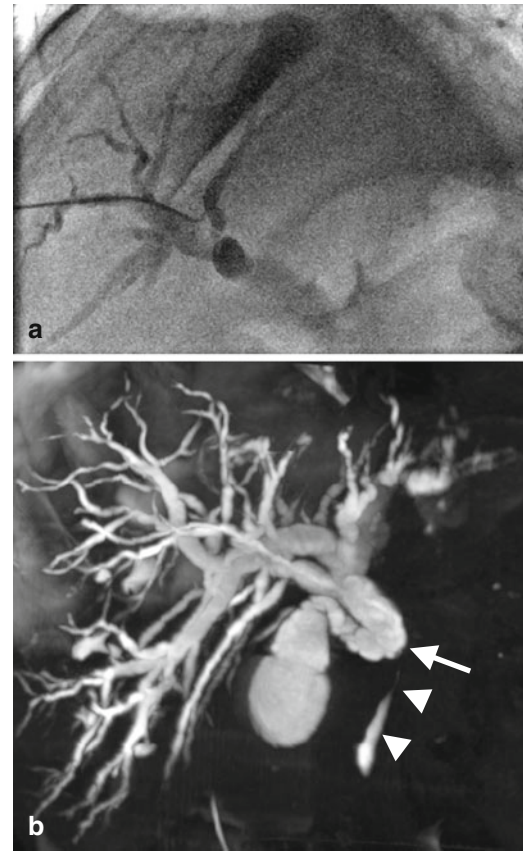

Fig. 16.15 (**a**, **b**) PTC and direct C-arm CT cholangiography. (**a**) Fluoroscopic image after puncture of a right hepatic bile duct, contrast injection, and insertion of a guidewire. (**b**) C-arm CT cholangiography after injection of diluted contrast material through the drainage catheter shows the subtotal stenosis of the common bile duct (*arrow*) followed by a filiform stenosis of the subsequent segment (*arrowhead*) caused by a tumor in the pancreas head. Due to the high endoluminal contrast, a high window level allows for a clear delineation of the small bile duct branches even with MIP

16.4.3.2 Results of Catheter-Based Interventions Using C-Arm CT

Several potential benefits of C-arm CT during catheter-based interventions have been investigated since C-arm CT has been introduced. In small series, C-arm CT was instrumental for the creation of TIPS (Sze et al. 2006), for the detection of intracranial hemorrhage (Heran et al. 2006), and for the confirmation of the catheter position during adrenal vein blood sampling (Fig. 16.16) (Georgiades et al. 2007).

The majority of publications investigated the use of contrast-enhanced C-arm CT during embolization studies. Advantages of C-arm CT guidance have been demonstrated for embolization of head, neck, and abdominal tumor embolization. In a study of Kakeda et al., the anatomic detail on

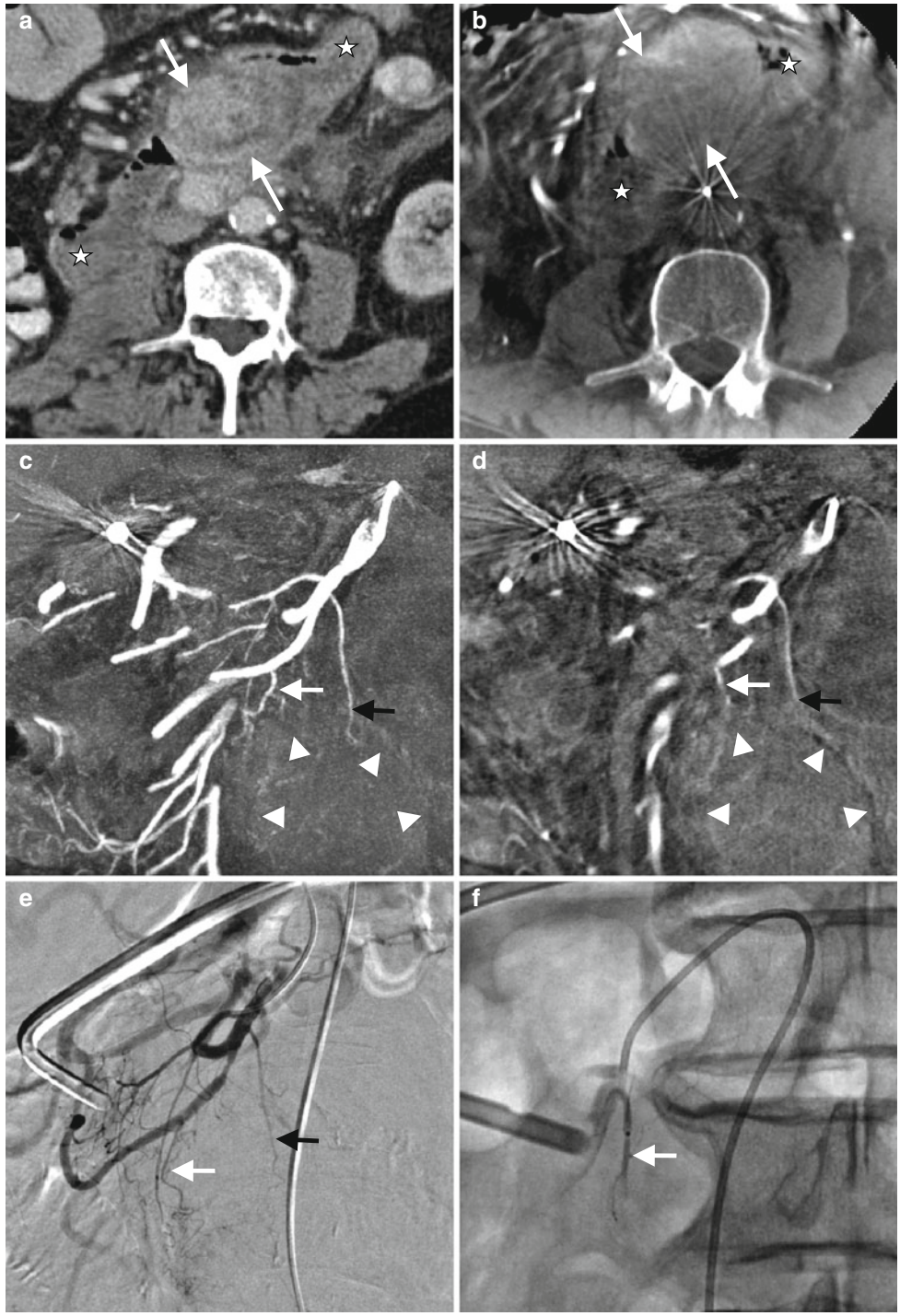

Fig. 16.16 (**a**–**d**) Embolization of a liposarcoma infiltrating the duodenum. (**a**, **b**) MSCT and C-arm CT of the abdomen show a large tumor (*arrows*) infiltrating the duodenum (*asterisk*). (**c**, **d**) MIP (15 mm, **c**) and MPR (5 mm, **d**) of the C-arm CT in the arterial phase provides information on both feeding vessels as well as soft tissue of the tumor (*arrowheads*) and the surrounding structures. This enables clear-cut identification of two tumor-feeding arteries (*white and black arrow*). (**e**) DSA of the SMA shows multiple small branches, but conclusive identification of tumor-feeding vessels is not provided. (**f**) Selective angiogram proves successful embolization of one of the feeding vessels (*white arrow*, same vessel as in (**c**–**e**), from Meyer et al. (2007))

continuous cross-sectional C-arm CT imaging was advantageous over DSA alone in patients with advanced head and neck tumors for superselective intra-arterial chemotherapy, thus enabling higher concentrations of chemotherapeutic agents within the tumor bed with fewer systemic toxic effects than normally seen with systemic chemotherapy (Kakeda et al. 2007a).

The same was true for embolization procedures in abdominal tumors (Meyer et al. 2007). Here, C-arm CT in combination with the intra-arterial contrast injection leads to improved visualization of smaller vessels that compares favorably to MSCT during intravenous administration of contrast medium (Figs. 16.17 and 16.18).

Fig. 16.17 (**a**–**d**) Embolization of a renal metastasis for pain management. (**a**) Coronal T1-weighted fat-saturated post-contrast MRI acquired prior to the intervention shows hepatic metastases and renal metastasis in the upper third of the left kidney (*arrow*). (**b**) C-arm CT of the upper abdomen in the portal venous phase. Disseminated hepatic metastases and renal metastasis in the upper third of the left kidney (*arrow*). (**c**, **d**) C-arm CT images acquired after chemoembolization of the left kidney. The perfusion defect in the upper pole of the kidney can clearly be appreciated. A segmental artery feeding the upper pole is still opacified (*black arrow*). C-arm CT allows differentiation of the perfusion defect (*black arrowhead*), metastasis (*white arrowhead*), and the normally perfused renal parenchyma (*asterisk*). Note the excellent visualization of the small left adrenal gland vein (*white arrow*; from Meyer et al. (2007))

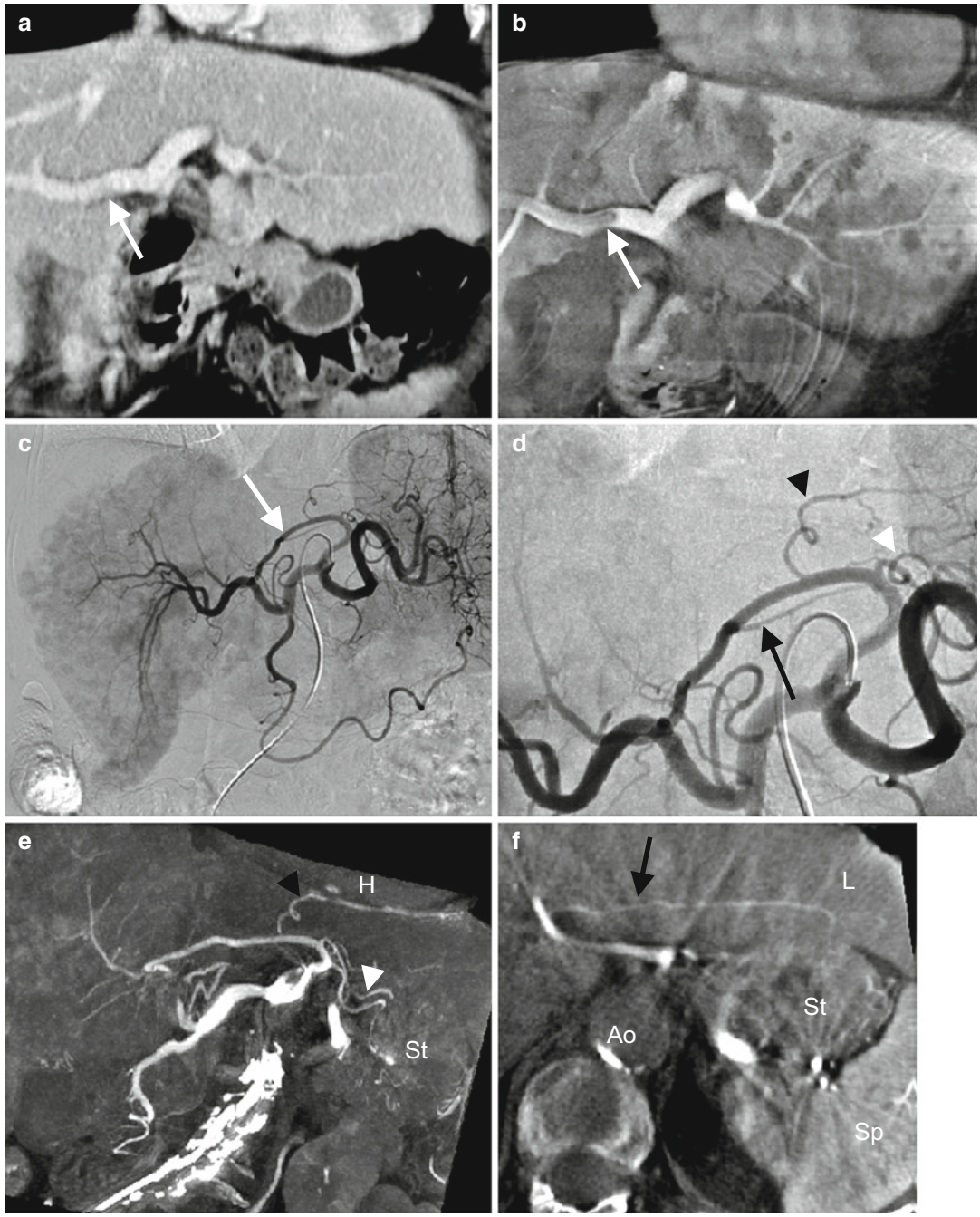

Fig. 16.18 (**a**–**f**) TACE of the liver (**a**, **b**). Coronal MPR (3 mm) of the MSCT (**a**) and the C-arm CT (**b**), both in the portal venous phase. The disseminated hepatic metastasis as well as the segmental partial thrombosis of the portal vein (*arrow*) can be better appreciated with C-arm CT. (**c**) DSA shows the left hepatic artery feeding liver segments 2, 3, and 4 (*arrow*) coming off the prominent left gastric artery. (**d**) Enlarged view of the DSA shown in (**c**). Clear classification of the three proximal side branches of the left gastric artery could not be achieved on a single projection. (**e**, **f**) Coronal curved MPR of the C-arm CT with simultaneous presentation of both the soft tissue as well as the arteries facilitates clear identification of the gastric branches (*white arrowhead* in **d** and **e**), a phrenic branch *(black arrowhead* in **d** and **e**), and a hepatic branch *(black arrow* in **d** and **f**) feeding liver segments 2 and 3. Based on these findings, the catheter for chemoembolization of the left liver lobe was positioned at the *arrowhead* shown in (**c**). *St* stomach, *Ao* aorta, *L* liver, *Sp* spleen, *H* heart (From Meyer et al. (2007))

Iwazawa et al. used C-arm CT to identify tumor-feeding arteries and observed that C-arm CT is superior to DSA for identifying tumor-feeding arteries during superselective TACE for HCC (Iwazawa et al. 2009). In a study from our group, in 50 % of the patients, the catheter position for TACE was changed after considering C-arm CT compared to DSA alone (Meyer et al. 2009). Wallace et al. demonstrated that C-arm CT provides additional imaging information beyond DSA during hepatic arterial interventions (approximately 60 %) and that this information impacted procedure management in 19 % of cases. C-arm CT offered the greatest opportunity for additional information during chemoembolization procedures and was responsible for a significant but acceptable increase in procedure time for this type of hepatic intervention (Wallace et al. 2007). The high impact of C-arm CT on the TACE procedure demonstrated in these studies suggests the benefits of its routine use for all patients undergoing their first TACE.

The quality of soft tissue visualization during intra-arterial contrast administration was initially investigated by two groups (Kakeda et al. 2007b; Meyer et al. 2008a). The setting is comparable to CTHA and CTAP using conventional CT, which rely on selective delivery of contrast material to the liver via the hepatic artery and the portal vein and are known to have sensitivities around 90 % for the detection of hypervascular liver lesions (Spreafico et al. 1997). Both the cumbersome patient handling of CTAP and the success of MR imaging of the liver led to a sustained decline in usage of CTHA and CTAP over the last decade.

With C-arm CT, however, no patient transfer is necessary after the catheter is placed into the respective arteries. Even when catheter repositioning becomes necessary, this can be performed without moving the patient or the patient table. Kakeda et al. observed that intra-arterially enhanced C-arm CT can provide clinically acceptable image quality in the assessment of HCC, thereby improving the detection of tumor staining due to HCC and the visualization of the extent of contrast medium perfusion (Kakeda et al. 2007b). In a study from our group in patients undergoing transarterial chemoembolization of the liver, the angiographic C-arm was used to perform the procedure under fluoroscopic control as well as to acquire C-arm CT images during contrast injection into the hepatic and superior mesenteric artery (Fig. 16.19). Interobserver agreement for segmental tumor involvement in

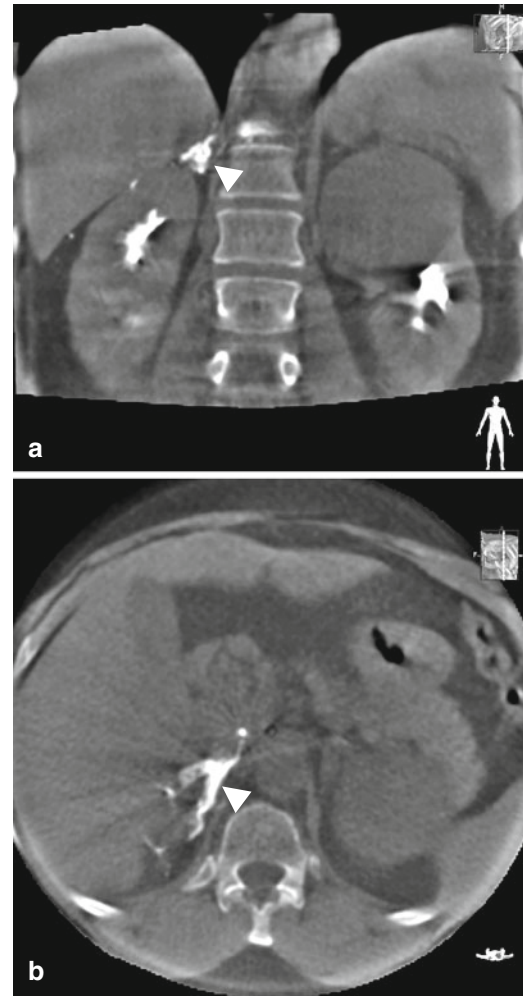

Fig. 16.19 (**a**, **b**) C-arm CT of the adrenal gland. (**a**, **b**) Coronal and axial MPR of C-arm CT performed during hand injection of contrast medium via a catheter in the adrenal vein demonstrate opacification of the right adrenal gland (*white arrowhead*), confirming proper catheter position. The medial and lateral limbs of the gland are clearly identified. (Images courtesy of Christos Georgiadis, Johns Hopkins School of Medicine, The Russell H. Morgan Department of Radiology and Radiological Science)

the liver was very good during intra-arterial contrast administration and compared favorably to that of MSCT (Meyer et al. 2008a).

Recently, a paper on the use of C-arm CT for radioembolization has been published by Becker et al. (Becker et al. 2011). For radioembolization planning, C-arm CT provided some additional information in 31.9 % or had an impact on the procedure in 25.6 % of patients, respectively. The authors conclude that C-arm CT may add decisive information in patients scheduled for RE.

Potential disadvantages of C-arm CT include increased amounts of contrast agent, additional radiation exposure, and additional time required for setup, C-arm CT run, and reconstruction. In our experience, however, the detailed information on vascular anatomy provided by C-arm CT helps to avoid additional oblique DSA runs, thus reducing radiation and amount of contrast with the interventional procedure. It remains to be seen if this compensates for the time, dose, and contrast agent used for C-arm CT during catheter-based interventions.

16.4.4 Complications

C-arm CT is a relatively new technique with only few reports on clinical applications. Most of them use C-arm CT during catheter-based interventions, and only few papers exist on percutaneous punctures using C-arm CT. Complications are more likely to be related to the procedure itself, and specific complications of C-arm CT have, to the best of our knowledge, not yet been reported.

Based on the overall image properties of C-arm CT, one could hypothesize that certain procedures, such as percutaneous punctures of small structures with a low contrast to the surrounding tissue (e.g., small liver lesions), might be associated with a higher rate of unsuccessful punctures, more puncture attempts per patient, and higher complication rate due to the inferior contrast resolution and the limited field of view. On the other hand, the ability to perform double oblique punctures with more access options to lesions that are difficult to reach with MSCT might reduce the number of complications. For endovascular procedures, the additional information provided by contrast-enhanced C-arm CT might reduce the number of additional selective angiographic series needed and provide additional soft tissue information. This could lead to reduced number of DSA runs and shorter procedure time as well as decreased complication rate with endovascular C-arm CT-guided procedures. Since there are no studies directly comparing MSCT and C-arm CT yet, the actual complication rate of C-arm CT remains to be determined.

Summary

The increasing complexity of minimally invasive procedures requires a continuous improvement in imaging technologies that guide and monitor such procedures. Modern FD C-arms with C-arm CT technology combine 3D soft tissue imaging, 2D real-time fluoroscopy, and high-resolution angiography without the need for transferring the patient to another imaging modality. Since C-arm CT is a relatively new technique, a standardized workflow is not yet established. Its benefits for interventional procedures have been demonstrated in a small number of studies, and only few reports exist on actual clinical applications. However, based on the preliminary results obtained so far, its potential goes beyond just copying existing procedures currently performed in an angiography or CT suite toward the guidance of minimally invasive techniques that need the full breadth of information available in an C-arm with C-arm CT capabilities.

Key Points

- Flat Panel Detector: C-arm CT requires FD angiographic systems to produce cross-sectional images with soft tissue information.
- 3D Soft Tissue Information: In the course of an interventional procedure,

C-arm CT provides 3D soft tissue information similar to MSCT without the need for transferring the patient.

- CT-Like Soft Tissue Images: C-arm CT currently provides CT-like soft tissue images with slightly higher spatial but slightly lower contrast and temporal resolution and a limited field of view when compared to MSCT.
- Detailed Depiction of Vascular Territories: C-arm CT acquisition during intra-arterial contrast administration provides a more detailed depiction of the vasculature and the supplied tissue compared to MSCT.
- C-arm CT is beneficial for percutaneous as well as for endovascular procedures. For some indications, such as transarterial embolizations, influence on the course of the intervention has been reported in several studies.

16.5 Hybrid Interventional CT/Angio System

Toshihiro Tanaka

16.5.1 Introduction

An interventional CT/angio system was developed in 1992, and Arai first introduced it in Aichi Cancer Center (Nagoya, Japan) (Inoue 1993; Inaba et al. 1996). This system integrates a computed tomography (CT) scanner and an angiography unit, which are arranged in line using a common patient table (Fig. 16.20). It permits CT, conventional fluoroscopy, and angiography on the same table without moving the patient, thereby omitting the risk of needle and catheter dislocation or losing sterile conditions due to patient transportation. Currently, about 150 systems are introduced in the world, and almost 90 % of them are in Japan. This system is used for various diagnostic and therapeutic interventions. In this chapter, the usage and advantages of a hybrid interventional CT/angio system are described for several common procedures.

16.5.2 CT During Arterial Portography (CTAP) and CT During Arterial Hepatic Arteriography (CTHA)

16.5.2.1 Indication

An interventional CT/angio system is quite convenient for conducting CT arterioportography (CTAP) and CT hepatic arteriography (CTHA) (Inaba et al. 2000). Combination of CTAP and CTHA is considered one of the most sensitive techniques for detection of hepatic tumors including hepatocellular carcinoma (HCC) and metastatic lesions. In addition, it is useful for imaging the multistep human hepatocarcinogenesis (Matsui et al. 2011) (Fig. 16.21). Although CTAP/CTHA is less routinely performed for liver metastases due to the recent progress in other image modalities, it still plays an important role particularly for small and early stage of HCC.

16.5.2.2 Technique

Usually, CTAP is chosen as the initial examination before angiography because an excellent contrast between the hepatic nodules with lack of the portal venous flow and the hepatic parenchyma can be achieved. Under fluoroscopic guidance, an angiographic catheter is inserted into the superior mesenteric or splenic artery. Kutlu et al. reported (Kutlu et al. 2004) that CTAP via splenic artery demonstrated lower prevalence of non-tumoral perfusion defects in the left hepatic lobe. By test injection of the contrast material, anatomic variations are excluded. In case an anatomical variation such as a transposition of the right hepatic artery arising from the superior mesenteric artery or hepatopetal flow of the gastroduodenal artery is found, the catheter must be inserted deeper beyond the orifice of the replaced right hepatic artery or distally from the origin of the pancreaticoduodenal

Fig. 16.20 Example of an interventional CT/angio system introduced in Nara Medical University in Japan (Infinix Activ, Toshiba Medical Systems) consisting of a CT scanner and an angio unit which are placed in line and use the same patient table

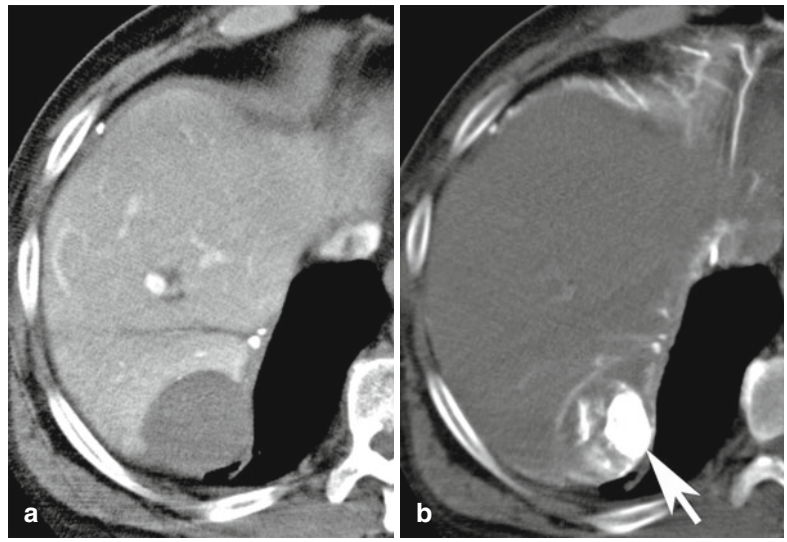

Fig. 16.21 HCC which shows "nodule-in-nodule" appearance. (**a**) CTAP shows portal perfusion-defective nodule. (**b**) CTHA shows a slightly hypervascular nodule with a central hypervascular focus (*arrow*). (**c**) Macro- and microscopic examinations proved a mostly well-differentiated HCC with sections of moderately differentiated HCC

artery. Thereafter, the patient table is slide into the CT gantry, and contrast medium diluted to 150 mg I/ml is injected through the catheter at a flow rate of 2–3 ml/s (total volume: 80–100 ml). The scan is started 25–35 s after initiation of the contrast injection. Administration of prostaglandin E1 (5–10 μg) is recommended to improve the homogeneity of the contrast enhancement of the liver parenchyma.

For CTHA, after fluoroscopically guided catheterization of the common or proper hepatic artery, the diluted contrast medium (100–150 mg I/ml) is injected at a flow rate of 1.5–2 ml/s (total volume: 20–30 ml), and the CT scan is started with a delay of about 5–10 s. In case of aberrant vessels, such as the right hepatic artery arising from the superior mesenteric artery, these aberrant arteries need to be selectively catheterized, too.

Fig. 16.21 (continued)

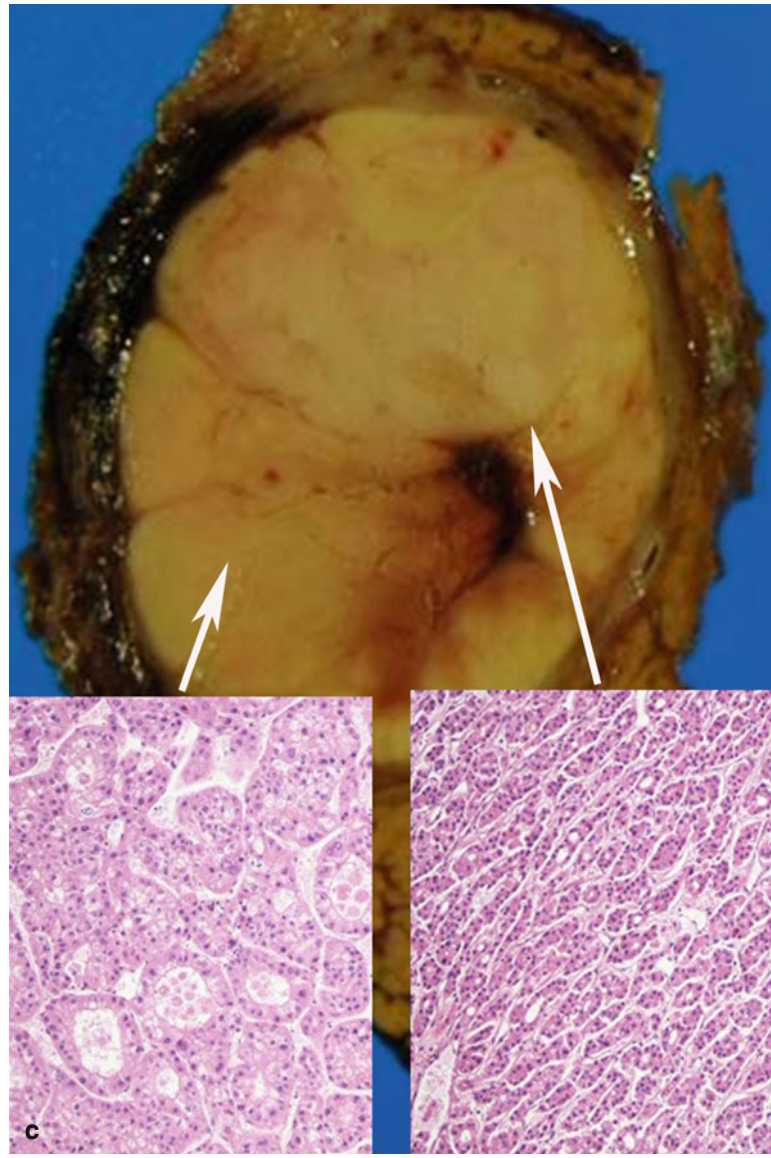

16.5.2.3 Results

The noninvasive diagnostic tools recommended by EASL (European Association for the study of the Liver), using contrast-enhanced CT, magnetic resonance (MR) imaging, and ultrasound (US), are restricted to HCC larger than 2 cm (Bruix et al. 2001). Accordingly, below this cutoff, a biopsy diagnosis is mandatory. Furthermore, two prospective studies demonstrated these modalities to be unsatisfactory for the diagnosis of small HCC (<2 cm), with a sensitivity of 44 % for CT and US (Bolondi et al. 2005) and 67 % with MR imaging and US (Forner et al. 2008). In contrast, the sensitivity of CTHA and CTAP for HCC smaller than 2 cm are 83 % in each, and the combination of them improves it to 94 % (Murakami et al. 1997). A report (Imai et al. 2008) showed that the combination of dynamic MDCT and SPIO-enhanced MR imaging provided an accuracy comparable to CTAP/CTHA; however, it was limited for detecting HCC

smaller than 1.5 cm. The latest report (Mita et al. 2010) demonstrated the sensitivity of detecting moderately differentiated HCC (<2 cm) by Sonazoid-enhanced US, Gd-EOB-DTPA-enhanced MR imaging, and CTAP/CTHA to be 79.2, 75.0, and 95.8 %, respectively, whereas the combination of Sonazoid US and Gd-EOB-DTPA MR imaging showed a sensitivity of 94.1 %. These data indicate CTAP/CTHA has highest accuracy, as single imaging modality, for small HCC (<2 cm).

Fig. 16.22 HCC recurrence in high-risk patient (Child-Pugh score 8). (**a**) Intravenously contrast-enhanced CT shows a slightly hypervascular tumor in segment VI. (**b**) It is difficult to depict the tumor stain during angiography (*arrow*). (**c**) A microcatheter is inserted into the suspected feeding branch (**d**), and selective CT arteriography demonstrates the tumor enhancement and the surrounding nontumorous embolization area. (**e**) Unenhanced CT immediately after TACE shows the dense Lipiodol retention inside and around the tumor

Fig. 16.22 (continued)

For liver metastases, previous prospective studies have shown MDCT to be equally accurate as MRI with lower false-positive rates in MDCT (Bhattachariya et al. 2006). Although current indications for CTAP/CTHA have been reduced, it remains an option if noninvasive imaging studies remain inconclusive (Choi 2006).

16.5.3 Transarterial Chemoembolization (TACE)

16.5.3.1 Subsegmental/Segmental TACE

Indication

Subsegmental/segmental TACE is widely performed for HCC and hypervascular liver metastases, that is, neuroendocrine tumor and gastrointestinal stromal tumor.

The ideal TACE should be a superselective catheterization of the feeding artery of the target lesion in order to inject large amounts of Lipiodol emulsion or particles containing chemoagent into the target lesion, thereby reducing the damage to the surrounding nontumorous liver parenchyma (Uchida et al. 1990). Subsegmental/segmental TACE has been a widespread procedure, and recent microcatheter technology allows more selective catheterization (Miyayama et al. 2007). An interventional CT/angio system is helpful for subsegmental/segmental TACE, especially in the small and slightly hypervascular tumors, which are difficult to identify on angiography (Fig. 16.22).

Technique

Based on a diagnostic angiography from the common or proper hepatic artery, the tumor-feeding artery is identified. A 1.7–2.7-F microcatheter is advanced through a 4–5.5-F mother catheter into the peripheral portion of the feeding artery as close to the targeted tumor as possible under fluoroscopic guidance. Then, selective CT arteriography is performed (the injection speed and total volume of contrast material are decided according to the selective angiography obtained before CT arteriography). If the contrast-enhanced area includes large zones of nontumorous hepatic parenchyma, the microcatheter tip is advanced into the more peripheral part of the feeding artery under fluoroscopy and selective CT arteriography is performed again. Afterward, Lipiodol emulsion or particles are injected (Table 16.9). In Lipiodol-TACE, after the injection of Lipiodol emulsion followed by embolization, we can immediately confirm the Lipiodol retention not only in the tumor but also the tumor-surrounding nontumorous hepatic parenchyma by unenhanced CT.

Results

The 2-year local control rates of subsegmental/segmental TACE are around 54 %, and the overall 1-, 3-, and 5-year survival rates are around 92, 67, and 44 %, respectively. There are several reports which demonstrate the value of an interventional CT/angio system for superselective TACE (Takayasu et al. 2001). A report by Toyoda et al. (2009) showed that longer survival was accomplished by TACE using an interventional CT/angio system when compared with using a conventional angiography system alone. This improvement was attributed to the more selective catheter placement and therefore better deposition of the drug and embolic agent in the target lesion.

Table 16.9 Chemo-agents and embolic material for subsegmental/segmental TACE (bland TAE) for HCC

Drug delivery	Chemo-agents	Embolic material	Authors	Year
Lipiodol	Epirubicin (10–20 mg) Mitomycin (2–4 mg)	Gelatin sponge particle (0.5 mm)	Miyayama	2007
Ethiodol	Cisplatin (100 mg), doxorubicin(50 mg), and mitomycinC(10 mg)	Embosphere (100–300 μm)	Kothary	2007
None	None	Embozene (40 μm)	Bonomo	2010
DC beads	Doxorubicin (25–75 mg)	DC beads (300–500 μm)	Sadick	2010

16.5.3.2 Collateral TACE

Indication

In patients with HCC, various extrahepatic collateral vessels may develop and contribute to the blood supply of the tumor. TACE of extrahepatic collaterals is considered to be useful for the control of tumor and prolonged overall survival (Miyayama et al. 2006). However, occasionally, it is difficult to detect the tumor-feeding artery on angiography. In addition, one has to consider the risk of nontarget embolization which can lead to severe complications, such as skin necrosis and gastrointestinal ulcer. CT arteriography via extrahepatic collateral vessels is useful to confirm the feeding artery and predict areas of nontarget embolization (Takeuchi et al. 1998 and Ishijima et al. 1999) (Fig. 16.23).

Technique

When a target lesion is not enhanced by CTHA, it is necessary to consider the extrahepatic collateral supply. There is a close relationship between the tumor location and the feeding extrahepatic collateral. Particularly if it is difficult to detect tumor staining on angiograms of the suspected collateral, CT arteriography should to be attempted. According to the technique of selective TACE, the repeated selective angiography and CT arteriography have the potential to advance a microcatheter more peripherally and perform the collateral TACE as safe as possible.

16.5.4 Arterial Infusion Chemotherapy

16.5.4.1 Indication

Arterial infusion chemotherapy has the advantage of decreasing the adverse events of any chemo-agent while achieving a good tumor response due to increased drug concentration in the target lesions. It has successfully been applied for hepatic, pancreatobiliary, gynecologic, and head and neck cancer. In regional chemotherapy, it is vital to achieve optimal drug distribution to the tumor to obtain the best possible therapeutic outcome. The combination of angiography and CT arteriography via the chemoinfusion catheter is useful to evaluate the drug distribution and the management of the arterial catheter-port system (Arai et al. 2007; Tanaka et al. 2009, and Kahiwagi et al. 2010) (Fig. 16.24).

16.5.4.2 Technique

During the arterial infusion chemotherapy with implantable catheter-port systems (Table 16.10), surveillance of the catheter position, arterial stenosis, and drug distribution are required at least

Fig. 16.23 HCC supplied from the left gastroepiploic artery. (**a**) CT arteriography from the common hepatic artery shows that multiple HCC nodules in the liver are enhanced, whereas the tumor protruding into the hepatogastric ligament is not (*arrow*). (**b**) The splenic artery is one of the suspected feeding arteries. (**c**) However, CT arteriography from the splenic artery demonstrates the contrast enhancement in a part of the protruding tumor (*arrow*). (**d**) On the basis of the left gastroepiploic angiography, a microcatheter was advanced into the tumor-feeding collateral branch (*arrow*). (**e**) Unenhanced CT after collateral TACE from the left gastroepiploic artery shows Lipiodol retention, with an enhancement defect in the ventral parts of the tumor (*arrow*). (**f**) Additional TACE from the left inferior phrenic artery (*arrow*). (**e**) Final unenhanced CT shows the complete embolization of the tumor (*arrow*)


a

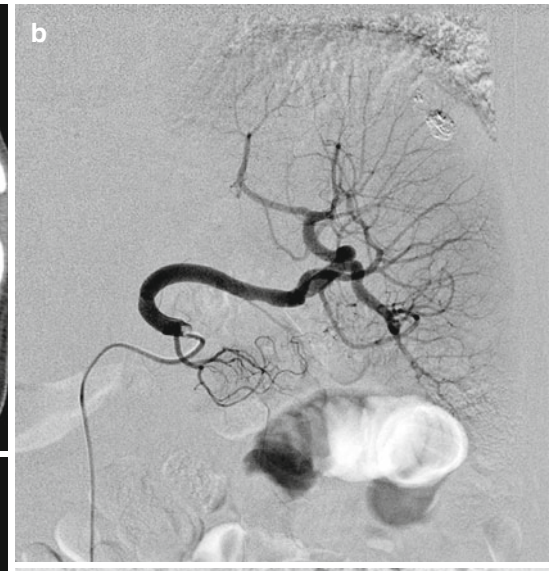
b

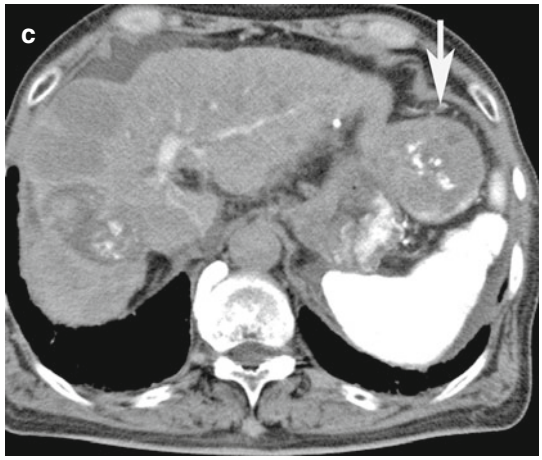
c

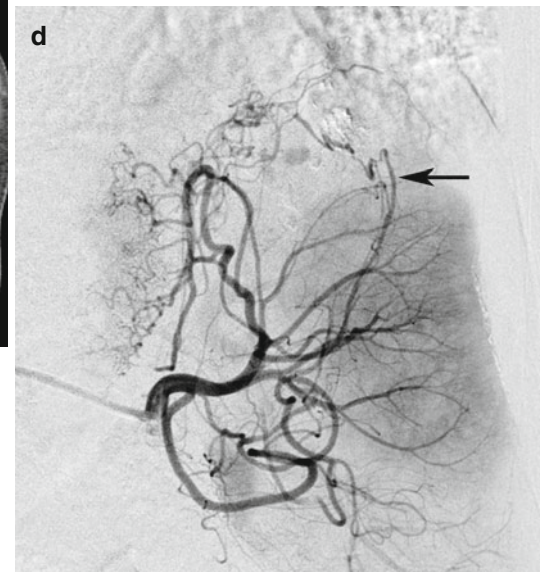
d

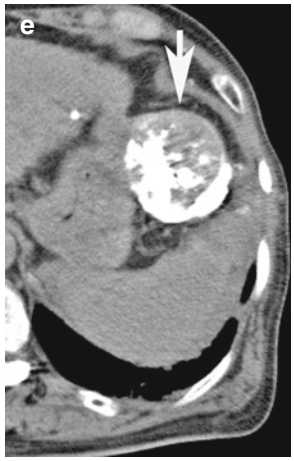
e


f

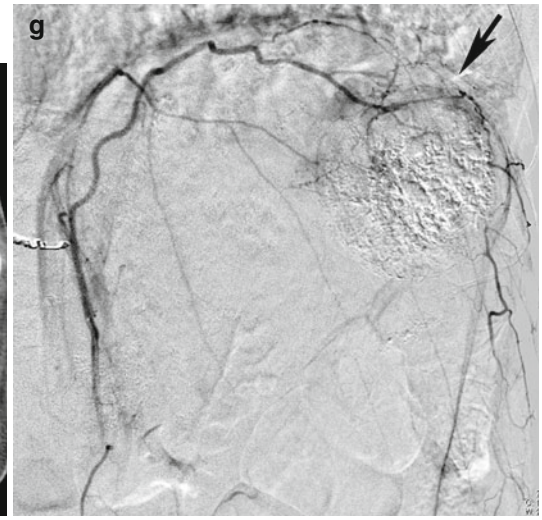
g

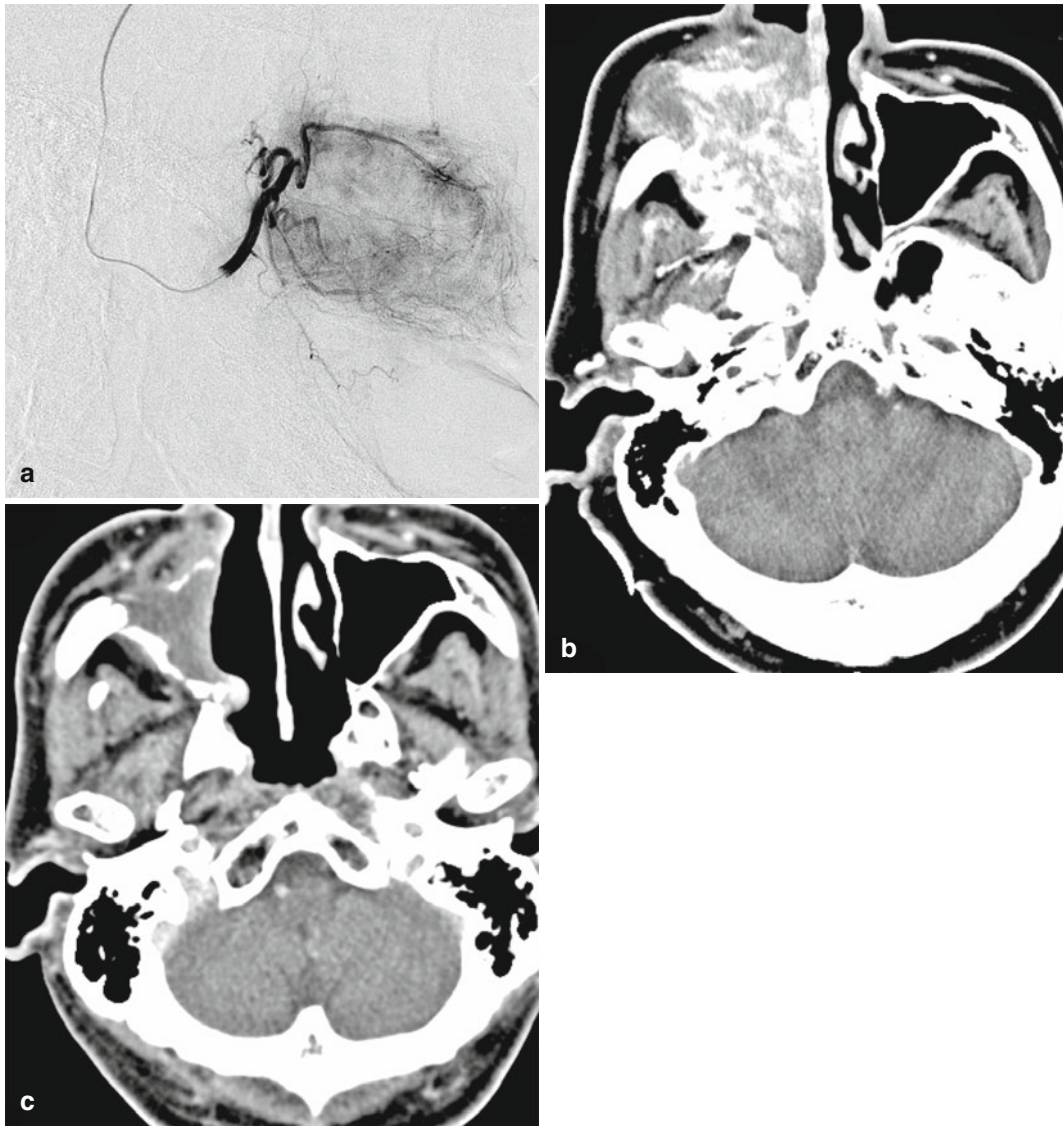

Fig. 16.24 Arterial infusion chemotherapy for advanced maxillary sinus cancer. (**a**) Selective angiography from the maxillary artery (the superficial temporal arterial approach) shows tumor stain. (**b**) CT arteriography shows entire tumor is contrast enhanced. (**c**) CT obtained 3 months after arterial infusion of a total dose of 100 mg cisplatin combined with radiotherapy shows almost complete tumor remission

every 3 months. Initially, angiography by hand injection of contrast material from the port is performed to check for arterial patency. Then, CT arteriography is conducted by injection of a total volume of 20–30 ml diluted contrast material (1:4) at a flow rate of 0.5–1.0 ml/s. In hepatic arterial infusion chemotherapy, contrast enhancement of the whole liver without distribution in extrahepatic organs is necessary (Fig. 16.25).

16.5.4.3 Results

A report by Seki et al. (1996) showed that perfusion abnormalities were found in 60 % of patients when a combination of angiography and

Table 16.10 Chemoregimens for arterial infusion chemotherapy

Cancer	Chemo-agents	Authors	Year
Colorectal cancer	5-FU (1,000 mg/m^2) weekly	Arai	1997
HCC	Cisplatin (7 mg/m^2),5-FU (170 mg/m^2)day1–5 every week	Ando	2002
Pancreatic cancer	5-FU (1,000 mg/m^2) combined with systemic gemcitabine (1,000 mg/m^2), day 1, 8, and 15 every 28 days	Tanaka	2011
Uterine cervical cancer	Cisplatin (120 mg) 4-week interval combined with RT (50 Gy)	Nagai	2009
Maxillary sinus cancer	5-FU (125–250 mg) daily, cisplatin (30–60 mg) weekly combined with RT (30–40 Gy)	Nibu	2002

5-FU 5-fluorouracil, *Cis* cisplatin, *Gem* gemcitabine, *RT* radiotherapy

CT arteriography was used for the management of hepatic arterial infusion chemotherapy.

16.5.5 Percutaneous Drainage

16.5.5.1 Indication

Percutaneous drainage is conducted using a variety of image guidance techniques, including US, conventional fluoroscopy, CT, and MR imaging. Since each of these methods has its specific advantages and disadvantages, the combination of these modalities should be beneficial. Conventional CT- and real-time CT fluoroscopy-guided punctures are established as precise interventional techniques. However, they are limited along the patient's z-axis. Hence, in percutaneous drainage procedures, the insertion of guidewires and drainage catheters frequently remains difficult after the successful needle puncture of the target. Several reports have shown the utility of the combined use of CT and fluoroscopy for percutaneous abscess drainage (Froelich et al. 2000), biliary drainage (Laufer et al. 2001), and nephrostomy (Sommer et al. 2011), although, in the majority of reports, a mobile C-arm fluoroscopy device was used. Compared with these mobile devices, an interventional CT/angio system has several advantages in handling the C-arm and moving the table position (Tanaka et al. 2002) (Fig. 16.26). This hybrid modality permits a variety of complicated interventions which depend on precise CT-guided needle puncture with subsequent fluoroscopy-guided procedures (Mahnken et al. 2008).

16.5.5.2 Technique

The puncture is performed under CT guidance with a 17–19-G needle. After confirming the correct needle position with CT, for example, in the abscess cavity, bile duct, or renal calyx, a 0.035-in. guidewire is inserted and a 8–12-F drainage catheter is placed under fluoroscopic guidance. When a 22-G fine needle is used for the puncture, the insertion of a coaxial catheter introducer system followed by the replacement with a 0.035-in. guidewire is conducted under fluoroscopic guidance. In the case of complex cavities such as an abscess or the other fluid collections separated by septae, CT immediately after catheter placement accompanied with aspiration or contrast material injection is useful to assess the position of the drainage catheter.

16.5.5.3 Results

Froelich et al. (2000) reported that abscess drainage under CT fluoroscopic guidance combined with C-arm fluoroscopy had advantages when compared with CT fluoroscopy alone. The procedure time was shorter (9 vs. 14 min; $P<0.005$), less drainage catheter revisions were needed (2/20patients vs. 8/20patients). and the post-interventional drainage period was shorter (13 vs. 19 days; $P<0.001$). Laufer et al. (Laufer et al. 2001) reported that transhepatic biliary drainage under the CT fluoroscopy combined with fluoroscopy reduced the number of punctures and puncture times when compared with conventional fluoroscopic guidance alone. Recently, Sommer et al. (Sommer et al. 2011) reported that combined CT- and fluoroscopy-guided nephrostomy

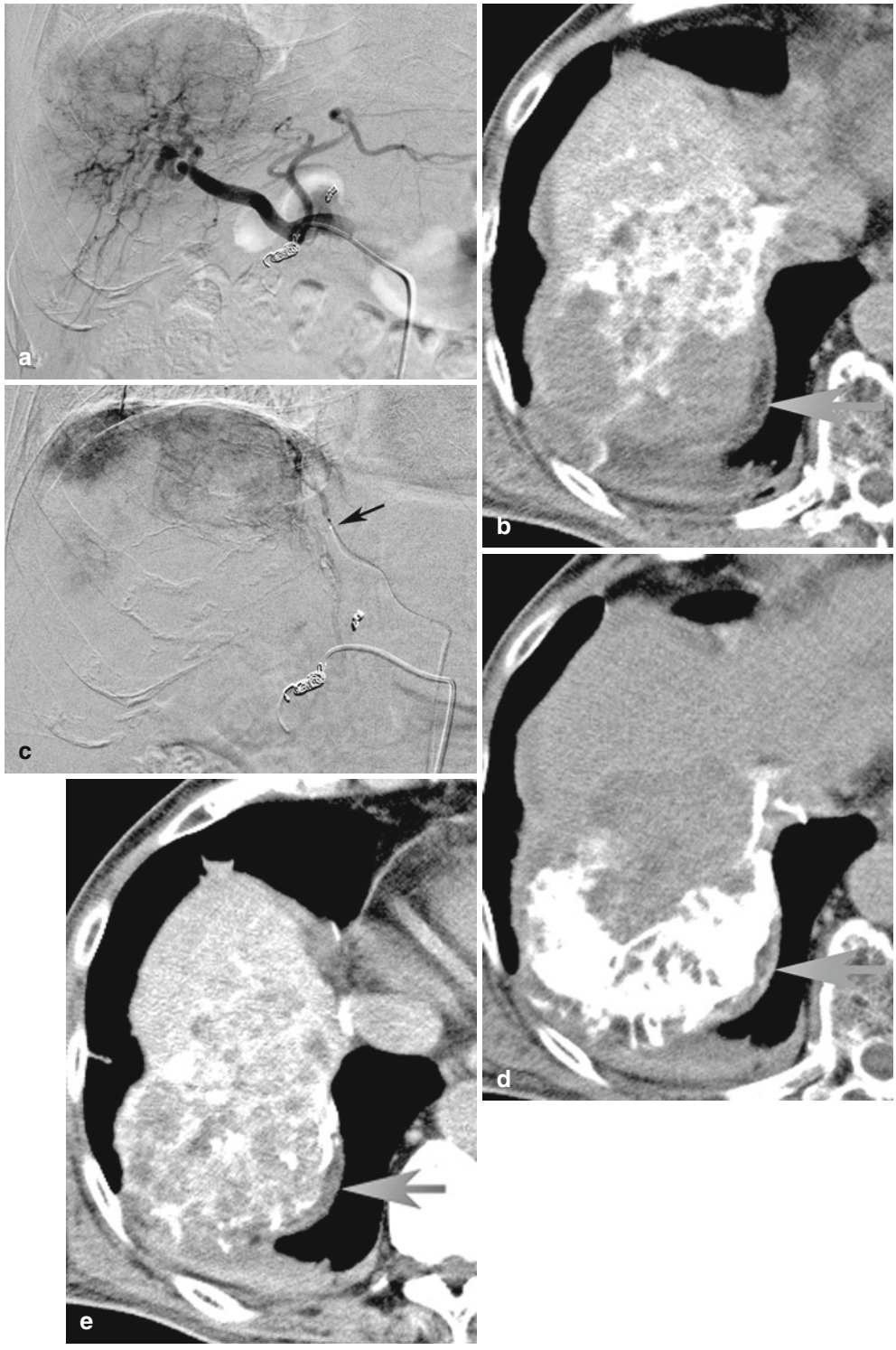

Fig. 16.25 Management and reintervention for hepatic arterial infusion chemotherapy. (**a**) Angiography from implanted catheter-port system for HCC with portal venous thrombus. (**b**) CTA from the port shows an unenhanced area in segment VII. (**c**) Angiography from the right inferior phrenic artery (rIPA) (*arrow*). (**d**) CT arteriography from rIPA shows the enhancement of the unenhanced segment VII at CT arteriography from the port. (**e**) CT arteriography from the port after embolization of the rIPA with NBCA-Lipiodol mixture shows a markedly improved drug distribution

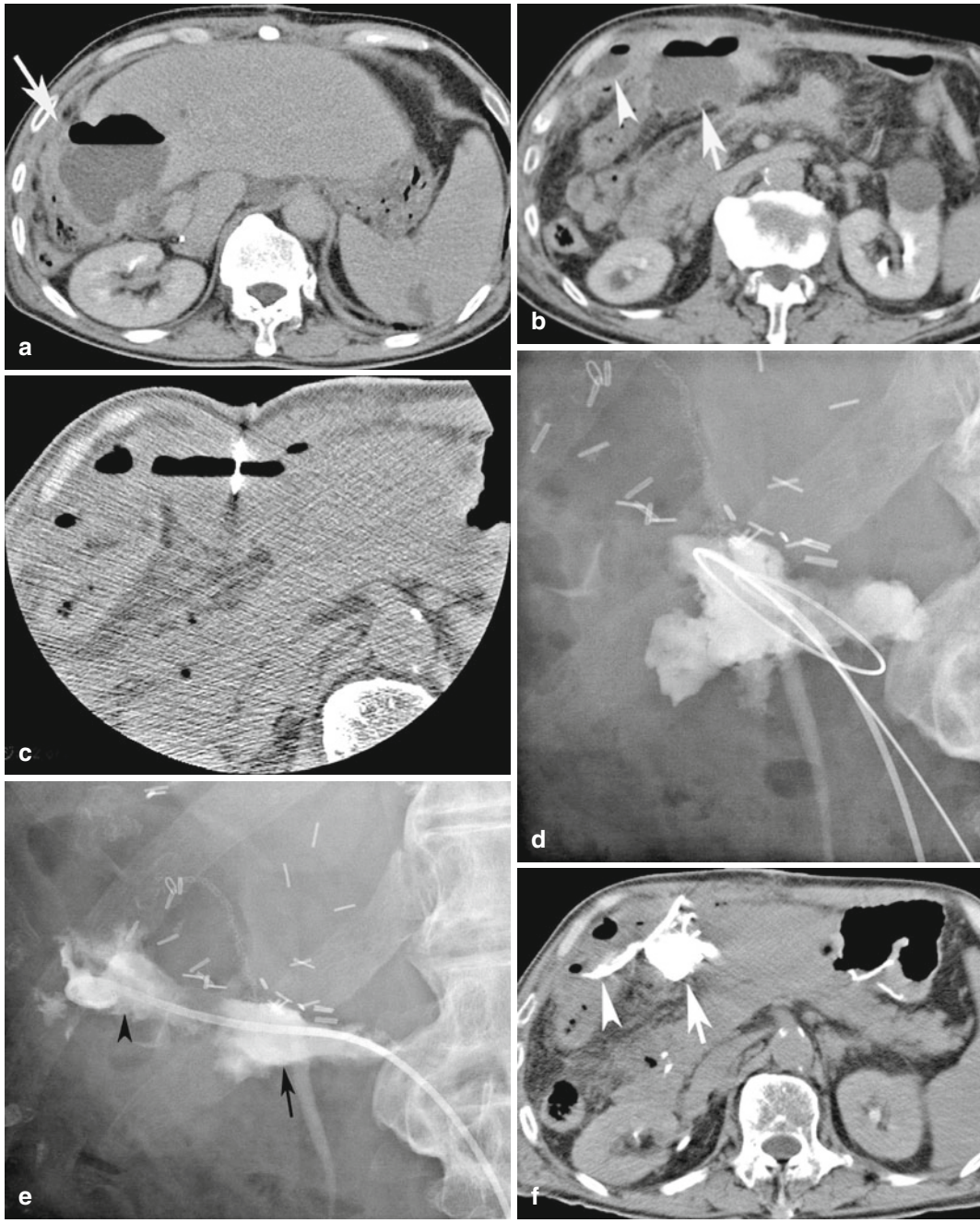

Fig. 16.26 Intra-abdominal abscess after surgery. (**a**, **b**) CT before drainage shows complex abscess cavities close to the resection margin after hepatectomy (*arrows* and *arrowhead*). (**c**) One of the cavities was punctured under CT fluoroscopic guidance. (**d**) A seeking catheter and a safety guidewire were inserted into the cavity under conventional fluoroscopy. (**e**) A hydrophilic guidewire was introduced through the seeking catheter and successfully passed into the adjoining cavity (*arrowhead*), and a drainage catheter which had additional proximal side holes (*arrow*) was placed in these cavities. (**f**) CT after the drainage catheter placement suggests the drainage for two cavities could be accomplished (*arrow* and *arrowhead*); however, it was necessary to perform an additional puncture for another cavity. (**g**) Additional transhepatic CT-guided needle puncture was performed (**f**), and another drainage tube was placed (**h**)

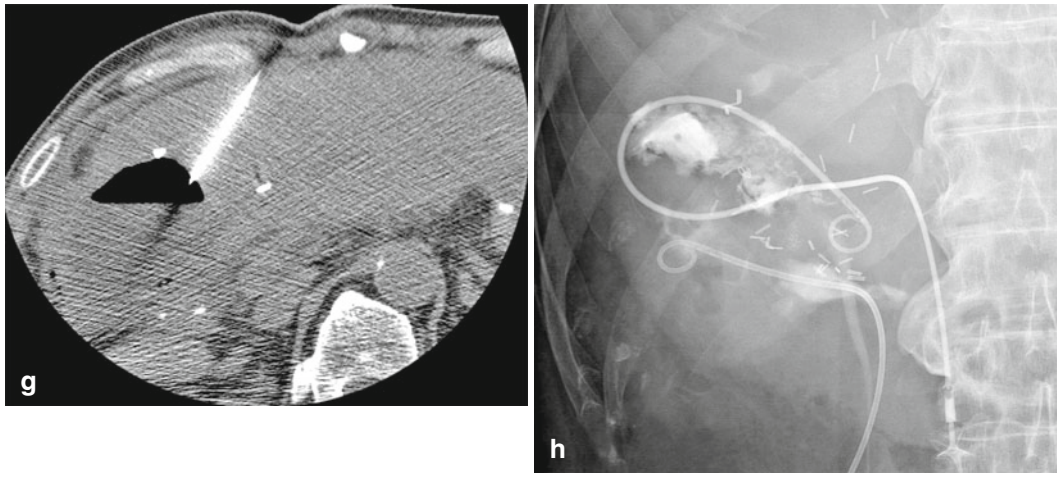

Fig. 16.26 (continued)

for nonobstructive uropathy due to urine leaks was successful in 91 % of patients.

16.5.6 Radiofrequency (RF) Ablation

16.5.6.1 Indication

RF ablation combined with TACE is effective not only for medium or large size tumors to create large ablation zones but also for small tumors invisible on US and unenhanced CT. US guidance is most frequently used for percutaneous RF ablation; however, sometimes small nodules are not sufficiently depicted. On the other hand, CT is a well-established alternative guidance tool, whereas the US occult lesions are usually small and therefore invisible on unenhanced CT, too. In such a setting, RF ablation after Lipiodol-TACE is useful, because the accumulation of iodinated oil helps to unmask the lesion on unenhanced CT (Lee et al. 2009). Despite the controversy about the interval between TACE and RF ablation, an interventional CT/angio system allows these procedures to be conducted at the same day without patient transportation (Fig. 16.27).

16.5.6.2 Technique

Lipiodol-TACE is performed through segmental and subsegmental hepatic artery according to the technique described above. CT-guided RF ablation with a wide window width image is usually helpful to depict the Lipiodol-stained tumor.

16.5.6.3 Results

Yamakado et al. (2008) reported that RF ablation combined with TACE for early-stage HCC equals surgery with respect to survival. The 1-, 3-, and 5-year overall survival rates were 98, 94, and 75 %, and recurrence-free survival rates were 92, 64, and 26 %, respectively. Takayasu et al. (1999) demonstrated the utility of CT-guided ethanol injection after marking by CTHA or arterial injection of Lipiodol using an interventional CT/angio system. Lee et al. (2009) reported that 14 % of HCC nodules were invisible on both US and unenhanced CT (average size of 1.2 cm), and in 71 % of them, RF ablation could be successfully conducted after TACE (including CT, fluoroscopy, and US guidance).

16.5.7 Percutaneous Vertebroplasty (PVP)

16.5.7.1 Indication

In 1994, Gangi et al. (1994) demonstrated the advantage of combining CT and fluoroscopic guidance for the PVP. CT-guided puncture to vertebra is useful for the visibility of bone and sur-

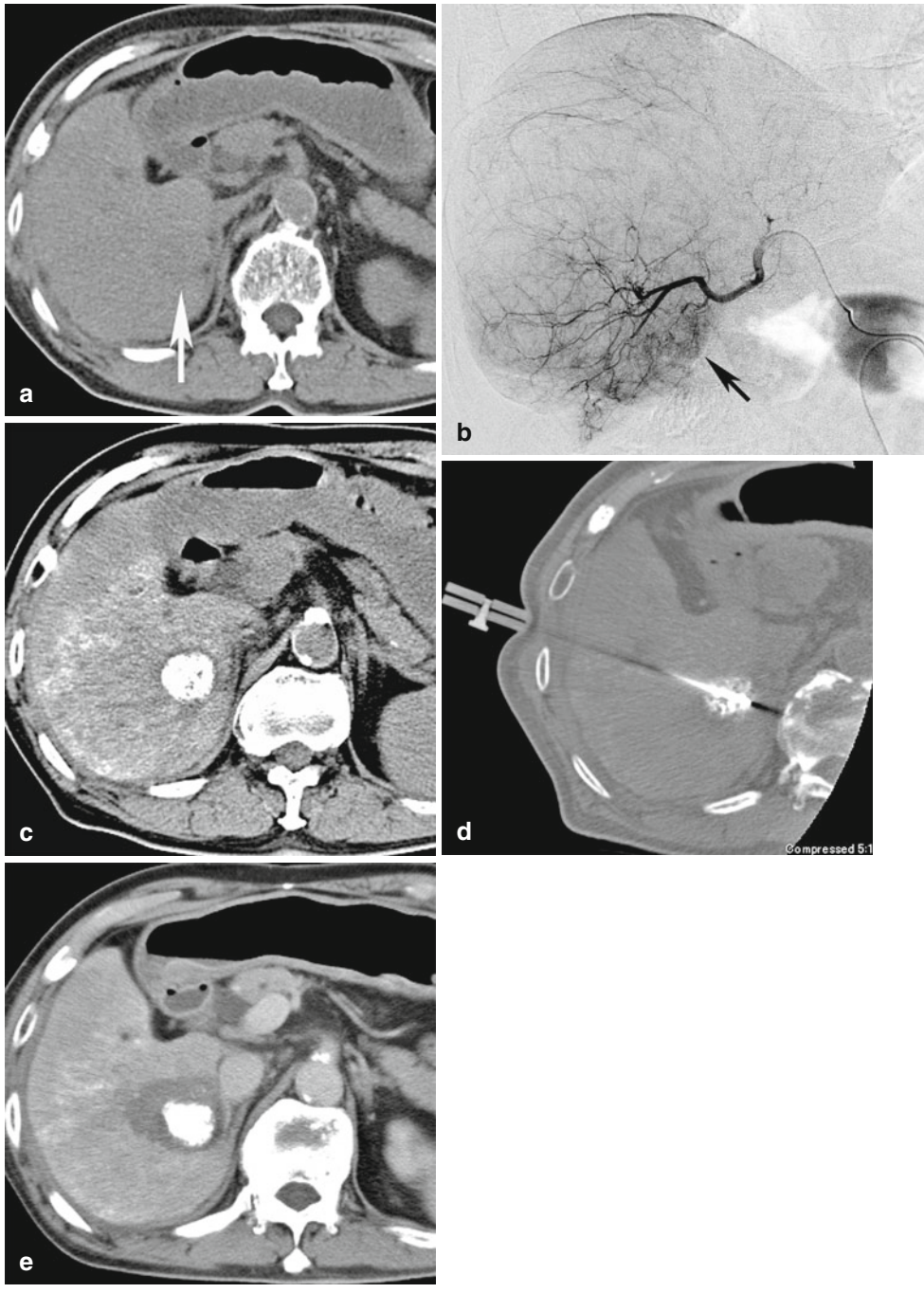

Fig. 16.27 RF ablation after segmental Lipiodol-TACE for an HCC which was invisible on US and hardly detectable on unenhanced CT. (**a**) Unenhanced CT before treatment shows a slightly hypodense tumor in segment VI (*arrow*). (**b**) Selective arteriography shows a hypervascular area with a badly defined margin (*arrow*). After confirmation by CT arteriography, segmental Lipiodol-TACE was conducted. (**c**) Unenhanced CT after TACE shows Lipiodol accumulation in the tumor. (**d**) CT fluoroscopy-guided RF ablation was performed, (**e**) and the final contrast-enhanced CT after RF ablation shows a completely ablated tumor

rounding soft tissue, and it prevents damage to adjacent vascular, nerval, and visceral structures. Although there is an ongoing controversy whether PVP should be performed under fluoroscopic guidance alone or with a combination of CT and fluoroscopic guidance, several authors showed the advantage of the combined approach for reducing the radiation exposure during the procedure (Trappero et al. 2009).

16.5.7.2 Technique

With the patient in a prone position, a 10- to 12-gauge trocar needle is introduced into the vertebral body via a transpedicular or lateral approach under CT guidance. After the needle is in the optimal position (needle tip in the anterior third of the vertebral body), vertebral venography is performed by the injection of 10–15 ml of iodized contrast material under fluoroscopic guidance. The injection of bone cement is monitored by lateral fluoroscopic guidance, and monitoring of the distribution of bone cement under CT fluoroscopy is also very useful to prevent complications.

16.5.7.3 Results

Trappero et al. (in 2009) reported that operator radiation exposure dose during PVP with a combination of CT and fluoroscopic guidance could be reduced compared with fluoroscopic guidance alone (0.8 vs. 5.8 mSv), provided that the puncture was conducted sequentially under conventional CT guidance, not using real-time CT fluoroscopy.

16.5.8 Special Techniques

In the emergency setting, an interventional CT/angio system offers the possibility for CT diagnosis and interventional treatment on the same patient table (Gross et al. 2010). For example, in the case of unstable pelvic fractures, the initial CT scan plays an important role in the screening for damage of internal organs, while external fixation can be conducted immediately after the diagnostic scan under fluoroscopic guidance. If necessary, additional transcatheter internal iliac artery embolization can also be performed without patient transportation.

There are further special techniques, which require CT-guided needle puncture to access the target vessel followed by an endovascular intervention, for example, TIPS recanalization (Tanaka et al. 2011a). Another recent report showed (Iguchi et al. 2010) a case with bleeding ilial varices successfully treated by percutaneous transhepatic sclerotherapy using a hybrid CT/angio system.

Appraisal

With the recent progress of interventional radiology, including knowledge, technique, and new devices, more precise and complicated procedures became feasible utilizing the simultaneous use of multiple image guidance techniques. From almost 20 years of experience, there is no doubt that an interventional CT/angio system has an enormous impact on interventional strategies. These systems do not only facilitate routine interventions, for example, selective TACE, percutaneous drainage, and RF ablation, but have a great potential to be applied in particularly complex and challenging cases.

Key Points

- CTAP and CTHA, which are useful particularly for the diagnosis of small and early stage of HCC, can be performed conveniently.
- In superselective TACE and arterial infusion chemotherapy, the embolization area and the drug distribution area can precisely be predicted by CT arteriography.
- In the field of nonvascular intervention such as percutaneous drainage or vertebroplasty, CT-guided needle punctures followed by conventional fluoroscopic-guided interventions are possible.
- One-step TACE followed by CT-guided RF ablation without patient transportation became feasible with hybrid CT/angio systems.

Acknowledgments The help of Dr. Satoru Sueyoshi, Dr. Nishiofuku Hideyuki, and Dr. Hiroshi Anai from Nara Medical University for preparing the images is gratefully acknowledged.

16.6 A Primer on MR-Guided Endovascular Procedures

Gabriele A. Krombach

16.6.1 Introduction

Interventional magnetic resonance (MR) imaging is clinically established for biopsies of lesions which are hard to delineate, not delineable, or impossible to reach using other imaging modalities. Most often, lesions of the breast and liver lesions fall into the first category, while subdiaphragmatic liver lesions represent those which benefit from the free choice of imaging planes.

MR-guided endovascular interventions are appealing due to the high soft tissue contrast of MRI; the ability to perform luminographic angiography with and without the application of contrast medium; the inherent option to assess physiologic function, such as flow velocity and ventricular function; and most recently, the promises of "molecular imaging." Despite of very encouraging results derived from animal studies, reports of endovascular interventions in human remain low in number and are generally limited to small series of patients. So far, not a single endovascular procedure has been well established in clinical routine. The strongest and most obvious obstacle to a broader clinical acceptance is the lack of commercially available MR-safe instruments. Only a handful of devices that are routinely applied in conventional angiography are MR safe. Most catheters are braided with metal to improve torque and steerability. Braiding renders catheters unsafe, since it bears the potential to turn catheters into RF antennae, increases the risk of heating and patient burns, and introduces strong image artifacts. Nitinol guidewires face the same problem (Fig. 16.28). Standard devices without braiding, such as multipurpose balloon catheters can be applied in the MR environment safely, although such devices lack steerability. Up to now, it is very common to employ self-made devices for animal studies or dedicated prototypes manufactured by industrial partners, but not readily available on the market, for interventions in human. In the very recent years, the collaboration of researchers and industrial partners with the declared goal to develop and release MR-safe instruments to the market has led to several instruments, which are now commercially available or in the process of CE certification (Krueger et al. 2008; Kos et al. 2009; Tzifa et al. 2010).

Over the last decades, the claimed indication of endovascular MR-guided interventions was merely saving of X-ray radiation by replacing fluoroscopy with real-time MRI. In many animal studies, interventions, which are routinely carried out using X-ray only, have been duplicated under MR guidance. These intermediate steps were certainly essential to develop the technique of MR-guided interventions and to provide the interventional and diagnostic imaging community with experience. The perspective of decreasing X-ray exposure for adult patients and interventionalists is hardly convincing radiologists to transfer well-established X-ray-guided interventions into the MR suite. Consequently, the method has not made the critical step from the experimental lab into the clinical arena with the exception of diagnosis and treatment in patients with congenital heart disease.

Recently, technical maturation of interventional MR imaging and simultaneous development of MR imaging in other areas, namely, the development of MR-safe conductors and the advent of molecular imaging, promise to open up the avenue of MR-guided interventions that cannot be carried out in another imaging environment. Consequently, MR-guided endovascular procedures that have their own indications are rapidly emerging. Currently, three applications that are on the rise are the following: 1. interventions for the endovascular treatment of congenital heart diseases, 2. electrophysiological interventions, and 3. local delivery of drugs, cells, or genes targeted at the recovery of damaged tissue or tumor therapy. However, almost all of these techniques are in a preclinical stage.

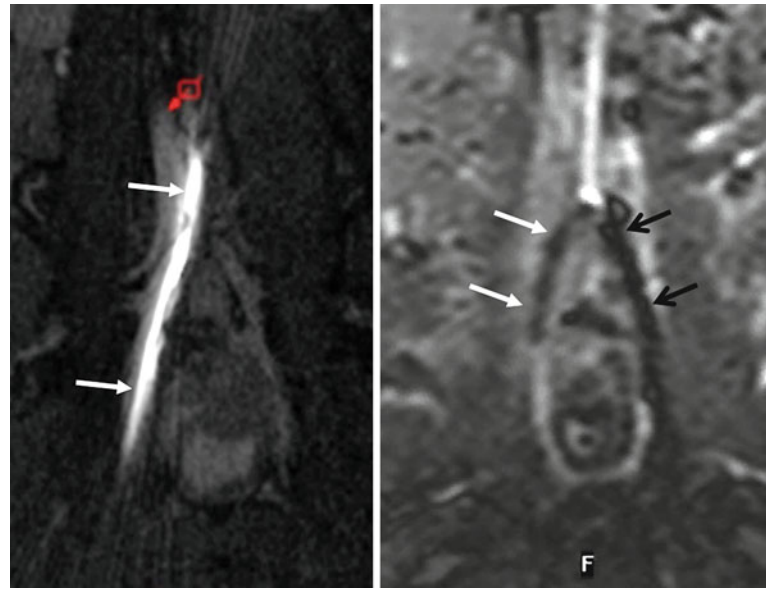

Fig. 16.28 Real-time imaging using a true-FISP sequence. *Left image* shows a standard nitinol guidewire introduced into the iliac artery and aorta. Common mode lighting is visible, resulting from deferral of electrons. The wire appears bright (*arrows*), and the surrounding anatomy is masked, due to this effect. The *right image* shows an MR-safe wire (*white arrows*). A crossover probing of the common iliac artery has been performed with the aid of a catheter (*open black arrows*). The devices do not introduce artifacts that disturb the surrounding anatomic structures

16.6.2 Technical Requirements

Endovascular interventions require real-time imaging with a temporal resolution close to that of conventional angiography in order to monitor manipulation of instruments and potentially assess complications. For safe guidance of catheters, a frame rate of approximately six images per second is necessary. Real-time MR imaging is usually obtained by combining rapid imaging strategies such as radial or spiral techniques which are rather insensitive to motion and fill the data space (k-space) in an efficient way with smart reconstruction methods that increase the apparent frame rate. The sliding window technique is one of numerous possibilities to accomplish this challenge. In a time series of continuous radial data acquisition, k-space lines are shared between frames. For this purpose, the oldest k-space lines are replaced by newly incoming k-space lines (Fig. 16.29).

In general, two strategies for visualization of devices on MR images are established, active and passive instrument visualization:

1. Passive visualization relies on the inherent imaging features of the devices. Currently, with passive visualization, devices are delineated as signal voids on bright blood images (true FISP or FLASH). Small markers consisting of iron particles, nitinol, or dysprosium can be added to the device in order to enhance visualization (Fig. 16.30). The advantage of this strategy is the immediate applicability of these devices: hardware or software modifications of the scanner are not required. If nonconducting materials are used, the devices are MR safe. Interactive catheter tracking is a considerable drawback of passive visualization. The tip of passive devices must be followed by manually adjusting the slice position. If the catheter tip is not distinctively labeled, it might be confused with parts of the catheter shaft, if the catheter tip is not captured by the imaging slice.
2. Active visualization makes use of small radiofrequency coils, which are integrated in the interventional devices. The location of the tip can be automatically tracked and detected so that the slice position can be automatically adjusted to the course of the device. Wire connection to the scanner is required, and usually, hardware modification is necessary to allow for such a connection. Another drawback is that active devices are very expensive, which is a major disadvantage in disposables.

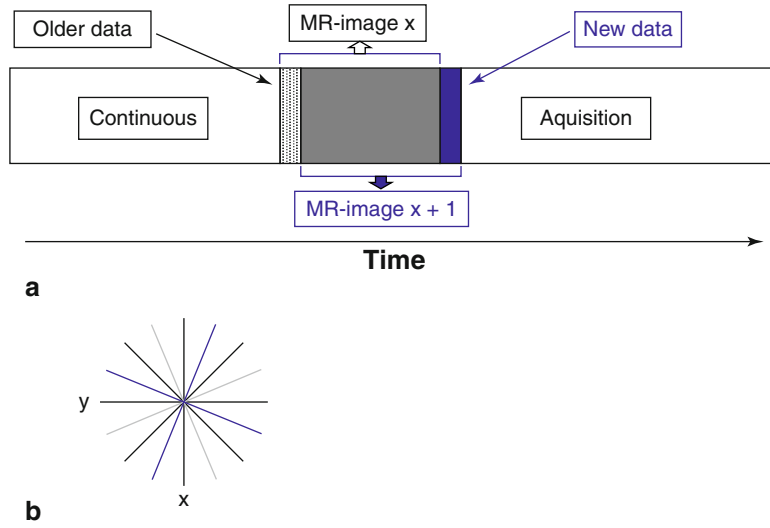

Fig. 16.29 Principle of the sliding window approach: MR data are continuously acquired, and images are reconstructed after an initially chosen percentage of the oldest k-space lines of the n replaced with new k-space lines (**a**). K-space lines can be acquired using a radial trajectory (**b**) and interleaved acquisition

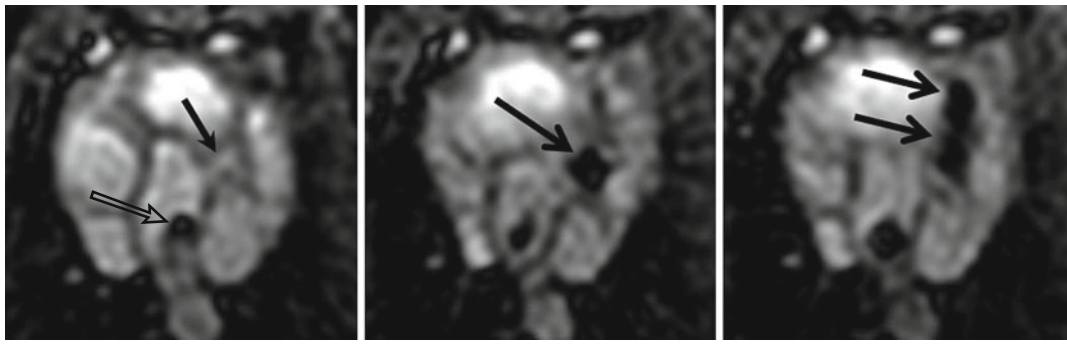

Fig. 16.30 The left coronary artery (*left image*, *arrow*) is probed with a MR-compatible guidewire and an iron-marked catheter (*long arrows*). The catheter is introduced into the ostium of the LAD (*middle image*) and advanced into the left coronary artery (*right image*). The catheter has been marked with dots of iron oxide particles, which cause signal void

Semi-active tracking is a third way, which combines the best of both worlds: a tunable coil, which is not wire connected with the scanner is mounted on a catheter. The signal arising from the coil can be modified by changing the flip angle. Hardware modification is not necessary, the location of the coil can automatically be tracked, and slice position automatically adjusted accordingly. The limitation of this technique is that the size of the coil must be relatively large, in order to render adequate signal intensity. Thus, semi-active tracking can be applied for relatively large devices such as cava filters (Kramer et al. 2011) or potentially for valved stents.

For many procedures, monitoring of the vital parameters needs to be ensured during scanning. For this purpose, dedicated equipment is commercially already available.

16.6.3 Applications

16.6.3.1 Congenital Heart Disease

Treatment options for patients with congenital heart disease have considerably improved in the last decades, and patients reach adulthood as a result of these improvements. The clinical examination and noninvasive imaging methods can guide the decision on the therapeutic regime. However,

in order to capture the right time for reinterventions or follow-up operations, cardiac catheterization for measurement of physiologic parameters is repeatedly required, starting from early age. This patient group is highly vulnerable to the sequelae of ionizing radiation as a single cardiac catheterization imposes a risk of 1 in 1,000 to develop a solid tumor in children of 5 years or younger (Bedetti et al. 2008; Razavi et al. 2003). The considerable accumulation of radiation dose in this patient group makes the efforts of saving radiation exposure by transferring cardiac catheterization to MR imaging worthwhile. In addition, the individual anatomy of patients with congenital heart disease is usually highly complex, especially after palliative surgery. The group of Razavi in London has clinically established a protocol for cardiac catheterization of patients, including calculation of pulmonary vascular resistance (Razavi et al. 2003). Standard multipurpose non-braided balloon catheters, which are MR safe, can be employed. Diagnostic cardiac catheterizations entirely guided by MR are currently established as the gold standard approach for assessment of pulmonary vascular resistance in children and adults. The excellent soft tissue contrast of MR imaging and the inherent visualization of the individual anatomy of the patients facilitate catheterization. Even more, MR-guided diagnostic catheterization provides more information compared to fluoroscopy, since it offers the possibility of measuring flow. Kuehne et al. performed MR-guided cardiac catheterization in patients with pulmonary hypertension (Kuehne et al. 2005). Another breakthrough was dilatation of coarctation in human using MR-compatible devices including a prototype guidewire (Krueger et al. 2006). Here, the traits of MR imaging help to avoid radiation exposure but facilitate assessment of cardiac and vessel anatomy, measurement of physiological parameters, such as flow, and support combination of these data with invasive pressure measurements (Krueger et al. 2006). MR-safe pacemakers have recently been developed and might be used if dilatation of the aortic valve is performed. By rapid pacing, damage to the valve from movement of the balloon catheter during dilatation can be avoided (Neizel et al. 2010).

The combination of data obtained from hemodynamic catheterization, MR (flow and ventricular function), and delineation of anatomy beyond luminography strongly improves the diagnostic and interventional capabilities in patients with complex congenital heart disease. In this area, endovascular MR-guided interventions have been introduced into the clinic in very few pioneering institutions.

16.6.3.2 Electrophysiological Interventions Including Radiofrequency Ablation

Radiofrequency (RF) ablation is the first-line therapy for supraventricular arrhythmias. Electrophysiological studies and interventions aiming at identification of arrhythmic substrate and ablation of such foci are currently performed using X-ray fluoroscopy with the aid of electrophysiological mapping. X-ray fluoroscopy capabilities for visualization of anatomical structures and verification of correct ablation catheter positioning are rather limited due to the missing soft tissue contrast. However, ablation strategies have been shifted from barely electrical substrates to anatomical targets. The need of visualizing anatomical structures, such as the pulmonary veins, in order to deliver multiple lesions circling the veins has lead clinicians to obtain CT or MR imaging days or weeks prior to the procedure in order to match these images with the mapping system. Results were not completely satisfying, since registration errors hampered guiding of catheters. In parallel, advances in ablation strategies, such as the ablation of chunks of vital myocardium within scar tissue in the ventricles, which might be involved in the tachycardia circuit, have raised the demand for an on-line imaging modality that can visualize such areas during the ablation procedure. Consequently, real-time MR imaging has been suggested to suit the clinical needs of ablation procedures. Images acquired during the procedure present the actual anatomy, and an extra co-registration with fiducial markers is not required. Ventricular scars can be visualized in 3D using delayed contrast enhancement so that the areas of catheter tissue contact with subsequent ablation can directly be assessed.

Performing MR-guided ablation procedures requires reliably catheter visualization together with contact recording of the intracardiac electrocardiogram, which is in the range of millivolts, during scanning and ablation. Signal-to-noise ratio of the intracardial ECG signal can be significantly enhanced by ECG signal filtering (Nazarian et al. 2008). The development of safe conductors for intracardial ECG mapping and ablation is key for the success of MR-guided electrophysiological procedures. Image distortion resulting from RF ablation can be avoided using special RF filters and shielding (Lardo et al. 2000). The contact electrocardiogram obtained from the catheter tip must be reliably co-registered to its location in the cardiac chamber. So far, this goal has been achieved using active catheter tracing, where coordinates of the signals from the catheter microcoils can be superimposed to the anatomic images obtained simultaneously (Dukkipati et al. 2008). The ablation lesions can be immediately detected in T2-weighted images and in T1-weighted images after intravenous injection of contrast medium (Lardo et al. 2000).

In summary, MR-guided electrophysiological procedures allow for clear delineation of anatomic structures, simultaneous registration of the intracardiac ECG and matching of position, RF ablation, and monitoring of lesion size. MR-guided electrophysiological procedures overcome the drawbacks of fluoroscopic guidance and pave the way for further development of RF ablation including more complicated interventional procedures. Examples for future applications are ablation of arrhythmogenic foci in patients with congenital heart disease, such as single ventricles treated after Fontan operation or anatomical bases ablation strategies, such as isolation of pulmonary veins. MR guidance of RF ablation will decrease procedure time so that the overall number of complications, which has been demonstrated to correlate with lengthy procedures, will be reduced. Currently, MR-safe ablation systems are under development, and the reported studies have assessed feasibility in animals.

16.6.3.3 Local Delivery of Drugs, Genes, or Cells

Revascularization therapy for coronary artery occlusion has matured over many decades; bypass operation and stent placement have become ubiquitously available at a high standard, but the prognosis of patients with myocardial infarction is still poor, due to remodeling of the left ventricle. Consequently, not only prevention but reduction of scar tissue after myocardial infarction has become a target of therapeutic efforts. Intramyocardial injection of stem cells previously collected from the patient is currently explored in clinical trials in order to increase the amount of contractile myocytes and/or supplying capillaries. First, clinical studies demonstrated that intramyocardial injection of stem cells results in an improved global left ventricular function (Beeres et al. 2006). In parallel, genes, precursors, proteins, and drugs are explored. A catheter-based approach for injection of cells or other substances is appealing, since it allows for repeated and more targeted injections, instead of single-shot injections during surgery. An eligible imaging modality should support delineation of the target area, which is the myocardial infarction and its borders, and catheter visualization together with the depiction of the spatial distribution of the injected material. While fluoroscopy and ultrasound fulfill only single aspects of these requirements, MR imaging is capable to delineate myocardial infarction, to visualize and track catheter in real time, and to monitor the distribution of contrast media-doped injectates (Kraitchman et al. 2003; Saeed et al. 2006; Krombach et al. 2005). In current practice, two approaches are commonly used to mark the injected substance: fluids are doped with extracellular contrast media (Saeed et al. 2006), while cells have been labeled with ultrasmall particles of iron oxide (USPIO) (Kraitchman et al. 2003). Cells, marked with USPIOs, can be followed up with MRI even weeks after the initial injection (Kraitchman et al. 2005).

Another indication for delivery of substances is the application of drugs to the vessel wall during angioplasty of peripheral arteries. Recently, it has been demonstrated in a longitudinal study with an observation period of 24 month that restenosis

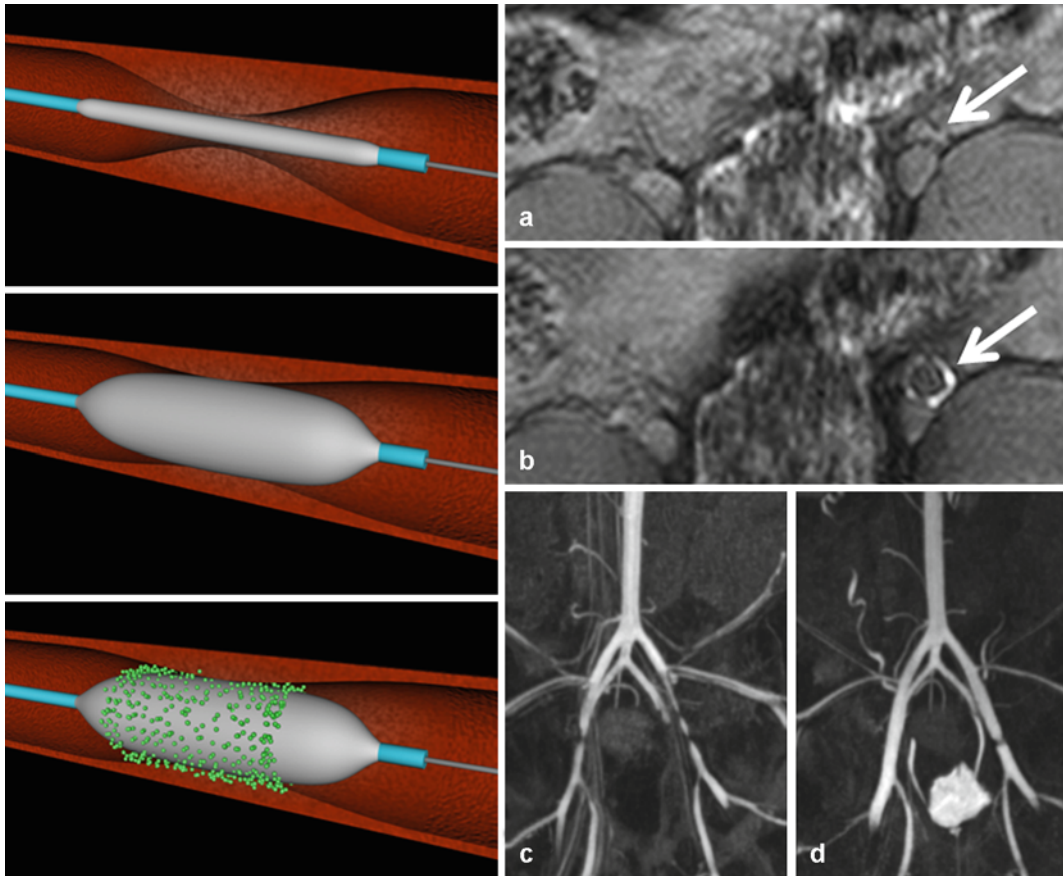

Fig. 16.31 *Left*: basic principle of the local delivery of a fluid mixture. (**a**–**d**) In pigs, surgically induced stenosis in the iliac arteries (**a**, T1-weighted gradient echo image, *arrow*: stenotic artery) were dilatated with a fluid-eluting balloon catheter. A contrast medium-doped solution was administered. After the intervention, the vessel wall is enriched with contrast medium (*arrow* in **b**). MR angiography prior to dilatation shows the stenosis (**c**, *arrows*), which is almost completely resolved after the intervention (**d**, *arrow*: small residual stenosis)

after angioplasty with drug-eluting balloons can be significantly decreased (Tepe et al. 2008). In another animal study, peripheral vascular stenoses were dilatated in concert with the application of contrast medium and tissue due solution to the vessel wall using a microporous balloon catheter (Krombach et al. 2008). Distribution of the contrast medium in the vessel wall was visible on MR images (Fig. 16.31) and resembled that of tissue due and hence facilitated the assessment of the delivery location. An optimistically inclined practitioner can imagine that future MR procedures will include vessel wall imaging with the ultimate goal of plaque characterization followed by selection and local supply of the indicated drug together with monitoring of sufficient delivery at the intervention. Such a concept cannot be followed using X-ray guidance, since the vessel wall cannot be sufficiently delineated, but recent MR studies are very encouraging. For example, injection of pancreatic islet cells, immunoisolated by encapsulating in magnetocapsules into the portal vein, has been successfully guided and visualized by MR imaging in a preclinical setting (Barnett et al. 2007). The extent of engraftment of the magnetocapsules into the liver could be monitored over time. Such an approach would be valuable for the treatment of patients with type I diabetes.

The different strategies of local delivery of therapeutics are currently developing and are likely to culminate in a concept that can be

applied with interventional MR imaging exclusively. This approach can certainly benefit from the traits of high-field MR imaging.

Appraisal

MR-guided endovascular interventions are attractive since MR imaging provides high soft tissue contrast, the ability to perform angiography with and without the application of contrast medium, the possibility of assessing physiologic function, and most recently, the concept of "molecular imaging." Actually, three groups of indications emerge: MR guidance of endovascular interventions is attractive for the treatment of patients with congenital heart disease, electrophysiological interventions, and local delivery of drugs or other therapeutics. Currently, different groups assemble the elements necessary for MR-guided endovascular interventions and develop dedicated protocols and procedures. However, these endovascular MR-guided interventions are being developed and have not yet entered the clinical arena.

Key Points

- The technical requirements, such as availability of real-time imaging and dedicated sequences, designed for endovascular interventions are already fulfilled. MR-safe equipment for monitoring of the patient during scanning is available.
- MR-safe interventional instruments are currently being developed and start to be available on the market.
- Catheters and other interventional instruments can be delineated by means of passive, active, or semi-active tracking. These techniques have different advantages and drawbacks and must be applied tailored to the intervention performed.

References

Sclerosing Therapy in Cysts and Parasites

Akhan O, Özmen MN (1999) Percutaneous treatment of liver hydatid cysts. Eur J Radiol 32:76–85

Akhan O, Baykan Z, Oguzkurt L et al (1997) Percutaneous treatment of a congenital splenic cyst with alcohol: a new therapeutic approach. Eur Radiol 7:1067–1070

Akinci D, Akhan O, Ozmen M et al (2005) Long-term results of single session percutaneous drainage and ethanol sclerotherapy in simple renal cysts. Eur J Radiol 54:298–302

Anon R, Guijarro J, Amoros C et al (2006) Congenital splenic cyst treated with percutaneous sclerosis using alcohol. Cardiovasc Intervent Radiol 29:691–693

Bean WJ (1981) Renal cysts: treatment with alcohol. Radiology 138:329–331

Caremani M, Vincenti A, Benci A et al (1993) Ecographic epidemiology of non-parasitic hepatic cysts. J Clin Ultrasound 21:115–118

Choi YD, Ham WS, Kim WT et al (2009) Clinical experience of single-session percutaneous aspiration and OK-432 sclerotherapy for treatment of simple renal cysts: 1-year follow-up. J Endourol 23(6):1001–1006

Frisell J, Rojdmark S, Arvidsson H et al (1979) Compression of the inferior caval vein – a rare complication of a large non-parasitic liver cyst. Acta Med Scand 205:541–542

Gharbi HA, Hassine W, Brauner MW et al (1981) Ultrasound examination of the hydatid liver. Radiology 139:459–463

Gigot JF, Legrand M, Hubens G et al (1996) Laparoscopic treatment of nonparasitic liver cysts: adequate selection of patients and surgical technique. World J Surg 20:556–561

Kabaalioglu A, Ceken K, Alimoglu E et al (2006) Percutaneous imaging-guided treatment of hydatid liver cysts: do long-term results make it a first choice? Eur J Radiol 59:65–73

Klee FE, Osswald BR, Wysocki S (1996) Splenic cyst – a classical "incidental finding". Zentralbl Chir 121:805–816 [German]

Larssen TB, Rosendahl K, Horn A et al (2003) Single-session alcohol sclerotherapy in symptomatic benign hepatic cysts performed with a time of exposure to alcohol of 10 min: initial results. Eur Radiol 13: 2627–2632

Mueller PR, Dawson SL, Ferrucci JT et al (1985) Hepatic echinococcal cyst: successful percutaneous drainage. Radiology 155:627–628

Ogita S, Tsuto T, Nakamura K et al (1996) OK-432 therapy for lymphangioma in children: why and how does it work? J Pediatr Surg 31:477–480

Saini S, Mueller PR, Ferrucci JT Jr et al (1983) Percutaneous aspiration of hepatic cysts does not provide definitive therapy. Am J Roentgenol 141:559–560

Sawhney R, D'Agostino HB, Zinck S et al (1996) Treatment of postoperative lymphoceles with percutaneous drainage

and alcohol sclerotherapy. J Vasc Interv Radiol 7: 241–245
Smego RA, Bhatti S, Khaliq AA et al (2003) Percutaneous aspiration-injection-reaspiration drainage plus albendazole or mebendazole for hepatic cystic echinococcosis: a meta-analysis. Clin Infect Dis 37:1073–1083
Thanos L, Mylona S, Ntai S et al (2005) Percutaneous treatment of true splenic cysts: report of two cases. Abdom Imaging 30:773–776
Tikkakoski T, Mäkelä JT, Leinonen S et al (1996) Treatment of symptomatic congenital hepatic cysts with single-session percutaneous drainage and ethanol sclerosis: technique and outcome. J Vasc Interv Radiol 7:235–239
Üstünsöz B, Akhan O, Kamiloglu MA et al (1999) Percutaneous treatment of hydatid cysts of the liver: long-term results. Am J Roentgenol 172:91–96
Völk M, Rogler G, Strotzer M et al (1999) Post-traumatic pseudocyst of the spleen: sclerotherapy with ethanol. Cardiovasc Intervent Radiol 22:246–248
WHO Informal Working Group on Echinococcosis – PAIR network (1996) Guidelines for treatment of cystic and alveolar echinococcosis in humans. Bull World Health Organ 74:231–242
WHO Informal Working Group on Echinococcosis (2000) Percutaneous drainage of echinococcal cysts (PAIR—puncture, aspiration, injection, reaspiration): results of a worldwide survey for assessment of its safety and efficacy. Gut 47:156–157

Percutaneous Management of Endoleaks

Ayuso JR, de Caralt TM, Pages M, Riambau V et al (2004) MRA is useful as a follow-up technique after endovascular repair of aortic aneurysms with nitinol endoprostheses. J Magn Reson Imaging 20:803–810
Baum RA, Carpenter JP, Golden MA et al (2002) Treatment of type 2 endoleaks after endovascular repair of abdominal aortic aneurysms: comparison of transarterial and translumbar techniques. J Vasc Surg 35:23–29
Cuypers P, Buth J, Harris PL et al (1999) Realistic expectations for patients with stent-graft treatment of abdominal aortic aneurysms. Results of a European multicentre registry. Eur J Vasc Endovasc Surg 17:507–516
Gambaro E, Abou-Zamzam AM Jr, Teruya TH et al (2004) Ischemic colitis following translumbar thrombin injection for treatment of endoleak. Ann Vasc Surg 18:74–78
Golzarian J, Murgo S, Dussaussois L et al (2002) Evaluation of abdominal aortic aneurysm after endoluminal treatment: comparison of color Doppler sonography with biphasic helical CT. AJR Am J Roentgenol 178:623–628
Görich J, Rilinger N, Sokiranski R et al (1999) Leakages after endovascular repair of aortic aneurysms: classification based on findings at CT, angiography, and radiography. Radiology 213:767–772
Parent FN, Meier GH, Godziachvili V et al (2002) The incidence and natural history of Type I and II endoleak: a 5-year follow-up assessment with color duplex ultrasound scan. J Vasc Surg 35:474–481
Rial R, Serrano FJ, Vega M et al (2004) Treatment of type II endoleaks after endovascular repair of abdominal aortic aneurysms: translumbar puncture and injection of thrombin into the aneurysm sac. Eur J Vasc Endovasc Surg 27:333–335
Rosenblit AM, Patlas M, Rosenbaum AT et al (2003) Detection of endoleaks after endovascular repair of abdominal aortic aneurysms: value of unenhanced and delayed CT acquisitions. Radiology 227:426–433
Sarac TP, Gibbons C, Vargas L et al (2012) Long-term follow-up of type II endoleak embolization reveals the need for close surveillance. J Vasc Surg 55:33–40
Schmid R, Gurke L, Aschwanden M et al (2002) CT-guided percutaneous embolization of a lumbar artery maintaining a Type II endoleak. J Endovasc Ther 9:198–202
Stavropoulos SW, Park J, Fairman R et al (2009) Type 2 endoleak embolization comparison: translumbar embolization versus modified transarterial embolization. J Vasc Interv Radiol 20:1299–1302
van den Berg JC, Nolthenius RP, Casparie JW et al (2000) CT-guided thrombin injection into aneurysm sac in a patient with endoleak after endovascular abdominal aortic aneurysm repair. AJR Am J Roentgenol 175:1649–1651
van Marrewijk C, Buth J, Harris PL et al (2002) Significance of endoleaks after endovascular repair of abdominal aortic aneurysms: the Eurostar experience. J Vasc Surg 35:461–473
Zarins CK, White RA, Hodgson KJ et al (2000) Endoleak as a predictor of outcome after endovascular aneurysm repair: AneuRx multicenter clinical trial. J Vasc Surg 32:90–107

Percutaneous Gastrostomy, Gastrojejunostomy, and Direct Jejunostomy

Beaver ME, Myers JN, Griffenberg L, Kimberly W (1998) Percutaneous fluoroscopic gastrostomy tube placement in patients with head and neck cancer. Arch Otolaryngol Head Neck Surg 124:1141–1144
Cope C, Davis AG, Baum RA et al (1998) Direct percutaneous jejunostomy: techniques and applications-ten years experience. Radiology 209:747–754
David VS, Gupta A, Zegel HG et al (1998) Investigation of antibiotic prophylaxis usage for vascular and nonvascular interventional procedures. J Vasc Interv Radiol 9:401–406
Gauderer MW, Ponsky JL, Izant RJ (1980) Gastrostomy without laparotomy: a percutaneous endoscopic technique. J Pediatr Surg 15:872–875
Given MF, Lyon SM, Lee MJ (2004) The role of the interventional radiologist in enteral alimentation. Eur Radiol 14:38–47

Given MF, Hanson JJ, Lee MJ (2005) Interventional radiology techniques for provision of enteral feeding. Cardiovasc Intervent Radiol 28:692–703
Gottschalk A, Strotzer M, Feuerbach S et al (2007) CT-guided percutaneous gastrostomy: success rate, early and late complications. Fortschr Röntgenstr 179:387–395
Gray RR, Chia-Sing H, Allan Y et al (1987) Direct percutaneous jejunostomy. AJR Am J Roentgenol 149: 931–932
Halkier BK, Ho CS, Yee ACN (1989) Percutaneous feeding gastrostomy with seldinger technique: review of 252 patients. Radiology 171:359–362
McDermott VG, Schuster MG, Smith TP (1997) Antibiotic prophylaxis in vascular and interventional radiology. AJR Am J Roentgenol 169:31–38
Neeff M, Crowder VL, McIvor NP et al (2003) Comparison of the use of endoscopic and radiologic gastrostomy in a single head and neck unit. ANZ J Surg 73:590–593
Pershaw RM (1981) A percutaneous method for inserting a feeding gastrostomy tube. Surg Gynaecol Obstet 152:659–660
Rieker O, Pitton M, Herber S, Vomweg T, Teifke A, Düber C (2005) Direct percutaneous radiologic jejunostomy (PRJ) and duodenostomy: a retrospective analysis. Fortschr Röntgenstr 177:393–398
Seitz J, Gmeinwieser M, Strotzer M et al (1997) CT-guided gastrostomy and gastroenterostomy: a reliable nonsurgical method also when percutaneous endoscopic gastrostomy is contraindicated or has failed. Dtsch Med Woschenschr 122:1337–1342
Wollmann B, D'Agostino HB, Walus-Wigle JR et al (1995) Radiologic, endoscopic, and surgical gastrostomy: an institutional evaluation and meta-analysis of the literature. Radiology 197:699–704

Interventions Using C-Arm Computed Tomography

Becker C, Waggershauser T et al (2011) C-arm computed tomography compared with positron emission tomography/computed tomography for treatment planning before radioembolization. Cardiovasc Intervent Radiol 34(3):550–556
Becker HC, Meissner O et al (2009) C-arm CT-guided 3D navigation of percutaneous interventions. Radiologe 49(9):852–855
Braak SJ, van Strijen MJ et al (2010) Real-time 3D fluoroscopy guidance during needle interventions: technique, accuracy, and feasibility. AJR Am J Roentgenol 194(5):W445–W451
Capasso P, Trotteur G et al (1996) A combined CT and angiography suite with a pivoting table. Radiology 199(2):561–563
Dick AJ, Raman VK et al (2005) Invasive human magnetic resonance imaging: feasibility during revascularization in a combined XMR suite. Catheter Cardiovasc Interv 64(3):265–274
Fahrig R, Holdsworth DW (2000) Three-dimensional computed tomographic reconstruction using a C-arm mounted XRII: image-based correction of gantry motion nonidealities. Med Phys 27(1):30–38
Fahrig R, Dixon R et al (2006) Dose and image quality for a cone-beam C-arm CT system. Med Phys 33(12): 4541–4550
Froelich JJ, El-Sheik M et al (2000a) Feasibility of C-arm-supported CT fluoroscopy in percutaneous abscess drainage procedures. Cardiovasc Intervent Radiol 23(6): 423–430
Froelich JJ, Wagner HJ et al (2000b) Comparison of C-arm CT fluoroscopy and conventional fluoroscopy for percutaneous biliary drainage procedures. J Vasc Interv Radiol 11(4):477–482
Georgiades CS, Hong K et al (2007) Adjunctive use of C-arm CT may eliminate technical failure in adrenal vein sampling. J Vasc Interv Radiol 18(9):1102–1105
Heran NS, Song JK et al (2006) The utility of DynaCT in neuroendovascular procedures. AJNR Am J Neuroradiol 27(2):330–332
Iwazawa J, Ohue S et al (2009) Identifying feeding arteries during TACE of hepatic tumors: comparison of C-arm CT and digital subtraction angiography. AJR Am J Roentgenol 192(4):1057–1063
Jin KN, Park CM et al (2010) Initial experience of percutaneous transthoracic needle biopsy of lung nodules using C-arm cone-beam CT systems. Eur Radiol 20(9):2108–2115
Kakeda S, Korogi Y et al (2007a) A cone-beam volume CT using a 3D angiography system with a flat panel detector of direct conversion type: usefulness for superselective intra-arterial chemotherapy for head and neck tumors. AJNR Am J Neuroradiol 28(9): 1783–1788
Kakeda S, Korogi Y et al (2007b) Usefulness of cone-beam volume CT with flat panel detectors in conjunction with catheter angiography for transcatheter arterial embolization. J Vasc Interv Radiol 18(12):1508–1516
Kalender WA (2006) X-ray computed tomography. Phys Med Biol 51(13):R29–R43
Kalender WA, Kyriakou Y (2007) Flat-detector computed tomography (FD-CT). Eur Radiol 17(11):2767–2779
Kang SE, Lee JW et al (2010) Percutaneous sacroplasty with the use of C-arm flat-panel detector CT: technical feasibility and clinical outcome. Skeletal Radiol 40(4): 453–460
Meyer BC, Frericks BB et al (2007) Contrast-enhanced abdominal angiographic CT for intra-abdominal tumor embolization: a new tool for vessel and soft tissue visualization. Cardiovasc Intervent Radiol 30(4): 743–749
Meyer BC, Frericks BB et al (2008a) Visualization of hypervascular liver lesions during TACE: comparison of angiographic C-arm CT and MDCT. AJR Am J Roentgenol 190(4):W263–W269
Meyer BC, Peter O et al (2008b) Electromagnetic field-based navigation for percutaneous punctures on C-arm CT: experimental evaluation and clinical application. Eur Radiol 18(12):2855–2864

Meyer BC, Witschel M et al (2009) The value of combined soft-tissue and vessel visualisation before transarterial chemoembolisation of the liver using C-arm computed tomography. Eur Radiol 19(9):2302–2309
Mohlenbruch M, Nelles M et al (2010) Cone-beam computed tomography-guided percutaneous radiologic gastrostomy. Cardiovasc Intervent Radiol 33(2):315–320
Morimoto M, Numata K et al (2010) C-arm cone beam CT for hepatic tumor ablation under real-time 3D imaging. AJR Am J Roentgenol 194(5):W452–W454
Ohnesorge B, Flohr T et al (2000) Efficient correction for CT image artifacts caused by objects extending outside the scan field of view. Med Phys 27(1):39–46
Pedicelli A, Rollo M et al (2009) Percutaneous vertebroplasty with a high-quality rotational angiographic unit. Eur J Radiol 69(2):289–295
Spreafico C, Marchiano A et al (1997) Hepatocellular carcinoma in patients who undergo liver transplantation: sensitivity of CT with iodized oil. Radiology 203(2):457–460
Sze DY, Strobel N et al (2006) Transjugular intrahepatic portosystemic shunt creation in a polycystic liver facilitated by hybrid cross-sectional/angiographic imaging. J Vasc Interv Radiol 17(4):711–715
Tam A, Mohamed A et al (2009) C-arm cone beam computed tomographic needle path overlay for fluoroscopic-guided placement of translumbar central venous catheters. Cardiovasc Intervent Radiol 32(4):820–824
Tam AL, Mohamed A et al (2010) C-arm cone beam computed tomography needle path overlay for fluoroscopic guided vertebroplasty. Spine (Phila Pa 1976) 35(10):1095–1099
Vanderschelden P, Flandroy P et al (1998) Comparative evaluation of cerebral aneurysms with selective arterially enhanced CT and DSA. Eur Radiol 8(7):1181–1186
Vogl TJ, Balzer JO et al (2002) Hybrid MR interventional imaging system: combined MR and angiography suites with single interactive table. Feasibility study in vascular liver tumor procedures. Eur Radiol 12(6): 1394–1400
Wallace MJ, Murthy R et al (2007) Impact of C-arm CT on hepatic arterial interventions for hepatic malignancies. J Vasc Interv Radiol 18(12):1500–1507
Wiesent K, Barth K et al (2000) Enhanced 3-D-reconstruction algorithm for C-arm systems suitable for interventional procedures. IEEE Trans Med Imaging 19(5):391–403

Hybrid Interventional CT/Angio System

Ando E, Tanaka M, Yamashita F et al (2002) Hepatic arterial infusion chemotherapy for advanced hepatocellular carcinoma with portal vein tumor thrombosis: analysis of 48 cases. Cancer 95:588–595
Arai Y, Inaba Y, Takeuchi Y, Ariyoshi Y (1997) Intermittent hepatic arterial infusion of high-dose 5FU on a weekly schedule for liver metastases from colorectal cancer. Cancer Chemother Pharmacol 40:526–530
Arai Y, Takeuchi Y, Inaba Y et al (2007) Percutaneous catheter placement for hepatic arterial infusion chemotherapy. Tech Vasc Interv Radiol 10(1):30–37
Bhattachariya S, Bhattachariya T, Baber S et al (2006) Prospective study contrast-enhanced computed tomography during arterioportography, and magnetic resonance imaging for staging colorectal liver metastases for liver resection. Br J Surg 91:1361–1369
Bolondi L, Gaiani S, Celli N et al (2005) Characterization of small nodules in cirrhosis by assessment of vascularity: the problem of hypovascular hepatocellular carcinoma. Hepatology 42:27–34
Bonomon G, Pedicini V, Monfardini L et al (2010) Bland embolization in patients with unresectable hepatocellular carcinoma using precise, tightly size-calibrated, anti-inflammatory microparticles: first clinical experience and one-year follow-up. Cardiovasc Intervent Radiol 33:552–559
Bruix J, Sherman M, Llovet JM et al (2001) Clinical management of hepatocellular carcinoma. Conclusion of the Barcelona-2000 EASL conference. European Association for the Study of the Liver. J Hepatol 35:421–430
Choi J (2006) Imaging of hepatic metastases. Cancer Control 13:6–12
Forner A, Vilana R, Ayuso C et al (2008) Diagnosis of hepatic nodules 20 mm or smaller in cirrhosis: prospective validation of the noninvasive diagnostic criteria for hepatocellular carcinoma. Hepatology 47:97–104
Froelich JJ, Ei-Scheik M, Wagner HJ, Achenbach S, Scherf C, Klose KJ (2000c) Feasibility of C-arm-supported CT fluoroscopy in percutaneous abscess drainage procedures. Cardiovasc Intervent Radiol 23:423–430
Gangi A, Kastler BA, Dietemann JL (1994) Percutaneous vertebroplasty guided by a combination of CT and fluoroscopy. AJNR Am J Neuroradiol 15:83–86
Gross T, Messmer P, Amsler F et al (2010) Impact of a multifunctional image-guided therapy suite on emergency multiple trauma care. Br J Surg 97:118–127
Iguchi T, Yabushita K, Sakaguchi K et al (2010) Percutaneous transhepatic sclerotherapy for bleeding ilial varices associated with portal hypertension and previous abdominal surgery. Jpn J Radiol 28:169–172
Imai Y, Murakami T, Hori M et al (2008) Hypervascular hepatocellular carcinoma: combined dynamic MDCT and SPIO-enhanced MRI versus combined CTHA and CTAP. Hepatol Res 38:147–158
Inaba Y, Arai Y, Kanematsu M et al (2000) Revealing hepatic metastases from colorectal cancer: value of combined helical CT during arterial portography and CT hepatic arteriography with a unified CT and angiography system. AJR 174:955–961
Inaba Y, Arai Y, Takeuchi Y et al (1996) Clinical effectiveness of a newly developed interventional-CT system. J Jpn Soc Angiography Interv Radiol 11:34–49
Inoue A (1993) Development of a hybrid CT/angiography system. Med Rev 43:9–15
Ishijima H, Koyama Y, Aoki J et al (1999) Use of a combined CT-angiography system for demonstration of

correlative anatomy during embolotherapy for hepatocellular carcinoma. J Vasc Interv Radiol 10:811–815
Kahiwagi N, Nakanishi K, Kozuka T et al (2010) Vascular supply with angio-CT for superselective intra-arterial chemotherapy in advanced maxillary sinus cancer. Br J Radiol 83:171–178
Kothary N, Weintraub JL, Susman J et al (2007) Transarterial chemoembolization for primary hepatocellular carcinoma in patients at high risk. J Vasc Interv Radiol 18:1517–1522
Kutlu R, Akbulut A, Siqirci A et al (2004) Lower prevalence of non-tumoral perfusion defects in left hepatic lobe during CT arterial portography with splenic arterial injection. Eur J Radiol 49:262–267
Laufer U, Kirchner J, Kickuth R, Adams S, Jendreck M, Liermann D (2001) A comparative study of CT fluoroscopy combined with fluoroscopy versus fluoroscopy alone for percutaneosu transhepatic biliary drainage. Cardiovasc Intervent Radiol 24:240–244
Lee MW, Kim YJ, Park SW et al (2009) Percutaneous radiofrequency ablation of small hepatocellular carcinoma invisible on both ultrasonography and unenhanced CT: a preliminary study of combined treatment with transarterial chemoembolization. Br J Radiol 82:908–915
Mahnken AH, Günther RW, Winograd R (2008) Percutaneous transgastric snaring for repositioning of a dislocated internal drain from pancreatic pseudocyst. Cardiovasc Intervent Radiol 31:S217–S220
Matsui O, Kobayashi S, Sanada J et al (2011) Hepatocellular nodules in liver cirrhosis: hemodynamic evaluation (angiography-assisted CT) with special reference to multi-step hepatocarcinogenesis. Abdom Imaging 36(3): 264–272
Mita K, Kim SR, Kudo M et al (2010) Diagnostic sensitivity of imaging modalities for hepatocellular carcinoma smaller than 2 cm. World J Gastroenterol 16:4187–4192
Miyayama S, Matsui O, Taki K et al (2006) Extrahepatic blood supply to hepatocellular carcinoma: angiographic demonstration and transcatheter arterial chemoembolization. Cardiovasc Intervent Radiol 29:39–48
Miyayama S, Matsui O, Yamashiro M et al (2007) Ultraselective transcatheter arterial chemoembolization with a 2-F tip microcatheter for small hepatocellular carcinomas: relationship between local tumor recurrence and visualization of the portal vein iodized oil. J Vasc Interv Radiol 29:39–48
Murakami T, Oi H, Hori M et al (1997) Helical CT during arterial portography and hepatic arteriography for detecting hypervascular hepatocellular carcinoma. AJR 169:131–135
Nagai N, Kaneyasu Y, Komatsu M et al (2009) Distribution of platinum in the female genital tract and efficacy of radiotherapy combined with transcatheter arterial infusion of cisplatin for locally advanced stage IIIb carcinoma of uterine cervix. Oncol Rep 21:585–591
Nibu K, Sugasawa M, Asai M et al (2002) Results of multimodality therapy for squamous cell carcinoma of maxillary sinus. Cancer 94:1476–1482
Sedick M, Haas S, Loehr M et al (2010) Application of DC beads in hepatocellular carcinoma: clinical and radiological results of a drug delivery device for transcatheter superselective arterial embolization. Onkologie 33:31–37
Seki H, Kimura M, Kamura T, Miura T, Yoshimura N, Sakai K (1996) Hepatic perfusion abnormalities during treatment with hepatic arterial infusion chemotherapy: value of CT arteriography using an implantable port system. J Comput Assist Tomogr 20:343–348
Sommer CM, Huber J, Radeleff BA et al (2011) Combined CT- and fluoroscopy-guided nephrostomy in patients with non-obstructive uropathy due to urine leaks in cases of failed ultrasound-guided procedures. Eur J Radiol 80(3):686–691
Takayasu K, Muramatsu Y, Asai S, Muramatsu Y, Kobayashi T (1999) CT fluoroscopy-assisted needle puncture and ethanol injection for hepatocellular carcinoma: a preliminary study. AJR 173:1219–1224
Takayasu K, Muramatsu Y, Maeda T et al (2001) Targeted transarterial oily chemoembolization for small foci of hepatocellular carcinoma using a unified helical CT and angiography system: analysis of factors affecting local recurrence and survival rates. AJR 176:681–688
Takeuchi Y, Arai Y, Inaba Y, Ohno K, Meda T, Yuji I (1998) Extrahepatic arterial supply to the liver: observation with a unified CT and angiography system during temporary balloon occlusion of the proper hepatic artery. Radiology 209:121–128
Tanaka T, Günther RW, Isfort P, Kichikawa K, Mahnken AH (2011a) Pull-through technique for recanalization of occluded portosystemic shunt (TIPS): technical note and review of the literature. Cardiovasc Intervent Radiol 34(2):406–412
Tanaka T, Nishiofuku H, Sho M et al (2011b) Phase I/II study of arterial infusion with 5-fluorouracil combined with systemic gemcitabine for unresectable pancreatic cancer. J Clin Oncol 29 (suppl 4; abstr 307)
Tanaka T, Inaba Y, Arai Y, Matsueda K, Aramaki T, Dendo S (2002) Mediastinal abscess successfully treated by percutaneous drainage a unified CT and fluoroscopy system. Br J Radiol 75:470–473
Tanaka T, Sakaguchi H, Sho M et al (2009) A novel interventional radiology technique for arterial infusion chemotherapy against advanced pancreatic cancer. Am J Roentgenol 192:W168–W187
Toyoda H, Kumada T, Sone Y (2009) Impact of a unified CT angiography system on outcome of patients with hepatocellular carcinoma. AJR 192:766–774
Trappero CT, Barbero S, Costantino S et al (2009) Patient and operator exposure during percutaneous vertebroplasty. Radiol Med 114:595–607
Uchida H, Ohishi H, Matsuo N et al (1990) Transcatheter hepatic segmental arterial embolization using lipiodol mixed with an anticancer drug and gelfoam particle for hepatocellular carcinoma. Cardiovasc Intervent Radiol 13:140–145
Yamakado K, Nakatsuka A, Takaki H et al (2008) Early-stage hepatocellular carcinoma: radiofrequency ablation combined with chemoembolization versus hepatectomy. Radiology 247:260–266

A Primer on MR-Guided Endovascular Procedures

Barnett BP, Arepally A, Karmarkar PV et al (2007) Magnetic resonance-guided, real-time targeted delivery and imaging of magnetocapsules immunoprotecting pancreatic islet cells. Nat Med 13:986–991

Bedetti G, Botto N, Andreassi MG et al (2008) Cumulative patient effective dose in cardiology. Br J Radiol 81:699–705

Beeres SL, Bax JJ, Kaandorp TA et al (2006) Usefulness of intramyocardial injection of autologous bone marrow-derived mononuclear cells in patients with severe angina pectoris and stress-induced myocardial ischemia. Am J Cardiol 97:1326–1331

Dukkipati SR, Mallozzi R, Schmidt EJ et al (2008) Electroanatomic mapping of the left ventricle in a porcine model of chronic myocardial infarction with magnetic resonance-based catheter tracking. Circulation 118:853–862

Kos S, Huegli R, Hofmann E et al (2009) Feasibility of real-time magnetic resonance-guided angioplasty and stenting of renal arteries in vitro and in swine, using a new polyetheretherketone-based magnetic resonance-compatible guidewire. Invest Radiol 44:234–241

Kraitchman DL, Heldman AW, Atalar E et al (2003) In vivo magnetic resonance imaging of mesenchymal stem cells in myocardial infarction. Circulation 107:2290–2293

Kraitchman DL, Tatsumi M, Gilson WD et al (2005) Dynamic imaging of allogeneic mesenchymal stem cells trafficking to myocardial infarction. Circulation 112:1451–1461

Kramer NA, Immel E, Donker H et al (2011) Evaluation of an active vena cava filter for MR imaging in a swine model. Radiology 258:446–454

Krombach GA, Pfeffer JG, Kinzel S et al (2005) MR-guided percutaneous intramyocardial injection with an MR-compatible catheter: feasibility and changes in T1 values after injection of extracellular contrast medium in pigs. Radiology 235:487–494

Krombach GA, Wehner M, Perez-Bouza A et al (2008) Magnetic resonance-guided angioplasty with delivery of contrast-media doped solutions to the vessel wall: an experimental study in swine. Invest Radiol 43:530–537

Krueger JJ, Ewert P, Yilmaz S et al (2006) Magnetic resonance imaging-guided balloon angioplasty of coarctation of the aorta: a pilot study. Circulation 113:1093–1100

Krueger S, Schmitz S, Weiss S et al (2008) An MR guidewire based on micropultruded fiber-reinforced material. Magn Reson Med 60:1190–1196

Kuehne T, Yilmaz S, Schulze-Neick I et al (2005) Magnetic resonance imaging guided catheterisation for assessment of pulmonary vascular resistance: in vivo validation and clinical application in patients with pulmonary hypertension. Heart 91:1064–1069

Lardo AC, McVeigh ER, Jumrussirikul P et al (2000) Visualization and temporal/spatial characterization of cardiac radiofrequency ablation lesions using magnetic resonance imaging. Circulation 102:698–705

Nazarian S, Kolandaivelu A, Zviman MM et al (2008) Feasibility of real-time magnetic resonance imaging for catheter guidance in electrophysiology studies. Circulation 118:223–229

Neizel M, Kramer N, Bonner F et al (2010) Rapid right ventricular pacing with MR-compatible pacemaker lead for MR-guided aortic balloon valvuloplasty in swine. Radiology 255:799–804

Razavi R, Hill DL, Keevil SF et al (2003) Cardiac catheterisation guided by MRI in children and adults with congenital heart disease. Lancet 362:1877–1882

Saeed M, Martin AJ, Lee RJ et al (2006) MR guidance of targeted injections into border and core of scarred myocardium in pigs. Radiology 240:419–426

Tepe G, Zeller T, Albrecht T (2008) Local delivery of paclitaxel to inhibit restenosis during angioplasty of the leg. N Engl J Med 358:689–699

Tzifa A, Krombach GA, Kramer N et al (2010) Magnetic resonance-guided cardiac interventions using magnetic resonance-compatible devices: a preclinical study and first-in-man congenital interventions. Circ Cardiovasc Interv 3:585–592

Part IV

Economics in Interventional Radiology

Quality Management in Interventional Radiology

17

Joachim E. Wildberger

Contents

J.E. Wildberger
Department of Radiology,
University Hospital Maastricht,
P.O. Box 5800, Maastricht NL 6202 AZ,
The Netherlands
e-mail: joachim.wildberger@maastrichtuniversity.nl

17.1 Introduction

Quality in business, engineering, and manufacturing is pragmatically defined as "the non-inferiority or superiority of something" (Wikipedia 2011). Many different techniques and concepts are available to reach a dedicated quality level. Maintenance of a given quality level is also important ("quality assurance").

The first question that might come up with this rather theoretical definition is whether a quality management (QM) is really needed for interventional radiology. The answer to that question certainly is "yes." Each of us has faced situations where a certain device was needed and was not available at that time. Subsequent searching, nervous acting, and even misunderstanding may lead to hazardous situations and will endanger the patient. Another example out of the clinical practice is the misunderstanding between the referring physician and the interventional radiologist by not following standardized pathways; e.g., a certain laboratory test is requested in the forefront of the procedure and personally addressed. On the day of the intervention, the results of the test are not available, and the colleague is not on duty. Therefore, the whole procedure has to be postponed, or the intervention will become some kind of a risky "off-label procedure."

One of the primary ambitions of QM is to set-up standards, e.g., by establishing "standard operating procedures (SOP)" and/or clinical pathways. Standardization is helpful in many respects: It facilitates comparability, appropriate treatment

A.H. Mahnken et al. (eds.), *CT- and MR-Guided Interventions in Radiology*,
DOI 10.1007/978-3-642-33581-5_17, © Springer-Verlag Berlin Heidelberg 2013

and reporting, as well as effective communication. This may lead to an effective usage of time and will improve the cost-benefit ratio. A critical incident reporting system (CIRS) might be useful as well. For instance, the latter is implemented for nuclear power plants (e.g., International Atomic Energy Agency – IAEA), aviation (e.g., International Air Transport Association – IATA), and aerospace (e.g., National Aeronautics and Space Administration – NASA). It increases awareness of actual and potential problems before critical endpoints or even harmful events are met. For patients, however, the variety and complexity of human conditions make it impossible to always reach the most appropriate diagnosis or to predict with certainty a particular response to treatment American College of Radiology et al. (2005). Nevertheless, internal review and structured audits will help to understand potential risks and lead to further optimization of workflow issues. Therefore, QM is a prerequisite in modern interventional radiology.

Probably everyone is practicing some kind of QM, even without trying to get to the bottom of the question. Most of us do procedures according to a (individual) guideline.

Major interventional radiological societies like the "Society of Interventional Radiology (SIR)" and the "Cardiovascular Interventional Radiological Society of Europe (CIRSE)" have published practical guidelines and standards of clinical practice on the web (http://www.sirweb.org/clinical/quality.shtml; http://www.cirse.org/index.php?pid=412#sops). Standards of practice are currently available on different issues for image-guided interventions. It should be stressed that these guidelines have to be adapted individually according to the local facilities and profiles, as these are some kind of "minimal consensus." Some recommendations deal with this issue in a comprehensive manner, e.g., establishing a quality improvement program in interventional radiology (http://www.sirweb.org/clinical/cpg/0810-1.pdf; Steele et al. 2010) and establishing a general guideline for interventional clinical practice (American College of Radiology et al. 2005). Other standards refer to terminology and reporting criteria for image-guided tumor ablation (Goldberg et al. 2009), quality improvement guidelines for percutaneous drainage, aspiration of abscess and fluid collections (http://www.sirweb.org/clinical/cpg/0810-4.pdf; Wallace et al. 2010), quality improvement guidelines for percutaneous needle biopsy (http://www.sirweb.org/clinical/cpg/0810-5.pdf; Gupta et al. 2010), antibiotic prophylaxis during vascular and interventional procedures (http://www.sirweb.org/clinical/cpg/QI32.pdf; Venkatesan et al. 2010), as well as for management of coagulation status and hemostasis risk in percutaneous image-guided interventions (http://www.cirse.org/files/File/SOP/Periprocedural.pdf; Malloy et al. 2009).

Evidence-based medicine will play an important role; however, there is also a tendency for too much evaluation, with a new term arising, the so-called evaluitis (Frey and Bruno 2006). Therefore, the main goal is to keep it simple, rational, and productive. Applying the triad of structure, process, and outcome according to Donabedian (1980) is one of various possible approaches to QM that should be applied also to interventional radiology. Ideally, the steps "quality control" and "quality assurance" will lead to "quality improvement." According to Donabedian (Donabedian 1980), three objective dimensions always have to be met:

1. Quality of structure
2. Quality of process
3. Quality of outcome

17.2 Quality of Structure

Quality of structure describes all infrastructural measures in an interventional radiology department. One striking example is the organization of logistics, which is particularly complex due to the broad variability of medical devices needed for interventional procedures. A standardized logistic division and stock-keeping is advantageous for

all kinds of interventions. Staff members with and without expert knowledge will profit from SOPs and the computer-based supply of materials under emergency conditions. In addition, an intelligent stock-keeping will provide information such as remaining periods of use and adequate stockage on the basis of a valid estimate. Compiling emergency kits with the necessary interventional devices are modules that have delivered an optimal performance in practice, e.g., for diagnostic punctures and abscess drainage procedures. Customized checklists with the individual preferences are favorable and should be updated on a regular basis.

Setting up individual SOPs again works best in a team approach, with technicians, interventional radiologists, and all other member of staff available that are responsible for the patient. A decision tree in terms of good medical practice avoids time-consuming discussions and may serve as a guiding line for less experienced colleagues, e.g., for on-call procedures.

17.3 Quality of Process

At first the indication for the intervention should be checked. Usually imaging diagnostics, the clinical course of the patient, and all additional information available (laboratory tests, previous results, etc.) form the basis for a rational decision-making ("assessment" and "decision to treat"). Especially cross-sectional image-guided procedures have profited from the tremendous technical development over the past years. Complex and challenging procedures have become technically feasible on the basis of 3D-data acquisition. A standardized examination protocol will guarantee a consistent image quality and will allow for proper decision. This course of action is nearly indispensable for follow-up studies in interventional oncology. Consistent imaging quality improves comparability and reporting safety at any rate (standardization of contrast material delivery [indispensable? If so: Which kind of CM, amount, delay] and standardization of the examination protocol [late-arterial/portal-venous/optional native scans/late phase scanning; perfusion studies – 4D imaging]).

Nowadays, the usage and the specification of an interventional procedure will be discussed by an internal review board, for instance a tumor board or a local reference centre for certain diseases. It is the responsibility of the interventional radiologist to advice the other members of the committee. Opportunities and potential drawbacks of the anticipated technique should be reflected so that the best decision for the individual patient can be put on a firm footing (central question: Is there enough evidence in order to allow for a clear cut indication management that meets objective criteria? ("treatment selection")).

Also the anticipated pathology is of major importance, as this will influence the intervention itself; e.g., a core biopsy will be mandatory if a lymphoma is the most likely diagnosis, while a fine-needle aspiration biopsy will be adequate for suspected bronchial cancer (Böcking 1991).

The patient's informed consent has to be taken in the forefront of the intervention, usually requiring a written education. A preprinted *standardized* form can be used as a starting basis for an *individual* preoperative interview and customizing. The whole spectrum of therapeutic options including interventional diagnostics and therapy should be reflected from this perspective as well ("patient-related factors").

When it comes to the procedure itself, one has to consider that interventional radiology is an individual and interactive supply of service. Therefore, the demands and personal skills of the interventional radiologist also have to be part of the process negotiation and delivery. To guarantee an acceptable quality of process, the interventional procedure also needs to be performed in a standardized manner, according to the local conditions (imaging techniques, availability of staff, etc.) and the individual experience of the interventional radiologist. This also includes the management of the corporate and the individual knowledge within the interventional team (Fig. 17.1).

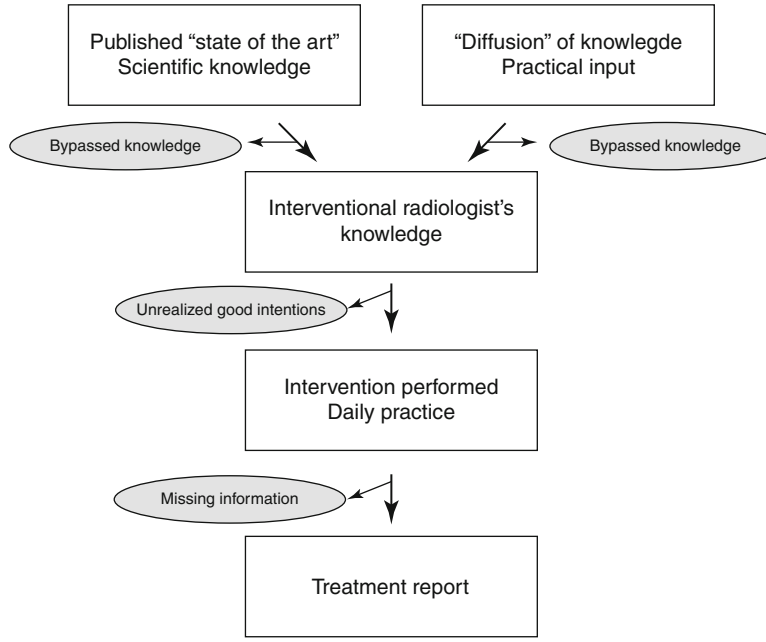

Fig. 17.1 Managing the explicit (e.g., literature) and the implicit knowledge (e.g., personal experience) as an inherent part of QM in interventional radiology

17.4 Quality of Outcome

Finally, the outcome of the interventional procedure should also be reflected. Typical questions that might be answered by a standardized questionnaire include:

- Must this type of policy also be put into practice, e.g., by cross-checking the results (anticipated pathology met)?
- Is additional imaging needed?
- Did the chosen method prove to be feasible in terms of outcome?
- Is another therapeutic option mandatory yet?
- Are there alternate options?
- Can the procedure itself be changed for the better?

A clear-cut responsibility assignment will optimize post-interventional treatment and prevent patients from falling through the cracks (especially in oncologic patients). This ensures fulfillment in treatment and diagnostics with continuity and sustainability in patient management.

Many sequences of action have become established over time and are not dealt with critically any more. This is regarded problematic, as radiology and interventional options are substantially advancing over time. Therefore, prospective implementation of an individually customized QM profile usually starts with an analysis of the present situation.

17.5 Setup of Individual Guidelines

The following nine step proposition of quality aspects according to the "Joint Commission on Accreditation of Healthcare Organizations (JCAHO 1990)" might serve as a basis for further discussion if the reader wants to set up an individual guideline for image-guided interventions or wants to reflect on the existing workflow within a department:

Accessibility of care

The ease with which patients can obtain the care that they need when they need it.

Appropriateness of care

The degree to which the correct care is provided, given the current state of the art.

Continuity of care

The degree to which the care needed by patients is coordinated among practitioners and across organization and time.

Effectiveness of care

The degree to which care (e.g., an interventional procedure) is provided in the correct manner given the current state of the art.

Efficacy of care

The degree to which a service has the potential to meet the need for which it was used.

Efficiency of care

The degree to which a service has the potential to meet the need for which it was used.

Patient perspective issues

The degree to which patients (and their families) are involved in the decision-making processes in matters pertaining to their health, and the degree to which they are satisfied with their care.

Safety of the care environment

The degree to which the environment is free from hazard or danger.

Timeliness of care

The degree to which care is provided to patients when it is needed.

Standardization can also be achieved by an internal or external certification and helps to structure the specified pathway in the particular setting. Some of these certificates are valid throughout the US/Europe and even worldwide (http://www.efqm.org/en/; http://www.din.de/cmd;jsessionid=323F70A217D9B80F7F0FA29967CE0723.4?level=tpl-home&languageid=en; http://www.jointcommissioninternational.org/).

Development of training charters for interventional radiology, including noninvasive vascular imaging, diagnostic angiography/venography and vascular, as well as nonvascular interventions, will be beneficial as well. Such guidelines have been set up, e.g., in a detailed curriculum for subspeciality training by the European Society of Radiology (http://www.myesr.org/html/img/pool/ESR_brochure_06.pdf; ESR Board 2005a, b). These might also serve as a good starting point for internal discussions, in combination with a proper definition of required technical, communication, and decision-making skills.

Finally, a large number of preventable adverse events are related to patient's admission and are particularly seen around the procedure itself (de Vries et al. 2009). Therefore, multidisciplinary aviation-style checklists, as, e.g., the SURPASS checklist for surgery, might be developed for radiology as well to cover the entire process from admission to discharge.

Summary

In summary, prospectively organized quality management needs to become an integrated part of interventional radiology. Standardization as its primary tool will have valuable advantages: it makes examination techniques, procedures, outcome, and the long-time course of the patients more comparable and will, therefore, be beneficial for interventional radiology in the long run. Moreover, QM establishes a beneficial link between the quality of the procedure and its efficiency. Therefore, QM has also important economic impact. Lapses in the standards of care may lead to harm to the patient and will be avoided in many cases by a functioning QM system. Completely unexpected errors, however, cannot be avoided in all cases. Finally, the goal of risk management as an integral part of QM will be to reduce and, where possible, to safeguard the patient, the radiologist, and the organization in which the radiologist works (http://www.myesr.org/html/img/pool/ESR_2006_IV_Riskmanagement_Web.pdf; ESR Board 2004).

Key Points

- Prospectively organized QM is needed in interventional radiology.
- The triad of structure, process, and outcome is well suited to establish QM in interventional radiology.
- SOPs and clinical pathways are effective tools of QM that can also be used in interventional radiology, ideally from admission to discharge of the patient.
- QM improves the clinical as well as the economic outcome of interventional therapy.

References

American College of Radiology; American Society of Interventional and Therapeutic Neuroradiology; Society of Interventional Radiology (2005) Practice guideline for interventional clinical practice. J Vasc Interv Radiol 16:149–155

Böcking A (1991) Cytological vs histological evaluation of percutaneous biopsies. Cardiovasc Intervent Radiol 14:5–12

De Vries EN, Hollmann MW, Smorenburg SM, Gouma DJ, Boermeester MA (2009) Development and validation of the SURgical PAtient Safety System (SURPASS) checklist. Qual Saf Health Care 18:121–126

Donabedian A (1980) Explorations in quality assessment and monitoring. In: The definition of quality and approaches to its assessment, vol 1. Health Administration Press, Ann Arbor

ESR Board (2004) Risk management in radiology in Europe, vol IV, Publications and media. European Society of Radiology, Vienna

ESR Board (2005a) Interventional radiology. In: Detailed curriculum for the initial structured common programme, vol VI, Publications and media. European Society of Radiology, Vienna, pp 28–30

ESR Board (2005b) Interventional radiology. In: Detailed curriculum for subspeciality training, vol VI, Publications and media. European Society of Radiology, Vienna, pp 58–60

Frey, Bruno S (2006) Evaluitis - A New Illness (Evaluitis - Eine Neue Krankheit). Available at SSRN: http://ssrn.com/abstract=914123 or http://dx.doi.org/10.2139/ssrn.914123

Goldberg SN, Grassi CJ, Cardella JF, Society of Interventional Radiology Technology Assessment Committee and the International Working Group on Image-guided Tumor Ablation et al (2009) Image-guided tumor ablation: standardization of terminology and reporting criteria. J Vasc Interv Radiol 20(7 Suppl):S377–S390

Gupta S, Wallace MJ, Cardella JF, Society of Interventional Radiology Standards of Practice Committee et al (2010) Quality improvement guidelines for percutaneous needle biopsy. J Vasc Interv Radiol 21:969–975

http://www.cirse.org/index.php?pid=412#sops. Accessed 2 Dec 2010

http://www.din.de/cmd;jsessionid=323F70A217D9B80F7F0FA29967CE0723.4?level=tpl-home&languageid=en. Accessed 2 Dec 2010

http://www.efqm.org/en/. Accessed 2 Dec 2010

http://www.jointcommissioninternational.org/. Accessed 2 Dec 2010

http://www.sirweb.org/clinical/quality.shtml. Accessed 2 Dec 2010

Joint Commission on Accreditation of Healthcare Organisations (JCAHO) (1990). Primer on indicator development and application. Measuring quality in health care. The joint commission on accreditation of healthcare organization, (Hrsg.). Oakbrooke Terrace, Illinois

Malloy PC, Grassi CJ, Kundu S, Standards of Practice Committee with Cardiovascular and Interventional Radiological Society of Europe (CIRSE) Endorsement et al (2009) Management of coagulation status and hemostasis risk in percutaneous image-guided interventions. J Vasc Interv Radiol 20(7 Suppl): S240–S249

Steele JR, Wallace MJ, Hovsepian DM et al (2010) Guidelines for establishing a quality improvement program in interventional radiology. J Vasc Interv Radiol 21:617–625

Venkatesan AM, Kundu S, Sacks D et al (2010) Practice guideline for adult antibiotic prophylaxis during vascular and interventional radiology procedures. J Vasc Interv Radiol 21:1611–1630

Wallace MJ, Chin KW, Fletcher TB, Society of Interventional Radiology Standards of Practice Committee et al (2010) Quality improvement guidelines for percutaneous drainage/aspiration of abscess and fluid collections. J Vasc Interv Radiol 21:431–435

Wikipedia (2011) http://en.wikipedia.org/wiki/Quality_(business). Accessed 2 Dec 2011

Cost-Effectiveness in Interventional Radiology

18

Mathias Bosch

Contents

M. Bosch
Boston Scientific Medizintechnik GmbH,
Daniel-Goldbach-Straße 17-27,
Ratingen D-40880, Germany
e-mail: boschm@bsci.com

18.1 Introduction

Cost-effectiveness is a term most radiologists did not know some years ago and some of them still do not, although cost-effectiveness analyses of imaging procedures are performed for more than 20 years (Otero et al. 2008)! However, it will become more and more important in the future, and physicians can no longer afford to leave this field to economists and controllers only! In most other areas of life, it is accepted that resources are limited, and therefore, a lot of effort is made to use it optimally, to "produce" at minimal costs. Only in medicine where the well-being (and sometimes indeed the life) of patients is at stake does this seem to be unethical while in fact it is unethical to waste resources thoughtlessly which are missing to treat another patient who much needs them.

Before we proceed, let me quickly explain what you can and cannot expect in this short chapter. Certainly, you will be disappointed if you just want to know whether, for example, radiofrequency ablation of the liver is cost-effective. The answer to this complex question depends on so many variables (such as: What other procedure do you compare it with? What are the local costs and outcomes of both procedures? What time horizon do you chose? At what rate do you discount future costs and health benefits? What view do you take if you compare costs: the view of the hospital, the sickness fund, or society) that it just cannot be answered globally. On the other hand you will learn:

A.H. Mahnken et al. (eds.), *CT- and MR-Guided Interventions in Radiology*,
DOI 10.1007/978-3-642-33581-5_18, © Springer-Verlag Berlin Heidelberg 2013

- What the difference is between efficacy, effectiveness, and cost-effectiveness.
- What the definition of cost-effectiveness is.
- An easy graphic model of cost-effectiveness.
- What kind of resource allocations have to be identified, collected, and valued.
- How the systematic cost calculation is done annually in the German DRG system.
- How important the point of view (society as a whole, sickness fund, hospital, private practice, patient) as well as the time horizon chosen is for the result of a cost-effectiveness analysis.
- Why we have to discount future costs.
- Why models can help you in assessing cost-effectiveness.
- How to ask the right questions.

18.2 Hurdles on the Way to the Market

Here are the three consecutive steps every pharmaceutical drug or interventional procedure normally has to go through:

1. The evaluation of a new procedure (or drug) starts with clinical studies to prove its *efficacy*. The patient group in those clinical studies on purpose is made very homogenous by strict inclusion and exclusion criteria. The question which can be answered after this step is: "Does it work?" Only if the answer to this question is a clear "yes," it will be approved and put on the market.
2. The evaluation typically continues with registries or all-comer studies to prove its *effectiveness*. This step is important in order to come closer to real world conditions. The patient population in this stage has to be as inhomogeneous as the patients a doctor sees every day. At the end it is clear, whether the intervention is effective, that is, whether it works in regular patients under regular conditions (which among others also means "in the hands of average physician") and therefore has an advantage for them.
3. Only after these first two steps have been successful the question of *cost-effectiveness* (or efficiency) comes up. Now the question to be answered is: "How much effect do we get at what cost?" Unfortunately, for most interventions, valid data on cost-effectiveness in real-world patients are still lacking, but much needed.

It is the constant price pressure of every national health-care system (due to various factors such as an aging population, costly innovations, less revenue of the sickness funds due to unemployment in countries where their revenue is defined as a percentage of wage) that puts cost-effectiveness on the forefront of health-political discussions with organizations like NICE (National Institute for Health and Clinical Excellence) in the UK or IQWiG (Institut für Qualität und Wirtschaftlichkeit im Gesundheitswesen) in Germany. For them, cost-effectiveness is a means of ensuring that the least-cost interventions are utilized given the allocated budget. An economic evaluation informs what additional costs society has to spend for an additional improvement in medical benefits (Aidelsburger et al. 2007).

Clearly, policy makers cannot and should not scrutinize every minor change in medical practice. In the United States, the Centers for Medicare and Medicaid Services (CMS), for example, reserves its national coverage determinations for types of technologies that (Hollingworth and Jarvik 2006):

1. Affect a large number of beneficiaries
2. Represent a significant medical advantage
3. Have a potential for rapid diffusion or overuse
4. Are subject to substantial controversy
5. Local carriers have inconsistent coverage policies for

It is generally accepted that minimally invasive procedures such as they are performed in interventional radiology do have many advantages in comparison to, for example, open surgery. This is true for the patient (less trauma, shorter stay in hospital, quicker recovery), the sickness fund and society as a whole (shorter stay in hospital, sooner back to work), and the hospital/doctor if adequately reimbursed (good image, high patient satisfaction). Therefore, their number is growing in virtually all medical fields. However, according to evidence-based medicine,

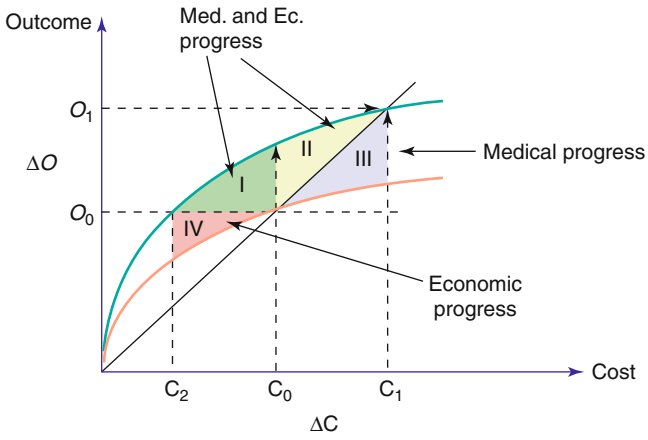

I	II	III	IV
Medical and economic progress	Medical and economic progress	Only medical progress	Only economic progress
$O_1 > O_0$	$O_1 > O_0$	$\Delta O > 0$	$\Delta O_1 > O_0$
$C_2 < C_0$	$C_1 > C_0$	$\Delta C > 0$	$\Delta C_1 > C_0$
$\Delta O > \Delta C$	$\Delta O > \Delta C$	$\Delta O > \Delta C$	$-\Delta O > -\Delta O$

Fig. 18.1 Model of cost-effectiveness: the two production functions (*upper one*: with the innovation; *lower one*: conventional procedure for comparison) show the relationship between the different inputs (i.e., costs, *C*) and the outcomes (*O*) of the intervention. *I* "ideal situation," *II* typical "cost-effective" innovation, *III* typical "costly" innovation, *IV* only economic progress (modified according to (Bundesverband Medizintechnologie e.V 2003))

their superiority needs to be shown in well-made cost-effectiveness studies.

18.3 Definition of Cost-Effectiveness

Since there are various similar terms, let us start by defining what cost-effectiveness is. Cost-effectiveness analysis (CEA) is a form of economic analysis that compares the relative expenditure (costs) and outcomes (effects) of two or more courses of action. It is important which procedure is chosen as the comparator: this can be the most frequently performed procedure, the most effective, or the most cost-effective procedure. Sometimes it is also essential to compare a new procedure to doing nothing ("watchful waiting" as, e.g., in the case of prostate cancer).

The difference between the effects (*E*) of an intervention (I) and an alternative intervention (A) in relation to the difference of cost (*C*) results in the incremental cost-effectiveness ratio (ICER) (Drummond et al. 1997; Gold et al. 1996):

$$\text{ICER} = (C_1 - C_A) / (E_1 - E_A) \qquad (18.1)$$

The four general results which a cost-effectiveness analysis can potentially have are illustrated in Fig. 18.1. The two production functions show the relationship between the different inputs (i.e., costs, *C*) and the outcomes (*O*) of the intervention.

I – "*Ideal situation*" *which probably is rare in the real world.* The new procedure (blue curve) is a medical progress since its outcome (O_1) is higher (better) than the outcome of the compared procedure (O_0). At the same time, it is also an economic progress since its costs (C_2) are lower than the costs of the compared procedure (C_0).

II – *Typical* "*cost-effective*" *innovation.* Again, it is a medical progress since its outcome (O_1) is higher (better) than the outcome of the compared procedure (O_0). However, this time there is a price to pay for this progress, its costs (C_1) are somewhat higher than the costs of the compared procedure (C_0). Please note that additional outcome is greater (*above* the 45°

line) than the additional costs ($\Delta O > \Delta C$). Such a procedure should be acceptable to most health economists.

III – Typical "costly" innovation. Here we have almost the same situation as in case No. II: a higher outcome ($\Delta O > 0$) at higher costs ($\Delta C > 0$). The minor, however, important difference is that the additional outcome is smaller (*below* the 45° line) than the additional costs ($\Delta O < \Delta C$). Such a procedure will be looked at very intensely by health economists who will ask: Should we pay this higher price for this amount of better outcome or should be better spend this money in other fields where we can get more additional outcome for it?

IV – Only economic progress. Here is a result not many physicians and patients will like: The outcome is worse ($\Delta O < 0$)! Why then is it still considered to be an economic progress? Simply because costs are more reduced than outcome ($-\Delta C > -\Delta O$). In cases of very scarce resources, one therefore might decide to go for a procedure which "only" brings economic progress.

18.4 What Kind of Resource Allocations Have to Be Identified, Collected, and Valued?

If we look at the costs of an intervention, the challenge is to identify, measure, and value all resources which are needed for a certain intervention. Obviously there are various groups of costs as far as the time is concerned: costs incurred before the intervention (e.g., before hospital), in hospital, and after hospital. The same applies to the various benefits. The general difficulty of collecting cost/benefit data is partly due to that fact. If a country (like Germany) has two totally separated sectors, hospitals (inpatient), and private practices (outpatient), the task of collecting cost data becomes almost impossible.

Costs and benefits may be separated in direct and indirect costs which can be divided in tangible and intangible. Figure 18.2 summarizes some (by far not exhaustive) examples of what costs and benefits we could think of.

On the other hand, there are various cost categories which you will have to look at when calculating the cost of a procedure:

- Material costs (such as implants, catheters, contrast medium, etc.)
- Drugs
- Costs of labor (time of physicians, assistant medical technicians, nurses, etc.)
- (Virtual) renting costs of, for example, a computed tomography (CT) or magnetic resonance (MR) scanner
- Overhead costs (e.g., for the hospital administration)

If you do not restrict your view to the time in hospital, you might also have the following costs:

- Future medical costs that are a consequence of the intervention (such as medication the patient has to take after an intervention or adjuvant medical devices such as crutches or a wheelchair).
- Rehabilitation.
- Medical treatment in private practice.
- Lack of work due to sick certificate (indirect cost).
- Home care by professionals or family members (indirect cost).
- Invalidity pension (indirect cost).
- Time losses from activities which might not receive a wage, but which may be valued by society or the individual none the less (intangible cost).

There is one more outcome parameter which needs to be measured (by questionnaires which have proven their effectiveness such as the SF-36): quality of life (QoL) (Ware and Sherbourne 1992). It is obvious that one of the main advantages of (minimally invasive) interventional radiology is that QoL in most cases should be better than in the case of open (and more invasive) surgery.

But how can one measure and compare the lifetime gained by different procedures if the QoL is different because of the different procedures (e.g., bypass vs. percutaneous coronary intervention). The answer is quality-adjusted life years, or QALYs, a way of measuring both the quality and the quantity of life lived, as a means of quantifying the benefit of a medical intervention. They are based on the number of years of life that would be added by the intervention. Each year in perfect

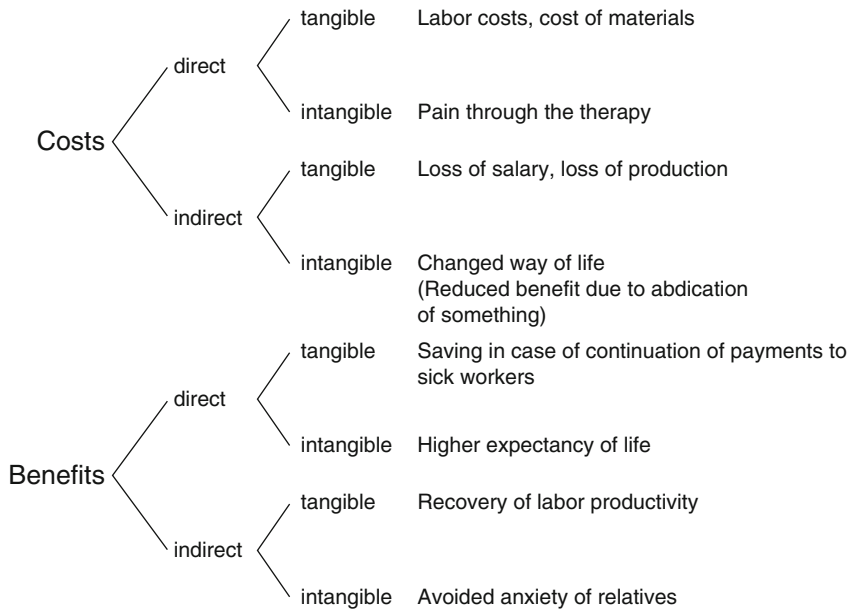

Fig. 18.2 Various costs and benefits (Ujlaky 2005)

health is assigned the value of 1.0 down to a value of 0 for death. If the extra years would not be lived in full health, for example, if the patient would lose a limb or be blind or be confined to a wheelchair, then the extra life years are given a value between 0 and 1 to account for this (e.g., major stroke ~ 0.35, post-MI ~ 0.683). The calculation of QALY therefore depends on the health state (QoL score) and time spent in that state.

Example:

- 1 year in perfect health = 1 QALY
- 1 year after major stroke = 0.35 QALY
- 0.5 year in perfect health + 0.5 year dead = 0.5 QALY

QALYs are used in cost-utility analyses to calculate the ratio of cost to QALYs gained for a particular health care intervention. This information is used to allocate health-care resources, with an intervention with a lower cost to QALY-saved ratio being preferred over an intervention with a higher ratio. This method is controversial because it means that some people will not receive treatment as it is calculated that cost of the intervention is not warranted by the benefit to their quality of life. However, its supporters argue that, since health-care resources are inevitably limited, this method enables them to be allocated in the way that is most beneficial to society.

The meaning and usefulness of QALY is debated for some other reason too. Perfect health is hard, if not impossible, to define. (The WHO has tried to do so and came up with "Health is a state of complete physical, mental, and social well-being and not merely the absence of disease or infirmity"; but its definition is of no practical use) (WHO 1948) Some argue that there are health states worse than death and that therefore there should be negative values possible on the health spectrum (indeed, some health economists have incorporated negative values into calculations). Determining the level of health depends on measures that some argue places disproportionate importance on physical pain or disability over mental health. The effects of a patient's health on the quality of life of others – caregivers, family, etc. – also do not figure in these calculations.

18.5 Systematic Cost Calculation in the German DRG System: An Example

The various kinds of costs become much more practical if we look for an example at the German DRG (diagnosis related groups) system where costs are calculated every year anew.

Although relatively new and "imported" from Australia, the German DRG system which is mandatory for all German acute care hospitals is already rather refined and (in contrast to, for example, the USA and Italy) updated every year. The basis for cost calculations is about 250 hospitals which collect their full-year cost data (according to the specifications of a detailed calculation handbook) and give it to the German DRG institute (called InEK). InEK makes a quality check, annually calculates the roughly 1,200 various DRGs, and publishes the aggregated data afterward (InEK 2007).

Let us demonstrate this point with radiofrequency ablation of the liver. In 2010 this leads to the DRG H41A (Table 18.1) if the patient has so many side diagnoses that he has a PCCL (patient clinical complexity level, i.e., the total weight of all his side diagnoses) of 4.

The different columns show the different cost categories:

1. Doctors
2. Nurses
3. Assistant medical technicians
4. Drugs
5. Implants
6. Other medical equipment
7. Medical infrastructure
8. Nonmedical infrastructure

Cost categories 1–3 obviously are labor costs, 4–6 are material costs, 7 and 8 are a mixture of both.

The different lines outline the various *cost centers*:

1. Regular ward
2. Intensive care unit
3. Operating room
4. Anesthesia
5. Cardiology diagnosis and therapy
6. Endoscopic diagnosis and therapy
7. Radiology
8. Laboratory
9. Other diagnosis and therapy
10. Basic cost center

Total costs of the DRG add up to €5301.80 with €301.80 of this being in radiology.

Despite the fact that this DRG (called "complex therapeutic ERCP with extremely severe clinical complexity or photodynamic therapy") contains many more patients than just those who received a radiofrequency ablation of the liver, these costs are considered more and more as norm costs. The consequence is that many heads of radiology departments in Germany are confronted with the norm costs of their department given all the various DRGs of a hospital. This figure is then compared with the actual costs of the radiology department in order to assess its overall "cost-effectiveness."

A rough calculation of all DRGs (weighting the costs of each DRG with its number in the calculation data) shows this picture (own data on file): the cost of radiology (cost center No. 9) in 2007 was €206,000,000,00 representing 3.8 % of a total of €5,400,000,000,00 since this percentage is constantly rising from 3.5 % in 2006 to 5.3 % in 2010.

18.6 The Importance of the Point of View and the Time Horizon of a Cost-Effectiveness Analysis

Although it is useful in cost-effectiveness analyses to take the perspective of the society in evaluating alternative allocations of health resources (i.e., by measuring aggregate health cost and aggregate health benefits across all members of society), it is also important that the particular objectives of the actual decision maker are considered. For example, total costs might be of concern to a sickness fund or health maintenance organization, whereas only in-hospital costs might concern a hospital administrator receiving a certain DRG reimbursement. Society as a whole bears all the costs, whether through insurance premiums or out-of-pocket payments, but the organizations and individuals who actually make resource-allocation decisions usually have varying objectives that should be recognized in a realistic cost-effectiveness analysis (Weinstein and Stason 1977).

It is also vital to choose the right time horizon for the study. As all effects and costs related to an intervention should be included into the economic evaluation, a long-term time horizon for the evaluation might become necessary. In these

Table 18.1 Model of cost-effectiveness

	Personnel expenditure			Non-personnel costs					Personnel and non-personnel costs		
	Doctors	Nurses	Assistant medical technicians	Drugs		Implants	Other medical equipment		Medical infrastructure	Non-medical infrastructure	
	1	2	3	4a	4b	5	6a	6b	7	8	Sum
Regular ward	464.5	990.0	54.3	152.0	65.5	0.0	89.3	9.6	252.2	901.1	2978.3
Intensive care unit	62.6	136.8	2.3	20.7	8.7	0.0	22.9	0.6	23.8	69.3	347.7
Operating room	26.9	0.0	23.1	1.1	0.7	6.3	18.4	6.3	11.6	18.6	113.0
Anesthesia	27.5	0.0	18.8	2.4	0.1	0.0	6.6	0.1	3.5	7.6	66.7
Cardiology diagnosis and therapy	1.6	0.0	1.9	0.1	0.0	1.5	1.1	3.0	1.1	1.6	11.8
Endoscopic diagnosis and therapy	185.2	0.0	197.4	9.7	1.6	66.9	120.3	56.9	93.6	151.4	882.9
Radiology	59.8	0.0	77.2	1.0	0.8	6.1	24.9	42.9	31.9	57.2	301.8
Laboratory	24.1	0.0	118.3	3.4	54.0	0.0	90.8	39.0	14.1	60.3	404.0
Other diagnosis and therapy	55.1	1.8	68.2	2.6	0.0	0.0	10.3	1.4	12.5	44.1	195.8
Sum	907.2	1128.5	561.5	193.1	131.4	80.8	384.4	159.8	444.2	1311.0	5301.8

cases the usage of data from randomized clinical trials (RCT) are not sufficient (even if they should contain cost data) as they usually do not cover this long-term time horizon for cost containment reasons. Mathematical models which utilize data from different sources can be applied to overcome this limitation.

The importance of the time horizon chosen can be easily illustrated by the following example. If you compare the cost-effectiveness of an arrhythmic drug with the cost-effectiveness of a pacemaker or internal defibrillator, no doubt the drug will be superior in a short time frame. However, if you set the end point of the study at 7–8 years, the result might be the opposite (Aidelsburger et al. 2007).

A totally different question to cost-effectiveness is whether the costs of an intervention (the total stay of a patient in hospital) are adequately reimbursed.

Literature about the cost-effectiveness of certain interventions is not easily found; the number of patients included is generally too low (e.g., 7 and 6, respectively, in a study comparing the cost of MR-guided laser ablation and surgery in the treatment of osteoid osteoma), and its quality is not satisfactory (Ronkainen et al. 2006). Blackmore and Smith (1998) have evaluated the methodological quality of economic analyses of radiological procedures published in the non-radiology medical literature during the years 1990–1995. Of the 56 articles, only 8 (14 %) conformed to all ten methodological criteria:

1. Comparative options stated
2. Perspective of analysis defined
3. Outcome measure identified
4. Cost data included
5. Source of cost data stated
6. Long-term costs included
7. Discounting employed
8. Summary measure provided
9. Incremental computation method used
10. Sensitivity analysis used

One of the peculiarities in comparison to clinical studies is that cost-effectiveness studies should be national (since the health-care systems and their incurred costs vary so much across different countries) and recent (since prices vary considerably over time).

This can be demonstrated by a recent cardiologic cost-effectiveness study (Brunner-La Rocca et al. 2007) from Switzerland which was intended to find out whether in percutaneous coronary interventions and stenting the use of drug-eluting stents (DES) instead of bare-metal stents (BMS) is cost-effective. They found that overall costs were higher for patients with drug-eluting stents (€11,808) than for patients with bare-metal stents (€10,450) due to higher stent costs. They calculated an incremental cost-effectiveness ratio (ICER) of €64,732 to prevent one major adverse cardiac event and stated that an unrealistic reduction of the cost of DES of about 29 % would have been required to achieve the arbitrary threshold ICER of €10,000. Sounds logical; however, what prices did they assume? Swiss list prices of 2004 are certainly much higher than, for example, present DES prices in Germany. Therefore, their findings are only valid for Switzerland in 2004 and cannot be extrapolated to all of Europe, let alone across the whole world.

18.7 Why We Have to Discount Future Costs

In finance and economics, discounting is the process of finding the present value of an amount of cash at some future date. To calculate the present value of a single cash flow, it is divided by one plus the interest rate for each period of time that will pass. If we assume a 12 % per year interest rate, the present value of €100 that will be received in 5 years time is only about €56.74. Therefore, a procedure which incurs exactly the same costs as an alternative procedure – but does it at a later point in time – is more cost-effective.

However, not only do costs have to be discounted. Benefits have to be discounted too for at least three reasons (Cairns 2001):

- Diminished marginal utility (in the temporal context).
- The risk that, whether as a result of death or some other circumstances, future consumption opportunities may not be available.
- Individuals simply have a preference for earlier consumption compared to later consumption.

18.8 Why Models Can Help You in Assessing Cost-Effectiveness

Economic evaluations (such as cost-effectiveness) depend on the evidence on cost and health effects of medical and public health interventions. This evidence can be derived from clinical studies, registries, meta-analysis, databases, administrative records (e.g., from sickness funds), and case reports. Of course the level of evidence found in these various sources is quite different.

Because the evidence required on consequences and cost of interventions is never present in a single source and the time horizon of most clinical studies is far too short, practitioners of cost-effectiveness analysis use mathematical models to synthesize data on costs and benefits of alternative clinical strategies. Economic evaluations that have been piggybacked on clinical trials often require almost as much modeling in order to extend the time horizon. If one fails to consider health and economic outcomes that may occur beyond the time frame of the observed data, there is an implicit assumption being made that all arms of the trial are equivalent.

A model makes explicit assumptions about the incidence and/or prognosis of a disease, the magnitude and duration of risks and benefits of prevention and/or treatment, the determinants of utilization of health-care resources, and health-related quality-of-life. Of particular value to clinicians and policy makers is that the models allow one to investigate how cost-effectiveness ratios might change if the values of key parameters in a model are changed (Kuntz and Weinstein 2001).

Models often used are decision trees (or probability trees), Markov models, and state-transition models (Gazelle et al. 2004). A decision tree has one decision node at the root. The branches of the initial decision node represent all interventions that are to be compared. Markov models are analytical structures that represent key elements of a disease and are commonly used in economic evaluations. They are particularly useful for diseases in which events can occur repeatedly over time such as acute myocardial infarction for patients with stable angina or cancer recurrence. For more detailed information see Sonnenberg and Beck (1993).

In both cases there is a trade-off between building a complicated model that accurately reflects all the important aspects of a disease and its treatment and building a simple model that is more transparent. At any rate, the input probabilities, utilities, and costs, as well as the key assumptions that underlie the model, should be carefully documented.

Zowall is a nice example of such a model comparing the cost-effectiveness of MR-guided focused ultrasound surgery (MRgFUS) for the treatment of uterine fibroids with uterine artery embolization, myomectomy, and hysterectomy (Zowall et al. 2008). O'Sullivan et al. present a quite different model for the same question (O'Sullivan et al. 2009). They even discuss in what ways their model differs from Zowall's considerably. The two articles seem to perfectly demonstrate the fact that models heavily depend on their assumptions. If costly equipment like MR is involved (like in MRgFUS), one of the most important assumptions is the assumed patient throughput.

Summary

Economic questions (such as cost-effectiveness of alternative procedures) become more and more important in medicine due to increasing pressure to curb health-care costs. Every radiologist is well advised to open his mind to such questions and to start finding what the costs of his clinical pathway are. In countries with a fixed payment (DRG) per patient, this is a must anyhow. Physicians need to learn how to ask the right questions when building up an interventional radiology program. These questions could be:

- What are the alternatives to my intervention (including wait and see)?
- What are the cost and the outcome of my intervention and the alternatives?
- What is the cost per QALY gained?
- What is the perspective of the patient, provider, payer, health maintenance organization, health care system, and society?

Should the radiologist initiate a clinical study? it is generally a good idea to include cost data in order to be able to answer economic questions which might arise later. As with clinical studies, the design of which has improved over the last few years, so will cost-effectiveness studies improve as more physicians become aware of the methodological standards of such studies.

Key Points

- Health economics become more and more important due to limited resources for health care.

Cost-effectiveness analyses are generally complex studies requiring a multidisciplinary team with expertise in the clinical problem, clinical epidemiology, decision analysis, economics, and statistics.

Collecting the various cost and asking the right questions is a reasonable first step.

In order to improve our knowledge about the cost-effectiveness of interventional radiological procedures, cost data (and well-made cost-effectiveness analyses) should be included in all future clinical studies.

References

Aidelsburger P, Grabein K, Klauss V et al (2007) Cost effectiveness of cardiac resynchronization therapy in combination with an implantable cardioverter defibrillator (CRT-D) for the treatment of chronic heart failure from a German health care system perspective. Clin Res Cardiol 97:89–97

Blackmore CC, Smith WJ (1998) Economic analyses of radiological procedures: a methodological evaluation of the medical literature. Eur J Radiol 27:123–130

Brunner-La Rocca HP, Kaiser C, Bernheim A et al (2007) Cost-effectiveness of drug-eluting stents in patients at high or low risk of major cardiac events in the Basel Stent Kosten Effektivitäts Trial (BASKET): an 18-month analysis. Lancet 370:1552–1559

Bundesverband Medizintechnologie e.V. (2003) Leitfaden für eine lokale und dezentrale Marktetablierung innovativer und neuer Medizinprodukte. MedInform c/o BVMed, Berlin

Cairns J (2001) Discounting in economic evaluations. In: Drummond M, McGuire A (eds) Economic evaluation in health care, merging theory with practice. Oxford University Press, Oxford, p 236

Drummond M, Sculpher MJ, Torrance GW (1997) Methods for the economic evaluation of health care programmes. Oxford University Press, New York

Gazelle GS, McMahon PM, Beinfeld MT et al (2004) Metastatic colorectal carcinoma: cost-effectiveness of percutaneous radiofrequency ablation versus that of hepatic resection. Radiology 233:729–739

Gold MR, Siegel JE, Weinstein MC (1996) Cost-effectiveness in health and medicine. Oxford University Press, New York

Hollingworth W, Jarvik JG (2006) Evidence on the effectiveness and cost-effectiveness of vertebroplasty: a review of policy makers' responses. Acad Radiol 13: 550–555

InEK (2007) Institut für das Entgeltsystem im Krankenhaus. Homepage (http://www.g-drg.de). Report browser 2005/2007, published 15 Dec 2006

Kuntz KM, Weinstein MC (2001) Modeling in economic evaluation. In: Drummond M, McGuire A (eds) Economic evaluation in health care, merging theory with practice. Oxford University Press, Oxford, p 141

O'Sullivan AK, Thompson D, Chu P et al (2009) Cost-effectiveness of magnetic resonance guided focused ultrasound for the treatment of uterine fibroids. Int J Technol Assess Health Care 25:14–25

Otero HJ, Rybicki FJ, Greenberg D et al (2008) Twenty years of cost-effectiveness analysis in medical imaging: are we improving? Radiology 249:917–925

Preamble to the Constitution of the World Health Organization as adopted by the International Health Conference, New York, 19–22 June, 1946; signed on 22 July 1946 by the representatives of 61 States (Official Records of the World Health Organization, no. 2, p. 100) and entered into force on 7 April 1948

Ronkainen J, Blanco Sequeiros R, Tervonen O (2006) Cost comparison of low-field (0.23 T) MRI-guided laser ablation and surgery in the treatment of osteoid osteoma. Eur Radiol 16:2858–2865

Sonnenberg FA, Beck JR (1993) Markov models in medical decision making: a practical guide. Med Decis Making 13:322–338

Ujlaky R (2005) Innovations-Risikomanagement im Krankenhaus. Frankfurt/Main, p 133

Ware JE, Sherbourne CD (1992) The MOS 36-item short-form health survey (SF-36): conceptual framework and item selection. Med Care 30:473–483

Weinstein MC, Stason WB (1977) Foundations of cost-effectiveness analysis for health and mental practices. N Engl J Med 296:716–721

WHO: Preamble to the Constitution of the World Health Organization as adopted by the International Health Conference, New York, 19–22 June, 1946; signed on 22 July 1946 by the representatives of 61 States (Official Records of the World Health Organization, no. 2, p. 100) and entered into force on 7 April 1948

Zowall H, Cairns JA, Brewer C et al (2008) Cost-effectiveness of magnetic resonance-guided focused ultrasound surgery for treatment of uterine fibroids. BJOG 115:653–662

Building an Interventional Department

19

Philip Ditter and Kai E. Wilhelm

Contents

Interventional radiology plays an increasingly important role in today's medicine. Not only because of a general trend away from invasive to minimally – or even noninvasive procedures – but also due to increasing technical capabilities giving way for image-guided interventions, which a few years ago could not be performed. For this reason, it is more and more important that interventional radiology is established as an independent unit (Keeling et al. 2009; Lammer 2008). So far, interventional radiologists mostly just perform a procedure requested from referring physicians. They are only very little – and sometimes not at all – involved in pre- and postinterventional patient care (Tomashek 2002; Murphy 2003; Siskin et al. 2004; Lammer 2008). Hence, the interventional radiologist acts more like a technician than a clinician (Tomashek 2002). In a long-term perspective, it is desirable to change these circumstances. The role of interventional radiology should be reconsidered, and a more clinically oriented, longitudinal approach to patient care should be ensured: from preprocedural assessment, the procedure itself, to postprocedural follow-up – everything should be performed under the "roof" of interventional radiology (White et al. 1989; Tomashek 2002; Murphy 2003; Pentecost 2003; Siskin et al. 2004; Swischuk et al. 2004; Lammer 2008; Keeling et al. 2009). Concerning a successful physician-patient relationship, it is not least important to provide effective and satisfactory communication in order to actively involve patients in treatment processes and medical decision making (Tomashek 2002; Murphy 2003; Pentecost 2003; Siskin et al. 2004;

P. Ditter (✉) • K.E. Wilhelm
Department of Radiology, University Hospital Bonn, Sigmund-Freud-Str. 25, D- 53127 Bonn, Germany
e-mail: philip.ditter@ukb.uni-bonn.de; wilhelm@uni-bonn.de

A.H. Mahnken et al. (eds.), *CT- and MR-Guided Interventions in Radiology*,
DOI 10.1007/978-3-642-33581-5_19, © Springer-Verlag Berlin Heidelberg 2013

Swischuk et al. 2004). Various studies show that especially clinical outcome and patient compliance are improved due to a successful physician-patient relationship (Hulka et al. 1975; Ring and Kerlan 1985; Greenfield et al. 1988; Adams et al. 2001; Siskin et al. 2004).

On the one hand, this approach might lead to an increasing competition arising with referring physicians, especially with those providing similar procedures (e.g., cardiologists or vascular surgeons) (Swischuk et al. 2004; Keeling et al. 2009). On the other hand, however, this aspect can be seen as a promising challenge in order to optimize quality and efficiency of radiological interventions that finally benefits the patients (Tomashek 2002; Lammer 2008).

Up to now, there are only few randomized prospective studies performed by interventional radiologists. Publications – especially concerning peripheral angioplasty – are highly dominated by other medical disciplines such as cardiology or angiology. Thus, emerging competition with other departments might have a positive influence on this situation in the future and thus contribute to interventional radiology's establishment as a serious competitor in patient care.

Interventional radiologists are often "afraid" of independent patient care – maybe because of an (assumed) lack of clinical experience (Smith et al. 1989; Ring and Kerlan 1985; Keeling et al. 2009). Radiological training typically includes a 12-month clinical internship and another – in some countries voluntary and in other countries mandatory – year in clinical medicine before or during the radiology fellowship. In addition, there is a mandatory interventional training within a radiological fellowship, and 74 % of European interventional radiologists have more than 10 years experience in interventional radiology according to a study by Keeling et al. (Keeling et al. 2009). Yet, there are several authors that argue that clinical training is underrepresented in radiological training and that training programs should be reconsidered (Keeling et al. 2009; Ahmed et al. 2010). But still, interventional radiologists should not be reluctant competing with specialists from other disciplines as they already have a highly specialized, both clinical and interventional trainings (Lammer 2008). Of course, there are unexpected medical problems (e.g., exacerbation of hypertension or hyperglycemia) that may require other medical services. Under these circumstances, the interventional radiologist can either consult a specialist or refer the patient to a specialized department. This approach will reverse current clinical practice by keeping the interventional radiologist as the patient's primary physician (Lammer 2008).

Despite of all efforts to be perceived as independent department, cooperation with general radiology should not be neglected as profound knowledge of imaging techniques is essential for successful interventions. A further development of MR-guided interventions, for example, will only be possible if experiences and insights from general radiology are well considered.

Moreover, patients usually consider invasive surgical procedures as risky and painful. So, if they have the choice, many patients tend to less invasive treatments with low morbidity and mortality. This advantage should be used by interventional radiologists to promote their services (Lammer 2008). In addition, minimal invasive procedures contribute to cost reduction: They allow shorter hospital stays (e.g., compared to open surgery) or in many cases, outpatient treatment (Nolte-Ernsting et al. 2006). Furthermore, early interventions often help to prevent occurrence or exacerbation of subsequent diseases. This aspect should be clearly emphasized as cost efficiency plays an increasing role in today's medicine.

The following chapter will provide a brief overview of how an interventional unit can be designed and offers aspects which might be considered when building an interventional unit – as a hospital-based in- and outpatient service as well as in private practice.

19.1 General Considerations

The role of interventional radiologists can be seen from different perspectives.

First, from a more passive or "traditional" view, patients are referred only for a certain procedure and thereafter return to the referring department. The interventional radiologist is only involved in the procedure itself and not part of the further treatment process (Teng et al. 2008; Keeling et al. 2009). This is a very passive approach as interventional

radiologists depend on referring departments and not actively run their schedules by having "own" radiological patients (Tomashek 2002).

Second, from a more active or "progressive" view, interventional radiologists act as the patient's primary doctor providing a full standalone medical service. Interventional radiologists offer longitudinal patient care including not only an intervention as such but also pre- and postinterventional care (Katzen et al. 1989; White et al. 1989: Tomashek 2002; Pentecost 2003; Swischuk et al. 2004; Lammer 2008; Keeling et al. 2009).

As mentioned above, the latter way might be a more promising option for the future. In this context, it is necessary to mention that interventional radiologists should not only receive referrals for just an intervention but also develop their own "patient contingent" that is admitted and discharged independently (Katzen et al. 1989; White et al. 1989; Barth and Matsumoto 1991; Becker 2001; Tomashek 2002; Murphy 2003; Pentecost 2003; Siskin et al. 2004; Swischuk et al. 2004; Lammer 2008). This is a necessary step because optimal patient care can hardly be achieved in a dependent relationship with other departments.

Moreover, billing of consultations, examinations, and interventions should be coordinated by interventional radiologists themselves (Tomashek 2002; Siskin et al. 2004; Lammer 2008).

19.1.1 Information

Of course, it is still mandatory to accept referrals from other departments or primary care physicians. Yet, it is crucial that interventional radiologists are seen as primary consultants for an entire treatment by both patients and practitioners (Katzen et al. 1989; Tomashek 2002; Lammer 2008).

For this reason, interventional radiologists need to present themselves as independent experts in a certain clinical field. They have to emphasize their specialization (e.g., vascular interventions) and promote themselves as a reasonable alternative to other disciplines (e.g., vascular surgery) (Swischuk et al. 2004). Therefore, it is essential that detailed information on the spectrum of examinations and interventions as well as on the technical equipment is given not only to patients but also to referring physicians (White et al. 1989; Tomashek 2002; Siskin et al. 2004; Lammer 2008).

In addition, extended preprocedural assessments should predict possible results, benefits, and complications. Adequate postprocedural follow-up is needed to fulfill the criteria of longitudinal patient care. The objective of this concept should be to develop an entire treatment regimen – in accordance with the patient (White et al. 1989; Tomashek 2002; Murphy 2003; Siskin et al. 2004). Various studies confirm that this approach to clinical care benefits the patients by improving compliance and clinical outcome (Hulka et al. 1975; Ring and Kerlan 1985; Greenfield et al. 1988; Adams et al. 2001; Siskin et al. 2004). Other departments should be consulted only for certain issues (e.g., concomitant diseases) that cannot be handled by an interventional radiologist alone (Tomashek 2002; Murphy 2003; Siskin et al. 2004; Lammer 2008).

19.1.2 Office

Prerequisite for organizing an independent interventional in- or outpatient service is to establish an office. The office serves as a unit's center where all essentials are covered (Pentecost 2003; Siskin et al. 2004; Lammer 2008):

19.1.2.1 Communication

Proper communication is essential – not least for workflow efficiency. If there is a central office with a contact person (receptionist, office coordinator), many issues can be managed quickly and easily, for example, without wasting time on unrequited phone calls.

Moreover, building a reliable, long-term partnership between interventional radiologist, patients, and referring physician is hardly possible without having a fixed drop-in center (Murphy 2003; Siskin et al. 2004; Lammer 2008).

19.1.2.2 Schedule Coordination

A central office is also essential to ensure a reasonable and well-functioning schedule. Appointments can be made, postponed, or cancelled in an uncomplicated way – important for workflow efficiency and for binding patients or referrers on the interventional unit (Siskin et al. 2004; Lammer 2008).

19.1.2.3 Management of Patient Records

Solid management of patient records plays a crucial role for efficient patient care. It is necessary that addresses, contact numbers (of patients, referring departments, general practitioners), insurance information, prior medical history, pre- and postinterventional assessments, previous and current imaging studies, laboratory reports, letters from referring physicians, and obligatory consent forms (patient agreement to intervention) are collected in one place (Becker 2001; Siskin et al. 2004).

Furthermore, reports of the intervention itself as well as preprocedural evaluations, postprocedural follow-ups and therapy plans have to be documented, and reports have to be sent – not only to patients but also to all referring departments and to the responsible general practitioners (Tomashek 2002; Lammer 2008).

19.1.2.4 Billing

Provided services have to be coded and billed. Very often, this is a very complex issue, and experts have to be consulted. Yet, establishing an office can be helpful concerning billing and coding as patients' insurance and procedural information is easily accessible (Siskin et al. 2004).

An office serves as a "pivotal point" of an interventional unit: Communication with the in- and outside is coordinated, and the unit schedule as well as patient records is centrally managed. This helps to establish an efficient workflow by saving resources, especially time. Ultimately, there is a benefit for all who are involved: interventional radiologists, referring physician, and, above all, patients (Tomashek 2002; Siskin et al. 2004; Lammer 2008).

Incidentally, this is not a new development in medicine. Other disciplines (e.g., cardiology, gastroenterology, dermatology, or surgery) have offered services like this for many years.

19.2 Practical Considerations

19.2.1 Hospital-Based Interventional Unit

As mentioned before, it is recommended to install a central office in order to provide an efficient clinical service. On the one hand, a hospital-based interventional unit should take care of inpatients. On the other hand, it should also serve as a hospital-based outpatient clinic (Lammer 2008; Keeling et al. 2009). Not least for economic reasons, outpatient treatment yields additional revenue to the hospital (Nolte-Ernsting et al. 2006).

For many reasons, preprocedural assessments should take place in a well-coordinated clinic. Some of the reasons are (Siskin et al. 2004; Lammer 2008):

- Patients can be interviewed and examined in a calm setting.
- Additional examinations can easily be performed (imaging studies, laboratory reports, etc.).
- Time to inform patients about the intervention, its risks, its benefits, and possible alternatives.
- Time to obtain informed consent.
- Time to inform patients about follow-ups.

Not forgetting that during a detailed pre- or postprocedural assessment, patients have the opportunity to express their problems and fears. This helps to develop a faithful relationship between patient and interventional radiologist and finally improves patient comfort (Siskin et al. 2004).

19.2.1.1 Premises

For a proper clinical service, it is mandatory to have a defined location with at least two or three rooms for (Siskin et al. 2004; Lammer 2008):

- Office/reception including a waiting area
- Consultation
- Examination

Appropriate equipment should be available (e.g., examination table, computer terminal, ECG machine, ultrasound, treadmill, etc.) (Lammer 2008). Preferably these rooms should be located close to the room(s) where interventions take place (e.g., angiography lab) (Siskin et al. 2004).

19.2.1.2 Staff

Obviously, the number of staff members depends on the number of treated patients and – not least – on individual financial resources. However, there is a minimum of necessary staff to successfully run an interventional unit (Tomashek 2002; Pentecost 2003; Siskin et al. 2004; Lammer 2008; Keeling et al. 2009):

- An interventional radiologist
- Two nurse(s), nurse practitioner(s), or clinical junior doctor(s) with experiences in interventional radiology
- A receptionist/coordinator

19.2.1.3 Beds

Some interventions are day-case procedures, some require a hospital stay of 2–3 days, and there might be few cases that need longer hospitalization. Hence, it is absolutely essential for an independent interventional unit to have beds available (Lammer 2008; Keeling et al. 2009).

A recent study by Keeling et al. showed what the actual situation in Europe is like (Keeling et al. 2009): Only very few European institutions provide own interventional radiology beds (Keeling et al. 2009); just 31 % of the centers have day-case beds, and only 17 % provide inpatient beds (Keeling et al. 2009). Numbers from Canada are similar (Baerlocher et al. 2006). The major reason for this situation lies in the fact that the hospital management refuses access to needed beds (Keeling et al. 2009). A lack of assisting junior doctors and a big workload (due to also providing diagnostic imaging) are further reasons (Keeling et al. 2009). Yet, experience from China and Japan shows that successfully running more dedicated interventional radiology beds is feasible: More than 50 % of interventional radiology departments provide own beds in these countries (Yamashita et al. 1994; Teng et al. 2008; Keeling et al. 2009).

Practically the number of needed beds depends on the size of the hospital, the number of patients treated by the unit, and complexity of treated cases (Lammer 2008).

There are several options in providing beds (Lammer 2008; Keeling et al. 2009):

- Own beds exclusively for interventional radiology patients
- Beds from other departments where interventional patients are admitted, treated, and discharged independently by interventional radiologists
- Day-case beds

Although it is comfortable to run an own ward with interventional beds, it should be considered that the number of interventional patients might be fluctuating, more administration is required, and the costs are higher, not least because of an increased number of staff members.

For this reason, it makes sense to have a minimum number of interventional beds (depending on the size of your hospital, the average number of interventional cases, and the case mix). Exceed requests for interventional radiology services should be covered by using vacancies of other departments (Lammer 2008).

After all, "Liason with hospital management and cooperation with other clinicians may increase hospital patient bed availability" (Keeling et al. 2009).

19.2.1.4 Schedule

It is important to establish an efficient time management in close cooperation with the office coordinator. Procedures should never take place during clinical hours. More time should be estimated for initial assessments than for follow-ups (e.g., 30 vs. 10 min), and waiting time should be kept to a minimum (Siskin et al. 2004; Lammer 2008).

19.2.1.5 Technical Equipment

Depending on the spectrum of treated diseases and personal specialization, it is necessary to have appropriate imaging modalities available (CT, MRI, angiography, ultrasound, stereotaxis). However, one should be aware that complex imaging devices such as CT or MR scanners are major investments and full utilization by interventions only is hardly possible. For these reasons, a close collaboration with general radiologist or joint usage is advisable.

The interventional radiologist should be aware that different modalities might need different interventional equipment. Especially, performance of MR-guided procedures demands special, magnetization compatible kits (e.g., certain vascular stents). Furthermore, it is important that a sufficient number of necessary interventional tools are available while performing an intervention – including alternative tools that might be needed. It is very unpleasant for all involved persons if a procedure has to be interrupted and postponed due to missing equipment (Lammer 2008).

19.2.2 Private Interventional Practice

Building up a private office is a possible alternative to a hospital-based outpatient clinic. There are some advantages of running a private practice, not least that the interventional radiologist can act beyond sustaining hospital politics and the income perspective might be better (Lammer 2008).

Basically most facts mentioned above are relevant for a private practice as well. However, there are several points that have to be considered.

In private practice, there might be interventions in which complications that cannot be handled by the interventional radiologist him- or herself. These cases require immediate consultation of a dedicated hospital department (e.g., surgery). Such "worst-case scenarios" are under better and faster control in a hospital-based unit where the relevant departments are available. A potential solution to this problem could be a contract with a hospital about a certain number of beds for treating patients as a visiting consultant (Lammer 2008).

Although the income might be higher in a private practice, one should be aware of higher corresponding costs at the same time: Technical equipment as well as staff and monthly rents has to be paid. A subleasing contract with another radiologist could be a solution of this aspect (Lammer 2008).

Furthermore, referring departments or colleagues are often not located in the same building. For this reason, promotion and marketing are likely to play a bigger role for a private practice than it does for a hospital-based interventional unit. The interventional services need to be promoted continuously using different media such as internet, print brochures, or information events (Siskin et al. 2004; Lammer 2008).

References

Adams RJ, Smith BJ, Ruffin RE (2001) Impact of the physician's participatory style in asthma outcomes and patient satisfaction. Ann Allergy Asthma Immunol 86:263–271

Ahmed K, Keeling AN, Khan RS, Ashrafian H, Arora S et al (2010) What does competence entail in interventional radiology? Cardiovasc Intervent Radiol 33:3–10

Baerlocher MO, Asch MR, Hayeems E, Collingwood P (2006) The clinical interventional radiologist: results of a national survey by the Canadian Interventional Radiology Association. Can Assoc Radiol J 57:218–223

Barth KH, Matsumoto AH (1991) Patient care in interventional radiology: a perspective. Radiology 178:11–17

Becker GJ (2001) 2000 RSNA annual oration in diagnostic radiology: the future of interventional radiology. Radiology 220:281–292

Greenfield S, Kaplan SH, Ware JE Jr, Yano EM, Frank HJ (1988) Patients' participation in medical care: effects on blood sugar control and quality of life in diabetes. J Gen Intern Med 3:448–457

Hulka BS, Kupper LL, Cassel JC, Mayo F (1975) Doctor-patient communication and outcomes among diabetic patients. J Community Health 1:15–27

Katzen BT, Kaplan JO, Dake MD (1989) Developing an interventional radiology practice in a community hospital: the interventional radiologist as an equal partner in patient care. Radiology 170:955–958

Keeling AN, Reekers JA, Lee MJ (2009) The clinical practice of interventional radiology: a European perspective. Cardiovasc Intervent Radiol 32:406–411

Lammer J (2008) Clinical practice in interventional radiology. Vol 1. Version 0.1. CIRSE, Vienna, Austria

Murphy TP (2003) Clinical interventional radiology: serving the patient. J Vasc Interv Radiol 14:401–403

Nolte-Ernsting C, Abel K, Krupski G, Lorenzen J, Adam G (2006) Wirtschaftliche Evaluation angiographischer Interventionen einschließlich einer radiologischen stationären und ambulanten Patientenbetreuung. Fortschr Röntgenstr 178:78–89

Pentecost MJ (2003) American college of radiology: clinical practice of interventional radiology and neurointerventional radiology white paper. ACR, Reston

Ring EJ, Kerlan RK (1985) Inpatient management: a new role for interventional radiologist. Radiology 154:543

Siskin GP, Bagla S, Sansivero GE, Mitchell NL (2004) The interventional radiology clinic: key ingredients for success. J Vasc Interv Radiol 15:681–688

Smith TP, Cragg AH, Berbaum KS (1989) Political trends in vascular and interventional radiology: a randomized survey. Radiology 170:941–944

Swischuk JL, Sacks D, Pentecost MJ, Mauro MA, Moresco K et al (2004) Clinical practice of interventional and cardiovascular radiology: current status, guidelines for resource allocation, future directions. J Am Coll Radiol 1:720–727

Tomashek JP (2002) The interventional radiology clinic: back to basics and into the future. Appl Radiol 31(8): 20–28

Teng GJ, Xu K, Ni CF, Li LS (2008) Interventional radiology in China. Cardiovasc Intervent Radiol 31:233–237

White RI Jr, Denny DF Jr, Osterman FA, Greenwood LH, Wilkinson LA (1989) Logistics of a university interventional radiology practice. Radiology 170:951–954

Yamashita Y, Takahashi M, Hiramatsu K, Ishikawa T, Suzuki S et al (1994) Current status of angiography and interventional radiology in Japan: survey results. J Vasc Interv Radiol 5:299–304

Medical Education in Interventional Radiology

20

Patrick Stumpp

Contents

20.1 Introduction

This chapter about medical education in interventional radiology seems a bit unusual at first sight. People who are about to do their first steps in interventional radiology will probably be more interested in the first three parts of this book.

However, there are people that do have more routine in interventional radiology and use this book mostly for looking up details while preparing special interventions. These people usually are also responsible for teaching (interventional) radiology. This chapter will try to give them some helpful suggestions for an effective teaching.

This chapter will mainly focus on two important parts of medical education: undergraduate and postgraduate studies.

One can ask whether interventional radiology should already be part of undergraduate studies or if this should not be restricted to postgraduate education.

At this stage, one should not forget that teaching radiology in undergraduate medical education is an important opportunity to present this interesting and fascinating specialty to the students. Teaching interventional radiology can direct students' attention to the many different facets our field has to offer (Baerlocher and Asch 2006).

Three main factors are especially important for teaching of interventional radiology in undergraduate studies:

1. Image-guided interventional procedures have continued to grow during the past decades and will certainly offer an interesting and challenging

P. Stumpp
Department of Diagnostic Radiology,
University Hospital Leipzig,
Liebigstraße 20, D-04103 Leipzig, Germany
e-mail: patrick.stumpp@medizin.uni-leipzig.de

A.H. Mahnken et al. (eds.), *CT- and MR-Guided Interventions in Radiology*,
DOI 10.1007/978-3-642-33581-5_20,

field for every young medical student in the near future. Awareness for this potential has to be created amongst the medical students.
2. Interventional radiology gives radiologists the opportunity to take an active role in the therapeutic process – radiology is not longer "just a way to diagnosis".
3. It also includes a closer contact to patients, compared to other areas of radiology. Up to now, a lot of undergraduates name "not enough contact to patients" as an important reason not to choose radiology as a subspecialty.

Many medical students that so far had a sceptic attitude towards radiology will find interest in this specialty when they see the *therapeutic options*, the fascinating aspects of *minimally invasive image-guided techniques* and the opportunity for a closer *doctor-patient interaction*. These statements are supported by recent findings in a survey amongst second-year medical students (Ghatan et al. 2010) and similar results in a survey amongst radiology residents (Baerlocher et al. 2005).

Therefore, teaching interventional radiology in undergraduate medical education has to cover two important aspects. First, one has to stimulate the students' interest in radiology as explained above. Second, the students have to know what therapeutic and minimally invasive option radiology has to offer in the treatment of many different diseases and conditions so that they know when to contact the radiologist as a therapeutic partner.

In Sect. 21.2, some basic thoughts for planning a radiological curriculum will be presented as a help for achieving these two goals. Some guidelines for the formulation of learning goals and objectives will also be given.

Section 21.3 deals with different aspects in teaching interventional radiology, namely, the postgraduate education. In this setting, the challenge is to compete with the interesting diagnostic modalities from conventional x-rays up to powerful magnets. At this point, it is necessary to define which interventional procedures have to be mastered by every radiologist and which should be reserved for the interventional-radiology specialist.

Although this definition will probably vary between different countries, all together have the challenge to teach newcomers in two radiology aspects about interventions. The most important point certainly is the "when and why" of an intervention. But for the teaching of skills that are necessary to do interventions, the "how to" also is of great importance.

Section 21.3 will introduce the so-called 4-step method for teaching practical skills that can help especially in the "how to"– aspect of teaching interventional radiology.

20.2 Interventional Radiology in Undergraduate Medical Education

20.2.1 Active and Passive Learning

Basically, one can differentiate two learning styles that (not only) students are directed to, the so-called active and passive learning. While in passive learning, the knowledge is only presented to the student; active learning gives the students specific tasks and motivates them to gather new knowledge from different sources and synthesise this knowledge to solve the task.

Passive learning is mostly receptive in style and favoured by the classic lecture (ex cathedra teaching). Knowledge is brought to the student by the teacher and has to be memorised somehow. This "teacher-centred" approach confronts students with knowledge, but the processing of the knowledge and the connection with already adopted knowledge is not encouraged in this learning situation. Typical recall rates of knowledge presented in lectures after 3 months lie round about 3–5 % (Bruner 1966). For IR, an example could be a lecture about organ biopsies that systematically lists all amenable organs and enumerates indications and contraindications for each organ.

In an *active learning* situation, the students are challenged to work with their already acquired knowledge, and they have to connect that with new information presented to them. In this "student-centred" approach, the teacher acts as a facilitator to help the student with the integration of new knowledge into the pre-existing body of knowledge. This type of knowledge processing leads to 3-month recall rates of ≥50 %. In the former example of

biopsies, this could be realised by giving different groups of students the task to prepare a patient briefing for liver biopsy, lung biopsy, kidney biopsy, etc. This compels the students to work up indications, contraindications and technique of biopsies. The following teaching session can be used to highlight similarities and differences for biopsies in different organs.

The tenfold difference between the recall rates of active and passive learning should be enough motivation to implement teaching methods that favour an active learning style. For teaching radiology in undergraduate medical education, an appropriate course was already published in the 1980s (Edeiken-Monroe et al. 1988). They favoured a tutor-guided setting, in which students had to prepare radiological cases and explain and discuss the images and findings to their peers. After all cases were discussed in this small-group setting with a radiologist supervising three groups at the same time, the remaining open questions were reviewed by all three groups with the attending radiologist.

Our own findings with a similar technique show positive effects of active learning and support results of other studies. If you want to design a (new) curriculum that favours active learning, the "Kern cycle" can be of use and is introduced in the following section.

20.2.2 The "Kern Cycle"

In their book "Curriculum Development For Medical Education", Kern et al. describe a six-step approach for successful curriculum development (Kern et al. 1998). These steps are neither surprisingly new nor very complicated, but it surely is a great help to envision them while planning a curriculum.

The following paragraphs will list the six steps and explain their meaning using interventional radiology as an example.

The six steps are titled:

1. Problem identification and general needs assessment
2. Needs assessment of targeted learners
3. Goals and objectives
4. Educational strategies
5. Implementation
6. Evaluation and feedback

1. Problem identification and general needs assessment
   Concerning interventional radiology, the problem about teaching contents of this subspecialty and thoughts about general need were discussed in detail in the introduction section of this chapter. At this stage, let us agree that teaching interventional radiology in undergraduate medical education is reasonable.
2. Needs assessment of targeted learners
   Assessing the needs of medical students concerning interventional radiology may reveal different needs at different institutions, depending on the content students have been taught in other classes like vascular surgery, oncology or angiology.

   Probably, all students will need to know facts about contrast media and their contraindications, different interventional materials and general treatment options (e.g. revascularisation, vascular occlusion, local chemotherapy, coiling of aneurysms).
3. Goals and objectives
   Definition of goals and objectives is a crucial step in designing a curriculum. One should spend enough time for the definition of these, as very often the process of exactly phrasing learning objectives helps to get a clearer view on what actually is or is not necessary to teach.

   Broader goals in interventional radiology could be:
   - To acquaint students with opportunities and risks of contrast media
   - To familiarise students with interventional treatment options
   - To enable students to explain the technique of digital subtraction angiography

   The definition of specific objectives can include cognitive, affective or psychomotor objectives. In undergraduate teaching, one will probably emphasise more cognitive objectives. For postgraduate teaching, there will be a stronger focus on the psychomotor objectives. Concerning interventional radiology, one could state that after a course the students should:

- Be able to explain the Seldinger technique
- Be able to describe six steps of an image-guided biopsy (planning, aiming, disinfection, advancement of needle, tissue sampling, (complication) control)
- Be able to explicate two indications and three contraindications for liver biopsies
- Have seen examples of at least three common angiographic imaging procedures and interventions

A precise wording is crucial for the definition of goals and objectives. Especially the correct operationalisation of objectives helps in different ways: the staff in planning the course, the students in finding the right things to learn and the examiners in asking the right questions. A learning objective "liver biopsy" would be very unspecific and leave a large room for interpretation. Differences about the essentials of this objective are foreseeable. The above-named example of "being able to explicate two indications and three contraindications for liver biopsies" is specific and measurable for teachers, students and examiners.

Anderson and Krathwohl's revision of Bloom's "taxonomy of educational objectives" provides a guide for phrasing objectives (Anderson et al. 2001).

4. Educational strategies
   It is only after step 3 that the specific educational strategy can be selected, which will be most effective in achieving the defined goals and objectives.

   Concerning the above-mentioned objectives, one could think about a short introductory talk about contrast media, followed by a case example about a patient with a contrast reaction and a discussion about preventive treatment options.

   For the Seldinger technique, a video could be shown, and one could provide the real devices used for an arterial access so students can see and touch them. In a Skills Lab, students could even be taught the procedure itself, but then the objective would have to be defined in a different manner.
5. Implementation
   For the very important step of implementing a curriculum, one has to consider a variety of different aspects.

   The process should be supported by the institutions' leaders. Resources in facilities and staff members have to be checked. Possible barriers for implementation should be identified and handled before starting the process. Information about the curriculum has to be spread amongst the involved personnel, meaning both faculty members *and* students! Careful scheduling is necessary to avoid a negative connotation of the curriculum caused by insufficient organisation.
6. Evaluation and feedback
   Having introduced a curriculum, its effects have to be evaluated. This includes different aspects of evaluation.

   Students can be evaluated in their performance by an examination. Under the assumption, that the exam itself has a good quality, the results can reflect if our teaching was effective. This can be used for adjusting the curriculum.

   The curriculum itself can be evaluated by interviewing students and faculty about the course of action and the experienced strengths and weaknesses of the curriculum. If problems are identified, proper adjustments can be made in time to continuously improve the curriculum.

Not all of the above-mentioned steps necessarily have to be passed in the presented order, although, for a successful curriculum, one has to be sure that each step has been completed at least once. And at this stage, the importance of clearly expressed goals and objectives for both planning the curriculum and guiding the learner through a course needs to be emphasised again.

20.3 Interventional Radiology in Postgraduate Medical Education

When teaching interventional radiology in a postgraduate setting, the focus certainly lies more on psychomotor skills and the knowledge about indications and contraindications for a given procedure. Handling of typical complications should also be an issue.

For recruiting new interventional radiologists, it seems to be advantageous to confront trainees with interventional radiology early in their training (Baerlocher et al. 2005;

McGuinness and Holden 2008). Kothary et al. even claim increased responsibility and ownership (realised by first assistance and on-call times) for radiology residents as a successful way to recruit more interventional radiologists (Kothary et al. 2010).

20.3.1 Simulation

Considering the six-step approach explained in detail in the previous section, this method can be used just as well for designing a curriculum for postgraduates. Here, the differing learning goals and objectives have to be kept in mind. Having defined different objectives, the educational strategies and surroundings used will be different as well.

As the postgraduate setting is most likely the one in which the "how to" question has to be answered, the surrounding might well be a simulator laboratory. Traditionally, training in interventional radiology started with handling of catheters and guidewires, which could be practised in diagnostic angiographies. Nowadays, many purely diagnostic procedures are performed with cross-sectional imaging modalities like ultrasound, CT or MRI. Many patients enter the IR suite only for an interventional procedure. Consecutively, trainees have less opportunity to practise their psychomotor skills with the catheter on patients.

Preparation of residents and fellows for this task can take place in a safe surrounding like a simulator laboratory instead. Various simulators for interventional radiology exist and reach from simple homemade synthetic models to very sophisticated virtual reality simulators with haptic feedback. These simulators have been evaluated thoroughly (Neequaye et al. 2007), and it was found that especially the existing virtual reality simulators already give a good opportunity to practise technically challenging tasks like carotid artery stenting. Their use can result not only in significant improvement of in vitro performance of interventional procedures but also in improvement of in vivo performance (Berry et al. 2007; Chaer et al. 2006). But also the synthetic models can be of great use in training, especially for practising simpler tasks like changing catheters over a guidewire (Gould 2010).

In an extensive meta-analysis of studies about the use of high-fidelity models, Issenberg et al. came to the conclusion that any model has to be used within a clearly structured curriculum, should represent different levels of difficulties, has to give the opportunity to repeat the task and has to include feedback to result in a valuable learning experience (Issenberg et al. 2005).

A simulator laboratory can also be the surrounding for team training, in which the normal workflow with all team members can be practised. Going even further, training in the sense of crew resource management – as known from the aviation industry – can be implemented here as well (Miguel et al. 2011).

20.3.2 4-Step Method

Simulator laboratories can also be a good place for the implementation of the 4-step method (Peyton's method) for teaching psychomotoric proficiencies. Far too long, the "see one, do one, teach one" method has been used to "teach" practical skills. While this might be all right for simpler tasks like palpation of the radial pulse, it already overstrains a learner when it comes to an easy medical procedure like the insertion of an intravenous line. When such practical skills have to be taught, the 4-step method described by Peyton can help to reassure teachers and learners of the knowledge and skills of the learner (Walker and Peyton 1998).

The four steps were summarised under the following headlines (Lake and Hamdorf 2004):

- Demonstration. Trainer demonstrates at normal speed, without commentary.
- Deconstruction. Trainer demonstrates while describing steps.
- Comprehension. Trainer demonstrates, while learner describes steps.
- Performance. Learner demonstrates while describing steps.

The *first step* is intended to give the learner the full picture of what is expected from him later on. The learner has the opportunity to view the procedure and perceive all involved persons and instruments.

The *second step* is the real challenge for the teacher. He has to break up a sometimes complicated task into manageable actions that can be understood and reproduced by the learner. This part actually requires a most conscious preparation as the teacher has to step back and reflect what he is doing routinely in everyday practice. It is as if one had to rethink about what he or she has to do, for riding a car. To explain this to a person that never rode a car before will take some time to reflect the action and explain the succeeding steps. The explanations have to be easy to understand and follow for a beginner. The same holds true for different medical skills that can range from measuring blood pressure to completing a liver transplant. Off course, the complexity of these skills varies and so does the complexity of the teaching. But still, even the most complex task can be broken down into understandable, teachable and manageable actions.

In the *third step*, the teacher can check what the learner already understands. As the teacher still has to perform the activity, it is a safe step. Sticking to the examples named above, it is safe for the engines and gears of the car and – more important in our case – safe for the patient. If there have been misunderstandings, the teacher can correct these now.

Before the learner goes on practising his newly learnt skill on his own, the *fourth step* requires him to vocalise the different actions *before* he completes them. This step allows the teacher once more to convince himself of the learners' level of understanding.

Certainly, any of these steps can be repeated, and one can also go back one step to make sure that the learner actually gets all things right. This is why especially for skills that put patients at risk (what basically all interventional-radiology procedures do) Peyton's 4-step method gives an extra amount of safety to teaching.

Key Points

1. In modern medical education, an active learning approach should be favoured. The learner needs to get actively involved for a better processing and retention of knowledge as well as more self-confidence.
2. Teaching always requires the thorough preparation of an appropriate curriculum. The Kern cycle is an established tool to complete everything needed for a successful curriculum planning.
3. Precise phrasing of learning goals and objectives is of utmost importance. It will help learners *and* teachers.
4. Simulation laboratories can be valuable tools for learning skills in IR but should be embedded into a comprehensive curriculum to have maximum effect.
5. For teaching practical skills, Peyton's 4-step method is recommended as an easy and robust technique.

References

Anderson LW, David R, Krathwohl DR et al (2001) A taxonomy for learning, teaching, and assessing: a revision of Bloom's taxonomy of educational objectives. Allyn & Bacon, Boston

Baerlocher MO, Asch MR, Eran H, Canadian Interventional Radiology Association (CIRA) (2005) Attitudes of and influences on residents in English Canadian radiology programs regarding interventional radiology: results of a national survey by the Canadian Interventional Radiology Association (CIRA). J Vasc Interv Radiol 16(10):1349–1354

Baerlocher MO, Asch M (2006) Protecting the future: attracting interventional radiology trainees–a medical student's perspective. Can Assoc Radiol J 57(3):147–151

Berry M, Lystig T, Beard J, Klingestierna H, Reznick R, Lonn L (2007) Porcine transfer study: virtual reality simulator training compared with porcine training in endovascular novices. Cardiovasc Intervent Radiol 30:455–461

Bruner JS (1966) Towards a theory of instruction. Harvard University Press, Cambridge

Chaer RA, DeRubertis BG, Lin SC, Bush HL, Karwowski JK, Birk D et al (2006) Simulation improves resident performance in catheter-based intervention – results of a randomized, controlled study. Ann Surg 244:343–352

Edeiken-Monroe BS, Harris JH, Jackson H (1988) Diagnostic radiology. One week prelude to the clinical continuum. Invest Radiol 23:945–949

Ghatan CE, Kuo WT, Hofmann LV, Kothary N (2010) Making the case for early medical student education in interventional radiology: a survey of 2nd-year students

in a single U.S. institution. J Vasc Interv Radiol 21(4): 549–553

Gould DA (2007) Interventional radiology simulation: prepare for a virtual revolution in training. J Vasc Interv Radiol 18(4):483–490

Gould D (2010) Using simulation for interventional radiology training. Br J Radiol 83:546–553

Issenberg SB, McGaghie WC, Petrusa ER et al (2005) Features and uses of high fidelity medical simulations that lead to effective learning: a BEME systematic review. Med Teach 27:10–28

Kern DE, Thomas PA, Howard DM, Bass EB (1998) Curriculum development for medical education: a six-step approach. The Johns Hopkins University Press, Baltimore

Kothary N, Ghatan CE, Hwang GL, Kuo WT, Louie JD, Sze DY, Hovsepian DM, Desser TS, Hofmann LV (2010) Renewing focus on resident education: increased responsibility and ownership in interventional radiology rotations improves the educational experience. J Vasc Interv Radiol 21(11):1697–1702

Lake FR, Hamdorf JM (2004) Teaching on the run, Part 5. Med J Aust 181(6):327–328

McGuinness B, Holden A (2008) Interventional radiology: a survey of trainees. J Med Imaging Radiat Oncol 52(2): 155–160

Miguel K, Hirsch JA, Sheridan RM (2011) Team training: a safer future for neurointerventional practice. J Neurointerv Surg 3(3):285–287

Neequaye SK, Aggarwal R, Van Herzeele I, Darzi A, Cheshire NJ (2007) Endovascular skills training and assessment. J Vasc Surg 46(5):1055–1064

Walker M, Peyton JWR (1998) Teaching in theatre. In: Peyton JWR (ed) Teaching and learning in medical practice. Manticore Europe Limited, Rickmansworth, pp 171–180

Index

A.H. Mahnken et al. (eds.), *CT- and MR-Guided Interventions in Radiology*,
DOI 10.1007/978-3-642-33581-5, © Springer-Verlag Berlin Heidelberg 2013